

Realistic LOCA Evaluation Methodology Applied to the Full Spectrum of Break Sizes (FULL SPECTRUM LOCA Methodology)

Appendices Requests for Additional Information, Audit Summaries, and Other Licensing Documentation



Westinghouse Electric Company
Engineering, Equipment and Major Projects
1000 Westinghouse Drive, Building 3
Cranberry Township, Pennsylvania 16066
USA

U.S. Nuclear Regulatory Commission
Document Control Desk
11555 Rockville Pike
Rockville, MD 20852

Direct tel: (412) 374-4643
Direct fax: (724) 940-8560
e-mail: greshaja@westinghouse.com

LTR-NRC-15-24

April 14, 2015

Subject: Submittal of Westinghouse WCAP-16996-P Volume I, Revision 1 and WCAP-16996-NP Volume I, Revision 1, 'Realistic LOCA Evaluation Methodology Applied to the Full Spectrum of Break Sizes (FULL SPECTRUM LOCA Methodology) - WCOBRA/TRAC-TF2 Models and Correlations' (Proprietary/Non-Proprietary), Project 700, TAC No. ME5244

Enclosed are copies of the proprietary and non-proprietary versions of the report 'Westinghouse WCAP-16996-P Volume I, Revision 1 and WCAP-16996-NP Volume I, Revision 1, Realistic LOCA Evaluation Methodology Applied to the Full Spectrum of Break Sizes (FULL SPECTRUM LOCA Methodology) - WCOBRA/TRAC-TF2 Models and Correlations'.

The updates from Revision 0 of the topical report are generally tracked, with the exceptions noted below; additions and deletions are marked with change bars, and text additions are shown in blue (except for equations which only have change bars). In order to improve readability and make the updates readily identifiable, the following types of updates were not tracked:

- Any shifting of proprietary markings due to repagination.
- Equation numbering and consistency formatting (any changes to the equations are tracked).
- Reference consistency formatting and minor error correction (any additions or deletions from the reference list are tracked).
- The updates previously transmitted to the Nuclear Regulatory Commission in LTR-NRC-13-75.

Revision 1 of the topical report reflects all the updates to the FULL SPECTRUM LOCA™ (FSLOCA™) evaluation model which occurred as a result of the methodology licensing. The following additional changes are also implemented and tracked consistent with the updates associated with the methodology licensing:

- Any inconsistencies that were identified as part of updating the topical report are corrected.
- The application range of the HRM break flow model is modified (Section 5.12) to alleviate spurious premature unchoking in pressurized water reactor simulations.

FULL SPECTRUM and FSLOCA are trademarks of Westinghouse Electric Company LLS, its subsidiaries and/or its affiliates in the United States of America and may be registered in other countries throughout the world. All rights reserved. Unauthorized use is strictly prohibited. Other names may be trademarks of their respective owners.

- The vapor flow at the top of a cell (rather than the cell average vapor flow) is used for the reflood entrainment model (Section 5.6.3), as it better represents the vapor flow which would carry droplets into the cell above.
- Updates are made in Section 5.4 to maintain consistent agreement with select separate effects tests after the interfacial drag package was updated as a result of the licensing process.

Also enclosed are:

1. An Application for Withholding Proprietary Information from Public Disclosure, AW-15-4146 (Non-Proprietary), with Proprietary Information Notice and Copyright Notice
2. An Affidavit (Non-Proprietary).

This submittal contains proprietary information of Westinghouse Electric Company LLC. In conformance with the requirements of 10 CFR Section 2.390, as amended, of the Commission's regulations, we are enclosing with this submittal an Application for Withholding Proprietary Information from Public Disclosure and an Affidavit. The Affidavit sets forth the basis on which the information identified as proprietary may be withheld from public disclosure by the Commission.

Correspondence with respect to the proprietary aspects of the Application for Withholding or the Westinghouse Affidavit should reference AW-15-4146 and should be addressed to James A. Gresham, Manager, Regulatory Compliance, Westinghouse Electric Company, 1000 Westinghouse Drive, Building 3 Suite 310, Cranberry Township, Pennsylvania 16066.

Very truly yours,

Handwritten signature of James A. Gresham, with the text "FOR" written to the right of the signature.

James A. Gresham, Manager

Regulatory Compliance

Enclosures

cc: Ekaterina Lenning (NRC)

bcc: James A. Gresham
Cheryl Robinson
Anne M. Stegman
Amy J. Colussy
Jeffrey R. Kobelak
Ryan S. Lenahan
Thomas Rodack
Marianne P. Rudakewiz

Internal References: LTR-FSLOCA-14-95



Westinghouse Electric Company
Engineering, Equipment and Major Projects
1000 Westinghouse Drive, Building 3
Cranberry Township, Pennsylvania 16066
USA

U.S. Nuclear Regulatory Commission
Document Control Desk
11555 Rockville Pike
Rockville, MD 20852

Direct tel: (412) 374-4643
Direct fax: (724) 940-8560
e-mail: greshaja@westinghouse.com

AW-15-4146

April 14, 2015

APPLICATION FOR WITHHOLDING PROPRIETARY
INFORMATION FROM PUBLIC DISCLOSURE

Subject: LTR-NRC-15-24 P-Attachment, 'Westinghouse WCAP-16996-P Volume I, Revision 1 and WCAP-16996-NP Volume I, Revision 1, Realistic LOCA Evaluation Methodology Applied to the Full Spectrum of Break Sizes (FULL SPECTRUM LOCA Methodology) - WCOBRA/TRAC-TF2 Models and Correlations' (Proprietary)

Reference: Letter from James A. Gresham to Document Control Desk, LTR-NRC-15-24, dated April 14, 2015

The Application for Withholding Proprietary Information from Public Disclosure is submitted by Westinghouse Electric Company LLC (Westinghouse), pursuant to the provisions of paragraph (b)(1) of Section 2.390 of the Commission's regulations. It contains commercial strategic information proprietary to Westinghouse and customarily held in confidence.

The proprietary information for which withholding is being requested is identified in the proprietary version of the subject report. In conformance with 10 CFR Section 2.390, Affidavit AW-15-4146 accompanies this Application for Withholding Proprietary Information from Public Disclosure, setting forth the basis on which the identified proprietary information may be withheld from public disclosure.

Accordingly, it is respectfully requested that the subject information which is proprietary to Westinghouse be withheld from public disclosure in accordance with 10 CFR Section 2.390 of the Commission's regulations.

Correspondence with respect to the proprietary aspects of the Application for Withholding or the accompanying Affidavit should reference AW-15-4146 and should be addressed to James A. Gresham, Manager, Regulatory Compliance, Westinghouse Electric Company, 1000 Westinghouse Drive, Building 3 Suite 310, Cranberry Township, Pennsylvania 16066.

Very truly yours,

W. J. Gresham / FOR

James A. Gresham, Manager
Regulatory Compliance

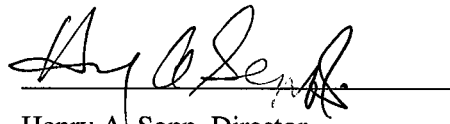
AFFIDAVIT

COMMONWEALTH OF PENNSYLVANIA:

SS

COUNTY OF BUTLER:

I, Henry A. Sepp, am authorized to execute this Affidavit on behalf of Westinghouse Electric Company LLC (Westinghouse), and that the averments of fact set forth in this Affidavit are true and correct to the best of my knowledge, information, and belief.

A handwritten signature in black ink, appearing to read "H. A. Sepp", is written over a horizontal line.

Henry A. Sepp, Director

MCRE-Engineering Services

- (1) I am Manager, Regulatory Compliance, Westinghouse Electric Company LLC (Westinghouse), and as such, I have been specifically delegated the function of reviewing the proprietary information sought to be withheld from public disclosure in connection with nuclear power plant licensing and rule making proceedings, and am authorized to apply for its withholding on behalf of Westinghouse.
- (2) I am making this Affidavit in conformance with the provisions of 10 CFR Section 2.390 of the Commission's regulations and in conjunction with the Westinghouse Application for Withholding Proprietary Information from Public Disclosure accompanying this Affidavit.
- (3) I have personal knowledge of the criteria and procedures utilized by Westinghouse in designating information as a trade secret, privileged or as confidential commercial or financial information.
- (4) Pursuant to the provisions of paragraph (b)(4) of Section 2.390 of the Commission's regulations, the following is furnished for consideration by the Commission in determining whether the information sought to be withheld from public disclosure should be withheld.
 - (i) The information sought to be withheld from public disclosure is owned and has been held in confidence by Westinghouse.
 - (ii) The information is of a type customarily held in confidence by Westinghouse and not customarily disclosed to the public. Westinghouse has a rational basis for determining the types of information customarily held in confidence by it and, in that connection, utilizes a system to determine when and whether to hold certain types of information in confidence. The application of that system and the substance of that system constitute Westinghouse policy and provide the rational basis required.

Under that system, information is held in confidence if it falls in one or more of several types, the release of which might result in the loss of an existing or potential competitive advantage, as follows:

 - (a) The information reveals the distinguishing aspects of a process (or component, structure, tool, method, etc.) where prevention of its use by any of

Westinghouse's competitors without license from Westinghouse constitutes a competitive economic advantage over other companies.

- (b) It consists of supporting data, including test data, relative to a process (or component, structure, tool, method, etc.), the application of which data secures a competitive economic advantage, e.g., by optimization or improved marketability.
 - (c) Its use by a competitor would reduce his expenditure of resources or improve his competitive position in the design, manufacture, shipment, installation, assurance of quality, or licensing a similar product.
 - (d) It reveals cost or price information, production capacities, budget levels, or commercial strategies of Westinghouse, its customers or suppliers.
 - (e) It reveals aspects of past, present, or future Westinghouse or customer funded development plans and programs of potential commercial value to Westinghouse.
 - (f) It contains patentable ideas, for which patent protection may be desirable.
- (iii) There are sound policy reasons behind the Westinghouse system which include the following:
- (a) The use of such information by Westinghouse gives Westinghouse a competitive advantage over its competitors. It is, therefore, withheld from disclosure to protect the Westinghouse competitive position.
 - (b) It is information that is marketable in many ways. The extent to which such information is available to competitors diminishes the Westinghouse ability to sell products and services involving the use of the information.
 - (c) Use by our competitor would put Westinghouse at a competitive disadvantage by reducing his expenditure of resources at our expense.

- (d) Each component of proprietary information pertinent to a particular competitive advantage is potentially as valuable as the total competitive advantage. If competitors acquire components of proprietary information, any one component may be the key to the entire puzzle, thereby depriving Westinghouse of a competitive advantage.
- (e) Unrestricted disclosure would jeopardize the position of prominence of Westinghouse in the world market, and thereby give a market advantage to the competition of those countries.
- (f) The Westinghouse capacity to invest corporate assets in research and development depends upon the success in obtaining and maintaining a competitive advantage.
- (iv) The information is being transmitted to the Commission in confidence and, under the provisions of 10 CFR Section 2.390, it is to be received in confidence by the Commission.
- (v) The information sought to be protected is not available in public sources or available information has not been previously employed in the same original manner or method to the best of our knowledge and belief.
- (vi) The proprietary information sought to be withheld in this submittal is that which is appropriately marked in LTR-NRC-15-24 P-Attachment, "Westinghouse WCAP-16996-P Volume I, Revision 1 and WCAP-16996-NP Volume I, Revision 1, 'Realistic LOCA Evaluation Methodology Applied to the Full Spectrum of Break Sizes (FULL SPECTRUM LOCA Methodology) - WCOBRA/TRAC-TF2 Models and Correlations" (Proprietary), for submittal to the Commission, being transmitted by Westinghouse letter, LTR-NRC-15-24, and Application for Withholding Proprietary Information from Public Disclosure, to the Document Control Desk. The proprietary information as submitted by Westinghouse is that associated with Westinghouse's request for NRC approval of WCAP-16996-P, and may be used only for that purpose.

- (a) This information is part of that which will enable Westinghouse to:
 - (i) Obtain NRC approval of the FULL SPECTRUM LOCA Methodology documented in WCAP-16996-P, "Realistic LOCA Evaluation Methodology Applied to the Full Spectrum of Break Sizes (FULL SPECTRUM LOCA Methodology).
- (b) Further this information has substantial commercial value as follows:
 - (i) Westinghouse plans to sell the use of similar information to its customers for the purpose of assisting customers in obtaining license changes for a Westinghouse pressurized water reactor (PWR).
 - (ii) Westinghouse can sell support and defense of FULL SPECTRUM LOCA Methodology documented in WCAP-16996-P, "Realistic LOCA Evaluation Methodology Applied to the Full Spectrum of Break Sizes (FULL SPECTRUM LOCA Methodology)".
 - (iii) The information requested to be withheld reveals the distinguishing aspects of a methodology which was developed by Westinghouse.

Public disclosure of this proprietary information is likely to cause substantial harm to the competitive position of Westinghouse because it would enhance the ability of competitors to provide similar technical evaluation justifications and licensing defense services for commercial power reactors without commensurate expenses. Also, public disclosure of the information would enable others to use the information to meet NRC requirements for licensing documentation without purchasing the right to use the information.

The development of the technology described in part by the information is the result of applying the results of many years of experience in an intensive Westinghouse effort and the expenditure of a considerable sum of money.

In order for competitors of Westinghouse to duplicate this information, similar technical programs would have to be performed and a significant manpower effort, having the requisite talent and experience, would have to be expended.

Further the deponent sayeth not.

PROPRIETARY INFORMATION NOTICE

Transmitted herewith are proprietary and non-proprietary versions of documents furnished to the NRC for approval of WCAP-16996-P, and may be used only for that purpose.

In order to conform to the requirements of 10 CFR 2.390 of the Commission's regulations concerning the protection of proprietary information so submitted to the NRC, the information which is proprietary in the proprietary versions is contained within brackets, and where the proprietary information has been deleted in the non-proprietary versions, only the brackets remain (the information that was contained within the brackets in the proprietary versions having been deleted). The justification for claiming the information so designated as proprietary is indicated in both versions by means of lower case letters (a) through (f) located as a superscript immediately following the brackets enclosing each item of information being identified as proprietary or in the margin opposite such information. These lower case letters refer to the types of information Westinghouse customarily holds in confidence identified in Sections (4)(ii)(a) through (4)(ii)(f) of the Affidavit accompanying this transmittal pursuant to 10 CFR 2.390(b)(1).

COPYRIGHT NOTICE

The reports transmitted herewith each bear a Westinghouse copyright notice. The NRC is permitted to make the number of copies of the information contained in these reports which are necessary for its internal use in connection with generic and plant-specific reviews and approvals as well as the issuance, denial, amendment, transfer, renewal, modification, suspension, revocation, or violation of a license, permit, order, or regulation subject to the requirements of 10 CFR 2.390 regarding restrictions on public disclosure to the extent such information has been identified as proprietary by Westinghouse, copyright protection notwithstanding. With respect to the non-proprietary versions of these reports, the NRC is permitted to make the number of copies beyond those necessary for its internal use which are necessary in order to have one copy available for public viewing in the appropriate docket files in the public document room in Washington, DC and in local public document rooms as may be required by NRC regulations if the number of copies submitted is insufficient for this purpose. Copies made by the NRC must include the copyright notice in all instances and the proprietary notice if the original was identified as proprietary.



Westinghouse Electric Company
1000 Westinghouse Drive
Cranberry Township, Pennsylvania 16066
USA

U.S. Nuclear Regulatory Commission
Document Control Desk
11555 Rockville Pike
Rockville, MD 20852

Direct tel: (412) 374-4643
Direct fax: (724) 940-8560
e-mail: greshaja@westinghouse.com

LTR-NRC-15-54

June 29, 2015

Subject: Submittal of WCAP-16996-P Volume II, Revision 1 and WCAP-16996-NP Volume II, Revision 1, "Realistic LOCA Evaluation Methodology Applied to the Full Spectrum of Break Sizes (FULL SPECTRUM LOCA Methodology)," (Proprietary/Non-Proprietary)

Enclosed are the proprietary and non-proprietary versions of WCAP-16996 Volume II, Revision 1, "Realistic LOCA Evaluation Methodology Applied to the Full Spectrum of Break Sizes (FULL SPECTRUM LOCA Methodology)," dated June 2015, submitted for review and approval under the NRC's licensing topical report program for referencing in licensing actions.

The updates from Revision 0 of the topical report are all tracked, with the exceptions noted below; additions and deletions are marked with change bars, and text additions are shown in blue. In order to improve readability and make the updates readily identifiable, the following types of updates were not tracked:

- Any shifting of proprietary markings due to repagination
- Equation numbering and consistency formatting (any changes to the equations are tracked)
- Reference consistency formatting and minor error correction (any additions or deletions from the reference list are tracked)

Revision 1 of the topical report reflects all the updates to the FULL SPECTRUM LOCA™ (FSLOCA™) evaluation model which occurred as a result of the methodology licensing. Additionally, it is noted that additional liquid velocity cases were included in the Northwestern perforated plate simulation plots (Section 19) which were inadvertently omitted in Revision 0.

Also enclosed are:

1. An Application for Withholding Proprietary Information from Public Disclosure, AW-15-4214 (Non-Proprietary) with Proprietary Information Notice and Copyright Notice
2. An Affidavit (Non-Proprietary).

This submittal contains proprietary information of Westinghouse Electric Company LLC. In conformance with the requirements of 10 CFR Section 2.390, as amended, of the Commission's regulations, we are enclosing with this submittal an Application for Withholding Proprietary Information from Public Disclosure and an Affidavit. The Affidavit sets forth the basis on which the information identified as proprietary may be withheld from public disclosure by the Commission.

Correspondence with respect to the proprietary aspects of the Application for Withholding or the Westinghouse Affidavit should reference AW-15-4214 and should be addressed to James A. Gresham, Manager, Regulatory Compliance, Westinghouse Electric Company, 1000 Westinghouse Drive, Building 3 Suite 310, Cranberry Township, Pennsylvania 16066.

A handwritten signature in black ink, appearing to read 'J. Gresham', with a stylized flourish at the end.

James A. Gresham, Manager
Regulatory Compliance

Enclosures

cc: Ekaterina Lenning (NRC)

bcc: James A. Gresham
Cheryl Robinson
Anne M. Stegman
Amy J. Colussy
Jeffrey R. Kobelak
Ryan S. Lenahan
Thomas Rodack
Marianne P. Rudakewiz

Internal Reference: LTR-FSLOCA-15-47



Westinghouse Electric Company
1000 Westinghouse Drive
Cranberry Township, Pennsylvania 16066
USA

U.S. Nuclear Regulatory Commission
Document Control Desk
11555 Rockville Pike
Rockville, MD 20852

Direct tel: (412) 374-4643
Direct fax: (724) 940-8560
e-mail: greshaja@westinghouse.com

AW-15-4214

June 29, 2015

APPLICATION FOR WITHHOLDING PROPRIETARY
INFORMATION FROM PUBLIC DISCLOSURE

Subject: WCAP-16996-P Volume II, Revision 1, "Realistic LOCA Evaluation Methodology Applied to the Full Spectrum of Break Sizes (FULL SPECTRUM LOCA Methodology)" (Proprietary)

Reference: Letter from James A. Gresham to Document Control Desk, LTR-NRC-15-54, dated June 29, 2015

The Application for Withholding Proprietary Information from Public Disclosure is submitted by Westinghouse Electric Company LLC (Westinghouse), pursuant to the provisions of paragraph (b)(1) of Section 2.390 of the Commission's regulations. It contains commercial strategic information proprietary to Westinghouse and customarily held in confidence.

The proprietary information for which withholding is being requested is identified in the proprietary version of the subject report. In conformance with 10 CFR Section 2.390, Affidavit AW-15-4214 accompanies this Application for Withholding Proprietary Information from Public Disclosure, setting forth the basis on which the identified proprietary information may be withheld from public disclosure.

Accordingly, it is respectfully requested that the subject information which is proprietary to Westinghouse be withheld from public disclosure in accordance with 10 CFR Section 2.390 of the Commission's regulations.

Correspondence with respect to the proprietary aspects of this Application for Withholding or the accompanying Affidavit should reference AW-15-4214 and should be addressed to James A. Gresham, Manager, Regulatory Compliance, Westinghouse Electric Company, 1000 Westinghouse Drive, Building 3 Suite 310, Cranberry Township, Pennsylvania 16066.

A handwritten signature in black ink, appearing to read "James A. Gresham".

James A. Gresham, Manager
Regulatory Compliance

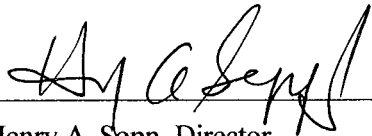
AFFIDAVIT

COMMONWEALTH OF PENNSYLVANIA:

ss

COUNTY OF BUTLER:

I, Henry A. Sepp, am authorized to execute this Affidavit on behalf of Westinghouse Electric Company LLC (Westinghouse), and I declare under penalty of perjury that the foregoing is true and correct.


Henry A. Sepp, Director

CRE-Systems and Components Engineering

- (1) I am Director, CRE-Systems and Components Engineering, Westinghouse Electric Company LLC (Westinghouse), and as such, I have been specifically delegated the function of reviewing the proprietary information sought to be withheld from public disclosure in connection with nuclear power plant licensing and rule making proceedings, and am authorized to apply for its withholding on behalf of Westinghouse.
- (2) I am making this Affidavit in conformance with the provisions of 10 CFR Section 2.390 of the Commission's regulations and in conjunction with the Westinghouse Application for Withholding Proprietary Information from Public Disclosure accompanying this Affidavit.
- (3) I have personal knowledge of the criteria and procedures utilized by Westinghouse in designating information as a trade secret, privileged or as confidential commercial or financial information.
- (4) Pursuant to the provisions of paragraph (b)(4) of Section 2.390 of the Commission's regulations, the following is furnished for consideration by the Commission in determining whether the information sought to be withheld from public disclosure should be withheld.
 - (i) The information sought to be withheld from public disclosure is owned and has been held in confidence by Westinghouse.
 - (ii) The information is of a type customarily held in confidence by Westinghouse and not customarily disclosed to the public. Westinghouse has a rational basis for determining the types of information customarily held in confidence by it and, in that connection, utilizes a system to determine when and whether to hold certain types of information in confidence. The application of that system and the substance of that system constitute Westinghouse policy and provide the rational basis required.

Under that system, information is held in confidence if it falls in one or more of several types, the release of which might result in the loss of an existing or potential competitive advantage, as follows:

- (a) The information reveals the distinguishing aspects of a process (or component, structure, tool, method, etc.) where prevention of its use by any of

Westinghouse's competitors without license from Westinghouse constitutes a competitive economic advantage over other companies.

- (b) It consists of supporting data, including test data, relative to a process (or component, structure, tool, method, etc.), the application of which data secures a competitive economic advantage, e.g., by optimization or improved marketability.
 - (c) Its use by a competitor would reduce his expenditure of resources or improve his competitive position in the design, manufacture, shipment, installation, assurance of quality, or licensing a similar product.
 - (d) It reveals cost or price information, production capacities, budget levels, or commercial strategies of Westinghouse, its customers or suppliers.
 - (e) It reveals aspects of past, present, or future Westinghouse or customer funded development plans and programs of potential commercial value to Westinghouse.
 - (f) It contains patentable ideas, for which patent protection may be desirable.
- (iii) There are sound policy reasons behind the Westinghouse system which include the following:
- (a) The use of such information by Westinghouse gives Westinghouse a competitive advantage over its competitors. It is, therefore, withheld from disclosure to protect the Westinghouse competitive position.
 - (b) It is information that is marketable in many ways. The extent to which such information is available to competitors diminishes the Westinghouse ability to sell products and services involving the use of the information.
 - (c) Use by our competitor would put Westinghouse at a competitive disadvantage by reducing his expenditure of resources at our expense.

- (d) Each component of proprietary information pertinent to a particular competitive advantage is potentially as valuable as the total competitive advantage. If competitors acquire components of proprietary information, any one component may be the key to the entire puzzle, thereby depriving Westinghouse of a competitive advantage.
- (e) Unrestricted disclosure would jeopardize the position of prominence of Westinghouse in the world market, and thereby give a market advantage to the competition of those countries.
- (f) The Westinghouse capacity to invest corporate assets in research and development depends upon the success in obtaining and maintaining a competitive advantage.
- (iv) The information is being transmitted to the Commission in confidence and, under the provisions of 10 CFR Section 2.390, it is to be received in confidence by the Commission.
- (v) The information sought to be protected is not available in public sources or available information has not been previously employed in the same original manner or method to the best of our knowledge and belief.
- (vi) The proprietary information sought to be withheld in this submittal is that which is appropriately marked in WCAP-16996-P Volume II, Revision 1, "Realistic LOCA Evaluation Methodology Applied to the Full Spectrum of Break Sizes (FULL SPECTRUM LOCA Methodology)" (Proprietary), dated June 2015, for submittal to the Commission, being transmitted by Westinghouse letter, LTR-NRC-15-54, and Application for Withholding Proprietary Information from Public Disclosure, to the Document Control Desk. The proprietary information as submitted by Westinghouse is that associated with Westinghouse's request for NRC approval of WCAP-16996, and may be used only for that purpose.

- (a) This information is part of that which will enable Westinghouse to:
 - (i) Obtain NRC approval of WCAP-16996, “Realistic LOCA Evaluation Methodology Applied to the Full Spectrum of Break Sizes (FULL SPECTRUM LOCA Methodology)”.
- (b) Further this information has substantial commercial value as follows:
 - (i) Westinghouse plans to sell the use of similar information to its customers for the purpose of assisting customers in obtaining license changes for a Westinghouse pressurized water reactor (PWR).
 - (ii) Westinghouse can sell support and defense of industry guidelines and acceptance criteria for plant-specific applications.
 - (iii) The information requested to be withheld reveals the distinguishing aspects of a methodology which was developed by Westinghouse.

Public disclosure of this proprietary information is likely to cause substantial harm to the competitive position of Westinghouse because it would enhance the ability of competitors to provide similar technical evaluation justifications and licensing defense services for commercial power reactors without commensurate expenses. Also, public disclosure of the information would enable others to use the information to meet NRC requirements for licensing documentation without purchasing the right to use the information.

The development of the technology described in part by the information is the result of applying the results of many years of experience in an intensive Westinghouse effort and the expenditure of a considerable sum of money.

In order for competitors of Westinghouse to duplicate this information, similar technical programs would have to be performed and a significant manpower effort, having the requisite talent and experience, would have to be expended.

Further the deponent sayeth not.

PROPRIETARY INFORMATION NOTICE

Transmitted herewith are proprietary and non-proprietary versions of documents furnished to the NRC in connection with requests for generic and/or plant-specific review and approval.

In order to conform to the requirements of 10 CFR 2.390 of the Commission's regulations concerning the protection of proprietary information so submitted to the NRC, the information which is proprietary in the proprietary versions is contained within brackets, and where the proprietary information has been deleted in the non-proprietary versions, only the brackets remain (the information that was contained within the brackets in the proprietary versions having been deleted). The justification for claiming the information so designated as proprietary is indicated in both versions by means of lower case letters (a) through (f) located as a superscript immediately following the brackets enclosing each item of information being identified as proprietary or in the margin opposite such information. These lower case letters refer to the types of information Westinghouse customarily holds in confidence identified in Sections (4)(ii)(a) through (4)(ii)(f) of the Affidavit accompanying this transmittal pursuant to 10 CFR 2.390(b)(1).

COPYRIGHT NOTICE

The reports transmitted herewith each bear a Westinghouse copyright notice. The NRC is permitted to make the number of copies of the information contained in these reports which are necessary for its internal use in connection with generic and plant-specific reviews and approvals as well as the issuance, denial, amendment, transfer, renewal, modification, suspension, revocation, or violation of a license, permit, order, or regulation subject to the requirements of 10 CFR 2.390 regarding restrictions on public disclosure to the extent such information has been identified as proprietary by Westinghouse, copyright protection notwithstanding. With respect to the non-proprietary versions of these reports, the NRC is permitted to make the number of copies beyond those necessary for its internal use which are necessary in order to have one copy available for public viewing in the appropriate docket files in the public document room in Washington, DC and in local public document rooms as may be required by NRC regulations if the number of copies submitted is insufficient for this purpose. Copies made by the NRC must include the copyright notice in all instances and the proprietary notice if the original was identified as proprietary.



Westinghouse Electric Company
1000 Westinghouse Drive
Cranberry Township, Pennsylvania 16066
USA

U.S. Nuclear Regulatory Commission
Document Control Desk
11555 Rockville Pike
Rockville, MD 20852

Direct tel: (412) 374-4643
Direct fax: (724) 940-8560
e-mail: greshaja@westinghouse.com

LTR-NRC-15-83

October 1, 2015

Subject: Submittal of WCAP-16996-P Volume III, Revision 1 and WCAP-16996-NP Volume III, Revision 1, "Realistic LOCA Evaluation Methodology Applied to the Full Spectrum of Break Sizes (FULL SPECTRUM LOCA Methodology)" (Proprietary/Non-Proprietary)

Enclosed are the proprietary and non-proprietary versions of WCAP-16996 Volume III, Revision 1, "Realistic LOCA Evaluation Methodology Applied to the Full Spectrum of Break Sizes (FULL SPECTRUM LOCA Methodology)," dated October 2015, submitted for review and approval under the NRC's licensing topical report program for referencing in licensing actions.

The updates from Revision 0 of the topical report are all tracked, with the exceptions noted below; additions and deletions are marked with change bars, and text additions are shown in blue. In order to improve readability and make the updates readily identifiable, the following types of updates were not tracked:

- Any shifting of proprietary markings due to repagination.
- Any text which was moved, but not modified.
- Equation numbering and consistency formatting (any changes to the equations are tracked).
- Reference consistency formatting and minor error correction (any additions or deletions from the reference list are tracked).

Revision 1 of the topical report reflects all the updates to the FULL SPECTRUM LOCA™ (FSLOCA™) evaluation model which occurred as a result of the methodology licensing. Additionally, the containment discussion was clarified to reflect that the LOTIC2 code, not the COCO code, is used for ice condenser containment designs. The LOTIC2 code version used within the FSLOCA evaluation model is the same as for the approved ASTRUM evaluation model, except for the changes reported under "General Code Maintenance" and "LOTIC2 Error Corrections" in LTR-NRC-12-37 (ML12207A081), and under "General Code Maintenance" in LTR-NRC-13-16 (ML13101A189).

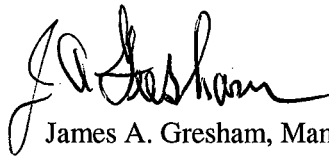
Also enclosed are:

1. An Application for Withholding Proprietary Information from Public Disclosure, AW-15-4292 (Non-Proprietary), with Proprietary Information Notice and Copyright Notice
2. An Affidavit (Non-Proprietary).

FULL SPECTRUM and FSLOCA are trademarks of Westinghouse Electric Company LLC, its subsidiaries and/or its affiliates in the United States of America and may be registered throughout the world. All rights reserved. Unauthorized use is strictly prohibited. Other names may be trademarks of their respective owners.

This submittal contains proprietary information of Westinghouse Electric Company LLC. In conformance with the requirements of 10 CFR Section 2.390, as amended, of the Commission's regulations, we are enclosing with this submittal an Application for Withholding Proprietary Information from Public Disclosure and an Affidavit. The Affidavit sets forth the basis on which the information identified as proprietary may be withheld from public disclosure by the Commission.

Correspondence with respect to the proprietary aspects of the Application for Withholding or the Westinghouse Affidavit should reference AW-15-4292 and should be addressed to James A. Gresham, Manager, Regulatory Compliance, Westinghouse Electric Company, 1000 Westinghouse Drive, Building 3 Suite 310, Cranberry Township, Pennsylvania 16066.



James A. Gresham, Manager

Regulatory Compliance

Enclosures

Cc: Ekaterina Lenning - NRC

bcc: James A. Gresham
Cheryl Robinson
Anne M. Stegman
Amy J. Colussy
Jeffrey R. Kobelak
Ryan S. Lenahan
Thomas Rodack
Marianne P. Rudakewiz

Internal Reference: LTR-FSLOCA-15-79, LTR-FSLOCA-15-81, LTR-FSLOCA-15-84 and LTR-FSLOCA-15-85.



Westinghouse Electric Company
1000 Westinghouse Drive
Cranberry Township, Pennsylvania 16066
USA

U.S. Nuclear Regulatory Commission
Document Control Desk
11555 Rockville Pike
Rockville, MD 20852

Direct tel: (412) 374-4643
Direct fax: (724) 940-8560
e-mail: greshaja@westinghouse.com

AW-15-4292

October 1, 2015

APPLICATION FOR WITHHOLDING PROPRIETARY
INFORMATION FROM PUBLIC DISCLOSURE

Subject: WCAP-16996-P Volume III, Revision 1, "Realistic LOCA Evaluation Methodology Applied to the Full Spectrum of Break Sizes (FULL SPECTRUM LOCA Methodology)" (Proprietary)

Reference: Letter from James A. Gresham to Document Control Desk, LTR-NRC-15-82, dated October 1, 2015

The Application for Withholding Proprietary Information from Public Disclosure is submitted by Westinghouse Electric Company LLC (Westinghouse), pursuant to the provisions of paragraph (b)(1) of Section 2.390 of the Commission's regulations. It contains commercial strategic information proprietary to Westinghouse and customarily held in confidence.

The proprietary information for which withholding is being requested is identified in the proprietary version of the subject report. In conformance with 10 CFR Section 2.390, Affidavit AW-15-4292 accompanies this Application for Withholding Proprietary Information from Public Disclosure, setting forth the basis on which the identified proprietary information may be withheld from public disclosure.

Accordingly, it is respectfully requested that the subject information which is proprietary to Westinghouse be withheld from public disclosure in accordance with 10 CFR Section 2.390 of the Commission's regulations.

Correspondence with respect to the proprietary aspects of the Application for Withholding or the accompanying Affidavit should reference AW-15-4292 and should be addressed to James A. Gresham, Manager, Regulatory Compliance, Westinghouse Electric Company, 1000 Westinghouse Drive, Building 3 Suite 310, Cranberry Township, Pennsylvania 16066.

A handwritten signature in black ink, appearing to read 'J. A. Gresham'.

James A. Gresham, Manager

Regulatory Compliance

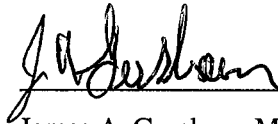
AFFIDAVIT

COMMONWEALTH OF PENNSYLVANIA:

SS

COUNTY OF BUTLER:

I, James A. Gresham, am authorized to execute this Affidavit on behalf of Westinghouse Electric Company LLC (Westinghouse), and that the averments of fact set forth in this Affidavit are true and correct to the best of my knowledge, information, and belief.

A handwritten signature in black ink, appearing to read "J. A. Gresham", is written over a horizontal line.

James A. Gresham, Manager
Regulatory Compliance

- (1) I am Manager, Regulatory Compliance, Westinghouse Electric Company LLC (Westinghouse), and as such, I have been specifically delegated the function of reviewing the proprietary information sought to be withheld from public disclosure in connection with nuclear power plant licensing and rule making proceedings, and am authorized to apply for its withholding on behalf of Westinghouse.
- (2) I am making this Affidavit in conformance with the provisions of 10 CFR Section 2.390 of the Commission's regulations and in conjunction with the Westinghouse Application for Withholding Proprietary Information from Public Disclosure accompanying this Affidavit.
- (3) I have personal knowledge of the criteria and procedures utilized by Westinghouse in designating information as a trade secret, privileged or as confidential commercial or financial information.
- (4) Pursuant to the provisions of paragraph (b)(4) of Section 2.390 of the Commission's regulations, the following is furnished for consideration by the Commission in determining whether the information sought to be withheld from public disclosure should be withheld.
 - (i) The information sought to be withheld from public disclosure is owned and has been held in confidence by Westinghouse.
 - (ii) The information is of a type customarily held in confidence by Westinghouse and not customarily disclosed to the public. Westinghouse has a rational basis for determining the types of information customarily held in confidence by it and, in that connection, utilizes a system to determine when and whether to hold certain types of information in confidence. The application of that system and the substance of that system constitute Westinghouse policy and provide the rational basis required.

Under that system, information is held in confidence if it falls in one or more of several types, the release of which might result in the loss of an existing or potential competitive advantage, as follows:

 - (a) The information reveals the distinguishing aspects of a process (or component, structure, tool, method, etc.) where prevention of its use by any of

Westinghouse's competitors without license from Westinghouse constitutes a competitive economic advantage over other companies.

- (b) It consists of supporting data, including test data, relative to a process (or component, structure, tool, method, etc.), the application of which data secures a competitive economic advantage, e.g., by optimization or improved marketability.
 - (c) Its use by a competitor would reduce his expenditure of resources or improve his competitive position in the design, manufacture, shipment, installation, assurance of quality, or licensing a similar product.
 - (d) It reveals cost or price information, production capacities, budget levels, or commercial strategies of Westinghouse, its customers or suppliers.
 - (e) It reveals aspects of past, present, or future Westinghouse or customer funded development plans and programs of potential commercial value to Westinghouse.
 - (f) It contains patentable ideas, for which patent protection may be desirable.
- (iii) There are sound policy reasons behind the Westinghouse system which include the following:
- (a) The use of such information by Westinghouse gives Westinghouse a competitive advantage over its competitors. It is, therefore, withheld from disclosure to protect the Westinghouse competitive position.
 - (b) It is information that is marketable in many ways. The extent to which such information is available to competitors diminishes the Westinghouse ability to sell products and services involving the use of the information.
 - (c) Use by our competitor would put Westinghouse at a competitive disadvantage by reducing his expenditure of resources at our expense.

- (d) Each component of proprietary information pertinent to a particular competitive advantage is potentially as valuable as the total competitive advantage. If competitors acquire components of proprietary information, any one component may be the key to the entire puzzle, thereby depriving Westinghouse of a competitive advantage.
 - (e) Unrestricted disclosure would jeopardize the position of prominence of Westinghouse in the world market, and thereby give a market advantage to the competition of those countries.
 - (f) The Westinghouse capacity to invest corporate assets in research and development depends upon the success in obtaining and maintaining a competitive advantage.
- (iv) The information is being transmitted to the Commission in confidence and, under the provisions of 10 CFR Section 2.390, it is to be received in confidence by the Commission.
- (v) The information sought to be protected is not available in public sources or available information has not been previously employed in the same original manner or method to the best of our knowledge and belief.
- (vi) The proprietary information sought to be withheld in this submittal is that which is appropriately marked in WCAP-16996-P Volume III, Revision 1, "Realistic LOCA Evaluation Methodology Applied to the Full Spectrum of Break Sizes (FULL SPECTRUM LOCA Methodology)" (Proprietary), dated October 2015, for submittal to the Commission, being transmitted by Westinghouse Letter LTR-NRC-15-83 and Application for Withholding Proprietary Information from Public Disclosure, to the Document Control Desk. The proprietary information as submitted by Westinghouse is that associated with Westinghouse's request for NRC approval of WCAP-16996-P and may be used only for that purpose.

- (a) This information is part of that which will enable Westinghouse to:
 - (i) Obtain NRC approval of the FULL SPECTRUM LOCA Methodology documented in WCAP-16996-P, "Realistic LOCA Evaluation Methodology Applied to the Full Spectrum of Break Sizes (FULL SPECTRUM LOCA Methodology).
- (b) Further this information has substantial commercial value as follows:
 - (i) Westinghouse plans to sell the use of similar information to its customers for the purpose of assisting customers in obtaining license changes for a Westinghouse pressurized water reactor (PWR).
 - (ii) Westinghouse can sell support and defense of industry guidelines and acceptance criteria for plant-specific applications.
 - (iii) The information requested to be withheld reveals the distinguishing aspects of a methodology which was developed by Westinghouse.

Public disclosure of this proprietary information is likely to cause substantial harm to the competitive position of Westinghouse because it would enhance the ability of competitors to provide similar technical evaluation justifications and licensing defense services for commercial power reactors without commensurate expenses. Also, public disclosure of the information would enable others to use the information to meet NRC requirements for licensing documentation without purchasing the right to use the information.

The development of the technology described in part by the information is the result of applying the results of many years of experience in an intensive Westinghouse effort and the expenditure of a considerable sum of money.

In order for competitors of Westinghouse to duplicate this information, similar technical programs would have to be performed and a significant manpower effort, having the requisite talent and experience, would have to be expended.

Further the deponent sayeth not.

PROPRIETARY INFORMATION NOTICE

Transmitted herewith are proprietary and non-proprietary versions of documents furnished to the NRC in connection with requests for generic and/or plant-specific review and approval.

In order to conform to the requirements of 10 CFR 2.390 of the Commission's regulations concerning the protection of proprietary information so submitted to the NRC, the information which is proprietary in the proprietary versions is contained within brackets, and where the proprietary information has been deleted in the non-proprietary versions, only the brackets remain (the information that was contained within the brackets in the proprietary versions having been deleted). The justification for claiming the information so designated as proprietary is indicated in both versions by means of lower case letters (a) through (f) located as a superscript immediately following the brackets enclosing each item of information being identified as proprietary or in the margin opposite such information. These lower case letters refer to the types of information Westinghouse customarily holds in confidence identified in Sections (4)(ii)(a) through (4)(ii)(f) of the Affidavit accompanying this transmittal pursuant to 10 CFR 2.390(b)(1).

COPYRIGHT NOTICE

The reports transmitted herewith each bear a Westinghouse copyright notice. The NRC is permitted to make the number of copies of the information contained in these reports which are necessary for its internal use in connection with generic and plant-specific reviews and approvals as well as the issuance, denial, amendment, transfer, renewal, modification, suspension, revocation, or violation of a license, permit, order, or regulation subject to the requirements of 10 CFR 2.390 regarding restrictions on public disclosure to the extent such information has been identified as proprietary by Westinghouse, copyright protection notwithstanding. With respect to the non-proprietary versions of these reports, the NRC is permitted to make the number of copies beyond those necessary for its internal use which are necessary in order to have one copy available for public viewing in the appropriate docket files in the public document room in Washington, DC and in local public document rooms as may be required by NRC regulations if the number of copies submitted is insufficient for this purpose. Copies made by the NRC must include the copyright notice in all instances and the proprietary notice if the original was identified as proprietary.

WCAP-16996-NP-A
Revision 1

**Realistic LOCA Evaluation Methodology Applied to the
Full Spectrum of Break Sizes
(FULL SPECTRUM LOCA Methodology)**

Jeffrey R. Kobelak	LOCA Integrated Services
Dr. Katsuhiro Ohkawa	LOCA Integrated Services
Dr. Liping Cao	LOCA Integrated Services
Aaron M. Everhard	LOCA Integrated Services
Dr. Jun Liao	LOCA Integrated Services
Nikolay P. Petkov	LOCA Integrated Services
Michael A. Shockling	LOCA Integrated Services

November 2016

Prepared by: Jeffrey R. Kobelak*
LOCA Integrated Services

Reviewer: Kevin J. Barber*
LOCA Integrated Services

Approved: Amy J. Colussy*, Manager
LOCA Integrated Services

FSLOCA and FULL SPECTRUM are trademarks of Westinghouse Electric Company LLC, its affiliates and/or its subsidiaries in the United States of America and may be registered in other countries throughout the world. All rights reserved. Unauthorized use is strictly prohibited. Other names may be trademarks of their respective owners.

*Electronically approved records are authenticated in the electronic document management system.

Westinghouse Electric Company LLC
1000 Westinghouse Drive
Cranberry Township, PA 16066, USA

© 2016 Westinghouse Electric Company LLC
All Rights Reserved

TABLE OF CONTENTS**APPENDICES**

A	REQUESTS FOR ADDITIONAL INFORMATION AND RESPONSES	A-1
	LTR-NRC-13-37	A-7
	LTR-NRC-13-45	A-138
	LTR-NRC-13-33	A-157
	LTR-NRC-13-31	A-220
	LTR-NRC-14-17	A-261
	LTR-NRC-13-32	A-477
	LTR-NRC-13-40	A-501
	LTR-NRC-13-73	A-533
	LTR-NRC-13-75	A-638
	LTR-NRC-13-41	A-769
	LTR-NRC-14-12	A-845
	LTR-NRC-14-19	A-927
	LTR-NRC-14-21	A-1073
	LTR-NRC-14-33	A-1111
	LTR-NRC-14-70	A-1118
	LTR-NRC-14-9	A-1225
	LTR-NRC-14-4	A-1288
B	NUCLEAR REGULATORY COMMISSION AUDIT SUMMARIES	B-1
	LTR-NRC-13-70	B-3
	LTR-NRC-14-55	B-489
	LTR-NRC-14-29	B-515
	LTR-NRC-14-38	B-660
	LTR-NRC-14-60	B-726
	LTR-NRC-15-6	B-770
	LTR-NRC-15-11	B-930
	LTR-NRC-15-67	B-974
	LTR-NRC-15-70	B-994
	LTR-NRC-15-85	B-1016
	LTR-NRC-15-82	B-1028
	LTR-NRC-15-88	B-1048
C	MISCELLANEOUS LICENSING DOCUMENTS	C-1
	LTR-NRC-15-91	C-2
	LTR-NRC-15-102, Revision 2	C-94
	LTR-NRC-16-14	C-145
	LTR-NRC-16-58	C-155

A REQUESTS FOR ADDITIONAL INFORMATION AND RESPONSES

This section contains all the documents which transmitted the requests for additional information (RAIs) and associated responses on the **FULL SPECTRUM™** LOCA (**FSLOCA™**) evaluation model (EM). The transmittal documents are listed in the included order below, along with the RAIs which were contained in each document.

LTR-NRC-13-37: 1-8, 10-11, 13-19

LTR-NRC-13-45: 9, 12

LTR-NRC-13-33: 20-29

LTR-NRC-13-31: 30-35

LTR-NRC-14-17: 36-39

LTR-NRC-13-32: 40-44

LTR-NRC-13-40: 45

LTR-NRC-13-73: 46-58, 75, 77 (note that two separate RAI-77s were received)

LTR-NRC-13-75: 59-71

LTR-NRC-13-41: 72-74, 76

LTR-NRC-14-12: 77-82, 86-87, 93, 112

LTR-NRC-14-19: 83-85, 88-92, 94-95, 113-119

LTR-NRC-14-21: 96-105, 107

LTR-NRC-14-33: 108, 120-121

LTR-NRC-14-70: 109-111

LTR-NRC-14-9: 122-126, 128-131, 136

LTR-NRC-14-4: 127, 132-135, 137-139

A summary of the transmittal letters and subject for all of the RAI responses is contained in Table A1.

Table A1		
RAI #	Transmittal Document	Subject
1	LTR-NRC-13-37	WCOBRA/TRAC MOD7A Revision 7
2	LTR-NRC-13-37	TRAC-PF1/MOD2
3	LTR-NRC-13-37	LBLOCA and SBLOCA PIRTs
4	LTR-NRC-13-37	End of Blowdown
5	LTR-NRC-13-37	Gap Conductance
6	LTR-NRC-13-37	Pressurizer Response
7	LTR-NRC-13-37	Long-Term Cooling and PIRT
8	LTR-NRC-13-37	SBLOCA Boundary and Region I to Region II Boundary
9	LTR-NRC-13-45	Worst SBLOCA
10	LTR-NRC-13-37	Loss-of-Offsite Power versus Reactor Coolant Pumps Operating
11	LTR-NRC-13-37	Loop Seal Behavior
12	LTR-NRC-13-45	Worst Break Sampling
13	LTR-NRC-13-37	Decay Heat Multiplier / Sampling
14	LTR-NRC-13-37	Number of SBLOCA Cases Sampled
15	LTR-NRC-13-37	SBLOCA Upper Limit Break Size
16	LTR-NRC-13-37	Long-Term Cooling Restriction
17	LTR-NRC-13-37	Swelled or Two-Phase Mixture Level versus Collapsed Level
18	LTR-NRC-13-37	High Pressure Safety Injection Curve Basis and Uncertainty
19	LTR-NRC-13-37	SBLOCA Axial Power Shape
20	LTR-NRC-13-33	Uranium and Plutonium Decay Heat Uncertainty Fits to ANS 5.1-1979
21	LTR-NRC-13-33	Uranium and Plutonium Decay Heat and Uncertainty Comparison to ANS 5.1-1979
22	LTR-NRC-13-33	Uranium and Plutonium Decay Heat Uncertainty Comparison to ANS 5.1-1979
23	LTR-NRC-13-33	Burnup Limit in Assessing Kinetics Parameters
24	LTR-NRC-13-33	Editorial Comments
25	LTR-NRC-13-33	Codes Utilized for Decay Heat Calculations
26	LTR-NRC-13-33	Actinides Decay Heat Power
27	LTR-NRC-13-33	Decay Heat in Demonstration Plant Analyses
28	LTR-NRC-13-33	Decay Heat Uncertainty Distribution
29	LTR-NRC-13-33	Decay Heat Sampling Approach
30	LTR-NRC-13-31	Scaling of Westinghouse Vertical COSI Test Facility and Tests
31	LTR-NRC-13-31	Westinghouse Vertical COSI Downcomer Condensation
32	LTR-NRC-13-31	Westinghouse Vertical Condensation on Safety Injection Heat Loss
33	LTR-NRC-13-31	Westinghouse Vertical Condensation on Safety Injection Data and Condensation Outside the Jet Region
34	LTR-NRC-13-31	Westinghouse Vertical Condensation on Safety Injection Data Qualification

Table A1 (cont'd)		
RAI #	Transmittal Document	Subject
35	LTR-NRC-13-31	Scale Impact on Cold Leg Condensation
36	LTR-NRC-14-17	Fuel Thermal Conductivity Model
37	LTR-NRC-14-17	Burnup Impact on Fuel Thermal Conductivity and Initial Stored Energy
38	LTR-NRC-14-17	Treatment of Fuel Burnup Dependent Parameters
39	LTR-NRC-14-17	Fuel Burnup Sampling
40	LTR-NRC-13-32	Fuel Burnup Limit in FSLOCA Methodology
41	LTR-NRC-13-32	Nuclear Fuel Rod Special Model Changes
42	LTR-NRC-13-32	Nuclear Fuel Rod Special Model Validation
43	LTR-NRC-13-32	I ^{a,c} Component Models
44	LTR-NRC-13-32	Fuel Rod Material Properties
45	LTR-NRC-13-40	Validity of Wilks Theorem
46	LTR-NRC-13-73	Containment Pressure Analysis Code COCO Component
47	LTR-NRC-13-73	TRAC-PF1 One-Dimensional Component Models
48	LTR-NRC-13-73	Steam Generator Modeling
49	LTR-NRC-13-73	T-Junction Component
50	LTR-NRC-13-73	Component Multipliers
51	LTR-NRC-13-73	Fluid Properties for Nusselt Number in Dispersed Droplet Flow
52	LTR-NRC-13-73	Nusselt Number Correlation Applicability for Dispersed Droplet Flow
53	LTR-NRC-13-73	Interfacial Heat Transfer in Inverted Annular and Liquid Slug Flows
54	LTR-NRC-13-73	Interfacial Heat Transfer to Droplet / Bubble
55	LTR-NRC-13-73	Droplet Diameter for Interfacial Heat Transfer in Dispersed Droplet Flow
56	LTR-NRC-13-73	Droplet-Wall Direct Contact Heat Transfer in Dispersed Flow Film Boiling
57	LTR-NRC-13-73	Large Break LOCA Heat Transfer Package in <u>W</u> COBRA/TRAC-TF2
58	LTR-NRC-13-73	Flow Regime Map Selection Criterion for Vessel Component
59	LTR-NRC-13-75	<u>W</u> COBRA/TRAC-TF2 Flow Maps for Vessel and One-Dimensional Components
60	LTR-NRC-13-75	PWR Core Two-Phase Mixture Level and Sensitivity to Axial Nodalization
61	LTR-NRC-13-75	ORNL THTF Mixture Level Predictions and Axial Nodalization Sensitivity
62	LTR-NRC-13-75	ORNL THTF <u>W</u> COBRA/TRAC-TF2 Detailed Prediction Results
63	LTR-NRC-13-75	Interfacial Drag Correlations in <u>W</u> COBRA/TRAC-TF2
64	LTR-NRC-13-75	Interfacial Area in Inverted Slug Flow
65	LTR-NRC-13-75	Interfacial Drag for Inverted Slug Flow
66	LTR-NRC-13-75	Annular Film Flow Interfacial Drag

Table A1 (cont'd)		
RAI #	Transmittal Document	Subject
67	LTR-NRC-13-75	Bubbly Flow Interfacial Drag Ramping to Hot Wall Inverted Annular Drag
68	LTR-NRC-13-75	Approach to Interfacial Drag Ramping Between Cold Wall and Hot Wall Regimes
69	LTR-NRC-13-75	Calculation Results for Bubbly Flow Interfacial Drag
70	LTR-NRC-13-75	Film Flow Drag Assessment Using THTF Test Data
71	LTR-NRC-13-75	Film Drag Impact on Bubbly Flow Void Predictions for THTF Tests
72	LTR-NRC-13-41	Bubbly Flow Drag Assessment Using THTF Test Data
73	LTR-NRC-13-41	Bubbly Flow Drag Assessment Using G-1 and G-2 Test Data
74	LTR-NRC-13-41	Interfacial Drag Sampling Approach
75	LTR-NRC-13-73	Interfacial Drag Sampling Impact on ROSA-IV LSTF Test Predictions
76	LTR-NRC-13-41	<u>W</u> COBRA/TRAC-TF2 Interfacial Drag Assessment
77 ¹	LTR-NRC-13-73	Summary of Uncertainty Parameters
77 ¹	LTR-NRC-14-12	Loop Seal Clearance in LSTF Test SB-CL-18
78	LTR-NRC-14-12	Loop Seal Clearance in LSTF Tests SB-CL-14 and SB-CL-18
79	LTR-NRC-14-12	<u>W</u> COBRA/TRAC-TF2 Assessment for LSTF Test SB-CL-14
80	LTR-NRC-14-12	LSTF Test SB-CL-14 Data Qualification
81	LTR-NRC-14-12	ROSA-IV LSTF <u>W</u> COBRA/TRAC-TF2 Assessment Results Presentation
82	LTR-NRC-14-12	Break Equivalent Diameter in LSTF Tests SB-CL-01, SB-CL-02, and SB-CL-03
83	LTR-NRC-14-19	Stratified Flow Multiplier HS_SLUG
84	LTR-NRC-14-19	Stratified Flow Multiplier HS_SLUG Application
85	LTR-NRC-14-19	Stratified Flow and Inclination Limitation
86	LTR-NRC-14-12	MSTRTX, STRTX, STRTX1, and STRTX2 Multipliers
87	LTR-NRC-14-12	<u>W</u> COBRA/TRAC-TF2 Non-Sampled Modeling Multipliers
88	LTR-NRC-14-19	LSTF Loop Seal Nodalization
89	LTR-NRC-14-19	Modeling of LSTF Loop Seal Horizontal Section and Bend Regions
90	LTR-NRC-14-19	<u>W</u> COBRA/TRAC-TF2 Features Applied in LSTF Loop Seal Modeling
91	LTR-NRC-14-19	V. C. Summer and Beaver Valley Unit 1 Loop Seal Models
92	LTR-NRC-14-19	PWR Loop Seal Horizontal Section and Bends Modeling
93	LTR-NRC-14-12	Editorial Findings
94	LTR-NRC-14-19	Interpolation for Stratified Flow and C_{HS_SLUG} Parameter
95	LTR-NRC-14-19	Interpolation for Stratified Flow and C_{STFRU} Parameter
96	LTR-NRC-14-21	PWR Upper Head Spray Nozzle Bypass Design Data
97	LTR-NRC-14-21	PWR Upper Head Spray Nozzle Bypass Flow Tune-Up

1. Two separate RAI-77s were received.

Table A1 (cont'd)		
RAI #	Transmittal Document	Subject
98	LTR-NRC-14-21	PWR Upper Head Temperature Tune-Up
99	LTR-NRC-14-21	PWR Upper Head Spray Nozzle Bypass in <u>W</u> COBRA/TRAC-TF2 Pilot Plant Models
100	LTR-NRC-14-21	Upper Head Spray Nozzle Bypass in LSTF Tests
101	LTR-NRC-14-21	Upper Head Spray Nozzle Bypass in LSTF <u>W</u> COBRA/TRAC-TF2 Model
102	LTR-NRC-14-21	LSTF Upper Head Spray Nozzle Bypass Relevance to PWR
103	LTR-NRC-14-21	Pressure Vessel Internal Leaks in LSTF Tests
104	LTR-NRC-14-21	Hot Leg-to-Downcomer Bypass Modeling in LSTF and PWR LOCA Analyses
105	LTR-NRC-14-21	Representation of LSTF Bypasses in <u>W</u> COBRA/TRAC-TF2 LSTF Test Simulations
106	No RAI 106 was received	
107	LTR-NRC-14-21	PWR Hot Leg Bypass in <u>W</u> COBRA/TRAC-TF2 Plant Simulations
108	LTR-NRC-14-33	<u>W</u> COBRA/TRAC-TF2 Assessment Using Counter-Current Flow Data by Costigan et al.
109	LTR-NRC-14-70	Semiscale Test S-LH-1 Assessment of <u>W</u> COBRA/TRAC-TF2
110	LTR-NRC-14-70	Semiscale Test S-LH-2 Assessment of <u>W</u> COBRA/TRAC-TF2
111	LTR-NRC-14-70	Sensitivity of <u>W</u> COBRA/TRAC-TF2 Semiscale Predictions to Steam Generator Nodalization
112	LTR-NRC-14-12	Sensitivity of <u>W</u> COBRA/TRAC-TF2 SBLOCA Predictions to Steam Generator Nodalization
113	LTR-NRC-14-19	<u>W</u> COBRA/TRAC-TF2 UPTF Loop Seal Nodalization
114	LTR-NRC-14-19	UPTF TRAM Loop Seal Instrumentation and <u>W</u> COBRA/TRAC-TF2 UPTF Model
115	LTR-NRC-14-19	<u>W</u> COBRA/TRAC-TF2 Sampled Parameters and Special Options in Loop Seal Modeling
116	LTR-NRC-14-19	UPTF TRAM Loop Seal Clearance Data and <u>W</u> COBRA/TRAC-TF2 Assessment
117	LTR-NRC-14-19	<u>W</u> COBRA/TRAC-TF2 UPTF Loop Seal Nodalization Sensitivity Study
118	LTR-NRC-14-19	<u>W</u> COBRA/TRAC-TF2 UPTF Loop Seal Modeling Options Sensitivity Study
119	LTR-NRC-14-19	<u>W</u> COBRA/TRAC-TF2 UPTF Loop Seal Time Step Limit Sensitivity Study
120	LTR-NRC-14-33	IVO Loop Seal Clearance Data and <u>W</u> COBRA/TRAC-TF2 Assessment
121	LTR-NRC-14-33	ECTHOR Loop Seal Clearance Data and <u>W</u> COBRA/TRAC-TF2 Assessment

Table A1 (cont'd)		
RAI #	Transmittal Document	Subject
122	LTR-NRC-14-9	Upper Bound Approach to Reactor Coolant Pump Trip Time During a LOCA with Offsite Power Available
123	LTR-NRC-14-9	Factors Affecting Reactor Coolant Pump Trip Time for LOCA Analyses with Offsite Power Available
124	LTR-NRC-14-9	Reactor Coolant Pump Trip Time for SBLOCA Analyses with Offsite Power Available
125	LTR-NRC-14-9	Reactor Coolant Pump Trip Time for LBLOCA Analyses with Offsite Power Available
126	LTR-NRC-14-9	Delay in Operator Action to Trip Reactor Coolant Pumps During SBLOCAs
127	LTR-NRC-14-4	Single Failure Assumption in LOCAs
128	LTR-NRC-14-9	Prolonged Reactor Coolant Pump Operation During SBLOCAs
129	LTR-NRC-14-9	Early Reactor Coolant Pump Trip During SBLOCAs
130	LTR-NRC-14-9	Break Location Impact in Previous SBLOCA Analyses
131	LTR-NRC-14-9	Break Location Impact in SBLOCA Analyses Using <u>W</u> COBRA/TRAC-TF2
132	LTR-NRC-14-4	Steam Generator Decay Heat Removal During SBLOCAs
133	LTR-NRC-14-4	Steam Generator Heat Transfer Modeling
134	LTR-NRC-14-4	Steam Generator Tube Plugging Levels
135	LTR-NRC-14-4	Steam Generator Tube Plugging Impact on Core Flow Stagnation for LBLOCAs
136	LTR-NRC-14-9	Reactor Coolant Pump Trip Impact on Core Initial Thermal-Hydraulic Response for LBLOCAs
137	LTR-NRC-14-4	Steam Generator Tube Plugging Impact on Steam Generator Reversed Heat Transfer for LBLOCAs
138	LTR-NRC-14-4	Safety Injection Pump Flow During LOCAs
139	LTR-NRC-14-4	Asymmetrical Predictions in Modeling of Parallel Flow Configurations

**WCAP-16996-P, “Realistic LOCA Evaluation Methodology Applied to the Full Spectrum of Break Sizes
(FULL SPECTRUM LOCA Methodology)”
Requests for Additional Information – (Non-Proprietary)
RAIs 1-8, 10, 11 and 13-19**

June 2013

Westinghouse Electric Company LLC
1000 Westinghouse Drive
Cranberry Township, PA 16066

©2013 Westinghouse Electric Company LLC
All Rights Reserved

Question 1: WCOBRA/TRAC MOD7A Revision 7

Coding, scaling, applicability and uncertainty (CSAU) methodology Step 4 emphasizes the identification and use of a frozen version of a mature code and Step 5 requires proper documentation consistent with the frozen code, which is used to determine the code maturity and applicability. Westinghouse's current methodology WCAP-16009-P-A "Realistic Large-Break LOCA Evaluation Methodology Using the Automated Statistical Treatment of Uncertainty Method (ASTRUM)" (2005) is based on the frozen code version WCOBRA/TRAC MOD7A Revision 6. Applicant's previously approved best-estimate Large-break (LBLOCA) methodology was approved based on the frozen code version WCOBRA/TRAC MOD7A Revision 1. It is described in WCAP-12945-P-A "Code Qualification Document for Best Estimate LOCA Analysis" (1998) for Westinghouse designed 3- and 4-loop plants with emergency core cooling system (ECCS) injection into the cold legs and in WCAP-14449-P-A "Application of Best Estimate Large Break LOCA Methodology to Westinghouse pressurized water reactors (PWRs) with Upper Plenum Injection" (1999) for Westinghouse designed 2-loop plants with upper plenum injection. WCAP-16009-P-A Appendix B, "Validation of WCOBRA/TRAC MOD7A Revision 6," describes the differences between these two frozen versions and includes the evaluations performed to ensure that the prior code assessments against experimental data remained valid.

WCAP-16996-P/WCAP-16996-NP, Volumes I, II, and III, Revision 0, Section 1.2.7, "EMDAP Element 3 (Steps 10, 11 and 12): Develop Evaluation Model," states that the development of WCOBRA/TRAC-TF2 started from WCOBRA/TRAC MOD7A Revision 7. The section explains that this revision was released to reflect error corrections and minor improvements, including such related to additional features for special applications. It also clarifies that these changes were reported under the Section 50.46 of Title 10 of the *Code of Federal Regulations (CFR)* reporting requirements process. Please provide a list of the changes made in WCOBRA/TRAC MOD7A Revision 7 from the last approved version and identify those that are germane to WCOBRA/TRAC-TF2. In addition, describe the resolution of the changes in this category and provide specific references documenting their approval by the U.S. Nuclear Regulatory Commission (NRC).

Response:

The last approved version of WCOBRA/TRAC for best estimate LOCA (BELOCA) analysis was WCOBRA/TRAC M7AR6, approved as part of the ASTRUM evaluation model (Reference [1]). Changes between WCOBRA/TRAC M7AR6 and M7AR7 which were applicable to NRC-approved Westinghouse BELOCA methodologies were reported to the NRC as:

GENERAL CODE MAINTENANCE in LTR-NRC-06-8 [3]

GENERAL CODE MAINTENANCE in LTR-NRC-07-51 [4]

The changes associated with this general code maintenance are listed (changes germane to WCOBRA/TRAC-TF2 as part of the FULL SPECTRUM LOCA™ (FSLOCA™) methodology are in **bold**):

- **Improved input diagnostics for boundary condition inputs, channel input, and gap input**
- **Automated calculation and printout of peak linear heat rate and hot rod integral power**
- **Increase dimensions for the code**
- Include library routines as part of Unix operating system updates
- Print pellet radial power in the HOTSPOT input file generated by WCOBRA/TRAC

FULL SPECTRUM™ and **FSLOCA™** are trademarks of Westinghouse Electric Company LLC, its affiliates and/or its subsidiaries in the United States of America and may be registered in other countries throughout the world. All rights reserved. Unauthorized use is strictly prohibited. Other names may be trademarks of their respective owners.

Westinghouse Non-Proprietary Class 3

These changes are considered discretionary changes in accordance with Section 4.1.1 of WCAP-13451 [5].

Also, in WCOBRA/TRAC M7AR7, additional options for modeling of UO₂ fuel pellet thermal conductivity were implemented. These options were implemented for special applications of the ASTRUM methodology outside of the United States (U.S.). These options do not impact U.S. applications of approved Westinghouse BELOCA methodologies and therefore were not reported to the NRC. (It is noted that procedures are in place to preclude the use of these options for U.S. applications.) WCAP-16996-P [2] Section 11.4.1 describes UO₂ thermal conductivity model options in the as-submitted FSLOCA methodology.

References

- 1) WCAP-16009-P-A Revision 0, "Realistic Large Break LOCA Evaluation Methodology Using the Automated Statistical Treatment of Uncertainty Method (ASTRUM)," January 2005.
- 2) WCAP-16996-P Revision 0, "Realistic LOCA Evaluation Methodology Applied to the Full Spectrum of Break Sizes (FULL SPECTRUM LOCA Methodology)," November 2010.
- 3) LTR-NRC-06-8 Revision 0, Letter from B. M. Maurer (WEC) to J. S. Wermiel (NRC), "10 CFR 50.46 Annual Notification and Reporting for 2005," March 16, 2006.
- 4) LTR-NRC-07-51 Revision 0, Letter from B. M. Maurer (WEC) to J. S. Wermiel (NRC), "10 CFR 50.46 Annual Notification and Reporting for 2006," May 15, 2007.
- 5) WCAP-13451 Revision 0, "Westinghouse Methodology for Implementation of 10 CFR 50.46 Reporting," October 1992.

Question 2: TRAC-PF1/MOD2

WCAP-16996-P/WCAP-16996-NP, Volumes I, II, and III, Revision 0, Section 2.5, “WCOBRA/TRAC-TF2 Development Strategy,” explains that the full spectrum LOCA (FSLOCA) code architecture was developed by inserting the WCOBRA/TRAC 3D Module based on COBRA-TF into the TRAC-PF1/MOD2 code while deactivating the 3D component in TRAC-PF1/MOD2. WCAP-16996-P/WCAP-16996-NP, Volumes I, II, and III, Revision 0, Section 2.4, “Requirement Analysis/Assessment for WCOBRA/TRAC-TF2 Models,” asserts that the 1D six-equation two fluid formulation of TRAC-PF1/MOD2 extended to the loops provides adequate formulation for both stratified flow simulation, required for SBLOCA, and limiting the mass error during slow draining transients in comparison to the 1D five-equation drift-flux formulation of WCOBRA/TRAC (based on TRAC-PD2). Additionally, TRAC-PF1/MOD2 featured a non-condensable transport model.

WCAP-16996-P/WCAP-16996-NP, Volumes I, II, and III, Revision 0, Section 2.4 refers to “Open Literature, Theory Manual [1], and Assessment Report [2]” when discussing TRAC-PF1 expected capabilities (see WCAP-16996-P/WCAP-16996-NP, Volumes I, II, and III, Revision 0, Volume 1 page 2-44). Explain what “Open Literature, Theory Manual [1], and Assessment Report [2]” stand for in Section 2.4. Please identify the frozen code version of TRAC-PF1/MOD2 that was used in the development of WCOBRA/TRAC-TF2 and provide a complete set of references that document this code version. In addition, explain why this code version was considered to be mature for the purpose of WCOBRA/TRAC-TF2 development and describe the technical basis that was considered and evaluated in reaching this conclusion.

Response:

Question 2 has been split into three parts (a, b, c) based on the second paragraph of Question 2, and each part is reiterated and responded to below.

a. Explain what “Open Literature, Theory Manual [1], and Assessment Report [2]” stand for in Section 2.4.

As noted, the Section 2.4 fourth paragraph initial sentence and fragment are poorly formed with unidentifiable references as follows:

Open Literature, Theory Manual [1], and Assessment Report [2] were surveyed for expected capabilities of TRAC-PF1 relative to the requirements listed in Section 2.3. The assessment report ...

This sentence and fragment should be replaced with the following:

The TRAC-M Theory Manual (Spore, et al., 2000) and TRAC-M Assessment Manual (Boyack, et al., 2001) were surveyed for expected capabilities relative to the requirements listed in Section 2.3. The assessment manual ...

The following two references should be added to those in Section 2.7:

Spore, J. W., et al., 2000, "TRAC-M/Fortran 90 (Version 3.0) Theory Manual," LA-UR-00-910.
Boyack, B. E., et al., 2001, "TRAC-M/F77, Version 5.5, Developmental Assessment Manual, Volume 1: Assessments," and "Volume 2: Appendices," LA-UR-01-2105.

b. Please identify the frozen code version of TRAC-PF1/MOD2 that was used in the development of WCOBRA/TRAC-TF2 and provide a complete set of references that document this code version.

TRAC-P Version 5.4.28 for HP is the frozen version transmitted to Westinghouse by the USNRC via Information Systems Laboratories with letter:

ISL-TRAC-04-002 Transmittal of TRAC-P Version 5.4.28 (9/2004)

The following are the references identified as documentation of the frozen version:

LA-UR-99-2312	Steinke, R. G., et al., 1999, "TRAC-M/Fortran 77, Version 5.5, Programmer's Guide"
LA-UR-00-803	Adams, B. T., et al., 2000, "TRAC-M/Fortran 90 (Version 3.0) Programmer's Manual"
LA-UR-00-834	Steinke, R. G., et al., 2000, "TRAC-M/Fortran 90 (Version 3.0) User's Manual"
LA-UR-00-910	Spore, J. W., et al., 2000, "TRAC-M/Fortran 90 (Version 3.0) Theory Manual"
LA-UR-01-2105(1)	Boyack, B. E., et al., 2001, "TRAC-M/F77, Version 5.5, Developmental Assessment Manual, Volume 1: Assessments"
LA-UR-01-2105(2)	Boyack, B. E., et al., 2001, "TRAC-M/F77, Version 5.5, Developmental Assessment Manual, Volume 2: Appendices"
LA-UR-01-921	Dearing, J. F., et al., 1998, "XTV User's Guide, Release 2.3c"

c. In addition, explain why this code version was considered to be mature for the purpose of WCOBRA/TRAC-TF2 development and describe the technical basis that was considered and evaluated in reaching this conclusion.

The TRAC-PF1/MOD2 code version (TRAC-P) was considered to be mature for the purpose of WCOBRA/TRAC-TF2 development because it was the final TRAC code version available in a format compatible with the Fortran 77 structure of the WCOBRA/TRAC code (WC/T) in use at Westinghouse for predicting the response of a pressurized water reactor (PWR) to a loss of coolant accident (LOCA), and it provided additional capabilities not present in WC/T, based on the TRAC-M Theory Manual (Spore, et al., 2000) and TRAC-M Assessment Manual (Boyack, et al., 2001).

WC/T was previously qualified for the realistic analysis of PWR Large Break (LB) LOCAs. TRAC-P provided additional capabilities to potentially expand the application of WC/T to the full spectrum of breaks: small, medium, and large. The TRAC-P 1D module provided enhanced LBLOCA features, e.g. non-condensable gas transport, and added capabilities to properly capture the important processes and phenomena identified for small and intermediate break scenarios. It featured expanded fundamental field equations and closure relationship models which are essential to extend the WC/T code capabilities. The TRAC-P six equation two fluid solution provides adequate formulation for horizontally stratified flow simulation required for SBLOCA analysis, in comparison to the formulation in WC/T (based on TRAC-PD2).

The TRAC-P developmental assessment documentation (Boyack, et al., 2001) demonstrated that TRAC-P was a viable tool for analyzing PWRs during a LOCA and other operational transients, by successful comparisons to analytical solutions, separate effect tests, and integral effect tests.

Based on this information, it was determined that the coupling of the WC/T 3D module with the TRAC-P 1D modules was a technically sound base to begin development of the new WCOBRA/TRAC-TF2 code.

Assessments that have been performed for the WCOBRA/TRAC-TF2 components used within the FULL SPECTRUM method are documented in WCAP-16996-P as follows:

- Section 16: Horizontal stratified flow (PIPE and TEE components)
- Section 17: Cold leg condensation (PIPE and TEE)
- Section 18: Loop seal clearing (PIPE)
- Section 19.6: Cylindrical Core Test Facility (integral test facility)
- Section 20.1: Accumulator (PIPE, VALVE)
- Section 20.2: PUMP
- Section 20.3: 1D/3D Junction
- Section 21: ROSA (integral test facility)
- Section 22: LOFT (integral test facility)
- Section 23.2: Numerical thought problems (PIPE, FILL, BREAK)

Question 3: LBLOCA and SBLOCA PIRTs

WCAP-16996-P/WCAP-16996-NP, Volumes I, II, and III, Revision 0, Revision 0 Section 2.3, “Phenomena Identification and Ranking Table (EMDAP Steps 3 and 4),” explains that the FSLOCA PIRT was developed using “existing LBLOCA and SBLOCA PIRTs as the starting point.” With regard to the previously existing LBLOCA PIRT, Section 2.3 stated that it was “the subject of NRC review.” Please identify this existing LBLOCA PIRT, as approved by NRC, and provide a table that compares and documents all differences between the original approved LBLOCA PIRT and the FSLOCA PIRTs for LBLOCA and intermediate break (IBLOCA). In addition, explain the conversion process between the ranking system used in the existing LBLOCA (ranks from 1 to 9) and the system adopted in the new FSLOCA PIRTs (“Low,” “Medium,” and “High”).

With regard to the previously existing SBLOCA PIRT, Section 2.3 clarifies that it was a subject of “independent peer review.” Please identify this original SBLOCA PIRT along with its technical basis and supporting references describing its development. In addition, provide a brief summary of all major findings from the “independent peer review.” Please present a table that compares and documents all differences between the original SBLOCA PIRT and the FSLOCA PIRT for SBLOCAs.

Response:

Comparison to Existing Westinghouse Large Break LOCA (LBLOCA) Phenomena Identification and Ranking Table (PIRT)

The original ranking of the LBLOCA PIRT for 3 and 4 loop Westinghouse plant was developed as part of the Westinghouse Best Estimate LBLOCA methodology development, and is documented in Section 1-3-3-3 of WCAP-12945-P-A [3]. The PIRT for the upper plenum injection (UPI) PWRs was later developed and presented in the Table 2-3 in Section 2-4 of WCAP-14449-P-A [8], which is identical to Table 1-1 in Section 1-2-3 of WCAP-16009-P-A [2]. Table A-1 in Appendix-A of WCAP-16009-P-A contains an extension to Combustion Engineering type PWRs. The combined PIRT (Tables 1-1 and A-1 from WCAP-16009-P-A) was then converted from the numerical ranking of 5 through 9 to Medium (5-6), and High (7-9), and added to the LBLOCA portion of the integrated PIRT contained in WCAP-16996-P [1] with clarifying comments when the ranking of a particular phenomenon is different between the two sets of PIRT. The conversion process is explained in the sections that follow. Where the ranking is different between WCAP-16009-P-A and WCAP-16996-P, the cell is highlighted with yellow (Item). If the item is added or removed, it is highlighted. If items are added, they are highlighted in green (Item) and comments are added to the comparison table to note the changes. If items are removed they are noted and explanation is provided on why it was removed, or how it was incorporated into existing items in the remark to the region heading.

The FSLOCA PIRT contains phenomena for all break sizes, and thus many items were considered in LBLOCA that were not considered in the previous LBLOCA PIRT.

Comparison to Existing Westinghouse SBLOCA PIRT

The same process of comparison was performed for the SBLOCA portion of the integrated PIRT contained in WCAP-16996-P [1]. The previous SBLOCA PIRT was originally documented in Section 1-4 of WCAP-14936 [4].

Review of SBLOCA by an independent panel of experts

Westinghouse developed a PIRT for a small break LOCA, which was then reviewed by an independent external review team of experts: P. Griffith (MIT), Y. Hassan (Texas A&M), T. Fernandez (EPRI), and D. Speyer (consultant). Attachment A to WCAP-14936 [4] contains the team’s review comments on the

preliminary SBLOCA PIRT. Note that the preliminary PIRT is different from the final SBLOCA PIRT given in Table 1-9 of WCAP-14936. While the independent PIRT Review Team's rankings were incorporated in the final PIRT, there were some exceptions as noted in Section 1-4-6 of WCAP-14936. The independent review of the Westinghouse SBLOCA PIRT was also published in Reference 5.

References:

1. WCAP-16996-P, "Realistic LOCA Evaluation Methodology Applied to the Full Spectrum of Break Sizes (FULL SPECTRUM LOCA Methodology)," November 2010.
2. WCAP-16009-P-A, "Realistic Large-Break LOCA Evaluation Methodology Using the Automated Statistical Treatment of Uncertainty Method (ASTRUM)," January 2005.
3. WCAP-12945-P-A, "Westinghouse Code Qualification Document for Best Estimate Loss of Coolant Analysis," March 1998.
4. WCAP-14936, "Code Qualification Document for Best Estimate Small Break LOCA Analysis," August 2001. (SBLOCA PIRT is included in Appendix A), attachment to ML031560746, "Transmittal of WCAP-14936, "Code Qualification Document for Best Estimate Small Break LOCA Analysis," Revision 0, August 2001 (Proprietary) and WCAP-14936-NP, Revision 0, April 2003 (Non-Proprietary)," June 16, 2003.
5. S. M. Bajorek, A. Ginsberg, D. J. Shimeck, K. Ohkawa, M. Y. Young, L. E. Hochreiter, P. Griffith, Y. Hassan, T. Fernandez, and D. Speyer, "SMALL BREAK LOSS OF COOLANT ACCIDENT PHENOMENA IDENTIFICATION AND RANKING TABLE (PIRT) FOR WESTINGHOUSE PRESSURIZED WATER REACTORS," Ninth International Topical Meeting on Nuclear Reactor Thermal Hydraulics (NURETH-9), San Francisco, California, October 3 - 8, 1999.
6. NUREG/CR-5249, "Quantifying Reactor Safety Margins – Application of Code Scaling, Applicability, and Uncertainty Evaluation Methodology to a Large-Break, Loss-of-Coolant Accident," December 1989.
7. NUREG/CR-5074, "Development of a Phenomena Identification and Ranking Table (PIRT) for Thermal-Hydraulic Phenomena During a PWR Large-Break LOCA," November 1988.
8. WCAP-14449-P-A Rev.1, "Application of Best Estimate Large Break LOCA Methodology to Westinghouse PWRs With Upper Plenum Injection," October 1999.
9. Wang, M. and Mayinger, F., 1995, "Simulation and Analysis of Thermal-Hydraulic Phenomena in a PWR Hot Leg Related to SBLOCA," Nuclear Engineering and Design, Vol. 15, pp. 643-652.

1 Comparison of FSLOCA PIRT against WCAP-12945-P-A/WCAP-16009-P-A PIRT

The ranking provided in the large break LOCA portion of the FSLOCA PIRT in Table 1-1 of this attachment has been mostly based on the previous LBLOCA PIRT shown in Table 1-2. In general, rankings of 7-9 in Table 1-2 are reflected as high (H) rankings in Table 1-1 and rankings of 5-6 are medium (M) rankings. In the previous LBLOCA PIRT, no ranking below 5 was provided. Rankings below 5 were converted, based on the ranking definitions provided in Section 2-3 of Reference 1, to either Medium (M), low (L) or not-applicable (N/A) in Table 1-1. In all these cases, justification is provided in Section 2.3.2 of Reference 1.

Beside this conversion, the LB LOCA input in Table 1-1 differs from that provided in Table 1-2 in some areas, which are discussed as follows. Note that in the following sections only those ranking and phenomena that don't directly correspond to the conversions presented above will be discussed. For more detailed information on the specific phenomena, see Section 2.3 in WCAP-16996-P.

1-1-1 Fuel Rod

(See Section 2.3.2.1 in WCAP-16996-P for additional discussion regarding the phenomena associated with this system/component/process and rankings.)

Clad Deformation (Burst Strain, Relocation) is new in FSLOCA PIRT, and was not included explicitly in the previous LBLOCA PIRT as seen in Table 1-2. Although these processes were not explicitly included in the previous large break LOCA PIRT, their modeling was recognized as implicit in several other core heat transfer processes and as such their models were part of the LBLOCA Methodology. For the FSLOCA PIRT, it was considered more appropriate to explicitly capture these phenomena in the fuel rod ranking. Also in Table 1-1, ranking changes are presented, which reflect the thermal conductivity degradation (TCD) effects which were not accounted for in the original submittal. A more comprehensive PIRT for the impact of TCD effects will be given in the response to RAI-36 through 39.

1-1-2 Core

(See Section 2.3.2.2 in WCAP-16996-P for additional discussion regarding the phenomena associated with this system/component/process and rankings.)

DNB: In the FSLOCA PIRT, the more generic term CHF is used. Ranking is consistent between Table 1-1 and Table 1-2.

In the LBLOCA PIRT, Reflood Heat Transfer was ranked []^{a,c} during reflood, and was meant to provide a comprehensive definition of all the heat transfer modes occurring in the core during reflood. For this reason, Post-CHF and Rewet were left unranked during reflood, as their effects were considered within the generic reflood heat transfer multiplier. For the FSLOCA PIRT, it was necessary, considering the range of break sizes and relative periods considered, to provide a more specific ranking. Reflood Heat Transfer is a combination of several other more fundamental processes such as Post-CHF, Rewet, heat transfer to covered core and entrainment/de-entrainment. In particular, the ranking for Rewet and Post-CHF in the FSLOCA PIRT has been assigned as []^{a,c} consistent with the ranking of Reflood Heat Transfer in the LBLOCA PIRT. Thus, the ranking between Table 1-2 and Table 1-1 is equivalent.

Rewet/Tmin: In the FSLOCA PIRT, the ranking for Rewet is provided as a []^{a,c} during blowdown and reflood in recognition that the low and average power rods would rewet and provide cooling to the hot assembly rods while a []^{a,c} was assigned in the previous LBLOCA PIRT. The ranking in refill was changed to []^{a,c}. The reason for this modification is discussed in Section 2.3.2.2 of Reference 1: “[

] ^{a,c}” This modification is the result of

additional knowledge acquired with the application of the LBLOCA Best-Estimate methodology by Westinghouse. Ranking for the reflood period has been discussed above as part of the decomposition of the Reflood Heat Transfer in the FSLOCA PIRT.

Two additional phenomena are included in the FSLOCA PIRT, Flow Resistance and Water Storage in Barrel/Baffle Region. As observed in Table 1-1, these are both considered of []^{a,c} importance for large breaks, with justification provided in Section 2.3.2.2 of Reference 1.

1-1-3 Upper Head

(See Section 2.3.2.3 in WCAP-16996-P for additional discussion regarding the phenomena associated with this system/component/process and rankings.)

While the FSLOCA PIRT distinguishes between upper head and upper plenum, the LBLOCA PIRT included only an Upper Plenum ranking. The refined subdivision used for the FSLOCA is mostly due to the slower drain of the upper head for the smaller breaks, such that it was considered more appropriate to separate the two regions.

The ranking for the FSLOCA PIRT is provided in Table 1-1 and is justified in Section 2.3.2.3 of Reference 1. It can be observed that two main processes are associated with the upper head. The first is the contribution to core cooling during blowdown (Draining/Flashing/Mixture Level and Initial Fluid Temperature). These effects were only implicitly captured in the previous LBLOCA PIRT for their influence on heat transfer in the core during blowdown (see for example the discussion on Core 3-D Flow in Section 1-2-3-2 of Reference 2 (or Section 1-3-3-3 of Reference 3), and the relative importance of downflow from the upper plenum and upper head during blowdown).

The second relevant effect associated with the upper head is the venting during reflood. The ranking justification is provided as in Section 2.3.2.3 of Reference 1. While not explicitly captured in the previous LBLOCA PIRT this is part of the overall vent path flow resistance, captured for example as two-phase loop DP in the previous LBLOCA PIRT.

1-1-4 Upper Plenum

(See Section 2.3.2.4 in WCAP-16996-P for additional discussion regarding the phenomena associated with this system/component/process and rankings.)

The only differences between the large break LOCA part of the FSLOCA PIRT provided in Table 1-1 and the LBLOCA PIRT provided in Table 1-2 are relative to two additional phenomena that have been included in the FSLOCA PIRT.

The Hot Leg-Downcomer Gap Flow was not included in the previous LBLOCA PIRT, as it was recognized that not modeling this gap would be conservative. However, it is recognized that the expected flow through the Hot Leg-Downcomer gap is []^{a,c}. Therefore, in the FSLOCA PIRT it was decided to include this effect in the PIRT to capture its significance to a realistic LOCA analysis, []^{a,c}. Ranking rationale is provided in Section 2.3.2.4 of Reference 1.

Metal Heat Release: The ranking rationale is provided in Section 2.3.2.4 of Reference 1. While not explicitly captured in the UPI LBLOCA PIRT, these effects were considered as part of the CCF Drain/Fallback in the LBLOCA PIRT, consistent with the ranking rationale provided for the FSLOCA PIRT.

1-1-5 Hot Leg

(See Section 2.3.2.5 in WCAP-16996-P for additional discussion regarding the phenomena associated with this system/component/process and rankings.)

Although some additional phenomena are included in the FSLOCA PIRT, the ranking remains of either low or not-applicable for large break LOCA. Ranking is consistent with that provided for the previous LBLOCA PIRT, as discussed in Section 2.3.2.5 of Reference 1.

1-1-6 Pressurizer/Surge Line

(See Section 2.3.2.6 in WCAP-16996-P for additional discussion regarding the phenomena associated with this system/component/process and rankings.)

Although some additional phenomena are included in the FSLOCA PIRT, the ranking remains of either []^{a,c} for large break LOCA. Ranking is consistent with that provided for the previous LBLOCA PIRT, as discussed in Section 2.3.2.6 of Reference 1. The only difference between the ranking in Table 1-1 and Table 1-2 is relative to the early quench. The original CSAU [6] expert team ranking of (High) was from the LOFT tests that indicated that liquid from the pressurizer and its surge line could flow back into the vessel during the reverse flow period of blowdown, contributing to the top down cooling [7]. In the previous Westinghouse LBLOCA PIRT, a ranking of []^{a,c} was assigned.

Additionally, “Early Quench” is a combined effect of Surge line flow and the “Flow Reversal” at the Upper Plenum/hot leg interface, and both of these items are included in the current table. Thus, based on Westinghouse’s experience with realistic LBLOCA analysis, and the fact that phenomena controlling “early quench” behavior are already included in the table, this entry is removed.

1-1-7 Steam Generator

(See Section 2.3.2.7 in WCAP-16996-P for additional discussion regarding the phenomena associated with this system/component/process and rankings.)

Several phenomena associated with the steam generators are included in Table 1-1 for the FSLOCA PIRT. Most of these phenomena assume some significance only for the small breaks, where the steam generators act as a heat sink for a significant portion of the transient. For large breaks, a ranking of []^{a,c} is assigned to most of the steam generator phenomena, as justified in Section 2.3.2.7 of Reference 1. The only two phenomena for which ranking are different than []^{a,c} (Steam Binding and Flow Resistance) are present in both Table 1-1 and Table 1-2.

For Steam Binding, ranking is consistent between the two PIRTs.

For Flow Resistance, a ranking of []^{a,c} is provided for the blowdown phase. The ranking rationale is provided in Section 2.3.2.7 of Reference 1. In the LBLOCA PIRT, the Loop was considered as a separate entry in the PIRT, and flow split was defined as the split of flow between the vessel side and loop side of the break due to the relative flow resistance of the two flow paths. In the FSLOCA PIRT, it was considered more appropriate to identify separately the flow resistance in the various components of the flow path, and rank the importance of this flow resistance on the basis of its influence on the flow split.

While not explicitly represented in the previous LBLOCA PIRT this ranking is therefore considered consistent with the flow split ranking during blowdown and, due to the influence of the venting path flow resistance on the core flooding rate during reflood, with reflood heat transfer during reflood.

1-1-8 Pump Suction Piping/ Loop Seal Clearance

(See Section 2.3.2.8 in WCAP-16996-P for additional discussion regarding the phenomena associated with this system/component/process and rankings.)

These phenomena are all ranked of low importance for the large breaks in the FSLOCA PIRT, and they are included for their importance in the smaller break sizes. For this reason, the FSLOCA PIRT is consistent with the previous LBLOCA PIRT provided in Table 1-2, where no pump suction piping phenomena is considered. Ranking for the FSLOCA PIRT is justified in Section 2.3.2.8 of Reference 1.

As stated in the response to RAI 7, the FSLOCA methodology is not applicable to the long term cooling period. However, it is recognized that the loop seals could possibly replug during the “short term” and is addressed in Section 2.3.2.9 of WCAP-16996-P for intermediate breaks where the broken loop accumulator or SI water could conceivably backflow during the second phase of this scenario.

1-1-9 Pump

(See Section 2.3.2.9 in WCAP-16996-P for additional discussion regarding the phenomena associated with this system/component/process and rankings.)

Ranking for the pump phenomena relative to large breaks is consistent between the FSLOCA PIRT and LBLOCA PIRT. Coastdown performance was included in Two-Phase performance in the previous Large Break LOCA PIRT, while a separate ranking is provided in the FSLOCA PIRT.

Flow Resistance has a ranking consistent in the FSLOCA PIRT with that provided in the previous LBLOCA PIRT, although a lower ranking is provided for the refill and reflood phases than the ranking provided for blowdown. The reason for this choice is that other loop resistances are separately captured, and thus the pump resistance is only one of the components of the overall loop resistance, and is not expected to be a dominating contributor. A ranking of []^{a,c} is assigned for refill and reflood, and a ranking of []^{a,c} is assigned for blowdown, consistent with the ranking for the steam generator flow resistance.

1-1-10 Cold Leg / Safety Injection

(See Section 2.3.2.10 in WCAP-16996-P for additional discussion regarding the phenomena associated with this system/component/process and rankings.)

Ranking for the FSLOCA and LBLOCA PIRT is consistent. The main difference between the two PIRTs is the inclusion of the Spilling Flow Treatment (Pumped SI) in the FSLOCA PIRT, which is assigned a ranking of []^{a,c} for the reflood phase of large break LOCA. This item was not captured in the LBLOCA PIRT since flow to the broken loop was assumed spill to the break, and the total amount of spilled SI flow was to be conservatively estimated in the LBLOCA methodology. In the FSLOCA PIRT it is instead explicitly recognized that, independent from the modeling approach selected, the treatment of spilled SI flow has a significant impact on the reflood portion of the LBLOCA transient, as discussed in Section 2.3.2.10 of Reference 1.

1-1-11 Accumulator

(See Section 2.3.2.11 in WCAP-16996-P for additional discussion regarding the phenomena associated with this system/component/process and rankings.)

The Accumulator was included with the Cold Leg in the LBLOCA PIRT. For the FSLOCA PIRT, it was considered more appropriate to consider the Accumulator as a separate PIRT item. Ranking rationale is discussed in Section 2.3.2.11 of Reference 1. Aside from the phenomena ranked as []^{a,c}, the following can be observed on the ranking of accumulator phenomena in the FSLOCA PIRT.

The ranking for Nitrogen Discharge is consistent with the LBLOCA ranking of non-condensable gases in the cold leg and elsewhere in the system, and is therefore implicitly included in the LBLOCA PIRT. It is also recognized that Nitrogen discharged into the reactor coolant system from the accumulator may impact steam binding through the primary-to-secondary heat transfer process during reflood, if the non-condensable gas is present in the steam generator tubes.

For the Broken Loop Accumulator Treatment, the same considerations provided in Section 2.3.2.10 of Reference 1 to the Spilling Flow Treatment apply.

The accumulator injection rate is explicitly captured in the FSLOCA PIRT, with ranking rationale provided in Section 2.3.2.11 of Reference 1. In the previous LBLOCA PIRT, accumulator injection is implicitly considered in several different phenomena related to ECC bypass and core reflood.

1-1-12 Downcomer

(See Section 2.3.2.12 in WCAP-16996-P for additional discussion regarding the phenomena associated with this system/component/process and rankings.)

Ranking for the downcomer is consistent between the FSLOCA and LBLOCA PIRTs, with the following differences.

Non-Condensable Effects. These are explicitly captured in the FSLOCA PIRT because of their potential, and short lived, effect on downcomer condensation. The ranking is consistent with that provided for non-condensable effects in the Cold Leg.

Flow Resistance. In the FSLOCA PIRT flow resistance is explicitly captured because of its effect on ECC bypass (see ranking justification in Section 2.3.2.12 of Reference 1). The ranking is qualitatively consistent with that provided in the LBLOCA PIRT for Countercurrent / Slug / Non-equilibrium Effect, but was captured as a separate phenomenon in the FSLOCA PIRT for consistency with other parts of the system, where flow resistance was explicitly accounted for.

Mixture Level/Flashing/Void Fraction / Void Generation / Void Distribution is explicitly included in the FSLOCA PIRT, while in the LBLOCA PIRT it was included with the Hot Wall. In the FSLOCA PIRT the stored energy in the wall and its effect on the fluid are separately captured. The Ranking for the Mixture Level/Flashing also accounts for ECC bypass related processes, which were generically included in Countercurrent / Slug / Non-equilibrium Effect in the LBLOCA PIRT. Thus the ranking of []^{a,c} is provided for the refill period. Detailed description and ranking justification for the Countercurrent / Slug / Non-equilibrium Effect, Flow Resistance, Mixture Level/Flashing is provided in Section 2.3.2.12 of Reference 1.

The Counter-Current, Slug, and Non-equilibrium Flows are characteristic of the ECC bypass phenomena during the refill period and are the same for the Westinghouse 2-, 3-, 4-loop and CE designed PWRs. This item was missing from the FSLOCA PIRT but present in the previous LBLOCA PIRT. This item will be reinstated in the revised PIRT. While the phenomena are the same, there are geometric differences. These phenomena ranked []^{a,c} begin at the end of blowdown and end at the conclusion of the refill period when the lower plenum is filled and there is no longer any steam flow up the downcomer.

1-1-13 Lower Plenum

(See Section 2.3.2.13 in WCAP-16996-P for additional discussion regarding the phenomena associated with this system/component/process and rankings.)

Ranking is consistent for the FSLOCA and LBLOCA PIRT. Ranking justification for the FSLOCA PIRT is provided in Section 2.3.2.13 of Reference 1.

1-1-14 Break

(See Section 2.3.2.14 in WCAP-16996-P for additional discussion regarding the phenomena associated with this system/component/process and rankings.)

Ranking is consistent for the FSLOCA and LBLOCA PIRT. Ranking justification for the FSLOCA PIRT is provided in Section 2.3.2.14 of Reference 1.

The only significant difference is due to an explicit entry of Cold Leg Nozzle Flow Resistance in the FSLOCA PIRT. This addition is due to the fact that the LBLOCA PIRT includes in the Loop an effect indicated as Flow Split. Two flow paths are available to the fluid to reach the break: the flow path through the hot leg, steam generator, and broken loop pump and the flow path through the core, downcomer, and broken loop cold-leg nozzle to the break. The resistance difference between the two flow paths determines the amount of downflow through the core during blowdown, and the amount of core cooling. In the FSLOCA PIRT, flow split is not considered as a separate phenomenon, but rather as a result of the relative flow resistances of the two flow paths discussed above. Thus, flow resistance at critical components along the flow path was ranked, rather than a generic flow split.

It is noted that in the FSLOCA PIRT, Cold Leg Nozzle Flow Resistance is also ranked []^{a,c} during reflood, due to the influence of the venting path flow resistance on the core flooding rate during reflood.

Table 1-1: Comparison of FSLOCA LBLOCA PIRT to combined PIRT (Table 1-1 and Table A-1) in WCAP-16009-P-A

] ^{a,c}

Table 1-1: Comparison of FSLOCA LBLOCA PIRT to combined PIRT (Table 1-1 and Table A-1) in WCAP-16009-P-A (cont.)

Table 1-1: Comparison of FSLOCA LBLOCA PIRT to combined PIRT (Table 1-1 and Table A-1) in WCAP-16009-P-A (cont.)

[

] ^{a,c}

Table 1-1: Comparison of FSLOCA LBLOCA PIRT to combined PIRT (Table 1-1 and Table A-1) in WCAP-16009-P-A (cont.)

Table 1-1: Comparison of FSLOCA LBLOCA PIRT to combined PIRT (Table 1-1 and Table A-1) in WCAP-16009-P-A (cont.)

] ^{a,c}

Table 1-1: Comparison of FSLOCA LBLOCA PIRT to combined PIRT (Table 1-1 and Table A-1) in WCAP-16009-P-A (cont.)

[

] ^{a,c}

Table 1-1: Comparison of FSLOCA LBLOCA PIRT to combined PIRT (Table 1-1 and Table A-1) in WCAP-16009-P-A (cont.)

]^{a,c}

(1) Cold leg injection/Upper Plenum Injection.

Table 1-2: PIRT for Large-Break LOCA (Table 1-1 and Table A-1 in WCAP-16009-P-A and Table 1-14 in WCAP-12945-P-A)

]^{a,c}

Westinghouse Non-Proprietary Class 3

Table 1-2: PIRT for Large-Break LOCA (Table 1-1 and Table A-1 in WCAP-16009-P-A and Table 1-14 in WCAP-12945-P-A) (Cont.)

[

] ^{a,c}

Table 1-2: PIRT for Large-Break LOCA (Table 1-1 and Table A-1 in WCAP-16009-P-A and Table 1-14 in WCAP-12945-P-A) (Cont.)

[

]^{a,c}

Table 1-2: PIRT for Large-Break LOCA (Table 1-1 and Table A-1 in WCAP-16009-P-A and Table 1-14 in WCAP-12945-P-A) (Cont.)

[

]^{a,c}

*Ranking for CE Design if different from W/3-4 Loop PWRs (Appendix A in WCAP-16009-P-A)

2 SMALL BREAK LOCA PIRT COMPARISON

2-1 SBLOCA Portion of FSLOCA

The SBLOCA portion of the FSLOCA PIRT was compared to the previously developed SBLOCA PIRT in Table 2-1. The previously developed PIRT with ranking rationale is provided in Table A-1 of Appendix A for comparison. Similar to the LBLOCA PIRT comparison shown in the previous section, where the ranking is different between the previous SBLOCA PIRT (duplicated in Appendix A) and the one contained in WCAP-16996-P, the cell is highlighted with yellow (**Item**). If the item is added or removed, it is highlighted. If items are added, they are highlighted in green (**Item**) and comments are added to the comparison table to note the changes. If items are removed they are noted in the remark to the region heading.

2-2 Justification of FSLOCA PIRT against SBLOCA PIRT

The ranking provided in the small break LOCA portion of the FSLOCA PIRT in Table 2-1 has been mostly based on the small break LOCA PIRT provided in Table A-1 and discussed above. In general, in the FSLOCA PIRT it was decided to eliminate the “scenario dependent rankings” indicated with H*, M* or L*. This was based on the fact that essentially all rankings provided would be somewhat scenario dependent and it is considered more adequate to define rankings in such a way that they represent the largest possible impact from a specific phenomenon on the figures of merit considered.

Aside from this difference, the ranking for small breaks in the FSLOCA PIRT in Table 2-1 is directly obtained from Table A-1, with only a limited number of changes that are discussed as follows. For more detailed information on the specific phenomena, see Section 2.3 in WCAP-16996-P.

2-2-1 Fuel Rod

(See Section 2.3.2.1 in WCAP-16996-P for additional discussion regarding the phenomena associated with this system/component/process and rankings.)

Gap Conductance is not explicitly included in the FSLOCA PIRT as it is considered a component of the Stored Energy, consistent with the approach used for the LBLOCA PIRT discussed.

Local Power is not explicitly included in the FSLOCA PIRT, as it is considered included in the Stored Energy and Decay Heat, since the local power influences the spatial distribution of decay heat.

2-2-2 Core

(See Section 2.3.2.2 in WCAP-16996-P for additional discussion regarding the phenomena associated with this system/component/process and rankings.)

3-D Power Distribution is not explicitly included in the FSLOCA PIRT, as it is considered included in the Decay Heat, since the local power influences the spatial distribution of decay heat, and 3-D Flow/Core Natural Circulation.

DNB. In the FSLOCA PIRT, the more generic term CHF is used. Ranking is consistent between Table 2-1 and Table A-1.

Heat Transfer to Covered Core. A ranking of []^{a,c} is used in the FSLOCA PIRT also for blowdown.

[]^{a,c}

Void Generation / Void Distribution. In the FSLOCA PIRT, this terminology is preferred over the mixture level definition used in the SBLOCA PIRT. Ranking is consistent between Table 2-1 and Table A-1.

Top Nozzle / Tie Plate CCFL. This is included with Draining/Fallback/CCFL in the upper plenum, and is therefore not listed separately in the FSLOCA PIRT.

2-2-3 Upper Head

(See Section 2.3.2.3 in WCAP-16996-P for additional discussion regarding the phenomena associated with this system/component/process and rankings.)

Draining / Mixture Level. The ranking of low for the last three phases in the SBLOCA PIRT is modified to N/A in the FSLOCA PIRT since the upper head is expected to be completely drained during the first two phases.

Initial Fluid Temperature. The ranking of low for the last three phases in the SBLOCA PIRT is modified to N/A in the FSLOCA PIRT since the upper head is expected to be completely drained during the first two phases.

Venting. Venting through the upper head is explicitly captured in the FSLOCA PIRT, with a ranking consistent with that provided for Hot Leg-Downcomer Gap Flow. The rationale for this added phenomenon is provided in Section 2.3.2.3 of Reference 1.

2-2-4 Upper Plenum

(See Section 2.3.2.4 in WCAP-16996-P for additional discussion regarding the phenomena associated with this system/component/process and rankings.)

Condensation for the FSLOCA PIRT was ranked as N/A rather than low as in the SBLOCA PIRT. The rationale for a ranking of N/A is that condensation is not expected to occur in the upper plenum, and even for UPI plants it is only the low head safety injection that would be delivered to the upper plenum, and low head SI is not actuated during the small break scenario until after or during the recovery phase.

Horizontal Stratification and Counter-Current Flow & CCFL have been removed from the upper plenum and are now part of Horizontal Stratification/Flow Regime in the hot leg.

Phase Separation in tee at Pressurizer was considered in the FSLOCA PIRT as Phase Separation at Branch Tee under Pressurizer/Surge Line. Ranking is consistent between Table 2-1 and Table A-1.

2-2-5 Hot Leg

(See Section 2.3.2.5 in WCAP-16996-P for additional discussion regarding the phenomena associated with this system/component/process and rankings.)

Differences between Table 2-1 and Table A-1 is the ranking of Horizontal Stratification and Counter-Current Flow which are ranked low (L) in FSLOCA PIRT while they are ranked medium (M) in the previous SBLOCA PIRT. These are ranked low because of low vapor velocity expected in SBLOCA, and because full scale tests showed that there is no evidence of CCFL [9], this phenomenon was removed.

2-2-6 Pressurizer/Surge Line

(See Section 2.3.2.6 in WCAP-16996-P for additional discussion regarding the phenomena associated with this system/component/process and rankings.)

In general, all rankings relative to the pressurizer volume have been changed from low in the SBLOCA PIRT to N/A in the FSLOCA PIRT for the periods when the pressurizer is expected to be empty of liquid. Rationale for each phenomenon is provided in Section 2.3.2.6 of Reference 1.

The remaining ranking is consistent between Table 2-1 and Table A-1. Ranking for Phase Separation at Branch Tee has been discussed in Section 2-2-4.

2-2-7 Steam Generator

(See Section 2.3.2.7 in WCAP-16996-P for additional discussion regarding the phenomena associated with this system/component/process and rankings.)

The only difference between the FSLOCA and the SBLOCA PIRTs is that Steam Binding is included in the FSLOCA PIRT due to its relevance in intermediate and large break scenarios. For small breaks, a ranking of low or not applicable is provided for all phases, as justified in Section 2.3.2.7 of Reference 1.

In addition, it is recognized that tube plugging can influence the phenomena and processes identified in Section 2.3.2.7 of Reference 1 through the impact on fluid volume, momentum area and heat transfer area. While increased tube plugging will reduce the fluid volume and momentum area (and therefore increase the resistance through the loop), it will also reduce the heat transfer area between the primary and secondary sides. During the phases when heat transfer in the steam generator is from the secondary side to the primary side, this has a potential impact of reduced Steam Binding and vapor superheating. However, the impact due to the difference in heat transfer area is less important than the impact on the loop resistance (e.g., influence on loop seal clearing, level swell and reflood rate) due to the reduction in fluid volume and momentum area. As stated in Section 25.1 of Reference 1, [

] ^{a,c}.

2-2-8 Pump Suction Piping / Loop Seal Clearance

(See Section 2.3.2.9 in WCAP-16996-P for additional discussion regarding the phenomena associated with this system/component/process and rankings.)

There is no difference between the FSLOCA PIRT in Table 2-1 and the SBLOCA PIRT in Table A-1.

It is recognized that partial clearing of the loop seals and liquid hold-up in the uphill side of the loop seal region can have an influence on the thermal-hydraulic response during the boil-off period. The degree of liquid hold-up is a result of Horizontal Stratification (i.e., does the liquid in the horizontal section stratify or is it pushed to the uphill section of the loop seal region) and CCFL and Entrainment/Flow Regime/Interfacial Drag (is the liquid pushed out, carried out or partially remain in the loop seal region). The overall impact of liquid being retained in the loop seal region is on the Flow Resistance through a given loop after it has cleared.

2-2-9 Pump

(See Section 2.3.2.9 in WCAP-16996-P for additional discussion regarding the phenomena associated with this system/component/process and rankings.)

Mixing was removed in the FSLOCA PIRT. Mixing is considered as a consequence of the pump operation, captured elsewhere, and is already captured as cold leg Flow Regime. Also, during blowdown the cold leg remains water solid, and thus the effect of mixing generated by the pumps is not considered of any importance.

The Two Phase Performance definition was modified to include also the single phase performance. Also, ranking for the natural circulation phase was modified from [] ^{a,c} in the SBLOCA PIRT to [] ^{a,c} in the FSLOCA PIRT to reflect the possibility that for some of the “larger” small breaks the pumps may still be running in the natural circulation phase.

Analogously, Coastdown ranking for the natural circulation phase was modified from [] ^{a,c} in the SBLOCA PIRT to [] ^{a,c} in the FSLOCA PIRT to reflect the possibility that for some of the “larger” small breaks the pumps may still be running in the natural circulation phase.

See the response to RAI 10 for discussion on reactor coolant pump trip.

2-2-10 Cold Leg / Safety Injection

(See Section 2.3.2.10 in WCAP-16996-P for additional discussion regarding the phenomena associated with this system/component/process and rankings.)

Cold Leg and Safety Injection have been combined in the FSLOCA PIRT. Ranking is consistent with that provided in the SBLOCA PIRT. However, Flow Resistance was removed in the FSLOCA PIRT for consistency with the hot leg flow resistance (loop piping flow resistance is small compared to other flow resistances in the system, for example in the steam generators or pumps). Also, Water Hammer was removed from the FSLOCA PIRT. Per the SBLOCA PIRT in Appendix A-1-2-11, "The possible consequences of a condensation-induced water hammer would not alter the scenarios for the small break LOCA event." Thus, it was not considered necessary to maintain this inconsequential phenomenon in the FSLOCA PIRT.

The main difference between the two PIRTs is however the inclusion of the Spilling Flow Treatment (Pumped SI) in the FSLOCA PIRT. This item was not captured in the SBLOCA PIRT since the total amount of spilled SI flow was to be conservatively estimated in the SBLOCA methodology. In the FSLOCA it is instead explicitly recognized that, independent from the modeling approach selected, the []^{a,c}, as discussed in Section 2.3.2.10 of Reference 1.

It is recognized that the Metal Heat can be a higher percentage of total heat added to the RCS for a small break and the smaller breaks of an intermediate break transient, which can influence the liquid temperature from the safety injection when it reaches the downcomer. However, this mode of heating the liquid is not as dominant as Interfacial Heat Transfer (Condensation), which is reflected by the difference in ranking between the two phenomena.

2-2-11 Accumulator

(See Section 2.3.2.11 in WCAP-16996-P for additional discussion regarding the phenomena associated with this system/component/process and rankings.)

Injection Flow Rate and Line Resistance are merged in the FSLOCA PIRT given their strict interrelation. The Interfacial Heat Transfer ranking was modified from []^{a,c} for the SBLOCA PIRT to []^{a,c} for the FSLOCA PIRT. This is due to the fact that very low heat transfer is expected to occur at the liquid/nitrogen interface, and the fact that accumulator injection will essentially terminate the small break LOCA transient.

For the Broken Loop Accumulator Treatment, the same considerations provided in Section 2-2-10 to the Spilling Flow Treatment apply.

2-2-12 Downcomer

(See Section 2.3.2.12 in WCAP-16996-P for additional discussion regarding the phenomena associated with this system/component/process and rankings.)

Downcomer and Lower Plenum are merged together in the SBLOCA PIRT, while they are separated in the FSLOCA PIRT due to different considerations and phenomena that apply in these two regions for the larger breaks.

3-D Effect was ranked as []^{a,c} during blowdown in the FSLOCA PIRT, versus a []^{a,c} ranking assigned in the SBLOCA PIRT. Per Appendix A-1-2-12, this may be important for breaks closer to intermediate size, in which the downcomer may be partially depleted during the blowdown period and a non-uniform mixture level may result around the downcomer. The consideration put forth in the

FSLOCA PIRT is that []^{a,c}, that are explicitly included in the PIRT and for which a ranking consistent of []^{a,c} is provided.

As stated in Section 1-1-12, Countercurrent / Slug / Non-equilibrium Flow Effect was missing in the original FSLOCA PIRT and will be re-instated. This and Liquid Level Oscillations are specific ECC bypass related phenomena that have been included in the FSLOCA PIRT due to their importance for larger breaks. These phenomena do not occur for small breaks and are therefore ranked as N/A for all phases.

2-2-13 Lower Plenum

(See Section 2.3.2.13 in WCAP-16996-P for additional discussion regarding the phenomena associated with this system/component/process and rankings.)

Downcomer and Lower Plenum are merged together in the SBLOCA PIRT, while they are separated in the FSLOCA PIRT due to different considerations and phenomena that apply in these two regions for the larger breaks.

Sweep-Out is a specific phenomenon that has been included in the FSLOCA PIRT due to its importance for larger breaks. This phenomenon does not occur for small breaks and is therefore ranked as N/A for all phases.

Hotwall Effects has a ranking []^{a,c} in the FSLOCA PIRT consistent with that []^{a,c} provided for RPV Internals / Vessel Wall Stored Energy Heat Release in the SBLOCA PIRT.

2-2-14 Break

(See Section 2.3.2.14 in WCAP-16996-P for additional discussion regarding the phenomena associated with this system/component/process and rankings.)

Containment Pressure is included in the FSLOCA PIRT due to its importance for larger breaks. Flow is expected to remain critical for small break throughout the transient, and thus a ranking of N/A is assigned to all phases, except the final phase where flow can become unchoked.

Upstream Fluid Mixing has been added to the PIRT to distinguish the Upstream Flow Regime and the mixing of two streams coming from the two side of the break. Ranking justification is provided in Section 2.3.2.14 of Reference 1. Note that the ranking for Upstream Flow Regime for blowdown has been modified in the FSLOCA PIRT to a ranking of not-applicable, since in this phase mostly single phase liquid will be present in the cold leg.

Cold Leg Nozzle Flow Resistance is included in the FSLOCA PIRT due to its importance for larger breaks. It is considered of []^{a,c} significance for small breaks, as justified in Section 2.3.2.14 of Reference 1.

2-3 Previously Developed SBLOCA PIRT and Its Independent Review

The previously developed SBLOCA PIRT with the ranking rationale is documented in Section 1-4 of WCAP-14936 [4]. Before the final SBLOCA PIRT, an independent review of the preliminary SBLOCA PIRT was performed. The independent external review team of experts included, P. Griffith (MIT), Y. Hassan (Texas A&M), T. Fernandez (EPRI), and D. Speyer (consultant). Attachment A to WCAP-14936 [4] contains the team's review comments on the preliminary SBLOCA PIRT. The summary result of the independent review of the Westinghouse SBLOCA PIRT was also published in Reference 5. Note that the preliminary PIRT is different from the final SBLOCA PIRT given in Table 1-9 of WCAP-14936. While the independent PIRT Review Team's rankings were incorporated in the final PIRT, there were some exceptions as noted in Section 1-4-6 of WCAP-14936.

Westinghouse Non-Proprietary Class 3

Table 2-1: Comparison of FSLOCA SBLOCA PIRT to the one presented in WCAP-14936

Table 2-1: Comparison of FSLOCA SBLOCA PIRT to the one presented in WCAP-14936 (Cont.)

[

]^{a,c}

Westinghouse Non-Proprietary Class 3

Table 2-1: Comparison of FSLOCA SBLOCA PIRT to the one presented in WCAP-14936 (Cont.)

[

] ^{a,c}

Westinghouse Non-Proprietary Class 3

Table 2-1: Comparison of FSLOCA SBLOCA PIRT to the one presented in WCAP-14936 (Cont.)

[

] ^{a,c}

Westinghouse Non-Proprietary Class 3

Table 2-1: Comparison of FSLOCA SBLOCA PIRT to the one presented in WCAP-14936 (Cont.)

[

] ^{a,c}

Westinghouse Non-Proprietary Class 3

Table 2-1: Comparison of FSLOCA SBLOCA PIRT to the one presented in WCAP-14936 (Cont.)] ^{a,c}

Westinghouse Non-Proprietary Class 3

Table 2-1: Comparison of FSLOCA SBLOCA PIRT to the one presented in WCAP-14936 (Cont.)] ^{a,c}

Question 4: End of Blowdown Westinghouse Non-Proprietary Class 3

WCAP-16996-P/WCAP-16996-NP, Volumes I, II, and III, Revision 0 Subsection 2.3.1.2, “Large Break LOCA (LBLOCA) Periods Specification,” explains that a large break LOCA transient can be characterized by three distinct periods: blowdown, refill, and reflood. It is further stated that the blowdown period extends from the initiation of the break until the primary side depressurizes to the point when “emergency core cooling (ECC) water can start to penetrate the downcomer.” Subsection 27.2.1, “CGE Large Break Reference Transient Description,” suggests that the end of blowdown the primary system pressure approaches the containment pressure, the break flow and consequently the downward core flow are reduced, the core begins to heat up, and the vessel begins to fill with emergency core cooling system (ECCS) water. In this regard, the CSAU report (NUREG/CR-5249) describes the end of blowdown by the initiation of accumulator injection in the intact loops.

Please explain if there is any difference in these definitions with regard to the end of blowdown phase. As it remains unclear how the timing when ECC water “can start to penetrate the downcomer” is determined, please clarify if the time when the primary system pressure approaches the containment pressure (and when depressurization basically ceases) is appropriate to describe the end of blowdown. In addition, please explain what input the defined timing of end of blowdown has on ECCS performance and predicted peak cladding temperature (PCT).

Response:

Contrary to previous Westinghouse Best-Estimate LOCA evaluation models (EMs) (ASTRUM and CQD), in the Full Spectrum LOCA EM, there is a difference between the relevance and purpose of the period specifications in the phenomena identification and ranking table (PIRT) and in the context of the actual plant analysis and uncertainty methodology.

For the purpose of the PIRT exercise, Section 2.3.1.2 describes a typical large break LOCA scenario. The transient is divided into the three typical periods: a rapid blowdown followed by a refill period and reflood period.

The purpose of the period definition in the PIRT is to provide a qualitative description of the evolution of the transient in order to identify the phenomena pertinent to each time period occurring in each component of the system. The ranking of importance for each phenomenon proceeds from there. When it comes to the Large Break LOCA scenario there are different but practically equivalent descriptions of the processes occurring as the transient proceeds from blowdown to refill and into reflood. The blowdown extends to the point when the ECC water penetrates to the lower plenum to initiate refill (as presented in Section 2.3.2.1) and also corresponds to the time when the primary system pressure approaches the containment pressure as indicated in Section 27.2.1.

The PIRT is instrumental in identifying the evaluation model functional requirements as well as the requirements for the code assessment matrix. However, an exact definition of the time period is not required in the FSLOCA EM uncertainty propagation step. The reason is that biases and uncertainties are based on the particular processes that occur during the transient rather than the transient phase or period. The timing is captured if the code is shown to predict the sequence of events adequately during a particular scenario.

This aspect is new in FSLOCA EM. Previous EMs (ASTRUM and CQD) had a more simplistic means (the HOTSPOT heat conduction code) to propagate local uncertainties over time, and a clear definition of the time period was required by the mechanics of the methodology.

Section 29.4.3 of WCAP-16996-P describes how uncertainties in the post-CHF heat transfer are treated and how this component fits within the overall uncertainty analysis. As stated in the section *“There are several heat transfer regimes that affect the cladding temperature during a postulated LOCA accident, which depend on the fluid conditions as well as the cladding temperature itself. Models are included in the code to characterize each heat transfer regime, as described in Section 7. During a simulation, models are properly selected depending on the local flow regime, void fraction and surface temperature. Such models have been derived from a large data base which describes the fundamental heat transfer processes. The heat transfer package is then validated and assessed against prototypical data which was intended to recreate conditions expected in the reactor core during an accident, as discussed in Sections 14 and 15.*

[

] ^{a,c}

Section 29.4.3.1 describes how the uncertainties on [

] ^{a,c}

From the previous discussion, it is clear that the exact definition of end of blowdown, which would be dependent on specific attributes of the scenario (break size being a key factor) is irrelevant in the context of the FSLOCA EM uncertainty methodology because the propagation of uncertainties is based on the actual processes occurring during the scenario.

Other aspects of the biases and uncertainties, such as the capability of the FSLOCA EM to adequately predict the depressurization during blowdown, the end of blowdown, the ECCS bypass, and the penetration of the accumulator water in the lower plenum during a Large Break LOCA are demonstrated by assessing the EM prediction of integral and separate system effect tests such as LOFT (Section 22) and the full-scale UPTF-6 (Section 19.3.5). In particular Section 19.3.5.6 concludes that [

] ^{a,c}

From an overall system behavior stand point an adequate prediction of timing of events is shown in Section 22. In particular Section 22.5.4 concludes that “*The WCOBRA/TRAC-TF2 computer code [*

]^{a,c}

Thus, the definition of the end of blowdown is only important in the development of the PIRT, where the qualitative aspects of the transient progression are used to define the functional requirements of the EM. In the analysis, there is no explicit definition of the end of blowdown, and it therefore is of no consequence to the calculation of ECCS performance or PCT.

Question 5: Gap Conductance

NUREG/CR-5249 CSAU Table 6, "Summary of Highest-Ranked Processes," listed the gap conductance as a separate process. Furthermore, CSAU Table 16, "Thermal Response of Fuel and Peak Cladding Temperature Change," illustrated that the effect of gap conductance on the blowdown PCT was the largest one. It was recognized that during blowdown the impact on the PCT from stored energy release to cladding prevails over that from decay heat generation. Accordingly, the gap conductance was considered in the uncertainty analysis. The CSAU PIRT, as presented in NUREG/CR-5249 Table 1, "Summary of Expert Rankings and AHP-calculated Results," rated this process low during the blowdown and refill periods and high during the reflood period as the CSAU report was probably documenting the process as it evolved. WCAP-16009 Table 1-1, "PIRT for Large-Break LOCA," while including the gas conductance, provides no ranking for this factor besides the CSAU ranking of 8 during blowdown.

WCAP-16996-P/WCAP-16996-NP, Volumes I, II, and III, Revision 0, Table 2-1, "PIRT for Full Spectrum LOCA for Westinghouse and Combustion Engineering Plants," does not include and rank fuel gap conductance. Studies show that gap resistance dominates at the beginning of irradiation (until closure) and becomes again important at increased burnup levels close to 70 GWd/tU due to significant gap conductivity decrease (see results by C.B. Lee et al. as reproduced by M.T. Del Barrio et al., "Analysis of FRAPCON-3 Models Related to High Burnup Fuel," 2006 International Meeting on Light Water Reactor Fuel Performance "Nuclear Fuel: Addressing the Future," October 22-26, 2006, Salamanca, Spain).

Please explain why WCAP-16996-P /WCAP-16996-NP, Volumes I, II, and III, Revision 0, Table 2-1, "PIRT for Full Spectrum LOCA for Westinghouse and Combustion Engineering Plants," does not include and rank fuel gap conductance and its impact on fuel stored energy and predicted PCT. Please also identify the codes and methods for determining fuel gap conductance, fuel pin pressure, fuel temperatures, and stored energy versus burnup and explain their application and use in the FSLOCA methodology.

Response:

As described in the question, pellet-clad gap conductance is important through its influence on the steady state pellet average temperature. Following the postulated LOCA, the primary influence of the gap conductance is on the initial conditions. Section 1-2-3-1 of WCAP-16009 explains that "[t]he stored energy is most important (rank=9) during blowdown since the resulting pellet temperature distribution undergoes a readjustment that determines the heatup of the cladding after departure from nucleate boiling (DNB). The stored energy also reflects the power level at which the hot rod is operating before the initiation of the transient. In the Westinghouse analysis, items such as the gas gap conductance, fuel conductivity, effects of pellet radial power, or pellet cracking are considered as part of the initial stored energy used in the plant calculation. The stored energy effects diminish during refill but are still important since they represent the power history (peak kW/ft) of the hot rod." Later in that section, it is stated that "[t]he gas conductance is important because it helps establish the initial stored energy. It is accounted for in the assumed value used for the pellet stored energy."

Given this rationale, WCAP-16009 Table 1-1, "PIRT for Large-Break LOCA," while showing the CSAU rankings for Oxidation, Decay Heat, and Gas Conductance, provides the Westinghouse rankings for Stored Energy. Gas conductance can influence peak clad temperature by influencing the initial Stored Energy (pellet

average temperature), and is therefore captured in that category as described in Section 1-2-3-1 of WCAP-16009-P-A.

Section 2.3.2.1 of WCAP-16996-P describes the treatment of Stored Energy and its influence on the fuel rod. As described there, “[t]he stored energy is primarily a function of axial and radial power distributions throughout the core, pellet-clad gap conductance, and fuel thermal conductivity. [

]”^{a,c}

This is reflected in the rankings in Table 2-1 of WCAP-16996-P, where Gap Conductance is implicitly included through its influence on Stored Energy. The omission of Gap Conductance from Table 2-1 is due to the removal of the CSAU rankings, not because Gap Conductance is no longer considered to be important in determining the initial pellet stored energy.

A description of the codes and methods for determining fuel gap conductance, fuel pin pressure, fuel temperatures, and stored energy versus burnup and an explanation of their application and use in the FSLOCA methodology, will be provided as part of the response to Questions 36 and 37.

Question 6: Pressurizer Response

WCAP-16996-P/WCAP-16996-NP, Volumes I, II, and III, Revision 0, Revision 0 Subsection 2.3.2.6, “Pressurizer/Surge Line,” discusses processes related to the reactor pressurizer. Accordingly, WCAP-16996-P/WCAP-16996-NP, Volumes I, II, and III, Revision 0, Revision 0, Table 2-1, “PIRT for Full Spectrum LOCA for Westinghouse and Combustion Engineering Plants,” provides the ranking for processes related to pressurizer level/liquid flashing. During blowdown, [

] ^{a,c}

Subsection 2.3.2.6, “Pressurizer/Surge Line,” recognizes that the pressurizer level or pressure can initiate reactor trip. With regard to safety injection actuation, Subsection 2.3.1.3, “LBLOCA Periods Specification,” explains that the ECCS is aligned for delivery following the generation of an “S” signal when the pressurizer low/low-pressure setpoint is reached with some delay. Although Subsection 2.3.2.6 states that reactor trip is not credited for large breaks, please explain if possible impact on the safety injection actuation was considered in the adopted ranking with regard to the pressurizer level swell/flashing for large and intermediate breaks.

When considering the pressurizer component, it is also recognized that the broken loop is not known in advance. Please explain why WCAP-16996-P/WCAP-16996-NP, Volumes I, II, and III, Revision 0, Subsection 2.3.2.6, “Pressurizer/Surge Line,” provides no consideration with regard to possible effects associated with the break occurring in a loop connected to the pressurizer versus a break in a remaining loop without a pressurizer.

Response:

Following a large or intermediate break, the pressurizer drains rapidly and the system pressure drops to the low-low pressure setpoint around 1750 psia quickly, initiating the safety injection signal. See Figure 27.1.1.2-3 of WCAP-16996-P Revision 0 for the CGE intermediate break spectrum response; large breaks tend to depressurize even faster as illustrated in Figure 27.1.1.1-4. [

] ^{a,c}

For intermediate breaks, the timing of high pressure safety injection is also of low importance. As described in Section 2.3.2.11 of WCAP-16996-P Revision 0, it is the accumulator injection that quenches the core if any heatup occurs. Imprecision in the timing of high pressure safety injection initiation is therefore expected to not have a significant effect on the peak cladding temperature for intermediate breaks.

Also note that [

] ^{a,c}

Regarding the effects of a break occurring in the pressurizer loop, little influence is expected. For a break in the cold leg, communication with the pressurizer and surge line in the hot leg is indirect. The pressure in the pressurizer itself is largely insensitive to the location of the break, as is the time at which the setpoint pressure near 1750 psia is reached. As such, the influence on the predicted timing of the safety injection initiation is negligible.

Question 7: Long-Term Cooling and PIRT

WCAP-16996-P/WCAP-16996-NP, Volumes I, II, and III, Revision 0, Subsection 2.3.1, "LOCA Scenario Specification," identifies distinct periods that are used to characterize each LOCA sub-scenario. These periods also used to identify and rank participating phenomena in the proposed PIRT. When discussing the 10 CFR 50.46(b) acceptance criteria for emergency core cooling systems for light-water nuclear power reactors in WCAP-16996-P/WCAP-16996-NP, Volumes I, II, and III, Revision 0, Section 30.1, "Statistical Methodology Roadmap," the applicant states that the last two criteria, 10 CFR 50.46(b)(4) "Coolable geometry" and 10 CFR 50.46(b)(5) "Long-term cooling," are typically "satisfied outside the LOCA analysis once the LOCA calculation is demonstrated to be in compliance with the first three criteria." Section 32.3.1 "Regulatory Position 4, "Estimation of Overall Calculational Uncertainty"" further explains that Westinghouse methodology used to satisfy the long-term cooling criterion defined in 10 CFR 50.46(b)(5) is unaffected by the use of best-estimate techniques for the short-term transient calculation."

Phenomena germane to long-term cooling can have important impact on LOCA safety analyses. Thus, NUREG-0800 Standard Review Plan Section 15.6.5, "Loss-of-Coolant Accidents Resulting from Spectrum of Postulated Piping Breaks within the Reactor Coolant Pressure Boundary," requires analyses of both LBLOCAs and SBLOCAs performed to identify the timing for boric acid precipitation. Another phenomenon is re-plugging of the loop seals by SI water as recognized in Subsection 2.3.2.9 "Pump." The long-term cooling phase is not identified as a separate period in the general LOCA characterization provided in Subsection 2.3.1, "LOCA Scenario Specification." It is also not included as a separate LOCA in the FSLOCA PIRT provided in Table 2-1, "PIRT for Full Spectrum LOCA for Westinghouse and Combustion Engineering Plants." Please explain why such a period is not considered in the proposed FSLOCA PIRT and if the WCOBRA/TRAC-TF2 evaluation model is applicable for post-LOCA long-term cooling analysis.

In the context of long term cooling, the NRC staff finds that use of WCOBRA/TRAC-TF2 should be limited only to demonstration that sufficient coolant (i.e. in excess of boil-off) is added to the core to maintain it covered with two-phase mixture and keep fuel temperatures acceptably low during the long term after core quench. Since the FSLOCA methodology does not treat boric acid precipitation, long-term cooling can not be completely addressed with this methodology. Therefore, the long-term cooling criterion defined in 10 CFR 50.46(b)(5) can not be stated as being satisfied by application of the FSLOCA methodology. Accordingly, this will be a limitation applied to this methodology.

Response:

As stated in Section 1.2.1, "the scenario being addressed by the FSLOCA methodology is a postulated loss of coolant accident that is initiated by an instantaneous rupture of a reactor coolant system (RCS) pipe. The break type considered is either a double-ended guillotine, defined as a complete severance of the pipe resulting in unimpeded flow from either end, or a split break, defined as a partial tear. The break size considered for a split break ranges from the break size at which the break flow is beyond the capacity of the normal charging pumps up to a size equal to the area of a double ended guillotine rupture"

The PIRT developed in Section 2 is intended to be comprehensive and therefore to cover the same power plant classes included in the previous methodology (ASTRUM). This includes Westinghouse designed 3- and 4-loop plants with ECCS injection into the cold legs, Westinghouse designed 2-loop plants with upper plenum injection (UPI) and Combustion Engineering designs"

The FSLOCA methodology was designed to support the short term of a LOCA event, which for a Large Break LOCA event (FSLOCA Region II) corresponds to a complete quench of the core. For smaller breaks (Region I) the transient is terminated after the boil-off is terminated and core is recovered essentially by the injection of the accumulators. Therefore the long-term cooling phase was not identified as a separate period in the general LOCA characterization provided in Subsection 2.3.1.

The methodology was NOT intended to be applicable to a longer time frame which would include the identification of the timing for boric acid precipitation for example and consistently the long-term cooling phase was not identified as a separate period in the general LOCA characterization provided in Subsection 2.3.1 (the PIRT).

On the other hand phenomena such as tube re-plugging of the loop seals were considered as a possibility during the “short term” as stated in Section 2.3.2.9 for intermediate breaks where the broken loop accumulator or SI water could conceivably backflow during the second phase of this scenario.

Although the PIRT did not explicitly identify long term cooling as a separate phase, the WCOBRA/TRAC-TF2 code models, their assessment, and conclusions on the model biases and uncertainties are aimed to be as generic as possible. However, it is recognized that the methodology is not applicable to the long term cooling period, and it is consistent with the Staff’s conclusion that the use of the Evaluation Model should be limited only to demonstration that sufficient coolant, i.e. in excess of boil-off, is added to the core to maintain it covered with two-phase mixture and keep fuel temperatures acceptably low during the long term after core quench. The FSLOCA methodology does not treat boric acid precipitation, and long-term cooling cannot be completely addressed with this methodology. Therefore, the long-term cooling criterion defined in 10 CFR 50.46(b)(5) cannot be stated as being satisfied by application of the FSLOCA methodology.

However, there is no apparent reason to restrict the code only to cases where the loop seals do not refill, because this phenomenon was considered in the PIRT and could also occur in the near term for some scenario or breaks. For example Figure 27.3.3-9 shows the loop seal replugging (loop 2) at about 2600 seconds for DLW reference transient while other loops (Figure 27.3.3-8 and 27.3.3-10) do not show the replugging. Therefore, the code is capable of predicting the phenomenon if appropriate conditions exist.

Question 8: SBLOCA Boundary and Region-I to Region-II Boundary

The proposed Westinghouse **FSLOCA** methodology includes any break size causing a leakage beyond the capacity of the normal charging pumps up to and including a double ended guillotine rupture with a break flow area equal to two times the pipe area. WCAP-16996-P/WCAP16996-NP, Volumes I, II, and III, Revision 0, Section 2.3.1 “LOCA Scenario Specification,” identifies three different LOCA sub-scenarios with regard to break area: small breaks, intermediate breaks, and large breaks. Subsection 2.3.1.3 “IBLOCA Periods Specification” clarifies that the IBLOCA break sizes, although somewhat plant dependent, generally range from 10-inch to 13.5-inch equivalent diameter (0.55 ft² to 1.0 ft²). A proposed hybrid position for treatment of break type and size, described in Subsection 29.2.3 “Break Type, Split Break Area and Break Flow Model Uncertainty Methodology,” divides the full spectrum of break sizes in two contiguous regions identified as Region-I and Region-II. [

] ^{a,c} The subsection further explains that break sizes historically classified as intermediate breaks are included in both Region I and Region II. Thus, “Region-I provides coverage of what typically are defined as Small Break LOCA scenarios and stretch into Intermediate Break LOCA whereas Region-II starts from Intermediate Break size and include what typically are defined Large Break LOCA scenarios” as stated in WCAP-16996-P/WCAP-16996-NP, Volumes I, II, and III, Revision 0, “Executive Summary”.

WCAP-16996-P/WCAP-16996-NP, Volumes I, II, and III, Revision 0, Section 31.3, “Analysis of Results for Region I,” presents a demonstration analysis of the **FSLOCA** methodology for a selected three-loop Westinghouse PWR. Subsection 31.1.1 “Break Area Ranges” employs a mechanistic model using WCT-TF2 to determine the minimum small break as [

] ^{a,c} As discussed in Subsection 2.3.1.3, IBLOCAs generally range from 10-inch to 13.5-inch equivalent diameter (0.55 ft² to 1.0 ft² or 13.2 percent to 24.2 percent cold leg area). Please explain if there is inconsistency with regard to the intended coverage of the entire SBLOCA range in Region-I as proposed in the **FSLOCA** methodology.

To assess the adequacy of the proposed position for applying the uncertainty analysis to the full break spectrum and related treatment of the break size, the staff needs the following additional information. Please explain if an approach for determining an upper limiting break size for SBLOCAs, based on major controlling plant characteristics, has been considered for the **FSLOCA** methodology. The staff finds that the break size, selected to separate Region-I from Region-II, lacks relevant evidence to governing LOCA phenomena inherent to and defining the major LOCA categories. The staff finds it important that the upper break boundary for SBLOCA is based on phenomenological considerations that allow for the determination of such boundaries based on the scaling of major contributing parameters, such as reactor coolant system volume, power level, etc., on a plant specific basis. Accordingly, any division of the entire break spectrum into sub-regions in the uncertainty analysis should be based on similar considerations. Please address these items for the **FSLOCA** methodology.

Response:

There are two main topics embedded in the question. The first topic is to determine if there is an inconsistency regarding the intended coverage of the entire small break loss-of-coolant accident (LOCA)

Westinghouse Non-Proprietary Class 3

range in Region-I vs. the as-analyzed range. The second topic is to clarify if the upper limiting break size for small break LOCA based on major controlling plant characteristics has been considered. These topics are addressed herein.

The intent of the two Regions is to develop probabilistic statements with respect to peak cladding temperature (PCT) and maximum local oxidation (MLO) for the possible break sizes within each region of the spectrum.

The key distinction between Region-I and Region-II is [

] ^{a,c}

From Table 29-1 in WCAP-16996-P (Reference 1), there is [

] ^{a,c} (the breaks in consideration here are the

Split breaks). As such, there are no gaps at the boundary between the two Regions. This is further demonstrated by looking at the break sizes sampled for the demonstration analysis (plant [] ^{a,c}) in Section 31 of WCAP-16996-P (see also Table Q8-1 at the end of the response). The largest effective break area sampled in Region-I (calculated using Equation 31-1 in WCAP-16996-P) is [

] ^{a,c}. The smallest effective break area in Region-II (calculated using Equation 31-3 in WCAP-16996-P) is [

] ^{a,c}. As seen, there is an inconsequential gap [] ^{a,c} between the largest Region-I effective break area and the smallest Region-II effective break area. It is also observed that [

] ^{a,c}

The boundary between Region-I and Region-II [

] ^{a,c}

Based on the above, the statements in WCAP-16996-P related to small and intermediate breaks falling within Region-I is [

Westinghouse Non-Proprietary Class 3

] ^{a,c}

For Westinghouse NSSS plants, [

] ^{a,c} Within the range of volume-to-power ratio, a lower volume-to-power ratio will tend to result in a smaller, small break size being limiting; likewise a higher volume-to-power ratio will tend to result in a larger, small break size being limiting. This is due to a higher power resulting in more vapor generation, which results in a slower depressurization and reduced safety injection, and/or due to a lower volume resulting in a deeper core uncover.

The four-loop plants have the highest volume-to-power ratio, but also have [

] ^{a,c}

Therefore, [

] ^{a,c} The 2-loop and 3-loop plants have similar volume-to-power ratios, [

] ^{a,c}

There are two three-loop plant break spectrum studies presented in Section 27. These will be discussed further to show the potential impact of [] ^{a,c}. This will be followed by a review of the demonstration analysis.

- Break Spectrum Study 1 ([] ^{a,c})

The pressure response for the small and intermediate breaks executed is shown in Figures 27.1.1.3-2 and 27.1.1.2-3, respectively, of WCAP-16996-P. Both figures include the 8-inch break for comparison. The figures show that the 8-inch break [

] ^{a,c}

- Break Spectrum Study 2 ([] ^{a,c})

The pressure response for small and intermediate breaks is shown in Figures 27.1.2.3-1 and 27.1.2.2-3, respectively, of WCAP-16996-P. Both figures include the 8-inch break for comparison. The figures show that the 8-inch break [

] ^{a,c}

- Demonstration Analysis

To demonstrate the effect of Region-I vs. Region-II on PCT, several cases from the demonstration analysis are presented in Table Q8-1. These cases are the Region-I cases near the Region-I/II boundary and the Region-II cases with an effective break area less than 1 ft². As seen from Table Q8-1, [

] ^{a,c}

In summary, the Regions cover the intended break size ranges, and the Region I/II boundary is defined with controlling plant characteristics in mind.

Table Q8-1: Results Comparison Near Region I / II Boundary from Demonstration Analysis

Region	RUN	Break Area Multiplier	CDV2	CDP2	PCT (F)	Effective Break Area (ft2)	Effective Break Diameter (in)
--------	-----	-----------------------	------	------	---------	----------------------------	-------------------------------

a,c

Reference

1. WCAP-16996-P, "Realistic LOCA Evaluation Methodology Applied to the Full Spectrum of Break Sizes (FULL SPECTRUM™ LOCA Methodology)," November 2010.

Question 10: LOOP vs. RCPs Operating

If LOOP is assumed at break time, please justify that this assumption is appropriate since LOOP at time of pressurizer low/low-pressure trip setpoint produces a more severe result for SBLOCA. Furthermore, if there is no LOOP during SBLOCA, what is the limiting break size and location with PCT identified, using the FSLOCA methodology? How is the emergency operating procedure trip timing modeled including operator error and uncertainty when simulating SBLOCAs with RCPs running? Please explain and show the break spectrum with RCPs running. Furthermore, it is not clear that cold leg breaks are always the limiting location as stated in Section 2.3.1, "LOCA Scenario Specification," given the effects of operating RCPs during the event. With RCPs operating, the limiting break may be a hot leg break. Please also describe any changes to the models for key SBLOCA phenomena that are impacted if RCPs are operating for SBLOCAs. In addition, please explain why the PIRT did not specifically include SBLOCA phenomena with the RCPs running. In this regard, it is explained in WCAP-16996-P/WCAP-16996-NP, Volumes I, II, and III, Revision 0, Section 2.3.1 "LOCA Scenario Specification" that "the availability of the RCPs following reactor trip is considered, so variability in the pump trip time does exist."

Response:

LOOP Assumption

[

]^{a,c}

RCP Trip Time

[

]^{a,c}

[

]^{a,c}

Break Spectrum

[

]^{a,c}

Hot Leg Considerations

[

] ^{a,c}Modeling Changes

[

] ^{a,c}PIRT

[

] ^{a,c}**References:**

1. WCAP-16996-P, "Realistic LOCA Evaluation Methodology Applied to the Full Spectrum of Break Sizes (FULL SPECTRUM LOCA Methodology)," November 2010. (Westinghouse Proprietary)
2. WCAP-9584, "Analysis of Delayed Reactor Coolant Pump Trip During Small Loss of Coolant Accidents for Westinghouse Nuclear Steam Supply Systems," August 1979. (Westinghouse Proprietary)
3. OG-110, "Evaluation of Alternate RCP Trip Criteria," September 1983.
4. OG-117, "Justification of Manual RCP Trip for Small Break LOCA Events," March 1984.
5. EGG-LOFT-5480, "Four-inch Equivalent Break Loss-of-Coolant Experiments: Posttest Analysis of LOFT Experiments L3-1, L3-5, (PUMPS OFF), and L3-6 (PUMPS ON)," October 1981.

Question 11: Loop Seal Behavior

Loop seal clearing is a major physical phenomenon that controls PCT for small break LOCAs. Integral test data shows that for break sizes less than 5-inch equivalent diameter in the discharge cold leg, only one loop seal clears. And for example, for Semiscale Test S-O7-10D, there is also residual water remaining in the horizontal section of the suction legs that clear. Furthermore, loop seal clearance following small breaks is very difficult to predict with T/H codes and as such, modeling break sizes less than 5-inch diameter should only credit the clearing of one loop seal. Table 31.3-1b shows the limiting PCT to be 906 °F for Case 059. Case 059 predicted three loop seals clearing. Test data shows that break sizes less than 5-inch diameter do not exhibit more than one loop seal clearing. Please repeat the analysis for Case 059 with only one loop seal cleared. Also, if residual water remains in the horizontal section, how is the vapor flow area in this region modeled and computed? Please explain. In addition, please describe if the hot leg nozzle gaps and core barrel leak paths are credited. Please repeat 059 with the nozzle gaps and core barrel leakage paths closed. What is the impact of these assumptions on the Beaver Valley Region I break spectrum, particularly the limiting small break as identified in Question 9?

Response:**Loop Seal Clearing Observed in ROSA-IV LSTF Tests**

The Rig-of-Safety Assessment Number 4 (ROSA-IV) program conducted a series of experiments to investigate the thermal-hydraulic behavior of a Westinghouse-designed four-loop PWR during small break LOCAs and operational transients using the Large Scale Test Facility (LSTF). The LSTF is a 1/48 volume scale representation of a Westinghouse four-loop 3423 MWt Pressurized Water Reactor (PWR). The Westinghouse FSLOCA program specifically incorporated the ROSA-IV test facility in its assessment of the WCT/FT-2 code in Section 21 of Reference 1 due to the scaling relative to a Westinghouse four-loop PWR. A review of the tests performed at this facility indicates that break sizes less than a 5-inch equivalent break size may clear multiple loop seals. For example, for the 2.5% Cold Leg Break orientation studies (Reference 4), multiple loop seal clearings, either partial or full clearing, were observed as demonstrated by the measured loop seal differential pressures shown in the following figures taken from Reference 4.

Westinghouse Non-Proprietary Class 3

a.c

ROSA-IV LSTF 2.5% Cold Leg Break Test SB-CL-01

Westinghouse Non-Proprietary Class 3

a.c

ROSA-IV LSTF 2.5% Cold Leg Break Test SB-CL-02

Westinghouse Non-Proprietary Class 3

a.c

ROSA-IV LSTF 2.5% Cold Leg Break Test SB-CL-03

In addition, there is evidence of multiple loop seal clearing, at least for a partial duration of the transient, in the 0.5% Cold Leg Break orientation studies (Reference 5) as well.

Therefore, the statement regarding test facilities only clearing single loop seals for breaks below 5-inches is not clearly supported by available test data.

Loop Seal Clearance Observed in Semiscale Tests S-07-10 and S-07-10D

Per Reference 2, Semiscale test S-07-10 and S-07-10D simulated a 10% equivalent cold leg break (~8.7-inch) without emergency core coolant (ECC) (until elevated core heater rod temperatures were achieved) to determine the system behavior leading to and accompanying dryout and heat-up of a core during a small break transient. This break size is equivalent to an accumulator line break in a PWR. The break was located on the centerline of the broken loop cold leg between the pump and the vessel. Test S-07-10D differed from test S-07-10 in that the broken loop steam generator was allowed to blow down throughout the transient.

The major features of Mod-3 version in which experiment S-07-10D was performed are:

- Full scale elevation
- 1:1705.5 volume scale
- Maintained component layout and relative elevations of various components between plant and test facility
- Full length (3.66m) 5×5 electrically-heated rods
- External downcomer
- Full length upper plenum and upper head with simulated reactor internals
- High-pressure and low-pressure coolant injection pumps and accumulator injection in intact loop
- Pressure suppression system simulating the containment response.

Per Table 3 of Reference 2, it is indicated that for test S-07-10 the intact loop pump suction piping cleared first, followed by the broken loop. For test S-07-10D, only the intact loop pump suction piping was predicted to clear. As noted in the report, the non-symmetric behavior between the intact and broken loop is attributed to differences in pump characteristics, loop hydraulic resistances and steam generator heat transfer and condensation.

The first two figures presented below (Figures 20 and 21 from Reference 2) compare the measured cold leg fluid densities upstream of the break for Tests S-07-10 and S-07-10D. Figure 20 indicates that there is little vapor venting through the broken loop for Test S-07-10D (plugged during most of the transient) and the broken loop vents later in the transient for Test S-07-10. Figure 21 shows that the measured vessel side fluid density is very similar for both tests and indicates that venting occurred through the intact loop seals from approximately 120 seconds onward.

Westinghouse Non-Proprietary Class 3

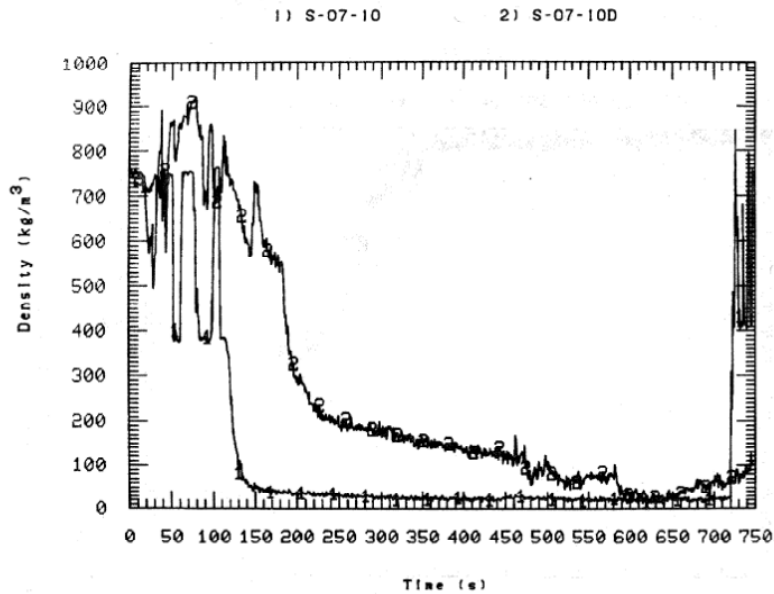


Figure 20. Comparison of fluid density measurements between the broken loop pump and break for Tests S-07-10 and S-07-10D.

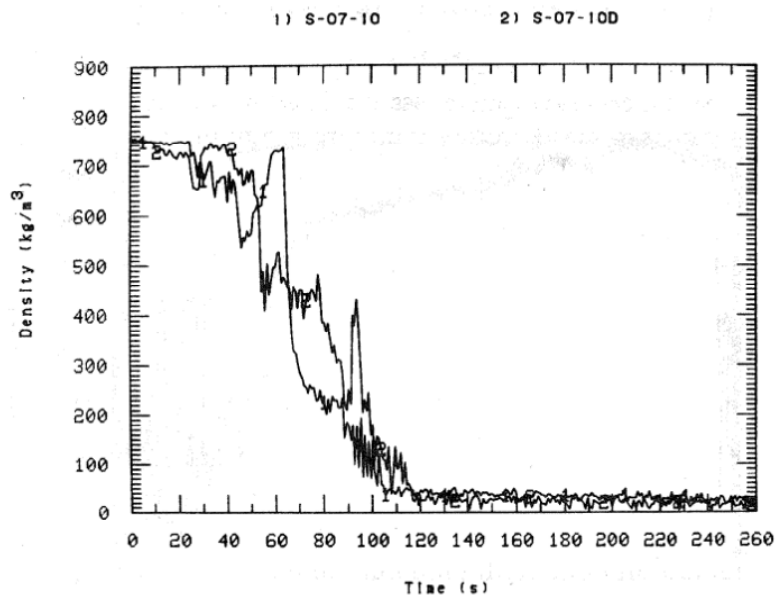


Figure 21. Comparison of fluid density measurements between the break and vessel for Tests S-07-10 and S-07-10D.

The test results indicate that the intact loop pump suction retains slightly more residual water following the loop seal clearing in Test S-07-10D as compared to S-07-10 (Figure 28 of Reference 2). The broken loop pump suction piping did not clear for Test S-07-10D (Figure 29 of Reference 2).

The primary observation from these two tests is the suppression of the broken loop seal from clearing and the delayed prediction of the intact loop seal clearing in Test S-07-10D which is attributable to the blowdown of the broken loop steam generator. In addition, makeup flow which

Westinghouse Non-Proprietary Class 3

was to be terminated at transient initiation actually continued for 150s into the transient for test S-07-10D which could also have contributed to some of the residual water in the pump suction piping of the broken loop.

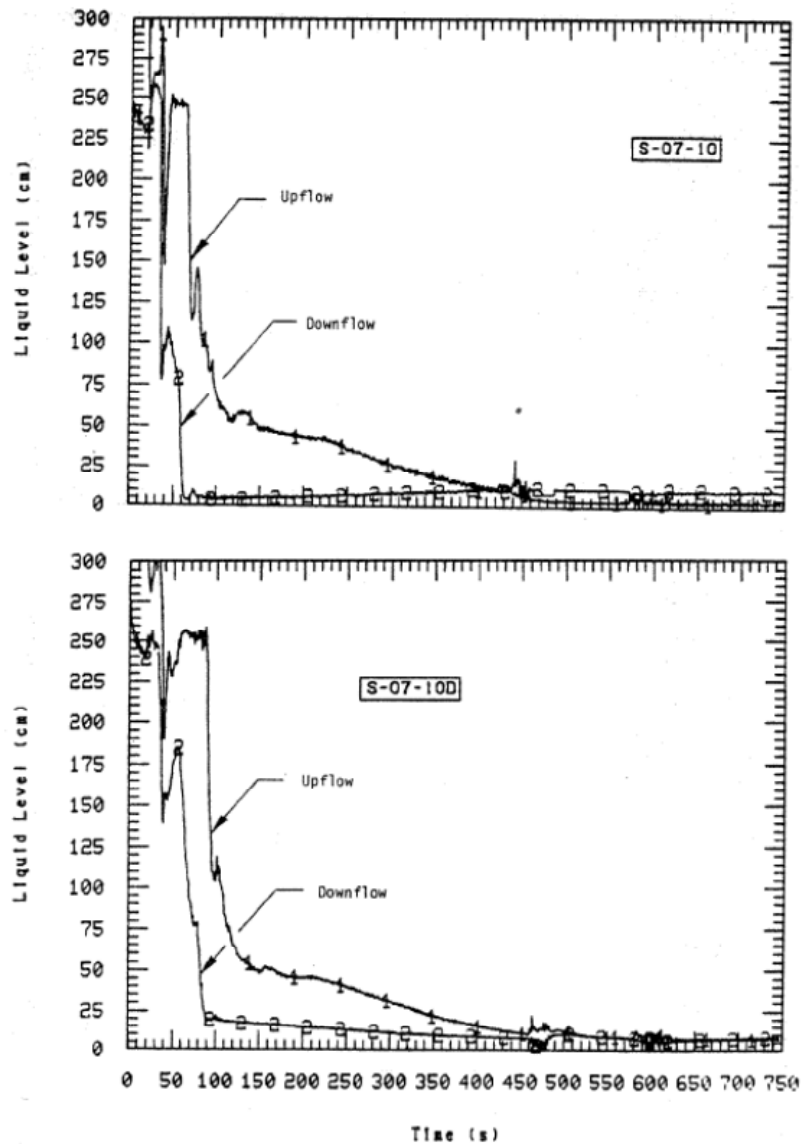


Figure 28. Calculated collapsed liquid levels in the intact loop pump suction for Tests S-07-10 and S-07-10D.

Westinghouse Non-Proprietary Class 3

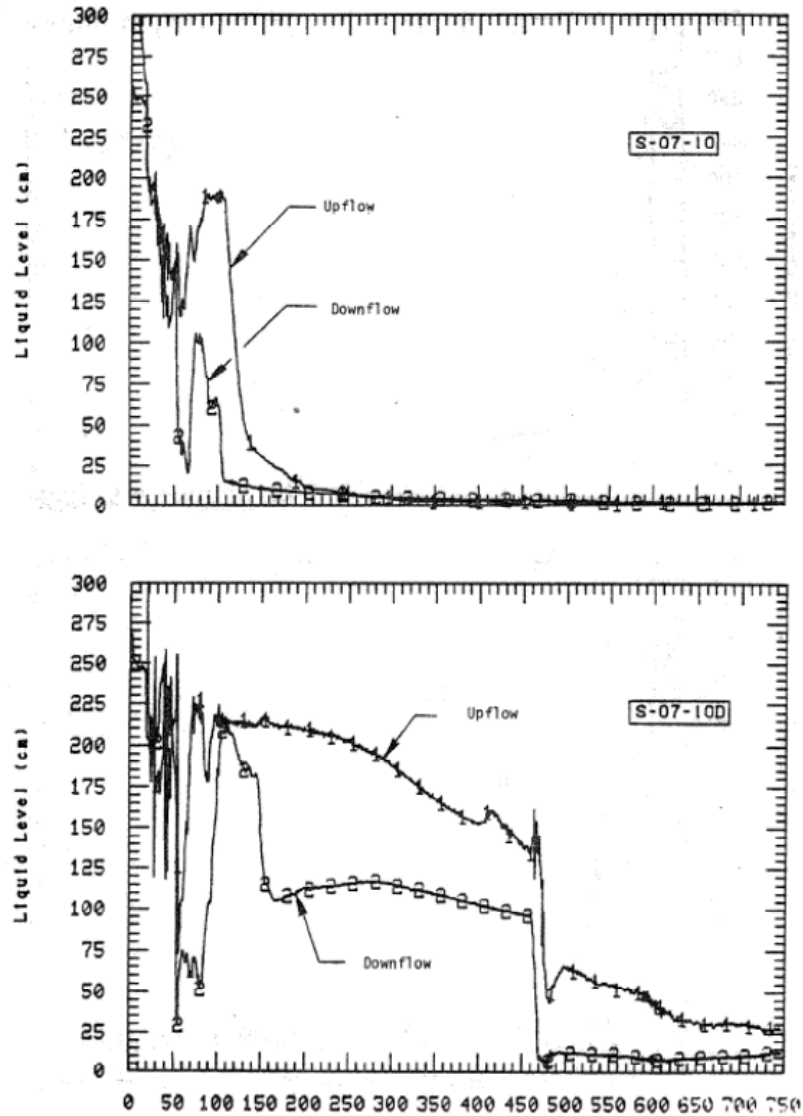


Figure 29. Calculated collapsed liquid levels in the broken loop pump suction for Tests S-07-10 and S-07-10D.

WCT/TF-2 loop seal model validation

The loop seal clearing validation work performed for the WCOBRA/TRAC-TF2 (WCT-TF2) code utilized in the FULL SPECTRUM LOCA (FSLOCATM) is documented in Section 18 of Reference 1. Based on this work, the FSLOCATM approach adopted is to not restrict loop seal clearing to a single loop. This is also supported by the results of the test series cited previously (Semiscale Test S-07-10) which indicate the occurrence of multiple loop seal clearing with the intact loop seal clearing first. The ROSA-IV LSTF 2.5% and 0.5% cold break tests, References 4 and 5, further support this modeling approach.

The WCT-TF2 loop seal clearing validation section describes the important phenomena and available experiments used to assess the performance of the WCT-TF2 code. The important aspects of the loop seal clearing process are noted to depend on the following factors:

- Core steam generation rate
- Bypass steam flow rate through various vent paths
- Rate of accumulation of liquid in the pump suction piping

Various experiments (both air/water and steam/water) have shown that the basic physical process is controlled by:

- The extent to which a stratified flow regime can be maintained in the horizontal leg
- The degree to which liquid pushed into the downstream vertical leg can be entrained out of the loop seal

Review of the experiments indicates that the loop seal behavior can be explained in terms of three regimes. These are:

- Droplet entrainment
- Wave Instability and Vertical CCFL
- Slug/Oscillatory

The effect of scale was also assessed. [

] ^{a,c}

Two ROSA tests (1/48 volume scale) were examined, followed by scaled loop seal experiments [^{a,c} (Reference 3), and full-scale (Reference 6)). The scaled tests were utilized to highlight the important physical and scaling features of the loop seal clearing process. Finally, WCOBRA/TRAC-TF2 simulated large scale UPTF tests (References 7 and 8) to assess the models and correlations in the code. The factors considered to be important for the assessment of the UPTF loop seal predictions are as follows:

- Overall loop seal pressure drop as a function of steam flow
- Liquid distribution in the loop seal as a function of steam flow

The validation work performed with the UPTF full-scale steam-water test, (Section 18.3 of Reference 1) [

] ^{a,c}

Westinghouse 3-loop plant loop model

[

] ^{a,c}

Case 059 and loop seal clearing

As noted in Figure 31.3-7 of Reference 1, [

] ^{a,c} As

seen in Figure 31.3-7 of Reference 1, this implies that [

] ^{a,c}

Modeling of bypass flow paths

[

] ^{a,c}

Modeling of horizontal pump suction piping in FSLOCA

Residual water in the horizontal loop seal regions are predicted following loop seal clearing. The interfacial drag in the stratified flow directly controls the time period for the loop clearance and the level of residual water in the loop seal. It is recognized that the vapor flow in this region involves multi-dimensional/complex liquid flow and to model it using a one-dimensional model completely mechanistically is not possible (Reference 8). However, as discussed earlier, the remaining residual water in the horizontal section of the loop seal and the pressure losses (resistance) over the loop seal are relatively well simulated using WCT-TF2 (Section 18.3 of Reference 1).

The WCT-TF2 flow regime maps and the calculation of interfacial areas in the one-dimensional components are discussed in Section 4.4 of Reference 1.

The horizontal stratified flow and wavy dispersed flow is discussed in Section 16 of Reference 1. An improved horizontal flow regime map is included in the 1D module of WCOBRA/TRAC-TF2 to expand the applicability of the code to small break LOCA scenarios. The 1D module is based on the TRAC-PF1 formulation. TRAC-PF1 shortcomings are identified and improvements were implemented with a revised model which better describes the conditions expected in a PWR during postulated LOCA scenarios. The improved model includes a hybrid transition criterion for the transition from horizontal stratified flow to non-horizontal stratified flow, [

] ^{a,c} A wavy-dispersed

model, [

] ^{a,c} which in TRAC-PF1/MOD2 is applied

generically regardless the orientation of the pipe. A detailed discussion on the flow regime, transition criteria and applicability can be found in Section 4 of Reference 1.

At the relatively low flow rates associated with the break size range of small break LOCA, the horizontal two-phase flow is expected to be in the horizontal stratified or wavy-dispersed flow regimes most of the time. Once flow regime is identified to be horizontal stratified or wavy-dispersed, the appropriate closure relations are selected for the interfacial area, the interfacial drag, and the interfacial heat transfer. The selection criterion for either the horizontal

stratified or wavy-dispersed flow regimes is discussed in Section 4 of Reference 1, while Sections 5 (interfacial and wall drag) and 6 (interfacial heat transfer) of Reference 1 provide the closure relationships associated with these flow regimes. Scaling and applicability of those models were also discussed in these sections. Section 16 of Reference 1 compares the void fraction prediction for horizontal stratified flow with relevant test data to assess the stratified flow interfacial drag model, wall drag model, and influence of inlet and outlet boundaries.

[]^{a,c}

Loop seal clearing effect on Beaver Valley Region I

The effect of loop seal clearing behavior on the Beaver Valley Region I break spectrum will be discussed in the response for RAI Question 9.

References

1. WCAP-16996-P, "Realistic LOCA Evaluation Methodology Applied to the Full Spectrum of Break Sizes (FULL SPECTRUM LOCA Methodology)," November 2010.
2. EGG-SEMI-5201, "Analysis of Semiscale Mode-3 Small Break Test S-07-10 and S-07-10D," U. S. Department of Energy, D. J. Shimeck, July, 1980.
3. Boileau, H., and Bourteele, J. P., 1985, "ECHTOR Program, PWS 2.3: Small Size Break, Final Report," EP/TA/DC 533.
4. Koizumi, Y., et al., 1987, "ROSA-IV/LSTF 2.5% Cold Leg Break LOCA Experiment Data Report for Runs SB-CL-01, 02 and 03," JAERI memo 62-399.
5. Koizumi, Y. and Tasaka, K., 1988, "Quick Look Report for ROSA-IV/LSTF 0.5% Cold Leg Break LOCA Tests, SB-CL-15 and SB-CL-16," JAERI memo 63-344.
6. Tuomisto, H. and Kajanto, P., 1988, "Two Phase Flow in a Full Scale Loop Seal Facility," Nuclear Eng. and Design, 107, 295-305.
7. Liebert, J. and Emmerling, R., 1998, "UPTF Experiment Flow Phenomena During Full-Scale Loop Seal Clearing of a PWR," Nuclear Engineering and Design, Vol. 179, pp. 51-64.
8. Ohvo, J., et al., 1998, "Simulation of Full-Scale UPTF Loop Seal Experiments with APROS, CATHARE and RELAP," 6th International Conference on Nuclear Engineering, ICONE6-6090.

Question 13: Decay Heat Multiplier/Sampling

It is not clear how the decay heat multiplier is computed. Please provide a detailed explanation of the methods used to compute the nominal decay heat curve and then show how the uncertainty is computed as a multiplier (multiplication factor) applied to the total decay heat. Choosing an initial multiplier and applying it throughout the entire transient is not considered realistic or justified. Decay heat multipliers less than 1.0 are not considered acceptable. There are many decay chains comprising the total decay heat and as such, the applied decay heat multiplier during the transient should be sampled between 1.0 and the upper 2- σ level. σ may change with time but this must be justified. Furthermore, use of the 1979 American Nuclear Society (ANS) decay heat standard (as well as all other standards) may not be appropriate for best-estimate determinations because the data from the standard was not developed for best-estimate determinations other than Appendix K 'type' assessments and analysis. Lastly, it is not clear how one determines the nominal curve using the ANS standards. In view of these concerns, please describe an approach that accounts for all known uncertainties in arriving at a decay heat curve that represents the nominal plus the upper 2- σ interval.

Response:

The response to RAI-21 (LTR-NRC-13-33 [2]) describes the WC/T-TF2 implementation and validation of the nominal decay heat power according to the ANS 1979 Standard [3] calculation method. The response to RAI-22 (LTR-NRC-13-33 [2]) describes the WC/T-TF2 implementation and validation of calculation of decay heat power uncertainty ANS 1979 Standard [3] calculation method. The application of decay heat uncertainty is detailed in the response to RAI-28 (LTR-NRC-13-33 [2]).

The decay power uncertainty methodology samples a multiplier to the standard deviation of the decay power uncertainty. The absolute decay power associated with this uncertainty changes as a function of time after shutdown according the ANS 1979 standard [3], which is considered adequate for the best estimate LOCA analysis [4]. Decay power multipliers less than 1.0 can be sampled if the sampling is consistent with the uncertainty distribution. As stated in the ANS 1979 Standard [3], "...the uncertainty is expressed in a statistical sense as one standard deviation in a normal distribution." Therefore, it is appropriate to sample from the normal distribution with the standard deviation as formulated in the standard.

RG 1.157 [4] states that the ANS 1979 standard [3] is adequate for use in best estimate LOCA analysis. WCOBRA/TRAC-TF2 (WC/T-TF2) decay heat power model is described in Section 9 of [1] and in the response to RAIs 20 through 28 in detail. The validation confirmed that the model in WC/T-TF2 is an accurate implementation of the ANS 1979 standard and thus is adequate for use in FSLOCA.

The uncertainty in the contribution from actinides is conservatively accounted for in the FSLOCA method as described in the response to RAI-26 [2]. [

]^{a,c} It is therefore concluded that the decay heat power and its uncertainty are conservatively modeled in WC/T-TF2 for the purpose of Best Estimate LOCA analysis.

References:

Westinghouse Non-Proprietary Class 3

1. WCAP-16996-P, “Realistic LOCA Evaluation Methodology Applied to the Full Spectrum of Break Sizes (FULL SPECTRUM LOCA Methodology),” November 2010.
2. LTR-NRC-13-33, ‘Submittal of Westinghouse Responses to “WCAP-16996-P, ‘Realistic LOCA Evaluation Methodology Applied to the Full Spectrum of Break Sizes (FULL SPECTRUM LOCA Methodology)’ Request for Additional Information – Second Set” (Proprietary/Non-Proprietary), Project 700, TAC No. ME5244’ dated May 31, 2013.
3. ANSI/ANS-5.1-1979, “American National Standard for Decay Heat Power in Light Water Reactors.”
4. Regulatory Guide 1.157, “Best-Estimate Calculations of Emergency Core Cooling System Performance,” May 1989.

Question 14: Number of SBLOCA Cases Sampled: []^{a,c}

What is the basis for the []^{a,c} chosen for the SBLOCA Region-I sample size described in WCAP-16996-P/WCAP-16996-NP, Volumes I, II, and III, Revision 0 Subsection 30.3.1 “Tolerance Intervals and Sample Size?” Given the PCT and oxidation criteria, at least 124 cases are necessary to properly capture the limiting break with the 95/95 probability statement. However, given the concerns with regard to resolving the worst break as discussed above in Question 11, please either propose a strategy that incorporates a deterministic identification of the worst break or propose additional sampling cases that will always capture this worst break size. If a sampling approach is chosen, it should be shown to identify the same limiting break size as that for the deterministic approach.

Response:

In the FSLOCA methodology, []

[]^{a,c}

10 CFR 50.46 requires that “[...] uncertainty must be accounted for, so that, when the calculated ECCS cooling performance is compared to the criteria set forth in paragraph (b) of this section, there is a high level of probability that the criteria would not be exceeded.”

In addition to clarifying that 95% is sufficient for “high probability,” Regulatory Guide 1.157 explains that “[...] The revised paragraph 50.46(a)(1)(i) requires that it be shown with high probability that none of the criteria of paragraph 50.46(b) will be exceeded, and is not limited to the peak cladding temperature criterion. However, since the other criteria are strongly dependent on peak cladding temperature, explicit consideration of the probability of exceeding the other criteria may not be required if it can be demonstrated that meeting the temperature criterion at the 95% probability level ensures with an equal or greater probability that the other criteria will not be exceeded.”

[]

Westinghouse Non-Proprietary Class 3

] ^{a,c}

Aspects of this question that refer to the deterministic identification of a worst break will be addressed in the response to Question 12.

Question 15: SBLOCA Upper Limit Break Size

The upper limit to the break size in Region-I []^{a,c} The small break spectrum should include break sizes up to approximately 1.0 ft². This upper limiting small break needs to be identified and justified. A small break spectrum that ends at []^{a,c} is missing the remaining portion of the small break spectrum. As such, use of the selected []^{a,c} break as an upper limit is inappropriate. Furthermore, the upper limit should be scaled based on power and plant physical characteristics such as volume. For example, a 0.15 ft² break for a high power and large RCS volume plant will produce the same result as that for a smaller break size for a plant with a lower power and a smaller RCS volume with all other inputs being scaled correspondingly. Please identify and justify the small break spectrum and show how the small break spectrum upper limit changes with proper scaling of key plant parameters (power and volume).

Response:

See response to Question 8.

Question 16: Long-Term Cooling Restriction

The staff does not agree that the WCAP 16996-P/WCAP-16996-NP, Volumes I, II, and III, Revision 0, FSLOCA methodology completely satisfies the long-term cooling requirement even if it addresses 50.46(b)(1) through 50.46(b)(5) criteria. To satisfy criterion 50.46(b)(5), the prevention of boric acid precipitation should be addressed and shown to be prevented for all break sizes. This is currently done using Appendix K models and analyses. Boric acid precipitation was not addressed in the WCAP 16996-P/WCAP-16996-NP, Volumes I, II, and III, Revision 0, FSLOCA methodology. Therefore, the staff will restrict the use of the FSLOCA methodology to only addressing criteria 1 through 4. The FSLOCA methodology should, of course, demonstrate that, once the core temperature have been reduced to an acceptably low temperature, the FSLOCA thermal hydraulic analysis predicts that the injection exceeds boil-off after core quench and therefore the core remains covered with two-phase mixture. It must also be demonstrated that the loop seals do not refill with liquid and depress the level into the core during the long term. The WCAP 16996-P/WCAP-16996-NP, Volumes I, II, and III, Revision 0, FSLOCA methodology document in Section 2.3.2.9 “Pump” and in Section 31.3 “Analysis of Results For Region I” explains that []^{a,c} Show this behavior and demonstrate that during the long-term cooling phase heat up does not cause reheating of the fuel cladding.

Response:

See the response to related Question 7.

Question 17: Swelled or Two-Phase Mixture Level versus Collapsed Level

The WCAP-16996-P/WCAP-16996-NP, Volumes I, II and III, Revision 0, mentions the collapsed liquid level in many assessments and analysis. It is important to emphasize that the key parameter determining core uncover and heat up is the two-phase mixture level. That is, the same liquid level could have different mixture levels and rates of attendant heat up. Therefore, all calculations should show the two-phase mixture level versus time as the key figure of merit for small breaks and not the liquid level. Please describe how this mixture level is determined for all small breaks. Describe the treatment of steam cooling heat transfer and heat up in the cell containing the two-phase mixture surface. How is the vapor superheat computed when the two-phase mixture surface is very near the bottom of the cell? Do all cells containing saturated liquid, regardless of whether the cell contains the two-phase mixture surface, treat the vapor as saturated also? Since T/H codes can artificially entrain liquid from the surface and expel drops into the upper vapor region of the core, please explain and demonstrate that liquid drops are not artificially expelled into the vapor region during long-term uncover of the core for small breaks. Please explain what is done in the code to prevent such behavior in the WCOBRA/TRAC-TF2 vessel model.

Response

As described in Section 7.2 of WCAP-16996-P (Reference 17-1), the heat transfer regime selection logic is determined based on [

]^{a,c} A small break loss-of-coolant accident (SBLOCA) will tend to move laterally through the heat transfer regime map shown in Figure 7.2-3 of WCAP-16996-P, (i.e., from the pre-CHF regimes to single phase vapor (SPV), rather than pre-CHF to annular/film boiling). This requires good accounting of the two-phase mixture level location in a given channel and cell, as well as the vapor temperature and steam cooling above the two-phase mixture level.

The response to this question is segregated as follows. First the determination of the two-phase mixture level in WCOBRA/TRAC-TF2 is discussed. This is followed by a discussion of the vapor temperature and heat transfer to vapor above the two-phase mixture level. Lastly, prevention of entrainment above the two-phase mixture level is discussed.

Two-Phase Mixture Level

It is recognized that the two-phase mixture level is a key figure of merit for a SBLOCA transient. However, as discussed in Section 13.3 of WCAP-16996-P, [

]^{a,c}

Westinghouse Non-Proprietary Class 3

[

] ^{a,c}

Westinghouse Non-Proprietary Class 3

[

] ^{a,c}

[

] ^{a,c}Vapor Temperature and Steam Cooling

[

] ^{a,c}

[

] ^{a,c}

Entrainment

[

] ^{a,c}

[

] ^{a,c}Conclusion

[

] ^{a,c}References

- 17-1 WCAP-16996-P, "Realistic LOCA Evaluation Methodology Applied to the Full Spectrum of Break Sizes (FULL SPECTRUM LOCA Methodology)," November 2010. (*Westinghouse Proprietary*)
- 17-2 Cheremisinoff, N. P., Ed., *Encyclopedia of Fluid Mechanics, Volume 3, Gas-Liquid Flows*, Gulf Publishing Company, Houston, 1986.

Westinghouse Non-Proprietary Class 3

a,c

Figure 17-1: Pictorial Representation of Vapor Fraction Sharpener



a,c

Figure 17-2: Comparison of Vapor Fraction Resolution to Estimate the Two-Phase Mixture Level

**Figure 17-3a: Vapor Temperature and Vapor Fraction Profile Comparison for run012
when Mixture Level is in a Cell**

**Figure 17-3b: Vapor Temperature and Vapor Fraction Profile Comparison for run059
when Mixture Level is in a Cell**

a,c

Figure 17-4: Entrainment Fraction Profile from run059 of Demonstration Analysis at Various Times Before, During and After PCT Time

a,c

**Figure 17-5a: Entrainment Fraction Profile from run012 of Demonstration Analysis
Before PCT Time**

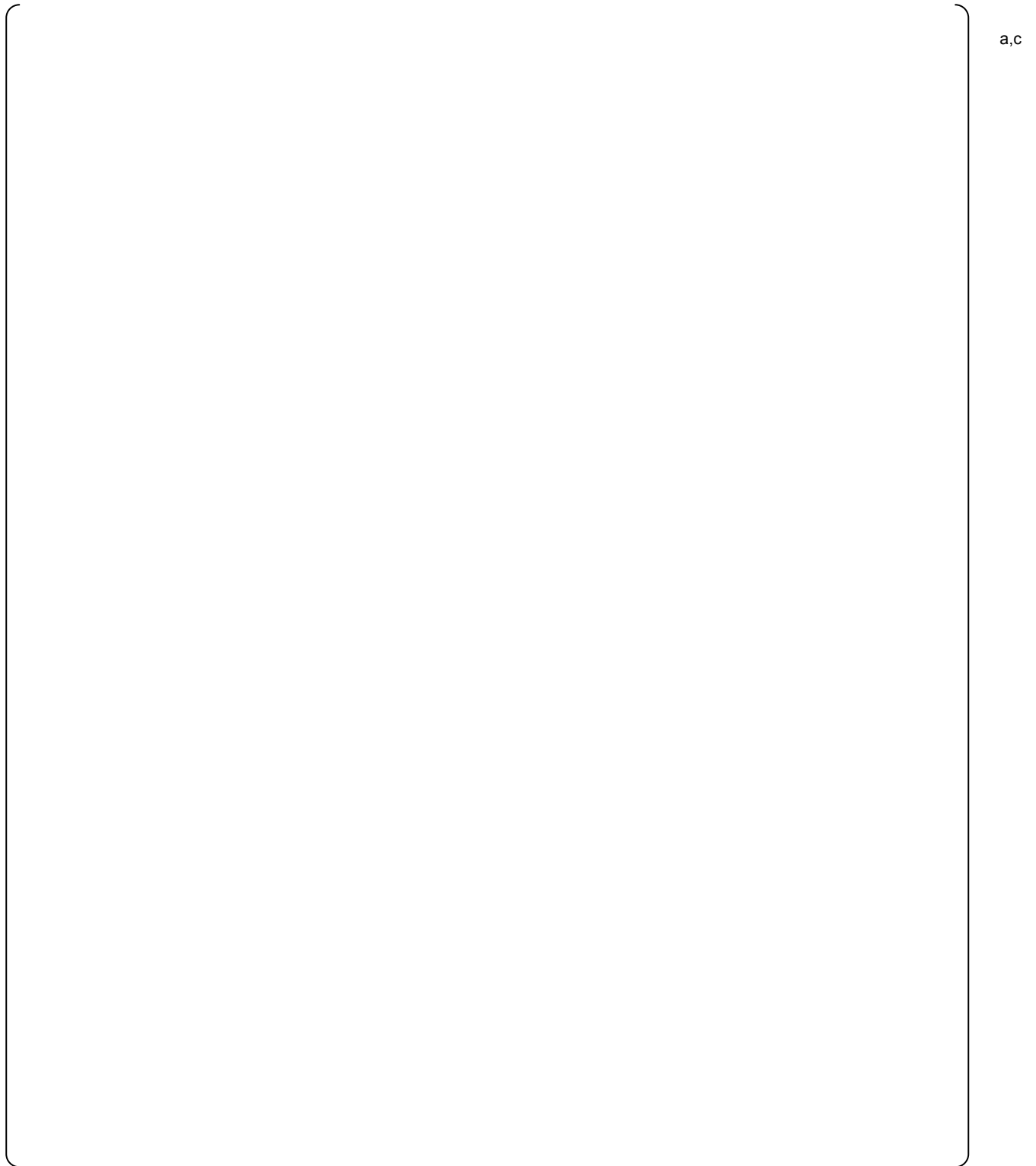
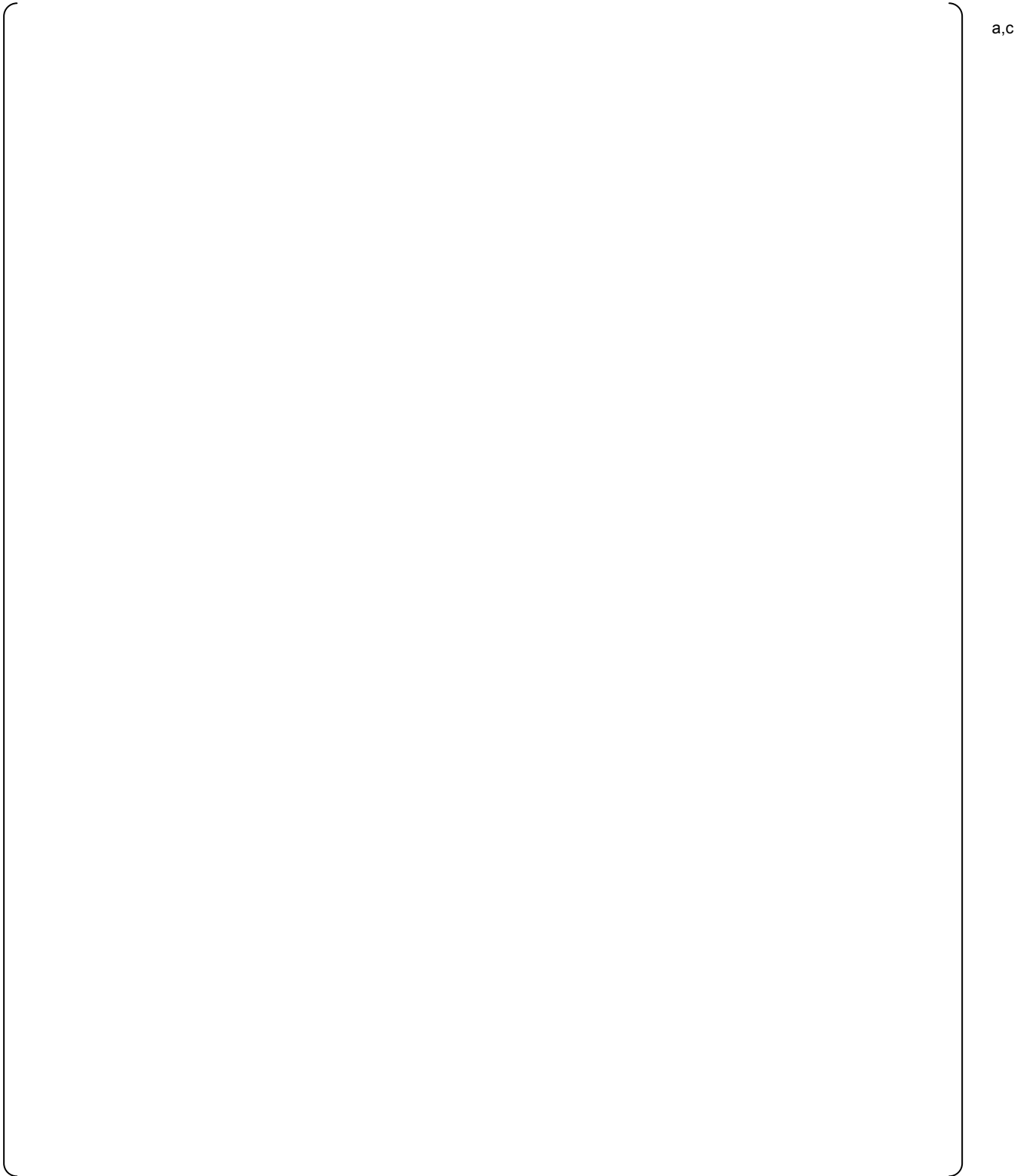


Figure 17-5b: Entrainment Fraction Profile from run012 of Demonstration Analysis Before PCT Time

a,c

**Figure 17-5c: Entrainment Fraction Profile from run012 of Demonstration Analysis
Near PCT Time**

Westinghouse Non-Proprietary Class 3



**Figure 17-5d: Entrainment Fraction Profile from run012 of Demonstration Analysis
After PCT Time**

a,c

Figure 17-6a: Heat Transfer Mode for Conduction Nodes in Hot Assembly Cell 13 for run012

Westinghouse Non-Proprietary Class 3

a,c

Figure 17-6b: Heat Transfer Mode for Conduction Nodes in Hot Assembly Cell 14 for run012

Figure 17-6c: Heat Transfer Mode for Conduction Nodes in Hot Assembly Cell 15 for run012

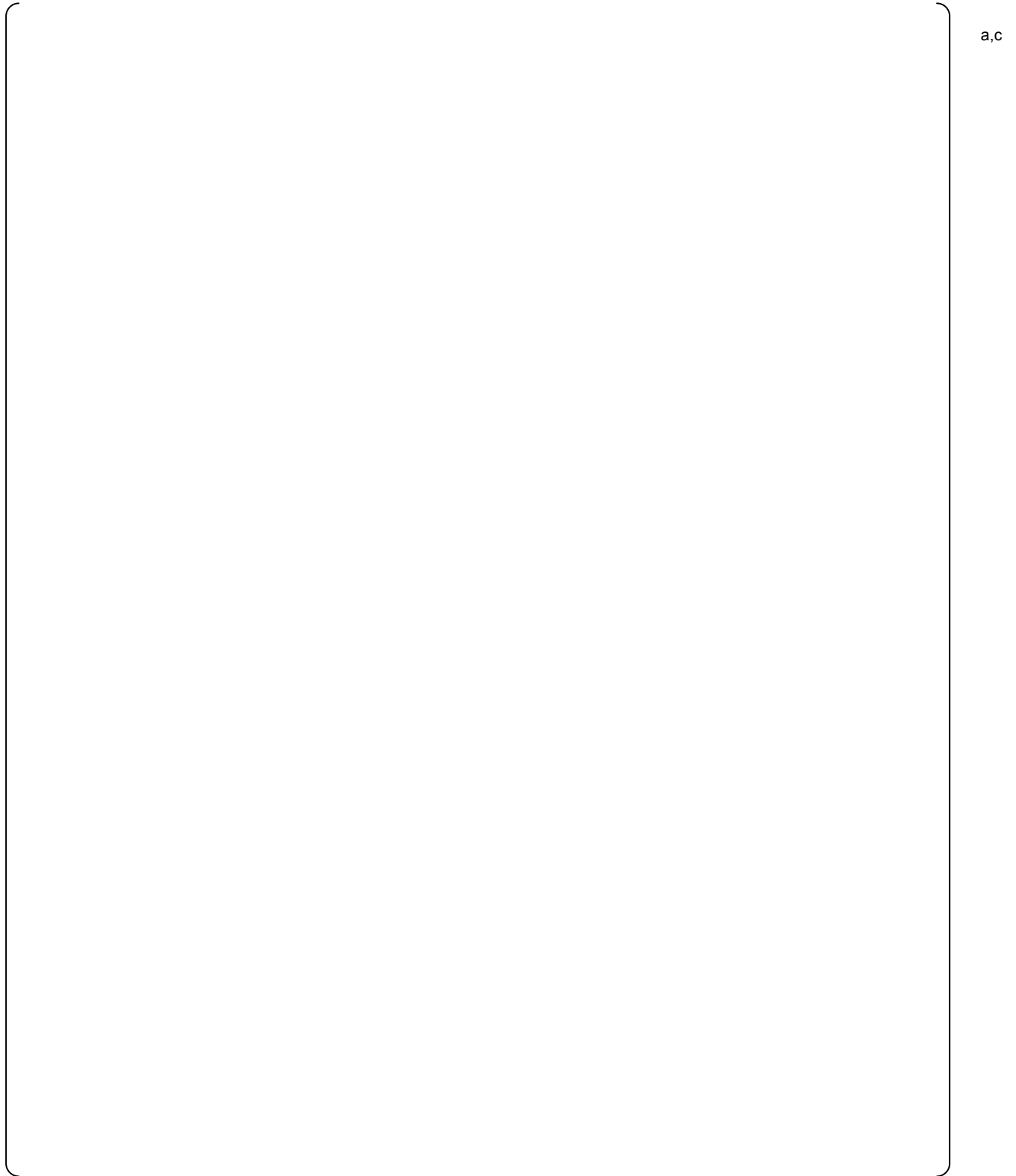


Figure 17-7a: Heat Transfer Mode for Conduction Nodes in Hot Assembly Cell 11 for run059

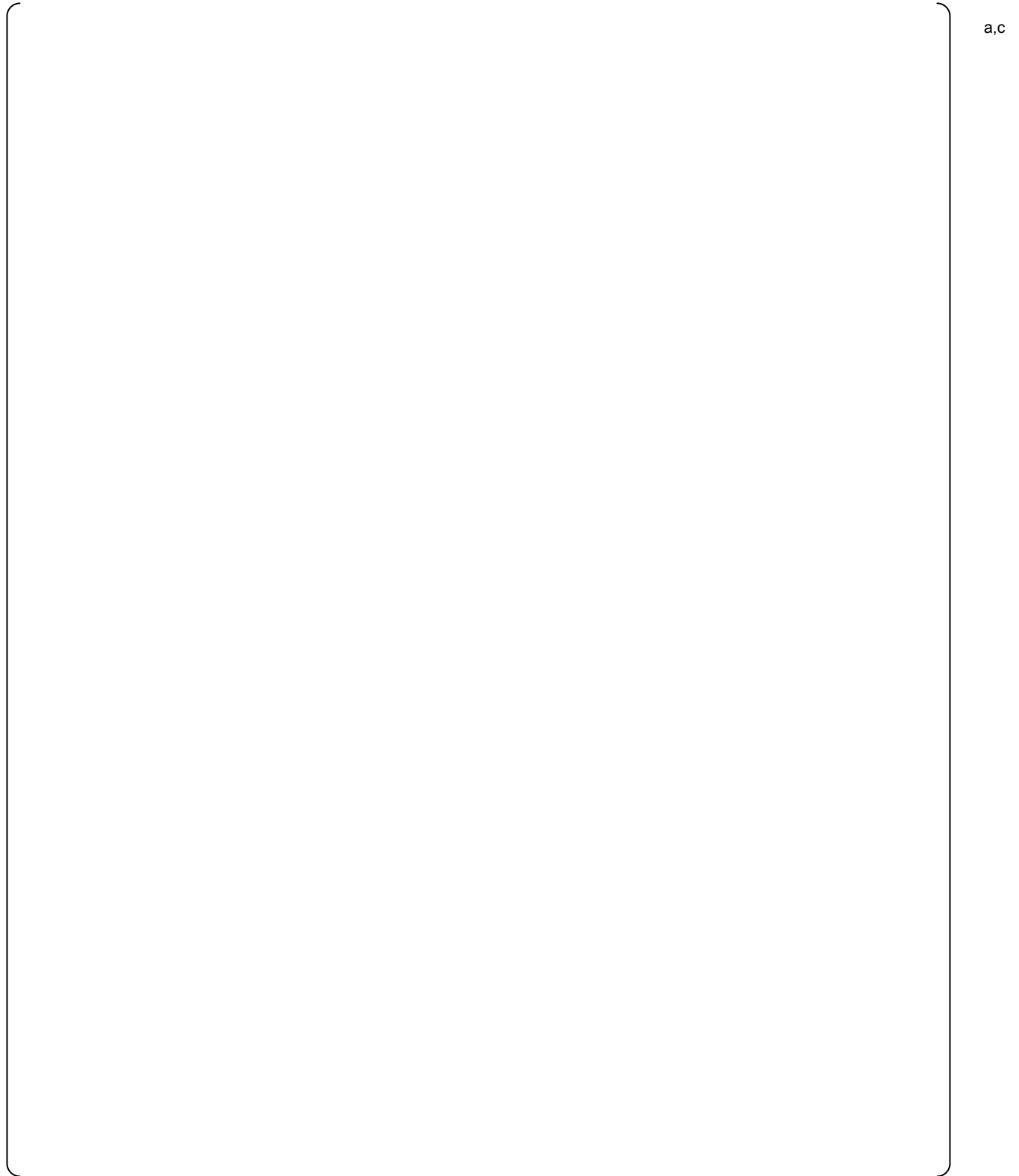


Figure 17-7b: Heat Transfer Mode for Conduction Nodes in Hot Assembly Cell 12 for run059

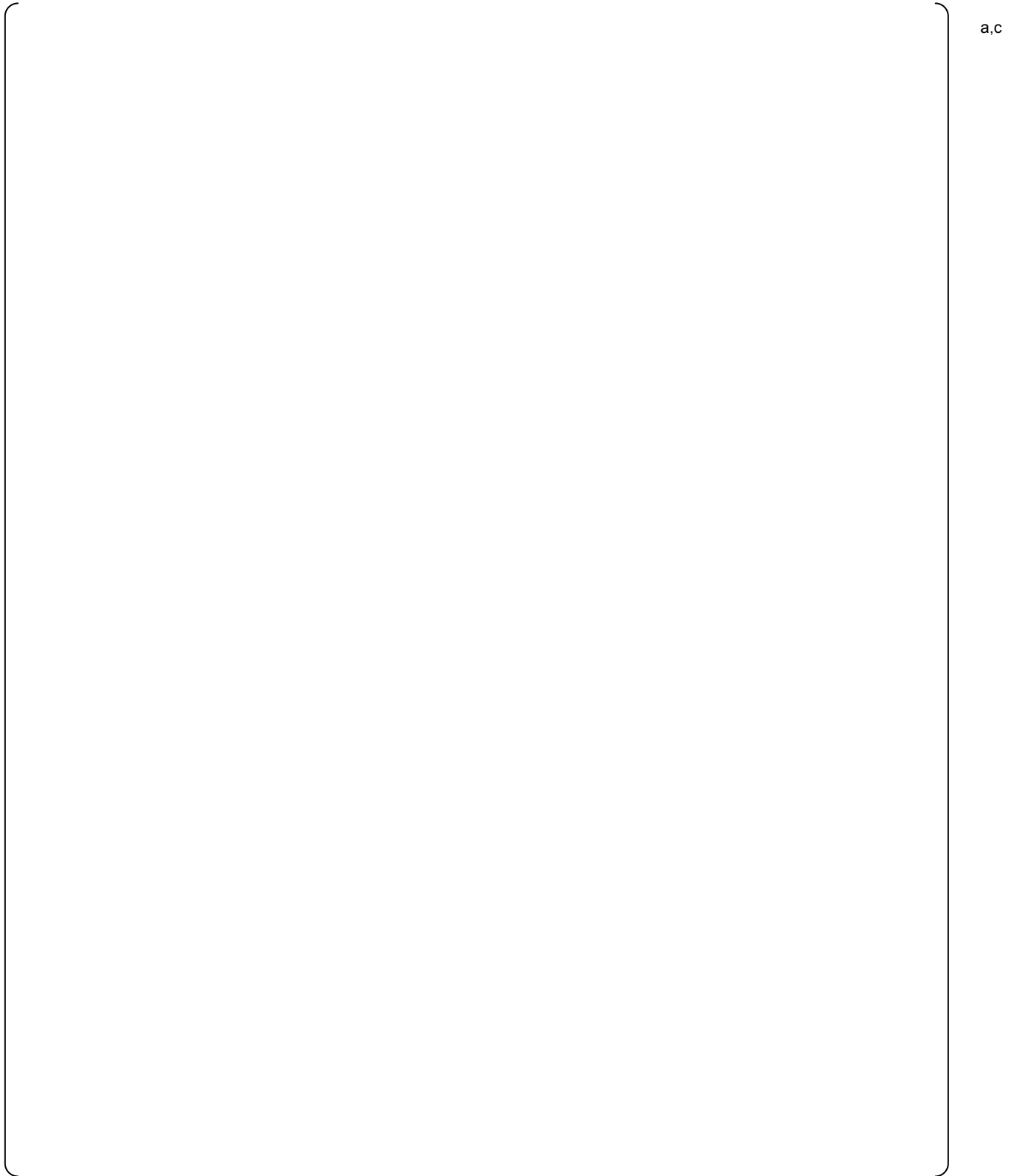


Figure 17-7c: Heat Transfer Mode for Conduction Nodes in Hot Assembly Cell 13 for run059

a,c

Figure 17-7d: Heat Transfer Mode for Conduction Nodes in Hot Assembly Cell 14 for run059

Westinghouse Non-Proprietary Class 3

a,c

Figure 17-7e: Heat Transfer Mode for Conduction Nodes in Hot Assembly Cell 15 for run059

Appendix 17-A: Approximated Two-Phase Mixture Level Plots

a,c

a,c

a,c

a,c

a,c

a.c

[

]

a,c

Question 18: HPSI Curve Basis and Uncertainty

Please explain how the HPSI curve is generated for SBLOCA analyses and show that the uncertainty in pressure and flow is accounted for based on the HPSI surveillance measurements. Show a representative HPSI curve used in the FSLOCA SBLOCA evaluation and explain how it relates to the surveillance head and flow measurement considering and including all uncertainties.

Response:

All Safety Injection (SI) curves utilized in the Full-Spectrum Loss of Coolant Accident (FSLOCA) plant analyses, including the high pressure safety injection (HPSI) curves, are based on the minimum safety injection flow characteristics. [

] ^{a,c}

Curve Development Methodology

In general, the following method is used to define the minimum HPSI pump curve used to generate minimum emergency core cooling system (ECCS) flows for the small break LOCA analyses. The utility and Westinghouse co-operatively define a base pump performance curve which bounds the performance of the operating pumps at the station. The utility and Westinghouse also agree on an amount to reduce the base pump curve in order to develop the analysis pump curve; the amount of the reduction is typically on the order of 5-10% of the HPSI pump design developed head. The analysis minimum flow rates are then based on the analysis pump curve. The utility then takes the analysis pump curve, modifies it to account for uncertainties associated with surveillance test measurements and diesel generator speed uncertainties, and compares the modified curve to the surveillance test results to ensure the pump exceeds what was used in the LOCA analysis. The method of adjusting the analysis pump curve for diesel generator speed is consistent with WCAP-17308-NP (References 1 and 2).

The analysis pump curve is adjusted to account for uncertainties in measurement of pump developed head and pump flow rate, as discussed below.

Pump Developed Head Measurement Uncertainty

The pump developed head is the difference in static pressure head (PH), velocity head (VH), and elevation head (EH) across the pump (Equation 1). Therefore, the uncertainty in ΔH will be the combined uncertainty in the measurement of these values. In general, this measurement uncertainty will be a function of the flow rate and different values will be applied at different points on the pump curve.

$$\Delta H = \frac{144}{\rho} (P_D - P_S) + \frac{V_D^2 - V_S^2}{2g} + (Z_D - Z_S) \quad \text{Equation 1}$$

where:

ρ	=	fluid density, lb/ft ³
g	=	gravitational acceleration, ft/sec ²
P_D	=	pump discharge pressure, psig
P_S	=	pump suction pressure, psig
V_D	=	pump discharge velocity, ft/sec
V_S	=	pump suction velocity, ft/sec
Z_D	=	pump discharge pressure sensor elevation, ft
Z_S	=	pump suction pressure sensor elevation, ft

The total uncertainty in pump head is the square root of sum of the squares (SRSS) of the composite terms, as discussed below.

1. Uncertainty in measured pressure head, ΔPHM
The uncertainty in pressure head is associated with the uncertainty in suction and discharge pressure measurements. Since the suction and discharge pressure measurements are made independently of each other, and there are no error effects that affect both instruments, the overall differential pressure uncertainty is taken as the suction and discharge pressure error combined by SRSS.
2. Uncertainty in measured velocity head, ΔVHM
The uncertainty in velocity head is associated with the uncertainty in pump flow measurement. As conservatism, the velocity head error is found by calculating the velocity head with the discharge and suction velocity terms biased with the velocity error such that the velocity head is maximized. The velocity head error is much smaller than the pressure head uncertainty and can be ignored without significant impact.
3. Uncertainty in measured elevation head, ΔEH
This is the error associated with the elevation of the suction and discharge pressure measurements. There is no error associated with this term.
4. Total uncertainty in measured pump head, ΔHM
The total uncertainty in pump head is taken as the SRSS of the uncertainty in pressure head measurement and velocity head measurement (Equation 2).

$$\Delta HM = \sqrt{(\Delta PHM)^2 + (\Delta VHM)^2} \quad \text{Equation 2}$$

where:

ΔHM	=	measurement uncertainty in pump head, ft
ΔPHM	=	measurement uncertainty in pump pressure head, ft
ΔVHM	=	measurement uncertainty in pump velocity head, ft

Pump Flow Rate Measurement Uncertainty

The pump flow rate is typically measured by summing the measured flow rates of one or more paths; for example, the total pump flow rate may be the combination of the ECCS header flow plus the reactor coolant pump (RCP) seal injection flow rate. Since the flow measurements are independent, the overall flow measurement is the SRSS of the uncertainties of the individual measurements (Equation 3).

$$\Delta Q_{MT} = \sqrt{(\Delta Q_{M1})^2 + (\Delta Q_{M2})^2 + \dots + (\Delta Q_{Mi})^2} \quad \text{Equation 3}$$

where:

ΔQ_{MT}	=	measurement uncertainty of total pump flow rate, gpm
ΔQ_{M1}	=	measurement uncertainty of flow rate in path 1, gpm
ΔQ_{M2}	=	measurement uncertainty of flow rate in path 2, gpm
ΔQ_{Mi}	=	measurement uncertainty of flow rate in path i, gpm

Determination of Pump Variation Due to Flow Measurement Variation

The pump developed head varies with pump flow rate. Therefore, there is an uncertainty in pump developed head associated with the uncertainty in measured flow rate. The rate of change of pump ΔH with respect to flow is a function of the flow rate. The uncertainty in pump ΔH due to flow measurement uncertainty is calculated by Equation 4. Note that the absolute value of $\frac{d(\Delta H)}{dQ}$ is used in the equation.

$$\Delta H_Q = \left| \frac{d(\Delta H)}{dQ} \right| \Delta Q_{MT} \quad \text{Equation 4}$$

where:

ΔH_Q	=	uncertainty in pump developed head due to flow uncertainty, ft
$\frac{d(\Delta H)}{dQ}$	=	rate of change of pump developed head with flow, ft/gpm

Uncertainty in Pump Head due to Uncertainty in Diesel Generator Speed

The uncertainty in pump head due to uncertainty in diesel generator speed (ΔH_S) is calculated using the methodology defined in WCAP-17308-NP.

Overall Pump Head Uncertainty

The overall pump head uncertainty is the SRSS of the uncertainty in pump developed head measurement, the uncertainty in pump developed head due to uncertainty in flow measurement, and the uncertainty in pump head due to the uncertainty in diesel generator speed (Equation 5).

$$\Delta HT = \sqrt{(\Delta HM)^2 + (\Delta HQ)^2 + (\Delta HS)^2} \quad \text{Equation 5}$$

The surveillance criteria ensures/adjusts the analysis pump curve to account for the overall pump head uncertainty.

Example FSLOCA HPSI Curves

Example HPSI injection curves, calculated by utilizing the aforementioned methodology, are provided in the following figures. Figure 1 presents the HHSI flow for []^{a,c} whereas

Figure 2 presents the HHSI flows for []^{a,c}. The methodology utilized to generate these curves bounds the operation of the pumps at the station.

Westinghouse Non-Proprietary Class 3

a,c

References

1. WCAP-17308-NP, Rev. 0 (Non-Proprietary) "Treatment of Diesel Generator (DG) Technical Specification Frequency and Voltage Tolerances," April 2012.
2. OG-12-162 "PWR Owners Group Submittal of WCAP-17308-NP, Revision 0, Treatment of Diesel Generator (DG) Technical Specification Frequency and Voltage Tolerances," May 1, 2012.

Question 19: SBLOCA Axial Power Shape

Please provide the axial power shapes in the FSLOCA SBLOCA evaluations and explain how they are generated and sampled in the evaluation. In addition, please show the limiting axial power shape for the limiting SBLOCA size.

Response:

1.0 SBLOCA Power Distributions

The axial power shapes analyzed in the V. C. Summer example plant analysis for the small break region are provided in Figure RAI-19-A. In the example analysis for the small break region, only three transients exhibited core uncover and a corresponding cladding temperature heatup. The power shapes associated with these cases are presented as bold, dashed lines in Figure RAI-19-A.

2.0 Process to Generate Power Distributions

The PSHAPE code uses a []^{a,c} to calculate the power shapes used within the FULL SPECTRUM™ LOCA (FSLOCA) Evaluation Model (EM). The following sections provide a description of the []^{a,c} and the process used by PSHAPE to calculate a power shape.

2.1 []^{a,c}

[

] ^{a,c}

[

]^{a,c}

[

]^{a,c}

[

]^{a,c}

[

]^{a,c}

[

]^{a,c}

[

]^{a,c}

[

]^{a,c}

[

]^{a,c}

[

]^{a,c}

[

] ^{a,c}**Step 3a: Shape Accepted**

If shape passes all of the above checks, it is judged to be an acceptable shape.

Step 3b: Shape Rejected

If the shape was rejected for any of the above checks, [

] ^{a,c}

3.0 Comparison of Sampled to Predicted Power Distributions for V. C. Summer

The following illustration is provided based on V. C. Summer to compare the analyzed axial power distributions compared to those predicted by the core design.

Maximum baseload (without uncertainty) axial power distributions were generated at beginning-of-cycle (BOC), near BOC, middle-of-cycle (MOC), and end-of-cycle (EOC) burnups. These distributions are compared to the sampled distributions in Figure RAI-19-B; it can be seen that [

] ^{a,c}

Representative transient shapes were then generated following the Westinghouse relaxed axial offset control (RAOC) methodology which envelope any transients expected during reactor operation. These transient distributions were then increased to include the maximum uncertainty, and a subset of these transient shapes based on the MOC cases are compared against the analyzed power distributions in Figures RAI-19-C (initial negative offset) and RAI-19-D (initial positive offset). It can be seen that [

] ^{a,c}

4.0 Conclusions

The as-submitted sampling approach for the axial power distributions assumes that [

] ^{a,c}

a,c

Figure RAI-19-A **Axial Power Distributions for the V. C. Summer Small Break LOCA
Example Pressurized Water Reactor (PWR) Analysis**

a,c

Figure RAI-19-B **Range of Axial Power Distributions for the V. C. Summer Small Break
LOCA Example PWR Analysis Compared to Steady-State Distributions**

a,c

Figure RAI-19-C

**Comparison of MOC Axial Shapes with Maximum Uncertainty for
Transient Event with Initial Negative Offset to Analyzed Axial Power
Distribution Range for V. C. Summer**

a,c

Figure RAI-19-D

**Comparison of MOC Axial Shapes with Maximum Uncertainty for
Transient Event with Initial Positive Offset to Analyzed Axial Power
Distribution Range for V. C. Summer**

a,c

Figure RAI-19-E **F_Q Histogram for Full Power points of Load Follow Maneuver for sample plant included in the Code Qualification Document (CQD); Solid Line Indicates Uniform Range Assumed**



Figure RAI-19-F **F_Q Histogram for All Power points of Load Follow Maneuver for sample plant included in the CQD**

a,c

Figure RAI-19-G**F_Q Histogram for Full Power points of Load Follow Maneuver for 6 combined CAOC plants; Solid Line Indicates Uniform Range Assumed**

a,c

Figure RAI-19-H **F_Q Histogram for All Power points of Load Follow Maneuver for 6 combined CAOC plants**

a,c

Figure RAI-19-I

F_Q Histogram (3-Loop RAOC Plant) for full power points of all Condition I maneuvers (only transient conditions included). Solid Line indicates the uniform range assumed for corresponding Best-Estimate LOCA (BELOCA) Analysis

Figure RAI-19-J

F_Q Histogram (3-Loop CAOC Plant) for full power points of all Condition I maneuvers (only transient conditions included). Solid Line indicates the uniform range assumed for corresponding BELOCA Analysis

Figure RAI-19-K

F_Q Histogram (4-Loop CAOC Plant) for full power points of all Condition I maneuvers (only transient conditions included). Solid Line indicates the uniform range assumed for corresponding BELOCA Analysis

Figure RAI-19-L **F_Q Histogram (4-Loop RAOC Plant) for full power points of all Condition I maneuvers (only transient conditions included). Solid Line indicates the uniform range assumed for corresponding BELOCA Analysis**

**WCAP-16996-P, "Realistic LOCA Evaluation Methodology Applied to the Full Spectrum of Break Sizes
(FULL SPECTRUM LOCA Methodology)"
Request for Additional Information – (Non-Proprietary)
RAIs 9 and 12**

June 2013

Westinghouse Electric Company LLC
1000 Westinghouse Drive
Cranberry Township, PA 16066

©2013 Westinghouse Electric Company LLC
All Rights Reserved

Question 9: Worst SBLOCA

The WCAP-16996-P/WCAP-16996-NP, Volumes I, II, and III, Revision 0, Section 29.2.3 “Break Type, Split Break Area and Break Flow Model Uncertainty Methodology,” proposes a position for the treatment of the break type and size [

]^{a,c} Section 29.2.3 claims that “this approach provides an adequate coverage of all possible LOCA scenarios” and Section 30.1 “Statistical Methodology Roadmap” asserts this is done [

]^{a,c} According to Section 30.5 “Overview of Full Spectrum LOCA Statistical Procedure (ASTRUM-FS)”, when generating a representative sample of the LOCA scenarios population, [

]^{a,c} WCAP-16996-P/WCAP-16996-NP, Volumes I, II and III, Revision 0 Section 31.3, “Analysis of Results for Region I,” presents a demonstration analysis of the FSLOCA™ methodology for a selected three-loop Westinghouse PWR. For Region I, the break area is sampled between [

]^{a,c}

To assess the appropriateness of the proposed position in the FSLOCA methodology regarding SBLOCA resolution and treating the worst break size in Region I, please present the results from an additional analysis for the demonstration three-loop Westinghouse plant (V. C. Summer (CGE)) examined in Section 31.3. In this analysis, please assume that the examined breaks range from 2.0-inch to 6.0-inch equivalent diameter (0.022 ft² to 0.196 ft² or 0.5 percent to 4.8 percent break area), [

]^{a,c} Please present the updated Figures 31.3-4 to 31.3-7 and Tables 31.3-1a and 31.3 1b to illustrate the obtained results. If this approach does not guarantee adequate resolution of the worst break, please consider an alternative method as discussed in the following paragraph. Please be aware that for some plants the PCT can

FULL SPECTRUM™ and **FSLOCA™** are trademarks of Westinghouse Electric Company LLC, its affiliates and/or its subsidiaries in the United States of America and may be registered in other countries throughout the world. All rights reserved. Unauthorized use is strictly prohibited. Other names may be trademarks of their respective owners.

increase by a few hundred degrees Fahrenheit when the break size changes from 0.05 ft² to 0.06 ft². Thus, it has been shown for some plants that the PCT can increase by approximately 100 °F for a small break area increase of 0.005 ft² so that the 0.055 ft² break PCT is higher than both the 0.05 ft² and 0.06 ft² break. This limiting break is characterized by an RCS pressure that just depressurizes to a pressure within several psi of the safety injection tank (SIT) actuation pressure. Because such behavior characterizes most plants, it is necessary to resolve the size of the worst break controlled entirely by the HPSI injection only. While this low range of small break sizes is most pronounced under Appendix K analysis assumptions, it still needs to be evaluated in the best estimate space since future increased power levels and linear heat generation limits will also produce such a temperature spike for such a small break window. The included figure illustrates the described PCT behavior. In addition, sometimes this worst break size can be just slightly larger than that at which SIT injection is prevented. In this case, a small amount of injection after a deeper core uncover can often lead to the worst break because SIT injection quickly terminates with only a small increase in core level as the RCS pressure can quickly increase with the small level change.

To assess the appropriateness of the proposed position in the FSLOCA methodology regarding SBLOCA resolution and treating the worst break size in Region I, please present the results from an additional analysis for the three-loop Westinghouse plant examined in Section 31.3. In this analysis, please assume that Region I breaks range from 2.0-inch to 6.0-inch equivalent diameter (0.022 ft² to 0.196 ft² or 0.5 percent to 4.8 percent break area) and vary the break in increments of 0.2 inch. Please perform the analysis assuming nominal values for all remaining sampled parameters including the break discharge coefficients. In addition, show the effect of key parameter variations from the nominal values over this detailed range and present the updated Figures 31.3-4 to 31.3-7 and Tables 31.3-1a and 31.3-1b using the obtained results.

In both approaches the Region I [

]^{a,c}

Please also show the spectrum evaluation for the Beaver Valley Unit 1 three-loop PWR plant considered in WCAP-16996-P/WCAP-16996-NP, Volumes I, II, and III, Revision 0, Section 26.3 "Beaver Valley Unit 1 Nuclear Power Plant" and compare the break spectrum results with the Appendix K more limiting analysis.

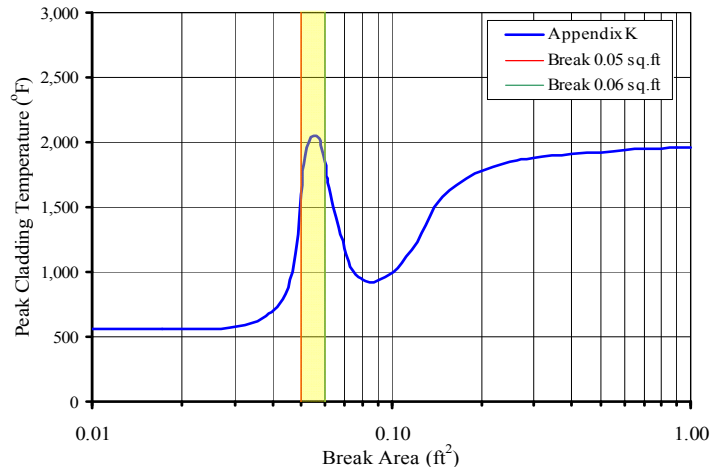


Figure: Illustration of PCT Response to Break Size Variation for Appendix K SBLOCA Analysis

Response:

The sampling of the break area as a random parameter (break spectrum) for the purpose of a best-estimate loss-of-coolant accident (LOCA) analyses is currently employed in licensed methodologies in the industry and has a regulatory precedence. For example, the break type (double-ended guillotine of the cold leg (DEGCL) vs. Split) is sampled in the ASTRUM Evaluation Model (EM) (WCAP-16009-P-A [1]), which covers the large break LOCA spectrum, and for the Split breaks, the break area is also sampled. In other words, the break area is assumed to be a random parameter in the uncertainty analysis for the purpose of demonstrating with “high probability” that the 10 CFR 50.46 limits are not exceeded. As stated in Section 3.3.1.1 of the ASTRUM EM Safety Evaluation Report (SER), the staff reviewed the break sampling approach and found it acceptable.

Region II of the **FSLOCA**[™] EM essentially follows the same approach considered in the ASTRUM EM with the only difference being the lower bound of the break spectrum is now set to []^{a,c}, instead of the generic value of 1 ft².

For Region I, a similar approach to the Split breaks of Region II was considered. The intent is to develop a probabilistic statement with respect to peak cladding temperature (PCT) and maximum local oxidation (MLO) for the possible break sizes within that region of the spectrum. The rationale is that the break size at the onset of a LOCA event is unknown, and therefore a stochastic variable considered in the analysis. The probabilistic statement is correct, as long as the code is shown to be capable of predicting all possible scenarios adequately within the spectrum (Region I in this case).

The second part of the RAI 9 focuses on this “code capability” aspect, recognizing that the limiting break sizes could be confined within a small sub-region of Region I. An equivalent in mechanics (vibrations) is the small resonance region within the spectrum of possible forcing functions.

The approach in this response is therefore the following:

- 1) Restate the reasoning of sampling break size as a random variable, which as stated above has regulatory precedence
- 2) Demonstrate code capability of predicting limiting scenarios within the spectrum of break sizes.

Given the complexity of the response and recognizing that the current focus of the response is limited to the second item above, Westinghouse discussed this topic with the Staff on December 3 and 4, 2012 and February 21 and 22, 2013. The response here provides an extension to the information presented at those meetings.

As stated previously, sampling break size has regulatory precedence, with the break size being a legitimate random variable during a LOCA event. The limiting scenario is predicted to the extent of its probability weight within the spectrum of possible break sizes, and the sampling methodology is selected to [

]^{a,c}

[

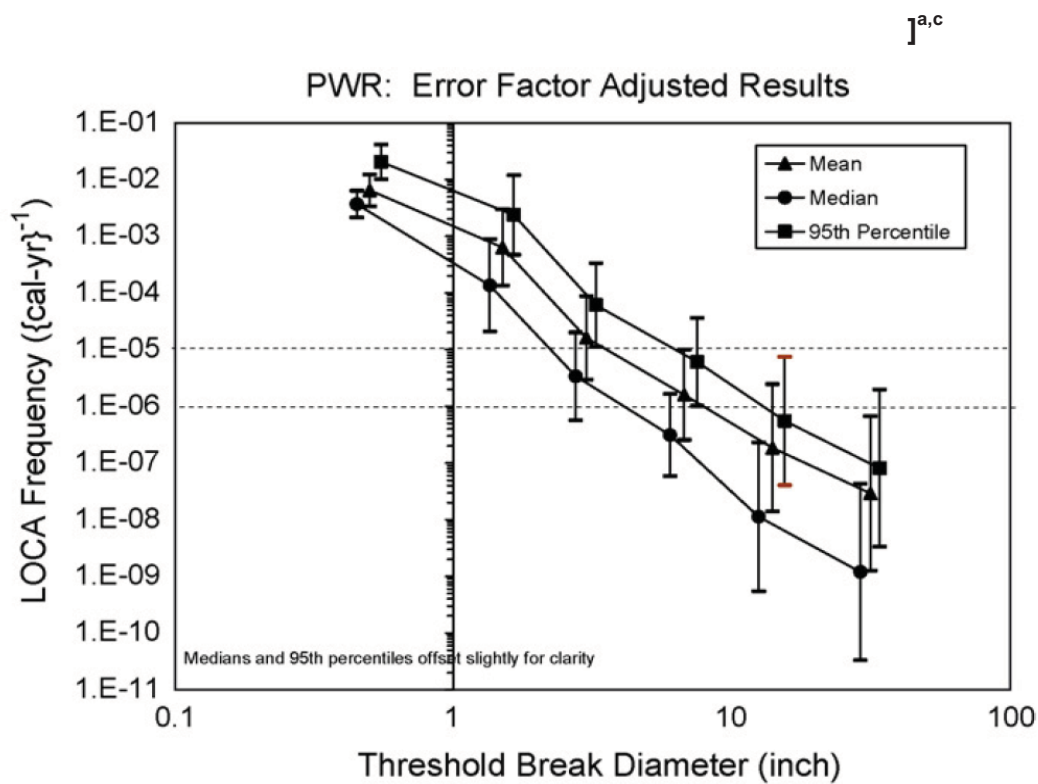


Figure A: LOCA Frequency as a Function of Break Diameter (Figure 7.37 of NUREG-1829 V1 [2])

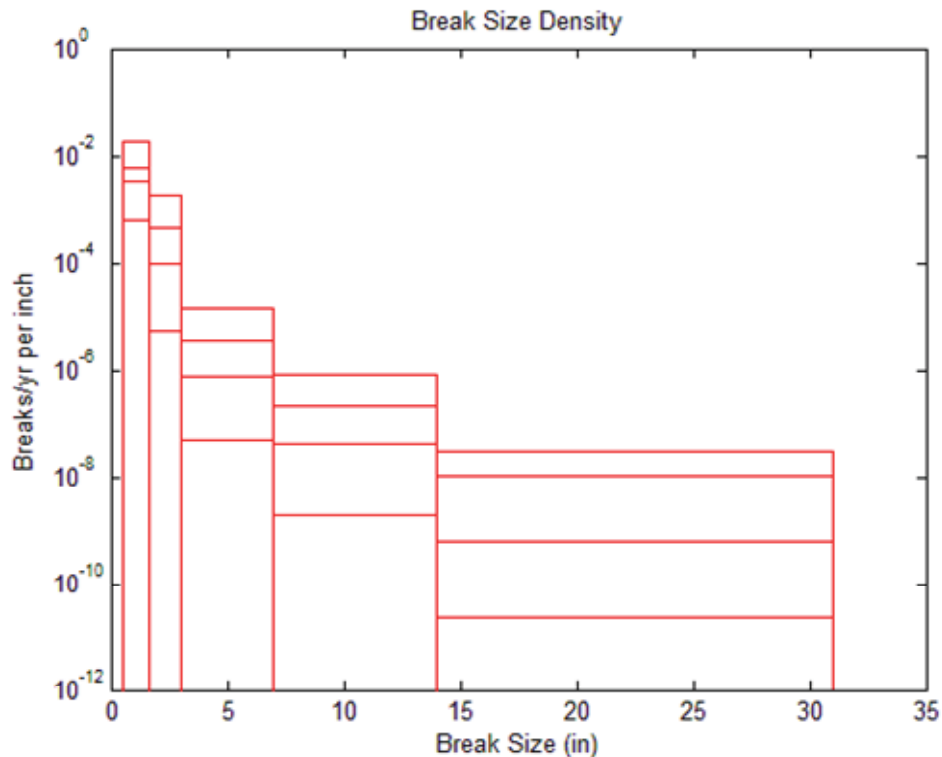


Figure B: LOCA Frequency as a Function of Break Diameter (taken from Los Alamos National Lab presentation, May 9, 2012 ACRS transcripts [3])

To demonstrate code capability of predicting limiting scenarios within the spectrum of break sizes, the following studies were performed using a different 3-loop plant from that used for the demonstration analysis:

- A. A deterministic break study from []^{a,c} to []^{a,c} in increments of []^{a,c} with as-coded models (i.e., no uncertainty or bias applied)
- B. Same deterministic break study performed in A, but with the core interfacial drag uncertainty parameters (YDRAG) set to []^{a,c}, respectively, and the high pressure single-phase vapor heat transfer coefficient multiplier (SPV2_MULT) set to []^{a,c}; both are used to force a more severe core uncover. This study will demonstrate the code's capability to predict the impact of decreasing the key parameters which control level swell and heat transfer to vapor, respectively.
- C. Same deterministic break study performed in B, but forcing loop seal clearing of the broken loop by deepening the loop seals of the two intact loops. This study will show the impact of "controlling" the loop seal clearing behavior by forcing the clearing of the broken loop.
- D. Same deterministic break study performed in B, but forcing the multiplier on the criterion for transition to stratified flow to be at its lowest allowed sampled values (Study D-1) or the highest allowed sampled value (Study D-2).

The following provides a discussion based on the calculation results.

Study A: Base Case

Figure 1 presents the PCT and number of loop seals venting vapor at the time of PCT versus equivalent break diameter. The following observations are made: [

] ^{a,c}

Study B: Biased Case

Figure 2 presents the PCT and number of loop seals venting vapor at the time of PCT versus equivalent break diameter. The following observations are made: [

] ^{a,c}

Study C: Biased Case Plus Force Broken Loop, Loop Seal Clearing

Figure 3 presents the PCT and number of loop seals venting vapor at the time of PCT versus equivalent break diameter. As seen from the figure, [

] ^{a,c}

Study D-1: Biased Case Plus HS_SLUG=[]^{a,c}

Figure 4 presents the PCT and number of loop seals venting vapor at the time of PCT versus equivalent break diameter. As seen from the figure, [

]^{a,c}

Study D-2: Biased Case Plus HS_SLUG=[]^{a,c}

Figure 5 presents the peak cladding temperature versus equivalent break diameter. As seen from the figure, the results are very similar to Study B, which suggests that [

]^{a,c}

Based on the observations, further investigation and discussion on the effects of loop seal clearing behavior was performed. The [

]^{a,c}

The following is provided in response to the request of comparing the break spectrum results with an Appendix K type analysis.

Comparison with Appendix K Analysis

The results from an Appendix K analysis are compared to the results of Study B. The comparison is performed to determine if similar trends in break size are observed as in the Appendix K method. This is shown in Figure 6. In the break sizes of interest, Study B does follow a similar trend as the Appendix K method, and due to the limiting nature of the Appendix K analysis, the PCTs of Study B are much lower.

Conclusion

With the **FSLOCA** evaluation method, [

] ^{a,c}

References

- 1) WCAP-16009-P-A, "Realistic Large-Break LOCA Evaluation Methodology Using the Automated Statistical Treatment Of Uncertainty Method (ASTRUM)," January 2005.
- 2) NUREG-1829, Volume 1, "Estimating Loss-of-Coolant Accident (LOCA) Frequencies Through the Elicitation Process: Main Report," April 2008.
- 3) Presentation by Bruce Letellier of Los Alamos National Laboratory, "South Texas Project, Containment Accident Stochastic Analysis – CASA Grande –,” attached to transcripts to the May 9, 2012 ACRS Thermal Hydraulic Phenomena Subcommittee Meeting (*ADAMS Accession number ML121520429*).

a,c

Figure 1: Peak Cladding Temperature vs. Break Diameter for Study A (Base Case)

a,c

Figure 2: Peak Cladding Temperature vs. Break Diameter for Study B (Biased Case)

a,c

Figure 3: Peak Cladding Temperature vs. Break Diameter for Study C (Loop Seal Case)

a,c

Figure 4: Peak Cladding Temperature vs. Break Diameter for Study D-1 (HS_SLUG=[]^{a,c})

a,c

Figure 5: Peak Cladding Temperature vs. Break Diameter for Study D-2 (HS_SLUG=[]^{a,c})

a,c

Figure 6: Peak Cladding Temperature vs. Break Diameter for Study B and Appendix K Analysis

a,c

Figure 7: Peak Cladding Temperature and Collapsed Liquid Level of the Hot Assembly vs. Time, Study B []^{a,c} Break

a,c

Figure 8: Peak Cladding Temperature and RCP Speed vs. Time, Study B []^{a,c} Break

a,c

Figure 9: Comparison of Study B and Study C Peak Cladding Temperature vs. Time, []^{a,c} Break

a,c

Figure 10: Comparison of Study B and Study C Vessel Mass vs. Time, []^{a,c} Break

a,c

Figure 11: Comparison of Study B and Study C RCS Pressure vs. Time, []^{a,c} Break

a,c

Figure 12: Comparison of Study B and Study C Total Vapor Flow through Loop Seals vs. Time, []^{a,c} Break

a,c

Figure 13: Comparison of Study B and Study C Vapor Velocity through Individual Loop Seals vs. Time, []^{a,c} Break

a,c

Figure 14: Comparison of Study B and Study C Void Fraction in Horizontal Section of Individual Loop Seals vs. Time, []^{a,c} Break

Question 12: Worst Break Sampling

The small break spectrum for many PWRs will show the limiting small break to be in the range from 0.05 ft² to 0.2 ft² in the cold leg (3.03 inch to 6.06 inch). Depending on the axial power distribution, SIT pressure, core power (decay heat), and HPSI injection flow capacity, PCTs can increase significantly within a small window of break sizes of plus or minus 0.01 ft² to 0.005 ft². In this break range, the worst break size is the largest small break that does not actuate SITs as the RCS depressurizes to values just slightly above the SIT actuation pressure (within a couple psi). Sampling the break spectrum in Region-I as it is described in WCAP-16996-P/WCAP-16996-NP, Volumes I, II, and III, Revision 0, Section 29.2.3 "Break Type, Split Break Area and Break Flow Model Uncertainty Methodology" will not adequately resolve this detail or identify this worst break. Break sizes of plus or minus 0.005 ft² in the above range about this break size, which is often thought to be limiting but identified with too coarse a spectrum of analyzed breaks, can show an increase of 100°F - 200°F when the worst break is found. The concern is that the proposed approach for Region I is not adequate in identifying this limiting break. [

]^{a,c} Either much more sampling is required or this break should be first found deterministically assuming nominal initial conditions and then statistics is applied appropriately for a spectrum of sizes about this peak to assure the limiting break is found. Since power level is a key ingredient driving the PCT, use of the current power levels may not show this distinct peak or narrow spike behavior. As such, please find this break size for the Beaver Valley demonstration plant and increase the thermal power by 15 percent – 20 percent to show future expected behavior for possible power uprates using the FSLOCA methodology. This analysis should allow only one loop seal to clear if the break size is less than 5 inches. For this analysis, please use a decay heat multiplier with an upper 2- σ multiplier. For the purpose of finding this limiting break size, the limiting conditions for PLHGR, core power (decay heat nominal plus 2- σ), limiting top skewed shape, minimum HPSI head flow curve, one loop seal cleared, no hot leg nozzle gap and core barrel leakage paths open, and closed upper head venting should be assumed. This question is closely related to Question 9.

Response:

See response to Question 9. In addition, [

]^{a,c}

**WCAP-16996-P, "Realistic LOCA Evaluation Methodology Applied to the Full Spectrum of Break Sizes
(FULL SPECTRUM LOCA Methodology)"
Requests for Additional Information – Second Set (Non-Proprietary)**

May 2013

Westinghouse Electric Company LLC
1000 Westinghouse Drive
Cranberry Township, PA 16066

©2013 Westinghouse Electric Company LLC
All Rights Reserved

Question 20: ^{235}U , ^{238}U , and ^{239}Pu Decay Heat Uncertainty Fits to ANS 5.1-1979

Decay heat is an important factor in the analysis of postulated LOCAs and ECCS performance evaluation and an accurate assessment of both the decay heat and its uncertainty is necessary. WCAP-16996-P/WCAP-16996-NP, Volumes I, II and III, Revision 0, Section 9.2, "Decay Heat Source," explains that WCOBRA/TRAC-TF2 solves the time-dependent decay activity differential equation accounting for ^{235}U thermal, ^{239}Pu thermal, and ^{238}U fast fissions. The energy yield constants are weighted by the appropriate fission rate fractions as a function of initial enrichment and burnup within WCOBRA/TRAC-TF2. Section 9.2 states that the WCOBRA/TRAC-TF2 decay heat model was benchmarked against the ANSI/ANS 5.1-1979 Standard. Results of decay heat for ^{235}U computed by WCOBRA/TRAC-TF2 and using the American Nuclear Standards Institute (ANSI)/ANS 5.1-1979 Standard are presented in Table 9-2, which shows that the difference between the values calculated from both approaches is negligible for decay time up to 10^3 s. The section also states that similar comparisons exist for ^{239}Pu and ^{238}U .

The decay heat uncertainty modeling in WCOBRA/TRAC-TF2 is discussed in WCAP-16996-P/WCAP-16996-NP, Volumes I, II and III, Revision 0, Section 9.7, "Decay Heat Uncertainty Evaluation," which explains that WCOBRA/TRAC-TF2 models decay heat uncertainty through the use of pseudo-isotope energy yield augmentation factors generated using a least squares fit to the uncertainty data provided in ANSI/ANS 5.1-1979. The section claims that the results, as provided in Table 9-14, "provide a conservative representation of the standard's quoted uncertainties." Although Table 9-14 presents the computed factors, a description of the uncertainty modeling equations and their implementation in WCOBRA/TRAC-TF2 is not provided. Please provide the equations used in WCOBRA/TRAC-TF2 to compute the decay heat uncertainties for the considered isotopes and explain how the individual uncertainties are used in predicting the overall decay heat uncertainty in plant analyses.

Response:

Equation 9-2 of WCAP-16996-P Revision 0 is solved by WCOBRA/TRAC-TF2 to determine the time dependent decay heat power for a given pseudo-isotope. This equation is as follows:

$$\frac{d}{dt}DH^i = \alpha_i(\Sigma_F\phi) - \Gamma_iDH^i \quad (1)$$

In WCOBRA/TRAC-TF2, the decay heat uncertainty is modeled by [

]^{a,c} The total decay heat uncertainty is dependent upon the cumulative uncertainty contributions due to each of the pseudo-nuclides. Their relative contributions will

change with burnup and, to a lesser extent, enrichment since the fission fractions of the fissile isotopes (the w_n factors in equation 9-3 of Section 9.2) will change as function of burnup and enrichment.

ANSI/ANS 5.1-1979 requires accounting for the uncertainty in the energy per fission. This uncertainty, which has been determined in WCOBRA/TRAC-TF2 using uncertainty data from ENDF/B-V, is convoluted with the decay heat uncertainty. The uncertainty in the prompt energy per fission is a function of the channel burnup and enrichment since the fission fractions for each of the fissionable isotopes is a function of these variables. Table RAI-20-1 below provides the fitting data for κ and the one sigma uncertainty in κ , σ_κ . Both κ and σ_κ are fitted as functions of burnup, enrichment, and H/U ratio.

Section 9.7 of WCAP-16996-P Revision 0 explains that the A_i terms in equation (2) were determined through a least squares fit of the uncertainty data in ANSI/ANS 5.1-1979. Effectively, these A_i terms reproduce, to a high degree of accuracy, the ANSI/ANS 5.1-1979 decay power with 2σ uncertainty over the range of cooling times given in Tables 4-6 of ANSI/ANS 5.1-1979 for the three fissionable isotopes.

From ANSI/ANS 5.1-1979, the decay heat power is given by the following for a single fissionable isotope:

$$F(t_j, T) = \sum_{i=1}^{23} \frac{\alpha_i}{\Gamma_i} e^{-\Gamma_i t_j} (1 - e^{-\Gamma_i T}) \quad (3)$$

where the summation is over the 23 pseudo-nuclides, α_i and Γ_i are energy yield fraction and decay constant values from ANSI/ANS 5.1-1979, respectively, T is the operation time (taken to be 10^{13} seconds in the standard), and t_j is the cooling time. Tables 4, 5, and 6 of the standard give decay heat power values for U-235, Pu-239, and U-238, respectively, for 55 cooling times in each table. Thus, there are effectively 55 t_j values for which the standard provides one sigma uncertainty values. [

] ^{a,c}

a,c

[

Table RAI-20-1 Fitting Data for κ and σ_{κ}					
Term	C_i^{κ}	$C_i^{\sigma\kappa}$	L	M	N

]

a,c

[

]

a,c

Question 21:**(^{235}U , ^{238}U , and ^{239}Pu Decay Heat and Uncertainty Comparison to ANS 5.1-1979)**

WCAP-16996-P/WCAP-16996-NP, Volumes I, II and III, Revision 0, Section 9.7, “Decay Heat Uncertainty Evaluation,” in discussing the decay heat uncertainty modeling in WCOBRA/TRAC-TF2, refers to Figures 9-26 to 9-28 for comparison of “predicted decay heat with uncertainties to the standard decay heat plus 2σ uncertainties” for cooling times from 1 s to 10^9 s. Figure 9-26 shows the decay heat for ^{235}U , Figure 9-27 exhibits the decay heat for ^{239}Pu , and Figure 9-28 plots the decay heat for ^{238}U as functions of cooling time after shutdown and each plot identifies three data sets. The first data set is labeled “DH Standard” and the second data set is labeled “DH Standard + 2 Sigma” in all three plots. The third data set is labeled as “DH Fitted” in Figure 9-26 and as “DH Calculated” in Figures 9-27 and 9-28.

Please clarify and address, as needed, the following comments related to Section 9.7 and Figures 9-26 to 9-28.

- (1) It is believed that the units for decay heat on the Y-axis in each figure should be “MeV/fission” (MeV/fission=[MeV/s]/[fission/s]). Instead, the decay heat units appear as “MeV/sec/fission”.
- (2) It appears that that Figure 9-26 exhibits the decay heat function $F_i(t,T)$ for thermal fission of ^{235}U , Figure 9-27 plots $F_i(t,T)$ for thermal fission of ^{239}Pu , and Figure 9-28 shows $F_i(t,T)$ for fast fission of ^{238}U for infinite irradiation time ($T=10^{13}$ s) in all three plots. However, description for the plotted quantities is not provided in Section 9.7.
- (3) Only two data sets (curves) are seen in each of the plots. A third data set (curve) is not distinguishable and using symbols to indicate overlapping curves can be used if appropriate.

Please provide updated plots that represent the WCOBRA/TRAC-TF2 decay heat predictions for ^{235}U , ^{239}Pu , and ^{238}U for decay time from 0.1 s to 10^6 s. In each plot, please show the standard decay heat values $F_i(t,\infty)$ for ^{235}U , ^{239}Pu , and ^{238}U as tabulated in ANSI/ANS 5.1-1979 Tables 4, 5, and 6 representing each value by a symbol with a two-sided Y-error bar corresponding to $\pm 2\sigma$ uncertainty using the uncertainty data in the ANSI/ANS 5.1-1979 tables. The uncertainties in both ANSI/ANS 5.1-1979 and ANSI/ANS 5.1-2005 are currently represented in tabular form for the decay heat functions $f_i(t)$ and $F_i(t,\infty)$ and values for intermediate times are obtained by interpolation. The included figure presents the $F_i(t,\infty)$ ANSI/ANS 5.1-1979 Standard decay heat and uncertainty data for ^{235}U , ^{239}Pu , and ^{238}U . In each figure, plot a curve that shows the “nominal” WCOBRA/TRAC-TF2 decay heat prediction as a continuous function of time and then show two additional curves that represent uncertainties predicted by WCOBRA/TRAC-TF2 and representing the decay heat “upper bound” (nominal plus 2σ) and “lower bound” (nominal minus 2σ). Explain how the code predicts the uncertainties for $t < 1$ s as no standard data are provided.

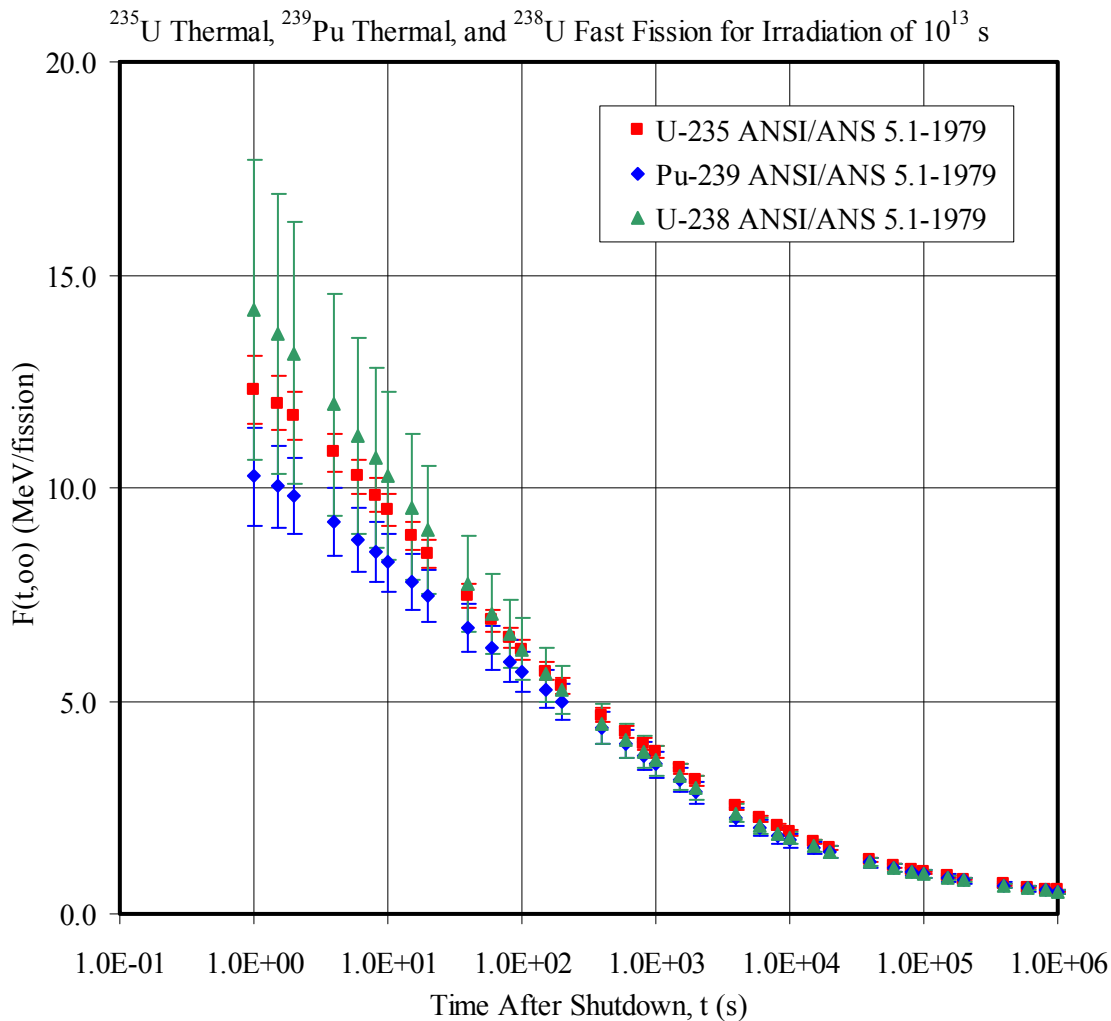


Figure: ANSI/ANS 5.1-1979 Tabular Data for Standard Decay Heat Power and Uncertainty for Thermal Fission of ^{235}U and ^{239}Pu and Fast Fission of ^{238}U for Irradiation of 10^{13} s

Response:

The following responses pertain to the numbered questions/comments in RAI-21:

- (1) The units for decay heat power on the Y-axis in Figures 9-26 through 9-28 should be MeV/fission.
- (2) Figures 9-26 through 9-28 display the comparison of decay heat power functions $F_i(t,T)$ for thermal fission of ^{235}U , thermal fission of ^{239}Pu , and fast fission of ^{238}U for infinite irradiation time calculated with WCOBRA/TRAC-TF2 and the ANSI/ANS-5.1-1979 standard .
- (3) See Figures RAI-21-1 through RAI-21-3 for updated plots with more visible lines.

Figures RAI-21-1 through RAI-21-3 provide curves that represent the nominal WCOBRA/TRAC-TF2 decay heat power predictions as continuous functions of time, as well as two additional curves that represent the decay heat power “upper bound” (nominal plus 2σ) and “lower bound” (nominal minus 2σ) for ^{235}U , ^{239}Pu , and ^{238}U for decay time from 0.1 s to 10^6 s. In addition, each plot includes the standard

decay heat power values $F_i(t, \infty)$ for ^{235}U , ^{239}Pu , and ^{238}U as tabulated in ANSI/ANS 5.1-1979 Tables 4, 5, and 6, representing each value by a symbol with a two-sided Y-error bar corresponding to $\pm 2\sigma$ uncertainty using the uncertainty data in the ANSI/ANS 5.1-1979 tables.

To calculate the decay heat power uncertainty prior to 1 second after shutdown, Equation 4 of the response to RAI Question 20 is used.

It is noted that the WCOBRA/TRAC-TF2 code version used to generate the data presented in Figures RAI-21-1 through RAI-21-3 corrects several errors in the existing configured WCOBRA/TRAC-TF2 code version relevant to this RAI response. The identified WCOBRA/TRAC-TF2 code errors are as follows:

1. The decay group uncertainty factors (in Table 9-14 of WCAP-16996-P) for ^{239}Pu are applied to ^{238}U , and the decay group uncertainty factors for ^{238}U are applied to ^{239}Pu .
2. The decay group uncertainty factor for Group 6 of ^{235}U is erroneously coded as 2.5% instead of 2.25%.
3. The yield fraction directly from fission (α) for Group 19 of ^{239}Pu is erroneously coded as 5.703E-11 instead of 5.730E-11.

Figures RAI-21-4 through RAI-21-6 provide the same curves as RAI-21-1 through RAI-21-3, except that they are produced using a WCOBRA/TRAC-TF2 code version containing the errors described above. By comparing Figures RAI-21-4 through RAI-21-6 to Figures RAI-21-1 through RAI-21-3, the following observations are made:

- Error 2 identified above has a negligible impact based on the WC/T Nominal $\pm 2\sigma$ lines in Figures RAI-21-1 and RAI-21-4 (maximum deviation of less than 0.09%).
- Error 3 identified above has a negligible impact based on the WC/T Nominal lines in Figures RAI-21-2 and RAI-21-5 (maximum deviation of less than 0.07%).
- The WC/T Nominal $\pm 2\sigma$ lines in Figures RAI-21-5 and RAI-21-6 show that Error 1 identified above causes over-prediction of uncertainty in decay power from ^{239}Pu and under-prediction of uncertainty in decay power from ^{238}U . Figures RAI-21-7 and RAI-21-8 compare the normalized 1σ uncertainty factor with and without the errors as a function of burnup and enrichment immediately after shutdown. These curves are calculated taking the fission fractions for each isotope into account. Figure RAI-21-9 shows a comparison of the 5 w/o enrichment curves with and without the errors. From these figures, it is concluded that this error results in an over-prediction of decay heat power uncertainty for fuel rods with burnup greater than about 5000 MWD/MTU and positive sampled uncertainty. For fuel rods with burnup less than 5000 MWD/MTU and positive sampled uncertainty, the under-prediction of decay heat power uncertainty varies from about 0.4% to 0 between about 0 and 5000 MWD/MTU.

a,c

Figure RAI-21-1 Comparison of Decay Heat Power Predictions for Thermal Fission of U-235 between ANSI/ANS 5.1 – 1979 Decay Heat Standard and WC/T with Errors Corrected

a,c

Figure RAI-21-2 Comparison of Decay Heat Power Predictions for Thermal Fission of Pu-239 between ANSI/ANS 5.1 – 1979 Decay Heat Standard and WC/T with Errors Corrected

a,c

Figure RAI-21-3 Comparison of Decay Heat Power Predictions for Fast Fission of U-238 between ANSI/ANS 5.1 – 1979 Decay Heat Standard and WC/T with Errors Corrected

a,c

Figure RAI-21-4 Comparison of Decay Heat Power Predictions for Thermal Fission of U-235 between ANSI/ANS 5.1 – 1979 Decay Heat Standard and WC/T with Errors

a,c

Figure RAI-21-5 Comparison of Decay Heat Power Predictions for Thermal Fission of Pu-239 between ANSI/ANS 5.1 – 1979 Decay Heat Standard and WC/T with Errors

a,c

Figure RAI-21-6 Comparison of Decay Heat Power Predictions for Fast Fission of U-238 between ANSI/ANS 5.1 – 1979 Decay Heat Standard and WC/T with Errors



Figure RAI-21-7 Comparison of Normalized 1σ Uncertainty Factor as a Function of Burnup and Enrichment with Errors Corrected

a,c

Figure RAI-21-8 Comparison of Normalized 1σ Uncertainty Factor as a Function of Burnup and Enrichment with Errors

a,c

Figure RAI-21-9 Comparison of Normalized 1σ Uncertainty Factor for 5 w/o Enrichment as a Function of Burnup

Question 22:**(²³⁵U, ²³⁸U, and ²³⁹Pu Decay Heat Uncertainty Comparison to ANS 5.1-1979)**

The determination of decay heat uncertainties is an important area and the modeling of decay heat uncertainty in WCOBRA/TRAC-TF2 is discussed in WCAP-16996-P/WCAP-16996-NP, Volumes I, II and III, Revision 0, Section 9.7, "Decay Heat Uncertainty Evaluation." WCOBRA/TRAC-TF2 models decay heat uncertainty through the use of pseudo-isotope energy yield augmentation factors generated using a least squares fit to the uncertainty data provided in ANSI/ANS 5.1-1979. The section refers to Figures 9-23 to 9-25 stating that they "illustrate the fit deviation in both energy and decay heat versus cooling time." According to the figure captions, the plots represent "percent fit deviations" for ANSI/ANS 5.1-1979 plus 2σ for ²³⁵U, ²³⁹Pu, and ²³⁸U.

It is seen from Figures 9-23 to 9-25 that the plotted discrepancies exhibit most pronounced deviation during the first 100 s of cooling time. At the same time, approximately 25% of the residual decay energy is released in the first 10 s after the fission process ends and about 50% is released by 100 s after fission (see I. Gauld, "Validation of ORIGEN-S Decay Heat Predictions for LOCA Analysis," PHYSOR-2006, ANS Topical Meeting on Reactor Physics, Vancouver, BC, Canada, September 10-14, 2006).

Please explain how the quantity labeled "Deviation" and shown along the vertical Y-axis in Figures 9-23 to 9-25 for cooling time from 10^{-1} s to 10^9 s was computed and define the parameters "energy" and "decay heat" for which the results were plotted. Please provide updated plots that compare the WCOBRA/TRAC-TF2 uncertainty predictions for ²³⁵U, ²³⁹Pu, and ²³⁸U for cooling time from 0.1 s to 10^6 s. In each plot, please show the uncertainty presented as $1+2\sigma$ and computed using the tabulated σ uncertainty percent values provided in ANSI/ANS 5.1-1979 Tables 4, 5, and 6. The included figure presents the ANSI/ANS 5.1-1979 Standard decay heat uncertainty data for ²³⁵U, ²³⁹Pu, and ²³⁸U. In each figure, plot a curve that shows the WCOBRA/TRAC-TF2 decay heat uncertainty prediction as a continuous function of time. Explain how the code predicts the uncertainties for $t < 1$ s as no standard uncertainty data are provided. If the WCOBRA/TRAC-TF2 decay heat uncertainty model underestimates any of the ANSI/ANS 5.1-1979 Standard values, a correction factor needs to be implemented to ensure that the code calculates uncertainties that are not less than the standard values.

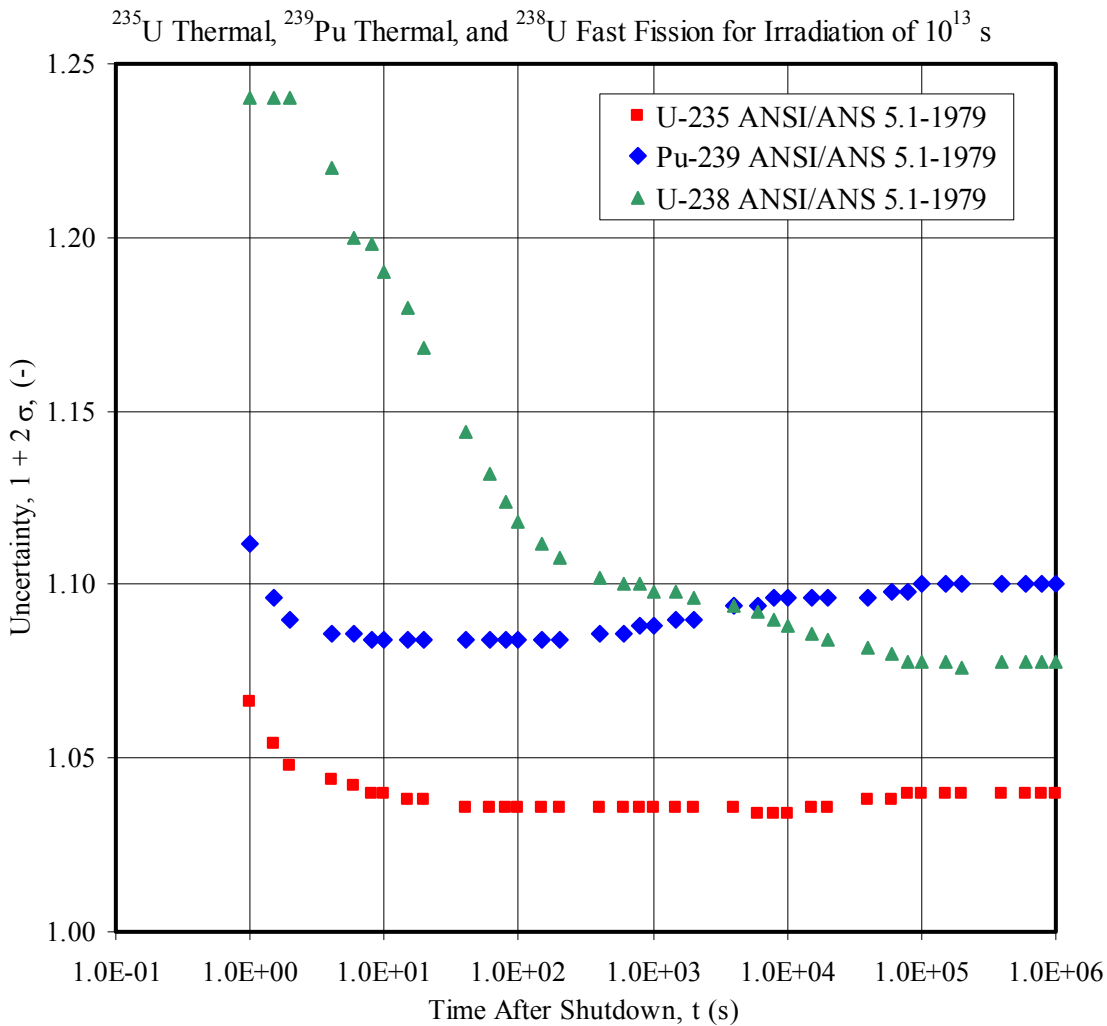


Figure: ANSI/ANS 5.1-1979 Tabular Data for Standard Decay Heat Power Uncertainty for Thermal Fission of ^{235}U and ^{239}Pu and Fast Fission of ^{238}U for Irradiation of 10^{13} s

Response:

The lines designated as decay heat in Figures 9-23 through 9-25 represent the percent deviation between the WCOBRA/TRAC-TF2 decay heat power predictions in Mev/fission and the standard decay heat power values $F_i(t, \infty)$ from ANSI/ANS 5.1-1979 in Mev/fission. The percent deviation is calculated according to Equation (1).

$$\%Dev_{DH} = \frac{DH_{WC/T} - DH_{Standard}}{DH_{Standard}} * 100 \quad (1)$$

The lines designated as decay energy in Figures 9-23 through 9-25 represent the percent deviation in decay power integrated over the cooling time between WCOBRA/TRAC-TF2 and the standard decay heat power values $F_i(t, \infty)$ from ANSI/ANS 5.1-1979. Specifically, to calculate the decay energy between any two cooling times, t_1 and t_2 :

$$DE(t_2 - t_1) = \int_{t_1}^{t_2} DH(t) dt \quad (2)$$

Equation (2) produces decay energy results with units of MeV/fission/sec. [

] ^{a,c}

Finally, to obtain the percent deviation given in Figures 9-23 through 9-25, Equations (1) and (7) are used at each time step for decay heat power and decay energy, respectively.

$$\%Dev_{DE} = \frac{DE_{WC/T} - DE_{Standard}}{DE_{Standard}} * 100 \quad (7)$$

Figures RAI-22-1 through RAI-22-3 show the nominal WCOBRA/TRAC-TF2 decay heat power predictions plus 2σ uncertainty as continuous functions of time for ²³⁵U, ²³⁹Pu, and ²³⁸U, presented normalized to the nominal values. In addition, the ANSI/ANS 5.1-1979 standard decay heat power uncertainty data for ²³⁵U, ²³⁹Pu, and ²³⁸U is presented in the same format.

To calculate the decay heat power uncertainty prior to 1 second after shutdown, Equation (4) of the response to Draft RAI number 20 is used.

[

]^{a,c}

As discussed in the RAI-21 and RAI-27 responses, ²³⁸U contributes less decay heat than ²³⁵U and ²³⁹Pu. As a result, it is judged that the [

]^{a,c}

Based on the decay heat discussion in Section 2.3.2.1 of WCAP-16996-P Revision 0, decay heat is [

Additionally, at about 10 seconds, the decay energy deviations for each isotope in Figures 9-23 through 9-25 of WCAP-16996-P Revision 0 are positive, which indicates that the total decay energy is over-predicted. The decay energy remains over-predicted until about 400 seconds for ²³⁵U, and past 1000 seconds for ²³⁸U and ²³⁹Pu. [

]^{a,c}

It is noted that the WCOBRA/TRAC-TF2 code version used to generate the data presented in Figures RAI-22-1 through RAI-22-3 is the same as that used to generate Figures RAI-21-1 through RAI-21-3 and thus has the same error corrections described in the response to RAI 21.

a,c

Figure RAI-22-1 Comparison of Decay Heat Power Uncertainty Predictions for Thermal Fission of U-235 between ANSI/ANS 5.1 – 1979 Decay Heat Standard and WC/T

a,c

Figure RAI-22-2 Comparison of Decay Heat Power Uncertainty Predictions for Thermal Fission of Pu-239 between ANSI/ANS 5.1 – 1979 Decay Heat Standard and WC/T

a,c

Figure RAI-22-3 Comparison of Decay Heat Power Uncertainty Predictions for Fast Fission of U-238 between ANSI/ANS 5.1 – 1979 Decay Heat Standard and WC/T

Question 23: Burnup Limit in Assessing Kinetics Parameters

WCAP-16996-P/WCAP-16996-NP, Volumes I, II and III, Revision 0, Section 9, “WCOBRA/TRAC-TF2 Reactor Kinetics and Decay Heat Models,” includes Figures 9-1 through 9-3, Figures 9-5 through 9-15, and Figures 9-32 through 9-34 that illustrate the dependence of various important physical parameters on the fuel burnup. With regard to neutron kinetics, WCAP-16996-P/ WCAP-16996-NP, Volumes I, II and III, Revision 0, Section 9.3, “Fission Heat,” states that WCOBRA/TRAC-TF2 explicitly models the burnup and initial enrichment dependence of kinetics data. Such data, generated for typical Westinghouse fuel lattice designs, are presented in Figures 9-5 through 9-14.

In all identified figures, the burnup range is limited to 60 MWD/MTU. Please explain if the application of the FSLOCA™ methodology is limited by this burnup level. If this is not the case, please show revised plots that cover the entire expected range of fuel burnup levels.

Response:

Westinghouse fuel is currently licensed to a peak rod burnup of 62,000 MWD/MTU. [

] ^{a,c} In general, the fuel with the highest burnup is modeled on the core periphery. In typical core loading patterns, high burnup fuel is placed on the core periphery to improve fuel economy. [

] ^{a,c} Should Westinghouse seek approval to increase the peak rod burnup beyond 62,000 MWD/MTU at some future time, the adequacy of the fitting parameters and the 0-60,000 MWD/MTU burnup range will be revisited.

FULL SPECTRUM™ and **FSLOCA™** are trademarks of Westinghouse Electric Company LLC, its affiliates and/or its subsidiaries in the United States of America and may be registered in other countries throughout the world. All rights reserved. Unauthorized use is strictly prohibited. Other names may be trademarks of their respective owners.

Question 24: Editorial

WCAP-16996-P/WCAP-16996-NP, Volumes I, II and III, Revision 0, Section 9.10, “Generalized Energy Deposition Model (GEDM) Validation,” refers to Table 9-19 for a comparison [] Table 9-19 is not found in WCAP-16996-P Revision 0. It is believed that the referenced table should be Table 9-18 instead of Table 9-19. Please clarify and correct accordingly.

WCAP-16996-P/WCAP-16996-NP, Volumes I, II and III, Revision 0, Subsection 9.9.2, “WCOBRA/TRAC-TF2 Fission Energy Accounting,” refers to Table 9-18 with regard to the prompt fission energy release, radiative capture release, and average fission neutron energy utilized in the evaluation of the composite prompt energy release per fission. It is believed that the referenced table should be Table 9-17 instead of Table 9-18. Please clarify and correct accordingly.

WCAP-16996-P/ WCAP-16996-NP, Volumes I, II and III, Revision 0, Subsection 9.9.1, “Actinide Decay Power,” with regard to physical data for []^{a,c} used in calculations performed to evaluate the impact of the total actinide heat source. It is believed that the referenced table should be Table 9-16 instead of Table 9-17. Please clarify and correct accordingly.

Response:

Westinghouse agrees that the items noted in RAI #24 are incorrect. Revisions to reflect the correct cross-references will be made as part of the overall topical report revision.

Question 25: Utilized Codes

WCAP-16996-P/WCAP-16996-NP, Volumes I, II and III, Revision 0, Section 9.2, "Decay Heat Source," explains that WCOBRA/TRAC-TF2 solves the time-dependent decay activity differential equation accounting for ^{235}U and ^{239}Pu thermal fission as well as for ^{238}U fast fission. The energy yield constants are weighted by the appropriate fission rate fractions as a function of initial enrichment and burnup within WCOBRA/TRAC-TF2. It is explained that the fission rate weighting was obtained from detailed physics evaluations of PWR fuel lattice designs and the results from these evaluations are presented in Figure 9-1 for ^{235}U thermal fission and in Figures 9-2 and 9-3 for ^{239}Pu thermal fission and ^{238}U fast fission weightings, respectively. Thus, WCOBRA/TRAC-TF2 solves for the composite decay heat of the reactor of interest using the fission rate fractions derived from specific physics calculations for the fuel lattice design. Please identify the codes used to perform these calculations, explain if they have been approved by NRC, and provide appropriate references.

WCAP-16996-P/WCAP-16996-NP, Volumes I, II and III, Revision 0, Section 9.3, "Fission Heat," states that a series of detailed space/energy calculations have been performed for a typical fresh assembly to quantitatively evaluate fission rate per unit neutron density for water densities that occur during a LOCA transient. Figure 9-4 shows the calculated coolant density dependence of the macroscopic cross section. Please identify the codes used to perform these calculations, explain if they have been approved by NRC, and provide appropriate references. In addition, please identify and explain the values for the physical parameters "KSF," "NSF," and "SIGA" that are used to identify each of the three curves shown in Figure 9-4. Which of the results was used to model the fission frequency in WCOBRA/TRAC-TF2?

WCAP-16996-P/WCAP-16996-NP, Volumes I, II and III, Revision 0, Subsection 9.6.2, "GEDM," explains that the DOT code was used as the dimensional particle transport code for the examples presented in this report. Please explain if this code has been approved by NRC and provide appropriate references.

WCAP-16996-P/WCAP-16996-NP, Volumes I, II and III, Revision 0, Subsection 9.9.1, "Actinide Decay Power," explains that detailed calculations have been performed to evaluate the impact of the total actinide heat source. Please identify the codes used to perform these calculations, explain if they have been approved by NRC, and provide appropriate references.

Response:

The fission rate fractions and coolant density dependence of the macroscopic cross sections were generated using a Westinghouse unit cell depletion program (ARK) which evolved from the codes LEOPARD and CINDER and additionally included a higher order matrix exponential method option for calculation of depletion isotopics. The references for these codes are provided below:

R. F. Barry, "LEOPARD - A Spectrum Dependent Non-Spatial Depletion Code for the IBM-7094," WCAP-3269-26, Westinghouse Electric Corporation (September, 1963).

T. R. England, "CINDER - A One-Point Depletion and Fission Product Program," WAPD-TM-334, Westinghouse Electric Corporation Bettis Atomic Power Laboratory (August, 1962).

LEOPARD and CINDER have not been formally generically approved, but their use has been documented and licensed in FSAR's dating back to the 1970's.

The values for the physical parameters "KSF," "NSF," and "SIGA" that are used to identify each of the three curves shown in Figure 9-4 are simply the normalization factors for each of the curves. Each curve

is normalized to a value of 1.0 at a water density of 0.7 gm/cm^3 . So, for example, the Σ_A curve ("SIGA") is normalized using the factor $[\Sigma_A]^{a,c}$ which is the value of Σ_A in units of cm^{-1} at 0.7 gm/cm^3 .

The fission frequency, which is $\nu\kappa\Sigma_F$, $[\Sigma_F]^{a,c}$ using the specific curves given in Figure 9-4. The density dependence of the fission frequency, $[\Sigma_F]^{a,c}$ the formulation given in Table 9-5. This formulation accounts for the density dependence of the $\kappa\Sigma_F$ portion of the fission frequency. The average neutron velocity, v , increases as density decreases. So, the density dependence of $\nu\kappa\Sigma_F$ is not the same as the density dependence of $\kappa\Sigma_F$.

The DOT code, which was the basis for the DORT code, is a radiation transport code that employs a standard industry method. Use of DORT has been approved by the NRC in the following topical report:

Anderson, S. L., "Benchmark Testing of the FERRET Code for Least Squares Evaluation of Light Water Reactor Dosimetry," WCAP-16083-NP-A, Westinghouse Electric Company, LLC, May 2006.

In WCAP-16083-NP-A, DORT has the following reference:

RSICC Computer Code Collection CCC-650, "DOORS 3.1, One- Two- and Three-Dimensional Discrete Ordinates Neutron/Photon Transport Code System," Radiation Safety Information Computational Center, Oak Ridge National Laboratory (ORNL), August 1996.

The actinide decay power heat source was determined using actinide number densities generated using the above-mentioned Westinghouse unit cell depletion program with the matrix exponential method employed.

Question 26: Actinides Decay Heat Power

In treating actinide decay heat power, ANSI/ANS 5.1 explicitly considers only decay heat power from ^{239}U and ^{239}Np . These two actinide isotopes are the dominant actinide decay heat for cooling times for which the standard is routinely applied to calculate decay heat for thermal-hydraulic safety system analyses. This limitation of the standard necessitates consideration of its augmentation with actinide values obtained from other calculations as actinide contribution, with ^{239}U and ^{239}Np excluded, increases from approximately 1 percent of the fission product decay heat power after 1 s up to approximately 10 percent after 10^5 s following shutdown (I.C. Gauld et al., "Proposed Revision of the Decay Heat Standard ANSI/ANS-5.1-2005," ORNL Publication No. 24753, October 2011). WCAP-16996-P/WCAP-16996-NP, Volumes I, II and III, Revision 0, Subsection 9.9.1, "Actinide Decay Power," presents results from detailed calculations performed to evaluate the impact of the total actinide heat source. As seen from Figures 9-32 and 9-33 [

] ^{a,c} Please present the analysis

results that quantify the impact of [

] ^{a,c} Identify the assumptions applied in this analysis and

show the results for the predicted actinide power for both cases [

] ^{a,c} Illustrate the impact from major parameters over their

entire range of interest for decay heat predication.

Response:

The actinide decay heat power at any particular core position is dependent upon the power density history of that core position. The half-lives of ^{239}U and ^{239}Np are 0.39 hr and 56.4 hr, respectively. Because the half-life of ^{239}U is relatively short, decay heat due to ^{239}U will reach its equilibrium value within a few hours after a step change in the local power density. This is not the case for ^{239}Np . For ^{239}Np , the decay heat only approaches its equilibrium value after several days following a step change in local power density. The decay heat from ^{239}Np represents about 47% of the total decay heat from both isotopes in equilibrium. Consequently, after any change in local power density, the total actinide decay heat from both isotopes will lag the equilibrium actinide decay heat primarily because of the lag in the contribution from ^{239}Np .

The kinds of peak local power densities that are limiting from a LOCA perspective are caused by non-equilibrium operation of the core, e.g., due to load follow. Changes in the core power level and core power distribution cause changes in the core xenon distribution. The result, in the absence of tight reactor control, is a dynamic reactor response which can lead to highly peaked power shapes. Such power shapes, however, occur over shorter time scales than the half-life of ^{239}Np . The time scale for load follow is 24 hours. Therefore, a core performing continuous load follow will cycle between peak power densities over a 24 hour period. The time scale for xenon changes is determined by the half-life of ^{135}Xe , which is about 9 hours. Consequently, the power shapes and local power densities that are limiting from a LOCA perspective are not stable and will naturally exist for only a few hours before other dynamic effects, such as xenon destruction, decay, or production, cause the power distribution to change.

To quantify the decay heat effects of non-equilibrium operation, it is necessary to make assumptions about the power density history. In the discussion below, the response of the actinide decay heat to a step change in power density and to power density changes typical of daily load follow will be described. Of

course, the number of possible power density histories is infinite. The examples provided serve to illustrate a range of possible decay heat responses relative to the assumption of equilibrium actinide decay heat.

To quantify the temporal behavior of the ^{239}U and ^{239}Np decay heat for a power density history, it is useful to solve the differential equations (9-12) and (9-13) given in Section 9.4 of WCAP-16996-P Revision 0. These equations are repeated below as equations (1) and (2):

$$\frac{dP_u}{dt} = \bar{R}\alpha_u[v\Sigma_F n(t)] - \lambda_u P_u(t) \quad (1)$$

$$\frac{dP_n}{dt} = \frac{\lambda_u P_u(t)\alpha_n}{\alpha_u} - \lambda_n P_n(t) \quad (2)$$

where:

$v\Sigma_F n(t)$ = time-dependent fission rate (proportional to power density),

$\lambda_u = ^{239}\text{U}$ decay constant = $4.91\text{E-}4 \text{ sec}^{-1}$,

$\lambda_n = ^{239}\text{Np}$ decay constant = $3.41\text{E-}6 \text{ sec}^{-1}$,

$\bar{R}(\text{BU}, \epsilon) = ^{238}\text{U}$ capture-to-fission ratio, function of initial enrichment ϵ , and burnup (BU),

$P_u(t)$ = time dependent decay power due to ^{239}U decay,

q_u = energy release per ^{239}U decay = 0.474 MeV,

$P_n(t)$ = time dependent decay power due to ^{239}Np decay,

q_n = energy release per ^{239}Np decay = 0.419 MeV,

$\alpha_u = q_u \lambda_u$ decay power yield per capture (MeV/sec/capture) for ^{239}U , and

$\alpha_n = q_n \lambda_n$ decay power yield per capture (MeV/sec/capture) for ^{239}Np .

[

]^{a,c}

a,c

(3)

(4)

Equations (1) and (2) can be readily solved if one assumes a constant fission rate over a short time step Δt . If we specify the constant fission rate as Q , the solutions for the time dependent decay powers over the time step are given by the following expressions:

a,c

(5)

(6)

[

 $I^{a,c}$

Suppose a step change in power density is assumed from a relative power density of 1.0 to 1.4, i.e., Q in the above expression increases instantaneously from a steady state value of 1.0 to 1.4 at time 0 and then remains at this value. (This is analogous to the local F_Q *Power value increasing, e.g., from a steady state value of 1.8 to 2.52 since $2.52/1.8 = 1.4$). Figure RAI-26-1 shows the resulting time dependent decay heat values for ^{239}U and ^{239}Np and for the sum of both. [

$I^{a,c}$ are also given. This figure assumes an \bar{R} value (^{238}U capture/fission ratio) of 0.6, corresponding to low burnup, high enrichment fuel. As will be shown later, the value for \bar{R} is not important to the relative difference between [

 $I^{a,c}$

[

 $I^{a,c}$

The above step change is not a realistic case since such a large increase in local power density above the natural steady-state value cannot be maintained for such an extended period, i.e., days. A more realistic, but still conservative, assumption is to assume a periodic variation in power density such as would be experienced for continuous daily load follow. Figure RAI-26-2 shows four power density (or fission rate) profiles (i.e., $Q(t)$ profiles) that will be examined to determine how the maximum decay heat experienced during the load follow day compares with the decay heat value resulting from the [

 $I^{a,c}$

These power profiles correspond to a 12-3-6-3 load follow scheme, i.e., 12 hours at the peak power density followed by a 3 hour ramp to the minimum power density, followed by 6 hours at the minimum power density, followed by 3 hour ramp back to the peak power density. This profile mimics a typical load follow schedule. It is conservatively assumed that the peak Q value remains constant for 12 hours during the load follow day. This is equivalent to assuming that the peak F_Q peaking factor (the peak to average power density) in the core is maintained at a constant value while the core is at full power. (Effectively, one can view the power density profiles as having a constant F_Q value throughout but with core power level cycling over a 24 hour period. The power density and the fission rate are proportional to F_Q *Power.) This assumption is conservative since it would be very difficult, due to xenon feedback, to maintain the local power density at a large non-equilibrium peak value for 12 hours. Also, this kind of operation would not be consistent with recommended axial power distribution control strategies. For present purposes, however, [

 $I^{a,c}$

Equations (5) and (6) were used to determine the time dependent decay heat values for an equilibrium load follow cycle. To achieve equilibrium, the load follow decay heat cycle was repeated until equilibrium was achieved. A time step size of 1 minute was used. This time step is very small relative to the time constants for both ^{239}U and ^{239}Np and, thus, will generate accurate results. A predictor-corrector scheme was also used to minimize any error due to the assumption of a constant Q value over the small

time step. [

] ^{a,c}

Figure RAI-26-3 show the time dependent decay heat results for the 1.0-0.50-1.0 Q(t) profile. The maximum decay heat for the load follow cycle occurs at 12 hours, the time at which Q begins to decrease. This is due to the decrease in the decay heat contribution from ²³⁹U that begins after hour 12. During the equilibrium cycle, the maximum decay heat value reached 0.492 MeV/fission. [

] ^{a,c}

All of the profiles produce results that are qualitatively similar to Figure RAI-26-3. However, the profiles with larger differences between the maximum and minimum Q values also produce larger decay heat differences [^{a,c} Table RAI-26-1 compares the maximum decay heat for all four of the Q(t) profiles. Note that the range of the ratio of the [

] ^{a,c} In actual operation, power profiles with large differences between the maximum and minimum power densities will tend to be limiting from a LOCA standpoint since these profiles represent the largest departure from the equilibrium state.

The maximum Q value and power profile are the major parameters affecting the maximum decay heat value and the [

] ^{a,c} The other variable that can affect the maximum decay heat is \bar{R} . Table RAI-26-2 gives decay heat values for a range of \bar{R} values. The 1.0-0.50-1.0 profile was assumed for this table. As the table shows, a higher \bar{R} increases the decay heat (as expected since more atoms of ²³⁹U and ²³⁹Np are produced), but the [

] ^{a,c}

Table RAI-26-1
Transient and Maximum Equilibrium Actinide Decay Heat (MeV/fission)
for Four Power Density Profiles

[

]

a,c

Note: These decay heat values assume an \bar{R} value of 0.6.

Table RAI-26-2
Transient and Maximum Equilibrium Actinide Decay Heat (MeV/fission)
for a 1.0-0.50-1.0 Power Density Profile and Various \bar{R} Values

[

]

a,c

Figure RAI-26-1 Relative Decay Heat for ^{239}U and ^{239}Np for a Step Change in Relative Power Density from 1.0 to 1.4

a,c

Note: Equilibrium values are for a Q of 1.4

Figure RAI-26-2 Q Profiles used for Study of ^{239}U and ^{239}Np Transient Decay Heat

a,c

Note: Q is the relative local power density or fission rate where a Q of 1 corresponds to the maximum power density or fission rate over the cycle. Absolute power density or fission rate values can be determined by multiplying the profile by the peak power density or peak fission rate over the cycle.

Figure RAI-26-3 Relative Total Decay Heat (MeV/Fission) for ^{239}U and ^{239}Np for a Power Density Profile of 1.0-0.50-1.0



Question 27: Decay Heat in Demonstration Plant Analyses

WCAP-16996-P/WCAP-16996-NP, Volumes I, II and III, Revision 0 Section 9, “WCOBRA/TRAC-TF2 Reactor Kinetics and Decay Heat Models,” describes the models for heat sources from fission heat, fission product decay heat, and actinide decay heat. However, the section does not show a calculated reactor power curve used in any of the analyses discussed in WCAP-16996-P Revision 0.

For the demonstration Westinghouse plant (V. C. Summer) examined in WCAP-16996-P/WCAP-16996-NP, Volumes I, II and III, Revision 0, Section 31, “Full Spectrum LOCA Demonstration Analysis,” please present graphs that show the WCOBRA/TRAC-TF2 predicted total residual power relative to the operating power (total reactor power or local power as appropriate) for the Region I and Region II limiting cases (Run 059 and Run 119). Use logarithmic scales for both the X-axis showing time after shutdown or break occurrence from 0.1 s to 10^6 s and for the Y-axis showing relative power from 10^{-3} to 10^0 . In each plot, please show with separate curves the residual fission power from the point kinetics model, the individual decay power contributions accounting for fission product decay power, actinide decay power, and decay power due to neutron capture by fission products during irradiation using the ANSI/ANS 5.1-1979 decay heat model, and the resulting total residual power. Present the “nominal” WCOBRA/TRAC-TF2 decay heat curve along with the upper (nominal plus 2σ) and lower (nominal minus 2σ) bounds in the plots. Please include two tables that document all utilized input parameters to the applied WCOBRA/TRAC-TF2 models to compute the contributing residual powers for both runs as plotted in the presented graphs (e.g., energy per fission). For each appropriate input parameter, please show its identifier, units, numerical or logical value, and the way in which the input value was determined. In the same manner, please document also all relevant uncertainty factors applied for both runs. Please explain if suggestions contained in NRC Information Notice 96-39, “Estimates of Decay Heat Using ANSI 5.1 Decay Heat Standard May Vary Significantly,” dated July 5, 1996, are of relevance when determining any ANSI/ANS 5.1-1979 Standard input model parameters for WCOBRA/TRAC-TF2.

Response:

1.0 Description of Figures

Figure RAI-27-1 presents the total residual power, as well as the individual contributions from the point kinetics model, thermal fission of ^{235}U , thermal fission of ^{239}Pu , fast fission of ^{238}U , actinide decay power, and power production due to neutron capture for the limiting case (Run 59) of Region I in the Westinghouse demonstration plant calculations. These curves are all normalized to initial core power, and they are all calculated using the sampled decay heat power uncertainty value from the demonstration plant analysis.

Figure RAI-27-2 presents the total residual power for Region I, Run 59, normalized to initial core power. The Actual Power curve represents the power calculated using the sampled decay heat power uncertainty value from the demonstration plant analysis. The Nominal Power curve represents the power calculated using no decay heat power uncertainty, and the Nominal $\pm 2\sigma$ curves represent the power modeling nominal $\pm 2\sigma$ decay heat power uncertainty.

Figures RAI-27-3 through RAI-27-5 present power generated by thermal fission of ^{235}U , thermal fission of ^{239}Pu , and fast fission of ^{238}U , respectively, for Region I, Run 59. The curves are all normalized to initial core power. The Actual Power curves represent the power calculated using the sampled decay heat power uncertainty value from the demonstration plant analysis. The Nominal Power curves represent the power calculated using no uncertainty, and the Nominal $\pm 2\sigma$ curves represent the power modeling nominal $\pm 2\sigma$ uncertainty.

Figures RAI-27-6 through RAI-27-8 present the power calculated with the point kinetics model, the actinide power, and power production due to neutron capture, respectively, for Region I, Run 59. The curves are all normalized to initial core power. The Actual Power curves represent the power calculated using the sampled decay heat power uncertainty value from the demonstration plant analysis. The Nominal Power curves represent the power calculated using no uncertainty, and the Nominal $\pm 2\sigma$ curves represent the power modeling nominal $\pm 2\sigma$ uncertainty.

The decay heat power uncertainty sampled for Region I, Run 59 is []^{a,c} Therefore, it is expected that the Actual Power curves in Figures RAI-27-2 through RAI-27-5 show []^{a,c} From Figure RAI-27-2, it can be seen that the initial deviation between the Actual Power and the Nominal Power is very small; however, as the fission power becomes less dominant around 100 seconds, the deviation due to decay heat power uncertainty begins to become more pronounced as decay heat power begins to make up more of the total power. It is shown in Figures RAI-27-6 and RAI-27-7 that decay power uncertainties cause negligible changes to the fission power and actinide power. []

[]^{a,c}

Figure RAI-27-9 presents the total residual power, as well as the individual contributions from the point kinetics model, thermal fission of ^{235}U , thermal fission of ^{239}Pu , fast fission of ^{238}U , actinide decay power, and power production due to neutron capture for the limiting case (Run 119) of Region II in the Westinghouse demonstration plant calculations. These curves are all normalized to initial core power, and they are all calculated using the sampled decay heat power uncertainty value from the demonstration plant analysis.

Figure RAI-27-10 presents the total residual power for Region II, Run 119, normalized to initial core power. The Actual Power curve represents the power calculated using the sampled decay heat power uncertainty value from the demonstration plant analysis. The Nominal Power curve represents the power calculated using no decay heat power uncertainty, and the Nominal $\pm 2\sigma$ curves represent the power modeling nominal $\pm 2\sigma$ decay heat power uncertainty.

Figures RAI-27-11 through RAI-27-13 present power generated by thermal fission of ^{235}U , thermal fission of ^{239}Pu , and fast fission of ^{238}U , respectively, for Region II, Run 119. The curves are all normalized to initial core power. The Actual Power curves represent the power calculated using the sampled decay heat power uncertainty value from the demonstration plant analysis. The Nominal Power curves represent the power calculated using no uncertainty, and the Nominal $\pm 2\sigma$ curves represent the power modeling nominal $\pm 2\sigma$ uncertainty.

Figures RAI-27-14 through RAI-27-16 present the power calculated with the point kinetics model, the actinide power, and power production due to neutron capture, respectively, for Region II, Run 119. The curves are all normalized to initial core power. The Actual Power curves represent the power calculated using the sampled decay heat power uncertainty value from the demonstration plant analysis. The Nominal Power curves represent the power calculated using no uncertainty, and the Nominal $\pm 2\sigma$ curves represent the power modeling nominal $\pm 2\sigma$ uncertainty.

The decay heat power uncertainty sampled for Region II, Run 119 is []^{a,c} Therefore, it is expected that the Actual Power curves in Figures RAI-27-10 through RAI-27-13 show []^{a,c} It is shown in Figures RAI-27-6 and RAI-27-7 that decay power uncertainties cause negligible changes to the fission power and actinide power. []

] ^{a,c}

2.0 Description of the Calculation of Total Residual Core Power

The total core power is the sum of the fission power calculated by the point kinetics model and the total decay heat power, which is calculated as a sum of the contributions from thermal fissions of ^{235}U and ^{239}Pu , fast fission of ^{238}U , actinide decay, and neutron capture. The input and selected computed parameters related to the fuel rod power calculations for the demonstration plant runs (Run 59 and Run 119) are listed in Tables 1 and 2.

2.1 Calculation of Fission Power with the Point Kinetics Model

The calculation of fission power with the point kinetics model is described in Section 9.3 of WCAP-16996-P, Revision 0. The reactivity in the point kinetics model is coupled with WCOBRA/TRAC-TF2 core thermal hydraulics, and it is also a function of the core-averaged fuel temperature accounting for all of the rods.

2.2 Calculation of Actinide Power

The calculation of actinide decay power is discussed in Sections 9.4 and 9.9.1 of WCAP-16996-P, Revision 0. As discussed in WCAP-16996-P, Revision 0, the capture to fission ratio, \bar{R} , is calculated based on the fuel rod burnup and enrichment inputs using Westinghouse correlations developed for its typical PWR fuel lattice design.

2.3 Calculation of Power from Neutron Capture

The calculation of power from neutron capture is described in Section 9.9.3 of WCAP-16996-P, Revision 0. The fissions per initial fissile atom, ψ , is calculated based on correlations developed for typical Westinghouse PWR fuel lattice design, [

] ^{a,c}

2.4 Calculation of Decay Heat Power

The calculations of thermal fissions of ^{235}U and ^{239}Pu , and fast fission of ^{238}U are described in Section 9.2 of WCAP-16996-P, Revision 0. The fission fraction for each fissile isotope, w_n , is calculated as a function of rod burnup and enrichment inputs. Additionally, under WCOBRA/TRAC-TF2 user input guidance, the burnups for the hot rod and hot assembly rod are converted to irradiation time (in seconds) and [

] ^{a,c} Additionally, the decay heat power uncertainty multipliers in Tables 1 and 2 are used to obtain the decay heat power for each isotope for each WC/T rod, as described in RAI response 21.

3.0 Examination of NRC Information Notice 96-39

NRC Information Notice 96-39 discusses the potential variation in decay heat power predictions using the ANSI/ANS-5.1-1979 Decay Heat Power Standard through user input parameters. In particular, Actinides, R-factor, G-factor, SI, Power history, and Fissile Elements are discussed in the Information Notice. Based on the discussions in Sections 2.2 through 2.4, these parameters are adequately modeled in WCOBRA/TRAC-TF2.

4.0 Known Errors Involved in the Original Calculations

The WCOBRA/TRAC-TF2 code version used to generate the data presented in Figures RAI-27-1 through RAI-27-16 corrects several errors in the existing configured WCOBRA/TRAC-TF2 code version, three of which are discussed in the response to RAI 21. Additionally, the calculation of decay heat power uncertainty in the code is missing the extra term to account for the 1σ uncertainty in the prompt energy per fission (σ_k/k), as described in the response to RAI 20. The inclusion of the extra uncertainty associated with the prompt energy per fission results in a slightly more conservative estimation of the total decay heat power uncertainties.

Table 1: Input and Selected Computed Parameters Used to Compute Residual Power for Region I, Run 59

Parameter	Hot Rod ($\frac{WC}{T}$ Rod 1)	Hot Assembly Rod ($\frac{WC}{T}$ Rod 2)	Core Average Rods ($\frac{WC}{T}$ Rods 3 and 4)	Low Power Rod ($\frac{WC}{T}$ Rod 5)

a,c

Table 2: Input and Selected Computed Parameters Used to Compute Residual Power for Region II, Run 119

Parameter	Hot Rod ($\frac{WC}{T}$ Rod 1)	Hot Assembly Rod ($\frac{WC}{T}$ Rod 2)	Core Average Rods ($\frac{WC}{T}$ Rods 3 and 4)	Low Power Rod ($\frac{WC}{T}$ Rod 5)

a,c

a,c

**Figure RAI-27-1 Total Power and Power Contributors Normalized to the Initial Core Power
for Region I, Run 59**



Figure RAI-27-2 Total Core Power Normalized to the Initial Core Power for Region I, Run 59

a,c

Figure RAI-27-3

Power Generated by Thermal Fission of U235 Normalized to the Initial Core Power for Region I, Run 59

a,c

**Figure RAI-27-4 Power Generated by Thermal Fission of Pu239 Normalized to the Initial
Core Power for Region I, Run 59**

a,c

Figure RAI-27-5 Power Generated by Fast Fission of U238 Normalized to the Initial Core Power for Region I, Run 59

a,c

Figure RAI-27-6

Fission Power Calculated by the Point Kinetics Model Normalized to the Initial Core Power for Region I, Run 59

a,c

Figure RAI-27-7 Actinide Power Normalized to the Initial Core Power for Region I, Run 59

a,c

**Figure RAI-27-8 Power Generated by Neutron Capture Normalized to the Initial Core Power
for Region I, Run 59**

a,c

**Figure RAI-27-9 Total Power and Power Contributors Normalized to the Initial Core Power
for Region II, Run 119**

a,c

Figure RAI-27-10

Total Core Power Normalized to the Initial Core Power for Region II, Run 119

a,c

Figure RAI-27-11 Power Generated by Thermal Fission of U235 Normalized to the Initial Core Power for Region II, Run 119

a,c

**Figure RAI-27-12 Power Generated by Thermal Fission of Pu239 Normalized to the Initial
Core Power for Region II, Run 119**

a,c

Figure RAI-27-13**Power Generated by Fast Fission of U238 Normalized to the Initial Core Power for Region II, Run 119**



Figure RAI-27-14 Fission Power Calculated by the Point Kinetics Model Normalized to the Initial Core Power for Region II, Run 119

a,c

Figure RAI-27-15 Actinide Power Normalized to the Initial Core Power for Region II, Run 119

a,c

Figure RAI-27-16**Power Generated by Neutron Capture Normalized to the Initial Core Power
for Region II, Run 119**

Question 28: Decay Heat Uncertainty Distribution

As described in WCAP-16996-P/WCAP-16996-NP, Volumes I, II and III, Revision 0, Subsection 25.2.1.4, “The Effect of Fuel Burnup on Power Distributions,” the time-in-cycle impacts the decay heat as a burnup-dependent parameter. Furthermore, Subsection 29.5.1, “Fuel Rod,” explains that the decay heat uncertainties, based on the ANSI/ANS 5.1-1979 standard, “vary with time in cycle as the decay heat contribution from each fissionable isotope changes.” Also, Subsection 29.4.1.2, “Reactor Core Power Distributions and Global Uncertainties,” states that “uncertainty in decay heat is considered through the application of ANSI/ANS 5.1-1979 Standard (DH, normal distribution).” Table 29-4, “Uncertainty Elements – Power-Related Parameters Defined in Section 29.4.1,” describes the decay heat uncertainty distribution as normal and characterizes it with a mean value and a standard deviation σ defined as a function of burnup and enrichment, $\sigma = f(\text{burnup}, \text{enrichment})$. Please explain the method of calculating the dependency of the standard deviation σ for the decay heat uncertainty distribution on the fuel burnup and enrichment and present results to illustrate the predicted effect on σ over the entire range of expected burnup levels and enrichments.

Tables 31.3-1a and 31.3-2a in WCAP-16996-P/ WCAP-16996-NP, Volumes I, II and III, Revision 0, Section 31.3, “Analysis of Results for Region I,” and Table 31.4-1a in Section 31.4, “Analysis of Results for Region II,” include the uncertainty attribute “DECAY HT (-)” along with the values used in the documented runs. If this or any other attributes are related to the decay heat uncertainty characterization, please explain their meaning and relationship to the characteristics defined in WCAP-16996-P/ WCAP-16996-NP, Volumes I, II and III, Revision 0, Table 29-4 to describe the decay heat uncertainty distribution. Also, please explain how “DECAY HT” or any other decay heat related uncertainty attributes are applied in executing the runs and obtaining the WCOBRA/TRAC-TF2 predictions.

Please explain how the ANS 5.1 uncertainties, represented in tabular form in ANSI/ANS 5.1-1979 Tables 1 to 6 for the decay heat functions $f_i(t)$ and $F_i(t, \infty)$, the fission product decay heat power for a pulse and infinite irradiation as a function of time after fission, relate to the decay heat uncertainty distribution parameters and the decay heat related uncertainty attributes considered above. In particular, please explain if dependence of the decay heat uncertainty distribution standard deviation σ or of the decay heat related uncertainty attributes on the cooling time following reactor shutdown is considered in the FSLOCA methodology.

Response:

As discussed in the response to Question 20, the [

$$\left[\begin{array}{c} \\ \\ \\ \end{array} \right]_{\text{a,c}}$$

^{a,c} The effective 1σ uncertainty in the total decay power is determined by the uncertainty in the relative contributions of each of the pseudo-nuclides to the total decay heat. In turn, these contributions will be dependent on burnup and, to a lesser extent, enrichment since the fission fractions for the fissile isotopes are functions of these variables.

To illustrate the dependence of the 1σ uncertainty factor on burnup and enrichment, the total decay heat power with and without uncertainty was calculated for a representative fuel lattice. A 0 second cooling time was assumed; consequently, the decay powers calculated were initial condition values. The decay heat powers were calculated over a range of burnups and enrichments. The ratio of the total decay heat power with and without uncertainty was then determined at each burnup and for each enrichment. Figure RAI-28-1 gives the results.

As this figure shows, the effective 1σ uncertainty factor [

] ^{a,c} As the ANS 5.1 Standard shows, the decay power uncertainty for ^{39}Pu is much larger than for ^{235}U . [^{a,c}

The decay heat power uncertainty attribute DECAY HT is the variable N_σ in equation 2 of RAI-20. Effectively, the decay heat power uncertainty factor for a given pseudo-nuclide has the following form:

$$\left[\frac{\text{DECAY HT}}{N_\sigma} \right]^{a,c}$$

The value for DECAY HT (N_σ) is sampled and employed in the above expression to determine the decay heat uncertainty factor for each pseudo-nuclide.

With respect to the decay heat power uncertainties given in the ANS 5.1 tables, these uncertainties were used to determine the values of the A_i decay group 1σ uncertainties for the various pseudo-nuclides such that the decay power with 2σ uncertainty was reproduced over the range of cooling times. The resulting decay heat power fit deviations relative to ANS 5.1 are given in Figures 9-23, 9-24, and 9-25. The fit deviations are quite small, indicating that the A_i factors accurately reproduce the ANS 5.1 decay powers including uncertainty.

[

] ^{a,c}

To illustrate this, Figure RAI-28-2 gives the effective decay heat power uncertainty factor versus burnup for 5 w/o fuel over cooling times ranging from 0 to 400 seconds. As ANS 5.1 shows, the decay heat power uncertainties decrease over cooling times of several hundred seconds as the short-lived pseudo-nuclides decay. This behavior is captured in WCOBRA/TRAC-TF2, as Figure RAI-28-2 illustrates.

Figure RAI-28-1 Effective 1σ Decay Heat Power Uncertainty Factor as a Function of Burnup and Enrichment

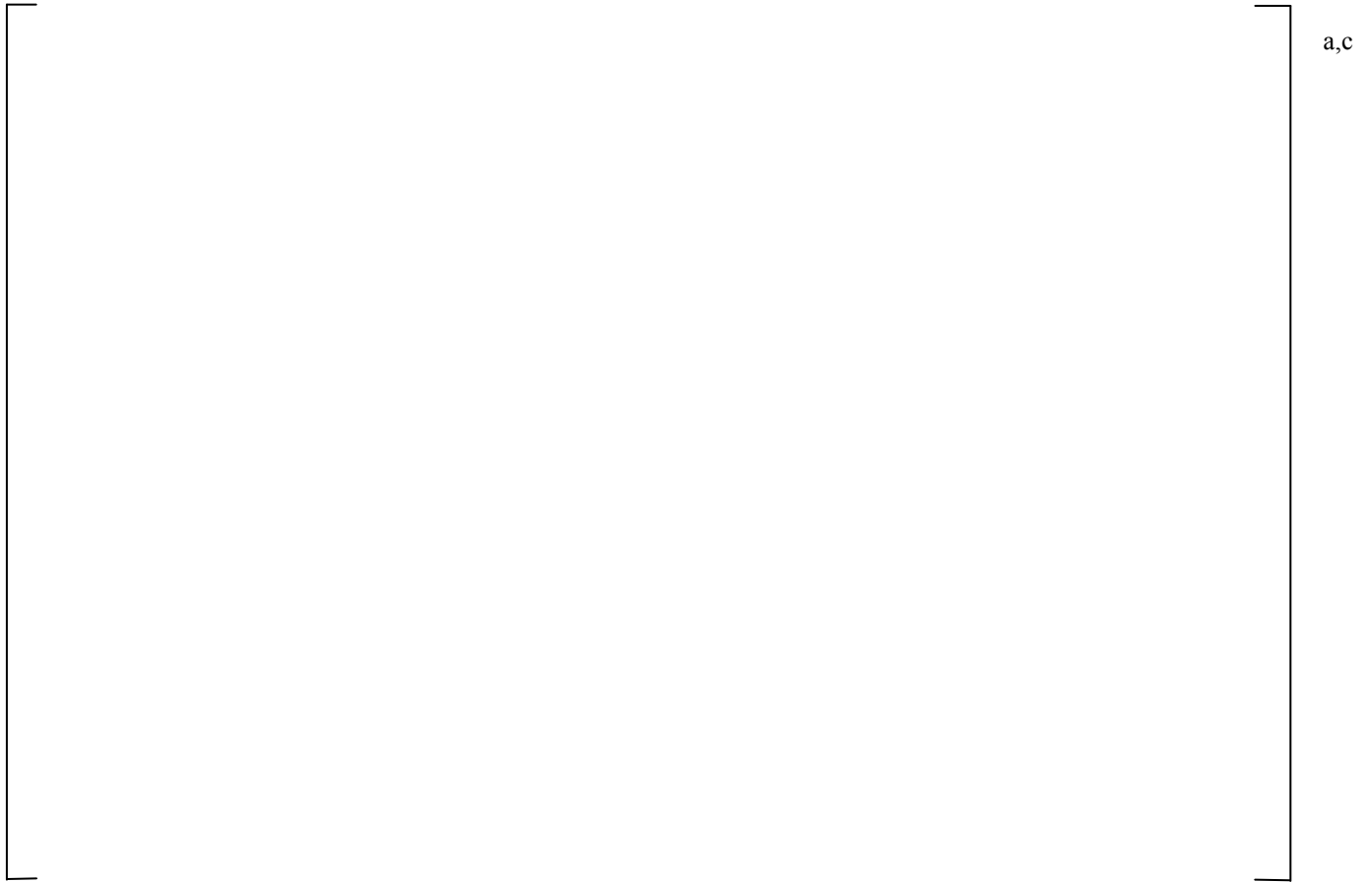


Figure RAI-28-2 Effective 1σ Decay Heat Power Uncertainty Factor as a Function of Burnup and Cooling Time



Question 29: Decay Heat Sampling Approach

WCAP-16996-P/WCAP-16996-NP, Volumes I, II, and III, Revision 0 Subsection 26.2.2, “V. C. Summer Reference Case and Allowable Plant Operating Conditions,” explains that the best-estimate methodology establishes a sampling of the distribution of potential uncertainty contributors, which occur due to changes in plant or model variables. The input values for V. C. Summer and Beaver Valley Unit 1 reference cases considered in Section 26, “WCOBRA/TRAC-TF2 Model of Pilot Plants,” are divided in three categories: 1) plant physical description, 2) plant initial operating conditions, and 3) accident boundary conditions. Decay heat is not included in the lists of categorized parameters. The parameters in these categories are sampled once for each run in order to initialize the input values needed to analyze the case.

Decay heat generation is a process that occurs in time and as such it differs from the parameters considered in the above identified categories of input parameters. Decay heat measurement data is characterized by experimental uncertainties. Detailed calculations of decay heat bear the uncertainties that originate from errors in the nuclear data and the yields of individual fission products. As a result, uncertainties are inherent to the decay heat generation process and its quantification at any point in time during the cooling period following reactor shutdown. In this regard, please explain the technique, appropriateness, and applicability of the FSLOCA methodology sampling approach in accounting for uncertainties in the decay heat prediction. This RAI question is related to Question 13.

Response:

The decay heat uncertainty is primarily driven by the uncertainties in the number densities of fission product nuclides at the time of the event and the uncertainties in the energy yields resulting from decay of those fission products. The number density uncertainties result from uncertainties in the fission product yields and nuclear data. The uncertainty in the decay heat power as codified in the decay heat standard [1] is an aggregate uncertainty that accounts for the uncertainty in the initial number densities and the uncertainty in the energy yields of the individual pseudo-nuclides. The aggregate uncertainty is a function of cooling time because the energy yields and decay constants of the individual pseudo-nuclides differ from nuclide to nuclide. Consequently, the decay power contribution of any individual fission product nuclide will vary with cooling time, and so its contribution to the total decay power uncertainty will also vary with cooling time.

Since the decay heat uncertainty is driven by uncertainties in the initial concentrations of fission product nuclides, the decay heat uncertainty is related to a physical property of the system at the time of the event. That physical property is the initial number density distribution among the fission product nuclides. By sampling the number of decay heat uncertainty sigmas for each case, the FSLOCA methodology is effectively sampling from a population of different initial number density combinations of fission product nuclides. Since the FSLOCA methodology reproduces the aggregate decay power uncertainties as codified in the standard as a function of cooling time, the methodology will appropriately capture the time-dependent decay power uncertainty that results from uncertainties in the initial fission product number densities.

Detailed descriptions of the nominal value and uncertainty in the decay power calculations are found in the responses to RAIs-13, 21, 22. The examination of each component of decay power for a sample calculation is given in the response to RAI-27.

References:

1. ANSI/ANS-5.1-1979, "American National Standard for Decay Heat Power in Light Water Reactors."

**WCAP-16996-P, “Realistic LOCA Evaluation Methodology Applied to the Full Spectrum of
Break Sizes (FULL SPECTRUM LOCA Methodology)”
Requests for Additional Information – Third Set (Non-Proprietary)**

May 2013

Westinghouse Electric Company LLC
1000 Westinghouse Drive
Cranberry Township, PA 16066

© 2013 Westinghouse Electric Company LLC
All Rights Reserved

RAI #30 – Scaling of the Westinghouse Vertical COSI Test Facility and Tests

WCAP-16996-P/WCAP-16996-NP, Volumes I, II and III, Revision 0, “Realistic LOCA [Loss-of-Coolant-Accident] Evaluation Methodology Applied to the Full Spectrum of Break sizes (FULL SPECTRUM™ LOCA [(FSLOCA™)] Methodology),” Subsection 6.3.6, “Special Model: Cold Leg Condensation Model,” describes the model for predicting direct contact condensation on the Safety Injection (SI) water for both small-break LOCA (SBLOCA) and large-break LOCA (LBLOCA) applications. The model employs an []^{a,c} that was derived from a best fit to a set of data points derived from tests at the Westinghouse Condensation on Safety Injection (COSI) test facility. The facility is referred to as the Westinghouse vertical COSI test facility and the tests as the Westinghouse vertical COSI tests. [

] ^{a,c}

a,c

WCAP-16996-P/WCAP-16996-NP, Volumes I, II and III, Revision 0, Subsection 6.3.6 states that the Westinghouse vertical COSI test facility “geometrically is a 1:100 scale of a pressurized water reactor (PWR) cold leg.” Additional information on scaling of a similar test facility is provided by P. Coste et al., “Status of a Two-Phase computational fluid dynamics (CFD) Approach to the PTS Issue,” Proc. OECD/NEA & IAEA Workshop “Experiments and CFD Code Applications to Nuclear Reactor Safety,” September 10-12, 2008, Grenoble, France. This reference explains that “COSI represents a PWR cold leg with the safety injection at the scale of 1/100 for volume and power, and conservation of Froude number” from a PWR under SBLOCA conditions.

WCAP-16996-P/WCAP-16996-NP, Volumes I, II and III, Revision 0, Subsection 17.2.1, “Test Facilities and Tests Description,” explains that a large matrix of tests was conducted over the course of the COSI program by both Westinghouse and Framatome and that “some reconfigurations of the facility test section were performed with regard to the length of the main pipe in the test assembly and the angle and size of the injection piping.” Please clarify and address, as appropriate, the following items related to the scaling of the Westinghouse vertical COSI test facility and test matrix conditions used to produce the data set for fitting the FSLOCA methodology cold condensation correlation.

FULL SPECTRUM™ and FSLOCA™ are trademarks in the United States of Westinghouse Electric Company LLC, its subsidiaries and/or its affiliates. This mark may also be used and/or registered in other countries throughout the world. All rights reserved. Unauthorized use is strictly prohibited.

- (1) Please describe the scaling of the Westinghouse vertical COSI test facility geometry and test matrix conditions used to produce the cold leg condensation rates. For this purpose, provide specific scaling relationships and criteria that are considered appropriate for investigation of SI cold leg condensation. Include specific consideration of cold leg diameter and cold leg length. Explain how the defined relationships and criteria apply to the Westinghouse vertical COSI test facility geometry and test matrix conditions. Explain which parameters and criteria support the scalability of the Westinghouse vertical COSI test data to prototypical conditions and which limit their applicability to such conditions.
- (2) Based on the applied experimental procedures and conditions, data analysis, and scaling, describe the impact of involved major experimental distortions, test limitations, contributing processes, and uncertainties, related to the COSI test geometry and test conditions, on the applicability of the derived condensation data set to prototypical PWR conditions. In particular, please address such impacts related to the cold leg diameter scale.

Response:

The COSI test facility was intended to investigate the condensation in the cold leg caused by the high head safety injection (SI) during a small break LOCA. The test facility was designed to properly downscale the cold leg of a Westinghouse PWR, as well as the steam flow rate, and SI rate to replicate the thermal hydraulics phenomena in the PWR cold leg.

As discussed in Section 6.3.6 of WCAP-16996-P, a special cold leg condensation model was developed from a subset of the data generated from the COSI test facility, specifically the Westinghouse vertical COSI test facility. The model was then validated by an independent data set spanning of different scales.

The scaling and applicability of the cold leg condensation model is based on the following principles which will be further elaborated in this response:

1) [

2)

3)

4)

]^{a,c}

1. Geometrical Scaling

The cold leg test section of the Westinghouse COSI facility was shown in Figure 17-2 of WCAP-16996-P. The inner diameter of the cold leg pipe is 0.118m (4.65 inch) and its length is approximately 4.9 m (16ft). The prototypical cold leg inner diameter in Westinghouse PWRs is 0.7m (27.5inch). The cold leg diameter scaling factor between the COSI test facility and a PWR cold leg is 1/6,

$$\frac{D_T}{D_P} = \frac{0.118}{0.7} \cong \frac{1}{6}$$

where the subscript T refers to the COSI test facility and the subscript P refers to the prototype, which is a Westinghouse PWR. The flow area scaling factor between the COSI test facility and a PWR cold leg is thus obtained,

$$\frac{A_T}{A_P} = \left(\frac{D_T}{D_P}\right)^2 \cong \frac{1}{35}$$

The diameter of the COSI SI line attached to the cold leg is scaled based on the geometrical similarity between the cold leg and SI line. Thus, its scaling factor is the same as the cold leg.

$$\frac{(D_{SI})_T}{(D_{SI})_P} = \frac{D_T}{D_P} \cong \frac{1}{6}$$

$$\frac{(A_{SI})_T}{(A_{SI})_P} = \left(\frac{(D_{SI})_T}{(D_{SI})_P} \right)^2 \cong \frac{1}{35}$$

The diameters of a typical high head SI line, a typical charging line and an accumulator line are []^{a,c}, respectively. The corresponding diameters in the COSI test facility are 0.9 inch (0.023m), 0.22 inch (0.0056m) and 1.5 inch (0.0381m), respectively. The scaling factors of those SI lines confirm the scaling factor of 1/6 (Table 1).

Table 1. Scaling Factors of SI lines Attached to Cold Leg

	a,c
--	-----

Note that the reported volume scaling of 1/100 (Sections 6.3.6 and 17.2.1 of WCAP-16996-P) is misleading and for the purpose of the scaling analysis it is more appropriate to focus on the specific geometric components:..[^{a,c}

2. Adequacy of Jet Re Number as Main Scaling Parameter

The historical path leading to the cold leg direct contact condensation model and the theoretical basis of the model are presented herein to facilitate the discussion. Asaka et al. [1] proposed a direct contact condensation model for TRAC-PF1/MOD 1 using turbulent liquid jet condensation model. Bestion and Gros d'Aillon [2] studied direct contact condensation in the cold leg with the data from the COSI test facility. They developed a mixing zone concept and assumed the vicinity of injection plays the most important role in the cold leg condensation. Janicot and Bestion [3] did further theoretical study on turbulence induced condensation in the vicinity of SI injection. A more accurate condensation model was developed by Janicot and Bestion using the COSI test data and the model was incorporated into the CATHARE reactor safety analysis code and validated against COSI experimental data [3]. A cold leg condensation model was incorporated into the Westinghouse NOTRUMP Appendix-K small break LOCA safety analysis code [12]. The NOTRUMP model also assumes the majority of condensation takes place immediately around the zone of the injection point based on findings from the COSI tests and a correlation was developed based on the assumed jet surface area. The development of a best-estimate small break LOCA evaluation model drove Westinghouse to develop a more scalable

WCAP-16996-NP-A November 2016 NP-4

cold leg condensation model than existing models for the FULL SPECTRUM™ LOCA (FSLOCA™) methodology. According to the surface renewal theory [4, 5, 6], the condensation heat transfer is controlled by the turbulent characteristics at the liquid side interface.

An accurate prediction on the condensation heat transfer relies on correlating liquid side heat transfer coefficient with the turbulent Reynolds number, which is shown in recent computational fluid dynamics simulations on the cold leg condensation problem [7, 8, 9]. In a coarse two fluid model, the detail of turbulent structure is beyond the resolution of the code. Instead, the SI jet Reynolds number, which is the kinetic source of the turbulence in the cold leg, becomes the controlling parameter.

The cold leg condensation correlation, which is used to predict the cold leg condensation rate in the cold leg condensation model was developed using the experiments from the Westinghouse vertical COSI test facility that represents a small break LOCA cold leg condensation scenario. Then, in the FSLOCA methodology, the cold condensation model is applied to the large break LOCA prediction. As addressed in Section 6.3.6 and Section 17.3 of WCAP-16996-P, the cold leg condensation scenario in a large break LOCA is different from that of a small break LOCA. As such, the application of the developed cold leg condensation model to large break LOCA is supported by the validation against the full scale cold leg condensation tests, UPTF 8A and UPTF 25A (Section 17.3 and Section 19.3 of WCAP-16996-P). [

]^{a,c}

The following sections discuss the effect of [

]^{a,c}

3. Adequacy of Cold Leg Diameter Scaling

In the cold leg condensation theory in WCAP-16996-P, [

]^{a,c}

One arguable effect caused by the 1/6 scaling factor of cold leg diameter in the COSI test facility is [

]^{a,c} The effect was illustrated in Figure 6-13 of WCAP-16996-P. To demonstrate that []^{a,c} when the cold leg condensation phenomenon is scaled up to a PWR cold leg, a comparison of []^{a,c} in the COSI test facility and the Beaver Valley Unit 1 cold leg was conducted using a computational fluid dynamics (CFD) tool in Westinghouse. The computational domain is displayed in Figure 1. The simulated COSI case is W012-1, which is a charging line case with the minimum SI flow rate, the most challenging COSI test in term of the SI jet penetration. The SI diameter and flow rate are scaled using scaling factors of 1/6 and []^{a,c}, respectively. Note, the flow rate scale is larger than the scaling factor between the COSI facility and Beaver Valley Unit 1, but that leads to an even smaller SI flow in the Beaver Valley Unit 1 CFD case, which would tend to

show a []^{a,c} The major parameters for the CFD computation are listed in Table 2. To []

The mesh was created by the TrueGrid mesh generation code. There are []^{a,c} cells in the COSI W012-1 CFD case and []^{a,c} cells in the Beaver Valley Unit 1 CFD case. The simulations were conducted using the Ansys CFX software.

Figure 2 shows the velocity profile at the cross section of the cold leg in the Westinghouse COSI test facility. The corresponding case in the cold leg of DLW is shown in Figure 3. In both cases,

Table 2. Major Parameters Used in the CFD Study

4. Impact of Cold Leg and SI line Area Scaling on Flow Regime

The COSI facility is properly designed to []^{a,c} The []^{a,c} in all Westinghouse COSI test was supported by the flow regime study using the well-recognized Taitel-Dukler flow regime map [11]. []

 $\mathbf{J}^{a,c}$

To determine the flow regime in the COSI SI line, the Froude number scaling factor of the SI line is evaluated [

1^{a,c}

5. Impact of Cold Leg Length Scaling

A noticeable feature of the COSI test facility is the length of the cold leg. The scaling factor of the cold leg length between Westinghouse COSI and PWRs is []^{a,c} The scaling factor is much larger than the scaling factor of the cold leg diameter. As discussed in Section 6.3.6 of WCAP-16996-P, the majority of cold leg condensation, when flow is stratified, is caused by the safety injection and occurs in the mixing zone. Outside the mixing zone, the stratification suppresses the interfacial heat transfer. [

] ^{a,c} This will be further addressed in Section 5.

More evidence supporting that the condensation occurs in the mixing zone comes from the COSI tests. The temperature profile from thermocouple rakes showed similarity between the profile near the SI jet and the profile further downstream. Furthermore, Shimeck [10] indicated that the Framatome COSI test facility considered a much shorter cold leg length than the Westinghouse test facility, but comparison between the Framatome test data and the Westinghouse test data showed that a shorter cold leg only led to a moderate decrease in the condensation heat transfer rate. These points support the assumption of the majority of the condensation is in the mixing zone, and the assumption has been adopted by several existing cold leg condensation models by both Westinghouse and Framatome.

[

] ^{a,c}

With respect to the validation of the cold leg condensation model, a favorable prediction of the Framatome tests (shorter cold leg) and ROSA SB-CL-05 (a better scaled cold leg length) is obtained. The validation against Framatome COSI was provided in WCAP-16996-P. In the response to RAI 33, an evaluation will be provided that shows [

] ^{a,c}.

6. Impact of Jet Re Scaling

The geometry scaling was determined to maintain prototypical conditions with respect to flow regimes and SI jet to stratified cold leg impingement mechanisms as discussed in the previous sections. However, [

] ^{a,c} as shown in Table 6-2 of WCAP-16996-P.

Figure 7 shows the ratio between the estimated condensation rate in the entire cold leg and measured value for the set of validation cases as a function of the SI Re number. Note that [

] ^{a,c}

The analysis of the figure leads to the following observations:

1) [

2)

3)

4)

$J^{a,c}$

Further evidence of the $J^{a,c}$ is provided in the response to RAI 33. It shows that the cold leg condensation rate predicted $J^{a,c}$

7. Summary on Scaling of COSI Facility

In summary, multiple aspects of scaling analyses on the diameter, flow area, length, superficial velocity, Reynolds number of both cold leg and SI line, and Froude number of SI line in the Westinghouse COSI test facility are provided. The scaling factor of SI jet Reynolds number and the cold leg diameter was further investigated. $J^{a,c}$

$J^{a,c}$

References:

1. Asaka, H., Murao, Y., and Kukita, Y., "Assessment of TRAC-PF1 Condensation Heat Transfer Model for Analysis of ECC Water Injection Transition," Journal of Nuclear Science and Technology, 26 (11), pp. 1045-1167, 1989.
2. Bestion, D., and Gros d'Aillon, L., "Condensation Tests Analysis and Correlation for the CATHARE Code," Proceeding of 4th International Topical Meeting on Nuclear Reactor Thermal-Hydraulics, Karlsruhe, Germany, October 1989.
3. Janicot, A., and Bestion, D., "Condensation modeling for ECC injection," Nuclear Engineering and Design, Vol. 145, pp. 37-45, 1993.
4. Theofanous, T., Houze, R., and Brumfield, "Turbulent Mass Transfer at Free Gas-Liquid Interface, with Applications to Open-Channel, Bubble and Jet Flows," International Journal of Heat and Mass Transfer, 19 (9), pp. 613-624, 1976.
5. Banerjee, S., "A Surface Renewal Model for Interfacial Heat and Mass Transfer in Transient Two-Phase Flow," International Journal of Multiphase Flow Vol. 4, pp. 571-573, 1978.
6. Hughes, E.D., and Duffey, R.B., "Direct Contact Condensation and Momentum Transfer in Turbulent Separated Flows," International Journal of Multiphase Flow Vol. 17 pp. 599-619, 1991.

7. Coste, P., et al., "Status of a Two-Phase CFD Approach to the PTS Issue," Proc. OECD/NEA & IAEA Workshop "Experiments and CFD Code Applications to Nuclear Reactor Safety," 10-12 September 2008, Grenoble, France.
8. Glantz, T., "COSI Test Case Simulation with CFX Code", Proceedings of the 17th International Conference on Nuclear Engineering (ICONE17), July 12-16, 2009, Brussels, Belgium.
9. Labois, M., and Lakehal, D., "PTS Prediction Using the CMFD Code TransAT: the COSI Test Case," Computational Fluid Dynamics (CFD) for Nuclear Reactor Safety Applications Workshop Proceedings, CFD4NRS-3, Bethesda, Maryland, USA, September 14-16, 2010.
10. WCAP-11767, "COSI SI/Steam Condensation Experiment Analysis," March 1988.
11. Taitel, Y., and Dukler, A., "A Model for Predicting Flow Regime Transitions in Horizontal and Near Horizontal Gas-Liquid Flow," AIChE Journal, Vol. 22, No. 1, pp. 47-54, 1976.
12. WCAP-10054-P, Addendum 2, Revision 1, "Addendum to the Westinghouse Small Break ECCS Evaluation Model Using the NOTRUMP Code: Safety Injection into the Broken Loop and COSI Condensation model," October 1995.



Figure 1. The COSI computational domain.



Figure 2. Total velocity contour at the cross section of the cold leg in Westinghouse COSI test facility (W012, point 1).



Figure 3. Total velocity contour at the cross section of the cold leg of Beaver Valley Unit 1 (SI flow rate scale of 1/14).



Figure 4. Plot of j_g and j_l in the Westinghouse COSI tests (both vertical and horizontal COSI tests) at 4.2MPa against the Taitel- Dukler flow regime map. The horizontal stratified flow regime is inside the solid line.



Figure 5. Plot of j_g and j_l in the Westinghouse COSI tests (both vertical and horizontal COSI tests) at 5.6MPa against the Taitel- Dukler flow regime map. The horizontal stratified flow regime is inside the solid line.



Figure 6. Plot of j_g and j_l in the Westinghouse COSI tests (both vertical and horizontal COSI tests) at 7.0MPa against the Taitel- Dukler flow regime map. The horizontal stratified flow regime is inside the solid line.



Figure 7. Ratio between Estimated Cold Leg Condensation Rate and Measured Value for Validation Cases as a Function of Jet Re Number.

RAI #31: Westinghouse Vertical COSI Downcomer Condensation

WCAP-16996-P/WCAP-16996-NP, Volumes I, II and III, Revision 0, Subsection 17.2.1, "Test Facilities and Tests Description," describes the approach in deriving the Westinghouse vertical COSI cold leg condensation data used to develop the correlation for SI jet condensation in the FSLOCA methodology. It explains that "the COSI experimental data report only gives boiler power and heat loss for the entire test loop." The boiler power was measured and the integral heat loss from the test section, boiler, and pipelines to the environment was estimated. The net total condensation heat transfer rates in the tests were obtained as difference between the boiler power and the heat loss as "steam from the inlet was completely condensed in the Westinghouse COSI tests." To obtain the cold leg condensation test data, the net total condensation rate was split into two parts: (1) condensation rate due to condensation in the cold leg and (2) condensation rate due to condensation in the downcomer. The first part included direct contact condensation on the SI jet in the cold leg and the second part accounted for condensation due to a possible "water fall" in the test section downcomer.

[

Subsection 17.2.1 Equation (17-2) provides the expressions for the downcomer condensation rate Q_{DC} (in kW) as function of the SI rate m_{SI} (in kg/s):

[

]^{a,c}
]^{a,c}

Assuming that the identified downcomer water levels were based on the lengths of the corresponding downcomer water falls, the water fall length ratio is assessed as:

[

]^{a,c}

SI rates were equal in the tests and Equation (17-2) gives the downcomer condensation rate ratio:

[

]^{a,c}

The downcomer condensation rate ratio is practically equal to the water fall length ratio for the Westinghouse vertical COSI tests used to establish the downcomer condensation rate.

Please provide additional information and clarification with regard to the following items.

- (1) Please define the reference elevation used to determine the downcomer levels in []^{a,c} test series. Explain how the downcomer water level was measured and how well was it controlled and maintained in testing.
- (2) Please explain if Equation (17-2) was based on the assumption that the condensation rate in the downcomer region was proportional to the length of a free water fall in the steam-filled upper downcomer region. This would allow attributing the difference in the boiler power between the corresponding []^{a,c} tests to difference in the water fall lengths (1.6 m – 0.3 m = 1.3 m) and establishing Equation (17-2).
- (3) Please explain if all []^{a,c} runs in each test series were used in establishing Equation (17-2) and present the corresponding test data used.
- (4) The expressions in Equation (17-2) were based on information from two Westinghouse []^{a,c} tests that differed only with regard to the downcomer water level. Equation (17-2) correlates the downcomer condensation rate only with the SI

rate and does not take into consideration other important parameters such as SI temperature, pressure, and variations in cold leg and downcomer conditions. If Equation (17-2) was used for all tests listed in WCAP-16996-P/WCAP-16996-NP, Volumes I, II and III, Revision 0, Table 17-2, "Westinghouse Vertical COSI Tests Data," please explain the basis for applying Equation (17-2) under different test conditions and possible implications with regard to the validity of the derived cold leg condensation rates.

Response:

(1) Per WCAP-11767 [1], the reference elevation is the bottom of the test section and the downcomer water level is measured by [

] ^{a,c}

(2) The estimation of condensation rate in the downcomer was based on the assumption that the condensation heat transfer rate in the downcomer is [

] ^{a,c}

To address this concern, the data reduction process for the COSI tests is revised to more accurately capture the cold leg condensation rate and address the scalability issue. There are two major changes in the revised data reduction process. First, [

] ^{a,c} Second, the downcomer condensation rate is evaluated at [] ^{a,c} using different pairs of tests and the uncertainty of the downcomer condensation rate is applied to the evaluation of the cold leg condensation rate. The process of the data reduction is listed below for the Westinghouse COSI tests.

1. The net condensation heat transfer rate, Q , in the test section (including downcomer) is [] ^{a,c} (see response to RAI32)
2. The net condensation efficiency is calculated using the following equation

$$\eta_{net} = \frac{Q_{net}}{m_{SI}(h_f - h_{SI})}$$

where Q_{net} is net condensation heat transfer in the test section, m_{SI} is the SI flow rate and h_f and h_{SI} are the enthalpy of saturated water and the SI water (at the test pressure and SI temperature).

3. The net condensation efficiency is [] ^{a,c} in several runs. The test report did not provide an explanation. In this data reduction process, the net condensation in those cases is [] ^{a,c}
4. The condensation heat transfer rate in the test section is split into two portions, the condensation in the cold leg and the condensation in the downcomer. The condensation heat transfer rate in the downcomer is evaluated using 3 pairs of tests with only differences being the [

There are 3 pairs of tests identified for difference pressures, []^{a,c}

All 5 runs in each pair are used to establish the downcomer condensation efficiency at the particular pressure. The []^{a,c} is the nominal condensation efficiency at the pressure and the maximum and minimum values provide the uncertainty of the downcomer condensation efficiency. The downcomer condensation efficiency and its uncertainty at []^{a,c} are calculated as shown in Tables 1 through 3.

5. The net condensation efficiency minus the efficiency caused by downcomer condensation is the cold leg condensation efficiency. []

6. The cold leg condensation heat transfer rate is evaluated using the cold leg condensation efficiency and the condensation potential with the formula below.

$$Q_{cond} = \eta_{cond} m_{SI} (h_f - h_{SI})$$

7. []

[]^{a,c}

A similar data reduction process is also applied to the Framatome COSI tests using the downcomer condensation efficiency shown in Tables 1 through 3. It is noted that []

However, the averaged downcomer condensation efficiency in Tables 1 through 3 reduces when the pressure drops from []^{a,c} Thus, the downcomer condensation efficiency of []

It is also noted that the SI injection rate in the Framatome COSI tests is generally higher than those in the Westinghouse COSI tests. However, the downcomer condensation efficiencies in Tables 1 through 3 []

[]^{a,c}

The final results of the cold leg condensation rate and its upper bound and lower bound in the Westinghouse COSI cases and the Framatome COSI cases are collected in Table 4 and Table 5, respectively. Those Tables will replace Table 17-2, Table 17-3 and Table 17-5 in the approved version of WCAP-16996-P.

[]

[]^{a,c}

It is worthwhile to point out that the condensation heat transfer rate could be interpreted from the measured downcomer temperatures (see Tables 4 and 5) in the tests using the following equation.

$$Q_{net} = m_{SI} (h_{DC} - h_{SI})$$

[]

] ^{a,c}

In summary, the approach to evaluate the condensation rate in the downcomer is revised to better capture the condensation heat transfer rate in the cold leg of COSI facility and to quantify the uncertainties of the condensation heat transfer rate. The revised Westinghouse COSI and Framatome COSI data are shown in Table 4 and Table 5, respectively.

(3) In current submittal of WCAP-16996-P, all the 5 runs in the pair of [] ^{a,c} tests were utilized to establish the condensation rate in the downcomer [] ^{a,c}. In the revised data reduction process in the response to question (2), all the 5 runs in the pairs of [] ^{a,c} are utilized to establish the nominal downcomer condensation efficiency and its uncertainty at three different pressures.

4) When the condensation rate in the downcomer was revisited, the influence of [] ^{a,c} were recognized. Among the parameters, [] ^{a,c} are primary. Regarding the SI temperature, [] ^{a,c} In the Framatome COSI tests, [] ^{a,c} However, the high downcomer water level in the Framatome COSI tests significantly reduced the magnitude of the downcomer condensation rate such that the influence of [] ^{a,c} Other parameters, such as [] ^{a,c} are judged as the secondary effect for the evaluation of the downcomer condensation rate.

Reference:

1. WCAP-11767, "COSI SI/Steam Condensation Experiment Analysis," March 1988.



Figure 1. Comparison between the nominal measured Nusselt number and the Nusselt number predicted from correlation. The measured Nusselt number is reduced from the boiler power.



Figure 2. Comparison between the nominal measured Nusselt number and the Nusselt number predicted from correlation. The measured Nusselt number is reduced from the downcomer temperature.

Table 1. Evaluation of Downcomer Condensation Efficiency at []^{a,c}

a,c

Table 2. Evaluation of Downcomer Condensation Efficiency at []^{a,c}

A large empty rectangular box with a black border, intended for a drawing or diagram.

a,c

a,c

Table 4. Westinghouse COSI Test Data

Table 4. Westinghouse COSI Test Data (continued)

--

--

Table 4. Westinghouse COSI Test Data (continued)

Table 5. Framatome COSI Test Data

RAI #32: Westinghouse Vertical Condensation on Safety Injection Heat Loss

The Westinghouse COSI test data average heat loss and associated uncertainty used to derive the cold leg condensation rates are shown in WCAP-16996-P/WCAP-16996-NP, Volumes I, II and III, Revision 0, Table 17-1, 'Westinghouse COSI Test Data Average Heat Loss and Uncertainty.' [

]^{a,c}

Please provide additional information and clarification with regard to the following items.

- (1) Please explain how the values for the heat loss uncertainty in Table 17-1 were determined. As the heat loss matched the boiler power, please clarify if the heat loss uncertainties corresponded to the uncertainties in the boiler power. [

]^{a,c}

- (2) [

]^{a,c}

- (3) Please explain how the boiler power was measured and provide the measurement accuracy.

- (4) As seen from Table 17-2 in WCAP-16996-P/WCAP-16996-NP, Volumes I, II and III, Revision 0, Subsection 17.2.1, "Test Facilities and Tests Description," the cold leg condensation rates range between []^{a,c}

Considering uncertainties related to heat loss estimates, downcomer condensation rate estimates, and boiler power, please provide estimates for the overall uncertainty of the cold leg condensation data and explain why the data included in Table 17-2 were considered representative and acceptable for the purpose of defining the cold leg condensation correlation.

Response:

- (1) Per the COSI test report [1], the heat loss of a test series was measured by []

[]^{a,c} There were total 15 heat loss measurements at []^{a,c} in Westinghouse COSI tests. In WCAP-16996-P, the heat loss was assumed to be primarily a function of the system pressure. The heat losses at the same pressure were []^{a,c} The results were shown in Table 17-1 of WCAP-16996-P. []

[]^{a,c}

In the response to RAI 31, the data reduction process is revised by utilizing []^{a,c}. The approach is consistent to the test procedure and leads to a reduced uncertainty of the heat loss.

- (2) The "estimated average heat loss" value is []^{a,c} It is different from the mean value of the uncertainty range. Nevertheless, in the revised data reduction process in the response to RAI 31, the averaged heat loss is not used.

- (3) The boiler power is measured by the []^{a,c} Though the detail of the []^{a,c} is not available in WCAP-11767 [1], the uncertainty of the boiler power is given as []^{a,c} The boiler power uncertainty is considered to be a minor factor compared with the uncertainty of the downcomer condensation rate, which is as large as []^{a,c}

- (4) The experimental uncertainties related to condensation heat transfer rate in the cold leg are []

[]^{a,c} As the Westinghouse vertical COSI data were used to generate the correlation and the Westinghouse horizontal COSI data and Framatome COSI data were used for the validation of the cold leg condensation model, the approaches to account for the experimental uncertainty are different.

[

]^{a,c}

Reference:

1. WCAP-11767, "COSI SI/Steam Condensation Experiment Analysis," March 1988.

RAI #33: Westinghouse Vertical Condensation on Safety Injection Data and Condensation outside the Jet Region

WCAP-16996-P/WCAP-16996-NP, Volumes I, II and III, Revision 0, Subsection 6.3.6, "Special Model: Cold Leg Condensation Model," clarifies that "the cold leg condensation model assumes that the majority of condensation occurs in a small region near the SI injection port and the condensation outside the mixing zone is negligible." Accordingly, the cold leg SI condensation rates, described in WCAP-16996-P/WCAP-16996-NP, Volumes I, II and III, Revision 0, Subsection 17.2.1 "Test Facilities and Tests Description," and presented in Table 17-2, "Westinghouse Vertical COSI Tests Data," were derived as integral condensation rates accounting for the condensation processes in the entire cold leg test section. The characteristic of the Westinghouse Vertical COSI condensation rates is further exacerbated by the fact that the Westinghouse Vertical COSI cold leg test section was significantly oversized in length in comparison to a typical PWR []^{a,c}

In WCOBRA/TRAC-TF2 calculations, the cold leg condensation model is applied to the []^{a,c}

Please explain if this can lead to over-prediction of the condensation rate for the entire cold leg region in WCOBRA/TRAC-TF2 PWR LOCA analyses due to condensation in the remaining cold leg cells.

Response:

The length of the cold leg in the Westinghouse COSI facility is over-scaled as discussed in the response to RAI30. The development of the correlation assumes that all the condensation (the net condensation rate after removal of heat losses and downcomer condensation) occurs at the mixing zone.

When the cold leg condensation model is applied to separated effects tests, integral effects tests and PWR LOCA, the special condensation model is []^{a,c}

Additionally, the special condensation model is active only []^{a,c}

The ROSA separate effects test in the validation matrix features a larger cold leg diameter and a properly scaled cold leg length (see the response to RAI 35). The measured condensation heat transfer rate in the cold leg, the predicted cold leg condensation heat transfer rate in the []^{a,c}, and the condensation heat transfer rate of []^{a,c} in the cold leg are collected in Table 1. The measured condensation heat transfer rates are compared with the predicted condensation heat transfer rates of the entire cold leg in Figure 1. []^{a,c}

When the cold leg condensation model is applied to PWR LOCA, in which the cold leg scale is larger than both the ROSA and COSI facility, []^{a,c}. To confirm this, the condensation heat transfer rate in the cold leg of Beaver Valley Unit 1 is studied. []

[]^{a,c}

Figure 2 compares the cold leg condensation heat transfer rate of []^{a,c} in the cold leg starting at the boil-off stage. The condensation heat transfer caused by the SI injection is shown as the solid line and the condensation heat transfer at the accumulator injection node is the blue dashed line. []

[]^{a,c}

The results of ROSA tests and Beaver Valley Unit 1 SBLOCA run show that the flow in the cold leg is mostly horizontal stratified with a low interfacial heat transfer rate. []

[]^{a,c}

During the refill and reflood stages of a large break LOCA, the cold leg flow regime could be []^{a,c} The interfacial heat transfer rate of the []

[]^{a,c} The application of the COSI model to the []^{a,c} prediction of cold leg condensation in the validation against the full scale UPTF 8A and UPTF 25A tests as shown in Sections 17.3 and 19.3 of WCAP-16996-P.

In summary, []

[]^{a,c}

Table 1. ROSA SB-CL-05 SI Condensation Heat Transfer Rate.

	a,c
--	-----

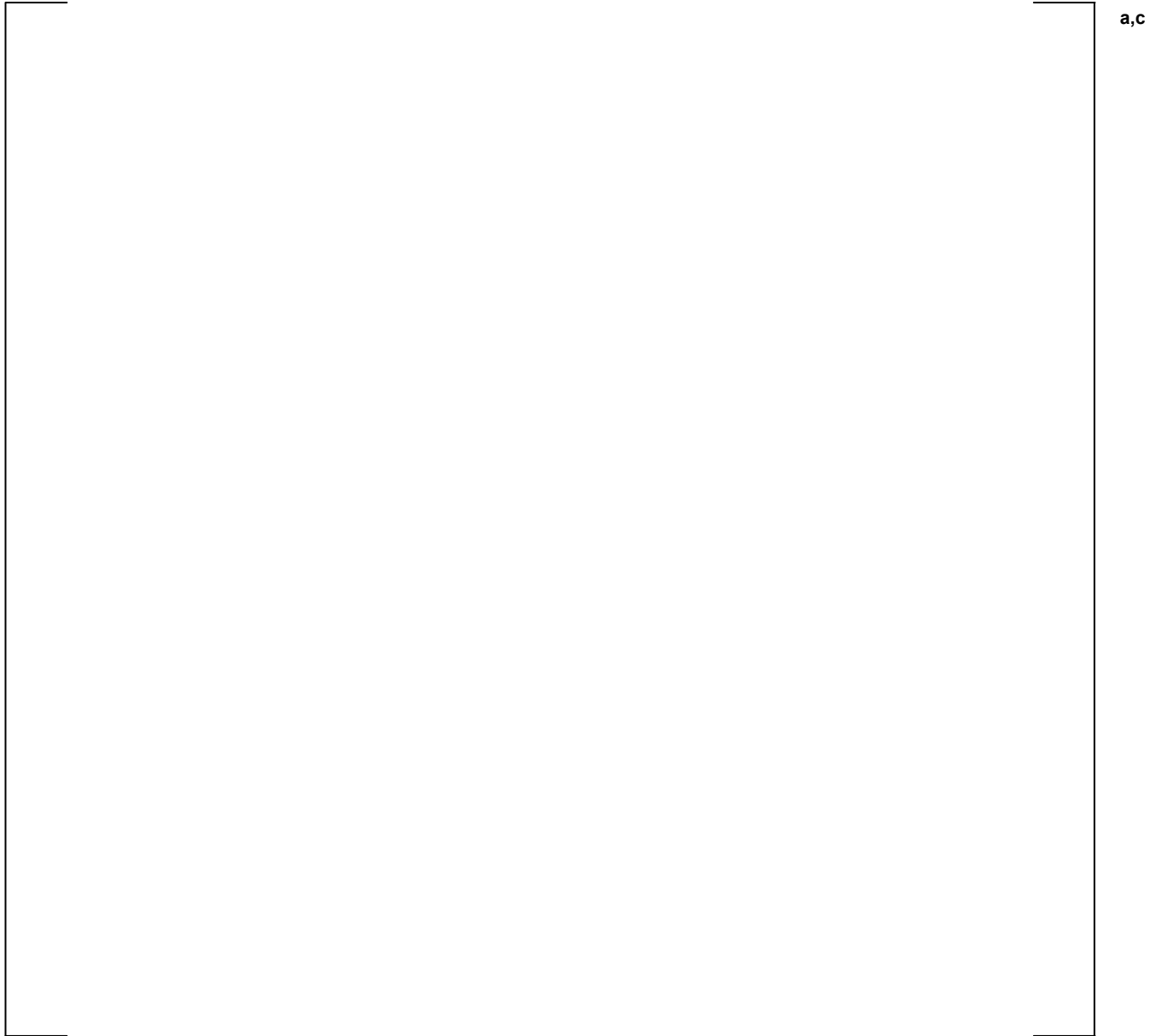


Figure 1. Comparison between the measured cold leg condensation rate in ROSA and the predicted condensation heat transfer rate of the entire cold leg.

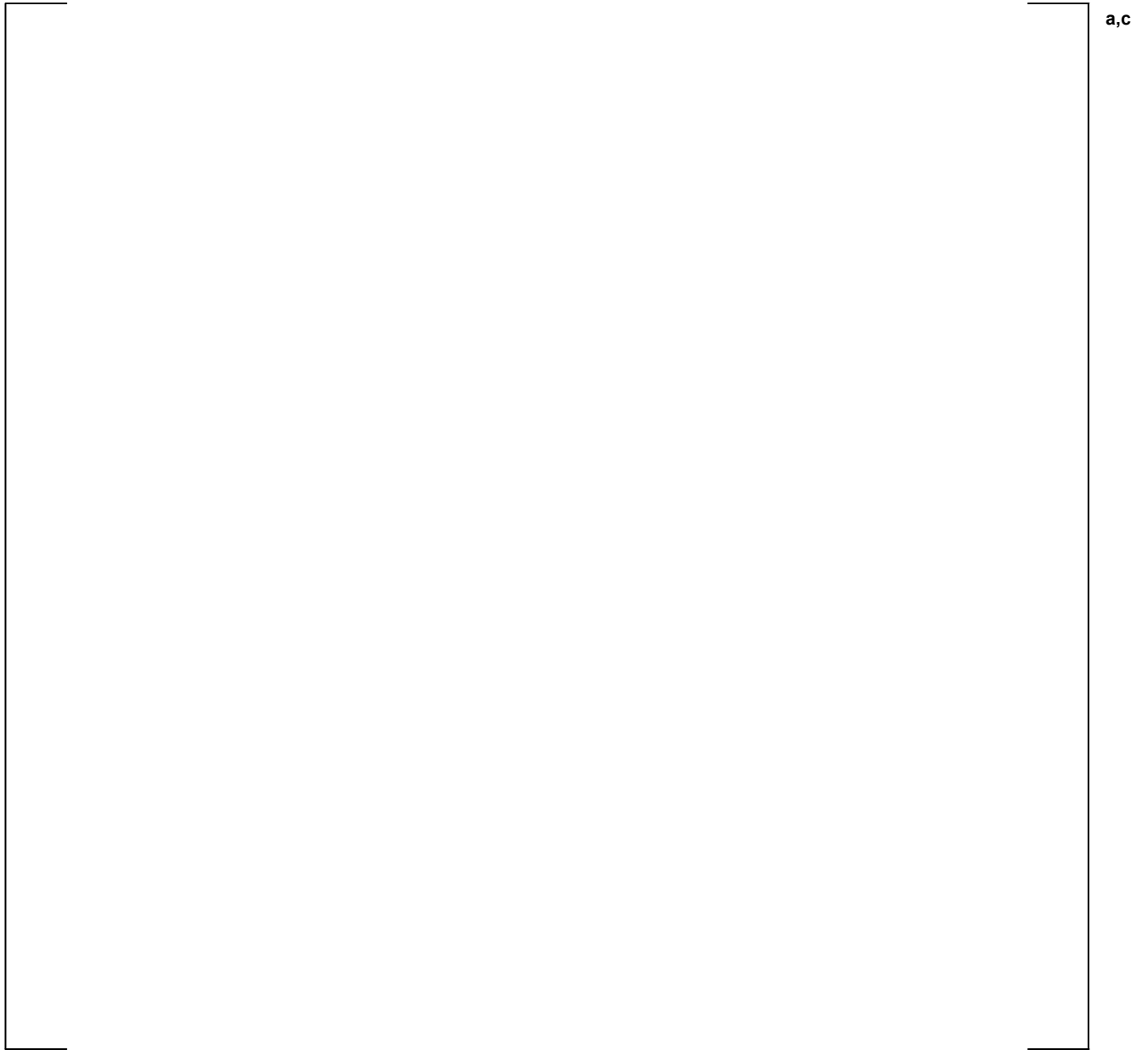


Figure 2. The cold leg condensation heat transfer rate in the []^{a,c} transient.

RAI #34: Westinghouse Vertical Condensation on Safety Injection Data Qualification

With regard to the Westinghouse COSI facility, WCAP-16996-P/WCAP-16996-NP, Volumes I, II and III, Revision 0, Subsection 17.2.1, "Test Facilities and Tests Description," states that "a core series of 15 tests, with 75 individual data, from Westinghouse configuration was conducted." The Westinghouse vertical COSI cold leg condensation rates used to define the empirical correlation for prediction of direct contact condensation on SI water in the cold legs are presented in WCAP-16996-P/WCAP-16996-NP, Volumes I, II and III, Revision 0, Table 17-2, "Westinghouse Vertical COSI Tests Data." The table contains 60 data points. In addition, Figure 6-15 in WCAP-16996-P/WCAP-16996-NP, Volumes I, II and III, Revision 0, presents a comparison between the calculated Nusselt number and the measured Nusselt number for the fitted data points.

Please clarify and address, as needed, the following items related to the set of Westinghouse vertical COSI data, which was utilized to define the SI condensation correlation.

- (1) Please explain if all available Westinghouse vertical COSI test runs were assessed and reported as "points" in the second column of WCAP-16996-P/WCAP-16996-NP, Volumes I, II and III, Revision 0, Table 17-2. Clarify if any estimated condensation rates were disregarded and not included as "points" in Table 17-2 and if so please explain the reasons. In addition, please clarify if all data points in Table 17-2 were plotted in Figure 6-15.
- (2) Table 17-2 provides only the derived condensation rates and does not include the measured boiler power, estimated downcomer condensation rate, and downcomer level. Please provide an expanded table that includes also these test parameters.

Response:

- (1) In Westinghouse COSI tests, there is a total of 75 data points [

]^{a,c}

(2) The measured boiler power and downcomer water level are shown in Table 4 in the response to RAI 31. Table 17-2 will be updated to include the measured boiler power and downcomer water level in the approved version of WCAP-16996-P. The estimated downcomer condensation rate is given in Tables 1 through 3 in the response to RAI 31 and was used to calculate the nominal lower bound and upper bound Qcond values in Table 4.

RAI #35: Scale Impact on Cold Leg Condensation

WCAP-16996-P/WCAP-16996-NP, Volumes I, II and III, Revision 0, Subsection 6.3.6, "Special Model: Cold Leg Condensation Model," and Subsection 17.2.1, "Test Facilities and Tests Description," explain that the Westinghouse horizontal injection COSI dataset, Framatome COSI dataset and ROSA-IV large scale test facility (LSTF) Test SB-CL-05 SI condensation separate effects test dataset were used "to independently perform the validation" of the cold leg condensation model.

The cold leg diameter of the Westinghouse and Framatome test sections was []^{a,c}. The length of the Framatome cold leg test section was only []^{a,c} from the inlet to the downcomer compared with []^{a,c} in the Westinghouse test section. The Westinghouse horizontal COSI test section had an SI line attached at []^{a,c} longitudinal angles with an increased diameter of []^{a,c}. The Framatome COSI test section had an SI line with a diameter of []^{a,c} and was oriented at []^{a,c} azimuthal angle and []^{a,c} longitudinal angles. The downcomer water level in the Framatome COSI tests was at []^{a,c} and the downcomer condensation rate was evaluated using Equation (17-2). A subset of qualified Framatome COSI test runs that had zero break flow vented out of the test facility exiting the cold leg test section were used in the validation process are shown in the Table 17-5.

The LSTF was a 1/48 volumetrically scaled model of a Westinghouse-type 3423 MWt four loop PWR. The cold legs were sized to preserve the volumetric ratio and the pipe length-to-square root of diameter, $L/(D)^{0.5}$, ratio for the reference PWR. The table below summarizes major geometric parameters for the test facility.

Table: Major Geometry Parameters for LSTF ROSA-IV

Parameter	LSTF	Prototype	Length Ratio
Cold leg diameter (in)	8.15	27.5	3.4
SI line diameter (in)	3.44	5.20	1.5
Cold leg pipe length (ft)	12.1	22.9	1.9
Azimuthal angle (deg)	90°	90°/45°	-
Longitudinal angle (deg)	45°	90°	-

For the purposes of validating the cold leg condensation model in the FSLOCA methodology, a simple modeling approach using a TEE component as shown in Figure 17-9, was applied to both the Westinghouse horizontal COSI and Framatome COSI test facilities. The nodding diagram for the ROSA-IV SB-CL-05 safety injection tests was similar to that of the Westinghouse vertical COSI facility. A separate nodding diagram, shown in Figure 17-10, was used for Framatome counter-current COSI tests.

Please clarify the following items related to the validation of the cold leg condensation model in the FSLOCA methodology that was derived from Westinghouse vertical COSI test data.

- (1) Both the Westinghouse and Framatome COSI experiments were performed with the same cold leg diameter of []^{a,c} and with the same downcomer geometry. Key geometry differences involved only the orientation and diameter of the SI injection line. The calculation for the heat loss, downcomer condensation, and upper and lower bound of the cold leg condensation rates for the Framatome tests followed the same procedure that used for the Westinghouse COSI data reduction. Please explain how the Westinghouse horizontal injection COSI dataset and the Framatome COSI dataset contribute to the validation of the FSLOCA methodology cold leg condensation model. Provide the resolution

of identified open items pertaining to the Westinghouse vertical COSI tests that are also applicable to the Westinghouse horizontal injection COSI dataset and the Framatome COSI dataset.

- (2) ROSA-IV LSTF Test SB-CL-05 was used as a separate effects test for cold leg SI condensation by modeling only the cold leg and SI injection portion in ROSA-IV and using test measurements of instantaneous flow conditions in the cold leg at four selected instances []^{a,c} Please explain which of the flow parameters in Table 17-7, "ROSA SB-CL-05 SI Condensation Test Data for separate effects tests (SETs)," were measured and how the provided experimental values were established and qualified. For example, test measurements can exhibit noticeable oscillations in time. For all remaining parameters in Table 17-7, if any, please provide the expressions used for their calculation.
- (3) WCAP-16996-P/WCAP-16996-NP, Volumes I, II and III, Revision 0, Subsection 17.2.2, "Description of WCOBRA/TRAC-TF2 Models," explains that in the cold leg condensation model validation studies based on the Westinghouse horizontal COSI test facility, Framatome COSI test facility, and ROSA-IV LSTF, a simple modeling approach with a TEE component was applied to simulate only "the scaled part of the cold leg" with the side TEE junction representing the injection port. Please explain how "the scaled part of the cold leg" was determined in the assessment studies and show that the applied scaling has no impact on the assessment results.
- (4) The comparison between the calculated condensation rates and the experimentally derived rates for LSTF ROSA-IV SB-CL-05 cold leg condensation test, shown in Figure 17-13, indicates that WCOBRA/TRAC-TF2 under-predicted all four rates. WCAP-16996-P/WCAP-16996-NP, Volumes I, II and III, Revision 0, Section 17, "Cold Leg Condensation: COSI Experiments, ROSA-IV SB-CL-05 Experiment, and UPTF-8A Experiment," does not provide direct comparison of WCOBRA/TRAC-TF2 predictions for the SI condensation rate against test data from test facilities other than COSI and LSTF. Please demonstrate that the WCOBRA/TRAC-TF2 cold leg condensation model will not inherently and systematically over-predict the cold leg condensation rate in PWR LOCA analyses if such a model is based on indirect measurements in a single scaled test facility with regard to PWR cold leg geometry.

Response:

- (1) Both the Westinghouse horizontal COSI tests and the Framatome COSI tests are part of validation matrix for the cold leg condensation model. The only difference between the Westinghouse horizontal COSI tests and the vertical COSI tests is the SI line diameter and the injection angle. Other parameters, such as the system pressure, SI flow rate and boiler power are similar in both tests. It was discussed in the response to RAI 30 that the diameter of SI line is [

]^{a,c}

Framatome COSI shared the same testing facility with Westinghouse COSI but with a shorter cold leg test section as shown in Figure 17-5 of WCAP-16996-P. The shorter cold leg is more appropriate from a scaling standpoint. The scaling effect of the cold leg diameter in the response to RAI 30 is applicable to the Framatome COSI test facility. [

1 of the response to RAI 30, which is []^{a,c} in Westinghouse COSI shown in Table

[]^{a,c}

[]^{a,c}

Since the cold leg diameter is the same for both the Westinghouse COSI tests and the Framatome COSI tests, the discussion on the cold leg diameter effect in the response to RAI 30 is applicable to the Framatome COSI test.

[

] ^{a,c}



Figure 1. Plot of j_g and j_l in the Framatome COSI tests at 7.0 MPa against the Taitel Dukler flow regime map. The horizontal stratified flow regime is inside the solid line.



Figure 2. Plot of j_g and j_l in the Framatome COSI tests at 2.0 MPa against the Taitel Dukler flow regime map. The horizontal stratified flow regime is inside the solid line.

(2) The ROSA SB-CL-05 experiment is an integral effects test featuring high head safety injection toward the cold leg. Unlike the COSI experiment, there was no steady state in the cold leg during the ROSA test. However, it is found that the cold leg flow condition in the boil off stage of SB-CL-05 is stable and the transient is slow. [

] ^{a,c}

The ROSA SB-CL-05 data reduction process included the use of raw data, establishing data points and converting test data to condensation heat transfer rates. First, the measured pressure transient of the experiment was used. [

] ^{a,c}

[

] ^{a,c}

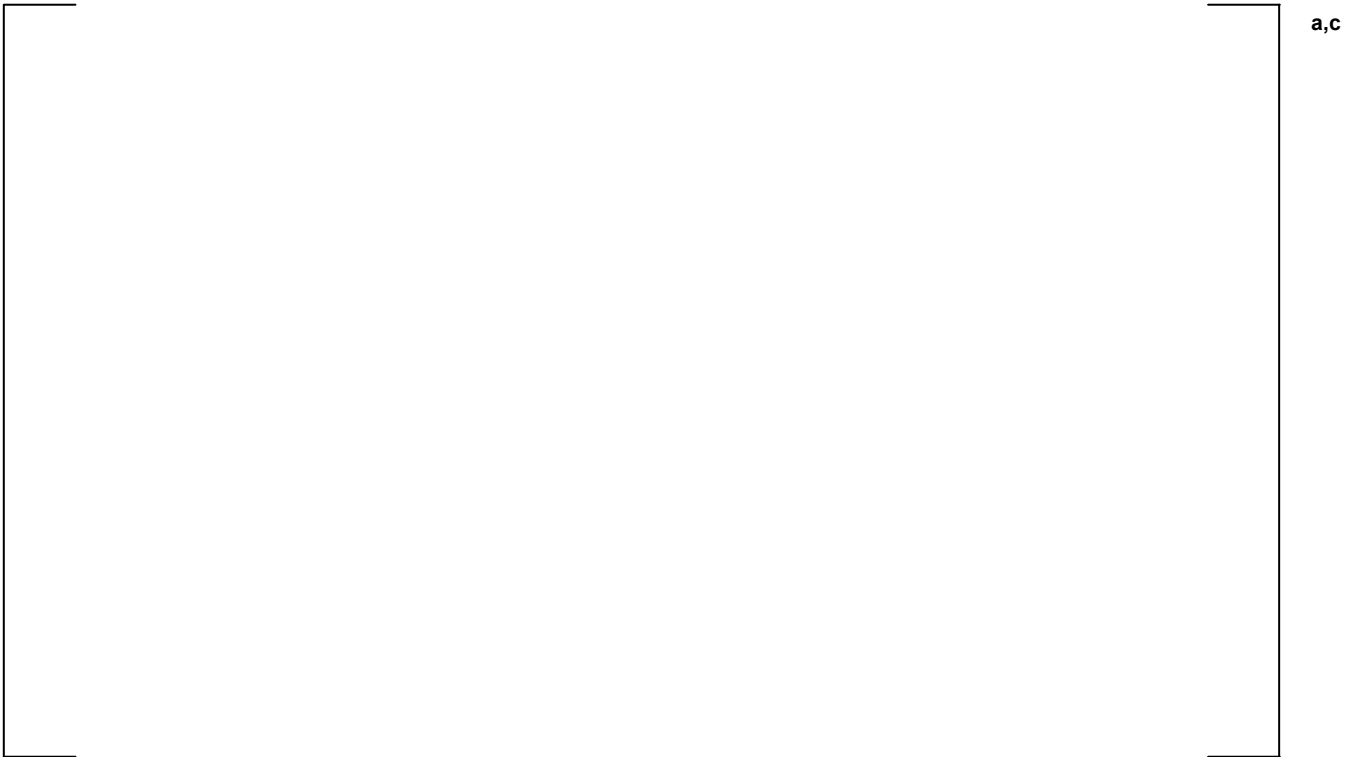


Figure 3. Pressurizer pressure transient in ROSA SB-CL-05 (Figs. 5.7 and 5.8 in Reference [2]).



Figure 4. Measured fluid temperature in the cold leg and SI temperature. (Reference [2]).

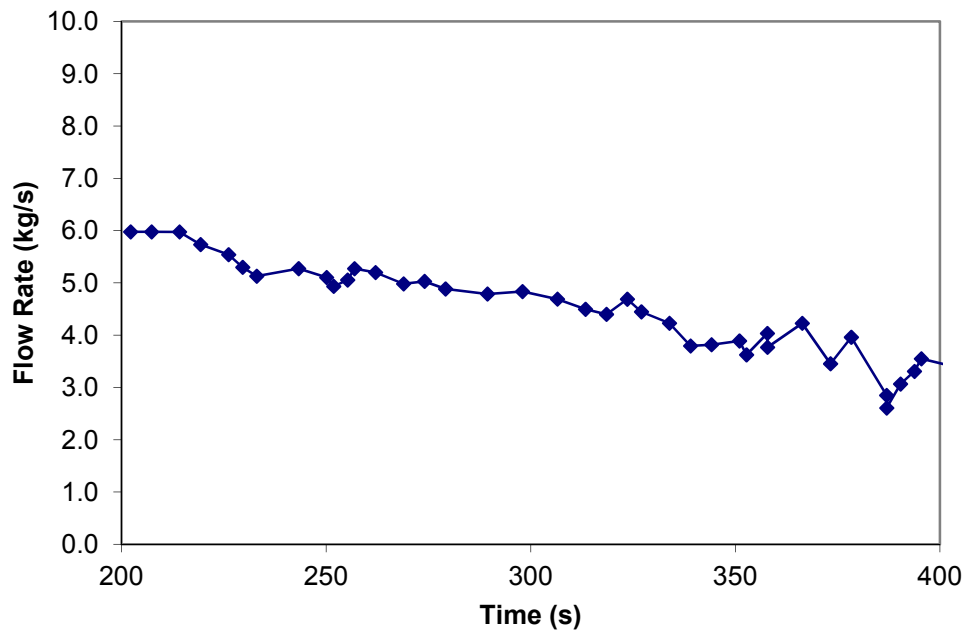


Figure 5. Measured Intact loop (Loop A) steam flow rate in ROSA SB-CL-05. (Reference [2]).

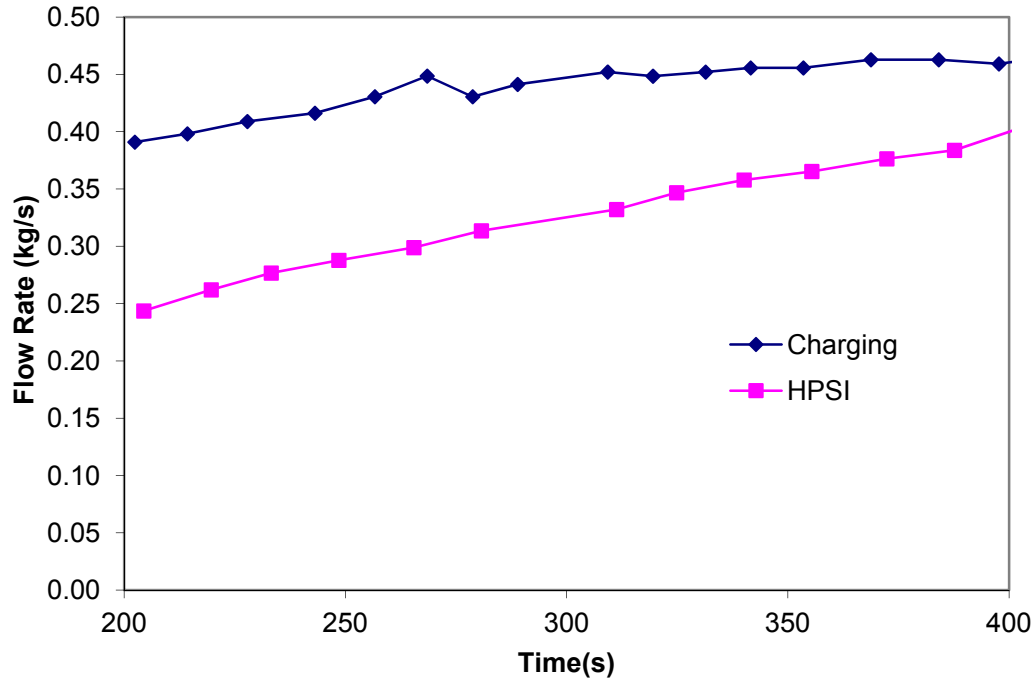


Figure 6. Measured Intact loop (Loop A) ECC flow rates in ROSA SB-CL-05. (Reference [2]).

(3) It is clarified that, in the validation cases, both the Westinghouse horizontal COSI tests and the Framatome COSI tests were simulated with [

] ^{a,c} In the response to RAI 30, it was shown that the extra length of the cold leg in the COSI facility is a secondary effect on the cold leg condensation rate though a bias was introduced. The results of ROSA prediction presented in the response to RAI 33 indicates that the total condensation rate of the properly scaled ROSA cold leg is [

] ^{a,c} The Beaver Valley Unit 1 cold leg condensation prediction also shows that [

] ^{a,c}

(4) The condensation heat transfer rates were compared to the Westinghouse COSI tests, the Framatome COSI tests, and the ROSA SB-CL-05 tests to demonstrate the performance of the cold leg condensation model. However, the data reduction to obtain condensation heat transfer rate followed different approaches. [

] ^{a,c} A detailed data reduction process has been provided in the response to question (2).

The main reason the condensation heat transfer rate comparison was not provided for the assessment of UPTF 8A and UPTF 25A is that, unlike SBLOCA tests of COSI and ROSA SB-CL-05, the temperature measurements in LBLOCA tests such as UPTF 8A showed excessive oscillations. The oscillations impact the data reduction process when converting the cold leg temperature to the condensation heat transfer rate. It is more appropriate to compare the measured cold leg temperature and the predicted cold leg temperature to assess the condensation prediction in LBLOCA cases. [

] ^{a,c} If the condensation heat transfer rate is [

] ^{a,c} Section 17.3 in WCAP-16996-P shows the water temperature at the outlet of the cold leg was [

] ^{a,c}

However, the condensation effect can be indirectly compared with the steam condensation rate. The predicted steam condensation rate in the UPTF 8A loop 2 cold leg is compared with the estimated steam condensation rate by MPR [3]. The steam condensation rate is defined as the steam flow rate difference between the inlet and the outlet of cold leg. Figure 7 shows the predicted values [

] ^{a,c} The steam condensation rate is [

] ^{a,c} Those behaviors are consistent with the cold leg temperature prediction in Section 19.3.8 of WCAP-16996-P.



a,c

Figure 7. Comparison between the predicted steam condensation rate and the measured steam condensation rate in UPTF 8A experiment. The ECC flow rate points (100kg/s to 600kg/s) correspond to UPTF 8A stages 6 through 1.

References:

1. WCAP-11767, "COSI SI/Steam Condensation Experiment Analysis," March 1988.
2. JAERI-memo 61-056, ROSA-IV/LSTF 5% Cold Leg Break LOCA Experiment Data Report: Run SB-CL-05, March 20, 1986.
3. MPR-1208, Summary of Results from the UPTF Cold Leg Flow Regime Separate Effects Tests, Comparison to Previous Scaled Tests, and Application to U.S. Pressurized Water Reactors, MPR Associates, 1992.

**WCAP-16996-P, “Realistic LOCA Evaluation Methodology Applied to the Full Spectrum of Break Sizes
(FULL SPECTRUM LOCA Methodology)”
Request for Additional Information – (Non-Proprietary)
RAIs 36-39**

March 2014

Westinghouse Electric Company LLC
1000 Westinghouse Drive
Cranberry Township, PA 16066

©2014 Westinghouse Electric Company LLC
All Rights Reserved

1 Background

This document provides an overview of the responses to Requests for Additional Information (RAIs) 36-39 [1] on the **FULL SPECTRUM™** LOCA (**FSLOCA™**) Methodology [2] and the updates to the **FSLOCA** methodology related to fuel pellet thermal conductivity degradation (TCD) [

]^{a,c} Along with this overview, the following materials are also provided:

- Responses to RAIs 36-39
- Updates to Sections 2, 8, 11, 25, 26, 29, 30, and 32 of the **FSLOCA** topical report

In RAIs 36-39 [1], further information was requested regarding:

- RAI 36: the modeling of fuel TCD in WCOBRA/TRAC-TF2 (WCT-TF2),
- RAI 37: the effects of TCD on initial stored energy and the modeling of fuel rod burnup,
- RAI 38: the treatment of fuel rod related parameters that are burnup dependent, and
- RAI 39: the fuel burnup sampling approach in the **FSLOCA** methodology.

[

]^{a,c}

Westinghouse has recently submitted the PAD5 fuel rod design methodology [4] that includes explicit treatment of fuel TCD. In conjunction with responding to RAIs 36-39, [

]^{a,c}

The following sections provide a high level summary of the updates made to the **FSLOCA** methodology in each of these categories. The final section provides a summary of the updates made in each of the **FSLOCA** topical sections.

Throughout this overview, items in (*italics*) refer to further detail provided in the attached RAI responses and updated **FSLOCA** topical sections.

ZIRLO is a registered trademark and Optimized ZIRLO, FULL SPECTRUM and FSLOCA are trademarks of Westinghouse Electric Company LLC, its affiliates and/or its subsidiaries in the United States of America and may be registered in other countries throughout the world. All rights reserved. Unauthorized use is strictly prohibited. Other names may be trademarks of their respective owners.

2 []^{a,c}

The Modified Nuclear Fuels Industries (NFI) fuel thermal conductivity model, as included in FRAPCON 3.3 [5], includes explicit treatment of fuel TCD. The **FSLOCA** methodology has been updated to use the Modified NFI model in all analyses with nuclear fuel, including plant analyses. PAD5 calculations are used in initializing WCT-TF2 fuel rods in plant analyses; PAD5 also explicitly accounts for TCD and includes detailed fuel rod models important for predicting initial fuel pellet temperatures and rod internal pressures over the life of the fuel. [

]^{a,c} (Section 11.4, RAI

36, RAI 37)

The consideration of fuel TCD [

]^{a,c}

3 []^{a,c}

[

] ^{a,c} The calculation of MLO includes both pre-accident corrosion and the oxidation occurring during the LOCA, consistent with NRC Information Notice 98-29 [7]. [

] ^{a,c} The NRC has initiated the formal process to revise 10 CFR 50.46, and it is anticipated that the MLO criterion will be replaced with an Equivalent Cladding Reacted (ECR) limit based on cladding hydrogen content (along with other considerations). A submittal (Appendix A) will be provided at a later date that describes how the **FSLOCA** evaluation model (EM) will comply with the known elements of the 10 CFR 50.46c rulemaking when the rulemaking process is complete. (*RAIs 38 and 39, Sections 29.4, 30.1, and 32*)

[

] ^{a,c}

4 []^{a,c}

Because [

] ^{a,c}

[

] ^{a,c}

5 Summary

The updates to the **FSLOCA** methodology to explicitly consider TCD have prompted a set of closely related updates and improvements. The updates to the **FSLOCA** topical sections included in this response package are as follows:

Section 2: (Section 2.3.2.1)

- Updates to [

] ^{a,c}

Section 8: (Sections 8.4, 8.4.1, and 8.6)

- Updates related to [

] ^{a,c}

Section 11: (Section 11.4)

- Update to identify the use of the Modified NFI fuel thermal conductivity model.

Section 25: (Introduction, Sections 25.1, 25.2, 25.8)

- Updates related to [

] ^{a,c}

Section 26: (Sections 26.4, 26.5)

- Updates for [

] ^{a,c}

Section 29: (Introduction, Sections 29.4.1, 29.4.2, 29.5.1, and 29.7)

- Updates for [

] ^{a,c}

[

] ^{a,c}Section 30: (Sections 30.1, 30.4, 30.5, 30.6, and 30.7)

- Updates to identify that MLO is calculated as the sum of pre-accident oxidation and the oxidation occurring during the LOCA.
- Updates to [

] ^{a,c}Section 32: (Sections 32.1, 32.2, and 32.4)

- Updates to identify that MLO is the sum of pre-accident oxidation and the oxidation occurring during the LOCA.

References:

1. Letter from E. Lenning to J. Gresham, "Request for Additional Information Re: Westinghouse Electric Company Topical Report WCAP-16996-P Volumes I, II, and III, Revision 0/WCAP-16996-NP, Volumes I, II, and III, Revision 0, 'Realistic LOCA Evaluation Methodology Applied to the Full Spectrum of Break Sizes (FULL SPECTRUM™ LOCA Methodology),' – FOURTH SET (TAC No. ME5244)," August 15, 2012.
2. WCAP-16996-P (Proprietary), WCAP-16996-NP (Non-Proprietary), "Realistic LOCA Evaluation Methodology Applied to the Full Spectrum of Break Sizes (FULL SPECTRUM LOCA Methodology)," November 2010.
3. WCAP-15063-P, Revision 1 (Proprietary), WCAP-15064-NP, Revision 1 (Non-Proprietary), "Westinghouse Improved Performance Analysis and Design Model (PAD 4.0)," 1999.
4. WCAP-17642-P (Proprietary), WCAP-17642-NP (Non-Proprietary), "Westinghouse Performance Analysis and Design Model (PAD5)," 2013.
5. NUREG/CR-6534, Volume 4, "FRAPCON-3 Updates, Including Mixed-Oxide Fuel Properties," Pacific Northwest National Laboratory, 2005.
6. LTR-NRC-13-37, "Submittal of Westinghouse Responses to "WCAP-16996-P, 'Realistic LOCA Evaluation Methodology Applied to the Full Spectrum of Break Sizes (FULL SPECTRUM LOCA Methodology)' Request for Additional Information" (Proprietary/Non-Proprietary), Project 700, TAC No. ME5244." June 5, 2013.
7. Roe, J., "NRC Information Notice 98-29: Predicted Increase in Fuel Rod Cladding Oxidation," August 3, 1998.

Question #36: Fuel Thermal Conductivity Model

WCAP-16996-P/WCAP-16996-NP, Volumes I, II and III, Revision 0, Section 11.4, "Thermal Properties of Nuclear Fuel Rod Materials," explains that the COBRA/TRAC-TF2 default nuclear fuel rod model computes the UO_2 thermal conductivity from a MATPRO-9 correlation to reduce computer time. It is also explained that this correlation has the same error band of 0.2 W/(m-K) and gives very nearly the same conductivity over the expected operating range of 500 K to 3,000 K when compared to the more complex version in MATPRO-11. Section 11.4 also states that an additional optional model is also provided in WCOBRA/TRAC-TF2 to account for the effects of burnup on thermal conductivity. The model, referred to as "the modified Nuclear Fuel Industries (NFI) model," is described as based on the Nuclear Fuels Industries (NFI) model by Ohira and Itagaki, on pages 541-549 of "Thermal Conductivity Measurements of High Burnup UO_2 Pellet and a Benchmark Calculation of Fuel Center Temperature," in Proceedings of the ANS international topical meeting on LWR Fuel Performance, Portland, Oregon, March 2-6, 1997. Section 11.4 also provides the range of applicability of the modified NFI correlation with regard to temperature, rod-average burnup and as-fabricated density in accordance with NUREG/CR-6534, "FRAPCON-3 Updates, Including Mixed-Oxide Fuel Properties," Vol. 4, 2005.

Please clarify the following items related to the default nuclear fuel rod model in WCOBRA/TRAC-TF2 and the modeling approach to account for the effects of burnup on fuel thermal conductivity in LOCA analyses.

- (1) The default thermal conductivity model in WCOBRA/TRAC-TF2, based on a MATPRO-9 correlation, does not explicitly account for fuel thermal conductivity degradation with burnup. Please describe the purpose of this model and state the conditions under which its application in LOCA analyses is considered acceptable and justify so. If overestimation of thermal conductivity can be associated with the application of the model for such analyses, are there any other code adjustments in WCOBRA/TRAC-TF2 to compensate for this limitation.
- (2) The additional optional model implemented in WCOBRA/TRAC-TF2 to account for the effects of burnup on thermal conductivity is based on a modification of the NFI correlation, which agrees with Equation (2.3-9) in NUREG/CR-7024, "Material Property Correlations: Comparisons between FRAPCON-3.4, FRAPTRAN 1.4, and MATPRO," March 2011. Such a burnup dependant model was not available in the previous ASTRUM LBLOCA methodology documented in WCAP-16009-P-A (Nissley, M. E., et al., 2005). Please describe the conditions under which this "additional optional model" is considered applicable in FSLOCA LOCA analyses and provide justification.
- (3) Please explain how the WCOBRA/TRAC-TF2 nuclear fuel rod model was evaluated for predicting degradation of fuel thermal conductivity with burnup. Describe how contributions from other processes and models such as gap conductance, fission gas release, and radial power profile were taken into consideration in the evaluation. Present analysis results, if available, and provide references to existing assessments that demonstrate the applicability of the model for the purposes of the FSLOCA methodology applications. Include findings from benchmarking against measured data, if available.

- (4) The current Westinghouse fuel rod design methodology (approved by NRC in July 2000) is based on the Performance Analysis and Design (PAD) 4.0 fuel performance code, “Westinghouse Improved Performance Analysis and Design Model (PAD 4.0),” WCAP-15063-P-A/WCAP-15064-NP-A, Revision 1. The PAD 4.0 code has a thermal conductivity model with no burnup dependence. Please explain if specialized fuel performance codes were used in support of the evaluation of the WCOBRA/TRAC-TF2 nuclear fuel rod model for predicting fuel thermal conductivity degradation with burnup. If this was the case, please present the assessment results and include comparison of prediction results for fuel temperatures and rod internal pressures obtained by the codes using the same input conditions. Provide references to the available assessment documentation.

Response:

In conjunction with the response to RAIs 36-39, the aspects of Section 11 and 29 of the FSLOCA Topical report [1] related to fuel rod burnup and pellet thermal conductivity have been updated. Along with those updates, the response to RAI 36 describes the updated fuel thermal conductivity treatment. When referring to the contents of Sections 11 and 29, this response is referring to the updated section.

Response to Parts (1) and (2) of the RAI

The revised Section 11.4.1 of WCAP-16996-P describes a version of the Nuclear Fuels Industries (NFI) thermal conductivity model as modified in FRAPCON 3.3 [2], which explicitly accounts for thermal conductivity degradation (TCD) with burnup. This modified NFI model will be used in FSLOCA plant analyses and in the simulation of validation tests (e.g. LOFT) involving UO₂ fuel pellets.

The MATPRO-9 correlation described in the original Section 11.4.1 of WCAP-16996-P is no longer included in the FSLOCA analysis methodology.

Response to Part (3) of the RAI

As stated in the revised Section 11.4.1, the modified NFI fuel thermal conductivity model is applicable over the following range of conditions (see also Section 2.4 of [2]):

Temperature	=	300 – 3000K
Rod-Average Burnup	=	0 – 62 GWD/MTU
As-fabricated Density	=	92 – 97% Theoretical Density

The above conditions cover the range expected for the FSLOCA EM.

The updated Figure 11-29 of WCAP-16996-P, taken from Figure 2.4 of [2], shows that the thermal conductivity model compares well to unirradiated pellet material data. Section 2.3 of [2] also shows that the model is adequate for predicting the conductivity of irradiated material.

Westinghouse has recently developed, and submitted to the USNRC, an updated version of the PAD fuel performance code, PAD5 [3]. The updated fuel performance code is designed to supersede PAD 4.0 and

FATES3B. Among other features, PAD5 includes an explicit treatment of burnup-related phenomena such as fuel TCD.

The final, approved version of PAD5 will be the fuel performance interface to the FSLOCA EM. As described in Section 4.3 of [3], the PAD5 code includes models for accurate prediction of fission gas release. Section 3.6.2 of [3] describes the PAD5 pellet radial power distribution model. [

] ^{a,c}

Figure RAI36-1 shows a comparison of the modified NFI conductivity model used in WCOBRA/TRAC-TF2 (WCT-TF2) and the model in PAD5 [3]. [

] ^{a,c}

As described in Section 11.4.4 of [1], the gas conductance is calculated based on the individual species' mole fractions and their respective thermal conductivity correlations. The thermal conductivity correlations for the fill and fission gases, taken from MATPRO-11 Rev.1 and shown in Section 11.4.4 of [1], [

] ^{a,c}

In WCT-TF2, a temperature jump distance is used in Equation 8-29 of [1] to compensate for the nonlinearity of the temperature gradient near the walls and the temperature discontinuities on the wall surface that result from incomplete thermal mixing of the gas molecules near the surface. Similarly, considerations are made in the PAD5 code as described in Sections 3.5.2 and 3.5.3 of [3], although this effect is neglected for all gases except Helium.

The pellet-cladding contact conductance model is described in Section 8.3.2 of [1], and was chosen based on its agreement with a wide range of contact conductance data. [

] ^{a,c}

Response to Part (4) of the RAI

[

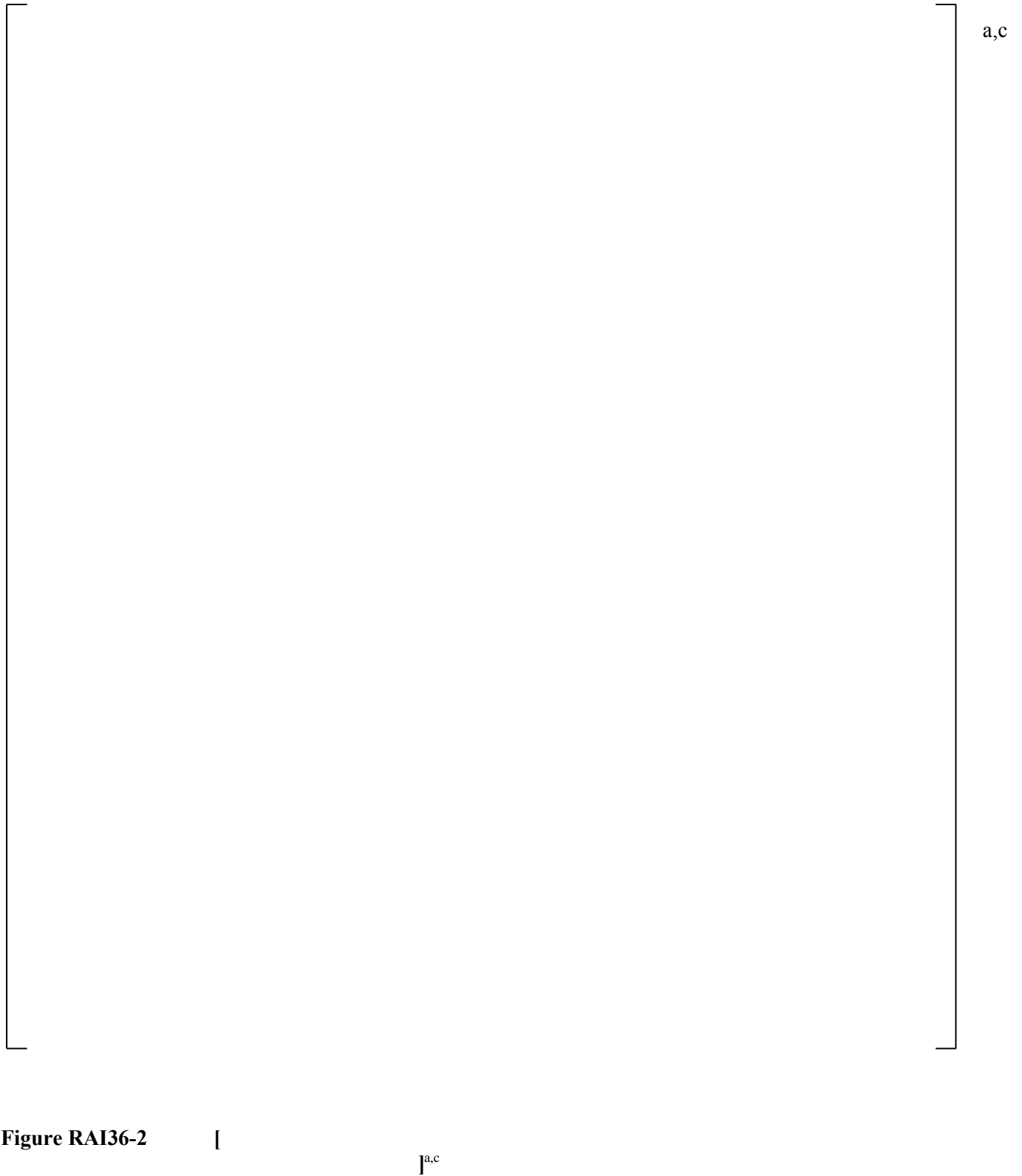
]^{a,c} The thermal conductivity model for the pellet in WCT-TF2 relies on an industry-accepted correlation that has been benchmarked to test data and has been found to be applicable over the range of conditions expected in the FSLOCA EM in [2]. Similarly, [

]^{a,c}**References:**

1. WCAP-16996-P, “Realistic LOCA Evaluation Methodology Applied to the Full Spectrum of Break Sizes (FULL SPECTRUM LOCA Methodology),” November 2010.
2. NUREG/CR-6534, Volume 4, “FRAPCON-3 Updates, Including Mixed-Oxide Fuel Properties,” Pacific Northwest national Laboratory, 2005.
3. WCAP-17642-P (Proprietary), WCAP-17642-NP (Non-Proprietary), “Westinghouse Performance Analysis and Design Model (PAD5),” 2013.
4. NUREG/CR-1845, “FRAPCON-2: A Computer Code for the Calculation of Steady State Thermal-Mechanical Behavior of Oxide Fuel Rods,” January, 1981.

a,c

Figure RAI36-1**Comparison of WCOBRA/TRAC-TF2 and PAD5 UO₂ Pellet Thermal Conductivity Models**



Question #37: Burnup Impact on Fuel Thermal Conductivity and Initial Stored Energy

Concerned about the impact of irradiation on fuel thermal conductivity, the U.S. Nuclear Regulatory Commission (NRC) issued Information Notice (IN) 2009-23 dated October 8, 2009 (ML091550527). In particular, IN 2009-23 states that “safety analyses performed for reactors using pre-1999 methods may be less conservative than previously understood.” WCAP-16996-P/WCAP-16996-NP, Volumes I, II and III, Revision 0, Section 11.4, “Thermal Properties of Nuclear Fuel Rod Materials,” explains that the WCOBRA/TRAC-TF2 nuclear fuel rod model uses a default UO_2 thermal conductivity model based on a MATPRO-9 correlation that does not account for the effect of degradation with burnup. An additional optional model based on the Nuclear Fuels Industries (NFI) model by Ohira and Itagaki (1997) is provided to account for the effects of burnup on thermal conductivity.

With regard to LOCA applications, WCAP-16996-P/WCAP-16996-NP, Volumes I, II and III, Revision 0, Section 8.6 explains that the steady state fuel temperature is calibrated against the PAD code and refers to WCAP-16996-P Section 29. Subsection 29.4.2.2, “Initial Calibration of the Steady-State Condition for the Nuclear Rods,” explains that the initial fuel temperature and rod internal pressure for Westinghouse pressurized water reactors (PWRs) are calibrated against the PAD 4.0 fuel performance code, “Westinghouse Improved Performance Analysis and Design Model (PAD 4.0),” WCAP-15063-P, Revision 1, 1999. The calibration for Combustion Engineering (CE) PWRs is performed against the FATES3B code, “Improvements to Fuel Evaluation Model,” CEN-161(B)-P, Supplement 1-P-A, CE, 1992. Subsection 29.4.2.2 of WCAP-16996-P/WCAP-16996-NP, Volumes I, II and III, Revision 0, Section 29, also states that “the initial fuel temperature is a function of the peak linear heat rate and burnup.”

Please clarify the following items related to the nuclear fuel rod model and modeling approach in WCOBRA/TRAC-TF2 with regard to accounting for the effects of fuel burnup in LOCA analyses.

- (1) Please explain how the FSLOCA methodology accounts for fuel burnup effects in obtaining core thermal-hydraulic parameters and fuel thermal response under steady state for the purpose of initialization of LOCA analyses. Include consideration of factors related to different reactor fuel cycles, reactor operation time in a cycle, and core nodalization. The FSLOCA methodology core nodalization scheme models a single hot rod and a hot assembly and represents the rest of the core by 3 separate assembly groupings: (1) low power assemblies on core periphery, (2) average power interior assemblies under guide tube structures, and (3) average power interior assemblies located under other structures. Please explain how WCOBRA/TRAC-TF2 accounts for individual fuel assembly burnup levels for each of the fuel rods that model the reactor core and justify any assumptions.
- (2) If results from any other codes are used in the FSLOCA methodology to initialize, calibrate, benchmark, match, or in other way alter WCOBRA/TRAC-TF2 calculated results that have an impact on the initial pellet stored energy, please identify these codes, the frozen code versions used, and their approval status with the NRC. In addition, please document in details and explain such calibrating techniques and describe related algorithms, expressions, criteria, limitations, and

assumptions. Justify the applicability and appropriateness of such techniques to account for the effects of fuel thermal conductivity degradation with burnup. Clearly explain how results from the PAD 4.0 or FATES3B codes are used if the code has a thermal conductivity model with no burnup dependence.

- (3) If the FSLOCA methodology employs initial calibration of the steady state condition for the nuclear rods by altering the initial fuel temperature and rod internal pressure, please explain why WCOBRA/TRAC-TF2 predictions results for LOCAs should be considered acceptable in terms of describing the core fuel transient responses. In this regard, please present any supporting analyses, if available.

Response:

In conjunction with the response to RAIs 36-39, the aspects of Section 11, 26, and 29 of the FSLOCA Topical report [1] related to fuel rod burnup, pellet thermal conductivity, and pellet average temperatures have been updated. Along with those updates, the response to RAI 37 describes the updated fuel thermal conductivity treatment and the initialization of the fuel rod in WCOBRA/TRAC-TF2 (WCT-TF2).

Response to Part (1) of the RAI

The response to RAI 39 describes the updated fuel burnup sampling methodology. Please see the response to RAI 39 and the updated Section 29.4.1.1 for a detailed description of how fuel burnup effects are considered in defining the various rods (hot rod, hot assembly rod, core balance rods, and low-power rod). [

] ^{a,c}

Response to Part (2) of the RAI

[^{a,c} PAD5 was recently submitted to the USNRC [2], and is designed to supersede PAD 4.0 and FATES3B. The fuel pellet thermal conductivity models in WCT-TF2 and PAD5 both explicitly account for the effects of fuel thermal conductivity degradation. [

^{a,c} The applicability of the pellet thermal conductivity model used in WCT-TF2 is established in [3], which has shown the model to be applicable within the range expected for the FSLOCA EM.

[

] ^{a,c}

[

] ^{a,c}

Response to Part (3) of the RAI

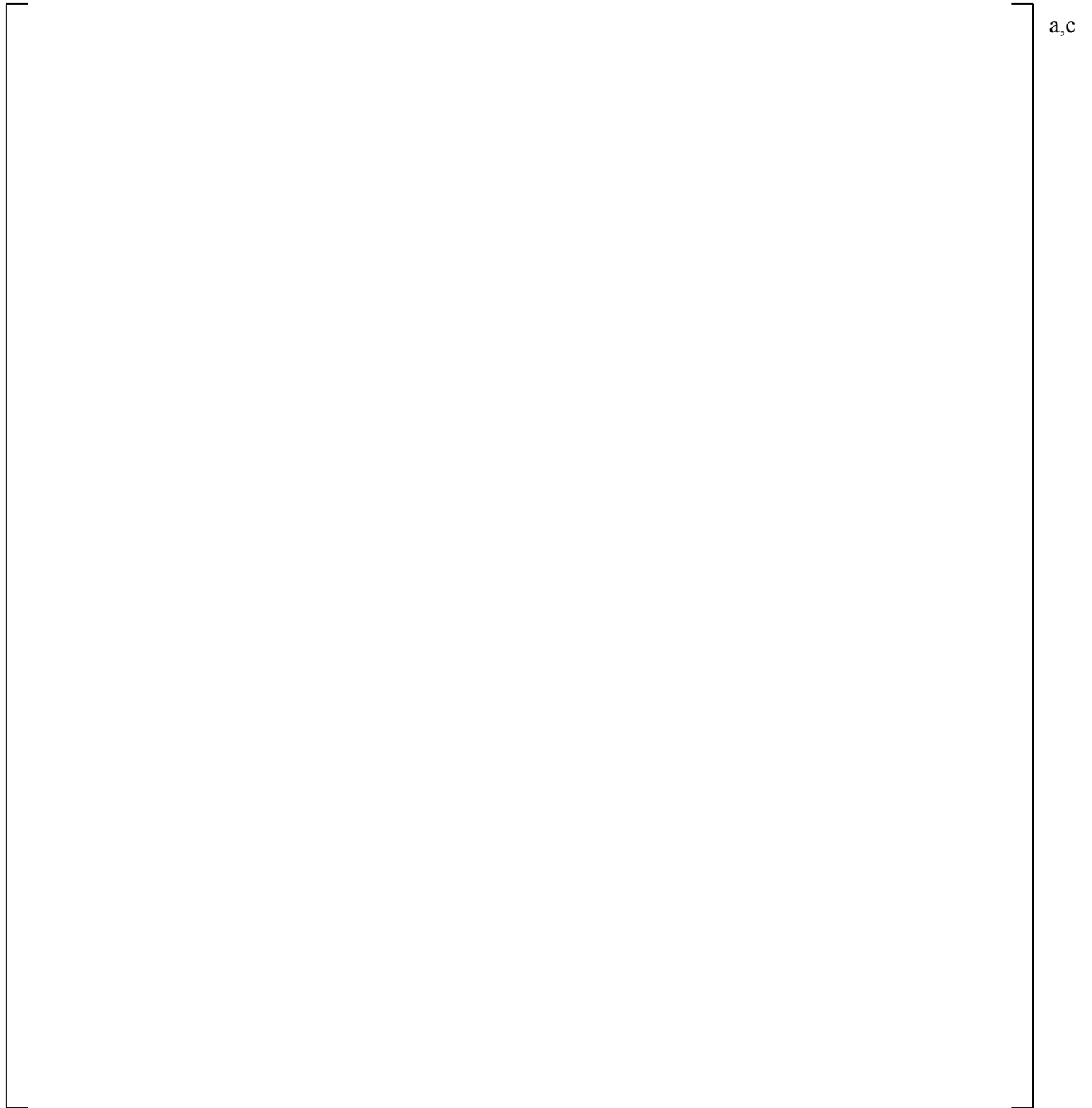
[

] ^{a,c}

[

] ^{a,c}**References:**

1. WCAP-16996-P, "Realistic LOCA Evaluation Methodology Applied to the Full Spectrum of Break Sizes (FULL SPECTRUM LOCA Methodology)," November 2010.
2. WCAP-17642-P (Proprietary), WCAP-17642-NP (Non-Proprietary), "Westinghouse Performance Analysis and Design Model (PAD5)," 2013.
3. NUREG/CR-6534, Volume 4, "FRAPCON-3 Updates, Including Mixed-Oxide Fuel Properties," Pacific Northwest National Laboratory, 2005.



a,c

Figure RAI37-1

[

] ^{a,c}



a,c

Figure RAI37-2

[

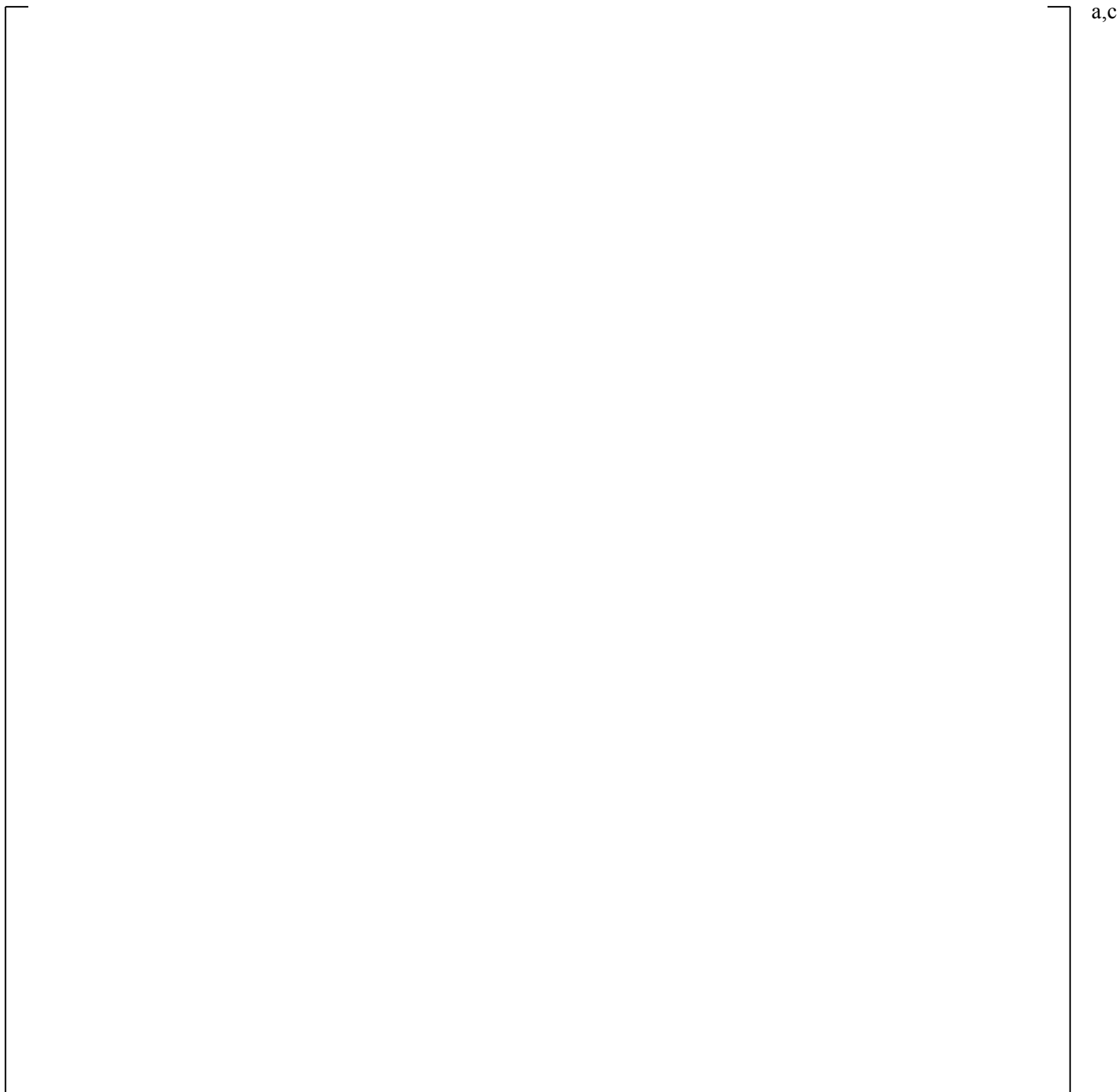
] ^{a,c}



Figure RAI37-3

[

] ^{a,c}

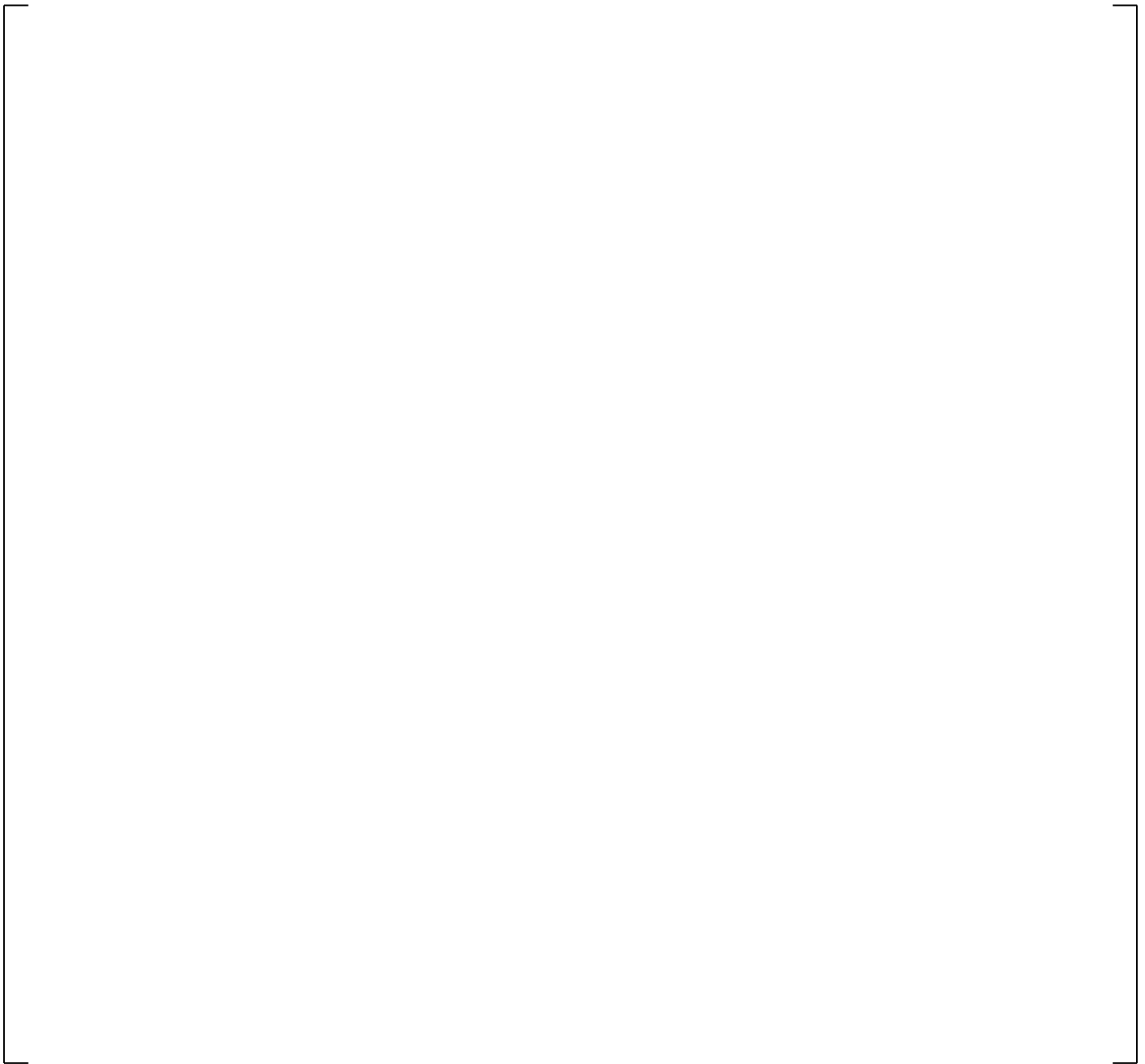


a,c

Figure RAI37-4

[

] ^{a,c}



a,c

Figure RAI37-5

[

] ^{a,c}

a,c

Figure RAI37-6

[

] ^{a,c}

Question #38: Treatment of Fuel Burnup Dependant Parameters

WCAP-16996-P/WCAP-16996-NP, Volumes I, II, and III, Revision 0, Section 29, “Assessment of Uncertainty Elements,” states that “many fuel related parameters are a function of burnup.”

Please clarify the following items related to the consideration of burnup effects on nuclear fuel rod related parameters in the FSLOCATM methodology and the accounting for such effects in LOCA analyses.

- (1) Please identify the parameters that have been identified as dependant on variability in the fuel burnup. Describe the importance of each parameter with regard to its possible impact on steady state initialization results and on LOCA transient predictions obtained by using the FSLOCA methodology.
- (2) Please explain how the functional dependence of each of the identified parameters on the fuel burnup accounts for variability in burnup and provide the burnup range that was considered. Describe how the burnup sampling process proposed for the FSLOCA methodology affects the treatment of each of these parameters.
- (3) From the list of parameters identified as burnup dependant, please identify those that are sampled on their own in the FSLOCA methodology. Explain how burnup is accounted for in the definition of the sampling ranges and sampling distributions for each of these burnup dependant parameters.
- (4) Please provide a table that summarizes the findings in response to the above identified items.

Response:

In conjunction with the response to requests for additional information (RAI) 36-39, the aspects of Section 29 of the FULL SPECTRUM LOCA Topical report [1] related to fuel rod burnup have been updated. Along with those updates, the response to RAI 39 describes the updated fuel burnup sampling methodology. Within that context, many fuel-related parameters remain a function of rod burnup, and so it is within that context that a response is provided here. When referring to the contents of Sections 25, 29 and 30, this response is referring to the updated section.

The treatment of the important burnup-related parameters is summarized in Table RAI38-1. The following discussion provides details specific to each of the listed parameters.

[

] ^{a,c}

[

] ^{a,c}

[

] ^{a,c}

As described in Section 30.1, the FSLOCA methodology demonstrates compliance with the 10 CFR 50.46(b)(2) oxidation criterion by showing that the sum of pre-accident oxidation and the oxidation occurring during the LOCA remains below the 17% limit. [

] ^{a,c}

Other nuclear fuel rod parameters are dependent upon the rod average burnup, but are of secondary importance for the steady-state and transient predictions. These parameters are included in the models to ensure reasonable agreement between WCOBRA/TRAC-TF2 (WCT-TF2) and PAD5 with respect to steady state initialization, and their uncertainty is not considered in the FSLOCA methodology.

- Pellet-Cladding Gap Gas Composition (Section 11.4.4): The gas composition as a function of rod average burnup []^{a,c}
- Pellet-Cladding Gap Conductance (Section 8.3.2): The gap conductance is the sum of thermal radiation conductance, conductance of the fill gas, and conductance due to pellet-clad contact pressure. It is calculated using the models in WCT-TF2 []^{a,c}
- Pellet-Cladding Gap Width: []

[]^{a,c}

In summary, one independently sampled parameter in the FSLOCA uncertainty methodology is []

[]^{a,c}

Reference:

1. WCAP-16996-P, “Realistic LOCA Evaluation Methodology Applied to the Full Spectrum of Break Sizes (FULL SPECTRUM LOCA Methodology),” November 2010.

Table RAI38-1 Summary of Important Fuel-Burnup-Dependent Parameters

Parameter	Sampling Approach	Basis
I		
		I ^{a,c}

Question #39: Fuel Burnup Sampling

Please describe the process of fuel burnup sampling as proposed in the FSLOCA methodology. Describe the sampling technique and explain how the proposed sampling approach accounts for fuel burnup variability with regard to space in consideration of fuel assemblies with different burnup in the core (e.g., fresh, once-burned, and twice-burned fuel) as well as for fuel burnup variability with regard to time in consideration of different fuel cycles (non-equilibrium and equilibrium) and reactor operation time in a cycle. In addition to the information in WCAP-16996-P/WCAP-16996-NP, Volumes I, II, and III, Revision 0, Subsection 29.4.1.1, "Time in Cycle," please explain if any such aspects due to burnup variability in space and time have been simplified or ignored in the proposed FSLOCA methodology fuel burnup sampling approach and provide justification.

Response:

In conjunction with the response to RAIs 36-39, the aspects of Section 29 of the FSLOCA Topical report [1] related to fuel rod burnup have been updated. Along with those updates, the response to RAI 39 describes the updated fuel burnup sampling methodology.

As described in the updated Section 29.4.1.1, and further in the response to RAI #38, one parameter that is independently sampled in the FSLOCA uncertainty methodology [

] ^{a,c}

[

] ^{a,c} Regardless of its actual location, the hot assembly is always assumed to reside in the most limiting location relative to the upper internals such that blowdown cooling is minimized and the most limiting LOCA results are calculated. [

] ^{a,c}

Reference:

1. WCAP-16996-P, "Realistic LOCA Evaluation Methodology Applied to the Full Spectrum of Break Sizes (FULL SPECTRUM LOCA Methodology)," November 2010.

Updates to Section 2.3.2.1 of WCAP-16996-NP

“Realistic LOCA Evaluation Methodology Applied to the

Full Spectrum of Break Sizes

(FULL SPECTRUM LOCA Methodology)”

2.3.2 Identification of System, Components, Processes and Ranking

2.3.2.1 Fuel Rod

Stored Energy

The stored energy is the total energy content of the fuel rods, and its spatial distribution, at the initiation of the transient. The stored energy is primarily a function of axial and radial power distributions throughout the core, pellet-clad gap conductance, and fuel thermal conductivity. The time in the fuel cycle at which the transient occurs affects the stored energy primarily through the [fuel thermal conductivity and the gap conductance](#). [

] ^{a,c}

Clad Oxidation

At high temperatures the zirconium base metal in the clad undergoes an exothermic reaction with the steam. [

] ^{a,c}

[

] ^{a,c}**Decay Heat**

Fission product decay heat is calculated using the American National Standards Institute/American Nuclear Society (ANSI/ANS) 5.1-1979 model. Implementation of the model includes consideration of the spatial distribution, and uncertainty of the decay heat itself. The power history during the transient is also considered in the Westinghouse analysis methodology. This affects the local power of all fuel rods included at the PCT location.

[

] ^{a,c}**Clad Deformation (Burst Strain, Relocation)**

As the system depressurizes below the rod internal pressure, clad swelling and burst can occur. Fuel pellet fragments can relocate into the ballooned section of the clad at the burst location, thereby increasing the local heat generation rate. The clad burst temperature depends on the differential pressure across the clad. Burst strain depends on the metallurgical phase of the clad at the time of burst. [

] ^{a,c}

[

] ^{a,c}

Table 2-1 PIRT for Full Spectrum LOCA for Westinghouse and Combustion Engineering Plants

a,c

Table 2-1 PIRT for Full Spectrum LOCA for Westinghouse and Combustion Engineering Plants
(cont.)

a,c

Table 2-1 PIRT for Full Spectrum LOCA for Westinghouse and Combustion Engineering Plants (cont.)
--

a,c

Table 2-1 PIRT for Full Spectrum LOCA for Westinghouse and Combustion Engineering Plants
(cont.)

a,c

Table 2-2	Requirement Assessment Against FSLOCA PIRT: Model Availability and Need
------------------	--

a,c

Table 2-2 (cont.)	Requirement Assessment Against FSLOCA PIRT: Model Availability and Need
------------------------------------	--

a,c

Table 2-2 (cont.)	Requirement Assessment Against FSLOCA PIRT: Model Availability and Need
------------------------------------	--

a,c

Table 2-2	Requirement Assessment Against FSLOCA PIRT: Model Availability and Need
(cont.)	

a,c

Table 2-2	Requirement Assessment Against FSLOCA PIRT: Model Availability and Need
(cont.)	

a,c

Table 2-2 (cont.)	Requirement Assessment Against FSLOCA PIRT: Model Availability and Need
------------------------------------	--

a,c

Table 2-2	Requirement Assessment Against FSLOCA PIRT: Model Availability and Need
(cont.)	

a,c

Table 2-2	Requirement Assessment Against FSLOCA PIRT: Model Availability and Need
(cont.)	

a,c

Table 2-2	Requirement Assessment Against FSLOCA PIRT: Model Availability and Need
(cont.)	

a,c

Table 2-2	Requirement Assessment Against FSLOCA PIRT: Model Availability and Need
(cont.)	

a,c

Table 2-2	Requirement Assessment Against FSLOCA PIRT: Model Availability and Need
(cont.)	

a,c

Table 2-2	Requirement Assessment Against FSLOCA PIRT: Model Availability and Need
(cont.)	

a,c

Table 2-2	Requirement Assessment Against FSLOCA PIRT: Model Availability and Need
(cont.)	

a,c

Updates to Sections 8.4, 8.4.1 and 8.6 of WCAP-16996-NP

“Realistic LOCA Evaluation Methodology Applied to the

Full Spectrum of Break Sizes

(FULL SPECTRUM LOCA Methodology)”

8.4 FUEL ROD DEFORMATION MODEL

Model Basis

Fuel pellet and cladding dimensional changes will occur during a loss-of-coolant accident, as a result of the thermal and mechanical stresses present in a nuclear fuel rod. The fuel rod deformation model calculates these changes and their effects on the core transient thermal-hydraulics. WCOBRA/TRAC-TF2 calculates the effects of fuel rod deformation on the pellet-cladding gap conductance, the cladding dimensions used in the conduction equation and the calculation of cladding oxidation, the cladding surface heat transfer area, and the continuity and momentum areas of the fluid cells associated with the fuel rods. The modeling of each of these effects is discussed in this section.

Model as Coded

The fuel rod deformation mechanisms which are modeled in WCOBRA/TRAC-TF2 are described in Section 8.4.1. The effects of fuel rod deformation on the core transient thermal-hydraulics are discussed in Section 8.4.2.

8.4.1 Deformation Mechanisms

Fuel Pellet Thermal Expansion

The axial and diametral thermal expansion of the fuel is calculated using the MATPRO-11 (Revision 1) (Hagman, Reymann, and Manson, 1980) FTHEXP subroutine correlation for thermally induced strain in UO_2 . The correlation was simplified by omitting the corrections for molten fuel and mixed oxide (Pu). FTHEXP will return the same numerical value as the correlation in WCOBRA/TRAC-TF2, when FCOMP (weight percent PuO_2) is equal to zero, and when T (fuel temperature) is less than FTMELT (fuel melting temperature). This is apparent by inspection of the subroutine listing in MATPRO.

In this model, the radial cracks in the fuel are assumed to relieve the hoop and radial stresses, allowing unrestrained radial movement of the fuel in each concentric radial node. The total radial movement at the fuel pellet surface is the sum of the expansion in all the fuel nodes.

$$(\Delta r_{th})_{fuel} = \sum_{i=1}^{NFUEL} \epsilon_r(T_i)_j \Delta r_i \quad (8-36)$$

where:

$$\begin{aligned} \epsilon_r(T_i)_j &= \text{thermal strain at axial node } j \text{ and radial node } i \\ &= 1 \times 10^{-5} T_i + 0.04 \exp(-5000/T_i) - 0.003 \\ T_i &= \text{node temperature (K)} \\ \Delta r_i &= \text{thickness of radial node } i \\ NFUEL &= \text{number of radial nodes in the fuel} \end{aligned}$$

The stress-free axial thermal expansion of the fuel pellet stack is calculated in an analogous manner. The fuel pellet stack length change due to the thermal expansion is:

$$(\Delta \ell_{th})_{fuel} = \sum_{j=1}^{NDX} \epsilon_z(\bar{T}_j) \Delta X_j \quad (8-37)$$

where:

$$\begin{aligned} \epsilon_z(\bar{T}_j) &= \text{thermal strain at axial node } j \text{ based on volume-averaged radial node} \\ &\quad \text{temperatures} \\ \Delta X_j &= \text{height of axial node } j \\ NDX &= \text{number of axial nodes} \end{aligned}$$

Cladding Thermal Expansion

The axial and radial thermal expansion of the cladding are calculated using the CTHEXP subroutine correlations from Hargman, Reymann, and Manson (1980). The radial thermal expansion is calculated as:

$$(\Delta r_{th})_{clad} = \epsilon_r(\bar{T}_j) \bar{r} \quad (8-38)$$

where:

$$\begin{aligned} \epsilon_r(\bar{T}_j) &= \text{radial thermal strain at axial node } j \text{ based on the average cladding temperature} \\ &\quad \text{(Table 8-1)} \\ \bar{r} &= \text{cladding mean radius (cold)} \end{aligned}$$

The axial thermal expansion of the cladding is:

$$(\Delta \ell_{th})_{clad} = \sum_{j=1}^{NDX} \varepsilon_Z(\bar{T}_j) \Delta X_j \quad (8-39)$$

where:

$\varepsilon_Z(\bar{T}_j)$ = axial thermal strain at axial node j based on average cladding temperature at node j (Table 8-1)

ΔX_j = height of axial node j

Cladding Elastic Deformation

When the pellet-cladding gap is open, elastic deformation of the cladding is driven by the difference between the fill gas and system pressures. If the gap closes, the cladding deformation is caused by the radial motion of the fuel. In both cases, the cladding is assumed sufficiently thin for the stress, strain, and temperature to be uniform throughout the cladding thickness.

In the open gap elastic deformation model, the cladding is considered as a thin cylindrical shell loaded by internal and external pressures. (Axisymmetric loading and deformation are assumed.) The radial and axial elastic deformation is the result of hoop stress and axial stress caused by pressure difference. These stresses are given by the following equations:

$$\sigma_{\theta} = \frac{r_i P_i - r_o P_o}{\tau_c} \quad (8-40)$$

$$\sigma_Z = \frac{\pi r_i^2 P_i - \pi r_o^2 P_o}{\pi(r_o^2 - r_i^2)} \quad (8-41)$$

where:

r_o = cladding outside radius

r_i = cladding inside radius

τ_c = cladding thickness

P_i = internal fill gas pressure (P_G if the gap is open, Equation 8-46; P_{int} if the gap is closed, Equation 8-49)

P_o = system pressure

The radial stress component is neglected, yielding the following relationships from Hook's Law:

$$\varepsilon_{\theta} = \frac{\Delta r}{r} = \frac{1}{E} (\sigma_{\theta} - \nu \sigma_z) \quad (8-42)$$

$$\varepsilon_z = \frac{\Delta \ell}{\ell} = \frac{1}{E} (\sigma_z - \nu \sigma_{\theta}) \quad (8-43)$$

where:

ε_{θ}	=	hoop strain
ε_z	=	axial strain
E	=	modulus of elasticity (Young's modulus)
ν	=	Poisson ratio, $E / 2G - 1$ where G = shear modulus

The modulus of elasticity and the shear modulus are shown in Table 8-2.

The relations for the cladding radial and axial elastic deformations, then, are:

$$(\Delta r_{el})_{clad} = \varepsilon_{\theta} \bar{r} \quad (8-44)$$

$$(\Delta \ell_{el})_{clad} = \sum_{j=1}^{NDX} \varepsilon_z \Delta X_j \quad (8-45)$$

where:

ε_{θ}	=	hoop strain at axial node j
\bar{r}	=	cladding mean radius
ε_z	=	axial strain at axial node j
Δx_j	=	height of axial node j

The internal fill gas pressure used to determine the cladding elastic deformation when the gap is open is calculated from the relation:

$$P_G = \frac{M \cdot R}{\frac{V_P}{T_P} + \sum_{j=1}^{NDX} \pi \Delta X_j \frac{r_{ci}^2 - r_{fo}^2}{T_G} + \sum_{j=1}^{NDX} \pi \Delta X_j \frac{r_v^2}{T_V} + \sum_{j=1}^{NDX} \pi \Delta X_j \frac{r_{fvoid}^2}{T_F}} \quad (8-46)$$

where:

M	=	gram-moles of gas in fuel rod
---	---	-------------------------------

V_p	= gas plenum volume, including effects of fuel and cladding axial expansion (ft ³) (from Equations 8-37, 8-39, and 8-45)
T_p	= gas plenum temperature (K) (defined as the temperature of the cladding at the top of the fuel rod + 10 K)
ΔX_j	= computational cell length at axial level j (ft)
r_{ci}	= cladding inside radius including thermal and elastic expansion, and creep deformation (ft) (from Equations 8-38, 8-44, and 8-59)
r_{fo}	= fuel outside radius including thermal expansion (ft) (from Equation 8-36)
R	= gas constant (6.1313 ft-lbf/g-mole-K)
r_v	= radius of central void (ft) (from input data)
T_G	= gas gap temperature (K)
T_v	= central void temperature (K)
T_F	= averaged fuel pellet temperature
r_{fvoid}	= radius of additional fuel void in the fuel pellet

This is a static lumped pressure model, similar to those in FRAP or GAPCON. The pressure is assumed uniform throughout the fuel rod, with constant fission gas inventory.

In the closed gap deformation model, the cladding is considered as thin-wall tubing with a specified displacement at the inside and pressure loading at the outside surface. The radial fuel displacement at which contact occurs can be calculated as:

$$(\Delta r_{th})_{fuel} = (\Delta r_{th})_{clad} + (\Delta r_{cr})_{clad} + \tau_{g,cold} - \tau_g|_L \quad (8-47)$$

where:

$\tau_g _L$	= fuel cladding gap width that defines the closed gap (i.e., $3.6 (R_1 + R_2)$ as in Equation 8-33)
$\tau_{g,cold}$	= user-input cold fuel cladding gap width (including burnup-dependent effects)
$(\Delta r_{th})_{fuel}$	= fuel radial thermal expansion (Equation 8-36)

$$(\Delta r_{th})_{clad} = \text{cladding radial thermal expansion (Equation 8-38)}$$

$$(\Delta r_{cr})_{clad} = \text{cladding creep deformation (Equation 8-59)}$$

Fuel radial displacement due to contact is assumed negligible, so the radial elastic deformation of the cladding must be equal to the applied fuel displacement on the inside surface,

$$(\Delta r'_{th})_{fuel} = (\Delta r_{th})_{fuel} - (\Delta r_{th})_{clad} - (\Delta r_{cr})_{clad} + \tau_g|_L - \tau_{g,cold}$$

$$(\Delta r_{el})_{clad} = (\Delta r'_{th})_{fuel} \quad (8-48)$$

The pellet-cladding interfacial pressure generated by the applied displacement can be computed using the equilibrium stress (Equations 8-40 and 8-41), Hook's Law (Equations 8-42 and 8-43), and the applied displacement $(\Delta r'_{th})_{fuel}$. The interfacial pressure is:

$$P_{int} = \frac{(\Delta r'_{th})_{fuel} E \tau_c (r_o^2 - r_i^2)}{\bar{r} [r_i (r_o^2 - r_i^2) - r_i^2 \tau_c \nu]} + P_o \frac{r_o (r_o^2 - r_i^2) - r_o^2 \tau_c \nu}{r_i (r_o^2 - r_i^2) - r_i^2 \tau_c \nu} \quad (8-49)$$

where:

$$(\Delta r'_{th})_{fuel} = \text{applied fuel displacement in cladding (from Equation 8-48)}$$

$$E = \text{modulus of elasticity}$$

$$\tau_c = \text{cladding thickness}$$

$$r_o = \text{cladding outside radius}$$

$$r_i = \text{cladding inside radius}$$

$$\bar{r} = \text{cladding mean radius}$$

$$\nu = \text{Poisson's ratio for the cladding}$$

$$P_o = \text{system pressure (on the outside surface of the cladding)}$$

The elastic deformation when the gap is closed is evaluated using the relation in Equation 8-44, but the internal pressure P_i is defined as the interfacial pressure P_{int} from Equation 8-49 instead of the fill gas pressure P_G from Equation 8-46.

Cladding Creep Deformation

The high-temperature creep model is based on tests performed at the Berkeley Nuclear Laboratories in the United Kingdom. Three cladding material options are available. The first is used for analyses of Westinghouse manufactured Zircaloy-4 cladding, and is based on the work of Donaldson, Healey, and Horwood (1985). The second is used for analyses of Westinghouse manufactured ZIRLO[®] cladding, and is based on the work of Donaldson and Barnes (1989), and Donaldson, Barnes, and Hall (1989). An additional option is available for analyses of the Sandvik manufactured Zircaloy-4 cladding used in the NRU experiments, and is based on the work of Donaldson, Horwood, and Healey (1982).

The Berkeley test data indicate that high-temperature creep of the cladding materials of interest is well described by a power law stress dependence and an Arrhenius temperature dependence.

$$de/dt = A' \sigma^n \exp(-Q/RT) \quad (8-50)$$

where:

de/dt	=	creep rate (sec^{-1})
σ	=	hoop stress (MPa)
Q	=	activation energy, cal/gm-mole
R	=	gas constant, 1.987 cal/gm-mole/K
T	=	temperature (K)
t	=	time

and A', n are material-specific functions of T and σ . This relationship for creep is commonly referred to as the Norton creep equation.

The time-dependent hoop stress is given by:

$$\sigma(t) = (d(t)/2\tau(t)) P(t) \quad (8-51)$$

where:

$d(t)$	=	mid-wall cladding diameter
	=	$d_o(1 + \varepsilon(t))$, where d_o = initial mid-wall cladding diameter
$\tau(t)$	=	cladding thickness
	=	$\tau_o / (1 + \varepsilon(t))$, where τ_o = initial cladding thickness
$P(t)$	=	cladding pressure differential
$\varepsilon(t)$	=	engineering strain

If the pressure is assumed to vary linearly over a small increment of time, such that,

$$P(t) = P_o + (dP/dt)\Delta t,$$

where:

P_o	=	cladding pressure differential at the beginning of the timestep
-------	---	---

the time-dependent stress is given by:

$$\sigma(t) = \sigma_o (1 + \varepsilon(t))^2 (1 + ((dP/dt)/P_o)\Delta t), \quad (8-52)$$

where:

$$\sigma_o = \text{hoop stress at the beginning of the timestep}$$

If the temperature is assumed to vary linearly over a small increment of time, such that:

$$T(t) = T_o + (dT/dt)\Delta t,$$

where:

$$T_o = \text{temperature (K) at the beginning of the timestep}$$

Then:

$$\exp(-Q/RT(t)) = \exp(-Q/RT_o(1 + ((dT/dt)/T_o)\Delta t)) \quad (8-53)$$

A good approximation to this expression is:

$$\exp(-Q/RT(t)) = \exp(-Q/RT_o)(1 + (dT/dt)(Q/RT_o^2)\Delta t) \quad (8-54)$$

provided that $|(dT/dt)(Q/RT_o^2)|\Delta t \leq 0.01$.

Substituting Equations 8-52 and 8-54 into 8-50 and allowing for the possibility of negative cladding pressure differentials yields:

$$\begin{aligned} d\epsilon/dt = & (|P_o|/P_o) A' \exp(-Q/RT_o) |\sigma_o|^n (1 + \epsilon)^{2n} \\ & (1 + ((dP/dt)/P_o)\Delta t)^n (1 + (dT/dt)(Q/RT_o^2)\Delta t) \end{aligned} \quad (8-55)$$

The true strain is related to the engineering hoop strain by $\epsilon = \ln(1 + \epsilon)$. Therefore, $d\epsilon = d\epsilon/(1 + \epsilon)$. If we define:

$$\begin{aligned} C_1 &= (|P_o|/P_o) A' \exp(-Q/RT_o) |\sigma_o|^n \\ C_2 &= (dT/dt)(Q/RT_o^2) \\ C_3 &= (dP/dt)/P_o \end{aligned}$$

Equation 8-55 may be rewritten as:

$$d\epsilon/(1 + \epsilon)^{2n+1} = C_1((1 + C_2\Delta t)(1 + C_3\Delta t)^n)dt$$

or

$$(1 + \epsilon)^{-(2n+1)} d\epsilon = C_1(1 + C_3\Delta t)^n dt + C_1 C_2 \Delta t (1 + C_3\Delta t)^n dt \quad (8-56)$$

Integration may be performed using standard integral tables (for example, Beyer, 1978) which yields:

$$(-1/2n)((1+\varepsilon)^{-2n}-1) = C_1/C_3^2((C_3-C_2)((1+C_3\Delta t)^{n+1}-1)/(n+1) \\ + C_2((1+C_3\Delta t)^{n+2}-1)/(n+2)) \quad (8-57)$$

The engineering hoop strain in the timestep Δt is therefore:

$$\varepsilon = [(1 - 2n(\text{Right Hand Side of Equation 8-57}))^{-1/2n} - 1] \quad (8-58)$$

The creep model used in WCOBRA/TRAC-TF2 calculates the incremental engineering hoop strain over a timestep Δt using Equation 8-58. The cladding creep deformation is then calculated as:

$$(\Delta r_{cr})_{clad} = \varepsilon(t) \bar{r} \quad (8-59)$$

where:

$$\begin{aligned} \varepsilon(t) &= \text{engineering hoop strain at end of timestep} \\ \bar{r} &= \text{cladding mean radius} \end{aligned}$$

The maximum timestep for the integration of the Norton creep equation is limited so that $|C_2| \Delta t \leq 0.01$, and the approximation to $\exp(-Q/RT(t))$ remains valid. Details of the model application for the three available cladding options are summarized below.

[

]^{a,c}

Westinghouse Zircaloy-4 Cladding

Donaldson, Healey, and Horwood (1985) report Westinghouse manufactured Zircaloy-4 creep data obtained under constant pressure, constant temperature test conditions. Test specimens were heated to the specified temperature and the temperature was held constant for 10 minutes prior to pressurization. The creep test results indicate the existence of two types of creep behavior (Figure 8-14). Creep in the alpha and beta phases, and part of the mixed phase region, exhibits high stress sensitivity typical of a dislocation climb mechanism. In the low stress/low temperature portion of the mixed phase region the stress sensitivity is significantly reduced. In this region, the creep mechanism is superplastic creep.

Donaldson, Healey, and Horwood (1985) report additional creep test data for [

]^{a,c}

The creep rates shown in Figure 8-14 are programmed in WCOBRA/TRAC-TF2 in the form:

$$de/dt = A\sigma^n \quad (8-60)$$

where the coefficients A and n are functions of temperature and the creep mechanism (Table 8-3). To determine the coefficients A', Q and n for integration of Equation 8-50, the following procedure is used:

$$1. \quad \left[\frac{de/dt}{\sigma^n} \right]^{a,c} \quad (8-61)$$

where:

$$2. \quad \left[\frac{de/dt}{\sigma^n} \right]^{a,c} \quad (8-62)$$

3. Calculate n from:

$$4. \quad \left[\frac{de/dt}{\sigma^n} \right]^{a,c} \quad (8-63)$$

5. Calculate Q from:

$$6. \quad \left[\frac{de/dt}{\sigma^n} \right]^{a,c} \quad (8-64)$$

Westinghouse ZIRLO® Cladding

Donaldson and Barnes (1989) and Donaldson, Barnes, and Hall (1989) report Westinghouse manufactured ZIRLO® cladding creep data obtained under similar test procedures as were used for the Zircaloy-4 tests, with the following notable exception. [

] ^{a,c}

The ZIRLO® cladding creep rates shown in Figure 8-15 are programmed in the form of Equation 8-60, with the coefficients **A** and **n** defined in Table 8-4. The procedure used to obtain the coefficients for the integration of the Norton creep equation is identical to that used for the Westinghouse Zircaloy-4 cladding option.

The ZIRLO® cladding creep model used in WCOBRA/TRAC-TF2 has previously been incorporated into the 1981 Evaluation Model with BASH and the NOTRUMP Evaluation Model (Davidson and Nuhfer, 1990). That reference describes a correction to the creep rate integration which is used in the alpha phase and the portion of the mixed phase region which exhibits dislocation creep, to more accurately predict the measured strain versus time. That correction is also used in WCOBRA/TRAC-TF2. Following integration of the Norton creep equation in the alpha phase and the mixed phase/dislocation creep regions, the strain accumulated during the timestep is reduced by an empirical expression which is a function of the strain accumulated in these regions, i.e.,

$$\varepsilon_e = \frac{\varepsilon}{(1+x)^m} \quad (8-65)$$

where:

ε_e	=	effective strain increment
ε	=	strain increment calculated by Equation 8-58
x	=	summation of ε_e in the strain hardening regimes
m	=	[] ^{a,c} for the alpha phase, [] ^{a,c} for the mixed phase/dislocation creep region

Sandvik (NRU) Zircaloy-4 Cladding

Donaldson, Horwood, and Healey (1982) report creep data for Sandvik Zircaloy-4 cladding specimens in the alpha phase. Testing was confined to the high alpha phase temperature range, based on the expected range of interest for the NRU Materials Test program.

The alpha phase Sandvik Zircaloy-4 cladding creep rates shown in Figure 8-16 are programmed in the form of Equation 8-60, with the coefficients **A** and **n** defined in Table 8-5. [

] ^{a,c}

[]^{a,c} The procedure used to obtain the coefficients for the integration of the Norton creep equation is identical to that used for the Westinghouse Zircaloy-4 cladding option.

Cladding Rupture

Loss of coolant accidents result in depressurization of the reactor coolant system and heatup of the nuclear fuel rods, due to insufficient cooling. The resulting stresses on the cladding may be sufficiently high to cause rupture of the cladding. Correlations which predict the occurrence of cladding rupture and the resulting cladding strains have been incorporated into WCOBRA/TRAC-TF2 for Zircaloy-4 cladding and for ZIRLO[®] cladding. These correlations are described below.

Zircaloy-4 Cladding

Powers and Meyer (1980) have reviewed zircaloy cladding rupture data from a wide range of experimental facilities and have recommended the cladding rupture correlation developed by Chapman (1979). The correlation is given by:

$$T_R = 3960 - \frac{20.4\sigma_E}{1+H} - \frac{8.51 \times 10^6 \sigma_E}{100(1+H) + 2790 \sigma_E} \quad (8-66)$$

where:

T_R	=	rupture temperature (°C)
σ_E	=	engineering hoop stress (kpsi)
H	=	min (1.0, HUR/28°C/sec)
HUR	=	heatup rate

This correlation has been incorporated into WCOBRA/TRAC-TF2, and is used to predict the occurrence of cladding rupture for nuclear fuel rods clad with Zircaloy-4.

The cladding heatup rate in WCOBRA/TRAC-TF2 is treated in the same way as in the LOCTA-IV code (Bordelon et al., 1974). The approach can be explained by using Figure 8-17 which illustrates a number of potential scenarios. The instantaneous heatup rate is used until the cladding temperature is within []^{a,c} of the cladding burst temperature. When this condition is reached (Point A) the cladding temperature and time are recorded to be used as a reference for the calculations. As long as the cladding temperature is []^{a,c}

$$\left[\begin{array}{c} \text{ } \end{array} \right]^{a,c} \quad (8-67)$$

where: []^{a,c}

[]^{a,c}

[

]^{a,c}

[

]^{a,c}

ZIRLO® Cladding

Westinghouse has conducted single rod burst tests of ZIRLO® cladding over a wide range of cladding pressure differentials (100 to 2000 psi), and heatup rates (5 to 50°F/sec) (Davidson and Nuhfer, 1990). The test results have been correlated in the form of rupture temperature as a function of engineering hoop stress, consistent with the Chapman approach. However, the ZIRLO® cladding rupture temperature correlation is not dependent on the heatup rate, as the data show no systematic heatup rate dependence.

The ZIRLO® cladding rupture correlation was defined using the mean of the 10°F/sec heatup rate data. Figure 8-19 shows a comparison of the measured burst temperatures and those predicted by the correlation. The correlation predicts the data well over the entire range of heatup rates included in the test matrix.

A correlation for the ZIRLO® cladding strain following rupture has been developed using the single rod burst test data reported in Davidson and Nuhfer (1990). The resulting correlation is shown with the database in Figure 8-20. The WCOBRA/TRAC-TF2 correlation reflects the alpha phase and beta phase peaks, and [

]^{a,c}

[

] ^{a,c}

8.6 []^{a,c} MODEL

[

] ^{a,c}

The FSLOCA methodology will model the hot assembly rods as []^{a,c}

1. Hot Assembly (HA) Rod Component – A type of active nuclear fuel rod that describes all fuel rods in the hot assembly but the hot pin. []^{a,c} A hot assembly rod is a fully functional fuel rod coupled with the thermal-hydraulic solution and core kinetics. The HA rod will consider all local uncertainty models at their nominal (as coded) value. The HA rod will deform consistently with the fuel rod deformation model discussed in Section 8.4, including creep deformation and rupture deformation. []^{a,c}
2. Hot Rod (HR) Component – A type of active nuclear fuel rod that describes the single fuel pin in the hot assembly, which represents a high power fuel pin. A hot rod is a partially functional fuel rod coupled with the thermal hydraulic solution and core kinetics. All the functions of the HA rod are applied to hot rod except the creep deformation and the rupture deformation are disabled for hot rod. The hot rod considers all applicable local uncertainty models at their nominal value.
3. []

] ^{a,c}

[

] ^{a,c}

A summary of functions of rods in the hot assembly is given in Table 8-6. The local uncertainties in Table 8-6 will be explained in Section 29.

The details of [^{a,c} model are listed below.

[

] ^{a,c}

[

] ^{a,c}

[

 $\text{I}^{\text{a,c}}$

[

 $\text{I}^{\text{a,c}}$

(8-86)

[

 $\text{I}^{\text{a,c}}$

[
] ^{a,c}
[] ^{a,c} (8-86a)
[] ^{a,c}
[] ^{a,c}
[] ^{a,c}

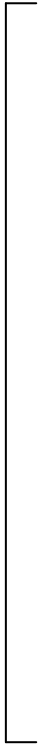
] ^{a,c}

[

] ^{a,c}

Table 8-6	I	J^{a,c}
------------------	----------	------------------------

a,c



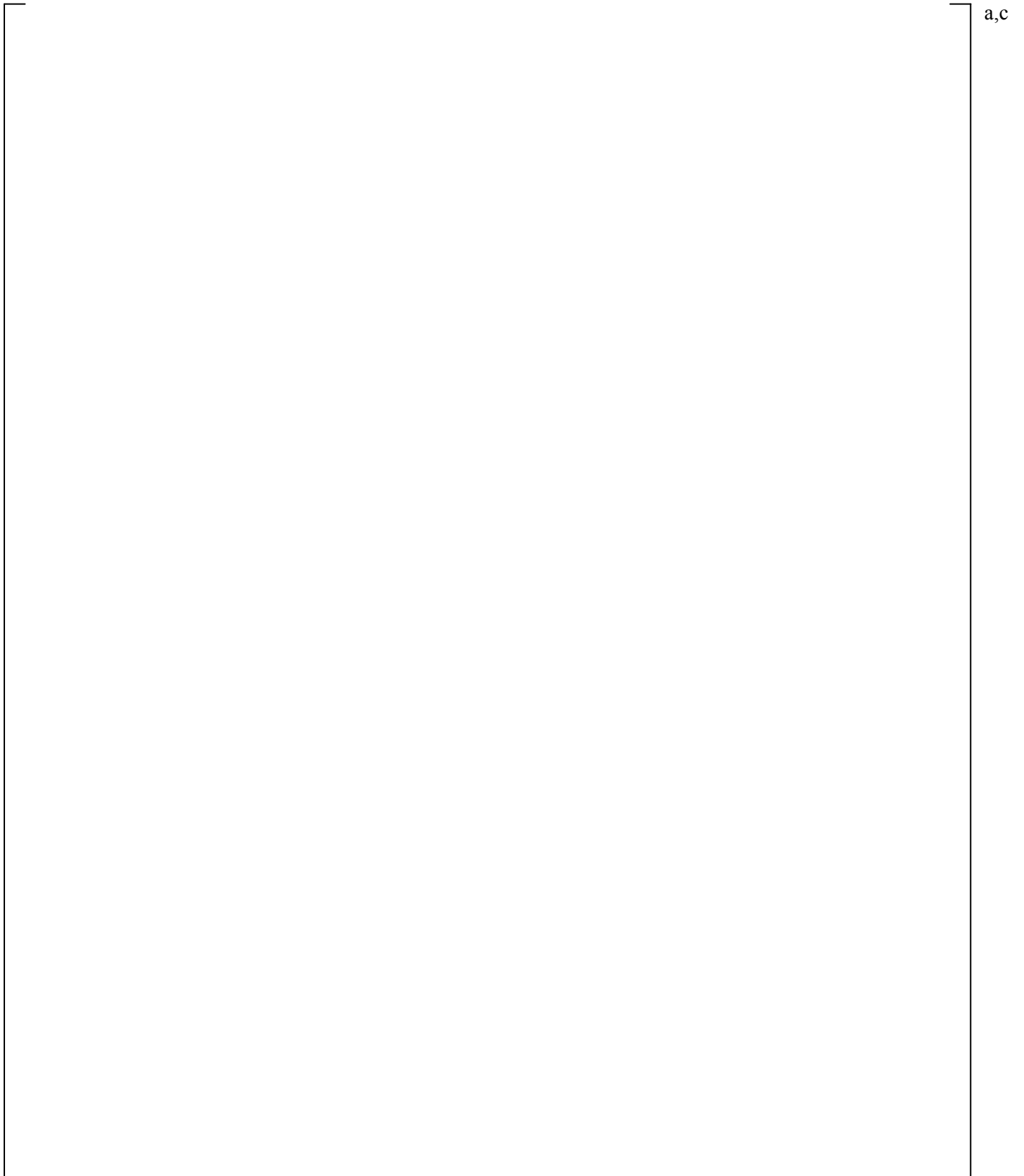


Figure 8-24 [

] ^{a,c}

Updates to Section 11.4 of WCAP-16996-NP

“Realistic LOCA Evaluation Methodology Applied to the

Full Spectrum of Break Sizes

(FULL SPECTRUM LOCA Methodology)”

11.4 THERMAL PROPERTIES OF NUCLEAR FUEL ROD MATERIALS

A typical nuclear fuel rod is composed of uranium-dioxide fuel pellets and a zirconium based clad material. The gap between the fuel pellets and the clad is filled with the initial backfill gas and fission gas. As part of the WCOBRA/TRAC-TF2 default nuclear fuel rod model, the material properties of uranium-dioxide, Zircaloy-4, ZIRLO[®] alloy, and of gas mixtures are included. This section describes the calculation of the thermal properties for these fuel rod materials.

[

] ^{a,c}

11.4.1 Uranium Dioxide

Model Basis

The material properties of uranium dioxide are based on MATPRO-9 (MacDonald et al., 1976) and on MATPRO-11, Rev. 1 (Hagman, Reymann, and Mason, 1980) calculations, with exception to the thermal conductivity model, which is the Nuclear Fuels Industries (NFI) model as modified in FRAPCON 3.3 (Lanning et al., 2005).

Density

The (cold) density for uranium-dioxide is assumed to be:

$$\rho_{\text{UO}_2} = 684.86f_D \quad (11-145)$$

where f_D is the fraction of theoretical density and is input by the user. The density ρ_{UO_2} has units of lbm/ft³.

Thermal Conductivity

The UO₂ thermal conductivity model accounts for the effects of burnup on thermal conductivity. The Nuclear Fuels Industries (NFI) model (Ohira and Itagaki, 1997) was selected as the starting point for a replacement of the Lucuta model (Lucuta et al., 1996) for FRAPCON 3.3 (Lanning et al., 2005). The Lucuta formula for uranium oxide pellet thermal conductivity was found to have two inaccuracies. First, it predicts values at high temperature (>2200 K) that are too large relative to credible modern data for un-irradiated fuel pellet material (Ronchi et al., 1999). Secondly, it has too little burnup degradation compared to both in-cell laser-flash diffusivity measurements on high-burnup pellet samples and in-reactor fuel temperatures measured at nominal to high burnup. For especially this second reason, the NFI model as modified in FRAPCON 3.3 is considered most appropriate. Section 2.3 in (Lanning et al., 2005) shows that the modified NFI model compares well against zero burnup (unirradiated) and irradiated test results.

The NFI model, similar to most other thermal conductivity models utilized in fuel performance codes, consists of a lead term that is inversely proportional to a temperature function $A + BT$ (phonon term), with burnup dependence factors in its denominator, plus terms that model the electronic contribution to fuel heat transfer at high temperature. The modified NFI model implemented in WCOBRA/TRAC-TF2 is defined as follows:

$$K_{95} = \frac{1}{A + B \cdot T + f(\text{Bu}) + (1 - 0.9 \cdot \exp(-0.04 \cdot \text{Bu})) \cdot g(\text{Bu}) \cdot h(T)} + \frac{E}{T^2} \cdot \exp(-F/T) \quad (11-146)$$

where:

K_{95} = Thermal Conductivity, W/m-K, for as fabricated fuel density of 95% of theoretical density (TD)

T = Temperature, K

Bu = Burnup, GWD/MTU

$f(\text{Bu})$ = effect of fission products in crystal matrix (solution)

$$= 0.00187 \cdot \text{Bu} \quad (11-147)$$

$g(\text{Bu})$ = effect of irradiation defects,

$$= 0.038 \cdot \text{Bu}^{0.28} \quad (11-148)$$

$h(T)$ = Temperature dependence of annealing on irradiation defects

$$= \frac{1}{1 + 396 \cdot \exp(-Q/T)} \quad (11-149)$$

Q = Temperature dependence parameter = 6380 K

A = 0.0452 m-K/W

B = 2.46E-4 m/W

E = 3.5E9 W-K/m

F = 16361 K

The model is adjusted for ‘as fabricated’ fuel densities different from 95% TD using the Lucuta recommendation for spherical-shaped pores (Lucuta et al., 1996), as follows:

$$K_d = 1.0789 \cdot K_{95} \cdot \{d/[1.0 + 0.5 \cdot (1 - d)]\} \quad (11-150)$$

where:

K_d = Thermal Conductivity, W/m-K, for as-fabricated fuel density “d”
 d = density in fraction of TD

The range of applicability of the modified NFI correlation is provided by volume 4 of the NUREG/CR-6534 (Lanning et al., 2005) as follows:

Temperature = 300 – 3000 K
 Rod-Average Burnup = 0 – 62 GWD/MTU
 As-fabricated Density = 92 – 97 % TD

Specific Heat

The specific heat in Btu/lbm-°F for uranium dioxide is given by:

$$c_{P_{UO_2}} = \left(2.388 \times 10^{-4} \right) \left\{ \frac{K_1 \theta^2 \exp(\theta/T_K)}{T_K^2 [\exp(\theta/T_K) - 1]^2} + K_2 T_K + \frac{F_{OM}}{2} \frac{K_3 E_D}{RT_K^2} \exp(-E_D/RT_K) \right\} \quad (11-151)$$

where T_K is the temperature in degrees K and

θ = Einstein temperature (535.285 K)
 R = 8.3143 (J/mol-K)
 K_1 = 296.7 (J/kg-K)
 K_2 = 2.43×10^{-2} (J/kg-K²)
 K_3 = 8.745×10^7 (J/kg)
 E_D = 1.577×10^5 (J/mol)
 F_{OM} = oxygen/metal ratio (2.0)

Model as Coded

The equations representing the density, thermal conductivity and specific heat for uranium dioxide are coded into WCOBRA/TRAC-TF2 as described by Equations 11-145 through 11-151 without modification.

Calculations for uranium dioxide density are performed in subroutine SETUP, those for thermal conductivity in subroutines SSTEMP and TEMP, and those for specific heat in subroutines TEMP and MOVE. Values of conductivity and specific heat versus temperature are shown in Figures 11-29, 11-30 and 11-31.

Scaling Considerations

Not applicable.

Conclusions

The WCOBRA/TRAC-TF2 correlations for UO₂ density and specific heat are based on MATPRO-9 and MATPRO-11. The correlation for UO₂ thermal conductivity is the modified NFI model used in FRAPCON 3.3. The models and correlations for these properties were used in simulations of LOFT. Therefore, the uncertainty and reliability of these models is accounted for in the overall code bias and uncertainty.

11.4.2 Zircaloy-4

Model Basis

The material properties of Zircaloy-4 are based on MATPRO-9 and MATPRO-11 calculations.

Density

The (cold) density of Zircaloy-4 clad material is assumed to be $\rho_{Zr} = 409.0 \text{ lbm/ft}^3$.

Thermal Conductivity

The thermal conductivity in Btu/hr-ft-°F for Zircaloy-4 clad is given by:

$$k_{Zr} = 0.5779 \cdot \left[7.51 + 0.0209T_K - (1.45 \times 10^{-5})T_K^2 + (7.67 \times 10^{-9})T_K^3 \right] \quad (11-152)$$

where T_K is temperature in degrees Kelvin.

Specific Heat

WCOBRA/TRAC-TF2 calculates the specific heat for Zircaloy-4 by linearly interpolating between values from a built-in table. Table 11-14 lists the values used to determine the specific heat of Zircaloy-4.

Model as Coded

The equations for the density, thermal conductivity and specific heat of Zircaloy-4 are coded into WCOBRA/TRAC-TF2 as described above without modification. Density is calculated in subroutine SETUP and HEAT, conductivity in subroutines STEMP, TEMP, and HEAT and specific heat in subroutines TEMP, HEAT, and MOVE. Curves of conductivity and specific heat versus temperature are shown in Figures 11-32 and 11-33.

Scaling Considerations

Not applicable.

Conclusions

The WCOBRA/TRAC-TF2 correlations for the density, thermal conductivity, and specific heat of Zircaloy-4 are based on MATPRO-9 and MATPRO-11. These property relations were used in simulations of LOFT.

11.4.3 ZIRLO[®] Alloy

Model Basis

The ZIRLO[®] alloy developed by Westinghouse represents a modification to Zircaloy-4 which was achieved by reducing the tin and iron content, eliminating the chromium, and adding a nominal one percent niobium. Table 11-15 shows a comparison of the two alloys.

Since tin is an alpha phase stabilizer and niobium is a beta phase stabilizer, the reduction in tin and the addition of niobium result in reductions in the temperatures at which the ZIRLO[®] alloy undergoes the alpha to beta phase change, relative to Zircaloy-4. Measurements performed by Westinghouse show that the ZIRLO[®] alloy starts the transformation at 1023 K and ends at 1213 K.

Since the ZIRLO[®] and Zircaloy-4 alloys are both about 98 percent zirconium, it should not be expected that the material properties are significantly different, except to the extent that they are affected by the differences in the phase change temperatures. Density, thermal expansion, thermal conductivity, and specific heat of both alloys have been measured by the Properties Research Laboratory using samples cut from Westinghouse production tubing (Taylor, Groot, and Larimore, 1989). Evaluation of the test results indicated that the materials are sufficiently similar that the Zircaloy-4 material properties can be used for the ZIRLO[®] alloy, with the exception of the specific heat (Davidson and Nuhfer, 1990). The specific heat of the ZIRLO[®] alloy is based on an adjustment to Table 11-14, which considers the difference in phase change temperatures.

Density

The (cold) density of the ZIRLO[®] cladding material is taken to be identical to that of Zircaloy-4 (409.0 lbm/ft³).

Thermal Conductivity

The thermal conductivity of the ZIRLO[®] cladding material is taken to be identical to that of Zircaloy-4, given by Equation 11-152.

Specific Heat

The specific heat shown in Table 11-14 for Zircaloy-4 includes both the true specific heat and the alpha to beta phase heat of transformation. The specific heat for the ZIRLO[®] cladding material was obtained by adjusting Table 11-14 to account for the difference in phase change temperatures, assuming both the true specific heat and the heat of transformation are the same for the two alloys. The true specific heat is taken

to be equal to the total specific heat in Table 11-14 for $T \leq 1090$ K, 0.085 Btu/lbm-°F for $T \geq 1213$ K, and:

$$\left[\right]^{a,c} \quad (11-153)$$

$$\left[\right]^{a,c} \quad (11-154)$$

where:

$$\left[\right]^{a,c} \quad (11-155)$$

WCOBRA/TRAC-TF2 calculates the specific heat for the ZIRLO[®] cladding material using the resulting total specific heat values, shown in Table 11-16.

Model as Coded

The density, thermal conductivity, and specific heat of the ZIRLO[®] cladding material are coded into WCOBRA/TRAC-TF2 as described above, without modification. Figure 11-34 shows a comparison of specific heat for ZIRLO[®] cladding material with that of Zircaloy-4.

Scaling Considerations

Not applicable.

Conclusions

Comparisons of the material properties for the ZIRLO[®] and Zircaloy-4 cladding materials have shown that the Zircaloy-4 relations for density and thermal conductivity can also be applied to the ZIRLO[®] alloy. The difference in the phase change temperatures of the two alloys requires that different specific heat correlations be used. The specific heat correlation for the ZIRLO[®] alloy is based on an adjustment to the Zircaloy-4 correlation, which accounts for the different phase change temperature range. This correlation will be used for analyses of nuclear reactors which utilize the ZIRLO[®] cladding material.

$$\left[\right]^{a,c}$$

11.4.4 Fuel Rod Gas Mixtures

Model Basis

For the gas mixture in the fuel-clad gap, only the thermal conductivity is calculated. The fill gas in the WCOBRA/TRAC-TF2 fuel rod model assumes that the gas is a mixture composed of helium, xenon, argon, krypton, hydrogen, and nitrogen. The thermal conductivity of the gas mixture as a function of temperature is determined, as described in MATPRO-11 Rev. 1 (Hagrman, Reymann, and Mason, 1980), from the relation:

$$k_{\text{gas}} = \sum_{i=1}^N \frac{k_i}{1 + \sum_{\substack{j=1 \\ j \neq i}}^N \psi_{ij} \frac{n_j}{n_i}} \quad (11-156)$$

where N = number of component gases, and where:

$$\psi_{ij} = \Phi_{ij} \left[1 + 2.41 \frac{(M_i - M_j)(M_i - 0.142M_j)}{(M_i + M_j)^2} \right] \quad (11-157)$$

and

$$\Phi_{ij} = \frac{\left[1 + \left(\frac{k_i}{k_j} \right)^{1/2} \left(\frac{M_i}{M_j} \right)^{1/4} \right]^2}{2^{3/2} \left(1 + \frac{M_i}{M_j} \right)^{1/2}} \quad (11-158)$$

where:

- M_i = molecular weight of gas species i
- n_i = mole fraction of gas species i
- k_i = thermal conductivity of gas species i

The thermal conductivities of the six component gases are evaluated in Btu/hr-ft-°F as a function of temperature from the following relations:

<u>Gas</u>	<u>k(Btu/hr-ft-°F)</u>	
Helium	$(1.314 \times 10^{-3}) T_{\text{gas}}^{0.668}$	(11-159)
Argon	$(1.31 \times 10^{-3}) T_{\text{gas}}^{0.701}$	(11-160)

$$\text{Krypton} \quad \left(1.588 \times 10^{-5}\right) T_{\text{gas}}^{0.92331} \quad (11-161)$$

$$\text{Xenon} \quad \left(1.395 \times 10^{-5}\right) T_{\text{gas}}^{0.872} \quad (11-162)$$

$$\text{Hydrogen} \quad \left(5.834 \times 10^{-4}\right) T_{\text{gas}}^{0.8213} \quad (11-163)$$

$$\text{Nitrogen} \quad \left(7.35 \times 10^{-5}\right) T_{\text{gas}}^{0.846} \quad (11-164)$$

where:

$$T_{\text{gas}} = \text{gas temperature } (^{\circ}\text{R})$$

Model as Coded

Equations 11-156 through 11-164 for gap gas thermal conductivity are coded in WCOBRA/TRAC-TF2 as described without modification in subroutine GTHCON.

Scaling Consideration

Not applicable.

Conclusions

Thermal conductivity for the gas mixture in the fuel-clad gap is calculated using the equations in MATPRO-11 Rev. 1 (Hagrman, Reymann, and Mason, 1980).

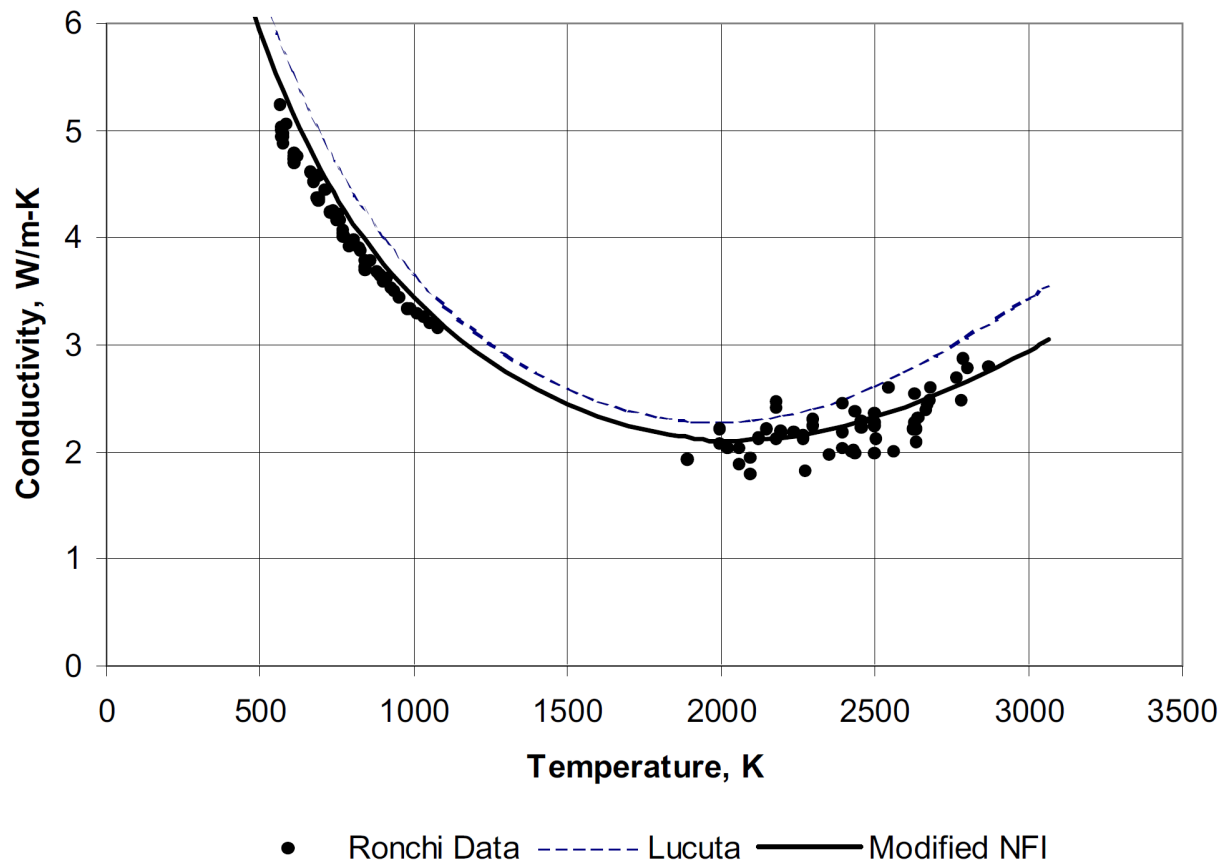


Figure 11-29 Modified NFI and Lucuta Model Predictions Compared to Measured Conductivity on Unirradiated Pellet Material (Ronchi et al., 1999), from Figure 2.4 of (Lanning et al., 2005)

Updates to Sections 25.1, 25.2 and 25.8 of WCAP-16996-NP

“Realistic LOCA Evaluation Methodology Applied to the Full

Spectrum of Break Sizes

(FULL SPECTRUM LOCA Methodology)”

25 PLANT SOURCES OF UNCERTAINTY

We have, to this point, assessed the ability of WCOBRA/TRAC-TF2 to simulate the key phenomena identified in the PIRT. In addition, it has been demonstrated that compensating errors or bias, due to the increase in scale from the experiments to the [pressurized water reactor \(PWR\)](#), result in a more conservative estimate of the LOCA analysis results relative to several key phenomena. However, there may be differences in PWR response to the LOCA, which may result in some models being more important for the PWR than for the experiment. In addition, variability in plant initial and boundary conditions introduce additional uncertainty. In this section, these additional aspects are discussed. The objective of this section is to develop a plan for performing various sensitivity or scoping studies with the PWR models described in Section 26, in order to identify those parameters which have an important influence on the calculation of the [peak cladding temperature \(PCT\)](#) in the PWR, and to make decisions about which variables should be considered for uncertainty propagation.

For some parameters, the uncertainty will be explicitly treated within the uncertainty analysis. For other parameters, a bounding approach may be employed (such as for the containment back-pressure).

25.1 PLANT PHYSICAL CONFIGURATION

The plant physical configuration consists of those parameters which define the geometrical and hydraulic configuration of the reactor at the time the LOCA occurs. These parameters are listed and defined below:

1. Dimensions
2. Flow resistances
3. Pressurizer location, relative to broken loop
4. Accumulator Tank Elevation
5. Hot assembly location, relative to vessel upper internals
6. Hot assembly type
7. Steam generator tube plugging level

Dimensions

Reactor dimensions, volumes, and surface areas are obtained directly from component drawings. Some variability exists in these dimensions due to tolerances and approximations which may have been made in geometrical calculations. Dimensions also vary from nominal due to thermal expansion. Thermal expansion is estimated to increase volumes by about [

] ^{a,c}

Fuel assembly grids, control rod guide tubes, and steam generator tubes may be affected, in some cases, by high stresses resulting from the combination of seismic and LOCA loads, an assumption required by 10 CFR 50, Appendix A, General Design Criterion 4. A dynamic analysis of the Reactor Coolant System (RCS) under combined seismic and LOCA loads is performed to demonstrate that key RCS components will continue to perform their safety function. Structural analyses performed as part of the original plant design basis have confirmed that Emergency Core Cooling System (ECCS) safety function and core

shutdown capability are maintained. These analyses have also indicated that for some plants, the pressure differentials and structural movements which are predicted may result in minor deformation of fuel assembly grids, control rod guide tubes, and/or steam generator tubes. In the case of the fuel assembly, some crushing of the grids in assemblies at the periphery of the core may be calculated. This may push fuel rods closer together, reducing the available flow area. Steam generator tubes may be slightly deformed at support plate locations, reducing the flow area through the tube bundle and increasing the flow resistance during reflood. For larger breaks, control rod guide tubes may be displaced from their nominal positions, preventing control rod insertion and causing the core to shutdown on voids early in the LOCA, and to remain shut down due to boron alone. These deformations, while not compromising safety functions, were found to affect the LOCA analysis results.

The combined effects of LOCA and seismic loads may potentially lead to some degree of grid crushing in the core, due to the baffle plates impacting the peripheral assemblies. If the impact on the peripheral assemblies is large enough, these assemblies may subsequently impact in-board assemblies, and so on. If the loads are large enough for grid damage to occur, test data and analyses show that the damage is typically limited to no more than two rows or rods per assembly, with elevations towards the mid-plane of the core.

[

] ^{a,c}

[

] ^{a,c}

[

] ^{a,c}Modeling Approach

[

] ^{a,c}**Flow Resistance**

The flow resistance in the vessel and loops during a LOCA is as much a function of the models used to calculate the friction factor, as it is the plant configuration. However, flow resistance is included in this category because some changes in plant configuration affect this parameter. The steady-state hydraulic resistance of virtually all the major components in a PWR was determined from scaled testing. The accuracy of the loss coefficients obtained from these tests has, over the years, been confirmed by the accurate prediction of steady-state flow and temperature conditions of operating reactors during numerous plant startup cycles. The accuracy of these predictions, using loss coefficients for subcomponents which are typically subject to large uncertainties may also be a result of the fact that the pressure distribution in a reactor circuit consists of many components. [

] ^{a,c} The uncertainty in

the pressure drop under LOCA transient conditions is discussed in Section 29.1.2.

When the LOCA occurs, reverse flow through some components and two-phase flow may significantly increase the uncertainty of the predicted flow resistance. One area in particular where reverse flow introduces additional resistance not present during normal operation is the broken cold leg inlet nozzle. Another area where additional resistance is introduced is the broken loop pump.

During several large scale ECCS tests conducted in the past years, it was observed that there was a significant pressure drop across the inlet nozzle of the broken cold leg. In the Cylindrical Core Test Facility (CCTF) reflood tests, this pressure drop was observed to result in a significant pressurization of the downcomer during reflood, resulting in increased reflood rates (Akimoto et al., 1984). Part of this loss was attributed to the increased dynamic head resulting from the reverse flow from a large reservoir, the reactor vessel, to the cold leg nozzle. Other contributors were losses associated with two-phase flow. A review of recent Upper Plenum Test Facility (UPTF) data has confirmed this finding as described in Section 29.1.2.

During a cold leg break, the flow rate through the broken loop pump increases substantially, to the point where the pump acts as a resistance. The effect of this additional flow resistance must also be taken into account, and is a source of additional uncertainty. The flow in the intact loop typically continues in the same direction at lower flow rates, therefore the predicted pressure drop is less subject to uncertainty.

Modeling Approach

[

]^{a,c}

Pressurizer Location

The pressurizer may be on the broken loop or one of the unbroken loops. Its location arises as a source of uncertainty because it may introduce some asymmetry into the reactor configuration at the time of the LOCA.

Modeling Approach

[

]^{a,c}

Accumulator Tank Elevation

The accumulator tanks may sit below, at, or above the cold leg elevation. The elevation of the accumulator relative to the cold leg will impact the maximum flow during accumulator injection, the duration of accumulator injection, and the amount of liquid which remains in the accumulator after accumulator injection into the cold leg terminates.

Modeling Approach

[

] ^{a,c}

Hot Assembly Location

Approximately 40 percent of the fuel assemblies in the core of a PWR lie beneath control rod guide tubes which extend into the upper head. These guide tubes, arranged in an approximate checkerboard pattern, house reactor control rods used for reactor control and shutdown, and extend into the reactor vessel upper head. The remaining fuel assemblies lie below open holes in the core plate, flow mixers attached to the core plate, or support columns of several possible designs (Section 26). As a result, for larger breaks (during the blowdown phase) the fuel assemblies will receive varying amounts of flow from the upper head and upper plenum depending on their position. [

] ^{a,c}

Modeling Approach

The configuration of the guide tubes is such that specific modeling of these flowpaths is considered necessary, particularly in view of the connection to the upper head, which contains a large volume of water. Consequently, the core and upper plenum geometry in the WCOBRA/TRAC-TF2 model is designed to specifically include separate channels for guide tubes and core plate open hole locations. As described in Section 26, each reactor internal layout is examined, and the hot assembly is located where reduced direct flow is expected to occur.

Hot Assembly Type

The basic design of a PWR fuel assembly has remained essentially unchanged through the years; the standard Westinghouse fuel assembly, for example, consists of an array of fuel rods in a 14x14, 15x15, 16x16 or 17x17 square matrix. Approximately 90 percent of the matrix is occupied by fuel rods; the remainder is occupied by thimble tubes. Five or more spacer grids hold the array together; some or all of the grids contain mixing vanes which serve to enhance flow turbulence, improving heat transfer during normal operation.

Variations in this standard design may occur to achieve improved fuel utilization. Typical changes made to a fuel assembly design are the following:

1. Changes in Fuel Rod Diameter – The fuel rod may be “optimized” by reducing its diameter, thus reducing the overall amount of fuel required. These changes are marginal in nature. For example, the standard Westinghouse 14x14 fuel rod diameter is 0.422 inches. For the optimized designs the diameter is 0.400 inches. Since smaller rods are designed to the same linear powers as standard rods, their surface heat fluxes and adiabatic heating rates are slightly higher. On the other hand, the amount of coolant in the core is also higher, because of the larger flow area.

2. Changes in Grid Design – The grid may be made of stainless steel, Inconel, or zirconium alloys. Typically, if the fuel rod diameter has been changed, the grids are modified slightly such that the overall hydraulic loss is the same as the standard design.

An additional design improvement is to incorporate additional mixing vane grids along portions of the rod, which further improve heat transfer characteristics, and offset reductions in departure from nucleate boiling (DNB) margin brought about by a smaller rod.

3. Changes in Fuel Enrichment – Axial and radial “blankets” are sometimes provided to reduce neutron leakage from the core. These blankets consist of regions of low reactivity fuel, or annular fuel. These blankets affect the axial and radial power distribution in the core, and are explicitly considered when these distributions are calculated.
4. Burnable Absorbers – Burnable absorbers are often used to reduce soluble boron requirements and improve power distributions. Burnable poisons may be **discrete** (i.e., loaded in thimbles) or integral (i.e., coatings or dopings of the fuel). Burnable absorbers affect axial and radial power distributions in the core, and are explicitly accounted for in core design calculations. Integral absorbers may also cause the internal pressure of the fuel rod, which generally increases with burnup, to increase at a different rate. Rod internal pressure causes swelling and possible burst during the LOCA.
5. Changes in Cladding Material – New alloys more resistant to corrosion are being developed. Their plastic strain characteristics may be different, and may therefore affect the LOCA results.
6. Other Changes – Minor modifications in upper and lower fuel assembly tie plates, mixing vane grid design, and removal of thimble plugging devices, are other changes which may occur from reload to reload, but which are not expected to change the LOCA results significantly.

Modeling Approach

[

] ^{a,c}

Steam Generator Tube Plugging Level

Steam generator tubes may require plugging for various reasons. Typically, tube plugging takes place during a normal outage. Plugs are inserted into each end of the degraded tube. This removes the tube completely from the RCS volume, and reduces the total flow area through the steam generator. The increased resistance and reduced volume may affect the blowdown transient and reflood behavior for larger breaks or the loop seal clearing in small breaks, and is a variation which must be considered in the LOCA analysis.

Modeling Approach

[

] ^{a,c}

25.2 PLANT INITIAL OPERATING CONDITIONS

Reactor operating conditions and their variations are described by two groups of parameters:

1. Core power parameters. These parameters define the core power distribution and fuel stored energy at the time of the LOCA.
 - a. Total core power
 - b. Peak linear heat rate (PLHR)
 - c. Hot assembly peak linear heat rate
 - d. Hot rod average power
 - e. Hot assembly average power
 - f. Axial power distribution
 - g. Low power region relative power
 - h. Time-in-Cycle
 - i. Reactor operating power history
 - j. Moderator temperature coefficient (MTC)
 - k. Hot full power (HFP) boron concentration

2. Reactor primary fluid conditions. These parameters describe the primary fluid thermodynamic state at the time of the LOCA.
 - a. Core average fluid temperature
 - b. Pressurizer pressure
 - c. Loop flow rate
 - d. Upper head fluid temperature
 - e. Pressurizer level
 - f. Accumulator water temperature
 - g. Accumulator pressure
 - h. Accumulator water volume
 - i. Accumulator line resistance
 - j. Accumulator boron concentration

The basis for the choice of these parameters is discussed in the following sections.

25.2.1 Core Power Parameters

A summary of the core modeling is given below. There are four core channels and [

] ^{a,c}

[]^{a,c} simulation the following fuel rods are modeled:

Rod 1: The rod with the highest linear heat rate []^{a,c} assumed to also have the highest average power and to reside in the assembly with the highest average power.

Rod 2: All the other (average) rods in the highest power assembly []^{a,c}

Rod 3: All the average rods in the assemblies residing under non-guide tube structures (e.g. support columns, free standing mixers, orifice plates, and open holes).

Rod 4: All the average rods in the assemblies residing under guide tubes.

Rod 5: All the average rods in the assemblies residing on the periphery of the core.

[]^{a,c}

There are three distinct regions (the hot assembly, the two average channels, and the low power channel) which serve to resolve the radial power distribution in the core.

Each fuel rod group has parameters describing the peak linear heat rate, the average linear heat rate, the axial distribution of power, and the number of physical rods modeled by the rod group. []

[]^{a,c}

The axial and radial core power distributions are of basic importance to the uncertainty analysis. The parameters which affect these distributions, and their variations, are described in the following section.

25.2.1.1 Core Power Distributions

The nuclear design of the reactor core meets constraints on the local power distribution in the fuel. Power distributions are typically characterized in terms of hot channel factors. These factors relate peak pellet power and hot rod power to core average quantities. These factors and other terms which will be used are defined below:

Core average heat flux (AFLUX) is the average thermal power produced per unit length of active fuel, kW/ft.

Peak linear heat rate (PLHR) is the maximum linear heat rate produced in the reactor, kW/ft.

Hot assembly peak heat rate (HAPHR) is the peak linear heat rate of an average rod in the hot assembly, kW/ft.

Hot assembly average power (HAFLUX) is the average power per unit length in the hot assembly, kW/ft.

Hot rod average power (HRFLUX) is the average power per unit length in the hot rod, kW/ft.

Total peaking factor (F_Q) is the ratio of the peak linear heat rate to the core average linear heat rate (PLHR/AFLUX).

Enthalpy rise peaking factor ($F_{\Delta H}$) is the ratio of hot rod average power to core average linear heat rate (HRFLUX/AFLUX).

PWR power distributions are often separated into their respective radial and axial components. The radial component is sensitive to the fuel and absorber loading pattern and the presence of control rods. Radial distributions change slowly with time and fuel depletion and are relatively insensitive to power level, xenon concentration/distribution, axial burnup distribution, and axial fuel design feature. By contrast, PWR axial distributions are relatively insensitive to the loading pattern but are quite sensitive to control bank position, xenon concentration/distribution, coolant density distribution, and reactor power.

The existence of this radial/axial power distribution separability has historically been utilized by the nuclear designer. As noted above, PWR radial power distributions are slowly varying in time, provided that the presence of control rods is accounted for accurately. Axial power distributions are dependent on cycle time as well as plant operating parameters such as current power level, recent changes in power level/distribution, prior operating history, control bank position (or operating strategy), and the time during a transient power maneuver (or the xenon distribution). These characteristics allow the analysis of transient three-dimensional power distributions to be performed by superposition of transient axial power distributions on steady-state, appropriately rodded, radial power distributions rather than the rigorous direct solution for the three-dimensional power distribution. While the methods and calculations used to design reload cores are extremely reliable, and have been confirmed by measurements taken in many operating reactors, it is a normal practice to design cores with some margin, such that measured power distributions will always fall below the core power limits, even when measurement uncertainties are added. These core power limits are determined from the body of safety analyses which support the FSAR and Technical Specifications, and ensure that regulatory limits will not be exceeded for any postulated transient.

Assembly power distributions in a typical Westinghouse designed PWR reload core are shown in Figures 25.2-1 and 25.2-2. The radial power distribution can typically be divided into three core regions: a low power peripheral region, high power assemblies distributed throughout the core (feed or non-feed), and average power regions also distributed throughout the core. These figures show the predicted power of assemblies in a reload core. This is a typical low leakage core loading pattern, in which low power assemblies are situated around the periphery of the core, while high power assemblies are in the interior of the core.

I^{a,c}

Within the fuel assembly, individual fuel rods vary in power due to the presence of burnable absorbers and water holes near the thimble tubes. Figure 25.2-3 is a histogram showing the distribution of rod powers within the high power assembly of several different Westinghouse fuel designs. The powers are expressed as a fraction of the maximum power allowed by the Technical Specifications. The maximum calculated rod power is therefore more than []^{a,c} lower than the maximum allowed value, to accommodate measurement uncertainties during surveillance and up to additional []^{a,c} for “good measure” or operational allowance. It can be seen that most of the fuel rods are at powers near the middle of the distribution, and that the hot assembly power distribution can be modeled with a single average rod and a single hot rod. The cumulative distribution is shown in Figure 25.2-4, and the average hot assembly power calculated from these distributions summarized in Table 25.2-1, and is seen to lie approximately []^{a,c} below the maximum calculated (hot rod) value.

The steady-state axial power distribution also varies as a function of time. Figure 25.2-5 shows the core average axial power distribution near the beginning of cycle, near the middle of cycle and near the end of cycle for a typical reload core. During the cycle, the steady-state axial peak moves away from the center of the core as the core is depleted. The depletion of the center of the core also affects any transient axial power distributions.

While a PWR is designed to easily follow load demand, the most likely state of the reactor is full power and equilibrium conditions. Under these conditions, the axial peaking is relatively low. Measurements taken of the maximum peaking factor at hot full power (HFP), nominal conditions are usually well below the Technical Specification limits. The margin to peaking factor limits is intended to allow for the less frequent occurrence of transient reactor operation, usually consisting of power reductions and increases to follow load. []^{a,c}

In summary, it is seen that the design of a core (its geometry, fuel enrichment, and loading pattern) establishes the maximum radial peaking in the core. The radial distribution is determined almost entirely by the core loading, and cannot be easily changed by external controls in normal operation. Hence, to assure that the measured hot rod power will always lie below the limit, core designs are set allowing for additional margin beyond the four percent required by Technical Specifications.

25.2.1.2 Transient Power Distributions

Short term changes in reactor power distributions are typically attributable to changes in reactor power level. Changes in power level may require control rod motion, and result in changes in coolant density profiles and xenon distribution. Changes in xenon distribution are a strong function of the magnitude and duration of the power change maneuver as well as the operating strategy used during the maneuver.

Westinghouse and Combustion Engineering (CE) core design methodologies used to generate axial power distributions have been previously reviewed by the USNRC. Distinct methods are employed in design based on the axial flux difference (AFD) Technical Specifications employed. (AFD is a measure of the axial power distribution, and is the axial flux difference between the top and bottom halves of the core.)

Westinghouse plants use the Constant Axial Offset Control (CAOC) or Relaxed Axial Offset Control (RAOC) core design method. The CAOC methodology (Morita et al., 1974) requires the core designer to

simulate various types of load follow maneuvers throughout the cycle to establish the limiting axial power distributions. The approach taken is conservative in that daily load follow swings to various power levels are assumed throughout the cycle. This method is used with plants whose AFD Technical Specification is defined as an allowable band (typically ± 5 percent) about a target AFD.

Another approach is used for plants with a fixed AFD Technical Specification. The RAOC methodology (Miller et al., 1983) considers the core parameters (power level, xenon distribution, and control rod position) that can affect power distributions and establishes the maximum variability possible in these parameters throughout a given cycle. These parameters are then treated as independent variables and all possible combinations are checked. Any axial shapes that are found to be within the AFD operating space defined by the Technical Specifications are taken to be possible.

CE plants do not control via AFD. Instead their monitoring and protective systems use the concept of axial shape index (ASI) (Combustion Engineering, 1986; Combustion Engineering, 1998; Combustion Engineering, 1975). ASI is similar to AFD, in that ASI is also a measure of the axial power distribution, and is the negative of percent axial offset divided by 100.

Typical transient distributions generated by the CAOC methodology are shown in Figures 25.2-6 through 25.2-8 for different times throughout the cycle. [

]^{a,c}

An additional characteristic of these transient power shapes is that fission products do not have sufficient time to build up in the high power region of the fuel rod. Consequently, if the reactor was shut down for any reason at the time the maximum transient linear shapes occurred, the decay heat generated is substantially lower at the peak power location than if the core had been operating indefinitely at these PLHR's. This phenomenon is not credited in the FULL SPECTRUM LOCA methodology.

The reactor heat source is made up of three major constituents. Fission energy is by far the largest component of the heat, comprising from roughly 93 to 100 percent of the total heat source for full power operation. The stored energy contribution to the LOCA transient is, therefore, directly related to the fission rate distribution at the time of the LOCA. The magnitudes of the decay and actinide heat sources make them a small contribution to the stored energy component. The decay and actinide components are, however, the principal contributors to core heat generation later in the LOCA transient since the fission rate during this portion of the transient is negligible. The decay and actinide heat sources are independent of the instantaneous fission rate at any given point in time but dependent upon the fission rate time history. Their concentrations determine the decay power available since the decay power for radionuclide decay is determined by the product of the energy release per decay, the decay constant, and the concentration. The concentration of a non-absorbing fission product is dependent upon the fission rate

time history, the fission product yield per fission, and the decay constant. Since the yield and time constant for a given fission product are constant for a specified isotope, the time dependent fission product concentration depends only upon the fission rate time history.

Decay heat is the result of a multitude of radionuclide decays (approximately 350 isotopes). These decay processes have been simplified in the ANSI/ANS 5.1-1979 decay heat standard to a summation of 23 exponentials for each fissile isotope. In the absence of significant absorption or isotope decay chain cross-coupling, the ANSI/ANS 5.1-1979 decay heat standard is a 23 group “pseudo-nuclide” representation of the fission product decay process. The magnitude of the decay heat source at any given point in the reactor, therefore, depends on the time history of the fission rate. The decay heat source for a given point in the reactor will be in effective equilibrium (production rate = decay rate) only if the fission rate has been maintained for the period of time corresponding to ten to twenty time constants for that nuclide. Figure 25.2-10 illustrates a point evaluation of decay equilibrium fraction versus sinusoidal fission rate period. [

]^{a,c}

25.2.1.3 Power Distribution Uncertainties

After a core has been designed and loaded, it is monitored to confirm that the core operates as designed, and to ensure that the reactor is operating within specified limits. The detailed reactor power distribution is monitored by means of in-core detectors. (There are several other core monitoring systems as well.) The readings from these detectors (which are fission chambers and convert the local neutron flux to a current signal) are transformed to fission rate distributions using analytical factors, based on the specific core design (Spier et al., 1988).

The core power distribution is measured during steady-state operation at regular intervals. The following quantities are typically obtained as the result of measurement and data processing:

- $F_{\Delta H}$ The enthalpy rise hot channel factor is the ratio of the integral of local power along the rod (pin) with the highest integrated power in the core to the average rod power.
- $F_{xy}(z)$ The elevation dependent radial peaking factor is the maximum local power density in the plane at elevation z divided by the average power density of the plane.
- $F_Q(z)$ The elevation dependent heat flux hot channel factor is the maximum local linear power density at elevation z divided by core average linear power density.

Because the above peaking factors are derived from a combination of instrument measurements and analytical model calculation, the uncertainty associated with these factors is a combination of the two factors.

The peaking factors defined above are typically measured on a monthly basis. In addition to the peaking factors defined above, the core axial flux difference is measured on a continual basis by the ex-core

nuclear detectors. This measurement is equivalent to the axial flux difference discussed previously, and provisions are incorporated in the plant computer to provide alarms if limits are exceeded.

The calculational uncertainty on radial power distribution ($F_{\Delta H}$) has been shown (Spier et al., 1988) to be bounded by a factor of []^{a,c} through benchmarks to critical experiments and other data. There is also an additional uncertainty associated with measuring the radial power distribution, which is bounded by a factor of four percent. It is desirable to assure that the plant will not routinely experience flux map measurements which exceed the ($F_{\Delta H}$) limit after a four percent uncertainty is applied due to combined effects of calculational and measurement uncertainties. To accomplish this, Westinghouse standard practice is to design the core such that it is predicted to be at least []^{a,c} below the ($F_{\Delta H}$) limit on a best-estimate basis. With this approach, the most probable condition is for the core to be measured at least []^{a,c} below the Technical Specification limit after measurement uncertainty is applied. Typical measurements shown in Figure 25.2-11 show this is indeed the case.

The margin inherent in the design as it relates to the total peaking factor $F_Q(z)$ is also reflected in typical measurements. Design calculations are performed to conservatively calculate the possible effects of adverse xenon distributions on the maximum total peaking factor. These penalty factors are generated assuming xenon transients are initiated in the core and shift the axial distribution to the full range allowed by the AFD Technical Specifications. The most probable condition for the core is at an equilibrium xenon condition which will produce F_Q values well below the limits. The total peaking factor measurement for a typical core during a cycle is shown in Figure 25.2-12. The maximum measured values include an uncertainty of 8.15 percent when compared to the Technical Specification.

Nuclear design calculations are performed assuming nominal pellet diameter, density, etc. These calculations form the basis of the analytic factors used to convert in-core measurements to rod power. Manufacturing uncertainties such as pellet diameter and the effects of rod bow introduce an additional uncertainty to point measurements. These uncertainties are accounted for in the FSLOCA methodology.

Rod bow and manufacturing uncertainties are both applied to the hot rod peaking factor measurement as described in the following paragraphs. These factors are not applied to measurements of the hot assembly and hot rod power. Local linear heat rate depends on the local mass of UO_2 per unit length, or more specifically, per pellet and also on the local channel geometry. The local mass varies as a result of manufacturing variations in pellet dimensions and fuel enrichment. []

[]^{a,c}

A similar statement can be made for rod bow. []

[]^{a,c}

A detailed study of the in-core flux mapping system and its accuracy was performed by Westinghouse (Spier et al., 1988). Because the “measured” values of $F_{\Delta H}$ and F_Q are actually inferred values obtained from the raw measurement using core model group constants, error contributions from both measurement

and modeling sources were considered. Two uncertainties are defined: a measurement uncertainty, to be applied to the inferred peaking factor during normal core surveillance such that the true values are bounded at a high confidence level, and a calculational uncertainty, to be applied to the calculated peaking factors during the core design such that the true values are bounded at a high confidence level. The two uncertainties contain several common components, and so are similar in magnitude. In the best-estimate LOCA methodology, we are concerned with the calculational uncertainty of the predicted peaking factors.

The calculational uncertainty is composed of several independent subcomponents which are summarized in Table 25.2-2. Some of these components are related to uncertainties which should be applied only to the hot rod. In subsequent application of these uncertainties (Section 29.4), these components will be applied separately when considering the calculational uncertainties associated with groups of fuel rods such as the hot assembly. [

] ^{a,c}

A final uncertainty related to the power distribution is that associated with the total core power. Core power is inferred from an energy balance using feedwater flow and temperature, and steam flow and pressure. The maximum error from this measurement is typically ± 2 percent, [^{a,c}. Some plants have employed improved uncertainty measurement systems which reduce this uncertainty below 2 percent.

25.2.1.4 Power Distribution Modeling Approach

Summarizing the preceding sections, the core power distribution is seen to exhibit the following characteristics:

1. The radial power distribution is primarily controlled by core geometry, fuel enrichment, burnable absorber loading, and core loading patterns. It is relatively insensitive to operational procedures such as load follow.
2. The axial power distribution is sensitive to operational procedures (such as load follow), which produce non-equilibrium xenon distributions in the core, and core burnup. Large axial power distribution variations have a small effect on the radial power distribution. Axial power distributions which produce the limiting F_Q occur during transient operation. [^{a,c}
3. The power distribution in the core is well described by the following parameters: the average linear heat rate, the hot assembly linear heat rate, the low power assembly linear heat rate, and the peak linear heat rate.

² Clarification on the determination of the rod bow uncertainty component was provided as part of RAID-6.4 in (Bajorek, et al., 1998) for prior Westinghouse best-estimate LOCA evaluation models.

4. The average power of the rods in the assembly which contains the hot rod is typically [$J^{a,c}$ or more lower than the hot rod.
5. The axial peak power may occur at any location within approximately two feet from the ends of the core, during both transient and steady-state conditions.

As described in Section 26, the PWR core is modeled with sufficient detail to resolve both the radial and axial power distributions present in the core. The radial power distribution is resolved using [

$J^{a,c}$

There are several parameters which play a role in the calculation of rod power in WCOBRA/TRAC-TF2. Each parameter, in turn, contributes some uncertainty. Based on the general discussion of power distributions, the parameters as used in WCOBRA/TRAC-TF2 are described in more detail below. A final summary of uncertainty contributors is presented later in this section, after the discussion of the fuel rod model.

As described previously, there are four core channels and [$J^{a,c}$ are defined as:

Rod 1: The rod with the highest linear heat rate [$J^{a,c}$ assumed to also have the highest average power and to reside in the assembly with the highest average power.

Rod 2: All the other (average) rods in the highest power assembly [$J^{a,c}$

Rod 3: All the average rods in the assemblies residing under non-guide tube structures (e.g. support columns, free standing mixers, orifice plates, and open holes).

Rod 4: All the average rods in the assemblies residing under guide tubes.

Rod 5: All the average rods in the assemblies residing on the periphery of the core.

[

$J^{a,c}$

Each fuel rod has input parameters describing the average linear heat rate, and the axial distribution of power relative to the core average linear heat rate. The important parameters used in WCOBRA/TRAC-TF2 for these fuel rods are described below. The “0” designates initial, or steady-state values of parameters which will change during the LOCA transient.

The reactor power parameters described below are directly related to several quantities which are also measured in the plant during normal operation. These are the total peaking factor (F_Q), the hot channel

factor ($F_{\Delta H}$), and the AFD. Other quantities of lesser importance are the moderator temperature coefficient (MTC) and the coolant boron concentration. The Technical Specifications call for specific uncertainties and margins to be applied to the measured values of some of these quantities before they are compared to the Technical Specification limit. In the discussion below, these quantities will normally be described in terms of calculated or expected values, without local uncertainties, and will be designated with subscript BE (Best-Estimate).

Initial Core Average Linear Heat Rate

The parameter defining core power in WCOBRA/TRAC-TF2 is the core average linear heat rate, calculated by:

$$AFLUX(0) = P(0)/(NFR * L) \quad (25-1)$$

where:

L	=	nominal active fuel length
P(0)	=	initial core power
NFR	=	total number of fuel rods

There is a tendency for the fuel pellet stack (L) to shrink during the cycle, which would increase AFLUX based on Equation 25-1. However, [

] ^{a,c} The only uncertainty affecting AFLUX is the core power measurement uncertainty, which results from calorimetric errors in measuring feedwater flow and temperature. As noted in Section 25.2.1.3, the range of this error is estimated as [

] ^{a,c}

The axial power distributions of the core average rods (Rods 3, 4, and 5) are [

] ^{a,c} These distributions will be illustrated later in the section, when the power distribution modeling is described.

Peak Linear Heat Rate (PLHR)

The peak linear heat rate (PLHR) for the hot rod (Rod 1) [

] ^{a,c} defined by:

$$\left[\right]_{a,c} \quad (25-2)$$

[

] ^{a,c}

[

] ^{a,c}

For the hot rod, the PLHR can also be expressed as,

[

] ^{a,c}

(25-3)

[

] ^{a,c}

The variation due to transient operation is the result of assumed load follow operations and other operational transients, which introduce relatively short lived skewed power shapes with relatively high peaking factors compared to equilibrium conditions, when the plant returns to full power. Limiting transient power distributions are generated during the core design analysis to confirm that maximum values remain below limits established in the Technical Specifications. The calculated maximum peaking factor is obtained from the [core design analysis using approved core design methods](#).

[

 $]^{a,c}$ **Hot Assembly Rod Peak Linear Heat Rate**

The hot assembly rod peak linear heat rate is defined as:

$$\left[\right]_{a,c} \quad (25-4)$$

[

 $]^{a,c}$

Therefore $HAPHR(0)$ can be written as:

$$\left[\right]_{a,c} \quad (25-5)$$

Typically, the relationship in power of the hottest rod in an assembly to the assembly average will depend upon details in the design of that assembly, such as the location of the hot rod in the assembly. In this

analysis, it is conservatively assumed that the []^{a,c} and the peak power is offset by a constant factor equal to the difference in average power. Further discussion of the validity of this assumption is provided in the next subsection.

There are two items to consider when developing the relationship between the hot rod, which is a single rod, and the hot assembly rod, which represents the average of all the rods in the hot assembly minus the hot rod. The first item is the actual difference between the hot rod and the hot assembly rod powers. The second is the difference in the uncertainty associated with various quantities for the hot rod and the hot assembly rod.

Examination of rod census data indicates that the minimum difference between the hot rod and the hot assembly average rod is []^{a,c}. Absent all uncertainties, this is a conservative estimate of the relationship which will exist between the hot rod and the hot assembly average rod during normal operation for the entire fuel cycle. As a general approach, the hot assembly average rod power will be calculated using the []^{a,c} difference. However, if additional information is available in the form of a core design limit, an alternative and less conservative approach may be taken to bound the hot assembly average power. In Equations 25-4 and 25-5 and the discussion that follows, it is assumed that the general approach (where the difference is []^{a,c}) is taken.

A second consideration is the uncertainty associated with the hot rod and with the hot assembly average rod. For a single rod at a single axial location, the following uncertainties exist:

1. Uncertainty in the actual linear heat rate, relative to what is predicted.
2. Uncertainty in the actual fuel pellet geometry. The pellet at a particular location may be slightly larger or be slightly more enriched than the value intended during manufacture.
3. Uncertainty in the hot rod subchannel geometry. The subchannel may be slightly distorted due to rod bow.

The overall uncertainty for the hot assembly average rod peaking factor should be less than that for the hot rod, since we are concerned with the average value over a number of rods, []^{a,c}. This is indicated in Table 25.2-2.

For a single axial location on a single rod, all of these uncertainties must be considered. Since the local axial linear heat rate as specified by F_Q is defined at a single location, all of these uncertainties must be considered for the hot rod, hence the full column of numbers in Table 25.2-2 for the hot rod F_Q . For integral quantities such as the rod total power as specified by $F_{\Delta H}$, local uncertainties such as pellet dimensions should not contribute significantly to the integral uncertainty. []^{a,c}

[a,c]

(25-6)

[

] a,c

[a,c]

(25-7)

[

] a,c

[a,c]

(25-8)

[

] a,c

$$\left[\frac{P_{\text{rod}}}{P_{\text{assembly}}} \right]^{a,c}$$

The result of the application of these different uncertainties is that the uncertainty associated with the power on the hot rod is typically larger than the uncertainty associated with the power in the hot assembly average rod. These uncertainties are discussed in Sections 29.4.1.2 and 29.4.2.1.

Hot Rod Average Linear Heat Rate

Since the hot rod has a very small effect on the hot assembly fluid conditions (it is only one rod among about 150), its total power is not as important as the power in the hot assembly rod. However, total power will affect hot rod gap pressure and cladding burst times.

$$\left[\frac{P_{\text{rod}}}{P_{\text{assembly}}} \right]^{a,c} \quad (25-9)$$

where:

$$\left[\frac{P_{\text{rod}}}{P_{\text{assembly}}} \right]^{a,c}$$

Therefore:

$$\left[\frac{P_{\text{rod}}}{P_{\text{assembly}}} \right]^{a,c} \quad (25-10)$$

$F_{\Delta H, BE}$ is defined as the maximum expected average linear heat rate of the highest power rod $\left[\frac{P_{\text{rod}}}{P_{\text{assembly}}} \right]^{a,c}$ relative to the core average linear heat rate. Typically, the calculated $F_{\Delta H, BE}$ for a core design is augmented by four percent to account for calculational and measurement uncertainties and up to an additional $\left[\frac{P_{\text{rod}}}{P_{\text{assembly}}} \right]^{a,c}$ for “good measure” or operational allowance. The reason for the application of additional margin in $F_{\Delta H}$ is that, unlike total peaking factor, there are few alternatives short of reducing power if the measured value exceeds the [Technical Specification](#).

Hot Assembly Average Linear Heat Rate

The hot assembly rod (Rod 2) average linear heat rate during steady-state is defined as:

$$\left[\frac{P_{\text{rod}}}{P_{\text{assembly}}} \right]^{a,c} \quad (25-11)$$

[

$$\left[\frac{P_{a,c}}{P_{H,BE}} \right]_{a,c} \quad (25-12)$$

The actual thermal power produced in the hot assembly rod relative to its nuclear power may be slightly different from the hot rod, due to different levels of redistribution. [

] ^{a,c}

As discussed in Section 25.2.1.1, a review of a large number of core designs indicates that the minimum difference between the hot rod and the hot assembly average rod is [^{a,c} lower (Figure 25.2-4). This is a conservative estimate of the relationship which will exist between the hot rod and the hot assembly average rod during normal operation, during the entire fuel cycle. The relative nuclear power generated in the hot assembly average rod is therefore assumed to be [^{a,c} lower than the best-estimate value of the hot rod relative nuclear power, $F_{\Delta H, BE}$. As previously discussed, however, if additional information is available in the form of a core design limit, an alternative and less conservative approach may be taken to bound the hot assembly average power.

Axial Power Distribution

Axial power distributions vary widely due to burnup and transient operation. The distributions have been considered in prior evaluation models using [

] ^{a,c}

[

] ^{a,c}**Low Power Region (PLOW)**

The power in the rod (Rod 5) representing the low power peripheral region of assemblies is determined from the core design and usually varies from [

]^{a,c} If this region has a low average power, the interior channels (Rods 3 and 4) have a higher power. A relative power []^{a,c} of the core average is typical of current and future low leakage loading patterns. An average value expected for future cycles is assumed as discussed in Section 29.3.1.

Time-in-Cycle

The time-in-cycle impacts a number of different parameters significant to the LOCA transient behavior. The fuel peaking factors, initial stored energy, rod internal pressure, corrosion, axial power distribution and decay heat are several examples of burnup dependent parameters. The impact of the time-in-cycle is considered in the uncertainty analysis as discussed in Section 29.4.1.1, Volume 3 of this topical.

Prior Operating History

As discussed previously, the power distributions which generate high peaking factors are relatively short lived. A detailed accounting of the buildup of fission products would show that after shutdown, the axial power distribution would revert back to the original, steady-state distribution. This effect will be [

] ^{a,c}

Transient Power Maneuver

[

] ^{a,c}

25.2.1.5 Moderator Temperature Coefficient (MTC)

The moderator temperature coefficient (MTC) affects reactor shutdown during the first few seconds of blowdown. The larger (more positive) this value, the less responsive the reactor is to the increased fluid temperature which occurs in the first second or two of the LOCA. [

] ^{a,c}

25.2.1.6 Hot Full Power (HFP) Boron Concentration

The initial primary fluid boron concentration coupled with the moderator temperature coefficient discussed previously dictate the core power response during the blowdown phase of a LOCA transient. The initial HFP boron concentration is modeled [

] ^{a,c}

25.2.1.7 Summary of Core Power Parameters

The consideration of the various core power distribution parameters described above is summarized as follows. [

] ^{a,c} (More details on this uncertainty treatment are provided in Section 29.4.) In Figure 25.2-14, a possible axial power distribution as input into the WCOBRA/TRAC-TF2 PWR model is shown. The hot rod peak power is offset by [^{a,c} from the hot assembly average rod power (assuming the general approach), and is offset from the average rod power by the total axial peaking ($F_{\Delta H}$). The low power rod is offset from the average rod power, in turn, by the factor PLOW.

25.2.2 Plant Fluid Conditions

The plant fluid conditions listed at the beginning of this section are those which are sufficient to define an overall thermodynamic state of the fluid. Since WCOBRA/TRAC-TF2 calculates a steady-state condition prior to the LOCA, the thermodynamic state cannot be over-specified. Thus, four basic quantities are defined for the primary fluid; its average temperature, pressure, volume, and flow rate. Then, the states of significant fluid regions which are isolated from the RCS during steady-state, but which subsequently become part of the RCS during the LOCA, such as the upper head and the accumulator, are defined. The section below is a brief description of how fluid conditions typically are controlled in a PWR.

25.2.2.1 Overview of Plant Fluid Conditions

A nuclear power plant is equipped with a variety of control systems. For example, the reactor control system in conjunction with the electric load demand program controls the neutron generation rate within the core such that core heat generation rates are proportional to the demanded electric power output. Other control systems are available for control of plant response to rapid disturbances arising from abnormal conditions and for the control of processes which maintain the plant in an economically desirable operating condition.

The static and dynamic behavior of the power production process can only be determined by reliable and accurate measurements of process variables. The application of these measurements by the control and protection systems is then accomplished in a manner which assures proper corrective action and provides protection for the plant and public against extreme accidents. This is normally accomplished by the feedback process where process variables are controlled to a predetermined value, commonly referred to as a setpoint. When measurements deviate from the setpoint, the deviation is noted as an error by the controller(s) and action is taken to restore the process to its correct state point or condition.

Setpoints generally represent either a desired, or “target,” value for a process control variable, or a limit or bounding value, that a process control variable may have. In the case of a “target” or control setpoint, variation from the desired value will result in some corrective action to return the plant to the control

setpoint. For example, the pressurizer water level control setpoint is approximately 35 percent of the full-scale reading of the measurement span, with either heaters or spray being actuated with a ± 5 percent variation of full span from the 35 percent span. Violation of limiting or bounding setpoints results in a more radical plant response.

From the preceding example of the pressurizer, it is readily seen that relatively small variations from control setpoints will result in plant control systems initiating corrective action. These small spans are called control bands. Thus, for a plant maintained at equilibrium conditions, the process control parameters may be taken to vary from their respective setpoints by no more than the bounds of their respective control bands. In particular, for process parameters which are subject to automatic control, such as the pressurizer level, the likelihood of the process parameter being significantly different from the target value is extremely small. For those process parameters subject to less frequent surveillance, the potential variation may be larger.

Trip setpoints define the limits within which the plant may operate. Again referring to the example of the pressurizer, the plant will continue to operate temporarily with a pressurizer water level between 17 and 92 percent of full-scale of the measured span, with the plant control systems acting to achieve a level of between 30 to 40 percent of full-scale reading. Owing to operator and/or automatic actions however, prolonged operation outside the control bands is extremely unlikely. The trip setpoints are established to allow the plant flexibility in responding to changes in operating conditions while providing for the health and safety of the public.

Plant operation parameter variations that are significant for LOCA analyses are listed in Table 25.2-4 for a typical PWR. All but primary side loop flow may be considered process control parameters for a nuclear power plant; direct controlling of primary coolant flow rate is not provided for. For a typical plant, the variability of these parameters about their nominal or setpoint values is seen to be small, with a control band of about []^{a,c} on primary loop pressure and fluid temperature, []^{a,c} on core power, and about []^{a,c} on water volumes.

25.2.2.2 Fluid Conditions Modeling Approach

In addition to the process parameters identified in Table 25.2-4, additional RCS fluid conditions have been found to be important in past LOCA analyses. The reactor vessel upper head is supplied by a small bypass flow from the upper downcomer. While the incoming fluid is at the temperature of the cold leg (T_{cold}), the upper head fluid may be at a different average temperature because of the low bypass flow rate which results in some flow from the upper plenum, which is at a higher temperature (T_{hot}). The initial temperature of the fluid in the upper head (T_{UH}) has been found to strongly affect the blowdown PCT in other evaluation models (for Large Break LOCA). Typically, plants can be separated into two categories: those with sufficient bypass flow to maintain (T_{UH}) near (T_{cold}), and those with low bypass flow, in which (T_{UH}) remains close to T_{hot} .

The bypass flow mentioned above is one component of several bypass flows, which reduce the core flow rate relative to the loop flow rate by about four to eight percent. This bypass flow has an indirect effect on the LOCA transient by affecting the fluid temperature rise through the core, but is not expected to affect the LOCA transient directly [by virtue of the different steady-state fluid conditions](#).

Not all the process parameters described in Section 25.2.2.1 are independent. Typically, if core power, primary flow, and secondary temperature and pressure are specified, the primary fluid temperature and pressure will seek appropriate levels consistent with these boundary conditions. In the modeling of these parameters, the secondary side conditions are adjusted as required to obtain primary side conditions consistent with the Technical Specifications and planned operation. Since the secondary-side model is rather detailed, the secondary-side conditions required to achieve the appropriate primary-side conditions are generally consistent with expected operational values.

Although the accumulator is isolated from the RCS by a check valve during normal operation, it is considered part of the RCS in this methodology. The performance of the accumulator during the LOCA depends on several factors including the water and cover gas initial pressure, temperature, and volume. These are all subject to some variation. Typically, pressure and volume are controlled to within plus or minus 10 percent or less. Since the accumulators reside within containment, the long term temperature of the containment atmosphere will affect the accumulator water temperature. The variation in containment temperature is likely to be seasonal to some degree, and is limited in most plants to a maximum value to avoid problems with equipment degradation. In general, therefore, the accumulator temperature range is plant specific. The accumulator line is subject to the same uncertainties as identified earlier for flow resistance; however, plant startup tests reduce this uncertainty to some extent as discussed in Section 29.3.2, Volume 3.

While accumulator boron concentration is not likely to have a significant effect on the LOCA PCT, it is modeled to ensure that recriticality does not occur in the short-term following a LOCA.

The parameters chosen to represent the reactor initial fluid conditions are:

1. Average fluid temperature (T_{avg}), degrees F
2. Pressurizer pressure (P_{RCS}), psia
3. Loop flow rate (W_{loop}), gpm per loop
4. Upper head fluid temperature (T_{UH}), degrees F
5. Pressurizer level (L_p), percent of full span
6. Accumulator temperature (T_{ACC}), degrees F
7. Accumulator pressure, (P_{ACC}) psia
8. Accumulator water volume, (V_{ACC}) cubic feet
9. Accumulator line fl/D (K_{ACC})
10. Accumulator boron concentration, (C_{ACC}) ppm

The effects that the above parameters have on the LOCA transient are considered as part of the uncertainty analysis. The treatment of the fluid condition uncertainties is discussed in Section 29.3.2, Volume 3.

Table 25.2-1 Hot Assembly Rod Power Census Summary for Westinghouse Fuel

a,c

Table 25.2-2 Peaking Factor Uncertainties

Notes:

1. Spier et al. (1988)
2. $J^{a,c}$
3. Uncertainties are given in terms of one standard deviation divided by average value (coefficient of variation), percent. The total uncertainty is the square root sum of squares of the components.

Table 25.2-3 Rod Bow F_Q Uncertainties

Notes:

1. Uncertainties are given in terms of one standard deviation divided by average value (coefficient of variation).
2. Argall et al. (1979)
3. $J^{a,c}$

Table 25.2-4 Typical Westinghouse Plant Operation Parameters

a,c

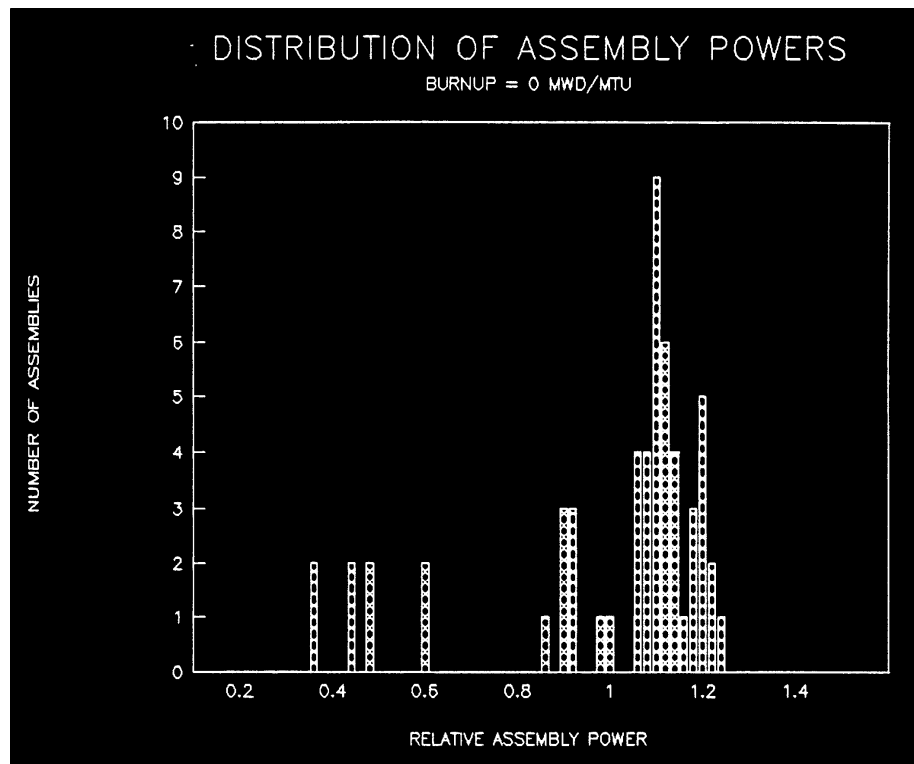
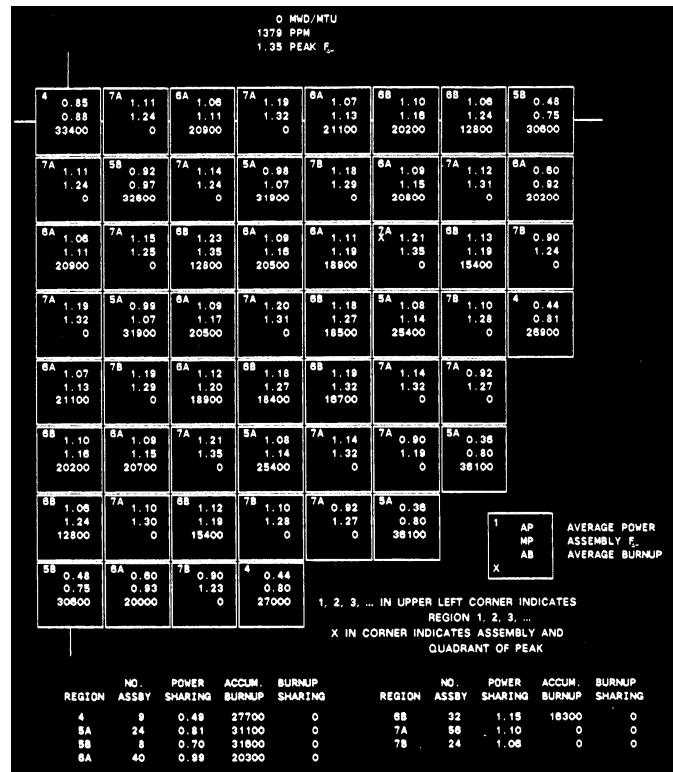


Figure 25.2-1 Typical Assembly Power Map and Assembly Power Distribution, Beginning of Cycle

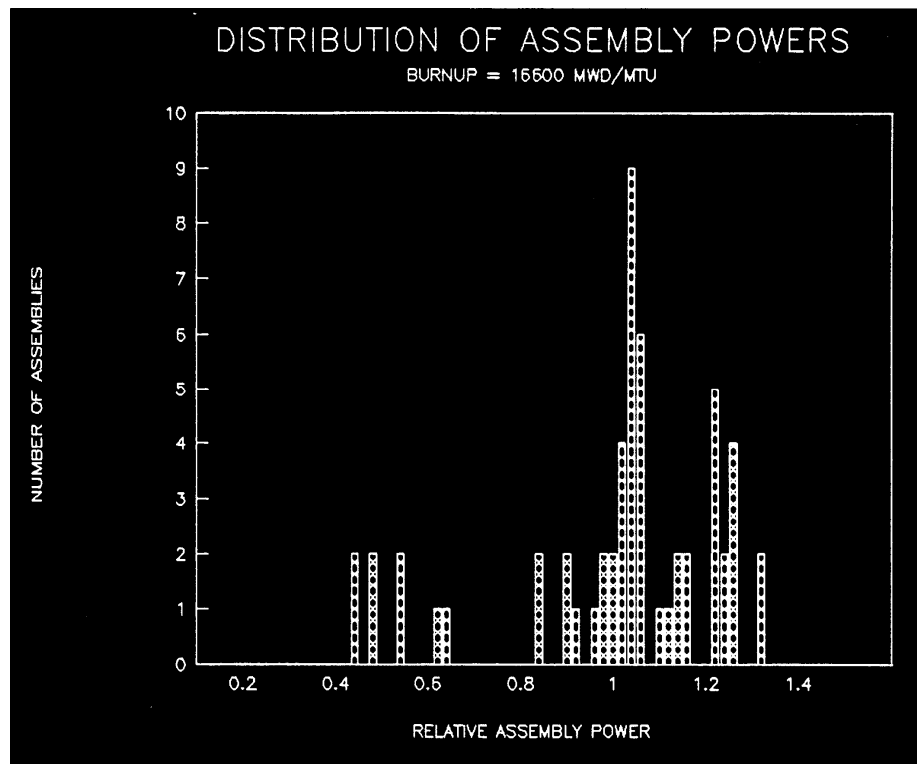
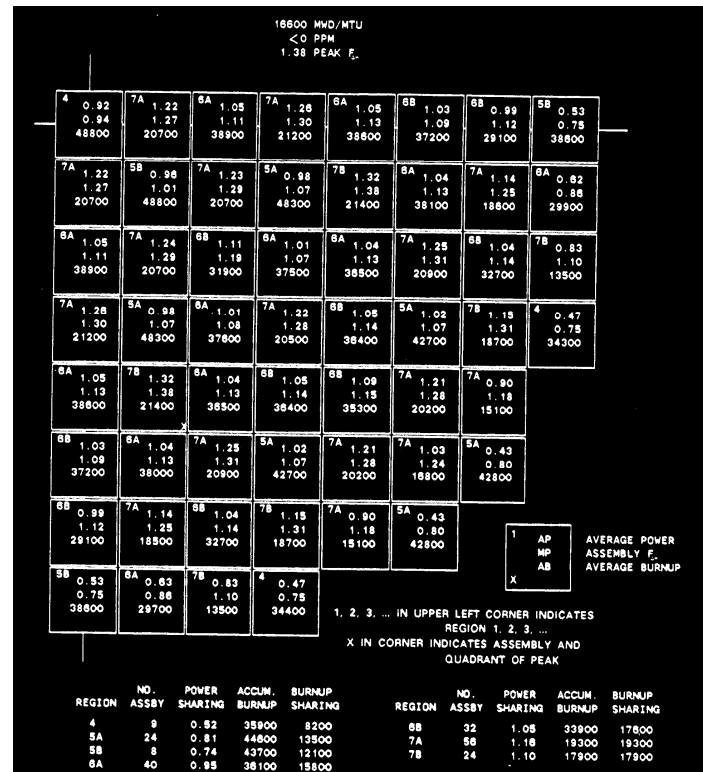


Figure 25.2-2 Typical Assembly Power Map and Assembly Power Distribution, End of Cycle

a,c

Figure 25.2-3 Typical Hot Assembly Fuel Rod Power Distribution

a,c

Figure 25.2-4 Hot Assembly Rod Power Census for Typical Westinghouse Fuel Designs

a,c

Figure 25.2-5 **Relative Axial Power Distribution** **near Beginning of Cycle, Middle of Cycle and End of Cycle** During Full Power Steady-State Conditions

a,c

Figure 25.2-6 Typical Transient Axial Power Distributions near Beginning of Cycle

a,c

Figure 25.2-7 Typical Transient Axial Power Distributions near Middle of Cycle

a,c

Figure 25.2-8 Typical Transient Axial Power Distributions near End of Cycle

a,c

Figure 25.2-9 [

] ^{a,c}

a,c

Figure 25.2-10 Effect of Load Follow Maneuver Period on Decay Heat Equilibrium Fraction for Various Times After Trip

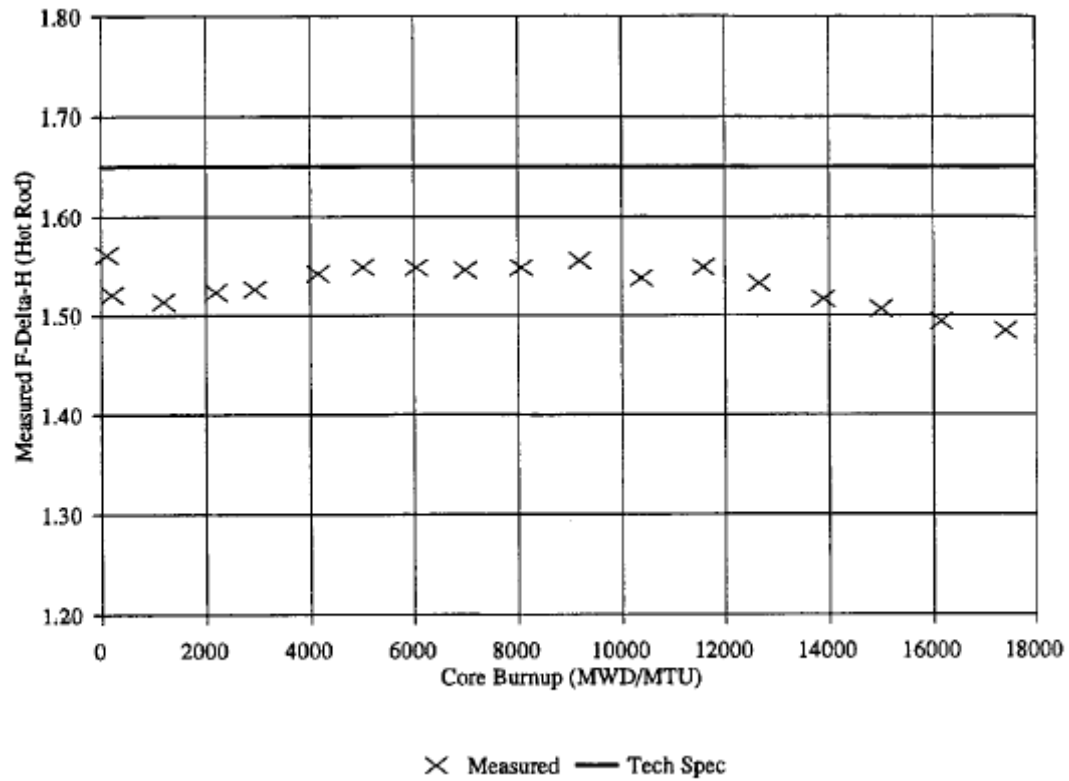


Figure 25.2-11 Typical Measurement of Enthalpy Rise Hot Channel Factor $F_{\Delta H}$

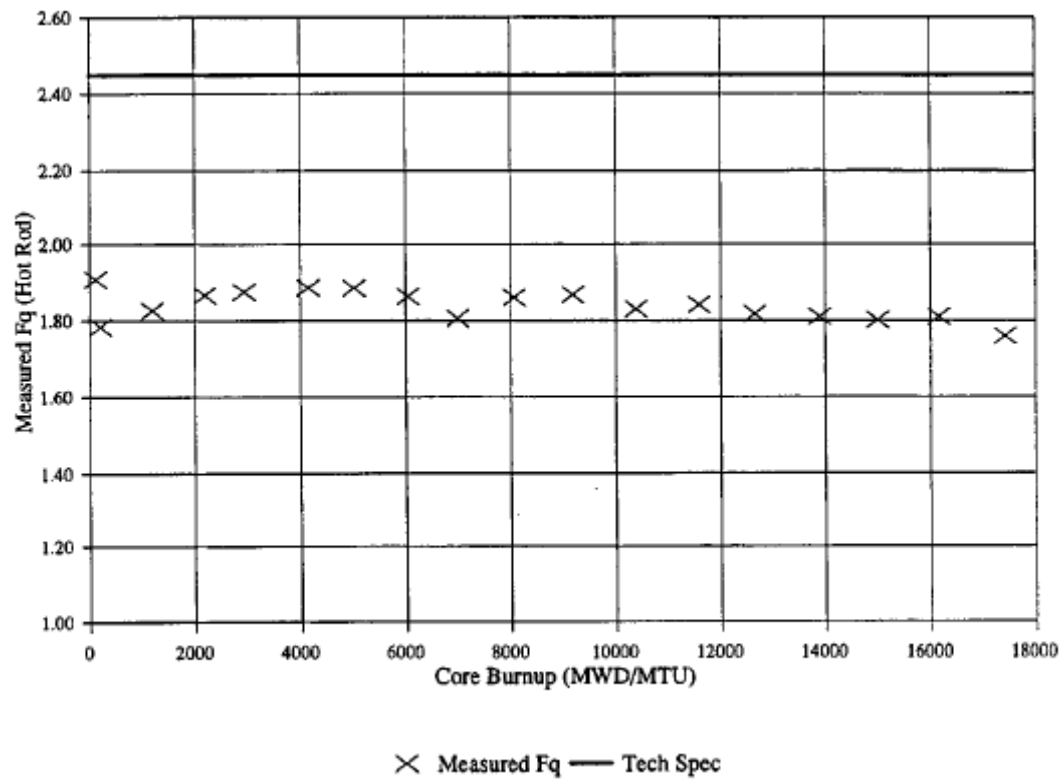


Figure 25.2-12 Typical Measurement of Total Peaking Factor F_Q

a,c

Figure 25.2-13 [

] ^{a,c}

a,c

Figure 25.2-14 Typical WCOBRA/TRAC-TF2 Axial Power Distribution

25.8 REFERENCES

1. American Nuclear Society, 1979, "American National Standard for Decay Heat Power in Light Water Reactors," ANSI/ANS-5.1-1979.
2. Akimoto, H., et al., 1984, "Pressure Drop through Broken Cold Leg During Reflood Phase of Loss-of-Coolant Accident of PWR," Journal of Nuclear Science and Technology, 21 [16].
3. Argall, B. M., et al., 1979, "Fuel Rod Bow Evaluation," WCAP-8691, Revision 1.
4. Bajorek, S. M., et al., March 1998, "Code Qualification Document for Best Estimate LOCA Analysis," Volume 1 Revision 2, and Volumes 2 through 5, Revision 1, WCAP-12945-P-A (Proprietary).
5. Bordelon, F. M. and Murphy, E. T., 1974, "Containment Pressure Analysis Code (COCO)," WCAP-8327 (Proprietary), WCAP-8306 (Non-Proprietary).
6. Bordelon, F. M., et al., 1974, "Westinghouse Emergency Core Cooling System Evaluation Model – Summary," WCAP-8339.
7. Bordelon, F. M., et al., 1975, "The Westinghouse ECCS Evaluation Model: Supplementary Information," WCAP-8471-P-A (Proprietary).
8. Combustion Engineering, 1975, "Assessment of the Accuracy of PWR Safety System Actuation as Performed by the Core Protection Calculators (CPC)," CENPD-170-P.
9. Combustion Engineering, 1986, "C-E Setpoint Methodology, C-E Local Power Density and DNB LSSS and LCO Setpoint Methodology for Analog Protection Systems," CENPD-199-P, Rev.1-P-A.
10. Combustion Engineering, 1998, "C-E Setpoint Methodology." CENPD-199-P, Rev.1-P-A, Supplement 2-P-A.
11. Letter from Johnson, W. J. to Richardson, J. E., December 1990, "Steam Generator Tube Deformation," NS-NRC-90-3557.
12. Mendler, O. J., 1975, "Method of Analysis and Evaluation of Jet Impingement Loads from Postulated Pipe Breaks," WCAP-8957.
13. Miller, R. W., et al., 1983, "Relaxation of Constant Axial Offset Control/F_q Surveillance Technical Specification," WCAP-10216-P-A.
14. Morita, T., et al., 1974, "Power Distribution Control and Load Following Procedures," WCAP-8385-P-A.

15. Nissley, M. E., et al., 2005, "Realistic Large-Break LOCA Evaluation Methodology Using the Automated Statistical Treatment Of Uncertainty Method (ASTRUM)," WCAP-16009-P-A and WCAP-16009-NP-A.
16. Salvatori, R., 1973, "Topical Report, Reactor Coolant Pump Integrity in LOCA," WCAP-8163.
17. Spier, E. M., et al., 1988, "Evaluation of Nuclear Hot Channel Factor Uncertainty," WCAP-7308-L-P-A.
18. U.S. Nuclear Regulatory Commission, 1989, "Best-Estimate Calculations of Emergency Core Cooling System Performance," Regulatory Guide 1.157.

Updates to Sections 26.4 and 26.5 of WCAP-16996-NP

“Realistic LOCA Evaluation Methodology Applied to the Full

Spectrum of Break Sizes

(FULL SPECTRUM LOCA Methodology)”

26.4 STEADY STATE CALCULATION/CALIBRATION

Steady-state acceptance criteria are necessary because the above-mentioned fluid and core conditions are likely to differ somewhat from plant-to-plant and the degree to which these parameters are matched in the WCOBRA/TRAC-TF2 simulation must be consistent. Table 26.4-1 shows the acceptance criteria used in WCOBRA/TRAC-TF2 for acceptable simulation of plant conditions. A checklist for a number of significant parameters is given below, which utilizes this table to verify whether these variables have reached their acceptable steady-state values.

[

] ^{a,c}

[

] ^{a,c}

Table 26.4-1 Criteria for an Acceptable Steady-State

[illegible]

a,c

26.5 REFERENCES

1. Bajorek, S. M., et al., March 1998, “Code Qualification Document for Best Estimate LOCA Analysis,” Volume 1 Revision 2, and Volumes 2 through 5, Revision 1, WCAP-12945-P-A (Proprietary).
2. Bordelon, F. M. and Murphy, E. T., 1974, “Containment Pressure Analysis Code (COCO),” WCAP-8327 (Proprietary), WCAP-8306 (Non-Proprietary).
3. Bordelon, F. M., et al., 1974, “Westinghouse Emergency Core Cooling System Evaluation Model – Summary,” WCAP-8339.
4. Bordelon, F. M., et al., 1975, “The Westinghouse ECCS Evaluation Model: Supplementary Information,” WCAP-8471-P-A (Proprietary).
5. Crede, T. M., et al., 2013, “Westinghouse Performance Analysis and Design Model (PAD5),” WCAP-17642-P (Proprietary), WCAP-17642-NP (Non-Proprietary).
6. Shimeck, D. J., March 1988, “COSI SI/Steam Condensation Experiment Analysis,” WCAP-11767 (Proprietary).

Updates to Sections 29.4.1, 29.4.2, 29.5.1 and 29.7

of WCAP-16996-NP

“Realistic LOCA Evaluation Methodology Applied to the

Full Spectrum of Break Sizes

(FULL SPECTRUM LOCA Methodology)”

29 ASSESSMENT OF UNCERTAINTY ELEMENTS

The list of dominant phenomena was identified by the PIRT discussed in Section 2. The PIRT included all processes covering the scenarios that span the full spectrum of break sizes. A summary of the important phenomena was provided in Section 2.3.3. The code models associated with such phenomena were then assessed against an independent dataset comprised of separate effect tests (SETs) and integral effect tests (IETs). This was the subject of Sections 12 through 23. Section 24 provides a synthesis of the assessment as well as an analysis of potential compensating errors.

The code assessment exercise leads to the determination and quantification of model biases and uncertainties (EMDAP Step 20). Consistent with the CSAU roadmap, the uncertainty has to be ultimately propagated or convoluted statistically during the plant analysis. The statistical procedure used to propagate the uncertainties is the subject of Section 30. The approach is based on a Monte Carlo convolution of the uncertainty contributors. The procedure is designed to generate a sample of the LOCA ‘population’ and then develop probabilistic statements that show compliance with the 10 CFR 50.46 criteria.

In general, the uncertainty parameters fall into three categories:

1. Nominal without Uncertainty – The nominal (expected or midpoint) value of the parameter is used without consideration of uncertainty when the variation in the parameter is tightly controlled, such as pressurizer level, or when the sensitivity of the transient to the value of the parameter is negligible, such as the initial [reactor coolant system \(RCS\)](#) boron concentration. An example of a model treated as nominal without uncertainty is the offtake model (Section 29.1.1.1).
2. Bounded – A conservative value of the parameter is used when the parameter varies gradually as a function of operating history, when the sensitivity of the transient to variations in the parameter is small, or when the effort to develop and justify a detailed uncertainty treatment is judged to exceed the benefits of doing so. Bounded plant parameters are discussed in Section 29.3.1. An example of a phenomenon treated in a bounding manner is steam binding.
3. Nominal with Uncertainty – The Westinghouse methodology includes three categories of uncertainty contributors to the overall uncertainty assessment. These are the thermal-hydraulic model uncertainties, the power-related parameter uncertainties, and the initial and boundary condition uncertainties.

Tables 29-1 through Table 29-5 provide the list of the uncertainty contributors or parameters that are explicitly considered in the FSLOCA methodology. The uncertainty contributors [

] ^{a,c}

[]^{a,c} For most models, ranging capabilities on key parameters has been included in the code such that the solution can be randomly biased during the Monte Carlo convolution of the uncertainties. The objective of Section 29.1 is to develop and justify the probability density function (PDFs) associated with such key parameters.

While a PDF was developed and justified for most of the models, in some instances a bounding approach was judged to be adequate for the purpose of the uncertainty analysis. This was the case when a complete characterization of the individual model biases and uncertainty could not be pursued, because of the complexity of the process, and/or because limitations in experimental data caused the effort of developing a detailed uncertainty treatment for each individual component to exceed the benefit of doing so. In those circumstances the objective of the exercise was to demonstrate that the biases associated with that specific complex phenomenon, albeit not quantified, are conservative with respect to engineering figures of merit in the context of a realistic but still conservative LOCA simulation. In those cases the validity of the approach was also supported by compensating error analyses (Section 24). []

[]^{a,c}

The analysis of the uncertainty on the break flow is []

[]^{a,c} The discussion of the break model methodology deserves a section itself and Section 29.2 is dedicated to this topic.

Core power related parameters are listed in Table 29-4. The time in cycle is the first parameter selected since many fuel related parameters are a function of burnup. The methodology is presented in Section 29.4.1.

Uncertainties associated with the fuel rod models are listed in Tables 29-3 and 29-4. Some of these parameters are characterized as local uncertainties since the effect is postulated to mainly affect the local [peak cladding temperature \(PCT\)](#) or [maximum local oxidation \(MLO\)](#) and the effect on the global T/H response is expected to be minimal. []

[]^{a,c}

All the other uncertainty parameters are associated with the plant parameters listed in Table 29-5. Section 29.3 is dedicated to the topic.

Section 29.5 provides a review of the PIRT and summarizes the conclusions from the perspective of model biases and uncertainty of all phenomena ranked high (H). This corresponds to EMDAP Step 20. Finally, Section 29.6 addresses experimental accuracy in the context of Step 9 of the EMDAP roadmap.

Table 29-1 Uncertainty Elements – Break Location, Type and Area Sampling Methodology

a,c

Table 29-2 Uncertainty Elements – Thermal-Hydraulic Models

a,c

[illegible]

Table 29-3b Burst Strain for []^{a,c}

a,c

Table 29-4 Uncertainty Elements – Power-Related Parameters Defined in Section 29.4.1

a,c

Note:

1. The uncertainty range may be less if the analysis assumes only the maximum of the range (for operational flexibility) or if a basis for a smaller uncertainty range exists (as in the case of a Measurement Uncertainty Recapture uprate).

Table 29-5 Initial and Boundary Conditions Considered in Uncertainty Methodology Defined in Section 29.3.2

a,c

29.4 CORE AND FUEL ROD MODEL UNCERTAINTIES

29.4.1 Initial Reactor State Uncertainties

29.4.1.1 Time in Cycle

[

] ^{a,c}

| [Hot Rod Burnup](#)

[

] ^{a,c}

[

] ^{a,c}

[

] ^{a,c}

| Hot Assembly Rod Burnup

[

] ^{a,c}

| Core Balance Rods

[

] ^{a,c}

29.4.1.2 Reactor Core Power Distributions and Global Uncertainties

Reactor core power distributions are characterized by radial and axial power distributions, as discussed in Section 25.2.1. The steady-state radial distribution is established by core loading pattern, fuel enrichment, fixed burnable poisons, etc., and is not subject to wide variation during normal operation (Section 25.2.1.1). The maximum of the radial distribution is defined by $F_{\Delta H}$ (hot rod average power divided by the core average rod average power). Predictions of $F_{\Delta H}$ are accurate to within []^{a,c} at > 95 percent probability (Section 25.2.1.3). []

[]^{a,c}

Steady-state axial distributions are established by core loading pattern and burnup. The axial distribution tends to vary widely as a result of changes in reactor power, xenon transients, boron or control rods. The maximum of the radial distribution times maximum of the axial distribution is F_Q (maximum linear heat rate divided by the core average linear heat rate). Transients are simulated in the core design process, yielding a wide range of possible power distributions and F_Q values. As described in Section 25, []

[]^{a,c}

Plants operate in “baseload” (i.e., full power, control rods out) nearly all the time. In baseload operation, F_Q varies slowly with time. However, the Technical Specifications allow for transient operation. Figure 29.4.1-4 shows the effect of a typical load follow maneuver on peaking factor ($F_Q \times$ power), for a plant with a Technical Specification (Tech Spec) F_Q limit of []^{a,c}. In the Westinghouse FSLOCA methodology, []

[]^{a,c}

[

] ^{a,c}

[

] ^{a,c}

[

] ^{a,c}

Other sources of uncertainty in the power related parameters involve: 1) the accuracy with which the power distribution in the hot assembly and remainder of the core can be defined; 2) the accuracy with which the power at the hot spot (most limiting elevation of the hot rod) can be defined, including local uncertainties. The latter is addressed in Section 29.4.2.

The following contributors are considered, [

] ^{a,c}.

- Radial power distribution
- Total peaking factor and axial power distribution
- Initial core power level
- Decay heat
- Gamma redistribution

Radial Power Distribution

The hot assembly and core radial power distribution is modeled by defining the following variables:

- Hot rod average relative power, $F_{\Delta H}$. The hot rod average relative power, $F_{\Delta H}$ will be ranged according to its calculational uncertainty. This global uncertainty, as shown in Table 25.2-2, has a standard deviation equal to [] ^{a,c} of the nominal value.
- Hot assembly average power is [] ^{a,c} lower than $F_{\Delta H}$, minimum (Section 25), [

] ^{a,c}

- Power in the assemblies in the core periphery (PLOW), as a percent of average assembly power ($P_{a,c}$ are typical lower and upper bounds). Variations in this parameter will have a small effect on the power of the core average rods surrounding the hot assembly. $P_{a,c}$

Total Peaking Factor and Axial Power Distribution

As previously discussed, the axial power distribution is $P_{a,c}$

The initial power generation rate, as a function of elevation, is specified for the hot rod by the initial axial and radial power distributions (peaking factors F_Q and $F_{\Delta H}$) on the hot rod. The uncertainty associated with the total peaking factor F_Q (Tables 25.2-2 and 25.2-3) can be divided into two components; one closely coupled to the uncertainty in the hot assembly power, and one associated only with local uncertainties and therefore independent of the hot assembly. Since there is a fixed radial power distribution in the assembly, a fluctuation in the hot assembly power results in a similar fluctuation in the hot rod. This situation is illustrated in Figure 29.4.1-12. Fluctuations in the hot assembly rod are assumed to also affect the thermal-hydraulics (i.e., they affect the heat transfer coefficient boundary condition), and so the uncertainties are considered in the global thermal-hydraulic solution accordingly. $P_{a,c}$

$P_{a,c}$

Initial Core Power, Decay Heat, Gamma Redistribution

The remaining variables, core average power, gamma redistribution, and decay heat, contribute additional uncertainty to the peak linear heat rate. The uncertainty in core power ($AFLUX_0$, $P_{a,c}$) was quantified in Section 25.2.1.3. Increases (decreases) in $AFLUX$ result in proportional increases (decreases) in rod powers for all rods as described in Section 25.2.1.4.

Uncertainty in decay heat is considered through the application of ANSI/ANS 5.1-1979 Standard (DH, normal distribution). See also Section 9.7.

[

$P_{a,c}$

[

] ^{a,c}

Table 29.4.1-1 []^{a,c}

a,c

a,c

Figure 29.4.1-1 Maximum Rod Average Power at a Given Rod Burnup at Various Times During a Typical Cycle



| **Figure 29.4.1-2** |

|^{a,c}

a,c

**Figure 29.4.1-3 Fuel Pellet Average Temperatures as a Function of Rod Average Burnup
for 0.422-inch Outer Diameter Fuel**

a,c

Figure 29.4.1-4 Effect of Load Follow on F_Q

a,c

| **Figure 29.4.1-5** |

] ^{a,c}

a,c

| **Figure 29.4.1-6** |

] a,c

a,c

| **Figure 29.4.1-7** |

] ^{a,c}

a,c

| **Figure 29.4.1-8** |

] ^{a,c}

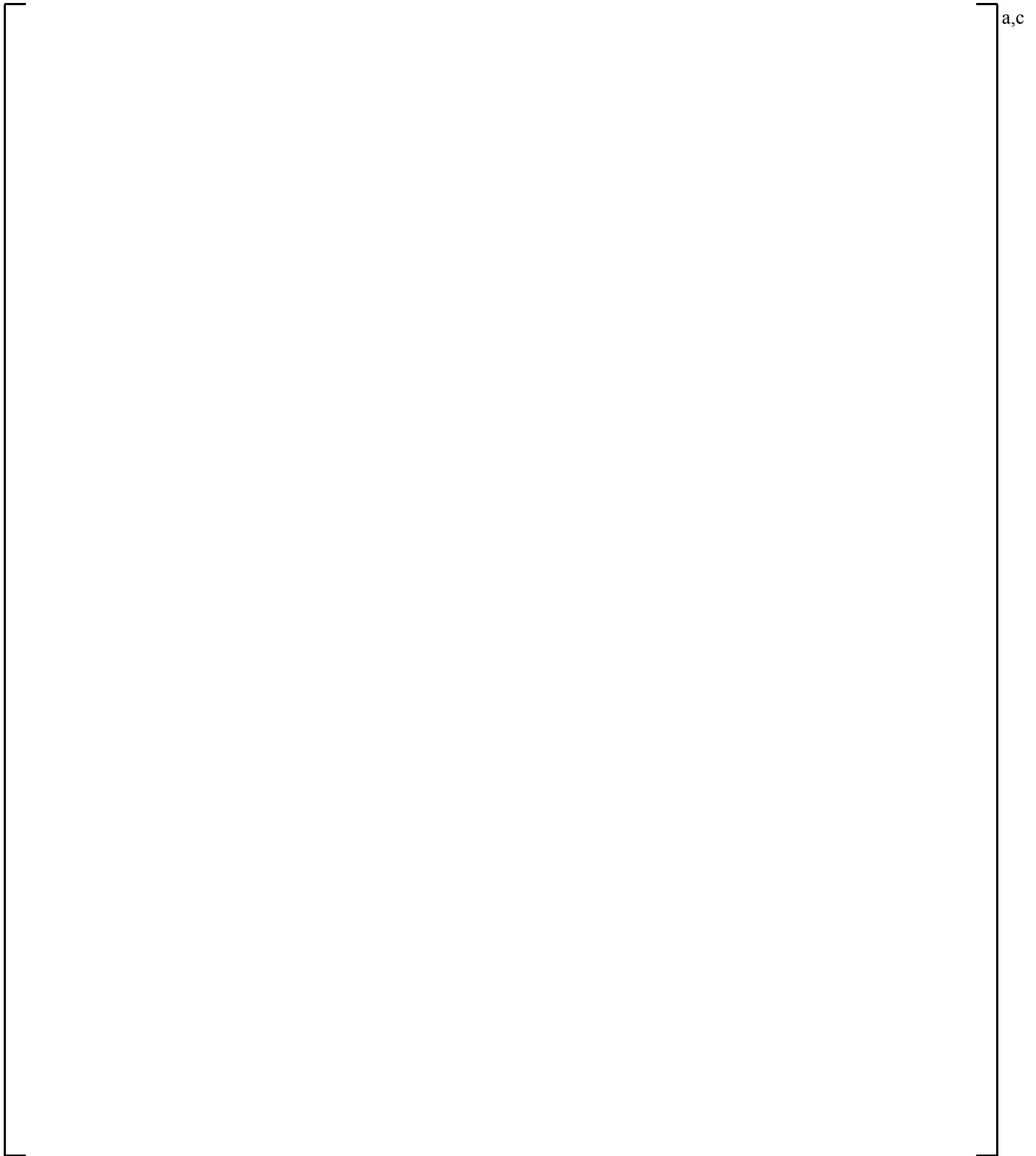


Figure 29.4.1-9 Example Bottom Skewed Axial Power Distribution [
]^{a,c}

a,c

Figure 29.4.1-10 Example Top Skewed Axial Power Distribution [
]^{a,c}

a,c

| **Figure 29.4.1-11** |

| ^{a,c}

a,c

| **Figure 29.4.1-12** |

]a,c

29.4.2 Hot Rod Local Models Uncertainty

Beside the uncertainty in hot rod local power discussed in the previous section, several other uncertainty contributors in the fuel rod models and heat transfer from the rod to the fluid contribute to the local hot spot uncertainty.

The fuel rod modeling was presented in Sections 8.3 through 8.6 (Volume 1). These included the fuel conduction model, the pellet-cladding gap conductance model, the fuel rod deformation model, the cladding reaction with water or steam models, and []^{a,c}. The heat transfer from the fuel rod to the fluid was discussed in Section 7 and its assessment is provided in Sections 14 and 15. The discussion in Sections 7 and 8 focuses on the models as coded, while here the discussion is expanded to describe the treatment of the uncertainty associated with those models.

In particular, the following contributors are considered:

- Hot rod peaking factor
- Hot rod radial peaking, [manufacturing tolerances](#), and rod bow uncertainties
- []^{a,c}
- Cladding burst temperature
- Cladding burst strain
- []^{a,c}
- Zirconium-water reaction
- Fuel relocation
- Convective heat transfer coefficient from the rod to the fluid

Models are considered ‘local’ when the effect of the uncertainty in those models has an effect limited to local processes, such as the local cladding temperature or local cladding oxidation, while the impact of such uncertainties on the ‘global’ thermal-hydraulic process is negligible. The hot rod peaking factor uncertainty reflects the power difference between the hot rod and the hot assembly rod. The additional uncertainty related to hot rod radial peaking, [manufacturing tolerances](#), and rod bow is captured by the local linear heat rate uncertainty. []

[]^{a,c} The uncertainties in the cladding burst temperature, the cladding burst strain, []^{a,c}, Zirconium-water reaction, fuel relocation, and convective heat transfer coefficient are incorporated into []^{a,c}.

In the previous ASTRUM methodology (Nissley, M. E., et al., 2005) the WCOBRA/TRAC solution was followed by the execution of a one-dimensional conduction code (HOTSPOT) []

[]^{a,c}

HOTSPOT is essentially a one-dimensional conduction code used to resolve the heat conduction []^{a,c}. Driven by boundary conditions on the fluid side calculated with WCOBRA/TRAC, HOTSPOT was used to simulate the transient conduction []^{a,c}. The models in HOTSPOT were consistent with the corresponding models in WCOBRA/TRAC.

[

] ^{a,c}

The uncertainty methodology for the heat transfer coefficients will be discussed in more detail in Section 29.4.3. The FSLOCA methodology for modeling the hot assembly rods was discussed in Section 8 and is briefly summarized here:

[

] ^{a,c}

29.4.2.1 []^{a,c}

[

] ^{a,c}

Fuel Internal Heat Generation – Local Uncertainty

As discussed in Section 29.4.1.2, the uncertainty in total peaking factor F_Q is comprised of components that are global in nature, and hence are closely coupled with hot assembly power, and components that are local in nature. The local uncertainties, which do not affect the global thermal-hydraulic solution, are accounted for []^{a,c}. From Tables 25.2-2 and 25.2-3, the local uncertainties in the

local heat generation arise from the combination of []^{a,c}. The total standard deviation (σ) can be expressed as:

$$\left[\left(\left[\right] \right)^2 + \left(\left[\right] \right)^2 \right]^{a,c} \quad (29.4.2-1)$$

[]^{a,c} The local uncertainty amounts to:

$$\left[\left(\left[\right] \right)^2 + \left(\left[\right] \right)^2 \right]^{a,c} \quad (29.4.2-2)$$

where []

[]^{a,c}

Cladding Burst Temperature

The rupture criteria for Zircaloy-4 cladding and ZIRLO[®] cladding introduced in Section 8.4.1 are applicable for both the hot assembly rod and []^{a,c}.

Cladding burst is calculated by monitoring the stress on the cladding and using the cladding rupture correlations to predict the rod burst as described in Section 8.4. The cladding burst temperature can be correlated fairly well as a function of hoop stress for ZIRLO[®] cladding as shown in Figure 8-19 in Section 8.4. Figure 29.4.2-1 is replication of Figure 8-19 with a band of []^{a,c} of the calculated burst temperature shown. The []^{a,c}.

The []^{a,c} uncertainty range on cladding burst temperature is used for both Zircaloy-4 and ZIRLO[®] cladding. The ZIRLO[®] data shown in Figure 29.4.2-1 actually indicates a smaller uncertainty than the assumed []^{a,c}. These data were obtained by Westinghouse using a consistent testing method. The zircaloy data from Powers and Meyer (1980), which were used to develop the zircaloy burst temperature and burst strain models in Section 8.4.1 (Volume 1), show scatter more consistent with the []^{a,c} range (Figure 1 of Powers and Meyer, 1980). This is believed to be at least partly attributable to the variety of testing methods used to obtain the Zircaloy-4 data. Although it is believed that the ZIRLO[®] cladding testing methods are as valid as those in Powers and Meyer, there may be some uncertainty due to the testing method, and the larger uncertainty for both cladding materials is used.

[]

[]^{a,c}

[

] ^{a,c}

a,c

Figure 29.4.2-1 ZIRLO® Cladding Burst Temperature Data and Correlation

Cladding Burst Strain

The burst strain discussed in Section 8.4, as shown in Figures 8-18 and 8-20 for the respective Zircaloy-4 and ZIRLO[®] cladding, is applied to hot assembly rod. However, the data in Figures 8-18 and 8-20 show wide scatter. Burman (1980) discussed how burst occurs randomly at “hot spots” which are the results of a wide range of azimuthal temperature gradients around the cladding. Burman also argued that in fuel rods these gradients can be larger due to random contact of the pellet against the cladding, which then causes smaller burst strains to occur.

For the cladding burst strain of the []^{a,c}, Figures 29.4.2-2 and 29.4.2-3 revisit the data of maximum burst strain as a function of burst temperature for the Zircaloy-4 and ZIRLO[®] cladding at different heatup rates to identify the influence of heat up rate. In both cases the scatter is very large for both alpha phase and beta phase, and low uncertainty for the alpha/beta transition region is observed. Thus, three burst temperature ranges are identified: []

[]^{a,c} Figures 29.4.2-4 to 29.4.2-6 show the Zircaloy-4 burst data in the form of histograms for burst temperature ranges []^{a,c}, indicating the frequency of occurrence of a particular burst strain within a range of burst temperatures. []

[]^{a,c} except for the difference in the transition temperature. The effect of heatup rate on cladding strain is evident []

[]^{a,c}

[

] ^{a,c}
$$\left[\quad \quad \right]^{a,c}$$

(29.4.2-3)

[

] ^{a,c}
$$\left[\quad \quad \right]^{a,c}$$

(29.4.2-4)

$$\left[\quad \quad \right]^{a,c}$$

(29.4.2-5)

[

] ^{a,c}

a,c

Figure 29.4.2-2 [

] ^{a,c}

a,c

Figure 29.4.2-3 [

] a,c

a,c

| **Figure 29.4.2-4** |] ^{a,c}

a,c

| **Figure 29.4.2-5** |

] ^{a,c}

a,c

| **Figure 29.4.2-6** |] ^{a,c}

a,c

| **Figure 29.4.2-7** |

] ^{a,c}

a,c

| **Figure 29.4.2-8** |

] a,c

a,c

| **Figure 29.4.2-9** |] ^{a,c}

a,c

Figure 29.4.2-10 |

a,c

Fuel Relocation Following Burst

The phenomenon of fuel relocation following cladding burst was discussed in Section 8.6.1. The fuel density at the burst region of []^{a,c} is measured by packing fraction. The packing fraction is the ratio of the volume of fuel within the burst region to the total volume within the burst region. The INEL (Broughton, 1981) studied data from several sources and used several measurement methods. In addition, NNC performed additional analyses using photographs of the fuel cross sections. These data are summarized in Table 29.4.2-1. A plot of this data versus burst strain (Figure 29.4.2-11) appears to confirm []^{a,c}. From these different measurement methods, the uncertainty on packing fraction was estimated.

The numbers of occurrences as a function of packing fractions are plotted in Figure 29.4.2-12. The range was calculated by taking the difference between the maximum and minimum value, and dividing by the average value. A histogram of the data is shown in Figure 29.4.2-12. []^{a,c}

Table 29.4.2-1 Packing Fractions Using Various Measurements				
Burst Strain Percent	Packing Fractions Percent (Various Measurement Methods)			
29	79	70	66	65
35	63	70	42	63
42	71	67	59	58
47	71	-	62	-
48	62	70	61	74
74	66	-	52	-

a,c

Figure 29.4.2-11 [

] a,c

a,c

Figure 29.4.2-12 Distribution of Packing Fraction Data

Zirconium-Water Reaction and its Uncertainty

The zirconium-water reaction rate calculations are performed using methods described in Volume 1, Section 8.5. When [

] ^{a,c} are from Cathcart and Pawel (1977). The prediction interval at 95 percent probability for these equations was calculated from the data using the following equation (Draper and Smith, 1981):

$$Y + t(95\%, n-2) \left[1 + \frac{1}{n} + \frac{(X - \bar{X})^2}{\sum (X_i - \bar{X})^2} \right]^{1/2} s \quad (29.4.2-6)$$

Where $t(95\%, n-2)$ is the 95 percentage point of a t-distribution with $n-2$ degrees of freedom, to account for sample size, \bar{X} is the average of the X values, and s^2 is the residual mean square of the data around the reaction equation line. The equation above is the prediction interval for the next “point estimate” of the reaction rate; the uncertainty interval for the prediction of the mean of the data is smaller (the equation is similar to that above except that the 1 is missing).

The “uncertainty” cited in [

] ^{a,c} A model is assumed of the form:

$$\ln(\delta^2 / 2) = A + B(1 / T(K)) \quad (29.4.2-7)$$

The regression output is shown in Table 29.4.2-2b. The output shows that the constants A and B are:

[
] ^{a,c}

These numbers compare to those in Table A2 of Cathcart and Pawel:

$A = -1.70986$
 $B = -20100$

[

] ^{a,c}

Pre-Accident Corrosion

NRC Information Notice 98-29 (Roe, 1998) provides clarification that the 10 CFR 50.46(b)(2) maximum local oxidation (MLO) criterion of 17% “includes both pre-accident oxidation and oxidation occurring during a LOCA.” In the FSLOCA uncertainty methodology, therefore, ‘MLO’ results are the sum of the two. At high rod average burnup, the uncertainty in pre-accident corrosion can become important when comparing the total calculated MLO against the 17% limit.

The approved corrosion models for ZIRLO[®] and Optimized ZIRLO[™] cladding (Garde et al., 2013) are incorporated into the PAD5 code as described in Section 3.3.1 of (Crede et al., 2013). The corrosion models were developed based on rod oxide measurements collected from cladding material in post-irradiation exams (PIEs), including data from operating plants. A calibration database was used to develop the model forms and for the determination of the final model coefficients, and a separate validation database was used to independently validate the models.

The corrosion model uncertainties were determined as a function of predicted thickness in order to cover 95% of the data over the entire measurement range. The actual uncertainty equation bounds more than 95% of the calibration data set.

In the FSLOCA methodology, [

1^{a,c}

Table 29.4.2-2a Zircaloy Rate Constants (Total Oxygen)				
T(°C)	$\delta^2/2=OX$	1/T(K)=X	(X-XBAR)²	LN(OX)=Y
1050	4.720E-08	0.000755	1.109E-08	-16.8689
1101	8.070E-08	0.000727	5.968E-09	-16.3325
1153	1.390E-07	0.000701	2.573E-09	-15.7888
1203	2.180E-07	0.000677	7.274E-10	-15.3388
1253	3.300E-07	0.000655	2.280E-11	-14.9242
1304	5.080E-07	0.000634	2.694E-10	-14.4928
1352	7.690E-07	0.000615	1.235E-09	-14.0782
1404	1.130E-06	0.000596	2.940E-09	-13.6933
1454	1.640E-06	0.000578	5.109E-09	-13.3208
1504	2.280E-06	0.000562	7.704E-09	-12.9913
NTESTS:		XBAR:	$\Sigma(X-XBAR)^2$:	
10		0.000650	3.764E-08	

Table 29.4.2-2b []^{a,c}	

Table 29.4.2-3 Predictions Using Equation 29.4.2-7 and Cathcart-Pawel

a,c

a,c

| **Figure 29.4.2-13** [

] a,c

a,c

| **Figure 29.4.2-14** [

] ^{a,c}

29.4.2.2 Initial Calibration of the Steady-State Condition for the Nuclear Rods

The initial fuel temperature and rod internal pressure for Westinghouse PWRs are calibrated against the PAD5 fuel performance code (Crede et al., 2013). The calibration of initial fuel temperature is performed for $I^{a,c}$ in FSLOCA.

The initial stored energy in the fuel is a direct function of the pellet average (radial) fuel temperature which we call TFUEL. The initial fuel temperature is a function of the local linear heat rate and burnup.

[

$$I^{a,c} = \left[\frac{I^{a,c}}{I^{a,c}} \right]_{a,c} \quad (29.4.2-8)$$

$$I^{a,c} = \left[\frac{I^{a,c}}{I^{a,c}} \right]_{a,c} \quad (29.4.2-9)$$

[

$I^{a,c}$

[

]^{a,c}

[]^{a,c}

(29.4.2-10)

[

]^{a,c}

[]^{a,c}

(29.4.2-11)

[

]^{a,c}

[

]^{a,c}

29.5 EVALUATION MODEL BIASES AND UNCERTAINTY (EMDAP STEP 20)

According to the Regulatory Guide 1.203, a singular uncertainty statement on the overall uncertainty results can only be achieved when the individual uncertainty contributions are determined. The procedure used to obtain the convolution of such uncertainties is the subject of Section 30. The development of the individual uncertainty contributors, ranges, and probability density functions has been the objective of this section.

The uncertainty contributors are divided in two main categories:

1. The first main category is the uncertainty associated with the code capability of representing phenomena and processes identified as highly important by the PIRT. The capability is established by assessing the code against SET/IET experiments that were designed to simulate such processes. The combined uncertainty will reflect the degree to which the individual models, correlations and methods used within the code represent the physical phenomena, the uncertainty associated with the use of such models, and the uncertainty associated with the experimental data itself and applicability of the data to PWRs.
2. The second main category is the uncertainty associated with the input boundary and initial conditions and all those parameters that define the plant state at the time of the postulated LOCA event, as well as the uncertainty associated with the break location, break type and size, etc. This uncertainty is not the result of the code capability of simulating the LOCA event, but rather the uncertainty associated with the LOCA scenario event itself.

The purpose of this section is to summarize the methodology for the treatment of the uncertainty contributors contained mainly in the first category. This is in line with the intent of Step 20 of the EMDAP, which asks for the determination of the EM biases and uncertainty. Since the process started by identifying the important phenomena with the PIRT, it is useful here to structure the review following the PIRT (Section 2), by describing how each of the phenomena was considered in the uncertainty methodology.

29.5.1 Fuel Rod

Stored Energy

Uncertainties in the initial stored energy of the hot rod and hot assembly are large. There is a wide range of possible peaking factors and power distributions that are allowed by the Technical Specifications. For a given power distribution, [

] ^{a,c} have been considered in the uncertainty methodology by explicitly ranging them as part of the uncertainty methodology.

Clad Oxidation

The metal-water reaction rate is ranged based on uncertainty estimates obtained from experimental data. This uncertainty is treated as a local uncertainty – see Table 29-3a for the numerical values.

[]^{a,c}

Decay Heat

The decay heat uncertainties from the American National Standards Institute/American Nuclear Society (ANSI/ANS) 5.1-1979 standard are applied as described in Section 9.7. []

^{a,c}

Clad Deformation (Burst Strain, Relocation)

These processes were ranked []

^{a,c} The uncertainty on cladding burst strain and temperature are obtained from the data scatter. The fuel pellet fragments packing fraction after relocation is also identified as an uncertainty contributor. Numerical values are provided in Table 29-3a and Table 29-3b.

29.7 REFERENCES

1. Akimoto, et al., 1984, J. Nucl. Sci. & Tech., 21[6], pp. 450-465, June 1984.
2. Bajorek, S. M., et al., 1998, "Code Qualification Document for Best Estimate LOCA Analysis," WCAP-12945-P-A, Volume 1 Revision 2, and Volumes 2 through 5 Revision 1, and WCAP-14747.
3. Boyack, B., et al., "Quantifying Reactor Safety Margins," NUREG/CR-5249, (1989).
4. American Nuclear Society, 1979, "Decay Heat in Light Water Reactors," ANSI/ANS 5.1.
5. Anklam, T. M., et al., 1982, "Experimental Investigations of Uncovered Bundle Heat Transfer and Two-Phase Mixture Level Swell Under High Pressure Low Heat Flux Conditions," NUREG/CR-2456.
6. Baum, A. J., 1977, "A Study of Transition and Film Boiling From Vertical Surfaces," Ph. D. Thesis, Carnegie-Mellon University.
7. Bordelon, F. M. and Murphy, E. T., 1974, "Containment Pressure Analysis Code (COCO)," WCAP-8327 (Proprietary), WCAP-8306 (Non-Proprietary).
8. Broughton, J. M., 1981, "PBF LOCA Test Series, Test LOC-3 and LOC-5 Fuel Behavior Report," NUREG/CR-2073.
9. Burman, D. L., 1980, "Comparison of Westinghouse LOCA Burst Tests Results with ORNL and Other Program Results," Specialist Meeting on Fuel Behavior Under Accident Conditions, September 1 – 4, Helsinki, Finland.
10. Cathcart, J. V., and Pawel, 1977, "Zirconium Metal-Water Oxidation Kinetics IV – Reaction Rate Studies," ORNL/NUREG-17, Oak Ridge National Laboratory, Oak Ridge, TN.
11. Combustion Engineering, 1981, "C-E ECCS Evaluation Model – Flow Blockage Analysis – ECCS Analysis," Enclosure 1-P-A (Proprietary) and Enclosure 1-NP-A (Non-Proprietary) to LD-81-095.
12. Crede, T. M., et al., 2013, "Westinghouse Performance Analysis and Design Model (PAD5)," WCAP-17642-P (Proprietary), WCAP-17642-NP (Non-Proprietary).
13. Crane Co., 1988, "Flow of Fluids Through Valves, Fittings, and Pipes," Technical Paper No. 410.
14. Dhir, V. K., Duffey, R. B., and Catton, I., 1981, "Quenching Studies on a Zircaloy Rod Bundle," ASME J. Heat Transfer, Vol. 103, pp. 293-299.
15. Draper, N. and Smith, H., 1981, "Applied Regression Analysis, Second Edition," John Wiley and Sons.

16. Frepoli, C., 2007, "Assessment of Rod-to-Rod Thermal Radiation Heat Transfer Contribution During Reflood in PWR Fuel Assemblies," ICAPP 2007, Nice, France, May 13-18, Paper 7323.
17. Garde, A., et al., "Westinghouse Clad Corrosion Model for ZIRLO and *Optimized ZIRLO*," WCAP-12610-P-A & CENPD-404-P-A, Addendum 2-A (Proprietary), WCAP-14342-A & CENPD-404-NP-A, Addendum 2-A (Non-Proprietary), October 2013.
18. Ganic, E. and Rohsenow, W. M., 1977, "Dispersed Flow Heat Transfer," Int. J. Heat Mass Transfer, Vol. 20, pp. 855-866.
19. Henry, R. E., 1974, "A Correlation for the Minimum Film Boiling Temperature," AICHE Symposium Series, Vol. 138, pp. 81-90.
20. Holmes, B. J., 1991, "ISP 25 Comparison Report," AEA-TRS-1043.
21. Lanning, D. D., Beyer, C. E., Geelhood, K. J., 2005, "FRAPCON-3 Updates, Including Mixed-Oxide Fuel Properties," Pacific Northwest National Laboratory, NUREG/CR-6534, Vol. 4.
22. Loftus, M. J., et al., 1980, "PWR FLECHT-SEASET Unblocked Bundle Forced and Gravity Reflood Task, Data Report," WCAP-9699.
23. Morita, T., et al., 1974, "Power Distribution Control and Load Following Procedures," WCAP-8385-P-A.
24. MPR, 1990, "Summary of Results From the UPTF Downcomer Separate Effects Tests, Comparison to Previous Scaled Tests, and Application to U.S. Pressurized Water Reactors," MPR Associates, MPR-1163.
25. Nissley, M. E., et al., 2005, "Realistic Large-Break LOCA Evaluation Methodology Using the Automated Statistical Treatment **Of** Uncertainty Method (ASTRUM)," WCAP-16009-P-A and WCAP-16009-NP-A.
26. Powers, D. A. and Meyer, R. O., 1980, "Cladding Swelling and Rupture Models for LOCA Analysis," NUREG/CR-0630.
27. Roe, J., 1998, "NRC Information Notice 98-29: Predicted Increase in Fuel Rod Cladding Oxidation."
28. Schueren, P., 2006, "Optimized ZIRLO™," WCAP-12610-P-A & CENPD-404-P-A, Addendum 1-A.
29. Shumway, R., 1985, "Return to Nucleate Boiling," ANS Proceedings National Heat Transfer Conference, Denver, CO, pp. 372-388.
30. Spier, E. M., et al., 1988, "Evaluation of Nuclear Hot Channel Factor Uncertainty," WCAP-7308-L-P-A.

31. Tasaka, K., et al., 1988, "The Results of 5% Small Break LOCA Tests and Natural Recirculation Tests at the ROSA-IV LSTF," Nuclear Engineering and Design, 108.
32. Tregoning, Abramson, Scott, and Chokshi, "LOCA frequency evaluation using expert elicitation," Nuclear Engineering and Design 237 (2007) 1429-1436.
33. Vijaykumar, R. and Dhir, V. K., 1992, "An Experimental Study of Sub-cooled Film Boiling on a Vertical Surface – Hydrodynamic Aspects," ASME J. Heat Transfer, Vol. 114, pp. 161-178.
34. Wong, S. and Hochreiter, L. E., 1981, "Analysis of the FLECHT-SEASET Unblocked Bundle Steam Cooling and Boiloff Tests," NRC/EPRI/Westinghouse-8.
35. Yoder, et al., 1982, "Dispersed Flow Film Boiling in Rod Bundle Geometry – Steady-State Heat Transfer Data and Correlation Comparisons," NUREG/CR-2435, ORNL-5822.

Updates to Sections 30.1, 30.4, 30.5, 30.6 and 30.7 of

WCAP-16996-NP

“Realistic LOCA Evaluation Methodology Applied to the Full

Spectrum of Break Sizes

(FULL SPECTRUM LOCA Methodology)”

30 TECHNICAL BASIS OF STATISTICAL PROCEDURES APPLIED IN FULL SPECTRUM LOCA UNCERTANTY METHODOLOGY

30.1 STATISTICAL METHODOLOGY ROADMAP

A realistic (best-estimate) safety analysis asks for the assessment of uncertainties associated with physical models, data uncertainties, and plant initial and boundary condition variability. The current safety regulations of the United States Nuclear Regulatory Commission (US NRC) are stipulated in 10 CFR Part 50, Section 50.46. Based on the 10 CFR 50.46 rule, an emergency core cooling system (ECCS) design is required to satisfy prescriptive criteria. The regulation identifies the following five criteria:

1. Peak cladding temperature (PCT) shall be less than 2200°F
2. Maximum local oxidation (MLO) shall be less than 17%
3. Core-wide oxidation (CWO) shall be less than 1% (to limit the maximum amount of hydrogen generated)
4. The core shall maintain a coolable geometry
5. Long term cooling shall be demonstrated

NRC Information Notice 98-29 (Roe, 1998) provides further clarification that the 10 CFR 50.46(b)(2) MLO criterion “includes both pre-accident oxidation and oxidation occurring during a LOCA.” In the FSLOCA uncertainty methodology, therefore, ‘MLO’ results are the sum of the two.

Code Scaling, Applicability, and Uncertainty (CSAU) Element 3, the sensitivity and uncertainty analysis element, aims to provide a simple Best-Estimate Plus Uncertainty (BEPU) statement (Boyack, et al. 1989) that satisfies the first three criteria above. To accomplish this objective, the effects of the important uncertainty contributors are determined. The uncertainty statement is based on the combined effect of the contributors.

The objective of a LOCA analysis is to address criteria (b)(1), (b)(2) and (b)(3) of 10 CFR 50.46, the determination of peak cladding temperature (PCT), maximum local oxidation (MLO) and core-wide oxidation (CWO). Typically the last two criteria (coolable geometry and long-term cooling), are satisfied outside the LOCA analysis once the LOCA calculation is demonstrated to be in compliance with the first three criteria. [

] ^{a,c}

Regarding the treatment of uncertainties within the CSAU framework, the most straightforward approach is to combine the uncertainties with a direct Monte Carlo simulation. The procedure is designed to generate a sample of the short term LOCA ‘population,’ and then non-parametric statistical inference procedures are used to develop probabilistic statements that show compliance with the 10 CFR 50.46 criteria.

The code (WCOBRA/TRAC-TF2) is the ‘black-box’ which receives as input a set of random values, one for each uncertainty parameter, and outputs the three values that characterize a specific LOCA scenario (PCT, MLO and CWO). [

] ^{a,c}

Several cases (scenarios) are executed until the sample size is large enough to represent the population and stabilize the estimates of the key parameters of interest. The issue is how results are interpreted to demonstrate compliance with the 10 CFR 50.46 requirements.

10 CFR 50.46 states that “[...] *uncertainty must be accounted for, so that, when the calculated ECCS cooling performance is compared to the criteria set forth in paragraph (b) of this section, there is a high level of probability that the criteria would not be exceeded.*” Paragraph (b) of 10 CFR 50.46 contains the list of the acceptance criteria. 10 CFR 50.46 does not explicitly specify how this probability should be evaluated or what its value should be.

Additional clarification as to the US NRC expectations on the acceptable implementation of the “high probability” requirement is provided in Section 4 of Regulatory Guide 1.157 (Best-Estimate Calculations of Emergency Core Cooling System Performance) that states: “*a 95% probability is considered acceptable to the NRC staff [...].*” Further, Regulatory Guide 1.157 introduced the concept of confidence level as a possible refinement to the uncertainty treatment, but did not expand further on this concept.

As statistical methods are implemented to perform LOCA safety analyses, a statistical statement which estimates or bounds the 95th quantile of the population with a 95% confidence level has been suggested by the NRC as acceptable to demonstrate the required “high probability.” In the previous approved methodology (ASTRUM, WCAP-16009-P-A) the 95th quantile of the joint-distribution of PCT, MLO and CWO is bounded with at least 95% confidence level. The Safety Evaluation Report (SER) of the Westinghouse Best-Estimate Large Break LOCA methodology (ASTRUM) states the following: “*the staff determined that a 95th percentile probability level based on best approximations of the constituent parameter distributions and the statistical approach used in the methodology is appropriately high for this application.*”

Consistently with the previously approved methodology, the 95/95 criterion is also considered for the FULL SPECTRUM LOCA (FSLOCA) methodology.

One key difference between the previous LBLOCA methodology (ASTRUM, WCAP-16009-P-A) and FSLOCA is that the FSLOCA methodology extends the break area spectrum considered in the analysis to cover the full range from what is historically defined as Small Breaks (SB) to Large Breaks (LB) including break sizes typically not analyzed and classified as Intermediate Breaks (IB).

As discussed in Section 29.4, a simple extension of the ASTRUM approach to smaller break sizes was considered not appropriate because SBLOCA would not be properly considered in the sample by simply

extending a uniform probability distribution of the split break sizes in the SB region. A more balanced approach has been developed and was discussed in Section 29.4.

[

] ^{a,c}

30.4 [

] ^{a,c}

[

] ^{a,c}

[

] ^{a,c}

[

] ^{a,c}

30.5 OVERVIEW OF FULL SPECTRUM LOCA STATISTICAL PROCEDURE

Sections 30.3 and 30.4 provided the theoretical basis for the various statistical procedures needed to:

1. Generate a representative sample of the LOCA scenarios population;
2. Analyze the results and infer figures of merit that can satisfy compliance with the 10 CFR 50.46 design criteria.

[

] ^{a,c}

[

] ^{a,c}

[

] ^{a,c}

30.6 CONCLUSIONS ON COMPLIANCE WITH 10 CFR 50.46 ACCEPTANCE CRITERIA

The previous Sections described the statistical theory used to determine the number of cases required to bound the 95th percentile of []^{a,c} with a joint probability of 95% confidence. This assures that there is a high probability that the first two acceptance criteria are met, consistent with the Code of Federal Regulations (CFR) 10 CFR 50.46 requirements and Regulatory Guide 1.157 guidance. Further insights on the full compliance with the 10 CFR 50.46 criteria are described below.

30.6.1 []^{a,c}

[

] ^{a,c}

30.6.2 []^{a,c}

[

] ^{a,c}

[

] ^{a,c}

30.7 REFERENCES

1. Boyack, B., et al., "Quantifying Reactor Safety Margins," NUREG/CR-5249, (1989).
 2. [
-] ^{a,c}
3. Guba, A., et al., "Statistical Aspects of Best Estimate Method-I," Reliability Engineering and System Safety, 80, (2003), pp. 217-232.

4. Montgomery, D. C., "Design and Analysis of Experiments," 5th Edition, 2000.
5. Press, W. H., et al., "Numerical Recipes in FORTRAN: The Art of Scientific Computing," 2nd Edition, Cambridge University Press, 1992, Chapter 7.
6. [Roe, J., "NRC Information Notice 98-29: Predicted Increase in Fuel Rod Cladding Oxidation," August 3, 1998.](#)
7. Wald, A., "An Extension of Wilks' Method for Setting Tolerance Limits," Annals of Mathematical Statistics, Vol. 14 (1943), pp. 45-55.
8. Wilks, S. S., "Determination of Sample Sizes for Setting Tolerance Limits," The Annals of Mathematical Statistics, Vol. 12 (1941), pp. 91-96.

Updates to Sections 32.1, 32.2 and 32.4 of WCAP-16996-NP

“Realistic LOCA Evaluation Methodology Applied to the Full

Spectrum of Break Sizes

(FULL SPECTRUM LOCA Methodology)”

32 METHODOLOGY SUMMARY

In this section, the FULL SPECTRUM LOCA (FSLOCA) evaluation model is assessed against applicable regulatory criteria and guidance.

32.1 COMPLIANCE WITH 10 CFR 50.46

1. (i) – This part briefly outlines the requirements for an acceptable evaluation model, and requires that demonstration be provided that the limits of the Code of Federal Regulations (CFR) 10CFR50.46 be met with a high degree of probability. Additional details concerning these requirements are spelled out in Regulatory Guides (RG) 1.157 (US Nuclear Regulatory Commission (NRC), 1989) and 1.203 (US Nuclear Regulatory Commission, 2005). Compliance of the best-estimate methodology with these requirements is addressed in detail in the next section.
2. Peak Cladding Temperature – The peak cladding temperature (PCT) is verified to remain below the limit of 2,200°F for loss-of-coolant accidents (LOCAs) of all break sizes, using the methods described in Section 30. A demonstrative application of the method is discussed in Section 31.
3. Maximum Cladding Oxidation – The maximum cladding oxidation (MLO) is verified to remain below the regulatory limit of 17 percent of cladding thickness, using the procedure described in Section 30. [Consistent with NRC Information Notice 98-29 \(Roe, 1998\), MLO is taken as the sum of pre-accident oxidation and the oxidation occurring during the LOCA.](#) A demonstrative application of the method is discussed in Section 31.
4. Maximum Hydrogen Generation – The hydrogen generated in the core, as determined by estimating the total volume of cladding oxidized for the limiting conditions, is verified to be less than the regulatory limit of 0.01 times the maximum theoretical amount, using the procedure described in Section 30. A demonstrative application of the method is discussed in Section 31.
5. Coolable Geometry – Westinghouse reload cores are analyzed using plant-specific or bounding seismic and LOCA loads to confirm that the core remains coolable during the LOCA. This acceptance criteria is met by compliance with acceptance criteria (b)(1), (b)(2), and (b)(3), and showing that grid crush due to combined seismic and LOCA loads does not extend to the in-board assemblies. Specific calculations are performed if grid crushing occurs in the in-board assemblies to assess the effects of the grid crush (Section 25.1).
6. Long-Term Cooling – Long-term cooling is dependent on the demonstration of continued delivery of cooling water to the core. The actions, automatic or manual, that are currently in place at these plants to maintain long-term cooling remain unchanged.

[The NRC has initiated the formal process to revise the ECCS acceptance criteria in § 50.46 via issuance of an Advance Notice of Proposed Rulemaking \(FR 40765\). In its current form, the FSLOCA EM shows compliance with the current 10 CFR 50.46 criteria. Changes to the method will be required to address the 10 CFR 50.46c rulemaking, with the expectation that the Maximum Cladding Oxidation criterion will be replaced with an allowable Equivalent Cladding Reacted \(ECR\) limit that is based on cladding hydrogen](#)

content (along with other considerations). Appendix A of this report describes how the FSLOCA EM will comply with known elements of the 10 CFR 50.46c rulemaking when the rulemaking process is complete.

32.2 COMPLIANCE WITH REGULATORY GUIDE 1.203

The FULL SPECTRUM LOCA Evaluation Model (FSLOCA EM) has been developed consistently with Regulatory Guide (RG) 1.203 which represents an evolution and extension to the 1989 RG 1.157. RG 1.203 provides guidance on the Evaluation Model Development and Assessment Process (EMDAP). RG 1.203 extends on the regulatory positions of RG 1.157 which has been the basis of previously approved methodologies (2004 ASTRUM EM, WCAP-16009-P-A and 1996 CQD, WCAP-12945-P-A).

The EMDAP is the process utilized to define the function requirements of the EM and to guide through its assessment such that a decision on the EM adequacy for the purpose of LOCA safety analysis can be made. The EMDAP comprises 4 Elements and a total of 20 Steps which represent the Regulatory Position on the matter.

The mapping of the FSLOCA EM to the EMDAP was already provided in Section 1.2. The purpose of this section is to summarize main conclusions relative to compliance with regulatory guide RG 1.203 and aspect of RG 1.157 that are not already considered in RG 1.203.

32.4 REFERENCES

1. Bajorek, S. M., et al., 1998, "Code Qualification Document for Best Estimate LOCA Analysis," WCAP-12945-P-A, Appendix C (Proprietary).
2. Nissley, M. E., et al., 2005, "Realistic Large Break LOCA Evaluation Methodology Using Automated Statistical Treatment of Uncertainty Method (ASTRUM)," WCAP-16009-P-A, Revision 0, and WCAP-16009-NP-A, Revision 0 (Non-Proprietary).
3. NRC, 1989, "Best-Estimate Calculations of Emergency Core Cooling System Performance," Regulatory Guide 1.157.
4. NRC, 2005, "Transient and Accident Analysis Methods," Regulatory Guide 1.203.
5. [Roe, J., "NRC Information Notice 98-29: Predicted Increase in Fuel Rod Cladding Oxidation," August 3, 1998.](#)

**WCAP-16996-P, "Realistic LOCA Evaluation Methodology Applied to the Full Spectrum of Break Sizes
(FULL SPECTRUM LOCA Methodology)"
Requests for Additional Information – Fourth Set (Non-Proprietary)**

May 2013

Westinghouse Electric Company LLC
1000 Westinghouse Drive
Cranberry Township, PA 16066

©2013 Westinghouse Electric Company LLC
All Rights Reserved

Question #40: Fuel Burnup Limit in FSLOCA Methodology

Please clarify if the FSLOCA™ methodology is limited to 62,000 megawatt-days per metric ton of uranium rod average burnup for LOCA licensing applications. If so, please explain how this burnup limit was established and where it is described in the FSLOCA methodology. In addition, please explain if the rod average burnup limit has been adequately and consistently accounted for in the proposed FSLOCA sampling methodology.

Response:

Westinghouse fuel is currently licensed to a peak rod burnup of 62,000 MWD/MTU based on the fuel rod design limit with the use of PAD 4.0 [1]. The burnup limit for FSLOCA also comes from several areas in the method itself. The burnup limit in the decay heat power modeling is discussed in the response to RAI-23. Also the model used for the Uranium Oxide thermal conductivity has its applicability limited to 62,000 MWD/MTU as stated in Section 11.4.1 of [2]. The rod burnup sampling in FSLOCA is performed consistent with this limitation as described in Section 29.4.1.1 of [2].

Westinghouse is currently in the process of developing and submitting to the USNRC an updated version of the PAD fuel performance code, PAD 5.0. []^{a,c} Among other features, PAD 5.0 will include an explicit treatment of burnup-related phenomena such as fuel TCD.

Once PAD 5.0 is approved, PAD 5.0 will replace PAD 4.0 as the current fuel performance interface to the FSLOCA EM. The FSLOCA EM may need to be updated to reflect the changes of the fuel performance code, as well as the 10 CFR 50.46 rule change. The rod burnup sampling method is expected to be revised based on PAD 5.0, however, the compliance to the burnup limitation will be strictly maintained.

References:

1. ADAMS Accession Number: ML061420458, "APPROVAL FOR INCREASE IN LICENSING BURNUP LIMIT TO 62,000 MWD/MTU (TAC NO. MD1486)."
2. WCAP-16996-P, "Realistic LOCA Evaluation Methodology Applied to the Full Spectrum of Break Sizes (FULL SPECTRUM LOCA Methodology)," November 2010.

Question #41: Nuclear Fuel Rod Special Model Changes

The nuclear fuel rod conductor in the FSLOCA methodology has several special models used for analyses of nuclear fuel rods. These models include a fuel rod quench front model, a dynamic pellet-cladding gap conductance model, a fuel rod deformation model, and a cladding reaction model. These models are described in WCAP-16996-P/WCAP-16996-NP, Volumes I, II and III, Revision 0, Section 8.3.1, Section 8.3.2, Section 8.4, and Section 8.5, correspondingly.

The previous ASTRUM LBLOCA Evaluation Model (EM) documented in WCAP-16009-P-A (Nissley, M. E., et al., 2005) describes the fuel rod quench front model in Section 7-3-1, the dynamic pellet-cladding gap conductance model in Section 7-3-2, the fuel rod deformation model in Section 7-4, and the cladding reaction model in Section 7-5.

Please clarify the following items related to the above identified models implemented in the fuel rod conductor in WCOBRA/TRAC-TF2.

- (1) The fuel rod quench front model in the ASTRUM **FSLOCA** EM is presented in WCAP-16996-P/ WCAP-16996-NP, Volumes I, II and III, Revision 0, Section 8.3.1, which contains Equations (8-25a) and (8-25a). The same model for the 2005 ASTRUM LBLOCA EM is presented in Section 7-3-1 of WCAP-16009-P-A, which contains Equation (7-25). Please identify and describe any changes introduced to the **FSLOCA** methodology model in comparison to the 2005 ASTRUM LBLOCA model.
- (2) The dynamic pellet-cladding gap conductance model in the ASTRUM **FSLOCA** EM is presented in WCAP-16996-P/WCAP-16996-NP, Volumes I, II and III, Revision 0, Section 8.3.2, which contains Equations (8-26) through (8-35). The same model for the 2005 ASTRUM LBLOCA EM is presented in Section 7-3-2 of WCAP-16009-P-A, which contains Equations (7-26) through (7-35). Although the models appear identical, please identify and describe any changes introduced to the **FSLOCA** methodology model in comparison to the 2005 ASTRUM LBLOCA model.
- (3) The fuel rod deformation model in the ASTRUM **FSLOCA** EM is presented in WCAP-16996-P/ WCAP-16996-NP, Volumes I, II and III, Revision 0, Section 8.4, which contains Equations (8-36) through (8-73). The same model for the 2005 ASTRUM LBLOCA EM is presented in Section 7-4 of WCAP-16009-P-A, which contains Equations (7-36) through (7-72). Some differences between both models were identified. Thus, the description in Section 8.4.2, "Effects of Fuel Rod Deformation on Core Thermal-Hydraulics," of WCAP-16996-P/WCAP-16996-NP, Volumes I, II and III, Revision 0, appears different in its last Subsection "Flow Blockage Due to Rod Deformation," which contains Equations (8-72) and (8-73) for blockage form loss. The corresponding Section 7-4-2 ends with a Subsection "Continuity and Momentum Cell Flow Areas," which only includes only Equation (7-72) for the flow area reduction factor. At the same time, Equation (7-69) for the outer radius of the heat transfer node containing the burst elevation in Section 7-4-2 is omitted in Section 8.4.2. Please identify and describe any changes introduced to the **FSLOCA** model in comparison to the 2005 ASTRUM LBLOCA model and present the validation base for the introduced modifications.
- (4) The cladding reaction model in the ASTRUM **FSLOCA** EM is presented in Section 8.5 of WCAP-16996-P/WCAP-16996-NP, Volumes I, II and III, Revision 0, which contains

Equations (8-74) through (8-85). The same model for the 2005 ASTRUM LBLOCA EM is presented in WCAP-16009-P-A Section 7-5, which contains Equations (7-73) through (7-87). Both model descriptions appear identical with the exception that the 2005 ASTRUM LBLOCA EM includes a description of the oxidation kinetics of **ZIRLO**[®] cladding material manufactured by Westinghouse at high temperatures based on a model by D. L. Burman, "**ZIRLO**[™] High Temperature Oxidation Tests," Appendix E to WCAP-12610, Westinghouse, Pittsburgh, PA, 1990. This model description along with the pertaining Equations (7-80) through (7-82) is not provided for the **FSLOCA** model. Please identify and describe any changes introduced to the **FSLOCA** model in comparison to the 2005 ASTRUM LBLOCA model and present the validation base for the introduced modifications.

Response:

(1) The fuel rod quench front model described in the ASTRUM Evaluation Model (EM) (WCAP-16009-P-A, Reference 1) is used in the **FSLOCA** EM (WCAP-16996-P, Reference 2). There are a few minor updates on the documented formulas in WCAP-16009-P-A and on the application of the model. Below is a list of differences between Section 8.3.1 in WCAP-16996-P and Section 7-3-1 in WCAP-16009-P-A:

- Because a heat transfer node could be []^{a,c} Eq. 7-25 in WCAP-16009-P-A was updated to be more generalized as shown in Eq. 8-25a in WCAP-16996-P. This change is limited to the documentation.
- Eq. 8-25b (Reference 2) was added to explicitly define the energy balance when a heat transfer node is removed (i.e., nodes coalesced). This change is limited to the documentation.
- In the **FSLOCA** EM, the []^{a,c} do not exist in the ASTRUM EM.
- As stated in Section 7-8 of WCAP-16009-P-A, []^{a,c} This is a new application of the model.

(2) The dynamic pellet-cladding gap conductance model in the ASTRUM EM (WCAP-16009-P-A) is continuously used in **FSLOCA** EM (WCAP-16996-P). There are a few corrections on the documented formulas in ASTRUM EM. Below is a list of differences between Section 7-3-2 in WCAP-16009-P-A and Section 8.3.2 in WCAP-16996-P.

- Eq. 8-34 in WCAP-16996-P corresponds to Eq. 7-34 in WCAP-16009-P-A. The unit of roughness in R1 and R2 has been corrected from inch to feet. The change is limited to the documentation.

¹ ZIRLO is a trademark or registered trademark of Westinghouse Electric Company LLC, its affiliates and/or its subsidiaries in the United States of America and may be registered in other countries throughout the world. All rights reserved. Unauthorized use is strictly prohibited. Other names may be trademarks of their respective owners.

- To complete Eq. 8-34, Eq. 8-34a was inserted to give the formula to evaluate the Meyer hardness. Eq. 8-34a is the same formula as in Eq. (B-16.1) in NUREG/CR-0497 (Reference 3). However, a typo in B-16.1 (Reference 3) was corrected in Eq. 8-34a. The sign in front of " $T(2.5621 \times 10^{-8})$ " should be a minus to match the curve in Fig. B-16.1 (Reference 3). The source code listed on p. 482 of NUREG/CR-0497 also shows the sign to be a minus. The change is limited to the documentation.
- In the **FSLOCA** EM, the overall calculated conductance of the gap after pellet and cladding contact in GAPHTC is limited by the value of $3.0 \text{ E5 BTU/hr-ft}^2\text{-F}$. This value is selected to be outside the normal gap conductance range, but be able to improve robustness of fuel rod conductance calculation. The limiter tends to conservatively reduce the gap conductance when it is applied.

(3) The majority of fuel rod deformation models in **FSLOCA** EM (WCAP-16996-P) are consistent with those in the ASTRUM EM (WCAP-16009-P-A). The differences between Section 7-4 in WCAP-16009-P-A and Section 8.4 in WCAP-16996-P are listed below:

- Eq. 8-46 in WCAP-16996-P corresponds to Eq. 7-46 in WCAP-16009-P-A. The contribution to the gap pressure from the additional fuel void in the fuel pellet is added. The change is only limited to the documentation. Note that the unit of averaged fuel pellet temperature is in Kelvin and the unit of radius of additional fuel void in the fuel pellet is ft in Eq. 8-46 of WCAP-16996-P.
- Text is inserted to p. 8-24 of WCAP-16996-P to note that Eq. 8-59 is also not applicable to [

]^{a,c}. The change is only limited to the

documentation.

- The transient gap conductance after rod ruptures, the burst strain and outer radius of the heat transfer node at the burst elevation in ASTRUM EM as documented in Section 7-4-2 of WCAP-16009-P-A is only applicable to [^{a,c} in **FSLOCA** EM (WCAP-16996-P), so the discussion has been moved from Section 8.4.2 to Section 8.6 of WCAP-16996-P.
- A difference between "flow blockage due to rod deformation" in ASTRUM EM (WCAP-16009-P-A) and **FSLOCA** EM (WCAP-16996-P) is the flow blockage due to rod rupture. The model in ASTRUM EM was described in the "Continuity and Momentum Cell Flow Areas" subsection on p. 7-32, and the model in **FSLOCA** EM is described in the "Flow Blockage Due to Rod Deformation" subsection on p. 8-31. This flow blockage due to creep is consistent between ASTRUM EM and **FSLOCA** EM. However, the flow blockage model due to rod rupture deformation is revised in **FSLOCA** EM. The revised flow blockage model due to rod rupture is based on [

J^{a,c}

(4) The majority of the cladding reaction model in the ASTRUM EM (WCAP-16009-P-A) is continuously used in **FSLOCA** EM (WCAP-16996-P). The changes between Section 7-5 in WCAP-16009-P-A and Section 8.5 in WCAP-16996-P are listed below:

- Burman oxidation model for the **ZIRLO**[®] cladding in the ASTRUM EM is removed from **FSLOCA** EM and is being replaced with the Cathcart-Pawel oxidation model.
- In **FSLOCA** EM, the Cathcart-Pawel oxidation model is applied to predict oxidation of both Zircaloy-4 and **ZIRLO**[®] cladding materials. [

J^{a,c}

[

J^{a,c}

References:

1. WCAP-16009-P-A, "Realistic Large-Break LOCA Evaluation Methodology Using the Automated Statistical Treatment Of Uncertainty Method (ASTRUM)," January 2005
2. WCAP-16996-P, Volumes I through III, "Realistic LOCA Evaluation Methodology Applied to the Full Spectrum of Break Sizes (**FULL SPECTRUM**[™] LOCA Methodology)," November 2010
3. NUREG/CR-0497, Hagrman, D.L., and Reymann, G.A., "MATPRO-Version 11: A Handbook of Material Properties for Use in the Analysis of Light Water Reactor Fuel Rod Behavior," Idaho National Engineering Laboratory, Idaho Falls, Idaho, February 1979
4. NUREG-0630, Powers, D. A., and Meyer, R. O., 1980, "Cladding Swelling and Rupture Models for LOCA Analysis," U.S. Nuclear Regulatory Commission, Washington, D.C.
5. Research Information Letter 0801, "Technical Basis for Revision of Embrittlement Criteria in 10 CFR 50.46," May 2008
6. NUREG/CR-6967, "Cladding Embrittlement during Postulated Loss-of-Coolant Accidents," July 2008

Question #42: Nuclear Fuel Rod Special Model Validation

The special models of the nuclear fuel rod conductor implemented in the **FSLOCA** methodology to analyze the nuclear fuel rods behavior include the fuel rod quench front model, dynamic pellet-cladding gap conductance model, fuel rod deformation model, and cladding reaction model. These models are described in WCAP-16996-P/WCAP-16996-NP, Volumes I, II and III Revision 0 Section 8.3.1, Section 8.3.2, Section 8.4, and Section 8.5, correspondingly. As explained in WCAP-16996-P/WCAP-16996-NP, Volumes I, II and III, Revision 0, Subsection 29.4.2.2, "Initial Calibration of the Steady-State Condition for the Nuclear Rods," specialized fuel performance codes are used by Westinghouse for stored energy and rod pressure inputs to LOCA analyses performed with the **FSLOCA** methodology.

Please clarify the following items related to the special models of the nuclear fuel rod conductor implemented in WCOBRA/TRAC-TF2 for describing the behavior of nuclear fuel rods.

- (1) Please explain if some of the nuclear fuel rod special models or major modeling features in these models have been previously reviewed by the U.S. NRC. In particular, clarify if this has been the case as part of the review of other fuel rod performance codes used by Westinghouse for LOCA analyses. If this is the case, please identify these codes, code versions, models and/or modeling features that apply to the WCOBRA/TRAC-TF2 nuclear fuel rod conductor model, provide the review outcome and summarize major relevant review findings and conclusions. Please provide references for the safety evaluations by the staff.
- (2) Please explain if specialized fuel performance codes were used as part of the evaluation of the WCOBRA/TRAC-TF2 nuclear fuel rod special models. In such a case, please present the assessment results and include comparison of prediction results for governing parameters obtained by the codes using the same input conditions. Provide references to the available assessment documentation.

Response:

(1) It has been discussed in the response to RAI 41 that the majority of nuclear fuel rod special models such as the fuel rod quench front model, the dynamic pellet-cladding gap conductance model, the fuel rod deformation model, and the cladding reaction model, in **FSLOCA** EM (WCAP-16996-P, Reference 1) are equivalent as the corresponding model in ASTRUM EM (WCAP-16009-P-A, Reference 2). Those models have been reviewed and approved by NRC. The differences between the models in ASTRUM EM and **FSLOCA** EM have been identified in the response to RAI 41, and the differences were justified by the evidences and validations provided in WCAP-16996-P or the response to RAI 41.

WCAP-16996-P Section 29.4.2.2 describes the initial calibration of fuel average temperature and rod internal pressure for the fuel rods against the PAD 4.0 fuel performance code (WCAP-15064-P-A, Revision 1, Reference 3) or FATES3B fuel performance code (CEN-161(B)-P, Supplement 1-P-A, Reference 4). Both are NRC approved fuel performance codes. However, it is worthwhile to point out that using the fuel average temperature and rod internal pressure data predicted by the PAD 4.0 or FATES3B codes is only limited to the

steady state condition calibration. Once the LOCA transient starts, the fuel rod behavior is predicted by the fuel rod models provided in Section 8 of WCAP-16996-P.

(2) As addressed in the response to part (1), the fuel performance code is only used to provide input for the fuel rod initial conditions (e.g., fuel rod average temperatures and rod internal pressures) in the steady state run. The fuel performance codes such as PAD 4.0 and FATES3B are not directly used to predict the fuel rod behavior in **FSLOCA** EM.

References:

1. WCAP-16996-P, Volumes I through III, "Realistic LOCA Evaluation Methodology Applied to the Full Spectrum of Break Sizes (**FULL SPECTRUM**™ LOCA Methodology)," November 2010.
2. WCAP-16009-P-A, "Realistic Large-Break LOCA Evaluation Methodology Using the Automated Statistical Treatment Of Uncertainty Method (ASTRUM)," January 2005.
3. WCAP-15063-P-A, Revision 1 with Errata, "Westinghouse Improved Performance Analysis and Design Model (PAD 4.0)," July 2000.
4. CEN-161(B)-P, Supplement 1-P-A, "Improvements to Fuel Evaluation Model," January 1992.

Question #43: Dummy Rod Component Models

As a major difference between the FSLOCA methodology and the previous ASTRUM LBLOCA Evaluation Model (EM) documented in WCAP-16009-P-A (Nissley, M. E., et al., 2005), WCOBRA/TRAC-TF2 features a dummy rod component, [

]^{a,c} WCAP-16996-P/WCAP-16996-NP, Volumes I, II and III, Revision 0, Section 8.6 describes the dummy rod component.

Please clarify the following items related to the new dummy rod component implemented in WCOBRA/TRAC-TF2.

- (1) Please explain if the dummy rod component models are consistent with the corresponding models in WCOBRA/TRAC-TF2. If corresponding models are not fully consistent, please identify only the differences and explain why such differing features in the dummy rod model are considered appropriate and valid for the intended functions of the dummy rod component.
- (2) Please identify the models in the dummy rod component that have no counterpart models in WCOBRA/TRAC-TF2. For each such model, please explain if the model or major modeling features in the model have been previously reviewed by the NRC. If this is the case, please identify these codes, code versions, models and/or modeling features that apply to the WCOBRA/TRAC-TF2 dummy rod component, provide the review outcome and summarize major relevant review findings and conclusions. Please provide references for the safety evaluations by the staff.
- (3) Please explain how the dummy fuel rod model in WCOBRA/TRAC-TF2 was evaluated. Present analysis results, if available, and provide references to existing assessments that demonstrate the applicability of the model for the purposes of LOCA analyses performed with the FSLOCA methodology. Please explain if the model was benchmarked against any available tests.

Response:

- (1) The purpose of introducing the dummy rod is to [

]^{a,c}

Section 8.6 of WCAP-16996-P and Table 8-6 explained the difference between the dummy rod, hot rod, and hot assembly rod. The hot assembly rod is a typical regular fuel rod in WCOBRA/TRAC-TF2, and the hot rod is the typical regular fuel rod [

]^{a,c}. The differences between a dummy rod and hot assembly rod (which is treated as a regular fuel rod) have been listed in Section 8.6 of WCAP-16996-P and are summarized herein following the same order.

[

]^{a,c}

[

]^{a,c}

(2) The relationship between the dummy rod and the regular rod in WCOBRA/TRAC-TF2 has been addressed in the response to part 1. The dummy rod model was developed to [

]^{a,c} The consistency and differences between the dummy rod model and the HOTSPOT code are discussed:

[

] ^{a,c}

(3) Most of the dummy rod models are [

] ^{a,c}

References:

1. WCAP-12945-P-A, Revision 2 (Vol. 2) and Revision 1 (Vols. 2 through 5), "Westinghouse Code Qualification Document for Best Estimate Loss of Coolant Accident Analysis," March 1998.

2. WCAP-16009-P-A, "Realistic Large-Break LOCA Evaluation Methodology Using the Automated Statistical Treatment Of Uncertainty Method (ASTRUM)," January 2005.
3. NUREG-1230, R4, "Compendium of ECCS Research for Realistic LOCA Analysis," December 1988.
4. NUREG-4166, "Analysis of FLECHT SEASET 163-Rod Blocked Bundle Data Using COBRA-TF," January 1986.

Question #44: Fuel Rod Material Properties

WCAP-16996-P/WCAP-16996-NP, Volumes I, II and III, Revision 0, Section 8.2, "Conductor Geometries Modeled in the Vessel," explains that the nuclear fuel rod model requires minimum user input and uses material properties specified by input or "defaulted to uranium-dioxide and zircaloy." The default properties are calculated using correlations from MATPRO-Version 11 (Revision 1) as documented in NUREG/CR-0497, Revision 1, 1980.

Subsection 8.3.2, "Pellet-Cladding Gap Conductance Model," of the Section 8.3, "Fuel Rod Modeling," states that the material property correlations in the simplified dynamic gap conductance model were taken exclusively from MATPRO-11 (Revision 1). In computing radiant heat transfer, the fuel emissivity and that of the cladding inner surface are based on data from MATPRO-11 (Revision 0). The gas mixture conductivity is determined from the conductivities of the constituent gases using a simplified version of the model in MATPRO-11 subroutine GTHCON. The conductivities of helium, xenon, argon, krypton, hydrogen, and nitrogen gases are calculated using correlations from MATPRO-11 (Revision 1). The interfacial pressure for the pellet-cladding contact conductance is calculated with the fuel rod deformation model and is non-dimensionalized using the Meyer hardness calculated from MATPRO-11 (Revision 1).

Subsection 8.4.1, "Deformation Mechanisms Fuel Pellet Thermal Expansion," of the Section 8.4, "Fuel Rod Deformation Model," explains that the axial and radial thermal expansion of the fuel is calculated using a MATPRO-11 (Revision 1) correlation for thermally induced strain in UO_2 . The correlation was simplified by omitting the corrections for molten fuel and mixed oxide. The axial and radial thermal expansion of the cladding is also calculated using correlations from MATPRO-11 (Revision 1).

The most recent version of the material properties library MATPRO is documented in NUREG/CR-6150, Vol. 4, Rev 2, "SCDAP/RELAP5/MOD 3.3 Code Manual: MATPRO-A Library of Materials Properties for Light-Water-Reactor Accident Analysis," 2001. A comparative study between the current versions of FRAPCON-3 and FRAPTRAN, which use a relatively consistent set of correlations for applied properties, and the latest MATPRO properties is documented in NUREG/CR-7024, "Material Property Correlations: Comparison between FRAPCON-3.4, FRAPTRAN 1.4, and MATPRO," 2011. In addition to comparing various correlations, correlation-to-data comparisons for FRAPCON-3, FRAPTRAN, and MATPRO properties are also provided in NUREG/CR-7024.

Please explain how material properties in the WCOBRA/TRAC-TF2 nuclear fuel rod model described in WCAP-16996-P/WCAP-16996-NP, Volumes I, II and III, Revision 0, Sections 8.2, 8.3, and 8.4 compare with the latest MATPRO library and data provided in NUREG/CR-6150 (Siefken et al., 2001) and NUREG/CR-7024 (Luscher and Geelhood, 2011). Please clarify which cladding materials can be modeled using the default material properties for zircaloy in the WCOBRA/TRAC-TF2 nuclear fuel rod model.

Response:

WC/T-TF2 fuel rod dynamic gap conductance and deformation models simulate the fuel rod dimensional changes and pellet-cladding gas conductance to calculate the fuel rod temperature response. In the WC/T-TF2 steady state calculation, [

]^{a,c} When the loss-of-coolant accident (LOCA) transient is initiated, the WC/T-TF2 fuel rod deformation model predicts the variations in the fuel rod structure and filling gas pressure at accident conditions, and these changes are accounted for in the gap conductance model to determine the fuel rod temperature.

The default WC/T-TF2 nuclear fuel rod models, with limited user inputs, feature UO₂ fuel. The cladding material is selected from either ZIRLO[®] or Zircaloy-4 cladding for plant calculations.

In this response, the WC/T-TF2 fuel rod properties in the gap conductance and fuel rod deformation models using MATPRO-11 (Reference 2) are compared to the latest versions of MATPRO (Reference 4), designated as MATPRO (2001), FRAPCON and FRAPRAN (Reference 3), designated as FRAP, as follows.

- Density (Fuel, Cladding)

The radial position of the fuel and cladding conduction nodes are fixed in WC/T-TF2, which ignores the node relocation due to thermal expansion. As such, the densities are evaluated at the [

]^{a,c} for fuel pellet (Uranium Dioxide) and cladding (Zircaloy-4, ZIRLO[®]) materials, respectively.

- Specific Heat (Fuel, Cladding)

The Specific Heat of the fuel pellet is calculated using the same correlation among MATPRO-11, MATPRO (2001) and FRAP.

WC/T-TF2 calculates the Zircaloy-4 specific heat by interpolating the tabulated values in a table consistent with MATPRO-11, MATPRO (2001) and FRAP. For ZIRLO[®] specific heat calculation, WC/T-TF2 modifies the Zircaloy-4 specific table [

]^{a,c}, while MATPRO (2001) and FRAP use the same table for ZIRLO[®] and Zircaloy-4. Figure 11-34 in Section 11 of Reference 1 shows the comparison of WC/T-TF2 specific heat models for Zircaloy-4 and ZIRLO[®].

- Thermal conductivity (Fuel, Cladding and fill gas)
 - + Fuel (Uranium Dioxide): the fuel thermal conductivity model in MATPRO-11 and MATPRO (2001) do not account for the degradation of thermal conductivity with increasing burnup, which is taken into consideration in FRAP fuel thermal conductivity model. The impact of the thermal conductivity degradation and the resolution to the issue will be discussed in the response to RAI 36.
 - + Cladding (Zircaloy-4, ZIRLO®): the same correlation is used to calculate cladding material thermal conductivity in WC/T-TF2, MATPRO (2001) and FRAP.
 - + Fill gas:

The thermal conductivity of the fuel rod pellet-cladding gap gas mixture is calculated from the thermal conductivities of the constituent gases, i.e. helium, argon, krypton, xenon, hydrogen and nitrogen based on a mixing law used consistently in WCT-TF2, MATPRO (2001) and FRAP.

The constituent gas thermal conductivities are calculated slightly different in WC/T-TF2, MATPRO (2001) and FRAP, as compared in the Figures RAI44-1 through RAI44-6 attached. It is shown in Figures RAI44-1 through RAI44-6 that [

]^{a,c}

For temperatures higher than []^{a,c}, the thermal conductivity for []^{a,c} in WCT-TF2 results, []^{a,c} when compared to the MATPRO (2001) results. This difference is considered small and acceptable [

]^{a,c} This is discussed in Section 29.4.2.2 of WCAP-16996-P.

- Surface Emissivity (Fuel, Cladding)

- + Fuel (UO_2): The same correlation is used to calculate fuel surface emissivity in WC/T-TF2, MATPRO (2001) and FRAP.

- + Cladding:

WC/T-TF2 uses a []^{a,c} for cladding surface emissivity, instead MATPRO (2001) and FRAP use the cladding surface emissivity model depending on the surface oxide layer thickness and temperature.

As shown in the model-to-data comparison performed in References 2 and 3 (Figure RAI44-8 is the duplication of Figure 3.4-1 in Reference 2), the []^{a,c} used in WC/T-TF2 is a []^{a,c} and MATPRO (2001), etc.

model prediction trend of 0.80 for temperature lower than 1500 °K (2240.3 °F) and surface layer thickness greater than 5µm (Note: It is believed that the title of the Figure 3.4-1 in Reference 2 should be 'Surface Layer Thickness (µm)' instead of 'Surface Layer Thickness (mm)', based on the model correlations enclosed therein).

- Cladding Meyer Hardness

Cladding Meyer Hardness number in WC/T-TF2 is modeled using the same correlation as that in MATPRO (2001) and FRAP packages.

- Thermal Expansion (Fuel, Cladding)

- + Fuel (UO_2): WC/T-TF2 uses the same correlation to calculate the thermal expansion of UO_2 as that in MATPRO (2001). The comparison of the MATPRO (2001) models to the models in FRAP are documented in Reference 3, which shows similar results between these models at temperatures lower than 1500 °K (2240.3 °F). The noticeable difference shown in the comparison results at a temperature near 2300 °K (3680.3 °F) is not a concern in WC/T-TF2 transient scenarios within the **FSLOCA**TM evaluation model.

- + Cladding

The circumferential and axial thermal expansions as functions of temperature are compared in Figures RAI44-9 and RAI44-10. The cladding thermal expansion models in WC/T-TF2 using MATPRO-11 []^{a,c}

- Cladding Modulus of Elasticity and Shear Modulus

WC/T-TF2 uses the models that []

$J^{a,c}$ that are included in the MATPRO (2001) and FRAP models. The temperature dependence of the elastic and shear modulus models in WC/T-TF2-TF2, MAPTRO (2001) and FRAP are the same.



Figure RAI44-1 Comparison of Helium Gas Thermal Conductivity

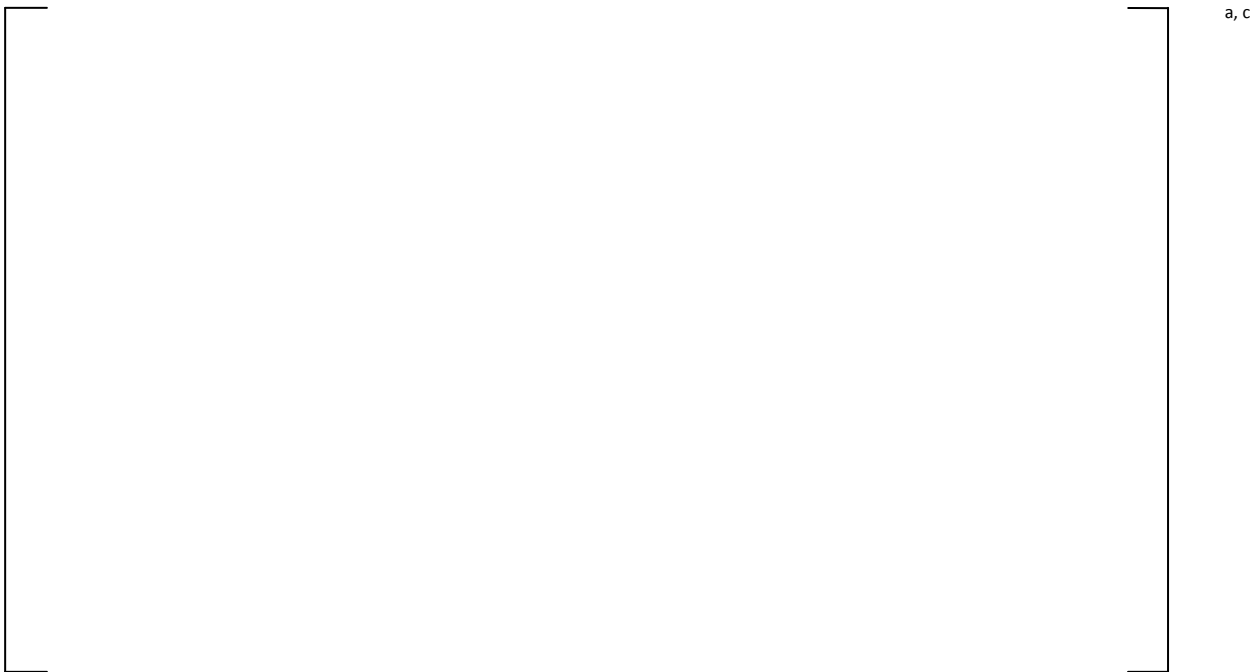


Figure RAI44-2 Comparison of Argon Gas Thermal Conductivity

a, c

Figure RAI44-3 Comparison of Krypton Gas Thermal Conductivity

a, c

Figure RAI44-4 Comparison of Xenon Gas Thermal Conductivity



Figure RAI44-5 Comparison of Hydrogen Gas Thermal Conductivity



Figure RAI44-6 Comparison of Nitrogen Gas Thermal Conductivity



Figure RAI44-7 Comparison of Gas Mixture Thermal Conductivity (Gas mixture of the mole fraction composition: Helium 63.8%; Argon 0.32%; Krypton 5.38%; Xenon 30.5%; Nitrogen 0.003%)

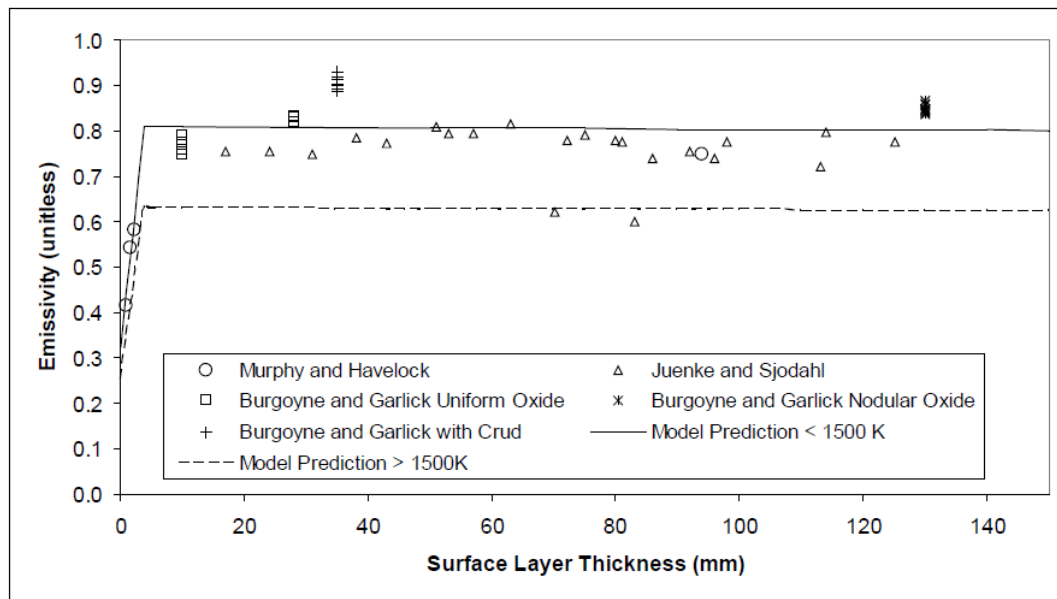


Figure 3.4-1 Model-to-data comparison for cladding oxide emissivity.

Figure RAI44-8 Data-to-Model Comparison on Cladding Surface Emissivity (Duplicated from References 3)



Figure RAI44-9 Comparison of Cladding Circumferential Thermal Expansion between WC/T-TF2 and FRAP



Figure RAI44-10 Comparison of Cladding Axial Thermal Expansion between WC/T-TF2 and FRAP

References:

1. WCAP-16996-P, "Realistic LOCA Evaluation Methodology Applied to the Full Spectrum of Break Sizes (FULL SPECTRUM™ LOCA Methodology)," November 2010
2. Hagrman, D. L., Reymann, G. A. and Mason, R. E., "MATPRO – Version 11 (Revision 1): A Handbook of Material Properties for Use in the Analysis of Light Water Reactor Fuel Rod Behavior," USNRC Report NUREG/CR-0497, Revision 1, 1980
3. NUREG/CR-7024, "Material Property Correlations: Comparisons between FRAPCON-3.4, FRAPTRAN 1.4, and MATPRO," March, 2011
4. NUREG/CR-6150, "SCDAP/RELAP5/MOD 3.3 Code Manual," Vol. 4, Rev. 2, January 2001

**WCAP-16996-P, “Realistic LOCA Evaluation Methodology Applied to the Full Spectrum of Break Sizes
(FULL SPECTRUM LOCA Methodology)”
Requests for Additional Information – (Non-Proprietary)
RAI 45**

June 2013

Westinghouse Electric Company LLC
1000 Westinghouse Drive
Cranberry Township, PA 16066

©2013 Westinghouse Electric Company LLC
All Rights Reserved

Question #45:

Please demonstrate that the assumption for the validity of Wilks Theorem holds with regard to the application of the code described in WCAP-16996-P/WCAP-16996-NP, Volumes I, II and III, Revision 0, in quantifying a single probabilistic statement of safety for the full spectrum of breaks, the full spectrum of model parameters and their variation, and the models of the engineered safety systems for small, intermediate and large break LOCAs. That is, there are no disjoint density functions of the figures of merit, or you can identify them and take them into account in the application of Wilks theorem.

Response:

1. Introduction

The issue raised with RAI-45 is broad and far reaching as it challenges the basis and best practices of approved best estimate LOCA methodologies as they are applied in the industry today (References 1, 2, 3, 4 and 6).

This request was motivated by the staff's concern that the FULL SPECTRUM™ LOCA (FSLOCA™)¹ Evaluation Model (EM) represents a "game changer" with respect to the method used to combine the uncertainties. It was pointed out that sampling uncertainties in this framework could lead to the *"the introduction of a continuous (rather than constant) parameter that can greatly alter in a discontinuous fashion the dynamics of the system. That is, there may appear multiple, stable, nonintersecting solutions, (i.e. bifurcations) that need to be taken into account in Wilks' theorem."*

The intent of the FSLOCA methodology is not to provide a singular statement that applies to the full spectrum of breaks as stated in the question above but rather to [

]^{a,c}

In the ASTRUM Safety Evaluation Report (SER) (Reference 1), the staff judged a 95/95 statement on the figures of merit as acceptable [

]^{a,c} The 95/95 criterion is also now de-facto a standard practice in the industry. [

]^{a,c}

Thus, if the question is limited to the possibility of generating disjoint density functions of Peak Cladding Temperature (PCT) [

]^{a,c}

In the following, the possibility of disjoint sets which may result from chaotic solutions will be discussed.

The intent here is to first define and clarify the problem statement such that Westinghouse can formally and logically address the reviewer's underlying concern. The response is constructed by following the steps below:

¹ **FULL SPECTRUM™** and **FSLOCA™** are trademarks of Westinghouse Electric Company LLC, its affiliates and/or its subsidiaries in the United States of America and may be registered in other countries throughout the world. All rights reserved. Unauthorized use is strictly prohibited. Other names may be trademarks of their respective owners.

- 1) Analyze the details of the question and restate the problem statement. Decompose the questions into elements that can be addressed in a logical and constructive manner (Section 2).
- 2) Define the scope and boundary of the questions within the envelope and purpose of the FSLOCA EM intended application, and consistent with 10 CFR 50.46 and applicable Regulatory Guides (RG 1.157 [23] and RG 1.203 [25]) (Section 3).
- 3) Address the question in each of the subtopics (Section 4).

2. Problem Statement Definition by Breaking Down RAI-45 into Elements

In order to facilitate the resolution of the issue, the RAI-45 question is broken down into four key elements. Westinghouse then provides a response to each element in Section 4. Here below are the elements:

- 45.1.** Model and Input uncertainties are randomly sampled in the plant analysis following a direct Monte Carlo propagation of uncertainty method using a validated code. The code simulation of a particular scenario is expected to represent a random realization of the Pressurized Water Reactor (PWR) transient response to the postulated event. The effect of varying model parameters in the process is questioned. One difference between the plant simulation and the methods used to validate the code against Integral Effects Tests (IETs) is that model parameters are kept constant in the latter and varied in the former. In other words, in the current WCAP-16996-P [11], the adequacy of the validation is based upon comparing IET test predictions by the code with models set at their coded nominal values to IET test data. Typically the code is shown to be more conservative than the data with respect to key Figures of Merit (say PCT). **QUESTION: Can the same conclusions be supported accounting for the propagation of model and input uncertainties in the IET simulation?**
- 45.2.** Sampling uncertainties in this framework could lead to the introduction of a continuous (rather than constant) parameter that could potentially alter in a discontinuous fashion the dynamics of the system. That is, there may appear multiple, stable, nonintersecting solutions, (i.e. bifurcations) that need to be taken into account in Wilks' theorem. **QUESTION: Are simulations of IETs affected by chaotic behaviors (bifurcations)? Can we still support a high probability statement that uncertainties are properly captured?**
- 45.3.** Part 45.2 addresses the IETs. Plant analysis models consider additional uncertainties (Plant Design Parameters). The same question applies here. **QUESTION: Are simulations of PWRs affected by chaotic behaviors (bifurcations)? Can we still support a claim that there is a high probability that our sample includes a limiting transient which bounds the 95% of the population with 95% confidence?**

- 45.4.** Addressing parts 45.2 and 45.3 explores the possibility of clustering solutions in disjoint, non-intersecting sets. Wilks' theorem (see Pal-Makai (2002) or Guba-Makai (2003), References 7 and 8) only requires the unknown cumulative distribution $G(y)$ to be continuous (in our application y can be the PCT value from a simulated transient - max clad temperature in time and space). The continuity can be ensured by satisfying uniqueness of the solution for given initial and boundary condition. Uniqueness of the solution and Chaos are two different issues and this part of this response is intended to clarify and elaborate on this argument. **QUESTION: Assuming a degree of Chaotic variability (or volatility) is real and properly captured by the model, is it still possible to rely on Wilks' theorem (and order statistics) to infer an upper tolerance limit for the PCT/Maximum Local Oxidation (MLO) and demonstrate compliance with the 10 CFR 50.46 regulation?**

3. Assumptions and Regulatory Guide Compliance

The response is developed starting from some key premises:

- 1) Principles of Regulatory Guide 1.157 and 1.203 are followed.
- 2) This is an engineering solution to a complex theoretical question.
- 3) Precedence and validity of approved license applications in the industry is considered.

In discussions with the staff, the reviewer sees the FSLOCA methodology as a "game change".

However, in Westinghouse's view, [

]^{a,c} Also, other vendors in the industry rely on similar approaches and similar computer codes architecture.

The new features in FSLOCA are predominantly [

]^{a,c}

The FSLOCA EM (WCAP-16996-P, Reference 11) employs [

]^{a,c} This is consistent with Regulatory guide 1.157 which states that "A 95% probability is considered acceptable to the NRC staff [...] to show that there is a high probability that the criteria [b.1 to b.3 of 10CFR50.46] will not be exceeded."

Westinghouse's intention is to address the issue stated in RAI-45 following the breakdown of the question suggested above (elements 45.1, 45.2, 45.3 and 45.4). However, in the resolution of these elements it will be assumed [

] ^{a,c}

4. Response to the elements of the question 45.1, 45.2, 45.3 and 45.4

Element 45.1

It is recognized that experiments (Separate Effects Tests (SETs) and IETs) used to validate the codes are representations of postulated events and potentially affected by distortions due to scaling biases or the limited number of tests. The fact that tools are validated by comparing code simulations to those individual tests has to be acknowledged. It is desirable to well-predict or to retain some degree of conservative biases in the code when assessing code predictions to IETs.

This is consistent with regulatory guidance. As stated in RG 1.157: *"...In practice, best-estimate codes may contain certain models that are simplified or that contain conservatism to some degree..."*. And further *"The introduction of conservative bias or simplification in otherwise best-estimate codes should not, however, result in calculations that are unrealistic, that do not include important phenomena, or that contain bias and uncertainty that cannot be bounded. Therefore, any calculational procedure determined to be a best-estimate code in the context of this guide or for use under paragraph 50.46(a)(i) should be compared with applicable experimental data to ensure that the calculation of important phenomena is realistic."*

The judgment on the adequacy of predicting IETs in the Topical Report (TR) (WCAP-16996-P) is based on setting the facility input model and code models at their best-estimate as-coded values, and simulating the test as it was executed to ensure that the key phenomena are properly accounted for. Section 24 of the TR also provides further analysis into the compensating errors to ensure that observed biases do not add undue distortion to the simulation.

Question 45.1 raises the issue if such adequate conclusions can be drawn after accounting for uncertainty propagation. If that is the case, then a similar argument can be extended to the plant analyses which do in fact consider propagation of all uncertainties.

To address the issue an analysis was conducted utilizing the CCTF-62 test. The CCTF-62 test is presented in Section 19.6 of the TR and is one of the key IETs utilized to demonstrate the code capabilities in modeling realistically the refill and reflood phases of a postulated LBLOCA in a PWR. The CCTF tests are the largest scale integral tests available to investigate these phenomena. CCTF has a flow area scaling of 1/21.4 of a four-loop PWR and includes a full-height (12 foot heated length) core section with three intact loops explicitly modeled. Its large scale makes the facility particularly well suited as verification of the code's ability to handle the

multi-dimensional thermal hydraulics in the core. In addition, the full-height scaling makes these tests important indicators []^{a,c}

As stated in Section 19 of the TR, WCOBRA/TRAC-TF2 was shown to []

[]^{a,c} The important phenomena to be addressed by the CCTF 62 simulation are water accumulation in upper plenum, steam binding effect, and core quenching during gravity reflood.

From the code assessment (with the nominal model), the adequacy of the EM is based on demonstrating the following conclusions:

- a. Important phenomena are adequately or conservatively predicted,
- b. Any miss-predictions (or conservative predictions) are acceptable and explained, and
- c. There is adequate evidence that when applied to the full scale PWR transient analysis of the same scenario, the EM is likely to produce reasonably accurate results.
- d. The conservative nature of the EM enables one to conclude that the confidence on the predicted 95% PCT for the plant analysis is 95% or higher.

The results presented in the TR were obtained with the code models at their nominal, as-coded settings and the question here is if same conclusions can be reached when uncertainties are ranged. The purpose of the analysis presented in this response is to demonstrate that this is the case. Preliminary results (fully documented herein) were already presented to the Staff in August 2012 for the purpose of addressing this part of the issue (Reference 12).

The following exercise was conducted:

- Code model parameters whose ranging may impact the prediction of CCTF data were identified.
- Uncertainties in test initial and boundary conditions were characterized.
- A random sample of simulations []^{a,c} was obtained, where uncertainties were sampled similarly to the procedure used in plant analysis.

² There is nothing specific to []

[]^{a,c} as described in the Topical Report (WCAP-16996-P).

- Code model ranging was based on the SET assessment and the sampling procedure is consistent to what would be followed in a plant analysis. Models include [

]^{a,c}

Initial and boundary conditions uncertainties were extracted from the test report (Reference 13) and sampled in the analysis. For example the initial temperature of the accumulator water was reported to be affected by uncertainty of +/- 1.5%. This uncertainty range was used as a basis for the sampling. The results of these []^{a,c} Monte Carlo simulations are discussed in the following.

Figure 1 shows the PCT(t) traces for []^{a,c}. Figures 2, 3 and 4 shows the following curves for all the three elevations in the bundle respectively (6.0, 8.0 and 10.0 ft):

- [

]^{a,c}

Figures 2, 3 and 4 show [

]^{a,c}

Figures 5, 6 and 7 show respectively [

] ^{a,c}

In conclusion these results address issue 45.1.



Figure 1 – [

] ^{a,c}



Figure 2 – Predicted [

] ^{a,c}

Figure 3 - Predicted [

] ^{a,c}



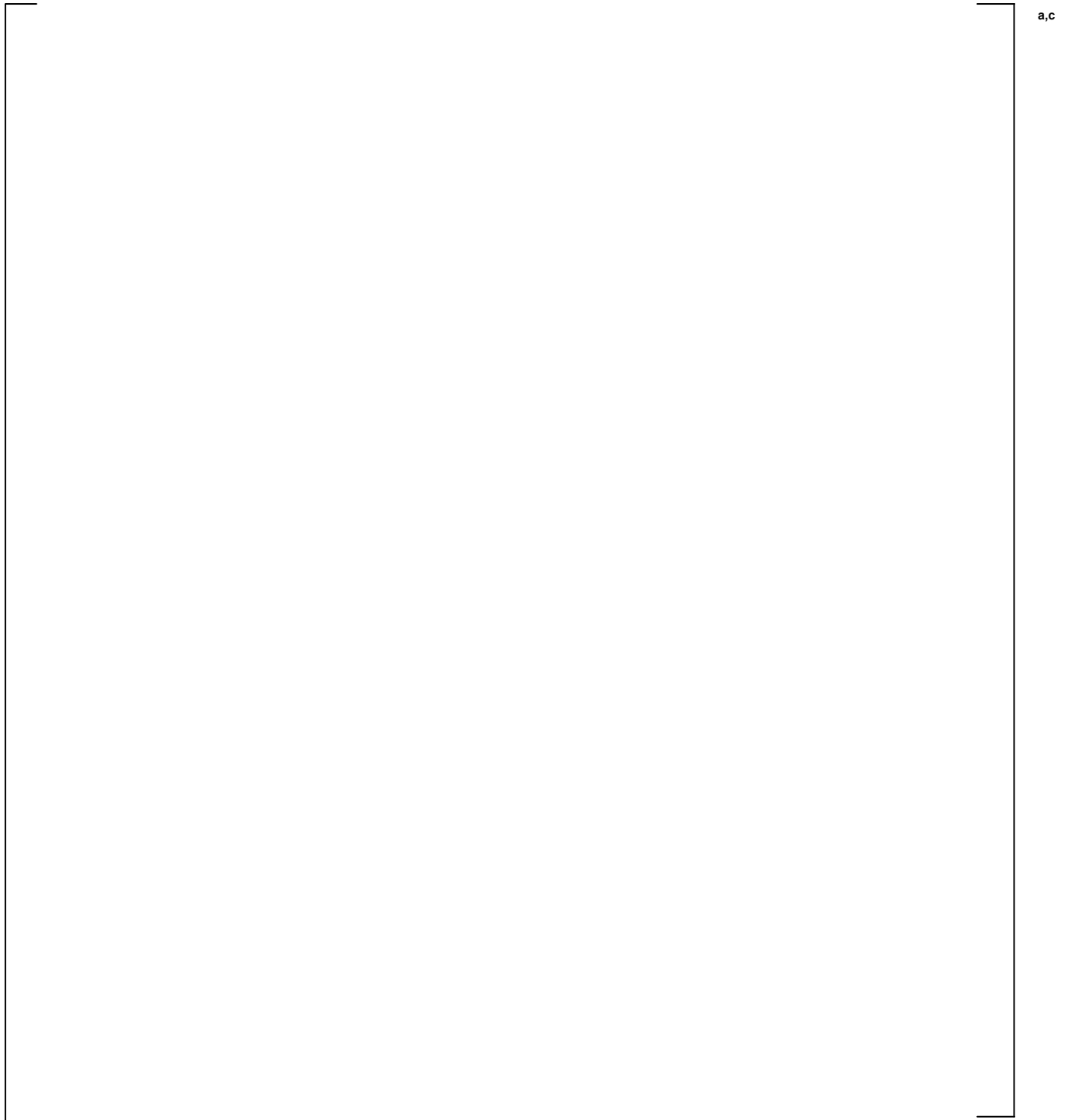
Figure 4 - Predicted [

] ^{a,c}

a,c

Figure 5 - Predicted [

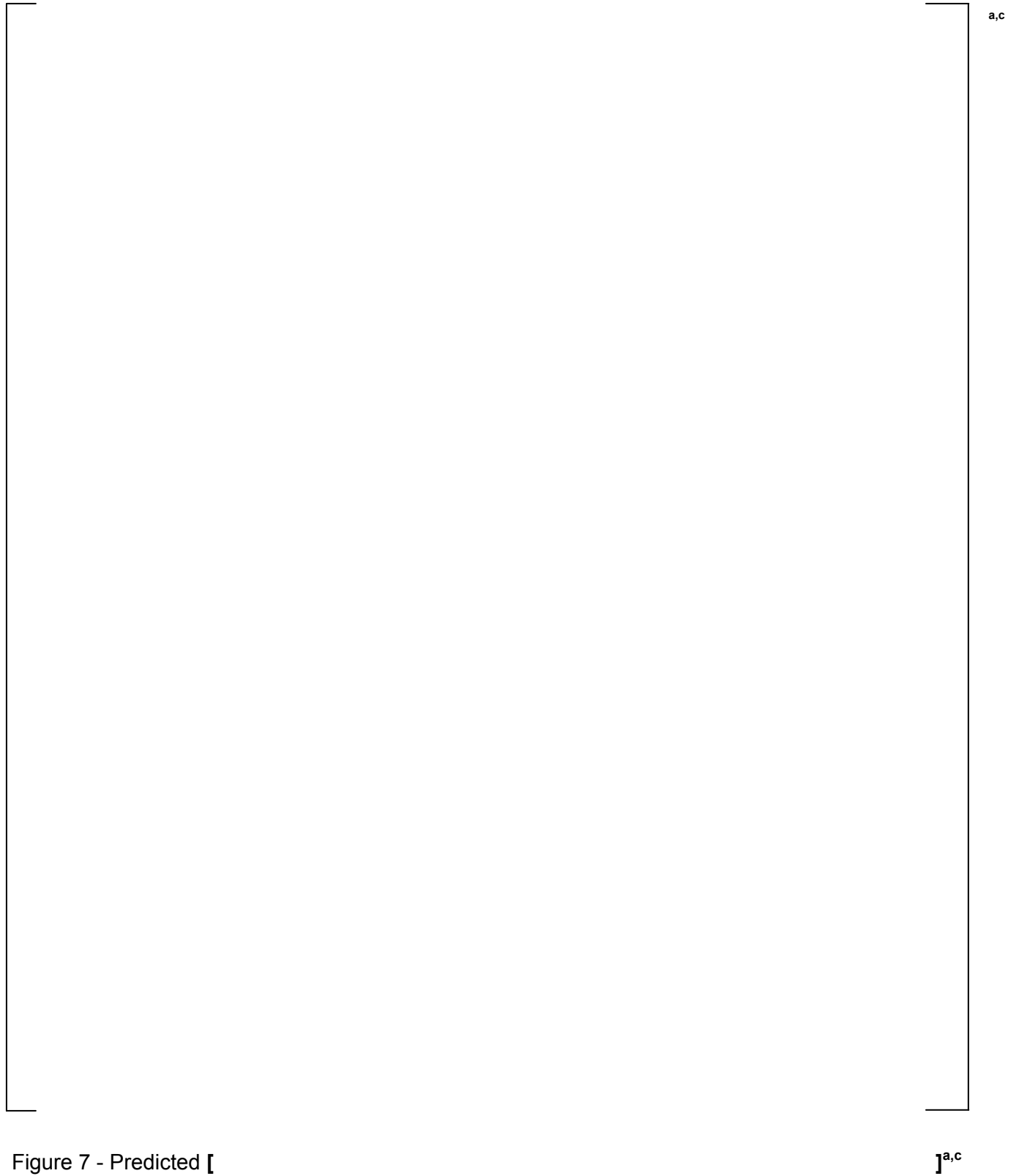
]a,c



a,c

Figure 6 - Predicted [

]a,c



a,c

Figure 8 – [

] ^{a,c}**Element 45.2**

The previous results were inspected to identify possible chaotic behavior which could arise by varying model parameters as stated in the question. For this set of IET simulations [

acceptance criteria as stipulated in the 10 CFR 50.46 regulation.] ^{a,c} not exceeding the

Element 45.3

CCTF-62 is intended to represent the PWR behavior (refill and reflood phases) in response to a large break LOCA event. For the PWR analysis the same approach is followed. However, note that while in a test (like CCTF) the initial and boundary conditions are quite controlled, for the plant analysis the number of parameters sampled is large and ranges are wider to reflect possible plant operating ranges [] ^{a,c}

Figure 9 shows [

50.46 regulation.]^{a,c} not exceeding the acceptance criteria as stipulated in the 10 CFR

a,c

Figure 9 – [

] ^{a,c}

Chaotic behaviors in the classical sense, i.e. high sensitivity to small perturbation to inputs, are a physical expectation in some cases. For example the interaction between system wide phenomena such as random loop seal clearing, venting capability and core level depression, etc. may lead to bifurcating events. These phenomena were observed and analyzed in response to RAI-9 and RAI-12.

In order to explore this further [

purpose of each study is presented next.

] ^{a,c} The description and

Study 1 (S1)

Description: This is [

] ^{a,c}

Purpose: Identify if [

] ^{a,c}

Study 2 (S2)

Description: This is a repeat of S1 with [

] ^{a,c}

Purpose: Assess the impact of [

] ^{a,c}

Analysis of the PWR Studies (Studies S1 and S2)

Figure 10 shows [

] ^{a,c}

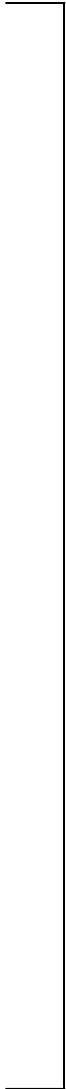
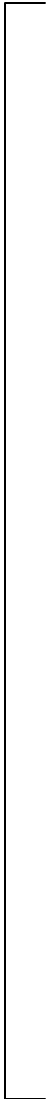
a,c

Figure 10 – [

] ^{a,c}

Figure 11 shows [

] ^{a,c}



a,c

Figure 11 – [

] ^{a,c}

Figure 12 shows [

] ^{a,c}

Figures 13 through 16 show [

] ^{a,c}

The concern with a chaotic solution is sometimes explained as the “volatility” in the solution, borrowing a term from the financial market. In other words, the concern is that a possible solution branch could be quite more severe than the solution in another more nominal branch. The distance between the solution disjoint sets could be a concern. A large distance between the sets casts some doubt on the sample size because of the possibility of missing some of those unlikely but very severe events. These studies shows [

] ^{a,c}

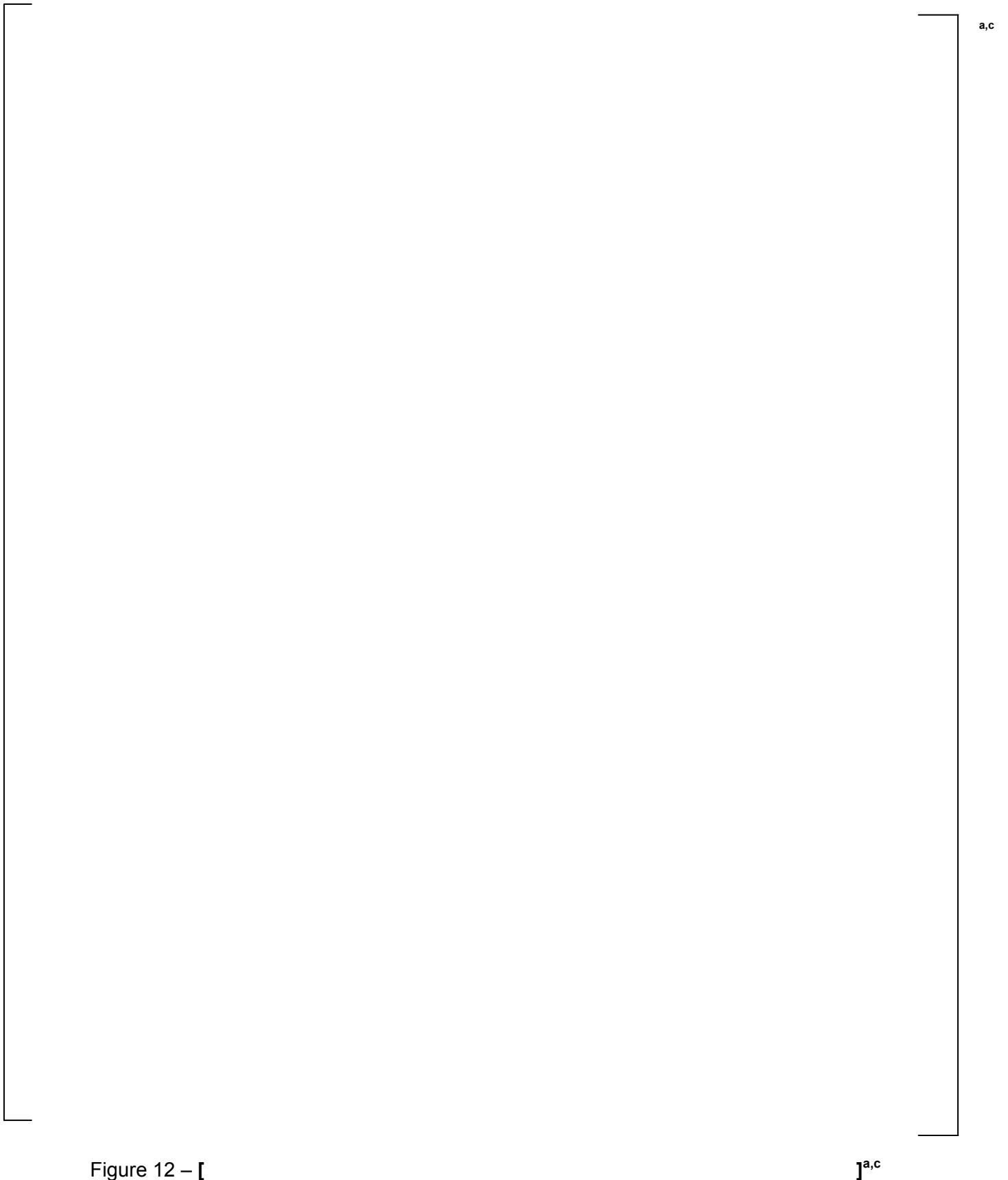


Figure 12 – [

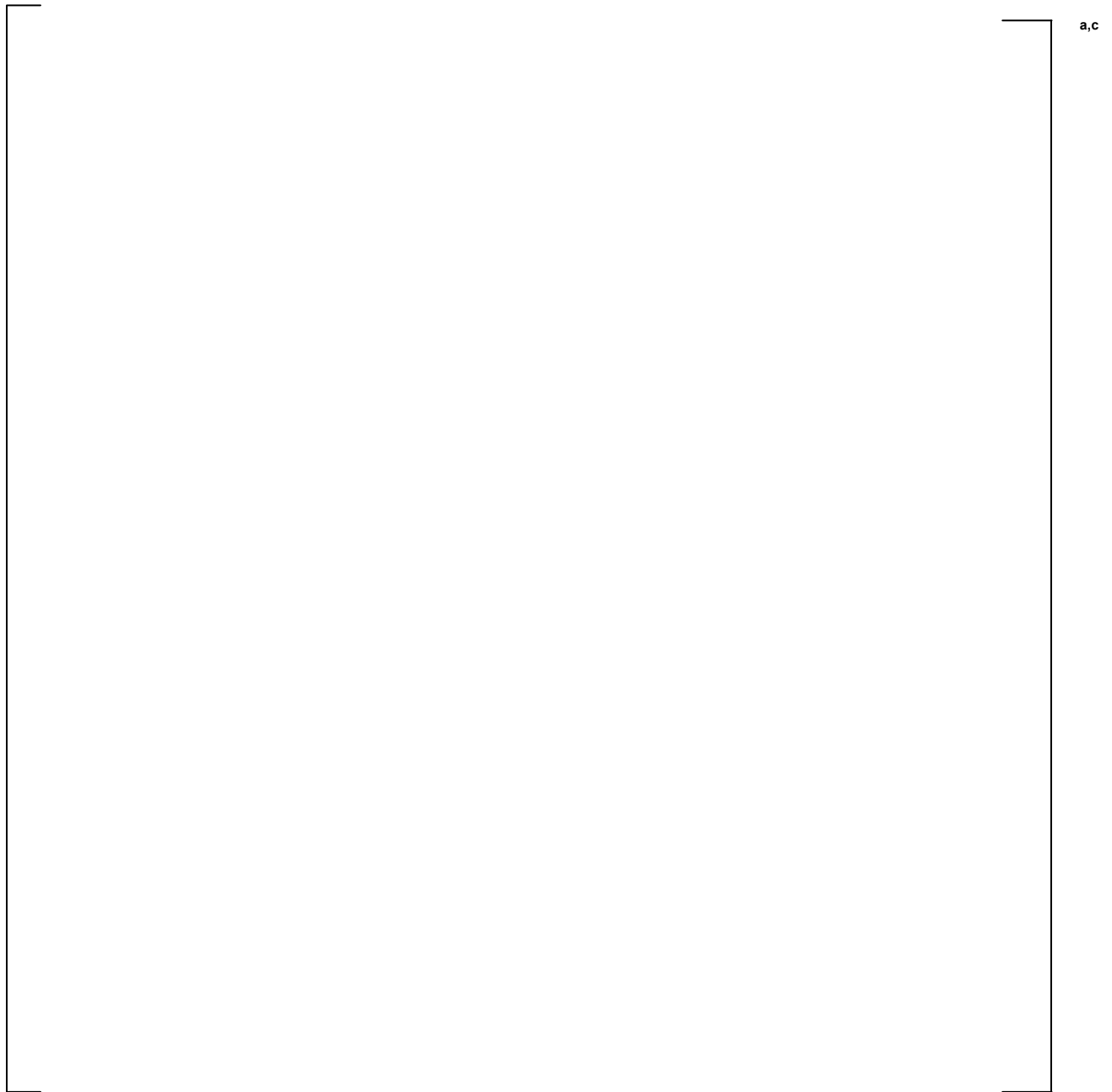


Figure 13 – [

] ^{a,c}

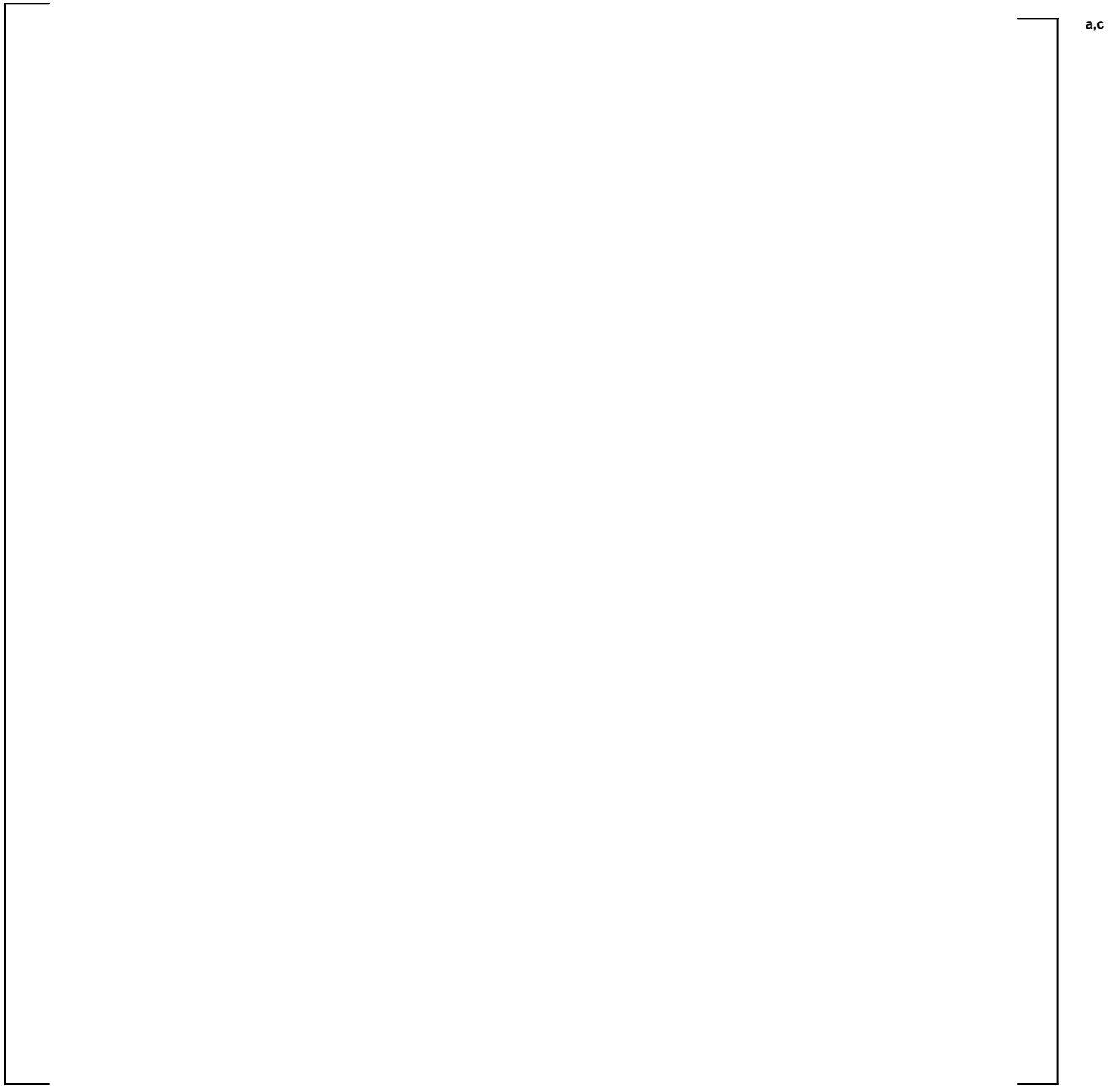


Figure 14 – [

] ^{a,c}

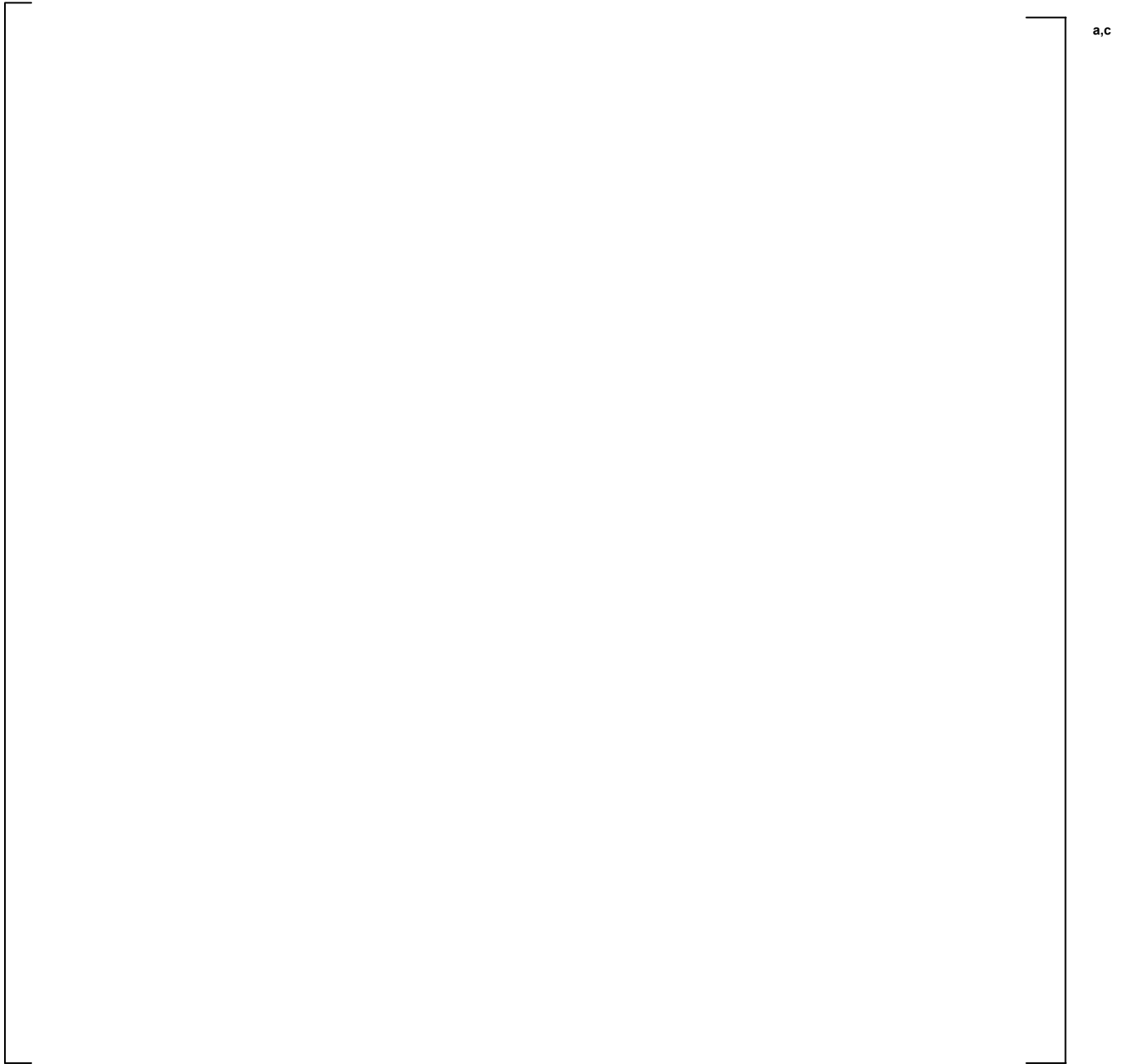


Figure 15 – [

]a,c

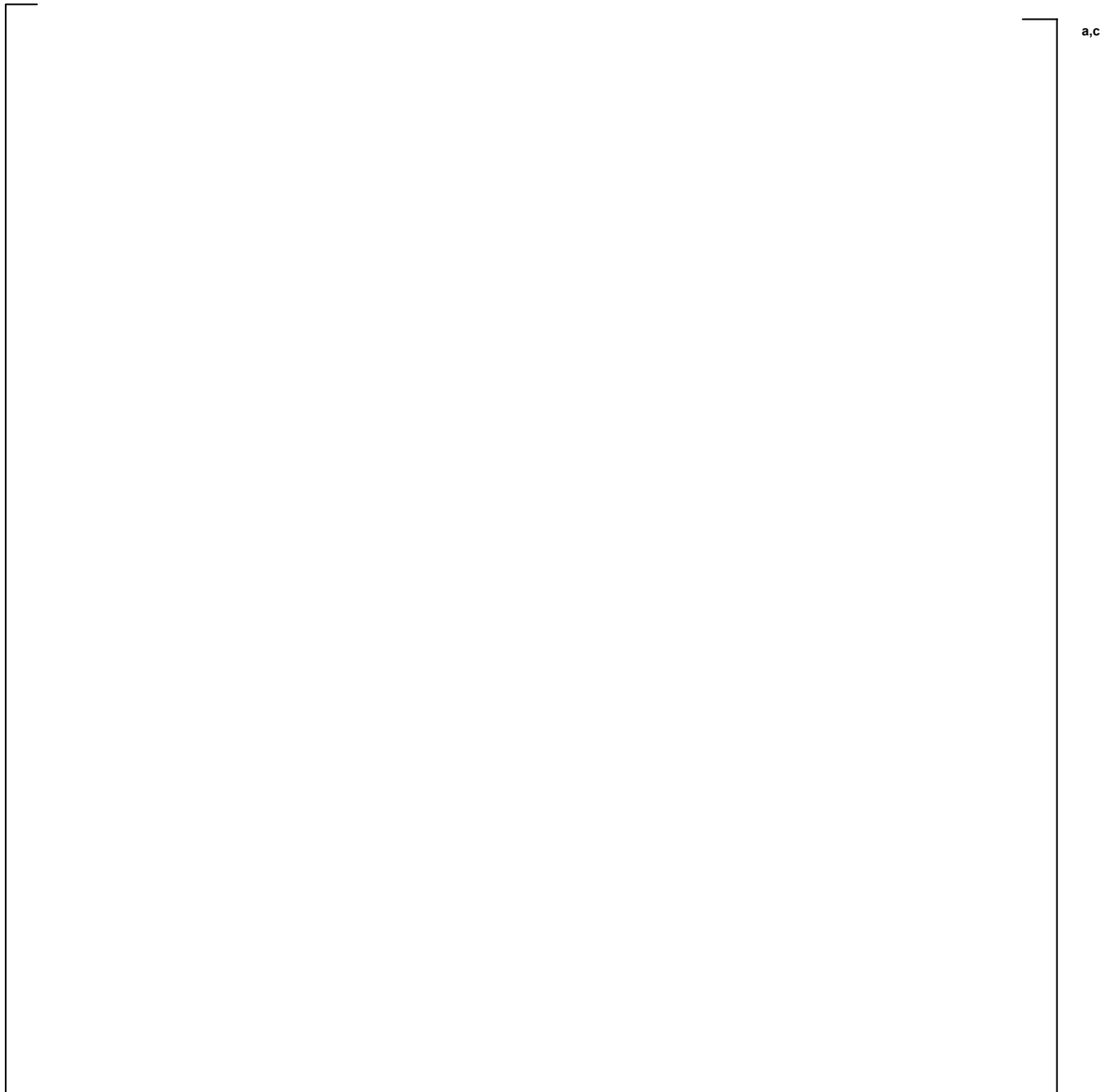


Figure 16 – [

] ^{a,c}

Figure 17 shows [

] ^{a,c}

a,c

Figure 17 – [

] ^{a,c}**Conclusions from the PWR Studies**

The following conclusions are drawn from the previous analysis:

- The code [

]^{a,c}

Element 45.4

It is recognized that the problem at hand is complex and non-linear in nature. Non-linear operators are known to exhibit chaotic behaviors. The work performed as part of 45.1 to 45.3 addresses the issue on the code applicability and capability to model such behaviors.

However the reviewer challenges the applicability of Wilks' theorem in the case that chaotic behaviors are possible in the plant. Similarly the Pal, Makai and Guba literature deals with the possibility of chaotic behavior of output variables which is observed in some computer simulations and poses the same questions.

There are two parts to this response. The first is to restate the problem by clarifying that for the LOCA safety analysis [

]^{a,c} The second part is to reflect on the mathematical assumptions which are actually at the basis of the Wilks' theorem. Review of pertinent literature shows [

]^{a,c} and the response will elaborate on these points.

The current practice in the industry to meet the NRC requirements in achieving the high level of probability required by the 10 CFR 50.46 rule is to bound 95% of the population of PCT and oxidation with 95% confidence. The procedure is a Monte Carlo sampling of the uncertainty attributes and the generation of a sample of scenarios from a hypothetical population of them. From each simulated transient in the sample specific figures of merits such as maximum clad temperature and oxidation are tallied.

The thermal-hydraulic computer code designed to simulate the transient is what the Guba-Makai-Pal (GMP) paper refers to as the 'black-box'. In this case the back box receives as input a set of random values, one for each uncertainty parameter, and outputs the selected figures of merit (PCT and oxidation). [

]^{a,c} The issue here is how the results are interpreted to demonstrate compliance with 10 CFR 50.46 requirements.

The currently approved LBLOCA methodology (ASTRUM) relies on a non-parametric order statistics procedure with a minimum sample size. The results are ranked and the top rank is selected as the estimator. [

]^{a,c}

Now, it is important to recognize that the only mathematical requirement for the applicability of the method is shown in the footnote of pg. 224 of GMP (2003) [8]: “The probability that equal values occur is zero” – i.e. a continuous CDF of the output.

The implementation of non-parametric techniques in the framework of LOCA safety analysis generated a vigorous debate in the industry in the previous decade [References 14 to 22]. Much of the debate in the early 2000's was given to the ‘sample size problem’, since most of the vendors were utilizing maximum order statistics estimators with small sample size (<150 cases) to infer upper tolerance limits. This issue is today much less important since computational capabilities allow larger sample sizes at reduced costs.

Instead the emphasis in RAI-45 is on more fundamental questions associated with the ‘mathematics’ and the fidelity of the computer codes used to analyze these complex scenarios [24], [25].

It is recognized that the problem at hand is complex and non-linear in nature. Non-linear operators are known to exhibit chaotic behavior. Section 4 of Guba-Makai-Pal (2003) deals with possibility of chaotic behavior of output variables and observed in some computer simulations. More specifically Section 5 of GMP (2003) states that “...we assume that the observed randomness of output variables is the result of the randomness of input variables, and the mapping $y(X)=C(t) X$ does not show chaotic behavior...”

GMP (2003) continues by providing stringent requirements for safety:

- *A state x is called safe if y is in the safety envelope for every x in $[X]$, where $[X]$ is the set of all possible values of x .*
- *If there is a value outside the safety envelope the state is unsafe independently of the fact that the nominal state may be safe.*

Obviously the above statement appears to point to the population of events and an ideal solution which aims in determining the safety of a design in a deterministic sense, i.e. 100% probability. In practice the requirements are different, because an engineering safety statement is made assuming some risk. For instance, the 50.46 regulation requires that there is a very low probability of falling outside the safety envelope (not “a value” as stated – i.e. zero probability).

The problems of bifurcation and cliff effects are also discussed by D’Auria (2000) (Reference 26). Their paper provides a good classification by distinguishing between bifurcations originated by the safeguard system (actuation of valves for example) and bifurcations originated by phenomena, which possibly are the ones to which the GMP work refers. Note that a combination of the two causes is also possible.

In other words it is reasonable to speculate about the existence of phenomena-driven bifurcation during a postulated (and simulated) LOCA event. However, we should differentiate true chaotic behaviors from threshold effects, like the occurrence of burst and swelling which may lead to a different scenario as far as the clad heat up and oxidation transient are concerned

local to the burst region; or the occurrence of dryout which determines the clad temperature excursion.

On the other hand phenomena such as [

]^{a,c} are rather chaotic and may lead to chaotic behaviors, or high sensitivity to small variation in the inputs according to the classic definition of Chaos. D'Auria (2000) concluded that phenomena-based bifurcations are implicitly accounted for in their method. Similarly Makai-Pal (2003) show that chaos in output may be predicted by thermal-hydraulic system codes (ATHLET in this case).

This leads to the conclusion that as long as the physics are properly modeled in the system code of choice, chaotic events are predicted and eventually captured in the uncertainty methodology which typically exercises the solution with random sampled inputs as discussed in the previous section.

The presence of disjoint-set data structures does not prevent the use of the Wilks' theorem which is simply a tool to infer a probabilistic statement from a sample of the population. The issue of having disjoint sets in itself does not prevent the applicability of non-parametric statistics, as long as the solution is unique. Order statistics only requires the CDF of the population to be continuous (References 8, 9 and 10) which can still be achieved even in the case of disjoint sets. As long as the population underneath a disjoint set (or multiple attractors) is sampled by the code by randomly sampling the inputs, disjoint sets and unlikely scenarios will be considered to the extent of their probability weight. Note that when dealing with computer codes the uniqueness of the solution is not violated, i.e. for exactly the same input, the same output is reproduced.

Sometimes large sensitivities to small perturbation of the inputs are claimed for some parameters like the level in the downcomer (per Reference 8). However for the purpose of safety inference it is more appropriate to examine the effect on figures of merit (outputs) that more directly relate to the 10 CFR 50.46 criteria, PCT for instance. Therefore, the conclusions in Reference 8 which describe clustering of predicted transient level in the downcomer may not be fully relevant in judging the impact on the PCT solution.

Ultimately, rather than challenging the applicability of the Wilks' theorem for the inference of the statistical measure in such a context, the issue should reside on the degree of belief that the simulation run-set sample represents with high fidelity an unknown population of 'real' PWR transient evolutions, once parameters are varied according to the sampling procedure. The work performed as part of this response and the observations from other authors (e.g. Reference 8) provide reassurance on the predictability of such behaviors and, once they are predicted, the extent of the chaotic volatility of the solution.

Finally, it has to be recognized that a mathematical proof or certainty with respect of the fidelity issue is unattainable given the complexity of the problem and the tools used to analyze the problem. The acceptability of the method resides in the realm of a reasonable demonstration that the code simulations are a good representation of the possible real scenarios. This will

ultimately lead to the engineering judgment that the design is safe within tolerances that satisfy the intent of the 10 CR 50.46 regulation.

Such reasonable demonstration can be drawn primarily from the code V&V against SETs and IETs provided in Volume 2 of the TR, and complemented by the studies presented in this response.

5. References

- [1] WCAP-16009-P-A, "Realistic Large-Break LOCA Evaluation Methodology Using the Automated Statistical Treatment Of Uncertainty," January 2005.
- [2] Young, M. Y., Bajorek, S. M., Nissley, M. E., and Hochreiter, L. E., 1998, "Application of code scaling applicability and uncertainty methodology to the large break loss of coolant," Nuclear Engineering and Design 186 (1998) 39-52.
- [3] Frepoli, C., 2008, "Review Article - An Overview of Westinghouse Realistic Large Break LOCA Evaluation Model," Science and Technology of Nuclear Installations, Vol. 2008, Hindawi Publishing Corporation, Article ID 498737.
- [4] Glaeser, H., Hofer, E., Kloos, M., and Skorek, T., 1998, "GRS Analyses for CSNI Uncertainty Methods Study (UMS)," in CSNI Report NEA/CSNI/R(97)35, Volume 1, June 1998.
- [5] NOT USED.
- [6] Martin, R. P. and O'Dell, L. D., 2005, "AREVA's Realistic Large Break LOCA Analysis Methodology", Nucl. Eng. Des., Vol. 235, pp. 1713-1725.
- [7] Pal, L. and Makai, M., 2002, "Remarks on statistical aspects of safety analysis of complex systems," physics-data-an
- [8] Guba, A., Makai, M., Pal, L., 2003, "Statistical aspects of best estimate method-I," Reliability Engineering and System Safety, Vol. 80, 217-232.
- [9] Makai, M., Pal, L., 2006, "Best estimate method and safety analysis II," Reliability Engineering and System Safety, Vol. 91, 222-232.
- [10] Wilks, S. S., 1941, "Determination of Sample Sizes for Setting Tolerance Limits," The Annals of Mathematical Statistics, Vol. 12, pp. 91-96.
- [11] WCAP-16996-P, "Realistic LOCA Evaluation Methodology Applied to the Full Spectrum of Break Sizes (FULL SPECTRUM LOCA Methodology)," November 2010.
- [12] LTR-NRC-12-66, "Transmittal of Meeting Presentation Materials Regarding WCAP-16996-P, Rev. 0, 'Realistic LOCA Evaluation Methodology Applied to the Full Spectrum of Break Sizes (FULL SPECTRUM LOCA Methodology)' (Proprietary/Non-Proprietary)," September 18, 2012.
- [13] JAERI-Memo 59-450, "Data Report on Large Scale Reflood Test-82, CCTF Core-II Test C2-4 (Run 62)," February 1985.
- [14] Frepoli C., Oriani L., "Notes on the Implementation of Non-Parametric Statistics within the Westinghouse Realistic Large Break LOCA Evaluation Model (ASTRUM)," Proceedings of ICAPP '06, Reno, NV USA, June 4-8, 2006, Paper 6257.
- [15] Frepoli C., Iyengar S., "A Comparison of Non-Parametric Tolerance Limits with Linear Combinations of Order Statistics in Safety Analysis," Proceedings of ICAPP '11, Nice, France, May 2-5, 2011, Paper 11430.
- [16] Wallis G.B., 2003, "Contribution to the paper 'Statistical Aspects of Best Estimate Method-I' by Attila Guba, Mihakly Makai, Lenard Pal," Reliability Engineering and System Safety, Vol. 80, 309-311.
- [17] Wallis, Graham B. and Nutt, William T., 2005, " Short Communication: Reply to 'Comments on 'Evaluation of Nuclear Safety from the Outputs of Computer Codes in the Presence of

- Uncertainties' by W.T. Nutt and G.B. Wallis,' by Y. Orechwa," Reliability Engineering and System Safety, Vol. 87, 137-145.
- [18] Wallis, G.B., 2005, "Uncertainties and Probabilities in Nuclear Reactor Regulation," The 11th International Topical Meeting on Nuclear Reactor Thermal-Hydraulics (NURETH-11), Avignon, France, October 2-6, 2005.
- [19] Orechwa, Yuri, 2004, "Best-Estimate Analysis and Decision Making Under Uncertainty," Proc. Best Estimates 2004, Washington, D.C., November 14-18, 2004.
- [20] Orechwa, Yuri, 2005, " Short Communication: Comments on 'Evaluation of Nuclear Safety from Outputs of Computer Codes in the Presence of Uncertainties' by W.T. Nutt and G.B. Wallis," Reliability Engineering and System Safety, Vol. 87, 133-135.
- [21] Nutt William T., Wallis Graham B., 2004, "Evaluation of Nuclear Safety from the Outputs of Computer Codes in the Presence of Uncertainties," Reliability Engineering and System Safety, Vol. 83, 57-77.
- [22] R. P. Martin and W. T. Nutt, "Perspectives on the application of order-statistics in best-estimate plus uncertainty nuclear safety analysis," Nuclear Engineering and Design, Vol. 241, Issue 1, pp. 274-284, 2011.
- [23] Regulatory Guide 1.157, "Best-Estimate Calculations of Emergency Core Cooling System Performance," USNRC, May 1989.
- [24] NUREG-0800, "Standard Review Plan - 15.0.2 Review of Transient and Accident Analysis Methods," December 2005.
- [25] Regulatory Guide 1.203, "Transient and Accident Analysis Methods," USNRC, December 2005.
- [26] D'Auria, F., Giannotti, W., Piagentini, A., 2000, "Consideration of Bifurcations within the Internal Assessment of Uncertainty," The 8th International Conference on Nuclear Engineering (ICONE-8), Baltimore, USA, April 2-6, 2000.

**WCAP-16996-P, “Realistic LOCA Evaluation Methodology Applied to the Full Spectrum of Break Sizes
(FULL SPECTRUM LOCA Methodology)”
Requests for Additional Information – (Non-Proprietary)
RAIs 46 – 58, 75, and 77**

October 2013

Westinghouse Electric Company LLC
1000 Westinghouse Drive
Cranberry Township, PA 16066

Question #46: Containment Pressure Analysis Code COCO Component

The Full Spectrum™ LOCA methodology uses the COCO containment code (Bordelon, F. M., Murphy, E. T., "Containment Pressure Analysis Code (COCO)," WCAP-8327 (Proprietary), WCAP-8306 (Non-Proprietary), 1974) to compute the containment backpressure [

] ^{a,c} The COCO code was integrated into WCOBRA/TRAC-TF2. WCAP-16996-P/WCAP-16996-NP, Volumes I, II and III, Revision 0, Section 10.11, "COCO Component," explains that "the COCO computer program (Bordelon and Murphy, 1974) is used to predict the containment pressure response to a LOCA for dry containment buildings, with modeling assumptions to conservatively minimize the back pressure as described in (Bordelon et al., 1974)." WCAP-16996-P/WCAP-16996-NP, Volumes I, II and III, Revision 0, Section 25.6, "Containment Response," further clarifies that COCO is used to calculate the containment pressure [

] ^{a,c} Section 25.6 states that input values are shared consistently between WCOBRA/TRAC-TF2 and COCO (i.e., safety injection temperature) with the exception of the single failure assumption. Whereas a failure of a single-train of ECCS is assumed for the LOCA transient calculations, all trains of containment spray, fan coolers, etc. are assumed to be in operation for the containment pressure calculation. Also, Section 25.6 states that "the values for inputs pertinent only to the containment model were typically selected to provide a minimum containment pressure (e.g. maximum heat transfer areas and volumes are modeled for containment heat sinks)." [

] ^{a,c}

Please clarify the following items related to the COCO containment component in WCOBRA/TRAC-TF2.

(1) Please identify the frozen code version of the stand-alone COCO containment code that was used to develop the integrated in WCOBRA/TRAC-TF2 and provide a complete set of references that document this code version. Explain if this code version has been approved by the U.S. Nuclear Regulatory Commission (NRC) and provide appropriate references. If any changes were made to the stand-alone code as part of its integration in to WCOBRA/TRAC-TF2, please describe these changes and explain if they have been previously reviewed and approved by NRC.

(2) Please describe briefly the balance equations used in the lumped parameter modeling approach and identify the subsystems included in the containment model. In addition, describe the implemented modeling assumptions and explain any possible non-conservatism in the modeling approach. Describe the modeling of engineered features, components and safety systems that can have an impact on the containment pressure response predictions and identify any modeling limitations in this regard.

FULL SPECTRUM and **FSLOCA** are trademarks of Westinghouse Electric Company LLC, its affiliates and/or its subsidiaries in the United States of America and may be registered in other countries throughout the world. All rights reserved. Unauthorized use is strictly prohibited. Other names may be trademarks of their respective owners.

(3) Please describe and present results from validation cases that demonstrate the applicability and appropriateness of the COCO component for the purposes of the FULL SPECTRUM™ LOCA methodology. Identify any modeling biases and their possible impact on LBLOCA prediction results.

(4) COCO is used to calculate the temperature and pressure inside a pressurized water reactor (PWR) dry containment following a LOCA for containment design (i.e., peak pressure) as well as for containment backpressure prediction for LOCA analyses. Please identify and provide a list of all parameters for which Section 25.6 states that “the values for inputs pertinent only to the containment model were typically selected to provide a minimum containment pressure” applies. In addition, please provide these selected values and explain the basis for their determination. Clarify if any of these input values are plant-specific and if so explain how it is ensured that appropriate inputs will be used for intended FULL SPECTRUM™ LOCA methodology applications.

(5) Please describe the modeling options for determining the heat transfer to containment walls and structures (e.g., input tables). Please describe any implemented heat transfer coefficient correlations along with their range of applicability and activation logic. Explain how [

]^{a,c} was determined and implemented in the COCO component.

(6) Please identify any parameters related to the COCO component that are subject to sampling in FULL SPECTRUM™ LOCA methodology applications. For each such parameter, define the sampling range and distribution and explain their determination for best-estimate plant LOCA applications.

(7) WCAP-16996-P/WCAP-16996-NP, Volumes I, II and III, Revision 0, Section 10.11, “COCO Component,” refers at its end to topical report Section 25.5, “Operator Actions.” It is believed that the reference in Section 10.11 should be to Section 25.6, “Containment Response,” instead of Section 25.5, “Operator Actions.”

Response:

Response to Question 1

The frozen code version of the stand-alone COCO version used to develop the integrated WCOBRA/TRAC-TF2 model is COCO_A Version 1.4, which was built using COCOLIB.A Version 1.2. The references that document this code version are WCAP-8327-P (Reference 1), Containment Pressure Analysis Code (COCO), and WCAP-8339 (Reference 8), Westinghouse Emergency Core Cooling System Evaluation Model. Reference 1 provides the code description and Appendix A of Reference 8 provides instructions as to how the code will be applied.

COCO was approved by the NRC as part of the LOCA 1975 Evaluation Model according to WCAP-8471-P-A (Reference 3), which references the COCO topical report (Reference 1). This COCO topical was also referenced in the BASH Evaluation Model in WCAP-10266-P-A (Reference 5). According to the SER, Section 3.5, Item I.D.2 in Reference 5, “The COCO and LOTIC codes are used in the same manner as previously approved by the NRC. Pressure reducing effects are maximized.” Also, according to Section 6.4 of Reference 5, “COCO is accepted for ECCS calculations and is described in detail in WCAP-8327.” In addition, page 2-8 of WCAP-9220-P-A, Revision 1 (Reference

4), specifies that paint may be modeled on the containment walls in the COCO code. This change was approved as part of the 1978 and 1981 versions of the Westinghouse ECCS Evaluation Models in Reference 4.

There are several changes made to the stand-alone code as part of its integration in WCOBRA/TRAC-TF2, which include the following:

- a) Coupling logic / Time-Step Treatment: The containment conditions are updated after each WC/T-TF2 time-step. In this case, COCO will use the mass and energy releases (M+Es) at the end of each successful WC/T-TF2 time-step as boundary conditions at the BREAK until the COCO calculations catch up to the WC/T-TF2 time-step. In most cases, COCO will need only one time-step to catch up, since the WC/T-TF2 time-step size is typically small compared to the typical COCO time-step size.
- b) Treatment of boundary conditions: COCO and WC/T-TF2 have been integrated to pass boundary condition information back and forth at each WC/T-TF2 time-step. This allows every break case to have immediate feedback with the containment, and allows each WC/T-TF2 run to have different containment pressure boundary conditions. There is no impact on the WC/T-TF2 solution matrix or numerical solution method as a result of this difference because the data is transferred as boundary conditions from the last time-step of one code feeding the new time-step of the other code.

In order to pass the boundary condition information between COCO and WC/T-TF2 at each time-step, the COCO “Air Addition” and “Steam – Air Removal” capabilities are used as the path to provide flow of non-condensable gases (NCD) from WC/T-TF2 to containment (Air Addition), and the path to supply steam and/or NCD from containment back to WC/T-TF2 (Steam – Air Removal). Therefore, the changes to COCO only involve provision for the new boundary conditions with WC/T-TF2 and do not represent a change to the numerical solution of COCO. At the end of each WC/T-TF2 time-step, the following boundary conditions are provided to COCO: []^{a,c} In addition, COCO provides the following boundary conditions back to WC/T-TF2 for its next time step: []^{a,c}

In order for WC/T-TF2 to interface with COCO, a new type of BREAK component is used to pass the boundary conditions between the codes. For a typical plant analysis, one BREAK would be needed for split breaks, and two for double-ended guillotine (DEG) breaks. Using the COCO containment conditions as a boundary condition means that there are no changes required to the WC/T-TF2 solution matrix, or numerics, and only the source and input of the BREAKs are modified.

- c) Change in treatment of non-condensable gases: According to page 2-3 of Reference 1, COCO has capabilities for modeling two NCD gases. One of the changes to the code is to pass non-condensable gas information between WC/T-TF2 and COCO at the BREAK interface. With the addition of a NCD in the TRAC PF1 components and the COBRA VESSEL component, changes are needed as follows;

- WC/T-TF2 must provide the NCD M+Es to COCO and accept the revised containment NCD conditions from COCO
- COCO must accept and use the NCD M+Es and pass the containment NCD conditions back to WC/T-TF2

As part of this change, it is necessary that flows from the containment to WC/T-TF2 are modeled. Thus, if WC/T-TF2 predicts flows from containment into the BREAK, COCO must recognize this condition and treat these flows appropriately. For flows from the BREAK to the containment, COCO accepts 2-phase mixture M+Es and separate NCD M+Es. For flows from the containment to the BREAK, only steam and NCD M+Es are considered, since the liquid modeled by COCO is only in the sump, with no communication path to the BREAK.

- d) Input changes are described in further detail in responses to Questions 4, 5, and 6. Specifically, there are changes to the safety injection water temperature and delay time inputs (see Question 6), the end-of-blowdown time and blowdown energy inputs (see Question 5), and a few other input updates due to the coupling of COCO and WC/T-TF2 (see Question 4).

These changes have not been previously reviewed and approved by the NRC, but are not considered significant changes to the code itself. The COCO-interface in WC/T-TF2 is behaving consistent with the stand-alone COCO_A Version 1.4 computer program.

Response to Question 2

COCO uses continuity and energy equations in a lumped parameter modeling approach as described in Section 2.2 of Reference 1. In addition, COCO uses volume equations, equations of state, and steam and water tables. The energy equations used for modeling the containment walls are described in Section 2.3 of Reference 1 and are discussed in more detail in the response to Question 5. The auxiliary systems in the containment model are described in Section 2.4 of Reference 1, and include flashing of break flow, heat sources, and venting. Modeling assumptions a) through d) are described in Section 2.1 of Reference 1, and include the following:

- a) The containment air-steam-water mixture is separated into two distinct systems. The first system is the air-steam phase, while the second is the water phase in the containment sump. COCO assumes uniform thermodynamic conditions in each of these systems, but this does not imply continual thermal equilibrium between the air-steam mixture and the water phase. COCO uses the fundamental laws of thermodynamics to solve for the containment conditions at any time.
- b) Air inside containment is treated as an ideal gas. The thermodynamic properties of steam as found in the 1967 ASME steam tables adopted by the Sixth International Conference on the Properties of Steam are used in COCO.
- c) For heat transfer through and heat storage in walls of the containment structure, only multi-layered flat walls are considered and heat transfer is neglected in any direction perpendicular to the wall surface. In addition, the thermal conductivity, density and specific heat of each heat layer are assumed to be constant.

- d) Two phase discharge flow is divided by assuming the liquid part to be saturated liquid at the total containment pressure, and the steam part to be saturated vapor at the steam partial pressure in the containment. For single discharge flow, the flow goes directly to the appropriate system.

It is noted that these four assumptions have always existed in the containment modeling approach, and originated in the as-approved COCO version. The changes to COCO as a result of coupling WC/T-TF2 and COCO are described in response to Question 1, and are considered modeling implementation approaches rather than modeling assumptions. As discussed in response to Question 6, the safety injection temperature and delay times are input to COCO [

] ^{a,c}

The engineered features, components and safety systems included in the COCO containment code are described in Section 2.5 of Reference 1, and are described in more detail in response to Question 4. The engineered safeguards modeled in COCO are containment ventilation fan coolers, internal spray system, recirculation cooling system, and external spray.

Response to Question 3

Section 3 of Reference 1 presents a validation case comparing the COCO code prediction to experimental test data. The COCO code performance was shown to be in good agreement with the corrected test temperatures from the work of Kolflat and Chittenden (Reference 6). In addition, the code was compared to other techniques including the CONTEMPT code, which is an independently derived containment analysis code used by the (former) Atomic Energy Commission (AEC) staff. The response to Question 1 shows that the COCO version in Reference 1 is very similar to the coupled COCO version in WC/T-TF2. Therefore, the results of this validation case still remain applicable to the COCO Version 1.4 used with WC/T-TF2.

To validate the coupled WC/T-TF2 and COCO code Version 1.4, several validation test cases were performed to ensure the implemented features were functioning as intended. In addition, the standalone COCO containment pressure calculations were compared with WC/T-TF2 coupled run calculations. The following validation test cases were performed:

a. [

b.

] ^{a,c}

c. [

d.

] ^{a,c}

Modeling biases in the COCO inputs are typically selected to conservatively minimize containment backpressure from a LOCA perspective. See the response to Question 4 for the parameters that are typically selected to provide a minimum containment pressure, and see the response to Question 5 for further information on the [^{a,c}

Response to Question 4

The COCO input parameters were reviewed to identify those that are intentionally selected to provide a minimum containment pressure.

COCO Inputs

- The standard COCO break flow model input results in break flow flashing into steam at steam partial pressure and water at total containment pressure. All of the steam from the break goes to the atmosphere, and all of the water from the break goes to the sump.
- Several inputs are used for coefficients and multipliers in the Tagami correlation.
 - As discussed in Appendix A, Section III.B.1 of Reference 8, the maximum condensing heat transfer coefficient at the end of blowdown is five times higher than that calculated using the Tagami correlation.
 - As discussed in Appendix A, Section III.B.3 of Reference 8, in the post-blowdown period of the transient, the coefficient for exponential decay in the Tagami correlation is specified as 0.05.
- The [^{a,c} respectively. These inputs are discussed further in the response to Question 5.

- The net free volume of containment is a plant-specific input, and is biased high to minimize containment backpressure.
- The initial state of containment has four possible modeling options, which are described in Section 2.2 of Reference 1. According to page 2-3 of Reference 1, the condition of superheated steam and subcooled water is intended to represent the containment atmosphere in the form of air with a small relative humidity. This condition is typically used for LOCA applications of COCO.
- Containment Passive Heat Sinks
 - The containment heat sink inputs are developed from plant-specific data. The surface area, thickness, and materials of each layer present (including paint), as well as the thermal conductivity, and volumetric heat capacity of each material is requested. Maximum values are conservative for all areas, thicknesses, etc, with the exception of paint layer thickness. A minimum value is conservative for paint layer thickness. Also, for thermal conductivity and specific heat, the maximum values are recommended for use. See the response to Question 5 for additional information about the heat sink modeling approach.
 - COCO has the capability to specify the heat transfer boundary condition at the outer surface of each layer of the walls. Options include specifying a constant heat transfer coefficient, modeling the outer surface of the layer of the wall as adiabatic, or inputting the surface emissivity for radiation heat transfer. Standard LOCA values for the various surfaces modeled in COCO include the following:
 - Heat transfer coefficient for steel/concrete interfaces of 300 BTU/hr-ft²-°F. According to pages A-3 and A-4 of Reference 8, preliminary results of experimental data show that the coefficient lies in the range of 10-100 BTU/hr-ft²-°F, but 300 BTU/hr-ft²-°F is used as a conservatively bounding value.
 - Heat transfer coefficient for paint/paint, paint/steel, paint/concrete, and concrete/concrete interfaces of []^{a,c} Therefore, the heat is able to flow through the paint layers, and is stored in the interior layers of the wall.
 - For the final layer of an internal wall, adiabatic conditions are modeled.
 - For the external surface of the containment building exposed to the atmosphere, an emissivity of []^{a,c} is modeled. According to Table A.11 of Reference 10, the emissivity of concrete is between 0.88 and 0.93, thus []^{a,c} is an adequate representative value for the emissivity of concrete.

- Initial Conditions

- COCO provides two options for the user to specify initial containment parameters. The first is to input initial containment parameters for water and steam (and then the code specifies or calculates the other initial conditions), or the initial conditions can be specified for air, hydrogen, steam, and water. In a typical LOCA analysis, the latter option is used with the following initial conditions specified for each biased to minimize the calculated containment pressure:

- Initial pressures are set by the user for air, hydrogen, steam, and water. The initial containment pressure for LOCA evaluation models has typically been set to [

]^{a,c} The initial water pressure is set to the initial containment pressure. The partial pressures for steam and air are then calculated using the initial containment pressure and the initial containment temperature, conservatively assuming []^{a,c} relative humidity. Finally, the initial hydrogen pressure is set to zero. The generic value of []^{a,c} is justified in ET-NRC-92-3699 (Reference 9).

- Gas constant and specific heat are set by the user for air and hydrogen only. Standard gas constants of 53.3 ft-lbf/lbm-°R and 767 ft-lbf/lbm-°R are used for air and hydrogen, respectively. Standard specific heats of 0.24 BTU/lbm-°F and 3.42 BTU/lbm-°F are used for air and hydrogen, respectively.

- Initial temperatures are set by the user for steam and water only. The initial containment temperature for LOCA evaluation models has typically been set to []^{a,c} for dry-atmospheric containments. This value is further justified in Reference 9.

- Fan Coolers

- []^{a,c} is a plant-specific input which is biased high in the COCO code. For a plant with fan coolers, the utility is recommended to specify [

]^{a,c} It is noted that if there are no fan coolers in the plant design, none are modeled.

- The minimum fan cooler initiation delay time is []^{a,c} For FSLOCA applications, [

]^{a,c} This is noted as a departure from prior COCO applications where the delay time was [

]^{a,c}

- The heat removal rate is [

]^{a,c}

- Recirculation Modeling

- This set of inputs is used to enter information related to recirculation modeling, which is used for plants with []^{a,c} and plants with [

]^{a,c}

- The recirculation modeling approach has not changed as a result of coupling COCO and WC/T-TF2; therefore, the recirculation cooling system described in Section 2.5.3 of Reference 1 is still applicable.
- The plant provides the minimum recirculation spray pump initiation time, and the delay time is []^{a,c} For FSLOCA applications, [

]^{a,c} This is noted as a departure from prior COCO applications where the delay time was []^{a,c} If the plant is not equipped with a recirculation containment spray system that can operate during ECC injection mode coincident with the containment spray system, or if the recirculation spray system only initiates after the large break LOCA transient has ended, then this input is not required. However, if the recirculation pumps come on before the LOCA transient has ended, then additional plant-specific inputs will be requested from the plant.

- Internal Spray

- The maximum containment spray flow rate []^{a,c} is a plant-specific input. [

]^{a,c}

- The containment spray start time (spray pump initiation delay) is []^{a,c} For FSLOCA applications, [

]^{a,c}

This is noted as a departure from prior COCO applications where the delay time was []^{a,c} The containment spray stop time is

typically entered as a value much greater than the transient end time to ensure continuous spray flow throughout the entire transient.

- The containment spray temperature input is []^{a,c} in the FSLOCA applications. The SI spray temperature will be modeled []^{a,c}. It is noted that this is a change from prior applications, where this input was typically taken as the []^{a,c}.
- In a typical LBLOCA analysis, the spray inputs are used to model the []

] ^{a,c}

- Wall Surface Heat Transfer Coefficient vs. Time Tables

- COCO has the capability to model a table of wall surface heat transfer coefficients vs. time. It is recommended that the inside surface film heat transfer coefficient is equal to []^{a,c} at all times. This generic coefficient value is generally used for walls in contact with the containment sump. This parameter is not expected to have much influence on the containment pressure calculation for FSLOCA, though it is assumed to be sufficiently high to adequately remove heat from the sump.

- Air Addition Input Capabilities

- A table of air addition mass flow rate and temperature vs. time can be input to COCO. The table contains values of []

] ^{a,c}

Note that the air addition table is used to model the emptying of the broken loop accumulator. Transport of the NCD gases from the intact loop accumulators is modeled in WC/T-TF2. When it travels through the RCS to the break, it is introduced to the COCO calculation.

Response to Question 5

The heat transfer to containment walls and structures is described in Section 2.7.2 of Reference 1. The modeling options to determine the heat transfer to the containment walls and structures have not changed as a result of integrating COCO in WC/T-TF2. Overall, the code has the capability to model []^{a,c} which was a minor change implemented into COCO_A, Version 1.4. Structural heat sinks are modeled as a series of layers, and there can be up to a maximum of []^{a,c} layers per heat sink. For each heat sink []

[]^{a,c} is input. In addition, the analyst can specify the method for calculating the wall heat transfer coefficient for structural heat sinks, and whether the heat sink is in contact with the sump or steam-air mixture. For the wall heat transfer coefficient, in a typical plant analysis, the Tagami Correlation for heat transfer to steel or to concrete is used, depending on the material of the structural heat sink. These coefficients are calculated internally. In addition, the code has the capability for time or temperature dependent user-specified heat transfer coefficient tables. Then, for each of the layers for all heat sinks, the thickness of the layer, the thermal conductivity, the volumetric heat capacity, and the heat transfer boundary condition at the outer surface of the layer is modeled.

COCO uses the Tagami correlation to describe the heat transfer coefficients between the containment atmosphere and the containment structures. To use the Tagami correlation in COCO, the time from the start of accident to the end of blowdown must be input. In addition, the coolant energy discharged from the beginning of the accident until the end of blowdown must be specified. For the FSLOCA application of COCO, []

[]^{a,c}

According to Equation 56 of Reference 1, the maximum heat transfer coefficient is proportional to the blowdown energy raised to a power of 0.6, and inversely proportional to the end-of-blowdown time raised to a power of 0.6. Therefore, minimizing the end-of-blowdown time and maximizing the blowdown energy will maximize the heat transfer coefficient, and minimize the calculated containment pressure. []

[]^{a,c}

The Demonstration Analysis, presented in Section 31 of Reference 7, used []

[]^{a,c} which was shown to be bounding for the Demonstration Analysis.

Response to Question 6

The response to RAI 77 describes the sampled parameters in an FSLOCA uncertainty analysis. These parameters were examined to determine which, if any, are also used as inputs in the LOCA containment pressure calculations. Based on a review of Table 1 of the response to RAI 77, [

] ^{a,c}

For a plant-specific application of FSLOCA, the [^{a,c} are determined by input from the plant. The sampling range is based on historical data provided by the plant per Table 29-5 of Reference 7. RAI 77 provides additional information regarding the [^{a,c}

In addition, there are other sampled parameters that have an impact on the containment response during a LOCA. Due to the implementation of coupling WCT-TF2 and COCO, the break M+Es are passed between the two codes during the transient. As a result, the break type, break area, and discharge coefficients are sampled parameters which indirectly influence the containment backpressure calculation as the size of the break will impact on the M+Es that are released to containment. It is noted that all of the sampled parameters in FSLOCA may indirectly have a minor impact on the containment backpressure calculation during a LOCA.

Response to Question 7

Westinghouse agrees with the observations noted in Question 7. Revisions to correct cross references will be made as part of the overall topical report updates.

References:

1. **WCAP-8327-P**, "Containment Pressure Analysis Code (COCO)," July 1974 (*Note that the non-proprietary version is available as WCAP-8326-NP*).
2. Not used.
3. **WCAP-8471-P-A**, "THE WESTINGHOUSE ECCS EVALUATION MODEL: SUPPLEMENTARY INFORMATION," April 1975.
4. **WCAP-9220-P-A, Revision 1**, "WESTINGHOUSE ECCS EVALUATION MODEL 1981 VERSION," February 1982.
5. **WCAP-10266-P-A, Revision 2**, "The 1981 Version of the Westinghouse ECCS Evaluation Model Using the BASH Code," March 1987.
6. **Kolflat, A., and Chittenden, W.**, "A New Approach to the Design of Containment Shells for Atomic Power Plants," Proceedings of American Power Conference, pg. 651, Vol. XIX, 1957.
7. **WCAP-16996-P, Volumes I through III**, "Realistic LOCA Evaluation Methodology Applied to the Full Spectrum of Break Sizes (FULL SPECTRUM LOCA Methodology)," November 2010.
8. **WCAP-8339**, "Westinghouse Emergency Core Cooling System Evaluation Model Summary," June 1974.
9. **ET-NRC-92-3699**, "Results of Technical Evaluation of Containment Initial Temperature Assumptions for Large Break Loss of Coolant Accident Analysis," June 1, 1992.
10. **Incropera, F. P., DeWitt, D. P., Bergman, T. L., and Lavine, A. S.**, "Fundamentals of Heat and Mass Transfer," Sixth Edition, John Wiley and Sons, 2007.

Question #47: TRAC-PF1 One-Dimensional Component Models

WCAP-16996-P/WCAP-16996-NP, Volumes I, II and III, Revision 0, Section 10, "WCOBRA/TRAC-TF2 One-Dimensional Component Models," explains that the one-dimensional components in WCOBRA/TRAC-TF2 used to model the reactor primary system are derived from TRAC-PF1. As stated in Subsection 10.1, "Introduction,"

"many of the base modules, such as PIPE, TEE, HTSTR, VALVE and PUMP are virtually unchanged from their original TRAC-PF1 versions, so their descriptions are very similar to those given by TRAC-PF1 user manual."

Please clarify the following items related to the one-dimensional component modules in WCOBRA/TRAC-TF2.

- (1) Please identify the frozen code version of TRAC-PF1, from which the one-dimensional component modules implemented in WCOBRA/TRAC-TF2 were taken and provide a reference to the cited TRAC-PF1 user manual. In addition, explain how it was determined that the existing TRAC-PF1 modules were adequate for the purposes of the WCOBRA/TRAC-TF2 code. If any changes were made to these modules as part of their integration in WCOBRA/TRAC-TF2, please document the changes and explain if they have been previously reviewed by NRC.
- (2) In describing the HTSTR component, WCAP-16996-P/WCAP-16996-NP, Volumes I, II and III, Revision 0, Subsection 10.10, "HTSTR Components," refers on several occasions to the TRAC-M code. TRAC-M was the predecessor of the TRACE code developed by the NRC. Please identify the code from which the HTSTR component was taken and explain how TRAC-M was used for the purpose of implementing this HTSTR component in WCOBRA/TRAC-TF2.

Response:

Text references to TRAC-M, TRAC-P, TRAC-PF1, or TRAC-PF1/MOD2 represent the same base (frozen) TRAC code version: TRAC-P Version 5.4.28. WCAP-16996-P/WCAP-16996-NP will be updated to replace the aforementioned code version references with a single TRAC-P code reference, which is TRAC-P Version 5.4.28. However, actual referenced documents may still point to other TRAC versions when they represent the best known available information.

TRAC-P Version 5.4.28 is the frozen version transmitted to Westinghouse by the USNRC via Information Systems Laboratories with the following letter:

ISL-TRAC-04-002 "TRAC-04-002: Transmittal of TRAC-P Version 5.4.28,"
September 2004.

The user manual cited for this frozen version is the following:

LA-UR-00-834 "TRAC-M/Fortran 90 (Version 3.0) User's Manual,"
Steinke, R. G., et al., February 2000.

The following are the other references identified as documentation of the frozen version:

LA-UR-99-2312 "TRAC-M/Fortran 77, Version 5.5, Programmer's Guide,"
Steinke, R. G., et al., October 1999.

LA-UR-00-803 "TRAC-M/Fortran 90 (Version 3.0) Programmer's Manual,"
Adams, B. T., et al., February 2000.

LA-UR-00-910 "TRAC-M/Fortran 90 (Version 3.0) Theory Manual," Spore, J. W., et al.,
July 2000.

LA-UR-01-2105(1) "TRAC-M/F77, Version 5.5, Developmental Assessment Manual,
Volume 1: Assessments," Boyack, B. E., et al., April 2001.

LA-UR-01-2105(2) "TRAC-M/F77, Version 5.5, Developmental Assessment Manual,
Volume 2: Appendices," Boyack, B. E., et al., April 2001.

The TRAC-PF1/MOD2 code version (TRAC-P) was considered to be mature for the purpose of WCOBRA/TRAC-TF2 (WCT-TF2) development. It was the final TRAC code version available in a format compatible with the Fortran 77 structure of the WCOBRA/TRAC (WC/T) code in use at Westinghouse for predicting the response of a pressurized water reactor (PWR) to a loss of coolant accident (LOCA), and it provided additional capabilities not present in WC/T, based on the TRAC-M Theory Manual (Spore, et al., 2000) and TRAC-M Assessment Manual (Boyack, et al., 2001).

WC/T was previously qualified for the realistic analysis of PWR Large Break (LB) LOCAs. TRAC-P provided additional capabilities to potentially expand the application of WC/T to the full spectrum of breaks: small, intermediate, and large. The TRAC-P 1D module provided enhanced LBLOCA features (e.g. non-condensable gas transport) and added capabilities to properly capture the important processes and phenomena identified for small and intermediate break scenarios. It featured expanded fundamental field equations and closure relationship models which are essential to extend the WC/T code capabilities. The TRAC-P six-equation two-fluid solution provides adequate formulation for horizontally stratified flow simulation required for Small Break (SB) LOCA analysis, in comparison to the formulation in WC/T (which is based on TRAC-PD2).

The TRAC-P developmental assessment documentation (Boyack, et al., 2001) demonstrated that TRAC-P was a viable tool for analyzing PWRs during a LOCA and other operational transients, by successful comparisons to analytical solutions, separate effect tests, and integral effect tests.

The adequacy of the WCT-TF2 individual 1D-components has been demonstrated by performing successful comparisons to analytical solutions, separate effect tests, and integral effect tests, as provided in WCAP-16996-P/WCAP-16996-NP.

Changes to 1D-Components

The following summarizes the source code changes made to the TRAC-P 1D-components during the development of the WCT-TF2 code, and identifies specific WCAP-16996-P/WCAP-16996-NP section numbers where each change is described and/or assessed, when appropriate:

1. **Generic** No further documentation in WCAP-16996-P/WCAP-16996-NP for these changes, unless noted.
 - a. Ported program to GNU Linux, using Intel Fortran (ifort).
 - b. Added and improved input checking logic for all 1D-components to consistently provide an ERROR or WARNING message when appropriate. Corrected and improved output information related to input.
 - c. []^{a,c} is described in Section 5.12, and demonstrated in Section 12.0.
 - d. []^{a,c}
2. **BREAK** See Section 10.9 and Section 10.11.
 - a. Added IBTY=101 option to interface with COCO for containment boundary conditions. Up to []^{a,c} BREAK components can interface with COCO.
3. **FILL** See Section 10.9. No FILL-specific changes.
4. **HTSTR** See Section 10.10 for HTSTR description, and Section 10.5 for use of HTSTR in steam generator model. No HTSTR-specific changes.
5. **PIPE** See Section 10.2.
 - a. Added []^{a,c} applied in TF1D.
 - b. Added []^{a,c} applied in PREPER.
 - c. Modified flow regime map (and use of inputs []^{a,c}). Horizontal stratification in a PIPE can be controlled by []^{a,c} input. Calculations in FEMOM and HTIF. See Section 4.4.
6. **PRIZER** See Section 10.6.
 - a. Added THTR optional time to []^{a,c} for control.
7. **PUMP** See Section 10.4.

- a. Added the []^{a,c} as OPTION=3. Modifications in PUMPI, RDCRVS, RDDIM. See Figures 10-4 through 10-7 for the []^{a,c}.
 - b. Included the WC/T production version (WC/T Version Mod.7A Revision 7) []^{a,c}, with input of TFROPT=1 on input card PUMP.7.
8. **TEE** See Section 10.3.
 - a. Added []^{a,c} applied in TF1D.
 - b. Added []^{a,c} applied in PREPER.
 - c. Modified flow regime map (and use of inputs []^{a,c}). Horizontal stratification in a TEE can be controlled by []^{a,c}. Calculations in FEMOM and HTIF. See Section 4.4.
 - d. Added new option under IOFFTK=1 to use []^{a,c}. See Section 6.3.6 for as-coded description and Section 17 for the assessment.
 - e. Modified []^{a,c}. Calculations in OFFTKE. See Section 5.13 for description of changes to the offtake model.
 - f. Added new IENTRN=4 option, with []^{a,c}.
9. **VALVE** See Section 10.7.
 - a. Added []^{a,c} applied in TF1D.
 - b. Added []^{a,c} applied in PREPER.

Question #48: Steam Generator Modeling

WCAP-16996-P/WCAP-16996-NP, Volumes I, II and III, Revision 0, Subsection 10.5, "Steam Generator," explains that PWR Steam Generator (SG) is modeled in WCOBRA/TRAC-TF2 with a combination of PIPE, TEE, and HTSTR components. The example nodding diagram for a U-tube SG shown in Figure 10-8, "Steam Generator Noding Diagram," includes a single PIPE component representing the entire U-tube bundle. The SG models in the plant examples discussed in WCAP-16996-P/WCAP-16996-NP, Volumes I, II and III, Revision 0, Section 26, "WCOBRA/TRAC-TF2 Model of Pilot Plants," follow the same modeling approach. As seen from Figure 26.2-9, "Virgil C. Summer Steam Generator Component Noding Diagram," and Figure 26.3-15, "Beaver Valley Unit 1 Steam Generator Component Noding Diagram," the U-tube bundle is modeled with a single PIPE component as well.

Although WCAP-16996-P/WCAP-16996-NP, Volumes I, II and III, Revision 0, Subsection 10.5, "Steam Generator," mentions that in the implemented approach the SG U-tube bundle is represented by "a single effective tube that has the heat transfer characteristics of the entire tube bank," the following related items need further clarification.

Using a single PIPE in combination with a HTSTR component allows preserving the heat transfer surface area of the entire SG U-tube bundle. At the same time, individual U-tubes in the bundle are characterized by various elevation heights of the apex points in their bending sections that range between the height of the apex of the shortest tube row and that of the longest tube row. It is recognized that the height of individual U-tubes in the bundle is an important factor under conditions involving natural circulation through the primary coolant loops. Such conditions are of importance when modeling small break LOCAs. Accordingly, several U-tube rows of different heights are used in integral PWR test facilities to represent the SGs. For example, the PKL III (abbreviation from Primärkreislauf, German for primary coolant circuit) 1:1 vertical scale replica of a 1,300 MegaWatt PWR employs seven different U-tube clusters of variable height to represent the SG U-tube bundle. The elevation difference between the apex of the longest tube cluster and that of the shortest one amounts to 2.020 m or 6.63 ft (see Figure 2.3, "Axial Locations of Thermocouples in SG Tubes," in NUREG/IA-0170, "RELAP5/MOD3.2 Post Test Calculation of the PKL-Experiment PKLIII-B4.3", December 1999). As reported by K. Umminger, T. Mull, and B. Brand, "Integral Effect Tests in the PKL Facility with International Participation," Nuclear Engineering and Technology, Vol. 41, No. 6, pp. 765-774, August 2009, representing the SG tubes by three lengths can be insufficient for adequate modeling of processes in the SG tubes that are of importance for specific accident conditions.

Please explain and provide the technical basis in support of using a single PIPE representation of the SG U-tube bundle in WCOBRA/TRAC-TF2 models of plants with such SGs. Discuss possible limitations of this approach with regard to modeling thermal-hydraulic phenomena that can take place during small break LOCA transients using the FULL SPECTRUM™ LOCA methodology. Explain how it is ensured that the SG U-tube bundle representation and SG modeling are adequate in resolving specific processes of safety importance that can occur during the course of a small break LOCA.

Response:**Issue Description:**

As noted in the RAI, the steam generator (SG) model used in the PWR plant examples in [1] uses a single PIPE component to model the entire primary side U-tube bundle; the primary-to-secondary heat transfer is modeled by using a HTSRT component connected inside to the U-tube PIPE and outside to the secondary side, modeled by the main pipe of a TEE component.

The particular concern of this RAI is that using a single PIPE component to model the steam generator U-tube bundle would not capture the effect of the possible flow stagnation or reversal in some of the U-tubes during the natural circulation (NC) phase of a small break loss of coolant accident (SBLOCA).

As stated in the RAI, results of some PKL mid-loop natural circulation tests investigating boron dilution have indicated the presence of unstable non-uniform SG U-tube behavior during the natural circulation phase of a mid-loop operation test. It is suggested in Section 4.3 of [2], based on benchmark simulation experience of PKL tests reported in [3], that more detailed multi-tube representation of the SG U-tubes is needed to capture the complex non-uniform multi-tube behavior during natural circulation. However, it has to be noted that this recommendation is made for the simulation of long-term boron dilution studies, not necessarily the early stages of LOCA accidents.

State of Knowledge (experimental and analytical):

Non-uniform U-tube flow behavior has been observed and reported by both the PKL boron dilution NC tests in [2] and [3] and the ROSA-IV LSTF natural circulation tests in [4],[5],[6], and [7].

As reported in Section 4.1 of [4], temperature measurements in the LSTF steam generator U-tubes during the high-pressure natural circulation test ST-NC-02 indicated that the flow in the longer U-tubes was stagnant or reversed in direction for mass inventories greater than 80%. More detailed discussion of the different flow modes observed in the LSTF U-tubes during the high-pressure NC test ST-NC-02 is presented in [5]. In particular, Fig.3 of [5] shows quite a complicated map of observed flow modes in the U-tubes at the different phases (system inventories) of natural circulation. For example, flow reversal is indicated to occur in the long and even some of the medium length U-tubes between 100% and 80% for system inventories. Cyclic fill&dump (F&D) is indicated to occur in all U-tubes for inventories between 80% and 62%, approximately. The process of emptying (E) occurs at inventories between 65% to 60%. Reflux condensation is established in all U-tubes for inventories less than 57% and in a typical SBLOCA would normally end when the loop seals clear.

As stated in [5], experience with modeling the LSTF natural circulation test ST-NC-02 with the RELAP5/MOD2 code using single-tube representation of the SG U-tube [6] suggested the need for more detailed multiple U-tube modeling for accurate prediction of the system overall response; the single-tube modeling approach resulted in over-prediction of the loop flow for single-phase NC and the loop flow oscillations were much larger than those observed in the test. However, the results of RELAP5/MOD3.3 simulations of the ST-NC-02 test with multiple SG U-tubes reported in [7] do not seem to have contributed much to the overall accuracy of the calculations. With a 9-tube

representation of the U-tubes, Fig.11 of [7], the average loop flow is still well over-predicted, for both single-phase and the two-phase period of the natural circulation. The effect of the 9-tube U-tube model is a significant reduction of the calculated loop flow oscillation, Fig.13 of [7], which can obviously be attributed to the 180-degree phase shift of the flows calculated in the 9 individual U-tubes, Fig.14 of [7], but not necessarily an ability to capture realistically the complex non-uniform U-tube flow modes observed in the test.

Calculations using the TRAC code and a 3-tube model of the U-tube SG bundle, reported in [8], appear to have resulted in only qualitative representation of the overall ST-NC-02 test results. However, although flow reversal was calculated to occur in the long U-tube during the single-phase NC period, and the peak flow was calculated to occur at the same system mass inventory as the test, the calculated overall maximum loop flow rate exceeded the measured by 50%. Uncertain and inconclusive explanation was offered in [8] to explain the discrepancies between the test and the simulation results.

In summary, it appears that the known attempts to explicitly model the non-uniform flow behavior in the SG U-tube bundle using a multi-tube representation do not add to substantial improvement of the accuracy in the calculated overall SG behavior during natural circulation.

Justification of the Single-PIPE Steam Generator U-tube Modeling Approach

The ROSA-IV Large Scale Test Facility (LSTF) is used as an important benchmark integral test facility to validate various component modeling techniques used by the PWR simulations within the Westinghouse FSLOCA Methodology [1], including that of the SG U-tube bundle model. Since the design and scaling of the ROSA-IV LSTF allows for the realistic reproduction of the most important small break thermo-hydraulic phenomena, the ROSA LSTF steam generator (SG) model was validated through the simulation of selected ROSA LSTF tests; consistent with the design similarity, the same SG modeling approach was adopted for the full scale PWR plant calculations as well, Section 26 of [1].

The significance and ranking of the steam generator multi-tube behavior during the different phases of the small, intermediate and large break LOCA is briefly discussed in Section 2.3.2.7 of [1].

Large and Intermediate Breaks:

As stated in Section 2.3.2.7 of [1], for intermediate and large breaks the multi-tube behavior has a low influence on the flow through the SG during all phases of the transient. A single-pipe representation of the SG U-tube bundle would be sufficiently to model the SG primary side behavior with respect to primary-to-secondary side heat transfer for intermediate and large break LOCA accidents.

Small Breaks, Blowdown Phase, (Single-Phase Natural Circulation):

With single-phase natural circulation complemented by the driving head of the reactor coolant pumps still coasting down, significant non-uniform U-tube behavior (flow stagnation and/or inversion observed in the PKL and the ROSA natural circulation tests) is unlikely to occur. Therefore, single-pipe modeling would be sufficient representation of the SG U-tube bundle thermal hydraulic behavior.

Small Breaks, Natural Circulation (Two-Phase):

For the purpose of the discussion herein, it is clarified that the “natural circulation (NC) period”, as described in Section 2.3.1.1 of [1], in fact refers to the period of two-phase NC followed by the reflux condensation, which typically includes the loop seal clearing phenomenon; as mentioned above, the single-phase NC occurs earlier during the blowdown period.

The results of the simulation of the ROSA-IV LSTF high-pressure natural circulation test ST-NC-02, documented in Section 21.9 of [1] demonstrate that with the single-tube model of the SG U-tubes the calculated general system behavior is consistent with that observed in the test. Sufficient accuracy is achieved in calculating the loop flow rate at different primary side fluid inventories and phases of the natural circulation, Figure 21.9-2 of [1]. The calculated void fraction distribution as a function of system inventory (Figures 21.9-11 and 21.9-12 for SGA, and Figure 21.9-13 and 21.9-14 for SGB, [1]) indicate that the code is even capable of predicting in general the “cyclic fill & dump” phenomenon observed in the U-tubes at the ST-NC-02 test, as described in [5] and [7]. At the same time, as pointed out in Section 21.9.4, the calculated effective heat transfer coefficient is []^{a,c} than the minimum measured at the LSTF post-natural circulation test ST-SG-02, reported in Section 4.2 of [4]. As a result, it is judged that with the current SG model (single-pipe U-tube) the code has the tendency to slightly []^{a,c} the primary system pressure. As seen in Figure 21.9-3 (system inventories less than 80%), this effect appears to be relatively small, 0.25 MPa (36 psi), but is still in a conservative direction – []^{a,c}.

The calculations (Figure 21.9-4 for ST-NC-02 and Figures 21.4-7 and -8 for SB-CL-18, [1]) also indicate somewhat excessive liquid holdup in the uphill side of the steam generator U-tubes during the NC phase; this contributes to deeper and longer core uncover and as a result higher rod heat-up during the loop seal clearance period.

In summary, it is concluded that the single-pipe modeling of the steam generator U-tubes represents reasonably well and in a conservative manner the most important thermo-hydraulic phenomena that might affect the key overall results (PCT, core coolability, etc.).

Small Break, Core Recovery and Boiloff:

During this phase of the SBLOCA accident the steam generator secondary side is a heat source, the tubes are essentially drained and vapor super-heating is the predominant phenomenon; non-uniform U-tube behavior is not expected to occur. Therefore, single-pipe U-tube bundle modeling is sufficient to model the secondary-to-primary side heat transfer.

Applicability and Limitations of the Single-PIPE SG Model:

It is obvious that the single-pipe representation of the SG U-tube model adopted for the FSLOCA methodology, as described in [1], is not capable to model localized non-uniform multi-tube behavior, in particular that related to boron dilution that might occur during long-term post-LOCA scenarios discussed in [2] and [3].

While the need to accurately represent the non-uniform U-tube behavior seems obvious for the purpose of boron dilution studies, that need is not as obvious for the class of LOCA transients considered within the Westinghouse FSLOCA methodology presented in [1], where the sequence of the NC phenomena developing during the accident are quite different. Therefore, based on the model validation, it is judged that the single-pipe SG U-tube model used for the PWR simulations represents conservatively and with sufficient detail key thermal hydraulic phenomena taking place in the SG during the different phases of the LOCA accidents considered by the Westinghouse FSLOCA Methodology [1], which exclude the long-term cooling period and associated boron dilution phenomena.

References:

1. WCAP-16996-P, "Realistic LOCA Evaluation Methodology Applied to the Full Spectrum of Break Sizes (FULL SPECTRUM™ LOCA Methodology)," November 2010.
2. Umminger, K., et.al., "Integral Effect Tests in the PKL Facility with International Participation," Nuclear Engineering and Technology, Vo.41, No.6, pp 765-774, August 2009.
3. A. Bucalossi, "Validation of Thermal-Hydraulic Codes for Boron Dilution Transients in the Context of the OECD/SETH Project", Seminar 2, EUROSAFE, Brussels, 2005.
4. Tasaka, K., et al., "The Results of 5% Small Break LOCA Tests and Natural Recirculation Tests at the ROSA-IV LSTF," Nuclear Engineering and Design, Vol.108, pp 37-44 (1988).
5. Y. Kukita, et.al., "Nonuniform Steam Generator U-Tube Flow Distribution During Natural Circulation Tests in ROSA-IV Large Scale Test Facility," Nuclear Science and Engineering: Vol. 99, pp 289-298 (1988).
6. JAERI-M 88-215, "Post-Test Analysis with RELAP5/MOD2 of ROSA-IV/LSTF Natural Circulation Test ST-NC-02," October 1988.
7. Yonomoto, T., "ROSA/LSTF Experiments of PWR Natural Circulation and Validation of RELAP5/MOD3.3," 2nd CRP RCM, Corvallis, Oregon (USA), Aug. 29–Sept. 2 (2005).
8. H. Stumpf, et.al., "Reverse Primary-Side Flow in Steam Generators During Natural Circulation Cooling," ASME Heat Transfer Division (HTD), Vol. 92. Submitted to ASME Winter Annual Meeting, Boston, Massachusetts, December 13-18 (1987).

Question #49: T-Junction Component

WCAP-16996-P/WCAP-16996-NP, Volumes I, II and III, Revision 0, Subsection 10.3, "TEE Component," explains that WCOBRA/TRAC-TF2 basically treats a TEE component as two PIPE components as shown in Figure 10-2, "TEE Component Noding." If the primary-side PIPE component, PIPE 1, has NCELL1 cells and the secondary-side PIPE component, PIPE 2, has NCELL2 cells, please explain the meaning of the parameter NCELLS, defined in Figure 10-2 by the expression $NCELLS = NCELL1 + 1 + NCELL2$.

Response:

The parameter NCELLS is defined by the expression $NCELLS = NCELL1 + 1 + NCELL2$, where NCELL1 is the number of cells in the main branch and NCELL2 is the number of cells in the side branch. There is one phantom cell in between the last index of the main branch and the first index of the side branch. The phantom cell represents [

]^{a,c} Users are not required to provide input related to the phantom cell, and the information of the phantom cell is not shown in the output file as well.

Question #50: Component Multipliers

WCAP-16996-P/WCAP-16996-NP, Volumes I, II and III, Revision 0, Section 10, “WCOBRA/TRAC-TF2 One-Dimensional Component Models,” states that additional user-defined multipliers were added that enable the code user to affect specific models and correlations in WCOBRA/TRAC-TF2.

The HS_SLUG multiplier, identified in Subsection 10.2, “PIPE Component,” can be used to affect the horizontal flow calculation for all WCOBRA/TRAC-TF2 one-dimensional hydraulic components, except the PUMP. According to Subsection 10.2, this multiplier ranges between 0.1 and 9.99. WCAP-16996-P/WCAP-16996-NP, Volumes I, II and III, Revision 0, Subsection 4.4.5, “Horizontal Stratified Flow,” provides a range from 0.1 to 9.9 for the same parameter. Its default input value is equal to []^{a,c} and, according to WCAP-16996-P/WCAP-16996-NP, Volumes I, II and III, Revision 0, Subsection 17.3.4, “WCOBRA/TRAC-TF2 Results: Sensitivity Studies,” its uncertainty range is from []^{a,c}

User specified allowances for horizontal stratification within a PIPE component can be provided through the MSTRTX and STRTX input. Similarly, the user has the option to specify allowance for horizontal stratification in the TEE main and side pipes through the STRTX1 and STRTX2 multipliers. The option to provide user specified allowance for horizontal flow is not available in the VALVE component model.

Interfacial drag multipliers YDRGX can be defined by the user at any cell faces of the PIPE, TEE and VALVE components. Similarly, interfacial condensation heat transfer at user selected cells can be modified by using the CNDNX multipliers for the PIPE and TEE components and the XCNDX multiplier for the VALVE component.

WCAP-16996-P Revision 0 Subsection 29.1.6, “Cold Leg Condensation (KCOSI),” identifies a cold leg condensation multiplier, KCOSI, that was added in the code to allow varying the cold leg condensation heat transfer rate for the purpose of the uncertainty analysis.

Please clarify the following items related to the use of user-defined multipliers in conjunction with the one-dimensional component models discussed in Section 10 of WCAP-16996-P/WCAP-16996-NP, Volumes I, II and III, Revision 0:

(1) Please provide a table that lists all user-defined multipliers that can be applied to the one-dimensional component models in WCOBRA/TRAC-TF2 presented in Section 10. For each multiplier, include its identifier, relevant one-dimensional component, applicable cells/interfaces, default value, and allowable range of input values as appropriate.

(2) Please identify the multipliers that are subject to sampling in the uncertainty analyses and provide a table that lists all such multipliers. For each such parameter, provide its identifier, sampling range and corresponding distribution. Explain the technical basis for establishing the provided sampling ranges and sampling distributions. Please explain each individual case for which the range of allowable input values for a multiplier is broader than the defined sampling range (e.g., HS_SLUG).

(3) For the multipliers that are not subject to sampling, if any, please explain the basis for introducing such multipliers. In addition, please clarify how the ranges of allowed input values were established and explain the process of determining the input values in performing plant analyses using the FULL SPECTRUM™ LOCA methodology. Explain if an input value in a plant model can fall outside of the documented range of allowable input values.

(4) Please address Items (1) through (3) above for user-defined multipliers that can be applied to VESSEL component models in WCOBRA/TRAC-TF2, as applicable.

Response:

Part (1)

Table 50-1 below provides a list of all user-defined multipliers that can be applied to the one-dimensional component models, as well as all user-defined multipliers that can be applied to VESSEL component models in WCOBRA/TRAC-TF2. [

] ^{a,c}

Table 50-1: User Defined Multipliers

[
] ^{a,c}

$$J^{a,c}$$

NP-28

J^{a,c}

Part (2)

Table 50-2 below specifies the multipliers from Table 50-1 that are subject to sampling in the uncertainty analysis. The first column in Table 50-2 specifies the multiplier name, and the second column provides a description of the multiplier. The third and fourth columns provide the sampling range and distribution of each multiplier, respectively. The final column in Table 50-2 (Reference) shows the section from WCAP-16996-P that explains the technical basis for establishing the provided sampling ranges and sampling distributions. If the applicable section from WCAP-16996-P does not provide a sufficient explanation, more detail is provided in the notes section of Table 50-2. It is noted that the basis for most of this information is the Westinghouse response to RAI 77.

Table 50-2: Multipliers Subject to Sampling in the Uncertainty Analysis

Acronym	Identifier	Sampling Range	Distribution	Reference
Multipliers Applicable to One-Dimensional Components				
[
				^{a,c}]

¹ []^{a,c}² []^{a,c}³ []^{a,c}

$$]^{a,c}$$

$\mathbf{J}^{a,c}$

Part (3)

Table 50-3 below lists the multipliers that are not subject to sampling in the uncertainty analysis. Additional information about each of these multipliers is in Table 50-1. In FSLOCA EM, the value for each of these multipliers is set at the default value, which is shown in both Table 50-1 and Table 50-3. The rationale for the default value which is fixed in the FSLOCA EM is provided in the 2nd column of Table 50-3. It is noted that there is a description for each of the multipliers that appears in Table 50-1 but does not appear in Table 50-2.

Table 50-3: Justification of Default Values for Multipliers Not Subject to Sampling in the Uncertainty Analysis

Identifier	Justification of the Default Value or the Value used in the FSLOCA EM
------------	---

] ^{a,c}

Identifier	Justification of the Default Value or the Value used in the FSLOCA EM
------------	---

[

] ^{a,c}

Question #51: Fluid Properties for Nusselt Number in Dispersed Droplet Flow

WCAP-16996-P/WCAP-16996-NP, Volumes I, II and III, Revision 0, Subsection 6.2.7, Dispersed Droplet Flow Regime,” provides the interfacial heat transfer coefficient between superheated vapor and dispersed droplets in Equation (6-70), which can be presented in terms of the Nusselt number as follows:

[]^{a,c}

WCAP-16996-P/WCAP-16996-NP, Volumes I, II and III, Revision 0, Subsection 6.2.7 identifies [

] ^{a,c}

Please clarify the following items related to the application of the above correlation for predicting the interfacial heat transfer from superheated steam to liquid droplets for dispersed droplet flow in WCOBRA/TRAC-TF2.

(1) Define the quantities used in Equation (6-71) to determine [

] ^{a,c} Explain if B reduces to zero when the steam superheat becomes negligible. Explain how WCOBRA/TRAC-TF2 determines the thermodynamic properties that are used to calculate [] ^{a,c} in Equation (6-71).

(2) Under high-temperature superheated steam conditions, the Reynolds, Prandtl, and Nusselt numbers become significantly dependent on the fluid properties that are used to calculate the values. The values for these dimensionless numbers evaluated at the free stream (ambient) temperature can differ significantly from those evaluated at the film temperature. Usually, the temperature of the film formed around the droplet from vaporization is defined as the mean of the droplet surface temperature and the ambient gas temperature. Please explain which thermodynamic properties are used in WCOBRA/TRAC-TF2 to calculate the Reynolds, Prandtl, and Nusselt numbers in Equation (6-70).

Equation (6-70) is basically the [

] ^{a,c}

Response:

WCT-TF2 calculates the interfacial heat transfer between the superheated steam and liquid droplets in the dispersed flow and film boiling (DFFB) flow regime using Equation (6-70) in Reference 1.

The mass transfer number, B , as shown in Equations (6-51) and (6-71) of Reference 1 involves typos and they should be corrected as follows:

[

$]^{a,c}$

With the correction as defined above, the mass transfer number, B , reduces to zero if no vapor phase superheating exists.

In Equation (6-70) of Reference 1, the Reynolds number Re_d and Prandtl number Pr_v are calculated

[

$]^{a,c}$

As function of flow Reynolds and Prandtl numbers without considering the correction to the vapor phase superheating, Equation (6-70) of Reference 1 is [

$]^{a,c}$. For example, the well-referenced Ranz and Marshall correlation (Reference

8) is presented in Equation RAI.5, among others recommended using different constants in front of the Reynolds number in the range of from 0.55 (Reference 2) to 0.74 (Reference 5).

$$Nu = 2.0 + 0.60 Re_f^{1/2} Pr_f^{1/3} \quad \text{RAI.5}$$

The Westinghouse topical report (Reference 1) refers Equation (6-70) therein as the [

Equation (6-70) of Reference 1 is different from the exact form of the []^{a,c} However,

impact of using the []^{a,c} To assess the potential

the WCT-TF2 DFFB interfacial heat transfer correlation, i.e. Equation (6-70) of Reference 1, is compared with the correlation recommended in Reference 5 in which the correlation is proposed for high temperature steam droplet flows, as shown in Figures RAI.1 and RAI.2 as follows. Please note that the Reference 5 correlation is recommended based on its comparison to the low pressure and high temperature air data available from Reference 3 and 4, which covers a pressure range lower than 30 psia and an air superheating range from 150 – 960 °C.



Figure RAI.1 Comparison of DFFB interfacial heat transfer correlations []^{a,c}

a,c

Figure RAI.2 Comparison of DFFB interfacial heat transfer correlations []^{a,c}

It is shown in the comparisons in these figures that WCT-TF2 predicts []

[]^{a,c}. In most of the DFFB flows occur in WCT-TF2 plant simulations, their void fraction is in the range of []^{a,c}. If the void fraction of []^{a,c} is used in the comparisons shown in Figures RAI.1 and RAI.2 above, the WCT-TF2 []^{a,c} would be less than []^{a,c} relative to the Reference 5 correlation. The uncertainties introduced by the interfacial heat transfer models will be accounted for in WCT-TF2 as part of the []^{a,c} for DFFB heat transfer (Section 29.4.3 of Reference 1)

References:

1. WCAP-16996-P, "Realistic LOCA Evaluation Methodology Applied to the Full Spectrum of Break Sizes (FULL SPECTRUM™ LOCA Methodology)," November 2010.
2. Forslund, R. P. and Rohsenow, W. M., "Dispersed Flow Film Boiling," J. Heat Transfer, Vol. 90, pp. 399-407, 1968.
3. Yuen, M. C. and Chen, L. W., "Heat-Transfer Measurements of Evaporating Liquid Droplets," Int. J. Heat Mass Transfer, Vol. 21, pp. 537-542, 1978.
4. Lee, K. and Ryley, D. J., "The Evaporation of Water Droplets in Superheated Steam," J. Heat Transfer, Vol. 90, pp. 445-451, 1968.
5. Ban, C. H. and Kim, Y., "Evaporation of a Water Droplet in High-Temperature Steam," J. Korean Nuclear Society, Vol. 32, pp. 521-529, 2000.
6. Ishii, M. and Chawla, T. C., "Local Drag Laws in Dispersed Two-Phase Flow," ANL-79-105, NUREG/CR-1230, 1979.
7. Wallis, G.B., "One Dimensional Two Phase Flow," McGraw Hill Book Company, 1969.
8. Crowe, C. T., Sommerfeld M. and Tsuji Y., "Multiphase Flows With Droplets and Particles," CRC Press LLC, 1998.

Question #52: Nusselt Number Correlation Applicability for Dispersed Droplet Flow

WCAP-16996-P/WCAP-16996-NP, Volumes I, II and III, Revision 0, Subsection 6.2.5, "Inverted Annular Regime," explains that the coefficient [

]^{a,c} The same coefficient appears in Equation (6-70) in WCAP-16996-P/WCAP-16996-NP, Volumes I, II and III, Revision 0, Subsection 6.2.7, Dispersed Droplet Flow Regime," which provides the interfacial heat transfer coefficient between superheated vapor and dispersed droplets. Equation (6-70) can be presented as:

[]^{a,c}

As mass transfer away from the drop has been found to decrease the heat transfer, the effect of evaporation on the interfacial heat transfer needs to be accounted for if the free stream gas phase is superheated. The shielding function []^{a,c} in Equation (6-70) accounts for steam superheating. Importantly, during the reflood phase of a PWR LOCA, the core seam flow conditions range from negligible to considerable steam superheating. For example, at a typical reflood pressure of 0.3 MPa and an assumed superheated steam temperature of 1,000 K (723 °C or 1,340 °F), the heat to increase the temperature of the evaporated steam to 1,000 K exceeds half of the latent heat of evaporation.

Yuen and Chen (1978) (M. C. Yuen and L. W. Chen, 1978, "Heat-Transfer Measurements of Evaporating Liquid Droplets," Int. J. Heat and Mass Transfer, Volume 21, Issue 5, pp. 537-542, May 1978) studied heat transfer to water and methanol droplets in an atmospheric vertical hot air tunnel and showed that the experimental data can best be correlated by:

$$Nu_f = (2 + 0.6 Re_M^{1/2} Pr_f^{1/3}) / (1 + B).$$

Their experiments were limited to the following range of flow conditions:

Reynolds number:	200 - 2,000
Pressure:	atmospheric
Free stream air temperature:	150 - 960 °C (302 - 1,760 °F)
Velocity:	2.1 - 11.4 m/s (6.9 - 37.4 fps)

Renksizbulut and Yuen (1983) (M. Renksizbulut and M. C. Yuen, "Experimental Study of Droplet Evaporation in a High-Temperature Air Stream," J. Heat Transfer, Volume 105, Issue 2, pp. 384-388, May 1983) measured heat transfer rates to liquid droplets of water, methanol and heptane in an atmospheric hot air tunnel in a Reynolds number range of 25 to 2,000 and a Spalding number range of 0.07 to 2.79. It was shown that the obtained experimental data along with data by others can best be correlated by:

$$Nu_f = (2 + 0.57 Re_M^{1/2} Pr_f^{1/3}) / (1 + B)^{0.7}.$$

Ban and Kim (2000) (Ch. Hw. Ban and Y. Kim, "Evaporation of a Water Droplet in High-Temperature Steam," J. Korean Nuclear Society, Volume 32, Number 5, pp. 521-529, October, 2000) proposed a modification to the Lee and Ryley (1968) correlation (K. Lee and D. J. Ryley, "The Evaporation of

Water Droplets in Superheated Steam,” J. Heat Transfer, Volume 90, Issue 4, pp. 445-451, November 1968):

$$Nu_f = (2 + 0.74 Re_M^{1/2} Pr_f^{1/3}) / (1 + B).$$

The proposed expression correlated well with data for a water droplet in gas flow for both negligible and considerable degree of superheating. Ban and Kim (2000) also explained that the necessity of the exponent 0.7 in the correlation by Renksizbulut and Yuen (1983) comes from the data of heptane and stated that water and methanol data can be well correlated with an exponent of 1.0. In this case, the correlation is identical with that by Yuen and Chen (1978) if radiation heat transfer is neglected in the calculation of the Spalding number as proposed by Renksizbulut and Yuen (1983).

A sensitivity study performed with the TRACE code by B. Belhouachi, S. P. Walker, and G. F. Hewitt, “Analysis and Computational Predictions of CHF Position and Post-CHF Heat Transfer,” NUREG/IA-0236, May 2010, illustrated the central role of the droplet Nusselt number in the PCT and CHF predictions. Please clarify the following items related to the use of the correlation for predicting the interfacial heat transfer from superheated steam to liquid droplets for dispersed droplet flow in WCOBRA/TRAC-TF2.

- (1) Identify the experimental data and provide the technical basis in support of the application of Equation (6-70) to calculate the interfacial heat transfer coefficient between superheated vapor and dispersed droplets in WCOBRA/TRAC-TF2. Describe the ranges of test conditions for which the applicable data sets were obtained and provide the applicability ranges for this equation.
- (2) Present the technical basis for using a shielding function of []^{a,c} in Equation (6-70). Applying different shielding functions to the same zero mass transfer Nusselt number can have a pronounced effect on the resulting heat transfer coefficient as the degree of superheating increases. For example, under typical reflood conditions at 0.3 MPa pressure and 1,000 K (1,340 °F) steam temperature, using a shielding function of []^{a,c} with the same zero mass transfer Nusselt number will increase the predicted heat transfer coefficient by more than 20 percent. Accordingly, this can have a pronounced impact on the calculated PCT.
- (3) Demonstrate the applicability of Equation (6-70) for prediction of interfacial heat transfer between water droplets and superheated steam under the range of conditions occurring in a PWR core following a LBLOCA. Provide the expected ranges for the controlling flow parameters of interest for PWR LBLOCA re-flood analyses and compare these ranges against the test data conditions used to establish Equation (6-70) and its range of applicability. Discuss effects related to the correlation's applicability to PWR core flow re-flood conditions considering each governing parameter.

Response:

The heat transfer in DFFB is important for predicting fuel cladding temperatures during the blowdown and reflood phases of a large break LOCA and during the safety injection and accumulator injection phases of an intermediate break LOCA. WCT-TF2 calculates the total wall heat transfer by solving simultaneously the heat transfers from the wall to vapor, wall to liquid (continuous and entrained liquid) and between the vapor and liquid phases (Section 15.2, Reference 1).

In similar form as Equation (6-70) of Reference 1, several heat transfer correlations of evaporation of liquid droplets were recommended by a number of researchers (References 2, 3, 4 and 5) based on the experiments conducted using different fluids and under different thermal and flow conditions. None of the past experiments published were performed in sufficient high pressure and vapor temperature conditions using the water and superheated steam as those encountered in LOCA blowdown and reflood phases. For example, the tests reported in Reference 3 was performed using air at atmospheric pressure; Reference 2 conducted nitrogen film boiling convective heat transfer test under low pressure (inlet pressure was measured at 25 psia); the water/steam system was used in the test of Reference 4 with low degrees of vapor superheat (5~61 °F) and low pressure (14.7~28.9 psia); the effects of high degree of superheated air (150~960 °C) was investigated in the tests in Reference 3. Despite the limitation on these operating conditions, the tests cited above covered a comparable range of Reynolds number from 200 to 2000 with that during a typical large break LOCA low pressure reflood phase for DFFB flows.

The limits for the controlling parameters of DFFB interfacial heat transfer expected from PWR large break LOCA reflood phase are:[

]^{a,c}

The calculation of interfacial heat transfer is flow regime dependent in WCT-TF2 (Section 6.1, Reference 1). Equation (6-70) of Reference 1 is applied in predicting the interfacial heat transfer between the vapor and liquid droplet in DFFB flows occurring in high (blowdown, []^{a,c}) and low (reflood, []^{a,c}) pressure ranges. The DFFB interfacial heat transfer models in WCT-TF2 are validated in Sections 15.5 and 15.6 of Reference 1, through the comparison of the heater rod cladding temperatures with the available test data representative of the blowdown and reflood parameter ranges. Since fuel rod temperature is a direct indicator of the overall heat transfer between the rod and fluid, the interfacial heat transfer is thus validated as one of the contributors to the overall wall heat transfer, among the droplet size model, entrainment model, etc.

The DFFB heat transfer uncertainties (wall to vapor/droplet mixture) is accounted for through the DFFB heat transfer multipliers derived respectively for the blowdown and reflood phases in Section 29.4.3 of Reference 1. It is evident that the derived heat transfer multipliers include the bias introduced through the interfacial heat transfer model. In taking this approach to treat the overall uncertainties as a result of several contributing sub-models, it is realized that there exists potential compensating errors which could lead to a good match of the overall predicted results, e.g. cladding temperatures, to the test data, as a result of the lucky combination of the offsetting sub-model errors

under limited range of conditions. For example, under fixed flow conditions, the total wall heat transfer could be predicted reasonably well with over-predicted interfacial heat transfer coefficient, and under-predicted wall-vapor heat transfer coefficient. In interacting with hydraulic conditions, total wall heat transfer could also be reasonable due to a well predicted interfacial heat transfer as a result of the under-predicted interfacial heat transfer coefficient and over-predicted interfacial area (more entrainment or smaller droplet size).

The DFFB validation test data and WCT-TF2 prediction are analyzed in Section 24.6 of Reference 1, for potential compensating errors involved in the DFFB heat transfer during the large break blowdown and reflood phases. The intention there is to compare more available performance measures from the test with the code prediction than just the principle figures of merit, and demonstrate the physical and reasonable results in other areas than just the principle objectives. Specific to DFFB interfacial heat transfer, the pertaining discussion of compensating errors is summarized as follows for high (blowdown) and low (reflood) phases, respectively.

- High pressure (Blowdown, []^{a,c})
 - DFFB validation using ORNL test data indicates that wall heat transfer is []^{a,c}. Since most of the heat is transferred from the wall to the vapor phase which supplies the energy required for evaporating the liquid droplet in DFFB, []^{a,c}.
The total uncertainty of the wall heat transfer is accounted for by heat transfer multipliers as documented in Section 29.4.3 of Reference 1. There is no indication of compensating errors relating to the interfacial heat transfer in the total wall heat transfer from this validation.
 - G-1 Blowdown film boiling tests and WCT-TF2 simulation were compared and analyzed in Section 24.6.3. Based on the available test data, it was concluded that the observed []^{a,c}.
- Low pressure (Reflood, []^{a,c})
 - Section 24.6.4 of Reference 1 investigated DFFB heat transfer in one of the FLECHT SEASAT reflood tests and simulations. It was indicated that both the vapor superheat and cladding temperature above the quench front is []^{a,c}, similar to several other forced reflood tests. Based on the comparison of vapor mass flow, droplet velocity, heat transfer to vapor and liquid phases above the quench front, the analysis therein shown that []^{a,c}.

The mass transfer from the liquid droplet during the evaporation has been found to decrease the heat transfer. To account for the effects of the mass transfer on the heat transfer process, the mass transfer number B is included in Equations (6-56), (6-57) and (6-70) of Reference 1 to extend their applicability in the case of high evaporation rate caused by superheated vapor. The form of the correction factor to the vapor phase superheating in Equation (6-70) of Reference 1, [

]^{a,c}. Yuen and Chen (Reference 3) and Ban and Kim (Reference 5) used a factor of $1.0/(1.0+B)$ to fit the experimental data in an attempt to account for the effect of vapor superheating on a heat transfer model assuming negligible mass transfer. However, no theoretical basis is provided in terms of using the form of $1.0/(1.0+B)$ to fit the test data, which validated the overall interfacial heat transfer models instead of just the correction factor of the vapor superheating.

It is true that under typical reflood conditions at 0.3 MPa pressure and 1,000 K (1,340 °F) steam temperature, using a shielding function of [^{a,c} instead of $1/(1+B)$ with the same zero mass transfer Nusselt number will increase the predicted heat transfer coefficient by more than 20%. However, for most of the applied range in the large break LOCA reflood phase, as shown in the comparison figures, Figure RAI.1 and RAI.2, in the response to RAI #51, [

]^{a,c}.

The comparison difference shown therein is due to [

]^{a,c}.

References:

1. WCAP-16996-P, "Realistic LOCA Evaluation Methodology Applied to the Full Spectrum of Break Sizes (FULL SPECTRUM™ LOCA Methodology)," November 2010.
2. Forslund, R. P. and Rohsenow, W. M., "Dispersed Flow Film Boiling", J. Heat Transfer, Vol. 87, pp. 399-407, 1968.
3. Yuen, M. C. and Chen, L. W., "Heat-Transfer Measurements of Evaporating Liquid Droplets," Int. J. Heat Mass Transfer, Vol. 21, pp. 537-542, 1978.
4. Lee, K. and Ryley, D. J., "The Evaporation of Water Droplets in Superheated Steam," J. Heat Transfer, Vol. 90, pp. 445-451, 1968.
5. Ban, C. H. and Kim, Y., "Evaporation of a Water Droplet in High-Temperature Steam," J. Korean Nuclear Society, Vol. 32, pp. 521-529, 2000.
6. Wallis, G.B, "One Dimensional Two Phase Flow," McGraw Hill Book Company, 1969.

Question #53: Interfacial Heat Transfer in Inverted Annular and Liquid Slug Flows

WCAP-16996-P/WCAP-16996-NP, Volumes I, II and III, Revision 0, Subsection 6.2.5, "Inverted Annular Regime," provides expressions for calculation of the interfacial heat transfer coefficient from both continuous liquid and droplets to superheated vapor for inverted annular flow in Equations (6-56) and (6-57). Subsection 6.2.6, "Inverted Liquid Slug Regime," defines the correlations for prediction of the interfacial heat transfer coefficient from the continuous liquid and droplets interface to superheated vapor for inverted liquid slug flow in Equations (6-65) and (6-66). The interfacial heat transfer coefficients given by the above identified equations can be presented in terms of the Nusselt number with a single expression:

[]^{a,c}

Please clarify the following items related to the use of the above correlation for predicting the interfacial heat transfer coefficient for inverted annular and inverted liquid slug flows in WCOBRA/TRAC-TF2.

- (1) Describe the way of determining the fluid properties in calculating the Reynolds, Prandtl, []^{a,c} and Nusselt numbers in Equations (6-56), (6-57), (6-65), and (6-66) as applied in WCOBRA/TRAC-TF2 in the case of inverted annular and inverted liquid slug flows.
- (2) Please present the technical bases and justify the applicability of Equations (6-56), (6-57), (6-65), and (6-66) for computing the interfacial heat transfer coefficient for inverted annular and inverted liquid slug flows in WCOBRA/TRAC-TF2.

Response:

WC/T-TF2 calculates the flow regime dependent interfacial heat transfer between the superheated vapor and the continuous liquid column and entrained droplets in the inverted annular and inverted liquid slug flow regimes using the Equations (6-56), (6-57), (6-65), (6-66) in Reference 1. In terms of flow regime, []

[]^{a,c}. In these two regimes, referred to as hot wall regimes, the continuous liquid is assumed to be liquid column or slug separated from the hot wall by a thin vapor film, into which liquid droplet could be entrained.

WC/T-TF2 total wall heat transfer is determined by the overall interactions of the wall to vapor, wall to liquid and vapor to liquid phases. The total heat transfer from the wall to the fluid determines the fuel rod cooling/heating, which is the ultimate concern of LOCA transient simulation. Under those flow regimes, the wall heat transfer modes is selected based on the cell void fraction. More specifically, the inverted annular film boiling (IAFB) and dispersed flow film boiling (DFFB) modes feature low void fraction []^{a,c} and high void fraction []^{a,c}, respectively. The interfacial heat transfer associated with the DFFB heat transfer mode is discussed in the Westinghouse Response to RAI 52. When []^{a,c}, the wall heat transfer calculation is a simple interpolation between the IAFB and DFFB models.

The discussion in this response complements the Response to RAI 52 for DFFB mode with the interfacial heat transfer for the inverted annular/liquid slug flow regimes.

- (1) Equations (6-57) and (6-66) are used to calculate interfacial heat transfer from the superheated vapor to the entrained liquid droplets in the vapor phase. The fluid properties involved in these correlations are assessed [

]^{a,c}.

The interfacial heat transfer between the superheated vapor and the continuous liquid column is evaluated using Equations (6-56) and (6-65), which are [

]^{a,c}. Details in evaluating the fluid properties involved in Equations (6-56) and (6-65) are presented as below:

[

]^{a,c}.

The impact of using [

]^{a,c} in the interfacial heat transfer models was evaluated in the Westinghouse response to RAI 51 for dispersed droplet flow regime. It was shown that WCT-TF2 [

]^{a,c} the interfacial heat transfer at extreme vapor superheat and high vapor Reynolds number. [

]^{a,c}

- (2) For interfacial heat transfer between the superheated vapor and liquid droplets, similar correlations as Equations (6-57) and (6-66) were developed by several researchers based on the experiments using different fluids, and more discussion of their models were presented in the Westinghouse Response to RAI 51 with respect to the interfacial heat transfer in the dispersed droplet flow regime.

In inverted annular and inverted liquid slug regimes, the continuous liquid column is assumed to be in the form of large liquid slugs, and [

] ^{a,c} are utilized to calculate the interfacial heat transfer between the vapor and liquid column, assuming [

] ^{a,c}. Reference 2 validated the application of Equation RAI.3 in air and water experiment with large droplets of up to 1.5 inches in diameter, which demonstrated that [

] ^{a,c}.

$$Nu = 2.0 + 0.69 Re_v^{1/2} Pr_v^{1/3} \quad \text{RAI.3}$$

In WC/T-TF2's applications to PWR plant simulation, the [

] ^{a,c}.

The WC/T-TF2 interfacial heat transfer correlations (Equations (6-56), (6-57), (6-65), (6-66) in Reference 1) for the inverted annular and inverted liquid slug flow regimes are validated as [

] ^{a,c}.

As explained in the WC/T-TF2 wall heat transfer models for the inverted annular film boiling in Section 7.2.6 of Reference 1, the total heat transfer from the wall is calculated using the [

] ^{a,c}.

[

]

^{a,c}

[

] ^{a,c}

[

]^{a,c}.

For WC/T-TF2 applications, the inverted annular and inverted liquid slug regimes are [

]^{a,c}. Section 15.6.1.1.5 of Reference 1 documents the high flooding rate (6.1 in/s) validation test FLECHT SEASET Test 31701, and it is shown that WC/T-TF2 predicts [

]^{a,c}.

References:

1. WCAP-16996-P, "Realistic LOCA Evaluation Methodology Applied to the Full Spectrum of Break Sizes (FULL SPECTRUM™ LOCA Methodology)," November 2010.
2. Rowe, P. N., Claxton K. T. and Lewis, J. B., "Heat and Mass Transfer from A Single Sphere in An Extensive Flowing Fluid," Trans. Inst. Chem. Engrs., Vol. 43, 1965.

Question #54: Interfacial Heat Transfer to Droplet/Bubble

WCAP-16996-P/WCAP-16996-NP, Volumes I, II and III, Revision 0, Subsection 6.2.3, "Churn-Turbulent Regime," provides an expression for the interfacial heat transfer coefficient from superheated vapor to liquid droplets that can appear in the flow from entrainment and from adjoining channels. It states that "the interfacial heat transfer coefficient is given by the Lee-Ryley (1968) correlation," which is given in Equation (6-26). The relationship can be presented in terms of the Nusselt number as:

$$Nu_d = 2 + 0.74 Re_d^{1/2} Pr_v^{1/3}$$

The correlation by K. Lee and D. J. Ryley, "The Evaporation of Water Droplets in Superheated Steam," J. Heat Transfer, Volume 90, Issue 4, pp. 445-451, November 1968, is given a special recognition in LOCA analyses as it was based on data for droplet evaporation in superheated steam in contrast to other experiments that studied liquid droplet evaporation in air. The droplet diameter and flow parameters were varied as follows:

Droplet diameter:	230 μm - 1,130 μm (9 mils - 44.5 mils)
Reynolds number:	64 - 250
Pressure:	101.4 - 200 kPa (14.7 - 29 psia)
Superheat:	2.8 - 33.9 K (5 - 61 $^{\circ}\text{F}$)
Velocity:	2.7 - 11.9 m/s (9 - 39 fps)

WCAP-16996-P/WCAP-16996-NP, Volumes I, II and III, Revision 0, Subsection 6.2.7, "Dispersed Droplet Flow Regime," refers to [

]^{a,c}

[

]^{a,c}

WCAP-16996-P/WCAP-16996-NP, Volumes I, II and III, Revision 0, Subsection 6.2.2, "Small to Large Bubble Regime," explains that the heat transfer coefficient for large bubbles of superheated vapor for the discussed flow regime is determined using the correlation by Lee and Ryley (1968) as given in Equation (6-14).

Please clarify the following items related to the prediction of the interfacial heat transfer from superheated steam to liquid droplets and from large superheated bubbles to the continuous liquid phase for different flow regimes in WCOBRA/TRAC-TF2.

- (1) Explain why two different existing correlations are provided in WCAP-16996-P/WCAP-16996-NP, Volumes I, II and III, Revision 0, Section 6, "WCOBRA/TRAC-TF2 Interfacial Heat and Mass Transfer Models," when describing the technical basis for predicting interfacial heat transfer from superheated steam to liquid droplets.
- (2) Equation (6-49) with small variations in the coefficient of the second term (0.552, 0.55, 0.60) is often cited in the technical literature. In the case of a liquid droplet falling through a moving airstream, Frössling (1938) developed an empirical relation of the same form for the mass transfer

number (Frössling, "Über die Verdunstung fallender Tropfen," Gerlands Beiträge Zur Geophysik, Volume 52, pp. 170-216, 1938). Ranz and Marshall (1952) used the heat transfer analogy to show that the heat transfer data can be correlated through the droplet Nusselt number using a relationship of the same form (see W. E. Ranz and W. R. Marshall, Jr.: "Evaporation from Drops: I," Journal of Chemical Engineering Progress, Volume 48, No. 3, pp. 141-146, March 1952. Also W. E. Ranz and W. R. Marshall, Jr.: "Evaporation from Drops: II," Journal of Chemical Engineering Progress, Volume 48, No. 4, pp. 173-180, April 1952). Please provide the reasons for its identification as "a correlation by Forslund and Rohsenow (1968)."

- (3) According to Abou Al-Sood (2010), the Frössling (1938) and Ranz and Marshall (1952) correlations are applicable to describe droplet evaporation in a laminar convective flow (see M. M. Abou Al-Sood, "Simple Model for Turbulence Effects on the Vaporization of Liquid Single Droplets in Forced Convective Conditions," 23rd Annual Conference on Liquid Atomization and Spray Systems, ILASS – Europe 2010, Brno, Czech Republic, September 2010). Please explain the applicability of the Lee-Ryley (1968) correlation under flow conditions expected in a PWR core following a LBLOCA.
- (4) The Lee and Ryley (1968) correlation was developed from data describing heat transfer from evaporating droplets. Although Subsection 6.2.2, "Small to Large Bubble Regime," recognizes that such bubbles are unlikely to occur extensively in a LOCA transient, please justify the technical basis for the use of the Lee and Ryley (1968) correlation for the description of heat transfer mechanisms in the case of large bubbles of superheated steam.

Response:

The RAI has four components. Part (1) of the questions asks to describe the technical basis for the different coefficient applied to the droplet Reynolds number Re_d in the calculation of the Nusselt number Nu_d . In particular a coefficient of [

]^{a,c}.

The first observation is that, as discussed in Section 6.2.3 of the TR, the Churn-Turbulent Regime is [

]^{a,c}.

Considering that a) []^{a,c} and b) [

]^{a,c} to the overall heat transfer from the vapor to the liquid.

On the contrary the Dispersed Droplet Flow Regime is one of the important hot wall flow regimes which are relevant to determine the heat transfer in proximity of the PCT location. In that regime the continuous liquid flow becomes completely entrained and the interfacial heat transfer is limited to the heat transfer between the superheated vapor and the droplets. Moreover, in the regime a high degree of superheating is anticipated.

As result, rather than addressing [

]^{a,c}, the focus in this response is to address the adequacy of the formulation used for the Dispersed Droplet Flow Regime which is the topic of parts (2) and (3) of this RAI.

Part (2) of the question acknowledges that [

]^{a,c}. Frossling (1938) (Reference 1) assumes 0.55, Ranz and Marshall (Reference 2) is based on 0.6 for example. [

]^{a,c}.

In part (3) the reviewer noted that Frossling-type of correlations, like Ranz-Marshall (Reference 2) and Lee-Ryley (Reference 4) correlations are applicable to droplet evaporation in a laminar convective flow. A review of the effect of turbulence on the combustion spray system evaporation rate of droplets is presented by Birouk (Reference 5) and a model is proposed in the cited reference of Abou Al-Sood (Reference 6) by the reviewers. In general, the review found that the turbulence acts as an enhancer to the interfacial heat and mass transfer, depending on the mean flow characteristics and the level of the turbulent intensity, among other spray droplet properties and spray environment conditions. Moreover, based on the review, the developed models to account for the turbulence effects on the interfacial heat and mass transfers requires the knowledge of the turbulent flow parameters, for example turbulent intensity, turbulent length scale, etc., [

]^{a,c}.

Section 24 further investigates the possibility of compensating errors which would originate by a bias on interfacial heat transfer in the DFFB regime. Section 24.6.3 discusses the observed [

]^{a,c}. However [

]^{a,c}.

Section 24.6.4 elaborates on the role of the interfacial heat transfer during reflood, by [

]^{a,c}.

Overall the potential for compensating error is understood and controlled and [

] ^{a,c}.

Finally point (4) of the question asks to justify the use of the [

] ^{a,c}.

Given the context in which it is used, the [^{a,c} is a reasonable [

] ^{a,c}.

References

1. Frossling, N., On the Evaporation of Falling Droplets. Gerlands Beitrage zur Geophysik, Vol. 52, 1938, pp. 170–216 (in German).
2. Ranz, W. E. and Marshall, W. R.,: Evaporation from Drops, Pt. 1. Chem. Eng. Prog., Vol. 48, 1952, pp. 141-146.
3. Forslund, R. P., and Rohsenow, W. M., “Dispersed Flow Film Boiling,” J. Heat Transfer, Vol. 87, 1968, pp. 399-407.
4. Lee, K., and Ryley, D. J., “The Evaporation of Water Droplets in Superheated Steam,” Trans A.S.M.E. J Heat Transfer, Vol. 90, 1968, pp. 445-451.
5. Birouk, M., and Gökalp, I., “Current status of droplet evaporation in turbulent flows,” Progress in Energy and Combustion Science, Vol. 32, 2006, pp. 408–423
6. M. M. Abou Al-Sood, “Simple Model for Turbulence Effects on the Vaporization of Liquid Single Droplets in Forced Convective Conditions,” ILASS – Europe 2010, 23rd Annual Conference on Liquid Atomization and Spray Systems, Brno, Czech Republic, September 2010

Question #55: Droplet Diameter for Interfacial Heat Transfer in Dispersed Droplet Flow

The liquid droplet diameter is an important parameter when computing the interfacial heat transfer for dispersed droplet flow. Considering single isolated droplet, the heat transfer coefficient decreases with increasing droplet diameter. However, the product of the heat transfer coefficient and the surface area will increase by virtue of surface area's higher order dependence on diameter. For a dispersed droplet flow at a certain flow quality, the product of the heat transfer coefficient and the integral droplet surface area will decrease when increasing the assumed droplet diameter as both the heat transfer coefficient and the integral surface area of all droplets will decrease.

WCAP-16996-P/WCAP-16996-NP, Volumes I, II and III, Revision 0, Subsection 6.2.7, "Dispersed Droplet Flow Regime," does not explain how the droplet size is determined for the purpose of predicting the interfacial heat transfer coefficient and associated heat transfer rate between the dispersed droplets and the continuous gas phase.

Please explain and justify the implemented modeling approach for calculating the droplet size in predicting the interfacial heat transfer between superheated steam and liquid droplets in addition to the information provided in Subsection 6.2.7, "Dispersed Droplet Flow Regime."

Response:

The dispersed droplet flow regime is one of the vessel hot wall flow regimes, characterized with the presence of a heated surface with a temperature exceeding that given by Equation 4-1. The heat transfer rate of the dispersed droplet is a product of the droplet heat transfer coefficient and the integral droplet surface area as shown by Eqs. 6-75 through 6-78 in Section 6.2.7. Both the heat transfer coefficient and droplet surface area depend on the droplet diameter. The dependence of the heat transfer coefficients on the droplet diameter is shown in both the Nusselt number and the Reynolds number. The interfacial area of droplets phase is explicitly tracked by the 3D module of WCOBRA/TRAC-TF2. Thus, the droplet transportation mechanism, droplet generation mechanisms, evaporation/condensation, and droplet break up mechanism all contribute to the droplets interfacial area distribution and in turn determines the droplet diameter in the droplet heat transfer calculation. In the response, the interfacial area transport model and heat transfer coefficient in the dispersed droplet flow regime are explained in details.

The calculation of the interfacial area of the droplet field in the dispersed droplet flow regime is provided in Section 4.3.4. The interfacial area concentration (interfacial area in a unit volume) is determined directly from solution of the droplets interfacial area transport equation as shown in Section 4.3.7. Eq. 4-68 of Section 4.3.7 describes that the rate change of interfacial area concentration is a result of the convection of the interfacial area concentration, interfacial area concentration generated by entrainment and de-entrainment and the interfacial area concentration change due to phase change. The spacer grid droplet break up model in Section 5.6.5 also contributes to the interfacial area concentration. The discretized form of Eq. 4-68 is given in Eq. 4-76. The total droplet interfacial area is the interfacial area concentration times the volume of node as shown in Eq. 4-78. In general, the droplet interfacial area concentration is inversely proportional to the droplet diameter with a given droplet volume. The droplet interfacial area transport model is based on

sound transport theory and mechanistically captures the evolution of the interfacial area of the dispersed droplet fields.

The interfacial heat transfer coefficient models for the dispersed droplet flow regime are described in Section 6.2.7. The interfacial heat transfer between the superheated steam and liquid droplets is a result of heat transfer to the superheated vapor and heat transfer to subcooled liquid droplet. The interfacial heat transfer coefficient to superheated vapor is given by the modified Forslund-Rohsenow correlation (Eq. 6-70), where the droplet diameter appears as a part of Nusselt number and the heat transfer coefficient shows a low order dependence on the Reynolds number. Further discussion on modifying Forslund-Rohsenow correlation has been provided in Section 6.2.5. The interfacial heat transfer coefficient to subcooled liquid droplets is calculated using Andersen's formula (Eq. 6-73), where the droplet diameter only appears as a part of the Nusselt number. In those heat transfer models, the drop diameter of the dispersed droplet flow regime is calculated from the droplet volumetric fraction and interfacial area concentration as shown by Eq. 4-48 in Section 4.2.5. The calculated droplet diameter is limited to [

$$]^{a,c}$$

In addition, the FSLOCA topical report provides an assessment on the droplet model in the 3-D vessel module of WCOBRA/TRAC-TF2 in Section 15.9.2, where the predicted droplet size is compared with the measured droplet size from [

$$]^{a,c}$$

Question #56: Droplet-Wall Direct Contact Heat Transfer in Dispersed Flow Film Boiling

WCAP-16996-P/WCAP-16996-NP, Volumes I, II, and III, Revision 0, Subsection 7.2.7, “Dispersed Flow Film Boiling,” explains that the VESSEL component wall heat transfer logic in WCOBRA/TRAC-TF2 invokes the Dispersed Flow Film Boiling (DFFB) heat transfer regime when the void fraction is greater than []^{a,c} and the wall temperature is greater than the minimum stable film boiling temperature, T_{MIN} as given in Equation (7-91). The subsection states that heat transfer in this post-dryout or post-CHF flow regime “is calculated as a “two-step” method where the dominant heat transfer mode is forced convection to superheated steam.” The code computes the dispersed flow film boiling heat flux as a sum of four components: (1) convective heat flux to vapor, (2) radiative heat flux to vapor, (3) radiative heat flux to droplets, and (4) drop-wall direct contact heat transfer. What is also important, Subsection 7.2.7 explains that “the steam superheat is then determined by the interfacial heat transfer rate to the entrained droplets as part of the hydrodynamic solution.”

Subsection 7.2.7 states that the drop-wall direct contact heat transfer that accounts for droplet impingement on the heated surface is calculated using the model by R. P. Forslund and W. M. Rohsenow, “Dispersed Flow Film Boiling,” J. Heat Transfer, Vol. 90, Issue 4, pp. 399-407, November 1968, as given in Equation (7-130).

WCOBRA/TRAC-TF2 implements []^{a,c}

Following the initial surge into the core, the PWR core re-flood after a LBLOCA takes place at low flow and low pressure conditions. Flooding rates are very low and typically stay below 1 in/s. Under such conditions, post-dryout heat transfer with dispersed flow film boiling in the upper core region controls the PCT. For example, a typical re-flood flow rate of 0.8 in/s (0.02 m/s) of safety injection water at 150 °F (65.6 °C or 338.7 K) and 20 psia (1.4 bar or 0.14 MPa) corresponds to a mass flux of:

$$pw (338.7 \text{ K}, 0.14 \text{ MPa}) \times V_{\text{Reflood}} = 980.3 \text{ kg/m}^3 \times 0.02 \text{ m/s} = 19.9 \text{ kg/m}^2\text{-s} = 14,687 \text{ lbm/ft}^2\text{-hr.}$$

For a fuel rod with a standard diameter of 0.422 inches (10.7×10^{-3} m) and an assumed peak LHGR of 15 kW/ft (49.2 kW/m), the linear heat rate and rod surface heat flux conditions for decay heat power ratios of 5 percent, 3 percent, and 2 percent (about 10 sec, 100 sec, and 1,000 sec after scram) are given in the Table 1 below.

Table 1: Fuel Rod LHGR and Surface Heat Flux Conditions

Parameter	Units	Value			
Decay Ratio	-	1.0	0.05	0.03	0.02
Decay Time	s	0.0	~10	~100	~1,000
LHGR	kW/ft	15	0.75	0.45	0.30

	kW/m	49.2	2.46	1.48	0.98
Heat Flux	Btu/(ft ² -hr)	463,298	23,165	13,899	9,266
	kW/m ²	1,461	73.1	43.8	29.2

Typical dispersed flow film boiling conditions at low reflood rate can be identified as:

Pressure: 1 to ~3 bar (0.1 to ~0.3 MPa or 14.5 to ~44 psia),

Mass Rate: ~1 in/s (0.0254 m/s) or ~25 kg/m²-s (18,700 lbm/ft²-hr),

Void Fraction: Higher than 80 percent.

A work by M. Andreani and G. Yadigaroglu, "Prediction Methods for Dispersed Flow Film Boiling," Int. J. of Multiphase Flow," Vol. 20, p. 1-51, 1994, and more recently a report by the International Atomic Energy Agency (IAEA), "Thermohydraulic Relationships for Advanced Water Cooled Reactors," IAEA-TECDOC-1203, April 2001, represent a comprehensive review of post-dryout heat transfer methods for water cooled reactors. NUREG/CR-6975, "Rod Bundle Heat Transfer Test Facility Test Plan and Design," July 2010, summarizes the available single-tube and rod bundle data and existing modeling approaches.

As discussed by M. Andreani and G. Yadigaroglu, "Difficulties in Modeling Dispersed-Flow Film Boiling," Wärme und Stoffübertragung, Volume 27, Number 1, pp. 37-49, 1992, the difficulties in the post-dryout heat transfer modeling are related to phenomenological characteristics of participating processes can be grouped into four major areas: (1) thermal non-equilibrium effects, (2) mechanical non-equilibrium effects, (3) flow history dependant heat transfer, and (4) sub-channel and spacer grid effects in fuel rod bundles. In addition, a major limitation is related to the area averaging aspect of any one-dimensional (1D) modeling approach that is used in LOCA analyses.

Thermal non-equilibrium effects are related to significant steam superheats have been measured in reflood experiments performed both with single-tube and rod bundle test sections. For example, Ghazanfari, A., Hicken, E. F., and Ziegler, A., "Unsteady Dispersed Flow Heat Transfer Under Loss-of-Coolant Accident Related Conditions," Nuclear Technology, Vol. 51, pp. 21-26, November 1980, measured vapor superheat of 260 K (468 °F) on average at the top of the test tube. More recent experiments by S.-Ki Moon et al., "An Experimental Study on Post-CHF Heat Transfer for Low Flow of Water in a 3x3 Rod Bundle," Nuclear Engineering and Technology, Vol. 37, No. 5, October 2005, also showed a significant degree of thermal non-equilibrium near the end of the heated length of a 3x3 test section. Mechanical non-equilibrium effects are related to the behavior of clusters of droplets in the continuous steam flow. M. Andreani and G. Yadigaroglu, "Effect of the Cross-Sectional Droplet Distribution in Dispersed Flow Film Boiling at Low Mass Flux," Proceedings of the 5th International Topical Meeting on Reactor Thermal-Hydraulics (NURETH-5), Volume III, pp. 823-831, September 21-24, 1992, Salt Lake City, Utah, USA, discuss related effects on prediction results obtained with 1D models. A recent work by F. B. Cheung and S. M. Bajorek, "Dynamics of Droplet Breakup Through a Grid Spacer in a Rod Bundle," Nuclear Engineering and Design, Vol. 241, pp. 236-244, 2011, focused on the dynamics of droplet breakup associated with the flow of a dispersed two-phase mixture through a rod bundle grid spacer during a PWR re-flood transient and presented new test data from the RBHT Facility.

Andreani and Yadigaroglu (1992) pointed out to modeling limitations related to the assumption of a uniform droplet distribution over the channel cross section. Importantly it was recognized that 1D models can overestimate the interfacial heat transfer between vapor and droplets if a cross-section averaged temperature difference between vapor and droplets is used instead of a temperature difference based on a lower mean temperature of vapor in the central core region where droplets tend to reside. As a result, such models can fail to adequately predict the wall surface temperature particularly at low flow conditions of interest for DFFB modeling.

Please clarify the following items related to the method of calculating the dispersed flow film boiling heat flux in WCOBRA/TRAC-TF2.

1. Explain what corrections and modeling features are applied in WCOBRA/TRAC-TF2 to overcome the major difficulties in modeling the dispersed flow film boiling with regard to both the interfacial and wall to fluid heat transfer processes. In addition, please explain how the limitation of the 1D approach stemming from the highly non-uniform steam temperature profile across the radial flow direction (maximum steam temperature near the wall with a cooler core region containing droplets) is rectified.
2. The Forslund-Rohsenow (1968) correlation is based on data for dispersed flow film boiling of nitrogen under the following conditions:

Mass flux:	70,000 to 190,000 lbm/ft ² -hr (94.9 kg/m ² -s to 257.7 kg/m ² -s)
Heat flux:	5,000 to 25,000 Btu/ft ² -hr (15.8 to 78.9 kW/m ²)
Test section inlet pressure:	25 psia (1.72 bar or 0.172 MPa)
Test section exit quality:	35 percent to 315 percent
Test section inner diameter:	0.228 in, 0.323 in, 0.462 in (5.79 mm, 8.20 mm, 11.73 mm)

Please present a table that includes typical ranges for conditions incurring during reflood dispersed flow film boiling in a PWR core and compare those against the Forslund-Rohsenow (1968) test data conditions. Present comparison against data that representative of prototypical reflood conditions to support the WCOBRA/TRAC-TF2 dispersed flow film boiling model for prediction of PWR reflood PCTs.

Heat transfer from a heated tube to dispersed steam-water flow under post-dryout conditions was studied experimentally by Ghazanfari, A., Hicken, E., and Ziegler, A., "Unsteady Dispersed Flow Heat Transfer Under Loss-of-Coolant Accident Related Conditions," Nuclear Technology, Vol. 51, pp. 21-26, November 1980. The test conditions varied as follows:

Mass flux:	10,300 to 26,500 lbm/ft ² -hr (14 to 36 kg/m ² -s)
Heat flux:	5,400 to 13,300 Btu/ft ² -hr (17 to 42 kW/m ²)
Pressure:	17.4 to 23.2 psia (1.2 to 1.6 bar)
Inlet quality:	0.50 to 1.00

As already mentioned, vapor superheat of 260 K (468 °F) on average was measured at the top of the test tube in the tests. It was also concluded that the wall droplet contribution to the total heat transfer rate was negligible at flow qualities greater than 50 percent.

The Forslund-Rohsenow (1968) correlation is based on an equilibrium model where the bulk vapor temperature is assumed to be equal to the local saturation temperature. As such, its validity as a model basis for predicting direct contact heat transfer for the dispersed droplet field in WCOBRA/TRAC-TF2 is questionable. In addition, the use of this correlation above the quench front where the clad temperature is above the minimum stable film boiling temperature, T_{MIN} , and significant steam superheating can take place is considered inappropriate. Once the liquid droplets enter into the central flow region, there can be insufficient lateral momentum that is needed for them to penetrate the highly superheated boundary layer and reach the wall. As a result, the droplets will have little influence on cooling the fuel rod surfaces at locations above the quench front where the cladding temperature is in excess of T_{MIN} .

3. Please explain why [

]^{a,c}

Accordingly, an increased heat transfer rate could lead to under predicting the PCT. Such changes in the coding of relations in WCOBRA/TRAC-TF2 that are implemented without providing the underlying technical basis or discussing possible impact on prediction results of safety relevance are found unacceptable. Please explain this specific case and clarify if such an approach has been applied with regard to other constitutive relations coded in WCOBRA/TRAC-TF2. Present a table that documents such deviations in as coded expressions and the actions taken to rectify or substantiate each individual occurrence of such a modification.

4. Please provide plots of WCOBRA/TRAC-TF2 prediction results for the parameters listed below for FLECHT SEASET Tests 31504, 35304, 31805, 34006, 34907, 35807, 34209, 34103, 33903, 31922, and 31108:
- a) forced convective heat transfer coefficient to vapor,
 - b) grid enhancement multiplier, F_{grid} ,
 - c) two-phase enhancement multiplier, $F_{2\phi}$
 - d) radiation heat transfer coefficient to vapor,
 - e) radiation heat transfer coefficient to droplets,

- f) Forslund-Rohsenow drop-wall direct contact heat transfer coefficient,
- g) interfacial heat transfer coefficient between the drops and the vapor,
- h) droplet number and diameter,
- i) minimum stable film boiling temperature, T_{MIN} .

Plot the above parameters as function of time for the elevation of PCT occurrence and for two additional elevations located approximately two and four feet below the hot spot. In addition, please show the steam and liquid flow rates, void fraction, steam temperature, liquid temperature, and clad temperature as function of time at all three locations. Please plot also a comparison of the measured local PCT against the code predictions as a function of the vertical test bundle axis.

5. Please provide plots of WCOBRA/TRAC-TF2 prediction results for the following FLECHT low flooding rate skewed power shape tests:

Parametric Effects:

Run Numbers:

Flooding rate (in/sec):	0.6, 0.8, 1.0, 1.5, 3, 6, 15606, 15305, 13404, 13303, 12102, 13001
Pressure (psia): 20, 40, 60	13609, 13404, 13711
Initial Cladding Temp ($^{\circ}$ F):	500; 1,000; 1,600 12816, 12515, 13303
Subcooling ($^{\circ}$ F): 5, 80, 140	15713, 13812, 13914
Peak Power (kW/ft): 0.45, 0.7, 1.0	11618, 13303, 16022
Initial (Variable) Flooding Rate:	15305, 15132, 15034

Include plots of the following quantities:

- a) forced convective heat transfer coefficient to vapor,
- b) grid enhancement multiplier, F_{grid} ,
- c) two-phase enhancement multiplier, $F_{2\phi}$,
- d) radiation heat transfer coefficient to vapor,
- e) radiation heat transfer coefficient to droplets,
- f) Forslund-Rohsenow drop-wall direct contact heat transfer coefficient,
- g) interfacial heat transfer coefficient between the drops and the vapor,
- h) droplet number and diameter,
- i) minimum stable film boiling temperature, T_{MIN} .

Plot the above parameters as function of time for the elevation of PCT occurrence and for two additional elevations located approximately two and four feet below the hot spot. In addition, please show the steam and liquid flow rates, void fraction, steam temperature, liquid temperature, and clad temperature at function of time as all three locations.

Present plots that show the parametric effects with regard to flooding rate, pressure, initial clad temperature, subcooling, peak power, and initial (variable) flooding rate on the WCOBRA/TRAC-TF2 capabilities to predict the FLECHT test data. Please plot also a

comparison of the measured local PCT against the code predictions as a function of the vertical test bundle axial position.

6. The WCOBRA/TRAC heat transfer from the fuel rod to the surrounding media does not consider rod-to-rod thermal radiation. Since the FLECHT and other heat transfer data contain thimbles, cooler neighboring rods, and wall bundle boundaries, etc. that absorb thermal radiation from the hot rod of interest, please explain how the convective heat transfer coefficient is extracted/determined from all test data where thermal radiation is a component heat transfer removal mechanism.

Response:

Part (1)

In WCOBRA/TRAC-TF2, the dispersed flow film boiling (DFFB) wall heat transfer regime is assumed when the void fraction is [

]^{a,c} The dispersed flow film boiling model as documented in WCAP-16996-P [1] is composed of four components, (1) convective heat transfer to vapor, (2) radiation heat transfer to vapor, (3) radiation heat transfer to droplets, and (4) the droplet-wall direct heat transfer. The heat transfer from the wall to vapor is further transferred to liquid droplets through liquid-vapor interfacial heat transfer. The DFFB wall heat transfer mechanism is detailed in Section 7.2.7 of WCAP-16996-P, and the dispersed droplet interfacial heat transfer is described in Section 6.2.7. Following a postulated large break loss-of-coolant accident (LBLOCA), the peak cladding temperature (PCT) typically occurs during the reflood phase of a LBLOCA, so the heat transfer process, which ultimately cools the hottest elevation of the fuel, is characterized by DFFB heat transfer and single phase vapor heat transfer.

Due to the significance of the DFFB heat transfer regime, it has been a consistent challenge to the nuclear thermal hydraulic community to develop a sound DFFB heat transfer model. Extensive experiments have been conducted, and numerous research articles have been published in the last 50 years. However, there still lacks mechanistic models that include an accurate description of all the thermal hydraulic phenomena characterizing the DFFB heat transfer process.

The thermal hydraulic model developed for a LOCA safety evaluation code is restricted by the resolution limit of the computer code, where the core is represented by multiple vertical channels with lateral connections between channels, and the 3-D effects are largely ignored (see Phenomena Identification and Ranking Table (PIRT) discussion on core 3-D effect in Section 2.3.2.2 of WCAP-16996-P). Thus, there is no ideal engineering solution to practically combine the LOCA safety evaluation code with the convoluted fluid flow or heat transfer models.

The DFFB models, as described in WCAP-16996-P, utilize the modified Forslund-Rohsenow correlation to predict the droplet-wall direct heat transfer and the droplet-vapor interfacial heat transfer. Those models are consistent with the corresponding models described in WCAP-12945-P-A [2]. The only update is [

]^{a,c}

Due to the limitation of the original Forslund and Rohsenow experiment and the models modified by Westinghouse to account for the thermal hydraulic condition in a LOCA, an extensive assessment matrix was developed for the DFFB regime. Those tests featured full height, full pressure, and prototypical fuel assemblies. The parameter ranges in the experiments cover the parameter ranges expected in a pressurized water reactor (PWR) LOCA (see the response to Request for Additional Information (RAI) 57). The assessments in Section 15 of WCAP-16996-P show that the DFFB wall heat transfer and interfacial heat transfer models are [

]^{a,c} and the uncertainty of the DFFB model is captured through the validation. The uncertainty in the DFFB model is quantified and is applied to the PWR analysis as described in Section 29.4 of WCAP-16996-P.

The uncertainty evaluation accounts for the potential over-prediction of heat transfer due to the DFFB model by the multipliers that are developed based on comparison of code results to test data. By using the overall heat transfer coefficient (HTC) to develop the multipliers, the effects of differences in local conditions are included. Thus, if the model results in over-predicting the HTC relative to the test data, the multiplier will account for this effect. Furthermore, the [

]^{a,c}

Part (2)

The Forslund-Rohsenow correlation was developed based on the dispersed flow film boiling data with nitrogen as the coolant. The experimental parameters, such as mass flux, heat flux, pressure, exit quality, etc., have been summarized in the RAI. The original Forslund-Rohsenow model was modified by Westinghouse to account for the thermal hydraulic condition in a PWR LOCA, and the modified model was applied to predict droplet-wall contact heat transfer in the DFFB regime as shown by Eq. 7-132 in Section 7.2.7 of WCAP-16996-P. In the modified model, [

]^{a,c}

Due to the limitation of the original Forslund and Rohsenow experiment and the modified model by Westinghouse, the DFFB wall heat transfer model has been validated against various test facilities that are full height and full pressure and have prototypical fuel assemblies as shown in Sections 15.5 and 15.6 of WCAP-16996-P. The assessment matrix on DFFB heat transfer in the blowdown phase is shown in Section 15.5 of WCAP-16996-P. The validation tests [

]^{a,c} The assessments on DFFB heat transfer during the reflood phase are provided by the reflood validation tests in Section 15.6 of WCAP-16996-P, [

]^{a,c} (It is noted that DFFB is not expected during a small break LOCA transient.)

A direct comparison of the parameters ranges in the original Forslund and Rohsenow experiments to the same parameters ranges in the PWR LOCA is not appropriate because the Forslund and Rohsenow experiment was based on a different coolant (nitrogen). The comparison would require

proper dimensionless numbers. For the purpose of a bottom-up review, the adequacy of the model is based on comparing flow conditions considered in the extensive DFFB validation tests, which are full height, full pressure, and with prototypical fuel assemblies, to the expected flow conditions in a PWR LOCA. This comparison is provided in Table 57-6 of the response to RAI 57. [

] ^{a,c}

It is worthwhile to note that the experimental study provided by Ghazanari et al. (1980) [4] concludes that at the high flow quality the wall-droplet contribution to the total wall heat transfer is negligible. This appears to be consistent with the expected scenario in a LBLOCA. In the limiting LBLOCA case, due to the low reflooding rate, the flow quality at the upper portion of core is high, and the steam Reynolds number tends to be low. Thus, the contribution of droplet-wall direct contact heat transfer to the overall DFFB heat transfer is small at the typical LBLOCA conditions. Previous sensitivity studies performed to support the licensing of the Code Qualification Document (WCAP-12945-P-A) showed that the Forslund-Rohsenow droplet-wall contact heat transfer (without modification) represents only [^{a,c} of the total heat transfer during DFFB. To demonstrate the contribution in a WCOBRA/TRAC-TF2 calculation, the local wall heat flux near the PCT location of the Beaver Valley Unit 1 LBLOCA double-ended guillotine (DEG) case with a break discharge coefficient (CD) equal to 1.0 is extracted to reveal the contribution of droplet-wall direct contact heat transfer. The ratio of droplet-wall heat transfer to the total wall heat transfer at each time step for the first [^{a,c} of the transient, which is sufficient to cover the PCT time, is calculated and the frequency of the ratios is plotted in a histogram as shown in Figure 56-1. The histogram shows the contribution of the droplet-wall direct contact heat transfer is [

] ^{a,c} In general, this study concludes that the contribution of droplet-wall direct contact heat transfer is insignificant compared with the convective and radiation heat transfer to vapor for a limiting LBLOCA case.

Since the predicted contribution of the droplet-wall contact during DFFB is small, it is being removed from the DFFB heat transfer regime model. Therefore, the dispersed flow film boiling model is now composed of three components, (1) convective heat transfer to vapor, (2) radiation heat transfer to vapor, and (3) radiation heat transfer to droplets. This change will be revised accordingly in the updated topical report.

Part (3)

As previously stated, the droplet-wall contact (i.e., the modified Forslund-Rohsenow correlation) is being removed from the DFFB heat transfer regime in WCOBRA/TRAC-TF2. As such, response to this question is no longer necessary.

Parts (4) and (5)

Of the tests listed, FLECHT SEASET 31504 and 31805 and FLECHT SKEWED 15305, 13609, 15713, 13812 and 13914 tests were simulated. In addition, FLECHT SEASET Tests 31203, 31701 and 32013 and FLECHT Low Flooding Rate Tests 04641, 05029 and 05132 were simulated.

Most of the information requested is not readily available (quantities are internally calculated within WCOBRA/TRAC-TF2 and not written to the output files); however, comparison of simulated results to test data are presented in Section 15.0 of WCAP-16996-P which does provide information requested, specifically as follows:

- Section 15.6.1 documents the simulations of FLECHT SEASET Tests 31203, 31504, 31701, 31805 and 32013 and provides comparison plots for:
 - Cladding temperature at several elevations
 - Vapor temperature at several elevations
 - Cladding temperature vs. axial elevation at two transient times near PCT time
 - Predicted PCT versus measured PCT for several thermocouples at various elevations
- Section 15.6.2 documents the simulations of FLECHT Low Flooding Rate Tests 04641, 05029 and 05132 and provides comparison plots similar to the ones provided for the FLECHT SEASET tests.
- Section 15.6.3 documents the simulation of FLECHT SKEWED Tests 13609, 13812, 13914, 15305 and 15713 and provides comparison plots similar to the ones provided for the FLECHT SEASET tests.
- Section 15.9.1 documents predicted versus measured PCT, quench times and PCT turnaround times for the FLECHT tests.
- Section 15.9.2 documents an assessment of the reflood droplet generation for Tests 31701 and 31805.
 - Section 15.9.3 documents a discussion regarding parametric effects due to flooding rate, pressure and subcooling for the FLECHT tests.

In addition to the results presented in Section 15.0, Sections 24.6.4, 24.6.5 and 24.6.6 provide results and discussion in support of the compensating error assessment related to Post-CHF heat transfer for FLECHT SEASET Tests 31504, 31805 and 31701, respectively. Lastly, Section 29.1.8 provides a discussion related to minimum film boiling temperature and predicted versus measured quench temperatures for the reflood tests simulated. It is noted that per Table 29-2 of WCAP-16996-P, the minimum film boiling temperature for the [

]^{a,c}

While all the information requested is not directly contained within the above cited sections of the topical report, the assessment regarding reflood heat transfer (which includes dispersed flow film boiling) is thorough and focuses on the overall behavior of the code during the reflood phase, which includes an assessment related to compensating errors.

It is noted that the comparisons provided in WCAP-16996-P are from the execution of a code version that includes the drop-wall direct contact heat transfer, which is no longer considered a component of the DFFB heat transfer model, as discussed in Part (2) previously. As reported in the response to RAI 77, the [

] ^{a,c}, respectively. With the removal of the drop-wall direct contact heat transfer, the [

] ^{a,c} This demonstrates that with the removal of the drop-wall direct contact heat transfer, the overall model is more conservative.

Part (6)

The effect of rod-to-rod radiation heat transfer is addressed in Section 29.4.3.4 of WCAP-16996-P, Volume III. In summary, [

] ^{a,c} See Section 29.4.3.4 of WCAP-16996-P for more information.



Figure 56-1: Contribution of droplet-wall contact heat transfer to the total wall heat transfer near the PCT location of Beaver Valley Unit 1 LBLOCA DEG Case with CD=1.0.

References

1. WCAP-16996-P/WCAP-16996-NP, Volumes I, II and III, "Realistic LOCA Evaluation Methodology Applied to the Full Spectrum of Break Sizes (FULL SPECTRUM LOCA Methodology)," November 2010.
2. WCAP-12945-P-A, Revision 2 (Volume 1) and Revision 1 (Volumes 2 through 5), "Code Qualification Document for Best Estimate LOCA Analysis," March 1998.
3. Removed.
4. Ghazanfari, A., Hicken, E.F., and Ziegler, A., "Unsteady Dispersed Flow Heat Transfer Under Loss-of-Coolant Accident Related Conditions," Nuclear Technology, Vol. 51, pp. 21-26, 1980.

Question #57: Large Break LOCA Heat Transfer Package in WCOBRA/TRAC-TF2

Please provide a summary table that presents the core heat transfer package that is implemented in WCOBRA/TRAC-TF2 and as it is applied in the modeling of LBLOCA transients. Include five columns identifying LBLOCA phases, pre-CHF, CHF, transition boiling, and dispersed flow film boiling correlations. Provide the implemented relations for the three major post-LBLOCA phases blowdown, refill, and reflood with each phase presented by a separate row in the table. Include the corresponding expressions for each correlation as coded in WCOBRA/TRAC-TF2, the range of applicability of the correlation, and a typical range of flow and heat transfer conditions as occurring in a PWR core following an LBLOCA. Justify the applicability of each model for prototypical reactor core analyses.

Response:

In this response, a summary of the core heat transfer package is presented for each wall heat transfer mode in WCOBRA/TRAC-TF2, in a format not exactly the same as that requested in the RAI question. For each heat transfer mode, its applicability in the applicable phases of the blowdown, refill and reflood phases of a LBLOCA is discussed in addition to other requested information related to the model itself. In doing so, it is an attempt to present the same requested information in a concise and clear format and avoid multiple duplications or cross references of the heat transfer discussion since there are multiple cases that one heat transfer mode is expected to occur and is important in not just one phase of the three phases of a LBLOCA.

In WCOBRA/TRAC-TF2, the vessel heat transfer package consists of a library of heat transfer correlations and the selection logic to determine which correlation is appropriate [

]^{a,c} The heat transfer mode selection logic can be found in Figure 7.2-2 of WCAP-16996-P (referred to herein as the topical report). The following list gives the heat transfer modes used in the WCOBRA/TRAC-TF2 core heat transfer package together with the index of the tables, in which the model description and model correlation range, typical ranges of flow and heat transfer conditions in a PWR LBLOCA, and justifications of the applicability are addressed. There are eight wall heat transfer modes in the core heat transfer package. In addition, the critical heat flux temperature as requested in this RAI is added to the list.

	Wall Heat Transfer Mode	Table Index
Mode 1	Single-phase liquid convection (SPL)	Table 57-1
Mode 2	Subcooled nucleate boiling (SUBC)	Table 57-2
Mode 3	Saturated nucleate boiling (NUCB)	Table 57-2
	Critical Heat Flux (CHF)	Table 57-3
Mode 4	Transition boiling (TRAN)	Table 57-4
Mode 5	Inverted annular film boiling (IAFB)	Table 57-5
Mode 6	Inverted annular dispersed flow (IADF)	Table 57-5

Mode 7	Dispersed droplet film boiling (DFFB)	Table 57-6
Mode 8	Single-phase vapor (SPV)	Table 57-7

Tables 57-1 through 57-7 describe, each wall heat transfer mode respectively, the model correlations, the equation numbers in the topical report, the applicable ranges of the correlation and its references, and the equation numbers of the as coded correlations in the topical report. A discussion on the correlation applicability of the correlation is also presented in each table, together with the typical PWR LBLOCA parameter ranges and the validation test parameter ranges.

The as-coded correlations in topical report (Sec. 7.2.1 through 7.2.8) include the []^{a,c} for each wall heat transfer mode, in addition to the model correlations. The as-coded correlation equation numbers as shown in the topical report are listed in Tables 57-1 through 57-7.

Table 57-8 provides a summary table that presents the expected heat transfer modes during the PWR LBLOCA for the blowdown, refill, and reflood phases.

According to the FSLOCA PIRT (Table 2-1 of the topical report), the importance of each wall heat transfer mode in the core heat transfer package is different for the PWR LBLOCA prediction. []

[]^{a,c} The post-CHF wall heat transfer mode include those of the transition boiling, inverted annular film boiling, inverted annular dispersed flow, dispersed droplet film boiling, and single phase vapor. As discussed in Section 14.1 of the topical report, []

[]^{a,c}

References

1. Rohsenow, W.M., et al. Handbook of Heat Transfer, 3rd edition, McGraw-Hill, 1998.
2. Leung, J.C.M., et al. "Critical Heat Flux Predictions during Blowdown Transients," Int. J. Multiphase Flow, Vol.7, pp. 677-701, 1981

Note: The references to this response include the two listed above and those in the topical report. The same reference style in the topical report is used herein for those references listed in the topical report.

Table 57-1: Single Phase Liquid (SPL) (Note 1)

Model Description	Topical Report Equation Number	Correlation Range	Correlation Reference	Typical LBLOCA Range in PWR	As-Coded Correlation Equations Numbers in Topical Report	Applicability
Kim's correlation for laminar flow	Equation : 7-1	Laminar Flow Regime	Kim (1979)	[] ^{a,c}	Equations: 7-1 through 7-7	Note 2,3
Dittus and Boelter correlation for fully developed turbulent flow	Equation : 7-2	Pr: 0.7 ~ 120 Re: 2.5 x 10 ³ ~ 1.24x10 ⁵ L/d: > 60	Table 5.11 of Reference 1			
Notes: 1. As one of the heat transfer modes occurring in the covered core, single phase liquid heat transfer is ranked [] ^{a,c} (Table 2-1 of the topical report) for all three phases of a LBLOCA. 2. The Dittus and Boelter correlation covers a wide range of turbulent flow conditions measured by the Reynolds and Prandtl numbers. The Kim's laminar flow correlation covers the laminar flows in the low end of the Reynolds number range. 3. [] ^{a,c}						

Table 57-2: Subcooled Nucleate Boiling (SUBC) / Saturated Nucleate Boiling (NUCB) (Note 1)						
Model Description	Topical Report Equation Number	Correlation Range	Correlation Reference	Typical LBLOCA Range in PWR	As-Coded Correlation Equation Numbers in Topical Report	Applicability
Chen's correlation	NUCB: Equations: 7-8 through 7-15 SUBC: Equations: 7-16 through 7-25	Pressure (psia): 8 ~ 505 Liquid Velocity (ft/s): 0.2~14.7 Quality (%): 1.0~ 71.0 Heat Flux (Btu/hr-ft ²): 1.3x10 ⁴ ~ 7.6x10 ⁵	Chen (1963)	<u>Blowdown</u> Note 2 <u>Reflood</u> [] ^{a,c}	Equations: 7-26 through 7-48 and 7-19	Note 2,3,4
Notes: 1. Both the subcooled nucleate boiling and saturated nucleate boiling are predicted by the Chen's correlation in <u>WCT-TF2</u> , and are addressed in one table here. 2. The SUBC and NUCB modes [] ^{a,c} (Table 2-1 of the topical report) for all three phases of a LBLOCA as part of the heat transfer to [] ^{a,c} 3. The Chen flow boiling heat transfer correlation assumes that both nucleation and convective mechanisms occur and it makes the transition to single-phase forced convection at low wall superheat, and to pool boiling at low flow rate. Though it was originally developed for saturated nucleate boiling, existing research by Moles and Shaw (1972) show that it can be applied with satisfactory agreement for low to moderate subcooling. 4. [] 5. [] ^{a,c}						

* For a gravity reflood situation, the inlet flooding rate is oscillatory in nature, due to manometric effects between the core and the downcomer.

Table 57-3: Critical Heat Flux (CHF)

Model Description	Topical Report Equation Number	Correlation Range	Correlation Reference	Typical LBLOCA Range in PWR	As-Coded Correlation Equations Numbers in Topical Report	Applicability	WCT-TF2 Validation Test Range
Modified Zuber's pool boiling CHF	Equation: 7-49	Pressure (atm): 1-10 Subcooling (°C): 5-60 (water, mass flux near zero)	Bjornard and Griffith (1977) Zuber et al. (1961)	Blowdown []] ^{a,c}	Equations: 7-51 through 7-62	Note 1,2,3	Note 3
Groeneveld CHF look-up table	Not Applicable	Tube Diameter (mm): 3-25 Pressure (MPa): 0.1-21 Mass Flux ($\text{kg m}^{-2}\text{s}^{-1}$): 0-8000 Vapor Quality: $X_{\text{CHF}} \sim 1.0$ L/D: >25	Groeneveld (2007)				

Notes:

- The CHF phenomenon is ranked []^{a,c} (Table 2-1 of topical report). []^{a,c} The Groeneveld CHF table was developed based on a large test database covering a wide range of the thermal hydraulic conditions (Groeneveld, 2007). Reference 2 confirms the wide application range of the modified Zuber's pool boiling model.
- The WCT-TF2 CHF model was assessed against prototypical rod bundle experiments in Section 15.3 of the topical report. The validation tests for LBLOCA include the ORNL dispersed flow film boiling tests and LOFT experiments. []^{a,c}
- The pressure range of ORNL dispersed flow film boiling tests reaches 2040psia and the LOFT tests reach the PWR pressure of 2250psia. []^{a,c}

Table 57-4: Transition Boiling (TRAN)

Model Description	Topical Report Equation Number	Correlation Range	Correlation Reference	Typical LBLOCA Range in PWR	As-Coded Correlation Equation Numbers in Topical Report	Applicability	WC/T-TF2 Validation Test Range
Maximum of Model 1 and Model 2 as described in Section 7.2.4 of the Topical Report	Equations: 7-63 through 7-72	Note 1	Iloeje et al. (1974)	Blowdown [] ^{a,c}	Equations: 7-79 through 7-86, 7-72, 7-70, 7-75, 7-76, 7-62, 7-78b, 7-66, 7-52, 7-160, 7-161, and 7-43	Note 2	Prototypical PWR rod bundles
Top-down quench transition boiling model	Equation: 7-73 through 7-76		Ganic and Rohsenow (1977)				Blowdown (Taken from Table 14.1-3 of the Topical Report)
	Equation: 7-77 through 7-78b		Forslund and Rohsenow (1968)	Reflood [] ^{a,c}			[] ^{a,c}
			Bjornard and Griffith (1977)				Reflood (Taken from Table 14.1-6 of the Topical Report)
			Bajorek et al. (1998)				[] ^{a,c}
			Zuber et al. (1961)				
<p>Notes:</p> <p>1. [] ^{a,c} Due to the unstable nature of transition boiling, the TRAN heat transfer mode involves complicated hydrodynamic and heat transfer phenomenon and is modeled with numerous correlations as shown in Sec. 7.2.4 of the topical report. [] ^{a,c}</p> <p>2. The validation of the transition boiling mode using WCT-TF2 is part of the overall post-CHF heat transfer validation to evaluate the blowdown rewetting and reflood quenching. Thus the transition boiling heat transfer is assessed against G1 blowdown tests in Section 15.5 of the topical report for the blowdown rewetting and the FLECHT tests in Section 15.6 of the topical report for the reflood quenching. To justify the applicability of the TRAN model in WCT-TF2, the ranges of important parameters of the transition boiling in the validation tests are compared with the typical ranges in PWR. [] ^{a,c}</p>							

^a For a gravity reflood situation, the inlet flooding rate is oscillatory in nature, due to manometric effects between the core and the downcomer.

Table 57-5: Inverted Annular Film Boiling (IAFB) / Inverted Annular Dispersed Flow (IADF)

Model Description	Topical Report Equation Number	Correlation Range	Correlation Reference	Typical LBLOCA Range in PWR	As-Coded Correlation Equation Numbers in Topical Report	Applicability	WC/T-TF2 Validation Test Range
Modified version of the Bromley correlation for IAFB ($\alpha_v < []^{a,c}$)	Equations: 7-92 through 7-95	Geometry: external horizontal tube with F-113 Pressure: Atmospheric $\Delta T(^{\circ}F)$: 200 ~ 500 Heat Flux (Btu/hr-ft ²): $5 \times 10^3 \sim 2.5 \times 10^4$	Pomerantz (1964)	<u>Reflood</u> [] ^{a,c}	Equations: 7-96 through 7-107	Note 1	Prototypical PWR rod bundles <u>Reflood</u> (Taken from Table 14.1-6 of the Topical Report) [] ^{a,c}
IADF is interpolated between IADF and DFFB if [] ^{a,c}					Equations: 7-108 through 7-111		
Notes: 1. [] ^{a,c} <u>WCT-TF2</u> extends the application of Pomerantz (1964) correlation to a steam-water system at a higher pressure than atmospheric, and the validation tests for these heat transfer modes aim to compare the quench front progressing between the code prediction and the test data. The IAFB and IADF heat transfer models are validated as part of the overall post-CHF model package that impacts the blowdown and reflood rewetting/quench behavior. Those validation tests are listed in Table 14.1-6 of the topical report. The ranges of important parameters in the validation tests are compared with the typical ranges in PWR. [] ^{a,c}							

* For a gravity reflood situation, the inlet flooding rate is oscillatory in nature, due to manometric effects between the core and the downcomer.

Table 57-6: Dispersed Flow Film Boiling (DFFB)

Model Description	Topical Report Equation Number	Correlation Range	Correlation Reference	Typical LBLOCA Range in PWR	As-Coded Correlation Equation Numbers in Topical Report	Applicability	WC/T-TF2 Validation Test Range
The total DFFB heat flux comprises of				<u>Blowdown/Refill</u>			<u>Blowdown/Refill</u>
1. Convective heat flux to vapor including the spacer grid and two phase enhancement	Equations: 7-113, 7-114 and 7-135 through 7-141	Note 1	[^{a,c} Kays (1966)]	Table 14.1-4 of Topical Report	Equations: 7-142 through 7-153	Note 2,3	Table 14.1-4 of Topical Report
2. Radiation heat transfer to vapor and droplets	Equations: 7-115 through 7-129	Note 1	Sun, Gonzalez, and Tien, (1976)	<u>Reflood</u> Table 14.1-5 of Topical Report			<u>Reflood</u> Table 14.1-5 of Topical Report

Notes:

1. [^{a,c} The DFFB heat transfer mode involves complicated hydrodynamic and heat transfer phenomena and is modeled with numerous correlations as shown in Sec. 7.2.7 of the topical report. [^{a,c}
2. The assessment of DFFB heat transfer in the blowdown phase is shown in Section 15.5 of the topical report. The validation tests (ORNL-THTF high pressure film boiling tests (Section 15.5.2.1), G-1 intermediate pressure blowdown heat transfer tests (Section 15.5.2.2), and G-2 low pressure refill heat transfer tests (Section 15.5.2.3)) indicate that [^{a,c} The assessments of DFFB heat transfer in reflood phase are provided by multiple reflood validation tests in Section 15.6, including FLECHT SEASET, FLECHT Low Flooding Rate, FLECHT skewed, and G-2 Reflood tests. [^{a,c}
3. To justify the applicability of the DFFB model in WC/T-TF2, the ranges of important parameters of DFFB in the validation tests are compared with the typical ranges in PWR. [^{a,c}

Table 57-7: Single Phase Vapor (SPV)

Model Description	Topical Report Equation Number	Correlation Range	Correlation Reference	Typical LBLOCA Range in PWR	As-Coded Correlation Equation Numbers in Topical Report	Applicability	WC/T-TF2 Validation Test Range
McAdams correlation for turbulent free convection	Equation:7-154	Ra: $10^9 \sim 10^{13}$ Re: < 2000	McAdams (1954)	Table 14.1-2 of the Topical Report	Equations: 7-160 through 7-166	Note 1	Table 14.1-2 of the Topical Report
Lee's Laminar forced convection heat transfer model	Equation: 7-157	Laminar flow regime	Lee (1981)				
Wong and Hochreiter forced turbulent heat transfer correlation	Equation: 7-159	Re: 2.5×10^3 - 2.52×10^4 Pressure (psia): 20-60	Wong and Hochreiter (1981)				
<p>Notes:</p> <p>1. []^{a,c} The Nusselt number in the laminar forced convection is suggested by Lee (1981) based on the rod bundle tests. []^{a,c} The Wong and Hochreiter (1981) correlation is similar to the Dittus-Boelter correlation, but the coefficients are generated by fitting the steam cooling heat transfer data in a 17X17 rod bundle at the reflood-type pressure.</p> <p>2. The assessment on SPV heat transfer is shown in Section 15.4 of the topical report. The validation tests include the ORNL-THTF uncovered bundle heat transfer tests and the FLECHT SEASET SPV tests and the SPV heat transfer coefficients and wall temperatures in the tests []^{a,c} Table 14.1-2 of the topical report shows that []^{a,c}</p>							

Table 57-8: Generally Expected Heat Transfer Modes During the Major LBLOCA Transient Phases

a,c

Question #58: Flow Regime Map Selection Criterion for Vessel Component

The mixture level swell in the reactor core governs the fuel cladding temperature response in the late stages of a small or intermediate break LOCA when the reactor core can uncover. The WCOBRA/TRAC-TF2 vessel component relies on flow regime maps in modeling the two-phase flow behavior including the response of the reactor core region. WCAP-16996-P/WCAP-16996-NP, Volumes I, II, and III, Revision 0, Section 4, "WCOBRA/TRAC-TF2 Flow Regime Maps and Interfacial Area," explains that the code vessel component utilizes two different flow regime maps: (1) a "Normal Wall" or also referred to as a "Cold Wall" flow regime map and (2) a "Hot Wall" flow regime map. The former is applied when a momentum cell contains heated surfaces that are expected to be fully wetted by liquid and the latter is used to describe the hydrodynamics of highly non-homogeneous and thermally non-equilibrium two-phase flow that can take place during blowdown and reflood. Subsection 4.2, "Vessel Component Normal Wall Flow Regimes," explains that the criterion for selecting a flow regime map, defined by Equation (4-1), is based on the surface temperature of the heated structures present within a computational cell. As described in Subsection 4.2, the transitional temperature is set equal to "the surface temperature at the critical heat flux," T_{CHF} , approximated as $T_w = T_{CHF} \approx (T_{sat} + 75) ^\circ F = (T_{sat} + 41.7) K$ and limited by the critical water temperature given as $705.3 ^\circ F$ ($374.1 ^\circ C$ or $647.2 K$). When the metal surface temperature exceeds the CHF criterion, it is assumed that the liquid can only partially wet the wall and the "Hot Wall" flow regime map is used. Below T_{CHF} , it is considered that the liquid fully wets the wall and the "Cold Wall" flow regime map is applied.

The "Cold Wall" flow regime map recognizes four different regimes: (1) SB with a flow regime indicator ISIJ of 1 (see Table 4.2-1, "Summary of Flow Regime Number in Vessel Components"), (2) SLB with ISIJ=2, (3) CT, and (4) FD with ISIJ=5. The "Hot Wall" flow regime map identifies five individual regimes: (1) Subcooled Inverted Annular, (2) Inverted Liquid Slug, (3) Dispersed Droplet, (4) Falling Film, and (5) Top Deluge with ISIJ=11. The selection of the vessel flow regime takes place in subroutine INTFR, which also computes the wall and interfacial drag coefficients.

- (1) Please explain the appropriateness and provide the technical basis in support of the implemented criterion in Equation (4-1) for selection between the "Cold Wall" and the "Hot Wall" flow regime maps in two-phase flow modeling for the vessel component. Clarify if the WCOBRA/TRAC-TF2 applies the same modeling approach to both plant designs with top down cooling (i.e., Upper Plenum Injection (UPI) plants) and bottom up re-flood. As different validation/qualification processes apply to both designs, please describe the technical bases that demonstrate the applicability of the modeling approach for each plant design.
- (2) As explained in Subsection 4.2, "It is assumed that for cells in which a metal surface temperature exceeds the criterion given by Equation (4-1), liquid can only partially wet the wall and the hot wall flow regime is used." The introduced phenomenological approach for flow regime map selection between the "Cold Wall" map and the "Hot Wall" map is based on surface wetting. At the same time, when surfaces are hot enough, liquid droplets are not

expected to even partially wet the metal wall. Please clarify how the phenomenon of hot surface wetting relates to the flow map identification criterion defined by Equation (4-1).

- (3) Please explain which heat transfer correlations are employed in WCOBRA/TRAC-TF2 to model partially wetted wall surfaces and describe the applicable technical basis. In particular, identify and describe the data used to validate the wetting of walls and related heat transfer when the wall surface temperature, T_w , is above the defined criterion for wall surface wetting.
- (4) Please explain how the criterion defined by Equation (4-1) and the assumed approximation for the CHF surface temperature as $T_{CHF} \approx (T_{sat} + 75)^\circ\text{F}$ relate to the Leidenfrost wall temperature limit, T_{Leid} . A simple correlation for the Leidenfrost temperature used by Bricard et al. (see Bricard, P., Péturaud, P. and Delhay, J. M., "Understanding and Modeling DNB in Forced Convective Boiling: Modelling of a Mechanism Based on Nucleation Site Dryout," Multiphase Science and Technology, No. 9, p. 329, 1997) gives $T_{Leid} = (T_{sat} + 150)^\circ\text{C}$. Similarly, a range of Leidenfrost wall superheat of 100 to 150 $^\circ\text{C}$ is provided by Celata et al. (see Celata, G. P., Cumo, M., Mariani, A. and Zummo, G., "Burnout in subcooled boiling of water. A visual experimental study," Int. J. Therm. Sci., No. 39, pp. 896-908, 2000).

Response:

The $T_{CHF} \approx T_{SAT} + 75^\circ\text{F}$ criterion was originally implemented in Westinghouse Best-Estimate LBLOCA evaluation models [1,2,3]. This criterion was found to provide reasonable agreement with well-accepted correlations and experimental data under LBLOCA reflood conditions.

Carbajo (Carbajo, J., 1985 [4]) noted that the most significant contributor to T_{CHF} was the pressure. He compared T_{CHF} to various correlations and experimental data as a function of pressure. This comparison is presented as Figure 1, with the addition of the $T_{CHF} \approx T_{SAT} + 75^\circ\text{F}$ criterion.

It is observed that for pressures less than 0.5 MPa (73 psia): $T_{SAT} + 75^\circ\text{F}$, Thom, Weatherhead, Jens and Lottes, and the experimental data are all in good agreement. At higher pressures which are more representative of SBLOCA conditions, $T_{SAT} + 75^\circ\text{F}$ tends to fall in between the correlations and the experimental data.

The value of T_{CHF} for selection of the flow regime is expected to be less significant under SBLOCA conditions. Given the interface between the two-phase level and single-phase vapor, the cladding will heatup, and the flow regime will switch from cold wall to hot wall at the point where the transition to single phase vapor occurs (Figure 2). As such, application of Equation 4-1 is also judged to be acceptable for SBLOCA conditions.

Sensitivity studies were executed with ROSA Test SB-CL-02 and a Beaver Valley PWR SBLOCA case with $T_{CHF} = T_{SAT} + 150^\circ\text{F}$ to illustrate the lack of sensitivity. The ROSA study results are presented in Figures 3 through 7. The red, solid lines are Equation 4-1 from WCAP-16996-P, and the green, dashed lines are with $T_{CHF} = T_{SAT} + 150^\circ\text{F}$. It is observed that the

[
^{a,c} The Beaver Valley PWR study results are presented in Figures 8 through 13. The red, solid lines are Equation 4-1 from WCAP-16996-P, and the green, dashed lines are with $T_{CHF} = T_{SAT} + 150^{\circ}\text{F}$. Again it is noted that [

^{a,c}

It is therefore concluded that based on the comparisons to data, correlations, and the sensitivity study described previously that the vessel flow regime selection is appropriate.

Supplemental Discussion Specific to Question 58, Part 1

The same models are used in WCOBRA/TRAC-TF2 for plants equipped with Upper Plenum Injection (UPI) as for non-UPI plants. This was the same approach used for prior best-estimate LBLOCA evaluation models. It is important to note that under LBLOCA transient conditions even plants equipped with UPI experience a bottom-up reflood rather than top-down cooling. The UPI water tends to preferentially drain through the low power assemblies, and then refill the core from the bottom (see Section 5-4-3-5 of WCAP-14449-P-A, Revision 1). The UPI is not of consequence for SBLOCA since the high head safety injection is into the cold legs for 2-loop Westinghouse-designed plants, and the reactor coolant system (RCS) pressure is above the low head safety injection cut-in pressure during the period of interest for the transient.

Supplemental Discussion Specific to Question 58, Part 3

[

^{a,c}

Supplemental Discussion Specific to Question 58, Part 4

There is no direct relationship between the criterion in Equation 4-1 of WCAP-16996-P and the Leidenfrost temperature. The Leidenfrost temperature is generally compared to the minimum film boiling temperature. It is expected that the critical heat flux temperature would be less than the Leidenfrost temperature (e.g. Equation 1 from Carbajo, J., 1985), which is the case given the discussion in the papers cited in the RAI.

References

- 1) WCAP-12945-P-A, Volume1, Revision 2, Volumes 2 through 5, Revision 1, "Code Qualification Document for Best Estimate LOCA Analysis," March 1998.
- 2) WCAP-14449-P-A, Revision 1, "Application of Best Estimate Large Break LOCA Methodology to Westinghouse PWRs With Upper Plenum Injection," October 1999.

- 3) WCAP-16009-P-A, "Realistic Large-Break LOCA Evaluation Methodology Using the Automated Statistical Treatment Of Uncertainty Method (ASTRUM)," January 2005.
- 4) Carbajo, Juan J., "A Study on the Rewetting Temperature," *Nuclear Engineering and Design*, Vol. 84, pp. 21-52, 1985.
- 5) WCAP-16996-P, "Realistic LOCA Evaluation Methodology Applied to the Full Spectrum of Break Sizes (FULL SPECTRUM LOCA Methodology)," November 2010.

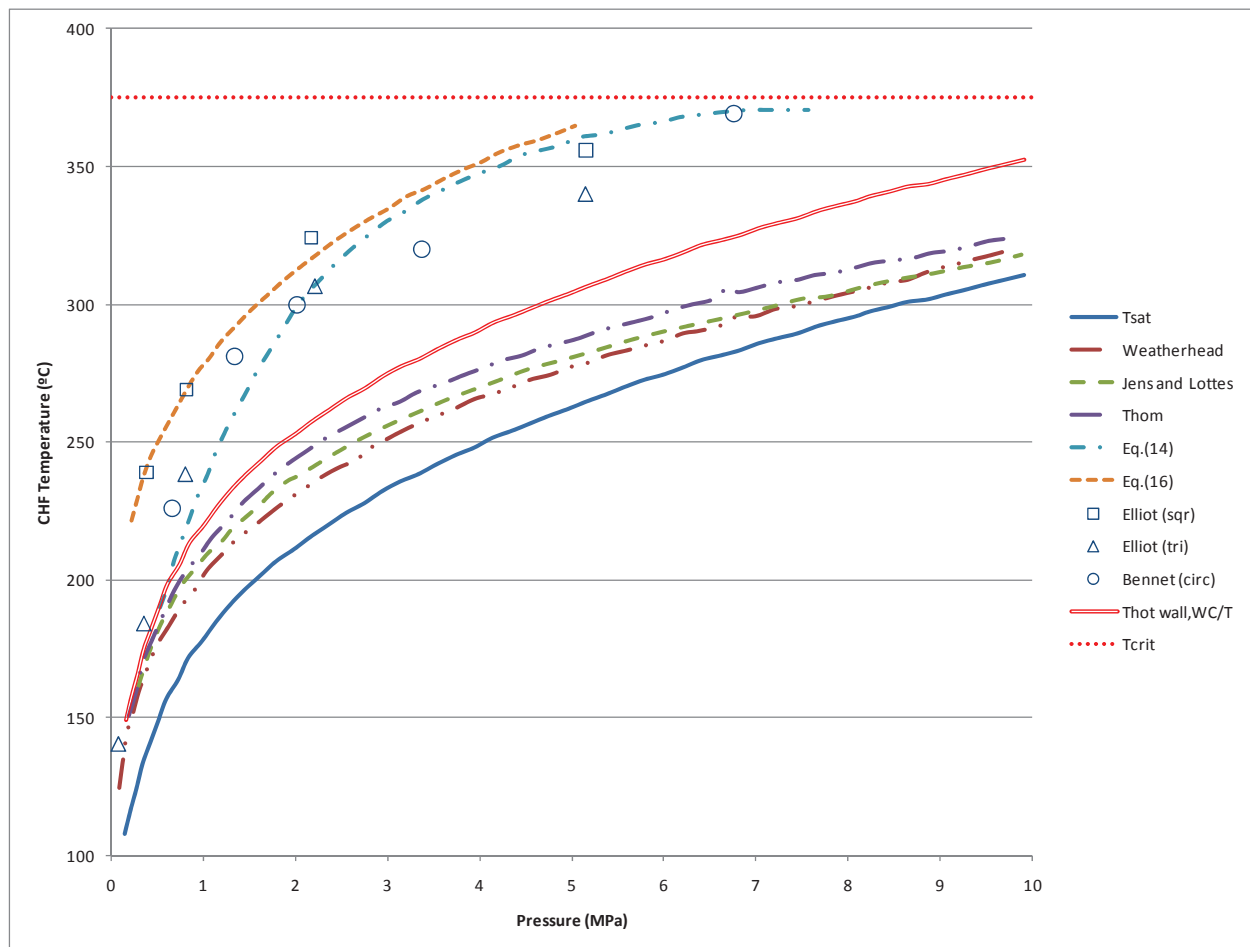


Figure 1: Comparison of WCOBRA/TRAC-TF2 T_{CHF} Criterion with Various Correlations and Experimental Data

a,c

Figure 2: Comparison of the Heat Transfer Mode and Cladding Temperature for the Simulation of G2 Test 715

a,c

Figure 3: Pressurizer Pressure for the ROSA SB-CL-02 Critical Heat Flux Temperature Sensitivity

a,c

Figure 4: Vessel Fluid Inventory for the ROSA SB-CL-02 Critical Heat Flux Temperature Sensitivity

a,c

Figure 5: Cladding Temperature at the 6-foot Elevation for the ROSA SB-CL-02 Critical Heat Flux Temperature Sensitivity

a,c

Figure 6: Cladding Temperature at the 8-foot Elevation for the ROSA SB-CL-02 Critical Heat Flux Temperature Sensitivity

a,c

Figure 7: Cladding Temperature at the 10-foot Elevation for the ROSA SB-CL-02 Critical Heat Flux Temperature Sensitivity

a,c

Figure 8: Pressurizer Pressure for the Beaver Valley Unit 1 PWR Critical Heat Flux Temperature Sensitivity

a,c

Figure 9: Vessel Fluid Inventory for the Beaver Valley Unit 1 PWR Critical Heat Flux Temperature Sensitivity



Figure 10: Cladding Temperature at the 8-foot Elevation for the Beaver Valley Unit 1 PWR Critical Heat Flux Temperature Sensitivity

a,c

**Figure 11: Cladding Temperature at the 9-foot Elevation for the Beaver Valley Unit 1 PWR
Critical Heat Flux Temperature Sensitivity**

a,c

**Figure 12: Cladding Temperature at the 10-foot Elevation for the Beaver Valley Unit 1 PWR
Critical Heat Flux Temperature Sensitivity**

a,c

**Figure 13: Cladding Temperature at the 11-foot Elevation for the Beaver Valley Unit 1 PWR
Critical Heat Flux Temperature Sensitivity**

Question #75: Interfacial Drag Sampling Impact on ROSA-IV LSTF Test Predictions

WCAP-16996-P/WCAP-16996-NP, Volumes I, II, and III, Revision 0, Section 29, "Assessment of Uncertainty Elements," identifies the bubbly flow drag multiplier, YDRAG, as a parameter that describes model uncertainties related to "thermal-hydraulic global models." YDRAG, described in WCAP-16996-P/WCAP-16996-NP, Volumes I, II, and III, Revision 0, Subsection 29.1.5 as being "applied directly to the small bubble, large bubble and hot wall interfacial drag calculations," is characterized by []^{a,c} According to Table 29-2, "Uncertainty Elements – Thermal-Hydraulic Models," it has []^{a,c}

WCAP-16996-P/WCAP-16996-NP, Volumes I, II, and III, Revision 0, Section 13, "Core Void Distribution and Mixture Level Swell," assesses WCOBRA/TRAC-TF2 interfacial drag and level swell prediction capabilities using SET data. An additional interfacial drag study is presented in WCAP-16996-P/WCAP-16996-NP, Volumes I, II, and III, Revision 0, Subsection 21.15, "YDRAG Sensitivity Calculations," also comparing code predictions against test data from an IET performed at the LSTF as part of the Rig-of-Safety Assessment No. 4 (ROSA-IV) Program. The effect of YDRAG variation for the core channels on transient calculations was analyzed and results compared against data for ROSA-IV LSTF Test SB CL-18 simulating a 5 percent cold leg break. The YDRAG multiplier in the core region was set []^{a,c}

[]^{a,c} and the sensitivity results are presented in Figures 21.15-1 through 21.15-6. The difference in the PCT predictions following core boiloff amounts to approximately 100° F (55.6 K) according to Figure 21.15-6, "Peak Cladding Temperatures." This ROSA-IV reference transient, Test SB-CL-18, is first analyzed in Subsection 21.4, "Simulation of SB-CL-18, 5-Percent Cold Leg Side Break," []^{a,c} in the core region. According to WCAP-16996-P/WCAP-16996-NP, Volumes I, II, and III, Revision 0, Subsection 21.3, this YDRAG value was used for all analyses presented in WCAP-16996-P/WCAP-16996-NP, Volumes I, II, and III, Revision 0, Section 21, "ROSA IV Test Simulations," except for the YDRAG sensitivity studies for Test SB-CL-18 discussed in Subsection 21.15. As explained in Subsection 29.1.5, []^{a,c}

[]^{a,c}

In assessing code compensating error, Subsection 24.8, "Core Level Prediction in SB-CL-18 Test," presents Figure 24.8.3-2, "Impact of YDRAG Variation on Predicted Level Swell," showing level swell predictions obtained with YDRAG values []^{a,c} for Test SB CL-18 and with YDRAG values []^{a,c} for Test SB-CL-01 (2.5 percent cold leg break) against the estimates from test measurements.

(1) Please provide two additional assessments for ROSA-IV LSTF Test SB-CL-18 using the YDRAG sampling range upper limiting value of []^{a,c} and its model nominal value of 1.0. Provide comparisons of WCOBRA/TRAC TF2 predictions against measured data including clad temperature measurements at deferent axial elevations. Include comparisons for the axial void

distribution in the core at the time of PCT occurrence as well as for the collapsed liquid level and two-phase mixture level as functions of time. Document the predicted maximum PCT values following core boiloff and compare them against the measured PCT value including the measurement accuracy as well.

(2) Please analyze and provide code predictions for ROSA-IV LSTF Test SB CL-01 (2.5 percent cold leg side break), Test SB-CL-02 (2.5 percent cold leg bottom break), and Test SB CL-03 (2.5 percent cold leg top break). In all three experiments, the measured PCTs reached a maximum value of approximately 1,205°F (925 K). In addition to the results obtained for these tests with []^{a,c} and presented in Subsection 21.7, please provide code predictions for YDRAG drag multipliers []^{a,c} and compare code results against test data. Include also comparisons for the axial void distribution in the core at the time of PCT occurrence as well as for the collapsed liquid level and two-phase mixture level as functions of time.

Response:

The question appears to address the apparent inconsistency between the established range of YDRAG uncertainty, []^{a,c} per Section 29.1.5 of [1], and the range of YDRAG sensitivities performed with the ROSA-IV LSTF 5% CL break test SB-CL-18 and the 2.5% CL break tests SB-CL-01, SB-CL-02 and SB-CL-03.

It is important to note that, while selected tests at the ROSA-IV LSTF integral test facility were used to validate the code capability to model the system response (overall and phenomenon specific), there is no specific intent to use the ROSA tests to establish uncertainty of separate effect phenomena; for example level swell, which is affected by the YDRAG multiplier. The YDRAG sensitivities with the ROSA test SB-CL-18, Section 21.15 of [1], were used to confirm that the code calculation response to the YDRAG variations are consistent with the expectations in terms of effect and direction of bias.

Furthermore, the YDRAG sensitivity calculations with the ROSA 5% break test SB-CL-18 reported in Section 21.15 of [1] bound the new reduced YDRAG uncertainty range []^{a,c} proposed in the response to RAI #74. Therefore, based on the revised range of YDRAG, and the YDRAG sensitivities with the ROSA test SB-CL-18 the requested analyses are not necessary.

References

1. **WCAP-16996-P, Volumes I through III**, "Realistic LOCA Evaluation Methodology Applied to the Full Spectrum of Break Sizes (FULL SPECTRUM LOCA Methodology)," November 2010.

Question #77: Follow-up to RAI #45

[

] ^{a,c}

Table 1: Parameters Treated as Sampled Variables in FSLOCA Calculations for RAI 77 Response

Table 1: Parameters Treated as Sampled Variables in FSLOCA Calculations for RAI 77 Response

Table 1: Parameters Treated as Sampled Variables in FSLOCA Calculations for RAI 77 Response

Table 1: Parameters Treated as Sampled Variables in FSLOCA Calculations for RAI 77 Response

Table 1: Parameters Treated as Sampled Variables in FSLOCA Calculations for RAI 77 Response

Table 2: Parameters Treated as Bounded in FSLOCA Calculations for RAI 77 Response

Acronym	PIRT	Physical Description	Modeling Approach (How Bounded)
---------	------	----------------------	---------------------------------

Table 2: Parameters Treated as Bounded in FSLOCA Calculations for RAI 77 Response

Acronym	PIRT	Physical Description	Modeling Approach (How Bounded)
---------	------	----------------------	---------------------------------

Table 2: Parameters Treated as Bounded in FSLOCA Calculations for RAI 77 Response

Acronym	PIRT	Physical Description	Modeling Approach (How Bounded)
---------	------	----------------------	---------------------------------

**WCAP-16996-P, “Realistic LOCA Evaluation Methodology Applied to the Full Spectrum of Break Sizes
(FULL SPECTRUM LOCA Methodology)”
Requests for Additional Information – (Non-Proprietary)
RAIs 59 -71**

November 2013

Westinghouse Electric Company LLC
1000 Westinghouse Drive
Cranberry Township, PA 16066

1. Introduction and Problem Statement

Requests for Additional Information (RAIs) 59 through 71 are focused on the WCOBRA/TRAC-TF2 interfacial drag models, regarding model basis as well as their validation test and Pressurized Water Reactor (PWR) plant simulations. Responses to these RAIs are provided in this letter. As an extension to Westinghouse's current approved methodology (Reference 1-1) for Large-Break loss-of-coolant accident (LBLOCA) analysis, WCOBRA/TRAC-TF2 is designed to be capable of predicting the LOCA event covering the full spectrum of break sizes. For small-break LOCA (SBLOCA), the interfacial drag models in the code directly impact the core two-phase mixture level and void fraction distribution, which are critical to predicting the fuel rod heat up. As such, the responses to the questions included in this set of RAIs focus on discussing the adequacy of the WCOBRA/TRAC-TF2 interfacial drag models and their key validation tests in the context of SBLOCA analysis, in direct association with the several key issues expressed in these RAIs.

The first issue is the nodalization sensitivity of the Oak Ridge National Laboratory (ORNL) Thermal-Hydraulic Test Facility (THTF) level swell and boil-off test validations and the PWR plant simulations, and the second is the interfacial drag model accounting for the effect of significant vapor generation at the wall in the small and small to large bubble flow regime. These two issues are discussed in Sections 2 and 3 that follow, respectively. The answers to the individual questions besides those involved in the aforementioned issues in these RAIs are found in Section 4 of this response. Section 5 of this letter includes an updated Section 5.4 of the Topical report (Reference 1-2). This updated topical section is provided as part of the response to RAI 66 (1) to resolve inconsistencies between the interfacial drag factor correlations as-written and the general form in technical publications, and inconsistencies between the topical description and the WCOBRA/TRAC-TF2 source code. The revised description of vessel component interfacial drag factors in topical report Section 5.4 as enclosed in Section 5 of this letter will be incorporated in Reference 1-2 when the topical report is updated.

The vessel component interfacial drag models in WCOBRA/TRAC-TF2 describe the momentum interaction of the three fields of vapor, continuous and dispersed liquid and are flow regime dependent. Section 4.0 of Reference 1-2 discusses the flow regimes and associated interfacial area, while the flow regime dependent interfacial drag models are described in Section 5.0 of Reference 1-2.

Reference 1-2 is interchangeably referred to as 'the Topical' in the discussion that follows.

Reference(s)

- 1-1. WCAP-12945-P-A, "Code Qualification Document for Best Estimate LOCA Analysis," March 1998.
- 1-2. WCAP-16996-P, "Realistic LOCA Evaluation Methodology Applied to the Full Spectrum of Break Sizes (FULL SPECTRUM LOCA Methodology)," November 2010.

2. Nodalization and Timestep Studies

A number of nodalization and maximum timestep size sensitivity studies were executed in order to show that the selected core nodalization and timestep size produce reasonable code convergence.

Oak Ridge National Laboratory Core Axial Noding Studies

Core axial noding sensitivity studies were run with ORNL Tests I, L, AA, and DD. The number of nodes in the core was doubled such that the hydraulic node length was reduced from about 12 inches to about 6 inches. The resulting core node sizes cover the range typically used for PWR analysis.

The results of these ORNL axial noding studies are presented in Figures 2-1 through 2-4. The void distributions presented are for channel 2, which is the interior core channel. Refer to Section 13.4.2 of WCAP-16996-P (Reference 2-1) for additional information regarding the ORNL noding.

The base cases are the red, solid lines and the sensitivity cases with increased core noding are the dashed, green lines. It is observed that the resulting void fraction profiles with the additional core nodes are comparable to the base case results; indicating that reasonable convergence is obtained relative to the core axial noding. Since the code results are comparable for this noding study, and the 6-inch to 12-inch nodes cover the typical PWR range (refer to Table 26.1-1 in WCAP-16996-P (Reference 2-1) for typical PWR core node lengths), it is judged that additional noding studies with finer core noding are not required. Furthermore, the inclusion of level sharpening logic (as described in the response to RAI-17 (Reference 2-2)) allows for resolution of the two-phase level beyond the hydraulic cell mesh at the rod heat-transfer node mesh. The maximum heat transfer node size for the fuel rods is 3-inches. The YDRAG range utilized in the uncertainty analysis is then biased low to produce a conservative prediction of the level swell for the uncertainty analysis, as described in the response to RAIs-72, 73 and 74 per LTR-NRC-13-41 (Reference 2-3).

Beaver Valley Unit 1 (DLW) PWR Core Axial Noding Study

A core axial noding sensitivity study was also run with the Beaver Valley PWR input deck. The base case was taken as one of the cases from Study C in the response to RAI-9, transmitted to the Nuclear Regulatory Commission (NRC) in LTR-NRC-13-45 (Reference 2-4). The number of hydraulic nodes used to model the active fuel region was increased, using two nodes for each original node (except for the top two nodes which were already less than eight-inches in the base case). The result is 26 hydraulic nodes in the active fuel region for the sensitivity study compared to 14 nodes in the case base.

Figures 2-5 through 2-9 present the lower plenum pressure, lower plenum liquid temperature, cladding temperature at NSAPLOT node 65, and cladding temperature at NSAPLOT node 75, and core axial void fraction profile near the Peak Cladding Temperature (PCT) time for the Beaver Valley PWR axial noding sensitivity, respectively. The base cases are the red, solid lines and the sensitivity cases with increased core noding are the dashed, green lines. These plots show little difference through the duration of the transient. The effect on the calculated cladding temperature is minimal (Figures 2-7 and 2-8); there is just a small difference in transient timing observed as the base case peaks higher at one elevation while the sensitivity case peaks higher at the other elevation. The timing difference is also observed in the core axial void fraction distribution (Figure 2-9). As such, it is concluded that solution is reasonably converged with the base case node size.

ORNL Maximum Timestep Size Studies

Maximum timestep size sensitivity studies were run with ORNL Tests I and CC. The maximum timestep size was reduced by an order of magnitude from 0.005 s to 0.0005 s. The resulting timestep sizes cover the range typically used for PWR analysis.

The results of these ORNL maximum timestep size studies are presented in Figures 2-10 and 2-11. The base cases are the red, solid lines and the sensitivity cases with decreased maximum timestep size are the dashed, green lines. It is observed that the resulting void fraction profiles with the reduced maximum timestep size are nearly identical to the base case results, indicating that the code is well converged with the base case timestep size.

Conclusion

The ORNL and PWR nodalization and maximum timestep size sensitivity studies executed indicate that the selected core nodalization and timestep size produce reasonable code convergence. Additional studies with 3-inch core nodes are judged unnecessary since the convergence was not sensitive to the noding studies already executed, and the PWR noding is covered by the noding studies already executed.

Reference(s)

- 2-1. WCAP-16996-P, "Realistic LOCA Evaluation Methodology Applied to the Full Spectrum of Break Sizes (FULL SPECTRUM LOCA Methodology)," November 2010.
- 2-2. LTR-NRC-13-37, "Submittal of Westinghouse Responses to 'WCAP-16996-P, 'Realistic LOCA Evaluation Methodology Applied to the Full Spectrum of Break Sizes (FULL

SPECTRUM LOCA Methodology)' Request for Additional Information' (Proprietary/Non-Proprietary), Project 700, TAC No. ME5244," June 5, 2013.

- 2-3. LTR-NRC-13-41, "Submittal of Westinghouse Responses to 'WCAP-16996-P, 'Realistic LOCA Evaluation Methodology Applied to the Full Spectrum of Break Sizes (FULL SPECTRUM LOCA Methodology)' Request for Additional Information – RAIs 72, 73, 74 and 76' (Proprietary/Non-Proprietary), Project 700, TAC No. ME5244," June 21, 2013.
- 2-4. LTR-NRC-13-45, "Submittal of Westinghouse Responses to 'WCAP-16996-P, 'Realistic LOCA Evaluation Methodology Applied to the Full Spectrum of Break Sizes (FULL SPECTRUM LOCA Methodology)' Request for Additional Information – RAIs 9 and 12' (Proprietary/Non-Proprietary), Project 700, TAC No. ME5244," June 26, 2013.

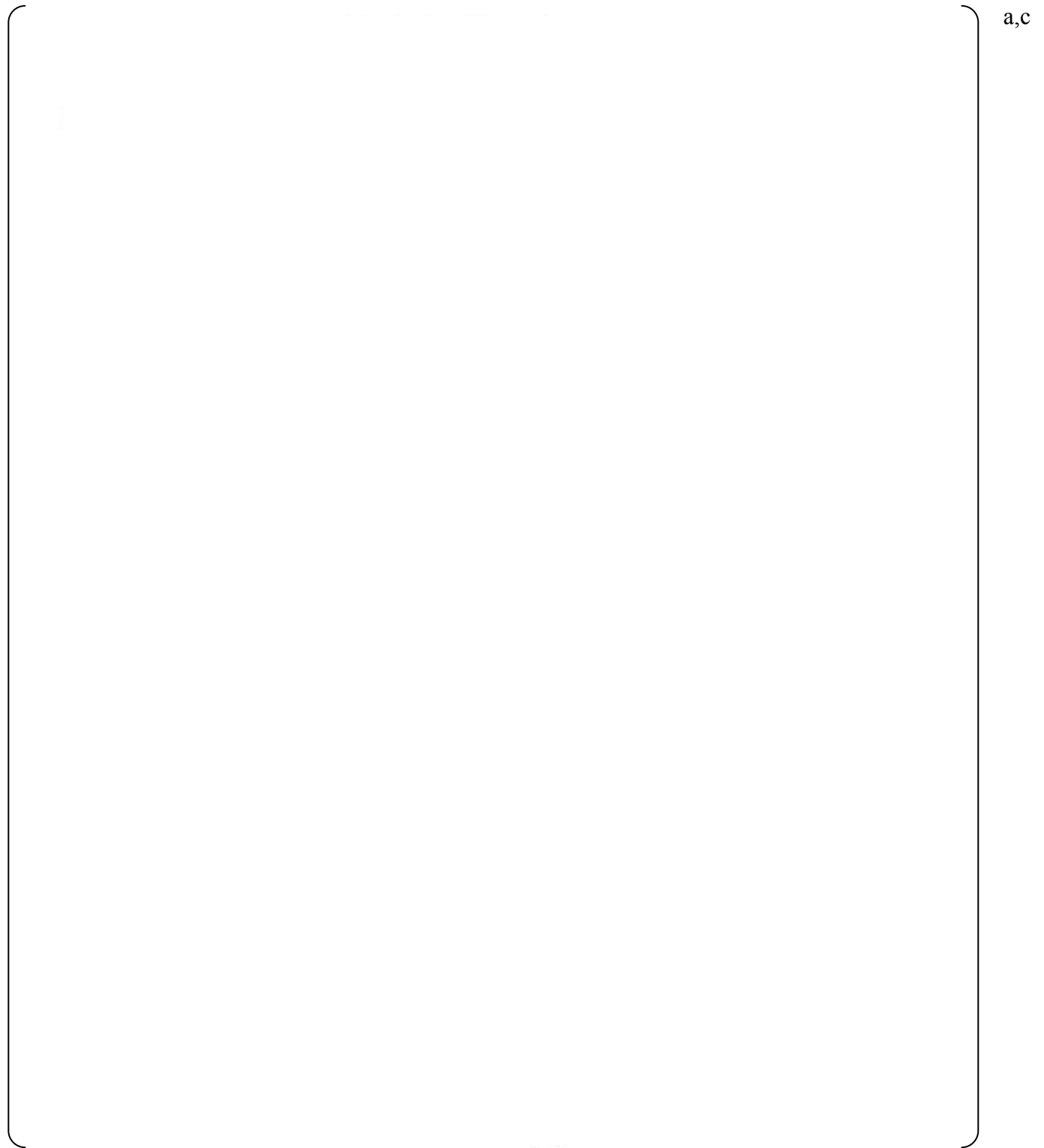


Figure 2-1 – Void Fraction Profile for ORNL Test 3.09.10I Axial Noding Sensitivity

a,c

Figure 2-2 – Void Fraction Profile for ORNL Test 3.09.10L Axial Noding Sensitivity

a,c

Figure 2-3 – Void Fraction Profile for ORNL Test 3.09.10AA Axial Noding Sensitivity

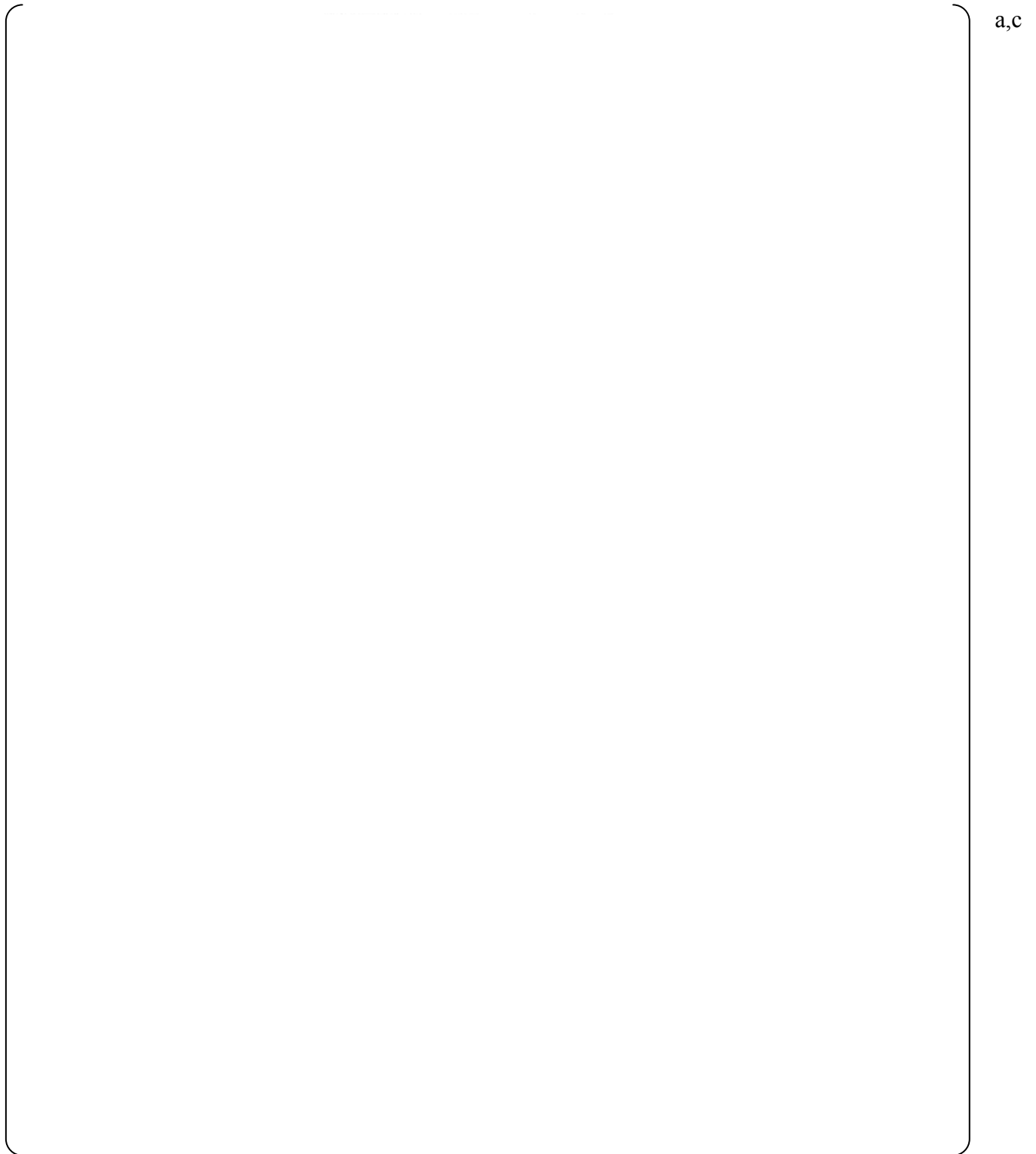


Figure 2-4 – Void Fraction Profile for ORNL Test 3.09.10DD Axial Noding Sensitivity

a,c

Figure 2-5 – Lower Plenum Pressure for the Beaver Valley PWR Axial Noding Study

a,c

Figure 2-6 – Lower Plenum Liquid Temperature for the Beaver Valley PWR Axial Noding Study

a,c

Figure 2-7 – NSAPLOT Node 65 Cladding Temperature for the Beaver Valley PWR Axial Noding Study

a,c

Figure 2-8 – NSAPLOT Node 75 Cladding Temperature for the Beaver Valley PWR Axial Noding Study

a,c

Figure 2-9 – Axial Void Fraction Profile in the Hot Channel Near the PCT Time for the Beaver Valley PWR Axial Noding Study

a,c

Figure 2-10 – Void Fraction Profile for ORNL Test 3.09.10I Timestep Size Sensitivity

a,c

Figure 2-11 – Void Fraction Profile for ORNL Test 3.09.10CC Timestep Size Sensitivity

a,c

**Figure 2-12 – Comparison of Predicted Void Profiles for FDRAG Sensitivity Study, ORNL
– THTF Test 3.09.10CC**

3. Hot Wall Ramp

By 'Hot wall ramp', it means a WCOBRA/TRAC-TF2 interfacial drag model to account for the vapor generation by wall heat transfer in Small Bubble flow regime. It is based on the premise that if boiling occurs at a solid boundary in a channel, the rate at which the vapor can be carried away from the wall is limited by the ability of the bubbles in the channel to perform this function. If more vapor is generated than can be carried away, vapor will begin to accumulate at the wall and the vapor/liquid interfacial geometry will take on the appearance of an inverted annular/slug regime. In consequence, the interfacial shear between the vapor and the bulk liquid is modeled ramping between the shear determined by the bubbly and inverted annular flow shear models.

In Small to Large Bubble flow regime, WCOBRA/TRAC-TF2 assumes large bubbles always co-exists with small bubbles, and the hot wall ramp algorithm is implemented for both Small Bubble and Small to Large Bubble flow regimes, as described in Sections 5.4.1 and 5.4.2 of Reference 3-1. However, effect is expected to diminish as the void fraction increases in this flow regime and results in more vapor flow area for vapor to be carried away from the boiling, as seen from Equation (5-69) of the Topical.

Further, for the Churn Turbulent flow regime, the interfacial drag force could potentially involve hot wall ramp effect since it is calculated by interpolating between the drag forces of the Small to Large Bubble and Film Mist flow regimes. Due to the associated high void fraction range in this regime, the chance to activate the hot wall ramp model is expected to be very small.

As a result of the detailed review of the hot wall ramp model on both the model description in the Topical (Reference 3-1) and how the model is coded in WCOBRA/TRAC-TF2, instances of inconsistency were identified between the coding and the topical report model descriptions, as well as between the design intent of the model and the coding. As a result, both the topical report and coded model need to be revised and they are detailed as follows.

- Based on the code review, Equation (5-67b) in the Topical will be revised to be consistent with WCOBRA/TRAC-TF2 coding as:

$$[\quad]^{a,c} \quad (5-67b)$$

where $K_{iX,v\ell,SB}$ is defined by (5-67a) in the Topical and revised to be consistent with the WCOBRA/TRAC-TF2 coding as:

$$[\quad]^{a,c} \quad (5-67a)$$

The term $[\quad]^{a,c}$ is included for Small Bubble regime to reduce the interfacial drag if relative velocity is high. This is to ensure that the drag coefficient remains reasonable for numerical stability reasons.

- It was found that U_{Γ} as defined by Equation (5-69) is not consistent with the physical meaning of wall heat transfer terms of Q_{wl} and Q_b , Equation (5-69) needs to be corrected as:

$$\left[\frac{Q_{wl} + Q_b}{A_x} \right]^{a,c} \quad (5-69)$$

where A_x is the cell momentum area in the axial direction and Q_{wl} and Q_b are the heat flow from wall to liquid and the subcooled boiling heat flow, respectively (Section 7.2), which represent the 'implicit' and 'explicit' portions of the boiling heat transfer to account for the vapor generation in the saturated and subcooled boiling applications.

The Γ_v term in Equation (5-69) of the Topical report is also removed as shown above after careful review of the model in the context of its applicable transient conditions. As pointed out in RAI 67 (4), the [

$$\left[\frac{Q_{wl} + Q_b}{A_x} \right]^{a,c}.$$

The interfacial drag models of the cold wall flow regimes play key roles in determining the level swell and rod heat up in SBLOCA applications; however their impacts to a LBLOCA transient are expected to be small. As part of the cold wall regime interfacial models, the hot wall ramping model is not validated directly by itself, instead the WCOBRA/TRAC-TF2 interfacial drag correlations including the hot wall ramping algorithm are validated through key SBLOCA tests, such as ORNL-THTF small break tests and G-1 and G2 core uncover tests (Section 13 of Reference 3-1). In order to assess the impact of the hot wall ramping model to the SBLOCA transients, the sensitivities of the validation results of selected ORNL-THTF small break tests and a sample PWR SBLOCA run are evaluated using interfacial drag models with and without implementing the hot wall ramping algorithm. These evaluation results are presented in Figures 3-1.1 through 3-1.12 for ORNL small break tests, and Figure 3-1.13 for Beaver Valley 2.6 inch small break run PCT. Please note that these sensitivity studies are performed without implementing the hot wall ramping model modifications discussed in this subsection.

The following conclusions are drawn through these sensitivity runs of the hot wall ramping model:

- [

$$\left[\frac{Q_{wl} + Q_b}{A_x} \right]^{a,c}$$

[

•

]^{a,c}

Reference(s)

- 3-1. WCAP-16996-P, "Realistic LOCA Evaluation Methodology Applied to the Full Spectrum of Break Sizes (FULL SPECTRUM LOCA Methodology)," November 2010.

a,c

Figure 3-1.1 Hot Wall Ramping Model Sensitivity of ORNL (Case i)
(Solid: No Hot Wall Ramping; Dashed: With Hot Wall Ramping)

a,c

Figure 3-1.2 Hot Wall Ramping Model Sensitivity of ORNL (Case j)

(Solid: No Hot Wall Ramping; Dashed: With Hot Wall Ramping)

a,c

Figure 3-1.3 Hot Wall Ramping Model Sensitivity of ORNL (Case k)

(Solid: No Hot Wall Ramping; Dashed: With Hot Wall Ramping)

a,c

Figure 3-1.4 Hot Wall Ramping Model Sensitivity of ORNL (Case I)

(Solid: No Hot Wall Ramping; Dashed: With Hot Wall Ramping)

a,c

Figure 3-1.5 Hot Wall Ramping Model Sensitivity of ORNL (Case m)
(Solid: No Hot Wall Ramping; Dashed: With Hot Wall Ramping)

a,c

Figure 3-1.6 Hot Wall Ramping Model Sensitivity of ORNL (Case n)
(Solid: No Hot Wall Ramping; Dashed: With Hot Wall Ramping)

a,c

Figure 3-1.7 Hot Wall Ramping Model Sensitivity of ORNL (Case aa)
(Solid: No Hot Wall Ramping; Dashed: With Hot Wall Ramping)

a,c

Figure 3-1.8 Hot Wall Ramping Model Sensitivity of ORNL (Case bb)

(Solid: No Hot Wall Ramping; Dashed: With Hot Wall Ramping)

a,c

Figure 3-1.9 Hot Wall Ramping Model Sensitivity of ORNL (Case cc)
(Solid: No Hot Wall Ramping; Dashed: With Hot Wall Ramping)

a,c

Figure 3-1.10 Hot Wall Ramping Model Sensitivity of ORNL (Case dd)
(Solid: No Hot Wall Ramping; Dashed: With Hot Wall Ramping)

a,c

Figure 3-1.11 Hot Wall Ramping Model Sensitivity of ORNL (Case ee)

(Solid: No Hot Wall Ramping; Dashed: With Hot Wall Ramping)

a,c

Figure 3-1.12 Hot Wall Ramping Model Sensitivity of ORNL (Case ff)

(Solid: No Hot Wall Ramping; Dashed: With Hot Wall Ramping)

a,c

Figure 3-1.13 Hot Wall Ramping Model Sensitivity of DLW SB
(Solid: No Hot Wall Ramping; Dashed: With Hot Wall Ramping)

4. RAI Questions and Responses

4.1 RAI 59

Question #59: WCOBRA/TRAC-TF2 Flow Maps for Vessel and One-Dimensional Components

WCAP-16996-P/WCAP-16996-NP, Volumes I, II, and III, Revision 0, Subsection 4.2.2, "Small Bubble Regime," explains that the SB regime is applied when the two-phase flow void fraction is less than 20 percent. As such, it models what is generally referred to as "bubbly flow" in the two-phase flow literature. In this regime, the vapor phase is assumed to exist as uniform spherical bubbles dispersed in a continuous liquid phase. The bubble radius is determined by Equation (4-15) using a critical Weber number of 10 and applying the vector sum of the maximum lateral relative velocity and the axial relative velocity for the cell. According to Equation 4-16, the bubble diameter is limited to the cell hydraulic diameter or $[\text{ }^{a,c}]$ whichever is smaller.

According to WCAP-16996-P/WCAP-16996-NP, Volumes I, II, and III, Revision 0, Subsection 4.2.3, "Small to Large Bubble Regime," this regime is applied for void fractions greater than or equal to 20 percent and less than or equal to 50 percent. In the SLB regime, the vapor phase is modeled by a SB field accounting for 20 percent void fraction with the remaining vapor content being attributed to one or more large bubbles. The large bubble radius is determined by Equation (4-24) and it cannot be larger than the cell hydraulic diameter or $[\text{ }^{a,c}]$ according to Equation (4-23).

WCAP-16996-P/WCAP-16996-NP, Volumes I, II, and III, Revision 0, Subsection 4.2.4, "Churn-Turbulent Flow Regime," explains that this regime is used when the void fraction is above 50 percent and remains below a certain critical void fraction at which a stable liquid film at the wall is formed. It is explained that this critical void fraction, determined by the flow channel size and the vapor velocity, is limited to a minimum void fraction of 80 percent as below this value waves are expected to bridge across the flow channel and cause a transition to CT flow. The CT regime as modeled as a combination of the Large Bubble and the FD regimes.

According to WCAP-16996-P/WCAP-16996-NP, Volumes I, II, and III, Revision 0, Subsection 4.2.5, "Film/Drop Flow Regime," this regime exists above a certain critical void fraction criterion. The liquid phase is present as a wall film and possibly droplets that can be entrained by the steam flow. The droplet diameter is determined by Equation (4-48) using the entrained liquid fraction and it is limited to $[\text{ }^{a,c}]$ Table 1 below presents major correlations used in the implementation of the "Cold Wall" flow regime map in WCOBRA/TRAC-TF2.

- (1) Please demonstrate the applicability of the value used for the critical Webber number in Equation (4-15) to predict the diameter of the small bubble, D_b^* . Provide the units for the SB radius as defined by this equation. Define the range of applicability of this expression with regard to hydraulic diameter, pressure, phase mass flow rates, and void fraction, along with supporting test data. Explain how the vector sum of relative velocities between the vapor

and continuous liquid phases, \underline{U}_{vl} , used in Equation (4-15), is calculated, and describe any limitations with regard to slip (velocity ratio). Please explain if Equations (4-15) and (5-60) define the same physical parameter.

- (2) Equation (4-24) defines the large bubble diameter, D_{LB}^* , as being proportionate to the volume of the hydraulic computational cell, $\Delta V = A_x \Delta X$:

$$D_{LB}^* \sim (A_x \Delta X)^{1/3}.$$

Please explain the appropriateness of defining a physical parameter that is introduced to describe a phenomenon of relevance for the core two-phase level swell modeling by making this diameter dependent upon the fluid volume in a computational mesh cell. Nodalization can vary and so will the predicted value of the relevant physical parameter describing the phenomenon of interest. Such an approach can introduce uncertainties and nonphysical behavior in code predictions through artificial distortions of physical models used in the prediction of safety relevant thermal-hydraulic process. Please estimate the bounding effect on core level-swell prediction results. Define the range of applicability of this expression with regard to hydraulic diameter, pressure, phase mass flow rates, void fraction, and slip along with supporting test data.

Table 1: Major Correlations in the WCOBRA/TRAC-TF2 "Cold Wall" Flow Regime Map

Flow Regime	Void Fraction, α (%)	Bubble/Droplet Diameter or Film Thickness	Size Limitations	Flow Structure
Small Bubble	$0 < \alpha \leq 20$	Small bubble diameter, Equation (4-15): $D_b^* = We_{crit} \sigma_c / (\rho_l \underline{U}_{vl}^2) + 0.00002$ \underline{U}_{vl} – vector sum of relative velocities between vapor and continuous liquid $We_{crit} = 10$	$[]^{a,c}$	Small bubble only
Small-to-Large Bubble	$20 < \alpha \leq 50$	Large bubble diameter, Equation (4-24): $D_{LB}^* = [3/(4\pi)(\alpha_v - V_{SB}/\Delta V)\Delta V]^{1/3}$ $\Delta V = A_x / \Delta X$ – cell volume V_{SB} – volume of small bubbles	$[]^{a,c}$	Small and large bubbles
Churn-Turbulent	$50 < \alpha \leq \alpha_{crit}$	Entrained droplet diameter, Equation (4-48): $[]^{a,c}$	$[]^{a,c}$	
Film/Drop	$\alpha_{crit} < \alpha \leq 100$	Critical layer thickness and void, Equation (4-39): $\delta_{crit} = C_l \sigma / (\rho_v \underline{U}_{vl} ^2)$ \underline{U}_{vl} – relative velocity between continuous liquid and vapor $\alpha_{crit} = 1 - 4\delta_{crit}/D_h - \alpha_c$ $C_l = 0.5$	$\alpha_{crit, min} = 80\%$	Liquid film and entrained drops, if any

- (3) According to Equation (4-16), the bubble diameter in the SB regime is limited to []^{a,c} or to the hydraulic diameter. A typical fuel assembly has a hydraulic diameter of 0.045 ft (0.53 in or 13.6×10^{-3} m). Based on Equation (4-23), the large bubble diameter in the SLB or CT flow regimes cannot be larger than the cell hydraulic diameter or []^{a,c} whichever is smaller. Accordingly, for a two-phase flow in a fuel bundle, the SB diameter would be limited to []^{a,c} and the large bubble diameter would be limited []

[]^{a,c} Please explain the appropriateness and applicability of the applied limits for the diameters of the small and large bubbles. Please explain the technical basis for the []^{a,c} limit for the large bubble diameter limit and its impact on two-phase level swell calculations.

- (4) Equation (4-41) defines the critical film thickness used in the CT flow regime modeling. Please define the range of applicability of this expression with regard to hydraulic diameter, pressure, and phase mass flow rates along with supporting test data. Explain how the relative velocity between the continuous liquid and the vapor phase, \underline{U}_{vl} , used in Equation (4-41), is calculated. Explain how the entrained liquid fraction, α_e , appearing in Equation (4-41) and Equation (5-80), is calculated. Please clarify why the critical void fractions, as defined in Equation (5-93) in WCAP-16996-P/WCAP-16996-NP, Volumes I, II, and III, Revision 0, Subsection 5.4.4, "Film/Drop Flow Regime," and in Equation (5-127) in Subsection 5.6.2, "Entrainment in Film Flow," do not take into account the entrained liquid fraction, α_e . Please address the threshold conditions for liquid entrainment and define the range of applicability of the correlations used to predict the entrained liquid fraction, α_e , with regard to hydraulic diameter, pressure, and phase mass flow rates, and void fraction along with supporting test data. In addition, please explain the way in which WCOBRA/TRAC-TF2 predicts the diameter of the entrained droplets, the number of droplets and the drop interfacial area density. Given these droplet diameters and associated interfacial areas, describe how this formulation is used in or related to the computation of interfacial heat transfer between the steam and liquid phases. Please explain if this model predicts entrained droplets leaving the two-phase surface and entering the steam region during periods of predicted core uncover for small breaks in the order of 0.02 to 0.01 ft².
- (5) WCAP-16996-P/WCAP-16996-NP, Volumes I, II, and III, Revision 0, Subsection 5.4.3, "Churn-Turbulent Flow Regime Interfacial Drag," explains that "The churn-turbulent regime is assumed to be a combination of the large bubble regime and the film/drop regime." Please explain how the CT flow is modeled in WCOBRA/TRAC-TF2 as a combination of LB and FD regimes. In particular, please explain the assumed forms of presence for each phase, e.g., small bubbles, large bubbles, droplets, slugs, continuous form.
- (6) Please provide a table that describes constitutive correlations used for flow regime identification by the "Cold Wall" and "Hot Wall" flow maps for a vessel component and the flow regime map for the one-dimensional components in WCOBRA/TRAC-TF2. For each

individual correlation, please provide information that describes the source reference, applicability range for defining parameters, extrapolations, and limitations outside of applicability ranges as appropriate, and the supporting technical basis including applicable test data and references to validation analyses. Include the flow regime indicator and number for each individual flow regime as Table 4.2-1 appears incomplete. In addition, please describe major differences in the modeling of corresponding flow regimes for the vessel and one-dimensional components.

Response:

Part (1)

In bubbly flow dynamics, an important dimensionless group to determine the stability of a single bubble is the Weber (We) number. The Weber number represents the ratio of inertia to surface tension. The inertia force tends to deform and break bubble while the surface tension tends to stabilize the bubble surface. The Weber number for bubbles is usually defined using liquid density, bubbly diameter, surface tension, and relative velocity or turbulent velocity. Eq. 4-15 of the topical report predicts the diameter of small bubbles by assuming a critical Weber number, which is an empirical value. The technical basis of adopting a critical Weber number to evaluate the interfacial drag in a two phase flow has been detailed by Wallis (Reference 4.1-1, Chapter 12) and Ishii (Reference 4.1-2, Chapters 11 and 12). In Chapter 11, Section 1.2.1 of Reference 4.1-2, the critical Weber number for bubble break up due to turbulent impact was determined to be 6.0 experimentally, and the critical Weber number is around 12 for droplet break up as shown in Chapter 12, Section 1.2.1 (Reference 4.1-2). For churn-turbulent flow regime, Section 1.2.2 of Chapter 12 (Reference 4.1-2) reported the critical Weber number is 8 for bubble and 12 for droplet. Eq. 4-15 in the topical report assumes a critical Weber number of []^{a,c} to the values by Ishii (Reference 4.1-2). With knowing the Weber number of []^{a,c}, one could calculate void fraction distribution in a vertical pipe using the small bubble interfacial drag model in the topical report and the force balance between the interfacial drag and buoyancy. Figure 4.1-1 and Figure 4.1-2 compare the calculated void fractions assuming []^{a,c} with the void fraction prediction based on the Zuber-Findlay drift flux model (Reference 4.1-10) at different vapor superficial velocities at low pressure (40 psia) and high pressure (1000 psia), respectively. The void fractions in the small bubble flow regime are []

]^{a,c}

Using a critical Weber number to predict bubble size is common in the thermal hydraulic codes. A review of those thermal hydraulic codes shows the critical Weber number of []^{a,c} is similar to the values selected by other thermal hydraulic codes. For example, TRAC-PF1 (Reference 4.1-3) uses a critical Weber number of 7.5 for bubbly flow, the critical Weber number is 10 in both RELAP5/MOD2 (Reference 4.1-4) and RELAP5/MOD3.3 (Reference 4.1-5), COBRA-TF (Reference 4.1-6) uses a critical Weber number of 10 for bubbly flow, and the same value of 10 is adopted by GOTHIC (Reference 4.1-7). Those thermal hydraulic codes

have been applied to a wide range of applications. Both TRAC-PF1 and RELAP5/MOD3.3 have been applied to small break and large break LOCA analysis of PWR. The COBRA-TF code has been applied to core thermal hydraulic analysis and transient analysis for both BWR and PWR. GOTHIC has been approved for the containment thermal hydraulic analysis. The diversified applications of those thermal hydraulic codes demonstrated the applicability of using the critical Weber number of $[\]^{a,c}$ to predict the bubble size.

In the FSLOCATM topical report, sufficient amount of validations against core level swell experiments in Section 13 demonstrate WCOBRA/TRAC-TF2 reasonably predicts the void fraction distribution compared with the test data at various pressure, mass flux and void fractions. Those tests featured prototypical rod bundle and the comparison of the testing conditions with typical PWR conditions has been provided in Table 13.4.1-1 of the topical report.

In the reactor thermal hydraulic codes, the interfacial drag model is a simplified model developed particularly for predicting thermal hydraulic in the reactor with a coarse nodalization. The simplified interfacial drag model and interfacial area model in WCOBRA/TRAC-TF2 together with the Weber number of $[\]^{a,c}$ produced reasonable void fraction distribution in the assessments documented in the topical report. The proper scaling between the facilities in the assessment and the PWR ensures the WCOBRA/TRAC-TF2 code is used within the parameter range of its assessments during the LOCA evaluations.

It is noted that both Eq. 4-15 and Eq. 5-60 define the same bubble radius using the critical Weber number. The radius in Eq. 4-15 is applied to the calculation of interfacial area, while the radius in Eq. 5-60 is used for the Reynolds number in the interfacial drag calculation. $[\]^{a,c}$

It is further clarified that, in the vessel component of WCOBRA/TRAC-TF2 code, $[\]^{a,c}$

$[\]^{a,c}$ is used for the calculation of the Reynolds number (Eq. 5-51), Weber number (Eq. 4-15), and the critical film thickness (Eq. 4-41) for the film/drop flow regime and churn turbulent flow regime. The vector sum of relative velocities is defined in Eq. 5-44. Note that vector sum of relative velocity in Eq. 5-44 is denoted with an asterisk. There is no additional limiter applied to the vector sum of relative velocities in Eq. 4-15.

Part (2) and Part (3)

Equation 4-23 sets reasonable upper limits to large bubble radius. The physical implications of three limits are discussed below.

¹ *FULL SPECTRUMTM and FSLOCATM are trademarks in the United States of Westinghouse Electric Company LLC, its subsidiaries and/or its affiliates. These marks may be used and/or registered in other countries throughout the world. All rights reserved. Unauthorized use is strictly prohibited. Other names may be trademarks of their respective owners.*

The upper limit of $[]^{a,c}$ ft for the bubble diameter reflects stability limit for the large bubble. Ishii (Reference 4.1-2) states, in a large diameter channel $D_h > 40\sqrt{\sigma/(g\Delta\rho)}$, slug and large cap bubbles cannot be sustained due to the interfacial instability and they disintegrate to smaller cap bubbles. Section F1.1 of the TRAC-M theory manual (Reference 4.1-8) has discussed the slug to cap bubble transition and assumes the critical bubble size is $D_h = 50\sqrt{\sigma/(g\Delta\rho)}$. This critical bubble size is only a weak function of pressure. $[$

$]^{a,c}$ (Figure 4.1-3, Figure 4.1-4, Figure 4.1-5, and Figure 4.1-6).

The second limit is the hydraulic diameter of the channel. The limit reflects $[$

$]^{a,c}$

The third limit r_{LB}^* , assumes one or more large bubbles accounts for the vapor left when the volume of small bubble vapor is subtracted. The derivation of the bubble radius is shown from Eq. 4-24 through Eq. 4-31. The definition r_{LB}^* involves the volume of the hydraulic cell. It is noted that due to the coarse nodalization implemented for the LOCA analysis, r_{LB}^* tends to be large.

Those 3 limits play a different role in the LOCA analysis depending on the geometry to be analyzed. $[$

$]^{a,c}$

To reduce the noding sensitivity in the LOCA analysis, a strict noding consistency between the validation tests and the pilot PWR has been established during the development of the FSLOCA evaluation model. The details of noding strategy and consistency of the FSLOCA Evaluation Model (EM) have been documented in Section 26.1 of the FSLOCA topical report. Particularly for the reactor core, the testing facilities in the level swell validation all featured full scale rod bundle and full pressure (the comparison of the testing conditions with typical PWR conditions has been provided in Table 13.4.1-1 of the topical report). $[$

$]^{a,c}$

Part (4) and Part (5)

The churn-turbulent flow regime is designed to be a simple transition between bubbly flow and film/drop flow. It is implemented as a linear interpolation of interfacial drag and interfacial heat transfer between two flow regimes. Section 5.4.3 of the topical report provides formulas for the interpolation of interfacial drag and Section 6.2.3 of the topical report provides formulas for the interpolation of interfacial heat transfer. The churn-turbulent regime as a part of the vessel component of WCOBRA/TRAC-TF2 has been validated against ORNL, G-1, G-2 and JAERI Two-Phase Test Facility (TPTF) level swell tests in Section 13 of the topical report, though the flow regime itself is shown to be much less significant for level swell than the bubbly flow regimes. [

] ^{a,c}

The upper bound of void fraction in the churn turbulent flow regime in Eq. 4-41 is established using the critical film thickness developed in NUREG/CR-0312 (Reference 4.1-9). [

] ^{a,c}

A major concern on the churn turbulent flow regime is the liquid entrainment in the churn turbulent flow regime and its possible impact to the core heat transfer in a small break LOCA. Thus, a study on entrainment and steam cooling above the two phase mixture level in a typical small break LOCA was conducted to address RAI 17. Figures 17-5a through 17-5d (Reference 4.1-11) provided a comparison of the vapor fraction and entrainment fraction profiles at several times before and after the PCT time. [

] ^{a,c} It can be concluded that the impact of the entrainment in churn turbulent flow to the core heat transfer is negligible in a SBLOCA evaluation.

Additional remarks for part (4) and part (5)

- As we explained in the response to part (1), the relative velocity in Eq. 4-41 is the vector sum of relative velocities between the vapor and continuous liquid phases.

- The vessel component of WCOBRA/TRAC-TF2 is modeled with a two-fluid three-field model, which utilizes a droplet interfacial area transportation model to predict interfacial area, droplet size and entrainment fraction. The theoretical basis, transportation equations and implementation of interfacial area transportation model have been summarized in the response to RAI 55 (Reference 4.1-12).
- The entrained liquid fraction α_e has been missed from both Eq. 5-93 and Eq. 5-127. However, the actual coding has been inspected to be correct for both equations.

Part (6)

In general, the vessel component and the one-dimensional component have its distinct set of governing equations and constitutive relations as a result that the vessel component is represented by two-fluid three-field model, and the one-dimensional component is represented by two-fluid (two-field) model. The benefit of each model and it's adequacy to the component have been discussed in Section 1 and Section 3 of the topical report. Inside the WCOBRA/TRAC-TF2 code, the vessel component and the one-dimensional component are solved by a different set of FORTRAN modules with the two components only coupled at the 1D/3D junctions. Section 3.6 of the topical report explained the coupling between the one-dimensional component and the vessel component. Due to the same physical laws governing the two phase flow, part of the formulas in the one-dimensional component and the vessel component share the same model, while some correlations are adjusted to address different concerns in the reactor pressure vessel and the reactor coolant system.

The details of flow regime maps, interfacial momentum transfer models, and interfacial heat transfer models, including formulas, technical basis, and scaling discussions, have been provided in Section 4, Section 5 and Section 6, respectively, in the topical report.

Note the churn turbulent flow regime is absent from Table 4.1-1. The current version of the WCOBRA/TRAC-TF2 code does not output the flow regime indicator for the churn turbulent flow regime to users. It is acceptable because of the insignificance of the churn turbulent flow regime in the PWR LOCA simulation.

a,c

Figure 4.1-1 Comparison of WCOBRA/TRAC-TF2 bubbly flow model with the Zuber-Findlay model with $C_0=1.2$. ($P=40$ psia, pipe ID=1.0 ft)

a,c

Figure 4.1-2 Comparison of WCOBRA/TRAC-TF2 bubbly flow model with the Zuber-Findlay model with $C_0=1.2$. ($P=1000$ psia, pipe ID=1.0 ft)

a,c

Figure 4.1-3 Comparison of reactor vessel inventories in ROSA SB-CL-18 with different large bubble radius limits.

a,c

Figure 4.1-4 Comparison of heater rod peak cladding temperatures in ROSA SB-CL-18 with different large bubble radius limits.

a,c

Figure 4.1-5 Comparison of reactor vessel inventories in Beaver Valley Unit 1 2.6 inch SBLOCA with different large bubble radius limits.

a,c

Figure 4.1-6 Comparison of fuel rod peak cladding temperatures in Beaver Valley Unit 1 2.6 inch SBLOCA with different large bubble radius limits.

References

- 4.1-1. Wallis, G.B., One-Dimensional Two-Phase Flow, 1969.
- 4.1-2. Ishii, M., and Hibiki, T., Thermo-Fluid Dynamics of Two-Phase Flow, 2ed, Springer, 2011.
- 4.1-3. Liles, et al., "TRAC-PF1/MOD1 Correlations and Models", NUREG/CR-5069, 1988.
- 4.1-4. Dimenna, R.A., et al., "RELAP5/MOD2 Models and Correlations," NUREG/CR-5194, 1988.
- 4.1-5. NUREG/CR-5535, Rev.1, Vol.4, "RELAP5/MOD3.3 Code Manual, Models and Correlations," 2001.
- 4.1-6. Salko, R., and Avramova, M.N., CTF Theory Manual, The Pennsylvania State University, 2012.
- 4.1-7. NAI 8907-06 Rev. 17, "GOTHIC Containment Analysis Package Technical Manual," EPRI, 2009.
- 4.1-8. LA-UR-00-910, TRAC-M/FORTRAN 90 (Version 3.0) Theory Manual, Los Alamos National Laboratory, 2000.
- 4.1-9. Richter, H.J., et al., Effect of Scale on Two-Phase Counter-Current Flow Flooding, NUREG/CR-0312, 1979.
- 4.1-10. Zuber, N., and Findlay, J.A., "Average Volumetric Concentration in Two-Phase Flow Systems," Journal of Heat Transfer, pp.453-468, 1965.
- 4.1-11. LTR-NRC-13-37, Submittal of Westinghouse Responses to "WCAP-16996-P, 'Realistic LOCA Evaluation Methodology Applied to the Full Spectrum of Break Sizes (FULL SPECTRUM LOCA Methodology)' Request for Additional Information" (Proprietary/Non-Proprietary), Project 700, TAC No. ME5244 dated June 5, 2013.
- 4.1-12. LTR-NRC-13-73, Submittal of Westinghouse Responses to "WCAP-16996-P, 'Realistic LOCA Evaluation Methodology Applied to the Full Spectrum of Break Sizes (FULL SPECTRUM LOCA Methodology)' Request for Additional Information – RAIs 46 – 58, 75 and 77" (Proprietary/Non-Proprietary), Project 700, TAC No. ME5244, dated October 28, 2013.

4.2 RAI 60

Question #60 Pressurized Water Reactor Core Two-Phase Mixture Level and Sensitivity to Axial Nodalization

WCAP-16996-P/WCAP-16996-NP, Volumes I, II, and III, Revision 0, Subsection 13.3, "WCOBRA/TRAC-TF2 Determination of the Mixture Level," explains that "WCOBRA/TRAC-TF2 does not include a specific model or pointer to identify the exact location of the mixture level. Rather, mixture level tracking is accomplished through detailed nodalization." It continues to say that " ... the ability of WCOBRA/TRAC-TF2 to track a mixture level is dependent upon the axial noding. In the core, the typical height of a hydraulic cell is 10 to 12 inches." With regard to the WCOBRA/TRAC-TF2 axial core noding strategy, Subsection 26.1.2, "Modeling Consistency," of WCAP-16996-P/WCAP-16996-NP, Volumes I, II, and III, Revision 0, explains that "the axial noding in a PWR core and in tests with simulated cores is established by the overall heated length and the location of spacer grids." According to noding details provided in Table 26.1-1, "Core Section Axial Cell Lengths," the PWR core models for V. C. Summer (CGE) and Beaver Valley Unit 1 (DLW), considered in Volume III, employed 14 axial cells with a minimum cell length of 7.78 in and 7.46 in, correspondingly, and a maximum cell length of 12.84 in. It is stated in Subsection 26.1.2 of WCAP-16996-P/WCAP-16996-NP, Volumes I, II and III, Revision 0, that "the average cell heights for all of the test models and the plant models fall within a narrow range."

NRC Regulatory Guide (RG) 1.157, Revision 0, "Best-Estimate Calculations of Emergency Core Cooling System Performance," requires that "sensitivity studies and evaluations of the uncertainty introduced by noding should be performed."

- (1) Please describe assessment studies that have been performed to examine sensitivity effects related to core axial nodalization on the mixture level predictions by WCOBRA/TRAC-TF2 under conditions of interest for SBLOCA analyses. Results from such studies should include quantification of nodalization effects on core mixture level predictions and the resulting impact on peak clad temperature predictions in WCOBRA/TRAC-TF2 analyses of test facilities and plant SBLOCA transients.
- (2) It is recognized that with cell heights of 10-12 inches, a very small quantity of liquid in the cell containing the two-phase level will cause the entire cell to saturate, thus greatly reducing the PCT as the mixture level is not tracked nor used to determine the axial elevation of the uncovered region in the core. Please explain the impact of cell height on PCT considering a cell containing the two-phase mixture surface when the mixture level is any small finite distance above the bottom interface of this cell. Given such possible circumstances and taking into account the fact that the two-phase mixture level is not tracked, it appears that finer axial nodalization involving many more cells is needed to properly capture the location of the two-phase mixture surface and the degree of superheat that is associated with the cell containing the mixture level once core uncover begins.

Response:

The response to this RAI is provided in Section 2 of this letter.

4.3 RAI 61

Question #61 Oak Ridge National Laboratory Thermal Hydraulic Test Facility Mixture Level Predictions and Axial Nodalization Sensitivity

WCAP-16996-P/WCAP-16996-NP, Volumes I, II, and III, Revision 0, Subsection 13.4.2, "ORNL-THTF Small Break Tests," presents WCOBRA/TRAC-TF2 prediction results for ORNL THTF tests. The analyzed tests include six bundle uncover tests (3.09.10I, 3.09.10J, 3.09.10K, 3.09.10L, 3.09.10M, 3.09.10N) and six level swell tests (3.09.10AA, 3.09.10BB, 3.09.10CC, 3.09.10DD, 3.09.10EE, 3.09.10FF) described in NUREG/CR-2456 (March 1982).

Figure 1.3.4.2-3, "WCOBRA/TRAC-TF2 Model of the ORNL-THTF," shows the noding of the WCOBRA/TRAC-TF2 model of ORNL THTF. [

] ^{a,c}

Subsection 13.4.2.5, "WCOBRA/TRAC-TF2 Model of the ORNL-THTF," also explains that "This section is divided into twelve axial nodes, in a manner consistent with the PWR core noding (Subsection 26.1.2, WCAP-16996-P/WCAP-16996-NP, Volumes I, II, and III, Revision 0, Volume III)." According to Table 26.1-1, "Core Section Axial Cell Lengths," all cells have practically an identical axial length of 12 inches.

- (1) Figures 13.4.2-4 through 13.4.2-15 show the results of WCOBRA/TRAC-TF2 void predictions for all 12 analyzed ORNL THTF bundle uncover and level swell tests. Please explain how the predicted void profiles shown in these figures relate to Channel 2 and Channel 3 results in the described WCOBRA/TRAC-TF2 THTF model.
- (2) Please provide results from a noding sensitivity study performed with WCOBRA/TRAC-TF2 when using "nominal" two-phase flow correlations (no bias or sampling) with the number of cells modeling the heated bundle length set to 24 and 48. The axial length of each cell in Section 2 of the ORNL THTF model shown in Figure 13.4.2-3 would amount to 6 and 3 inches, respectively. Include axial void fraction distribution, two-phase mixture level, and collapsed liquid level predictions as well as vapor and wall temperature profiles for the uncovered-bundle heat transfer tests. Compare the sensitivity results against those obtained with a cell height of 12 inches and presented in Figures 13.4.2-4 through 13.4.2-15 as well as against measured test data. In all comparisons, please use results that are representative for the entire test bundle flow area.
- (3) In analyzing WCOBRA/TRAC-TF2 capabilities in predicting level swell, Section 13, "Core Void Distribution and Mixture Level Swell," makes use of a mixture level swell parameter, S . This parameter is defined by Equation (13-1) through the two-phase mixture level, $Z_{2\phi}$, the elevation where the liquid reaches the saturation point, Z_{SAT} , and the collapsed liquid level,

Z_{CLL} , as follows:

$$S = [(Z_{2\Phi} - Z_{SAT}) - (Z_{CLL} - Z_{SAT})] / (Z_{CLL} - Z_{SAT}).$$

Please explain the way in which quantities $Z_{2\Phi}$ and Z_{SAT} are determined from code results and assess their uncertainties considering nodalization effects. Assess and provide the uncertainty of S that results from uncertainties associated with $Z_{2\Phi}$ and Z_{SAT} .

- (4) Please provide code results for the two-phase mixture levels in the THTF test bundle that are determined with the assumption that the void fraction in the computational cell containing the two-phase mixture level is equal to the void fraction in the neighboring cell located flow upstream. Compare the computed two-phase mixture levels against the measured data. Include data uncertainty bars in the comparison figures.

Response:

The response to this RAI is provided in Section 2 of this letter.

4.4 RAI 62

Question #62: Oak Ridge National Laboratory Thermal Hydraulic Test Facility WCOBRA/TRAC-TF2 Detailed Prediction Results

WCAP-16996-P/WCAP-16996-NP, Volumes I, II, and III, Revision 0, Subsection 13.4.2, "ORNL-THTF Small Break Tests," presents WCOBRA/TRAC-TF2 prediction results for ORNL THTF tests that included six bundle uncover tests (3.09.10I, 3.09.10J, 3.09.10K, 3.09.10L, 3.09.10M, 3.09.10N) and six level swell tests (3.09.10AA, 3.09.10BB, 3.09.10CC, 3.09.10DD, 3.09.10EE, 3.09.10FF).

To illustrate the performance of WCOBRA/TRAC-TF2 two-phase flow models, including flow regime maps, employed by the vessel component to predict the thermal hydraulic response of the reactor core region, please provide code prediction results for two THTF bundle uncover tests: 3.09.10J performed at 610 psia and 3.09.10M performed at 1,010 psia, and two level swell tests: 3.09.10AA at 590 psia and 3.09.10DD at 1,170 psia. For these tests, please provide code prediction results identified below and obtained with WCOBRA/TRAC-TF2 using "nominal" two-phase flow correlations (no bias or sampling) and the existing THTF model shown in Figure 13.4.2-3. Please include the following parameters: (1) predicted flow regime with flow regime indicator number, (2) pressure, (3) fluid phase temperatures, (4) wall temperature, (5) void fraction and its attributed components (e.g., SB, large bubbles, slugs, continuous field), (6) diameter and number of bubbles in each category (small, large), (7) liquid fraction and its attributed components (e.g., entrained drops, film, slugs, continuous field), (8) diameter and number of droplets, (9) phase mass flow rates for each field, and (10) phase velocities for each field and relative velocities as used in any related constitutive equation, e.g., Equation (4-15).

Please present the results in a table format for each of the twelve cells or associated interfaces, as appropriate, with the cells listed in the first column and each of the above parameters provided in a separate column. Please provide results that are representative for the entire test bundle cross sectional flow area based on results for individual channels.

Response:

The requested information was reviewed during an NRC audit of the WCOBRA/TRAC-TF2 calculations in July 2013 per LTR-NRC-13-70 (Reference 4.4-1).

Reference(s)

- 4.4-1. LTR-NRC-13-70, "Summary of July 2013 NRC Code Workshop and August 2013 NRC Audit of the FULL SPECTRUM LOCA (FSLOCA) Evaluation Model (Proprietary/Non-Proprietary)," October 10, 2013.

4.5 RAI 63

Question #63: Interfacial Drag Correlations in WCOBRA/TRAC-TF2

WCAP-16996-P/WCAP-16996-NP, Volumes I, II, and III, Revision 0, Subsection 5.4, "Vessel Component Interfacial Shear Models," describes the relationships used in WCOBRA/TRAC-TF2 to quantify interfacial friction forces between flow fields in various two-phase flow regimes by means of interfacial drag coefficients. The interfacial drag forces appear in the vessel component momentum conservation equations described in WCAP-16996-P/WCAP-16996-NP, Volumes I, II, and III, Revision 0, Section 3. The interfacial drag coefficients are calculated in subroutine INTFR to yield the average interfacial drag force per unit length when multiplied by the new time velocity difference between the fluid phases. Thus, Equation (5-42) defines the average interfacial drag force, F_D , exerted on the continuous liquid phase by vapor per unit length along the X axis, $F_D / \Delta X = \tau'_{iX, vl}$, as a product of the flow regime dependent interfacial drag coefficient, $K_{iX, v}$, and the axial relative velocity between the vapor and the continuous liquid, \underline{U}_{vl} :

$$F_D / \Delta X = \tau'_{iX, vl} = K_{iX, vl} \underline{U}_{vl}.$$

Thus defined dimensional drag coefficient, $K_{iX, vl}$, is calculated using a dimensionless drag coefficient, C_{Db} , commonly used in the literature. Equation (5-45) provides the relationship between $K_{iX, vl}$ and C_{Db} for a bubbly flow as:

$$K_{iX, vl} = C_{Db} \rho_l \underline{U}_{vl} A_{P,b} / 2 \Delta X ,$$

where $A_{P,b}$ is the total projected area of all bubbles in the volume. From the above equations, the drag force, F_D , is obtained from the dimensionless drag coefficient, C_{Db} , and relative velocity, \underline{U}_{vl} :

$$F_D = C_{Db} \rho_l \underline{U}_{vl} \left| \underline{U}_{vl} \right| A_{P,b} / 2.$$

Subsections 5.4.1 through 5.4.4 present the WCOBRA/TRAC-TF2 approach to interfacial drag calculation for vessel component "Cold Wall" two-phase flow regimes. Table 1 summarizes this modeling approach.

Table 1: WCOBRA/TRAC-TF2 Approach to Interfacial Drag for Vessel Component "Cold Wall" Two-Phase Flow Regimes

Flow Regime	Void Fraction α (%)	Major Constitutive Correlations	Note
Small Bubble	$0 < \alpha \leq 20$	$C_{Db} = 24 / Re_b (1 + 0.1 Re_b^{0.75})$	Equation (5-50)
		$C_{Db} = (2/9)^{1/2} N_{\mu} Re'_b (1 - \alpha_v)^2$	Equation (5-53)
		$C_{Db} = (8/3) (1 - \alpha_v)^2$	Equation (5-57)
		$C_{Db} = 0.45 (1 - \alpha_v)^2$	Equation (5-58)

Small-to-Large Bubble	$20 < \alpha \leq 50$	$C'_{Db} = C_{Db} (1 - \alpha_v)^2$ Interpolation between small bubble drag at 20% void and large bubble drag at 50% void.	Equation (5-71)
Churn-Turbulent	$50 < \alpha \leq \alpha_{crit}$	Interpolation between large bubble drag at 50% void and film/drop interfacial drag.	Equation (5-78)
Film/Drop	$\alpha_{crit} < \alpha \leq 100$	$f_{i,W} = 0.005[1+75(1 - \alpha_v)]$ $f_{i,W}^{a,c}$	Equation (5-92)

In a SB regime, the interfacial drag between the continuous liquid and the vapor is calculated from Equations (5-67a). For a SLB regime, the interfacial drag between the continuous liquid and vapor is calculated by interpolation between the SB drag at 20 percent void and the Large Bubble (LB) drag at 50 percent void in accordance with Equations (5-74a) and (5-74b). Similarly, for a CT flow, the drag is assumed to be a linear combination between the LB drag and the FD drag according to Equation (5-78). In a FD regime with a stable liquid film, the interfacial friction factor is calculated using Equation (5-92). In the case of an unstable wall film,

$f_{i,W}^{a,c}$

- (1) WCAP-16996-P/WCAP-16996-NP, Volumes I, II, and III, Revision 0, does not provide a complete description of individual interfacial drag correlations as implemented in the vessel component interfacial shear models. Thus, WCAP-16996-P/WCAP-16996-NP, Volumes I, II, and III, Revision 0, does not define applicability ranges for individual interfacial drag correlations nor does it provide supporting data and analysis that demonstrate the technical bases for individual models. Important description characteristics include, among others, applicability ranges for participating parameters, possible extrapolation beyond ranges for which correlations were developed or assessed and associated limitations, availability and quality of supporting test data and validation analyses, relevant source references as appropriate. Please provide a table that describes the interfacial drag correlations implemented in the two-phase flow regimes of the vessel component "Cold Wall" flow map. For each individual constitutive correlation, please describe the following items: (1) expressions for the dimensionless drag coefficient for an individual flow element (bubble, droplet, slug, film) in a form allowable to calculate drag force using element's characteristics such as projected cross-sectional or interfacial area and an appropriate relative velocity, (2) source references as appropriate, (3) applicability ranges for defining parameters, (4) extrapolation outside of applicability ranges as applicable and associated limitations, (5) qualified available test data, and (6) references to validation analyses.

Please include description for each item (1) to (6) above in a separate column with each constitutive correlation described in a separate row. Closure relations that are based on interpolation between distinct constitutive correlations should be provided at the end of the table following the description of all other constitutive correlations. Please define all participating quantities including participating dimensionless numbers, thermodynamic fluid

properties, and experimentally determined parameters. State and explain code implementation assumptions including phenomenological considerations related to treatment of characteristic sizes (e.g., bubble diameter or film thickness), ensemble numbers (e.g., number of drops or bubbles), distributions and categories (e.g., size distribution, large versus small bubbles). Please identify any quantities that are nodalization or input dependant or have other implementation conditions and restrictions.

- (2) Please provide information for the interfacial drag constitutive correlations implemented in the two-phase flow regimes of the vessel component "Hot Wall" flow map as requested in item (1) above for the "Cold Wall" flow map.
- (3) Please provide information for the interfacial drag constitutive correlations implemented in the drag models considered in Subsection 5.7, "One-Dimensional Component Interfacial Drag Models," for the one-dimensional component flow map as requested in item (1) above for the vessel component "Cold Wall" flow map.
- (4) Please provide the information related to items (1) to (3) above using a consistent nomenclature set with units for included dimensional parameters.

Response:

Table 1 in RAI Question #63 should be corrected as follows:

Table 1: WCOBRA/TRAC-TF2 Approach to Interfacial Drag for Vessel Component "Cold Wall"
Two-Phase Flow Regimes

Flow Regime	Void Fraction α (%)	Major Constitutive Correlations	Note
Small Bubble	$0 < \alpha \leq 20$	$C_{Db} = 24/Re_b (1+0.1Re_b^{0.75})$ $C_{Db} = (2/9)^{1/2} N_\mu Re'_b (1-\alpha_v)^2$ $C_{Db} = (8/3) (1-\alpha_v)^2$	Equation (5-50) Equation (5-53) Equation (5-57)
Small-to-Large Bubble	$20 < \alpha \leq 50$	$C'_{Db} = C_{Db} (1-\alpha_v)^2 = 24/Re_b (1+0.1Re_b^{0.75}) \cdot (1-\alpha_v)^2$ $C_{Db} = 0.45 (1-\alpha_v)^2$ Interpolation between small bubble drag and large bubble drag at local void fraction, using the interpolation factor defined as $F_{SB} = \alpha_{SB} (1-\alpha_v)/(1-\alpha_{SB})/\alpha_v$	Equation (5-71) Equation (5-58) Equation (5-76)
Churn-Turbulent	$50 < \alpha \leq \alpha_{crit}$	Interpolation between small to large bubble drag and film/drop interfacial drag at local void fraction, using the factor defined as $F_{CT} = (\alpha_v - \alpha_{LB})/(\alpha_{crit} - \alpha_{LB})$	Equation (5-78) Equation (5-79)
Film/Drop	$\alpha_{crit} < \alpha \leq 100$	$f_{i,w} = 0.005[1+75(1-\alpha_v)]$ $[\quad]^{a,c}$	Equation (5-92)

The other information is not provided in tabular format as it is available in the topical report as supplemented by the RAI responses.

4.6 RAI 64

Question #64: Interfacial Area in Inverted Slug Flow

WCAP-16996-P/WCAP-16996-NP, Volumes I, II, and III, Revision 0, Subsection 5.4.6, "Inverted Liquid Slug Regime," explains that for the liquid slug regime "the interfacial area is calculated assuming that the liquid slugs are spherical, and have a diameter []^{a,c} of the channel diameter, as described in WCAP-16996-P/WCAP-16996-NP, Volumes I, II and III, Revision 0, Section 4.3.3. The interfacial area is specified in Equation (5-104) as:

$$A_{i,IVS} = 4A_x\alpha_i / D_h .$$

Assuming that the above expression provides the interfacial slug area per unit length along the X axis, the volumetric concentration for the slug interfacial area is obtained from Equation (5-104):

$$A'''_{i,IVS} = A_{i,IVS} / A_x = 4\alpha_i / D_h .$$

WCAP-16996-P/WCAP-16996-NP, Volumes I, II, and III, Revision 0, Subsection 4.3.3, "Inverted Liquid Slug Flow Regime," estimates the interfacial area for the liquid slugs making the same assumption that continuous liquid slugs are spherical. An expression for the volumetric interfacial area concentration is provided in Equation (4-58):

$$A'''_{i,S} = 6\alpha_i / D_S .$$

Using the assumption that "the slugs have a diameter []^{a,c}" the volumetric concentration for the slug interfacial area is provided in Equation (4-59):

$$[]^{a,c}$$

The above assumed slug diameter of []^{a,c} is practically identical to a slug diameter of "[]^{a,c} of the channel diameter" used in WCAP-16996-P/WCAP-16996-NP, Volumes I, II, and III, Revision 0, Subsection 5.4.6.

From the above expressions for the volumetric concentration for the slug interfacial area, the ratio of the volumetric concentration for the slug interfacial area provided in WCAP-16996-P/WCAP-16996-NP, Volumes I, II, and III, Revision 0, Subsection 4.3.3, Equation (4-58) to the same quantity given in WCAP-16996-P/WCAP-16996-NP, Volumes I, II, and III, Revision 0, Subsection 5.4.6, Equation (5-104) is determined to be:

$$[]^{a,c}$$

Please explain why the slug interfacial area volumetric concentrations for the Inverted Liquid Slug flow regime, as defined in WCAP-16996-P/WCAP-16996-NP, Volumes I, II, and III, Revision 0, Subsection 4.3.3, "Inverted Liquid Slug Flow Regime," and Subsection 5.4.6, "Inverted Liquid Slug Regime," differ by []^{a,c} Please take into consideration that it

appears, as discussed above, that practically identical assumptions have been introduced and used for determining the slug interfacial area volumetric concentrations in both subsections.

Response:

The WCOBRA/TRAC-TF2 vapor/liquid film drag coefficient for Inverted Liquid Slug regime is defined as [Equation (5-103), Reference 4.6-1]

$$[\quad]^{a,c} \quad \text{RAI.64-1}$$

in which the interfacial friction coefficient $f_{i,IVS}$ is $[\quad]^{a,c}$ times the Wallis (Reference 4.6-2) equation given as Equation (5-92) of the Topical as follows:

$$[\quad]^{a,c} \quad \text{RAI.64-2}$$

Implicitly, WCOBRA/TRAC-TF2 means to model the interfacial drag force for the Inverted Annular Slug regime with $[\quad]^{a,c}$ times the Wallis equation is more than just defining the interfacial drag coefficient as shown in Equation RAI.64-2. The Wallis interfacial drag force is defined as Equation RAI.64-3 below as a function of interfacial drag coefficient, velocity head (based on relative velocity) and interfacial area, which is the general form of the interfacial drag force shown in most of the technical publications.

$$\tau_i = f_i \times \frac{\rho_v U_r^2}{2} \times A_i \quad \text{RAI.64-3}$$

In comparison with RAI.64-4, WCOBRA/TRAC-TF2 calculates the interfacial drag force (force per unit length) as:

$$[\quad]^{a,c} \quad \text{RAI.64-4}$$

As can be seen, there is a difference of a factor of 2 for the WCOBRA/TRAC-TF2 interfacial drag force equation, RAI.64-4, in comparison with the calculation of the drag force using the Wallis equation (Equation RAI.64-3). Therefore, in order to calculate the equivalent interfacial drag force using RAI.64-3 and RAI.64-4, the term $A_{i,IVS}$ in Equation RAI.64-4 should be calculated as half of the interfacial area, since $f_{i,IVS}$ is coded in WCOBRA/TRAC-TF2 as Equation RAI.64-2. The interfacial area for the Inverted Liquid Slug regime is defined in Equation (4-60) in Section 4.3.3 of the Topical, which can be converted to interfacial area per unit length and results in:

[

]^{a,c}

RAI.64-5

The $A_{i,IVS}$ derived as RAI.64-5 is the same as Equation (5-104) in Section 5 of the Topical.

Please note that Equation RAI.64-1 corrects the typographic error of $K_{iX,IVS}$ in Equation (5-103) in the Topical, which will be incorporated in the revised Section 5.4 of the Topical included in Section 5 of this letter.

Reference(s)

- 4.6-1. WCAP-16996-P, "Realistic LOCA Evaluation Methodology Applied to the Full Spectrum of Break Sizes (FULL SPECTRUM LOCA Methodology)," November 2010.
- 4.6-2. Wallis, G.B., One-Dimensional Two-Phase Flow, 1969.

4.7 RAI 65

Question #65: Interfacial Drag for Inverted Slug Flow

WCAP-16996-P/WCAP-16996-NP, Volumes I, II and III, Revision 0, Subsection 5.4.6, "Inverted Liquid Slug Regime," defines the interfacial drag coefficient for this "Hot Wall" flow regime in Equation (5-103):

$$K_{iX,IVS} = f_{i,IVS} \rho_v |\underline{U}_{vl}| A_{i,IVS} .$$

WCAP-16996-P/WCAP-16996-NP, Volumes I, II, and III, Revision 0, Subsection 5.4.6 explains that the interfacial friction factor "is calculated assuming an unstable liquid film surface exists on the large liquid ligaments or drops." To account for such flow conditions, the friction factor is assumed to be a factor []^{a,c} compared to the friction factor for stable liquid films defined in Equation (5-92) for the FD flow regime. Thus, Equation (5-102) provides the interfacial friction factor for Inverted Slug flow as:

$$[]^{a,c}$$

The interfacial slug area per unit length of the flow is defined in Equation (5-104):

$$A_{i,IVS} = 4A_X \alpha_i / D_h .$$

Further, Equation (5-105) calculates the interfacial drag coefficient, $K_{iX,vl,IVS}$, as the maximum value from two different expressions as follows:

$$[]^{a,c}$$

- (1) Please provide the technical basis for calculating the interfacial friction factor for unstable liquid films for Inverted Slug flow. In particular, please explain the basis for the assumed factor of []^{a,c} between the Inverted Slug liquid film friction coefficient, $f_{iX,IVS}$, given by Equation (5-102), and the annular film friction coefficient, $f_{i,W}$, defined by Equation (5-92).
- (2) Equation (5-105) that defines the interfacial friction factor in Inverted Slug flow $K_{iX,vl,IVS}$, as the maximum value from two expressions. As given, the first expression is provided by Equation (5-104), which defines the interfacial slug area as discussed above. At the same time, the second expression:

$$[]^{a,c}$$

does not include a relative velocity $|\underline{U}_{vl}|$, which is used in defining the interfacial drag coefficient, according to Equations (5-81), (5-103) and others. Please explain this apparent inconsistency. If necessary, please make corrections and provide justifications.

- (3) The interfacial drag coefficient is denoted in Equation (5-103) of WCAP-16996-P/WCAP-16996-NP, Volumes I, II, and III, Revision 0, Subsection 5.4.6 as $K_{iX,IVS}$ and, in Equation (5-105), as $K_{iX,vl,IVS}$. Please explain if both notations refer to the same parameter and, if

so, why the nomenclature is not consistent.

Response:

- (1) The factor of []^{a,c} between the Inverted Slug liquid film friction coefficient given by Equation (5-102) of Reference 4.7-1 does not have theoretical basis, it is instead ad hoc in the simple drag model of inverted annular/liquid slug hot wall flow regimes. The hot wall flow regimes occur in the refill and reflood periods at the core entrance region in LBLOCA transients. At beginning of the reflood, liquid enters into the core to cool the heated rod where inverted annular/liquid slug regimes occur downstream of the progressing rod quench front until the liquid in the inner region is all entrained in the vapor stream as droplets and the flow regime goes into Dispersed Droplet regime.

The interfacial drag model of the WCOBRA/TRAC-TF2 hot wall flow regimes is shown to be capable of adequately predicting the thermal hydraulics response of the reflood validation tests, as seen in three series of FLECHT reflood tests, as documented in Sections 15.6.1, 15.6.2, 15.6.3 and 19.5 of the Topical, and Cylindrical Core Test Facility (CCTF) test (Section 19.6 of the Topical).

The hot wall interfacial drag model directly influences the prediction of the void distribution in the core during the reflood phase, during which inverted annular/ liquid slug and dispersed drop regimes occur sequentially downstream of the progressing quench front with each regime lasting varied duration of time depending on the flooding rate, liquid subcooling, pressure and rod power. Except for the forced reflood test with the extremely high flooding rate, the core pressure drop is mostly attributed to the hydrostatic head of the vessel fluid and a good indicator of the integrated void distribution in the core. The WCOBRA/TRAC-TF2 simulations of the FLECHT reflood test are presented in Sections 15.6.1, 15.6.2 and 15.6.3 of the Topical where the comparison of the pressure drop measurement of the lower core, upper core and total core between the test measurement and code prediction shows satisfactory performance of the WCOBRA/TRAC-TF2 hot wall drag model in predicting the core void fraction. The same conclusion is also supported by comparing the differential pressure from the lower plenum to the upper plenum in the WCOBRA/TRAC-TF2 simulation of the CCTF reflood test (Figure 19.6-26, Section 19.6 of the Topical).

The drag model also impacts the entrainment during reflood which impacts the quench front progression and rod heat up. Specific to reflood entrainment, the WCOBRA/TRAC-TF2 drag model, altogether with its entrainment model and heat transfer model is demonstrated to perform adequately in predicting the FLECHT test carryover fraction as documented in Section 19.5 of the Topical.

- (2) There is no physical basis for the limit shown in Equation (5-105) of the Topical. It serves as an upper bound to the relative velocity, which is expected to be much larger than the calculated relative velocity in the Inverted Liquid Slug regime and only used rarely in WCOBRA/TRAC-TF2. This limit is part of the simple interfacial drag models used in WCOBRA/TRAC-TF2 for inverted liquid slug regime, and the overall hot wall drag model comprising inverted annular/liquid slug, dispersed droplet flow regimes is validated only as a whole using the FLECTH reflood tests as discussed in item (1) above, without specific validation on individual regimes and each part of the model. Please refer to Item (1) above for the discussion of the validation of the WCOBRA/TRAC-TF2 Inverted Liquid Slug regime.
- (3) Instances of typographic errors were identified in Equations (5-103) and (5-105) in Section 5 of Reference 4.7-1, which should be respectively corrected as follows:

$$[\qquad \qquad \qquad]^{a,c} \qquad (5-1)$$

$$[\qquad \qquad \qquad]^{a,c} \qquad (5-2)$$

Reference(s)

- 4.7-1. WCAP-16996-P, "Realistic LOCA Evaluation Methodology Applied to the Full Spectrum of Break Sizes (FULL SPECTRUM LOCA Methodology)," November 2010.

4.8 RAI 66

Question #66: Annular Film Flow Interfacial Drag

In a FD flow regime, the interfacial drag "between the vapor and continuous liquid for the wetted wall film flow regime" is calculated from Equation (5-81) in WCAP-16996-P/WCAP-16996-NP, Volumes I, II, and III, Revision 0, Subsection 5.4.4, "Film/Drop Flow Regime: Model Basis":

[]^{a,c}

The subsection clarifies that "when the vapor content in the flow exceeds a critical void fraction, and the wall is below the wetted wall temperature criteria, the film is assumed to become stable and liquid can no longer bridge the channel."

WCAP-16996-P/WCAP-16996-NP, Volumes I, II, and III, Revision 0, Subsection 5.4.4, "Film/Drop Flow Regime: Model as Coded," defines the interfacial drag also in Equation (5-94) as follows:

[]^{a,c}

The interfacial drag coefficient in the Falling Film regime of the "Hot Wall" flow map, $K_{IX,IV,FF}$, provided in Equation (5-114) in Subsection 5.4.8, "Falling Film Flow Regime," of WCAP-16996-P/WCAP-16996-NP, Volumes I, II, and III, Revision 0, is defined in a way consistent with Equation (5-94) above.

[]^{a,c}

[]^{a,c}

[]^{a,c}

[]^{a,c}

(1) As Equation (5-81) and Equation (5-94) apparently define the same interfacial drag quantity, please clarify if the parameters appearing on the right-hand side of these two equations and standing for the interfacial friction factor, relative velocity and interfacial area are defined in the same manner and mean the same physical quantity. If this is the case, please explain why different nomenclature is used in both equations. Please examine the nomenclature and revise as needed so that it is appropriately consistent throughout Volume I of the WCAP-16996-P/WCAP-16996-NP, Volumes I, II, and III, Revision 0 TR.

(2) If Equation (5-81) and Equation (5-94) define the same interfacial drag quantity, please

explain why the interfacial drag from Equation (5-81) and that from Equation (5-94) differ by a factor of 2:

$$[K_{iX,vi,FD} \text{ from Equation (5-94)}] / [K_{iX,vi,FD} \text{ from Equation (5-81)}] = 2.$$

- (3) Please provide the ranges of applicability for the interfacial friction factors as given by Equation (5-92) and attributed to stable films in annular flow and by Equation (5-86) and attributed to unstable films in co-current and countercurrent film flow. Please define the applicability range for each participating parameter. Describe the test conditions for the data that were used to develop these two correlations. Please compare these applicability ranges to typical flow conditions of interest for PWR LOCA analysis.
- (4) Please provide the technical basis for calculating the interfacial friction factor for unstable liquid films using Equation (5-90) as described in Subsection 5.4.4, "Film/Drop Flow Regime: Model as Coded."
- (5) According to WCAP-16996-P/WCAP-16996-NP, Volumes I, II, and III, Revision 0, Subsection 5.4.4, "Film/Drop Flow Regime: Model as Coded," the interfacial friction factor for unstable films is defined as []^{a,c} At the same time, WCAP-16996-P/WCAP-16996-NP, Volumes I, II, and III, Revision 0, Subsection 5.4.6, "Inverted Liquid Slug Regime," defines the interfacial friction factor in the case of an unstable liquid film surface as []^{a,c} times the annular flow friction factor defined in Equation (5-92) for stable liquid films in the FD flow regime. Please explain this discrepancy and compare the relevant technical bases used to demonstrate the validity of WCOBRA/TRAC-TF2 interfacial drag models for unstable liquid films as implemented in the FD flow of the "Cold Wall" flow regime map and in the Inverted Slug flow of the "Hot Wall" flow map.
- (6) Please describe availability and quality of test data, describing two-phase film flow, and any supporting analyses performed to demonstrate the applicability of WCOBRA/TRAC-TF2 interfacial drag models for FD flow prediction. Identify references for such validation analyses, if available, including source references for applied film flow test data. Present comparisons between model predictions for the friction factor and test data under typical conditions of relevance to PWR LOCA analyses.

Response:

- (1) Equations (5-81) and (5-94) in Section 5 of Reference 4.8-1 define the interfacial drag coefficients differing by a factor of []^{a,c}, albeit calculating the identical drag force. Equation (5-81) uses a more general form of interfacial drag coefficient as it typically shows in the technical publications, while Equation (5-94) defines an interfacial drag coefficient more in line with the interfacial drag coefficient variable for Film/Drop flow regime in the WCOBRA/TRAC-TF2 source code.

The drag coefficient $f_{iX,FD}$ in Equation (5-94) of Reference 4.8-1 is coded in WCOBRA/TRAC-TF2 as:

$$\left[\frac{1}{1 + 0.00015 \left(\frac{G}{G_{crit}} \right)^2} \right]^{a,c} \quad \text{RAI.66-1}$$

which is equivalent to $\left[\frac{1}{1 + 0.00015 \left(\frac{G}{G_{crit}} \right)^2} \right]^{a,c}$ times the coefficient developed by Wallis, shown as Equation (5-92) of Reference 4.8-1, taking into account the factor of $\left[\frac{1}{1 + 0.00015 \left(\frac{G}{G_{crit}} \right)^2} \right]^{a,c}$ in Equations (5-81) and (5-94) therein.

- (2) See explanation in (1) above.
- (3) The WC/T-TF2 interfacial drag coefficients for stable and unstable films are justified in Reference 4.8-2, in which the documented discussion justified the extension of the applicable ranges of the original models for WCOBRA/TRAC's intended applications, comparing the model predictions to the Westinghouse test data from the test geometries typical of some PWR components.
- (4) In Section 5 of the Topical, Equation (5-90) is used in lieu of Equation (5-91) to calculate the unstable film interfacial drag coefficient in WCOBRA/TRAC-TF2 due to the reasonable agreement of the two equations (<15%) over a Reynolds number range of 5,000 to 100,000, as explained in the Topical in the paragraph below Equation (5-91).
- (5) The interfacial friction factor for the unstable film in the Film/Drop flow regime is limited to be at least $\left[\frac{1}{1 + 0.00015 \left(\frac{G}{G_{crit}} \right)^2} \right]^{a,c}$ times the Wallis correlation, which predicts reasonable pressure drop and void fraction in the simulation study documented in Reference 4.8-2 for Film/Drop flow regime.

In the Inverted Liquid Slug regime, WCOBRA/TRAC-TF2 defines the interfacial drag factor of unstable liquid film surface to be equivalent to $\left[\frac{1}{1 + 0.00015 \left(\frac{G}{G_{crit}} \right)^2} \right]^{a,c}$ times the Wallis correlation (see Section 4.7 of this letter for discussion). However, the appearance of similarity of the interfacial drag factors defined for the Film/Drop and Inverted Liquid Slug regimes to be based on Wallis equation and to account for the unstable liquid-vapor interface using an empirical factor is an unrelated coincidence. The Film/Drop regime occurs in high void fraction region ($\alpha > \alpha_{crit}$) while the inverted liquid slug regime typically exists before the void fraction gets too high, with 'flipped' phase distribution on the two sides of the vapor-liquid interface in the flow channel.

The Wallis correlation defines the interfacial friction coefficient to be a linear function of liquid fraction, as shown in Equation (5-92) of the Topical, to correlate the data of the impact of the liquid film thickness on the interfacial friction factor (Reference 4.8-3) in annular flow. The phase topology and interface geometry of the Film/Drop flow regime is similar to the annular flow regime for which the Wallis model was developed using low pressure air water data; however, an empirical multiplier to the Wallis model is adopted

in WCOBRA/TRAC-TF2 to model Film/Drop regime interfacial drag to account for the extended application range of the original Wallis model, as well as the different flow characteristics from the ideal annular flow of 'wavy' interface, for example the entrained liquid droplets.

The interfacial factors defined for Inverted Liquid Slug regime in WCOBRA/TRAC-TF2 using []^{a,c} times the Wallis correlation is an empirical ad hoc model intended to be applicable only in the range of conditions under which the model is validated against the test data. The validation of the WCOBRA/TRAC-TF2 Inverted Annular/Liquid Slug regime is discussed in subsection 4.7 of this letter.

- (6) The WCOBRA/TRAC-TF2 Film/Drop model is specifically justified by the study documented in Reference 4.8-2 [See item (3) above]. In addition, as one of the flow regimes encountered in all of the ORNL small break boil-off and level-swell test cases, WCOBRA/TRAC-TF2 predicts reasonably well the void fraction profiles of these tests in this regime which can be mostly attributed to the adequate Film/Drop interfacial model.

Reference(s)

- 4.8-1. WCAP-16996-P, "Realistic LOCA Evaluation Methodology Applied to the Full Spectrum of Break Sizes (FULL SPECTRUM LOCA Methodology)," November 2010.
- 4.8-2. Resolution of Requests for Additional Information for WCAP-12945-P, Volume 1 RAI No.68. (Included following this response)
- 4.8-3. Wallis, G.B., One-Dimensional Two-Phase Flow, 1969.

Reference 4.8-2

a,c

234

a,c

a,c

a,c

[

a,c

]

a,c

a,c

**Figure 68-1. Variation of Interfacial Friction Factor with N
Dimensional Film Thickness for Various Pipe
Diameters**

a,c

Figure 68-2. Comparison of Five Times Wallis f_1 (----) with correlation from reference 1.

Figure 68-3. Crosssection View of WDR and RCC Guide for APWR

a,c

Figure 68-4. Axial View of WDR Guide

a,c

Figure 68-5. Crossection Views of Typical Operating Plant Guide Tube.

Top Figure: Normal Plate geometry.

Bottom Figure: Plate geometry at bottom of Guide Tube

a,c

Figure 68-6. Flow Regimes in WDR and RCC Downflow Tests

a,c

Figure 68-7. Predicted vs Measured Static Pressure Gradient in the WDR Guide During Two Phase Downflow.

a,c

**Figure 68-8. Predicted vs Measured Static Pressure Difference
for Various Flow Qualities in the WDR Guide.**

a,c

**Figure 68-9. Predicted vs Measured Static Pressure Difference
for Various Flow Qualities in the RCC Guide.**

a,c

**Figure 68-10. Predicted vs Measured Void Fraction Distribution
for Downflow in the WDR Guide.**

a,c

**Figure 68-11. Predicted vs Measured Void Fraction Distribution
for Downflow in the RCC Guide.**

a,c

Figure 68-12. Flooding Curve for WDR Guide



Figure 68-13. Flooding Curve for RCC Guide

a,c

68. Westinghouse stated Eqn. 4-92 was taken from Reference 8. Review of Wallis indicated Eqn. 4-92 was for thin films in pipes; therefore, justify the applicability of this equation to the vessel geometry where it is applied in WCOBRA/TRAC.

Additional comments:

4. Westinghouse's response to question 68 discussed the effect of scale on the use of Eqn. 4-92 in PWR calculations and started to address the effects of the differences in geometry between the tests used to develop Eqn. 4-92 (thin films in pipes) and the intended use of the equation in WCOBRA/TRAC (vessel geometry). However, to help close question 68, clarify if the Wallis model was used in the WCOBRA/TRAC results compared to data in your latest response. If not, are there other assessments that could be performed to justify the extension of the Wallis model to the vessel geometry? If yes, provide appropriate comparisons for review. If no, provide other information to justify the extension.

Additional information:

a,c

69. Provide a reference or derivation for Eqn. 4-93. Also, provide the basis for the minimum value of 0.8 applied to Eqn. 4-93.

a,c

4.9 RAI 67

Question #67: Bubbly Flow Interfacial Drag “Ramping” to “Hot Wall” Inverted Annular Drag

WCAP-16996-P/WCAP-16996-NP, Volumes I, II, and III, Revision 0, Subsection 5.4.1, "Small Bubble Flow Regime Interfacial Drag," explains that in a SB regime of the "Cold Wall" flow map, the interfacial drag is calculated by interpolation between the SB value and the value for an Inverted Liquid Slug regime of the "Hot Wall" flow map "if there is significant vapor generation at the wall." To account for the presence of "significant vapor generation at the wall," the interfacial drag coefficient, $\bar{K}_{iX,vi,SB}$, is computed from Equation (5-67b) by interpolating or "ramping" between the drag coefficient for SB flow, $K_{iX,vi,SB}$, given by Equation (5-67a), and the drag coefficient for Inverted Annular regime of the "Hot Wall" flow map, $K_{iX,vi,HW}$, defined by Equation (5-105):

$$[\quad]^{a,c}$$

In the above equation, the interpolated drag coefficient is multiplied by the ratio of the limited relative velocity, U_{Γ} , found in Equation (5-66), to the absolute value of the axial relative phase velocity, $|\underline{U}_v|$. The dimensionless interpolation factor, F_{Γ} , is calculated from Equation (5-68) using the terminal relative velocity, U_{rb} , between a bubble with a Webber number of 10 and the liquid as determined by Equations (5-59) and (5-60):

$$[\quad]^{a,c}$$

The axial vapor velocity accounting for vapor generation in a computational cell, U_{Γ} , is calculated from Equation (5-69) as follows:

$$[\quad]^{a,c}$$

In the above equation, α_v is the vapor void fraction with an upper limit of 0.2 for SB flow, ρ_v is the vapor density, A_x is the cell momentum flow area in the axial direction, and Γ_v is the interfacial vapor generation rate for the cell calculated in accordance with Equation (6-101). Q_{wl} is the rate of heat transfer between the wall and the combined liquid fields (continuous liquid and entrained liquid) and Q_b is the rate of heat transfer at the wall that results in vapor generation from subcooled boiling. Both heat transfer rates correspond to the entire node surface area present in a computational cell.

- (1) To take account for "significant vapor generation at the wall," WCOBRA/TRAC-TF2 computes the interfacial drag coefficient for the SB regime, $\bar{K}_{iX,vi,SB}$, through interpolation between a bubbly flow drag coefficient calculated without the assumption of vapor film existence at the wall, $K_{iX,vi,SB}$, and a drag coefficient for "Hot Wall" Inverted Annular flow, $K_{iX,vi,HW}$. The dimensionless interpolation factor, F_{Γ} , accounts for wall heat transfer and associated vapor generation through a velocity parameter U_{Γ} . The rate of vapor generation at the wall surface in the cell is divided by the void fraction, α_v , and axial momentum flow area, A_x , to compute an equivalent axial vapor velocity, which is used to determine U_{Γ} . As U_{Γ} and F_{Γ} are based on the vapor generation rate at wall surfaces associated with a certain

cell size, these parameters are nodalization dependant. Thus, for a cell in the core region with a defined axial area, A_x , the interfacial vapor generation rate, Γ_v , the wall heat transfer rates, Q_{wl} and Q_b , are dependent on the axial cell length, ΔX :

$$\Gamma_v \sim \Delta X, Q_{wl} \sim \Delta X, Q_b \sim \Delta X.$$

Accordingly, F_Γ and $\bar{K}_{iX,vl,SB}$ will depend on ΔX : $U_\Gamma \sim \Delta X$ and $\bar{K}_{iX,vl,SB} \sim \Delta X$. Please demonstrate that the implementation of nodalization dependant parameters in the WCOBRA/TRAC-TF2 interfacial drag model for SB flow is appropriate considering the intended purposes of obtaining best estimate code predictions. Provide results from relevant sensitivity studies examining the effect of noding.

- (2) Please provide the technical basis that demonstrates the applicability of the interpolation correlation in Equation (5-67b) and used for "ramping" the SB flow drag coefficient in the presence of "significant vapor generation at the wall," $\bar{K}_{iX,vl,SB}$, and define the applicability conditions for this correlation:

$$[\quad]^{a,c}$$

Define the validity ranges for the parameters used to calculate it from the above equation. Please clarify if such "ramping" technique is also applied to surfaces associated with passive heat structures.

- (3) Please provide the technical basis that demonstrates the applicability of the correlation for computing the dimensionless interpolation factor, F_Γ , defined by Equation (5-68):

$$[\quad]^{a,c}$$

Define the acceptable range for F_Γ and the validity ranges for the parameters used to calculate it from the above equation.

- (4) The axial vapor velocity accounting for vapor generation in a computational cell, U_Γ , is calculated from Equation (5-69) using the minimum of two quantities. Accordingly, under saturated liquid boiling conditions when vapor is being generated only at the wall surface, the lack of interfacial vapor generation rate in a cell will produce a zero outcome for U_Γ regardless of the wall vapor generation. Please explain the appropriateness of the relationship defined by Equation (5-69) and used to calculate U_Γ and demonstrate its applicability.

Response:

- (1) The calculation of U_Γ for hot wall ramping in bubbly flow regimes will be revised as follows based on the discussion in Section 3 of this letter.

[] ^{a,c}

It is true that $Q_{w\ell}$ and Q_b are wall heat transfer rates and linearly depend on axial cell length ΔX , but their dependence is reduced due to the dependence of α_v on ΔX in the region of interest. Mostly, the hot wall ramping is only in effect at the entrance of the boiling channel where α_v starts to ramp up and U_T is thus calculated high (small α_v), as can be seen from the plots shown in Figures 3-1.1 through 3-1.12 in Section 3 of this letter.

In WCOBRA/TRAC-TF2 applications, consistency of the node sizes between the intended applications in PWR plant and validation test simulations has always been maintained to the extent practical, so that the applicable range of the models validated through the validation tests can be extended to the PWR plant simulations with minimum impact resulting from the node size. In all WCOBRA/TRAC-TF2 validation test and the demonstration PWR plant simulations, the node size spans in the range from 0.5~1.0 ft as seen in Table 26.1-1 of the Topical.

The core axial nodalization sensitivity studies conducted for the selected ORNL-THTF small break tests and Beaver Valley plant as documented in Section 2 in this response indicate the hot wall ramping model works properly for typical range of axial node size in the intended WCOBRA/TRAC-TF2 applications.

- (2) See Section 3 of this letter.
- (3) The interpolation end points as defined in Equation (5-68) of the Topical is ad hoc and demonstrated to provide reasonable prediction agreement with the validation tests of the overall code wall flow regime interfacial drag models. (See Section 3 of this letter)
- (4) The U_T will be redefined for the hot wall ramping model as explained in Section 3 of this letter.

4.10 RAI 68

Question #68: Approach to Interfacial Drag “Ramping” Between “Cold Wall” and “Hot Wall” Regimes

WCAP-16996-P/WCAP-16996-NP, Volumes I, II, and III, Revision 0, Subsection 5.4.1, "Small Bubble Flow Regime Interfacial Drag," states that in a SB regime of the "Cold Wall" flow map, the interfacial drag is calculated by interpolation between the SB value and the value for an Inverted Liquid Slug regime of the "Hot Wall" flow map "if there is significant vapor generation at the wall." It is explained that the "Hot Wall" drag coefficient used for the purpose of SB flow drag "ramping" is calculated from Equation (5-105). Equation (5-67b) defines how the interfacial drag is "ramped:"

$$\left[\frac{\mu_{SLB} - \mu_{SB}}{\mu_{SLB} - \mu_{CT}} \right]^{a,c}$$

Subsection 5.4.2, "Small-to-Large Bubble Flow Regime Interfacial Drag," clarifies that "for conditions in which there is a large vapor generation rate at the wall, the bubble drag coefficient is ramped to the interfacial drag used in the hot wall flow regime." It is explained that the "Hot Wall" drag coefficient used for the purpose of SLB flow drag "ramping" is calculated from Equation (5-106). The SLB drag "ramping" is performed according to Equation (5-73):

$$\left[\frac{\mu_{SLB} - \mu_{SB}}{\mu_{SLB} - \mu_{CT}} \right]^{a,c}$$

According to Subsection 5.4.3, "Churn-Turbulent Flow Regime Interfacial Drag," interfacial drag ramping is applied for the CT flow regime as well.

It is explained that "The same ramp as in Section 5.4.2 of WCAP-16996-P/WCAP-16996-NP, Volumes I, II, and III, Revision 0, is applied to consider the vapor generation rate at the wall-by-wall heat transfer."

Table 1 below summarizes the approach to interfacial drag "ramping" used in various flow regimes modeling by WCOBRA/TRAC-TF2.

Table 1: Approach to Interfacial Drag Ramping Between "Cold Wall" and "Hot Wall" Flow Regimes in WCOBRA/TRAC-TF2 Vessel Component

"Cold Wall" Flow Regime	Drag Ramping Criterion	"Hot Wall" Regime Cited in Ramping	Referenced "Hot Wall" Drag Coefficient
Small Bubble	"Significant vapor generation at the wall"	Inverted Liquid Slug	Equation (5-105). Related drag factor: $\left[\frac{\mu_{SLB} - \mu_{SB}}{\mu_{SLB} - \mu_{CT}} \right]^{a,c}$ (Equations (5-92) and (5-102))
	"A large vapor generation rate at	Dispersed	Equation (5-106). Related drag factor:

Small-to-Large Bubble	the wall"	Droplet	$K_{iX,ve,DD} = 0.375 C_{Db} \alpha_v \rho_v \underline{U}_{ve} / r_b$ $[\quad]^{a,c}$ (Equations (5-106) and (5-108))
Churn-Turbulent	"The vapor generation rate at the wall-by-wall heat transfer"	Dispersed Droplet	Equation (5-106). Related drag factor: $K_{iX,ve,DD} = 0.375 C_{Db} \alpha_v \rho_v \underline{U}_{ve} / r_b$ $[\quad]^{a,c}$ (Equations (5-106) and (5-108))

- (1) Interfacial drag "ramping" between "Cold Wall" and "Hot Wall" drag coefficients is used to account for wall vapor generation in modeling SB, SLB, and CT two-phase flow regimes when recognized by the "Cold Wall" flow map. In the case of Small Bubble flow, film drag for "Hot Wall" Inverted Liquid Slug flow, as suggested by Equation (5-105), is used to "ramp" the bubbly flow drag as described in WCAP-16996-P/WCAP-16996-NP, Volumes I, II, and III, Revision 0, Subsection 5.4.1 .

In contrast to this approach and as explained in Subsections 5.4.2 and Subsection 5.4.3, interfacial drag for both SLB and CT flow regimes is "ramped" using droplet drag for entrained liquid droplets in "Hot Wall" Dispersed Droplet flow defined by Equation (5-106) and calculated using $[\quad]^{a,c}$ which is representative for a solid sphere in the Newton regime at high Reynolds numbers.

Please clarify this modeling disparity. If Subsection 5.4.2 erroneously refers on page 5-20 to Equation (5-105) instead of Equation (5-106), please provide a proper modeling description. Otherwise, please justify the difference in the modeling approaches.

- (2) Please explain the technical rationale behind interfacial drag ramping for "Cold Wall" SB, SLB, and CT flow regimes using interfacial drag defined for "Hot Wall" flow regimes. Present supporting phenomenological considerations and refer to specific experimental observations and data. Please provide and explain the criterion used for detection of "significant vapor generation at the wall" in SB flow and that applied for identification of "a large vapor generation rate at the wall" in SLB flow. In the case of CT flow, please define and explain the criterion used to identify the need "to consider the vapor generation rate at the wall-by-wall heat transfer" and clarify the meaning of the expression "vapor generation rate at the wall-by-wall heat transfer" on page 5-21 in WCAP-16996-P/WCAP-16996-NP, Volumes I, II and III, Revision 0, Subsection 5.4.3.
- (3) Please explain if the criteria for recognition of "significant vapor generation at the wall," as considered in item (2) above, were used to classify existing two-phase flow data sets into separate groups that can be used to validate "Cold Wall" interfacial drag models with no drag ramping, such that are appropriate for "Hot Wall" interfacial drag model validation, and data sets that are applicable for validation of "Cold Wall" interfacial drag models with drag

ramping. Please provide references to such validation analyses, if available, and summarize analysis results that demonstrate the applicability of the applied interfacial drag "ramping" approach in WCOBRA/TRAC-TF2 for each individual flow regime. Please present comparisons of code predictions obtained with interfacial drag "ramping" being present and absent against void fraction data measurements. In particular, consider an appropriate data set for which interfacial drag "ramping" is supposed to be applied and present code comparisons obtained with and without drag "ramping" versus measured data.

Response:

- (1) A review of Reference 4.10-1 and WCOBRA/TRAC-TF2 code found that there is a typo in the paragraph below Equation (5-73) in the Topical (Reference 4.10-1), which should be corrected as:

[

]^{a,c}.

Through the above correction, it clarifies that the 'hot wall ramping' for the small bubble and small to large bubble flow regimes is ramped to the same hot wall interfacial drag of the inverted liquid slug regime.

- (2) See Section 3 of this letter for 'Hot Wall Ramp' discussion.

- (3) See Section 3 of this letter for 'Hot Wall Ramp' discussion.

Reference(s)

- 4.10-1. WCAP-16996-P, "Realistic LOCA Evaluation Methodology Applied to the Full Spectrum of Break Sizes (FULL SPECTRUM LOCA Methodology)," November 2010.

4.11 RAI 69

Question #69: Calculation Results for Bubbly Flow Interfacial Drag

WCAP-16996-P/WCAP-16996-NP, Volumes I, II, and III, Revision 0, Subsection 5.4.1, "Small Bubble Flow Regime Interfacial Drag," refers to Figure 5-3(a), "Effect of Ramps on Interfacial Friction Factor: (a) SB Regime," as an illustration of the effect of ramps and limits, described in this subsection, on the interfacial drag for the SB flow regime. The figure plots a quantity denoted K_i referred to as "interfacial drag factor" versus relative velocity $U_v - U_l$. It is explained that the drag factor is plotted in Figure 5-3(a) for "typical fluid conditions." As seen from the graph, the two-phase flow conditions correspond to a SB flow regime with a vapor void fraction of $\alpha_v = 0.1$ and a pressure of 40 psia (0.276 MPa). The plot depicts four curves for the interfacial drag factor calculated at different cell vapor generation rates that correspond to values of 0, 1, 1.1, and 1.2 for the ratio between the axial velocity of vapor generation in a computational cell and the terminal relative velocity, U_l/U_{rb} .

Figure 5-3(a), "Effect of Ramps on Interfacial Friction Factor: (a) SB Regime," does not provide units for both plotted quantities: the interfacial drag factor, K_i , and the relative velocity, $U_v - U_l$. The figure also does not include geometric characteristics that describe channel geometry, heated surfaces and cell nodalization parameters nor does it define inlet and boundary conditions related to mass flow rates and surface heat flux. As such, the results presented in the figure are not amenable to assessment.

- (1) Please provide, in a table format, prediction results presented in Figure 5-3(a) to document the following information: (i) parameter, (ii) unit, (iii) correlation used to calculate the parameter, (iv) range of applicability, (v) values and units for input parameters, and (vi) calculated result. Include each of the identified items in a separate column and use a separate row to present individual parameters. Analyze and include results for three U_l/U_{rb} ratio values of 0, 1, and 1.2. Please provide the results at relative velocities equal, in units used for the horizontal axis in Figure 5-3(a), to 0 (or an appropriately defined low value), 0.5, the value at which the gradient of the curves, shown in Figure 5-3(a) for U_l/U_{rb} of 0, 1, and 1.1, changes a sign from positive to negative (value appears very close to unity), and 10. Please include the results for $K_{iX,vl,SB}$, $K_{iX,vl,HW}$, and $\bar{K}_{iX,vl,SB}$, as computed from Equations (5-67a), (5-105), and (5-67b). The numerical results provided should be self-contained and allow for independent verification of the values. For this purpose, all applied inlet and boundary conditions need to be given along with other assumed parameters such as bubble diameter or terminal relative velocity. Please include used fluid properties as well.
- (2) Using the obtained results for $\bar{K}_{iX,vl,SB}$ from Equation (5-67b), please calculate and provide the values for the corresponding dimensionless drag coefficient, \bar{C}_{Db} , that is commonly used in the relevant literature to calculate drag force for a single dispersed element through its projected cross-sectional area and continuous phase kinetic head corresponding to the relative velocity. To obtain \bar{C}_{Db} , please use the general form of the interfacial drag coefficient for bubbly flow as given by Equations (5-45) and (5-67a):

$$\left[\frac{\rho_l (U_v - U_l)^2}{\sigma} \right]^{a,c}$$

In addition, please calculate the dimensionless drag coefficient, C_{Db} , which corresponds to

the drag coefficient, $K_{iX,VI,SB}$, determined from Equation (5-67a) prior to "ramping" in order to account for "significant vapor generation at the wall:"

[]^{a,c}

Include the results for \bar{C}_{Db} , C_{Db} , and $f_{iX,IVS}$ in the tables prepared according to item (1) above.

- (3) Please provide figures that plot the results for the following parameters as functions of the relative velocity, U_v-U_l , including the units for the displayed quantities: (1) "ramped" dimensionless drag coefficient, \bar{C}_{Db} , (2) uncorrected for wall vapor generation dimensionless drag coefficient, C_{Db} , (3) interfacial friction factor for "Hot Wall" Inverted Liquid Slug flow, $f_{iX,IVS}$, as applied in bubbly flow drag "ramping," (4) $K_{iX,VI,SB}$ drag coefficient, (5) $K_{iX,VI,HW}$ drag coefficient, and (6) $\bar{K}_{iX,VI,SB}$ drag coefficient.
- (4) Please provide results for the WCOBRA/TRAC-TF2 interfacial drag model for the vessel component SLB flow regime by providing prediction results as requested in items (1) through (3) above for SB flow. Apply the same conditions as those used to produce Figure 5-3(b), "Effect of Ramps on Interfacial Friction Factor: (b) Large Bubble Regime."
- (5) Please provide results for the WCOBRA/TRAC-TF2 interfacial drag model for the vessel component CT flow regime by providing prediction results as requested in items (1) through (3) above for SB flow. Apply the same conditions as those used to produce Figures 5-3(a) and 5-3(b) except for using a void fraction of 0.6 instead of 0.1 and 0.4, respectively.

Response:

- (1) Interfacial drag factor for small bubble flow regime

The calculation in this subsection explains how Figure 5-3(a) in Section 5 of the Topical was generated.

- Input parameters:

Pressure: []^{a,c}
 Void fraction (α): []

Liquid velocity (U_l): []^{a,c}
 Flow Area (A_{mom}): []
 Hydraulic Diameter (D_h): []

- Properties (Saturation at given pressure):

$$\left[\begin{array}{c} \text{[Empty Box]} \end{array} \right]_{a,c}$$

- Calculation correlations:

Each curve in Figure 5-3(a) is calculated for a given U_r/U_{rb} , with each point of the curve for a given vapor-liquid relative velocity.

The relative velocity is limited as described in Section 5.4.1 of the Topical [Equations (5-62) through (5-66)], and calculated as:

$$\left[\begin{array}{c} \text{[Empty Box]} \end{array} \right]_{a,c}$$

where

$$\left[\begin{array}{c} \text{[Empty Box]} \end{array} \right]_{a,c}$$

The small bubble drag factor calculation is done in equations as follows, consistent with Sections 5.4.1 and 4.2.2 of the Topical.

$$\left[\text{Equation} \right]_{a,c}$$

The 'if' statement in the CD_{SB} calculation above is used to cap the CD_{SB} value at $CD_{SB,2}$ if $CD_{SB,tmp}$, the maximum of the $CD_{SB,0}$ and $CD_{SB,1}$, is over the limit of $CD_{SB,2}$.

The hot wall drag factor calculation is done through the equations as follows, consistent with Section 5.4.6 of the Topical.

For Inverted Liquid Slug Regime, the drag factor is calculated as:

$$\left[\text{Equation} \right]_{a,c}$$

The 'Ramp' in the equation below is identical to F_r as defined in Equation (5-68) of the Topical,

$$\left[\text{Equation} \right]_{a,c}$$

Based on this definition of 'Ramp', as well as the fact that liquid velocity is assumed to be zero in the calculation, it is evident that the four curves in Figure 5-3(a) of the Topical corresponding to the U_r equals to 0, $1.0U_{rb}$, $1.1U_{rb}$ and $1.2U_{rb}$ can be obtained by setting the 'Ramp' values to be 0.0, 0.5, 0.75 and 1.0.

Table RAI69-1 shows the results of the calculated drag coefficients as well as other selected parameters for each of the data points for the curve of ' $U_r = 0$ ' in Figure RAI69-1, which is a duplication of Figure 5-3(a) of the Topical. The units of the ordinate parameters are included in Figure RAI69-1.



Figure RAI69-1 Small Bubble Regime Interfacial Drag Factor with Hot Wall Ramping Effects

Please note that []^{a,c} term shown in Equation (5-67b) of the Topical is incorporated in the above equation in the $K_{IX,VI,SB}$, thus the equation for K_{SB} above is the same as Equation (5-67b) of the Topical.

Please also note that there is a typographical error in Equation (5-67b) of the Topical, which should be corrected as pointed out in Section 3 of this letter.

(2) Interfacial drag factor for small to large bubble flow regime

This subsection explains how Figure 5-3(b) in Section 5 of the Topical was generated first, then a corrected calculation consistent with the WCOBRA/TRAC-TF2 coding of the large bubble interfacial drag factor is provided together with the revised Figure 5-3(b).

The input parameter and property values are the same as those listed in subsection (1) for Figure 5-3(a) except that the void fraction is assumed to be 0.4 instead of 0.1 in the input parameter.

WCOBRA/TRAC-TF2 calculates the interfacial drag factor for the small to large bubble regime ([]^{a,c}) interpolating the interfacial drag factor for the small bubbles and large bubbles, []^{a,c}. The detailed model is explained in Sections 5.4.2 and 4.2.3 of the Topical.

To calculate the interfacial factor at $[\quad]^{a,c}$ for small to large bubble regime, the steps described in (1) are first followed to obtain the small bubble drag factor at $[\quad]^{a,c}$, which are followed by calculating the drag factor using the large bubble drag correlations as described as follows.

$$[\quad]^{a,c}$$

Large bubble radius is calculated consistently with Equation (4-24) of the Topical and its limits [Equation (4-23) in the Topical]. A cell axial length of $[\quad]^{a,c}$.

$$[\quad]^{a,c}$$

$$\left[\begin{array}{c} \text{---} \\ \text{---} \end{array} \right]^{a,c}$$

Please note that the equation for $K_{IX,VI,LB}$ above uses [

$$\left[\begin{array}{c} \text{---} \\ \text{---} \end{array} \right]^{a,c} \quad \text{---}^{a,c} \quad \left[\begin{array}{c} \text{---} \\ \text{---} \end{array} \right]^{a,c}$$

The results of these two ways of defining $K_{IX,VI,LB}$ is shown in Figures RAI69-2 and RAI69-3. It can be seen that Figure RAI69-2 duplicates Figure 5-3(b) in the Topical. The drag factor shown in Figure RAI69-3 is consistent with the code implementation in WCOBRA/TRAC-TF2. The calculation results of selected parameters are listed in Tables RAI69-2 and RAI69-3 corresponding to Figures RAI69-2 and RAI69-3, respectively.

The interfacial drag factor for small to large bubble regime is obtained by [

$$\left[\begin{array}{c} \text{---} \\ \text{---} \end{array} \right]^{a,c} \quad \text{---}^{a,c} \quad \left[\begin{array}{c} \text{---} \\ \text{---} \end{array} \right]^{a,c}$$



Figure RAI69-2 Small to Large Bubble Regime Interfacial Drag Factor with Hot Wall Ramping Effects (Using []^{a,c})



Figure RAI69-3 Small to Large Bubble Regime Interfacial Drag Factor with Hot Wall Ramping Effects (Using []^{a,c})

From the parameter values provided in Tables RAI69-1, RAI69-2 and RAI69-3, it is straightforward to obtain the dimensionless interfacial drag coefficients for bubbly flow regimes of small and small to large bubbles, as are commonly used in relevant literature to calculate drag forces, either prior to “ramping” or after “ramping” to [

]^{a,c}

As a final note, churn turbulent regime is modeled simplistically in WCOBRA/TRAC-TF2 as [

]^{a,c} flow drag model provides reasonable simulation results in these validation tests in the regime of the churn turbulent flow.

Table RAI69-1 Interfacial Drag Factor of Small Bubble Flow Regime (Case $U_T = 0.0$)

a,c

Table RAI69-2 Interfacial Drag Factor of Small to Large Bubble Flow Regime using limited relative velocity (Case $U_r = 0.0$)

a,c

Table RAI69-3 Interfacial Drag Factor of Small to Large Bubble Flow Regime Using Local Relative Velocity (Case $U_r = 0.0$)

a,c

4.12 RAIs 70 and 71

Question #70: Film Flow Drag Assessment Using Thermal Hydraulic Test Facility Test Data

WCAP-16996-P/WCAP-16996-NP, Volumes I, II, and III, Revision 0, Subsection 29.1.5, "Interfacial Drag in the Core Region," presents the treatment of film flow interfacial drag in WCOBRA/TRAC-TF2 uncertainty assessments. It is explained that "The FDRAG multiplier is the sole contributor for void fractions α_v greater than $\alpha_{crit} \sim 0.8$." In addition, "in the interpolation region between the small and small-to-large bubbly flow regime ($\alpha_v < 0.5$) and the annular film flow regime ($\alpha_v > \alpha_{crit} \sim 0.8$) both YDRAG and FDRAG have an effect." According to WCAP-16996-P/WCAP-16996-NP, Volumes I, II, and III, Revision 0, Subsection 29.1.5, the film drag multiplier, FDRAG, is applied directly to the interfacial drag as calculated for the FD flow regime using Equation (5-81) in Subsection 5.4.4, "Film/Drop Flow Regime: Model Basis":

[]^{a,c}

WCAP-16996-P/WCAP-16996-NP, Volumes I, II, and III, Revision 0, Subsection 13.4.2, "ORNL-THTF Small Break Tests," explains that "the parameter FDRAG has been introduced to facilitate WCOBRA/TRAC-TF2 ranging of film interfacial drag, which tends to impact the drag most significantly in the transition and annular flow regimes. It is specified on an individual cell basis." The subsection also describes the approach to determining FDRAG in plant calculations. It involved sensitivity calculations performed with WCOBRA/TRAC-TF2 for 12 ORNL THTF tests. The FDRAG sensitivity studies included 6 bundle uncover and 6 level swell tests as summarized in Table 1.

Table 1: ORNL THTF Tests Used in FDRAG WCOBRA/TRAC-TF2 Sensitivity Analysis

Test Facility	Test Bundle	Test Runs	Number and Type of Test Runs		FDRAG and Number of Test Runs Analyzed	
			Bundle Uncover	Level Swell	[] ^{a,c}	[] ^{a,c}
ORNL THTF	8x8	12	6	6	12	12

The WCOBRA/TRAC-TF2 void fraction predictions with []^{a,c} are compared against ORNL THTF bundle void fraction measurements in Figures 13.4.2-4 through 13.4.2-15. From the results predicted in these figures, it was concluded []

[]^{a,c}

[]^{a,c} It is also explained that [

] ^{a,c}

- (1) Figures 13.4.2-4 through 13.4.2-15 contains 9 measured void fraction data points for each of the analyzed THTF test runs. Please identify the void fraction data points measured in these THTF tests, for which WCOBRA/TRAC-TF2 predicts an annular flow configuration with a stable liquid film at the wall based on the interfacial drag model and document the data in a table. For each point, provide the measured void fraction value, void fraction measurement uncertainty (shown in Figures 13.4.2-4 through 13.4.2-1), corresponding liquid, vapor and entrained liquid mass flow rates, liquid film thickness, criteria used to identify the data points, such as α_{crit} and entrained liquid fraction, α_e , along with their numerical values, predicted nominal interfacial drag coefficient, f_i . Include corresponding void fraction predictions for []^{a,c} Please document each data point in a separate row and present the above identified quantities in separate columns. Please provide a plot comparing predicted void fractions (with []^{a,c}) versus measured data showing void fraction measurement accuracy. Please explain why the identified data points were considered representative of a stable film configuration. Please apply the nominal YDRAG value (YDRAG=1) in code predictions. In a separate table, please compare the flow conditions characterizing each measured data point against the applicability range for the interfacial drag correlations used in the code void fraction predictions.
- (2) Please identify the measured void fraction data points in the analyzed THTF test runs, for which the unstable liquid film model was used in predicting the interfacial drag coefficient. For these data points, please provide the information as requested in item (1) above for annular flow with a stable liquid film at the wall. Please apply the nominal YDRAG value (YDRAG=1) in code predictions and provide a separate table, which compares the flow conditions characterizing each measured data point against the applicability range for the interfacial drag correlations used in the code void fraction predictions.
- (3) Please identify the measured void fraction data points in the analyzed THTF test runs, for which the flow is predicted to exist in a CT flow regime ($0.50 < \alpha \leq \alpha_{crit}$). For these data points, please provide the information requested in item (1) above for annular flow. Please apply the nominal YDRAG value (YDRAG=1) in code predictions and provide a separate table, which compares the flow conditions characterizing each measured data point against the applicability range for the interfacial drag correlations used in the code void fraction predictions.
- (4) Please clarify what was the value for the YDRAG multiplier that was used in the code predictions shown in Figures 13.4.2-4 through 13.4.2-15.
- (5) Considering items (1) through (4) above, please explain why the ORNL THTF test data, analyzed in WCAP-16996-P/WCAP-16996-NP, Volumes I, II, and III, Revision 0, Subsection

13.4.2, "ORNL-THTF Small Break Tests," represent a suitable and sufficient technical basis to demonstrate the applicability and treatment of film flow interfacial drag in WCOBRA/TRAC-TF2 PWR LOCA analyses. Please provide validation results for the WCOBRA/TRAC-TF2 film drag model based on appropriately selected data describing annular film flow under conditions typical for PWR LOCA analyses.

Question #71: Film Drag Impact on Bubbly Flow Void Predictions for Thermal Hydraulic Test Facility Tests

WCAP-16996-P/WCAP-16996-NP, Volumes I, II, and III, Revision 0, Subsection 29.1.5, "Interfacial Drag in the Core Region," states that "The YDRAG multiplier is the sole contributor for void fractions α_v less than 0.5." Explaining the development of a proposed PDF for the film drag multiplier FDRAG, the subsection refers to WCOBRA/TRAC-TF2 ORNL THTF void fraction predictions obtained with []^{a,c} and compared against ORNL THTF test bundle void fraction measurements as described in WCAP-16996-P/WCAP-16996-NP, Volumes I, II, and III, Revision 0, Subsection 13.4.2, "ORNL-THTF Small Break Tests," and illustrated in Figures 13.4.2-4 through 13.4.2-15. In particular, Figure 13.4.2-12 shows the comparison between WCOBRA/TRAC-TF2 code predictions and void fraction measurements for THTF Test 3.09.10CC. In this test, both the measured void fractions and the code prediction results are less than 0.5. As seen from Figure 13.4.2-12, changing the FDRAG multiplier []^{a,c} had a significant impact on the predicted void fraction results under flow conditions corresponding to SB and SLB flow regimes used in the WCOBRA/TRAC-TF2 vessel component "Cold Wall" flow map. Such an effect, although to a smaller degree, is also seen in Figure 13.4.2-11 for Test 3.09.10BB, in Figure 13.4.2-5 for Test 3.09.10J, in Figure 13.4.2-7 for Test 3.09.10L, and in Figure 13.4.2-13 for Test 3.09.10DD.

- (1) Please explain why changing the interfacial drag multiplier for film flow, FDRAG, causes such a pronounced effect on WCOBRA/TRAC-TF2 void fraction predictions for the identified ORNL THTF tests at elevations below the two-phase mixture level where measured void fractions are less than 0.5. Relate the explanation to the statement in WCAP-16996-P/WCAP-16996-NP, Volumes I, II, and III, Revision 0, Subsection 29.1.5, "Interfacial Drag in the Core Region," that "The YDRAG multiplier is the sole contributor for void fractions α_v less than 0.5."
- (2) WCAP-16996-P/WCAP-16996-NP, Volumes I, II, and III, Revision 0, Subsection 5.4.1, "Small Bubble Flow Regime Interfacial Drag," explains that in a SB regime of the "Cold Wall" flow map, the interfacial drag is calculated by interpolation between the SB value and the value for an Inverted Liquid Slug regime of the "Hot Wall" flow map "if there is significant vapor generation at the wall." Similarly, WCAP-16996-P/WCAP-16996-NP, Volumes I, II, and III, Revision 0, Subsection 5.4.2, "Small-to-Large Bubble Flow Regime Interfacial Drag," clarifies that "for conditions in which there is a large vapor generation rate at the wall, the bubble drag coefficient is ramped to the interfacial drag used in the hot wall flow regime." Please clarify if interfacial drag "ramping" caused the observed effect on WCOBRA/TRAC-

TF2 void fraction predictions as exhibited by varying the film flow interfacial drag multiplier, FDRAG, in the code simulation for THTF Test 3.09.10CC for flow conditions with void fractions less than 0.5 that correspond to SB and SLB flow regimes.

- (3) Please explain what is unique for THTF tests, such as 3.09.10CC, for which FDRAG variation had a pronounced impact on the void fraction predictions at low voids according to Figure 13.4.2-12, in comparison to other analyzed THTF tests as seen in Figure 13.4.2-6 for Test 3.09.10K, in Figure 13.4.2-8 for Test 3.09.10M, in Figure 13.4.2-9 for Test 3.09.10N, in Figure 13.4.2-10 for Test 3.09.10AA, in Figure 13.4.2-11 for Test 3.09.10BB, in Figure 13.4.2-14 for Test 3.09.10EE, and in Figure 13.4.2-15 for Test 3.09.10FF.
- (4) If interfacial drag "ramping" caused the exhibited effect on WCOBRA/TRAC-TF2 void fraction predictions for the identified THTF tests, please present the technical basis that validates the implemented approach to interfacial drag "ramping" in WCOBRA/TRAC-TF2 for applications aimed at obtaining realistic thermal-hydraulic predictions of PWR core level swell under typical SBLOCA conditions.

Response:

[

] ^{a,c} A brief explanation of the sensitivity was provided in LTR-NRC-13-70 (Reference 4.12-2). A more detailed explanation follows.

The ORNL test simulations are initially in a transient condition. The transient condition exists until the quasi steady-state is reached, at which point the results of the simulation are extracted. The initialization of the simulations is such that the void in the top cells of the core is initially [^{a,c} would impact the results during the initial transient

behavior. For the particular simulation of ORNL Test CC presented in the topical, the different transient behavior resulted in a different void fraction profile once the quasi steady-state condition was reached. The initialization of this simulation was then changed such that the initial void fraction in the top cells of the core was set lower. This resulted in the expected non-sensitivity of the results to []^{a,c}, as presented in Figure 2-12.

As such, it is concluded that there is no sensitivity of the ORNL Test CC results to ranging []^{a,c}. Figure 13.4.2-12 in WCAP-16996-P should be replaced with an updated figure based on this response.

The introduction of []

[]^{a,c} It was observed that application of []^{a,c} in the core provided a better prediction of the data in the upper regions of the bundle from the ORNL test series. As such, a decision was made to utilize []^{a,c} in the core region. Not only does this cause a better prediction of the data, but since []^{a,c} which is considered conservative relative to the calculation of peak cladding temperature and oxidation for a SBLOCA transient. Since []^{a,c} is only applied in a conservative direction and only in the core, no additional validation is considered necessary. Note that all the IET validation was performed with []^{a,c}

It is also relevant to note that the YDRAG multiplier is ranged within the uncertainty analysis, while the FDRAG multiplier is held constant. Under SBLOCA boil-off core uncover conditions, where there is a clear interface between the two-phase mixture and single-phase vapor, it is not expected that the FDRAG multiplier would have a significant impact. This was already shown in the FDRAG sensitivity studies for ORNL Tests K, N, and FF. Rather, it was observed that the YDRAG multiplier tends to control the two-phase level (Figures 13.4.2-18, 13.4.2-21, and 13.4.2-27 of WCAP-16996-P, Reference 4.12-1).

[]^{a,c} was utilized in the sensitivity studies presented in Figures 13.4.2-4 through 13.4.2-15 of WCAP-16996-P.

Reference(s)

- 4.12-1. WCAP-16996-P, "Realistic LOCA Evaluation Methodology Applied to the Full Spectrum of Break Sizes (FULL SPECTRUM LOCA Methodology)," November 2010.
- 4.12-2. LTR-NRC-13-70, "Summary of July 2013 NRC Code Workshop and August 2013 NRC Audit of the FULL SPECTRUM LOCA (FSLOCA) Evaluation Model (Proprietary/Non-Proprietary)," October 10, 2013.

5. Revised Section 5.4 of the Topical

Section 5.4 of the Topical is updated as follows to clarify the definition of the vessel component interfacial drag factors. A limited number of small, grammatical corrections are also included.

5.4 VESSEL COMPONENT INTERFACIAL SHEAR MODELS

Flow regime maps used in the vessel component of WCOBRA/TRAC-TF2 are described in Section 4. The vessel momentum equations described in Section 3 require the interfacial drag coefficient in units which, when multiplied by the new time velocity difference between the phases, will yield force per unit length for that phase. During the numerical solution, these coefficients are divided by the appropriate phasic densities, when the phasic mass flow rate is solved for. In subroutine INTFR, the interfacial drag coefficients are defined based on phasic velocity, as shown below. The average interfacial drag force per unit length between the vapor and continuous liquid is defined as:

$$\tau'_{iX,v\ell} = K_{iX,v\ell} \underline{U}_{v\ell} \quad (5-42)$$

where:

$$\begin{aligned} \tau'_{iX,v\ell} &= \text{the force per unit length on the liquid by the vapor} \\ K_{iX,v\ell} &= \text{the flow regime dependent interfacial drag coefficient} \\ \underline{U}_{v\ell} &= \text{the axial relative velocity between the vapor and the continuous liquid} \end{aligned}$$

A similar expression exists for the drag force between the vapor and entrained liquid. This expression is given as:

$$\tau'_{iX,ve} = K_{iX,ve} \underline{U}_{ve} \quad (5-43)$$

where:

$$\begin{aligned} \tau'_{iX,ve} &= \text{the force per unit length on the entrained liquid phase by the vapor} \\ K_{iX,ve} &= \text{the flow regime dependent interfacial drag coefficient} \\ \underline{U}_{ve} &= \text{the axial relative velocity between the vapor and the entrained phase} \end{aligned}$$

When accounting for the relative velocity between the phases in some calculations, for example the Reynolds number in Equation 5-51, the relative velocity value generally assumed is the [

^{a,c}:

$$\left[\begin{array}{c} \underline{W}_{v\ell,max} \\ \underline{U}_{v\ell} \end{array} \right]^{a,c} \quad (5-44)$$

where $\underline{W}_{v\ell,max}$ is the maximum lateral relative velocity and $\underline{U}_{v\ell}$ is the axial relative velocity for the cell.

However, in some cases, this value is modified as described in the Model as Coded sections. When the value has been modified, it is expressed as U_r .

5.4.1 Small Bubble Flow Regime Interfacial Drag

Model Basis

For the bubbly regime, the general form of the interfacial drag coefficient is:

$$K_{iX,v\ell} = C_{Db} \frac{\rho_\ell |U_{v\ell}|}{2} A_{p,b} / \Delta X \quad (5-45)$$

where $A_{p,b}$ is the total projected area of the bubbles in the volume. For spherical bubbles, this results in:

$$A_{p,b} = N_b \pi r_b^2 \quad (5-46)$$

where N_b is the number of bubbles in the cell, and r_b is the bubble radius. This can be shown to be equivalent to:

$$\left[\begin{array}{c} \text{ } \\ \text{ } \\ \text{ } \end{array} \right]_{a,c} \quad (5-47)$$

where $A_{i,b}$ is the bubble interfacial area, described in Section 4. Two alternate forms of the interfacial drag coefficient are obtained:

$$\left[\begin{array}{c} \text{ } \\ \text{ } \\ \text{ } \end{array} \right]_{a,c} \quad (5-48a)$$

(5-48b)

Similarly, for lateral flow,

$$\left[\begin{array}{c} \text{ } \\ \text{ } \\ \text{ } \end{array} \right]_{a,c} \quad (5-49a)$$

(5-49b)

Expressions for the bubble drag coefficient (C_{Db}) are discussed by Ishii (1977) and Ishii and Chawla (1979). The drag coefficients are Reynolds number dependent and closely related to the drag coefficients for single bubbles and drops in an infinite medium. The drag coefficient for a single bubble in an infinite liquid medium is shown in Figure 5-2. The bubble is considered to behave as a solid sphere in the viscous

regime. At a higher Reynolds number, the bubble is characterized by a distorted shape and irregular motion. In this distorted particle regime the drag coefficient decreases with the Reynolds number. As the Reynolds number further increases, the bubble becomes spherical-cap shaped and the drag coefficient becomes constant.

As discussed by Ishii (1979), in the viscous regime the drag coefficient of a single particle in a multi-particle system may be assumed to have the same functional form as that of a single particle in an infinite medium, provided that the Reynolds number is computed using the appropriate mixture viscosity. Therefore, in the viscous regime the drag coefficient on a bubble is given by:

$$C_{Db} = \frac{24}{Re_b} (1.0 + 0.1 Re_b^{0.75}) \quad (5-50)$$

where:

$$Re_b = \frac{2r_b \rho_\ell \underline{U}_{v\ell}^*}{\mu_{mb}} \quad (5-51)$$

and

$$\mu_{mb} = \mu_\ell (1 - \alpha_v)^{-2.5 \frac{(\mu_v + 0.4\mu_\ell)}{(\mu_v + \mu_\ell)}} \quad (5-52)$$

In the distorted particle regime, it is again assumed that the drag coefficient for a particle in a multi-particle system is the same as that of a single particle in an infinite medium with the Reynolds number based on a mixture viscosity. In addition, it is assumed that churn-turbulent flow always exists in the distorted particle regime. Under these conditions, a particle tends to move in the wake caused by other particles. Therefore, the velocity used in the drag coefficient and Reynolds number should be the drift velocity, $\underline{U}_{vj} = (1 - \alpha_v) \underline{U}_{v\ell}$. The drag coefficient in the distorted particle regime is then,

$$C_{Db} = \frac{\sqrt{2}}{3} N_\mu Re'_b (1 - \alpha_v)^2 \quad (5-53)$$

where:

$$N_\mu = \frac{\mu_\ell}{\left[\rho_\ell \sigma \sqrt{\frac{\sigma}{g(\rho_\ell - \rho_v)}} \right]^{1/2}} \quad (5-54)$$

$$Re'_b = \frac{2r_b \rho_\ell (1 - \alpha_v) |\underline{U}_{v\ell}|}{\mu_m} \quad (5-55)$$

and

$$\mu_m = \frac{\mu_\ell}{(1 - \alpha_v)} \quad (5-56)$$

The $(1 - \alpha_v)^2$ in the expression for the drag coefficient results from using the drift velocity to compute the drag force.

Churn-turbulent flow is also assumed for the cap bubble regime where:

$$C_{Db} = \frac{8}{3} (1 - \alpha_v)^2 \quad (5-57)$$

For the large-bubble flow regime, Equation 5-50 is assumed to apply down to the limit of Newton's regime where the drag coefficient for a single solid sphere becomes constant at a value of 0.45. Within Newton's regime the large bubbles are assumed to move with respect to the average volumetric flux and, therefore,

$$C_{Db} = 0.45 (1 - \alpha_v)^2 \quad (5-58)$$

The mixture viscosity is used in Re'_b in Equation 5-55 because a particle moving in a multi-particle system experiences a greater resistance than a single particle in an infinite medium. As it moves it must deform not only the fluid, but the neighboring particles as well. The effect is seen by the particle as an increased viscosity.

The terminal relative velocity between the bubble and liquid is also calculated from a bubble rise model given by Ishii (1977) as:

$$U_{rb} = 1.414 \left[\sigma g_c (\rho_\ell - \rho_v) / \rho_\ell^2 \right]^{0.25} / (1 - \alpha_v) \quad (5-59)$$

The bubble size is assumed to depend on a Weber number criterion:

$$r_b = 0.5 We_b \sigma g_c / (\rho_\ell U_{v\ell}^2) \quad (5-60)$$

where:

$$We_b = 10$$

[

$$\left[\begin{matrix} \text{a,c} \\ \text{a,c} \end{matrix} \right] \quad (5-61)$$

If large heat releases exist at a solid boundary within the cell, then vapor is assumed to concentrate as a film at the wall. The interfacial shear between the vapor film and the bulk liquid is then determined by assuming a transition inverted slug regime described in Section 5.4.6.

Model as Coded

The WCOBRA/TRAC-TF2 coding logic uses the above correlations with consistency checks to establish limits on parameters such as relative velocities and bubble size before the interfacial drag is calculated. The relative velocity is compared using different methods and the minimum value is used in the bubble Weber number and drag coefficient. The reason for this is that in the small bubble regime the interfacial area is large and would lead to excessively large forces if a large relative velocity were used.

The relative velocity to be used in Equation 5-45 is initially set at the local vector sum value ($U_r = \underline{U}_{v\ell}$), given in Equation 5-44. It is then limited as follows.

The first limit is calculated by [

$$\left[\frac{C_{D1} \rho_l U_{v\ell}^2}{\sigma} \right]^{a,c} \quad (5-62)$$

[

$$\left[\frac{C_{D2} \rho_l U_{v\ell}^2}{\sigma} \right]^{a,c} \quad (5-63)$$

and the drift velocity is determined by:

$$\left[\frac{C_{D3} \rho_l U_{v\ell}^2}{\sigma} \right]^{a,c} \quad (5-64)$$

The second limit is calculated by [

$$\left[\frac{C_{D4} \rho_l U_{v\ell}^2}{\sigma} \right]^{a,c} \quad (5-65)$$

[

$$\left[\frac{C_{D5} \rho_l U_{v\ell}^2}{\sigma} \right]^{a,c} \quad (5-66)$$

[

$\left. \right]^{a,c}$

$$\left[\frac{C_{D,b}}{C_{D,b} + C_{D,w}} \right]^{a,c}$$

Next, the bubble drag coefficient is calculated, using Equations 5-50, 5-53, 5-57, and 5-58. [

]^{a,c}

The interfacial drag between the continuous liquid and the vapor in the small bubble regime is calculated as:

$$\left[\frac{C_{D,b}}{C_{D,b} + C_{D,w}} \right]^{a,c} \quad (5-67a)$$

where the interfacial area $A_{i,SB}$ is given in Equation 4-17. If there is significant vapor generation at the wall, the interfacial drag is ramped between the small bubble value calculated from Equation 5-67a and the inverted slug value as:

$$\left[\frac{C_{D,b}}{C_{D,b} + C_{D,w}} \right]^{a,c} \quad (5-67b)$$

The hot wall drag coefficient, $K_{iX,v\ell,HW}$ is calculated from Equation 5-105.

The value of F_{Γ} is given as:

$$\left[\frac{C_{D,b}}{C_{D,b} + C_{D,w}} \right]^{a,c} \quad (5-68)$$

where U_{tb} is calculated from Equation 5-59 and:

$$\left[\frac{C_{D,b}}{C_{D,b} + C_{D,w}} \right]^{a,c} \quad (5-69)$$

where A_x is the cell momentum area in the axial direction and Γ_v (Equation 6-101) is the cell vapor generation rate and $Q_{w\ell}$ and Q_b are the heat flow from wall to liquid and the subcooled boiling heat flow, respectively (Section 7.2). To illustrate the effect of the ramps and limits described above, Equation 5-67b was evaluated as a function of $\underline{U}_{v\ell}$ for typical fluid conditions, and plotted in Figure 5-3a. It can be seen that, at high heat flux and high relative velocities, the interfacial drag factor approaches a value more typical of separated, rather than bubbly, flow.

For lateral flow through gaps, the procedure is similar, with the following differences: the relative velocity is limited to a maximum value of []^{a,c}. The more complicated channel model is not used because, in general, gaps tend to have a large flow area, and the flow velocities are relatively small. [

$$]^{a,c}$$

The lateral flow interfacial drag uses the same expression for bubble drag coefficient except that the vector sum relative velocity is used in the Reynolds number as described earlier. The bubble drag coefficient for lateral flow uses the same logic as the axial or vertical flow. The interfacial area is calculated in the same fashion for the lateral flow as the axial flow, except the velocity is the lateral relative velocity for the gap flow. The lateral flow interfacial drag is given as:

$$\left[\frac{C_{D,b} \rho_f V_b}{A_{i,b}} \right]^{a,c} \quad (5-70)$$

Scaling Considerations

The formulation used in the small bubble regime is scale independent, since it is based on an individual bubble in the flow stream. Therefore, no scale dependence or bias would be introduced into the calculation by this model. Since the small bubble regime would be only a small region in the reactor core, before the flow regime would transition to other regimes, the noding selection used could influence the size of this regime and how it is weighted with other regimes. However the model is assessed against prototypical rod bundle data in Volume 2 of this report.

Conclusions

The small bubble regime models are based on the work of Ishii and Chawla (1979), which represents the current state of knowledge in this area. The same coding logic is used to represent the axial bubble behavior as well as the gap or lateral bubble effects.

5.4.2 Small-to-Large Bubble Flow Regime Interfacial Drag

Model Basis

The approach used for the large bubble regime is similar to that for the small bubble regime. The small bubbles are primarily in the viscous regime where $1.0 \leq Re_b \leq 1000$ whereas the larger bubbles may be in Newton's Regime where $Re_b \geq 1000$. In the Newton Regime the large bubbles are assumed to move with the average volumetric flux in the flow.

[

$]^{a,c}$

As discussed by Ishii (1977) the presence of other particles affects the resulting drag for a multi-particle system. This effect is corrected by using the appropriate mixture viscosity for multi-particle systems. As a single bubble moves in a multi-particle system, it deforms not only the neighboring fluid, but the other

particles as well. The individual particle or bubble is, in turn, distorted by its neighbors as it moves through the fluid. This effect is seen as an increased fluid viscosity. The bubble Reynolds number is defined as Equation 5-51 with the mixture viscosity correction given as Equation 5-52.

[

$\mathbf{]}^{a,c}$ In the Newton regime, the large bubbles are assumed to move relative to the average volumetric flux such that:

$$C'_{Db} = C_{Db}(1 - \alpha_v)^2 \quad (5-71)$$

where the $(1 - \alpha_v)^2$ term results from using the drift velocity to calculate the drag force, and C_{Db} is the maximum drag from Equation 5-50 or a value of $\mathbf{[}^{a,c}$.

The same basis is used for the transverse drag relationships in this regime. $\mathbf{[}$

$\mathbf{]}^{a,c}$

Model as Coded

The interfacial drag between the continuous liquid and vapor in the small-to-large bubble regime is calculated as:

$$\left[\quad \right]^{a,c} \quad (5-72)$$

where $A_{i,LB}$ is given by Equation 4-34. The calculation for the large bubble regime follows the same general procedure as the small bubble model, where $|\underline{U}_{v\ell}|$ is modified by the limits described by Equation 5-66.

For conditions in which there is a large vapor generation rate at the wall, the $\mathbf{[}^{a,c}$:

$$\left[\quad \right]^{a,c} \quad (5-73)$$

[

$\mathbf{]}^{a,c}$

The interfacial drag coefficient between the continuous liquid and vapor for the small to large bubble regime is then calculated by $\mathbf{[}^{a,c}$

$\mathbf{]}^{a,c}$

$$\left[\begin{array}{c} \text{ } \\ \text{ } \end{array} \right]^{a,c} \quad (5-74a)$$

or:

$$\left[\begin{array}{c} \text{ } \\ \text{ } \end{array} \right]^{a,c} \quad (5-74b)$$

$$\left[\begin{array}{c} \text{ } \\ \text{ } \end{array} \right]^{a,c} \quad (5-75)$$

which can be shown to be the as-coded expression:

$$\left[\begin{array}{c} \text{ } \\ \text{ } \end{array} \right]^{a,c} \quad (5-76)$$

The term α_{SB} represents the upper bound of the small bubble regime, assumed to be $\left[\begin{array}{c} \text{ } \\ \text{ } \end{array} \right]^{a,c}$.

The bubble drag relationship for the lateral flow through the gaps for the small-to-large bubble and large bubble regime are the same as the axial flow coding logic. As mentioned earlier, the lateral relative velocity along with the gap bubble radius is used to calculate the bubble Reynolds number for the bubble drag coefficient. The small-to-large bubble range is the same for the lateral flow as the axial flows given in Equation 5-72.

The effect of the models, ramps, and limits on the axial interfacial drag factor for this flow regime is shown in Figure 5-3b, and indicates similar trends as the small bubble regime.

Scaling Considerations

As described in Section 5.4.1, the noding selection could influence this flow regime and how it is weighted with other regimes. The verification of this model with noding similar to PWR noding is considered in the code assessment presented in Volume 2.

Conclusions

The bubble drag coefficient and interfacial drag relationships are consistent between lateral flow and axial flow in the WCOBRA/TRAC-TF2 model. The drag relationships are based on the extensive work by Ishii and Chawla (1979). A number of prototypical rod bundle experiments with different rod array sizes are considered in Volume 2 to assess the interfacial drag model in the small to large bubble flow regime.

5.4.3 Churn-Turbulent Flow Regime Interfacial Drag

Model Basis

The churn-turbulent regime is assumed to be a combination of the large bubble regime and the film/drop regime. The model basis for the film/drop regime is described in Section 5.4.4.

Model as Coded

The interfacial drag is calculated from the selected drag coefficient and the relative velocity as previously described in Section 5.4.2:

$$\left[\frac{C_D}{\rho_L} \right]_{a,c} \quad (5-77)$$

where the interfacial area $A_{i, LB}$ is given by Equation 4-34. The same ramp as in Section 5.4.2 is applied to consider the vapor generation rate at the wall-by-wall heat transfer.

The interfacial drag relationships for the film/drop component are described in Section 5.4.4.

For the churn-turbulent regime, a $\left[\frac{C_D}{\rho_L} \right]_{a,c}^{a,c}$:

$$\left[\frac{C_D}{\rho_L} \right]_{a,c} \quad (5-78)$$

where:

$$\left[\frac{C_D}{\rho_L} \right]_{a,c} \quad (5-79)$$

where $\alpha_{LB} = \left[\frac{C_D}{\rho_L} \right]_{a,c}^{a,c}$, and α_{crit} is given as:

$$\left[\frac{C_D}{\rho_L} \right]_{a,c} \quad (5-80)$$

The same logic is used in the lateral direction to combine large bubble and film/drop components.

Scaling Considerations

This model for interfacial drag has some scale dependence. Ishii (1977) attempted to compensate for the interaction effects of one bubble or groups of bubbles on each other through adjustments of the effective viscosity.

Conclusions

Although the model has some scale dependence, the coding logic will limit the bubble sizes based on the true physical dimensions for the problems.

5.4.4 Film/Drop Flow Regime

Model Basis

This section describes the interfacial drag models between the vapor and continuous liquid for the wetted wall film flow regime. The interfacial drag between the vapor and entrained liquid for this regime is the same as that for the hot wall dispersed droplet flow regime, and is discussed in Section 5.4.7. As shown in Section 4, when the vapor content in the flow exceeds a critical void fraction, and the wall is below the wetted wall temperature criteria, the film is assumed to become stable and liquid can no longer bridge the channel.

In the film regime, the general form of the interfacial drag coefficient is, for axial flow,

$$\left[\right]_{a,c} \quad (5-81)$$

where $A_{iX, \text{film}}$ is the interfacial area in the volume. For a thin liquid film, the interfacial area is:

$$\left[\right]_{a,c} \quad (5-82)$$

For lateral flow, the expression for interfacial area is:

$$\left[\right]_{a,c} \quad (5-83)$$

where the gap is viewed as a series of N_g vertical slots of height ΔX .

With the above equations, alternate versions of Equation 5-81 are defined:

$$\left[\right]_{a,c} \quad (5-84)$$

$$\left[\right]_{a,c} \quad (5-85)$$

The friction factor ($f_{i,FD}$) for film flow is dependent on whether the film is stable or unstable. It has been observed experimentally that the onset of film instability causes a sudden increase in system pressure drop. This is a result of increased roughness of the liquid film caused by large, unstable waves. The film friction factor for stable film flow in tubes has been studied by Wallis (1969), and Henstock and Hanratty (1976) have correlated a large amount of co-current and countercurrent film flow data for unstable films.

Henstock and Hanratty's correlation is of the form,

$$f_{i,HH} = f_s \left\{ 1 + 1400F \left[1 - \exp \left(- \frac{1}{G} \cdot \frac{(1 + 1400F)^{3/2}}{13.2F} \right) \right] \right\} \quad (5-86)$$

where:

$$G = \frac{\rho_\ell g D_h}{\rho_v U_v^2 f_s} \quad (5-87)$$

and

$$F = \frac{m^+}{\text{Re}_v^{0.9}} \frac{\mu_\ell}{\mu_v} \sqrt{\frac{\rho_v}{\rho_\ell}} \quad (5-88)$$

with:

$$m^+ = [(0.707 \text{Re}_\ell^{0.5})^{2.5} + (0.0379 \text{Re}_\ell^{0.9})^{2.5}]^{0.40} \quad (5-89)$$

and

$$\left[\quad \right]^{a,c} \quad (5-90)$$

[]^{a,c} The single-phase friction factor is different from that given in the Henstock and Hanratty (1976) paper which was:

$$f_s = 0.046 \text{Re}_v^{-.20} \quad (5-91)$$

[

] ^{a,c}

For stable films, the annular flow interfacial correlation developed by Wallis (1969) is used:

$$f_{i,W} = 0.005 [1 + 75(1 - \alpha_v)] \quad (5-92)$$

[

] ^{a,c}

As discussed in Section 4, the transition to churn-turbulent (large bubble) regime begins at a void fraction of []^{a,c} percent and continues until a stable film is achieved. The void fraction at which a stable liquid film will exist depends on the flow channel size and the vapor velocity. The critical void fraction is determined from a force balance between the disruptive force of the pressure gradient over the crest of waves on the film and the restraining force of surface tension. The resulting expression for the critical vapor fraction is:

$$\left[\frac{1}{\left(\frac{1}{\alpha} + \frac{1}{\beta} \right)} \right]^{a,c} \quad (5-93)$$

The critical void fraction is limited to a minimum value of $\left[\frac{1}{\left(\frac{1}{\alpha} + \frac{1}{\beta} \right)} \right]^{a,c}$, the value below which waves can be expected to bridge across the flow channel and cause a transition to churn-turbulent flow.

The interfacial drag logic for the lateral flow is simplified relative to the vertical flow since the film flow between the gaps is assumed to be stable and the Wallis interfacial friction factor given in Equation 5-92 is used. $\left[\frac{1}{\left(\frac{1}{\alpha} + \frac{1}{\beta} \right)} \right]^{a,c}$

Model as Coded

$\left[\frac{1}{\left(\frac{1}{\alpha} + \frac{1}{\beta} \right)} \right]^{a,c}$

$\left[\frac{1}{\left(\frac{1}{\alpha} + \frac{1}{\beta} \right)} \right]^{a,c}$ The interfacial drag is calculated as,

$$\left[\frac{1}{\left(\frac{1}{\alpha} + \frac{1}{\beta} \right)} \right]^{a,c} \quad (5-94)$$

where the interfacial area $A_{i, \text{film}}$ is given by Equation 4-51 and $f_{iX, \text{FD}}$ is given by Equation (5-92).

For lateral flow through the gaps, the interfacial friction factor is calculated using:

$$\left[\frac{1}{\left(\frac{1}{\alpha} + \frac{1}{\beta} \right)} \right]^{a,c} \quad (5-95)$$

where the factor of 2 in Equation 5-85 has been taken into account, and giving a lateral drag coefficient of:

$$\left[\frac{1}{\left(\frac{1}{\alpha} + \frac{1}{\beta} \right)} \right]^{a,c} \quad (5-96)$$

Scaling Considerations

The Wallis friction factor for film, Equation 5-92 has been examined for horizontal and vertical flow from pipe sizes ranging from 1-inch to 3-inch diameter as shown in Figure 5-4. The Hanstock and Hanratty film friction model has also been compared to vertical film flow data on diameter of 0.503 inches to 2.5 inches over a range of different fluid velocities and pressures. The comparison of their correlation to data is shown in Figure 5-5. This comparison shows that the correlation provides a good fit to the data over a range of scales.

Conclusions

The film wall drag models have been compared for both horizontal and vertical flows over a range of geometries and hydraulic diameters. WCOBRA/TRAC-TF2 has been used with these models to calculate the two-phase pressure drops in an annular film flow regime.

5.4.5 Inverted Annular Flow Regime

Model Basis

An inverted annular flow regime is assumed if the continuous liquid phase is subcooled and the surrounding surface is hot and dry. This regime consists of a liquid core surrounded by a vapor film.

For inverted annular flow, the interfacial friction factor is $f_{iX,IV}^{a,c}$:

$$\left[\frac{f_{iX,IV}^{a,c}}{f_{iX,IV}^{a,c}} \right]^{a,c} \quad (5-97)$$

Model as Coded

WCOBRA/TRAC-TF2 calculates the continuous liquid enthalpy and compares it to the saturated liquid enthalpy in the cell. If the liquid is subcooled and the wall is in the hot wall regime, the flow regime is inverted annular. If the liquid enthalpy is saturated or superheated, the code assumes the inverted liquid slug regime.

The interfacial drag for the axial momentum equation then is set to:

$$K_{iX,v\ell,IVA} = f_{iX,IVA} \frac{\rho_v |U_{v\ell}|}{2} A_{i,fil} / \Delta X \quad (5-98)$$

where the interfacial area $A_{i,fil}$ is given by Equation 4-54 and equal to $\frac{4\sqrt{\alpha_\ell} A_X \Delta X}{D_h}$.

The interfacial drag and friction models are simplified for the lateral flow in the inverted annular and inverted annular slug regimes. $f_{iX,IV}^{a,c}$

[
direction of:]^{a,c} A drag coefficient in the lateral

$$\left[\right]^{a,c} \quad (5-99)$$

is used, and the radius of the chunk of liquid is:

$$\left[\right]^{a,c} \quad (5-100)$$

The interfacial drag coefficient becomes:

$$\left[\right]^{a,c} \quad (5-100)$$

where $|\underline{W}_{v\ell}|$ is the lateral relative velocity between the continuous liquid and the vapor.

Scaling Considerations

Inverted annular flow can most commonly occur during a rapid reflood process when subcooled liquid is forced into the core either at the beginning of reflood, or when the nitrogen pressurizes the downcomer. When this situation occurs, the subcooled continuous liquid is forced into the bundle at a much higher velocity than the quench front velocity on the rods, and a thin vapor film exists on the rods' surface, separating it from the liquid core. Inverted annular flow was observed in the FLECHT and FLECHT-SEASET rod bundle experiments (Sections 14 and 15). These experiments are full-length tests using prototypical rod dimensions and spacing such that the geometric effects for this flow regime are preserved, and there are no scaling effects. The experimental conditions were varied over wide ranges to ensure that the PWR plant conditions were covered.

Conclusions

The inverted annular interfacial drag model used in WCOBRA/TRAC-TF2 is derived from the annular film flow model used for high void fraction wetted wall flows. The inverted annular interfacial drag model is assessed with full-scale prototypical rod bundle experiments for different rod arrays.

5.4.6 Inverted Liquid Slug Regime

Model Basis

As the liquid flow in the inverted annular flow regime is heated by wall heat transfer, the liquid core is accelerated by the increased vapor content of the flow. When the liquid reaches the saturation temperature, it no longer can condense the vapor and the liquid begins breaking into ligaments or chunks

into a dispersed droplet flow as it progresses up along the heated channel. The interfacial friction is calculated assuming an unstable liquid film surface exists on the large liquid ligaments or drops as:

$$\left[\right]^{a,c} \quad (5-102)$$

This equation is $\left[\right]^{a,c}$ times the Wallis (1969) equation for stable liquid films discussed earlier, given as Equation 5-92.

The interfacial area is calculated assuming that the liquid slugs are spherical, and have a diameter $\left[\right]^{a,c}$ of the channel diameter, as described in Section 4.3.3.

Model as Coded

The axial flow interfacial drag coefficient is calculated as:

$$K_{iX,IVS} = f_{i,IVS} \frac{\rho_v |U_{v\ell}|}{2} A_{i,IVS} / \Delta X \quad (5-103)$$

where the friction factor is calculated from Equation 5-102 and the interfacial area $A_{i,IVS}$ for the liquid slug regime is from Equation 4-60 as:

$$A_{i,IVS} = \frac{8.04\alpha_\ell}{D_h} A_X \Delta X \approx \frac{8\alpha_\ell}{D_h} A_X \Delta X \quad (5-104)$$

where α_ℓ is the minimum of the liquid void fraction in the mesh cell $\alpha_\ell(i,j)$ and the average liquid void is given by Equation 4-13.

Note that the ΔX term is absent from both equations, so the resulting expression is equivalent to that in Equation 5-81.

This is further modified by:

$$\left[\right]^{a,c} \quad (5-105)$$

The lower limit is necessary to allow for $\left[\right]^{a,c}$.

The lateral flow interfacial drag for the inverted slug regime is calculated in the same fashion as the inverted annular regime, as described in the previous section.

Scaling Considerations

As mentioned earlier in this subsection, the inverted annular flow regime is an evolution of the inverted annular flow regime as heat is transferred by the wall to the fluid. The inverted slug regime is a transition from the inverted annular flow regime, where the liquid column breaks up into ligaments or large liquid slugs, and into the dispersed droplets.

The interfacial drag in the inverted liquid slug regime will be somewhat sensitive to the number of heated surfaces per unit volume since the vapor layers along the heated rods will be growing. The liquid will not be continuous, but will still be trapped between the heated surfaces. Reflood experiments used to validate the WCOBRA/TRAC-TF2 code have full-height and full-scale subchannel dimensions prototypical of PWR fuel bundles. The inverted annular flow regime is expected to exist in those experiments so scaling effects if present will be evaluated as part of the code assessment.

Conclusions

The inverted slug regime is a transition hot wall regime where the liquid is breaking up into a dispersed droplet flow regime.

5.4.7 Dispersed Droplet Flow Regime

Model Basis

As discussed in Section 3, WCOBRA/TRAC-TF2 has a separate entrained liquid field. The droplet drag model is based on the work by Ishii (1977) using the analogy of a single drop in an infinite vapor medium to a single bubble in an infinite liquid field. The droplet drag models discussed in this section are used for both the hot wall and cold wall flow regimes. The interfacial friction coefficient used is:

$$\begin{aligned} K_{iX,ve,DD} &= C_{Dd} \frac{\rho_v |\underline{U}_{ve}|}{2} A_{p,d} / \Delta X \\ &= C_{Dd} \frac{\rho_v |\underline{U}_{ve}|}{2} \frac{A_{i,drop}}{4} / \Delta X \end{aligned} \quad (5-106)$$

where:

C_{Dd} = the droplet drag coefficient,

$|\underline{U}_{ve}|$ = the vector sum relative velocity between the vapor and the entrained droplet, and is given as

$$\underline{U}_{ve} = \sqrt{\max(\underline{W}_{ve})^2 + \underline{U}_{ve}^2} \quad (5-107)$$

$$A_{p,d} = \text{total projected area of the droplets, } \frac{3\alpha_e}{4r_d} A_X \Delta X$$

$$A_{i,\text{drop}} = \text{interfacial area of the droplets, } \frac{3\alpha_e}{r_d} A_X \Delta X$$

and

$$r_d = \text{the droplet radius,}$$

$$\alpha_e = \text{the entrained liquid fraction in the flow, and}$$

It can be seen that $A_{p,d} = \frac{A_{i,\text{drop}}}{4}$.

It is assumed that the drops are in the Newton Regime where the droplet Reynolds number is large. The droplet drag coefficient that is used in this is assumed to be:

$$\left[\right]_{a,c} \quad (5-108)$$

Bird, Stewart, and Lightfoot (1960) recommend a value of 0.44 for the droplet drag in the Newton Regime while Ishii and Chawla (1979) recommend a value of 0.45.

The droplet sizes used in WCOBRA/TRAC-TF2 are discussed in Section 4. The drop size is calculated as:

$$\left[\right]_{a,c} \quad (5-109)$$

Model As Coded

The current droplet diameter is first established via Equation 5-109.

The droplet interfacial drag is then calculated as:

$$K_{iX,ve,DD} = \left(C_{Dd} \frac{\rho_v |\underline{U}_{ve}|}{2} \frac{A_{i,\text{drop}}}{4} \right) / \Delta X \quad (5-110)$$

where:

$$A_{i,drop} = A_{i,d}''' A_X \Delta X \quad (5-111)$$

The droplet drag relationships for a cold wall are identical, except that there is no check on the drop size relative to the hydraulic diameters. If the drops were as large as the hydraulic diameter, they would intersect the liquid films on the wall and the channel would be filled with liquid. This would result in a different flow regime.

The lateral flow droplet calculation uses the average droplet radius calculated in each of the adjacent cells from Equation 5-109. The droplet drag coefficient for lateral flow is a constant value, $C_{Dd} = []^{a,c}$, and the lateral droplet drag coefficient is calculated as:

$$K_{iZ,ve,DD} = C_{Dd} \frac{\rho_v |W_{ve}|}{2} \frac{3\alpha_e}{4r_d} L_g \Delta X \quad (5-112)$$

Scaling Considerations

The droplet sizes have as their basis drop sizes measured in the FLECHT-SEASET program (Lee, N. et al., 1982). The interfacial drag is based on assuming spherical droplets to be in the Newton Regime (droplet Reynolds number is large). Since the rod bundle experiments have been performed on full-scale bundle simulations, the droplet interfacial drag models are applicable to the PWR.

Conclusions

There is consistency in how the droplet flow is modeled both axially and laterally. The same relationships for droplet drag are used for each drag coefficient formulation. Droplet size is derived from observations in prototypical rod bundle (FLECHT-SEASET) during reflood conditions, therefore the droplet interfacial drag models are applicable to the PWR.

5.4.8 Falling Film Flow Regime

Model Basis

As fuel rods quench from the top, a liquid film is formed on the rods behind the quench and sputtering front. Liquid is de-entrained from the upward flowing dispersed droplet flow to provide liquid source for the film on the rods. The interfacial drag relationships on the film behind the top quench front are the same as those for annular film flow except that the interfacial friction uses the Wallis (1969) friction factor given in Equation 5-92. [

$]^{a,c}$ Therefore, the interfacial friction coefficient for falling films is:

$$f_{iX,FF} = 0.005(1 + 75\alpha_\ell) \quad (5-113)$$

In the falling film regime, the gap or transverse flow film interfacial drag is calculated in the same fashion as the annular film flow drag discussed earlier in Section 5.4.4. The lateral flow of drops which are sputtered from the top down quench front would be handled in the same fashion as the droplet flow discussed in Section 5.4.7.

Model as Coded

The interfacial drag coefficient is given as:

$$C_{D,i} = \begin{cases} 0 & \text{if } \alpha_\ell > \alpha_{\ell,c} \\ f_{iX,FF} A_{i,film} & \text{if } \alpha_\ell \leq \alpha_{\ell,c} \end{cases} \quad (5-114)$$

where $f_{iX,FF}$ is from Equation 5-113 and $A_{i,film}$ is calculated from Equation 4-64.

The interfacial drag is always calculated if a cold wall is present in the cell. If the cell void fraction is greater than $\alpha_{\ell,c}$, then the flow regime is a falling film regime with upward flowing entrained droplets. If the void fraction is below $\alpha_{\ell,c}$ and the liquid flow is from the top, then the interfacial drag is ramped between the top deluge regime and the falling film regime. The top deluge interfacial drag coefficients will be discussed in Section 5.4.9.

Scaling Considerations and Conclusions

No major scaling issue was identified. The falling film flow regime was designed to simply approximate the behavior of the top quench front. The model is exercised as part of the assessment against prototypical rod bundle tests presented in Sections 14 and 15.

5.4.9 Top Deluge Flow Regime

Model Basis

When the walls are hot and a large amount of liquid flows downward into a computational cell, the flow regime is called the top deluge. This flow regime is similar to the liquid slug regime for upflow as discussed in Section 5.4.6. The top deluge regime is assumed present at void fractions less than $\alpha_{\ell,c}$. Physically, the top deluge regime could occur with large liquid injection rates in a PWR upper plenum due to upper plenum injection or upper head injection. The top deluge regime would also occur during blowdown when the core flow reverses and large amounts of liquid either drain out of the upper head or plenum and are forced into a hot core. PWR with combined injection, hot leg, and cold leg accumulators, where the hot leg accumulators inject large liquid flows in the upper plenum, could also experience the top deluge flow regime.

Model As Coded

The droplet drag coefficient is calculated as the maximum of:

$$C_{Dd} = \frac{24}{Re_v} \left[1.0 + 0.1 Re_v^{.75} \right] \quad (5-115)$$

where Re_v is the vapor Reynolds number in the cell based on local vapor properties; and:

$$\left[\quad \quad \quad \right]^{a,c} \quad (5-116)$$

The interfacial drag coefficient for top deluge regime is calculated as:

$$K_{iX,v\ell,TD} = C_{Dd} \frac{\rho_v |\underline{U}_{v\ell}|}{2} \frac{A_{i, \text{film}}}{4} / \Delta X \quad (5-117)$$

where the interfacial area is given by Equation 4-66.

The low vapor fraction for this regime implies that the liquid is filling most of the channel. Note that the velocity used in Equation 5-117 is the relative velocity between the continuous liquid and the vapor, rather than the entrained liquid to vapor, since the liquid slugs are modeled by the continuous liquid field. Again, the model represents large liquid slugs or chunks which would nearly fill the channel and would capture any small droplets in the channel.

[

]^{a,c}

Scaling Considerations and Conclusions

The top deluge model is similar to the liquid slug model for upflow. The basic correlations that are used are scale dependent because they depend on the channel hydraulic diameter. However, models have been assessed against prototypical rod bundle tests as discussed in Sections 14 and 15.

**WCAP-16996-P, “Realistic LOCA Evaluation Methodology Applied to the Full Spectrum of Break Sizes
(FULL SPECTRUM LOCA Methodology)”
Requests for Additional Information – (Non-Proprietary)
RAIs 72, 73, 74 and 76**

June 2013

Westinghouse Electric Company LLC
1000 Westinghouse Drive
Cranberry Township, PA 16066

©2013 Westinghouse Electric Company LLC
All Rights Reserved

Question 72: Bubbly Flow Drag Assessment Using Thermal Hydraulic Test Facility Test Data

WCAP-16996-P/WCAP-16996-NP, Volumes I, II, and III, Revision 0, Subsection 13.4.2, “ORNL-THTF Small Break Tests,” clarifies that “YDRAG is a multiplier on the interfacial drag value that is used to bias the value computed by the code. It is specified on an individual cell basis, and 1.0 is the default value.” The bubbly flow drag multiplier, YDRAG, is applied directly to the interfacial drag as calculated for SB flow from Equation (5-67a) and for Large Bubble flow from Equation (5-72):

$$I = I^{a,c}$$

WCAP-16996-P/WCAP-16996-NP, Volumes I, II, and III, Revision 0, Subsection 29.1.5 explains that “The YDRAG multiplier is the sole contributor for void fractions α_v less than 0.5.” It is also clarified that “in the interpolation region between the small and small-to-large bubbly flow regime ($\alpha_v < 0.5$) and the annular film flow regime ($\alpha_v > \alpha_{crit} \sim 0.8$) both YDRAG and FDRAG have an effect.” Subsection 29.1.5 of WCAP-16996-P/WCAP-16996-NP, Volumes I, II, and III, Revision 0, states that YDRAG “is applied directly to the small bubble, large bubble and hot wall interfacial drag calculations.”

Subsection 13.4.2 of WCAP-16996-P/WCAP-16996-NP, Volumes I, II, and III, Revision 0, examines [the effect of three different YDRAG values of $I^{a,c}$ on WCOBRA/TRAC-TF2 axial void fraction predictions for 12 ORNL THTF test runs as summarized in Table 1.

Table 1: ORNL THTF Tests Used in YDRAG WCOBRA/TRAC-TF2 Sensitivity Analysis

Test Facility	Test Bundle	Test Runs	Number and Type of Test Runs		YDRAG and Number of Test Runs Analyzed			
			Bundle Uncovery	Level Swell	YDRAG = $I^{a,c}$	YDRAG = $I^{a,c}$	YDRAG = $I^{a,c}$	YDRAG = $I^{a,c}$
THTF	8x8	12	6	6	12	12	12	12

The WCOBRA/TRAC-TF2 void fraction predictions with $I^{a,c}$ are compared against ORNL THTF bundle void fraction measurements in Figures 13.4.2-16 through 13.4.2-27. Sensitivity studies were performed with $I^{a,c}$ WCAP-16996-P/WCAP-16996-NP, Volumes I, II, and III, Revision 0, Subsection 13.4.2.7, “Summary and Conclusions,” states [

$I^{a,c}$ As such, it is concluded that the YDRAG range determined from the boiloff experiments adequately captures the data for the ORNL bundle uncovery and level swell simulations.”

- (1) Please identify the measured void fraction data points in the analyzed THTF tests, for which WCOBRA/TRAC-TF2 predicts a SB configuration and document the data in a table. For each point, provide the measured void fraction value, void fraction measurement uncertainty (shown in Figures 13.4.2-16 through 13.4.2-27), corresponding liquid and vapor mass flow rates, criteria used to identify the data points, predicted nominal interfacial drag coefficient, C_{Db} along with parameters that entered into its calculation. Include corresponding void fraction predictions for $I^{a,c}$. Please document each data point in a separate row and present the above identified quantities in separate columns. Please provide a plot comparing predicted void fractions versus measured data showing void fraction measurement accuracy. Please apply the nominal $I^{a,c}$ in code predictions. In a separate table, please compare the flow conditions characterizing each measured data point against the applicability range for the interfacial drag correlations used in the code void fraction predictions.

- (2) Please identify the measured void fraction data points in the analyzed THTF test runs, for which WCOBRA/TRAC-TF2 predicts existence of a SLB flow regime ($0.20 < \alpha \leq 0.50$). For these data points, please provide the information requested in item (1) above for SB flow. Please apply the []^{a,c} in code predictions and provide a separate table, which compares the flow conditions characterizing each measured data point against the applicability range for the interfacial drag correlations used in the code void fraction predictions.
- (3) Please explain predicted instances of decreasing void fraction with increasing bundle axial elevation as observed in void fraction results shown in Figure 13.4.2-6 for Test 3.09.10K, in Figure 13.4.2-12 for Test 3.09.10CC (at []^{a,c}), in Figure 13.4.2-14 for Test 3.09.10EE, and in Figure 13.4.2-15 for Test 3.09.10FF. Provide the causes for void fraction decrease at higher axial elevations taking into consideration, among other relevant factors, the fact that the flow area does not increase with height.
- (4) WCAP-16996-P/WCAP-16996-NP, Volumes I, II, and III, Revision 0, Subsection 29.1.5 states that YDRAG “is applied directly to the SB, large bubble and hot wall interfacial drag calculations.” Please provide a detailed description of and justification for YDRAG application to “Hot Wall” interfacial drag.

Question 73: Bubbly Flow Drag Assessment Using G-1 and G-2 Test Data

WCAP-16996-P/WCAP-16996-NP, Volumes I, II, and III, Revision 0, Subsection 13.4.3, “Simulation of G-1 Core Uncover Tests,” explains that 16 core uncover test runs conducted in the Westinghouse ECCS HPTF with the G-1 15×15 grid test bundle were used to define an uncertainty range for YDRAG. From the G-1 tests, 33 level swell data points were identified for the 10-foot, 8-foot, and 6-foot elevations, experiencing uncover, and were compared against WCOBRA/TRAC-TF2 predictions. The YDRAG uncertainty range study also included 9 core uncover test runs conducted in the Westinghouse ECCS HPTF with the G-2 19×19 grid test bundle (336 heater rods) as described in Subsection 13.4.4, “Simulation of G-2 Core Uncover Tests of WCAP-16996-P/WCAP-16996-NP, Volumes I, II, and III, Revision 0. From the G-2 tests, 18 level swell data points were identified for the 10-foot and 8-foot elevations, exhibiting uncover, and were compared against code predictions. Figures 13.4.3-9 and 13.4.4-8 compare measured versus predicted level swell using nominal YDRAG multiplier. Table 1 summarizes the Westinghouse ECCS HPTF G-1 and G-2 runs used to assess the bubbly flow interfacial drag.

Table 1: Westinghouse HPTF G-1 and G-2 Tests Used in YDRAG Range/Distribution Analysis

Test Facility	Test Bundle	Test Runs	Data Points	Note
Westinghouse ECCS HPTF	G-1 (15×15)	16	33	[] ^{a,c}
Westinghouse ECCS HPTF	G-2 (19×19)	9	18	[] ^{a,c}

Please provide additional information as described in the items below using the nominal YDRAG value ([]^{a,c}) in relevant analyses and, for consistency with previous results, with []^{a,c}

- (1) The YDRAG uncertainty study is based on calculated (or secondary) G-1 and G-2 test data representing the collapsed liquid level in the test bundle. As described in WCAP-16996-P/WCAP-16996-NP, Volumes I, II, and III, Revision 0, Subsection 13.4.3.6, “Simulation of G-1 Core Uncover Tests,” and in Subsection 13.4.4.6, “Simulation of G-2 Uncover Tests,” the collapsed level data were based on differential pressure/level transducer readings at points in time when heater rod thermocouples (TCs) located at selected axial elevations started indicating temperature rise above the saturation level due to mixture level falling below the TC elevations. Please provide the accuracy of the calculated collapsed liquid level data in the G-1 and G-2 tests using instrumentation accuracies for the measured test data. Derive the associated accuracy for the average level swell data provided in Table 13.4.3-3, “G-1 Simulation Results Summary at Model Nominal YDRAG,” and in Table 13.4.4-4, “G-2 Simulation Results Summary at Model Nominal YDRAG.” Present the results in a separate column in both tables and show accuracy bars for the data plotted in Figures 13.4.3-9 and 13.4.4-8.
- (2) Table 2 provides the TC elevations used to identify the mixture level and the associated collapsed liquid level in the examined G-1 and G-2 tests. In addition, the table lists the corresponding elevations reported in the WCOBRA/TRAC-TF2 runs in Tables 13.4.3-3 and Table 13.4.4-4. Also listed are elevations for cell interfaces nearest to the TC elevations according to the noding diagrams provided in Figure 13.4.3-6, “WCOBRA/TRAC-TF2 Model of the G-1 Test Bundle” and in Figure 13.4.4-6, “WCOBRA/TRAC-TF2 Model of the G-2 Test Bundle.” It is seen that there is a difference of up to about []^{a,c} between the TC elevations and those reported in the WCOBRA/TRAC-TF2 runs. A difference of up to []^{a,c} between the TC elevations and the nearest cell interface elevations in the WCOBRA/TRAC-TF2 G-1 model is evident. For the G2 model, this difference is smaller and it is limited to []^{a,c}. Please describe the reason for these discrepancies, which, in combination with a large cell size, can introduce errors in the comparison between data and code predictions for

level swell. Present analysis results obtained with modified G-1 and G-2 WCOBRA/TRAC-TF2 models in which TC elevations coincide with cell interface elevations and the heated conductors are modified accordingly and provide the updated Figures 13.4.3-9 and 13.4.4-8.

Table 2: G-1 and G-2 TC Elevations and Elevations Reported in WCOBRA/TRAC-TF2 Runs

Reference Elevation (ft)	TC Elevation				Elevations Reported in WCOBRA/TRAC-TF2 Runs				Cell Interface Elevations* in WCOBRA/TRAC-TF2 Models			
	G-1 Bundle		G-2 Bundle		G-1 Model		G-2 Model		G-1 Model		G-2 Model	
	(in)	(ft)	(in)	(ft)	(in)	(ft)	(in)	(ft)	(in)	(ft)	(in)	(ft)
10	[] ^{a,c}	118.9	9.908	[] ^{a,c}
8	[] ^{a,c}	94.3	7.858	[] ^{a,c}
6	[] ^{a,c}	69.7	5.808	[] ^{a,c}

× Elevation provided from the bottom of heated length.

+ Elevation did not uncover.

△ Nearest cell interface is below TC.

† Nearest cell interface is above TC.

- (3) It is seen from the predicted cladding temperature shown in Figure 13.4.4-7, “Collapsed Liquid Level and Predicted Cladding Temperatures at the 8- and 10- Foot Elevations, G-2 Test 716,” that the 7.96-ft elevation uncovers shortly after 1,200 seconds. From the plots of the liquid and mixture levels in the test bundle measured in G-2 Run 716 on pages 716-24 and 716-28 in EPRI Report AN-1692 Volume 2, it is estimated that the TC at the 94.3-inch elevation uncovers at approximately 1,900 s. Please explain this large timing discrepancy between test data and code prediction. Please clarify which void fraction value is plotted in Figure 13.4.3-8, “Void Fraction and Predicted Cladding Temperature at the 10- Foot Elevation, G-1 Test 62,” referring to the nodding diagram shown in Figure 13.4.3-6.
- (4) Using the G-2 TC elevations and the elevations reported in WCOBRA/TRAC-TF2 G-2 runs provided in Table 2, it is possible to reproduce both the data and code predictions for the level swell values provided in Table 13.4.4-4 assuming that the liquid is saturated at the bottom of heated length. However, the observed and predicted level swell values documented in Table 13.4.3-3 for G-1 test runs cannot be reproduced in the same manner. Please explain the reason for this inconsistency and provide corrected values if necessary.
- (5) The heated length of the G-1 test bundle is 144 inch (12.0 ft) and the G-2 test bundle heated length is 164 inch (13.667 ft). According to the nodding diagrams provided in Figures 13.4.3-6 and 13.4.4-6, this length is represented using 12 cells in the WCOBRA/TRAC-TF2 G-1 model and 16 cells in the WCOBRA/TRAC-TF2 G-2 model. After resolving the above identified items, please present code prediction results for the bundle level swell obtained with doubling the number of axial cells used to represent the heated bundle length for both test facilities. Present the updated Tables 13.4.3-3 and 13.4.4-4 with the obtained results and present them graphically by updating Figures 13.4.3-9 and 13.4.4-8.
- (6) Please provide comparisons of code predictions for clad temperatures and sink temperatures against test data for all test data axial locations for G-2 Test 718. Also show comparisons for the two-phase level

and collapsed liquid level predictions against test data for this test. Please provide comparisons of code predictions obtained with drag multipliers of []^{a,c} against test data.

Question 74: Interfacial Drag Sampling Approach

The capabilities of WCOBRA/TRAC-TF2 to predict the core void and the resultant mixture level swell for SBLOCAs are assessed in WCAP-16996-P/WCAP-16996-NP, Volumes I, II, and III, Revision 0, Section 13, “Core Void Distribution and Mixture Level Swell.” WCAP-16996-P/WCAP-16996-NP, Volumes I, II, and III, Revision 0, Subsection 13.2, “Physical Processes,” clarifies that “in SBLOCA scenarios, the steam velocities are too low to entrain droplets at the two-phase interface, and thus entrainment is negligible.” It is also explained that “...the liquid and vapor flow rates are low, which make wall drag due to form and friction losses negligible compared to the interfacial drag.” Thus, “...the mixture level swell is most directly affected by the interfacial drag between vapor and liquid, and the bubble rise velocity and bubble size.”

WCAP-16996-P/WCAP-16996-NP, Volumes I, II, and III, Revision 0, Section 29, “Assessment of Uncertainty Elements,” identifies three categories of uncertainty parameters: (1) nominal without uncertainty, (2) bounded, and (3) nominal with uncertainty. Model uncertainties related to “thermal-hydraulic global models” and belonging to the third category of uncertainty parameters are presented in Table 29-2, “Uncertainty Elements – Thermal-Hydraulic Models,” which includes the bubbly and film flow drag multipliers YDRAG and FDRAG, among others.

WCAP-16996-P/WCAP-16996-NP, Volumes I, II, and III, Revision 0, Subsection 29.1.5, “Interfacial Drag in the Core Region,” presents the PDFs proposed for the interfacial drag multipliers in WCOBRA/TRAC-TF2 uncertainty assessments. The subsection explains that “Rather than calibrating multipliers or adjustments to each individual closure relationships, the level swell is ‘globally’ ranged by applying the same multiplier to the interfacial drag coefficient calculated in each cell of the two-phase region.” Accordingly, “Two multipliers were added in the code to allow ranging capability on interfacial drag.” The multipliers, YDRAG and FDRAG, are applied directly to the drag coefficient in the expression for the interfacial drag force, $\tau'_{iX, vl}$:

$$\tau'_{iX, vl} = (YDRAG \times K_{iX, vl}) \underline{U}_{vl} \quad \text{and} \quad \tau'_{iX, vl} = (FDRAG \times K_{iX, vl}) \underline{U}_{vl}.$$

YDRAG and FDRAG are specified on an individual cell basis and apply to different flow regimes of the “Cold Wall” two-phase flow regime map in the WCOBRA/TRAC-TF2 vessel component.

Table 1 provides a summary description of the interfacial drag multipliers.

Table 1: “Global” Interfacial Drag Multipliers Used in Two-Phase Flow Regimes of the WCOBRA/TRAC-TF2 Vessel Component “Cold Wall” Flow Map

Flow Regime	Void Fraction α (%)	Applicable Multiplier	Applicable Drag Multiplier		Note
			YDRAG	FDRAG	
Small Bubble	$0 < \alpha \leq 20$	YDRAG	[] ^{a,c}	[] ^{a,c}	Specified on an individual cell basis
Small-to-Large Bubble	$20 < \alpha \leq 50$				
Churn-Turbulent	$50 < \alpha \leq \alpha_{crit}$	YDRAG FDRAG	[] ^{a,c}	[] ^{a,c}	Specified on an individual cell basis
Film/Drop	$\alpha_{crit} < \alpha \leq 100$	FDRAG	[] ^{a,c}	[] ^{a,c}	Specified on an individual cell basis

WCAP-16996-P/WCAP-16996-NP, Volumes I, II, and III, Revision 0, Subsection 29.1.5 describes the application of Westinghouse ECCS HPTF G-1 and G-2 test data to assess an uncertainty range for YDRAG. In code simulations of G-1 and G-2 test runs, [

] ^{a,c} For the G-1 simulations, [

] ^{a,c} In the calculations
for the G-2 data set, [

] ^{a,c} WCAP-16996-P/WCAP-16996-NP, Volumes I, II, and III, Revision 0, Subsection 29.1.5 concludes that [

] ^{a,c} Table 2 summarizes the Westinghouse ECCS HPTF G-1 and G-2 uncertainty assessment for YDRAG.

Table 2: Westinghouse HPTF G-1 and G-2 Tests Used in YDRAG Range/Distribution Analysis

Test Facility	Test Bundle	Test Runs	Data Points	Data Points and YDRAG Values to Recover Level Swell			Average YDRAG	Note
				[] ^{a,c}		
W ECCS HPTF	G-1 (15×15)	[] ^{a,c}
W ECCS HPTF	G-2 (19×19)	[] ^{a,c}

(×) [] ^{a,c}

- (1) RG 1.157 Revision 0, “Best-Estimate Calculations of Emergency Core Cooling System Performance,” states that “A best-estimate model should provide a realistic calculation of the important parameters associated with a particular phenomenon to the degree practical with the currently available data and knowledge of the phenomenon.” In addition, RG 1.157 requires that “If it is not possible or practical to consider a particular phenomenon, the effect of ignoring this phenomenon should not normally be treated by including a bias in the analysis directly, but should be included as part of the model uncertainty.”

Figure 1 below illustrates the impact of the proposed range limits and nominal YDRAG values on WCOBRA/TRAC-TF2 void fraction predictions for ORNL THTF Test 3.09.10CC according to results documented in WCAP-16996-P Revision 0 Figure 13.4.2-24. Please explain the technical rationale and requirements behind the approach of determining and assigning a sampling range to a physical quantity, which is amenable to quantification using experimental measurements, in quantifying the impact of its variation on assessing the uncertainty in predicting other physical parameters that can depend on that sampled quantity. Consider relevant factors such as: (a) state of knowledge, availability and accuracy of pertinent data, (b) uncertainty range versus measurement accuracy for individual physical parameters, (c) uncertainty assessment for individual governing parameters, (d) need for adequacy, quality and rigor of prediction tool qualification and assessment.

- (2) WCAP-16996-P/WCAP-16996-NP, Volumes I, II, and III, Revision 0, Subsection 29.1.5 states that YDRAG “is applied directly to the SB, large bubble and hot wall interfacial drag calculations.” Explain the rationale for assigning a sampling range “globally” to multiple parameters that describe different processes and phenomena (e.g., SB, large bubble, CT flow, “Hot Wall” interfacial drag) without qualifying uncertainties associated with each individual model considering the possibility for compensating errors.

a,c

Figure 1: Impact of Bubbly Flow Drag Multiplier YDRAG on WCOBRA/TRAC-TF2 Void Fraction Predictions for ONL THTF Test 3.09.10CC

- (3) The aspect of WCOBRA/TRAC-TF2 approach to interfacial drag calculation that involves implementation of “global” input drag multipliers, YDRAG and FDRAG, used to directly modify, also as part of the uncertainty sampling process, closure terms in the momentum conservation equations is questionable from a methodological point of view. The proposed approach to sampling of interfacial drag interferes with the quantification of specific physical quantities that have been a subject to extensive experimental and analytical studies aimed at their quantification using deterministically

established and experimentally validated constitutive models. The questionability of such an approach is particularly exacerbated by the safety relevance of these models as they impact level swell prediction, which, in turn, has a strong impact on SBLOCA PCT predictions. Equally relevant, availability of two-phase flow data measurements for interfacial drag quantification for both pipe and rod bundle geometries leaves little tolerance space for such an approach. Constitutive correlations need to be demonstrated as applicable and appropriate under the intended conditions of code applications. Please explain how the proposed interfacial drag sampling approach that effectively varies a physical quantity, otherwise amenable to quantification from measured physical parameters, by a factor of []^{a,c} applied across an entire spectrum of two-phase flow regimes, demonstrates the applicability of WCOBRA/TRAC-TF2 to predict realistically core level swell and resulting PCT predictions.

- (4) If WCOBRA/TRAC-TF2 is applied to quasi-steady unidirectional two-phase flow in a channel with well defined boundary and geometry conditions, thus rendering interfacial drag as the only thermal-hydraulic model parameter of relevance in assessing code uncertainty, how should void fraction and level swell predictions relate to accuracy of void/level measurements when drag has been subjected to sampling?
- (5) RG 1.157 Revision 0, states that “A best-estimate model should provide a realistic calculation of the important parameters associated with a particular phenomenon to the degree practical with the currently available data and knowledge of the phenomenon.” More specifically with regard to level swell prediction, RG 1.157, Revision 0 clarifies that “A correlation or model to be used in ECCS evaluation to calculate level swell should be checked against an acceptable set of relevant data and should recognize the effects of depressurization, boil-off, power level, fluid conditions, and system geometry.” As proposed in WCAP-16996-P/WCAP-16996-NP, Volumes I, II, and III, Revision 0, Subsection 29.1.5, “Interfacial Drag in the Core Region,” an interfacial drag multiplier ranging from []^{a,c} suggests that the two-phase flow drag models implemented in WCOBRA/TRAC-TF2 are deficient. It is recognized that even small variations in swelled levels amounting to 3 to 6 inches during protracted periods of core uncover under limiting break conditions can result in pronounced changes in PCT predictions. Improved physical models for two-phase flow interfacial drag prediction can be associated with a reduced drag sampling range or even eliminate the need for drag sampling altogether. Please discuss and provide a resolution approach for interfacial drag modeling and sampling in WCOBRA/TRAC-TF2.

1.0 Introduction and Problem Statement

The YDRAG parameter is used to account for uncertainty in the calculated core level swell by varying the interfacial drag in the core region. This parameter is meant to satisfy U.S. NRC Regulatory Guide 1.157 (Reference 4) by providing a means to bypass the convolutions of the uncertainties associated with the data (discussed in Section 2) and the models altogether, and use a single, global parameter to capture the uncertainties associated with a very important SBLOCA phenomenon. Considering both the uncertainty of the data sets as well as the model uncertainty, the resulting range is fairly large. YDRAG is meant to capture this somewhat large uncertainty range to satisfy the requirements of Reference 4 for level swell predictions.

The common theme among Requests for Additional Information (RAIs) 73 and 74 is the []^{a,c} Aside from some specific questions, the crucial areas in which the reviewers challenge the methodology are []

[]^{a,c}

In addition, parts (1) and (2) of RAI 72 asks for []^{a,c}

Section 2 of this response will address issues (a) and (b) above, and Section 3 will focus on responding to issues (c) and (d) above. Finally Section 4 will map specific questions contained in RAIs 72, 73, and 74 to the issues above.

2.0 Data Base Considered for the Bubbly Flow [

] ^{a,c}

2.1 Summary of Test Facilities Considering [

] ^{a,c}

As explained in Section 29.1.5 of Reference 1, [

] ^{a,c}

During a SBLOCA scenario, the cladding heatup usually begins with core uncover. Though the safety injection (SI) pumps begin injecting liquid to the reactor coolant system (RCS) early in the SBLOCA transient, the break flow outweighs this contribution until the accumulators inject. Thus, the liquid in the vessel gradually depletes and ultimately leads to core uncover while the core is in a boil-off scenario. As such, [

] ^{a,c}

The ORNL-THTF test is a quasi-steady state test in which the liquid mass flow rate matches the steam mass flow rate, and a steady mixture level is established. This is generally not the case in the SBLOCA transient, as the core liquid level generally decreases over time. [

] ^{a,c}

The GE Blowdown tests are rapid depressurization and flashing tests which are meant to simulate the blowdown phase of a transient with a relatively large hydraulic diameter. Due to the large hydraulic diameter, the GE Blowdown tests are not fully applicable to model the core region. [

] ^{a,c}

FULL SPECTRUM™ and **FSLOCA™** are trademarks of Westinghouse Electric Company LLC, its affiliates and/or its subsidiaries in the United States of America and may be registered in other countries throughout the world. All rights reserved. Unauthorized use is strictly prohibited. Other names may be trademarks of their respective owners.

2.2 Determination of Level Swell

[

] ^{a,c}

Equation 13-1 of Reference 1 is utilized (Equation 2-1 herein):

$$S = \frac{(Z_{2\Phi} - Z_{SAT}) - (Z_{CLL} - Z_{SAT})}{Z_{CLL} - Z_{SAT}} \quad (\text{Equation 2-1})$$

Each term of this equation has uncertainty associated with it, which will be discussed in the following subsections.

2.2.1 Two-Phase Mixture Level ($Z_{2\Phi}$)

[

] ^{a,c}

[

]^{a,c}

2.2.2 Collapsed Liquid Level (Z_{CLL})

[

]^{a,c}

2.2.3 Saturated Liquid Level (Z_{SAT})

[

]^{a,c}

[

] ^{a,c}

[

] ^{a,c}

2.2.4 Summary of the Uncertainty in the Level Swell Calculations

Based on the discussions in Sections 2.2.1 through 2.2.3, the following subsections discuss the uncertainties for the level swell calculations for each test facility.

2.2.4.1 G1 Boil-off Tests

[

] ^{a,c}

2.2.4.2 G2 Boil-off Tests

[

] ^{a,c}

[

] ^{a,c}

2.2.5 Other Sources of [

] ^{a,c}

[

] ^{a,c}

2.2.6 Conclusions Regarding the [

] ^{a,c}

Based on the discussions in Sections 2.2.1 through 2.2.5, [

] ^{a,c}

[

] ^{a,c}

2.3 Axial Void Fraction Profile and Average Void Fraction

[

] ^{a,c}

Table 2-1: Summary of the Uncertainty for the G1 Boil-Off Level Swell Calculations

a,c

Table 2-2: Summary of the Uncertainty for the G2 Boil-Off Level Swell Calculations

a,c

a,c

Figure 2-1: [

]^{a,c}

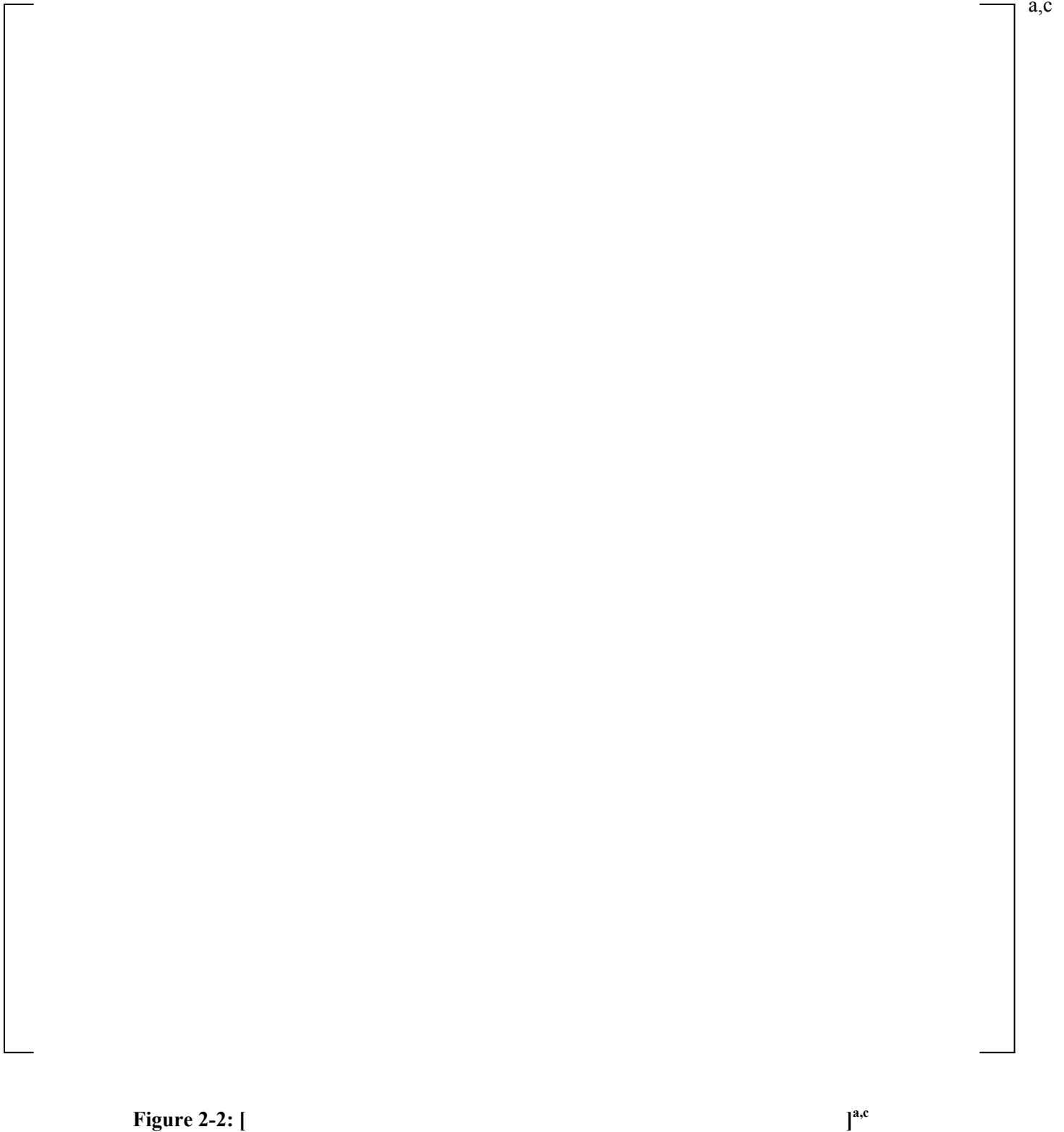




Figure 2-3: Uncertainty in the G1 Boil-Off Calculations for the []^{a,c}



Figure 2-4: Uncertainty in the G1 Boil-Off Calculations for the []^{a,c}

a,c

Figure 2-5: Uncertainty in the G1 Boil-Off Calculations for the []^{a,c}



Figure 2-6: Uncertainty in the G2 Boil-Off Calculations for the []^{a,c}



Figure 2-7: Uncertainty in the G2 Boil-Off Calculations for the []^{a,c}

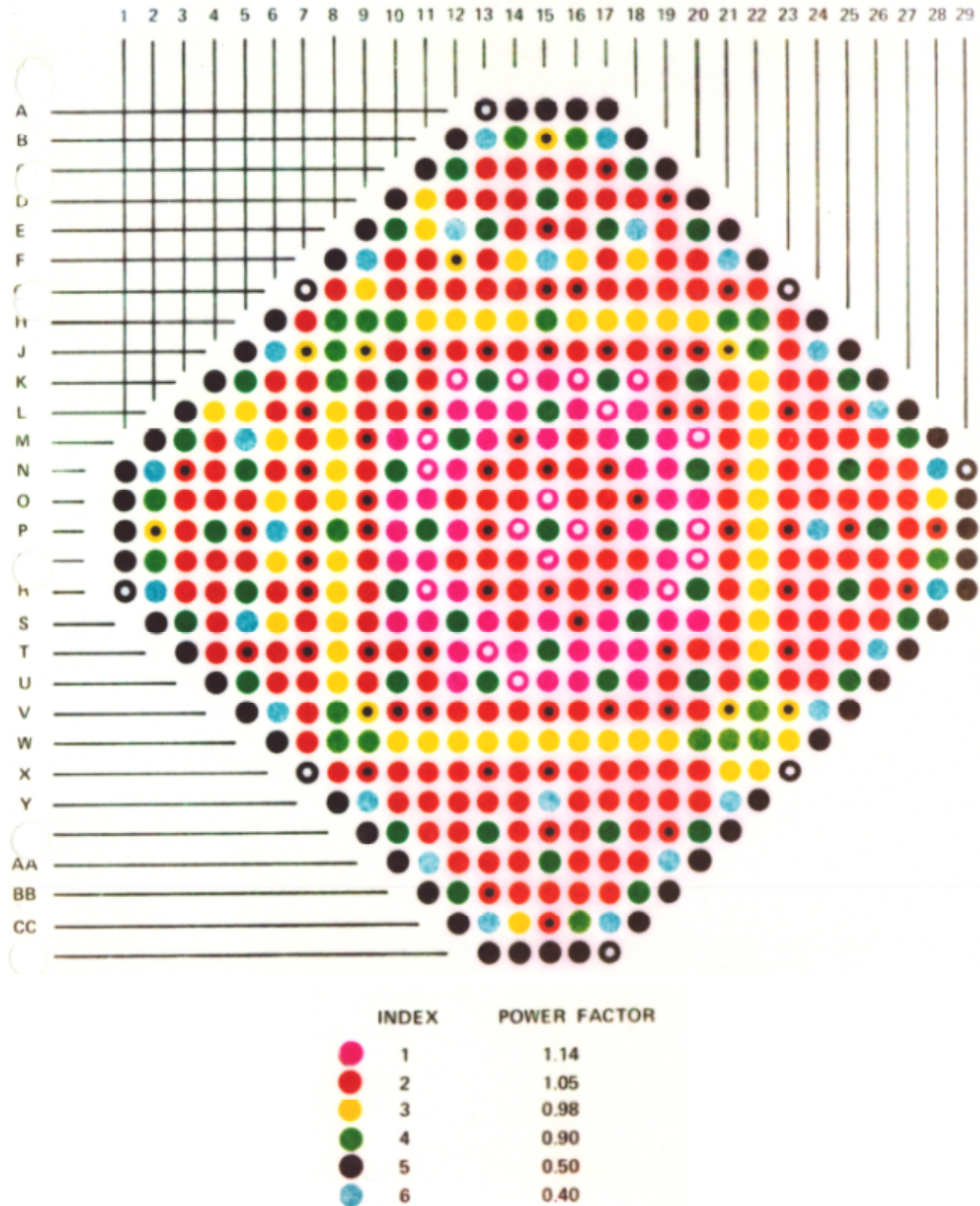


Figure 2-8: Radial Power Distribution in the G1 Boil-off Facility

Note: Black and white dots indicate instrumented rods.



Figure 2-9: G2 Boil-off [

]^{a,c}



Figure 2-10: G2 Boil-off [

]^{a,c}

3.0 Purpose and Applicability of []^{a,c}

[

] ^{a,c}

3.1 Discussion of the Effects of []^{a,c}

[

] ^{a,c}

3.2 Nonlinearity of []^{a,c}

[

] ^{a,c}

[

] ^{a,c}

3.3 Sensitivity of Drag Calculations to [] ^{a,c}

[

] ^{a,c}

[

] ^{a,c}

3.4 Summary of Purpose of []^{a,c}

In RAI 74, the reviewer refers to U.S. NRC Regulatory Guide 1.157 Revision 0 (Reference 4), which states that: "A best-estimate model should provide a realistic calculation of the important parameters associated with a particular phenomenon to the degree practical with the currently available data and knowledge of the phenomenon. If it is not possible or practical to consider a particular phenomenon, the effect of ignoring this phenomenon should not normally be treated by including a bias in the analysis directly, but should be included as part of the model uncertainty."

[

] ^{a,c}

3.5 Additional Study on Level Swell Predictions

[

] ^{a,c}

Reference 5 documents the results of a series of ROSA-IV LSTF tests, which were performed to investigate the void fraction distribution in the bundle at different pressure and power levels. Test ST-NC-06E was simulated with WC/T-TF2, [

] ^{a,c}

As described in Reference 5, this test was performed with the primary side partially filled with water and heated up by the core power which was set at the required level for each test. The core heat was removed by transferring heat from the primary to the secondary side through reflux condensation; this is a condition where the steam generators act as a heat sink. To achieve this condition, the secondary side pressure is maintained lower than the primary side and at saturation conditions such that all of the vapor generated in the core is condensed in the steam generator U-tubes and is drained back into the core in a quasi steady-state.

[

] ^{a,c}

Table 3-1: Comparison of the Level Swell Predictions for the G2 Boil-off Tests [
]^{a,c}

a,c

Table 3-2: Comparison of the Level Swell Predictions for the G2 Boil-off Tests [] ^{a,c}

a,c

a,c

Figure 3-1: Comparison of the Accuracy of Level Swell Predictions for the G2 Boil-off Tests [
]^{a,c}



Figure 3-2: Level Swell as a Function of [

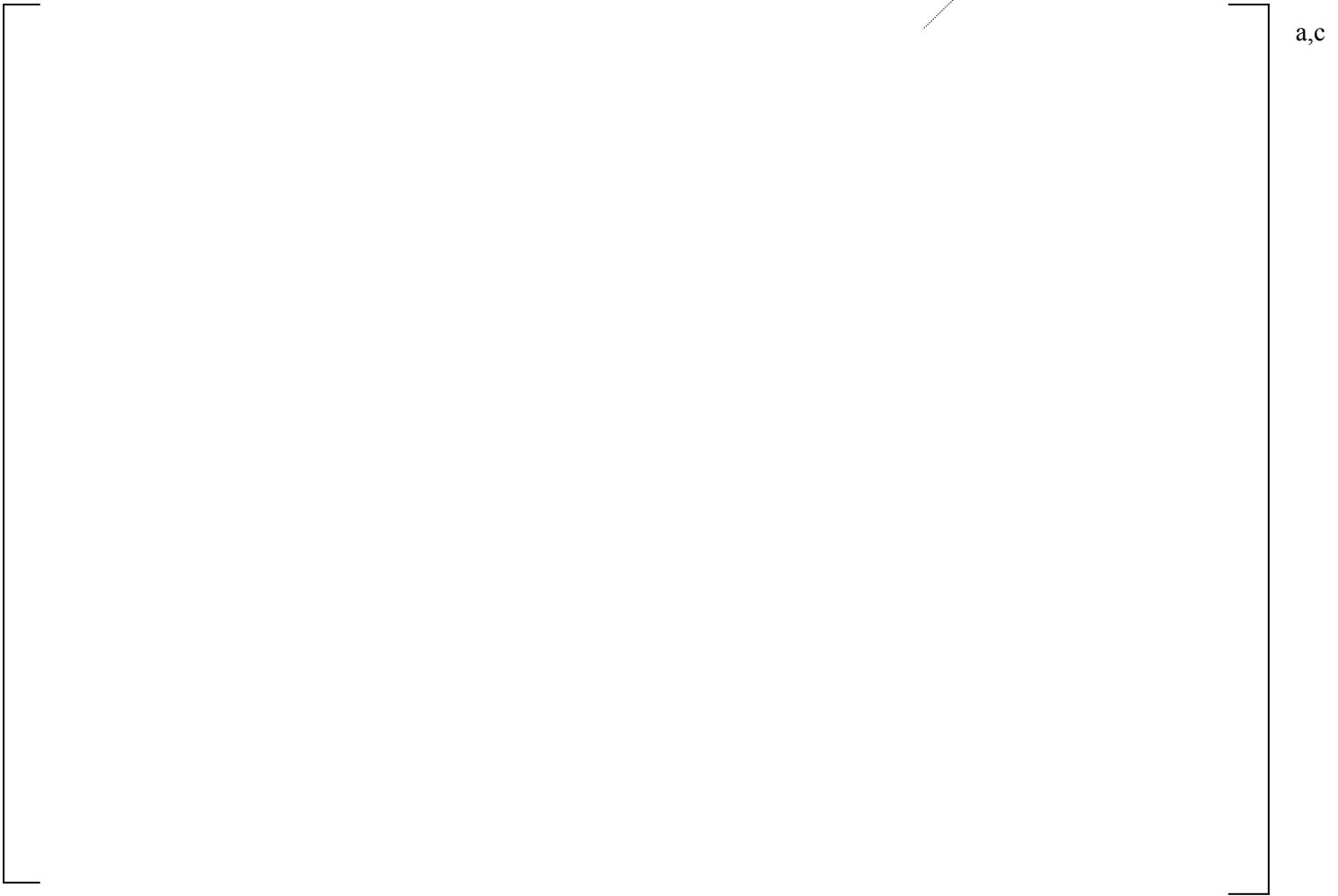
] ^a,c



Figure 3-3: Level Swell as a Function of [

] ^{a,c}





a,c

Figure 3-5: Comparison of the Accuracy of Level Swell Predictions for the G2 Boil-off Tests [

] ^{a,c}

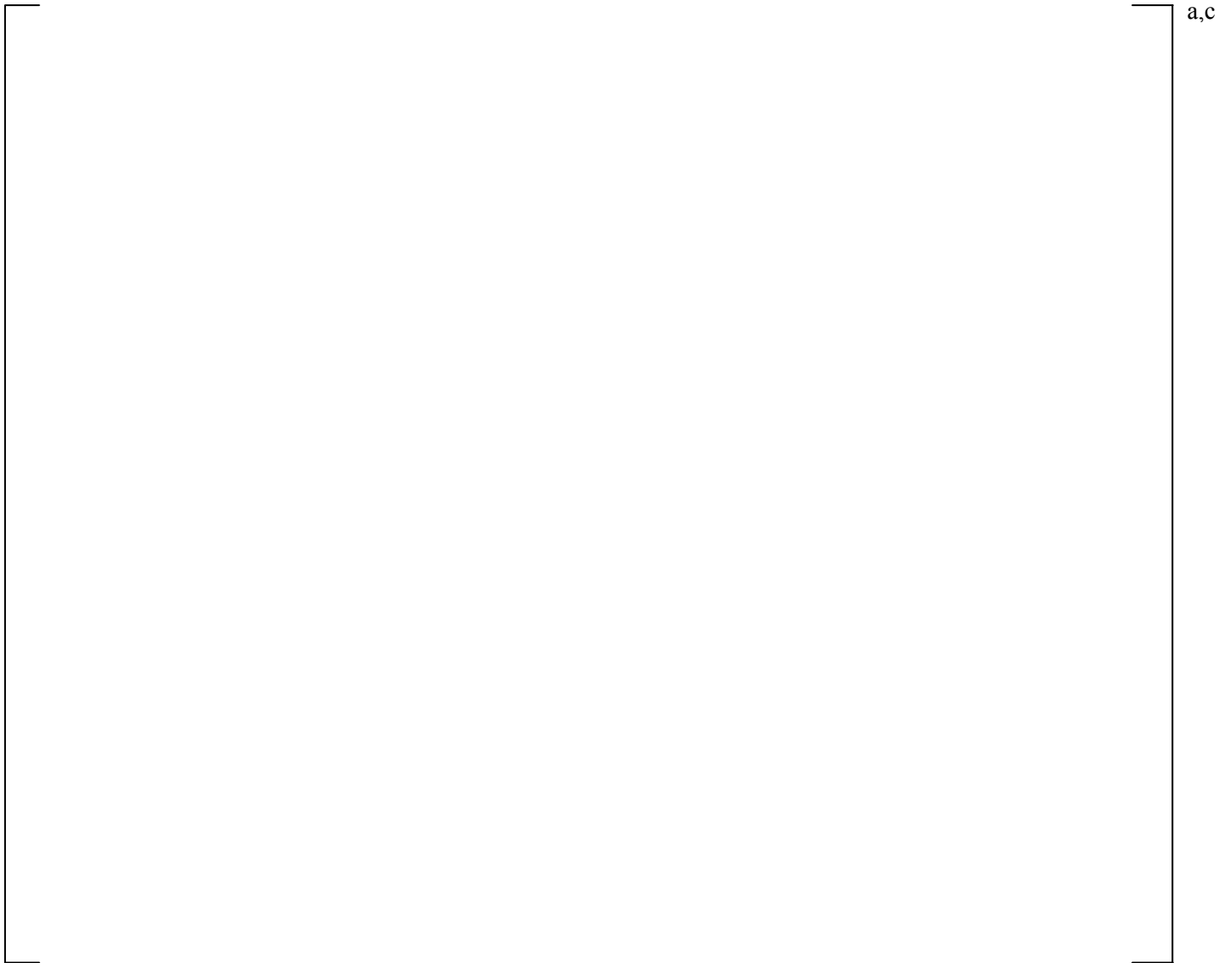


Figure 3-6 Comparison of [

]^{a,c}

4.0 Individual Responses to RAIs

This response was designed to only partially address RAI 72 and to completely address RAI 73 and RAI 74.

In this section the individual questions from the RAI are mapped to the overall discussion provided in Sections 2.0 and 3.0. The []^{a,c} for RAI 72 is performed for G2 boil-off tests in Section 3.1.

4.1 RAI 73

[]

[]^{a,c}

4.2 RAI 74

[]

[]^{a,c}

[

] ^{a,c}

5.0 Impact on the Topical Report (Reference 1)

At a minimum, the [^{a,c}] in Section 29.1.5 of Reference 1 must be revised to reflect the changes made herein. In addition, some of the wording throughout Sections 13 and 29.1.5 needs to be changed to reflect clarifications and changes. The clarifications and changes to the topical will be provided to the NRC with the remainder of the responses for Set 5.

6.0 References

1. WCAP-16996-P, "Realistic LOCA Evaluation Methodology Applied to the Full Spectrum of Break Sizes (FULL SPECTRUM LOCA Methodology)," November 2010.
2. EPRI NP-1692, Volumes 1 and 2, "Heat Transfer Above the two-Phase Mixture Level Under Core Uncovery Conditions in a 336-Rod Bundle," January 1981.
3. WCAP-9764, "Documentation of the Westinghouse Core Uncovery Tests and the Small Break Evaluation Model Core Mixture Level Model," July 1980.
4. U.S. NRC Regulatory Guide 1.157, "Best-Estimate Calculations of Emergency Core Cooling System Performance," May 1989.
5. Y. Anoda, Y. Kukita, K. Tasaka, "Void Fraction Distribution in Rod Bundle Under High Pressure Conditions," FED-Vol.99, HTD-Vol.155. Presented at the Winter Annual Meeting of the American Society of Mechanical Engineers, Dallas, Texas, November 25-30, 1990.

Question 76: WCOBRA/TRAC-TF2 Interfacial Drag Assessment

WCAP-16996-P/WCAP-16996-NP, Volumes I, II and III, Revision 0, Section 13, "Core Void Distribution and Mixture Level Swell," assesses WCOBRA/TRAC-TF2 level swell prediction capabilities using SETs that are mostly steady state and characterized by relatively low clad temperature. The analyzed tests include ORNL THTF uncovered bundle tests, Westinghouse G-1 and G-2 core uncover tests, and Japan Atomic Energy Research Institute (JAERI) TPTF critical heat flux bundle tests. To evaluate WCOBRA/TRAC-TF2 performance under test conditions that have not been addressed in WCAP-16996-P/WCAP-16996-NP, Volumes I, II and III, Revision 0, Section 13, Subsection 23.1.1, "GE Vessel Blowdown Tests," assesses WCOBRA/TRAC-TF2 prediction results for transient level swell during rapid depressurization (blowdown) while WCAP-16996-P/WCAP-16996-NP, Volumes I, II and III, Revision 0, Section 23.1.2, "Semiscale Tests," analyzes code level swell and post-CHF heat transfer prediction capabilities at high clad temperatures.

WCAP-16996-P/WCAP-16996-NP, Volumes I, II and III, Revision 0, Subsection 23.1.1, "GE Vessel Blowdown Tests," assesses WCOBRA/TRAC-TF2 prediction results for transient level swell during rapid depressurization (blowdown) using General Electric (GE) vessel blowdown test facility. The analyzed tests include 7 top-break blowdown experiments: 8-21-1, 8-25-1, 8-28-1, 9-1-1, 9-15-1, 1004-2, and 1004-3. The tests were performed with the small-tank blowdown vessel characterized by an inside diameter of 1 ft for the cylindrical portion of the vessel. The orifice opening diameters ranged from 3/8 to 1 in and a variety of different flow restrictions at the midpoint of the vessel were used. The figure of merit for the code assessment was the ability of WCOBRA/TRAC-TF2 to predict void distribution in the blowdown vessel. For this purpose, code predictions with []^{a,c} were obtained to examine the effect of interfacial drag on prediction results and compared against measured void fractions in Figures 23.1.1-4 through 23.1.1-45.

WCAP-16996-P/WCAP-16996-NP, Volumes I, II and III, Revision 0, Section 23.1.2, "Semiscale Tests," assesses WCOBRA/TRAC-TF2 level swell and post-CHF heat transfer prediction capabilities using IET data from Semiscale Mod-3 10% cold leg break integral effects Test S-07-10D. The test, designated as a U.S. NRC Small Break Experiment (SBE), featured deep core uncover and elevated heater rod temperatures due to manually delayed ECCS injection. WCAP-16996-P/WCAP-16996-NP, Volumes I, II and III, Revision 0, Section 23.1.2 does not provide assessment results with regard to interfacial drag and does not specify the value of YDRAG applied in the analysis.

Please provide additional assessment results for the WCOBRA/TRAC-TF2 vessel component interfacial drag model using available experimental data as described below.

- (1) Please compare WCOBRA/TRAC-TF2 predictions against the following tests performed with the CSE test facility: B-50TN, B-51TN, B-53BTN, and B-50MN. For test description, please see Battelle Northwest Laboratories Report BNWL-1463, "Coolant Blowdown Studies of a Reactor Simulator Vessel Containing a Perforated Sieve Plate Separator," February 1971, by R. T. Alleman et al. In addition, provide code assessment results for CSE Test B-10 as described in Battelle Northwest Laboratories Report BNWL-1411, "Experimental High Enthalpy Water Blowdown from a Simple Vessel through a Bottom Outlet," June 1970. Please provide comparisons against data for all of the above CSE tests using YDRAG drag multipliers of []^{a,c}
- (2) The GE Vessel Blowdown test facility was also used to perform level swell tests using a large-tank blowdown vessel with an inner vessel diameter of 47 in (1.194 m). The top-break, large-tank GE

level swell tests employed a blowdown venturi nozzle with a throat diameter ranging from 2.125 in (54 mm) to 3.625 in (92.1 mm). Please assess WCOBRA/TRAC-TF2 against GE large-tank level swell test data, including tests 5702-16, 5801-13, 5801-15, and 5801-19, using YDRAG drag multipliers of []^{a,c} Please provide history plots of time-dependent system pressure responses at the top of the blowdown vessel and two-phase mixture levels that compare code predictions and test data showing also accuracy bars for the two-phase mixture level measurements. In addition, please provide plots of axial void fraction profiles as a function of the axial vessel height, which compare core results with axial void fraction data along with accuracy bars for all seven axial levels as measured at the four transient points in time in each test. Assess the interfacial drag models in WCOBRA/TRAC-TF2 by presenting a plot, which compares axially-dependent void fraction data measured at the four transient times at all seven axial levels for each experiment against code predicted values. Please analyze and provide the code assessment for the GE large-tank level swell tests using YDRAG drag multipliers of []^{a,c}

- (3) Please provide comparisons of WCOBRA/TRAC-TF2 predictions against measured data including, among other important parameters, clad temperature measurements at deferent axial elevations for the following Semiscale IETs: Semiscale Mod-3 10 percent cold leg break Tests S-07-10 (SG secondaries isolated at 17 s into the transient) and S-07-10D (broken loop SG allowed to blowdown throughout the transient), Semiscale Mod-2A 5 percent cold leg break Test S-UT-08, Semiscale Mod-2C 5 percent centerline cold leg break Tests S-LH-1 (0.9 percent core bypass flow) and S-LH-2 (3.0 percent core bypass flow). Please analyze and provide the code assessment for these Semiscale tests using YDRAG drag multipliers of []^{a,c} Provide comparisons of WCOBRA/TRAC-TF2 predictions against measured data for PCTs at deferent axial elevations. In addition, please provide comparisons for the axial void distribution in the core at the time of PCT occurrence as well as for the collapsed liquid level and two-phase mixture level as functions of time. Document the predicted maximum PCT values following core boiloff and compare them against the measured PCT value including the measurement accuracy as well.

Response to Parts (1), (2), and (3) of RAI 76:**76.1. Parts (1) and (2)****Purpose of GE Blowdown Test within the Code V&V Matrix**

Section 13 describes the assessment of WCOBRA/TRAC-TF2 interfacial drag. However the focus is limited to ensure the code is capable of predicting with reasonable accuracy the core void fraction distribution and mixture level swell. Therefore the tests considered in the V&V matrix are limited to prototypical rod bundle data. Core interfacial drag biases and uncertainties are captured in the YDRAG multiplier - as discussed in Section 29 and responses to RAI 72, 73 and 74 - based on comparing code prediction against prototypical rod bundle data.

The GE Blowdown test is a rapid depressurization and flashing test which is meant to simulate the two-phase blowdown of a pressure vessel with a relatively large hydraulic diameter, and not fully applicable to model the core region. This test is not representative of the core level swell phenomena and conditions during the boil-off phase of a SBLOCA. As such, the GE Blowdown data was not and should not be considered in the development of the YDRAG range contrary to what is implied in RAI-76.

The GE Blowdown tests described in Section 23 were simply used as an additional benchmark, purely to investigate the effect of ranging YDRAG during rapid depressurization and subsequent flashing of the liquid in a tank. The phenomenon is quite different from boiling of liquid at the wall as result of wall-to-fluid heat transfer. Note that YDRAG ranging is only applied in the core region where the geometry of GE Blowdown would not be applicable.

Considering that the GE Blowdown tests are not applicable for the conditions under which the YDRAG multiplier is most important, and the volatile nature of the tests, the results show adequate agreement for their intended purpose.

76.2. Part (3)

76.2.a. Introduction/Problem Statement/Response Approach

Part (3) of RAI-76 requests simulation of a number of Semiscale tests. This request was motivated by the staff's concern that the validation matrix selected for WCT-TF2 is inadequate. In this response, the scale distortion and the parameter coverage of ROSA-IV LSTF test series included in the validation matrix are examined. Together with the consideration of scale distortion in Semiscale, the adequacy of ROSA-IV based validation matrix is discussed.

The scale distortion in ROSA-IV test SB-CL-02 was investigated in Appendix A. The review of scaling analysis and an additional scale distortion check for Semiscale were performed in Appendix B.

76.2.b. Scale Distortion in ROSA-IV LSTF Test

Top-down and bottom-up Scaling in blowdown (BLD), natural-circulation (NC), Loopseal-clearing (LSC), and boil-off (BO) phases in a ROSA-IV SBLOCA test, SB-CL-02 was investigated relative to an equivalent demonstration plant SBLOCA transient. The three loop demonstration plant will be referred to the plant identification, DLW in the subsequent texts in this document. SB-CL-02 has a 2.5% break at the bottom of the cold leg. [

]^{a,c} The scale distortion was investigated using the top-down scaling method used for AP600 by Banerjee (1997) [76.2-1] and for US-APWR by Mitsubishi Heavy Industries (2010) [76.2-2].

The top-down scaling analysis result indicated that there are minor scale distortions originating from the atypical steady state and transient initiation of ROSA-IV test SB-CL-02. In ROSA-IV, the steady state power is 14% of the scaled PWR value due to the power limitation for the facility (=10 MW). In order to achieve the same hot and cold leg loop temperatures as the PWR, the loop flow was also reduced to 14% of the scaled PWR value and the secondary side pressure was increased. The transient was initiated by a break opening followed by power transition to decay heat curve and the acceleration of pump speed until it reaches the expected coast down speed. After that the pump speed was programmed to follow the coast down curve.

The Bottom-up scaling analysis examined the pertinent loop geometry and expected flow conditions for the break flow during the BLD phase, the counter-current flow limit (CCFL) in the steam generator (SG) U-tube, CCFL in the SG/hot leg, and the residual liquid in cross-over leg in the LSC phase. The result indicated that there is no significant scale distortion in ROSA-IV SB-CL-02 test.

76.2.c. Parameter Coverage in IETs in Validation Matrix

In this section, the range of parameters investigated in the IETs in the validation matrix, which are important to SBLOCA is summarized.

Break Size and Break Orientation, SI Operation:

[

]^{a,c}

	Break Size (% of CL FA) Based on Equivalent 4 Loop PWR	
ROSA-IV	0.5, 2.5, 5.0, 10	High Pressure SI was active in SB-CL-05 (5%)
LOFT	2.5, 25	

Bypass from Inner to Outer Vessel and Downcomer:

The core collapsed liquid during the LSC phase is a result of how effective the bypass was in relieving the manometric pressure difference developed between the inner and outer vessel. ROSA-IV bypass values seen in the validation matrix is a typical value for PWRs. For Tcold plants, the bypass is larger and is near 2%.

	Bypass (% of Loop Flow)	
ROSA-IV	0.4%- 2.3%	Range covers typical PWRs.

Lowest Core Collapsed Liquid Level:

The lowest core collapsed liquid level measured in SB-CL-05 was reached during the LSC phase. The measured level was substantially lower than the loop seal elevation implying that there was significant liquid holdup in the hot leg/SG and uphill side of SG-tubes. For examining the level swell performance for an extreme low core liquid inventory, S-7-10D was simulated in the separate effects test (SET) mode which is discussed in Section 23 of the topical report.

	Lowest Core Collapsed Liquid Level (m)		
Phase	Measured from Bottom of Core	Level Relative to Loop Seal	
LSC	0.33	-1.465	SB-CL-05 (5% CL)
BO	0.63	N/A	SB-CL-02 (2.5% CL)
BO	~0	N/A	S-7-10D (SET)

Highest Rod Temperature:

The highest rod temperatures measured in ROSA-IV tests are relatively benign due to the operational procedure where the core power was turned off when the highest rod temperature reached 800C. In order to examine the code's predictive capability in the high temperature transients, S-7-10D was simulated in the SET mode.

Phase	Max Measured Clad Temperature	
LSC	~720 K (836F)	SB-CL-05 (5% CL)
BO	~870K (1106F)	SB-CL-02 (2.5% CL)
BO	~ 1060 K (1448F)	S-7-10D (SET mode)

Range of Parameters in Requested Semiscale Tests:

The range of parameters investigated in S-UT-8, S-7-10/10D, S-LH-1/2 experiments are shown in the table below. It is clear that the parameters are bounded by or comparable to the range examined in the validation matrix shown above with an exception of the bypass flow fraction for which the coverage by ROSA tests is shown to be adequate.

	Semiscale	
Break Size (% of CL FA)	5%, 10%	-
Bypass	0.9% - 3%	S-LH-1/S-LH-2 (5% CLB)
Lowest Core Collapsed Level	~0	S-7-10D (10% CLB)
Highest Temperature	~1145 K (1601F)	S-7-10 (10% CLB)

76.2.d. Scale Distortion in Semiscale Test

The scaling analyses and other similar investigations performed on the Semiscale test facility were reviewed in Appendix B for the facility's possible scale distortion in its SBLOCA transients.

Metal stored energy relative to the coolant volume and the heat loss to the environment were apparent scale distortions in the small scale facilities like Semiscale. In an effort to minimize environmental heat losses, external heaters were installed on the loop piping, downcomer, vessel, upper plenum, and secondary side shells. These heaters were controlled by independent variable power supplies, allowing the external heater power to be ramped down during the course of a transient in an attempt to not amplify the already atypical metal heat release to the primary fluid. Other scale distortions are seen in the CCFL behavior in the hot leg/SG interface and in the Loop seal where the clearing behavior is impacted and more residual liquid is expected in Semiscale tests compared to PWRs. Many of known distortions while some may be considered minor, are not correctable and the transient behavior requires careful examination to interpret and to extrapolate to the PWR behavior. The facility is still useful for code assessment however atypicalities and scale distortions in the facility are present which impacts the behavior of key phenomena such that the code may be exercised in an operating region different from what is expected in PWRs.

76.2.e. Adequacy of IETs in Validation Matrix

The validation matrix with 10 ROSA-IV IET simulations (9 SBLOCA plus 1 Natural Circulation test) with an additional S-07-10D SET simulation adequately covers important phenomena of SBLOCA over an expected range of DLW SBLOCA transients.

The scale distortion examination demonstrated that the ROSA-IV tests are well scaled IETs for examining the behavior of Westinghouse type PWRs under SBLOCA transient conditions, and are uniquely suited for the validation of WCT-TF2 for the application to SBLOCA analysis. Specifically, the IET set in the WCT-TF2 validation matrix includes 1 Natural Circulation test and 9 ROSA-IV SBLOCA tests with break sizes at 0.5%, 2.5%, 5% and 10% with different break orientations and with and without SI, supplemented by the level swell validation under an extremely low core liquid inventory using the S-7-10D high temperature Semiscale test, and 2 LOFT tests including 1 small break and 1 intermediate break tests. The IET set included in the WCT-TF2 validation matrix is believed to satisfy Step 8 of EMDAP described in RG 1.203 and is sufficient data base for validating the WCT-TF2 based evaluation model for the application of SBLOCA analysis.

Based on the comparison of parameter coverage in the validation matrix, simulation of requested Semiscale tests do not add any new phenomena nor exercise the code in ranges of importance that IETs in the validation matrix did not already cover.

References:

[76.2-1] S. Banerjee, M. G. Ortiz, T. K. Larson, D. L. Reeder, "Top-Down Scaling Analyses Methodology for AP600 Integral Tests," INEL-96/0040, May 1997

[76.2-2] ML103120255, "Scaling Analysis for US-APWR Small Break LOCAs," UAP-HF-10289-NP (R0), Mitsubishi Heavy Industries, Ltd., October 2010

Appendix-A: Examination of Scale Distortion in ROSA-IV Test, SB-CL-02

A.1 Introduction

The scale distortion in the SB-CL-02 (2.5% break at the bottom of cold leg) compared to the small break of an equivalent size for the demonstration plant (DLW). The equivalent break size of SB-CL-02 for DLW using []^{a,c} The scale distortion in SB-CL-02 relative to a []^{a,c} using the top-down scaling method used for AP600 by Banerjee (1997) [76.A-1] and for US-APWR by MHI (2010)[76.A-2].

In subsequent sections, the scaling analysis based on the non-dimensional mass and energy equations for the blowdown (BLD), natural circulation (NC), loop seal clearance (LSC), and boil-off (BO) phases developed in Ref [76.A-2] are presented. The non-dimensional coefficients derived from the non-dimensional mass, energy and momentum balance laws were then calculated and compared between the ROSA SB-CL-02 and the demonstration plant simulation results for identification and discussion of possible scaling distortions in SB-CL-02. To compute the non-dimensional coefficients, the SB-CL-02 simulation and the DLW SBLOCA transient of an equivalent break size are utilized for the parameters not available from the measurements, since the simulation of SB-CL-02 was found to be equivalent to the test in terms of the global mass and pressure transient as seen in Section 21 of the topical report. In addition to the top-down scaling analysis, the pertinent bottom-up scaling requirements for the phases were examined by comparing the geometry scaling and expected flow conditions based on appropriate correlations for high PIRT phenomena/processes.

A.2 Top-Down scaling of BLD, NC, LSC, and BO Phases

The system pressure and mass transients of DLW and ROSA were compared for the blowdown, natural circulation, Loopseal, and boil-off phases (see two figures below). []

] ^{a,c} the 2.5% cold leg break SB-CL-02 were selected for this investigation of scale distortion since among all ROSA test series, the 2.5% break size is the []

] ^{a,c} Since ROSA is a full pressure facility and the P/V scaling maintains 1:1 time scale, we can compare the system pressure vs. time directly as seen in Figure 76.A-1a. For mass, the normalized primary mass vs. time may be used for comparison as seen in Figure 76.A-1b. The scale distortion in ROSA may be identified through comparison of non-dimensional parameters.



Figure 76.A-1a: Pressure Transient Comparison

Figure 76.A-1b: Mass Transient Comparison

- Blowdown Phase []^{a,c}

Mass balance:

$$\frac{dM^*}{dt^*} = \Psi_{13} (-\dot{m}^*_{break})$$

Energy balance:

$$\frac{dP^*}{dt^*} = \Psi_2 C_{1,l}^* I_{b,l}^* + \Psi_6 C_{1,m}^* I_{c,m}^* + \Psi_{10} C_2^* H_l^*$$

Definition of non-dimensional coefficients is given in Appendix-C of [76.A-1] and listed in Table 76.A-1.

Table 76.A-1: Definition of Non-dimensional Parameters

Non-dimensionalized Parameters	Algebraic form	Note
M^*	M / M_0	Non-dimensionalized mass
t^*	t / t_0	Non-dimensionalized time
\dot{m}_{break}^*	$\dot{m}_{break} / \dot{m}_{break,0}$	Non-dimensionalized mass flow
P^*	P / P_0	Non-dimensionalized pressure
$I_{b,m}^*$	$\frac{I_{b,m}}{I_{b,m,0}} = \frac{\dot{m}_{break}(h_{break} - u_m)}{\dot{m}_{break,0}(h_{break} - u_m)_0}$	Non-dimensionalized saturated field energy change due to mass outflow
$I_{b,l}^*$	$\frac{I_{b,l}}{I_{b,l,0}} = \frac{\dot{m}_{break}(h_{break} - u_l)}{\dot{m}_{break,0}(h_{break} - u_l)_0}$	Non-dimensionalized subcooled field energy change due to mass outflow
$I_{c,m}^*$	$\frac{I_{c,m}}{I_{c,m,0}} = \frac{\dot{q}_{net,m}}{\dot{q}_{net,m,0}}$	Non-dimensionalized heat transfer
II_m^*	$\frac{II_m}{II_{m,0}} = \frac{v_m(-\dot{m}_{break})}{v_{m,0}(-\dot{m}_{break,0})}$	Non-dimensionalized saturated field volume flow due to mass outflow
II_l^*	$\frac{II_l}{II_{l,0}} = \frac{v_l(-\dot{m}_{break})}{v_{l,0}(-\dot{m}_{break,0})}$	Non-dimensionalized subcooled liquid field volume flow due to mass outflow
$C_{1,l}^*$	$C_{1,l} / C_{1,l,0}$	$C_{1,l} = \frac{\partial P / \partial u_l _{v_l} / \partial P / \partial v_l _{u_l}}{\sum_k (\rho_k V_k / \partial P / \partial v_k _{u_k})}$
$C_{1,m}^*$	$C_{1,m} / C_{1,m,0}$	$C_{1,m} = \frac{\partial P / \partial u_m _{v_m} / \partial P / \partial v_m _{u_m}}{\sum_k (\rho_k V_k / \partial P / \partial v_k _{u_k})}$
C_2^*	$C_2 / C_{2,0}$	$C_2 = \frac{1}{\sum_k (\rho_k V_k / \partial P / \partial v_k _{u_k})}$

The result of scaling analysis is summarized in the table below which compares the non-dimensional coefficients in the mass and energy equations for the demonstration plant (DLW) and ROSA SB-CL-02. As seen in the summary table, a scale distortion is seen in the ratio of pressure change due to change in specific energy of the saturated field from heat transfer. This distortion is due to the difference in the steady state operation between the DLW and ROSA. In ROSA, the steady state power is 14% of the scale due to the power limitation for the facility (=10 MW). In order to operate achieve the same loop temperatures, the loop flow was also set at 14% of the scaled PWR value. The transient was initiated by a break opening followed by power transition to decay heat curve and the acceleration of pump speed until it reaches the expected coast down speed. After that the pump follows the coast down curve.

The mass depletion during the blowdown phase is slower in DLW than in ROSA but is comparable.

Table 76.A-2: Non-dimensional Coefficients during Blowdown					
Dimensionless Group	Algebraic form	Physical Meaning	DLW	ROSA	DLW/ROSA
Ψ_2	$\frac{C_{1,l,0}(h_{break} - u_l)\dot{m}_{break,0}t_0}{P_0}$	Ratio of pressure change, due to change in specific energy of the subcooled liquid mass outflow, to the reference pressure	[$]^{a,c}$
Ψ_6	$\frac{C_{1,m,0}\dot{q}_{net,0}t_0}{P_0}$	Ratio of pressure change, due to change in specific energy of the saturated field from heat transfer, to the reference pressure	[$]^{a,c}$
Ψ_{10}	$\frac{C_{2,0}v_{l,0}\dot{m}_{break,0}t_0}{P_0}$	Ratio of pressure change, due to change in specific volume of the subcooled liquid from mass outflow, to reference pressure	[$]^{a,c}$
Ψ_{13}	$\frac{\dot{m}_{break,0}t_0}{M_0}$	Ratio of integrated mass flow to reference mass	[$]^{a,c}$

Table 76.A-3: Time Duration, Mass and Pressure in Blowdown Phase			
Reference Parameters	DLW	ROSA	Notes
t_0 (second)	[$]^{a,c}$	Time period
M_0 (kg)	[$]^{a,c}$	Initial RCS mass
P_0 (Pa)	[$]^{a,c}$	Initial RCS pressure

• **Natural Circulation Phase []^{a,c}**

Mass balance:

$$\frac{dM^*}{dt^*} = \Psi_{13} (-\dot{m}_{break}^*)$$

Energy balance:

$$\frac{dP^*}{dt^*} = \Psi_5 C_{1,m}^* I_{b,m}^* + \Psi_6 C_{1,m}^* I_{c,m}^* + \Psi_{11} C_2^* H_m^*$$

Definition of non-dimensional coefficients is given in Appendix-C of [76.A-1] and listed in Table 76.A-1.

The result of scaling analysis is summarized in the tables below which compare the non-dimensional coefficients in the mass, energy and driving force/resistance equations for the demonstration plant (DLW) and ROSA SB-CL-02. As seen in Table 76.A-4, a scale distortion is seen in the ratio of pressure change Ψ_6 due to change in specific energy of the saturated field from heat transfer. This distortion is due to the difference in the heat transfer rate from the primary to the secondary side of steam generators. It is believed that two factors contributed to this distortion. One factor is the hot leg enthalpy at the beginning of natural circulation phase. Because the pump in ROSA operated at the 14% during the steady state, while accelerated to the coast down curve following the initiation of the transient, combined with the delayed reactor trip, the upper plenum and hot leg stays hot for ROSA and the pressure is higher in ROSA at the beginning of natural circulation phase. Second factor is the steamline valve operation in ROSA. When the valve opens, the release rate is high enough to drop the secondary side so that the valve closes. The valve repeated this cycle which is in contrast to how DLW secondary side behaves. The difference then is the heat transfer rate from the primary to the secondary side. This difference, though notable, ends with the equilibration of the primary and the secondary pressures. At this point the heat transfer direction reverses as the primary pressure becomes lower than the secondary pressure. The scale distortion from this difference appears to impact slightly as the shorter natural circulation phase.

Table 76.A-4: Non-dimensional Coefficients during Natural Circulation					
Dimensionless Group	Algebraic form	Physical Meaning	DLW	ROSA	DLW/ROSA
Ψ_5	$\frac{C_{1,m,0} (h_{break} - u_m) \dot{m}_{break,0} t_0}{P_0}$	Ratio of pressure change, due to change in specific energy of the saturated field from mass outflow, to the reference pressure	[] ^{a,c}
Ψ_6		Ratio of pressure change, due to change in specific energy of the saturated field	[] ^{a,c}

Table 76.A-4: Non-dimensional Coefficients during Natural Circulation

Dimensionless Group	Algebraic form	Physical Meaning	DLW	ROSA	DLW/ROSA
	$\frac{C_{1,m,0} \dot{q}_{net,0} t_0}{P_0}$	from heat transfer, to the reference			
Ψ_{11}	$\frac{C_{2m,0} v_{m,0} \dot{m}_{break,0} t_0}{P_0}$	Ratio of pressure change, due to change in specific volume of the saturated field from break outflow, to reference pressure	[] ^{a,c}
Ψ_{13}	$\frac{\dot{m}_{break,0} t_0}{M_0}$	Ratio of integrated mass flow to reference mass	[] ^{a,c}

Table 76.A-5: Time Duration, and other pertinent parameters in Natural Circulation Phase

Reference Parameters	DLW	ROSA	Notes
t_0 (second)	[] ^{a,c}	Duration of Phase
M_0 (kg)	[] ^{a,c}	RCS mass at beginning of phase
P_0 (Pa)	[] ^{a,c}	Initial RCS pressure
$\dot{q}_{net,0}$ (W)	[] ^{a,c}	Average net heat source

Integrated Momentum Equation:

$$\frac{1}{2} \rho_{m,0}^2 v_{m,0}^2 \sum_i (N_{f,i} + N_{o,i}) \frac{1}{\rho_{m,i}} = \sum_i (\rho_{l,sat} - \rho_{m,i}) g \Delta H_i$$

where

$N_{f,i}$ is the non-dimensional parameter accounting for the two-phase frictional loss.

$N_{o,i}$ is the non-dimensional parameter accounting for the two-phase local loss.

The non-dimensional driving force can be obtained as:

$$N_{dr,i} = \frac{(\rho_{l,sat} - \rho_{m,i}) g \Delta H_i}{\rho_{l,sat} g L_h}$$

where L_h is the height of the difference between the middle of the core and the middle of average height of SG.

Table 76.A-6: Non-dimensional Coefficients in Loop Momentum Equation				
Dimensionless Group	Algebraic form	DLW	ROSA	ROSA /DLW
$\sum_i N_{f,i} + \sum_i N_{o,i}$ (Single Phase Region)	$N_{f,i} = f_l \left(\frac{l}{d} \right)_i \left(\frac{A_0}{A_i} \right)^2$ $N_{o,i} = K_i \left(\frac{A_0}{A_i} \right)^2$	[] ^{a,c}
$\sum_i N_{f,i} + \sum_i N_{o,i}$ (Two Phase Region)	$N_{f,i} = f_l \left(\frac{l}{d} \right)_i \frac{(1 + x \cdot \Delta\rho / \rho_g)}{(1 + x \cdot \Delta\mu / \mu_g)^{0.25}} \left(\frac{A_0}{A_i} \right)^2$ $N_{o,i} = K_i \left(1 + x^{1.5} \cdot \Delta\rho / \rho_g \right) \left(\frac{A_0}{A_i} \right)^2$	[] ^{a,c}
$\sum_i N_{dr,i}$	$N_{dr,i} = \frac{(\rho_{l,sat} - \rho_{m,i}) g \Delta H_i}{\rho_{l,sat} g L_h}$	[] ^{a,c}

• **Loopseal Clearing Phase []^{a,c}**

The mass and energy equations in loop seal clearance phase are the same as those of the natural circulation phase, with hydrostatic head in the RCS system as the driving force in loop seal clearance phase. Using the hydrostatic head as defined in Figure 6.3-12 of [76.A-2] and redefining L_{SGU} as L_{CCFL} and L_{SGD} as L_{UDS} , the following balance equation was derived,

RCS hydrostatic head balance equation:

$$L_{CUP}^* = \psi_1 L_{DC}^* - \frac{(\rho_l - \rho_g)^*}{\rho_l^*} (\psi_2 L_{SGU}^* + \psi_3 L_{LSU}^* - \psi_7 (L_{SGD}^* + L_{LSD}^*))$$

where $L_{CUP}^* = \frac{L_{CUP}}{L_{CUP,0}}$, $L_{DC}^* = \frac{L_{DC}}{L_{DC,0}}$, $L_{SGU}^* = \frac{L_{SGU}}{L_{SGU,0}}$, $L_{LSU}^* = \frac{L_{LSU}}{L_{LSU,0}}$, $L_{SGD}^* = \frac{L_{SGD}}{L_{SGD,0}}$,
 $L_{LSD}^* = \frac{L_{LSD}}{L_{LSD,0}}$, $(\rho_l - \rho_g)^* = \frac{(\rho_l - \rho_g)}{(\rho_l - \rho_g)_0}$, $\rho_g^* = \frac{\rho_g}{\rho_{g,0}}$, $\rho_l^* = \frac{\rho_l}{\rho_{l,0}}$

The result of scaling analysis is summarized in the tables below which compares the non-dimensional coefficients in the mass, energy and hydrostatic head equations for the demonstration

plant (DLW) and ROSA SB-CL-02. As seen in Table 76.A-7, no scale distortion is found. The ratio of non-dimensional parameter is found to be between []^{a,c}

Table 76.A-7: Non-dimensional Coefficients during Loop Seal Clearance					
Dimensionless Group	Algebraic form	Physical Meaning	DLW	ROSA	DLW /ROSA
Ψ_5	$\frac{C_{1,m,0} (h_{break} - u_m) \dot{m}_{break,0} t_0}{P_0}$	Ratio of pressure change, due to change in specific energy of the saturated field from mass outflows, to the reference pressure	[] ^{a,c}
Ψ_6	$\frac{C_{1,m,0} \dot{q}_{net,0} t_0}{P_0}$	Ratio of pressure change, due to change in specific energy of the saturated field from heat transfer, to the reference pressure	[] ^{a,c}
Ψ_{11}	$\frac{C_{2,m,0} v_{m,0} \dot{m}_{break,0} t_0}{P_0}$	Ratio of pressure change, due to change in specific volume of the saturated field from break outflow, to reference pressure	[] ^{a,c}
Ψ_{13}	$\frac{\dot{m}_{break,0} t_0}{M_0}$	Ratio of integrated mass flow to reference mass	[] ^{a,c}

Table 76.A-8: Time Duration, Mass and Pressure in Loop Seal Clearance Phase			
Reference Parameters	DLW	ROSA	Notes
t_0 (second)	[] ^{a,c}	Time duration of Phase
M_0 (kg)	[] ^{a,c}	Initial RCS mass at begin of phase
P_0 (Pa)	[] ^{a,c}	Beginning of phase

Table 76.A-9: Non-dimensional Liquid Hold-up in Loop Seal Clearance Phase				
Dimensionless Group	DLW	ROSA	DLW/ROSA	Algebraic form
ψ_1	[$]^{a,c}$	$\frac{L_{DC,0}}{L_{CUP,0}}$
ψ_2	[$]^{a,c}$	$\frac{(\rho_l - \rho_g)_0}{\rho_{l,0}} \frac{L_{SGU,0}}{L_{CUP,0}}$
ψ_3	[$]^{a,c}$	$\frac{(\rho_l - \rho_g)_0}{\rho_{l,0}} \frac{L_{LSU,0}}{L_{CUP,0}}$
ψ_7	[$]^{a,c}$	$\frac{(\rho_l - \rho_g)_0}{\rho_{l,0}} \frac{L_{SGD,0} + L_{LSD,0}}{L_{CUP,0}}$
L_{CUP}^*	[$]^{a,c}$	$\frac{L_{CUP,min}}{L_{CUP,0}}$

- Boiloff Phase [$]^{a,c}$

The mass and energy equations in boiloff phase are the same as those of the natural circulation and loop seal clearance phases.

The result of scaling analysis is summarized in the table below which compares the non-dimensional coefficients in the mass and energy equations for the demonstration plant (DLW) and ROSA SB-CL-02. As seen in the summary table, no scale distortion is found. The ratio of non-dimensional parameters is found to be between [$]^{a,c}$

Table 76.A-10: Non-dimensional Coefficients during Boil-off					
Dimensionless Group	Algebraic form	Physical Meaning	DLW	ROSA	DLW/ROSA
Ψ_5	$\frac{C_{1,m,0}(h_{break} - u_m)\dot{m}_{break,0}t_0}{P_0}$	ratio of pressure change, due to change in specific energy of the saturated field from mass outflows, to the reference	[$]^{a,c}$
Ψ_6	$\frac{C_{1,m,0}\dot{q}_{net,0}t_0}{P_0}$	Ratio of pressure change, due to change in specific energy of the saturated field from heat transfer, to the reference	[$]^{a,c}$

Table 76.A-10: Non-dimensional Coefficients during Boil-off

Dimensionless Group	Algebraic form	Physical Meaning	DLW	ROSA	DLW/ROSA
Ψ_{11}	$\frac{C_{2,m,0} v_{m,0} \dot{m}_{break,0} t_0}{P_0}$	Ratio of pressure change, due to change in specific volume of the saturated fluid from break outflow, to reference	[] ^{a,c}
Ψ_{13}	$\frac{\dot{m}_{break,0} t_0}{M_0}$	Ratio of integrated mass flow to reference mass	[] ^{a,c}

Table 76.A-12: Time Duration, Mass and Pressure in Boil-off Phase

Reference Parameters	DLW	ROSA	Notes
t_0 (second)	[] ^{a,c}	Duration of Phase
M_0 (kg)	[] ^{a,c}	RCS mass at beginning of phase
P_0 (MPa)	[] ^{a,c}	RCS pressure at beginning of phase

A.3 Bottom-Up scaling consideration of BLD, NC, LSC, and Boil-off Phases

For the bottom-up scaling discussion, we will focus on the controlling parameters for the important phenomena in BLD, NC, Loopseal clearing phase and the core collapsed liquid level during the boil-off phase.

I. Blowdown Phase [

]^{a,c}

Scaling at the Break - The break orifice flow area is determined from the ratio of flow area to volume scaling. The fluid enthalpy and pressure upstream of the break are equivalent based on the condition of the cold leg where the break is located for both ROSA and in the postulated plant transient at the initiation of SBLOCA transient. These two factors (flow path area, upstream fluid condition) are important and provide similarity between ROSA and the plant transient behavior during the blowdown phase.

II. Natural Circulation Phase [

]^{a,c}

The trajectory of operating point on the Jl^* - Jg^* plane during the natural circulation in the hot leg in DLW and in ROSA are compared in Figures 76.A-2a and -2b. The comparison shows that during the natural circulation phase, the operating point of ROSA case covers similar range of DLW operating points in the jl^* - yg^* plane implying that the similar flow regimes are expected in DLW and ROSA cases. The negative Jl^* is seen before the end of the natural circulation period which causes the vapor to accumulate at the top of U-tube to form a seal which is an indication of LCS phase.



Figure 76.A-2a: Jl^* vs. Jg^* in SB-CL-02

Figure 76.A-2b: Jl^* vs. Jg^* in DLW

III. Loopseal Clearing Phase [

] ^{a,c}

The manometric core depression during the Loopseal phase is determined by the elevation of top of X-over leg piping, the liquid hold up in the SG U-tubes and the SG/Hot Leg interface. Possible scale distortion relative to CCFL in SB-CL-02 and in DLW is examined below.

CCFL in SG U-tube

Using the ROSA facility Kukita et al. [76.A-3] developed a CCFL correlation applicable to the SG U-tube CCFL condition. Figure 76.A-3 shows the data and the correlation;

$$(j_g^*)^{1/2} + (j_f^*)^{1/2} = 0.88$$

This is based on Wallis correlation [Section 11.4 of 76.A-4]. This correlation will be used as the basis for scaling of SB-CL-02.

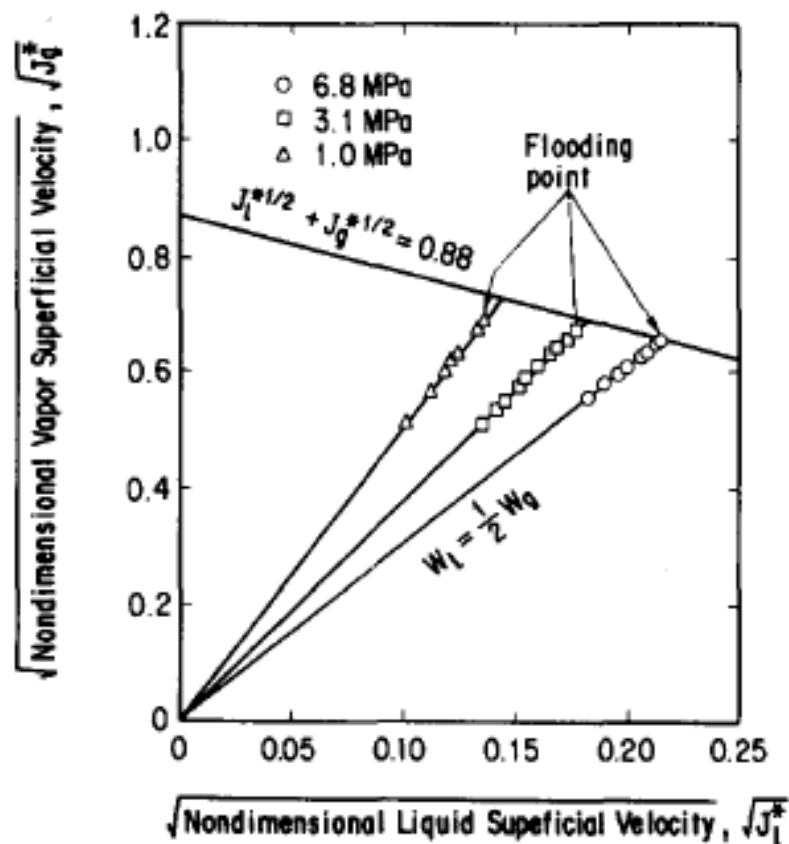


Figure 76.A-3: Steam generator U-tube CCFL characteristics [Figure 13 of 76.A-3]

As seen in the table below, the SG U-tube dimensions in ROSA and DLW are nearly identical. The pressure range and the fluid condition are prototypical of the full scale PWRs. Therefore the scale distortion in ROSA relative to the full scale PWRs for this phenomenon is not expected.

Table 76.A-13: SG U-tube Geometry Comparison			
	ROSA	3 Loop PWR	Remark
SG Tube Inner Diameter	19.6 mm	[] ^{a,c}
Average SG Tube height	9.86 m	[] ^{a,c}
Total Flow Area (all loops)	2x0.0425=0.085 m ²	[] ^{a,c}
Tube Sheet El. relative to HL centerline	2.461 m	[] ^{a,c}
Pressure	~SG Pressure	~SG Pressure	LSC Phase
Flow Condition	Liquid draining at saturation/subcooled against vapor upflow which is being condensed	Liquid draining at saturation/subcooled against vapor upflow which is being condensed	Draining of SG Tube against Vapor flow from core generated by decay heat

Based on the similarity of geometry and fluid conditions, it is concluded that the scale distortion is not expected in ROSA relative to the full scale PWRs.

CCFL at SG/HL interface

The CCFL correlation developed based on the UPTF data [76.A-5],

$$(j_g^*)^{1/2} + m \cdot (j_f^*)^{1/2} = C$$

where $m = 0.7 - 1.0$ and $C = 0.61 - 0.75$, is known to be applicable at the full scale pipe size at the low pressures (0.3 MPa and 1.5MPa). Ohnuki [76.A-6] confirmed the applicability of Wallis type correlation to small scale geometry. The pressure dependency was found to increase the C value with increasing pressure. Vallee et al. [76.A-7] confirmed Ohnuki's finding on the pressure dependency from 3 MPa data.

Table 76.A-14: Hot Leg/SG Interface Piping Geometry Comparison			
	ROSA	3 Loop PWR	Remark
SG HL Diameter (D)	0.207 m	[] ^{a,c}

Table 76.A-14: Hot Leg/SG Interface Piping Geometry Comparison			
	ROSA	3 Loop PWR	Remark
SG Elbow Length (ℓ)	0.8 m	[] ^{a,c}
HL Horizontal Run (L)	2.4 m	[] ^{a,c}
$\ln \left\{ \left(\frac{L}{D} \right) \cdot \left(\frac{1}{\ell} \right) \right\}^{-0.066} + 0.88$	0.7	[] ^{a,c}
Total HL Length	3.2 m	[] ^{a,c}
$(L + \ell)/\sqrt{D}$	7	[] ^{a,c}
Total Flow Area (all loops)	$2 \times 0.0337 = 0.0673 \text{ m}^2$	[] ^{a,c}
Pressure	~SG Pressure	~SG Pressure	LSC Phase
Flow Condition	Liquid draining at saturation or subcooled against vapor upflow which is being condensed	Liquid draining at saturation or subcooled against vapor upflow which is being condensed	Draining of SG Tube against Vapor flow from core generated by decay heat

Based on the similarity of geometry and fluid conditions, it is concluded that the scale distortion is not expected in ROSA relative to the full scale PWRs.

Residual Liquid in Cross-over Leg Piping

Loop Seal Clearing phase ends with clearing of loop seal and establishing the vent path for the vapor generated in the core to the break. The important phenomenon in this phase is maintenance of the presence of the residual liquid in the X-over leg piping which increases the resistance to the vapor flow from the core to the break. The presence of liquid in the cross-over leg piping results in the deeper core depression. As seen in the table below, the flow area in the loop seal region in ROSA is sized to be consistent with the volume scale which would result in the same velocity as in PWR. The basic mechanism of loop seal clearing was discussed, which included UPTF data analysis as seen in Figure 76.A-4, in Section 18 of the topical report. The impact of scale and pressure was examined in Section 18 as well. The scaling and analysis of limiting mechanisms indicate that the slugging criterion, the entrainment criterion, and the CCFL in the uphill piping are combined to result in determining the residual liquid presence. Since pipe diameter in ROSA is large enough such that the CCFL is limited by Kutateladze correlation as in the full scale PWRs, and the velocity is preserved, scale distortion is not expected in ROSA. There are flow meters and valve in the loop seal region which potentially have some impact. However, because no discernable impact on the clearing process is seen in the DP measurement due to the effect of area variations in the hardware, their impact on the residual liquid in transient is expected to be minimal.



Figure 76.A-4: Lines of Constant Gas Velocity Compared to UPTF Data for 3-Bar and 15-Bar Loop Seal Tests [Figure 18.2.3-2 from Topical Report]

Table 76.A-15: Cross-over Leg Piping Geometry Comparison			
	ROSA	3 Loop PWR	Remark
Cross-over Pipe Diameter	0.168 m	[] ^{a,c}
Cross-over Pipe Length	9.9 m	[] ^{a,c}
Cross-over Pipe Horizontal Run	2.17 m	[] ^{a,c}

Table 76.A-15: Cross-over Leg Piping Geometry Comparison			
	ROSA	3 Loop PWR	Remark
Elevation of Cross-over Pipe Centerline Relative to Core Bottom	1.785 m	[] ^{a,c}
Total Flow Area (all loops)	$2 \times 0.02217 = 0.0443 \text{ m}^2$	[] ^{a,c}
Pressure	Slightly above SG Pressure	Slightly above SG Pressure	LSC Phase
Flow Condition	Liquid draining at saturation or subcooled against vapor upflow which is being condensed	Liquid draining at saturation or subcooled against vapor upflow which is being condensed	Draining of SG Tube against Vapor flow from core generated by decay heat

IV. Boiloff Phase []^{a,c}

The local phenomena of importance for this period include the core level swell, SI condensation and the arrival of Accumulator injection. The core geometry is nearly identical to PWR except for the number of fuel assemblies. The designed power ratio was 1:48 originally relative to a 4 Loop PWR, but for this demonstration plant, the power ratio is []^{a,c} which is greater than the volume scale ratio of []^{a,c}. But the scale distortion is not expected since the difference is small.

A.4 Conclusion:

The scale distortion in ROSA-IV SB-CL-02 (2.5% Bottom of CL) is found to be minor and the SB-CL-series tests are suitable for the code validation. The code validation using the ROSA-IV data for SBLOCA application is considered adequate when the supplemental validation is performed for phenomena of importance not explicitly investigated in ROSA-IV tests selected for the WCT-TF2 validation matrix.

A.5 References

[76.A-1] S. Banerjee, M. G. Ortiz, T. K. Larson, D. L. Reeder, "Top-Down Scaling Analyses Methodology for AP600 Integral Tests," INEL-96/0040, May 1997

[76.A-2] ML103120255, "Scaling Analysis for US-APWR Small Break LOCAs," UAP-HF-10289-NP (R0), Mitsubishi Heavy Industries, Ltd., October 2010

[76.A-3] Y. Kukita, Y. Anoda, and K. Tasaka, "Summary of ROSA-IV LSTF first-phase test program – Integral simulation of PWR small-break LOCAs and transients," Nuclear Engineering and Design 131 (1991) 101-111

[76.A-4] G. B. Wallis, "One-dimensional Two-phase Flow," McGraw-Hill Book Company, 1969

[76.2-5] F. Mayinger, Weiss and K. Wolfert, "Two-phase flow phenomena in full-scale," Nuclear Engineering and Design 145 (1993) 47-61

[76.A-6] Akira OHNUKI, Hiromichi ADACHI and Yoshio MURAO, "SCALE EFFECTS ON COUNTERCURRENT GAS-LIQUID FLOW IN A HORIZONTAL TUBE CONNECTED TO AN INCLINED RISER," Nuclear Engineering and Design 107 (1988) 283-294

[76.A-7] Christophe Vallée, Tobias Seidel, Dirk Lucas, Matthias Beyer, Horst-Michael Prasser, Heiko Pietruske, Peter Schütz, Helmar Carl, "Counter-current flow limitation in a model of the hot leg of a PWR—Comparison between air/water and steam/water experiments," Nuclear Engineering and Design, 245 (2012) 113– 124

Appendix-B: Investigation of Scale Distortion in Semiscale Tests

B.1 Introduction

Several scaling analyses were performed on the earlier Semiscale facilities to identify scale distortions. Conclusions from these studies resulted in subsequent facility modifications to reduce scale distortions. Scale distortions identified in these studies will be reviewed first. Flow regime transition in Semiscale geometry will be examined next based on applicable CCFL correlations.

B.2 Review of Previous Scaling Analysis and Examination

Conclusions from scaling analyses by Rogers [76.B-1], Larson et al. [76.B-2], Zuber [76.B-3] and scaling examination captured in WCAP-10054-P-A [76.B-4] are summarized below;

1. 2D/3D effects [76.B-1]:

Differences in performance between a PWR and Semiscale Mod-3 are expected where two- and three-dimensional system effects influence controlling phenomena. Some particularly important phenomena influenced by two- and three-dimensional effects are core thermal performance and vessel lower plenum liquid level, upper head mixing, and downcomer counter-current flow. The Semiscale Mod-3 system cannot simulate the two- and three-dimensional temperature and flow distributions of the PWR core or the two- and three-dimensional velocity distributions of the PWR vessel downcomer and plenum regions.

2. Metal stored energy relative to the coolant volume:

The stored energy in the metal structure of Semiscale Mod-3 is greater per unit volume of system fluid than that in a PWR, and as a result, the released energy may adversely affect system response to some degree. Various types of insulation with low thermal capacitance and low thermal conductivity have been incorporated to reduce these effects [76.B-1]. During steady state operation this distortion will result in large environmental heat losses. During a small break LOCA transient the primary system's depressurization will result in the structural metal becoming heat sources, whose corresponding rates of heat release to the primary system will be atypically large. The secondary side's structural metal may become a heat source or sink during the course of a transient, depending upon the operation of the secondary side system [76.B-4].

3. Heat loss to the environment (the system heat loss to the environment is of the order of 130% of decay heat if unmitigated):

For the most part, analysis shows that first order effects during small break LOCA will be preserved in the Semiscale Mod-3 system relative to the PWR system. A possible exception to this is excess heat loss to the ambient in the Semiscale system [76.B-1]. In an effort to minimize environmental heat losses, external heaters were installed on the loop piping, down comer, vessel, upper plenum, and secondary side shells. These heaters were controlled by independent variable power supplies, allowing the external heater power to be ramped down during the course of a transient in an attempt to not amplify the already atypical metal heat release to the primary fluid [76.B-4].

4. Horizontal Two-phase flow regime transition:

Zuber [76.B-3] indicated that the intact loop's horizontal regime change in Semiscale is expected to be similar to that of PWRs. Despite the fact that the horizontal loop pipings are oversized relative to

the volume scale, Larson [76.B-2] pointed out that for boiloff period, hot legs in both PWRs and Semiscale are most likely stratified since the vapor flow from the decay heat is expected to be lower than the transition condition assuming the void fraction is higher than 0.7. It is suggested that while scale distortion exists, they are not likely to impact the 1st order effects of the SBLOCA transients in Semiscale. The flow regime transition and CCFL in the loop will be investigated further.

B.3 Further examination of CCFL and its implications

1. Vertical/inclined Two-phase flow regime transition:

Lee [76.B-5] identified the CCFL phenomena and their dependence on the pipe diameter as the possible source for scale distortion in scaled tests. This is illustrated in Figure 76.B-1. The figure shows that the CCFL in the full scale loop would follow Kutateladze type limit while smaller pipe would follow Wallis type limit which would be more restrictive, and that pipe sizes used in Semiscale may be in the Wallis type regime.

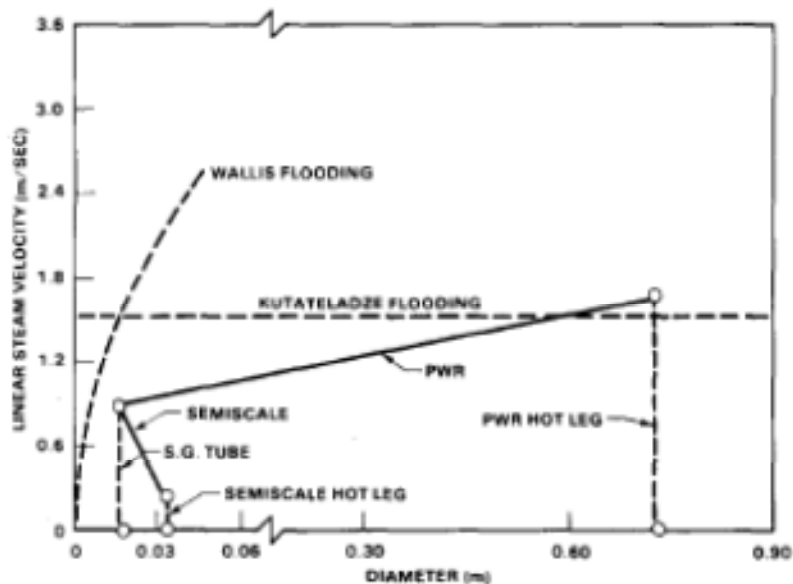


Figure 76.B-1: Comparison between linear velocities in hot leg and steam generator tubes for Semiscale and PWR [Figure 4 of 76.B-5]

Richter [76.B-6] investigated the flooding in tubes and annuli of various flow areas and clarified that starting from Kutateladze's correlation at the large pipe for Bond number $(N_B = D^2 \cdot \left(\frac{\sigma}{g \cdot (\rho_f - \rho_g)}\right)^{-1})$

larger than 3600 (or $D^* = D \cdot \left(\frac{\sigma}{g \cdot (\rho_f - \rho_g)}\right)^{-1/2} = 60$) the CCFL becomes more restrictive as the diameter becomes smaller and the limit line transitions to Wallis type correlation. This is illustrated in Figure 76.B-2 below (pipe diameter corresponding to D^* is evaluated at the atmospheric pressure). The triangle (Δ) marks are the measured vapor Kutateladze number at the point where there is no liquid downflow together with a group of no liquid flow curves based on Wallis's correlation with a varying coefficient.

Kutateladze Number vs. Non-dimensional Geometric Parameter and Experimental Results for Zero Penetration of Liquid

○	Ku0	0	0	0	Kg = 3.2
1	Ku1	0	0	0	(Jg*) ** 0.5 = 1
2	Ku2	0	0	0	(Jg*) ** 0.5 = 0.8
3	Ku3	0	0	0	(Jg*) ** 0.5 = 0.6
△	Meas	1	0	0	Test Measurement

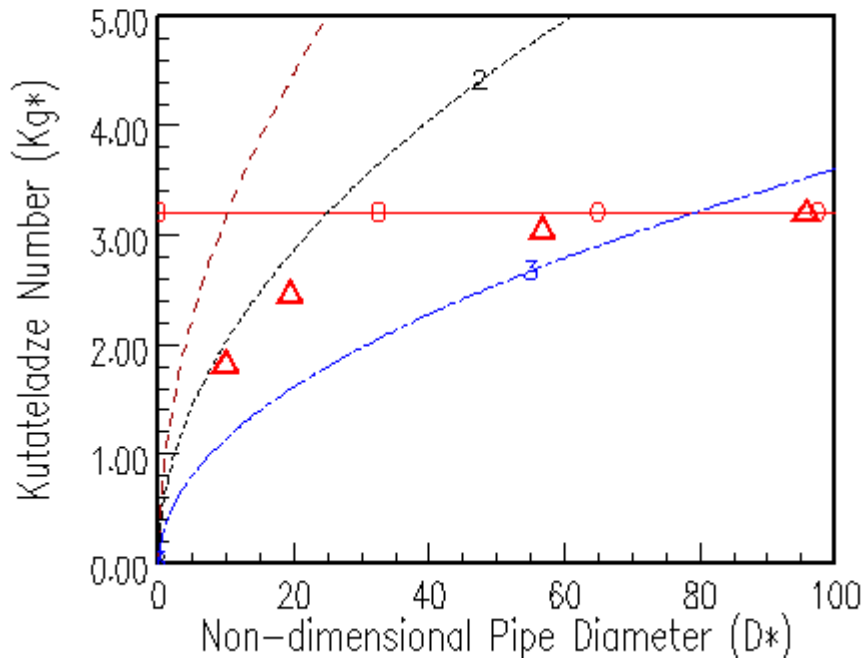


Figure 76.B-2: Kutateladze number vs. non-dimensional geometric parameter and experimental results for zero penetration of liquid [Figure 2 of 76.B-6 with correction]

It is interesting to note that $D^*=60$ for $D=9.6$ cm at $P=1000$ psia. This is larger than the size of both broken and intact loop piping of Semiscale Mod-3 and later modifications. This implies that the vertical flow regime transition in Semiscale facility at high pressures including the up-hill side of loop seal region would have the Wallis type CCFL criteria in contrast to PWRs which would have the Kutateladze type CCFL limit. However, because the loop seal []^{a,c} while the facility scale is 1600:1, the vapor velocity in the loop seal region is about []^{a,c} slower in Semiscale which would have a significant impact on how the loop seal clears. Therefore, it is expected that the loop seal clearing in Semiscale would be notably different from the PWR transient of an equivalent break size.

The SG/Hot Leg interface is another location where liquid hold-up is expected due to CCFL. For the full scale geometry, the following CCFL correlation based on the UPTF data is used [76.B-7].

$$(j_g^*)^{1/2} + m \cdot (j_f^*)^{1/2} = C$$

where $m = 0.7 - 1.0$ and $C = 0.61 - 0.75$.

This and Ohnuki's correlation [76.B-8] were found to be appropriate for small scales if the geometry is equivalent to PWR (HL horizontal run connected to an inclined pipe with an angle of ~50 degrees attached to the SG inlet plenum. "C" in Ohnuki's correlation is a function of the hot leg geometry.

$$C = \ln \left\{ \left(\frac{L}{D} \right) \cdot \left(\frac{1}{\ell} \right) \right\}^{-0.066} + 0.88$$

where L (m) is the length of horizontal run of Hot Leg, D (m) is the diameter, and ℓ (m) is the inclined pipe length. Though the correlation is not strictly applicable due to a significant difference in the geometry, it is illustrative to note that using the geometrical information, for Semiscale hot leg, C = 0.65 (Intact) and = 0.60 (Broken). These are low end of the possible range for the C value meaning that in Semiscale, the hot leg bend is more restrictive than PWR. The limiting location is believed to be the HL/Elbow connection area. However, the loop []^{a,c} than the volumetric scale, and the velocity is substantially lower. The SG/hot leg in Semiscale would therefore be less restrictive compared to the PWRs.

2. Axial Distribution of Liquid Inventory

Figure 76.B-3 below compares Volume distribution – elevation relationship between Semiscale and a PWR [76.B-1]. While the volume fraction at the loop level may be equivalent to PWR, Semiscale shows significant deviation at higher elevation. It is likely that the mixture level is notably impacted when the system becomes two-phase. It is expected that the loop flow during the natural circulation phase is more sensitive to the vapor generation in the system.

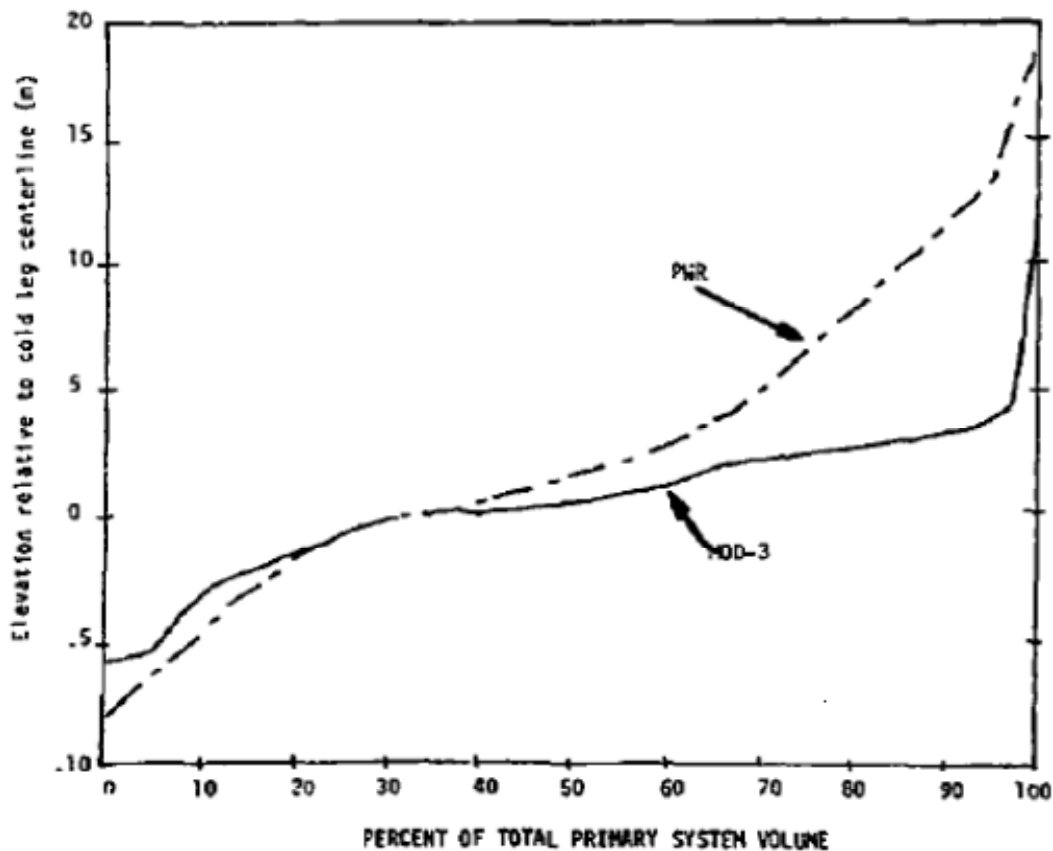


Figure 76.B-3: Comparison of PWR and Semiscale Liquid volume percentage relative to cold leg centerline [Figure 8 of 76.B-1]

3. Scale Impact on the Natural Circulation

D'Auria [76.B-9] discussed systematic scale effect on Natural Circulation. In SBLOCA the RCS inventory at the end of natural circulation phase is considered one of important parameter influencing the coolant inventory during the boil-off phase where the PCT most likely occurs. Figure 76.B-4 compares the normalized two-phase natural circulation mass flux vs. the residual mass in the primary system. Curves are from natural circulation tests from three difference scale IETs at 2% power level. It has been found that the smaller scale tests tended to terminate the natural circulation at the higher fraction of mass.

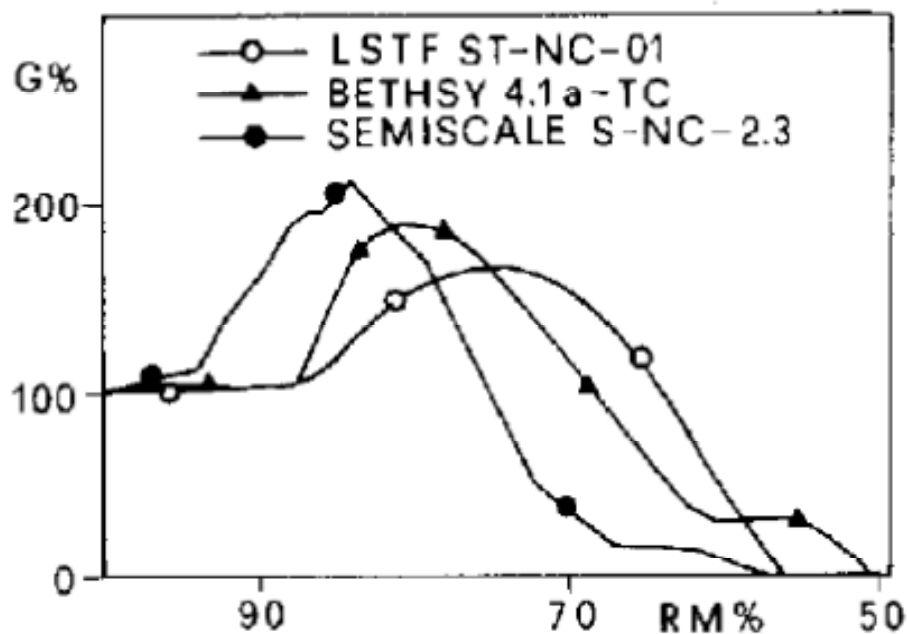


Figure 76.B-4: Scaling of two-phase natural circulation: effect of volume scale on the two-phase natural circulation mass flux relative to single phase natural circulation mass flux [Figure 19 of 76.B-9]

B.4 Conclusion:

Metal stored energy relative to the coolant volume and the heat loss to the environment were apparent scale distortions in the small scale facilities like Semiscale. In an effort to minimize environmental heat losses, external heaters were installed on the loop piping, downcomer, vessel, upper plenum, and secondary side shells. These heaters were controlled by independent variable power supplies, allowing the external heater power to be ramped down during the course of a transient in an attempt to not amplify the already atypical metal heat release to the primary fluid. Other scale distortions are seen in the CCFL behavior in the hot leg/SG interface and in the Loop seal where the clearing behavior is impacted and more residual liquid is expected in Semiscale tests compared to PWRs. Many of known distortions while some may be considered minor, are not correctable and the transient behavior requires careful examination to interpret and to extrapolate to the PWR behavior. The facility is still useful for code assessment however atypicalities and scale distortions in the facility are present which impacts the behavior of key phenomena such that the code may be exercised in an operating region different from what is expected in PWRs.

B.5 References

[76.B-1] G. M. Rogers, "ANALYSIS OF SCALING THE SEMISCALE MOD-3 SYSTEM TO A PRESSURIZED WATER REACTOR," EGG-SEMI-TR-005, APRIL 1979

[76.B-2] T. K. Larson, J. L. Anderson, D. J. Shimeck, "SCALING CRITERIA AND ANA ASSESSMENT OF SEMISCALE MD-3 SCALING FOR SMALL-BREAK LOSS-OF-COOLANT TRANSIENTS," EGG-M-21082, 1982

- [76.B-3] N. Zuber, "Problems in Modeling of Small Break LOCA," NUREG-0724, October, 1980
- [76.B-4] WCAP-10054-P-A, "WESTINGHOUSE SMALLBREAK ECCS EVALUATION MODEL USING THE NOTRUMP CODE, 1985
- [76.B-5] N. Lee, "LIMITING COUNTERCURRENT FLOW PHENOMENON IN SMALL BREAK LOCA TRANSIENTS," Nuclear Engineering and Design, 102 (1987) 211-216
- [76.B-6] H. J. Richter, "FLOODING IN TUBES AND ANNULI," International Journal of Multiphase Flow Vol.7, No. 6, pp.647-658, 1981
- [76.B-7] F. Mayinger, Weiss and K. Wolfert, "Two-phase flow phenomena in full-scale," Nuclear Engineering and Design 145 (1993) 47-61
- [76.B-8] Akira OHNUKI, Hiromichi ADACHI and Yoshio MURAO, "SCALE EFFECTS ON COUNTERCURRENT GAS-LIQUID FLOW IN A HORIZONTAL TUBE CONNECTED TO AN INCLINED RISER," Nuclear Engineering and Design 107 (1988) 283-294
- [76.B-9] D'Auria, "Scaling of natural circulation in PWR systems," Nuclear Engineering and Design, 1991

**WCAP-16996-P, “Realistic LOCA Evaluation Methodology Applied to the Full Spectrum of Break Sizes
(FULL SPECTRUM LOCA Methodology)”
Request for Additional Information – (Non-Proprietary)
RAIs 77-82, 86-87, 93 and 112**

March 2014

Westinghouse Electric Company LLC
1000 Westinghouse Drive
Cranberry Township, PA 16066

©2014 Westinghouse Electric Company LLC
All Rights Reserved

Question #77 (RAI Set 6): Loop Seal Clearance in LSTF Test SB-CL-18

WCAP-16996-P/WCAP-16996-NP, Volumes I, II and III, Revision 0, Section 18, "Loop Seal Clearance," Subsection 18.2, "Important Physical Processes and Scaling Laws," Subsection 18.2.1, "ROSA," considers experimental data from two integral effects, Test SB-CL-18 and Test SB-CL-14, performed at the LSTF as part of the ROSA No. 4 (ROSA-IV) test program. LSTF was a full-pressure facility and preserved major component elevations of the reference Westinghouse-type four-loop 3,423 MWt (1,110 MWe) PWR at Tsuruga Unit 2 of Japan Atomic Power Company. The LSTF had an overall volumetric scaling ratio of 1/48 and featured two equal-volume primary loops. The hot and cold legs had an ID of 0.207 m (8.15 inch) determined to preserve the loop volumetric scaling ratio 2/48 and the length to square-root-of-diameter ratio (L/\sqrt{D}) for flow regime simulation. The prototypical PWR hot and cold leg IDs were 0.7366 m (29 inch) and 0.6985 m (27.5 inch), respectively. The cross-over legs of the loop seals in LSTF had an ID of 0.1682 m (6.62 in), compared to a prototypical cross-over leg diameter of 0.7874 m (31 inch), to scale volume and preserve height. In Test SB-CL-18 and Test SB-CL-14, the break unit was connected horizontally to the cold leg between the RCP and the RPV in Loop B, which was not connected to the pressurizer.

Test SB-CL-18 simulated a 5 percent cold leg break, which corresponds to a break area of 0.205 ft² or a 6.1 inch equivalent break diameter based on the reference PWR cold leg diameter (27.5 inch). Test data is documented by H. Kumamaru et al., "ROSA-IV/LSTF Cold Leg Break LOCA Experiment Run SB-CL-18 Data Report," Japan Atomic Energy Research Institute Report JAERI-M 89-027, March 1989. Loop seal clearing occurred in both loops at approximately 140 s after the break. Core uncover took place temporarily between approximately 120 s and 155 s during loop seal clearing and most of the core heater rods experienced superheating of up to about 342 °F (190 K). PCT of approximately 872 °F (740 K) was observed during the core uncover just prior to loop seal clearing.

Figure A.2, "Primary Loop A Instruments (II)," in JAERI-M 89-027 shows the instrumentation in the intact loop and Figure A.4, "Primary loop B Instruments (II)," in the same report shows the instrumentation in the broken loop. JAERI-M 89-027, Figure 5.32, "Differential Pressure LSA, PCA," plots measurements from differential pressure transducer DPE070 in the loop seal downhill side (channel DPE070-LSA, DP 17) and from transducer DPE080 in the loop seal uphill side (data channel DPE080-LSA, DP 19). Figure 5.33, "Differential Pressure LSB, PCB," exhibits measurements from transducer DPE210 in the loop seal downhill side (channel DPE210-LSB, DP 41) and from transducer DPE220 in the loop seal uphill side (data channel DPE220-LSB, DP 42). As reflected by the DPE210 data in Figure 5.33, the liquid level in the descending loop seal section, connected to the SG exit chamber, reduces significantly from an initial quasi steady-state absolute value of about 43 kPa (6.3 psid) down to an absolute value of about 8 kPa (1.2 psid) at approximately 140 s after the break. At this point, loop seal clearance begins as seen from DPE220 signal for the ascending loop seal section. The process occurs during a time window of about 60 s and it is completed by 200 s after the break. During loop seal clearance, the DPE220 signal in the ascending loop seal section reduces sharply from an initial quasi steady-state value of about 24 kPa (3.5 psid) to approximately 2 kPa (0.3 psid) whereas the DPE210 signal in the descending loop seal section decreases further only slightly from 8 kPa to about 6 kPa (0.9 psid). The data measurements for the intact loop seal shown in Figure 5.32 exhibit a similar behavior.

Subsection 18.2.1 of the TR WCAP-16996-P/WCAP-16996-NP, Volumes I, II, and III, Revision 0, presents a single plot of Test SB-CL-18 data in Figure 18.2.1-1a, "Measured Pressure Drop in Broken Loop of ROSA 5 percent Break (Kumamaru, et al., 1989)." Figure 18.2.1-1a is a reproduction of Figure 5.33 in the JAERI-M 89-027 report. Referring to the Test SB-CL-18 data in Figure 18.2.1-1a, it is observed in Subsection 18.2.1 that "the liquid tends to be pushed towards the uphill bend and up the pump suction leg." Subsection 18.2.1 continues by stating that "this suggests that the remaining liquid after loop seal clearing will tend to be collected in the uphill side of the loop seal."

- (1) The DPE220 signal in the uphill loop seal section reproduced in Figure 18.2.1-1a, “Measured Pressure Drop in Broken Loop of ROSA 5 percent Break (Kumamaru, et al., 1989),” for Test SB-CL-18 shows only a very small differential pressure of about 2 kPa towards the end of the loop seal clearance phase at 200 s. During the following part of the transient, the measurement reduces gradually down to zero at approximately 650 s and remains at this level thereafter. The DPE210 signal in the descending loop seal section shows a relatively small, in absolute value, differential pressure, which reduces slightly from approximately 6 kPa down to 3.5 kPa during the depicted post-clearance period from 200 s to 900 s. Please clarify how the DPE210 and DPE220 differential pressure measurements shown in Figure 18.2.1-1a support the interpretation in WCAP-16996-P/WCAP-16996-NP, Volumes I, II and III, Revision 0, Subsection 18.2.1 that liquid remaining in the loop seal piping following the loop seal clearance “will tend to be collected in the uphill side of the loop seal.”
- (2) Based on “assessment of WCOBRA/TRAC-TF2 relative to the experiments indicates,” WCAP-16996-P/WCAP-16996-NP, Volumes I, II and III, Revision 0, Subsection 18.4, “Conclusions,” states, among other findings, that “the remaining liquid retained after loop seal clearing tends to collect in the uphill bend and RCP suction leg, as demonstrated in the ROSA tests (Section 21).” WCAP-16996-P/WCAP-16996-NP, Volumes I, II and III, Revision 0, Section 21, “ROSA-IV Test Simulations,” Subsection 21.4.3, “Results and Conclusions from the SB-CL-18 Simulation,” refers to Figures 21.4-1 through 21.4-20 when comparing code predictions against Test SB-CL-18 measurements. Figures 21.4-3 and 21.4-4 show a comparison of the calculated and measured loop seal differential pressures in both loops. It is stated in WCAP-16996-P/WCAP-16996-NP, Volumes I, II and III, Revision 0, Subsection 21.4.3 that [

]“^{a,c} and clarifies that “the test data and calculations also show that after the loop seals clear, steam venting is established through both crossover legs.” Please explain which evidence from Test SB-CL-18, as presented in WCAP-16996-P/WCAP-16996-NP, Volumes I, II and III, Revision 0, Section 21, Subsection 21.4, “Simulation of SB-CL-18, 5-Percent Cold Leg Side,” supports the conclusion in Subsection 18.4 that “assessment of WCOBRA/TRAC-TF2 relative to the experiments indicates that “the remaining liquid retained after loop seal clearing tends to collect in the uphill bend and RCP suction leg, as demonstrated in the ROSA tests (Section 21).” Please present any additional experimental measurements and specific analyses, as appropriate, in support of this conclusion.

Response:

The intent of the quoted text is to say that “the remaining liquid retained in the cross-over leg after the onset of the loop seal clearing tends to collect in the uphill bend and RCP suction leg.”

As noted in the RAI, the onset (beginning) of the loop seal clearing at the SB-CL-18 test does appear to be around 140 seconds after the break; this is when the differential pressures measured on the descending part of the cross-over leg (DPE070-LSA, Figure 21.4-3 and DPE210-LSB, Figure 21.4-4) are at about 8 kPa. During the following (~60-sec) loop seal clearing time window, the differential pressures measured on the ascending sides (DPE080-LSA and DPE220-LSB) gradually decrease from 25 kPa down to about 1-2 kPa; during the same time window the differential pressure on the descending side drops by only about 2 kPa – from 8 kPa down to 6 kPa. For the SB-CL-18 test this is evident from the loop seal differential pressure measurements shown in both Figure 21.4-3 and Figure 21.4-4 of [1]; note that Figure 18.2.1-1a in fact shows the DPE210-LSB and DPE220-LSB measurements for that test shown in Figure 21.4-4.

Similar observation can be made for the 5% break test SB-CL-05, based on the measured loop seal differential pressures shown in Figures 21.5-10 and 21.5-11.

The JAERI-M 62-399 test report for the 2.5% cold leg side break test SB-CL-01 shows that only the broken loop cleared completely; the differential pressures measured in the loop that cleared indicate a dynamics of the loop seal clearance similar to that observed at the 5% break tests SB-CL-05 and SB-CL-18, see Figure RAI.77-1.

Conclusion:

In the updated topical report, the text quoted by NRC in RAI #77, will be modified to state that *“the remaining liquid retained in the cross-over leg after the onset of the loop seal clearing tends to collect in the uphill bend and RCP suction leg”*. The updates will be applied in Section 18.2.1 and bullet 7 of Section 18.4.

References:

1. WCAP-16996-P, “Realistic LOCA Evaluation Methodology Applied to the Full Spectrum of Break Sizes (FULL SPECTRUM LOCA Methodology),” November 2010.
2. JAERI-M 89-027, “ROSA-IV/LSTF 5% Cold Leg Break LOCA Experiment Run SB-CL-18 Data Report,” March 1989.
3. JAERI-memo 62-399, “ROSA-IV/LSTF 2.5% Cold Leg Break LOCA Experiment Data Report for Runs SB-CL-01, 02 and 03,” November 1987.



a,c

Figure RAI.77-1 – Loop Seal Differential Pressures in the Broken Loop B at ROSA-IV 2.5% Cold Leg Break Test SB-CL-01

Note: This figure is digitized from the respective differential pressure plots shown in Fig.8.13 of the SB-CL-01 dataset in JAERI-M 62-399. Measurement uncertainty is $\pm 0.32\text{kPa}$.

Question #78: Loop Seal Clearance in LSTF Test SB-CL-14 and Test SB-CL-18

In addition to LSTF Test SB-CL-18, WCAP-16996-P/WCAP-16996-NP, Volumes I, II and III, Revision 0, Section 18, "Loop Seal Clearance," Subsection 18.2.1, "ROSA," presents data from LSTF Test SB-CL-14. Test SB-CL-14 simulated a 10 percent cold leg break, which corresponds to a break area of 0.413 ft² or an 8.7 inch equivalent break diameter based on the reference PWR cold leg diameter (27.5 in). Data from 6 ROSA-IV LSTF experiments, Test SB-CL-01, Test SB-CL-05, Test SB-CL-14, Test SB-CL-15, Test SB-CL-16, and Test SB-CL-18, were used for comparison with test predictions obtained with the NRC code TRACE as documented in "TRACE V5.0 Assessment Manual Appendix C: Integral Effects Tests," Agencywide Documents Accession and Management System (ADAMS) No. ML120060172. As indicated by the loop seal differential pressure measurements provided for Test SB-CL-14 in Subsection C.5.5.3, "Simulation of SB-CL-14," in this document, both loop seals experienced clearing between approximately 76 s and 100 s after the break opening. The core uncovered temporarily between approximately 60 s and 80 s just before loop seals clearing and the maximum observed heater rod temperature was about 72 °F (40 K) higher than the initial rod temperature.

WCAP-16996-P/WCAP-16996-NP, Volumes I, II and III, Revision 0, Subsection 18.2.1, "ROSA," includes a single plot of data from Test SB-CL-14, which is shown in Figure 18.2.1-1b, "Measured Pressure Drop in Broken Loop of ROSA 10 percent Break (Koizumi and Tasaka, 1988)." Figure 18.2.1-1b reproduces Figure 6.8, "Loop-B Crossover Leg Differential Pressures," from Reference 3 listed in Subsection 18.5, "References," as: Koizumi, and Tasaka, K., 1988, "Quick Look Report for ROSA-IV/ LSTF 10 percent Cold Leg Break LOCA Test, SB-CL-14," JAERI-memo 63-262. The curves in Figure 18.2.1-1b are marked with symbols labeled as "DP 41" and "DP 42" at the top of the plot. The vertical axis in the plot depicts differential pressure in units of kPa and has a label "DPE210-LSB." Referring to Figure 18.2.1-1b, Subsection 18.2.1 makes the observation that "the liquid tends to be pushed towards the uphill bend and up the pump suction leg" and continues stating that "this suggests that the remaining liquid after loop seal clearing will tend to be collected in the uphill side of the loop seal."

- (1) Figure 18.2.1-1b, "Measured Pressure Drop in Broken Loop of ROSA 10 percent Break (Koizumi and Tasaka, 1988)," in WCAP-16996-P/WCAP-16996-NP, Volumes I, II and III, Revision 0, Subsection 18.2.1 shows a reproduction of Figure 6.8 in JAERI-memo 63-262. The graph shown in Figure 18.2.1-1b is not entirely legible. Please provide a legible plot for the data presented in Figure 18.2.1-1b. Explain the availability of Reference 3 in Subsection 18.5 and clarify if electronically recorded data measurements were also available and used as part of the assessment process.
- (2) It appears that after the initial transitory period, one of the curves in Figure 18.2.1-1b shows practically zero differential pressure whereas the second one exhibits a rather high and persisting pressure difference, which slowly increases to reach about 30 kPa at the end of the displayed time interval. Some of the measurements from Test SB-CL-14 in Figure 18.2.1-1b are different, both in trend and in magnitude, when compared to the differential pressure measurements shown in Figure 18.2.1-1a, "Measured Pressure Drop in Broken Loop of ROSA 5 percent Break (Kumamaru, et al., 1989)," for Test SB-CL-18. Please explain the basis for asserting in Subsection 18.2.1, "ROSA," that data from both Test SB-CL-18 and Test SB-CL-14, as depicted in Figures 18.2.1-1a and 18.2.1-1b, respectively, support the interpretation that liquid remaining in the loop seal piping following the loop seal clearance "will tend to be collected in the uphill side of the loop seal," when there are obvious and significant disparities between the experimental responses shown in these two figures.

Response:

As observed by NRC, there is disparity between the measured loop seal differential pressures shown in JAERI-memo 63-262 (Fig. 6.7 and 6.8 therein) and those shown in the TRACE assessment in NRC Publication No. ML120060172 (Figures C.5-122 to C.5-125 therein).

Westinghouse is not aware of the origin and form of the SB-CL-14 test data used in the TRACE assessment (ML120060172). The observed disparity in the loop seal differential pressure measurements in SB-CL-14 is most likely due to inaccurate graphical presentation of the DPE070-LSA and DPE210-LSB measurements in Fig. 6.7 and 6.8 of JAERI-memo 63-262. Note that, as described in its title, JAERI-memo 63-262 is a quick look report and the qualification of the plots, Fig. 6.7 and 6.8 in particular, might not have been appropriate. For the DP 17 (DPE070-LSA) and DP 41 (DPE210-LSB) measurements shown in these two plots there must have been a zero-level shift which is estimated to be approximately 30 kPa, so that at about 340 sec the DPE070 and DPE210 measurements trend to <1 kPa.

The following Figures RAI.78-1 and RAI.78-2 show the loop seal differential pressures, obtained by digitizing the curves from Fig. 6.7 and 6.8 of JAERI-memo 63-262 and adjusting the DPE070-LSA and DPE210-LSB plots for the estimated 30 kPa zero-level shift. As seen, with the adjustment, the loop seal differential pressure curves are similar to those shown in Figures C.5-122 to C.5-125 of Appendix C to ML120060172.

Conclusion:

From 80 seconds to 90 seconds liquid holdup in the suction side of the cross-over leg is apparent and the dynamics of the loop seal clearance appears to be similar to that observed at the SB-CL-18 test (see response to RAI 77, Set 6).

Measured collapsed liquid levels in the ROSA 10% cold leg break test SB-CL-09, Fig.4-7 and Fig.4-23 of JAEA-Research 2008-087 [3] show similar loop seal clearance dynamics as well. Therefore, the interpretation that liquid remaining in the loop seal piping following the loop seal clearance will tend to be collected in the uphill side of the loop seal is considered valid. This interpretation is also supported by the full-scale IVO U-Tube test data, briefly discussed in Subsection 18.2.2.4 of [1].

As a result of this response, Figure 18.2.1-1b of the topical report [1] will be replaced with Figure RAI.78-2, presented herein. No other modification in Subsection 18.2.1 is needed as a result of this RAI response.

References:

1. WCAP-16996-P, "Realistic LOCA Evaluation Methodology Applied to the Full Spectrum of Break Sizes (FULL SPECTRUM LOCA Methodology)," November 2010.
2. JAERI-memo 63-262, "Quick Look Report for ROSA-IV/LSTF 10% Cold Leg Break LOCA Test, SB-CL-14," July 1988.
3. JAEA Research 2008-087, "A Study on Rosa/LSTF SB-CL-09 Test Simulating PWR 10% Cold Leg Break LOCA – Loop-seal Clearing and 3D Core Heat-up Phenomena," Japan Atomic Energy Agency, October 2008.



Figure RAI.78-1 – SB-CL-14 Loop Seal A Differential Pressures



Figure RAI.78-2 - SB-CL-14 Loop Seal B Differential Pressures

(Measurement uncertainty for DPE070-LSA and DPE210-LSB is ± 0.512 kPa, and for DPE080-LSA and DPE220-LSB it is ± 0.32 kPa.)

Question #79: WCOBRA/TRAC-TF2 Assessment for LSTF Test SB-CL-14

WCAP-16996-P/WCAP-16996-NP, Volumes I, II and III, Revision 0, Section 18, “Loop Seal Clearance,” Subsection 18.2.1, “ROSA,” refers to experimental observations from LSTF Test SB-CL-18 and Test SB-CL-14 when discussing loop seal clearance. Subsection 18.4, “Conclusions,” states that “assessment of WCOBRA/TRAC-TF2 relative to the experiments indicates” that, among other findings, “the remaining liquid retained after loop seal clearing tends to collect in the uphill bend and RCP suction leg, as demonstrated in the ROSA tests (Section 21).”

WCAP-16996-P/WCAP-16996-NP, Volumes I, II, and III, Revision 0, Section 21, “ROSA-IV Test Simulations,” Subsection 21.6.2, “Results and Conclusions for the SB-CL-14 Simulation,” presents comparisons of WCOBRA/TRAC-TF2 predictions against Test SB-CL-14 data in Figures 21.6-1 through 21.6-16. Each of Figures 21.6-1 through 21.6-14 and Figure 21.6-16 contain two parts: Part (a), “Code Calculation,” and Part (b), “Reported in JAERI-memo 63-262.” The graphs included in Part (a) in these figures show code predictions whereas the graphs in Part (b) reproduce data plots from JAERI-memo 63-262. Reference 3 in Subsection 18.5, “References,” lists JAERI-memo 63-262 as: Koizumi, and Tasaka, K., 1988, “Quick Look Report for ROSA-IV/LSTF 10% Cold Leg Break LOCA Test, SB-CL-14,” JAERI-memo 63-262. Reference 6 in Subsection 21.20, “References,” lists the same document as: Koizumi, Y. and Tasaka, K., 1988, “Quick Look Report for ROSA-IV/LSTF 10 percent Cold Leg Break LOCA Test, SB-CL-14,” JAERI-memo 63-262. Table 21.1-1, “Selected ROSA-IV Test Series Description and Related Technical Reports,” refers to “JAERI-memo 63-262 (’88, Koizumi).”

- (1) The excerpts from JAERI-memo 63-262 showing individual graphs in Part (b) in each of Figures 21.6-1 through 21.6-14 and in Figure 21.6-16, are not entirely legible. In addition, the horizontal and vertical axes in these reproduced plots use ranges and scales that are different from the corresponding ones used in the plots showing the code predictions in Part (a) of the assessment figures in Subsection 21.6.2. Some of these figures show only a single calculated parameter in Part (a) and several measured quantities in Part (b), making it unclear which measured quantity, if any, can be used as a legitimate reference parameter for code comparison assessments. Such an approach to analyzing code performance and assessing it against test data does not allow for proper examination of code predictions and their comparison and validation against experimental measurements. Even when a plot compares a single predicted variable against a single measured quantity, comparison is not always straightforward. Often, it is necessary to consider if the model supports a direct comparison between computational results and data. For example, adequate capturing of experimental measuring points and other relevant conditions can require specific nodalization. Please explain and justify the adequacy of the used approach to assessing WCOBRA/TRAC-TF2 best-estimate capabilities as exemplified by the identified assessment analyses presented in WCAP-16996-P/WCAP-16996-NP, Volumes I, II and III, Revision 0, Subsection 21.6, “Simulation of the 10 percent Side Break Test SB-CL-14.”
- (2) WCAP-16996-P/WCAP-16996-NP, Volumes I, II and III, Revision 0, Subsection 21.6.2, “Results and Conclusions for the SB-CL-14 Simulation,” Figure 21.6-7, “Comparison of Loop-B Cross-Over Leg Differential Pressures,” Part (a), “Code Calculation,” shows predictions for differential pressures in the downhill and uphill sections of the cold leg seal in the broken loop. The calculations presented in Figure 21.6-7 Part (a) appear remarkably different from the test data shown in Figure 21.6-7 Part (b), “Reported in JAERI-memo 63-2.” This disparity between code results and test data was not acknowledged in WCAP-16996-P/WCAP-16996-NP, Volumes I, II, and III, Revision 0 Subsection 21.6, “Simulation of the 10 percent Side Break Test SB-CL-14.” Please explain why such a pronounced discrepancy in describing an important phenomenon such

as the loop seal clearance remained unidentified and unexplained as part of the WCOBRA/TRAC-TF2 assessment analyses presented in Subsection 21.6.

- (3) The WCOBRA/TRAC-TF2 code qualification and assessment of its capabilities of capturing adequately important physical processes and predicting in a best-estimate manner associated governing parameters is found complicated by aspects of the assessment approach as those discussed in Items (1) and (2) above. Based on the resolution of these items, please describe modifications to specific aspects of the WCOBRA/TRAC-TF2 assessment approach in WCAP-16996-P/WCAP-16996-NP, Volumes I, II, and III, Revision 0, if such have been found appropriate for improving the clarity in demonstrating the technical basis for WCOBRA/TRAC-TF2 validation through proper presentation and documentation of results and findings from specific assessment studies. Include results and summarize outcomes from such modifications and revisions of the TR WCAP-16996-P/WCAP-16996-NP, Volumes I, II, and III, Revision 0, as appropriate.

Response:

The comparison plots for the 10% cold leg break test SB-CL-14 (Figures 21.6-1 through 21.6-16 in Section 21 of WCAP-16966-P) have been recreated to compare the code calculations and the test measurements in a single figure. The new set of plots is attached hereafter.

The comparisons of the code calculations against the test data do not change the essence of the discussion and the conclusions in Section 21.6.2 of the Topical Report [1]. However, for consistency with the new set of figures presented herein, the discussion in Section 21.6.2 of [1] is rewritten as follows.

21.6.2 Results and Conclusions for the SB-CL-14 Simulation

Table 21.6-3 summarizes the predicted and measured chronology of events for the 10-percent cold leg test.

Figures 21.6-1 and 21.6-2 show a comparison of the modeled vs. measured pump speed for the two pumps. [

]^{a,c} Beyond 80 seconds the loop flow measurements FE020A/B-LSA and FE160A/B-LSB are unreliable since the flow is two-phase.

The break flow comparison is shown in Figure 21.6-5; the figure presents the test break flow as calculated from the measured level in the catch tank. [

]^{a,c}

[

] ^{a,c}

[

] ^{a,c}

a,c

Figure RAI.79-1 – Loop-A Pump Speed Comparison
(*Measurement uncertainty is 0 Hz*)

(New Figure 21.6-1 for WCAP-16996-P)

a,c

Figure RAI.79-2 Loop-B Pump Speed Comparison
(Measurement uncertainty is 0 Hz)

(New Figure 21.6-2 for WCAP-16996-P)

a,c

Figure RAI.79-3 Loop-A Flow Rate Comparison
(Measurement uncertainty is ± 1.0008 kg/sec.)

(New Figure 21.6-3 for WCAP-16996-P)

Note: Beyond 80 seconds the loop flow measurements FE020A/B-LSA are unreliable since the flow is two-phase.

a,c

Figure RAI.79-4 Loop-B Flow Rate Comparison
(Measurement uncertainty is ± 1.0008 kg/sec.)

(New Figure 21.6-4 for WCAP-16996-P)

Note: Beyond 80 seconds the loop flow measurements FE160A/B-LSA are unreliable since the flow is two-phase.

a,c

Figure RAI.79-5 Comparison of Break Flows

(Measurement uncertainty for the break flow based on catch tank level is not available)

(New Figure 21.6-5 for WCAP-16996-P)

a,c

Figure RAI.79-6 Comparison of Fluid Density in the Break Spool*(Measurement uncertainty is not available)*

(New Figure 21.6-6 for WCAP-16996-P)

a,c

Figure RAI.79-7(a) Comparison of Loop-A Cross-Over Leg Differential Pressures
(Measurement uncertainty for DPE070-LSA is ± 0.512 kPa, and for DPE080-LSA it is ± 0.32 kPa)

(New Figure 21.6-7(a) for WCAP-16996-P)

a,c

Figure RAI.79-7(b) Comparison of Loop-B Cross-Over Leg Differential Pressures
(*Measurement uncertainty for DPE210-LSB is ± 0.512 kPa, and for DPE220-LSB it is ± 0.32 kPa*)

(New Figure 21.6-7(b) for WCAP-16996-P)

a,c

Figure RAI.79-8 Comparison of System Pressures (Pressurizer and Steam Generator Secondary)
(Measurement uncertainty for PE300-PR is ± 0.064 MPa and for PE430-SGA it is ± 0.032 MPa)

(New Figure 21.6-8 for WCAP-16996-P)

a,c

Figure RAI.79-9 Comparison of Steam Generator A (SGA) U-tube Inlet-to-top Differential Pressures

(Measurement uncertainty is ± 0.064 kPa)

(New Figure 21.6-9 for WCAP-16996-P)

a,c

Figure RAI.79-10 Comparison of Steam Generator B (SGB) U-tube Inlet-to-top Differential Pressures

(Measurement uncertainty is ± 0.064 kPa)

(New Figure 21.6-10 for WCAP-16996-P)

a,c

Figure RAI.79-11 Comparison of Steam Generator A (SGA) U-tube Outlet-to-top Differential Pressures

(Measurement uncertainty is ± 0.064 kPa)

(New Figure 21.6-11 for WCAP-16996-P)

a,c

Figure RAI.79-12 Comparison of Steam Generator B (SGB) U-tube Outlet-to-top Differential Pressures

(Measurement uncertainty is ± 0.064 kPa)

(New Figure 21.6-12 for WCAP-16996-P)

a,c

Figure RAI.79-13(a) Comparison of Steam Generator A (SGA) Inlet Plenum Differential Pressures
(*Measurement uncertainty is ± 0.256 kPa*)

(New Figure 21.6-13(a) for WCAP-16996-P)

a,c

Figure RAI.79-13(b) Comparison of Steam Generator B (SGB) Inlet Plenum Differential Pressures
(*Measurement uncertainty is ± 0.256 kPa*)

(New Figure 21.6-13(b) for WCAP-16996-P)

a,c

Figure RAI.79-14 Comparison of Core Collapsed Liquid Levels*(Measurement uncertainty is not available)*

(New Figure 21.6-14 for WCAP-16996-P)

a,c

Figure RAI.79-15(a) Calculated Accumulator A Injection Flow

(New Figure 21.6-15(a) for WCAP-16996-P)

a,c

Figure RAI.79-15(b) Calculated Accumulator B Injection Flow

(New Figure 21.6-15(b) for WCAP-16996-P)

a,c

Figure RAI.79-16 Comparison of High-Power Rod Cladding Temperatures at 6-ft (1830 mm) Core Axial Location

(Measurement uncertainty is $\pm 6.444K$)

(New Figure 21.6-16 of WCAP-16996-P)

Question #80: LSTF Test SB-CL-14 Data Qualification

WCAP-16996-P/WCAP-16996-NP, Volumes I, II and III, Revision 0, Section 18, "Loop Seal Clearance," Subsection 18.2.1, "ROSA," includes Figure 18.2.1-1b, "Measured Pressure Drop in Broken Loop of ROSA 10 percent Break (Koizumi and Tasaka, 1988)," which reproduces Figure 6.8, "Loop-B Crossover Leg Differential Pressures," from JAERI-memo 63-262. Section 21, "ROSA-IV Test Simulations," Subsection 21.6.2, "Results and Conclusions for the SB-CL-14 Simulation," includes Figure 21.6-7, "Comparison of Loop-B Cross-Over Leg Differential Pressures." Figure 21.6-7 Part (b), "Reported in JAERI-memo 63-262," reproduces the same Figure 6.8, "Loop-B Crossover Leg Differential Pressures," from JAERI-memo 63-262.

Subsection C.5.5.3, "Simulation of SB-CL-14," in "TRACE V5.0 Assessment Manual Appendix C: Integral Effects Tests," ADAMS Accession No. ML120060172, includes Figure C.5-124, "Differential Pressure along downhill Side of Loop-B Seal," and Figure C.5-125, "Differential Pressure along uphill Side of Loop-B Seal." The figures depict DPE210-LSB and DPE220-LSB data signals, respectively, for Test SB-CL-14.

- (1) There are apparent and significant disparities between parameters shown in Figure 18.2.1-1b in WCAP-16996-P/WCAP-16996-NP, Volumes I, II and III, Revision 0, Subsection 18.2.1, "ROSA," and in Figures C.5-124 and C.5-125 in "TRACE V5.0 Assessment Manual Appendix C: Integral Effects Tests." In addition, the WCOBRA/TRAC-TF2 calculations in Figure 21.6-7 Part (a), "Code Calculation," differ significantly from the test data in Figure 21.6-7 Part (b), "Reported in JAERI-memo 63-2," which are identical with the test data shown in Figure 18.2.1-1b. Please explain how Test SB-CL-14 measurements presented in Figure 18.2.1-1b, "Measured Pressure Drop in Broken Loop of ROSA 10 percent Break (Koizumi and Tasaka, 1988)," relate to the test data shown in Figures C.5-124, "Differential Pressure along downhill Side of Loop-B Seal," and in Figure C.5-125, "Differential Pressure along uphill Side of Loop-B Seal," in Appendix C, "Integral Effects Tests," of "TRACE V5.0 Assessment Manual."
- (2) Please describe test facility selection and test data qualification processes with regard to test data used in WCOBRA/TRAC-TF2 assessment studies if such processes have been considered and applied as part of the WCOBRA/TRAC-TF2 assessment approach implemented in WCAP-16996-P/WCAP-16996-NP, Volumes I, II and III, Revision 0. As part of these processes, please explain if availability of published test reports, documenting measured data, and electronic data files containing recorded measurements were considered and examined. When both types of data sources were available, clarify if a cross-check was performed to examine and qualify important measurements that were used to assess WCOBRA/TRAC-TF2.
- (3) Please explain reliance on and use of available information quantifying instrumentation accuracy for test data from experiments that have been selected and used in WCOBRA/TRAC-TF2 assessment studies. Please clarify if such considerations have been applied as part of the approach, implemented in WCAP-16996-P/WCAP-16996-NP, Volumes I, II and III, Revision 0, to assess WCOBRA/TRAC-TF2. Please explain how such aspects of the assessment approach relate to the analyses presented in Section 21, "ROSA-IV Test Simulations," Subsection 21.6, "Simulation of the 10 percent Side Break Test SB-CL-14," of WCAP-16996-P/WCAP-16996-NP, Volumes I, II and III, Revision 0, TR as an example.
- (4) Based on the resolution of Items (1) through (3) above, please describe modifications to specific aspects of the WCOBRA/TRAC-TF2 assessment approach in WCAP-16996-P/WCAP-16996-NP, Volumes I, II and III, Revision 0, if such have been found appropriate for improving the

clarity in demonstrating the technical basis for WCOBRA/TRAC-TF2 validation through proper, accurate, and adequate presentation and documentation of results and findings from specific assessment studies. Include results and summarize outcomes and revisions of the WCAP-16996-P/WCAP-16996-NP, Volumes I, II and III, Revision 0, TR from such modifications as appropriate.

Response:

Regarding Part (1), see responses to Questions 78 and 79.

Regarding Part (2), Westinghouse has provided a response to NRC Question 76 which uses scaling analysis to highlight the suitability of the ROSA-IV Large Scale Test Facility as the IET of choice for the WCOBRA/TRAC-TF2 code validation.

With regards to the ROSA test data qualification, I

^{a,c}

Regarding Part (3), each of the JAERI test reports documenting the simulated ROSA-IV tests includes detailed information on the accuracy of the instrument measurements and data qualification.

Westinghouse has relied on that information to make engineering judgments with respect to the validity of the test data but has not performed any additional instrument accuracy analysis or assessment beyond that already available in the respective JAERI reports.

Regarding Part (4), the updated topical report will include the revised figures and text, as stated in the responses to questions 77, 78 and 79.

Question #81: ROSA-IV LSTF WCOBRA/TRAC-TF2 Assessment Results Presentation

In RAI questions 78, 79, and 80, additional information was requested to clarify aspects related to both the use of ROSA-IV LSTF test data as well as the presentation and comparison of WCOBRA/TRAC-TF2 predictions against test data in WCAP-16996-P/WCAP-16996-NP, Volumes I, II and III, Revision 0, Section 18, "Loop Seal Clearance," and in Section 21, "ROSA-IV Test Simulations," to demonstrating and assessing the code performance. With regard to the experimental database used in WCAP-16996-P/WCAP-16996-NP, Volumes I, II and III, Revision 0, Section 21, Subsection 21.1, "Introduction," refers to Table 21.1-1, "Selected ROSA-IV Test Series Description and Related Technical Reports," and states: "Table 21.1-1 shows the list of tests used for the validation work. It contains relevant reports and articles related to the ROSA-IV LSTF and the different test considered herein." WCAP-16996-P/WCAP-16996-NP, Volumes I, II and III, Revision 0, Section 21, "ROSA-IV Test Simulations," Subsection 21.5.2, "Results and Conclusions from the SB-CL-05 Simulation," in discussing WCOBRA/TRAC-TF2 assessment results, states: "Unfortunately, the SB-CL-05 electronic data file available in Westinghouse does not contain any recorded fuel rod cladding temperature measurements so that direct graphical comparison cannot be presented. However, rod cladding temperatures measured at the test can be found in Figure 5.468 through Figure 5.484 of the SB-CL-05 test report (Kawaji, et.al.)." Subsection 21.20, "References," identifies only one work by Kawaji listed in Reference 3 as: "Kawaji, M., et al., 1986, "ROSA-IV/LSTF 5 percent Cold Leg Break LOCA Experiment Data Report, Run SB-CL-05," JAERI-memo 61-056."

In addition to addressing RAI questions 78, 79, and 80, the staff finds it necessary to request clarification of the following items.

- (1) Please present a table that documents the source and type of experimental data from experiments performed at the ROSA-IV LSTF integral effect test facility and used to assess WCOBRA/TRAC-TF2 for the purpose of the Full Spectrum LOCA Methodology development as presented in WCAP-16996-P/WCAP-16996-NP, Volumes I, II and III, Revision 0. The table should contain the following pieces of information, each presented in a separate column: (1) test run (experiment) identifiers, (2) identification of data channel identifiers (experimental instrument tags) for measurements used to assess WCOBRA/TRAC-TF2, (3) accuracies of the sensors used in each data channel, (4) availability of electronic test data files and if the files contain the identified experimental measurements, (5) test reports documenting the identified experimental measurements, (6) any other sources of information describing the identified experimental measurements, (7) if examination of the identified experimental measurements (data channel signals) was performed to qualify the data as appropriate for code assessment. Please list each separate experiment (test run) separately in the table. If appropriate, please group data channels based on the type of measurements (for example, temperature, differential pressure, etc.) and list the groups in separate rows when providing their characteristics (accuracies, data sources, examination status). Please provide the meaning of the symbols used in the instrument tags (for example, "TE" for fluid temperature, "DP" for differential pressure, "TW" for wall temperature, etc.).
- (2) When plotting WCOBRA/TRAC-TF2 code predictions against ROSA-IV LSTF test measurements that are considered of key importance for assessing the code capabilities, please explain why the depicted code predictions and test data represent a valid comparison for judging the code performance. In particular, it is important that the model nodalization reflects adequately experimental measuring points. For example, the computational node for a temperature prediction should closely match the location of the thermocouple used in the test. Also, when computing differential pressures for comparison against data, nodalization aspects and locations of

differential pressure taps in the experiment should be considered. As appropriate, please include diagrams showing model nodalization and sensor locations in the same figure.

- (3) Please redraw the figures that are used in WCAP-16996-P/WCAP-16996-NP, Volumes I, II and III, Revision 0, to compare WCOBRA/TRAC-TF2 prediction results against ROSA-IV LSTF test measurements so that both the data measurements and the code predictions are depicted in a single common graph. Please plot the error bars associated with the presented test data when information is available.
- (4) Please revise WCAP-16996-P/WCAP-16996-NP, Volumes I, II and III, Revision 0, to include the additional information requested in Items (1) through (3) above as found appropriate.

Response:

Regarding Parts (1) and (2) of the RAI:

All the requested information is already available in the JAERI reports. The noding of the ROSA test facility is fairly consistent with the location of the various measurement instruments. In the generated comparison plots for the ROSA test simulations, presented in WCAP-16996-P, code calculated pressures were adjusted wherever there was a significant mismatch between the hydraulic node center and the real physical location of the measurements.

Regarding Parts (3) and (4), the updated topical report will include the revised figures and text, as stated in the responses to questions 77, 78 and 79.

Question #82: Break Equivalent Diameter in LSTF Tests SB-CL-01, SB-CL-02, and SB-CL-03

WCAP-16996-P/WCAP-16996-NP, Volumes I, II and III, Revision 0, Section 21, “ROSA-IV Test Simulations,” Subsection 21.7.2.1, “2.5 percent Tests,” presents WCOBRA/TRAC-TF2 assessment results against three ROSA-IV LSTF tests simulating a 2.5 percent cold leg break with different break orientations. Test SB-CL-01 simulated a side break, Test SB-CL-02 studied a bottom break, and Test SB-CL-03 examined a top break. All three tests used an orifice with a 16.0 mm (0.63 inch) opening diameter to model the break. Assessment results are shown in Subsection 21.7.2.1 Figures 21.7-3 through 21.7-10. Subsection 21.7.2, “Discussion of Results,” states that Test SB-CL-01, Test SB-CL-02, and Test SB-CL-01-03 “simulated a 2.5 percent break in the cold leg, which approximates a 3 inch break in a PWR.”

The 16.0 mm (0.63 inch) ID orifice, used to simulate a 2.5 percent cold leg break in the identified ROSA-IV LSTF tests, had an opening area of 201.1 mm^2 (0.00216 ft^2). The LSTF reference PWR cold leg ID was 27.5 inch. Based on the LSTF volumetric scaling ratio, the 2.5 percent LSTF break size scales to a corresponding PWR cold leg break area, as follows:

$$\text{PWR Break Area} = 48 \times \text{LSTF Break Area} = 48 \times 0.00216 \text{ ft}^2 = 0.1037 \text{ ft}^2.$$

The above determined 2.5 percent PWR cold leg break area of 0.1037 ft^2 corresponds to an equivalent break diameter of 4.36 inch. This equivalent break diameter significantly differs from the 3 inch equivalent break diameter that is cited in WCAP-16996-P/WCAP-16996-NP, Volumes I, II and III, Revision 0, Subsection 21.7.2, “Discussion of Results.” Please explain how it was determined in Subsection 21.7.2, “Discussion of Results,” that ROSA-IV LSTF Test SB-CL-01, Test SB-CL-02, and Test SB-CL-01-03 “simulated a 2.5 percent break in the cold leg, which approximates a 3 inch break in a PWR.”

Response:

The statement in Section 21.7.2 of the FSLOCA™ Topical Report [1] that the ROSA-IV 2.5-percent break tests SB-CL-01, -02, and -03 approximate a 3-inch break in a PWR is too general and apparently inaccurate if applied specifically to a 4-loop Westinghouse PWR, which is volume-scaled 48:1 relative to the ROSA-IV LSTF. Westinghouse agrees with the NRC’s calculation that the ROSA 2.5% break tests represent an equivalent 4.36-inch diameter break of the reference 4-loop Westinghouse PWR.

At the same time, the 2.5% ROSA cold leg break would represent a 3.45-inch break if applied to the 3-loop Beaver Valley Unit 1 (DLW), which is approximately 30:1 volume-scaled relative to ROSA; for a 2-

FULL SPECTRUM™ and FSLOCA™ are trademarks or registered trademarks of Westinghouse Electric Company LLC, its affiliates and/or its subsidiaries in the United States of America and may be registered in other countries throughout the world. All rights reserved. Unauthorized use is strictly prohibited. Other names may be trademarks of their respective owners.

loop PWR the equivalent break size would be even smaller than the 3.45-inches determined for DLW. The relevant text in Section 21.7.2 of the FSLOCA Topical Report [1] will be modified by removing the 3-inch value provided for the equivalent break size of a PWR. The following text will be provided in Section 21.7.2 of the updated topical report.

In LSTF, the break unit can be configured such that the break orientation effect can be studied. Two sets of three experiments were conducted in the LSTF to investigate the effect of break orientation. The first three tests (SB-CL-01, -02, and -03; side, bottom and top respectively), simulated a 2.5 % break in the cold leg, which approximates a 3-inch break in a PWR. The second three tests (SB-CL-12, -15 and -16) simulated a 0.5% break in the cold leg. In this section these two sets of break orientation studies will be discussed.

References

1. WCAP-16996-P, "Realistic LOCA Evaluation Methodology Applied to the Full Spectrum of Break Sizes (FULL SPECTRUM LOCA Methodology)," November 2010.

Question #86: MSTRTX, STRTX, STRTX1, and STRTX2 Multipliers

WCAP-16996-P/WCAP-16996-NP, Volumes I, II, and III, Revision 0, Section 10, "WCOBRA/TRAC-TF2 One-Dimensional Component Models," Subsection 10.2, "Pipe Component," explains that in addition to the HS_SLUG multiplier, "user specified allowances for horizontal stratification within a PIPE component can be provided through the MSTRTX and STRTX input." Subsection 10.3, "TEE Component," states that "similar to the PIPE component, the user has the option to specify allowance for horizontal stratification in the main and side pipes through the STRTX1 and STRTX2 multipliers."

WCAP-16996-P/WCAP-16996-NP, Volumes I, II, and III, Revision 0, provides no description of the MSTRTX, STRTX, STRTX1, and STRTX2 multipliers. At the same time, Figure 21.3-9, "Hot Leg (Including Pressurizer), Steam Generator and Cross-Over Leg Noding," in Section 21, "ROSA-IV Test Simulations," of the WCAP-16996-P/WCAP-16996-NP, Volumes I, II and III, Revision 0, shows that specific values of STRTX linked to the common interface between the two adjacent cells used to model each of the 90° bends connecting the horizontal section of the LSTF loop seal to the downhill and uphill pipes of the cross-over leg.

- (1) The MSTRTX, STRTX, STRTX1, and STRTX2 multipliers appear to be related to the modeling of important process in horizontal two-phase flow such as flow stratification. Please explain why the MSTRTX, STRTX, STRTX1, and STRTX2 multipliers were not described in WCAP-16996-P/WCAP-16996-NP, Volumes I, II, and III, Revision 0.
- (2) Please explain the meaning of the MSTRTX, STRTX, STRTX1, and STRTX2 multipliers, their modeling impact, and intended use. Provide the definitions of these quantities and describe how they relate to specific WCOBRA/TRAC-TF2 models and expressions.
- (3) WCAP-16996-P/WCAP-16996-NP, Volumes I, II and III, Revision 0, Subsection 10.2, "Pipe Component," states that "user specified allowances for horizontal stratification within a PIPE component can be provided through the MSTRTX and STRTX input." Please clarify if MSTRTX, STRTX, STRTX1, and STRTX2 are user defined input parameters. Describe their initialization, default values, and allowable input ranges.
- (4) Please explain how the default values and allowable input ranges for MSTRTX, STRTX, STRTX1, and STRTX2 have been determined and present the technical basis for their validation for the purposes of PWR LOCA analyses using WCOBRA/TRAC-TF2. Describe how the values of these multipliers are assigned and controlled in PWR plant LOCA analyses. Please relate the responses to Items (2) and (3) above to specific features of PWR plant models used for LOCA analyses. Identify specific components in such models that are affected by these parameters. Please present diagrams from a reference plant model to explain and illustrate their application in PWR LOCA analyses.
- (5) Please revise WCAP-16996-P/WCAP-16996-NP, Volumes I, II, and III, Revision 0, to include the additional information as requested in Items (2) through (4) above.

Response:

- (1) The STRTX input flag is important to the modeling of flow stratification in the loop seal region. The description of this input flag is provided in Section 10.2 of WCAP-16696-P [1], and the application of the

input flag is alluded to in Section 29.5.6 of WCAP-16996-P. It is important to clarify that the MSTRTX, STRTX, STRTX1, and STRTX2 input flags are not multipliers, as described in part (2) of this response.

(2) The value of the MSTRTX input flag only determines whether additional inputs are specified for certain components; it does not directly impact the WCOBRA/TRAC-TF2 calculated results. MSTRTX can be input for PIPE and TEE components; the allowable input values are 0 and 1. If MSTRTX = 0 for a given PIPE or TEE component, then the STRTX, STRTX1, and STRTX2 flags are not specified as part of the component input. If MSTRTX = 1, then STRTX, STRTX1, and/or STRTX2 are included as part of the component input.

The STRTX, STRTX1, and STRTX2 input flags are all equivalent (i.e., they all have the same function); the differentiation is only in the component to which they are input. STRTX is input for PIPE components; STRTX1 for the main line of TEE components; and STRTX2 for the branch line of TEE components. [

] ^{a,c}

(3) The MSTRTX, STRTX, STRTX1, and STRTX2 input flags are all user defined. The default value of MSTRTX is 0, and by default the STRTX, STRTX1, and STRTX2 parameters are not input. The allowable entries for MSTRTX are 0 and 1, as described in Part (2) of this response. The allowable entries for STRTX, STRTX1, and STRTX2 (when MSTRTX = 1) are 0, 1, and 2: [

] ^{a,c}

(4) MSTRTX = 0 (STRTX, STRTX1, and STRTX2 not input) is specified for [

] ^{a,c} This modeling approach was selected for consistency with the supporting Separate Effects Test (SET) and Integral Effects Test (IET) simulations. The input values are controlled by code diagnostics and analyst guidance.

(5) The FSLOCA topical report will be updated to reflect the information discussed in this RAI response. The first paragraph in Section 29.5.6 of WCAP-16996-P under the “Horizontal Stratification” heading will be replaced with the following:

The prediction of the horizontal stratified flow regime in the loop seal piping was assigned a high (H) ranking in the loop seal clearance period of a small break LOCA. The flow is allowed to stratify at all cell faces in the loop seal region where the inclination angle is [

$I^{a,c}$ The uncertainty on the flow regime transition in and out from horizontal stratified (or wavy-dispersed) flow is treated as discussed in Section 29.1.7 (HS_SLUG). [

$I^{a,c}$

Additionally, the use of the user-specified input flag (STRTX = 1) will be described for all models where it is applied.

Reference(s)

- 1) WCAP-16996-P, “Realistic LOCA Evaluation Methodology Applied to the Full Spectrum of Break Sizes (FULL SPECTRUM LOCA Methodology),” November 2010.



Figure 86-1: Illustration of Flow Stratification Checks for a Pressurized Water Reactor Crossover Leg

Question #87: WCOBRA/TRAC-TF2 Non-Sampled Modeling Multipliers

As addressed in RAI question #86, the MSTRTX, STRTX, STRTX1, and STRTX2 multipliers, although related to the modeling of the highly ranked phenomenon of horizontal two-phase flow stratification, were not described in WCAP-16996-P/WCAP-16996-NP, Volumes I, II, and III, Revision 0. At the same time, it appears that one such parameter, STRTX, was applied in WCOBRA/TRAC-TF2 assessment studies as indicated in Figure 21.3-9, "Hot Leg (Including Pressurizer), Steam Generator and Cross-Over Leg Noding," in WCAP-16996-P/WCAP-16996-NP, Volumes I, II, and III, Revision 0, Section 21, "ROSA-IV Test Simulations."

- (1) Please provide a table that lists all parameters and multipliers related to the modeling of physical processes in WCOBRA/TRAC-TF2 and that are available for user input. The table should include separate columns that describe the following types of information: (1) the parameter identifier (for example, STRTX), (2) the PIRT ranking for the process to which the parameter applies, (3) the analytic expression for the relation where the parameter appears as coded in the code source, (4) a summary description of the physical phenomenon to which the parameter applies, and (5) default value and allowable input range for the parameter, as applicable. The parameters listed in the table should include all user defined quantities that are available in addition to the input parameters treated as random variables in the Full Spectrum LOCA methodology and described in WCAP-16996-P/WCAP-16996-NP, Volumes I, II, and III, Revision 0, Section 29, "Assessment of Uncertainty Elements."
- (2) Please explain how the default values and allowable input ranges for the parameters identified in the response to Item (1) above have been determined and present the technical basis for their validation. Describe how the values of these multipliers are assigned and controlled in PWR plant LOCA analyses using WCOBRA/TRAC-TF2.

Response:

The information requested was largely provided previously in response to Requests for Additional Information (RAIs) 50 and 77 on the FULL SPECTRUM LOCA (FSLOCA) Evaluation Model (EM) per LTR-NRC-13-73 [1]. A comprehensive list of the user-defined multipliers is provided in Table 50-1 of the response to RAI 50. The multipliers sampled in the uncertainty analysis (user-input or generic) are described in Table 50-2. These tables contain the parameter names, descriptions, ranges, default value (for user-input multipliers), and distribution (for sampled multipliers).

The Phenomena Identification and Ranking Table (PIRT) ranking, analytic expression, related physical phenomenon, and other information for the sampled variables are described in Table 1 of the response to RAI 77. There are several user-defined multipliers listed in Table 50-1 of the response to RAI 50 for which this information was not specified. This is generally because either a) the multiplier was part of the base TRAC-P Version 5.4.28 code and is not used within the FSLOCA methodology, or b) the multiplier was introduced during the method development and later determined to be unnecessary and therefore is unused for the FSLOCA methodology. An explanation of such parameters was provided in Table 50-3 of the response to RAI 50.

It is recognized that MSTRTX, STRTX, STRTX1, and STRTX2 do not appear in any of the tables in response to RAIs 50 and 77. These input flags were not included because they are not multipliers, but

rather allow the user to []^{a,c} as described in the response to RAI 86. Generally the application of such input flags is described in WCAP-16996-P [2]; however, in this particular case the topical report description was inadequate, and will be updated as discussed in the response to RAI 86.

There are a few other parameters which were not included in Table 50-2 of the response to RAI 50 since they are not direct multipliers within WCOBRA/TRAC-TF2; but they do modify code inputs. For example, the []^{a,c} which is input into the code. For completeness, the equivalent information for these parameters is provided in Table 87-1.

Table 87-1: Supplement to Table 50-2, Indirect Multipliers Subject to Sampling in the Uncertainty Analysis

Acronym	Identifier	Sampling Range	Distribution	Reference
I				
				I ^{a,c}

Reference(s)

- 1) LTR-NRC-13-73, “Submittal of Westinghouse Responses to ‘WCAP-16996-P, ‘Realistic LOCA Evaluation Methodology Applied to the Full Spectrum of Break Sizes (FULL SPECTRUM LOCA Methodology)’ Request for Additional Information – RAIs 46 – 58, 75 and 77’ (Proprietary/Non-Proprietary), Project 700, TAC No. ME5244,” October 28, 2013.
- 2) WCAP-16996-P, “Realistic LOCA Evaluation Methodology Applied to the Full Spectrum of Break Sizes (FULL SPECTRUM LOCA Methodology),” November 2010.

Question #93: Editorial Findings

Please address the findings identified below as they apply to various subsections of Section 21, "ROSA-IV Test Simulations," in Volume 2 of WCAP-16996-P/WCAP-16996-NP, Volumes I, II, and III, Revision 0.

- (1) Subsection 21.4.3 states on page 21-8 that "Figures 21.4-1 through 22.4-20 compare predicted and measured results for the 5-percent cold leg break test SB-CL-18." Please explain if Figure 22.4-20 has been referred to in error instead of Figure 21.4-20 on page 21-8 of WCAP-16996-P/WCAP-16996-NP, Volumes I, II, and III, Revision 0, and correct if appropriate.
- (2) WCAP-16996-P/WCAP-16996-NP, Volumes I, II, and III, Revision 0, Subsection 21.5.2, "Results and Conclusions from the SB-CL-05 Simulation," refers to Figures 21.6-7(a) and 21.6-7(b) on page 21-12 when discussing SG secondary side pressure in each loop. Please explain if Figures 21.6-7(a) and 21.6-7(b) have been referred to in error instead of Figures 21.5-7(a) and 21.5-7(b) on page 21-12 of WCAP-16996-P/WCAP-16996-NP, Volumes I, II, and III, Revision 0, and correct if appropriate.
- (3) WCAP-16996-P/WCAP-16996-NP, Volumes I, II, and III, Revision 0, Subsection 21.16.2 is entitled "HS_SLUG Sensitivity with 5 percent Top Break test SB-CL-18." The first sentence in this subsection reads: "Two simulations of the 5 percent side break test SB-CL-18 test were performed with setting the HS_SLUG multiplier at its maximum []^{a,c} and minimum []^{a,c} values." Please confirm the LSTF test run that is considered in Subsection 21.16.2, verify the break orientation angle for this test, and provide relevant corrections if appropriate. Please check the proper wording of the sentence cited above.
- (4) WCAP-16996-P/WCAP-16996-NP, Volumes I, II, and III, Revision 0, Section 21, "ROSA-IV Test Simulations," Subsection 21.11.2, "SB-CL-18 Simulation Without Hot Leg Nozzle Bypass Flow," states on page 21-33: "The results of this sensitivity, taken in conjunction with these presented in the previous Section 21.11.2, also shows that modeling lower overall bypass is conservative." Please confirm the subsection number referred to in this citation from Subsection 21.11.2 and correct the wording of the sentence as appropriate.

Response:

- (1) WCAP-16996-P/WCAP-16996-NP, Volume II, Revision 0, Subsection 21.4.3, paragraph five, first sentence will be corrected to read "Figures 21.4-1 through 21.4-20 compare predicted and measured results for the 5-percent cold leg break test SB-CL-18."
- (2) WCAP-16996-P/WCAP-16996-NP, Volume II, Revision 0, Subsection 21.5.2, paragraph eight, first and second sentences will be corrected to read []^{a,c}

[

]^{a,c}.

- (3) WCAP-16996-P/WCAP-16996-NP, Volume II, Revision 0, Subsection 21.16.2, the title will be corrected to read “HS_Slug Sensitivity with 5% Side Break test SB-CL-18”.
- (4) WCAP-16996-P/WCAP-16996-NP, Volume II, Revision 0, Subsection 21.11.2, paragraph four, last sentence will be corrected to read [

]^{a,c}

RAI Question #112: Sensitivity of WCOBRA/TRAC-TF2 Small Break LOCA Predictions to Steam Generator Nodalization

Please present sensitivity results for a reference four-loop Westinghouse plant using WCOBRA/TRAC-TF2, which examine the effect of SG nodalization on small break LOCA predication results. Show the sensitivity impact for the limiting small break size, which yields the most severe core level suppression for the selected PWR plant model and applying nominal input parameters.

- (1) Please present code results using a standard SG nodalization scheme, adopted for WCOBRA/TRAC-TF2 modeling of SGs with inverted U-tubes, and a refined noding in which the number of nodes representing the SG U-tube bundle is doubled. In particular, explain and present sensitivities to refined nodalization of the 180°-bend region of the U-tube bundle.
- (2) Please present sensitivity results as requested in Item (1) above when the SG U-tube bundle in each PWR primary loop is modeled using two and three pipe hydraulic components. In modeling the U-tubes in each SG bundle by multiple pipe components, please split the U-tubes into individual groups based on the U-tube apex elevations so that the tallest, middle, and shortest tubes are represented by individual hydraulic components.
- (3) In responding to Items (1) and (2) above, please include, among others, comparison plots for the SG U-tube upside and downside collapsed liquid levels in the broken and intact loops, uphill and downhill loop seal collapsed liquid levels in the broken and intact loops, vessel core-side and downcomer-side collapsed liquid levels, core void fractions, and peak clad temperatures.

Response:

The steam generator (SG) model used in the pressurized water reactor (PWR) examples in the FULL SPECTRUM™ LOCA (FSLOCA™) Topical Report [1] is based on a combination of PIPE, TEE, and HTSTR components. A single PIPE component is used to model the entire primary side U-tube bundle. The primary-to-secondary heat transfer is modeled by using a HTSTR component that connects the primary side PIPE and the secondary side, which is modeled by a TEE component. This steam generator model has been validated against test data from the ROSA-IV Large Scale Test Facility (LSTF) as shown in Section 21 of the topical report [1].

In this response, sensitivity studies have been performed to assess the impact of different steam generator nodalization to the PWR SBLOCA transient. The base case of this study is the most conservative [

]a,c SBLOCA case from Beaver Valley Unit 1, which is the reference 3-loop Westinghouse PWR for the SBLOCA parametric study to support an NRC audit on FSLOCA [2]. The postulated split break occurs in the cold leg of loop 1 with the break size of []a,c. With the most conservative parameters combined in the base run, severe core level suppression occurred and the PCT reached []a,c. There are two sensitivity studies performed per the RAI. The first sensitivity study is to refine the noding in the steam generator tubes and the second one utilizes three parallel PIPE components instead of one PIPE to model the steam generator tubes. The results of the studies will be presented followed by conclusive remarks.

FULL SPECTRUM™ and **FSLOCA™** are trademarks of Westinghouse Electric Company LLC, its affiliates and/or its subsidiaries in the United States of America and may be registered in other countries throughout the world. All rights reserved. Unauthorized use is strictly prohibited. Other names may be trademarks of their respective owners.

Sensitivity Study 1: Double the Nodes in the Steam Generator Tubes

In the first sensitivity study, the node size of the vertical tubes (both uphill and downhill) is reduced to a half of the original node size in the base run as shown in Figure 112-1. In the base run, [

] ^{a,c}

To demonstrate the water distribution in the steam generators and loop seals in the SBLOCA transient, in lieu of collapsed liquid level, an equivalent average void fraction is used in the steam generator and loop seal plots of the two sensitivity studies. Low void fraction indicates high collapsed liquid level while high void fraction means less water in the component. The results of this sensitivity study are presented in Figures 112-2 through 112-17. Figures 112-2, 112-3 and 112-4 show the average void fraction at the uphill side of U-tubes in the respective steam generator 1, steam generator 2, and steam generator 3. The SG noding difference only creates [

] ^{a,c}

Sensitivity Study 2: Three Parallel PIPEs Modeling the Steam Generator Tubes

In the base run, the SG U-tubes are modeled with one PIPE component. In this noding sensitivity study, the U-tube PIPE component is replaced by three parallel PIPE components. The three parallel PIPEs are merged to the steam generator inlet and outlet plenums similar to the physical layout of the steam generator as shown in Figure 112-18. [

] ^{a,c}

The results of this sensitivity study are presented in Figures 112-19 through 112-34. Similar to the first sensitivity study, average void fraction is used to demonstrate the water distribution in the steam generators and loop seals. Figures 112-19, 112-20 and 112-21 show the average void fraction at the uphill side of U-

tubes in the respective steam generator 1, steam generator 2, and steam generator 3. [

] ^{a,c}

Conclusive Remarks

The sensitivity studies on the steam generator nodalization indicate that in general the SBLOCA transient is not sensitive to the noding changes studied herein. [

] ^{a,c}

References:

1. WCAP-16996-P, "Realistic LOCA Evaluation Methodology Applied to the Full Spectrum of Break Sizes (FULL SPECTRUM™ LOCA Methodology)," November 2010.
2. LTR-NRC-13-70, "Summary of July 2013 NRC Code Workshop and August 2013 NRC Audit of the FULL SPECTRUM LOCA (FSLOCA) Evaluation Model (Proprietary/Non-Proprietary)," October 2013.
3. LTR-NRC-13-73, "Submittal of Westinghouse Responses to WCAP-16996-P, "Realistic LOCA Evaluation Methodology Applied to the Full Spectrum of Break Sizes (FULL SPECTRUM LOCA Methodology' Requests for Additional Information – RAIs 46 – 58, 75 and 77," (Proprietary)," November 2013.



a,c

Figure 112-1. Comparison of SG nodalization in the base run (left) and the revised one with doubled SG tube nodes (right). (Sensitivity Study 1)



a,c

Figure 112-2. Comparison of SG 1 U-tube uphill average void fraction. (Sensitivity Study 1)

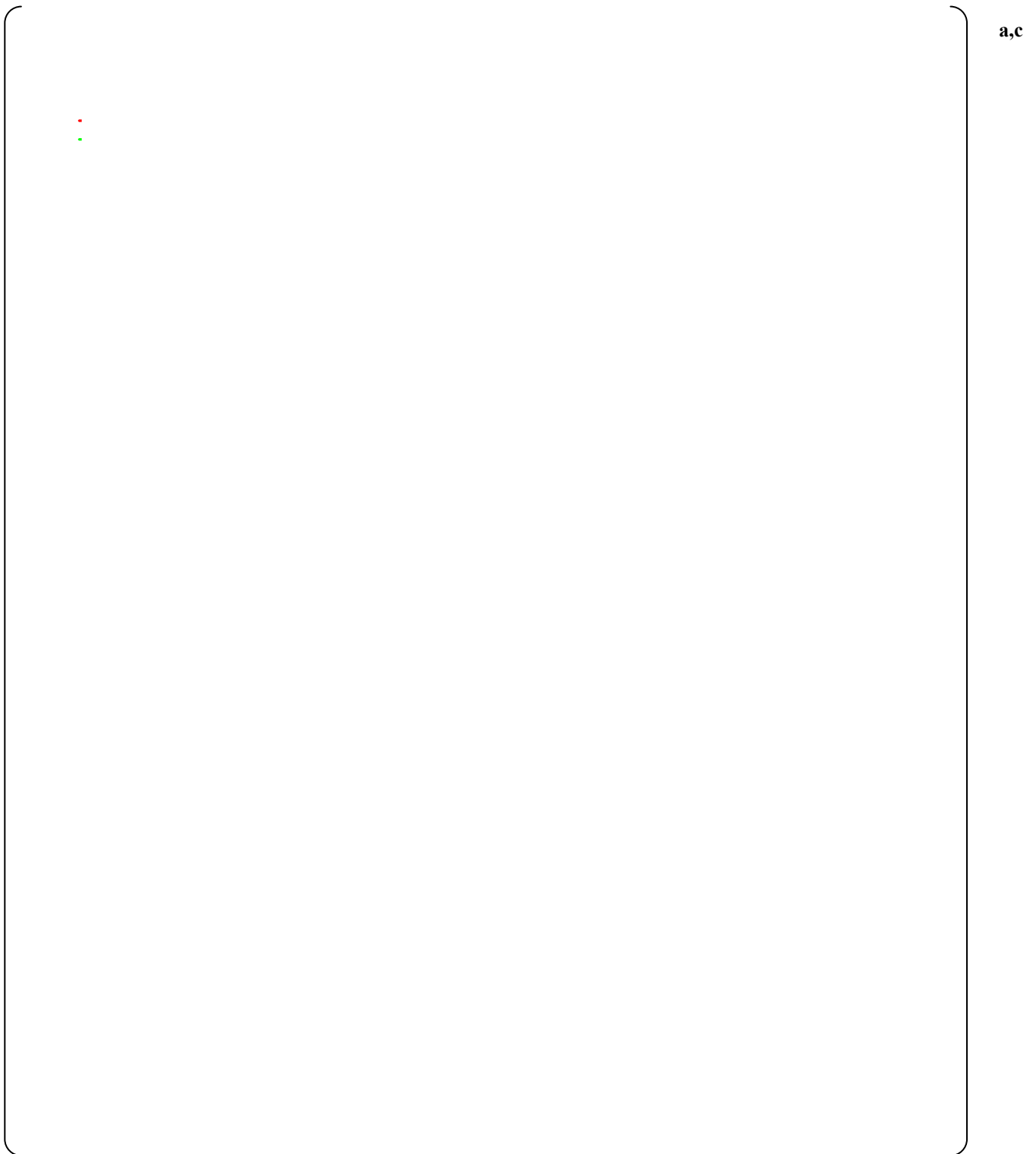


Figure 112-3. Comparison of SG 2 U-tube uphill average void fraction. (Sensitivity Study 1)



a,c

Figure 112-4. Comparison of SG 3 U-tube uphill average void fraction. (Sensitivity Study 1)



a,c

Figure 112-5. Comparison of SG 1 U-tube downhill average void fraction. (Sensitivity Study 1)



a,c

Figure 112-6. Comparison of SG 2 U-tube downhill average void fraction. (Sensitivity Study 1)



a,c

Figure 112-7. Comparison of SG 3 U-tube downhill average void fraction. (Sensitivity Study 1)

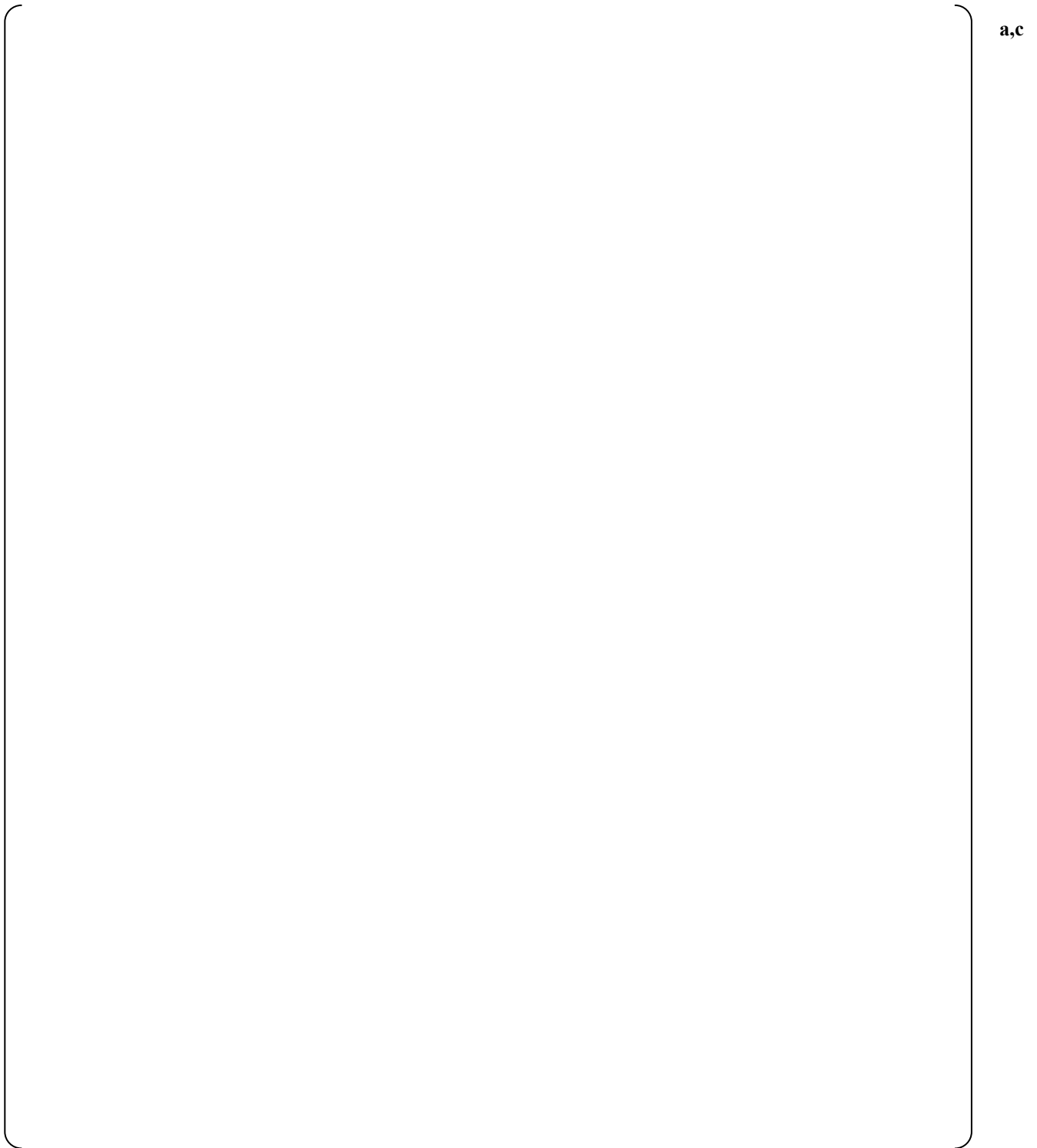


Figure 112-8. Comparison of loop seal 1 downhill average void fraction. (Sensitivity Study 1)

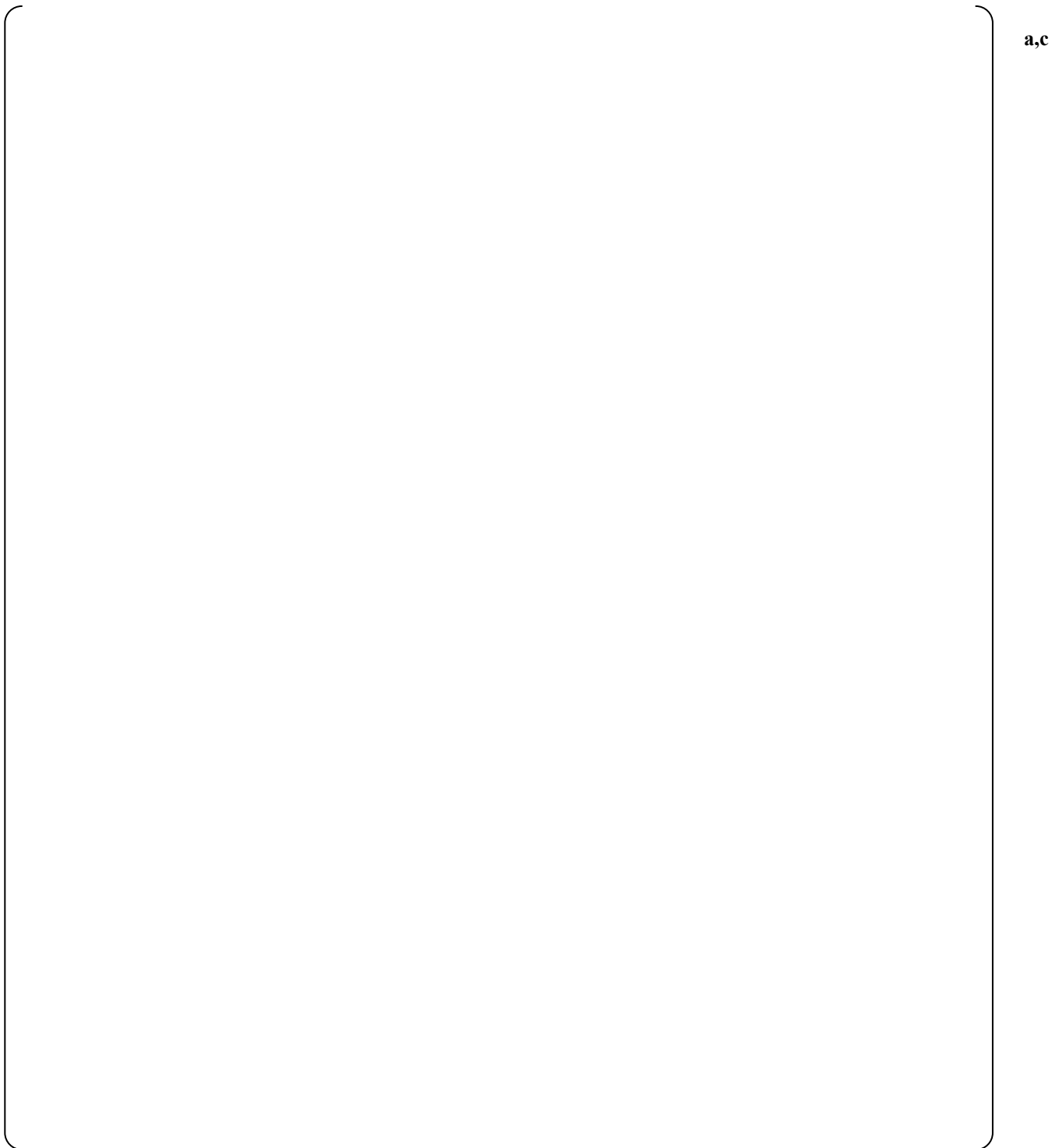


Figure 112-9. Comparison of loop seal 2 downhill average void fraction. (Sensitivity Study 1)



a,c

Figure 112-10. Comparison of loop seal 3 downhill average void fraction. (Sensitivity Study 1)



a,c

Figure 112-11. Comparison of loop seal 1 uphill average void fraction. (Sensitivity Study 1)

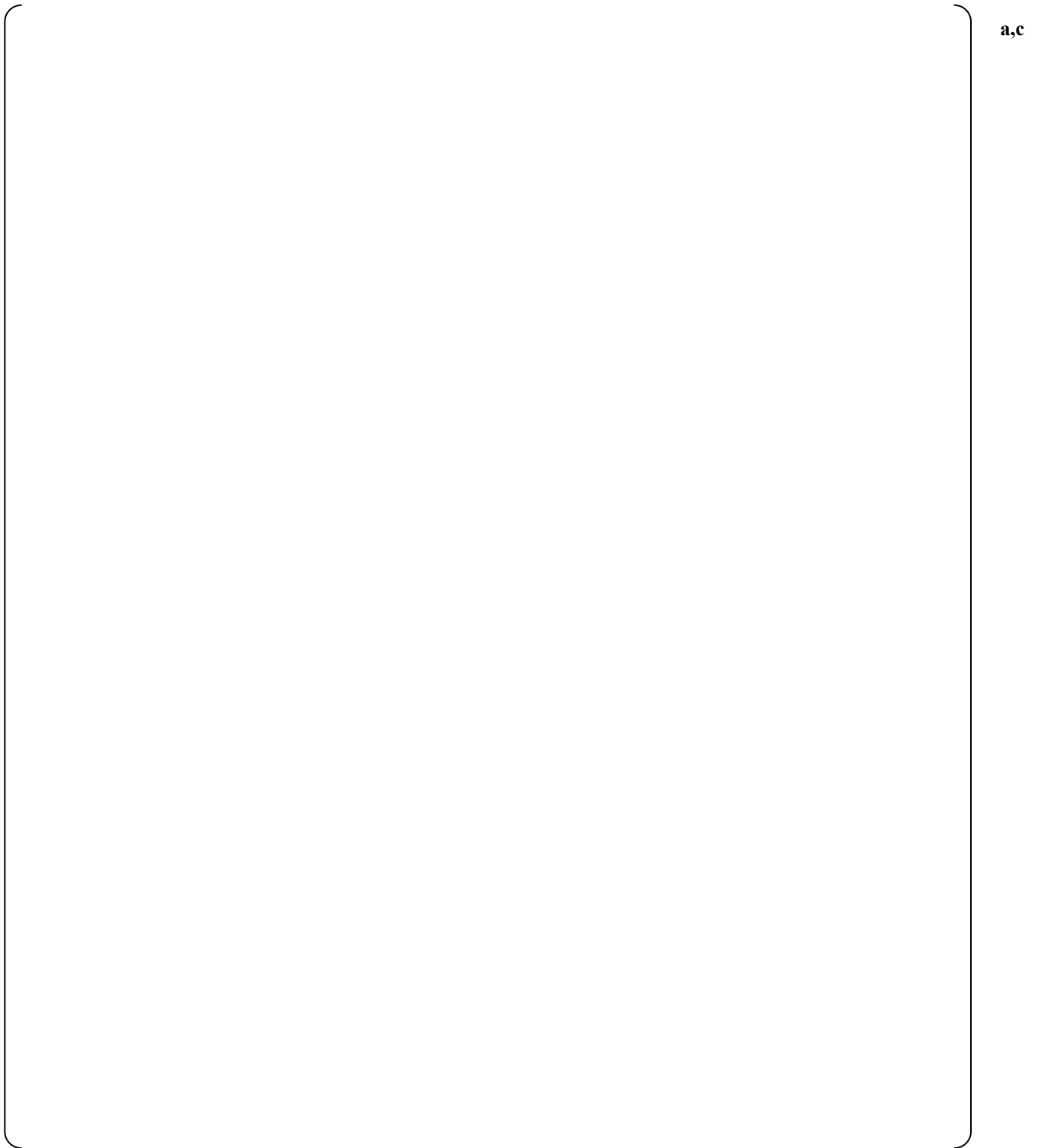


Figure 112-12. Comparison of loop seal 2 uphill average void fraction. (Sensitivity Study 1)

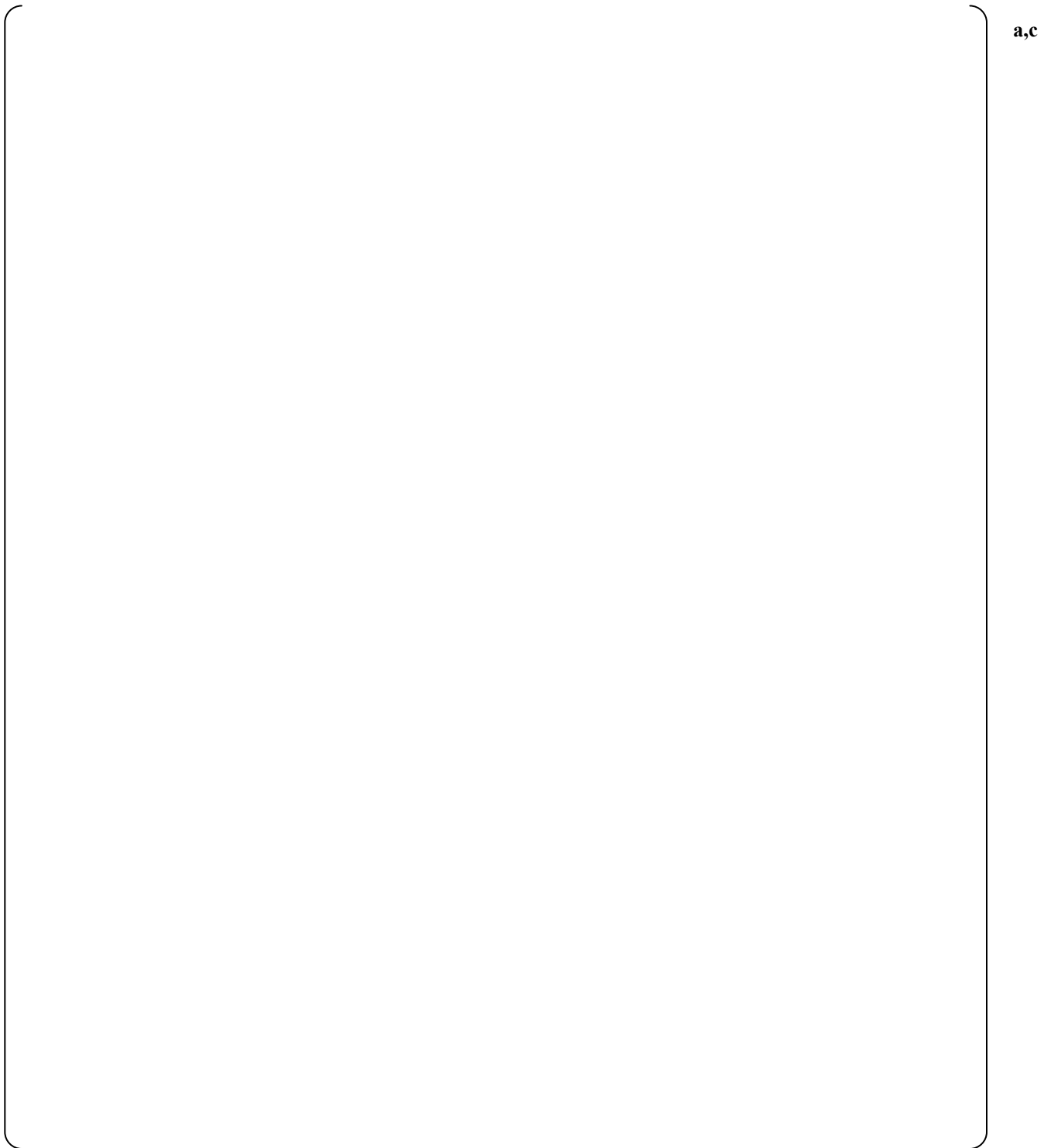


Figure 112-13. Comparison of loop seal 3 uphill average void fraction. (Sensitivity Study 1)



a,c

Figure 112-14. Comparison of core collapsed liquid level. (Sensitivity Study 1)



a,c

Figure 112-15. Comparison of core void fraction. (Sensitivity Study 1)



a,c

Figure 112-16. Comparison of downcomer collapsed liquid level. (Sensitivity Study 1)



a,c

Figure 112-17. Comparison of PCT. (Sensitivity Study 1)



a,c

Figure 112-18. Comparison of SG nodalization in the base input (left) and the revised one with three steam generator tube components (right). (Sensitivity Study 2)

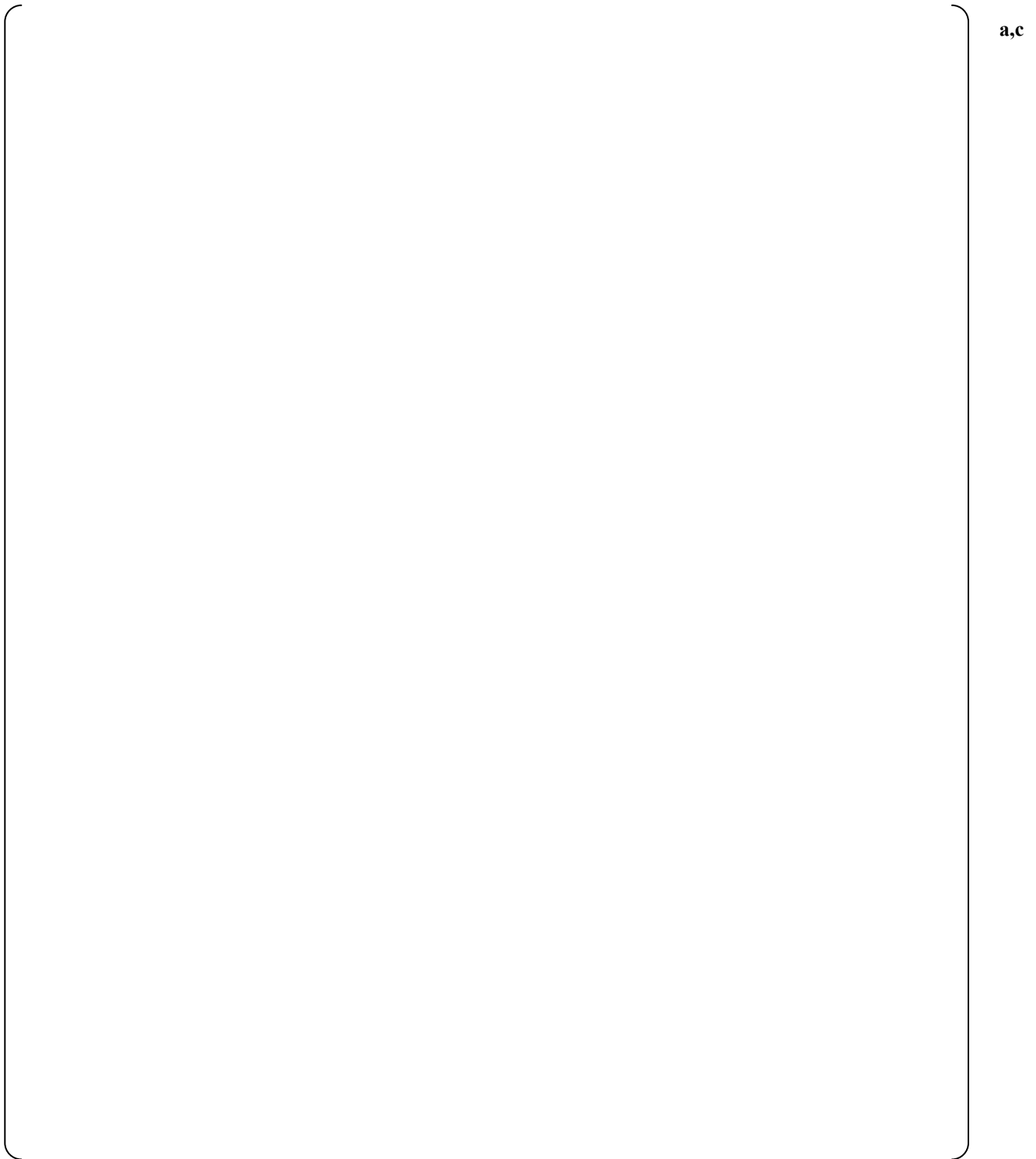


Figure 112-19. Comparison of SG 1 U-tube uphill average void fraction. (Sensitivity Study 2)

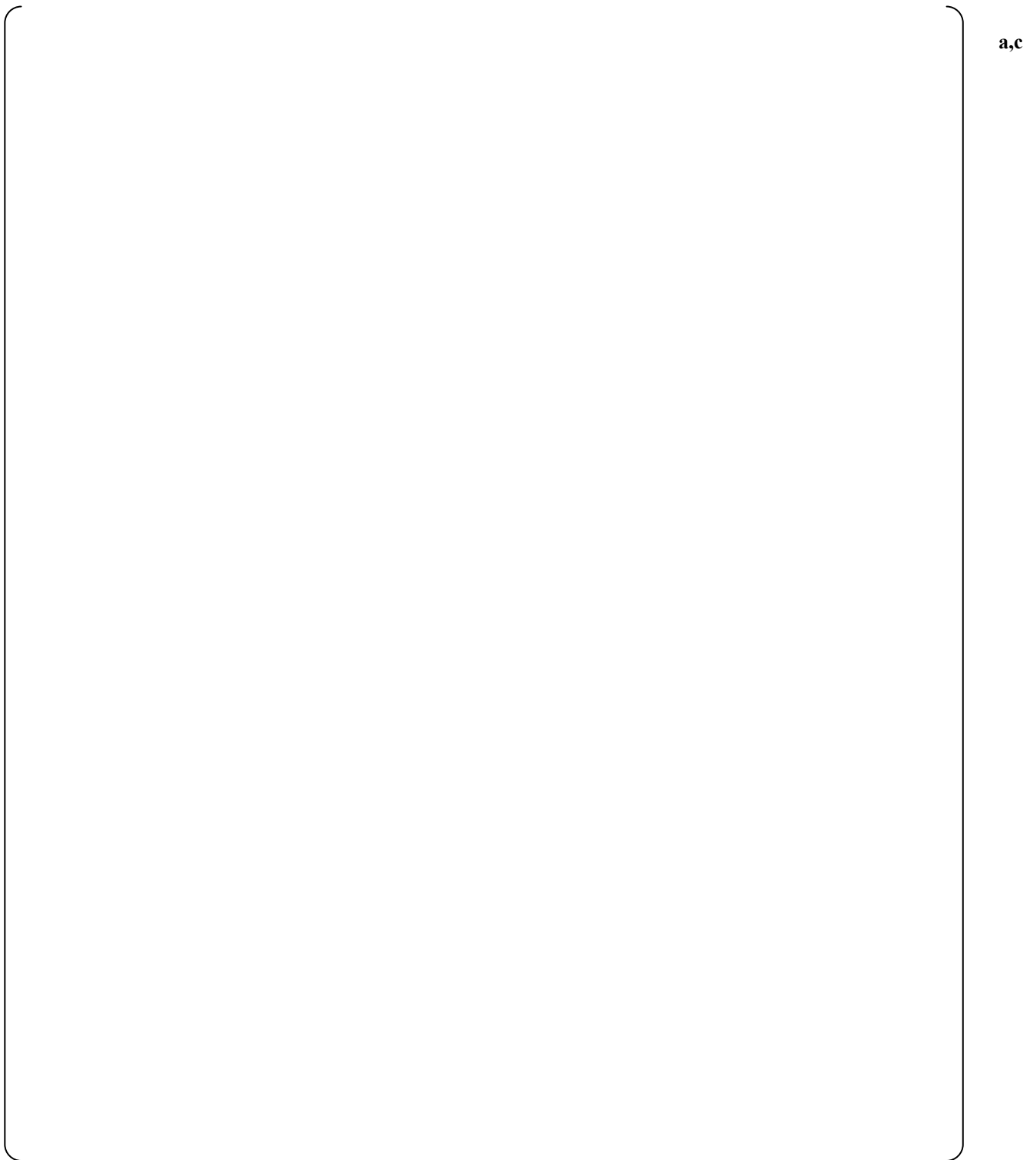


Figure 112-20. Comparison of SG 2 U-tube uphill average void fraction. (Sensitivity Study 2)



a,c

Figure 112-21. Comparison of SG 3 U-tube uphill average void fraction. (Sensitivity Study 2)



a,c

Figure 112-22. Comparison of SG 1 U-tube downhill average void fraction. (Sensitivity Study 2)



a,c

Figure 112-23. Comparison of SG 2 U-tube downhill average void fraction. (Sensitivity Study 2)



a,c

Figure 112-24. Comparison of SG 3 U-tube downhill average void fraction. (Sensitivity Study 2)



a,c

Figure 112-25. Comparison of loop seal 1 downhill average void fraction. (Sensitivity Study 2)



a,c

Figure 112-26. Comparison of loop seal 2 downhill average void fraction. (Sensitivity Study 2)



a,c

Figure 112-27. Comparison of loop seal 3 downhill average void fraction. (Sensitivity Study 2)

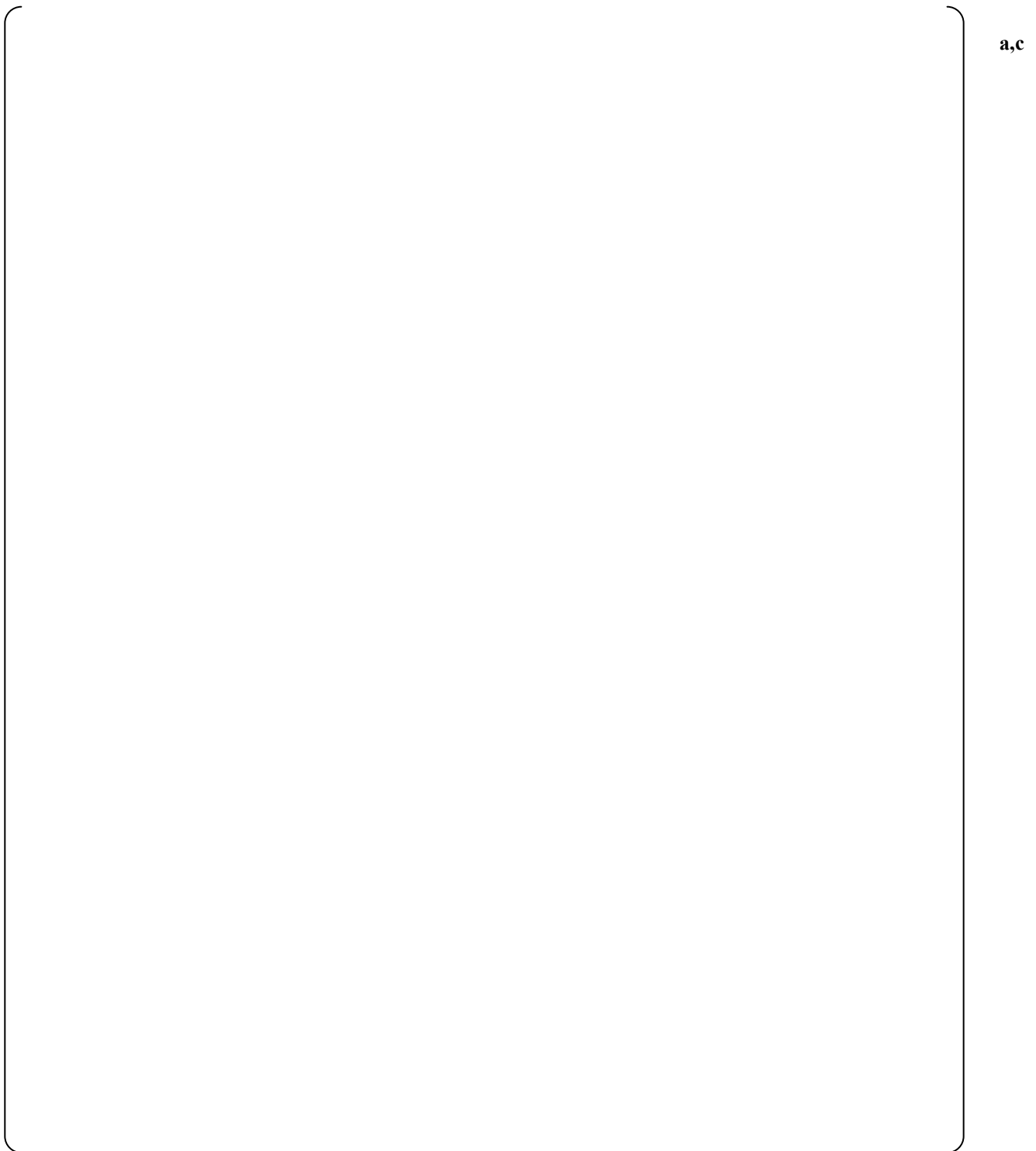


Figure 112-28. Comparison of loop seal 1 uphill average void fraction. (Sensitivity Study 2)

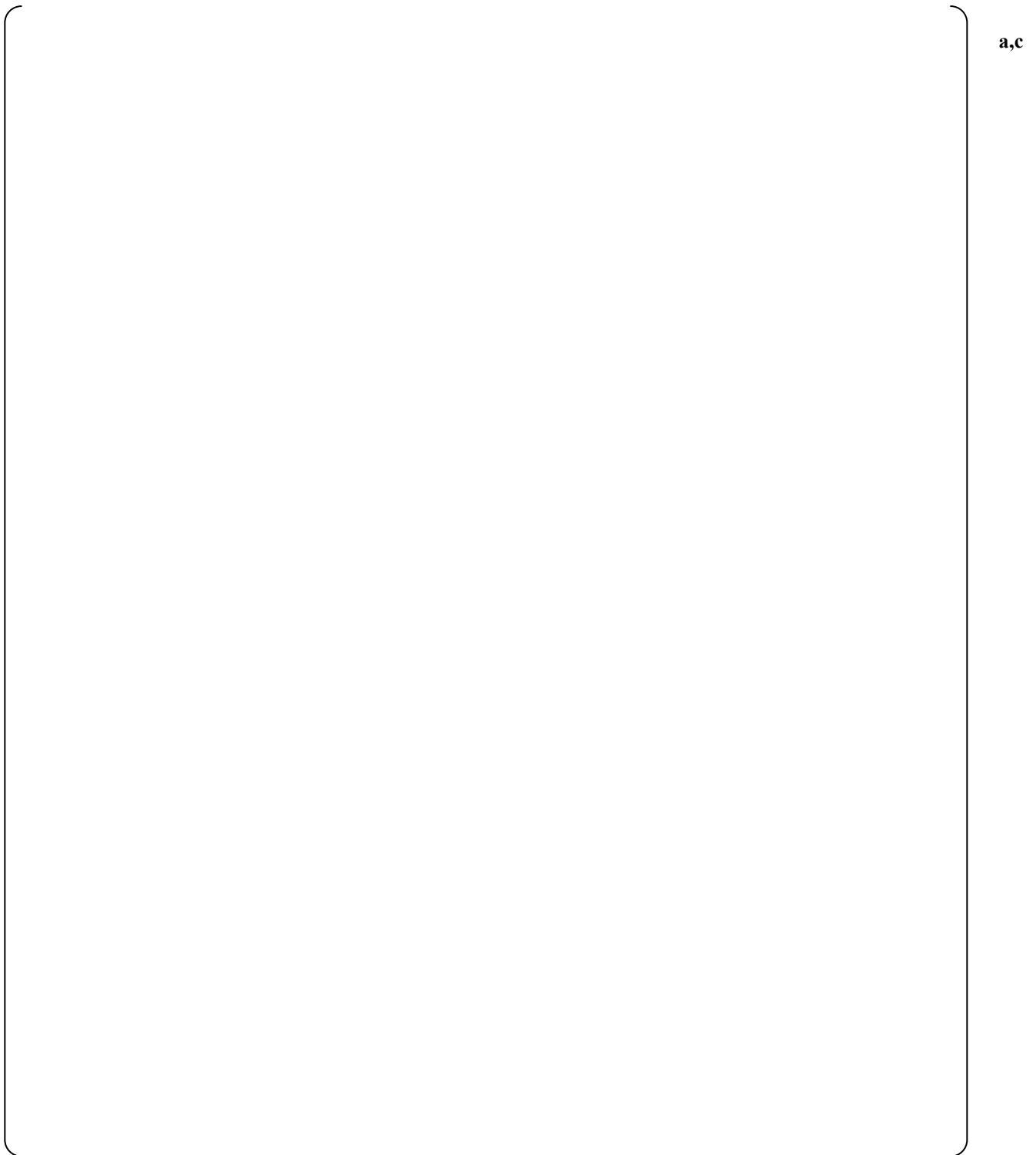


Figure 112-29. Comparison of loop seal 2 uphill average void fraction. (Sensitivity Study 2)

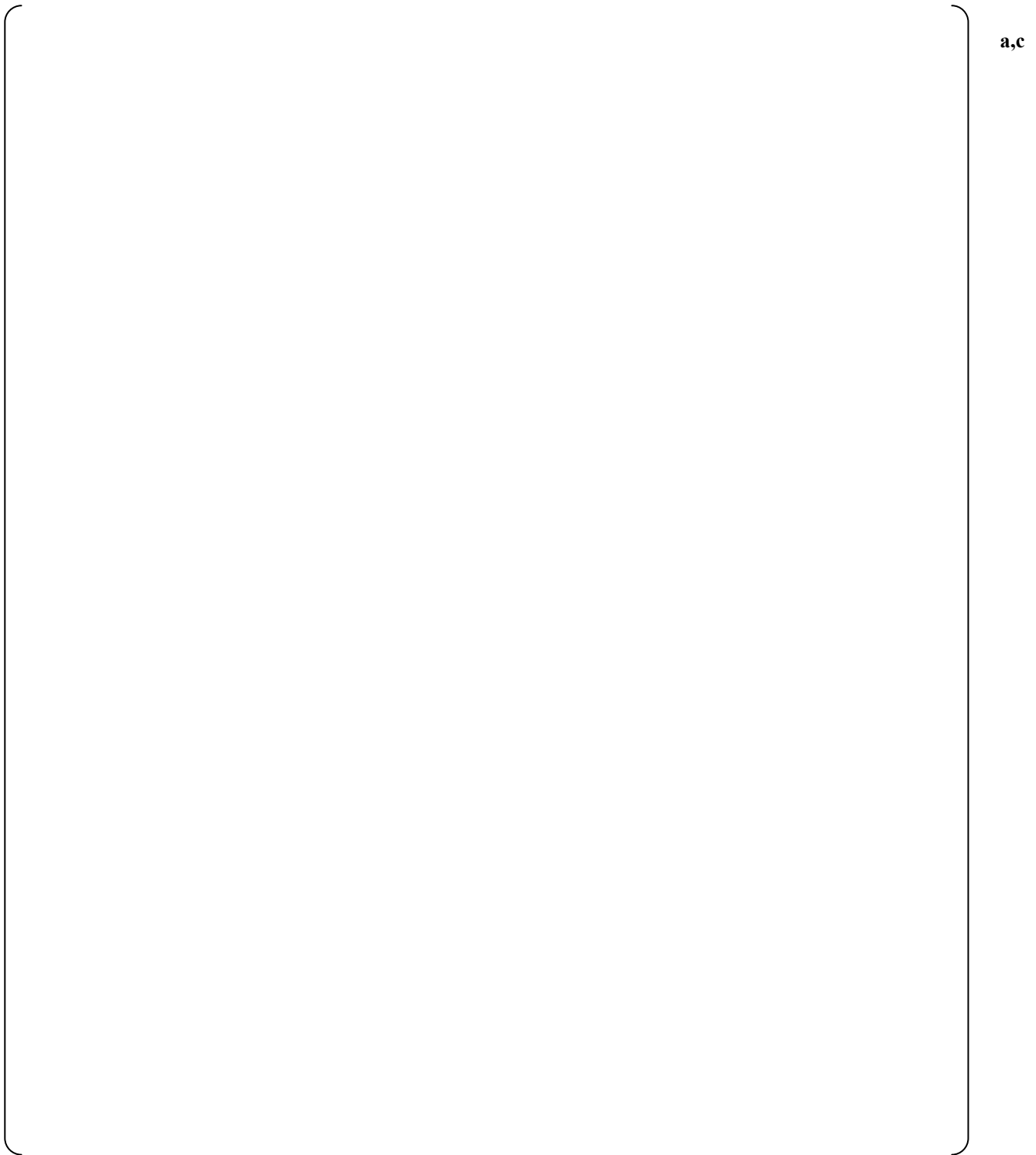


Figure 112-30. Comparison of loop seal 3 uphill average void fraction. (Sensitivity Study 2)



a,c

Figure 112-31. Comparison of core collapsed liquid level. (Sensitivity Study 2)



a,c

Figure 112-32. Comparison of core void fraction. (Sensitivity Study 2)



a,c

Figure 112-33. Comparison of downcomer collapsed liquid level. (Sensitivity Study 2)

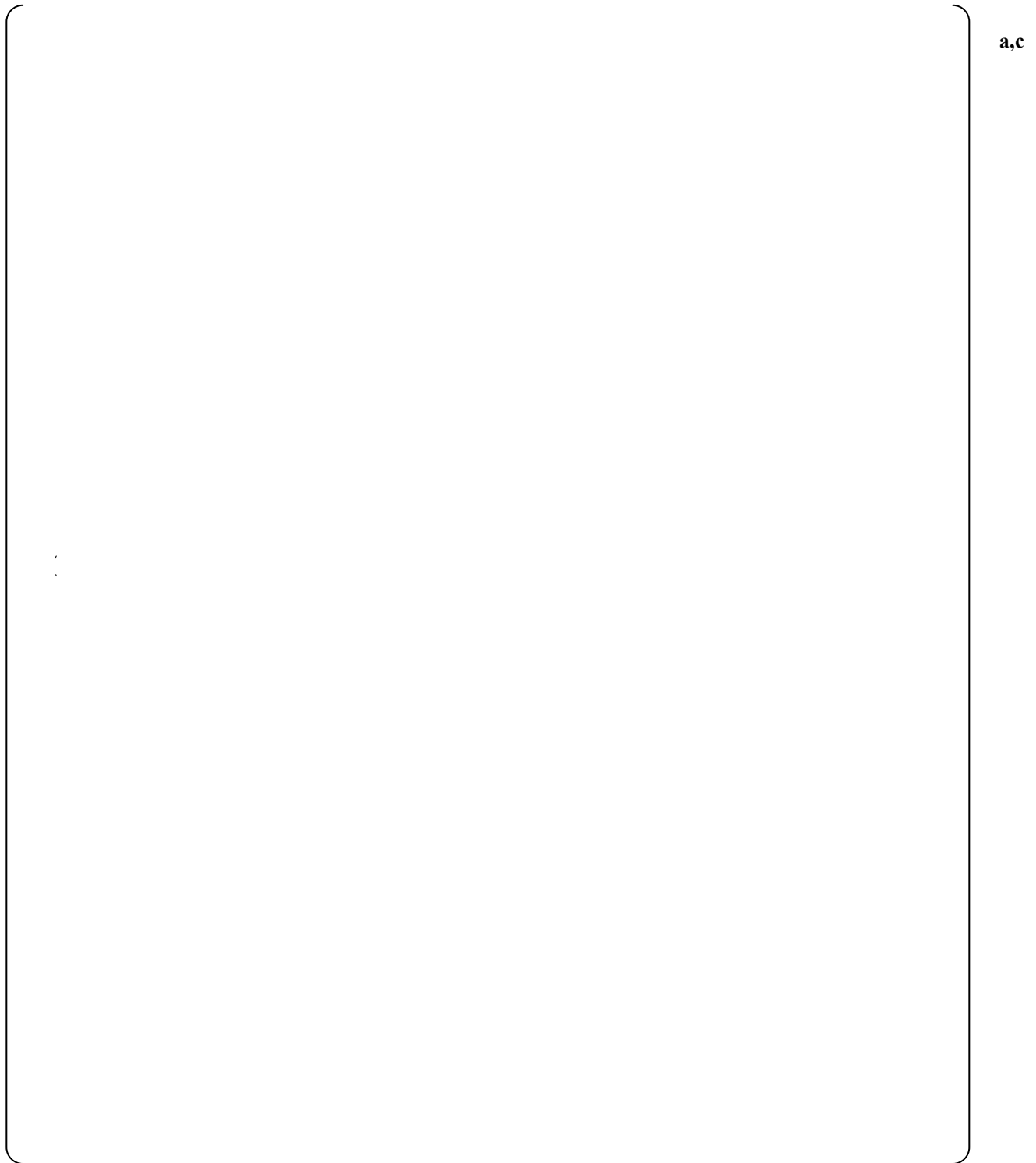


Figure 112-34. Comparison of PCT. (Sensitivity Study 2)

**WCAP-16996-P, “Realistic LOCA Evaluation Methodology Applied to the Full Spectrum of Break Sizes
(FULL SPECTRUM LOCA Methodology)”
Request for Additional Information – (Non-Proprietary)
RAIs 83-85, 88-92, 94-95 and 113-119**

April 2014

Westinghouse Electric Company LLC
1000 Westinghouse Drive
Cranberry Township, PA 16066

©2014 Westinghouse Electric Company LLC
All Rights Reserved

Question #83: Stratified Flow Multiplier HS_SLUG

WCOBRA/TRAC-TF2 superimposes horizontal stratified flow (including wavy-dispersed flow) onto the basic flow regime map. WCAP-16996-P/WCAP-16996-NP, Volumes I, II, and III, Revision 0, Section 4, "WCOBRA/TRAC-TF2 Flow Regime Maps and Interfacial Area," Subsection 4.4.5, "Horizontal Stratified Flow," analyzes test data by plotting modified Wallis numbers, as defined by Equation (4-108), versus void fraction in Figure 4-17, "Horizontal Stratified Flow Regime Transition and Relevant Data," and states that [

] ^{a,c} The critical relative phase velocity for horizontal flow, $\Delta u_c = |u_g - u_l|_c$, is given in Equation (4-112) using a criterion based on the Wallis parameter. Equation (4-117) introduces a weighting factor, W_{st} , which is determined from the critical velocity using two adjustable constants, C_{hs_slug} and C_{stfru} . W_{st} is used in Equation (4-116) to modify the interfacial flow area, A_i . According to Subsection 4.4.5, the allowable input range C_{hs_slug} is from 0.1 to 9.9 with unity being the default value for C_{hs_slug} in WCOBRA/TRAC-TF2.

Referring to the data presented in Figure 4-17, WCAP-16996-P/WCAP-16996-NP, Volumes I, II, and III, Revision 0, Section 29, "Assessment of Uncertainty Elements," Subsection 29.1.7, "Horizontal Stratified Flow Regime Transition Boundary (HS_SLUG)," states that [

] ^{a,c} Subsection 29.1.7 further explains that "the horizontal stratified flow regime transition boundary multiplier, HS_SLUG, is then introduced to adjust the critical relative velocity for horizontal stratified flow." It is also stated that "For the purpose of the uncertainty analysis a random value of HS_SLUG is sampled with [

] ^{a,c}

(1) Please clarify if the above cited sentence, appearing in the second paragraph of

WCAP-16996-P/WCAP-16996-NP, Volumes I, II, and III, Revision 0, Subsection 29.1.7, "Horizontal Stratified Flow Regime Transition Boundary (HS_SLUG)," on page 29-34 is in error and if it should be corrected as follows: "For the purpose of the uncertainty analysis a random value of HS_SLUG is sampled with [

] ^{a,c} Please explain and correct as appropriate.

(2) WCAP-16996-P/WCAP-16996-NP, Volumes I, II, and III, Revision 0, Section 10, "WCOBRA/TRAC-TF2 One-Dimensional Component Models," Subsection 10.2, "Pipe Component," explains: "The HS_SLUG multiplier affects the transition between non-stratified and stratified flow regimes and is described in detail in Section 4.4.5." Subsection 4.4.5, "Horizontal Stratified Flow," does not mention the HS_SLUG quantity nor does it provide a reference to HS_SLUG. It is in Subsection 29.1.7, "Horizontal Stratified Flow Regime Transition Boundary (HS_SLUG)," where it is explained: "The horizontal stratified flow regime transition boundary multiplier, HS_SLUG, is then introduced to adjust the critical relative velocity for horizontal

stratified flow. The multiplier is represented by the symbol C_{hs_slug} in Equation 4-117." This way of identifying and describing the HS_SLUG quantity in WCAP-16996-P/WCAP-16996-NP, Volumes I, II, and III, Revision 0, is found to be confusing and inappropriate as it lacks in accuracy, clarity, and adequacy of description. This represents one example when details, essential for the description of important quantities and features of the FSLOCA™ methodology, are found scattered among various sections in Volumes 1, 2, and 3 of WCAP-16996-P/WCAP-16996-NP, Volumes I, II, and III, Revision 0. Please describe the process of ensuring that important aspects of the FSLOCA methodology are described in a clear, systematic, and coherent manner in the voluminous content of WCAP-16996-P/WCAP-16996-NP, Volumes I, II, and III, Revision 0. In particular, please provide corrections, if such were deemed necessary, to improve the description provided with regard to HS_SLUG and C_{hs_slug} .

- (3) Subsection 4.4.5, "Horizontal Stratified Flow," explains that "the allowable input range of C_{hs_slug} is from 0.1 to 9.9. Subsection 10.2, "Pipe Component," states that "the default value of HS_SLUG is 1.0 and can be modified through the \$NAMELIST set of the model input within allowable range of $0.1 \leq HS_SLUG \leq 9.99$." As both subsections refer to the same quantity, please explain why the provided allowable input ranges differ somewhat. Provide the limiting values for HS_SLUG and C_{hs_slug} as coded in WCOBRA/TRAC-TF2.
- (4) Whereas HS_SLUG is sampled with []^{a,c} the \$NAMELIST set of the model input can be used to modify HS_SLUG within the allowable range of $0.1 \leq HS_SLUG \leq 9.99$. Please explain the large disparity between the sampling range and the range of allowable values for HS_SLUG in WCOBRA/TRAC-TF2 taking into consideration that this extremely broad range of allowable values for HS_SLUG lacks a technical basis. Please explain the rationale for defining the range of allowable values and its intended application. In particular, describe how the use of inappropriate HS_SLUG values within the allowable range is controlled and prevented in plant safety analyses.
- (5) WCAP-16996-P/WCAP-16996-NP, Volumes I, II, and III, Revision 0, Subsection 10.2, "Pipe Component," explains that "additional user defined multipliers have been added in WCOBRA/TRAC-TF2 that affect specific models and correlations" and describes HS_SLUG as one of them. With regard to HS_SLUG, Subsection 10.2 states that "besides the PIPE component, it also affects the horizontal flow calculation for all 1D hydraulic components, except the PUMP." Please clarify if HS_SLUG is imposed on a global basis for an entire input deck model, if it can be applied selectively to individual qualifying components in an input model, or if it can be activated for individual cells/interfaces within a specific qualifying component.

FULL SPECTRUM™ and FSLOCA™ are trademarks in the United States of Westinghouse Electric Company LLC, its subsidiaries and/or its affiliates. These marks may be used and/or registered in other countries throughout the world. All rights reserved.

Unauthorized use is strictly prohibited. Other names may be trademarks of their respective owners.

- (6) Please explain if WCOBRA/TRAC-TF2 allows excluding selected qualifying one-dimensional hydraulic components in an input deck model from the effect of variation of HS_SLUG on horizontal flow modeling. In such a case, please explain the basis for exclusion and clarify how horizontal flow is modeled in such selected one-dimensional hydraulic components.
- (7) Please relate the responses to Items (4) through (6) above to specific features of PWR plant models used for LOCA analyses. Identify specific components in such models that are affected by HS_SLUG. Present diagrams from a reference plant model to explain and illustrate the application of the HS_SLUG parameter in PWR LOCA analyses.

Response:

Part (1): The development of uncertainty range for the horizontal stratified flow follows Regulatory Guide 1.203 [1], Element 4 as a part of bottom up process to determine the bias and uncertainties of a closure relation. The uncertainty of transition from the horizontal stratified flow and non-stratified flow including the interpolation region was evaluated by comparing the prediction with the test data as shown in Fig. 4-17 of the topical report [2]. The range of uncertainty was determined to be []^{a,c} and then it is applied to the PWR LOCA evaluation. The uncertainty range is sampled and applied globally to the components in which the horizontal stratification is allowed. The process is presented in Sections 4.4.5 and 29.1.7 of the topical report, and is consistent with Regulatory Guide 1.203.

A clarification needs to be given on the allowable input range of []^{a,c} for C_{hs_slug} (HS_SLUG is the equivalent variable) in the WCOBRA/TRAC-TF2 computer code. As a part of Evaluation Model (EM) development following Regulatory Guide 1.203, the FSLOCA EM dictates that the range of C_{hs_slug} (HS_SLUG) in the LOCA evaluation is []^{a,c} based on the comparison with experimental data. Practically, the computer code usually accepts a sufficiently wider range of input than what EM requires to accommodate the possible input range adjustment during the EM development process.

Part (2): We agree with the observation. The variables of C_{hs_slug} and HS_SLUG can be used interchangeably in the topical report. It is clarified in Section 29.1.7. However, it was not clear in Section 10.2.

Part (3): We agree with the observation. In section 4.4.5, sentence []^{a,c}

Part (4): As discussed in part (1), the input range of []^{a,c} for C_{hs_slug} (HS_SLUG) is developed for the FSLOCA EM, while the WCOBRA/TRAC-TF2 computer code accepts the input range of []^{a,c} that is greater than the range required by the evaluation model. The default value of C_{hs_slug} (HS_SLUG) is 1.0 and it is applied to the majority of validations in the topical report. The value of C_{hs_slug} (HS_SLUG) could be adjusted using a FORTRAN namelist in the input. The input range developed for the FSLOCA EM is documented in the EM topical report. The LOCA analysts shall use the correct input parameter range. The quality assurance (QA) program implemented in Westinghouse is able to effectively prevent an inappropriate parameter from being used by the LOCA analyst in the LOCA safety evaluation.

Part (5): The range parameter C_{hs_slug} (HS_SLUG) is applied globally to 1-D components [

] ^{a,c}

Part (6): As explained in Part (5), the parameter C_{hs_slug} (HS_SLUG) and the horizontal stratification model are applied to every [

] ^{a,c}

Part (7): Figure 83-1 shows the nodalization of Beaver Valley Unit 1 PWR loop model. The solid line represents each 1-D component and the dash line separates each computational node of the component. The momentum equation is solved at the cell face (dash line), where the parameters of GRAV, C_{hs_slug} (HS_SLUG), etc., are applied.

Let's take the primary loop as the example to demonstrate the application of horizontal stratified flow to PWR. [

] ^{a,c}

[

] ^{a,c}**References:**

1. Regulatory Guide 1.203, “Transient and Accident Analysis Methods,” 2005.
2. WCAP-16996-P, “Realistic LOCA Evaluation Methodology Applied to the Full Spectrum of Break Sizes (FULL SPECTRUM™ LOCA Methodology),” November 2010.
3. LTR-NRC-14-12, “Submittal of Westinghouse Responses to “WCAP-16996-P, ‘Realistic LOCA Evaluation Methodology Applied to the Full Spectrum of Break Sizes (FULL SPECTRUM LOCA Methodology)’ Request for Additional Information – RAIs 77-82, 86-87, 93 and 112” (Proprietary/Non-Proprietary), Project 700, TAC No. ME5244.” March 2014.



a,c

Figure 83-1. Illustration of Nodalization of Beaver Valley Unit 1 PWR Loop Model. The solid line represents each component and the dashed line separates each computational node of the component. The momentum solution and GRAV, C_{hs_slug} (HS_SLUG),etc. are applied to the cell face (dashed line).

Question #84: Stratified Flow Multiplier HS_SLUG Application

WCAP-16996-P/WCAP-16996-NP, Volumes I, II, and III, Revision 0, Subsection 4.4.5, "Horizontal Stratified Flow," states that "the stratified flow regime is superimposed on the basic flow regime map." It also explains that if the flow is not fully stratified, i.e. the weighing factor W_{st} determined from Equation (4-116) is less than unity, "the code interpolates between the interfacial area determined for stratified flow, calculated as above, and the value otherwise determined with respect to the basic flow regime map." In the case of "fully horizontal stratified flow, the interfacial area can be calculated from the cell geometry." The expression for this interfacial area term, $A_{i, strat}$, is given by Equation (4-113).

WCAP-16996-P/WCAP-16996-NP, Volumes I, II, and III, Revision 0, Section 16, "Horizontal Stratified Flow and Wavy-Dispersed Flow," Subsection 16.5, "Assessment Results," explains that "the weighting factors $W_{st}=1$ indicates stratified flow, while $W_{st}=0$ indicates a non-stratified flow in the basic flow regime map. In the interpolation region, $0 < W_{st} < 1$."

- (1) W_{st} is used in Equation (4-116) to modify the interfacial flow area, A_i , when $0 \leq W_{st} \leq 1$. The equation appears as follows:

$$A_i = A_{i, st} = (1 - W_{st}) A_{i, map} + W_{st} A_{i, st}.$$

As provided, Equation (4-116) defines the quantity $A_{i, st}$, which appears simultaneously on both the left hand side and the right hand side of the equation. Please define the quantity $A_{i, st}$, appearing in Equation (4-116), and explain the meaning of this equation. In addition, please explain if the interfacial area for "fully horizontal stratified flow," $A_{i, strat}$, as defined by Equation (4-113), is used for interpolation purposes when $0 \leq W_{st} \leq 1$ and provide the corresponding expressions in such a case.

- (2) Besides the interpolation of the interfacial flow area, performed when $0 \leq W_{st} \leq 1$, please explain if the weighing factor W_{st} and the HS_SLUG multiplier are used for modification of other physical quantities used in WCOBRA/TRAC-TF2 for two-phase flow modeling in one-dimensional hydraulic components. In particular, please clarify if the calculation of interfacial friction and entrainment are affected due to variation of W_{st} and HS_SLUG. As applicable, please provide the corresponding relationships used for such modification purposes and describe the supporting technical basis.

Response:

Part (1): We agree with the observation. There are typographic errors in Eq. 4-113 and Eq. 4-116. These two equations will be corrected in the updated topical report [1] as follows:

$$A_i = A_{i,st} = S_i \cdot \Delta x = D_h \cdot \Delta x \sqrt{1 - \left(1 - \frac{2 h_l}{D_h}\right)^2}, \quad (4-113)$$

where $A_{i,st}$ replaced $A_{i, strat}$ to keep consistency with other equations in that section.

$$A_i = A_{i, map-st} = (1 - W_{st}) A_{i, map} + W_{st} A_{i, st}, \quad (4-116)$$

where $A_{i, map-st}$ is the interfacial area used for the interpolation region. A linear interpolation is used.

Part (2): The purpose of introducing the interpolation region between the horizontal stratified flow regime and the flow regimes in the basic flow regime map is to [

] ^{a,c}

There is no special physical meaning assigned to the interpolation region. A similar situation is the churn-turbulent regime in the basic flow regime map, in which a linear interpolation between bubbly slug flow and annular mist flow is used. Similarly, a simple linear interpolation between the horizontal stratified flow regime and the flow regimes in the basic flow regime map is implemented. The linear interpolation includes the flow area, Eq. 4-116 in topical report, interfacial drag coefficient, Eq. 5-250 in topical report, interfacial heat transfer factors, Eq. 6-211 in topical report, and wall drag factors, Eqs. 5-294 and 5-295 in topical report.

The interpolation region as a part of 1-D component flow regime map has been validated against the JAERI Two-Phase Test Facility (TPTF) tests in Section 16, the COSI tests in Section 17, the loop seal tests in Section 18, the UPTF and CCTF tests in Section 19, the ROSA IV tests in Section 21, and the LOFT tests in Section 22 of the topical report.

Reference:

1. WCAP-16996-P, "Realistic LOCA Evaluation Methodology Applied to the Full Spectrum of Break Sizes (FULL SPECTRUM™ LOCA Methodology)," November 2010.



a,c

Figure 84-1. Flow regime number of cell 17 of a horizontal PIPE flow with $C_{stfru}=1.01$.

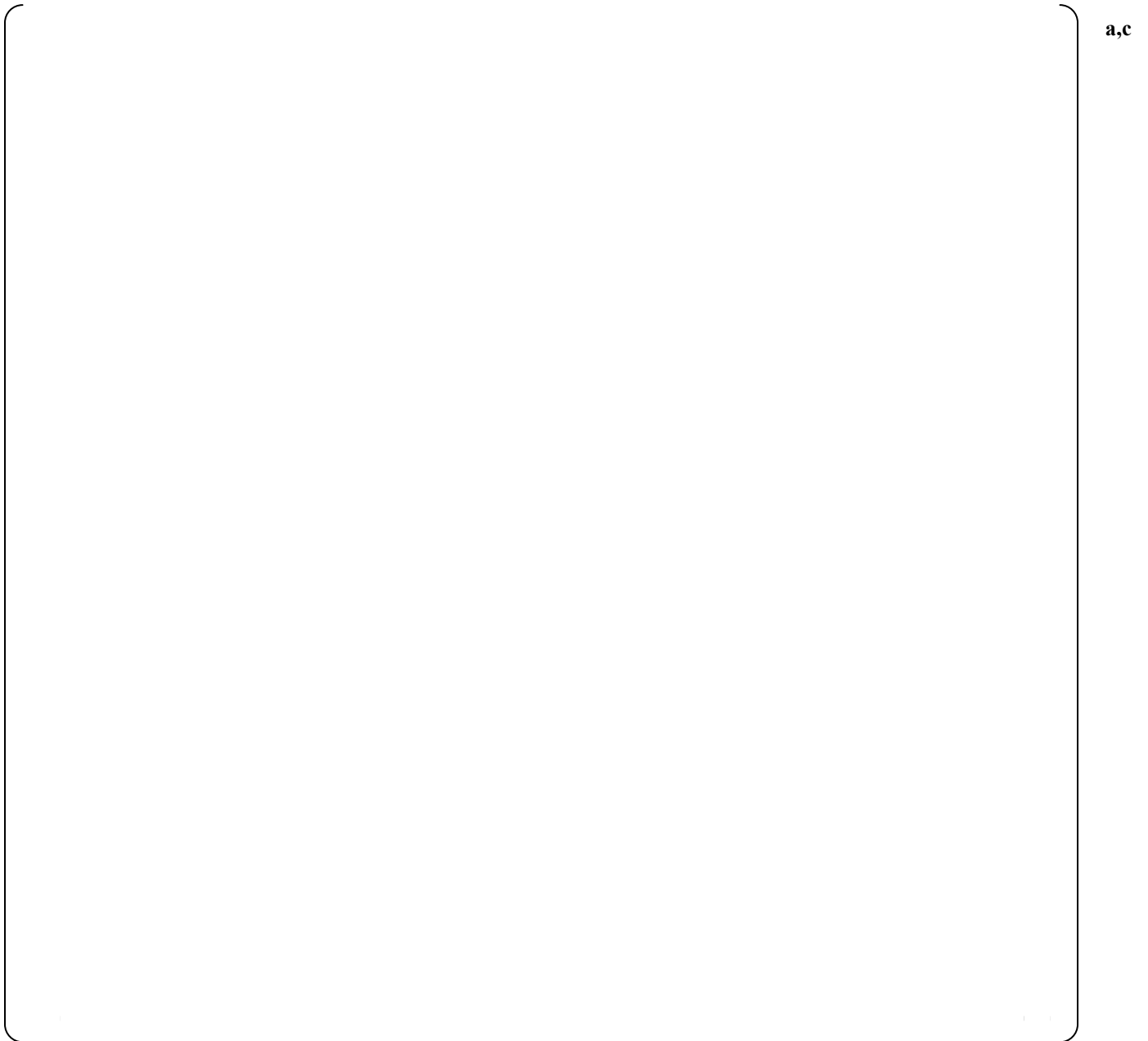


Figure 84-2. Flow regime number of cell 17 of a horizontal PIPE flow with $C_{stfru}=2.0$ (default).

Question #85: Stratified Flow and Inclination Limitation

WCAP-16996-P/WCAP-16996-NP, Volumes I, II, and III, Revision 0, Section 4, WCOBRA/TRAC-TF2 Flow Regime Maps and Interfacial Area," Subsection 4.4.5,

"Horizontal Stratified Flow," explains that the $[\cos\beta]^{a,c}$ limitation for the inclination angle of a channel, β , in the described approach to stratified flow modeling is based on the assumption that the cosine value of the limiting angle $[\cos\beta]^{a,c}$ is very close to unity. Thus, "the value can be approximated as 1.0 for simplicity, and $\cos\beta$ can be removed from the stratification transition criterion."

- (1) Please explain the WCOBRA/TRAC-TF2 approach to two-phase flow modeling in one-dimensional hydraulic components, including prediction of flow stratification, for channels of any inclination angle and present the applicable technical basis.
- (2) Figure 21.7-2, "WCOBRA/TRAC-TF2 Nodalization of LSTF Break Unit," shows that different values of the GRAV parameter apply to branches of different orientation that are used to model the break pipe. Please explain how the inclination angle is defined for each individual cell/interface in a one-dimensional hydraulic component. Provide the range of allowable input values and the parameter used to define the inclination angle.
- (3) If the horizontal flow calculation for a certain one-dimensional hydraulic component is affected by the HS_SLUG multiplier, please explain how input parameters, related to inclination, determine the application of the stratified flow model for the component. In addition, please clarify how the actual modeled flow piping inclination is accounted for.
- (4) Please relate the responses to Items (1) through (3) above to specific features of PWR plant models used for LOCA analyses. Identify specific components in such models that represent inclined sections of the primary coolant piping, such as the hot leg risers to the SG inlet chambers, and bend regions. In particular, please consider the representation of the bends in the PWR loop seals as well as the bends in the SG U-tube bundle. Show diagrams from a reference plant model to explain and illustrate the modeling of such inclined and bend regions in PWR plant models developed for WCOBRA/TRAC-TF2. Please present the technical basis in support of the modeling approach and any special modeling features implemented in WCOBRA/TRAC-TF2 to simulate these regions.

Response:

Part (1): The WCOBRA/TRAC-TF2 code and the FSLOCA EM are developed for the application of LOCA evaluation of Westinghouse PWRs. The inclination angle limit of $[\cos\beta]^{a,c}$

$[\cos\beta]^{a,c}$

[]^{a,c}

Due to the developed loop input model of the FSLOCA demonstration analyses, the significance of the inclination angle for the results of the LOCA analysis is limited. The loop input model of the FSLOCA demonstration PWR was shown in Figure 83-1. A consistent input model has been developed for the ROSA IV integral effects test as shown in Figure 21.3-8 of the topical report.

[

] ^{a,c}

Part (2): In the FSLOCA EM, the inclination angle of the components in the break model is consistent with the actual break unit configuration. Example is given using the ROSA break flow model. The break unit of the ROSA facility is shown in Figure 21.7-1 of the topical report, while the WCOBRA/TRAC-TF2 input model is shown in Figure 21.7-2. The actual inclination angles of the break unit were preserved in the input model. [

] ^{a,c} In the PWR model, the break orientation is consistent with the model for ROSA in Figure 21.7-2. This is discussed in Section 28.2.7 of the topical report.

Part (3): The C_{hs_slug} (HS_SLUG) uncertainty range was developed from the horizontal pipe flow data with negligible inclination angle in Section 4.4.5 of the topical report. The applicability of the C_{hs_slug} (HS_SLUG) range to a pipe flow with non-zero inclination angle may not be assumed. However, as addressed in part (1), the FSLOCA EM is developed for the particular PWR LOCA evaluation. The nodalization was given in Figure 83-1. [

] ^{a,c}

[

] ^{a,c}

Part (4): Response to this part is covered by the responses to parts (1) through (3).

Reference:

1. WCAP-16996-P, "Realistic LOCA Evaluation Methodology Applied to the Full Spectrum of Break Sizes (FULL SPECTRUM™ LOCA Methodology)," November 2010.

Question #88: LSTF Loop Seal Nodalization

WCAP-16996-P/WCAP-16996-NP, Volumes I, II, and III, Revision 0, Section 21, “ROSA-IV Test Simulations,” Subsection 21.3, “Description of WCOBRA/TRAC-TF2 Model for ROSA/LSTF-IV,” shows the one-dimensional loop noding diagram of the LSTF model in Figure 21.3-8, “WCOBRA/TRAC-TF2 Loop Noding Diagram of LSTF.” Components No. 13 and 23 are used to represent the loop seal piping in both primary loops. Figure 21.3-9, “Hot Leg (Including Pressurizer), Steam Generator and Cross-Over Leg Noding,” shows the one-dimensional nodalization of the loop seal region in the pressurizer loop modeled by Component No. 13 with []^{a,c} cells.

WCAP-16996-P/WCAP-16996-NP, Volumes I, II, and III, Revision 0, Subsection 5.2.4, “Primary Coolant Loop,” in “ROSA-IV Large Scale Test Facility (LSTF) System Description,” Japan Atomic Energy Research Institute Report JAERI-M 89-237, January 1985 explains that LSTF had two identical loops each representing two loops of the reference four-loop PWR. Pipes with 207 mm ID and 295 mm OD were used for the hot and cold legs and the cross-over leg pipes had 168.2 mm ID and 240.2 mm OD. The pipes were made of stainless steel SDS316L-TP. Important geometric dimensions of the loop seal piping are provided in Figure 5.2.34, “Primary Loop Dimensions (Elevation View),” in Figure 5.2.38, “Geometry of Primary Loop A,” and in Figure 6.11(c), “Locations of Selected Primary Loop A and B Instruments,” in the JAERI-M 89-237 report.

- (1) Please provide a table that documents geometric input data for each cell in Component No. 13 shown in Figure 21.3-9, “Hot Leg (Including Pressurizer), Steam Generator and Cross-Over Leg Noding,” and used to model the loop seal piping. Provide length, elevation, flow area, volume, and inclination angle for each cell/interface and explain how the cross-over leg input model accounts for relevant LSTF elevation data of critical importance. Include loss coefficients, if such were input as part of the loop seal model. Describe any disparities, if present, between Component No. 13 and Component No. 23 that model the cross-over legs in both loops.
- (2) Table 5.2.9, “Characteristics of Primary Loop Piping,” in JAERI-M 89-237 provides the length of the cross-over leg as 9.5498 m (31.331 ft) and the cross-over leg volume, excluding the RCP volume, as 0.2122 m³ (7.494 ft³). The provided length and volume data correspond to the cross-over leg flow area of 0.0222 m² (0.2392 ft²), which matches the 168.2 mm pipe ID. The total length of the cells of Component No. 13 in Figure 21.3-9, “Hot Leg (Including Pressurizer), Steam Generator and Cross-Over Leg Noding,” amounts to 30.8608 ft. Table 26.1-4 in WCAP-16996-P/WCAP-16996-NP, Volumes I, II, and III, Revision 0, Section 26, “WCOBRA/TRAC-TF2 Model of Pilot Plants,” Subsection 26.1.2, “Modeling Consistency,” lists the cross-over leg axial length, based on the LSTF noding model, as 30.86 ft. Please compare the cross-over leg integral cell length and volume based on the input data provided in response to Item (1) above against the geometric data for the LSTF cross-over leg provided in Table 5.2.9, “Characteristics of Primary Loop Piping,” in JAERI-M 89-237. Please explain any differences, if present.
- (3) Section 6.4.3, “Primary Loops Instruments,” in JAERI 89-237 explains that Venturi flow meters were installed at each cross-over leg to measure the flow rate of primary coolant. Figure 6.11(c), “Locations of Selected Primary Loop A and B Instruments,” in JAERI-M 89-237 shows the location of the flow meters in the uphill section of each loop seal. According to Table 5.7.4 in JAERI-M 89-

237, the flow meters had a contraction ratio of 0.505 corresponding to a Venturi throat diameter of 85 mm (3.34 in). As explained in Section 5.7, "Valves and Orifices," in JAERI-M 89-237, the flow meters installed in the facility acted as flow resistance for fluid in piping. Please clarify how the flow meter presence was accounted for in the LSTF loop seal models.

- (4) LSTF was equipped with flow control valves, installed upstream of the RCPs, to allow for considerable variation in the primary loop coolant flow during an experimental transient. As seen from Figure 6.11(c), "Locations of Selected Primary Loop A and B Instruments," in JAERI-M 89-237, the primary coolant flow control valves were installed in the horizontal sections of the loop seal cross-over legs in both loops. According to Figure 6.11(c), the length of the horizontal cross-over leg portion associated with the primary coolant flow control valves amounted to 2 mm + 762 mm + 2 mm = 766 mm (2.513 ft). Please clarify if the primary coolant flow control valves introduced additional flow resistance and if the presence of these valves was accounted for in the LSTF WCOBRA/TRAC-TF2 loop seal models.

Response:

A detailed nodding diagram of the loop seal region for the ROSA Large Scale Test Facility (LSTF) is presented in Figure 88-1. Only a single diagram is provided for the LSTF since there are no loop-to-loop differences within the model.

As noted in the Request for Additional Information (RAI), the total crossover leg length from the WCOBRA/TRAC-TF2 model is 30.861 ft compared to 31.331 ft cited in Table 5.2.9 of JAERI-M 84-237 [88-1]. The WCOBRA/TRAC-TF2 model was developed from the facility drawings provided in Sections 5 and 6 of JAERI-M 84-237. The observed difference could be the result of a small discrepancy in the calculation of the table entry, or in the definition of the crossover leg / pump interface. The drawings are considered to be an appropriate source of the facility geometry for the development of the WCOBRA/TRAC-TF2 model. Furthermore, the observed difference is small (about a 1.5% difference). It was confirmed that the elevation changes modeled are consistent with Figure 6.11(c) from JAERI-M 84-237.

The total loss through the loop for the base steady-state case was [

]^{a,c} A study is executed to illustrate the sensitivity of the key results from SB-CL-18 to additional losses in the loop seal region.

The base case is the nodding sensitivity study discussed in the response to RAI 89. This case was selected because the additional cell faces in the horizontal region are required for specification of the loss associated with the control valve. The sensitivity study applies loss coefficients to approximate the drag disks, control valve, and Venturi hydraulic losses, as well as the steam generator nozzle and loop seal bends.

The pressurizer pressures, loop seal differential pressures, inner vessel delta pressures, and peak cladding temperatures are compared in Figures 88-2 through 88-6. [

] ^{a,c}

Reference(s)

- 88-1) JAERI-M 84-237, "ROSA-IV Large Scale Test Facility (LSTF) System Description," January 1985.

a,c

Figure 88-1: Detailed Loop Seal Region Noding for ROSA LSTF

a,c

Figure 88-2a: Pressurizer Pressure without Additional Loop Seal Region Losses

a,c

Figure 88-2b: Pressurizer Pressure with Additional Loop Seal Region Losses

a,c

Figure 88-3a: Cross-Over Leg A Differential Pressures without Additional Loop Seal Region Losses

a,c

Figure 88-3b: Cross-Over Leg A Differential Pressures with Additional Loop Seal Region Losses



Figure 88-4a: Cross-Over Leg B Differential Pressures without Additional Loop Seal Region Losses



Figure 88-4b: Cross-Over Leg B Differential Pressures with Additional Loop Seal Region Losses

a,c

Figure 88-5a: Inner Vessel Differential Pressure without Additional Loop Seal Region Losses

a,c

Figure 88-5b: Inner Vessel Differential Pressure with Additional Loop Seal Region Losses



Figure 88-6a: Peak Cladding Temperature without Additional Loop Seal Region Losses



Figure 88-6b: Peak Cladding Temperature with Additional Loop Seal Region Losses

Question #89: Modeling of LSTF Loop Seal Horizontal Section and Bend Regions

[]^{a,c} in Component No. 13 in Figure 21.3-9, “Hot Leg (Including Pressurizer), Steam Generator and Cross-Over Leg Noding,” [

[]^{a,c} the length of the horizontal section of the cross-over leg, determined as 1.3817 m (2,383.7 mm – 2 x 501 mm = 1,381.7 mm = 1.3817 m), based on dimensions provided in Figure 5.2.34, “Primary Loop Dimensions (Elevation View),” and in Figure 5.2.38, “Geometry of Primary Loop A,” in JAERI-M 89-237. The primary coolant flow control valves, as shown in Figure 6.11(c), “Locations of Selected Primary Loop A and B Instruments,” in JAERI-M 89-237, occupy 2.513 ft of the 4.533-ft long horizontal sections of the LSTF loop seal cross-over legs.

- (1) It is determined that the length-to-diameter ratio (L/D) for horizontal section of the LSTF loop seal cross-over leg amounts to:

$$L / D = 1,381.7 \text{ mm} / 168.2 \text{ mm} = 8.21.$$

Please explain the rationale for representing the entire horizontal portion of the loop seal piping

[]^{a,c} in the WCOBRA/TRAC-TF2 model of LSTF.

- (2) As shown in Figure 21.3-9, “Hot Leg (Including Pressurizer), Steam Generator and Cross-Over Leg Noding,” each of the 90° bends connecting the cross-over leg horizontal section to the downhill and uphill sides of the loop seal are modeled by []^{a,c} Please explain how the noding of bend regions in the cross-over legs was determined and describe any special considerations taken with regard to the modeling of these regions. In particular, clarify the modeling approach with regard to capturing effects of inclination on the flow behavior. As inclination angles are associated with a specific noding scheme that is applied to a bend region, please explain how the noding relates to the two-phase flow being treated as horizontal, vertical or inclined as the flow transitions from horizontal to vertical (or vice versa) when it passes through the 90° bend.

Response:

The noding of the crossover leg bends and loop seal region was based on the following: [

[]^{a,c}

Sensitivity studies which were executed with the UPTF loop seal SET determined that one of the key parameters for [

[]^{a,c}

[

] ^{a,c} Justification for this modeling approach is provided in the response to RAI 115. This approach ensures consistency between the SET and Integral Effects Test (IET) facilities relative to where flow stratification is allowed to occur in the loop seal region.

For the LSTF, the previously described nodding approach resulted in a [

] ^{a,c} as shown in Table 89-1.

The pressurizer pressures are compared in Figure 89-1. It is observed that the [

] ^{a,c}

In summary, it is concluded that the nodding of the loop seal region of the ROSA facility is appropriate and consistent with the UPTF loop seal separate effects test. It is also concluded that the [

] ^{a,c}

Table 89-1: Facility L/D Comparison for Horizontal Section of Loop Seal Region

Facility	Length (ft)	Diameter (ft)	Approximate L/D (-)
I			
			I ^{a,c}

a,c

Figure 89-1a: Pressurizer Pressure (Figure 21.4-1 from WCAP-16996-P)

a,c

Figure 89-1b: Pressurizer Pressure with Additional Cells in Loop Seal Region

a,c

Figure 89-2a: Cross-Over Leg A Differential Pressures (Figure 21.4-3 from WCAP-16996-P)

a,c

Figure 89-2b: Cross-Over Leg A Differential Pressures with Additional Cells in Loop Seal Region

a,c

Figure 89-3a: Cross-Over Leg B Differential Pressures (Figure 21.4-4 from WCAP-16996-P)

a,c

Figure 89-3b: Cross-Over Leg B Differential Pressures with Additional Cells in Loop Seal Region

a,c

Figure 89-4a: Inner Vessel Differential Pressure (Figure 21.4-5 from WCAP-16996-P)

a,c

Figure 89-4b: Inner Vessel Differential Pressure with Additional Cells in Loop Seal Region

a,c

Figure 89-5a: Peak Cladding Temperature (Figure 21.4-6 from WCAP-16996-P)

a,c

Figure 89-5b: Peak Cladding Temperature with Additional Cells in Loop Seal Region

Question #90: WCOBRA/TRAC-TF2 Features Applied in LSTF Loop Seal Modeling

Figure 21.3-9, “Hot Leg (Including Pressurizer), Steam Generator and Cross-Over Leg Noding,” in WCAP-16996-P/WCAP-16996-NP, Volumes I, II and III, Revision 0, Section 21, “ROSA-IV Test Simulations,” Subsection 21.3, “Description of WCOBRA/TRAC-TF2 Model for ROSA/LSTF-IV,” shows one-dimensional nodalization of the loop seal region in the LSTF pressurizer loop. The overall one-dimensional loop noding diagram of the LSTF model is presented in Figure 21.3-8, “WCOBRA/TRAC-TF2 Loop Noding Diagram of LSTF.” Components Nos. 13 and 23 are used to represent the loop seal piping in both primary loops. WCOBRA/TRAC-TF2 assessment results using this model are presented in WCAP-16996-P/WCAP-16996-NP, Volumes I, II and III, Revision 0, Section 21, “ROSA-IV Test Simulations.”

- (1) Please explain which instrumentation devices, installed in the ROSA-IV LSTF loop seal cross-over leg, have been considered for the assessment of WCOBRA/TRAC-TF2 using ROSA-IV LSTF test data. If certain available and relevant measurements were not used in qualifying the code capabilities to predict loop seal clearing, please explain the reasons for this.
- (2) In addition to implementing an adequate noding model, meaningful assessment of code prediction results against experimental data requires that node or junction points, at which computational variables are computed by the code, relate properly to the location of experimental measuring points of interest. Please explain how this was taken into account in establishing the WCOBRA/TRAC-TF2 loop seal cross-over leg model for LSTF. In particular, please explain how the elevations were accounted for of the differential pressure tap locations, including the one in the horizontal section of the loop seal cross-over leg.
- (3) For the LSTF loop seal model, please describe any specific modeling features that were applied on Component Nos. 13 and 23, a component-wide basis to or to specific cells/interfaces of these components in representing the LSTF loop seal regions. Identify individual cells/interfaces where sampling of input quantities, for example HS_SLUG, was applied and identify all sampled parameters. In addition, please identify any non-sampled user defined parameters or multipliers, e.g. C_{strfu} and STRTX, related to the modeling of participating physical processes such as flow stratification, counter-current flow limitation (CCFL), or other relevant processes, that were applied in modeling the LSTF loop seals to assess WCOBRA/TRAC-TF2. Please provide a table that lists all such applied sampled and non-sampled user defined modeling parameters or multipliers applied in the LSTF loop seal modeling. Please include a brief description, the applied range, and the input values for each parameter listed in the table.

Response:

(1) From the ROSA LSTF design information found in JAERI-M 84-237 [90-1], it appears that there are numerous measurement devices installed in the loop seal crossover legs. According to Fig.6.1 (a) and (b) and 6.2 (a) and (b) there are video probes, gamma densitometers, drag disks, conductivity probes, temperature (wall and fluid) measurements, Venturi flow meters and differential pressure measurements. Among all of these, [

] ^{a,c} While the rest of the measurements could be used for validation purposes, they were either indicators of a secondary importance, had questionable reading, or were not qualified or used in the tests. Measurements that did not have sufficient design information to determine their exact location were generally not used, for example [^{a,c} in the downhill (steam generator) side of the crossover legs.

(2) The specific node sizes of the loop seal region (steam generator outlet plenum and crossover leg up to the pump inlet) were driven primarily by key mechanical design features and elevations of the ROSA LSTF. In addition, to the extent possible, consistency with the UPTF SET and PWR noding was desired especially at the bottom of the crossover legs. It was therefore impossible to achieve a perfect alignment of the centers of the hydraulic nodes with the exact locations of some measurement taps. Thus, there are some deviations between the hydraulic cell centers and the differential pressure taps.

For example, for the DPE070-LSA and DPE210-LSB differential pressure tags for SB-CL-18, the elevation of their higher tap (located at the exit of the steam generator U-tubes) was determined to be at elevation 7560.9 mm, Figure A.24 of JAERI-M 89-027 [90-2]. According to the ROSA noding diagram in Figure 21.3-9 of WCAP-16996-P [90-3], the elevation of the center of the respective hydraulic cell (cell 25 of component PIPE 12) is [

] ^{a,c} it is close enough for the code validation purpose given the fact that the gravity effect estimated above mostly disappears as the hydraulic cell is voided.

From Fig.6.11(c) in JAERI-M 84-237, it is seen that nozzle N-2c, used for the crossover leg differential pressure measurements DPE080-LSA and DPE070-LSA is located in the horizontal section of crossover leg A between the flow control valve and the pump-side elbow, but the exact location in terms of distance in mm from the valve outlet or orientation is not clear. The same is true for nozzle N-2h at the horizontal part of the crossover leg B; nozzle N-2h is used to measure DPE210 and DPE220. However, given that a [^{a,c} (Figure 21.3-9,

WCAP-16996-P), [

] ^{a,c} Early in the transient, before the loop seal clears, the gravity head is a predominant factor, hence correctly modeling the bottom elevation of the crossover leg is essential, and the elevation was indeed modeled consistent with the design. After the loop seal clears, the fluid retention in the pump-side defined by the detail in the 90-deg elbow and the vertical uphill part of the crossover leg is the defining phenomenon.

There is additional uncertainty with the lack of information for the exact elevation of the higher (pump-side) taps of DPE080-LSA and DPE220-LSB measurements. In Figure A.21 of JAERI-M 89-027, the tap elevation visually appears to be somewhere in the middle of the 702 mm spool pieces of both crossover legs. With this assumption, the elevation of the tap appears to be $702/2=351$ mm (1.15-ft) below the cold leg centerline (el. 5502.8 mm); this tap elevation falls within the span of the [

] ^{a,c}

(3) There is only one specific flag which is applied to the crossover leg component. [

] ^{a,c} is applied at the specific cell faces labeled 'STRTX = 1' in Figure 88-1 (response to RAI 88). This flag [

] ^{a,c} This flag is described in the response to RAI 86, and the basis for application of this flag is described in the response to RAI 115. Any other multipliers which would apply to the loop seal region (such as the multiplier to the [^{a,c} are retained at their nominal values so the as-coded models are applied in the simulation.

Reference(s)

- 90-1) JAERI-M 84-237, "ROSA-IV Large Scale Test Facility (LSTF) System Description," January 1985.
- 90-2) JAERI-M 89-027, "ROSA-IV/LSTF 5% Cold Leg Break LOCA Experiment Run SB-CL-18 Data Report," March 1989.
- 90-3) WCAP-16996-P, "Realistic LOCA Evaluation Methodology Applied to the Full Spectrum of Break Sizes (FULL SPECTRUM LOCA Methodology)," November 2010.

Question #91: V. C. Summer and Beaver Valley Unit 1 Loop Seal Models

Figure 6.2-8, “Virgil C. Summer Loop Model Noding Diagram,” and Figure 26.3-14, “Beaver Valley Unit 1 Loop Model Noding Diagram,” in WCAP-16996-P/WCAP-16996-NP, Volumes I, II, and III, Revision 0, Section 26, “WCOBRA/TRAC-TF2 Model of Pilot Plants,” show noding diagrams for the primary loops of the plant models across a horizontal plane. In both plant input models, Component Nos. 13, 23, and 33, represent the PWR cross-over legs in the primary coolant loops.

- (1) Please provide detailed noding diagrams across a vertical plane for the cross-over leg regions in both plant models similar to the one shown for the LSTF loop seal in Figure 21.3-9, “Hot Leg (Including Pressurizer), Steam Generator and Cross-Over Leg Noding.” In these diagrams, please show important elevations including the elevation of the axis of the horizontal bottom section of the loop seal. Provide the elevations data using the TAF elevation as the zero elevation point.
- (2) Please provide a table that documents geometric input data for each cell in Component Nos. 13, 23, and 33, used to model the loop seal piping for both plants. Provide length, elevation, flow area, volume, and inclination angle for each cell/interface and explain how the cross-over leg input models account for relevant elevations of critical importance. Include loss coefficients, if such were input as part of the loop seal models. Describe any disparities, if present, between Component No. 13, 23, and 33 for each plant.
- (3) For the loop seal models of the reference V. C. Summer and Beaver Valley Unit 1 PWR plants, please describe any specific modeling features that were applied to Component Nos. 13, 23, and 33 on a component-wide basis or to specific cells/interfaces of the loop seal components. Identify individual cells/interfaces where sampling of input quantities, e.g. HS_SLUG, was applied and identify all sampled parameters. In addition, please identify any non-sampled user defined parameters or multipliers, e.g. C_{strfu} and STRTX, related to the modeling of participating physical processes such as flow stratification, CCFL, or other relevant processes, that were applied to model the plant loop seals in the plant models. Please provide a table that lists all such applied sampled and non-sampled user defined modeling parameters or multipliers including brief descriptions, applied ranges, and input values for each listed parameter.

Response:

Detailed noding diagrams of the loop seal region for V. C. Summer and Beaver Valley Unit 1 are presented in Figures 91-1 and 91-2, respectively. Only a single diagram is provided for each PWR since there are no loop-to-loop differences within the individual models.

The noding of these components was developed based on the following concepts: [

]^{a,c}

[]^{a,c}

There are a few additional flags/models which are applied to the crossover leg component. The first is []^{a,c} which is applied at the specific cell faces labeled ‘STRTX = 1’ in Figures 91-1 and 91-2. This flag causes the code to []^{a,c} This flag is described in the response to RAI 86, and the basis for the application of this flag is discussed in the response to RAI 115. The multiplier to the []^{a,c} is also applied to all cell faces in the crossover leg where the code checks for stratification, since it is applied to the entire loop as discussed in the response to RAI 77 (transmitted in LTR-NRC-13-73, Reference 91-1). No other “special” flags or models are applied to the crossover leg. The values and ranges of all potential uncertainty contributors, including []^{a,c}, are discussed in the response to RAI 77 transmitted in LTR-NRC-13-73.

Reference(s)

- 91-1) LTR-NRC-13-73, “Submittal of Westinghouse Responses to ‘WCAP-16996-P, ‘Realistic LOCA Evaluation Methodology Applied to the Full Spectrum of Break Sizes (FULL SPECTRUM LOCA Methodology)’ Request for Additional Information – RAIs 46 – 58, 75 and 77’ (Proprietary/Non-Proprietary), Project 700, TAC No. ME5244,” October 28, 2013.



a,c

Figure 91-1: Detailed Loop Seal Region Noding for V. C. Summer



Figure 91-2: Detailed Loop Seal Region Noding for Beaver Valley Unit 1

Question #92: PWR Loop Seal Horizontal Section and Bends Modeling

WCAP-16996-P/WCAP-16996-NP, Volumes I, II, and III, Revision 0, Section 4, “WCOBRA/TRAC-TF2 Flow Regime Maps and Interfacial Area,” Subsection 4.4.5, “Horizontal Stratified Flow,” explains that the code allows horizontal flow when the pipe inclination angle is less than []^{a,c} In addition, WCAP-16996-P/WCAP-16996-NP, Volumes I, II, and III, Revision 0, Section 29, “Assessment of Uncertainty Elements,” Subsection 29.5.6, “Pump Suction Piping/Loop Seal,” clarifies that []

[]^{a,c}

Figure 21.3-9, “Hot Leg (Including Pressurizer), Steam Generator and Cross-Over Leg Noding,” shows the 1D nodalization of the loop seal region in the pressurizer loop, which is modeled by Component No. 13 using []^{a,c} Figure 6.2-8, “Virgil C. Summer Loop Model Noding Diagram,” and Figure 26.3-14, “Beaver Valley Unit 1 Loop Model Noding Diagram,” show the noding diagrams for the primary loops across a horizontal plane. In both plant input models, Component Nos. 13, 23, and 33 represent the cross-over legs in the primary coolant loops.

- (1) Please explain the noding of the horizontal section of the loop seal cross-over legs for both plant models. Provide the length-to-diameter ratio (L/D) for this horizontal section of the cross-over legs. Explain the rationale for the applied L/D ratio in the WCOBRA/TRAC-TF2 PWR models. Discuss any associated modeling guidelines along with analysis results that substantiate them, if available.
- (2) Please explain the noding of the bends in the loop seals for both plant models. Show the geometry of these regions along with relevant pipe geometrical dimensions such as ID and bend radii, and provide detailed noding diagrams.
- (3) In a piping bend region, inclination for individual cells/interfaces depends on and varies with the degree of refinement in the implemented nodalization scheme. Please explain the approach to nodalization of the bends in a PWR loop seal cross-over leg and clarify how the response to Item (2) above relates to this approach. Discuss any associated modeling guidelines along with analysis results used to develop them, if available. Identify any WCOBRA/TRAC-TF2 modeling features that can be used to account for effects due to channel curvature and inclination in bend regions on the flow behavior and describe them, if available.
- (4) Please explain if specific sensitivity analyses related to PWR loop seal cross-over leg modeling and realistic prediction of loop seal clearing have been performed to assess WCOBRA/TRAC-TF2 in this regard. If available, please summarize the results from such sensitivity analyses that are based on data from any integral effect test facilities, such the LSTF tests described in WCAP-16996-P/WCAP-16996-NP, Volumes I, II and III, Revision 0, Section 21, “ROSA-IV Test Simulations,” or performed using PWR plant models, e.g. the reference PWR plant models described in WCAP-16996-P/WCAP-16996-NP, Volumes I, II, and III, Revision 0, Section 26, “WCOBRA/TRAC-TF2 Model of Pilot Plants,” that demonstrate the WCOBRA/TRAC-TF2 capabilities to predict adequately PWR loop seal clearance and refill as related to modeling both SBLOCAs and LBLOCAs.

Response:

(1) Sensitivity studies which were executed with the UPTF loop seal SET determined that [

] ^{a,c}

In order to achieve the desired nodding consistency based on the UPTF SET simulation results and to preserve the PWR nodding, it was determined that the [

] ^{a,c} (shown in Table 89-1 in the response to RAI 89).

(2) The philosophy for the nodding of the loop seal bends is the same as explained in the part (1) response for the horizontal region. The resulting nodding guidance is to [

] ^{a,c}

A detailed nodding diagram of the crossover leg, including the loop seal region, was provided for each PWR in the response to RAI 91. The interior diameter of the crossover leg piping is 2.58 ft for both V. C. Summer and Beaver Valley Unit 1. The radius of curvature for the bends in the loop seal region is 4.27 ft for both V. C. Summer and Beaver Valley Unit 1.

(3) The loop seal nodding is [

] ^{a,c}

(4) No PWR loop seal nodding sensitivity studies were executed; however, a number of sensitivity studies were conducted with SET and IET facilities to compare the effect of nodding on the code predictions of the associated experimental data. Sensitivity studies with the UPTF loop seal SET model are discussed in the response to RAIs 117 and 119. Sensitivity studies with the ROSA LSTF IET facility are discussed in the response to RAIs 88 and 89. These sensitivity studies illustrate [

] ^{a,c} This modeling approach was used consistently across the SET, IET, and PWR models.

Question #94: Interpolation for Stratified Flow and C_{hs_slug} Parameter

Equation (4-117) defines the weighting factor, W_{st} , as a function of the relative phase velocity, $|u_g - u_l|$, the critical relative phase velocity, Δu_c , and two adjustable constants, C_{hs_slug} and C_{stfru} . Table 1 below shows the values for the ratio of the relative velocity to the critical relative velocity, $|u_g - u_l|/\Delta u_c$, at which the W_{st} weighting factor, as calculated from Equation (4-117), becomes equal to unity or zero for three different values of the C_{hs_slug} constant: []^{a,c}

In computing the results provided in Table 1, the constant C_{stfru} , appearing in Equation (4-117), was set equal to its default value of []^{a,c}

Table 1: Velocity Ratio Values when W_{st} Equals 0 or 1 for C_{hs_slug} Values of []^{a,c} and at the Nominal Value of $C_{stfru} = []$ ^{a,c}

Constant	Relative Velocity Ratio, $ u_g - u_l /\Delta u_c$ (-)	
	Stratified Flow,	Non-stratified
[] ^{a,c}		

Figure 1 plots W_{st} as a function of the relative velocity ratio, $|u_g - u_l|/\Delta u_c$, according to Equation (4-117) when the constant C_{hs_slug} is set equal to []^{a,c} as well as to its limiting values of 0.1 and 9.9. For the curves shown in Figure 1, the second adjustable constant C_{stfru} was set equal to its default value of []^{a,c}



Figure 1: Effect of Constant C_{hs_slug} (HS_SLUG) in Equation 4-117 on the Weighing Factor W_{st} at $C_{stfu} = []^{a,c}$

As seen from the results provided in Table 1 and the curves presented in Figure 1 above, the interpolation range $0 \leq W_{st} \leq 1$ for the weighting factor, W_{st} , as defined by Equation (4-117), corresponds to a relative velocity ratio, $|u_g - u_l|/\Delta u_c$, ranging from $[]^{a,c}$ when HS_SLUG varies between $[]^{a,c}$ with C_{stfu} being set at its default value of $[]^{a,c}$

Please explain the significant disparity between the proposed HS_SLUG sampling range from $[]^{a,c}$ and the relative velocity ratio range from $[]^{a,c}$ that corresponds to W_{st} values being $0 \leq W_{st} \leq 1$ when C_{stfu} is set equal to its proposed default value of $[]^{a,c}$. When $0 \leq W_{st} \leq 1$, an interpolation technique to account for the effect of stratification is applied WCOBRA/TRAC-TF2. Please relate the response to this request for additional information to the test data points that are plotted in Figure 4-17, "Horizontal Stratified Flow Regime Transition and Relevant Data." Also, please consider the statement provided in WCAP-16996-P/WCAP-16996-NP, Volumes I, II, and III, Revision 0, Section 4, "WCOBRA/TRAC-TF2 Flow Regime Maps and Interfacial Area," Subsection 4.4.5, "Horizontal Stratified Flow," that $[]^{a,c}$

$[]^{a,c}$

Response:

As explained in the response to RAI 83, the FSLOCA Evaluation Model (EM) dictates that the range of C_{hs_slug} (HS_SLUG) in the LOCA evaluation is []^{a,c} based on the comparison with the experimental data, and the size of the interpolation region is established using the C_{stfru} of []^{a,c}. Thus, the discussion herein will be limited to the C_{hs_slug} (HS_SLUG) range of []^{a,c}

Taking Figure 4-19 in the topical report [1] as an example, it is further clarified that the horizontal stratified flow regime is limited to $W_{st}=1.0$ and the transition boundary varies as a function of C_{hs_slug} (HS_SLUG). The transition boundary is compared with the test data in Figure 4-17 of the topical report. []^{a,c}

[]^{a,c}

Reference:

1. WCAP-16996-P, "Realistic LOCA Evaluation Methodology Applied to the Full Spectrum of Break Sizes (FULL SPECTRUM™ LOCA Methodology)," November 2010.

Question #95: Interpolation for Stratified Flow and C_{stfr} Parameter

Equation (4-117) defines a weighting factor, W_{st} , using two adjustable constants, C_{hs_slug} and C_{stfr} .

Discussing the weighting factor, W_{st} , and the corresponding interpolation range when $0 \leq W_{st} \leq 1$ in accordance with Equation (4-117), Subsection 4.4.5, "Horizontal Stratified Flow," explains that "the size of the interpolation region can be adjusted by the input variable C_{stfr} . The default value of C_{stfr} is [

] ^{a,c} The allowable input range of C_{stfr} is from [] ^{a,c} The impact of the C_{stfr} constant on W_{st} is illustrated in Figure 1 below for three different values of C_{stfr} : its default value of [] ^{a,c} and the lower and upper limiting values for the range of allowable input values for C_{stfr} , [] ^{a,c} For the curves shown in Figure 1, the second adjustable constant, C_{hs_slug} , was set equal to its default value of 1.0.



Figure 1: Effect of Parameter C_{stfr} in Equation 4-117 on the Weighing Factor W_{st} at $C_{hs_slug} = 1.0$

Please explain the rationale for selecting []^{a,c} as the default value for the C_{strfu} parameter. In addition, explain the reasons for defining a range from []^{a,c} as allowable input values for C_{strfu} and describe the intended application of this proposed range. Clarify the way in which the input value for C_{strfu} is defined and describe how the use of inappropriate C_{strfu} values within the allowable range of input values is controlled and prevented in PWR plant LOCA analyses using WCOBRA/TRAC-TF2.

Response:

As discussed in RAI 84 part (2), the presence of interpolation region in the 1-D component flow regime map is to improve numerical stability of the computation. The interpolation region itself does not imply physical interpretation. []^{a,c}

The allowable input range for C_{strfu} in the WCOBRA/TRAC-TF2 computer code is chosen to be []^{a,c}. The value of []^{a,c} leads a negligible interpolation region, while the value of []^{a,c} represents a very large interpolation region. []^{a,c}

In addition, a sensitivity study with []^{a,c}, which leads to a reduced interpolation region, was performed using the Beaver Valley Unit 1 2.6 inch SBLOCA case. The results indicate []^{a,c}

Reference:

1. WCAP-16996-P, "Realistic LOCA Evaluation Methodology Applied to the Full Spectrum of Break Sizes (FULL SPECTRUM™ LOCA Methodology)," November 2010.

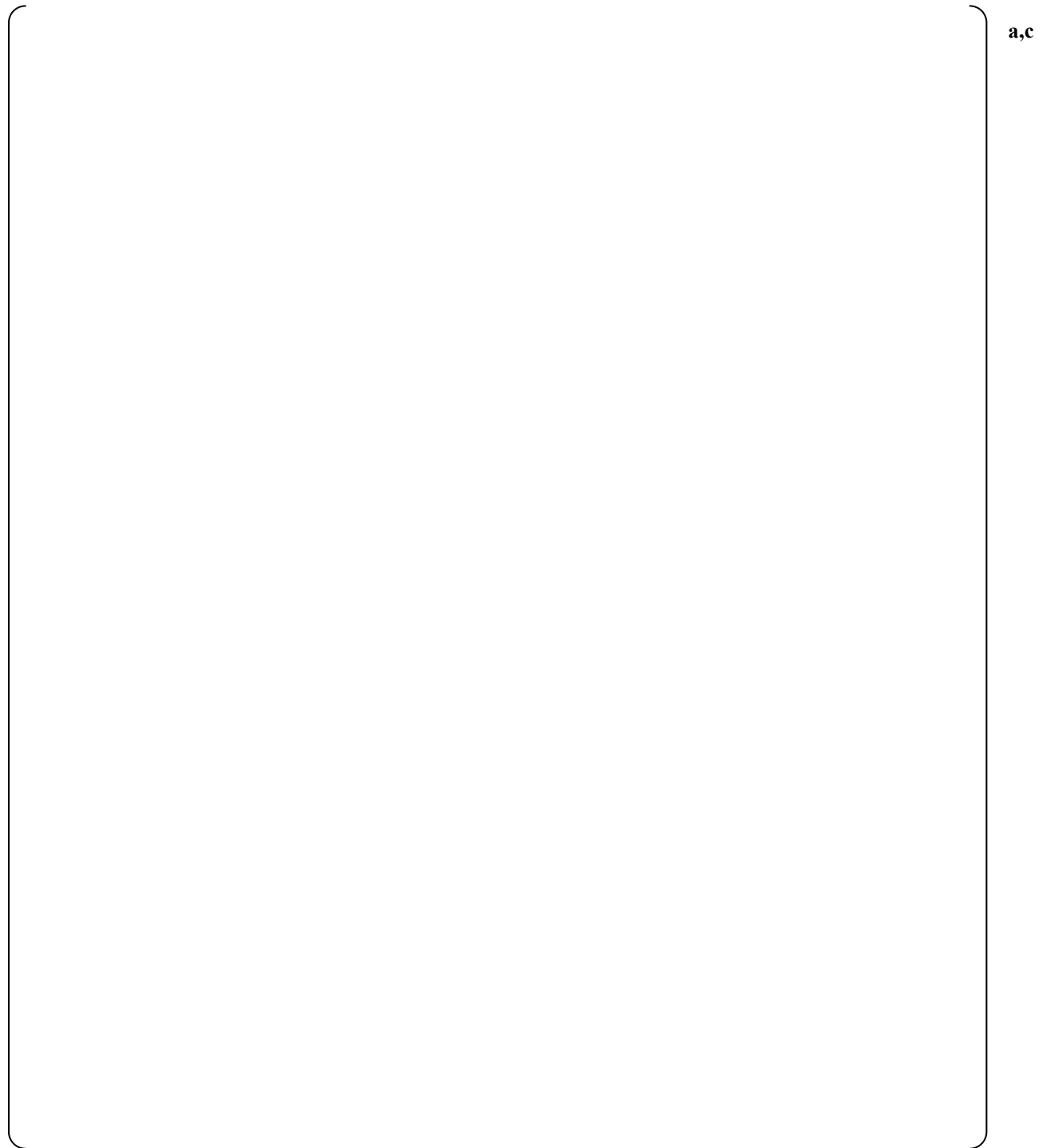


Figure 95-1. Comparison of reactor vessel inventories in Beaver Valley Unit 1 [
] ^{a,c}

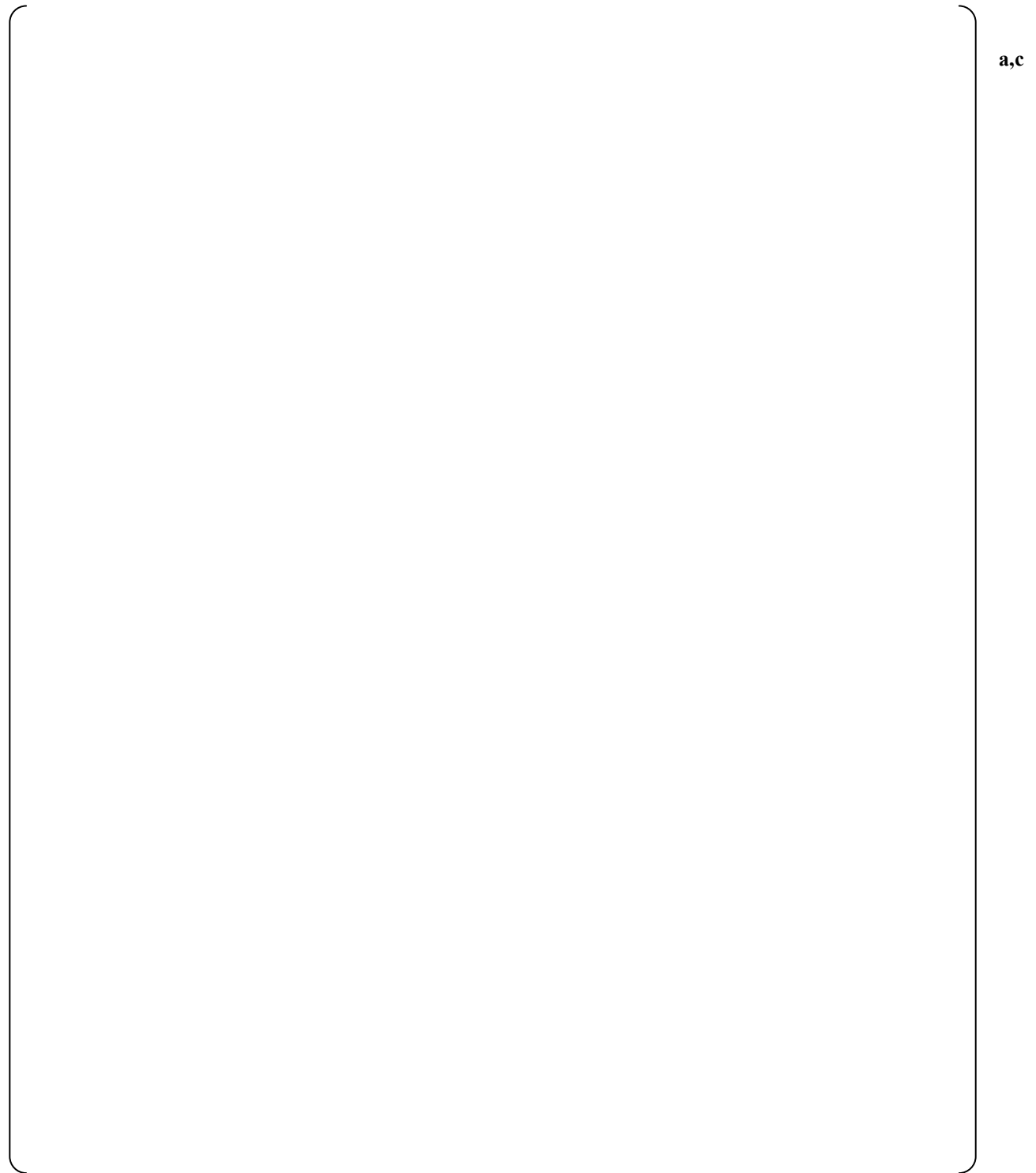


Figure 95-2. Comparison of fuel rod peak cladding temperatures in Beaver Valley Unit 1 [
] ^{a,c}

Preface

Table Preface-1 provides a list of acronyms used throughout the responses to the RAIs herein.

Table Preface-1: List of Acronyms	
Acronym	Definition
CCFL	Counter-Current Flow Limit
CGE	Virgil C. Summer Unit 1
DLW	Beaver Valley Unit 1
DTMAX	Maximum time step size
FSLOCA	FULL SPECTRUM LOCA
IET	Integral Effect Test
LOCA	Loss-of-Coolant Accident
PWR	Pressurized water reactor
RCP	Reactor Coolant Pump
SG	Steam Generator
TRAM	Transient and Accident Management
UPTF	Upper Plenum Test Facility

Table Preface-2 provides a list of symbols/variables used throughout the responses to the RAIs herein.

Table Preface-2: List of Symbols / Variables	
A	Area
D	Diameter (m)
g	Gravity (9.81 m/s ²)
hl/d	Residual Liquid Level
L/D	Ratio of Length over Diameter
α_v	Void / Vapor Fraction
Jg^*	Modified Froude Number = $\frac{\dot{m}_v}{A\sqrt{\rho_v(\rho_l - \rho_v)gD}}$
ρ_l	Liquid Density (kg/m ³)
ρ_v	Vapor Density (kg/m ³)

The following figures are provided here, as they are referenced in multiple RAI responses.

a,b,c

Figure Preface-1: Diagram of UPTF Primary System (taken from Figure 2 of NT33/94/011, “Versuch A5, Freiblasen des Pumpenbogens, Einzeleffekt- und Integralversuche,” December 1994.)

a,b,c

Figure Preface-2: Diagram of the UPTF Test Loop (taken from Figure 4 of NT33/94/011, “Versuch A5, Freiblasen des Pumpenbogens, Einzeleffekt- und Integralversuche,” December 1994.)

a,c

Figure Preface-3: Noding Diagram for WCOBRA/TRAC-TF2 Input for UPTF Loop Seal Test Simulations

RAI Question #113: WCOBRA/TRAC-TF2 UPTF Loop Seal Nodalization

Full-scale separate effect experiments describing the loop seal clearing process in a PWR primary loop during a LOCA were produced as part of the TRAM experimental program, carried out at the full-scale UPTF in Mannheim, Germany. The UPTF loop seal piping had an inner diameter of 0.750 m (33.46 inch or 2.8 ft) and the length of the bottom horizontal section of the loop seal piping was equal to 1.734 m (68.3 inch or 5.7 ft), which resulted in a length-to-diameter ratio (L/D) of 2.3 for this section. Also, the facility employed pump simulators to model the RCPs in a PWR.

WCAP-16996-P/WCAP-16996-NP, Volumes I, II, and III, Revision 0, Section 18, "Loop Seal Clearance," Subsection 18.3.1, "WCOBRA/TRAC-TF2 Simulation of the UPTF 3-Bar and 15-Bar Tests," presents assessment results based on UPTF TRAM loop seal clearance tests. Figure 18.3-1, "WCOBRA/TRAC-TF2 Model of the UPTF Separate Effects Loop Seal Clearing Tests," shows the implemented UPTF loop seal nodalization.

As described, PIPE component No. 2 with []^{a,c} cells was used to simulate the loop seal piping including the RCP simulator. In this model, []^{a,c} was used to represent the loop seal bottom horizontal section and []^{a,c} cells were used to model each of the 90° bends connecting the horizontal section of the loop seal to the downhill and uphill pipes of the cross-over leg.

- (1) Please provide a table that documents the WCOBRA/TRAC-TF2 input parameters for the WCOBRA/TRAC-TF2 UPTF loop seal model shown in Figure 18.3-1, "WCOBRA/TRAC-TF2 Model of the UPTF Separate Effects Loop Seal Clearing Tests." Describe each component separately and include a full description for PIPE Component No. 2 used to represent the UPTF loop seal piping. Provide length, elevation, flow area, volume, and inclination angle for each cell/interface and explain how the loop seal input model accounts for relevant UPTF geometry and instrumentation locations.
- (2) Please explain why the bend regions in the loop seal nodalization model appear as asymmetric in Figure 18.3-1. It is seen that the curvature of the uphill bend is much larger than the radius of the downhill bend. The UPTF loop seal piping had equal bend radii of 0.798 m (31.4 inch or 2.6 ft) for both bend regions.
- (3) If input parameters, such as pressure loss coefficients, were used to compute pressure losses as part of the specified WCOBRA/TRAC-TF2 UPTF loop seal model, please define these input quantities and provide the formulas used for their computation. Explain any assumptions used to determine the input values for these parameters.
- (4) Please explain how the UPTF RCP simulator, present in the simulated region of the UPTF primary circuit, was accounted for in the WCOBRA/TRAC-TF2 UPTF loop seal model. Provide any input parameters that were used to model the RCP simulator and explain how these parameters were computed. Provide and explain used formulas, applied assumptions, and calculated input values.

Response:

- (1) The WCOBRA/TRAC-TF2 input model for the UPTF loop seal tests was developed to preserve the length and volume of the piping in the loop seal region, including proper elevation changes. The model begins at the point where the vapor was injected in the experiment (JEC02SV010, Figure Preface-2). The component cell lengths were determined such that [

]^{a,c}

Figure Preface-3 provides the cell lengths and relevant elevations for the cells in the primary PIPE component used to simulate the tests; this can be compared to the test facility described in Figure Preface-2. [

]^{a,c}

Table 113-1 provides the inclination angles for the cell faces that are neither 0.0° (horizontal) nor 90° (vertical), as depicted in Figure Preface-3.

Table 113-1: Inclination Angles for Relevant Portions of the UPTF Loop Seal Model

Cell Face Number	Description	Inclination Angle

- (2) The reason for the asymmetric loop seal region is based on an interpretation of the figures provided in [113-1]. From Figure Preface-2, [

]^{a,b,c}

To demonstrate that the asymmetric nodding has a minimal impact on the calculated results, the 3-bar and 15-bar cases are executed with symmetric uphill and downhill bend modeling (i.e., cells' geometry mirrored). To preserve the overall length and volume, [

]^{a,c} and the corresponding volume updated.

The residual liquid levels versus the modified Froude number (Equation 18-1 of [113-2]) are presented in Figure 113-1 for the 3-bar cases and Figure 113-2 for the 15-bar cases. The differential pressures across the loop seal versus the modified Froude number are presented in Figure 113-3 for the 3-bar cases and Figure 113-4 for the 15-bar cases.

As seen from the figures, [

] ^{a,c}

(3) The only pressure loss coefficient used in the model is [

] ^{a,c}

(4) The pump simulator is modeled as [

] ^{a,c} Figures 113-5 to 113-7 provide a comparison of the liquid volume in the horizontal section (surrogate for residual liquid level), pressure difference across the loop seal region, and total system mass for the simulation. As seen in the figures, [

] ^{a,c}

Reference(s)

113-1) NT33/94/011, "Versuch A5, Freiblasen des Pumpenbogens, Einzeleffekt- und Integralversuche," December 1994.

113-2) WCAP-16996-P/WCAP-16696-NP, "Realistic LOCA Evaluation Methodology Applied to the Full Spectrum of Break Sizes (FULL SPECTRUM LOCA Methodology)," November 2010.



Figure 113-1: Symmetric Bend Study - Residual Liquid Level Comparison for the 3-bar Cases



Figure 113-2: Symmetric Bend Study - Residual Liquid Level Comparison for the 15-bar Cases



Figure 113-3: Symmetric Bend Study - Differential Pressure across the Loop Seal Region for the 3-bar Cases



Figure 113-4: Symmetric Bend Study - Differential Pressure across the Loop Seal Region for the 15-bar Cases



Figure 113-5: RCP Volume Study (15-bar, $J_{g^*}=0.178$) Liquid Volume in the Loop Seal Region



Figure 113-6: RCP Volume Study (15-bar, $J_{g^*}=0.178$) Pressure Drop across Loop Seal Region

a,c

Figure 113-7: RCP Volume Study (15-bar, $Jg^*=0.178$) Total System Mass

RAI Question #114: Upper Plenum Test Facility TRAM Loop Seal Instrumentation and WCOBRA/TRAC-TF2 Upper Plenum Test Facility Model

A valid and meaningful assessment of WCOBRA/TRAC-TF2 prediction results against UPTF TRAM separate effect loop seal clearance test data imposes, as part of a code assessment study, special requirements that the model accounts adequately for the type and location of test instrumentation and measuring locations. In turn, the data channels to be used for the purposes of the code assessment study should be determined considering available test instrumentation, relevance to the phenomena being assessed and code models used for their prediction, signal behavior and data accuracy, among other factors of relevance.

- (1) Please describe how the loop seal differential pressures were measured in the UPTF TRAM separate effect loop seal clearance tests. Explain how the locations of the differential pressure tap points were reflected in the WCOBRA/TRAC-TF2 UPTF loop seal models used to assess the code. Describe how the predicted loop seal differential pressure quantity was determined from the WCOBRA/TRAC-TF2 calculation results. Please identify nodes and/or cell interfaces in the WCOBRA/TRAC-TF2 UPTF loop seal model at which thermal hydraulic quantities were calculated by the code and used to determine the loop seal differential pressure predication for comparison against test data.
- (2) Please describe how the loop seal residual water levels were measured in the UPTF TRAM separate effect loop seal clearance tests. Explain how the locations of the differential pressure tap points were reflected in the WCOBRA/TRAC-TF2 UPTF loop seal models used to assess the code. Describe how the computed loop seal residual water levels, used for comparison against test data, were determined from the WCOBRA/TRAC-TF2 calculation results. Identify the thermal hydraulic quantities that were used to determine these predicted residual loop seal water levels. Please identify nodes and/or cell interfaces in the WCOBRA/TRAC-TF2 UPTF loop seal model at which these thermal hydraulic quantities were calculated by the code.

Response:

- (1) Per Section 6.1.3 of [114-1], the differential pressure is calculated [

] ^{a,b,c}

From Figure Preface-3, the center of [

] ^{a,c}

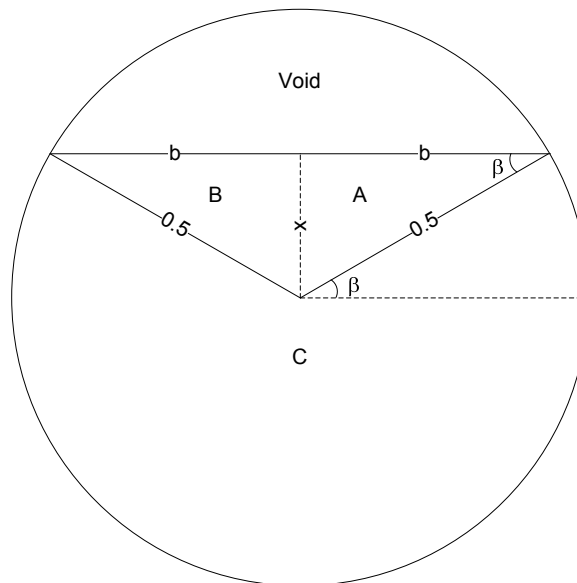
[

] ^{a,c} This is demonstrated in Figure 114-2.

(2) The UPTF residual liquid level data was calculated by [

] ^{a,b,c}The residual liquid level from the WCOBRA/TRAC-TF2 simulation is calculated [] ^{a,c} This is demonstrated in Figure 114-3.

The residual liquid level is calculated from the void fraction based on the following geometry for a circular pipe.



$$\frac{h_l}{d} = 0.5 + x \rightarrow x = \frac{h_l}{d} - 0.5 \text{ where, } -0.5 \leq x \leq 0.5$$

$$b = \sqrt{0.25 - x^2} = \sqrt{0.25 - \left(\frac{h_l}{d} - 0.5\right)^2} = \sqrt{0.25 - \left(\left(\frac{h_l}{d}\right)^2 - \frac{h_l}{d} + 0.25\right)} = \sqrt{\frac{h_l}{d} - \left(\frac{h_l}{d}\right)^2} = \sqrt{\frac{h_l}{d} \left(1 - \frac{h_l}{d}\right)}$$

$$\begin{aligned}
 Area_A &= Area_B = 0.5bx = 0.5 \left(\frac{h_l}{d} - 0.5 \right) \sqrt{\frac{h_l}{d} \left(1 - \frac{h_l}{d} \right)} \\
 Area_c &= \frac{\pi}{4} \left(0.5 + \frac{\beta}{\pi} \right) \\
 \beta &= \frac{\pi}{2} - \arccos \left(\frac{\frac{h_l}{d} - 0.5}{0.5} \right) \\
 \alpha_v &= \frac{Area_v}{Area} = 1 - \frac{Area_l}{Area} = 1 - \frac{Area_A + Area_B + Area_c}{Area} \\
 &= 1 - \frac{2 \left(0.5 \left(\frac{h_l}{d} - 0.5 \right) \sqrt{\frac{h_l}{d} \left(1 - \frac{h_l}{d} \right)} \right) + \frac{\pi}{4} \left(0.5 + \frac{\beta}{\pi} \right)}{\frac{\pi}{4}} \\
 &= 1 - \frac{\left(\frac{h_l}{d} - 0.5 \right) \sqrt{\frac{h_l}{d} \left(1 - \frac{h_l}{d} \right)}}{\frac{\pi}{4}} - \left(0.5 + \frac{\frac{\pi}{2} - \arccos \left(\frac{\frac{h_l}{d} - 0.5}{0.5} \right)}{\pi} \right)
 \end{aligned}$$

a,c

Figure 114-1: Differential Pressure Calculation Comparison

a,c

Figure 114-2: Demonstration of Determining Code Calculated Pressure Differential

a,c

Figure 114-3: Demonstration of Determining Code Calculated Residual Liquid Level

Reference(s)

- 114-1) NT33/94/011, "Versuch A5, Freiblasen des Pumpenbogens, Einzeleffekt- und Integralversuche," December 1994.
- 114-2) WCAP-16996-P/WCAP-16696-NP, "Realistic LOCA Evaluation Methodology Applied to the Full Spectrum of Break Sizes (FULL SPECTRUM LOCA Methodology)," November 2010.

RAI Question #115: WCOBRA/TRAC-TF2 Sampled Parameters and Special Options in Loop Seal Modeling

WCOBRA/TRAC-TF2 models and correlations that are relevant to predicting loop seal clearance in PWR plant LOCA analyses include such as those used for describing transition to non-stratified flow, CCFL, and liquid entrainment mechanisms. WCOBRA/TRAC-TF2 features user defined parameters and multipliers that can be applied to modify these models and criteria. Some of these user defined parameters and multipliers are sampled as part of the plant uncertainty analysis and others are not included in the sampling process.

Regarding relevant sampled parameters, WCAP-16996-P/WCAP-16996-NP, Volumes I, II, and III, Revision 0, Section 29, "29 Assessment of Uncertainty Elements," Subsection 29.1.7, "Horizontal Stratified Flow Regime Transition Boundary (HS_SLUG)," describes that a horizontal stratified flow regime transition boundary multiplier, HS_SLUG, is employed in WCOBRA/TRAC-TF2 to adjust the critical relative velocity for horizontal stratified flow. HS_SLUG is sampled []^{a,c} for the purpose of the uncertainty analysis.

Examples of WCOBRA/TRAC-TF2 parameters and multipliers that are not part of the sampling process include the parameters Cstfru and STRTX. For example, WCAP-16996-P Revision 0, Section 18, "Loop Seal Clearance," Subsection 18.3.1, "WCOBRA/TRAC-TF2 Simulation of the UPTF 3-Bar and 15-Bar Tests," states that []^{a,c}

- (1) Please provide a table that identifies and describes any user defined parameters, multipliers, and/or options, implemented as part of WCOBRA/TRAC-TF2 models and correlations that are used to predict loop seal clearance in PWR plant LOCA analyses, including such related to describing non-stratified flow transition, CCFL, and liquid entrainment mechanisms. Please explain if a parameter is implemented on a component-wide basis or it can be applied to specific cells/interfaces of hydraulic components used to represent the PWR loop seal region. In addition, identify if a parameter is being sampled or not as part of the plant uncertainty analysis. Include mathematical expressions that show modeling equations and quantities that can be modified through such user defined input parameters and/or special options. Present the technical rationale for the implementation of these special modeling options and provide the allowable input values. In addition, please explain how the input values for these options are determined for the purpose of performing PWR LOCA analysis using the Full Spectrum LOCA methodology.
- (2) Please identify which of the parameters, multipliers, and/or options, identified in Item (1) above, were used in the WCOBRA/TRAC-TF2 loop seal assessment study presented in Subsection 18.3.1, "WCOBRA/TRAC-TF2 Simulation of the UPTF 3-Bar and 15-Bar Tests." Present the technical rationale for applying or not applying a specific parameter, multiplier, or option. Explain if a specific parameter, multiplier, or option was applied on component-wide basis and/or to specific cells/interfaces only of component PIPE 2 used to represent the UPTF loop seal in the WCOBRA/TRAC-TF2 model. Provide a table that lists each individual modeling parameter, multiplier, and option such as the one used to prescribe that []^{a,c}

Response:Identification/Description of Parameters

Table 50-1 of the response to RAI 50 [115-1] provides a list of the user defined parameters, multipliers and/or options available in WCOBRA/TRAC-TF2, including their allowable input values. For the parameters that are not sampled as part of the FSLOCA method, justification for the value used is provided in Table 50-3 of the response to RAI 50 [115-1]. In addition, the response to RAI 86 provides clarification on MSTRTX/STRTX [115-2]. Of the parameters listed in Table 50-1 of the response to RAI 50 [115-1], the following directly influence the loop seal clearing calculation:

Table 115-1: Parameters that Directly Influence the Loop Seal Clearing Calculation

Parameter	Description	Default	Application	Sampled?

a,c

Discussion Regarding Parameters Which Directly Influence Loop Seal Clearing

[

] ^{a,c}

[

I^{a,c}



Figure 115-1: STFRU Study - Residual Liquid Level Comparison for the 3-bar Cases



Figure 115-2: STFRU Study - Residual Liquid Level Comparison for the 15-bar Cases



Figure 115-3: STFRU Study - Differential Pressure across the Loop Seal Region for the 3-bar Cases



Figure 115-4: STFRU Study - Differential Pressure across the Loop Seal Region for the 15-bar Cases

Reference(s)

- 115-1) LTR-NRC-13-73, “Submittal of Westinghouse Responses to ‘WCAP-16996-P, ‘Realistic LOCA Evaluation Methodology Applied to the Full Spectrum of Break Sizes (FULL SPECTRUM LOCA Methodology)’ Request for Additional Information – RAIs 46 – 58, 75 and 77’ (Proprietary/Non-Proprietary), Project 700, TAC No. ME5244,” October 28, 2013.
- 115-2) LTR-NRC-14-12, “Submittal of Westinghouse Responses to ‘WCAP-16996-P, ‘Realistic LOCA Evaluation Methodology Applied to the Full Spectrum of Break Sizes (FULL SPECTRUM LOCA Methodology)’ Request for Additional Information – RAIs 77-82, 86-87, 93 and 112’ (Proprietary/Non-Proprietary), Project 700, TAC No. ME5244,” March 12, 2014.
- 115-3) Takeuchi, K., Young, M. Y., and Gagnon, A. F., “Flooding in the pressurizer surge line of AP600 plant and analyses of APEX data,” *Nuclear Engineering and Design*, Volume 192, pp. 45-58, 1999.
- 115-4) WCAP-16996-P/WCAP-16696-NP, “Realistic LOCA Evaluation Methodology Applied to the Full Spectrum of Break Sizes (FULL SPECTRUM LOCA Methodology),” November 2010.

RAI Question #116: UPTF TRAM Loop Seal Clearance Data and WCOBRA/TRAC- TF2 Assessment

The UPTF TRAM loop seal clearance experiments comprise both integral effect and separate effect tests. The separate effect tests were performed using combined steam and water or steam injection only with various flow rates and at two different pressure levels of 0.3 MPa and 1.5 MPa (43.5 psia and 217.6 psia). As described in WCAP-16996-P/WCAP-16996-NP, Volumes I, II, and III, Revision 0, Section 18, "Loop Seal Clearance," Subsection 18.3.1, "WCOBRA/TRAC-TF2 Simulation of the UPTF 3-Bar and 15-Bar Tests," UPTF TRAM separate effect tests were used to assess the code. Regarding the test data, Subsection 18.3.1 refers to publications by J. Liebert and R. Emmerling, "UPTF Experiment: Flow Phenomena During Full-Scale Loop Seal Clearing of a PWR," Nuclear Engineering and Design, Vol. 179, No.1, pp. 51-64, 1998, and by J. Ohvo et al., "Simulation of Full-Scale UPTF Loop Seal Experiments with APROS, CATHARE and RELAP," ICONE6-6090, 6th International Conference on Nuclear Engineering, May 10-15, 1998, San Diego, California. The work by Ohvo, et al. includes a summary of the main parameters for the UPTF TRAM tests.

- (1) Please provide a table identifying the UPTF TRAM separate effect test data that were used to assess WCOBRA/TRAC-TF2 as described in Subsection 18.3.1. For each data point, provide the system pressure, steam and water injection flow rates, and corresponding measured test quantities. Please explain how the test boundary conditions were simulated in UPTF WCOBRA/TRAC-TF2 model and present separate assessments for the cases with and without water injection. Explain if any UPTF TRAM test data points were excluded from the assessment results presented in Figures 18.3-2, 18.3-4, and 18.3-5 in Subsection 18.3.1. Please clarify if Figure 18.3-5 includes all data points presented in Figure 18.3-2 and in Figure 18.3-4.
- (2) For each UPTF TRAM data point shown in Figures 18.3-2, 18.3-4, and 18.3-5 in Subsection 18.3.1, provide transient code prediction results for important thermal hydraulic quantities. In particular, please include plots for inlet and exit steam and liquid mass flow rates, liquid entrainment rates, phase velocities, void fractions in the horizontal section, bend regions, and downhill and uphill sections of the loop seal, as well as liquid coolant inventory residing in these simulated loop seal regions. In addition, please depict the two-phase flow regimes as identified in the loop seal nodes. Provide plots for the predicted volumetric concentrations of the interfacial friction force.
- (3) Please present plots showing WCOBRA/TRAC-TF2 calculation results against measured residual loop seal water levels and loop seal pressure losses observed at various injection flow rates. Provide consideration of measurement accuracies, observed hydraulic flow oscillations, and any other factors of relevance to the presented code assessment results.
- (4) For each UPTF TRAM data point shown in Figures 18.3-2, 18.3-4, and 18.3-5 in Subsection 18.3.1, provide plots comparing local transient thermal hydraulic conditions against corresponding critical conditions or criteria used in WCOBRA/TRAC-TF2 to describe phenomena of governing importance for predicting loop seal clearance including transition to non-stratified flow, CCFL, and participating liquid entrainment mechanisms. Plot the computed thermal hydraulic quantities and corresponding critical parameters as a function of transient time and at locations in the loop seal where such phenomena play a governing role.
- (5) In responding to Items (1) through (4) above, please assess UPTF TRAM 0.5 MPa tests and the 1.5 MPa tests separately. Provide detailed pressure scaling considerations based on contributing

WCOBRA/TRAC-TF2 models. Derive and provide corresponding pressure scaling relationships and explain how the UPTF TRAM full-scale loop seal clearance data support them.

Response:

- (1) Table 116-1 provides the experimental cases used for the code comparison of the differential pressure across the loop seal region and is taken from Table 14 of [116-1]. These cases were chosen as [

] ^{a,c}

Table 116-2 provides the experimental cases used for the code comparison of residual liquid level and is taken from Table 13 of [116-1]. Based on [

] ^{a,b,c}

Table 116-1: Differential Pressure Data from Table 14 of [116-1]			
3-bar Cases			
Run	Jg*	dP (kPa)	M _v (kg/s)
15-bar Cases			
Run	Jg*	dP (kPa)	M _v (kg/s)

Table 116-2: Residual Liquid Level Data from Table 13 of [116-1]			
3-bar Cases			
Run	Jg*	hl/d	M_v (kg/s)
15-bar Cases			
Run	Jg*	hl/d	M_v (kg/s)

(2) The requested figures have been generated for the following six cases:

Pressure	Jg*	Pressure	Jg*
3-bar	0.076	15-bar	0.070
	0.176		0.178
	0.283		0.299

The figures include vapor mass injected, total mass out, entrainment rate in the horizontal and uphill bend sections, phasic velocities around the loop seal bend and horizontal regions, void fractions around the loop seal bend and horizontal regions, total system mass, flow regimes around the loop seal bend and horizontal regions, and the volumetric interfacial friction force around the loop seal bend and horizontal regions and are presented in Figures 116-1 through 116-42.

As seen Figures 116-1, 116-8, 116-15, 116-22, 116-29 and 116-36, [

J^{a,c}

On the flow regime figures, it is noted that there are three y-axis coordinates for stratified flow. This is a result of how the code reports the momentum cell being in stratified flow (i.e., stratified flow from each of the non-stratified flow regimes). This creates the appearance of the flow regime being oscillatory, when in fact

the flow remains in stratified flow. This is demonstrated by the flow regime for momentum cell 8 in Figure 116-6.

Lastly, Figures 116-7, 116-14, 116-21, 116-28, 116-35 and 116-42 provide the interfacial friction force around the loop seal region. As expected, [

]^{a,c}

a,c

Figure 116-1: 3-bar, $J_g^*=0.076$ – Mass Flow Rate

a,c

Figure 116-2: 3-bar, $J_g^*=0.076$ – Total System Mass

a,c

Figure 116-3: 3-bar, $Jg^*=0.076$ – Void Fraction

Figure 116-4: 3-bar, $Jg^*=0.076$ – Phasic Velocities

Figure 116-5: 3-bar, $Jg^*=0.076$ – Liquid Entrainment Fraction

Figure 116-6: 3-bar, $J_g^*=0.076$ – Flow Regime

Figure 116-7: 3-bar, $J_g^*=0.076$ – Interfacial Friction Force

a,c

Figure 116-8: 3-bar, $J_g^*=0.176$ – Mass Flow Rate

a,c

Figure 116-9: 3-bar, $J_g^*=0.176$ – Total System Mass

Figure 116-10: 3-bar, $J_g^*=0.176$ – Void Fraction

Figure 116-11: 3-bar, $Jg^*=0.176$ – Phasic Velocities

Figure 116-12: 3-bar, $Jg^*=0.176$ – Liquid Entrainment Fraction

Figure 116-13: 3-bar, $J_g^*=0.176$ – Flow Regime

Figure 116-14: 3-bar, $J_g^*=0.176$ – Interfacial Friction Force

a,c

Figure 116-15: 3-bar, $J_g^*=0.283$ – Mass Flow Rate

a,c

Figure 116-16: 3-bar, $J_g^*=0.283$ – Total System Mass

Figure 116-17: 3-bar, $Jg^*=0.283$ – Void Fraction

Figure 116-18: 3-bar, $Jg^*=0.283$ – Phasic Velocities

Figure 116-19: 3-bar, $Jg^*=0.283$ – Liquid Entrainment Fraction

Figure 116-20: 3-bar, $J_g^*=0.283$ – Flow Regime

Figure 116-21: 3-bar, $J_g^*=0.283$ – Interfacial Friction Force

a,c

Figure 116-22: 15-bar, $J_g^*=0.070$ – Mass Flow Rate

a,c

Figure 116-23: 15-bar, $J_g^*=0.070$ – Total System Mass

Figure 116-24: 15-bar, $J_g^*=0.070$ – Void Fraction

Figure 116-25: 15-bar, $J_g^*=0.070$ – Phasic Velocities

Figure 116-26: 15-bar, $J_{g^*}=0.070$ – Liquid Entrainment Fraction

Figure 116-27: 15-bar, $J_g^*=0.070$ – Flow Regime

Figure 116-28: 15-bar, $J_g^*=0.070$ – Interfacial Friction Force

a,c

Figure 116-29: 15-bar, $J_g^*=0.178$ – Mass Flow Rate

a,c

Figure 116-30: 15-bar, $J_g^*=0.178$ – Total System Mass

Figure 116-31: 15-bar, $J_g^*=0.178$ – Void Fraction

Figure 116-32: 15-bar, $J_g^*=0.178$ – Phasic Velocities

Figure 116-33: 15-bar, $J_{g^*}=0.178$ – Liquid Entrainment Fraction

Figure 116-34: 15-bar, $J_g^*=0.178$ – Flow Regime

Figure 116-35: 15-bar, $J_g^*=0.178$ – Interfacial Friction Force

a,c

Figure 116-36: 15-bar, $J_g^*=0.299$ – Mass Flow Rate

a,c

Figure 116-37: 15-bar, $J_g^*=0.299$ – Total System Mass

Figure 116-38: 15-bar, $J_g^*=0.299$ – Void Fraction

Figure 116-39: 15-bar, $Jg^*=0.299$ – Phasic Velocities

Figure 116-40: 15-bar, $J_{g^*}=0.299$ – Liquid Entrainment Fraction

Figure 116-41: 15-bar, $J_g^*=0.299$ – Flow Regime

Figure 116-42: 15-bar, $J_g^*=0.299$ – Interfacial Friction Force

- (3) Specific uncertainties related to the residual liquid level data measurements are not readily available in the papers and reports that Westinghouse possesses. However, from the reports, the residual liquid levels are [

J^{a,c}

Table 116-3: Data hl/d Uncertainties				
3-bar				
Run	Jg*	hcl010/d	hcl011/d	hf/d

Table 116-3: Data hl/d Uncertainties _(cont)				
15-bar				
Run	Jg*	hcl010/d	hcl011/d	hf/d

[illegible]

Table 116-5: Symmetric Bend Results (Ranges)							
Pressure	Jg* (-)	UB h/d	NOM h/d	LB h/d	LB dP	NOM dP	UB dP



Figure 116-43: 3-bar Residual Liquid Level Comparison, Including Uncertainties



Figure 116-44: 15-bar Residual Liquid Level Comparison, Including Uncertainties



Figure 116-45: 3-bar Pressure Differential Comparisons, Including Uncertainties



Figure 116-46: 15-bar Pressure Differential Comparisons, Including Uncertainties

- (4) Figures 116-47 through 116-58 provide comparisons of the relative velocity vs. stratification and entrainment criteria, as well as Kutateladze values for the cells of interest. The cases represented are the same cases used for plotting results presented in part (2) of this response. See part (2) of this response for discussion related to these figures.

a,c

Figure 116-47: 3-bar, $Jg^*=0.076$ – Horizontal Stratification and Wavy Dispersed Criteria

a,c

Figure 116-48: 3-bar, $Jg^*=0.076$ – Kutateladze Number

Figure 116-49: 3-bar, $Jg^*=0.176$ – Horizontal Stratification and Wavy Dispersed Criteria

a,c

Figure 116-50: 3-bar, $J_g^*=0.176$ – Kutateladze Number

Figure 116-51: 3-bar, $Jg^*=0.283$ – Horizontal Stratification and Wavy Dispersed Criteria

a,c

Figure 116-52: 3-bar, $Jg^*=0.283$ – Kutateladze Number

Figure 116-53: 15-bar, $J_g^*=0.070$ – Horizontal Stratification and Wavy Dispersed Criteria

a,c

Figure 116-54: 15-bar, $Jg^*=0.070$ – Kutateladze Number

Figure 116-55: 15-bar, $J_g^*=0.178$ – Horizontal Stratification and Wavy Dispersed Criteria

a,c

Figure 116-56: 15-bar, $Jg^*=0.178$ – Kutateladze Number

Figure 116-57: 15-bar, $J_g^*=0.299$ – Horizontal Stratification and Wavy Dispersed Criteria

a,c

Figure 116-58: 15-bar, $J_g^*=0.299$ – Kutateladze Number

- (5) Even though the UPTF loop seal tests did not perform experiments at full pressure, simulations were performed at a pressure representative of the first main steam safety valve pressure. The results are presented in Section 18.3.1 of [116-2]. As part of the response to RAI 117, the pressure differential across the loop seal for the cases executed as part of the break spectrum study (Sections 27.1.1.3 and 27.1.2.3 of [116-2]) were examined. It was shown that the vapor flows (i.e., modified Froude number) and differential pressures from the plant cases were comparable to the UPTF loop seal data.

Reference(s)

- 116-1) NT33/94/011, "Versuch A5, Freiblasen des Pumpenbogens, Einzeleffekt- und Integralversuche," December 1994.
- 116-2) WCAP-16996-P/WCAP-16696-NP, "Realistic LOCA Evaluation Methodology Applied to the Full Spectrum of Break Sizes (FULL SPECTRUM LOCA Methodology)," November 2010.

RAI Question #117: WCOBRA/TRAC-TF2 Upper Plenum Test Facility Loop Seal Nodalization Sensitivity Study

Various nodalization approaches have been applied in analyzing loop seal clearance test data in assessing reactor safety codes. For example, in the work by J. Ohvo et al., "Simulation of Full-Scale UPTF Loop Seal Experiments with APROS, CATHARE and RELAP," Paper ICONE6-6090, 6th International Conference on Nuclear Engineering, May 10-15, 1998, San Diego, California, the bottom horizontal section of the UPTF the loop seal piping was represented by 2 nodes in the APROS model, by 7 nodes in the CATHARE model, and by 2 nodes in the RELAP5 model. Correspondingly, each of the 90° bend regions was represented by 3, 5, and a single node.

When describing the UPTF loop seal model, WCAP-16996-P/WCAP-16996-NP, Volumes I, II, and III, Revision 0, Section 18, "Loop Seal Clearance," Subsection 18.3.1, "WCOBRA/TRAC-TF2 Simulation of the UPTF 3-Bar and 15-Bar Tests," states that "the noding in this model is judged sufficient for simulation of the UPTF tests, and similar modeling is expected to be used in the plant simulations." At the same time, WCAP-16996-P/WCAP-16996-NP, Volumes I, II and III, Revision 0, Section 18, "Loop Seal Clearance," provides no justification for this statement.

The NRC Regulatory Guide 1.157, "Best-Estimate Calculations of Emergency Core Cooling System Performance," May 1989, Subsection 2.1.1, "Numerical Methods," requires that "Sensitivity studies and evaluations of the uncertainty introduced by noding should be performed." WCAP-16996-P/WCAP-16996-NP, Volumes I, II, and III, Revision 0, Section 18, "Loop Seal Clearance," does not examine the impact of noding on WCOBRA/TRAC-TF2 prediction results in assessing the code capabilities to predict loop seal clearance.

- (1) Please perform and present results from WCOBRA/TRAC-TF2 nodalization sensitivity studies that employ 2, 3, and 4 cells of an equal length to model the UPTF loop seal bottom horizontal section, which would correspond to cell length- to-diameter ratios (L/D) of 1.16, 0.77, and 0.58. Examine any additional nodalization schemes, as deemed appropriate. Show plots comparing both the residual loop seal levels and loop seal pressure losses against measured data.
- (2) Please perform and present results from WCOBRA/TRAC-TF2 nodalization sensitivity studies that employ 3, 4, and 5 cells to model each of the 90° bends connecting the bottom horizontal section of the loop seal to the downhill and uphill pipes of the UPTF cross-over leg. Show plots comparing both the residual loop seal liquid levels and loop seal pressure losses against measured data.
- (3) Present and discuss the technical basis used to establish the PWR loop seal nodalization approach considered adequate for predicting loop seal clearance in WCOBRA/TRAC-TF2 plant LOCA analyses as part of the Full Spectrum™ LOCA methodology. Describe the approach to PWR loop seal modeling implemented for LOCA analyses using the Full Spectrum™ LOCA methodology. Please explain how the results from the UPTF TRAM loop seal nodalization sensitivity study support this approach.

Response:

- (1) The sensitivity studies requested were executed, whereby the horizontal cell was split into two cells, three cells and four cells, respectively. The residual liquid levels versus the modified Froude number are presented in Figure 117-1 for the 3-bar cases and Figure 117-2 for the 15-bar cases. The differential pressures across the loop seal versus the modified Froude number are presented in Figure 117-3 for the 3-bar cases and Figure 117-4 for the 15-bar cases. As seen from the figures, [

] ^{a,c}



Figure 117-1: Horizontal Noding Study - Residual Liquid Level Comparison for the 3-bar Cases



Figure 117-2: Horizontal Noding Study - Residual Liquid Level Comparison for the 15-bar Cases



Figure 117-3: Horizontal Noding Study - Differential Pressure across the Loop Seal Region for the 3-bar Cases



Figure 117-4: Horizontal Noding Study - Differential Pressure across the Loop Seal Region for the 15-bar Cases

- (2) The sensitivity studies requested were executed, whereby the two cells representing the bend regions were split into three cells, four cells and five cells, respectively. Based on the discussion in the response to RAI 115 regarding [

] ^{a,c}

The residual liquid levels versus the modified Froude number are presented in Figure 117-5 for the 3-bar cases and Figure 117-6 for the 15-bar cases. The differential pressures across the loop seal versus the modified Froude number are presented in Figure 117-7 for the 3-bar cases and Figure 117-8 for the 15-bar cases. As seen from the figures [

] ^{a,c}

a,c

Figure 117-5: Bend Noding Study - Residual Liquid Level Comparison for the 3-bar Cases

a,c

Figure 117-6: Bend Noding Study - Residual Liquid Level Comparison for the 15-bar Cases



Figure 117-7: Bend Noding Study - Differential Pressure across the Loop Seal Region for the 3-bar Cases



Figure 117-8: Bend Noding Study - Differential Pressure across the Loop Seal Region for the 15-bar Cases

- (3) The PWR modeling is based on the model used for UPTF loop seal simulations (see response to RAIs 91 and 92) to ensure consistency with the assessment of loop seal clearing on residual liquid retention and pressure differential. While UPTF test data is not available at full pressure, the UPTF loop seal model was executed at a pressure representative of a PWR, with scaled flow rates. The results are discussed in Section 18 of [117-1].

In addition, the pressure drop across each of the loop seals is obtained from the break spectrum studies presented in Sections 27.1.1.3 and 27.1.2.3 of [117-1]. The results for all three loop seals of each break size are presented in Figures 117-9 through 117-16 (triangles represent loop 1; squares represent loop 2; pentagons represent loop 3). As seen from the figures, the pressure drops across the loop seal region from the plant break spectrum studies are within or slightly higher than those obtained from the UPTF loop seal simulations as well as the UPTF loop seal data (see Figures 117-7 and 117-8 for UPTF data points).



Figure 117-9: Loop Seal Pressure Differential with Results from CGE Plant Break Spectrum Study 2-inch Break



Figure 117-10: Loop Seal Pressure Differential with Results from CGE Plant Break Spectrum Study 3-inch Break



Figure 117-11: Loop Seal Pressure Differential with Results from CGE Plant Break Spectrum Study 4-inch Break



Figure 117-12: Loop Seal Pressure Differential with Results from CGE Plant Break Spectrum Study 6-inch Break

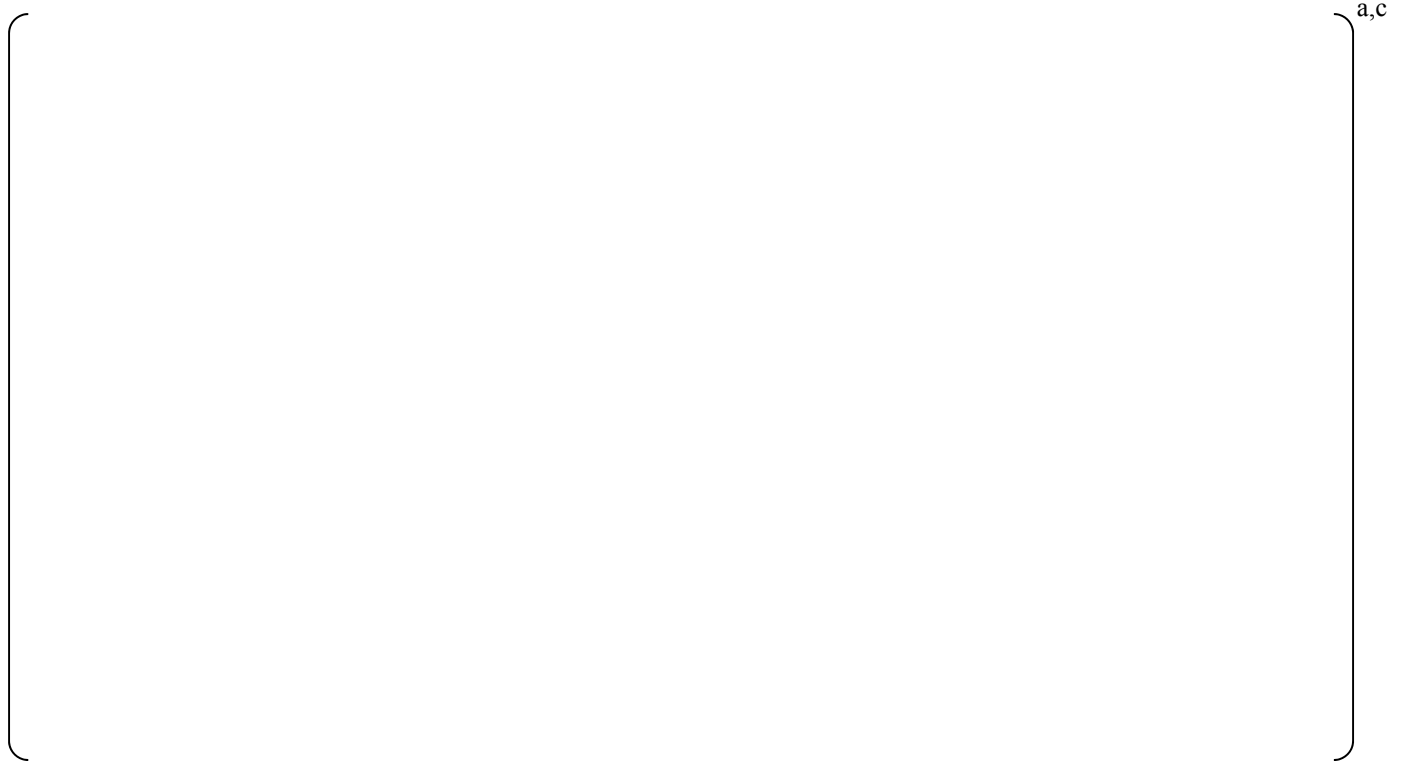


Figure 117-13: Loop Seal Pressure Differential with Results from DLW Plant Break Spectrum Study 2-inch Break



**Figure 117-14: Loop Seal Pressure Differential with Results from DLW Plant Break Spectrum Study
3-inch Break**



**Figure 117-15: Loop Seal Pressure Differential with Results from DLW Plant Break Spectrum Study
4-inch Break**



**Figure 117-16: Loop Seal Pressure Differential with Results from DLW Plant Break Spectrum Study
6-inch Break**

Reference(s)

- 117-1) WCAP-16996-P/WCAP-16696-NP, “Realistic LOCA Evaluation Methodology Applied to the Full Spectrum of Break Sizes (FULL SPECTRUM LOCA Methodology),” November 2010.

RAI Question #118: WCOBRA/TRAC-TF2 Upper Plenum Testing Facility Loop Seal Modeling Options Sensitivity Study

RAI Question No. 115 Item (1) requests information regarding user defined parameters, multipliers, and/or options, implemented in WCOBRA/TRAC-TF2 models and correlations relevant to predicting loop seal clearance in PWR plant LOCA analyses, including such related to describing non-stratified flow transition, CCFL, and liquid entrainment mechanisms.

Please provide results from WCOBRA/TRAC-TF2 sensitivity studies based on the UPTF TRAM full-scale separate effect loop seal clearance tests, which show the effect of varying or sampling of parameters, multipliers, and/or options relevant to the prediction of the loop clearance process. Examine each such user defined quantity and describe the bases for allowing variation or proposing sampling of input values. Provide a table, which lists all examined parameters. For the parameters, multipliers, and/or options being subject to variation or sampling, please provide the sampling range and distribution or proposed input values and allowed ranges. For the sampled parameters, such as HS_SLUG, apply the sampling approach used in PWR plant LOCA analyses. For all remaining user defined parameters, multipliers, and/or options, explain the basis for the proposed input values and ranges regardless if a specific user defined quantity is being described a subject to variation or not for the purpose of plant LOCA analyses using the Full Spectrum LOCA methodology. Analyze each parameter individually and independently from the remaining ones. In particular, demonstrate the effect of variation in Cstfru and STRTX input, if variation is allowed in plant LOCA analyses. Please present the WCOBRA/TRAC-TF2 sensitivity results and provide comparisons against UPTF TRAM full-scale separate effect loop seal clearance test data. In addition, provide comparisons among analyzed sensitivity cases, as appropriate.

Response:

See the response to RAI 115.

RAI Question #119: WCOBRA/TRAC-TF2 UPTF Loop Seal Time Step Limit Sensitivity Study

A special case of a user defined parameter of a global importance to code predictions, including loop seal clearance, is the maximum allowable time step size. WCAP-16996-P/WCAP-16996-NP, Volumes I, II, and III, Revision 0, Section 28, "Scoping and Sensitivity Studies," Subsection 28.2.4, "Time Step and Convergence Criteria Studies – SBLOCA," analyzes the impact of different DTMAX values on PWR plant LOCA predictions and notes that observed "differences among the cases arise from the prediction of loop seal clearance timing and extent of clearance." In the analyzed plant LOCA sensitivity studies, time step upper limits of 1 millisecond, 2 milliseconds, and 5 milliseconds were used.

Considering uncertainty in PWR plant LOCA analyses, WCAP-16996-P/WCAP-16996-NP, Volumes I, II, and III, Revision 0, Subsection 29.3.3, "Uncertainty Associated with Maximum Time Step Size," explains that the maximum allowable time step size in WCOBRA/TRAC-TF2 is set by the user through the DTMAX input parameter. The subsection states that "WCOBRA/TRAC-TF2 uses DTMAX as the time step throughout significant portions of the transient." It also explains that "in the analysis, a choice of DTMAX is made and is applied in all transients." Thus, DTMAX is not sampled in PWR plant LOCA analysis using the Full Spectrum™ LOCA methodology.

The NRC Regulatory Guide 1.157, "Best-Estimate Calculations of Emergency Core Cooling System Performance," May 1989, Subsection 2.1.1, "Numerical Methods," requires that "the effect of time-step size should also be investigated." WCAP-16996-P/WCAP-16996-NP, Volumes I, II, and III, Revision 0, Section 18, "Loop Seal Clearance," does not examine the impact of the maximum allowable time step size on WCOBRA/TRAC-TF2 prediction results in assessing the code capabilities to predict loop seal clearance.

Considering the importance WCOBRA/TRAC-TF2 capabilities to predict the loop seal clearance phenomenon, please present sensitivity results based on the UPTF TRAM full-scale separate effect loop seal clearance tests that show the effect of the maximum allowed time step size. Demonstrate if reduction of the maximum allowed time step size can lead to obtaining code predictions that remain insensitive, when considering major predicted quantities, to further restrictions of the maximum allowed time step size. Please plot the WCOBRA/TRAC-TF2 sensitivity results and provide comparisons against UPTF TRAM full-scale separate effect loop seal clearance test data. In addition, provide comparisons among examined sensitivity cases, as appropriate.

Response:

The original UPTF loop seal validation cases were performed with a maximum time step size of []^{a,c}, which is greater than the typical time step used for plant analyses, which generally range between []^{a,c}

A time step study was performed using the following maximum time step sizes for the symmetric bend cases used in response to RAI 113:

[

] ^{a,c}

Figure 119-1 provides a comparison of the residual liquid level versus the modified Froude number for the 3-bar cases, and Figure 119-2 provides a comparison of the residual liquid level for the 15-bar cases. Figure 119-3 provides a comparison of the differential pressure across the loop seal for the 3-bar cases, and Figure 119-4 provides a comparison of the differential pressure across the loop seal for the 15-bar cases. As seen from the figures [

] ^{a,c}



Figure 119-1: Time Step Study – Residual Liquid Level Comparison for the 3-bar Cases



Figure 119-2: Time Step Study – Residual Liquid Level Comparison for the 15-bar Cases



Figure 119-3: Time Step Study – Differential Pressure across the Loop Seal Region for the 3-bar Cases



Figure 119-4: Time Step Study – Differential Pressure across the Loop Seal Region for the 15-bar Cases

**WCAP-16996-P, “Realistic LOCA Evaluation Methodology Applied to the Full Spectrum of Break Sizes
(FULL SPECTRUM LOCA Methodology)”
Request for Additional Information – (Non-Proprietary)
RAIs 96-105 and 107**

April 2014

Westinghouse Electric Company LLC
1000 Westinghouse Drive
Cranberry Township, PA 16066

©2014 Westinghouse Electric Company LLC
All Rights Reserved

Question #96: PWR Upper Head Spray Nozzle Bypass Design Data

Upper head cooling spray nozzles are used in PWR to adjust the coolant temperature in the upper head plenum by providing a relatively small bypass flow of coolant at the cold leg temperature from the upper downcomer region into the upper head plenum. The exact configuration and bypass flow depend on the PWR design and the production line. WCAP-16996-P/WCAP-16996-NP, Volumes I, II, and III, Revision 0, Section 25, "Plant Sources of Uncertainty," Subsection 25.2.2.2, "Fluid Conditions Modeling Approach," explains that "typically, plants can be separated into two categories: those with sufficient bypass flow to maintain (T_{UH}) near (T_{cold}), and those with low bypass flow, in which (T_{UH}) remains close to T_{hot} ." Taking into account that the upper head-to-downcomer bypass flow affects the upper head initial temperature at steady-state, Subsection 25.2.2.2, states that "the initial temperature of the fluid in the upper head (T_{UH}) has been found to strongly affect the blowdown PCT in other evaluation models (for Large Break LOCA)." During small break LOCA, this bypass releases steam from the upper plenum and the resulting "venting has a high importance during the loop seal clearing period when it relieves some of the core two-phase level depression," as explained in WCAP-16996-P/WCAP-16996-NP, Volumes I, II, and III, Revision 0, Section 29, "Assessment of Uncertainty Elements," Subsection 29.5.3, "Upper Head." Subsection 29.5.3 also explains that "the ability to vent steam through the upper head is strongly dependent on the flow area of the spray nozzles, which is the flow path connecting the upper head and the downcomer" and states that "the spray nozzle bypass itself is modeled in a best-estimate manner."

- (1) Please explain if PWR upper head spray nozzle channels and relevant design features are modeled by implementing certain hydraulic components, component features, and/or activation of specific modeling options in WCOBRA/TRAC-TF2 vessel models of PWR plants and provide their corresponding description.
- (2) WCAP-16996-P/WCAP-16996-NP, Volumes I, II, and III, Revision 0, Section 26, "WCOBRA/TRAC-TF2 Model of Pilot Plants," Subsection 26.4, "Steady State Calculation/Calibration," states that "core bypass flow (including the thimble bypass flow and the spray nozzle flow) should closely match those provided by the mechanical design data." Please explain what "mechanical design data" of the upper head spray nozzles is used to simulate these nozzles in WCOBRA/TRAC-TF2 vessel models of PWR plants.
- (3) Please identify design data of upper head spray nozzles, including any relevant reactor features and conditions, such as number of spray nozzles, nozzle diameters, lengths, loss coefficients, flow areas, and other geometric dimensions and conditions, that are used for the upper head bypass simulation in WCOBRA/TRAC-TF2 vessel models. Explain the source, availability, and accuracy of data quantifying upper head bypass and explain how such bypass flow data is obtained for PWR plants of interest. Clarify how the design data is used in developing COBRA/TRAC-TF2 PWR plant models used for the purposes of LOCA analyses. Provide a table that provides the typical ranges for these parameters.
- (4) Please provide the range of spray nozzle bypass capacities for PWR plants included in the scope of intended WCOBRA/TRAC-TF2 applications for LOCA analyses and estimate the uncertainties associated with provided PWR upper head spray nozzle bypass capacities.

- (5) Please explain how Items (1) through (4) above relate to the statement that "the spray nozzle bypass itself is modeled in a best-estimate manner" in WCOBRA/TRAC-TF2 PWR plant LOCA analyses. Please explain how the information requested in Items (1) through (4) is taken into consideration in ensuring that "the spray nozzle bypass itself is modeled in a best-estimate manner." Describe any other relevant WCOBRA/TRAC-TF2 PWR plant model details and modeling features if implemented in the FSLOCA™ methodology in this regard.

Response:

- (1) The Pressurized Water Reactor (PWR) upper head spray nozzle design features are [

] ^{a,c} Please see
the responses to Items (2) and (3) below for additional information.

- (2) The "mechanical design data" being referred to in Subsection 26.4 of WCAP-16996-P [96-1] is the plant-specific best-estimate upper head spray nozzle bypass flow data generated by the Westinghouse Reactor Internals Design and Analysis group, using the PWR plant- specific upper head spray nozzle design data and features as discussed in the response to Item (3) below.

- (3) As noted in the response to Items (1) and (2) above, the [

] ^{a,c} from
Idelchik, I.E. "Handbook of Hydraulic Resistance" [96-2].

The typical upper head spray nozzle flow area and loss coefficient for Westinghouse- designed plants are provided below.

FULL SPECTRUM™ and FSLOCA™ are trademarks in the United States of Westinghouse Electric Company LLC, its subsidiaries and/or its affiliates. These marks may be used and/or registered in other countries throughout the world. All rights reserved. Unauthorized use is strictly prohibited. Other names may be trademarks of their respective owners

Westinghouse-Designed Plants	Upper Head Spray Nozzle Total Flow Area (in ²)	Upper Head Spray Nozzle Loss Coefficient (-)
[
Notes: 1.)] ^{a,c} 2.) UHI = Upper Head Injection. Note that UHI refers to the design of the plant, but is not active		

- (4) The range of upper head spray nozzle bypass capacities for Westinghouse-designed plants is shown below. The associated uncertainty on the upper head spray nozzle bypass flow provided below is [

] ^{a,c}

- (5) As discussed in the responses above, the plant-specific best-estimate upper head spray nozzle bypass flow is calculated by the Westinghouse Reactor Internals Design and Analysis group using the PWR plant-specific design data and features of the upper head spray nozzles at []^{a,c} To ensure that the upper head spray nozzle bypass is modeled in a best-estimate manner, the [

] ^{a,c}

References:

- 96-1) WCAP-16996-P, "Realistic LOCA Evaluation Methodology Applied to the Full Spectrum of Break Sizes (FULL SPECTRUM LOCA Methodology)," November 2010.
96-2) Idel'Chik, I. E., 1960, Handbook of Hydraulic Resistance," AEC-tv-6630.

Question #97: PWR Upper Head Spray Nozzle Bypass Flow Tune-up

Considering steady-state acceptance criteria for plant initial conditions, WCAP-16996-P/WCAP-16996-NP, Volumes I, II, and III, Revision 0, Section 26, "WCOBRA/TRAC-TF2 Model of Pilot Plants," Subsection 26.4, "Steady State Calculation/Calibration," provides Table 26.4-1, "Criteria for an Acceptable Steady-State," which contains a checklist with 17 significant parameters "to verify whether these variables have reached their acceptable steady-state values." Item (12) in this table lists the "Upper Head Nozzle Flow/Vessel Flow" variable and provides a corresponding acceptance criterion, according to which the "calculated value" should be within []^{a,c} of the "desired value."

Considering application aspects related to the spray nozzle bypass modeling, WCAP-16996-P/WCAP-16996-NP, Volumes I, II, and III, Revision 0, Section 21, "ROSA-IV Test Simulations," Subsection 21.11.3, "Spray Nozzle Bypass Ranging Sensitivity with the SB-CL-18 Test," states that "during the steady state tune-up procedure, the bypass flow through the spray nozzle is adjusted to be within []^{a,c} of the desired value, established for each plant."

- (1) Please explain how "the bypass flow through the spray nozzle is adjusted to be within []^{a,c} of the desired value, established for each plant" and describe the "steady state tune-up procedure" used to achieve this. Identify plant model input variables and related features that are subject to this "steady state tune-up" and describe how such parameters are varied. Explain if these parameters are subject to variation within certain allowable limits and, if this is the case, please describe how the corresponding limits are established.
- (2) Please explain how the "desired value" for the variable "Upper Head Nozzle Flow/Vessel Flow" identified in Table 26.4-1, "Criteria for an Acceptable Steady-State," is established for each plant and clarify how it is used in PWR LOCA analyses using WCOBRA/TRAC-TF2.
- (3) WCAP-16996-P/WCAP-16996-NP, Volumes I, II, and III, Revision 0, Subsection 26.4 states that "core bypass flow (including the thimble bypass flow and the spray nozzle flow) should closely match those provided by the mechanical design data, within the tolerances given in Table 26.4-1. The allowable variation is essentially equivalent to a 1 percent variation in the loop flowrate." Please explain the meaning of the statement that []^{a,c} Clarify how this statement relates to the criterion that the "calculated value" of the "Upper Head Nozzle Flow/Vessel Flow" parameter is within []^{a,c} of the "desired value."
- (4) The "steady state tune-up" procedure establishes the upper head bypass flow under the reactor initial conditions at steady-rate operation. Please explain how PWR vessel model hydraulic features implemented in WCOBRA/TRAC-TF2 PWR plant models and adjustments to such model features aimed at verifying that a certain "desired value" bypass flow is achieved at the end of an initial steady-state plant simulation ensure that the bypass flow is realistically modeled during a LOCA transient calculation.
- (5) Please explain how the information requested in Items (1) through (4) is taken into consideration in ensuring that "the spray nozzle bypass itself is modeled in a best-estimate manner." Describe any other relevant WCOBRA/TRAC-TF2 PWR plant

model details and modeling features if implemented in the Full Spectrum LOCA methodology in this regard.

Response:

- (1) As discussed in the responses to RAI #96, the PWR plant design features of the upper head spray nozzles are []^{a,c} in the WCOBRA/TRAC-TF2 PWR models. To achieve the desired upper head spray nozzle bypass flow at the end of the steady run, the []

[]^{a,c} of the desired value (D.V.) as shown in Table 26.4-1 of WCAP-16996-P. As noted in the responses to RAI #96, the desired value is obtained from the Westinghouse Reactor Internals Design and Analysis group, and is calculated based on the PWR plant-specific design data and features of the upper head spray nozzles at []^{a,c}

- (2) Please see the response to RAI #96.

- (3) This means that the []

[]^{a,c} An

example is provided below to illustrate this:

From Table 26.2-1 of WCAP-16996-P, the desired loop total flowrate for V. C. Summer []

[]^{a,c}

The typical upper head spray nozzle bypass ranges for Westinghouse-designed plants are provided in the response to RAI #96(4). The []^{a,c} criterion for the "Upper Head Nozzle Flow/Vessel Flow" is []

[]^{a,c} meet the tolerances provided in Table 26.4-1 of WCAP-16996-P.

- (4) See the response to RAI #107(2).

- (5) As discussed in the response to RAI #96, the plant-specific desired best-estimate upper head spray nozzle bypass flow is calculated by the Westinghouse Reactor Internals Design and Analysis group using the PWR plant-specific design data and features of the upper head spray nozzles at []^{a,c} To ensure that the upper head spray

nozzle bypass is modeled in a best-estimate manner, the calculated upper head spray nozzle bypass flow at the end of the PWR steady state run must agree with the plant-specific best-estimate value provided by the Westinghouse Reactor Internals Design and Analysis group within the tolerance shown in Table 26.4-1 of WCAP-16996-P. [

]^{a,c}

Reference:

- 97-1) WCAP-16996-P, "Realistic LOCA Evaluation Methodology Applied to the Full Spectrum of Break Sizes (FULL SPECTRUM LOCA Methodology)," November 2010.

Question #98: PWR Upper Head Temperature Tune-up

The upper head liquid temperature is dependent on the venting flow between the upper head and the reactor downcomer through the upper head spray nozzles.

WCAP-16996-PW/CAP-16996-NP, Volumes I, II, and III, Revision 0, Section 29, "Assessment of Uncertainty Elements," Subsection 29.5.3, "Upper Head," states that "the initial upper head liquid temperature is calibrated during the steady-state calculation." WCAP-16996-PW/CAP-16996-NP, Volumes I, II, and III, Revision 0, Section 26, "WCOBRA/TRAC-TF2 Model of Pilot Plants," Subsection 26.4, "Steady State Calculation/Calibration," Table 26.4-1, "Criteria for an Acceptable Steady-State," includes Item (14), which lists the "Upper Head Temperature" variable and provides a corresponding acceptance criterion, according to which the "calculated value" should be within []^{a,c} of the "desired value."

- (1) Please explain how the "desired value" for the variable "Upper Head Temperature" identified in Table 26.4-1, "Criteria for an Acceptable Steady-State," is established for each plant and describe how it is used in PWR LOCA analyses using WCOBRA/TRAC-TF2.
- (2) As explained in WCAP-16996-PW/CAP-16996-NP, Volumes I, II, and III, Revision 0, Subsection 29.5.3, "the initial upper head liquid temperature is calibrated during the steady-state calculation" so that it is within []^{a,c} of the "desired value." In addition, Subsection 29.5.3 states that "upper head liquid temperature uncertainty is considered by varying the temperature based on the ranging of vessel average temperature." As the upper head liquid temperature is influenced by the bypass flow between the upper head and the reactor downcomer through the upper head spray nozzles, please explain if the process of upper head initial temperature calibration and its uncertainty consideration have any effects on the spray bypass flow modeling.
- (3) For PWR small break LOCA analyses, adequate prediction of the upper head bypass flow is of primary importance. WCAP-16996-PW/CAP-16996-NP, Volumes I, II, and III, Revision 0, Section 29, "Assessment of Uncertainty Elements," Subsection 29.5.3, "Upper Head," states that "the spray nozzle bypass itself is modeled in a best-estimate manner" in plant LOCA analyses using WCOBRA/TRAC-TF2. Please explain how this is done for PWR small break LOCA analyses, taking into consideration the information requested in Items (1) and (2) above, to ensure that the upper head bypass flow is not inappropriately affected due to upper head temperature adjustments.

Response:

- (1) For Westinghouse-designed plants, the upper head region fluid temperature can [

]^{a,c} The plant-specific best-estimate

upper head temperature is calculated by the Westinghouse Reactor Internals Design and Analysis group at [

]^{a,c} used to calculate the plant-specific

best-estimate upper head spray nozzle bypass flow (see response to RAI #96). The

upper head spray nozzle flow passes vessel inlet temperature fluid into the upper head region. Generally speaking, however, this is [

]^{a,c}

The plant-specific best-estimate upper head temperature provided by the Westinghouse Reactor Internals Design and Analysis group is used as the target (i.e., desired) value for calibrating the PWR model. See the response to Item (2) below for additional information on the calibration process.

(2) The process of upper head initial temperature calibration [

]^{a,c} so that the calculated upper head temperature is within the []^{a,c} of the desired value per Table 26.4-1 of WCAP-16996-P at the end of the steady state run. In addition, note that [

]^{a,c} meet the tolerances provided in Table 26.4-1 of WCAP-16996-P.

(3) Please see the response to RAI #97(5) and the response to Item (2) above.

Reference:

98-1) WCAP-16996-P, "Realistic LOCA Evaluation Methodology Applied to the Full Spectrum of Break Sizes (FULL SPECTRUM LOCA Methodology)," November 2010.

Question #99: PWR Upper Head Spray Nozzle Bypass in WCOBRA/TRAC-TF2 Pilot Plant Models

Figures 26.2-3 through 26.2-6 in WCAP-16996-P/WCAP-16996-NP, Volumes I, II, and III, Revision 0, Section 26, "WCOBRA/TRAC-TF2 Model of Pilot Plants," Subsection 26.2.1, "V. C. Summer WCOBRA/TRAC-TF2 Nodalization," show the RPV nodalization for the three-loop V. C. Summer plant. As seen from Figure 26.2-3, "Virgil C. Summer Vessel Model Noding Diagram," the vessel is divided into nine vertical sections with Section 1 at the bottom and Section 9 at the top. In this model, Section 7, which contains two vertical cells, represents the uppermost region and "extends vertically from the top of the hot leg to the top of the upper support plate." The downcomer region in Section 7 is modeled by nine channels occupying the peripheral ring, Channels 40, 41, 42, 82, 83, 84, 85, 86, and 87. As described, each of these channels "represent one-ninth of the downcomer annulus volume between the vessel inner wall and the core barrel outer wall." Section 8, which has one vertical cell, models the lower section of the upper head region and "extends vertically from the top of the upper support plate to the top of the upper guide tube." As seen from Figure 26.2-6, "Virgil C. Summer Vessel Sections 7 through 9," this section is divided into two radial rings with the interface boundary "formed by the cylinder which intersects the inside of the upper head sphere at the top of the upper guide tube." Channels 47, 88, and 89 occupy the outer ring and each of them include one-third of the volume in the upper head outer region. Subsection 26.2.1 states that "Channels 40 through 42 and 82 through 87, however, connect vertically to vessel Section 8 via the upper head spray nozzles."

The Beaver Valley Unit 1 three-loop PWR RPV nodalization is described in WCAP-16996-P/WCAP-16996-NP, Volumes I, II, and III, Revision 0, Subsection 26.3.1, "Beaver Valley Unit 1 WCOBRA/TRAC-TF2 Nodalization." The spray nozzle bypass is modeled in a similar manner and the subsection repeats that "Channels 40 through 42 and 82 through 87, however, connect vertically to vessel Section 8 via the upper head spray nozzles."

- (1) Please describe how the bypass flow path through the spray nozzles connecting the downcomer and upper head regions were represented in the WCOBRA/TRAC-TF2 pilot models for the V. C. Summer and Beaver Valley Unit 1 PWR plants described in Section 26. Provide a table that lists the input parameters associated with hydraulic components and modeling features employed to simulate the spray nozzle passages. Provide noding details that show how Channels 40 through 42 and 82 through 87 "connect vertically to vessel Section 8 via the upper head spray nozzles" for each vessel model.
- (2) Please provide spray nozzles geometric data and drawings of the spray nozzles for both pilot plants and explain how plant design data was used in modeling the spray nozzle bypass flow passages in the WCOBRA/TRAC-TF2 vessel models for the V. C. Summer and Beaver Valley Unit 1 PWR plants. Please explain how spray nozzle design data was used to model the spray nozzle bypass and calculate the input parameters requested in Item (1) above.
- (3) Please explain how the "steady state tune-up procedure," used to "adjust" the bypass flow through the spray nozzle "within []^{a,c} of the desired value, established for each plant," was performed for the V. C. Summer and Beaver Valley Unit 1 pilot PWR plants. Describe how the "desired value" for the variable "Upper Head Nozzle Flow/Vessel Flow" listed in Table 26.4-1, "Criteria for an Acceptable Steady-State,"

was established for each plant and compare the "calculated value" versus the "desired value" at the end of the steady-state runs for both plants. Also, please provide a table that lists all parameters subject to modification "during the steady state tune-up procedure." For each such parameter, provide its values at the beginning and at the end of the "steady state tune-up procedure" as well as the allowable variation range listing each parameter in a separate column.

Response:

- (1) The upper head bypass flow path through the spray nozzles connecting the downcomer and upper head region is shown in Figures 26.2-3 and 26.3-3 of WCAP-16996-P [99-1] for V. C. Summer and Beaver Valley Unit 1, respectively. The top of the upper head spray nozzles is modeled at the top of downcomer Channels 40 through 42, and 82 through 87 in Vessel Section 7. Downcomer Channels 40 through 42, 82 through 84, and 85 through 87 in Vessel Section 7 are vertically connected to Upper Head Channels 47, 88 and 89 respectively in Vessel Section 8 via the upper head spray nozzles as shown in Figures 26.2-3 and 26.3-3 for V. C. Summer and Beaver Valley Unit 1, respectively. Additionally, the [

]^{a,c} so that the

calculated upper head bypass flow is within the []^{a,c} of the desired value per Table 26.4-1 of WCAP-16996-P at the end of the steady state run.

- (2) Please see the response to RAI #96.
- (3) Please see the response to RAI #97(1) for the steady state tune-up procedure performed to achieve the desired upper head spray nozzle bypass flow. Please see the response to RAI #96 for the establishment of the desired upper head spray nozzle bypass flow for each plant.

A table that lists all parameters subject to modification "during the SS tune-up procedure" for Beaver Valley Unit 1 was previously provided as Table 3-1 in LTR-NRC-13-70 [99-2]. In addition, desired values and calculated values from the last iteration step output are provided in Tables 3.4, 3.6 and 3.7 of LTR-NRC-13-70. The process and relative values for V. C. Summer would be similar.

References:

- 99-1) WCAP-16996-P, "Realistic LOCA Evaluation Methodology Applied to the Full Spectrum of Break Sizes (FULL SPECTRUM LOCA Methodology)," November 2010.
- 99-2) LTR-NRC-13-70, "Summary of July 2013 NRC Code Workshop and August 2013 NRC Audit of the FULL SPECTRUM LOCA (FSLOCA) Evaluation Model (Proprietary/Non-Proprietary)," October 10, 2013.

The series of NRC's questions that are addressed herein are related to the modeling of various core bypass flows in the ROSA LSTF tests selected to support the WCOBRA/TRAC-TF2 code validation. The requested information covers three types of bypass flows - flow through the spray nozzles, bypass leakage through the hot leg leak line and vessel internal leaks. Responses to individual parts of the various questions are provided as appropriate. Integral response is provided at the end to address topics that are common to multiple questions.

Question #100: Upper Head Spray Nozzle Bypass in LSTF Tests

To model the upper head spray nozzle bypass, the LSTF vessel featured 8 spray nozzle openings, each with a 3.4-mm (0.134-in) inlet ID, a 10-mm (0.394-in) exit inner diameter, and a 175-mm (6.9-in) length, where inlet and exit values correspond to normal flow direction from the downcomer into the upper head at normal operation. Based on the spray nozzle inlet diameter, the total spray nozzle bypass flow area amounts to 0.726 cm^2 ($7.826 \times 10^{-4} \text{ ft}^2$), which corresponds to an equivalent opening diameter of 0.961 cm (0.379 inch). Detailed geometrical data related to the upper head spray nozzles can be found in Figure 5.2.4, "Coolant Flow Path in Pressure Vessel," in Figure 5.2.6, "Downcomer-Upper Head Spray Nozzle Details," and in Figure 5.2.7, "Upper Head Cross Section," in "ROSA-IV Large Scale Test Facility (LSTF) System Description," Japan Atomic Energy Research Institute Report JAERI-M 84-237, January 1985.

- (1) Please provide a table that documents the spray nozzle bypass capacities as measured in the LSTF tests that are analyzed in WCAP-16996-P/WCAP-16996-NP, Volumes I, II, and III, Revision 0, Section 21, "ROSA-IV Test Simulations," and in Section 24, "Assessment of Compensating Error in Evaluation Model Using WCOBRA/TRAC-TF2." Describe each individual LSTF test in a separate row including the following parameters, each in a separate column: test identifier (e.g. SB-CL-05), test date, data source documents, upper plenum-to-upper head bypass unit, and experimental upper plenum-to-upper head bypass value. Explain the source, availability, and accuracy of data quantifying the LSTF upper head bypasses in these tests and explain if the bypass data was examined and qualified as part of the WCOBRA/TRAC-TF2 assessment.
- (2) Please compare LSTF upper head spray nozzle bypass data against downcomer-to-upper head bypass capacities simulated in WCOBRA/TRAC-TF2 LSTF test analyses presented in WCAP-16996-P/WCAP-16996-NP, Volumes I, II, and III, Revision 0, Section 21, "ROSA-IV Test Simulations," and in Section 24, "Assessment of Compensating Error in Evaluation Model Using WCOBRA/TRAC-TF2." In the table requested in Item (1) above, include an additional column, which documents the downcomer-to-upper head bypass values for all WCOBRA/TRAC-TF2 LSTF tests used in the simulations in consistent units. Clearly state if the downcomer-to-upper head bypass capacities in the WCOBRA/TRAC-TF2 LSTF test simulations were adjusted to account for any effects other than the downcomer-to-upper head bypass through the upper head spray nozzle openings present in the LSTF pressure vessel.

Response:

The requested information is provided in Table 2.3-1 of the integrated response.

Question #101: Upper Head Spray Nozzle Bypass in LSTF WCOBRA/TRAC-TF2 Model

WCAP-16996-P/WCAP-16996-NP, Volumes I, II, and III, Revision 0, Section 21, "ROSA-IV Test Simulations," describes the noding of the LSTF pressure vessel in Subsection 21.3, "Description of WCOBRA/TRAC-TF2 Model for ROSA/LSTF-IV." Figure 21.3-1, "WCOBRA/TRAC-TF2 Model of LSTF Pressure Vessel," Figure 21.3-5, "LSTF Pressure Vessel Sections 7 and 8," and Figure 21.3-6, "LSTF Pressure Vessel Sections 9 and 10," show nodalization details pertinent to modeling of the bypass flow path between the downcomer and the upper head.

- (1) Figure 21.3-1, "WCOBRA/TRAC-TF2 Model of LSTF Pressure Vessel," illustrates that the upper head bypass nozzles were modeled as []^{a,c} with a certain length. Please describe how the bypass flow paths through the upper head spray nozzles in the LSTF test vessel were represented in the WCOBRA/TRAC-TF2 vessel model of LSTF. Provide noding details that show how []^{a,c} connect vertically to hydraulic components in vessel Section 9 to represent the upper head spray nozzles. Include a table that lists the input parameters associated with hydraulic components and modeling features employed to model these bypass flow paths in the LSTF pressure vessel and provide the input values for all LSTF tests analyzed in WCAP-16996-P Revision 0 Section 21, "ROSA-IV Test Simulations," and in Section 24, "Assessment of Compensating Error in Evaluation Model Using WCOBRA/TRAC-TF2.
- (2) Please explain how the spray nozzles geometric and other design data were used to model the spray nozzle bypass flow passages between the downcomer and upper head in the WCOBRA/TRAC-TF2 model of the LSTF pressure vessel and to calculate the input parameters requested in Item (1) above.
- (3) Table 21.4-1, "Steady-State Parameter Checklist (Initial Conditions) for the SB-CL-18 Test," provides a downcomer-to-upper head flow rate of 0.30 percent of the core flow for both the "target (measured)" and "modeled" parameters. Table 21.5-1, "Steady- State Parameter Checklist (Initial Conditions) for the SB-CL-05 Test," lists a value of ~0.70 percent of "core flow" for the "modeled" downcomer-to-upper head flow rate and provides the "target (measured)" value as "N/A." Table 21.9-1, "Initialization of the SB-CL-02 Natural Circulation Test Simulation," gives a "target" value of 0.9% and a "calculated" value of 0.70 percent for the downcomer-to-upper head flow rate in percentage of "total core" at the end of Stage 1 of the LSTF experiment, which was run at nominal conditions. Please explain how the downcomer-to-upper head bypass flow rates, defined as "target (measured)" and "modeled" in Tables 21.4-1 and 21.5-1 and as "target" and "calculated" in Table 21.9-1, were established and explain the reported differences. Clarify why the "calculated" value, provided in Table 21.9-1, resulted in 0.70 percent.
- (4) The downcomer-to-upper head flow is provided in Table 21.9-1 in units of "kg/sec" and "percent total core." It appears that the provided percentage values correspond to the ratio of the downcomer-to-upper head flow rate to the total loop flow rate, which parameter is also listed in the table. At the same time, the downcomer-to- upper head flow is provided in Tables

21.4-1 and 21.5-1 in percentage units described as "percent core flow." The listed values correspond to the ratio of the downcomer-to-upper head flow rate to the core inlet flow rate, which quantity is also listed in these tables. Please explain why different definitions for the downcomer-to-upper head flow ratio were used for the percentage values in these tables.

- (5) Please explain if a "steady state tune-up procedure" was used to "adjust" the bypass flow through the spray nozzles in the WCOBRA/TRAC-TF2 model of the LSTF pressure vessel. In such a case, please describe how the "desired value" for the downcomer-to-upper head bypass flow was established for the analyzed LSTF experiments. Please provide a table that lists all parameters subject to modification "during the steady state tune-up procedure." For each listed parameter, provide the corresponding values at the beginning and at the end of the "steady state tune-up procedure" as well as the allowable variation range for the parameter. Please list each parameter in a separate column in the table.
- (6) Provide a table that documents the "calculated value" for the downcomer-to-upper head bypass at the end of the steady-state runs and the corresponding "desired values" for all LSTF tests analyzed in WCAP-16996-P/WCAP-16996-NP, Volumes I, II, and III, Revision 0, Section 21, "ROSA-IV Test Simulations," and in Section 24, "Assessment of Compensating Error in Evaluation Model Using WCOBRA/TRAC-TF2."

Response:

For the response to Part (1), see Downcomer-to-Upper Head Bypass Modeling in Section 2.1 of the integrated response.

Response to Part (2): The design data of the spray nozzle []^{a,c}; see Section 2.1 of the integrated response for further detail.

For the response to Part (3), see Section 2.1 of the integrated response and Note (4) of Table 2.3-1 therein.

Response to Part (4): The ST-NC-02 report (JAERI-M 88-215, Table 1) provides flow rate, without specifying whether this is loop or core flow rate; for the ST-NC-02 test it was assumed that Table 1 of JAERI-M 88-215 reports loop flows. Therefore the values of the DC-to-UH bypass flow provided in Table 21.9-1 are in "% of total loop flow". The usage of "% core flow" is incorrect; this statement will be corrected to read "% of total loop flow" in the updated topical report.

The difference in the definition of the downcomer-to-upper head flow ratio comes from the fact that for the 5% break test SB-CL-18 and SB-CL-05 the respective test reports (JAERI-M 89-027 and JAERI-memo 61-056) provided core inlet flows, which were then used as a basis for the downcomer-to-upper head bypass ratio.

Response to Part (5): [

]^{a,c}; see Downcomer-to-Upper Head Bypass Modeling in Section 2.1 of the integrated response for discussion of the spray bypass tune-up.

Response to Part (6): The requested information is included in Table 3.2-1 of the integrated response.

Question #102: LSTF Upper Head Spray Nozzle Bypass Relevance to PWR

As reported by Y. Kukita et al., "Quasi-Static Core Liquid Level Depression and Long-Term Core Uncovery During a PWR LOCA," Nuclear Safety, Vol. 34, No. 1, 1993, pp. 33-48, the LSTF pressure vessel bypasses included upper head spray nozzles and a hot-leg nozzle leak line between each hot leg and the downcomer that simulated bypass flow rates of about 0.3 percent and 0.2 percent (for both loops) of the total core flow rate at single-phase (liquid) steady-state operation, respectively. These normal LSTF bypass flow capacities were representative of the upper vessel bypasses of Japanese-built Westinghouse-type PWR plants with a total bypass flow rate of 0.5 percent. According to the same authors, spray nozzle bypass capacities, ranging typically from 1 percent to 4 percent, were representative for most of the U.S. Westinghouse PWR configurations. A bypass of 1.8 percent of the total downcomer mass flow rate for the Westinghouse standardized four-loop single-unit plant described in the Reference Safety Analysis Report (RESAR) RESAR-3S, sometimes referenced to as a "typical" Westinghouse plant, was provided by the authors. A special 0.5-inch tubing bypass line connected the downcomer to the upper head in the LSTF pressure vessel to simulate the leakage between these two components in commercial PWRs. A somewhat broader range from 0.5 percent to 4 percent of the total core flow for the leakage between the downcomer and the upper head in a commercial PWR is provided by G. G. Loomis and J. E. Streit, "Results of Semiscale Mod-2C Small-Break (5 percent) Loss-of-Coolant Accident Experiments S-LH-1 and S-LH-2," NUREG/CR-4438, EGG-2424, November 1985.

Based on LSTF design data provided in "ROSA-IV Large Scale Test Facility (LSTF) System Description," Japan Atomic Energy Research Institute Report JAERI-M 84-237, January 1985, the total flow area of the LSTF upper head bypass nozzles amounted to 0.726 cm^2 ($7.826 \times 10^{-4} \text{ ft}^2$), which scales to a 35.03 cm^2 (0.0377 ft^2 or 5.43 in^2) PWR bypass flow area with an equivalent opening diameter of 6.68 cm (2.63 inch) based on the volume scaling ratio for the LSTF pressure vessel upper head region.

- (1) Please provide the upper head spray nozzle bypass capacities as scaled to prototypical PWR conditions based on the LSTF upper head spray nozzle bypasses measured in each of the LSTF tests analyzed in WCAP-16996-P/WCAP-16996-NP, Volumes I, II, and III, Revision 0, Section 21, "ROSA-IV Test Simulations," and in Section 24, "Assessment of Compensating Error in Evaluation Model Using WCOBRA/TRAC-TF2." Explain how the LSTF bypass values were scaled to prototypical PWR conditions. List each LSTF test in a separate row and provide both the measured LSTF upper head spray nozzle bypass value and the scaled PWR bypass value.
- (2) Please explain how the PWR upper head spray nozzle bypass values as scaled from the LSTF test data and provided in the table requested in Item (1) above, represent the range of upper head spray nozzle bypass capacities of PWR plants that will be modeled for the purpose of LOCA analyses using WCOBRA/TRAC-TF2.
- (3) According to Y. Kukita et al., "Quasi-Static Core Liquid Level Depression and Long-Term Core Uncovery During a PWR LOCA," Nuclear Safety, Vol. 34, No.1, 1993, pp. 33-48,

ROSA-IV LSTF Test ST-LS-04 was conducted with a vent line connecting the upper plenum top region directly to the upper downcomer annulus to simulate a bypass flow rate of 4 percent compared to a 0.5 percent value in the standard LSTF test vessel bypass geometry. The experiment simulated conditions relevant to PWR plants with large bypass areas. The upper plenum vent line was equipped with a 44-mm (1.73-inch) inner diameter orifice and a valve. If the bypass capacity in ROSA-IV LSTF Test ST-LS-04 is within the range of spray nozzle bypass capacities of PWR plants to be analyzed with WCOBRA/TRAC-TF2, please provide WCOBRA/TRAC-TF2 prediction results for this test. Please compare the obtained results against the experimental measurements for ROSA-IV LSTF Test ST-LS-04 and assess the code performance.

Response:

For the response to Part (1) and (2), see the discussion in Section 2.1 of the integrated response.

For the response to Part (3), as an alternate approach to modeling ST-LS-04, Westinghouse will be presenting simulation results for the Semiscale test S-LH-1 and S-LH-2.

Question #103: Pressure Vessel Internal Leaks in LSTF Tests

According to Y. Kukita et al., "Data Report for ROSA-IV LSTF 5 percent Cold Leg Break LOCA Experiment Run SB-CL-08," Japan Atomic Energy Research Institute Report JAERI-M 89-220, January 1990, modifications to the LSTF design were made during the time period between March 27, 1986 and November 9, 1989 when Test SB-CL-08 was performed. As described in Subsection 2.3.1, "Sealing of Upper Pressure Vessel Internal Leaks," in the report, one modification was performed in May 1986 to seal off an unintentional small bypass leak between the upper plenum and the upper head, which was discovered at the control guide tube penetrations through the upper core support plate during facility checks.

Table 21.1-1, "Selected ROSA-IV Test Series Description and Related Technical Reports," in WCAP-16996-P/WCAP-16996-NP, Volumes I, II, and III, Revision 0, Section 21, "ROSA-IV Test Simulations," states that Test SB-CL-05 was performed on 26 June 1985 when the LSTF pressure vessel internal leak still existed. Therefore, as explained in Subsection 2.3.1, "Sealing of Upper Pressure Vessel Internal Leaks," in JAERI-M 89-220, "Run SB-CL-05 had an estimated flow rate through the upper head spray nozzles during the initial steady state of about 2.1 percent of the total core flow rate (vs. 0.3 percent for Run SB-CL-08)." K. Tasaka et al., "The Results of 5 percent Small-Break LOCA Tests and Natural Circulation Tests at the ROSA-IV LSTF," Nuclear Engineering and Design, Vol. 108, 1988, pp. 37-44, also report, in Table 2, "Test Conditions of 5 percent Break Tests," a 2.1 percent core flow downcomer-to-upper head bypass value for Test SB-CL-05.

Table 21.5-1, "Steady-State Parameter Checklist (Initial Conditions) for the SB-CL-05 Test," in WCAP-16996-P/WCAP-16996-NP, Volumes I, II, and III, Revision 0, Section 21, "ROSA-IV Test Simulations," gives a value of ~0.70 percent in "percent core flow" for the "modeled" downcomer-to-upper head flow rate and lists the "target (measured)" downcomer-to-upper head flow rate value as "N/A." With regard to the hot leg-to-downcomer "target (measured)" leakage flow rate, the table provides a value of ~0.10 kg/s (0.20 percent core flow), which agrees with the data provided in JAERI-M 89-220 (0.05 kg/s per loop) and the value identified by K. Tasaka et al., "The Results of 5 percent Small-Break LOCA Tests and Natural Circulation Tests at the ROSA-IV LSTF," Nuclear Engineering and Design, Vol. 108, 1988, pp. 37-44 (0.2 percent of core flow).

- (1) Please explain why the upper head-to-downcomer bypass, existent in ROSA-IV LSTF Test SB-CL-05 and documented in the above identified sources as amounting to a relatively high value of 2.1 percent of the core flow, was not identified in WCAP-16996-P/WCAP-16996-NP, Volumes I, II and III, Revision 0, Section 21, "ROSA-IV Test Simulations," for the purposes of WCOBRA/TRAC-TF2 assessment analyses based on this test. Please explain the technical basis for determining the appropriateness of an upper head-to-downcomer bypass of ~0.70 percent as documented in the steady-state parameter checklist for the initial conditions obtained for Test SB-CL-05 with WCOBRA/TRAC-TF2 and listed in Table 21.5-1 in WCAP-16996-P/WCAP-16996-NP, Volumes I, II, and III, Revision 0, Section 21.

- (2) Please provide a table that documents if unintentional bypasses between the LSTF upper head and the upper downcomer due to pressure vessel internal leaks existed in any of the LSTF tests analyzed in WCAP-16996-P/WCAP-16996-NP, Volumes I, II, and III, Revision 0, Section 21, "ROSA-IV Test Simulations," and in Section 24, "Assessment of Compensating Error in Evaluation Model Using WCOBRA/TRAC-TF2." Describe each individual ROSA-IV LSTF test in a separate row providing the following test parameters, each in a separate column: test identifier (e.g. SB-CL-05), test date, data source documents, bypass flow unit, unintentional bypass flow between the upper head and upper downcomer due to pressure vessel internal leaks if such were found to exist in the test. In an additional column, please provide the measured downcomer-to-upper head bypass value and state clearly if this downcomer-to-upper head bypass value includes the upper head spray nozzle bypass and any other bypass flows existing in the test. Include in a separate column the bypass value through the vent line connecting the upper plenum top region directly to the upper downcomer annulus to simulate larger spray nozzle bypass capacities or vent line between the upper plenum and the downcomer annulus or the operation of Babcock and Wilcox (B&W)-type core barrel vent valves as it was the case in ROSA-IV LSTF Test SB-CL-07. Explain the source, availability, and accuracy of the data quantifying the unintentional LSTF pressure vessel bypass in these tests. Please explain if the provided bypass data was examined and qualified as part of the WCOBRA/TRAC-TF2 assessment.
- (3) Compare LSTF experimental downcomer-to-upper head bypass data against downcomer-to-upper head bypass capacities simulated in the WCOBRA/TRAC-TF2 LSTF test analyses presented in WCAP-16996-P/WCAP-16996-NP, Volumes I, II, and III, Revision 0, Section 21, "ROSA-IV Test Simulations," and in Section 24, "Assessment of Compensating Error in Evaluation Model Using WCOBRA/TRAC-TF2." In the table requested in Item (2) above, include an additional column documenting, in consistent units, the downcomer-to-upper head bypass values calculated in the WCOBRA/TRAC-TF2 ROSA-IV LSTF test simulations. Clearly state if the downcomer-to-upper head bypass capacities in the WCOBRA/TRAC-TF2 ROSA-IV LSTF test simulations were adjusted to account for downcomer-to-upper head bypass through the upper head spray nozzle openings and any pressure vessel internal leaks, if such were known to exist.

Response:

For the responses to Parts (1) and (3) of the question, see Section 2.1 of the integrated response.

For the response to Part (2), with the exception of the natural circulation test ST-NC-02, [

]^{a,c}; see

discussion Uncontrolled Internal Vessel Leakages in Section 2.1 of the integrated response for more detail.

Question #104: Hot Leg-to-Downcomer Bypass Modeling in LSTF and PWR LOCA Analyses

A bypass leakage between the upper downcomer region and the upper plenum occurs in the PWR design via the gap opening along the periphery of the hot leg (HL) nozzles that penetrate through the downcomer. In the LSTF pressure vessel used in the ROSA-IV tests, the hot leg-to-downcomer (HL-to-DC) leakage was simulated by two dedicated hot leg leak lines. The bypass flow through these hot leg leak lines was one of the test variables in the LSTF SBLOCA tests according to Y. Kukita et al., "Data Report for ROSA-IV LSTF 5 percent Cold Leg Break LOCA Experiment Run SB-CL-08," Japan Atomic Energy Research Institute Report JAERI-M 89-220, January 1990.

Design details for the LSTF hot leg leak lines are provided in Tables 5.2.2, 5.2.4, 5.2.10, 5.7.1, 5.7.4, and A.1.1 in "ROSA-IV Large Scale Test Facility (LSTF) System Description," Japan Atomic Energy Research Institute Report JAERI-M 84-237, January 1985. According to the information provided in this report, each hot leg leak line was connected to the pressure vessel downcomer via a 21.2-mm (0.835-inch) inner diameter nozzle (Tags N-11a and N-11b) and to the hot leg via a Nominal Size 1 Schedule 160 nozzle (Tags N-1a and N-1b). The lines were equipped with a 0.687 contraction ratio orifice flow meter (Tags FE-010-HLA and FE-150-HLB) and a 0.24 kg/s normal flow capacity hand control valve (Tags HCV-010 and HCV-150) installed in each line.

WCAP-16996-P/WCAP-16996-NP, Volumes I, II, and III, Revision 0, Section 21, "ROSA-IV Test Simulations," Subsection 21.11.2, "SB-CL-18 Simulation Without Hot Leg Nozzle Bypass Flow," explains that the hot leg leakage was modeled in the WCOBRA/TRAC-TF2 pressure vessel model of LSTF with Gaps 21 and 22 as shown in Figure 21.3-4, "LSTF Pressure Vessel Sections 5 and 6."

- (1) According to H. Kumamaru et al., "ROSA-IV/LSTF Cold Leg Break LOCA Experiment Run SB-CL-18 Data Report," Japan Atomic Energy Research Institute Report JAERI-M 89-027, March 1989, Table 3.2, "Specified Operational Setpoints and Conditions for Run SB-CL-18," a HL-to-DC leakage of 0.049 kg/s per loop is provided as a "specified" operational setpoint for LSTF Test SB-CL-18. At the measured core inlet flow rate of 48.7 kg/s provided in Table 3.1, "Initial Conditions for Run SB-CL-18," in the same report, the resulting total HL-to-DC leakage via the gaps of both LSTF hot leg nozzles as a fraction of the core flow rate is:

$$\text{HL-to-DC leakage} = [(0.049 \text{ kg/s/loop}) \times (2 \text{ loops})] / (48.7 \text{ kg/s}) = 0.0020 = 0.20\%.$$

K. Tasaka et al., "The Results of 5 percent Small-Break LOCA Tests and Natural Circulation Tests at the ROSA-IV LSTF," Nuclear Engineering and Design, Vol. 108, 1988, pp. 37-44, report a downcomer-to-hot leg bypass of 0.2 percent of core flow for LSTF Test SB-CL-05 in Table 2, "Test Conditions of 5 percent Break Tests."

Table 21.4-1, "Steady-State Parameter Checklist (Initial Conditions) for the SB-CL-18 Test," provides a HL-to-DC leakage flow rate of 0.124 kg/s or 0.25 percent of the core flow rate for both the "target (measured)" leakage and the "modeled" leakage. Table 21.5-1, "Steady-State Parameter Checklist (Initial Conditions) for the SB-CL-05 Test," lists ~0.10 kg/s or 0.20 percent "core flow" for the "target (measured)" HL-to-DC leakage and 0.127 kg/s or 0.26 percent "core flow" rate for the "modeled" HL-to-DC leakage. Please clarify how the "target (measured)"

leakage and the "modeled" HL-to-DC leakage values provided in Tables 21.4-1 and 21.5-1 were established and explain the reported discrepancies between the measured and modeled values.

- (2) Please provide a table that documents the HL-to-DC leakage observed in the ROSA- IV LSTF tests analyzed in WCAP-16996-P/WCAP-16996-NP, Volumes I, II, and III, Revision 0, Section 21, "ROSA-IV Test Simulations," and in Section 24, "Assessment of Compensating Error in Evaluation Model Using WCOBRA/TRAC-TF2." Describe each individual ROSA-IV LSTF test in a separate row including the following test parameters, each in a separate column: test identifier (e.g. SB-CL-05), test date, data source documents, HL-to-DC leakage unit, and experimental HL-to-DC leakage value. Explain the source, availability, and accuracy of data quantifying the LSTF HL-to-DC leakage bypass in these tests and explain if the bypass data was examined for qualification purposes.
- (3) Please explain if a "steady state tune-up procedure" was used to "adjust" the HL-to- DC leakage in the WCOBRA/TRAC-TF2 model of the LSTF pressure vessel. In such a case, please describe how the "desired value" for the HL-to-DC leakage was established for the LSTF analyses. Please provide a table that lists all parameters subject to modification "during the steady state tune-up procedure." Describe each parameter in a separate row providing the corresponding values at the beginning and at the end of the "steady state tune-up procedure" as well as the allowable variation range.
- (4) Provide a table that documents the "calculated value" for the HL-to-DC leakage at the end of the steady-state runs and the corresponding "desired values" for the ROSA-IV LSTF tests considered in WCAP-16996-P/WCAP-16996-NP, Volumes I, II, and III, Revision 0, Section 21, "ROSA-IV Test Simulations," and in Section 24, "Assessment of Compensating Error in Evaluation Model Using WCOBRA/TRAC-TF2."
- (5) Compare LSTF HL-to-DC leakage test data against HL-to-DC leakage capacities simulated in WCOBRA/TRAC-TF2 ROSA-IV LSTF test analyses presented in WCAP-16996-P/WCAP-16996-NP, Volumes I, II, and III, Revision 0, Section 21, "ROSA-IV Test Simulations," and in Section 24, "Assessment of Compensating Error in Evaluation Model Using WCOBRA/TRAC-TF2." In the table requested in Item 2 above, include an additional column documenting, in consistent units, the leg-to-downcomer leakage values obtained in the WCOBRA/TRAC-TF2 ROSA-IV LSTF test simulations. Clearly state if the HL-to-DC leakage capacities in the WCOBRA/TRAC-TF2 ROSA-IV LSTF test simulations were adjusted to account for any effects other than the HL-to-DC leakage through the hot leg leak lines installed in the LSTF pressure vessel.

Response:

For the response, see Section 2.2 and Table 2.3-1 of the integrated response.

Question #105: Representation of LSTF Bypasses in WCOBRA/TRAC-TF2 LSTF Test Simulations

Analyzing WCOBRA/TRAC-TF2 prediction results for ROSA-IV LSTF Tests SB-CL-01, SB-CL-02, and SB-CL-03, WCAP-16996-P/WCAP-16996-NP, Volumes I, II, and III, Revision 0, Section 21, Subsection 21.7, "Break Orientation Study: Simulation of Top/Side/Bottom 0.5 percent (SB-CL-16/12/15) and 2.5 percent (SB-CL-03/01/02) Cold Leg Breaks," presents code predictions in Figures 21.7-3 through 21.7-10. Figure 21.7-5, "Comparison of Predicted and Measured Mixture Levels in Broken Cold Leg (ROSA-IV 2.5-Percent Cold Leg Break Runs), (a) Code Calculations" shows the predicted cold leg liquid levels and Figure 21.7-5 Part (b), "Reported in Reference 5," reproduces Figure 8, "Mixture levels in cold-leg B measured for side, bottom and top break experiments," appearing in a publication by Y. Koizumi et al., "Investigation of Break Orientation Effect during Cold Leg Small-Break LOCA at ROSA-IV LSTF," Journal of Nuclear Science and Technology, Vol. 25, No. 9, September 1988.

With regard to the comparison in Figure 21.7-5, Subsection 21.7 states: [

] ^{a,c}

Discussing WCOBRA/TRAC-TF2 calculation results for ROSA-IV LSTF Test ST-NC-02, WCAP-16996-P/WCAP-16996-NP, Volumes I, II, and III, Revision 0, Section 21, Subsection 21.9, "Simulation of ST-NC-02, 2 percent Power Natural Circulation Test," shows code calculations in Figures 21.9-2 through 21.9-8. Figure 21.9-8, "Downcomer- to-Upper Plenum Differential Pressure," shows a comparison of the downcomer-to-upper plenum differential pressures for the test. With regard to the comparison in Figure 21.9-8, Subsection 21.9 states: ["

] ^{a,c}

The above results illustrate the sensitivity of WCOBRA/TRAC-TF2 predictions to the modeling of flows through bypass flow paths between the downcomer and the upper head or plenum that existed in the LSTF pressure vessel when the ROSA-IV tests were performed. Such bypasses are particularly important for the progression of small break LOCA transients and their inaccurate modeling test simulations can affect the validity of comparing code predictions against test data in evaluating the WCOBRA/TRAC-TF2 performance.

Please assess the adequacy of modeling LSTF pressure vessel bypasses in WCOBRA/TRAC-TF2 analyses of ROSA-IV LSTF tests presented in WCAP-16996-P/WCAP-16996-NP, Volumes I, II, and III, Revision 0, Section 21, "ROSA-IV Test Simulations," in Section 24, "Assessment of Compensating Error in Evaluation Model Using WCOBRA/TRAC-TF2," or discussed elsewhere in WCAP-16996-P/WCAP-16996-NP, Volumes I, II, and III, Revision 0. As part of

this assessment, please identify test simulations in which the LSTF pressure vessel bypasses were not accurately modeled. Please reanalyze these cases with accurate representation of the LSTF pressure vessel bypasses and update WCAP-16996-P/WCAP-16996-NP, Volumes I, II, and III, Revision 0, sections in which ROSA-IV LSTF WCOBRA/TRAC-TF2 assessments are presented and/or discussed. Please provide a summary table, which lists the ROSA-IV LSTF tests that have been analyzed as part of the WCOBRA/TRAC-TF2 assessment and identify those that have been reanalyzed. Describe major results and summarize modifications in WCAP-16996-P/WCAP-16996-NP, Volumes I, II, and III, Revision 0, as applicable.

Response:

Westinghouse agrees that the modeling of the bypass is very important for the accurate prediction of SBLOCA scenarios. This is the reason for the dedicated bypass sensitivity presented in Section 21.11 of topical where the impact of variation in Hot Leg Nozzle Gap flow, and Spray Nozzle Bypass flow were investigated. The conclusion stated in Section 21.11 supports the decision to not model the Hot Leg Nozzle Gap flow and the modeling of the nominal Spray Nozzle bypass flow in PWRs. This decision is further supported by the response to RAI-107.

The target and the achieved bypass flows in the ROSA-IV LSTF test simulations are tabulated in Table 2.3-1 of this response. As seen in that table, the deviation between the target and actual bypass for the SBLOCA simulations is well within the range []^{a,c} used to study the impact of bypass uncertainty presented in Section 21.11 of the topical report where the impact was shown to be minor.

The impact of bypass on the ST-NC-02 natural circulation test simulation is as stated in note (4) of Table 2.3-1. For that test, the impact of the bypass change from []^{a,c} on other parameters is expected to be minor, as seen in the loop flow rate comparison of []^{a,c} bypass case, shown in Figure 105-1.



Figure 105-1 ST-NC-02 Loop Circulation Flows

**Integrated Response to NRC RAIs 100 through 105:
Modeling of the ROSA Large Scale Test Facility Bypass Flows**

1.0 Introduction

The design of the ROSA LSTF test facility allows for the simulation of various core bypass flow-paths that exist in a real PWR.

The upper head cooling spray nozzles provide a core bypass flow link (DC-to-UH) that allows for some amount of coolant to flow from the downcomer (DC) into the upper head (UH) and then into the upper plenum (UP) via the guide tubes (GT). The simulation of the effect of the upper head cooling spray nozzles that exist in the Westinghouse PWRs is achieved at the ROSA LSTF by using nozzles with similar design.

The effect of the HL nozzle-to-DC gap is simulated by two separate leak lines, each of which connects the downcomer and one of the hot legs; these are pipes equipped with orifice flow meters (FE010-HLA and FE150-HLB) and control valves (HCV-010 and HCV-150).

The LSTF also has the capability to simulate an UP-to-DC relief valve, which connects the top of the upper plenum to the downcomer. However, none of the tests included in the FSLOCA topical report had this valve operational and therefore this bypass flow path was not modeled in any of the ROSA LSTF tests discussed in the topical report WCAP-16996-P.

2.0 Vessel Core Bypass Flow Modeling in the ROSA LSTF Test Simulations

2.1 Downcomer-to-Upper Plenum Bypass

Spray Nozzle Bypass Flow

The upper head cooling spray nozzles, sometimes called downcomer (DC) spray nozzles, provide a “downcomer to upper head to upper plenum” (DC-UH-UP) core bypass flow path that allows for some amount of coolant to flow from the downcomer into the upper head and then into the bottom of the upper plenum via the guide tubes. Depending on the amount of this bypass flow, the upper head steady state temperature ranges between T_{hot} and T_{cold} .

The number of spray nozzles varies among the different Westinghouse PWR designs. For example, depending on the upper plenum-to-upper head flow paths, to maintain a sufficient spray nozzle bypass to

achieve Tcold upper head, a four-loop Westinghouse PWR with “inverted hat” upper support plate configuration may have spray nozzle flow areas ranging (approximately) from [

]^{a,c}

A three-loop Thot upper head plant like DLW, has a total spray nozzle flow area of only about [

]^{a,c}

At the ROSA-IV LSTF there are eight (3.4-mm diameter) DC spray nozzles with a total flow area of $7.26 \times 10^{-5} \text{ m}^2$ (72.6 mm^2 , or 0.097 in^2); based on the ROSA LSTF leakage tests (Section 4.3 of JAERI-M 89-113), the effective spray nozzle loss coefficient, normalized for the total spray nozzle flow area of 72.6 mm^2 , is estimated to be 1.72. According to Table 5.2.2 of JAERI-M 84-237, the flow area of the ROSA spray nozzle represents a PWR spray nozzle flow area of 3552 mm^2 (5.5 in^2), which area tends to be on the side typical for plants with Thot upper head conditions; this is 1748 mm^2 (2.7 in^2) for the Thot plant DLW, compared to the 18064 mm^2 to 41935 mm^2 (28 in^2 to 65 in^2) typical for plants with Tcold upper head. Thus, it is clear that, with respect to the spray nozzle bypass (by design and accounting for various unintended leakages), the ROSA-IV LSTF would represent a PWR with Thot upper head configuration. This conclusion is confirmed by the fact that the steady-state upper head temperatures measured at all ROSA LSTF tests, including the presumably “high DC leakage/bypass” SB-CL-05 test, tend to be slightly lower than Thot.

The measured upper head fluid temperatures at various ROSA tests (for example Fig.5.36 and 5.38 of JAERI-M 89-220 for SB-CL-08 and SB-CL-05 respectively) were only slightly lower than the hot leg (HL) temperature, which is an indication that although there might have been a net T_{CL} flow from the DC through the spray nozzles into the UH, most likely there was also a significant upper plenum to upper head (UP-UH) recirculation flow through a subset of the GTs that kept the UH temperature close to the HL temperature. This behavior is consistent with PWRs with T_{HOT} upper head. Note that the GT flow path between the upper head (UH) and the upper plenum (UP) is comprised by a total of 8 (parallel) guide tubes – six of them are located above the average- and high-powered assemblies, while two of them sit above low-powered (peripheral) assemblies, Figure 21.3-7 of the FSLOCA Topical. Therefore, it is quite plausible that the GT recirculation flow at the ROSA LSTF pre-transient steady states was non-uniform, due to the non-uniform fluid temperature distribution at the bottom of the UP (core exit) related to the radial power distribution in the core.

Uncontrolled Internal Vessel Leakages:

As noted in NRC question 103, unintended internal vessel leakages were identified at the ROSA-IV LSTF tests. Although repairs were performed to minimize them, they resulted in uncontrolled downcomer-to-

upper plenum bypass flow (capacity) in addition to the spray nozzle bypass. Since the capacity of these leakages was unquantifiable, they were not modeled explicitly. It was assumed that the desired DC-to-UH) spray bypass targets (Table 2.3-1 of the integrated response), estimated and quoted by various sources already include the effect of these uncontrolled leakages.

The unintended internal leakage around the guide tubes (repaired in May 1986) may have existed at the test preceding that repair. In the simulation of the natural circulation test ST-NC-02, conducted on 12/18/1985, this unintended leakage was explicitly modeled by opening a flow link between vessel channels 46 and 50, Figure 21.3-1 of WCAP-16996-P, with an estimated flow area of 12 in². This flow link does not have significant effect on the overall downcomer-to-upper head bypass since the most restrictive location is still modeled at the spray nozzle location at the top of the downcomer. In the ST-NC-02 simulation, it was modeled to eventually calculate better draining of the upper head.

Although it might have potentially existed, this leakage was not modeled in the simulations of the tests preceding ST-NC-02. However, the effect of this leakage on the upper head draining and on the transient as a whole is expected to be minimal due to the relatively small residual (drainable) volume at the bottom of the upper head.

Scaling of Downcomer-to-Upper Head (Spray) Bypass:

According to Table 5.2.2 of JAERI-M 84-237, the total spray nozzle flow area the scaling ratio (ROSA/PWR) is 1/48.91; while this number is consistent with the general ROSA/PWR ratio of 1/50, it does not represent scaling of the downcomer-to-upper plenum bypass flow. Given the uncertainty associated with the non-uniform guide tube recirculation flows and leakages it is difficult to scale the ROSA-IV downcomer-to-upper plenum bypass flows. At steady state conditions, the downcomer-to-upper head (spray) bypass flow can be defined as a net flow via the flow path “downcomer - spray nozzles – guide tubes – upper plenum”. At the same time, the primary flow path through the core is “downcomer – lower plenum – core – upper plenum”. At any time (steady state or transient) these two parallel flow paths would be subjected to the same pressure boundary conditions. Therefore, the ratio between their respective mass flows rates (spray bypass ratio) would be defined by their effective hydraulic resistances as:

$$(\dot{m}_{\text{spray}}/\dot{m}_{\text{core}}) = \sqrt[2]{(K_{\text{core}}/K_{\text{spray}})}$$

, where the resistances K are normalized to a flow area.

Both, a test facility or a PWR would have the similar spray bypass capacities if their $\sqrt[2]{(K_{\text{core}}/K_{\text{spray}})}$ ratios are similar.

As discussed earlier and based on the spray bypass capacities, summarized in Table 2.3-1 hereafter, the selected ROSA-IV LSTF tests in the WCOBRA/TRAC-TF2 validation set, presented in WCAP-16996-P

[1], appear to be scaled to a typical T_{HOT} upper head Westinghouse PWR. Combined with proper scaling of the various system sub-region volumes, upper plenum, upper head, core, hot leg, steam generator tubes and correct power scaling, these tests would demonstrate timing of key transient phenomena representative of the scaled PWR.

Downcomer-to-Upper Plenum Bypass Modeling:

Based on the ROSA design information, the most constricted location of the guide tubes is at their top – the total flow area at the top of the GTs is $8 \times 196 \text{ mm}^2 = 1568 \text{ mm}^2$, which is approximately 20 times larger than the area of the DC spray nozzles (72.6 mm^2); the area of the GT enclosures is even larger - $8 \times 5166 \text{ mm}^2 = 41328 \text{ mm}^2$. This implies that the resistance of the flow path (DC-UH-UP) would primarily be defined by the resistance of the DC spray nozzles. This design feature is implemented in a similar way in Westinghouse PWRs.

The effect of the DC spray nozzles at the ROSA LSTF is modeled fairly straightforward. As a first approximation, their effective form loss coefficient $K_{NZL} = 1.72$ (normalized for 0.097 in^2) is scaled for the modeled flow area at the top of the downcomer (151 in^2) and applied at the top of the downcomer channels 52, 53 and 67 through 70, Figure 21.3-1 of WCAP-16996-P. Then, iterative adjustment is made to that loss coefficient to achieve desired target DC-to-UH bypass flow (which includes the additional uncontrolled leakages). Note that this approach is similar to that implemented for the PWR spray bypass modeling, as described in the response to Part (1) of RAI-97.

[

$I^{a,c}$

2.2 Hot Leg Leakage Bypass

At the ROSA LSTF the effects of hot leg to downcomer (HL-to-DC) leakage is simulated by two separate lines which connect the downcomer to each of the hot legs. The lines contain isolation valves and flow rates are measured by FE010-HLA and FE150-HLB. The measured steady state HL-to-DC leakage flow rates at the different tests are very similar and typically around 0.05 kg/sec; for SB-CL-05 see Fig.5.61 and 5.64 of JAERI-memo 61-056, for SB-CL-01 see Fig.4.1 and 4.4 of JAERI-M 62-399.

The effect of the HL-to-DC leakage at the ROSA LSTF tests was modeled by using a flow links (transverse gap connections 21 and 22, in vessel Section 6), connecting the hot leg nozzle channels 25 and 35 to downcomer channels 61 and 60 respectively, see Figure 21.3-4 of WCQP-16996-P. The resistance of the two flow links is adjusted through the gap loss coefficient (WKR) to achieve the desired steady-

state HL-to-DC leakage target. The steady-state tune-up procedure for HL-to-DC leakage is iterative and, in essence, similar to the tune-up of the downcomer-to-upper head (spray) bypass. There were no additional adjustments of the HL-to-DC leakage capacity to account for any effects other than achieving the desired target.

The discrepancy in the established HL-to-DC leakage targets for the SB-CL-18 and SB-CL-05 tests, observed in Part (1) of NRC question 104 is discussed hereafter.

The HL-to-DC leakage target for the SB-CL-18 test (0.25%) was based on the measured leakage flow of 0.124 kg/sec, as measured by FE010-HLA and FE150-HLB; at the same time, Table 3.2 of JAERI-M 89-027 gives an approximate value of $2 \times 0.049 \approx 0.1$ kg/sec.

In Table 21.5-1 of WCAP-16996-P [1], the HL-to-DC leakage target for the SB-CL-05 test is reported as ≈ 0.1 kg/sec, which is based on the measured values shown in Fig. 5.61 and 5.64 of JAERI-memo 61-056 and is indeed consistent with the 0.2% ratio reported in Table 2 of Tasaka's paper [11].

For the SB-CL-18 and the SB-CL-05 tests, the resistance of the HL-to-DC leakage flow path was modeled the same without any re-tuning. The resulting deviation from the established target for the SB-CL-05 test is not considered significant from a code validation perspective.

2.3 Summary of Desired (Target) and Modeled ROSA LSTF Bypass Flows

Table 2.3-1 provides a summary of the desired and modeled spray bypass and Hot Leg to Downcomer (HL-to-DC) leakage capacities at the ROSA LSTF test reported in WCAP-16996-P. The notes to the table provide information regarding the values presented in the table. As seen in the summary table, the calculated values are close to the desired targets.

Table 2.3-1 Desired and Modeled ROSA LSTF Bypass Flows						
Test ⁽¹⁾	Date ⁽¹⁾	Test Report	Spray Bypass, % core flow		HL-to-DC Leakage, % core flow	
			Target	Modeled	Target	Modeled
SB-CL-01, 2.5%, side	5/30/85	JAERI-memo 62-399	[] ^{a,c}
SB-CL-05, 5%, side	6/26/85	JAERI-memo 61-056	[] ^{a,c}
SB-CL-02, 2.5%, bottom	7/18/85	JAERI-memo 62-399	[] ^{a,c}
SB-CL-03, 2.5%, top	8/8/85	JAERI-memo 62-399	[] ^{a,c}
ST-NC-02, Nat. circ.	12/18/85	JAERI-M 88-215	[] ^{a,c}
SB-CL-12, 0.5%, side	7/29/87	JAERI-memo 63-344	[] ^{a,c}
SB-CL-14, 10%, side	12/21/87	JAERI-memo 63-262	[] ^{a,c}
SB-CL-15, 0.5%,bottom	1/26/88	JAERI-memo 63-344	[] ^{a,c}
SB-CL-16, 0.5%, top	3/02/88	JAERI-memo 63-344	[] ^{a,c}
SB-CL-18, 5%, side	5/25/88	JAERI-M 89-027	[] ^{a,c}

Notes:

- (1) Break type and date are taken from JAERI-M 89-113.
- (2) Table 2 of Tasaka's paper [11] quotes 2.1% DC-to-UH bypass. However, this value is somewhat difficult to substantiate since such a high bypass value would result in upper head temperature close to T_{cold}. The measured upper head temperatures for the SB-CL-05 test appear to be only slightly below T_{hot}, Fig.5.250 of JAERI-memo 61-056.
- (3) The spray bypass of the SB-CL-05 test was adjusted [^{a,c}; thus achieving better downcomer differential pressure calculation. Thus, it

is higher than that of the SB-CL-18 test, also consistent with observations of increased leakage for the initial ROSA tests.

- (4) The spray bypass values for the ST-NC-02 test are % of total loop flow. Based on bypass data in Table 2 of Tasaka's paper [11] and information in JAERI-M 89-113, the target value for the ST-NC-02 test is estimated as being close to that of the SB-CL-06 test. The lower calculated value is a result of spray nozzle loss tuneup to achieve better calculation of the downcomer-to-upper plenum differential pressure.
- (5) According to JAERI-M 88-215, Section 2.1, the ST-NC-02 test was conducted with the HL-to-DC leakage line closed.
- (6) Spray bypass flow for SB-CL-18 is not quoted in JAERI-M 89-027; therefore the 0.3% value for the equivalent 5% break test SB-CL-08 is taken from Table 2 of Tasaka's paper [11].
- (7) The HL-to-DC leakage for SB-CL-18 is based on measured flow rates (FE010-HLA + FE150-HLB).
- (8) The DC-to-UH (spray) and HL-to-DC leakage desired targets for the three 2.5% break orientation test SB-CL-01, -02 and -03 were assumed the same as those of the SB-CL-05 test; since these test were conducted around the time when SB-CL-05 it was assumed that the bypasses will be similar.
- (9) The SB-CL-14 test was performed in the time period of the 0.5% break tests, and therefore it is assumed that the internal leakage and bypass flows in the ROSA vessel would have been similar to those of the three 0.5% break orientation tests.
- (10) The test report for the three 0.5% break orientation test SB-CL-12, -15 and -16, JAERI-memo 62-399 [8], did not quote any values for the DC-to-UH (spray bypass) or HL-to-DC leakage targets. Since these three tests were conducted shortly before the SB-CL-18 test it was decided to use the SB-CL-18 target as well.

3.0 References

- 1) WCAP-16996-P, "Realistic LOCA Evaluation Methodology Applied to the Full Spectrum of Break Sizes (FULL SPECTRUM LOCA Methodology)," November 2010.
- 2) JAERI-M 84-237, "ROSA-IV Large Scale Test Facility (LSTF) System Description," January 1985.
- 3) JAERI-M 89-113, "Supplemental Description of ROSA-IV/LSTF with No.1 Simulated Fuel-Rod Assembly," September 1989.
- 4) JAERI-M 89-220, "Data Report for ROSA-IV LSTF 5% Cold Leg Break LOCA Experiment Run SB-CL-08," January 1990.
- 5) JAERI-memo 61-056, "ROSA-IV/LSTF 5% Cold Leg Break LOCA Experiment Data Report, Run SB-CL-05," March 1986.
- 6) JAERI-memo 62-399, "ROSA-IV/LSTF 2.5% Cold Leg Break LOCA Experiment Data Report for Runs SB-CL-01, 02 and 03," November 1987.
- 7) JAERI-M 88-215, "Post-Test Analysis with RELAP5/MOD2 of ROSA-IV/LSTF Natural Circulation Test ST-NC-02," October 1988.
- 8) JAERI-memo 63-344, "Quick Look Report for ROSA-IV/LSTF 0.5% Cold Leg Break LOCA Tests, SB-CL-15 and SB-CL-16," September 1988.
- 9) JAERI-memo 63-262, "Quick Look Report for ROSA-IV/LSTF 10% Cold Leg Break LOCA Test, SB-CL-14," July 1988.
- 10) JAERI-M 89-027, "ROSA-IV/LSTF 5% Cold Leg Break LOCA Experiment, Run SB-CL-18 Data Report," March 1989.
- 11) Tasaka, K., et al., 1988, "The Results of 5% Small Break LOCA Tests and Natural Recirculation Tests at the ROSA-IV LSTF," Nuclear Engineering and Design, Vol.108, 1988, pp 37-44.

RAI Question #107: Pressurized Water Reactor Hot Leg Bypass in WCOBRA/TRAC-TF2 Plant Simulations

Addressing the modeling of bypass via gaps that exist at the interface of the core barrel and the hot leg nozzles, WCAP-16996-P/WCAP-16996-NP, Volumes I, II, and III, Revision 0, Section 29, "Assessment of Uncertainty Elements," Subsection 29.5.3, "Upper Head," states that "because the spray nozzle bypass itself is modeled in a best-estimate manner, neglecting the hot leg to downcomer gap, less bypass is modeled than is physically expected, so there is no need to range this parameter." As further explained in Subsection 29.5.4, "Upper Plenum," the gaps at the interface of the core barrel and the hot leg nozzles provide for leakage paths between the upper plenum and the upper downcomer region during all operating modes. It is explained that "for small breaks, these leakage paths are expected to have high importance during the loop seal clearing period when they provide alternative paths from the upper plenum to the cold leg break location to vent steam and relieve some two-phase level depression." Subsection 29.5.4, "Upper Plenum," concludes that "the ROSA sensitivity study in Section 21.11 shows that neglecting this gap is conservative." Accordingly, Section 21, "ROSA-IV Test Simulations," Subsection 21.11.2, "SB-CL-18 Simulation Without Hot Leg Nozzle Bypass Flow," states that "the results provided in this section clearly show that not modeling HL-to-DC bypass is a conservative modeling approach for the ROSA 5 percent small break transient."

The hot leg gaps in the LSTF pressure vessel were simulated by two dedicated hot leg leak lines. Based on the leak line 21.2-mm (0.835-inch) pressure vessel nozzle ID and the 0.687 contraction ratio of the orifice installed in each line, the LSTF hot leg gap bypass area for both loops amounted to 3.33 cm² (36.05x10⁻⁴ ft²) with an equivalent diameter of a 2.060 cm (0.811 inch). Based on the LSTF upper head volume scaling ratio, the LSTF hot leg gap bypass area corresponds to a PWR hot leg gap bypass area of 160.7 cm² (0.173 ft² or 24.9 in²) with an equivalent diameter of 14.3 cm (5.63 inch). For the reference Tsuruga Westinghouse-type four-loop Unit 2 PWR, the LSTF bypass area corresponds to a 0.068-inch gap width of the opening between the barrel and the vessel exit nozzle based on the hot leg ID of 29.0 inch specified in Table 5.2.9, "Characteristics of Primary Loop Piping," in "ROSA-IV Large Scale Test Facility (LSTF) System Description," JAERI-M 84-237, January 1985.

- (1) Please state clearly if no hot leg gap bypass is credited for the purposes of LOCA analyses of any PWR plant designs using the FSLOCA methodology. Also, clarify if no other features of WCOBRA/TRAC-TF2 PWR vessel models are somehow modified or adjusted because of not modeling hot leg bypass in PWR LOCA analyses.
- (2) WCAP-16996-P/WCAP-16996-NP, Volumes I, II and III, Revision 0, Section 29, "Assessment of Uncertainty Elements," Subsection 29.5.3, "Upper Head," states that "the spray nozzle bypass itself is modeled in a best-estimate manner" and explains that "there is no need to range this parameter" as "less bypass is modeled than is physically expected" due to "neglecting the hot leg to downcomer gap." The staff finds this justification insufficient. Please provide the range of upper head spray nozzle bypass capacities of PWR plants considered for intended WCOBRA/TRAC-TF2 LOCA analysis applications. Provide the uncertainties associated with this parameter and describe the plant conditions considered in assessing them. Then, provide the range of hot leg bypass

capacities along with their uncertainties for the considered PWR plants taking into account the variation of the hot leg gap during a LOCA transient. Explain which upper head spray nozzle bypass values are used in WCOBRA/TRAC-TF2 PWR models so that "the spray nozzle bypass itself is modeled in a best-estimate manner" and demonstrate that these values are conservative considering the provided hot leg bypass capacities and the uncertainties for the upper head spray nozzle bypass and the hot leg gap bypass.

Response:

(1) The Hot Leg Nozzle gap is [

]^{a,c} in the WCOBRA/TRAC-TF2 vessel models of the Virgil C. Summer and Beaver Valley Unit 1 PWRs [107-1]. The typical magnitude of the Hot Leg Nozzle gap flow is [

]^{a,c}

(2) The typical range of Upper Head (UH) Spray Nozzle bypass flow for Westinghouse 2, 3, and 4 Loop PWRs is given below;

[

]^{a,c}

It is clear that [

]^{a,c}

Figure 107-1 below shows the typical Spray Nozzle geometry. As seen in the figure, most of [

]^{a,c} Using a

typical nozzle design as shown in Figure 107-2 and Sections 3 and 11 of Idelchik [107-2], the

the Hot Leg Nozzle Gap flow in the WCOBRATRAC-TF2 PWR models.

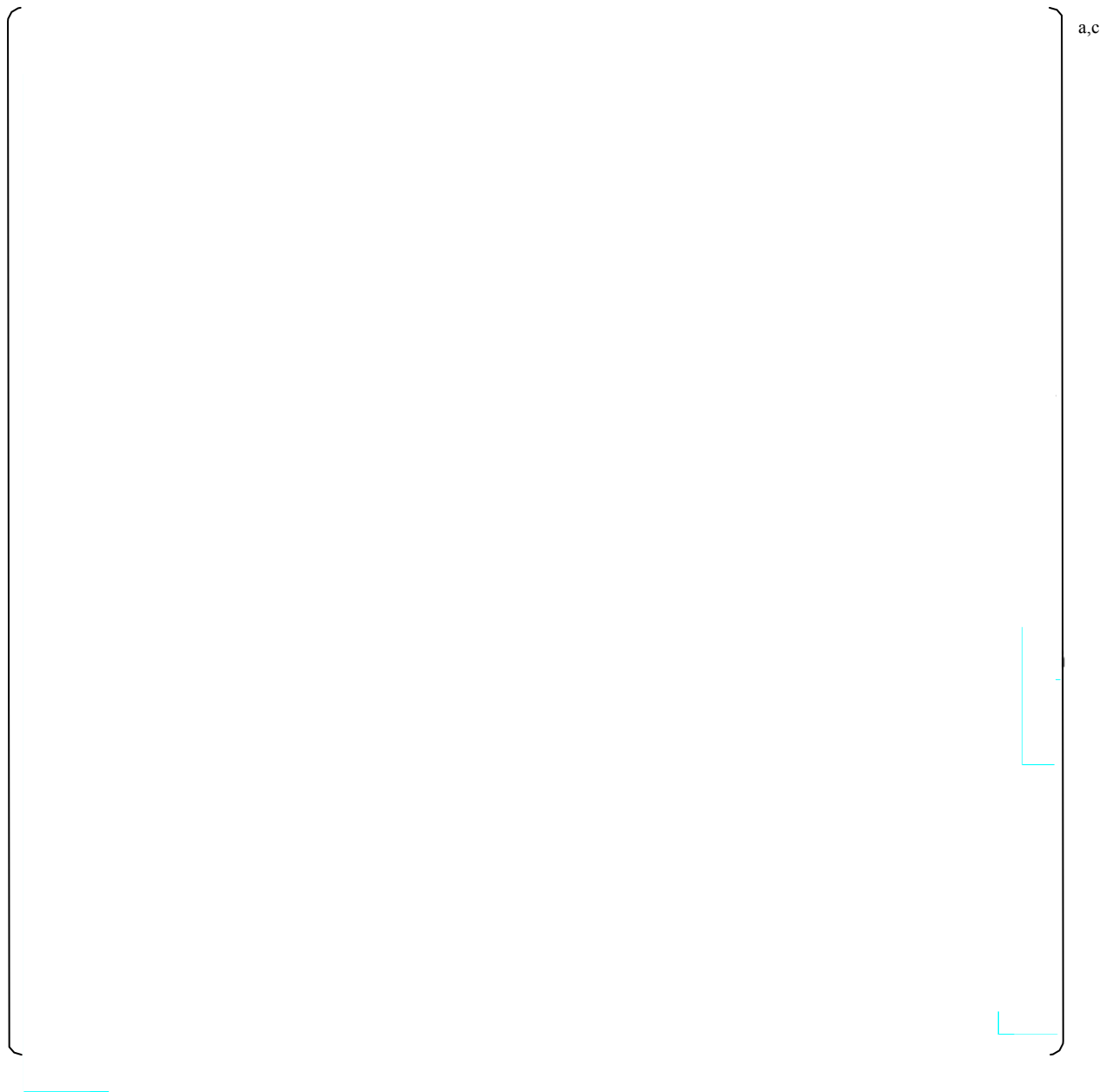


Figure 107-1: Typical Head Cooling Spray Nozzle

a,c

Figure 107-2: Typical Nozzle Design

References:

- 107-1) WCAP-16996-P, "Realistic LOCA Evaluation Methodology Applied to the Full Spectrum of Break Sizes (FULL SPECTRUM LOCA Methodology)," November 2010.
- 107-2) Idel'Chik, I. E., 1960, Handbook of Hydraulic Resistance," AEC-tv-6630.

**WCAP-16996-P, “Realistic LOCA Evaluation Methodology Applied to the Full Spectrum of Break Sizes
(FULL SPECTRUM LOCA Methodology)”
Request for Additional Information – (Non-Proprietary)
RAIs 108, 120 and 121**

June 2014

Westinghouse Electric Company LLC
1000 Westinghouse Drive
Cranberry Township, PA 16066

RAI Question #108: WCOBRA/TRAC-TF2 Assessment Using Counter-Current Flow Data by Costigan et al.

A simple experimental study of counter-current flow limitation was carried out at Harwell by Costigan et al., “Counter-current two-phase flow in horizontal channels of circular cross-section,” 2nd international Conference on Multiphase Flow, Paper F3, London, 1985. The apparatus operated at close to atmospheric pressure and consistent of a H-shaped test section. Water was injected into the left-hand limb, simulating the SG, and air into the right-hand limb representing the reactor upper plenum.

- (1) Please compare WCOBRA/TRAC-TF2 predictions of the observed flooding phenomena against the experimental data of Costigan et al. Present sensitivity studies showing the impact of the H_SLUG parameter variation. Plot the comparison results using the phase Wallis parameters or any other appropriately defined dimensionless number.
- (2) Please present sensitivity results illustrating the effect of nodalization refinement in representing the horizontal limb of the H-shaped test facility. For this purpose, please present code predictions using fine noding with cell length-to-hydraulic diameter ratio less than or equal to one and coarse noding with cell length-to-hydraulic diameter ratio greater two.

Response:

The cited experiment was an air-water test at near-atmospheric pressure designed to simulate counter-current flow limitation (CCFL) in a horizontal tube. CCFL in the hot leg and steam generator is of significance for the calculation of a Small Break LOCA (SBLOCA) transient.

A summary of the May 2014 Nuclear Regulatory Commission (NRC) audit of the FULL SPECTRUM™ LOCA (FSLOCA™) evaluation model was documented in LTR-NRC-14-29 [108-1]. As discussed in the presentation starting on page P-86 of the P-Attachment to LTR-NRC-14-29, [

^{a,c}

FULL SPECTRUM™ and FSLOCA™ are trademarks in the United States of Westinghouse Electric Company LLC, its subsidiaries and/or its affiliates. These marks may be used and/or registered in other countries throughout the world. All rights reserved. Unauthorized use is strictly prohibited. Other names may be trademarks of their respective owners.

In summary, a comparison of the UPTF facility versus the facility for the CCFL experiments carried out by Costigan reveals that the [

]^{a,c}

Reference(s)

- 108-1) LTR-NRC-14-29, "Summary of May 2014 NRC Audit of the FULL SPECTRUM LOCA (FSLOCA) Evaluation Model," June 5, 2014.
- 108-2) Glaeser, H., and Karwat, H., "The contribution of UPTF experiments to resolve some scale-up uncertainties in countercurrent two phase flow," *Nuclear Engineering and Design*, 145, pp. 63-84, 1993.
- 108-3) WCAP-16996-P, "Realistic LOCA Evaluation Methodology Applied to the Full Spectrum of Break Sizes (FULL SPECTRUM LOCA Methodology)," November 2010.
- 108-4) Ohnuki, A., "Experimental Study of Counter-Current Two-Phase Flow in Horizontal Tube Connected to Inclined Riser," *Journal of Nuclear Science and Technology*, 23(3), pp. 219-232, 1986.
- 108-5) Ohnuki, A., et al., "Scale Effects on Countercurrent Gas-Liquid Flow in a Horizontal Tube Connected to an Inclined Riser," *Nuclear Engineering and Design*, 107, pp. 283-294, 1988.

RAI Question #120: IVO Loop Seal Clearance Data and WCOBRA/TRAC-TF2 Assessment

A full-scale separate effect test facility, constructed by Imatran Voima Oy (IVO) in Finland, was used to study two-phase flow phenomena in a PWR loop seal region following a cold leg break LOCA. The full-scale loop seal test facility used a piping with an ID of 0.850 m (33.46 inch or 2.8 ft) and a length of the horizontal section of the seal of 4.3 m (169.3 inch or 14.1 ft), which resulted in a L/D of 5.1 for this section. The tests were conducted at atmospheric pressure and room temperature using air and water. As part of this experimental effort, two reduced-scale loop seal models were constructed using transparent pipes with an ID of 0.080 m (3.15 inch) to examine effects of scaling and geometry on the loop seal processes and flow regime transitions. Test data from these facilities were used for comparison against the full-scale loop seal geometry tests. The IVO tests are described by H. Tuomisto, "Large-Scale Air/Water Flow Tests for Separate Effects During LOCAs in PWRs," *Nuclear Engineering and Design*, Vol. 102, No.2, pp. 171-176, 1987 and by H. Tuomisto and P. Kajanto, "Two-Phase Flow in a Full-Scale Loop Seal Facility," *Nuclear Engineering and Design*, Vol. 107, No.3, pp. 295-305, 1988.

IVO separate effect loop seal clearance test data has have been used for assessing various reactor safety thermal hydraulic codes. Results from a RELAP5 assessment study are documented by O. Kymäläinen, "The Assessment of RELAP5/MOD2 against IVO Loop Seal Tests," NUREG/IA-0082, April 1992. In this work, RELAP5/MOD2 analyses for both the full-scale and the 1/10-scale atmospheric air-water loop seal facilities were performed. The calculated residual water levels differed from the measured data and the code yielded lower values. Also, the predicted gas superficial velocities, needed for loop seal clearing, was lower than the experimentally values. Even with interfacial drag modifications, agreement with the experimental data was not found. Results from a more recent TRACE assessment study are presented by S. Hillberg, "Full Scale Loop Seal Experiments with TRACE V5 Patch 1," NUREG/IA- 0403, December 2011. The assessment was focused on the code capability to predict the residual water level in the horizontal pipe section of the loop seal and examined the pressure behavior during the clearance of the loop seal. Effects related to loop seal nodalization, maximum time step size, and initial liquid levels were studied. The simulations revealed sensitivities to loop seal nodalization particularly with regard to representing the 90° bends of the seal piping.

IVO full-scale loop seal experiments are discussed in WCAP-16996-P/WCAP-16996-NP, Volumes I, II, and III, Revision 0, Section 18, "Loop Seal Clearance," Subsection 18.2.2.4, "Effect of Scale," and void fraction data points are compared against three different limiting lines in Figure 18.2.2-12, "IVO Full-Scale Final Void Fraction and Limit Lines." However, no assessment of WCOBRA/TRAC-TF2 prediction results against IVO separate effect loop seal experiments was reported.

- (1) Please perform an additional assessment study for WCOBRA/TRAC-TF2 using IVO separate effect atmospheric air-water test data obtained from both the full- scale and the 1/10-scale loop seal test facilities. Please describe the applied WCOBRA/TRAC-TF2 models for the IVO test facilities as requested in RAI Question No. 112 Items (1) through (4) with regard to the WCOBRA/TRAC-TF2 UPTF loop seal model. Also, describe the IVO loop seal tests instrumentation, test data, and assessed code predication results as requested in RAI Question No. 113, Items (1) and (2), with regard to the WCOBRA/TRAC-TF2 UPTF TRAM loop seal clearance test data. Document user defined parameters, multipliers, and/or options used in the WCOBRA/TRAC-TF2 IVO loop seal models as requested in RAI Question No. 114, Items (1) and (2), with regard to the WCOBRA/TRAC-TF2 UPTF TRAM loop seal model.
- (2) Please present detailed results from the WCOBRA/TRAC-TF2 assessment using IVO separate effect atmospheric air-water test data from the full-scale and the 1/10-scale loop seal test facilities as requested in RAI question #115 items (1) through (4) with regard to the WCOBRA/TRAC-TF2 UPTF TRAM loop seal tests assessment study.
- (3) Please perform and present results from sensitivity calculations assessing effects related to IVO the full-scale and 1/10-scale loop seal test facilities nodalization in the applied WCOBRA/TRAC-TF2 IVO loop seal models as requested in RAI question #116 items (1) through (3) with regard to the WCOBRA/TRAC-TF2 assessment using the UPTF TRAM

loop seal tests. The length of the bottom horizontal section of the full-scale IVO loop seal piping had an L/D ratio of 5.1, which was significantly larger than the corresponding ratio in the full-scale UPTF loop seal facility characterized by an L/D ratio of 2.3. Therefore, please adjust the number of cells in the WCOBRA/TRAC-TF2 IVO full-scale loop seal model so that the cell length-to-diameter ratios in the IVO full-scale loop seal model are close to the ratios examined in the UPTF full-scale loop seal model (L/D of 1.16, 0.77, and 0.58). Examine any additional nodalization schemes, as deemed appropriate.

- (4) Please provide results from WCOBRA/TRAC-TF2 sensitivity studies based on the IVO separate effect full-scale and 1/10-scale loop seal clearance tests, which show the effect of varying or sampling of parameters, multipliers, and/or options relevant to the prediction of the loop clearance process. Perform and document the code assessment results as requested in RAI question #118 with regard to the WCOBRA/TRAC-TF2 UPTF loop seal model.
- (5) Please provide results from WCOBRA/TRAC-TF2 sensitivity calculations based on the IVO separate effect full-scale and 1/10-scale loop seal clearance tests that show the effects related to the applied maximum allowed time step size (DTMAX). Perform and document the code assessment results as requested in RAI question #119 with regard to the WCOBRA/TRAC-TF2 UPTF TRAM loop seal assessment study.

Response:

See the response to RAI 121.

RAI Question #121: ECTHOR Loop Seal Clearance Data and WCOBRA/TRAC-TF2 Assessment

WCAP-16996-P/WCAP-16996-NP, Volumes I, II, and III, Revision 0, Section 18, "Loop Seal Clearance," Subsection 18.2.2, "PWS 2.3 Loop Seal Tests," discusses scaled air-water experiments examining the hydraulic behavior of a U-tube under conditions similar to those encountered in a PWR loop seal during a small break LOCA. The tests were performed as part of the ECTHOR (an acronym from French "Ecoulements dans des Tuyauteries Horizontales en Eau-Air," which stands for Water-Air Flow in Horizontal Pipes) Program carried out under an agreement between Framatome, Électricité de France, Commissariat à l'Energie Atomique, and Westinghouse. Description of the ECTHOR tests is provided by J. P. Bourteele, "Investigation of Stratified and Countercurrent Flows in Horizontal Piping during a Loss-of-Coolant Accident," European Two-Phase Flow Group Meeting, Glasgow, June 3-6, 1980, and by R. J. Skwarek, "Experimental Evaluation of PWR Loop Seal Behavior during Small LOCAs,"

Proceedings of the ANS Specialists Meeting on Small Break Loss-of-Coolant Accident Analyses in LWRs: Conference Papers, August 25-27, 1981, Monterey, California, pp. 5.1-5.12.

The ECTHOR separate effect air-water scaled loop seal tests were performed at atmospheric pressure in a U-tube pipe with an inner diameter of 0.25 m (9.84 inch or 0.82 ft) representing the geometry of a PWR loop seal at a scaling ratio of 0.32 (approximately 1/3). ECTHOR loop seal tests have been used in the past for interfacial drag model development and assessment of various reactor safety thermal hydraulic codes such as CATHARE (acronym from Code for Analysis of Thermalhydraulics during an Accident of Reactor and safety Evaluation) and RELAP5.

WCAP-16996-P/WCAP-16996-NP, Volumes I, II, and III, Revision 0, Section 18, "Loop Seal Clearance," Subsection 18.2.2, "PWS 2.3 Loop Seal Tests," Figures 18.2.2-3 shows residual liquid level data, Figures 18.2.2-4 and 18.2.2-5 depict average void fraction data, and Figure 18.2.2-9 plots U-tube differential pressure data from the ECTHOR tests. The test data are compared against limiting lines for governing participating processes in Figures 18.2.2-7 and 18.2.2-8. However, no assessment of WCOBRA/TRAC-TF2 prediction results against ECTHOR separate effect air-water scaled loop seal data was reported.

Please perform an additional assessment study for WCOBRA/TRAC-TF2 using ECTHOR separate effect air-water scaled loop seal test data. Perform this study and document the code assessment results as requested in RAI question #120 items (1) through (5) with regard to the WCOBRA/TRAC-TF2 IVO separate effect atmospheric air- water tests.

Response:

The IVO and ECTHOR loop seal clearing experiments were air-water tests at near-atmospheric pressure designed to study loop seal clearing behavior. The calculation of loop seal clearing is significant to the progression of a SBLOCA transient. As noted in the RAIs, the test data associated with these experiments was reviewed and discussed in the topical report. However, the experiments were not simulated with WCOBRA/TRAC-TF2. Rather, the Upper Plenum Test Facility (UPTF) loop seal clearing Separate Effects Tests (SETs) were simulated. The UPTF loop seal clearing SETs were selected because they were full-scale geometry, steam-water tests that were run at two different, elevated pressures.

A summary of a May 2014 Nuclear Regulatory Commission (NRC) audit of the FULL SPECTRUM LOCA evaluation model was documented in LTR-NRC-14-29 [121-1]. Additional investigation into loop seal clearing behavior observed in experimental data, as well as WCOBRA/TRAC-TF2 sensitivity studies are discussed in Section 3.0 of the P-Attachment to LTR-NRC-14-29. The FSLOCA methodology was then modified based on the results of the data investigation and WCOBRA/TRAC-TF2 sensitivity studies as described therein to better capture the behavior observed in the integral experiments.

In conclusion, the loop seal clearing phenomenon was evaluated by a review of the ECTHOR, IVO, and UPTF SET data. The code calculation of loop seal clearing was evaluated via simulation of the UPTF

loop seal clearing SETs with WCOBRA/TRAC-TF2. The loop seal clearing behavior was then evaluated as part of the integral SBLOCA response via the simulation of numerous Rig of Safety Assessment (ROSA) Large-Scale Test Facility (LSTF) experiments. Additional investigation of loop seal clearing in integral test facilities was performed, and the methodology was updated as described in LTR-NRC-14-29 to appropriately reflect the data. Given the SET and IETs simulated with WCOBRA/TRAC-TF2, and the methodology changes described in LTR-NRC-14-29, there is sufficient assurance that the loop seal clearing behavior is appropriately predicted with the WCOBRA/TRAC-TF2 code.

Reference(s)

- 121-1) LTR-NRC-14-29, "Summary of May 2014 NRC Audit of the FULL SPECTRUM LOCA (FSLOCA) Evaluation Model," June 5, 2014.

**WCAP-16996-P, “Realistic LOCA Evaluation Methodology Applied to the Full Spectrum of Break Sizes
(FULL SPECTRUM LOCA Methodology)”
Request for Additional Information – (Non-Proprietary)
RAIs 109-111**

October 2014

Westinghouse Electric Company LLC
1000 Westinghouse Drive
Cranberry Township, PA 16066

©2014 Westinghouse Electric Company LLC
All Rights Reserved

The series of NRC's questions addressed herein request simulations of the Semiscale Mod-2C tests S-LH-1 and S-LH-2 to further support the WCOBRA/TRAC-TF2 code validation. Responses to individual parts of the various questions are provided as part of an integrated response attached at the end.

RAI Question #109: Semiscale Test S-LH-1 Assessment of WCOBRA/TRAC-TF2

Semiscale test facility was based on the full-height full-pressure scaling concept. Semiscale Mod-2C was a scaled model representation of a Westinghouse four-loop PWR plant with a fluid volume scaling ratio of about 1/1,705. The pressure vessel featured an external downcomer, the intact primary loop simulated three combined unaffected loops and the broken primary loop simulated one loop with a break. Accordingly, the intact loop steam generator (SG) consisted of six inverted U-tubes and the broken loop SG had two inverted U-tubes. As documented in Table 1, "Comparison of Semiscale Systems," by G. G. Loomis, "Summary of the Semiscale Program (1965-1986)," NUREG/CR-4945, EGG-2509, July 1987, the Semiscale Mod-2C primary system piping was all stainless steel with the broken loop being 1.5-inch Schedule 160 pipe and most of the intact loop being 2.5-inch Schedule 160 pipe.

A special 0.5-inch tubing bypass line connected the downcomer to the upper head to simulate the leakage between these two components in commercial PWRs. According to G. G. Loomis and J. E. Streit, "Results of Semiscale Mod-2C Small-Break (5 percent) Loss-of-Coolant Accident Experiments S-LH-1 and S-LH-2," NUREG/CR-4438, EGG-2424, November 1985, this PWR leakage flow varies between 0.5 percent and 4 percent of the total core flow.

Test S-LH-1, which simulated a 5 percent cold leg, centerline, communicative break in the loop piping between the pump and the vessel downcomer, exhibited important small break LOCA phenomena including liquid holdup in SG U-tubes, consequent core uncover, and sequential loop seal clearance in the intact and broken loops. The upper head to downcomer bypass flow was calibrated at 0.9 percent of the recirculation flow by installing 0.125-inch thick flat plate orifice with 0.116-inch diameter hole in the bypass line to reduce steam venting through the spray nozzles during the transient. The experiment is described by G. G. Loomis and J. E. Streit, "Results of Semiscale Mod-2C Small-Break (5 percent) Loss-of-Coolant Accident Experiments S-LH-1 and S-LH-2," NUREG/CR-4438, EGG-2424, November 1985.

An early core uncover prior to loop seals clearance caused a first heater-rod heatup. The observed loop seal clearing in the intact loop at 171.4 s and in the broken loop at 262.3 s allowed the core to refill and cool after the first core uncover. During the period of the first core uncover, the uphill side of the SGs had liquid holdup, which was dependant on the heat transfer and CCFL phenomenon in the U-tubes. A second core uncover was caused by reduced system inventory later in the transient.

- (1) Please describe the WCOBRA/TRAC-TF2 model used to simulate Semiscale Mod-2C Test S-LH-1. Explain which special modeling features were activated in the analysis and describe any modeling parameter adjustments if such were employed in the analysis.
- (2) Please present WCOBRA/TRAC-TF2 assessment results using Semiscale
- (3) Mod-2C Test S-LH-1 experimental data. Show comparison plots for important parameters such as core collapsed and two-phase mixture levels, differential pressures reflecting manometric fluid head balance in both tests loops, and heater rod temperatures. In particular, please compare differential pressures and collapsed liquid levels in the uphill and downhill sides of the SGs, loop seal uphill and downhill differential pressures for both loops, rod surface temperature at the 208-cm elevation, break mass flow rate, and integrated break mass flow.

Response:

With regards to Item (1), the WCOBRA/TRAC-TF2 model of the Semiscale Mod-2C facility is described in Section 2.0 of the attached integrated response.

In response to the request in Items (2) and (3), Section 3.0 of the integrated response presents the steady-state and transient calculation results for the Semiscale S-LH-1 test.

RAI Question #110: Semiscale Test S-LH-2 Assessment of WCOBRA/TRAC-TF2

Semiscale Tests S-LH-1 and S-LH-2 were performed using the Semiscale Mod-2C facility configuration. Both tests simulated a 5 percent centerline communicative break in the cold leg piping between the pump exit and the vessel downcomer. For this purpose, the break was simulated by an orifice of a 0.20-ft² scaled area and an equivalent break diameter of 6.1 inch corresponding to a 4.92 percent break size based on a 27.5-inch PWR cold leg diameter.

In Test S-LH-1, a flat plate orifice with a 0.25 contraction ratio hole was installed in the special 0.5-inch tubing bypass line between the downcomer and the upper head. In Test S-LH-2, this orifice was removed. This resulted in initial condition core bypass flows of 0.9 percent and 3 percent in Test S-LH-1 and Test S-LH-2, respectively. Although these bypass flows differed by a ratio of 3.3, both values were thought to be within the range of possible PWR bypass flow. The bypass line hydraulic resistances for both tests are provided by G. G. Loomis and J. E. Streit, "Results of Semiscale Mod-2C Small-Break (5 percent) LOCA Experiments S-LH-1 and S-LH-2," NUREG/CR-4438, EGG-2424, November 1985.

As performed, Tests S-LH-1 and S-LH-2 examine the effect of the core bypass flow on the small break LOCA transient response. With regard to loop seal clearance in particular, Test S-LH-1, which had 0.9 percent bypass flow, exhibited loop seal clearance in both loops, first in the intact loop at 171.4 s followed by the broken loop at 262.3 s. In contrast, Test S-LH-2, which simulated 3 percent bypass flow, exhibited loop seal clearance only in the intact loop at 205.4 s with no clearance in the broken loop.

- (1) Please describe the representation of the special 0.5-inch tubing bypass line between the downcomer and the upper head in the WCOBRA/TRAC-TF2 model used to simulate Semiscale Mod-2C Test S-LH-1 and Test S-LH-2.
- (2) Please present WCOBRA/TRAC-TF2 assessment results using Semiscale Mod-2C Test S-LH-2 experimental data. Show comparison plots for important parameters such as core collapsed and two-phase mixture levels, differential pressures reflecting manometric fluid head balance in both tests loops, and heater rod temperatures. In particular, please compare differential pressures and collapsed liquid levels in the uphill and downhill sides of the SGs, loop seal uphill and downhill differential pressures for both loops, rod surface temperature at the 208-cm elevation, break mass flow rate, and integrated break mass flow.
- (3) Please present comparison results between WCOBRA/TRAC-TF2 predictions for Semiscale Mod-2C Test S-LH-1 and Test S-LH-2. Show comparison plots for important parameters such as core collapsed and two-phase mixture levels, differential pressures reflecting manometric fluid head balance in both tests loops, and heater rod temperatures. In particular, please compare differential pressures and collapsed liquid levels in the uphill and downhill sides of the SGs, loop seal uphill and downhill differential pressures for both loops, rod surface temperature at the 208-cm elevation, break mass flow rate, and integrated break mass flow. As part of the comparative analysis, use experimental

data from both tests when assessing the WCOBRA/TRAC-TF2 capabilities in modeling effects associated with core bypass flow, particularly with regard to impact on loop seal behavior.

Response:

In response to Item (1), Section 2.2 of the integrated response contains a description of the spray bypass line modeling approach.

For Item (2), Section 3.0 of the integrated response provides the results of the steady-state and transient calculations performed for the S-LH-2 test.

For Item (3), Section 3.2.3 of the integrated response provides a comparative analysis of the S-LH-1 and S-LH-2 test simulation results.

RAI Question #111: Sensitivity of WCOBRA/TRAC-TF2 Semiscale Predictions to SG Nodalization

The 5 percent SBLOCA Semiscale Test S-UT-8, performed with the Semiscale Mod-2A test facility system configuration, revealed the possibility for primary liquid holdup in the PWR SGs during a small break LOCA. In this test, condensation-induced filling of the SG tubes in the intact loop caused an extreme core liquid level suppression prior to the clearance of the liquid seal formed in the pump suction crossover piping. Test S-UT-8 data is reported by W. W. Tinkle, "Test data Report on Westinghouse Reactor Vessel Level Indicating System Performance during Semiscale Test S-UT-8," EGG-SEMI-5827, March 1982. The same effect was observed in Semiscale Mod-2C Tests S-LH-1 and S-LH-2 as reported by G. G. Loomis and J. E. Streit, "Results of Semiscale Mod-2C Small-Break (5 percent) Loss-of-Coolant Accident Experiments S-LH-1 and S-LH-2," NUREG/CR-4438, EGG-2424, November 1985.

The Semiscale Mod-2C intact loop was equipped with a Type II SG, which was a lumped representation of the three SGs in the intact loops of the reference Westinghouse four-loop plant. The affected Semiscale Mod-2C loop was equipped with a Type III SG featuring an external downcomer for γ -densitometer measurements. Accordingly, the intact loop Type II SG model had 6 inverted U-tubes: 2 short, 2 medium, and 2 long tubes representative of the range of bend elevations in a typical PWR SG, as described by Y. S. Bang et al., "Assessment of RELAP5/MOD3.2 With the Semiscale Natural Circulation Experiment, S-NC-8B," NUREG/IA-0144, August 1998. The affected loop Type III SG model had two inverted U-tubes with a 22.2-mm (0.87-inch) OD.

A simple sensitivity study on the nodalization of the SGs using an earlier version of RELAP5 was performed by C. Lee, T. Ito, and P. B. Abramson, "Sensitivity of SBLOCA Analysis to Model Nodalization," Paper CONF-830901-2, Anticipated and Abnormal Plant Transients in Light Water Reactors Conference, 26 September 1983, Jackson, Wyoming. The analysis examined a 4-inch cold leg break in a Westinghouse four-loop plant using a coarse SG nodalization with 4 vertically stacked secondary side nodes in the U-tube region and the corresponding 8 nodes in the U-tubes, 4 in the uphill side and 4 in downhill side. The U-tube bend sections were modeled with 2 nodes, one on each side. In the fine noding scheme, the number of nodes in the SGs was doubled while keeping the rest of the plant model identical. In this case, the U-tube bends were represented by 4 nodes, 2 on each side.

The study revealed that the predicted transient behavior was quite sensitive to the implemented SG nodalization schemes. While global system parameters, such as integrated break mass discharge, primary liquid inventory, and primary system pressure were relatively insensitive to the nodalization, the predicted distribution of coolant inventory in the primary loops was significantly affected by change in nodalization. In particular, more detailed nodalization led to prediction of higher liquid holdup in the SG U-tubes thus resulting in less coolant inventory in the reactor vessel and therefore causing earlier and more severe core uncover.

- (1) Please present sensitivity results for Semiscale Mod-2C Tests S-LH-1 and S-LH-2, which examine the effect of SG nodalization on small break LOCA predication results. For this purpose, please present test prediction results obtained with a SG nodalization scheme corresponding to the standard noding approach adopted in WCOBRA/TRAC-TF2 for modeling of SGs with inverted U-tube bundles. In addition, please present test prediction results obtained with a refined noding using a doubled number of nodes (cells) to represent the SG U-tube bundle. Also, please present sensitivity results examining the impact of refined nodalization of the 180°-bend region of the U-tube bundle by increasing further the number of cells representing this region. Compare the code test predictions against key measured quantities in each test.
- (2) Please present sensitivity results, as requested in Item (1) above, using SG models with split representation of the U-tube bundles. For this purpose, please model when the intact loop Type II SG U-tubes using three PIPE hydraulic components each representing two U-tubes. Please split the U-tubes in the SG bundle based on the U-tube apex elevations so that tubes with a different length are represented by individual hydraulic components. Please use two PIPE hydraulic components to model the broken loop Type III SG U-tubes individually.
- (3) When providing the information requested in Items (1) and (2) above, please include, among other important parameters, WCOBRA/TRAC-TF2 predictions for the SG U-tube bundle upside and downside collapsed liquid levels in the broken and in the intact loops, the uphill and downhill loop seal collapsed liquid levels in both loops, and the vessel core-side and downcomer-side collapsed liquid levels. Please compare obtained code predictions against test measurements as appropriate.

Response:

For Item 2, Westinghouse previously provided the justification and rationale of using single-pipe U-tube model in the response to RAI 48 (Steam Generator Modeling), transmitted to the NRC in LTR-NRC-13-73 [1]. The Semiscale simulations presented in this response use a single-pipe U-tube model of the steam generators.

For Items 1 and 3, see Section 3.2.4 of the integrated response.

Reference:

- 1) Letter from J. Gresham to NRC Document Control Desk, "Submittal of Westinghouse Responses to WCAP-16996-P, 'Realistic LOCA Evaluation Methodology Applied to the Full Spectrum of Break Sizes (FULL SPECTRUM LOCA Methodology)' Requests for Additional Information – RAIs 46 – 58, 75 and 77," (Proprietary), Project 700, TAC No.ME5244.

Integrated Response to NRC RAIs 109, 110 and 111:
**WCOBRA/TRAC-TF2 Simulations of the Semiscale Mod-2C Small Break
Loss-of-Coolant Tests S-LH-1 and S-LH-2**

1.0 Introduction

The Semiscale facility is a small scale (1:1705) replica of a 4-loop Westinghouse pressurizer water reactor (PWR) which includes all of the major components. The simulated reactor vessel houses an electrically heated bundle consisting of 25 rods (23 heated and 2 unheated) with a total power of 2 MW. The overall scaling philosophy used in designing the facility is the maintenance of the power-to-volume ratio, coupled with a 1:1 elevation scaling criteria (Larson, et al., 1982 [1] and Loomis, 1987 [2]). The facility is capable of operating at actual nuclear power plant pressures and temperatures, and therefore, a full range of pressures and fluid states occurs during a transient.

There are two loops in the facility, with one scaled as a single loop, and the other scaled to represent three combined loops. The facility evolved through several major modifications over the course of approximately a decade of testing and was used for both large and small break experiments. Later modifications to the facility focused on small break loss-of-coolant accident (LOCA) phenomena with extensive instrumentation installed to measure key parameters such as fluid density, liquid levels, break discharge rates, etc.

1.1 Key Phenomena

The purpose of the small-break LOCA experiments conducted at the Semiscale test facility was to provide information concerning the overall system behavior and interaction of phenomena that occur during the various stages of the accident in a complete integral reactor coolant system (RCS). Comparisons of calculated results to the experiments will be focused on general phenomena such as relative timing of events, magnitude of particular thermal-hydraulic parameters and factors which influence fluid distributions within the RCS.

One particular phenomenon that the facility can be used to address is the integral effects nature of loop seal clearing. While separate effects facilities like the Upper Plenum Test Facility (UPTF), Reference [3], address the 3-D phenomena in loop seal clearance given fixed fluid conditions, they do not provide information on the general aspects of how the loop seals behave over the course of a transient in relation to the fluid distribution in the entire RCS. The accuracy with which the code is able to calculate loop seal formation and clearing will be important in establishing its capability to model more complex system interactions, including phase separation and other phenomena for the nuclear power plant (NPP) calculations.

Another important phenomenon that influences the severity of small break transients is steam generator tube liquid holdup. This holdup phenomenon was first identified experimentally in a Semiscale small break LOCA experiment (Leonard, 1982 [4]); it has since been duplicated in other facilities such as ROSA (Osakabe, et al., 1987 [5]) and has been discussed extensively in the open literature (Leonard, 1982 [6]). Steam generator liquid holdup is the result of steam being condensed in the upflow side of the tubes relatively early during a small break LOCA transient. This liquid is unable to drain by gravity back through the hot leg into the upper plenum because it is impeded by high upward steam flowrates. The large pressure drop induced by this holdup, in turn, affects the hydrostatic head balances throughout the RCS. Whether the pump suction seal clearing phenomenon discussed above results in core uncover or

not, is significantly affected by the amount of liquid holdup in the steam generator U-tubes and the hot leg elbows as well.

Other important phenomena, investigated at the Semiscale tests, are break flow, vessel and downcomer collapsed and mixture levels and rod heatup.

1.2 Applicable Tests

The following are two small-break LOCA experiments conducted in the final Semiscale Mod-2C configuration (Loomis and Streit, 1985a [7]):

S-LH-1: A 6.1-inch equivalent cold leg break with downcomer-to-upper head bypass set to 0.9 percent at steady-state

S-LH-2: A 6.1-inch equivalent cold leg break with downcomer-to-upper head bypass set to 3 percent at steady-state

Both of these tests exhibited core uncoveries, which allows for investigation of in-bundle mixture level swell and rod heat transfer (Loomis and Streit, 1985b [8]). The purpose of varying the vessel upper head bypass was to investigate the influence of this relief path on the core liquid level depressions that occur due to manometric balances that form among various sections of the RCS: the core/downcomer, pump suction crossover legs, and steam generator tubes. The transients exhibited a notable difference in the amount of core uncover and rod heatup as a function of upper head bypass flow. The difference was attributed mainly to the timing of upper head drain, which clears a relief path between the upper plenum and the downcomer/cold leg.

1.3 Semiscale Facility Configuration for Tests S-LH-1 and S-LH-2

The loop arrangement of the Semiscale Mod-2C is shown in Figure 1.3-1. In conducting the small pipe break experiments, a break spool piece is inserted in the loop that is scaled to represent a single PWR loop and is designated as the broken loop; detail shown in Figure 1.3-2. The break orifice has a diameter of 0.1488 inches (3.78 mm) and is scaled to represent 5 percent of the area of a full-size (27.5-inch inside diameter) cold leg of a 4-loop Westinghouse PWR, which is equivalent to a 6.1-inch inside diameter break at full-scale. It is positioned at the horizontal centerline of the cold leg piping, so the break flow would be susceptible to flow regimes in the piping, such as stratification. All of the break discharge is passed through a system of condensing coils and is collected in a catch tank.

The layout of the vessel upper head area is depicted in Figure 1.3-3. A bypass line connects the top of the downcomer to the upper head at elevations representative of the reference PWR. A replaceable orifice is inserted in the bypass line and used to adjust the bypass flow ratio to the desired value for the particular experiment. A single tube is scaled to represent the flow area and elevations for the aggregate of all the control rod guide tubes (GT) in a PWR. There are also two tubes representing upper internals support columns, which connect the upper head to the upper core plate.

The core in the Semiscale facility (5x5 rod array) is composed of 2 unpowered and 23 electrically heated rods, each of which are geometrically similar to nuclear fuel rods in a PWR with 0.422-inch (1.072 cm) outside diameter cladding. The rods are capable of operating at the full steady-state power of a PWR nuclear rod. The resistive element windings of each heated rod are sized such that a stepped cosine axial

power profile is established, as shown in Figure 1.3-4, with a peak linear power of approximately 11.2 kW/ft at full power.

The steam generators are scaled to a full 1:1 elevation matching the reference PWR. There are a total of six U-tubes in the intact loop steam generator (each 7/8-inch outside diameter, 49-mil thick) and two U-tubes in the broken loop steam generator (each 7/8-inch OD, 65-mil thick) conserving the scaled heat transfer areas.

Elevation scaling is preserved 1:1 relative to the reference PWR. The Semiscale hot legs join together the vessel and the steam generator inlet plenums. The cold leg and hot leg centerline elevations are offset so that the HL centerline elevation is 8.5-in higher than that of the cold leg.

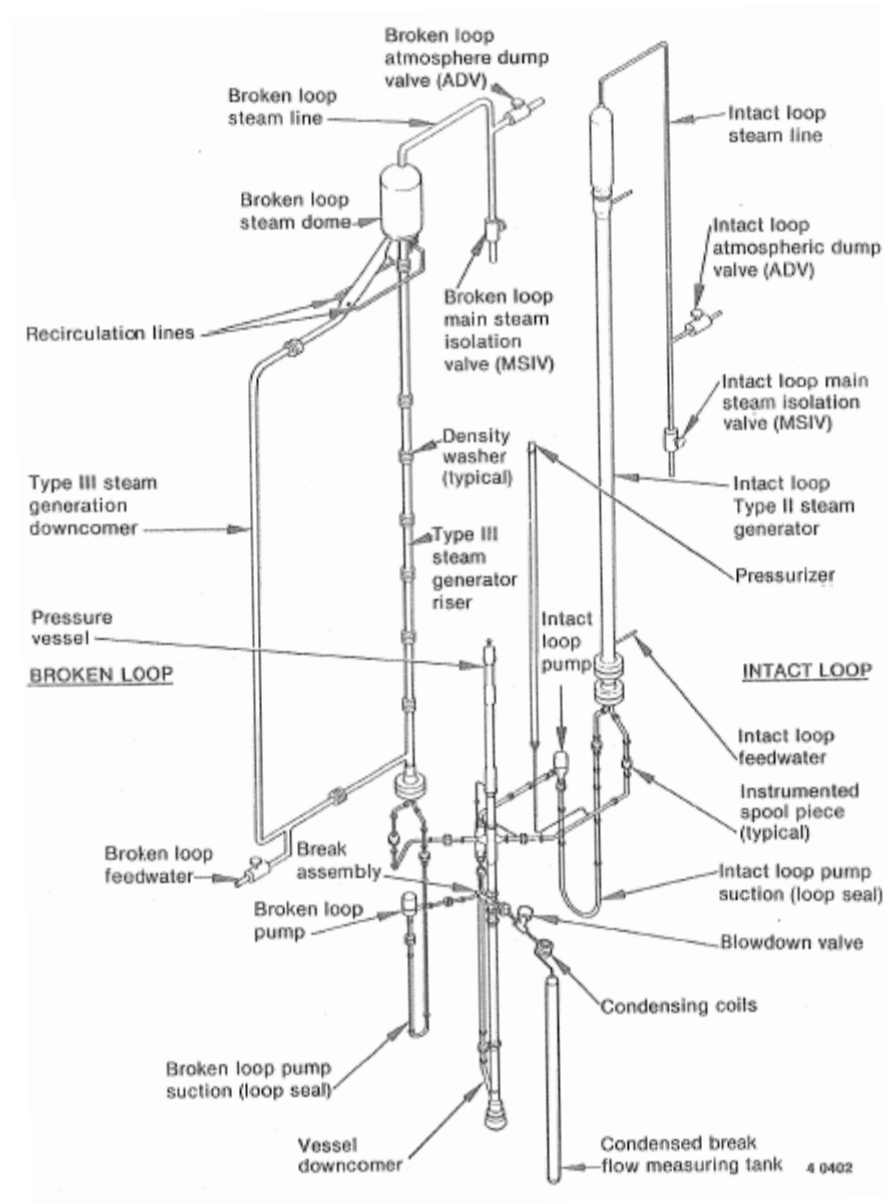


Figure 1.3-1 Semiscale Mod-2C System Configuration

(EGG-SEMI-6318, Figure 1)

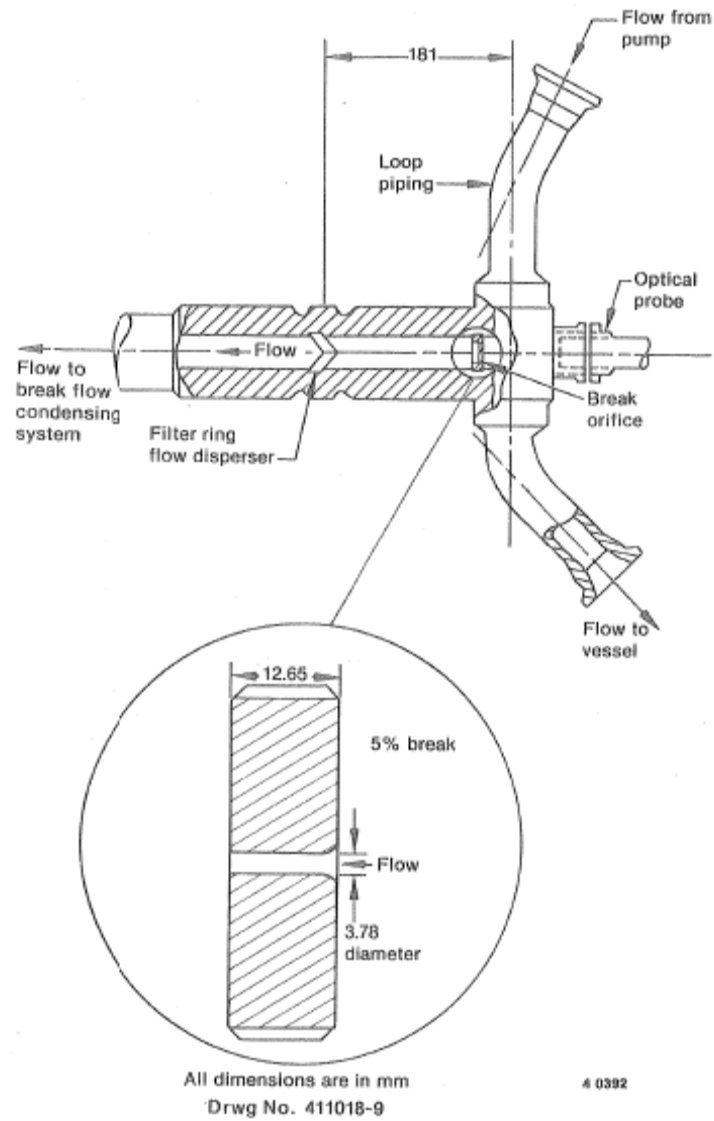


Figure 1.3-2 Break Spool Configuration for Semiscale Tests S-LH-1 and S-LH-2
(EGG-SEMI-6318, Figure 6)

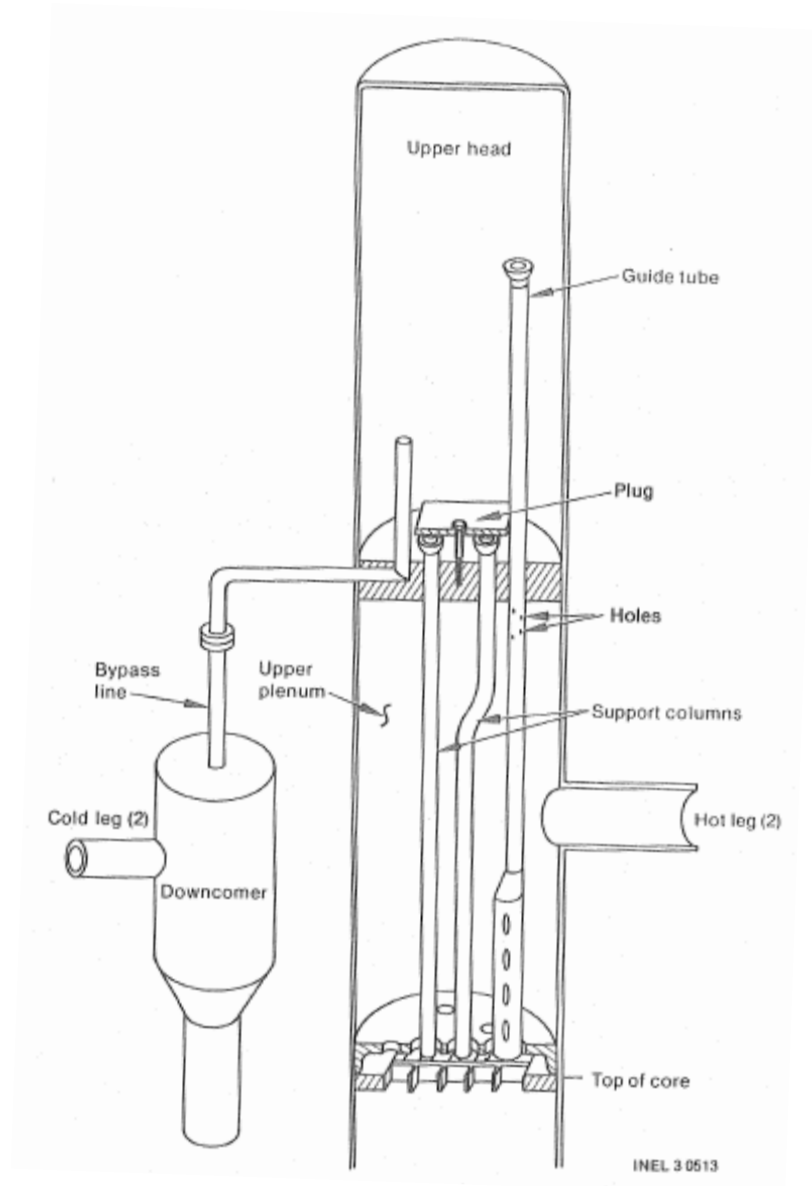


Figure 1.3-3 Vessel Upper Head Configuration for Semiscale Tests S-LH-1 and S-LH-2

(EGG-SEMI-6318, Figure 8)

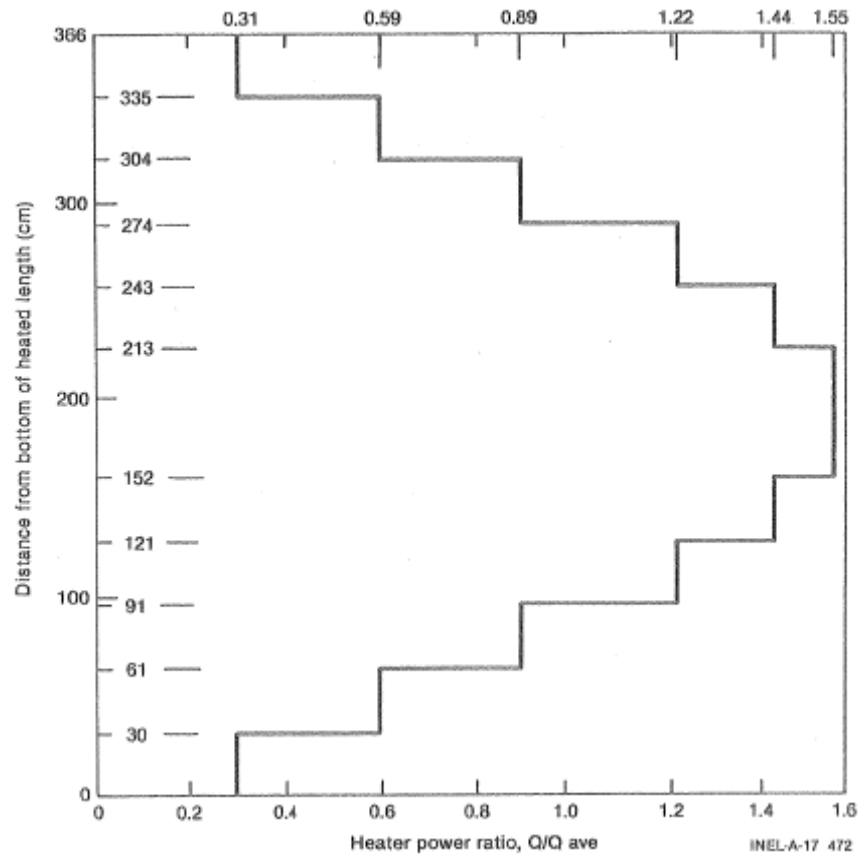


Figure 1.3-4 Axial Power Profile for the Semiscale Mod-2C Heater Core
(EGG-SEMI-6318, Figure 10)

2.0 Description of the WCOBRA/TRAC-TF2 Model of the Semiscale Mod-2C Configuration

Design information used to compile the Semiscale model presented herein was obtained largely through the review of available Semiscale reports. Key parameters were compared to the facility description in available Semiscale reports and RELAP5 model documented in NUREG/IA-0099 [9]. Utilization of the information in [9] assumes that the RELAP5 model documented therein adequately represents the key Semiscale Mod-2C facility detail, pertinent to the particular purpose of the WCOBRA/TRAC-TF2 model used for the Semiscale test simulations presented herein. Whenever possible, further confirmation of this assumption has been performed by using additional Semiscale Mod-2C and Mod-2A information from available test reports.

2.1 Semiscale Loop (1-D) Network Model

The primary loop piping and the steam generators are modeled using TRAC 1-D loop components. Figure 2.1-1 shows the general component layout of the WCOBRA/TRAC-TF2 model of the Semiscale Mod-2C system. The component numbers are enclosed in squares and junctions are identified by the numbered circles. In this figure, the vessel and downcomer, modeled using 3-D vessel channels (Figure 2.2-1) are only shown in general view.

Semiscale Hot Legs and Pressurizer Modeling:

The intact loop (IL) hot leg is modeled by the main pipe of TEE#10. The side pipe of TEE#10 represents the pressurizer surge line, which is attached to the bottom of the PRIZER#31 component. The broken loop (BL) hot leg is modeled by PIPE#20.

[

] ^{a,c}

Steam Generator Modeling:

[

] ^{a,c}

At the tests, SG secondary side is isolated by terminating the feedwater and closing the main steam isolation valves (MSIV) at low pressurizer pressure signal (12.6 MPa). To prevent secondary side overpressurization due to the MSIV closure, automatic dump valves (ADV) were installed on each steam generator. However, as mentioned in Section 2.2 and Section 3.1 of EGG-SEMI-6884 [7], at the tests the ADV were not actuated; thus the secondary side pressure response was defined by the balance between

the primary-to-secondary side heat transfer, the heat stored in the SG metal structures and the heat loss to the environment.

[

] ^{a,c}

Cross-Over Legs Modeling:

[

] ^{a,c}

Primary System Recirculation Pumps:

The standard PUMP component of WCOBRA/TRAC-TF2 is used to model the Semiscale recirculation pumps. A set of rated parameters (speed, head, and torque) and four quadrant homologous curves are supplied for each of the two pumps. Because the Semiscale pumps physically do not have a scaled moment of inertia, their rotational speed is controlled following a forced coastdown curve after the trip. This behavior is replicated in the pump input to WCOBRA/TRAC-TF2 for the simulation of the S-LH-1 and S-LH-2 tests. In general, because the pumps are tripped relatively early in the transient, the effective/active contribution of the pumps to the fluid redistribution within the primary system occurs primarily during periods in which they are pumping with a positive head of single-phase liquid. The pump homologous curves are consistent with those used in the RELAP5 model in NUREG/IA-0099 [9].

Cold Leg Noding:

[

] ^{a,c}

Emergency Core Cooling System (pumped safety injection and accumulator) Modeling

The Semiscale Mod-2C facility has an emergency core cooling safety injection system (ECCS) which uses high pressure positive displacement pumps. The pumps were controlled by a computer which used a pressure measurement from the RCS as input to vary the injection rate as a function of pressure. A prescribed curve was followed to simulate the performance of a centrifugal pump. Figures 2.1-2 and 2.1-3 show the injection rates for the intact and broken loop safety injection (SI) pumps as a function of pressure, as actually derived from the recorded experimental data for the S-LH-1 and S-LH-2 tests.

The curves for the intact loop pump for both tests show changes to the injection flow over the range of pressures from about 2.5 to 5.5 MPa. [

] ^{a,c}

The two accumulators inject into the respective ECCS header TEEs through their respective check VALVES. The individual accumulator capacities were modeled [

] ^{a,c}

Counter-current Flow Limitations:

[

] ^{a,c}Heat Loss to Environment:

As described in Section 2.1.5 of EGG-SEMI-6813 [11], to compensate for the heat loss to the environment, heater tapes were installed on the exterior of the primary system pressure boundary – the vessel, hot legs, cold legs, the intact and broken loop cross-over legs (pump suction) and the pressurizer. Power to the heater tapes was controlled separately. At the tests, the heater power delivered to the individual heaters was varied to compensate the estimated heat losses to the environment. The time-dependent heater power, implemented at each test, was predetermined such that it would compensate the expected heat losses to environment; [

] ^{a,c}

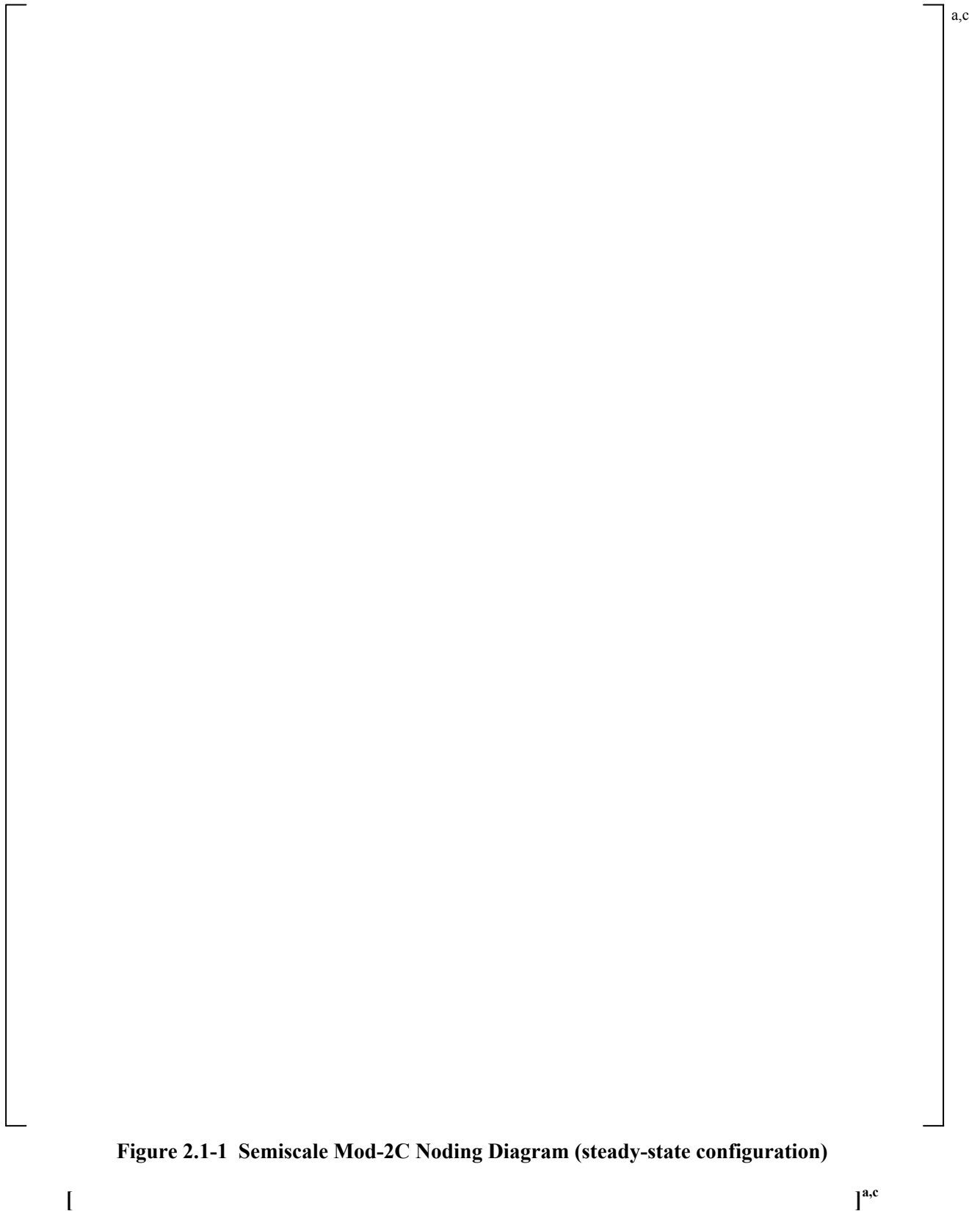




Figure 2.1-2 Modeled Pumped Safety Injection for S-LH-1



Figure 2.1-3 Modeled Pumped Safety Injection for S-LH-2

2.2 Semiscale Downcomer and Vessel Model

Figure 2.2-1 shows the nodalization of the simulated Semiscale vessel and downcomer using COBRA 3-D vessel channels. To the largest extent possible, the WCOBRA/TRAC-TF2 noding of the Semiscale facility is consistent with the nodalizations used for ROSA-IV LSTF and in the PWR demonstration calculations. Figure 2.2-1 shows the elevations within the vessel for the WCOBRA/TRAC-TF2 analysis; the section boundary elevations are relative to the inside of the bottom of the vessel. Values within squares are channel numbers, and values within circles are gap numbers.

[

] ^{a,c}

Core Region and Rod Power Simulation:

[

] ^{a,c}

[

] ^{a,c}

Noding Consistency with ROSA and PWR Models:

The Semiscale Mod-2C vessel model is designed to be generally consistent with the ROSA and PWR vessel noding [10] in key areas.

[

] ^{a,c}

2.3 Summary of Special Modeling Features

The following are the key special modeling features implemented in the WCOBRA/TRAC-TF2 model of Semiscale Mod-2C.



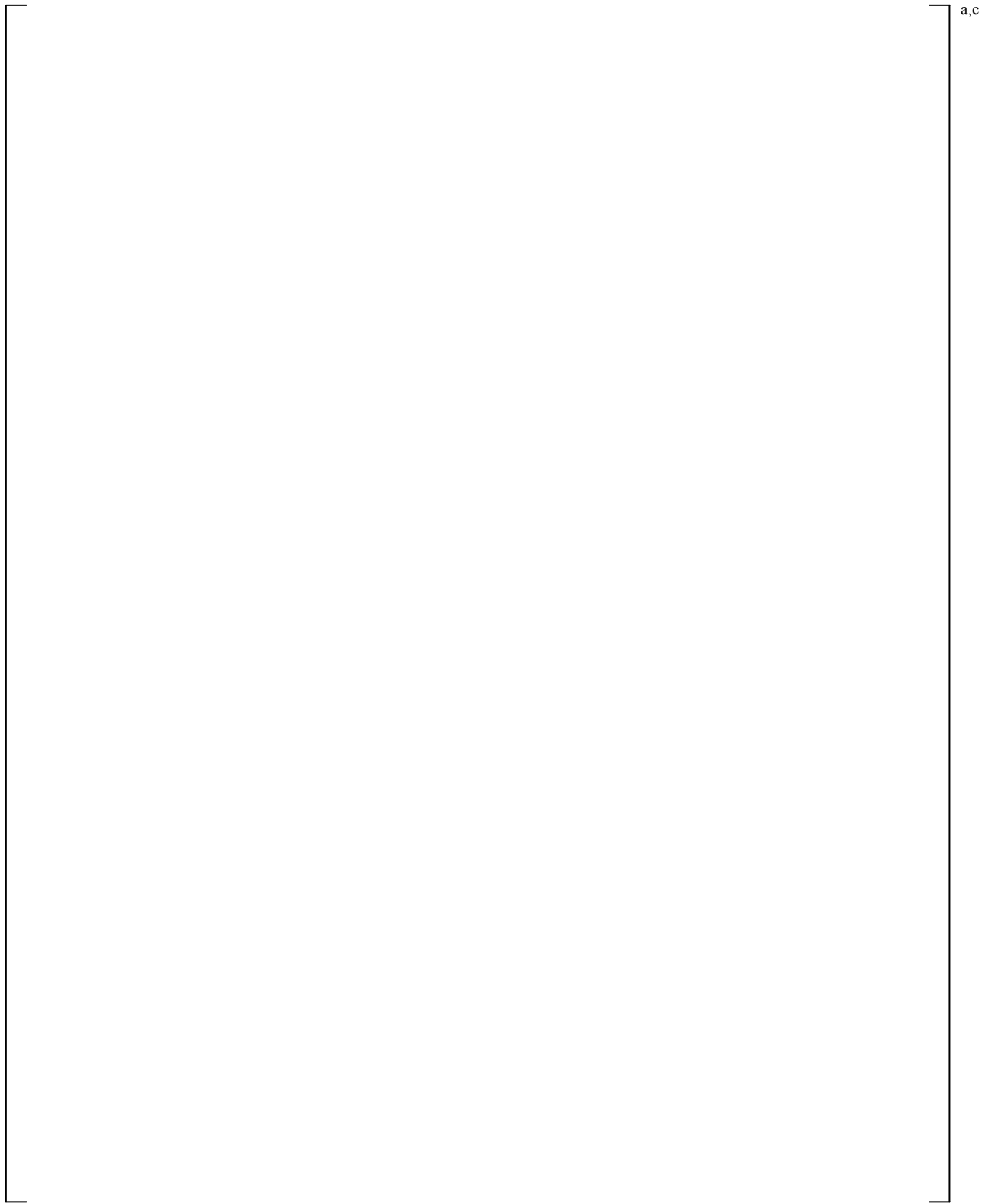


Figure 2.2-1 Semiscale Mod-2C Downcomer and Vessel Model Using COBRA 3-D Channels

3.0 Base Case Steady-State and Transient Calculations

3.1 Steady-State Calculations

Steady-state operating conditions are achieved in the WCOBRA/TRAC-TF2 model by running the code with no break in the system until conditions have stabilized. Table 3.1-1 compares the key parameters from test S-LH-1 to those obtained by the model; Table 3.1-2 provides the same information for test S-LH-2. Relative to the target values, the key parameters are within a range acceptable for conducting validation simulations. The vessel upper head bypass flow ratios in the WCOBRA/TRAC-TF2 steady-state simulation match the S-LH-1 and S-LH-2 experiments well. [

] ^{a,c}

Table 3.1-1 Steady-State Parameter Checklist (Initial Conditions) for the S-LH-1 Test			
Parameter	Target ⁽¹⁾	Modeled	
Pressurizer pressure, MPa (psia)	15.46 (2243)		a,c
Hot leg fluid temperature, K (°F)	599.0 (618.5)		
Cold leg fluid temperatures, K (°F)			
- Intact Loop	562.0 (552.0)		
- Broken Loop	564.1 (555.7)		
Core power, kW (MBTU/hr)	2014.75 (6.881)		
Primary loop flow rates, m ³ /min (gpm)			
- Intact Loop	0.572 (151.2)		
- Broken Loop	0.192 (50.7)		
Core inlet flow rate, m3/min (gpm) ⁽²⁾	0.757 (200.0) ⁽²⁾		
DC-to-UH Bypass Flow Rate,			
- m3/min (gpm)	0.0067 (1.776)		
- % core flow	0.88 ⁽³⁾		
Pressurizer water level, m (ft)	3.95 (12.96) ⁽⁵⁾		
Upper plenum to SG inlet (hot leg) ΔP, kPa (psi)			
- Intact loop	44.8 (6.5)		
- Broken loop	41.4 (6.0)		
Steam generator inlet to outlet, kPa (psi)			
- Intact loop	140.0 (20.3)		
- Broken loop	190.3 (27.6)		
Cross-Over Leg Down ΔP, kPa (psi)			
- Intact loop	15.0 (2.17)		
- Broken loop	-19.7 (-2.86)		
Cross-Over Leg Up ΔP, kPa (psi)			
- Intact loop	19.2 (2.79)		
- Broken loop	23.0 (3.34)		
Downcomer ΔP, kPa (psi)	13.1 (1.9)		
Inner vessel ΔP (including lower plenum, core and part of upper plenum), kPa (psi)	147.9 (21.45)		
Downcomer to upper head bypass ΔP, kPa (psi)	142.7 (20.7)		
Upper Head Temperature, K (°F)	562.5 (552.9)		

Table 3.1-1 Steady-State Parameter Checklist (Initial Conditions) for the S-LH-1 Test			
Steam generator secondary pressure, MPa (psia)			a,c
- Intact Loop	5.72 (830) ⁽⁴⁾		
- Broken Loop	6.08 (882) ⁽⁴⁾		
Steam generator feedwater temperature, K (°F)			
- Intact loop	508.8 (456.2)		
- Broken loop	507.2 (453.3)		
Steam generator feedwater flow rate, kg/sec (lbm/s)			
- Intact loop	0.81 (1.79) ⁽⁵⁾		
- Broken loop	0.27 (0.60) ⁽⁵⁾		

Notes:

- (1) All target values are as measured at the test, unless specified otherwise in the following notes.
- (2) Core inlet flow is calculated as (Total primary loop flow)-(DC-to-UH Bypass Flow Rate)
- (3) Table 1 of [12] shows a 0.9% core bypass flow value.
- (4) Table 1 of NUREG/IA-0064 [12].
- (5) Table 10 of EGG-SEMI-6813 [11].

Table 3.1-2 Steady-State Parameter Checklist (Initial Conditions) for the S-LH-2 Test			
Parameter	Target ⁽¹⁾	Modeled	
Pressurizer pressure, MPa (psia)	15.42 (2237)		a,c
Hot leg fluid temperature, K (°F)	598.5 (617.6)		
Cold leg fluid temperatures, K (°F)			
- Intact Loop	562.0 (551.9)		
- Broken Loop	564.3 (556.1)		
Core power, kW (MBTU/hr)	2006.2 (6.851)		
Primary loop flow rates, m ³ /min (gpm)			
- Intact Loop	0.590 (156.0)		
- Broken Loop	0.162 (42.74)		
Core inlet flow rate, m ³ /min (gpm) ⁽²⁾	0.729 (192.7) ⁽²⁾		
DC-to-UH Bypass Flow Rate,			
- m ³ /min (gpm)	0.0228 (6.013)		
- % core flow	~3.0 ⁽³⁾		
Pressurizer water level, m (ft)	3.93 (12.89) ⁽⁵⁾		
Upper plenum to SG inlet (hot leg) ΔP, kPa (psi)			
- Intact loop	44.9 (6.8)		
- Broken loop	33.1 (4.8)		
Steam generator inlet to outlet, kPa (psi)			
- Intact loop	147.5 (21.4)		
- Broken loop	136.5 (19.8)		
Cross-Over Leg Down ΔP, kPa (psi)			
- Intact loop	18.5 (2.68)		
- Broken loop	-25.0 (-3.62)		
Cross-Over Leg Up ΔP, kPa (psi)			
- Intact loop	19.4 (2.81)		
- Broken loop	21.4 (3.11)		
Downcomer ΔP, kPa (psi)	16.2 (2.35)		
Inner vessel ΔP (including lower plenum, core and part of upper plenum), kPa (psi)	140.7 (20.4)		
Downcomer to upper head bypass ΔP, kPa (psi)	120.0 (17.4)		
Upper Head Temperature, K (°F)	562.6 (553.0)		

Table 3.1-2 Steady-State Parameter Checklist (Initial Conditions) for the S-LH-2 Test			
Steam generator secondary pressure, MPa (psia)] a,c
- Intact Loop	5.70 (827) ⁽⁴⁾		
- Broken Loop	5.95 (863) ⁽⁴⁾		
Steam generator feedwater temperature, K (°F)			
- Intact loop	509.5 (457.4)		
- Broken loop	508.4 (455.5)		
Steam generator feedwater flow rate, kg/sec (lbm/s)			
- Intact loop	0.81 (1.79) ⁽⁵⁾		
- Broken loop	0.27 (0.60) ⁽⁵⁾		

Notes:

- (1) All target values are as measured at the test, unless specified otherwise in the following notes.
- (2) Core inlet flow is calculated as (Total primary loop flow)-(DC-to-UH Bypass Flow Rate)
- (3) Table 1 of [13] shows a 3.0% core bypass flow value.
- (4) Table 1 of NUREG/IA-0065 [13].
- (5) Table 10 of EGG-SEMI-6813 [11], no reference or measurement values for the feedwater flow rates are found for S-LH-2. Therefore, the target values are assumed to be the same as S-LH-1.

3.2 Base Case Transient Simulations

The simulations of tests S-LH-1 and S-LH-2 were initiated from the steady-state model conditions, as described in the previous section. In each of the test simulations, the cold leg break is modeled as proceeding from the break assembly location in the test facility. Similar to the ROSA-IV and the PWR approach, at the beginning of the transient calculation [

] ^{a,c}

Consistent with the ROSA and the PWR approach, [

] ^{a,c}

The following discussion will compare the code predictions to data from tests S-LH-1 and S-LH-2.

3.2.1 S-LH-1 Test Simulation Results

Figure 3.2.1-1(a) shows the pressurizer pressure from the WCOBRA/TRAC-TF2 test S-LH-1 calculation (PRZ PRESSURE curve) compared to test data (P*PRZ+632 curve). Overlaid on the same figure are curves comparing the secondary side pressures in the intact loop steam generator - simulated (PRESSURE) curve and the test (PIS+1117) curve. Figure 3.2.1-1(b) shows the overlay of the pressurizer pressures against the pressures in the broken loop steam generator; the (BL SG PRESS WCT) curve is the calculated pressure at the secondary side and the (PBG+1186) curve is the secondary side pressure measured at the test.

At the opening of the break, the model predicts [

] ^{a,c}

Once the primary system depressurizes to cold leg saturation (approximately 7.9 MPa), the depressurization rate slows appreciably both in the experiment and the calculation. The slowdown is primarily caused by the increase of the secondary side pressure due to the closure of the MSIV combined with heat removal by sustained primary-to-secondary side heat transfer. At these conditions the primary side pressure remains above the secondary side pressure with the break energy removal supplemented by continuing heat transfer to the steam generator secondary side fluid. The combined effect of these two processes defines the depressurization rate and the primary pressure holdup during the reflux condensation period. It is also noted that during the reflux condensation period loop seals are established in the cross-over legs and the break discharges primarily (low void) saturated liquid with fairly low volumetric flow. This further contributes to the pressure holdup observed at the test and the code predictions as well.

After the loop seals clear and the primary pressure falls below that at the SG secondary side, the calculated depressurization rate is slightly higher than that measured at the test.

Break Flow:

Figure 3.2.1-2(a) compares the calculated (MIXTURE MASS curve) and measured (MDOT*BREAK curve) break mass flow rates; Figure 3.2.1-2(b) compares the respective integrated break flows. In general, it is seen that the WCOBRA/TRAC-TF2 calculation [

] ^{a,c} At

the time when the intact loop seal clears at the test (~170sec), measured break flow drops suddenly due to [

] ^{a,c}

Steam Generator U-tube Draining:

The predicted draining of the steam generator U-tubes (primary side) is shown in Figure 3.2.1-3 (intact loop) and Figure 3.2.1-4 (broken loop). [

] ^{a,c}

Hot Leg Draining:

The draining of the hot legs is illustrated in Figures 3.2.1-5 and 3.2.1-6; in these figures (a) compares the predicted differential pressures and (b) compares the hot leg volumetric flows against the test data.

[

] ^{a,c}

The recorded increase in HL differential pressure prior to the loop seal clearance, 100-250 sec in Figure 3.2.1-6(a), indicates increased liquid holdup and is likely due to draining of the steam generator U-tubes,

100-250 sec in Figure 3.2.1-4(a). Following the broken loop clearance (250 sec), the recorded hot leg differential pressure indicates some liquid holdup in the broken hot leg, [

] ^{a,c} In the test data for the broken loop hot leg, Figure 3.2.1-6, there is an apparent discrepancy in that differential pressure is recorded while the measured volumetric flow rate is zero.

Loop Seal Clearance:

To illustrate the loop seal clearance, Figure 3.2.1-7 compares the differential pressures in the intact loop (a) and the broken loop (b) cross-over leg; the DPI and DPB curves represent the differential pressures measured at the test. [

] ^{a,c}

Downcomer and Vessel (core) Behavior:

The comparison of the downcomer differential pressures in Figure 3.2.1-8 is an indicator of the amount of liquid present in the downcomer. Just after the pumps stop rotating (~85 sec), the differential pressure measured at the test is about [

code calculates the level to be about [IL clearance (200 sec), the calculated [

] ^{a,c} At the same time, the
] ^{a,c} At the time of the onset of

] ^{a,c}

Figure 3.2.1-9 compares the differential pressure calculated in the vessel (core) region to the test data. Similar to the test, the simulation predicts two staggered level increases related to the occurrence of the intact and broken loop clearances, occurring at ~200 sec and ~260 sec, respectively.

[

] ^{a,c}

Upper Head Draining:

The draining of upper head is shown in Figure 3.2.1-10; it compares the upper head differential pressures as calculated by the code, curve (Upper Head dP), and the measured at the test, curve (LV+421+160).

[

] ^{a,c}

Core Mixture Level:

Figure 3.2.1-11 compares the calculated mixture levels in the two core channels to the mixture levels derived from the test data.

The test mixture levels shown in Figures 3.2.1-11 (a) and (b) are derived from the available data using two different methods. [

] ^{a,c}

[

] ^{a,c}Rod Heat-up:

Figure 3.2.1-12 compares the calculated rod heatup (TCLAD) for the heater rods in the core channel below the guide tube, to the test data. The rod heatup comparison is shown for three elevations relative to the bottom of the heated length. From the comparison it is observed that at about 250 sec the code calculates brief heatup [

] ^{a,c}

Figure 3.2.1-13 compares the calculated rod heatup (TCLAD) for the heater rods in the core channel below the open hole, to the test data. [

] ^{a,c}

[

] ^{a,c}

a,c

Figure 3.2.1-1 Pressurizer and Steam Generator Secondary Side Pressures

a,c

Figure 3.2.1-2 Break Flows

a,c

Figure 3.2.1-3 Intact Loop Steam Generator U-tube Differential Pressures

a,c

Figure 3.2.1-4 Broken Loop Steam Generator U-tube Differential Pressures

a,c

Figure 3.2.1-5 Intact Loop Hot Leg Draining

a,c

Figure 3.2.1-6 Broken Loop Hot Leg Draining

a,c

Figure 3.2.1-7 Cross-over Leg Differential Pressures



Figure 3.2.1-8 Downcomer Differential Pressures



Figure 3.2.1-9 Vessel (Core) Differential Pressures



Figure 3.2.1-10 Upper Head Differential Pressures

a,c

Figure 3.2.1-11 Core Mixture Level Comparison

a,c

Figure 3.2.1-12 Calculated Rod 1 Heatup (located under guide tube) vs. Test Data

a,c

Figure 3.2.1-13 Calculated Rod 2 Heatup (located under open hole) vs. Test Data

3.2.2 S-LH-2 Test Simulation Results

Figure 3.2.2-1(a) shows the pressurizer pressure from the S-LH-2 test calculation (PRZ PRESSURE curve) compared to the test data (P*PRZ+632 curve). Overlaid on the same figure are curves comparing the secondary side pressures in the intact loop steam generator - simulated (IL SG PRESS WCT) curve and the test (PIS+1117) curve; Figure 3.2.2-1(b) shows the overlay of the pressurizer pressures against the pressures in the broken loop steam generator.

[

] ^{a,c}

Once the primary system depressurizes to cold leg saturation (approximately 7.9 MPa), the depressurization rate slows appreciably both in the experiment and the calculation. The slowdown is primarily caused by the increase of the secondary side pressure due to the closure of the MSIV combined with heat removal by sustained primary-to-secondary side heat transfer.

After the loop seals clear and the primary pressure falls below that at the SG secondary side, [
] ^{a,c}

Break Flow:

Figure 3.2.2-2(a) compares the calculated (MIXTURE MASS curve) and measured (MDOT*BREAK curve) break mass flowrates; Figure 3.2.2-2(b) compares the respective integrated break flows. In general, it is seen that the WCOBRA/TRAC-TF2 calculation [
]

] ^{a,c}

Steam Generator U-tube Draining:

The predicted draining of the steam generator U-tubes (primary side) is shown in Figure 3.2.2-3 (intact loop) and Figure 3.2.2-4 (broken loop). The calculated draining is [
]

] ^{a,c}

Hot Leg Draining:

[

] ^{a,c}Loop Seal Clearance:

To illustrate the loop seal clearance, Figure 3.2.2-7 compares the differential pressures in the intact loop (a) and the broken loop (b) cross-over leg; the DPI and DPB curves represent the differential pressures measured at the test.

[

] ^{a,c}Downcomer and Vessel (core) Behavior:

The comparison of the downcomer differential pressures in Figure 3.2.2-8 is an indicator of the amount of liquid present in the downcomer. [

] ^{a,c}

Just after the pumps stop rotating (~85 sec), the differential pressure measured at the test is about 42 kPa, which is equivalent to about 5.86-m (586 cm) height, which indicates the downcomer level to be about 8 cm above the cold leg centerline. At the same time, the code calculates the level to be about 8 cm below the cold leg centerline. At the time of the onset of IL clearance (250 sec), the calculated deficit of the downcomer level (~5 kPa) relative to the test is roughly the same as the excess of fluid retained in the IL X-over leg, Figure 3.2.2-7(a). As the system inventory is depleted, the calculated downcomer level is reduced with a rate slightly lower than the test. The timing of the minimum level is consistent with the calculated intact loop accumulator injection.

[

] ^{a,c}Upper Head Draining:

The draining of upper head is shown in Figure 3.2.2-10; it compares the upper head differential pressures as calculated by the code, curve (Upper Head dP), and the measured at the test, curve (LV+421+160).

[

] ^{a,c}Core Mixture Level:

Figure 3.2.2-11 compares the calculated mixture levels in the two core channels to the mixture levels derived from the test data.

The S-LH-2 test mixture levels, curves Test (T ROD) and Test (Density), are derived from the test data using the methods implemented for the S-LH-1 test mixture levels, described in Section 3.2.1.

Figure 3.2.2-11(a) compares the calculated mixture level in the core channel under the guide tube to the test data. Consistent with the test, the code does not predict core uncover prior to boiloff.

During the boiloff period, the mixture level is generally [

] ^{a,c}

Figure 3.2.2-11(b) compares the calculated mixture level in the core channel under the open hole to the test data. Throughout the boiloff period and the rest of the transient, the calculated mixture level is very similar, if not identical, to the one shown in Figure 3.2.2-11(a); this similarity is expected given that at the time of boiloff there is no liquid draining predicted from the upper head or the upper plenum into the core.

Rod Heat-up:

Figures 3.2.2-12 and 3.2.2-13 show the calculated rod heatup (TCLAD) for the heater rods in the core channel below the guide tube and the open hole, respectively, compared to the test data. The rod heatup comparison is shown for three elevations relative to the bottom of the heated length.

During the boiloff, the onset of rod heatup at the different elevations is consistent with the time when mixture level reaches that elevation, which is earlier in the calculation than the test. The calculated heat-up rate is higher than the test, which is consistent with the calculated faster mixture level decrease and higher vapor superheat. Given that the predicted initiation of accumulator injection is very close to that observed at the test, the calculated peak rod temperatures are higher than the test at all three elevations.

From the comparison shown in both figures, it is observed that the calculated rod heat-up is consistent with the calculated mixture levels. Similar to the test, no rod heat-up was calculated to occur prior to loop seal clearance.

The cool-down rates and timing of rod quench at the three elevations are also consistent with the respective mixture levels, calculated or observed at the test.

a,c

Figure 3.2.2-1 Pressurizer and Steam Generator Secondary Side Pressures

a,c

Figure 3.2.2-2 Break Flows

a,c

Figure 3.2.2-3 Intact Loop Steam Generator U-tube Differential Pressures

a,c

Figure 3.2.2-4 Broken Loop Steam Generator U-tube Differential Pressures

a,c

Figure 3.2.2-5 Intact Loop Hot Leg Draining

a,c

Figure 3.2.2-6 Broken Loop Hot Leg Draining

a,c

Figure 3.2.2-7 Cross-over Leg Differential Pressures



Figure 3.2.2-8 Downcomer Differential Pressures



Figure 3.2.2-9 Vessel (Core) Differential Pressures



Figure 3.2.2-10 Upper Head Differential Pressure

a,c

Figure 3.2.2-11 Core Mixture Level Comparison

a,c

Figure 3.2.2-12 Calculated Rod 1 Heatup (located under guide tube) vs. Test Data

a,c

Figure 3.2.2-13 Calculated Rod 2 Heatup (located under open hole) vs. Test Data

3.2.3 Comparison of the S-LH-1 and S-LH-2 Test Simulations

This section presents a comparison of key parameters of the S-LH-1 and S-LH-2 test simulations, as requested by the NRC in Item 3 of RAI Question #110.

The comparison of the S-LH-1 and S-LH-2 test simulations demonstrates that the WCOBRA/TRAC-TF2 model of Semiscale is capable of predicting the effect of downcomer to upper head spray bypass capacity on key system phenomena.

The break flow comparisons in Figures 3.2.3-1 and 3.2.3-2, show that the simulation results are consistent with the test data. Similar to the test observations, the code predicts less integral break flow (inventory loss) for the higher spray bypass test S-LH-2.

The calculated draining of the upper head, Figure 3.2.3-3, is relatively consistent with the test, with the exception of the somewhat faster initial draining of the upper head, calculated for the S-LH-1 test. After reaching the top of the DC-to-UH bypass standpipe (~5.5 kPa) both test simulations show upper head inventory reduction somewhat lower than the test data.

The calculated downcomer and inner vessel (core) differential pressures, Figures 3.2.3-4 and 3.2.3-5 respectively, show that the predicted effect of the spray bypass capacity is consistent with the trends observed at the tests. The calculated levels however are lower than those measured at the test; these were discussed in more detail in Sections 3.2.1 (S-LH-1) and 3.2.2 (S-LH-2).

The comparison of the predicted vs. test rod cladding temperatures at the 207 cm elevation, Figure 3.2.3-6, indicates that overall effect of the DC-to-UH bypass capacity on the rod cladding temperature predicted by the code is in general agreement with the test. The same is true for the calculated core mixture levels as well, as shown in Figure 3.2.3-7.

The calculated steam generator differential pressures in the intact and broken loops for both tests, Figures 3.2.3-8 through 3.2.3-11, are consistent with the test data as well, with the exception of the predicted liquid holdup in the intact loop SG downhill side, Figure 3.2.3-9. The draining of the steam generator U-tubes does not seem to be affected by the DC-to-UH spray bypass capacity, as seen from the predictions and the test observations.

The predicted clearance of the cross-over legs (loop seals) is in good agreement with the test observations, as shown in Figures 3.2.3-12 and 3.2.3-13. Due to the higher DC-to-UH spray bypass capacity modeled (less loop vapor flow), the S-LH-2 simulation predicted clearance of the intact loop only, which is consistent with the test.

a,c

Figure 3.2.3-1 Break Flows

a,c

Figure 3.2.3-2 Integrated Break Flows

a,c

Figure 3.2.3-3 Upper Head Differential Pressures

a,c

Figure 3.2.3-4 Downcomer Differential Pressures

a,c

Figure 3.2.3-5 Inner Vessel (Core) Differential Pressures

a,c

Figure 3.2.3-6 Rod Cladding Temperatures at 207 cm Elevation

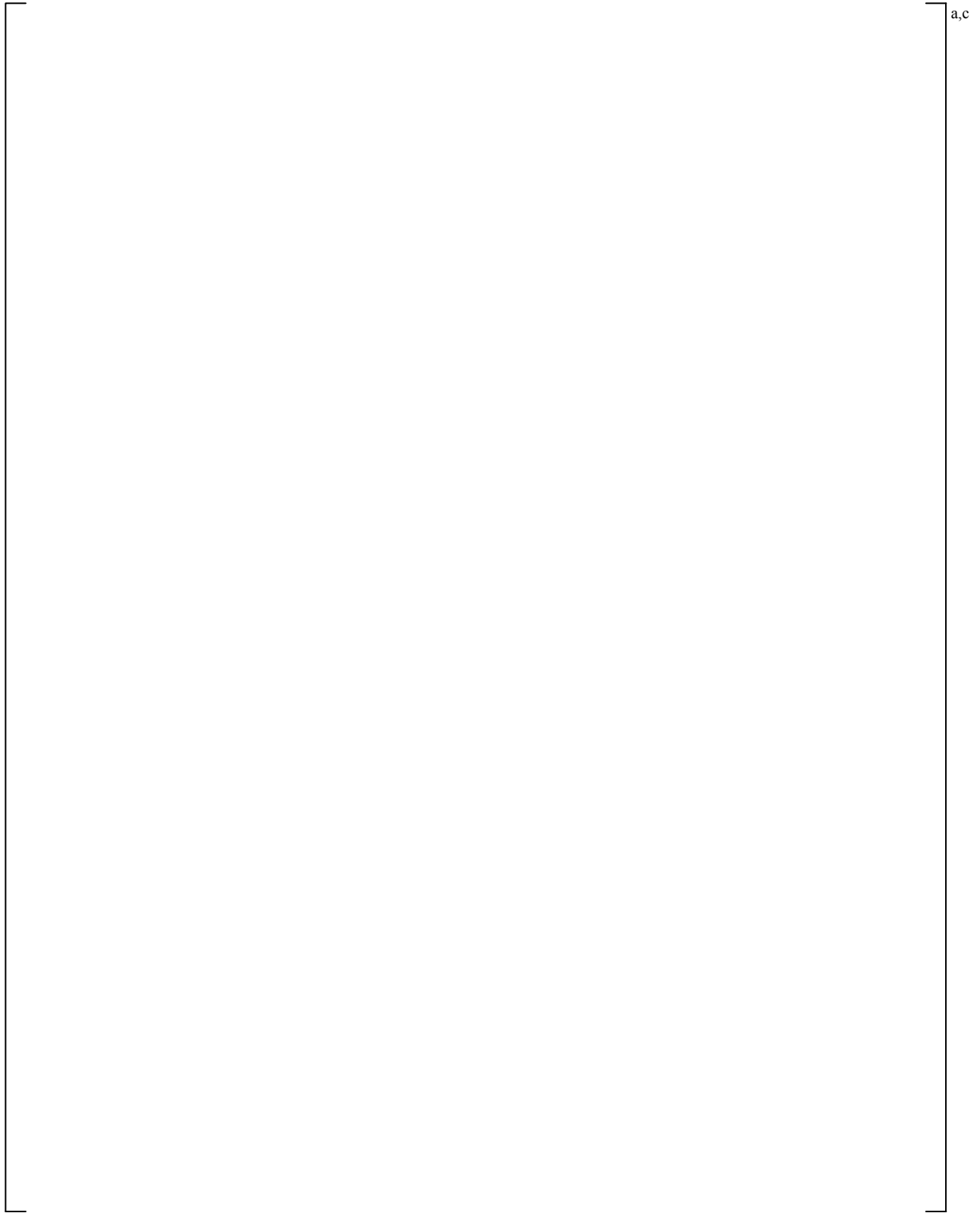


Figure 3.2.3-7 Core Mixture Levels

a,c

Figure 3.2.3-8 Intact Loop SG U-tube Uphill Differential Pressures

a,c

Figure 3.2.3-9 Intact Loop SG U-tube Downhill Differential Pressures

a,c

Figure 3.2.3-10 Broken Loop SG U-tube Uphill Differential Pressures

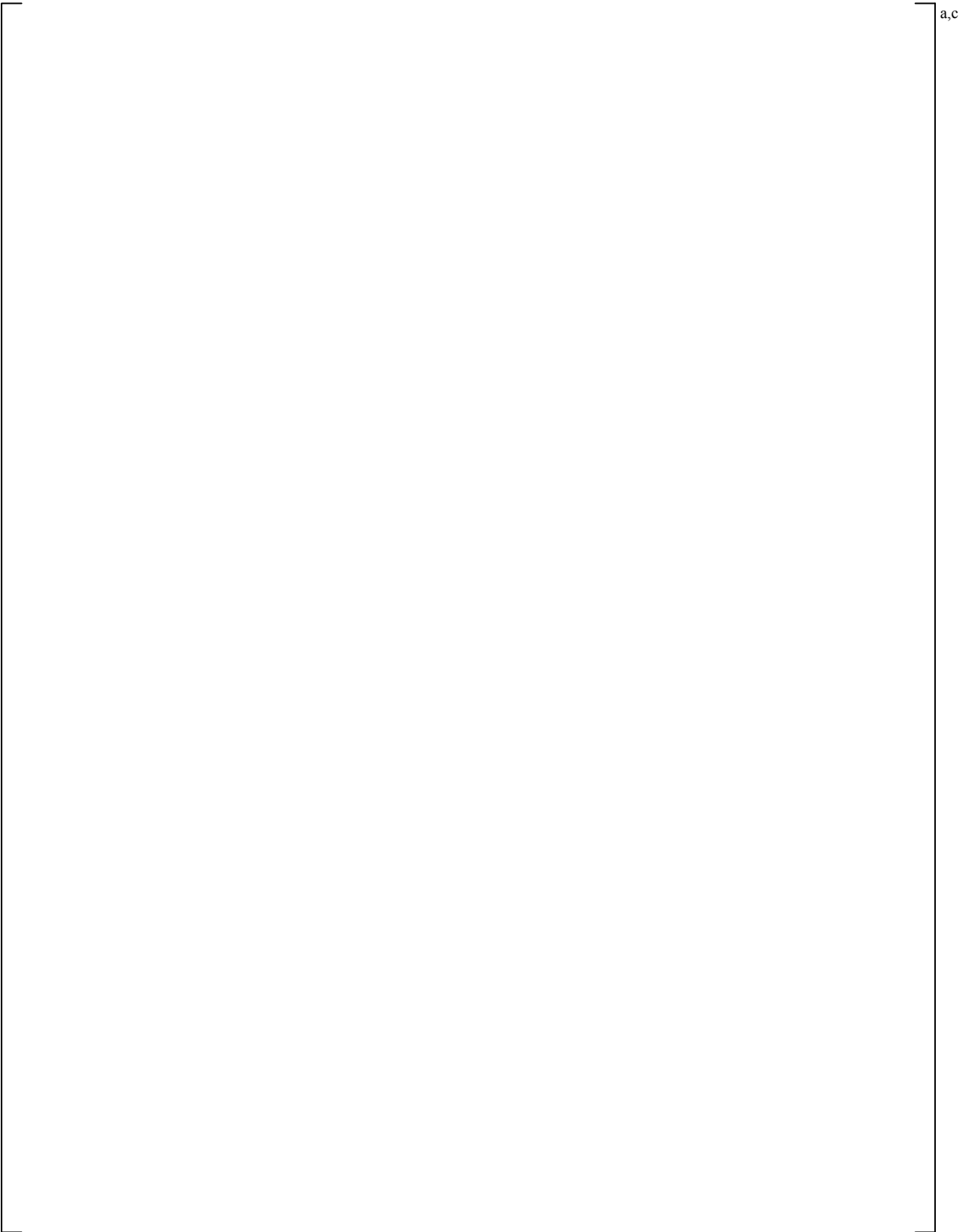


Figure 3.2.3-11 Broken Loop SG U-tube Downhill Differential Pressures

a,c

Figure 3.2.3-12 Intact Loop Cross-over Leg Differential Pressures

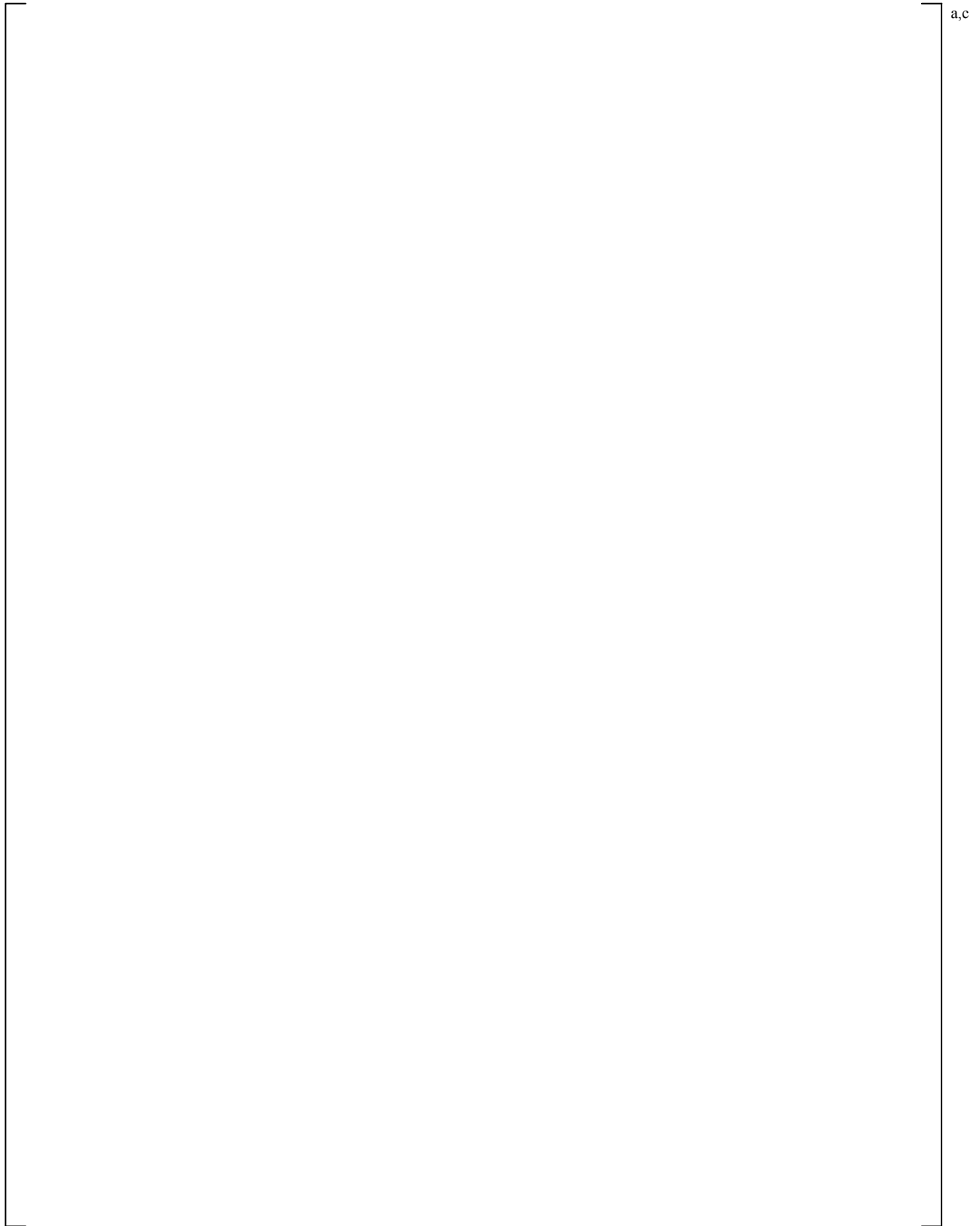


Figure 3.2.3-13 Broken Loop Cross-over Leg Differential Pressures

3.2.4 Steam Generator U-tube Noding Sensitivity Studies

As requested by the NRC, two sensitivities were performed with the nodalization of the steam generator U-tubes.

The first sensitivity is to double the number of hydraulic cells in the vertical part of the U-tubes. Thus the vertical part (uphill plus downhill) was modeled with a total of []^{a,c}

The number of the hydraulic cells in the secondary side boiler region and the number of nodes of the respective primary-to-secondary side heat conductors was modified accordingly.

The second sensitivity performed was modeling the vertical part of the U-tubes (uphill plus downhill) using []^{a,c}. In addition, the top (U-bend) hydraulic cell in the base case model was []^{a,c}. The number of nodes of the respective heat conductors was modified accordingly, but the noding of the boiler region remained unchanged from that used for the first sensitivity.

Simulations with the U-tube noding changes were performed for both the S-LH-1 and the S-LH-2 tests.

The results of the two sensitivity studies performed for the S-LH-1 test are presented in Figures 3.2.4-1 through Figure 3.2.4-7. This set of figures compares selected key parameters of the base case S-LH-1 test simulation against the results obtained with the aforementioned U-tube noding changes. The parameters of interest shown in the figures are the draining of the uphill and downhill of the steam generator U-tubes and the effect on the calculated downcomer and inner vessel (core) levels. In addition, comparison of the calculated rod cladding temperatures is presented in Figure 3.2.4-7.

As seen from the comparisons, the predicted U-tube draining and its effect on the overall system behavior is []^{a,c}. The predicted draining of the U-tubes and the effect on the core level depression is []

[]^{a,c}

The sensitivity calculation results for the S-LH-2 test, Figures 3.2.4-8 through Figure 3.2.4-14, show that the calculated steam generator U-tube draining and the overall system behavior is []^{a,c}

a,c

Figure 3.2.4-1 Intact Loop SG U-tube Uphill Differential Pressures (S-LH-1)

a,c

Figure 3.2.4-2 Intact Loop SG U-tube Downhill Differential Pressures (S-LH-1)

a,c

Figure 3.2.4-3 Broken Loop SG U-tube Uphill Differential Pressures (S-LH-1)

a,c

Figure 3.2.4-4 Broken Loop SG U-tube Downhill Differential Pressures (S-LH-1)

a,c

Figure 3.2.4-5 Downcomer Differential Pressures (S-LH-1)

a,c

Figure 3.2.4-6 Inner Vessel (Core) Differential Pressures (S-LH-1)

a,c

Figure 3.2.4-7 Rod Cladding Temperatures at 207 cm Elevation (S-LH-1)

a,c

Figure 3.2.4-8 Intact Loop SG U-tube Uphill Differential Pressures (S-LH-2)

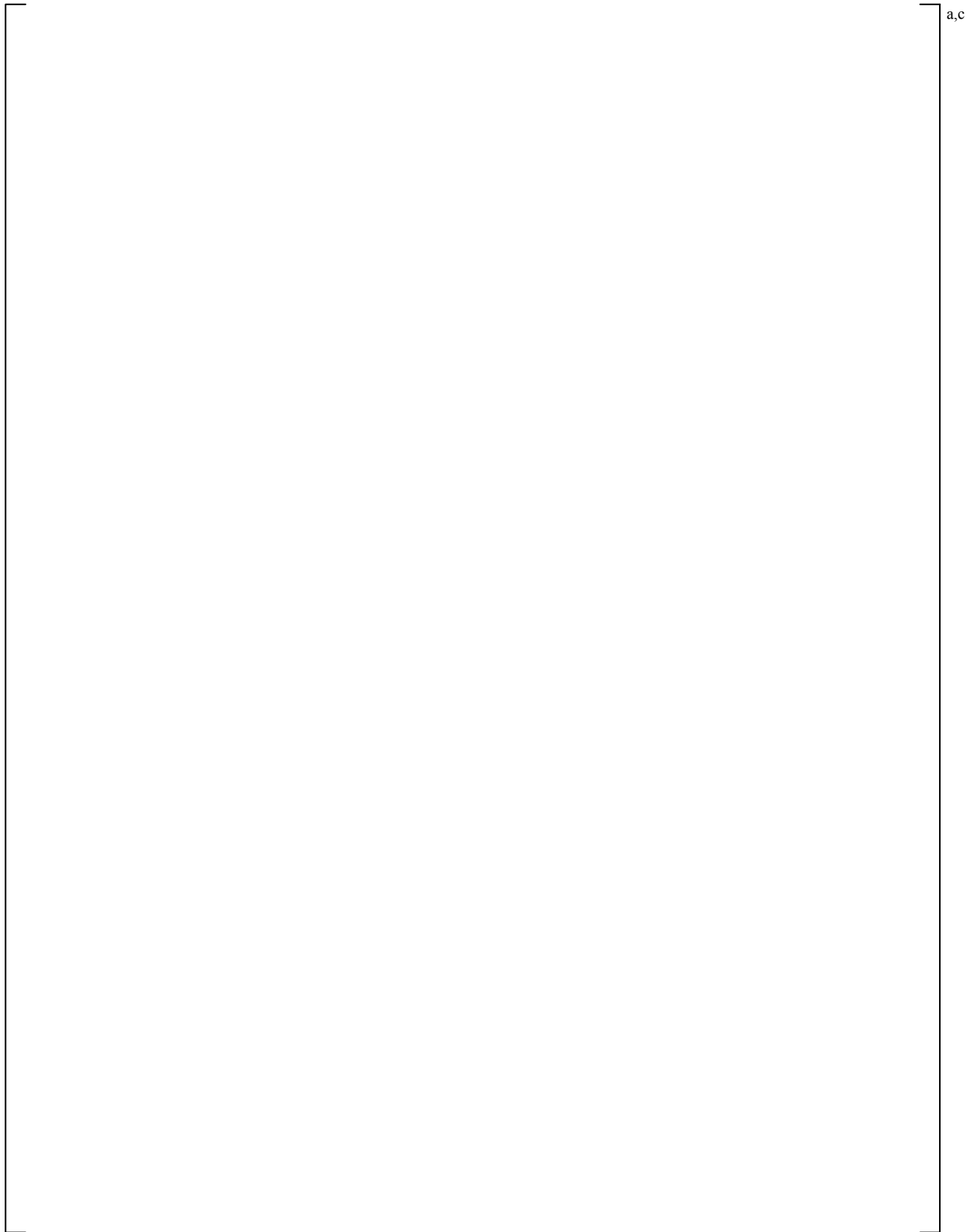


Figure 3.2.4-9 Intact Loop SG U-tube Downhill Differential Pressures (S-LH-2)

a,c

Figure 3.2.4-10 Broken Loop SG U-tube Uphill Differential Pressures (S-LH-2)

a,c

Figure 3.2.4-11 Broken Loop SG U-tube Downhill Differential Pressures (S-LH-2)

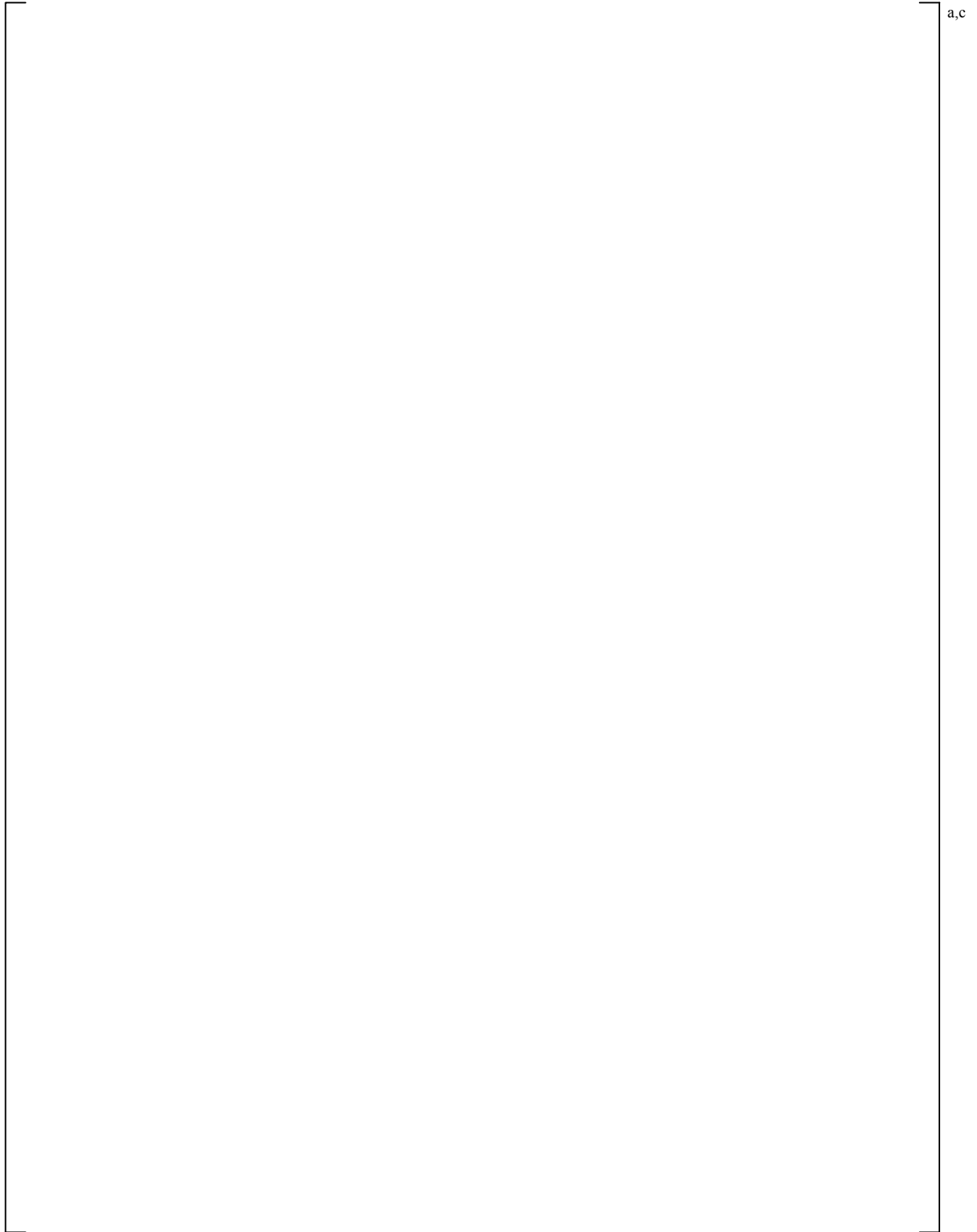


Figure 3.2.4-12 Downcomer Differential Pressures (S-LH-2)

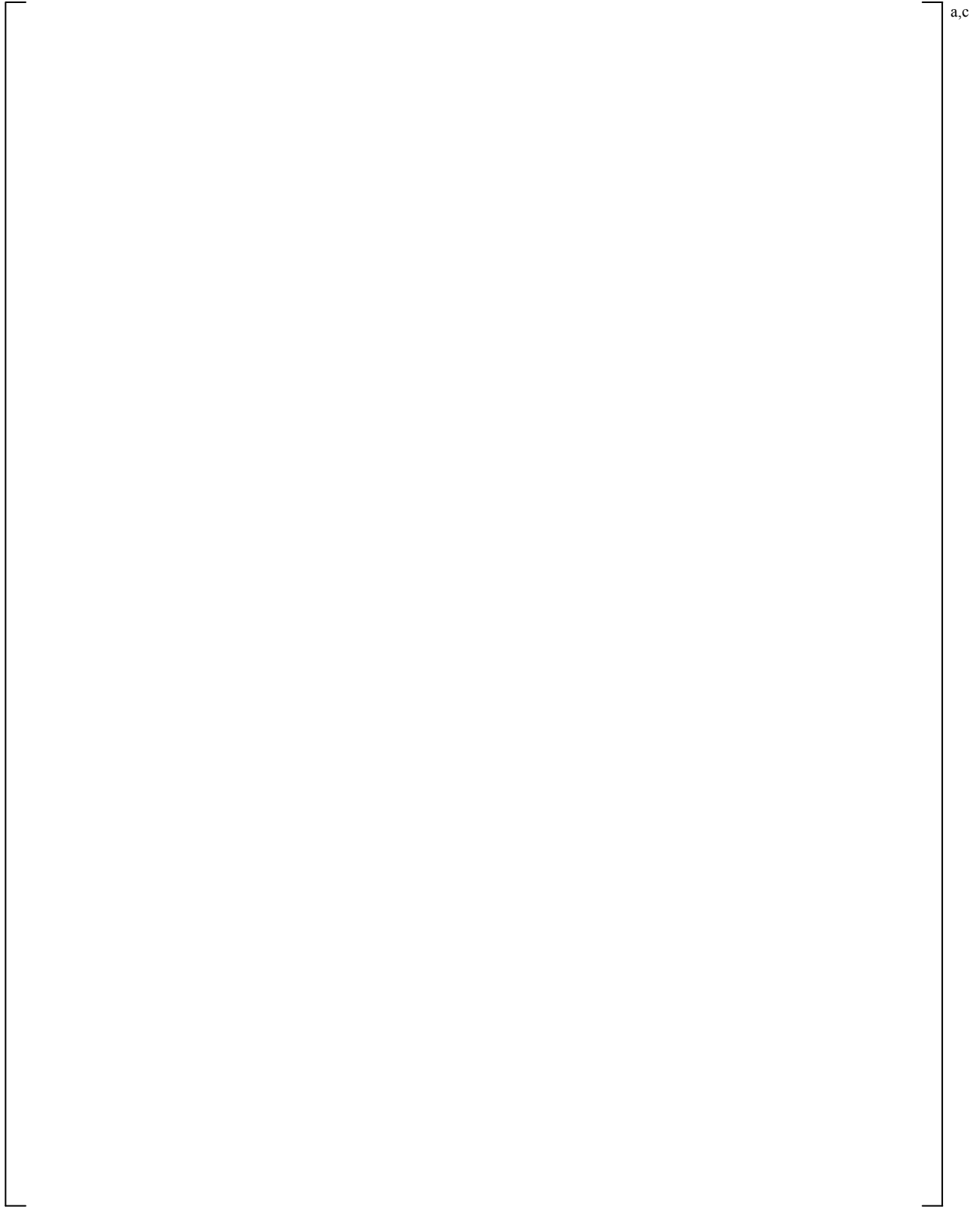


Figure 3.2.4-13 Inner Vessel (Core) Differential Pressures (S-LH-2)

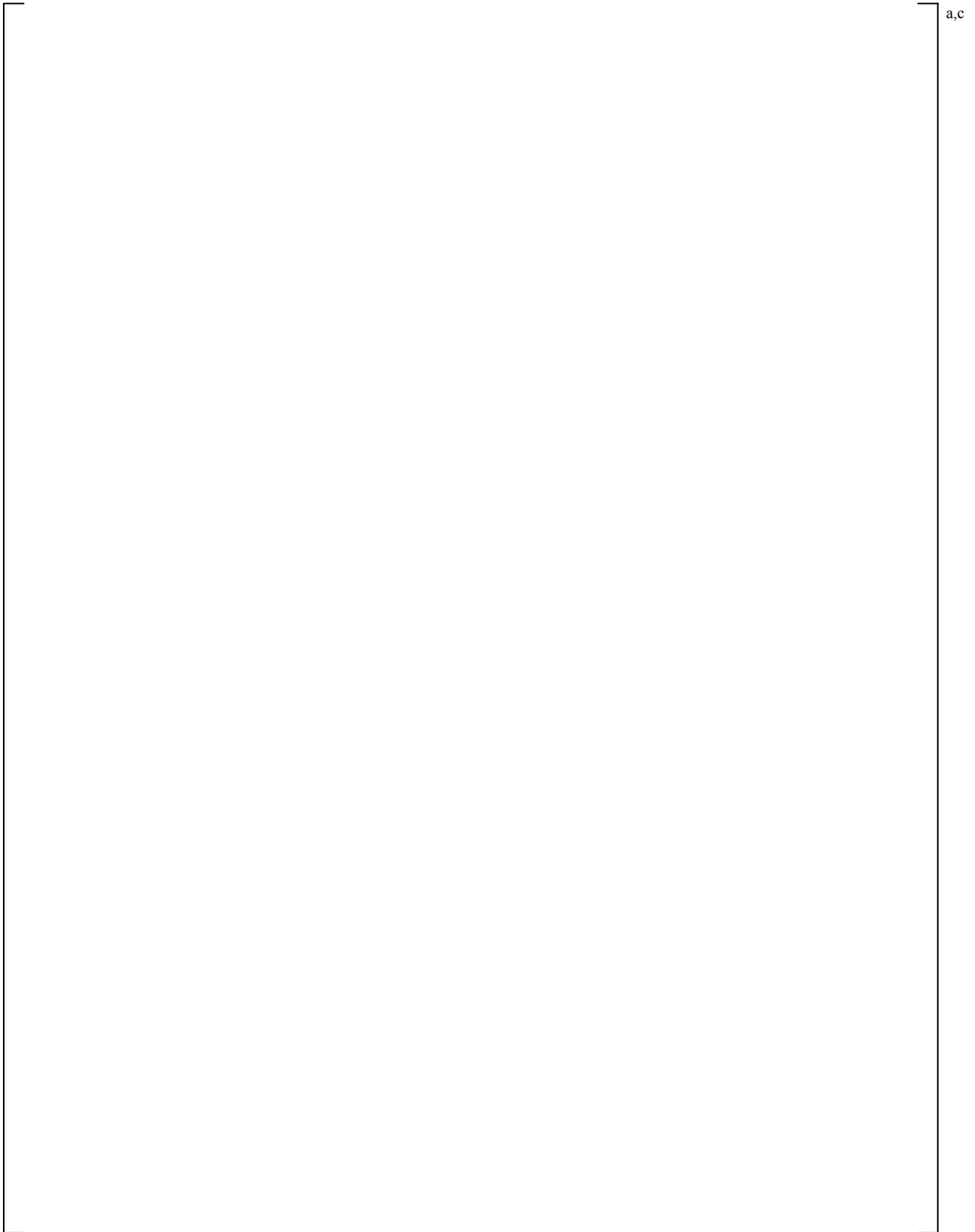


Figure 3.2.4-14 Rod Cladding Temperatures at 207 cm Elevation (S-LH-2)

3.2.5 Cross-Over Leg Modeling Sensitivity Studies

The two sensitivity studies presented here are needed to address the fact that the cross-over leg modeling used for the S-LH-1 and S-LH-2 simulations presented in the preceding sections is somewhat different than the one used for the ROSA and the PWR model described in WCAP-16996-P [10] due to the different facility geometry. The differences are in the number of hydraulic cells used to model both the vertical part and the bottom part of the cross-over legs.

3.2.5.1 Stratification at the Bottom of the Cross-Over Legs

This sensitivity is done to investigate the effect of not allowing the code to perform a stratification check at the bottom of the cross-over legs. To perform this sensitivity, STRTX=0 was specified at the two bottom cell faces of both cross-over leg components - PIPE#14 (intact loop cross-over) and PIPE 24 (broken loop cross-over). Since STRTX=0 and the inclination angle at those cell faces is greater than 10 degrees, the code cannot predict stratification at the bottom U-bend of the cross-over legs. This sensitivity study was performed with both the S-LH-1 and the S-LH-2 tests.

Figures 3.2.5.1-1 through 3.2.5.1-5 show results of the S-LH-1 test simulation with cross-over leg STRTX=0 compared against the base case S-LH-1 simulation; the key system parameters presented are intact and broken loop clearance (differential pressures in Figures 3.2.5.1-1 and 3.2.5.1-2), downcomer differential pressures (Figure 3.2.5.1-3), inner vessel (core) differential pressures (Figure 3.2.5.1-4) and the calculated rod cladding temperature at the 207 cm elevation, Figure 3.2.5.1-5. These parameters are considered to be most sensitive to the type of modeling change investigated here.

[

] ^{a,c}

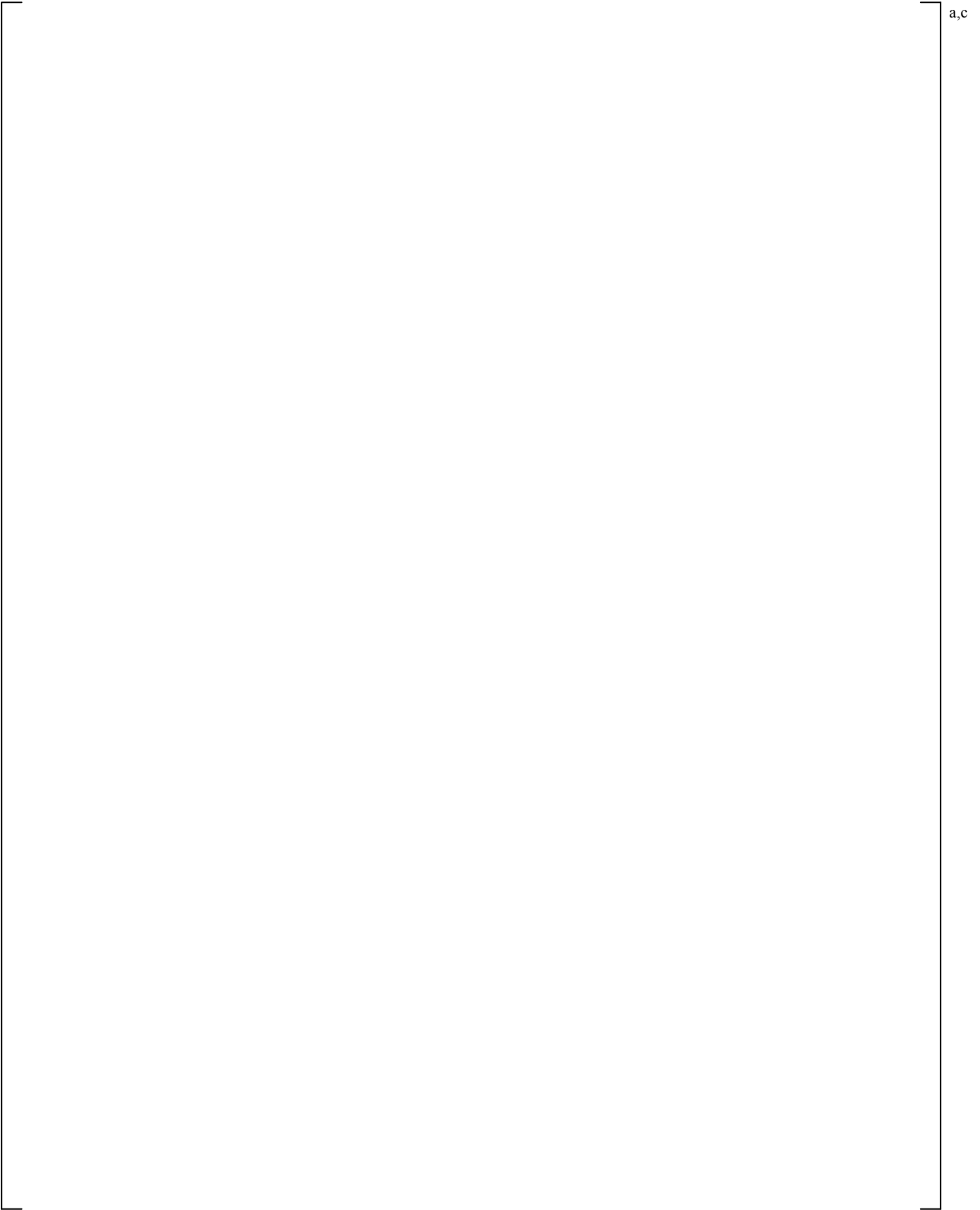


Figure 3.2.5.1-1 Intact Loop Cross-over Leg Differential Pressures

a,c

Figure 3.2.5.1-2 Broken Loop Cross-over Leg Differential Pressures

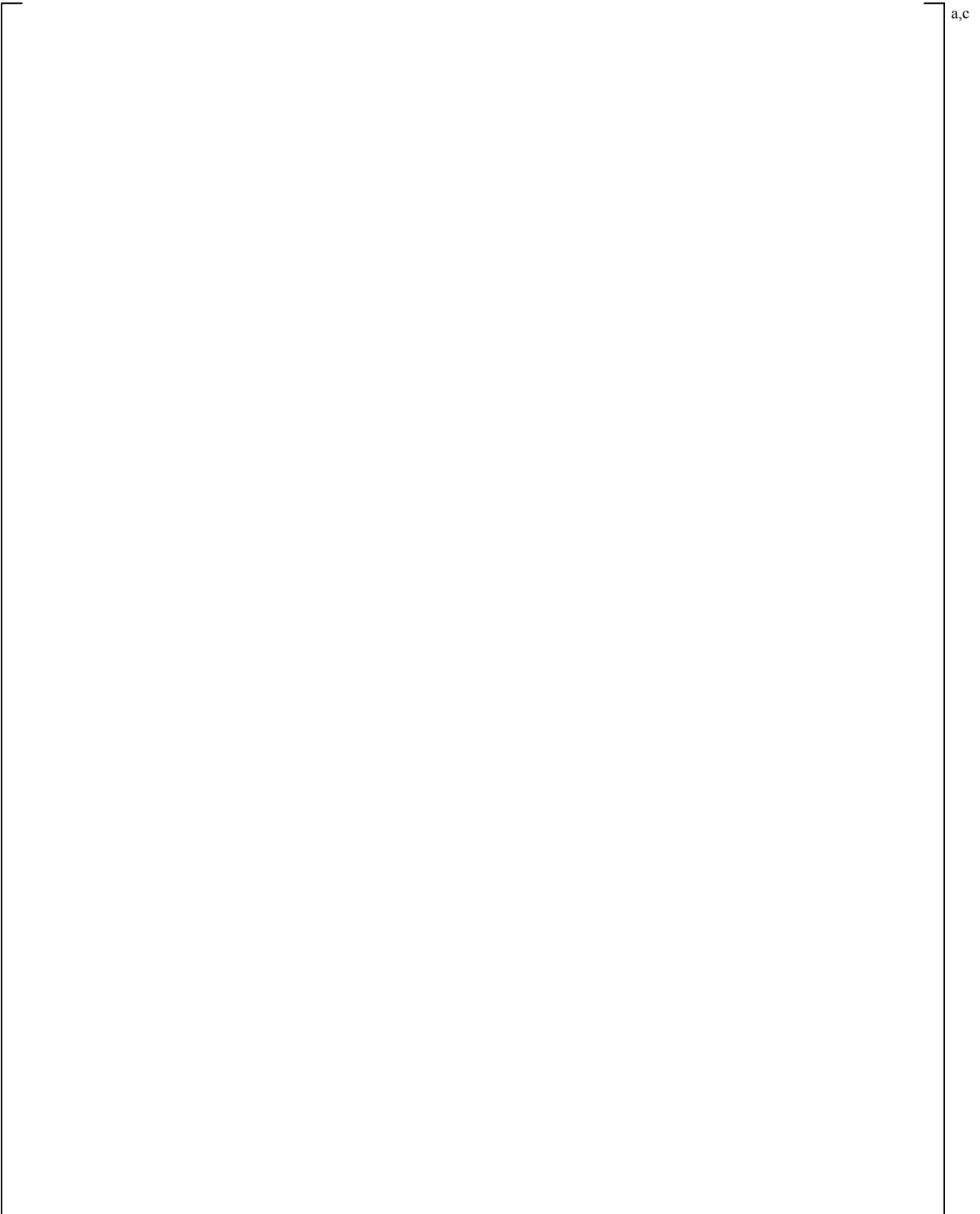


Figure 3.2.5.1-3 Downcomer Differential Pressures

a,c

Figure 3.2.5.1-4 Inner Vessel (Core) Differential Pressures

a,c

Figure 3.2.5.1-5 Rod Cladding Temperatures at 207 cm Elevation

3.2.5.2 Decreased Number of Cells in the Vertical Part of the Cross-over Legs

In this sensitivity the number of hydraulic cells in the vertical parts of the cross-over legs, PIPE 14 (intact loop) and PIPE 24 (broken loop), were reduced to match the number of cells used in the model of the ROSA tests facility, presented in Section 21 of WCAP-16996-P [10]. No changes were made to the nodding of the u-bend at the bottom of the cross-over legs. Thus, for this sensitivity the downhill (SG side) of the cross-over legs was modeled using 5 cells (compared to 9 cells in the base case) and the uphill (pump side) was modeled using 4 cells (compared to 5 cells in the base case).

Figures 3.2.5.2-1 through 3.2.5.2-5 show results of the S-LH-1 test simulation with reduced number of hydraulic cells in the cross-over leg compared against the base case S-LH-1 simulation; the key system parameters presented are intact and broken loop clearance (differential pressures in Figures 3.2.5.2-1 and 3.2.5.2-2), downcomer differential pressures (Figure 3.2.5.2-3), inner vessel (core) differential pressures (Figure 3.2.5.2-4) and the calculated rod cladding temperature at the 207 cm elevation, Figure 3.2.5.2-5. Similar to the cross-over leg stratification sensitivity study presented in Section 3.2.5.1, these parameters are considered to be most sensitive to the type of modeling change investigated here.

[

] ^{a,c}

a,c

Figure 3.2.5.2-1 Intact Loop Cross-over Leg Differential Pressures

a,c

Figure 3.2.5.2-2 Broken Loop Cross-over Leg Differential Pressures

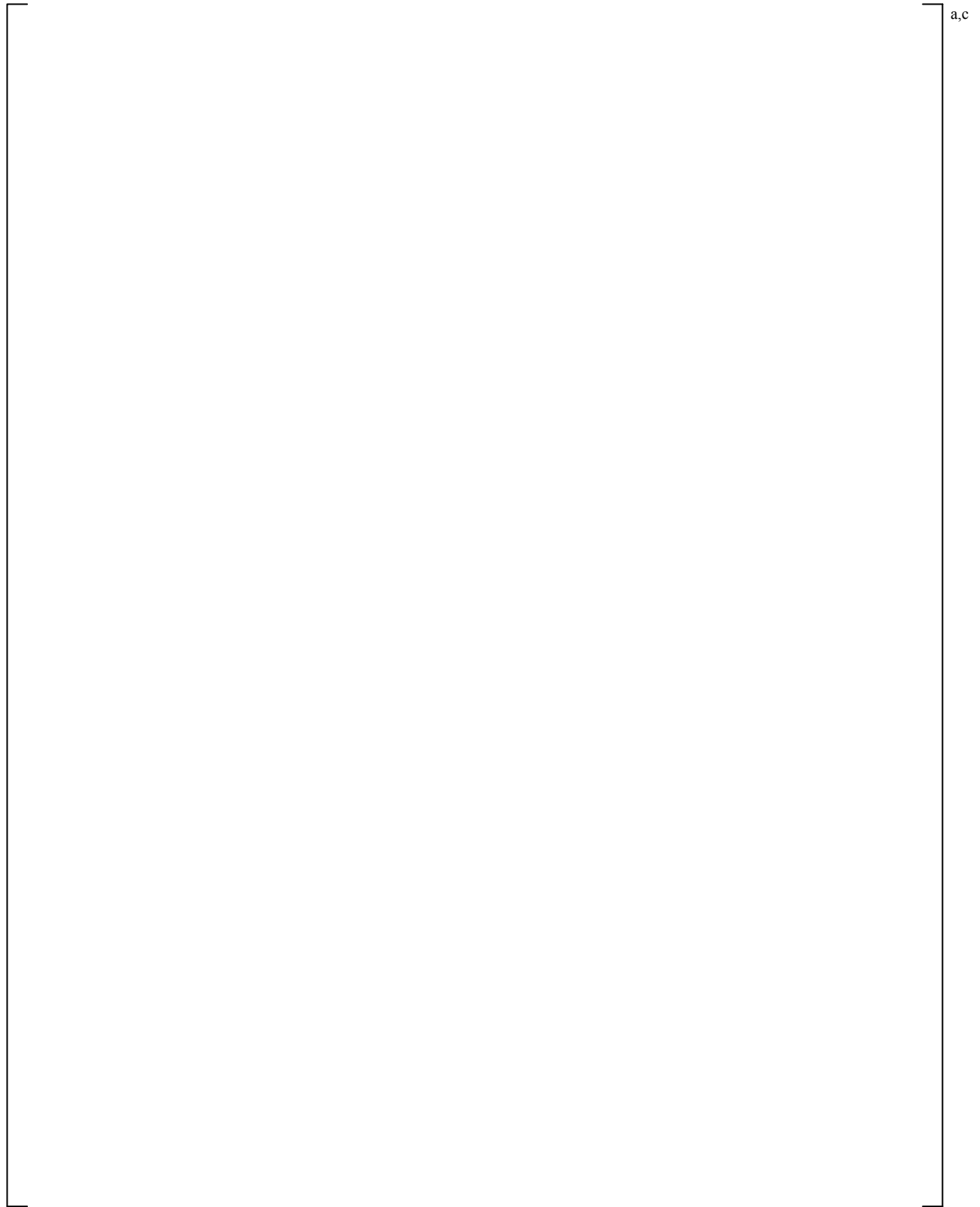


Figure 3.2.5.2-3 Downcomer Differential Pressures

a,c

Figure 3.2.5.2-4 Inner Vessel (Core) Differential Pressures

a,c

Figure 3.2.5.2-5 Rod Cladding Temperatures at 207 cm Elevation

3.3 Conclusions

A review of the calculation results indicates that the code is predicting the key small break LOCA phenomena well. Notably, the expected top-down drain of the system and the formation of quasi-equilibrium hydrostatic balances associated with liquid inventories in the vertical components, particularly the core/downcomer and pump suction loop piping, are quite reasonable and consistent with the test observations. Key transient parameters like break mass discharge and depressurization rate are predicted adequately as well.

Through review of the calculation results in comparison to the test data, it was determined that [

] ^{a,c}

[

] ^{a,c}

This set of 5-percent small break LOCA experiments conducted at the Semiscale MOD-2C facility addresses the sensitivity to the downcomer to upper head bypass capacity. The analysis of the S-LH-1 and S-LH-2 test simulations presented herein demonstrates that with the adopted Semiscale model, the WCOBRA/TRAC-TF2 code is capable of predicting fairly accurately the effects of the downcomer-to-upper head bypass capacities on the calculated system behavior.

3.4 References

1. Larson, T. K., et al., 1982, "Scaling Criteria and an Assessment of Semiscale Mod-3 Scaling for Small Break Loss Of Coolant Transients," EGG-M-21082.
2. Loomis, G. G., 1987, "Summary of the Semiscale Program (1965-1986)," NUREG/CR-4945 (EGG-2509).
3. Liebert, J. and Emmerling, R., 1998, "UPTF Experiment Flow Phenomena During Full-Scale Loop Seal Clearing of a PWR," Nuclear Engineering and Design, Vol. 179, pp. 51-64.
4. Leonard, M. T., 1982, "Vessel Coolant Mass Depletion During a Small Break LOCA," EGG-SEMI-6010.
5. Osakabe, M., et al., 1987, "Core Liquid Level Depression Due to Manometric Effect During PWR Small Break LOCA," J. of Nuclear Science and Technology 24(2), pp. 103-110.
6. Leonard, M. T., 1982, "An Analytical Study of a Small Break Loss-Of-Coolant Accident with Upper Head Injection," Nuclear Technology, Vol. 62.
7. Loomis, G. G. and Streit, J. E., 1985a, "Quick Look Report for Semiscale Mod-2C Experiments S-LH-1 and S-LH-2," EGG-SEMI-6884.
8. Loomis, G. G. and Streit, J. E., 1985b, "Results of Semiscale Mod-2C Small Break (5%) Loss-of-Coolant Accident Experiments S-LH-1 and S-LH-2," NUREG/CR-4438 (EGG-2424).
9. Euy-Joon Lee, et al., 1993, "RELAP5 Assessment Using Semiscale SBLOCA Test S-NH-1," NUREG/IA-0099.
10. Frepoli, C., et al., "Realistic LOCA Evaluation Methodology Applied to the Full Spectrum of Break Sizes (FULL SPECTRUM LOCA Methodology)," WCAP-16996-P, November 2010.
11. Loomis, G. G., 1985, "Experiment Operating Specification for Semiscale Mod-2C 5% Small Break Loss-of-Coolant Experiment S-LH-1," EGG-SEMI-6813.
12. P. C. Hall and D. R. Bull, 1992, "Analysis of Semiscale Test S-LH-1 Using RELAP5/MOD2," NUREG/IA-0064 (GD/PE-N/725).
13. P. Brodie and P. C. Hall, 1992, "Analysis of Semiscale Test S-LH-2 Using RELAP5/MOD2," NUREG/IA-0065 (GD/PE-N/745).
14. Letter from Thomas Rodack, LTR-NRC-13-41, June 2013, "Submittal of Westinghouse Responses to 'WCAP-16996-P, 'Realistic LOCA Evaluation Methodology Applied to the Full Spectrum of Break Sizes (FULL SPECTRUM LOCA Methodology)' Request for Additional Information - RAIs 72, 73, 74 and 76" (Proprietary/Non-Proprietary), Project 700, TAC No. ME5244."

**WCAP-16996-P, “Realistic LOCA Evaluation Methodology Applied to the Full Spectrum of Break Sizes
(FULL SPECTRUM LOCA Methodology)”
Request for Additional Information – (Non-Proprietary)
Set 8 RAIs 122-126, 128-131 and 136**

February 2014

Westinghouse Electric Company LLC
1000 Westinghouse Drive
Cranberry Township, PA 16066

RAI Question #122: Upper Bound Approach to Reactor Coolant Pump Trip Time during Loss-of-Coolant Accident with Offsite Power Available

WCAP-16996-P/WCAP-16996-NP, Volumes I, II, and III, Revision 0, Section 25, “Plant Sources of Uncertainty,” Subsection 25.3, “Reactor Accident Boundary Conditions,” explains that “offsite power determines whether RCS pumps initially remain on, and whether pumped safety injection (and containment safeguards) come on with only valve opening and alignment delays. The effect of the RCS pumps on the LOCA transient may be significantly different, depending on whether they are assumed to coast down or continue running (until operator action is taken, if applicable).” Section 30, “Technical Basis of Statistical Procedures Applied in FSLOCA Uncertainty Methodology,” Subsection 30.4, []^{a,c} describes a statistical approach for treatment of Offsite Power Availability (OPA) at the time of a postulated small or large break LOCA event (OPA=ON or OPA=OFF) in the FSLOCA methodology.

In analyzing LOCAs with offsite power available, WCAP-16996-P/WCAP-16996-NP, Volumes I, II, and III, Revision 0, Section 25, “Plant Sources of Uncertainty,” Subsection 25.5.2, “Variability of Plant Conditions Due to Operation Actions,” summarizes that []

[]^{a,c} The upper bound to operator action time to trip the RCPs is taken as []^{a,c} from the time reactor trip occurs, and this time is used in the reference break spectrum with offsite power available in Section 27, Volume 3 of this document.” WCAP-16996-P/WCAP-16996-NP, Volumes I, II, and III, Revision 0, Section 27, “Reference Break Spectrum Analysis,” describes representative LOCA analyses of small, intermediate, and large breaks for the reference V. C. Summer and Beaver Valley Unit 1 plants.

Please provide the following additional information regarding the approach to RCP trip time modeling with offsite power available as implemented in the FSLOCA methodology.

- (1) The analysis provided in Subsection 25.5.2 considers the short-term phase of a SBLOCA and refers to EOPs specific to Indian Point Unit 2, a four-loop Westinghouse PWR. At the same time, Subsection 25.5.2 states that the upper bound to operator action time to trip the RCPs, assessed at []^{a,c} from the time reactor trip occurs, is used in the LOCA analyses for large, intermediate, and small break sizes described in Section 27, “Reference Break Spectrum Analysis.” Please clarify if the described approach based on an upper bound to operator action time to trip the RCPs set at []^{a,c} from the time when reactor trip occurs is considered applicable on a generic basis for performing LOCA analyses with the FSLOCA methodology. Please provide a justification for the described approach.
- (2) Please describe the rationale for introducing “an upper bound to operator action time to trip the RCPs” as part of the approach for simulating RCPs operation during LOCAs with offsite power available in the FSLOCA methodology. Explain how such “an upper bound to operator action time to trip the RCPs” can be credited for modeling RCPs operation with offsite power available in

FULL SPECTRUM™ and FSLOCA™ are trademarks in the United States of Westinghouse Electric Company LLC, its subsidiaries and/or its affiliates. These marks may be used and/or registered in other countries throughout the world. All rights reserved. Unauthorized use is strictly prohibited. Other names may be trademarks of their respective owners.

performing best-estimate analyses of both small and large break LOCA. Describe the technical basis that demonstrates the validity of the approach implemented in the FSLOCA methodology.

RAI Question #123: Factors Affecting Reactor Coolant Pump Trip Time for Loss-of-Coolant Accident Analyses with Offsite Power Available

WCAP-16996-P/WCAP-16996-NP, Volumes I, II, and III, Revision 0, Section 2, "Evaluation Model Functional Requirements," Subsection 2.3.1, "LOCA Scenario Specification," recognizes the possibility of operator action in the accident scenario. Subsection 2.3.1 also explains that the availability of the RCPs following a reactor trip event is considered so that "variability in the pump trip time does exist."

Section 3.15, "Special Considerations for a Small-Break Loss-of-Coolant Accident in Pressurized Water Reactors," in the NRC RG 1.157, "Best-Estimate Calculations of Emergency Core Cooling System Performance," May 1989, requires that "the pump operation assumptions used in the calculations should be the most likely, based on operating procedures, with appropriate consideration of the uncertainty of the pump operation during an actual event."

Please provide additional information regarding the approach to model RCP trip time with offsite power available as part of the FSLOCA methodology as follows.

- (1) Explain specifically how the approach to model RCP trip time with offsite power available for LOCA analyses takes into consideration the following factors: (a) plant-specific design features, (b) relevant EOP requirements and applicable criteria, (c) break size, (d) plant monitored conditions, (e) availability, performance, and correct use of equipment, (f) operator recognition of the event and action, as well as any other factors considered of relevance.
- (2) Please provide an assessment for the uncertainties associated with each individual factor identified in Item (1) above with regard to the RCP trip time. Please consider each factor individually and assess its contribution to the overall uncertainty in the RCP trip time. Include appropriate ranges and associated uncertainties. Present examples of assessment results for PWR plant types with similar design features, EOP requirements, and other relevant factors, for which the FSLOCA methodology is considered applicable. Include a table that documents the assessed time contribution to RCP trip time due to each individual factor, the RCP trip time uncertainty range, and the RCP trip time credited in LOCA analyses. If appropriate, please provide a separate table for each plant type. Describe the introduced assumptions, explain and discuss the analysis results, and compare the assessments.

RAI Question #124: Reactor Coolant Pump Trip Time for Small Break Loss-of-Coolant Accident Analyses with Offsite Power Available

WCAP-16996-P/WCAP-16996-NP, Volumes I, II, and III, Revision 0, Section 25, "Plant Sources of Uncertainty," Subsection 25.5.1, "EOP Sequences for a Small Break LOCA," summarizes EOPs relevant to the short-term phase of a small break LOCA for Indian Point Unit 2. The procedures are summarized

in Table 25-1, “Condensed EOPs for Indian Point Unit 2, Short-Term Portion.” In particular, it is explained that [

] ^{a,c} The RCP trip time variability is caused by the time the operators take to identify that the trip conditions exist during their periodic scan of system parameters, and the small increment required to actually perform the trip.” Subsection 25.5.1 also states that “plants typically follow a generic template for the generation of EOPs, and plant-to-plant differences in the EOP structure are not expected to be important for the purpose of performing a LOCA safety analysis.”

Please provide the following additional information regarding the approach to RCP trip time modeling with offsite power available as implemented in the FSLOCA methodology for performing small break LOCA analyses.

- (1) Explain how the approach to modeling RCPs trip due to operator action in determining the boundary conditions for SBLOCA analyses is applied on a plant-by-plant basis in the FSLOCA methodology. In particular, identify relevant contributing factors and types of plant-specific information (for example, available data, EOPs and criteria, etc.) that are considered for modeling RCP trip time on a plant-by-plant basis in individual plant analyses. Provide and explain the uncertainty and significance, in terms of having an impact on the credited RCPs trip time, associated with such factors and plant-specific information.
- (2) Provide examples of assessed RCPs trip times considered applicable for small break LOCA analyses and determined for different PWR plant types based on design features, EOP requirements, and other pertinent factors. Present examples of assessment results for PWR plant types for which the FSLOCA methodology is considered applicable. Include a table that documents the assessment results for the examined cases. Describe the introduced assumptions, explain and discuss the analysis results, and compare the assessments.
- (3) The upper bound to operator action time to trip the RCPs of [] ^{a,c} from the time when reactor trip occurs, is provided in Subsection 25.5.2, “Variability of Plant Conditions Due to Operation Actions,” on the basis of small break LOCA considerations. Please provide the plant-specific values for the RCPs trip times used in the demonstration plant SBLOCA analyses for the FSLOCA methodology presented in WCAP-16996-P/WCAP-16996-NP, Volumes I, II, and III, Revision 0, Section 28, “Scoping And Sensitivity Studies,” and in Section 31, “Full Spectrum™ LOCA Demonstration Analysis.” Describe the introduced assumptions, explain and discuss the applicability of the analysis results, and compare the assessments. Explain the basis for the used RCPs trip times considering the response to the item (1) above.

RAI Question #125: Reactor Coolant Pump Trip Time for Large Break Loss-of-Coolant Accident Analyses with Offsite Power Available

WCAP-16996-P/WCAP-16996-NP, Volumes I, II, and III, Revision 0, Section 28, "Scoping and Sensitivity Studies," Subsection 28.1.2, "Offsite Power Availability – LBLOCA," analyzes effect of offsite power availability on RCPs behavior for LBLOCA analyses performed with WCOBRA/TRAC-TF2 for the reference V. C. Summer (CGE) and Beaver Valley Unit 1 (DLW) plants. Subsection 28.1.2 explains that "with LOOP, the RCP trip is modeled coincident with the reactor trip at the beginning of the transient, so the pumps in the intact loops coast down while the pump in the broken loop is accelerated by the flow toward the break." In the case "with offsite power available (OPA), the pumps continue to rotate at a fixed speed until operator trip."

The RCP rotational speeds in the intact loops and in the broken one the V. C. Summer (CGE) nominal DEG break demonstration plant analysis are shown in Figure 28.1.2-2, "Intact Loop Pump Speed, CGE Offsite Power Availability Sensitivity," and in Figure 28.1.2-3, "Broken Loop Pump Speed, CGE Offsite Power Availability Sensitivity," respectively. For the Beaver Valley Unit 1 (DLW) nominal DEG break demonstration plant analysis, the RCP rotational speeds in the intact loops and in the broken one are shown in Figure 28.1.2-8, "Intact Loop Pump Speed, DLW Offsite Power Availability Study," and in Figure 28.1.2-9, "Broken Loop Pump Speed, DLW Offsite Power Availability Study," accordingly. As it can be scaled from these graphs, the RCPs pump speeds in all loop start decreasing at about []^{a,c} following the break initiation in the analyses with offsite power available for both plants.

Please provide the following additional information regarding the approach to RCP trip time modeling with offsite power available as implemented in the FSLOCA methodology for performing large break LOCA analyses.

- (1) Explain how the approach to modeling RCPs trip due to operator action in determining the boundary conditions for large break LOCA analyses is applied on a plant-by-plant basis in the FSLOCA methodology. In particular, identify relevant contributing factors and types of plant-specific information (for example, available data, EOPs and criteria, etc.) that are considered for modeling RCP trip time on a plant-by-plant basis in individual plant analyses. Provide and explain the uncertainty and significance, in terms of having an impact on the credited RCPs trip time, associated with such factors and plant-specific information.
- (2) Provide examples of assessed RCPs trip times considered applicable for large break LOCA analyses and determined for different PWR plant designs based on design features, EOP requirements, and other pertinent factors. Present examples of assessment results for PWR plant types for which the FSLOCA methodology is considered applicable. Include a table that documents the assessment results for the examined cases. Describe the introduced assumptions, explain and discuss the applicability of the analysis results, and compare the assessments.
- (3) Please provide the plant-specific values for the RCPs trip times used in the demonstration plant large break LOCA analyses for the FSLOCA methodology presented in WCAP-16996-P/WCAP-16996-

NP, Volumes I, II, and III, Revision 0, Section 28, “Scoping And Sensitivity Studies,” and in Section 31, “Full Spectrum LOCA Demonstration Analysis.” Describe the introduced assumptions, explain and discuss the analysis results, and compare the assessments.

- (4) The upper bound to operator action time to trip the RCPs of []^{a,c} from the time when reactor trip occurs, provided in Subsection 25.5.2, “Variability of Plant Conditions Due to Operation Actions,” on the basis of small break LOCA considerations, agrees closely with the timing of about []^{a,c} following the break initiation when the RCP pump speeds were predicted to start decreasing with offsite power available in the large break demonstration plant analyses presented in Subsection 28.1.2. Please explain the basis for the implemented RCPs trip time considering the response to Item (1) above.

RAI Question #126: Delay in Operator Action to Trip Reactor Coolant Pumps during Small Break Loss-of-Coolant Accidents

WCAP-16996-P/WCAP-16996-NP, Volumes I, II, and III, Revision 0, Section 25, “Plant Sources of Uncertainty,” Subsection 25.5.2, “Variability of Plant Conditions Due to Operation Actions,” explains that []

[]^{a,c}

- (1) Please clarify if the above identified range of []^{a,c} expected in operator action to trip the RCP for small break LOCAs is considered applicable on a generic basis in performing LOCA analyses using the FSLOCA methodology.
- (2) Regarding the operator action to trip the RCPs during SBLOCAs, Subsection 25.5.2 clarifies that []
- []^{a,c} Please identify the “studies” described as []^{a,c} in the above provided citation from Subsection 25.5.2 and provide references for the source documents containing these studies. In particular, provide details and explain how the identified []^{a,c} demonstrates the acceptability and appropriateness of the provided delay time of []^{a,c} needed for operator action to trip the RCPs during a LOCA event.
- (3) Please explain if uncertainty in human reliability was considered in the approach to model the operator action to trip the RCPs implemented in the FSLOCA methodology.
- (4) If the approach for determining the delay time needed for operator action to trip the RCPs during a LOCA event will be applied in FSLOCA methodology on a plant-by-plant basis, please identify and describe the type of plant-specific information that will be considered in individual plant applications.

RAI Question #128: Prolonged RCP Operation during Small Break Loss-of-Coolant Accidents

J. Gonzalez-Cadelo, et al., “Applying Integrated Safety Assessment Methodology, Analysis of Cold Leg SBLOCA With Failed HPSI,” 21st International Conference Nuclear Energy for New Europe Ljubljana 2012, September 5-7, Ljubljana, Slovenia, provided results from the SBLOCA study of predicted PWR PCTs as a function of the break size and the RCPs trip delay. The work was performed for the Almaraz Unit I Nuclear Power Plant (NPP), a Westinghouse three-loop PWR, using the U.S. NRC code TRACE. Small breaks in the cold leg ranging between 1 inch and 5 inches of equivalent break diameter were analyzed with an increment as low as 0.25 inch. RCP trip delays ranging between zero and up to 10,000 seconds (~167 minutes) were examined with a time interval as low as 500 seconds. The study referenced Westinghouse EOPs EOP E-0, EOP E-1, and EOP ES-1.2 along with pertinent foldout pages related to small break LOCA sequences with early secondary-side depressurization and uncertain RCP trip time due to assumed failure of High Pressure Safety Injection (HPSI). The reported results exhibited a damage domain trend with PCTs in excess of 2,200 °F (1,204.4 °C or 1,477.6 K) at relatively short RCP trip times (about 500 seconds or less), for cold leg breaks between 2.5 inches and 3 inches in diameter.

- (1) Please identify and describe SBLOCA sequences and accident conditions under which RCPs can remain in operation for prolonged time periods. Such sequences can be characterized with large uncertainties in RCP trip time. In identifying and describing these LOCA sequences and related accident conditions, please provide consideration of initial plant conditions, plant design and safety features, availability and performance of equipment, single failure assumptions, EOP requirements, and other relevant factors.
- (2) Please explain how LOCA sequences, as identified in the response to Item (1) above, are accounted for in analyzing SBLOCAs using the FSLOCA methodology.
- (3) Please describe the analyses that established the technical basis for prolonged RCP operation for the LOCA transients identified in the response to Item (1) above. Explain how corresponding EOP requirements and criteria related to RCP operation and trip were developed. Summarize and present the results from such analyses and identify those performed with WCOBRA/TRAC-TF2, as applicable.
- (4) Please provide WCOBRA/TRAC-TF2 prediction results for a spectrum of break sizes that analyze SBLOCAs with prolonged RCP operation. In addition, please compare these predictions against results from WCOBRA/TRAC-TF2 analyses in which RCPs were tripped to illustrate the impact of RCP operation.

RAI Question #129: Early RCP Trip during Small Break Loss-of-Coolant Accidents

WCAP-16996-P/WCAP-16996-NP, Volumes I, II, and III, Revision 0, Section 25, “Plant Sources of Uncertainty,” Subsection 25.5.1, “EOP Sequences for a Small Break LOCA,” describes continuously monitored conditions that are used in EOP E-0 “Reactor Trip or Safety Injection” for comparison against

established RCP trip criteria when determining boundary conditions assumed for small break LOCA analysis calculations. It is mentioned in Subsection 25.5.1 that although the description is specific to Indian Point Unit 2, “plants typically follow a generic template for the generation of EOPs.”

- (1) Please identify and describe SBLOCA sequences and accident conditions under which RCPs are tripped early in the transient. In identifying and describing these LOCA sequences and related accident conditions, please provide consideration of initial plant conditions, plant design and safety features, availability and performance of equipment, single failure assumptions, EOP requirements, and other relevant factors.
- (2) Please describe the analyses that established the technical basis for tripping RCPs in the class of LOCA transients identified in the response to Item (1) above. Explain how corresponding EOP requirements and criteria related to RCP operation were established in the generic template used for generation of EOPs. Summarize and present the results from such analyses and identify those performed with WCOBRA/TRAC-TF2.
- (3) Please provide WCOBRA/TRAC-TF2 prediction results for a spectrum of break sizes that analyze SBLOCAs with RCPs tripped early in the transients. In addition, please compare these predictions against results from WCOBRA/TRAC-TF2 analyses in which RCPs were not tripped to illustrate the impact of RCP operation.

RAI Question #130: Break Location Impact in Previous Small Break Loss-of-Coolant Accident Analyses

WCAP-16996-P/WCAP-16996-NP, Volumes I, II, and III, Revision 0, Section 2, “Evaluation Model Functional Requirements,” Subsection 2.3.1, “LOCA Scenario Specification,” states: “Sensitivity studies based on Appendix K methods have identified a cold leg break to be the most limiting in terms of location. Since this was also true of earlier best-estimate cases analyzed, this is taken to be the limiting break location for the following PIRT discussion.”

- (1) Please identify and describe the conservative analyses of the effect of break location described as “sensitivity studies based on Appendix K methods” in the above given citation from Subsection 2.3.1. Summarize the findings from the performed analyses and present major prediction results using tables and graphs as appropriate. Include description of relevant modeling assumptions and computer codes used. Also, please provide a list of references identifying the source documents containing these studies.
- (2) Please identify and describe the best-estimate studies analyzing the effect of break location and described as “earlier best-estimate cases analyzed” in the above given citation from Subsection 2.3.1. As for Item (1) above, please summarize the findings from the performed analyses and present major prediction results using tables and graphs as appropriate. Include description of relevant modeling assumptions and computer codes used. Provide a list of references identifying the source documents containing these analyses.

RAI Question #131: Break Location Impact in Small Break Loss-of-Coolant Accident Analyses Using WCOBRA/TRAC-TF2

As pointed out in Section 4.4.2, “Break Location,” in NUREG-0623 (see B. Sheron, “Generic Assessment of Delayed Reactor Coolant Pump Trip during Small Break Loss-of-Coolant Accidents in Pressurized Water Reactors,” NUREG-0623, November 1979), vendor analyses identifying limiting breaks with regard to break location led to different findings. Thus, Westinghouse “concluded that a break in the cold leg discharge piping with the pumps running resulted in the limiting consequences” whereas Combustion Engineering concluded that “the breaks postulated in the hot leg with delayed pump trip or pumps running were the most limiting with regard to peak cladding temperatures.” Also, no best-estimate analyses of small break LOCAs by Westinghouse were identified in Section 4.4.6, “Best-Estimate Analysis,” in NUREG-0623.

Section 3.15, “Special Considerations for a Small-Break Loss-of-Coolant Accident in Pressurized Water Reactors,” in U.S. NRC RG 1.157, “Best-Estimate Calculations of Emergency Core Cooling System Performance,” May 1989, recognizes that “break flow may be greatly influenced by the location and specific geometry of the break.” Accordingly, “small-break loss-of-coolant accident calculations should, therefore, include various assumed break locations in the spectrum of breaks analyzed.”

Please provide the following additional information regarding WCOBRA/TRAC-TF2 analyses performed to examine sensitivity of code predictions to break location as part of substantiating and confirming the approach for treatment of break location for small break LOCA analyses implemented in the FSLOCA methodology.

- (1) Please identify best-estimate studies performed with WCOBRA/TRAC-TF2 to analyze the effect of break location in small break LOCAs. Provide a list of references that identify the source documents containing these analyses.
- (2) Please provide and describe WCOBRA/TRAC-TF2 prediction results for a spectrum of break sizes that analyze small breaks occurring in a cold leg piping between the RCP and the reactor pressure vessel as well as in a hot leg. For breaks located in a hot leg, please consider possible sensitivity with regard to the location of the pressurizer vessel connection. Include description of relevant modeling assumptions and the computer code versions used.
- (3) Present direct comparisons of prediction results for key parameters from small break LOCA analyses simulating transients with the same break sizes and different break locations. Present such comparison plots for different PWR plant types that will be analyzed with the FSLOCA methodology.
- (4) Provide and describe WCOBRA/TRAC-TF2 prediction results that examine the impact of RCPs trip delay with offsite power available on the limiting break location for small break LOCAs. Include analyses of small break LOCA sequences with RCPs tripped early in the transient and such with prolonged RCPs operation.

RAI Question #136: Reactor Coolant Pump Trip Impact on Core Initial Thermal-Hydraulic Response for Large Break Loss-of-Coolant Accidents

The time of RCP trip following a LBLOCA can have an impact on the initial thermal-hydraulic response in the reactor pressure vessel and in the reactor core region in particular. Among others, processes such as flow stagnation and possible flow reversal in the core can be affected by RCPs operation and time of RCP trip. WCAP-16996-P/WCAP-16996-NP, Volumes I, II, and III, Revision 0, Section 28, "Scoping and Sensitivity Studies," Subsection 28.1.2, "Offsite Power Availability – LBLOCA," presents LBLOCA analyses performed with WCOBRA/TRAC-TF2 for the reference V. C. Summer (CGE) and Beaver Valley Unit 1 (DLW) plants. The analyses examine the impact of offsite power availability on large break LOCA results.

WCAP-16996-P/WCAP-16996-NP, Volumes I, II, and III, Revision 0, Section 25, "Plant Sources of Uncertainty," Subsection 25.5.2, "Variability of Plant Conditions Due to Operation Actions," states that [

] ^{a,c}

Please provide the following additional information regarding WCOBRA/TRAC-TF2 analyses performed to examine sensitivity of the initial reactor core thermal-hydraulic response to RCP trip time with offsite power available.

- (1) Please identify best-estimate studies that have been performed with WCOBRA/TRAC-TF2 to analyze sensitivity of large break LOCA predictions to RCP trip time with offsite power available with a focus on the initial thermal-hydraulic response in the reactor pressure vessel and in the reactor core region. Provide a list of references that identify the source documents containing these analyses. In addition to the analyses discussed in Subsection 28.1.2, "Offsite Power Availability – LBLOCA," please present results from WCOBRA/TRAC-TF2 calculations to examine sensitivity to RCP trip time following a large break LOCA.
- (2) Please provide WCOBRA/TRAC-TF2 prediction results analyzing sensitivity of LBLOCA predictions to RCP trip time with offsite power available with a focus on the effect of core flow stagnation and possible flow reversal in the core.
- (3) In presenting the analyses requested in Item (1) above, please provide additional information addressing the following items: (a) the analyses should cover a spectrum of large break sizes over which the examined effect takes place and code predictions show most sensitivity to break change, if so observed, and (b) the analyses should cover a range of RCPs trip times that reflects the uncertainty associated with the pump trip event. Please provide consideration of different PWR plant types and show predictions results for a PWR plant design for which the sensitivity of examined parameters to RCPs trip time is most pronounced, as applicable. Show the impact on prediction results with relevance to the applicable safety criteria and include zoomed plots of computed results over a time window during which the stagnation effect is predicted to take place, as applicable.

1.0 Introduction and Problem Statement

The as-submitted FULL SPECTRUM LOCATM (FSLOCATM) evaluation model (EM) is based on the break occurring in the pump discharge cold leg as the limiting break location. The methodology considers both loss-of-offsite power (LOOP) and offsite power available (OPA) scenarios. For a loss-of-offsite power, the reactor coolant pumps are tripped coincident with the reactor trip. For offsite power available, the reactor coolant pumps are assumed to operate []^{a,c} after the reactor trip. The pumps are then tripped, since the operators are assumed to have tripped the pumps by this time.

This response addresses the Requests for Additional Information (RAIs) related to the reactor coolant pump (RCP) operation, as well as the limiting break location. The modeling of the RCP trip timing with offsite power available is discussed in Section 2 of this response. The modeling of the RCP trip timing is modified slightly as described in Sections 2.3 and 2.4.

A review of the limiting break location for other Small Break LOCA (SBLOCA) evaluation models is discussed in Section 3.1 of this response. Various sensitivity studies are presented in Section 3.2. It is shown that a break in the pump discharge cold leg is more limiting than a hot leg break for Westinghouse-designed Pressurized Water Reactors (PWRs). It is also shown that this conclusion remains valid with different RCP trip times when offsite power is available.

Some additional information requested in the RAIs is provided in Section 4 herein. Finally, a summary of the main conclusions is presented in Section 5.

2.0 Reactor Coolant Pump Trip with Offsite Power Available

2.1 Background

Following the accident at Three Mile Island Unit 2, the Nuclear Regulatory Commission (NRC) expressed concern about RCP operation during a SBLOCA. In response, the Westinghouse Owners' Group (WOG) sponsored analyses to determine when the RCPs must be tripped if offsite power remains available. It was determined that manually tripping the RCPs before RCS inventory is depleted to less than a "critical inventory" results in a peak cladding temperature (PCT) about the same as the PCT in the FSAR analysis (WCAP-9584 [1]).

The dialogue continued between the NRC and the industry until the NRC issued a revised position in NRC Generic Letters 83-10c [2] and 10d [3]. These NRC letters recognize that there are certain accident conditions for which the RCPs should be tripped, and others for which RCP operation should be continued if possible. Under either set of accident conditions, safety criteria must be met and maintained for those events within the plant design basis. In response, plants committed to implement RCP trip criteria early in the Emergency Operating Procedures (EOPs). In the 1980s, the WOG performed generic small break LOCA calculations with emergency power available to determine the impact of delayed RCP trip for LOCA and Non-LOCA conditions.

The WOG issued several documents (OG-110 [4] and OG-117 [5]) which recommended RCP trip criteria on a generic basis. This work was based on analyses presented in WCAP-9584, and subsequent follow-up work. The work in these documents strived, among other things, to establish generic RCP trip criteria that could be provided in the emergency response guidelines, thus not necessitating an automated RCP trip under SBLOCA conditions. Three different RCP trip criteria were presented that could be utilized by the plant staff in the EOPs; these are referred to as the alternate trip criteria. The criteria which were evaluated were RCS pressure, RCS subcooling, and secondary pressure dependent pressure (RCS/secondary pressure differential). The evaluation in OG-110 demonstrated that all three criteria are essentially equivalent in providing an indication for the operator to trip the pumps during an SBLOCA transient.

Per WCAP-9584, when considering the spectrum of possible small break sizes, there exists a critical time such that, if the RCPs are tripped no later than that time, PCTs will remain below 2200°F for that plant type regardless of the assumed break size. A []^{a,c} critical RCP trip time was determined for all Westinghouse NSSS designs. This was determined through an extensive analysis performed for the Westinghouse 3-Loop Plant which included many conservative analysis assumptions. In addition, the concept of an equivalent break size was utilized to conclude the critical time for 2-Loop and 4-Loop Plants. Therefore, it was determined this critical time could be applied on a generic basis. Note that in follow-up studies performed in OG-117, it was determined that the critical time could in some cases be as low as []^{a,c} for a specific break size. It was concluded that if the RCPs are tripped in conformance with the Westinghouse Emergency Response Guidelines (ERGs), the thermal-hydraulic system behavior and calculated peak clad temperature (or maximum clad temperature, PCT) will be almost identical to the FSAR calculation assuming RCP trip at reactor trip time.

In order to clarify the time critical nature of manual RCP trip following a small break LOCA and the time value associated with this action, the ERG Executive Volume, RCP TRIP/RESTART Generic Issue, Section 2.3.2, "Evaluation of Alternate RCP Trip Parameters" was updated as part of a Pressurized Water Reactor Owners' Group (PWROG) program (WCAP-17711-NP [6]) to note that manual RCP trip during a small break LOCA should be a Time Critical Action, which should be performed prior to the critical time after the trip criterion is met.

2.2 Treatment in Prior Westinghouse Best-Estimate SBLOCA Evaluation Model

The treatment of operator action associated with RCP trip for the prior Westinghouse Best-Estimate SBLOCA evaluation model was discussed in Section 25-3 of WCAP-14936 [7]. It was stated therein: [

] ^{a,c}

The reference for the database of studies discussed in WCAP-14936 is not readily available. The quoted []^{a,c} range in the RCP trip times is simply illustrative of the limited variance observed.

2.3 Updated Modeling for Manual RCP Trip within the FSLOCA Evaluation Model

Westinghouse issued a report (WCAP-17711-NP) for the PWROG with ERG critical tasks. The safety significance of manual RCP trip during SBLOCA is discussed in Appendix A.3 of WCAP-17711-NP, and CT-16 to manually trip the RCPs is provided in Appendix B.16 of WCAP-17711-NP. The following summary is extracted from the report:

“On a generic, owners group basis, manual tripping of RCPs during a SBLOCA should be retained as a critical task, provided that the particular set of plant conditions specified in worksheet CT-16 are met. The basis for retaining this task extends back to WCAP-9584, ‘Analysis of Delayed Reactor Coolant Pump Trip during Small-Break Loss of Coolant Accidents,’ and NRC Generic Letter 83-10d, ‘Resolution of TMI Action Item – Automatic Trip of RCPs.’”

It is likely that the FSLOCA EM could support a longer RCP trip time than the prior studies discussed in Section 2.1. However, for consistency with the industry position and current EOPs, the FSLOCA EM will []

[]^{a,c}

The EM will continue to assume that the RCPs trip coincident with the reactor trip for a LOOP.

2.4 Additional Discussion Regarding Impact on Region II (Large Break) Analysis

The most significant impact of pump trip and coastdown for the analysis of large breaks occurs []

[]^{a,c}

In the prior Automated Statistical Treatment of Uncertainty Method (ASTRUM) EM (WCAP-16009-P-A [9]), the RCPs were assumed to operate for the duration of the transient when offsite power was available. For FULL SPECTRUM LOCA, the manual RCP trip will be modeled for Region II (large breaks) in the same manner as for Region I (small breaks) discussed in the previous section. This approach is selected since: 1) the same criteria used for manual RCP trip under SBLOCA conditions will also be met for LBLOCA conditions, and 2) the LBLOCA transient results are []

[]^{a,c} (as reflected by the PIRT rankings, and also considering the duration of the large break transients, e.g., Figures 27.1.1.1-1 and 27.1.2.1-1 from WCAP-16996-P).

The treatment of loss-of-offsite power versus offsite power available is described in Section 30.4 of WCAP-16996-P. To paraphrase, [

] ^{a,c}

3.0 Limiting Break Location

It is stated in Section 2.3.1 of WCAP-16996-P that: [

] ^{a,c}

The RAIs question whether a hot leg break could be the limiting break location for the FSLOCA EM. It will be shown in the following sub-sections that hot leg breaks are non-limiting compared to cold leg breaks, consistent with the discussion and [^{a,c} in WCAP-16996-P.

3.1 Review of Prior Westinghouse Evaluation Models

Prior Westinghouse SBLOCA EMs (as well as studies performed to support the break location modeled in the EMs) are reviewed to determine the break location modeled in those EMs.

The NOTRUMP evaluation model (WCAP-10054-P-A [10]) is an Appendix K SBLOCA EM. The limiting break location is modeled in the pump discharge cold leg for the NOTRUMP EM. A study of different break locations, including a hot leg break, was executed with the NOTRUMP code in WCAP-11145-P-A (proprietary) [11] / WCAP-11372-A [12] (non-proprietary). The results of this study were presented in Table 3.3-4 of WCAP-11145-P-A / WCAP-11372-A, which is presented as Table 3.1-1 in this response. It can be seen in Table 3.1-1 that while the cold leg breaks experienced core uncover and a corresponding heatup, the hot leg break did not result in any core uncover.

Subsequent to the NOTRUMP EM, a Best-Estimate (BE) SBLOCA EM was developed by Westinghouse in the early 2000s. The evaluation model is documented in Volumes I through IV of WCAP-14936. While this EM was not approved by the NRC, a significant amount of validation was completed such that it can serve as another data point for the limiting break location. A break location study was executed with the Indian Point Unit 2 PWR model and is discussed in Section 28 of Volume III of WCAP-14936. The results of the hot leg break study are compared to a reference cold leg break study in Figures 28-2-13 through 28-2-15 of WCAP-14936, which are presented herein as Figures 3.1-1 through 3.1-3. It is observed in Figures 3.1-1 and 3.1-2 that the [

] ^{a,c}

Table 3.1-1: Presentation of Table 3.3-4 from WCAP-11145-P-A / WCAP-11372-A

<u>4-Loop Plant Category</u> <u>4-Inch Breaks</u> <u>Hot Rod Heatup Calculation Results</u>			
<u>Event</u>	<u>Break Location</u>		
	<u>Cold Leg</u>	<u>Pump Suction</u>	<u>Hot Leg</u>
Peak Cladding Temperature (F)	1253.0	1122.6	N/A
Peak Cladding Temperature Location (ft)	11.50	11.25	N/A
Local Zr/H ₂ O Reaction Maximum (%)	0.38	0.38	N/A
Local Zr/H ₂ O Reaction Location (ft)	11.50	11.25	N/A
Total Zr/H ₂ O reaction (%)	<0.3	<0.3	N/A
Hot Rod Burst Time (sec)	N/A	N/A	N/A
Hot Rod Burst Location (ft)	N/A	N/A	N/A

N/A Not Applicable



**Figure 3.1-1: Presentation of Figure 28-2-13 from WCAP-14936,
Break Location – Downcomer Collapsed Liquid Level Comparison, Break in Hot Leg**



**Figure 3.1-2: Presentation of Figure 28-2-14 from WCAP-14936,
Break Location – Inner Vessel Collapsed Liquid Level Comparison, Break in Hot Leg**



**Figure 3.1-3: Presentation of Figure 28-2-15 from WCAP-14936,
Break Location – PCT Comparison, Break in Hot leg**

3.2 Sensitivity Studies with the FSLOCA Evaluation Model

A review of prior Westinghouse SBLOCA evaluation models in Section 3.1 indicated that a cold leg break was consistently found to be limiting over a hot leg break for Westinghouse-designed plants. A more comprehensive series of break location sensitivity studies was executed with WCOBRA/TRAC-TF2 for the FSLOCA EM. First, a spectrum of cold leg and hot leg breaks from a 2-inch break to a 5-inch break was executed assuming OPA with an RCP trip time of []^{a,c} after reactor trip² (Section 3.2.1). Sensitivity studies for the RCP trip time were then conducted based on the 2.5-inch break cases, since the 2.5-inch cold leg break size produced the largest heatup from the cold leg break spectrum study (Section 3.2.2). Finally, a sensitivity study to the loop in which the hot leg break occurs (i.e. the loop with the pressurizer versus without) was conducted with the 2.5-inch hot leg break case (Section 3.2.3). The results of these sensitivity studies are discussed in the following subsections.

3.2.1 Cold Leg and Hot Leg Break Spectrums

Overview

A series of cold leg and hot leg break cases were executed with Beaver Valley Unit 1 based on Study B from the response to RAIs 9 and 12 previously transmitted in LTR-NRC-13-45 [13]. The studies included 2-inch, 2.5-inch, 3-inch, 3.5-inch, 4-inch, and 5-inch breaks. The hot rod Peak Cladding Temperature (PCT) from these twelve cases (six cold leg breaks and six hot leg breaks) is presented in Figure 3.2-1. []

[]^{a,c}

The general behavior of the 2.5-inch and 3-inch transients for the different break locations is now contrasted. []

[]^{a,c} A more detailed discussion of the transients, including plots which support the described behaviors, is provided in the following paragraphs.

² []

[]^{a,c}

Results Discussion

[

] ^{a,c}

[

] ^{a,c}

3.2.2 Reactor Coolant Pump Trip Sensitivity

[

] ^{a,c}

Hot Leg Break

[

] ^{a,c}

Cold Leg Break

[

] ^{a,c}

[

] ^{a,c}

3.2.3 Sensitivity to Loop with Pressurizer

[

] ^{a,c}

a,c

Figure 3.2-1: Hot Rod PCT for all the Hot Leg and Cold Leg Breaks

a,c

Figure 3.2-2: Pressurizer Pressure for the 2.5-inch and 3-inch Hot Leg and Cold Leg Breaks

a,c

Figure 3.2-3: Break Mass Flow Rate for the 2.5-inch Hot Leg and Cold Leg Breaks

a,c

Figure 3.2-4: Break Mass Flow Rate for the 3.0-inch Hot Leg and Cold Leg Breaks



Figure 3.2-5: Void Fraction at the Horizontal Section of the Loop Seal Region for the 2.5-inch Cold Leg Breaks



Figure 3.2-6: Comparison of Pressurizer Pressure and Void Fraction at the Break for the 2.5-inch Hot Leg and Cold Leg Breaks

a,c

Figure 3.2-7: Comparison of Pressurizer Pressure and Void Fraction at the Break for the 3-inch Hot Leg and Cold Leg Breaks

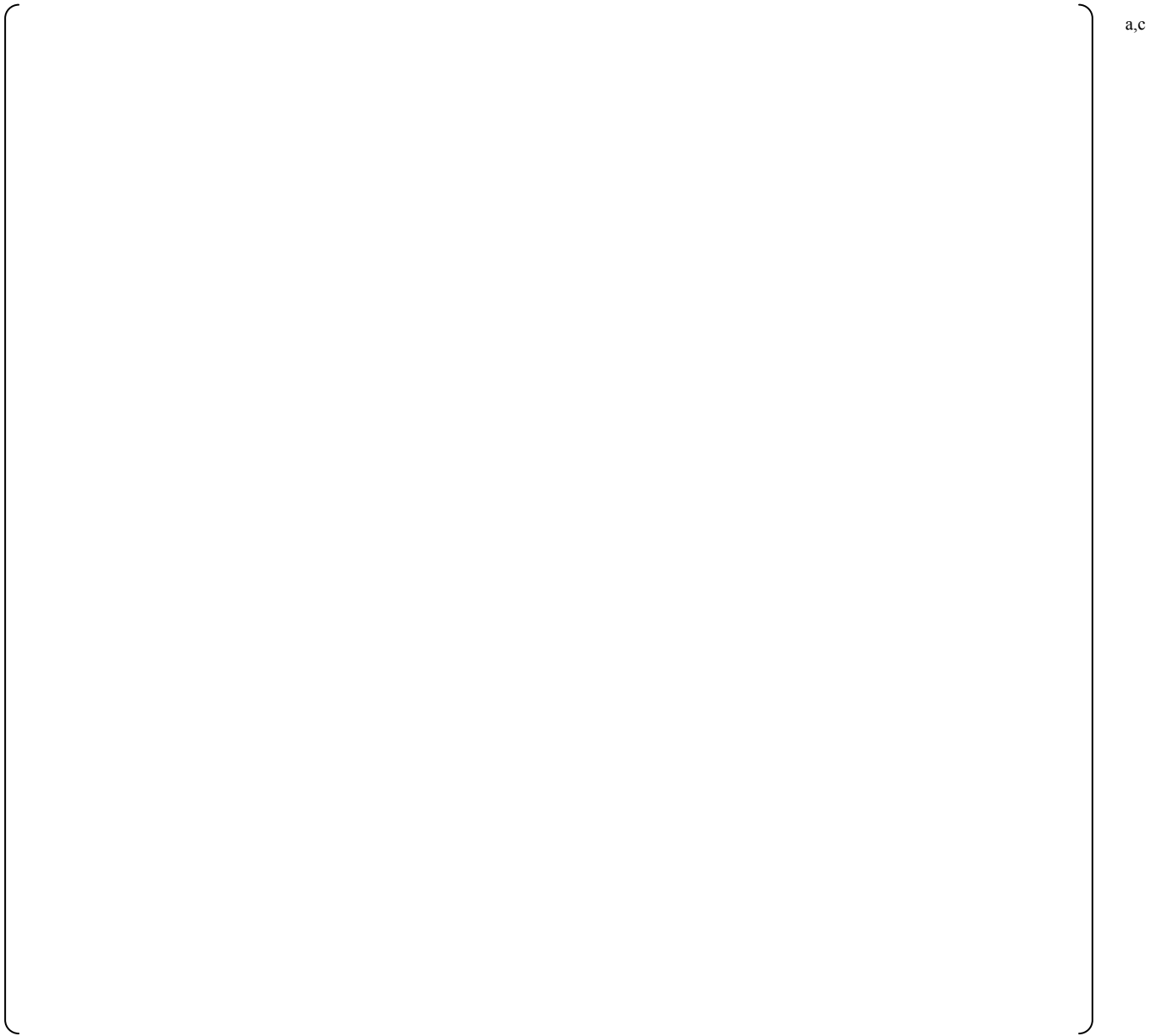


Figure 3.2-8: Void Fraction at the Horizontal Section of the Loop Seal Region for the 2.5-inch Hot Leg Breaks

a,c

Figure 3.2-9: Safety Injection Mass Flow Rate (Sum of all Loops) for the 2.5-inch and 3-inch Hot Leg and Cold Leg Breaks

a,c

Figure 3.2-10: Vessel Fluid Inventory for the 2.5-inch Hot Leg and Cold Leg Breaks

a,c

Figure 3.2-11: Vessel Fluid Inventory for the 3-inch Hot Leg and Cold Leg Breaks

a,c

Figure 3.2-12: Vessel Fluid Inventory and Integrated Accumulator Injection Flow for the 2.5-inch Hot Leg and Cold Leg Break

a,c

Figure 3.2-13: Vessel Fluid Inventory and Integrated Accumulator Injection Flow for the 3-inch Hot Leg and Cold Leg Breaks

a,c

Figure 3.2-14: Accumulator Injection Flow and Break Flow for the 2.5-inch Hot Leg Break

a,c

Figure 3.2-15: Accumulator Injection Flow and Break Flow for the 3-inch Hot Leg Break

a,c

Figure 3.2-16: Hot Rod PCT for the 2.5-inch and 3-inch Hot Leg and Cold Leg Breaks

a,c

Figure 3.2-17: Pressurizer Pressure for the Hot Leg Break RCP Trip Time Sensitivity Study

a,c

Figure 3.2-18: Pressurizer Pressure versus Core Inlet Liquid Mass Flow Rate for the Hot Leg Break RCP Trip Time Sensitivity Study

Figure 3.2-19: Pressurizer Pressure versus Vapor Generation in a Select Cell of the Hot Channel for the Hot Leg Break RCP Trip Time Sensitivity Study

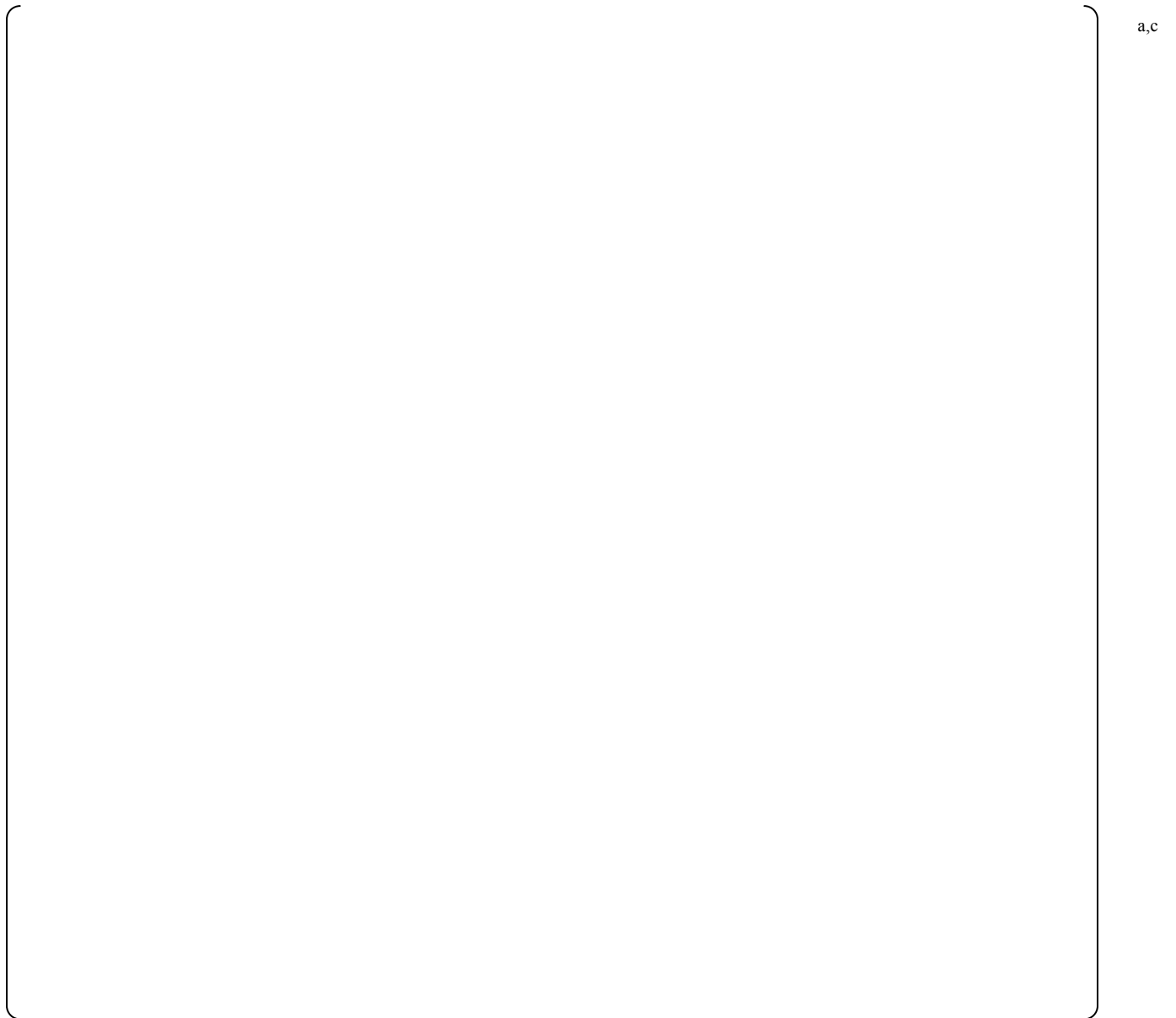


Figure 3.2-20: Void Fraction at the Horizontal Section of the Loop Seal Region for the 5-minute RCP Trip Time, Hot Leg Break

a,c

Figure 3.2-21: Void Fraction at the Horizontal Section of the Loop Seal Region for the 3-minute RCP Trip Time, Hot Leg Break



Figure 3.2-22: Void Fraction at the Horizontal Section of the Loop Seal Region for the 1-minute RCP Trip Time, Hot Leg Break

a,c

Figure 3.2-23: Vessel Fluid Inventory for the Hot Leg Break RCP Trip Time Sensitivity Study

a,c

Figure 3.2-24: Hot Rod PCT for the Hot Leg Break RCP Trip Time Sensitivity Study

a,c

Figure 3.2-25: Pressurizer Pressure for the Cold Leg Break RCP Trip Time Sensitivity Study

a,c

Figure 3.2-26: Pressurizer Pressure versus Core Inlet Liquid Mass Flow Rate for the Cold Leg Break RCP Trip Time Sensitivity Study

a,c

Figure 3.2-27: Pressurizer Pressure versus Vapor Generation in a Select Cell of the Hot Channel for the Cold Leg Break RCP Trip Time Sensitivity Study

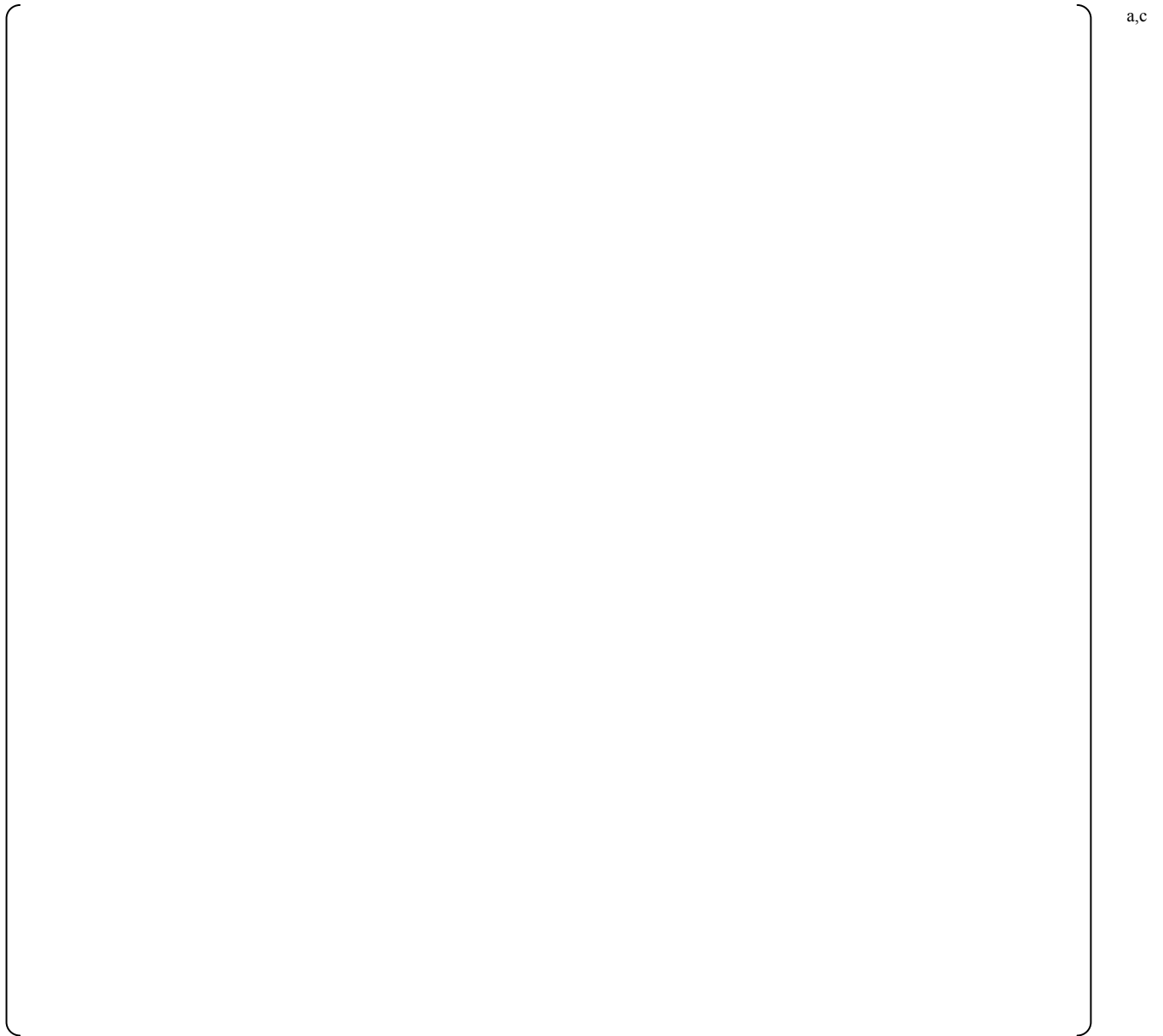


Figure 3.2-28: Void Fraction at the Horizontal Section of the Loop Seal Region for the 5-minute RCP Trip Time, Cold Leg Break

a,c

Figure 3.2-29: Void Fraction at the Horizontal Section of the Loop Seal Region for the 3-minute RCP Trip Time, Cold Leg Break

a,c

Figure 3.2-30: Void Fraction at the Horizontal Section of the Loop Seal Region for the 1-minute RCP Trip Time, Cold Leg Break

a,c

Figure 3.2-31: Void Fraction at the Horizontal Section of the Loop Seal Region for the No Delay RCP Trip Time, Cold Leg Break

a,c

Figure 3.2-32: Vessel Fluid Inventory for the Cold Leg Break RCP Trip Time Sensitivity Study

a,c

Figure 3.2-33: Hot Rod PCT for the Cold Leg Break RCP Trip Time Sensitivity Study

a,c

Figure 3.2-34: Void Fraction in the Bottom Cell of the Pressurizer for the Hot Leg Break, Broken Loop (Pressurizer versus Non-Pressurizer) Sensitivity Study

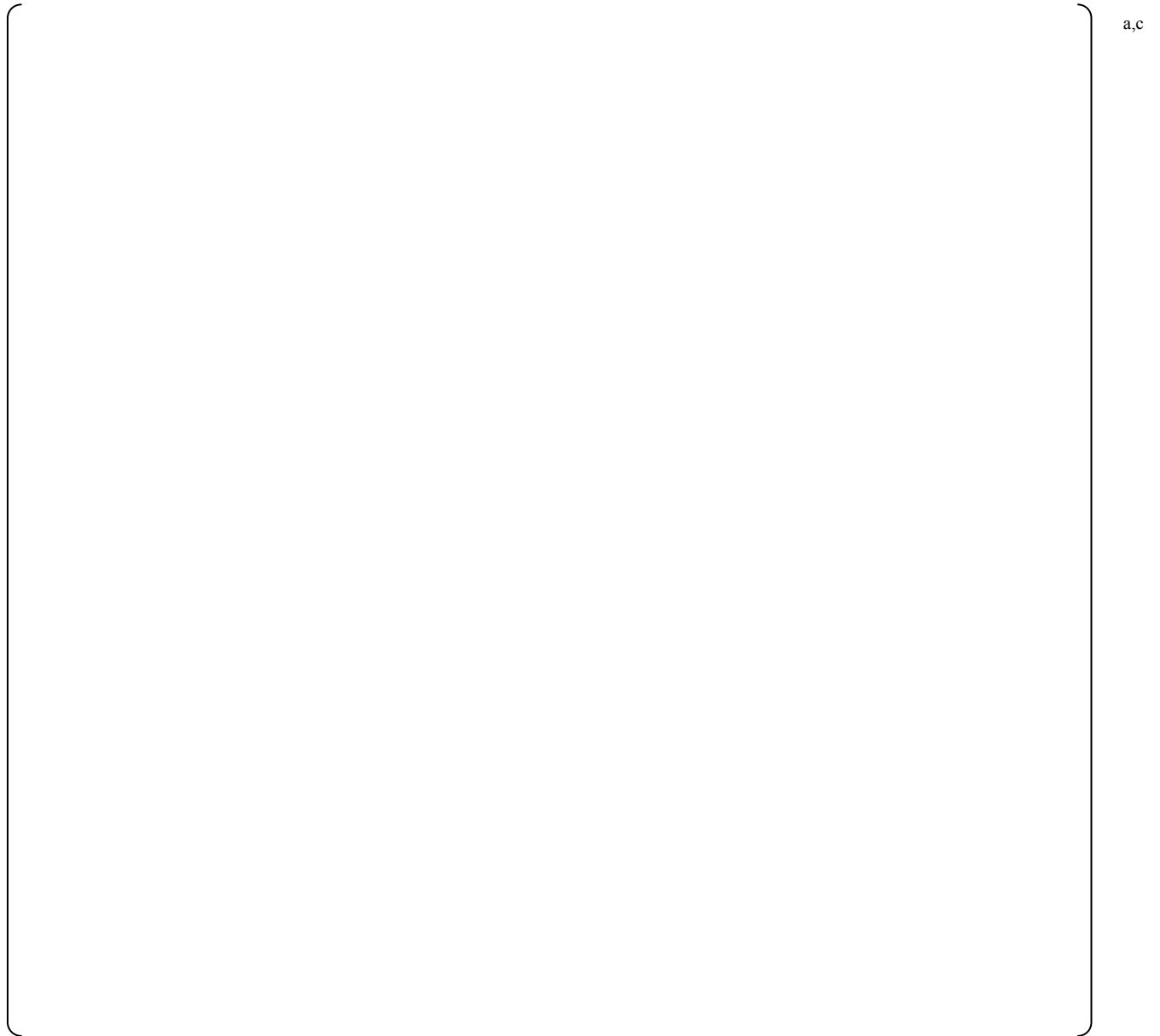


Figure 3.2-35: Pressurizer Pressure for the Hot Leg Break, Broken Loop (Pressurizer versus Non-Pressurizer) Sensitivity Study

a,c

Figure 3.2-36: Vessel Fluid Inventory for the Hot Leg Break, Broken Loop (Pressurizer versus Non-Pressurizer) Sensitivity Study

a,c

Figure 3.2-37: Hot Rod PCT for the Hot Leg Break, Broken Loop (Pressurizer versus Non-Pressurizer) Sensitivity Study

4.0 Additional Information for Specific RAI Questions

RAI-10: In the table with the resolution status of the responses to RAIs, there was a Westinghouse action cited for RAI-10 to show that the results of hot leg break studies are non-limiting. That action has been completed within the body of this response.

RAI-123: This RAI requests detailed information regarding factors which influence the modeling approach to RCP trip with offsite power available. However, the RCP trip is modeled deterministically in the FSLOCA EM. The only items from the cited list that are directly considered in the RCP trip time are the EOP requirements and applicable criteria, and the operator recognition of the event and action. The plant monitored conditions are inherent to the EOPs, and the break size influences the plant monitored conditions. The operator training at utilities ensures that the EOP requirements can be met by the operators. Aligning the FSLOCA modeling with the utility EOPs ensures that the actual time for RCP trip will not exceed that modeled by the FSLOCA EM. The sensitivity studies discussed in Section 3.2.2 of this response show that an [

] ^{a,c}

RAI-124: The Region I demonstration analysis presented in WCAP-16996-P modeled RCP trip [^{a,c} after the reactor trip for offsite power available. When the demonstration analysis results are updated to be consistent with the final evaluation model, the RCP trip will be modified as described in this response. [

^{a,c} The basis for the updated RCP trip time is described in the body of this response, as supplemented by the discussion for RAI-123 above.

RAI-125: The Region II demonstration analysis presented in WCAP-16996-P modeled RCP trip [^{a,c} after the reactor trip for offsite power available. When the demonstration analysis results are updated to be consistent with the final evaluation model, the RCP trip will be modified as described in this response.

RAI-126: The range of less than [^{a,c} was cited as an illustration of the operator response time, supported by the Indian Point Unit 2 simulator studies. However, it is clarified that the generic RCP trip time modeled for offsite power available is [^{a,c} as described in the body of the response (i.e., no range in the operator response time is modeled).

RAI-128: It is noted that the paper cited in this RAI studies the SBLOCA transient without any high pressure safety injection. Such a scenario requires multiple failures, and is beyond design basis. Prolonged RCP operation under SBLOCA conditions is precluded by the EOPs, to which the plant operators are trained. A [^{a,c} RCP trip time consistent with prior WOG studies and plant EOPs is modeled in the FSLOCA EM for offsite power available, as discussed in the body of the response.

RAI-136: A study of [

] ^{a,c}

5.0 Summary and Conclusions

[

] ^{a,c}

A cold leg break was shown to be more limiting than a hot leg break for a variety of different break sizes and RCP trip times. This conclusion is considered to be generically applicable for Westinghouse-designed PWRs.

6.0 References

- 1) WCAP-9584, "Analysis of Delayed Reactor Coolant Pump Trip during Small Loss of Coolant Accidents for Westinghouse Nuclear Steam Supply Systems," August 30, 1979.
- 2) NRC Generic Letter 83-10c, Resolution of TMI Action Item II.K.3.5, "Automatic Trip Of Reactor Coolant Pumps," February 8, 1983.
- 3) NRC Generic Letter 83-10d, Resolution of TMI Action Item II.K.3.5, "Automatic Trip Of Reactor Coolant Pumps," February 8, 1983.
- 4) OG-110, "Evaluation of Alternate RCP Trip Criteria," December 1, 1983.
- 5) OG-117, "Justification of Manual RCP Trip for SBLOCA Events," March 9, 1984.
- 6) WCAP-17711-NP, "Pressurized Water Reactor Owners Group Westinghouse Emergency Response Guideline Revision 2-Based Critical Tasks," March 2013.
- 7) WCAP-14936, Volumes 1 through 4, "Code Qualification Document for Best Estimate Small Break LOCA Analysis," August 2001.

- 8) WCAP-16996-P, "Realistic LOCA Evaluation Methodology Applied to the Full Spectrum of Break Sizes (FULL SPECTRUM LOCA Methodology)," November 2010.
- 9) WCAP-16009-P-A, "Realistic Large-Break LOCA Evaluation Methodology Using the Automated Statistical Treatment Of Uncertainty Method (ASTRUM)," January 2005.
- 10) WCAP-10054-P-A, "Westinghouse Small Break ECCS Evaluation Model Using the NOTRUMP Code," August 1985.
- 11) WCAP-11145-P-A, "Westinghouse Small Break LOCA ECCS Evaluation Model Generic Study with the NOTRUMP Code," 1986.
- 12) WCAP-11372-A, "Westinghouse Small Break LOCA ECCS Evaluation Model Generic Study with the NOTRUMP Code," 1986.
- 13) LTR-NRC-13-45, "Submittal of Westinghouse Responses to 'WCAP-16996-P, 'Realistic LOCA Evaluation Methodology Applied to the Full Spectrum of Break Sizes (FULL SPECTRUM LOCA Methodology)' Request for Additional Information – RAIs 9 and 12' (Proprietary/Non-Proprietary), Project 700, TAC No. ME5244," June 26, 2013.

**WCAP-16996-P, “Realistic LOCA Evaluation Methodology Applied to the Full Spectrum of Break Sizes
(FULL SPECTRUM LOCA Methodology)”
Request for Additional Information – (Non-Proprietary)
Set 8 RAIs 127, 132-135 and 137-139**

January 2014

Westinghouse Electric Company LLC
1000 Westinghouse Drive
Cranberry Township, PA 16066

RAI Question #127: Single Failure Assumptions in Loss-of-Coolant Accident Analyses

Criterion 35, “Emergency Core Cooling,” in Appendix A, “General Design Criteria for Nuclear Power Plants,” to Title 10 to Code of Federal Regulation Part 50, requires that a single failure be assumed when analyzing safety system performance. The NRC RG 1.157, “Best-Estimate Calculations of Emergency Core Cooling System Performance,” May 1989, states that “Appendix A to 10 CFR Part 50 requires that a single failure be considered when analyzing safety system performance and that the analysis consider the effect of using only onsite power and only offsite power.”

WCAP-16996-P/WCAP-16996-NP, Volumes I, II, and III, Revision 0, Section 25, “Plant Sources of Uncertainty,” Subsection 25.3, “Reactor Accident Boundary Conditions,” in its part “Single Failure Assumption,” states that “the loss of a train may be assumed for the determination of pumped ECCS flow during the LOCA, while the train will be assumed to operate in the calculation of containment backpressure.” It is also explained that “alternatively, a more complete analysis using consistent assumptions may be performed on a plant-by-plant basis.”

- (1) Please provide a table that lists single failure assumptions considered possible and applicable for the purposes of LOCA analyses using the FSLOCA™ methodology. Please use a separate row for each combination and formulate the single failure assumptions in two separate columns. Include the single failure assumption applicable for modeling the RCS response with WCOBRA/TRAC-TF2 in the first column and the one applicable for the containment backpressure modeling in the second column. Please consider small and large break LOCA analysis applications. Explain the identified single failure assumptions along with pertinent conditions and supporting considerations.
- (2) Subsection 25.3, “Reactor Accident Boundary Conditions,” in its part “Single Failure Assumption,” states that “a more complete analysis using consistent assumptions may be performed on a plant-by-plant basis.” Please explain what such “a more complete analysis,” when “performed on a plant-by-plant basis,” includes. Identify and describe the “consistent assumptions” that are considered applicable for performing the analysis. Describe the types of plant-specific information that are considered in individual plant analyses. If failure-related assumptions that can be identified and used in analyses on a plant-by-plant basis are not included in the response to Item (1) above, please provide a table that describes them. Explain the identified single failure assumptions along with pertinent conditions and supporting considerations.

Response:

Criterion 35, “Emergency Core Cooling,” in Appendix A, “General Design Criteria for Nuclear Power Plants,” to 10 CFR Part 50, requires suitable redundancy in components, features, interconnections, etc. such that the system safety function can be accomplished assuming a single failure. As such, when considering possible single failures, it is assumed that there is no single failure which can cause two independent trains of the Emergency Core Cooling System (ECCS) to be inoperable. Additionally, single failures are only considered for active components.

FULL SPECTRUM™ and FSLOCA™ are trademarks in the United States of Westinghouse Electric Company LLC, its subsidiaries and/or its affiliates. These marks may be used and/or registered in other countries throughout the world. All rights reserved. Unauthorized use is strictly prohibited. Other names may be trademarks of their respective owners.

A list of various single failures that could be of interest to different licensing-basis analyses is typically provided in a plant's Final Safety Analysis Report (FSAR). However, there are only a limited number of active systems credited for mitigating LOCA transients in the FULL SPECTRUM™ LOCA (FSLOCA) evaluation model (EM). [

] ^{a,c}

Therefore, many of the possible failures are not of significance for the LOCA analysis. Considering the previously discussed active systems, the resulting list of single failures considered relevant for the generic FSLOCA EM is presented in Table 127-1. The impact of the failure on both the RCS and containment is provided.

Table 127-1: Single-Failures Considered for the FULL SPECTRUM LOCA EM

Failure	RCS Impact	Containment Impact
---------	------------	--------------------

[

] ^{a,c}

[

] ^{a,c}

As stated in Section 25.3 of WCAP-16996-P, if additional margin is desired on a plant-specific basis, a more complete analysis using consistent assumptions may be performed. This statement refers to modeling the consistent RCS and containment impacts from a particular failure, rather than a bounding combination of the impacts. [

] ^{a,c}

Reference(s)

- 1) WCAP-16996-P, "Realistic LOCA Evaluation Methodology Applied to the Full Spectrum of Break Sizes (FULL SPECTRUM LOCA Methodology)," November 2010.
- 2) LTR-NRC-01-6, "10 CFR 50.46 Annual Notification and Reporting for 2000," March 13, 2001.

RAI Question #132: Steam Generator Decay Heat Removal during Small Break Loss-of-Coolant Accidents

The main steam safety valves (MSSVs) are direct-acting valves (actuated only by pressure) that provide overpressure design protection and backup decay heat removal capability when the steam dumps and secondary atmospheric dump valves cannot be used. Each main steam line has several safety valves with staggered set pressures to provide an increased relieving capacity with an increasing overpressure. As described by T. E. Wierman, et al., “Industry Performance of Relief Valves at U.S. Commercial Nuclear Power Plants through 2007,” NUREG/CR-7037, March 2011, the set pressures for these valves are a nominal 1170, 1200, 1210, 1220, and 1230 psig with the highest setpoint being less than 110 percent of the SG design pressure.

WCAP-16996-P/WCAP-16996-NP, Volumes I, II and III, Revision 0, Section 25, “Plant Sources of Uncertainty,” Subsection 25.3, “Reactor Accident Boundary Conditions,” in summarizing the modeling approach with regard to the SG secondary side boundary conditions, states that [

] ^{a,c} Specifically, it is explained that [

] ^{a,c}

Please provide additional information related to the modeling of SG secondary conditions in WCOBRA/TRAC-TF2 plant analyses to predict decay heat removal via primary to secondary heat transfer in the SGs during SBLOCAs as follows.

- (1) State the method of decay heat removal due to heat transfer from the RCS to the SG secondary sides in SBLOCA analyses with WCOBRA/TRAC-TF2 as credited in the FSLOCA™ methodology. Identify the credited systems, conditions for their operation, and introduced assumptions as applied in modeling decay heat removal via the SGs in SBLOCA analyses.
- (2) Describe the approach to determine the set pressures for the MSSVs. In particular, please explain how the implemented approach takes into consideration and models the following factors: (a) uncertainty in the setpoint characteristics of the safety valves, (b) pressure drop from the SG to the safety valves, (c) uncertainty in rated relief capacities of the safety valves, and (d) criteria for using the next highest pressure setpoint. For example, Section 7.2.2, “Westinghouse-Designed Plants,” in NUREG-0623 (see B. Sheron, “Generic Assessment of Delayed Reactor Coolant Pump Trip during Small Break Loss-of-Coolant Accidents in Pressurized Water Reactors,” NUREG-0623, November 1979), in discussing the system pressure for manual pump trip, describes that the next highest pressure setpoint for the secondary system safety valves is used when the calculated relief flow is greater than 60 percent of the rated valve capacity at the previous pressure setpoint.

- (3) Present a table that documents the parameters identified in Item (2) above and used in the demonstration plant small break LOCA analyses for the FSLOCA methodology presented in WCAP-16996-P/WCAP-16996-NP, Volumes I, II, and III, Revision 0, Section 28, “Scoping And Sensitivity Studies,” and in Section 31, “Full Spectrum LOCA Demonstration Analysis.” Subsection 31.1.1, “Break Area Ranges,” identifies only a quantity described as “the lowest MSSV set pressure” and provides its value as []^b for the V. C. Summer case analysis.

Response:

- (1) The only systems credited to remove decay heat due to heat transfer from the reactor coolant system (RCS) to the steam generator (SG) secondary-side after the reactor trips due to onset of the LOCA transient are []^{a,c}

- (2) The response to part (2) is separated into the setpoint uncertainties, the relief capacity, and the pressure drop.

Setpoint Uncertainties

[]^{a,c}

[]^{a,c}

Relief Capacity

[

] ^{a,c} for several cases from the V C Summer small break spectrum sensitivity studies (presented in Section 27.1.1.3 of WCAP-16996-P [132-1]) is considered. It is expected that the decay heat removal via the steam generator would be more significant for smaller breaks, since more energy is removed via the break for larger breaks.

[

] ^{a,c}

Pressure Drop

The pressure drop from the secondary-side of the SG to the safety valves is [

] ^{a,c} There was an information notice on this topic (IN-97-09 [132-2]) issued in 1997, where it was stated that MSSV configurations which have relatively long and relatively small piping between the SG and the valves could cause a full-flow pressure drop as high as 100 psi. [

] ^{a,c}

(3) Table 132-1 provides the MSSV parameters for V C Summer, and Table 132-2 provides the MSSV parameters for Beaver Valley Unit 1. Note that only the parameters []^{a,c} as described in part (2) of this response.

Table 132-1: Main Steam Safety Valve Parameters for V C Summer

[]				
] ^b

Table 132-2: Main Steam Safety Valve Parameters for Beaver Valley Unit 1

[]				
] ^b

Summary

In summary, the only systems modeled to remove energy from the secondary-side of the steam generators are []

[]^{a,c} As such, the modeling of the MSSVs and heat removal from the steam generator secondary within the FULL SPECTRUM LOCA evaluation model is judged to be acceptable.

Reference(s)

- 132-1) WCAP-16996-P, “Realistic LOCA Evaluation Methodology Applied to the Full Spectrum of Break Sizes (FULL SPECTRUM LOCA Methodology),” November 2010.
- 132-2) IN-97-09, “Inadequate Main Steam Safety Valve (MSSV) Setpoints and Performance Issues Associated with Long MSSV Inlet Piping,” March 12, 1997.

RAI Question #133: Steam Generator Heat Transfer Modeling

According to Section 3.2.7, “Primary to Secondary Heat Transfer (Not Applicable to Boiling Water Reactors),” in the NRC RG 1.157, “Best-Estimate Calculations of Emergency Core Cooling System Performance,” May 1989, “heat transferred between the primary and secondary systems through the steam generators should be considered in the calculation and should be calculated in a best-estimate manner.”

- (1) Please describe the mechanisms that participate in the primary to secondary heat transfer through the SG heat exchange tubes. Identify factors that can have an impact on the primary to the secondary heat transfer mechanisms during normal plant operation and under LOCA conditions. Include consideration of deposits fouling of SG heat transfer tubes and supporting structures and associated effects on the overall heat resistance and thermal performance degradation.
- (2) Please present a table that identifies the correlations used in WCOBRA/TRAC-TF2 to model the heat transfer mechanisms on the outer side of the SG heat transfer tubes. Identify the experimental database for each provided correlation and provide its applicability range. Compare the applicability ranges for the correlations against typical conditions expected during LOCAs. Explain how the factors affecting the heat transfer mechanisms as identified in Item (1) above are accounted for in the implemented heat transfer models. Summarize the technical basis for these models along with the supporting data and analyses. In particular, consider the effect of thermal performance degradation due to deposits fouling.
- (3) Please present a table that identifies the correlations used in WCOBRA/TRAC-TF2 to model the heat transfer mechanisms on the inner side of the SG heat transfer tubes. Identify the experimental database for each provided correlation and provide its applicability range. Compare the applicability ranges for the correlations against typical conditions expected during LOCAs. Explain how the factors affecting the heat transfer mechanisms as identified in Item (1) above are accounted for in the implemented heat transfer models. Summarize the technical basis for these models along with the supporting data and analyses. In particular, consider the effect of non-condensable gas on heat transfer inside the SG tubes.

Response**Heat Transfer Correlations**

The steam generator (SG) tubes are modeled with an HTSTR component in WCOBRA/TRAC-TF2. The WCOBRA/TRAC-TF2 HTSTR component is identical to the HTSTR component from the base TRAC-P Version 5.4.28 code.

The HTSTR component is described in Section 10.10 of WCAP-16996-P [1], which is largely based on the discussion in Section 4.3 of LA-UR-00-834 [2]. The HTSTR solution as described therein is dependent on the value of several parameter settings for the component. For convenience, the standard values utilized for the parameters described in Section 10.10 of WCAP-16996-P or Section 4.3 of LA-

UR-00-834 for the FULL SPECTRUM™ LOCA (FSLOCA™) Evaluation Model (EM) to model the SG tubes are provided as follows. [

] ^{a,c}

The calculation of heat conduction in the HTSTR component is described in Section 2.2.4 of LA-UR-00-910 [3]. There are four numerical calculation options described in this section; the [

] ^{a,c}

The wall heat transfer models utilized for the HTSTR component are described in Section 3.8 of LA-UR-00-910. A summary of the different correlations used to determine the heat transfer coefficients for the different regimes is provided in Table 3-7 on pages 3-23 and 3-24 of LA-UR-00-910. All of these regimes are encountered for the SG tubes in PWR analysis except for film boiling (regime 4). Additional information on the wall-to-fluid heat transfer solution is provided in Appendix F.2.1 of LA-UR-00-910 (Appendix F.2.2 does not apply since the core reflood model is not used for the SG tubes).

The set of correlations used to model the heat transfer on both the inside and outside of the steam generator tubes is the same.

Effect of Non-Condensables on Steam Generator Heat Transfer

There is a heat transfer suppression model resulting from non-condensables as described in Section 6.2.11 of WCAP-16996-P. This model will impact the heat transfer if non-condensables are transported to the steam generator tubes. The effect of non-condensable gas on heat transfer inside the steam generator tubes [^{a,c} of the Small Break LOCA (SBLOCA) transient behavior based on the following discussion.

The concern with non-condensable gas disrupting decay heat removal through the steam generator under SBLOCA conditions was addressed at least as far back as the late 1970's. This concern was studied in WCAP-9600 [4] and it was [

] ^{a,c}

The same situation is present for the FSLOCA EM. [

] ^{a,c}

[

] ^{a,c}

Effect of Fouling on Steam Generator Heat Transfer

The steam generators are modeled [

] ^{a,c}

The steam generators play a larger role in decay heat removal for smaller breaks as discussed and illustrated previously in this response. A sensitivity study was executed with the V C Summer 2-inch break case to illustrate the impact of SG fouling. [

] ^{a,c}

Summary

In summary, the heat transfer across the steam generator tubes is modeled using accepted correlations consistent with those in TRAC-P Version 5.4.28 code. The impact of []^{a,c} Overall, the modeling of the heat transfer across the steam generator tubes is judged to be acceptable for the FULL SPECTRUM LOCA evaluation model.

Reference(s)

- 1) WCAP-16996-P, "Realistic LOCA Evaluation Methodology Applied to the Full Spectrum of Break Sizes (FULL SPECTRUM LOCA Methodology)," November 2010.
- 2) LA-UR-00-834, "TRAC-M/FORTRAN 90 (Version 3.0) User's Manual," Steinke, R. G., et al., February 2000.
- 3) LA-UR-00-910, "TRAC-M/FORTRAN 90 (Version 3.0) Theory Manual," Spore, J. W., et al., July 2000.
- 4) WCAP-9600, "Report on Small Break Accidents for Westinghouse NSSS System," June 1979.



Figure 133-1: Void Fraction in the Bottom Cell of the Accumulator for the V C Summer 2-inch, 3-inch, 4-inch, and 5-inch Break Transients

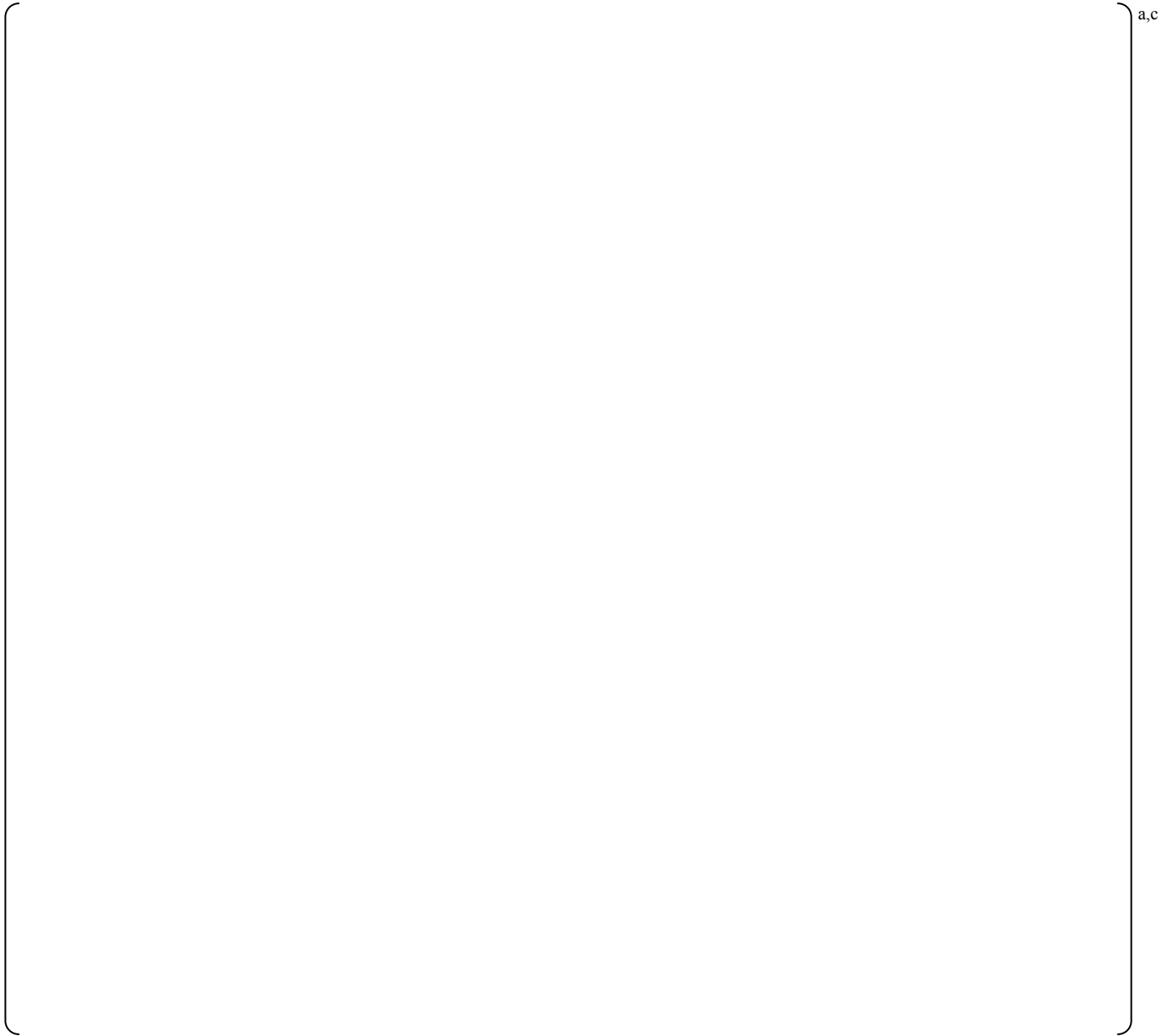


Figure 133-2: Partial Pressure of Non-Condensable Gas in the Steam Generator for the V C Summer 2-inch, 3-inch, 4-inch, and 5-inch Break Transients



Figure 133-3: Steam Generator Secondary-Side Pressure for the V C Summer 2-inch, 3-inch, 4-inch, and 5-inch Break Transients



Figure 133-4: Liquid Heat Transfer Coefficient on the Outside of the Steam Generator Tubes for the V C Summer 2-inch Break Steam Generator Fouling Sensitivity Study



Figure 133-5: Steam Generator Secondary-Side Pressure for the V C Summer 2-inch Break Steam Generator Fouling Sensitivity Study



Figure 133-6: Pressurizer Pressure for the V C Summer 2-inch Break Steam Generator Fouling Sensitivity Study



Figure 133-7: Vessel Fluid Inventory for the V C Summer 2-inch Break Steam Generator Fouling Sensitivity Study

RAI Question #134: Steam Generator Tube Plugging Levels

WCAP-16996-P/WCAP-16996-NP, Volumes I, II and III, Revision 0, Section 25, “Plant Sources of Uncertainty,” Subsection 25.1, “Plant Physical Configuration,” in summarizing the modeling approach with regard to SG tube plugging, states that [

] ^{a,c}

WCAP-16996-P/WCAP-16996-NP, Volumes I, II and III, Revision 0, Section 28, “Scoping and Sensitivity Studies,” Subsection 28.1.6, “Steam Generator Hydraulics: Tube Plugging – LBLOCA,” present results for tube plugging levels of 0 percent, 10 percent, and 20 percent for a nominal double-ended guillotine break demonstration plant analyses for V. C. Summer, a three-loop Westinghouse PWR plant.

Please provide the following additional information regarding the approach to SG tube plugging modeling implemented in the FSLOCA™ methodology for performing LOCA analyses.

- (1) Please explain how the [] ^{a,c} SG tube plugging fraction is established and used in determining relevant boundary conditions for performing LOCA analyses using the FSLOCA methodology.
- (2) WCAP-16996-P/WCAP-16996-NP, Volumes I, II and III, Revision 0, Section 28, “Scoping and Sensitivity Studies,” referring to [] ^{a,c} discussed in Section 28.1.6 and in Section 28.2.9 respectively, states that [] ^{a,c} Please identify and describe the type of plant-specific information that is considered in determining “a plant-specific [] ^{a,c} for the SG tube plugging used in LOCA and associated uncertainty analyses. In particular, please explain SG design-specific information and SG operational history are taken into account when determining the [] ^{a,c} SG tube plugging fraction on a plant-specific basis.
- (3) Please provide the information identified in Item (2) above and the plant-specific [] ^{a,c} for the SG tube plugging levels used in the demonstration plant analyses for the FSLOCA methodology presented in WCAP-16996-P/WCAP-16996-NP, Volumes I, II, and III, Revision 0, Section 28, “Scoping And Sensitivity Studies,” and in Section 31, “FSLOCA Demonstration Analysis.” Describe the introduced assumptions, explain and discuss the applicability of the analysis results, and compare the assessments.

RAI Question #135: SG Tube Plugging Impact on Core Flow Stagnation for Large Break Loss-of-Coolant Accidents

Considering the modeling approach with regard to SG tube plugging, WCAP-16996-P/WCAP-16996-NP, Volumes I, II, and III, Revision 0, Section 29, “Assessment of Uncertainty Elements,” Subsection 29.3.1, “Bounded Parameters,” explains that [

] ^{a,c}

Recognizing an additional phenomenon of importance for LBLOCA analyses, Subsection 29.3.1, “Bounded Parameters,” acknowledges that [

] ^{a,c} Specifically, Subsection 29.3.1 explains that [

] ^{a,c}

- (1) Please identify and describe the deterministic studies of SG tube plugging level that are referred to in the above provided citation from Subsection 29.3.1. Summarize and present results from such analyses that examine the impact of the assumed SG tube plugging level on large break LOCA predictions with a focus on core flow stagnation and possible flow reversal. Include plots that capture such predicted conditions for the core and the hot channel in particular. Analyze and show identified effects of flow stagnation on prediction results taking into consideration applicable safety criteria.
- (2) Please identify best-estimate studies that have been performed with WCOBRA/TRAC-TF2 to analyze the effect of SG tube plugging on LBLOCA predictions associated with core flow stagnation and possible flow reversal in the core. Provide a list of references that identify the source documents containing these analyses. In addition to the analyses discussed in Subsection 28.1.6, “Steam Generator Hydraulics: Tube Plugging – LBLOCA,” please present results from calculations obtained with WCOBRA/TRAC-TF2 that examine the impact of SG tube plugging on large break LOCA predictions due to core flow stagnation and possible flow reversal in the core.
- (3) In presenting the analyses requested in Item (2) above, please provide additional information addressing the following items: (a) the analyses should cover a spectrum of large break sizes over which the examined effect takes place and code predictions show most sensitivity to break change, if so observed, and (b) the analyses should cover the entire range of possible SG tube plugging levels. Please provide consideration of different PWR plant types and show predictions results for a PWR plant design for which the sensitivity to SG tube plugging due to core flow stagnation is expected to be most pronounced, as applicable. Show the impact on prediction results with relevance to the safety criteria and include zoomed plots of computed results over a time window during which the stagnation effect is predicted to occur, as applicable.

RAI Question #137: Steam Generator Tube Plugging Impact on Steam Generator Reversed Heat Transfer for Large Break Loss-of-Coolant Accidents

Considering the modeling approach with regard to SG tube plugging, WCAP-16996-P/WCAP-16996-NP, Volumes I, II, and III, Revision 0, Section 29, “Assessment of Uncertainty Elements,” Subsection 29.3.1, “Bounded Parameters,” explains that [

] ^{a,c}

Following a large break LOCA, liquid entrainment from the upper plenum through the hot legs and into the SG tube bundles can lead to significant evaporation of entrained liquid due to reversed heat transfer from the hot SG secondary systems to the primary side of the SG tubes. In turn, this process can cause a primary pressure increase thus impacting the core thermal response. Such reversed heat transfer through the SGs can be dependent on the available SG heat transfer area, which is directly affected by the assumed SG tube plugging level.

- (1) Please present results from calculations obtained with WCOBRA/TRAC-TF2 that examine the effect of the assumed SG tube plugging level on LBLOCA predictions with a focus on the effect of reversed heat transfer from the hot SG secondary systems and evaporation of entrained liquid on the SG tubes primary side.
- (2) In presenting the analyses requested in Item (1) above, please provide additional information addressing the following items: (a) the analyses should cover a spectrum of large break sizes over which the examined effect takes place and code predictions show most sensitivity to break change and (b) the analyses should cover the entire range of possible SG tube plugging levels. Please provide consideration of different PWR plant designs and show predictions results for a PWR plant design for which the sensitivity of primary pressure increase to SG tube plugging is expected to be most pronounced, as applicable. Show the impact on prediction results with relevance to the applicable safety criteria and include zoomed plots of computed results over a time window during which the examined effect is predicted to take place, as applicable.

Response:

1.0 Introduction and Problem Statement

The as-submitted FULL SPECTRUM LOCATM (FSLOCATM) evaluation model (EM) analyzes [^{a,c} as described in Sections 25.1 and 29.3.1 of WCAP-16996-P [1]. The Nuclear Regulatory Commission (NRC) requested additional information supporting the decision to [^{a,c} The additional information to support the modeling decision is provided in this response.

This response addresses Requests for Additional Information (RAIs) 134, 135, and 137 which are related to the [^{a,c}

2.0 Effects of Steam Generator Tube Plugging

Steam generator tube plugging can influence a number of phenomena during a LOCA transient. The phenomena which are impacted are dependent on the break size. The most important phenomena which could be influenced by the SGTP (regardless of break size) are considered to be the following (based on the Phenomena Identification and Ranking Table, Table 2-1 in WCAP-16996-P):

[

] ^{a,c}

The first four phenomena are primarily of significance for larger breaks. The fifth can impact both larger and smaller breaks. The sixth item is of significance for smaller breaks. These different phenomena are discussed in the following subsections. [

] ^{a,c}

2.1 Core Flow Stagnation Elevation (During Blowdown)

During the blowdown phase of a Large-Break LOCA (LBLOCA) transient, there are two primary paths from the core to the break. The first is out the bottom of the core, up the downcomer, into the broken cold leg and to the break. The second is up through the top of the core, through the upper plenum into the broken hot leg, around the loop and to the break. Any variations in relative resistance between these two paths will tend to impact the stagnation elevation.

The tube plugging level affects the resistance in the loop, so it will impact the stagnation point during blowdown. [

] ^{a,c}

This was shown in Sections 28.1.4.1 (V. C. Summer) and 28.1.4.2 (Beaver Valley Unit 1) of WCAP-16996-P []^{a,c} Please refer to these sections of WCAP-16996-P for additional discussion.

2.2 Mass and Energy Release to Containment

The SGTP level impacts the fluid volume on the primary side of the RCS. A higher tube plugging level reduces the RCS volume, which results in less mass and energy released from the break during the blowdown phase of a LOCA transient.

For smaller breaks, the containment pressure does not have a significant impact on the LOCA transient progression. However, the containment pressure becomes increasingly important for larger breaks. The reduced RCS primary side volume resulting from higher SGTP causes less mass and energy to be released into containment during blowdown, subsequently resulting in a lower containment pressure than for a lower tube plugging level. []^{a,c}

2.3 Loop Resistance to Reflood and Steam Venting

[]^{a,c}

[]^{a,c}

2.4 Steam Generator Heat Transfer Area and Steam Binding

The SGTP level impacts the heat transfer area between the primary side and secondary side of the reactor coolant system (RCS). For larger breaks, this can influence the vaporization of entrained liquid which is carried from the upper plenum into the steam generator (i.e. steam binding). The steam binding further serves to increase the resistance through the steam generator and thus slow the reflood rate.

Cylindrical Core Test Facility (CCTF) Run 62 is a prototypical integral effects test (IET) for LBLOCA. The predicted versus measured cold leg nozzle to upper plenum differential pressure is presented in Figure 19.6-28 of WCAP-16996-P. It is observed that the [

] ^{a,c}

A LBLOCA break spectrum study for Beaver Valley Unit 1 was presented in Section 27.1.2.1 of WCAP-16996-P. The average void fraction of the fluid flowing into and out of the steam generator is inspected for the largest and smallest break sizes of the break spectrum. The void fractions for all three loops are presented in Figure 2-1 for the largest break from the spectrum and in Figure 2-2 for the smallest break from the spectrum. [

] ^{a,c}

a,c

Figure 2-1: Average Post-Blowdown Void Fraction into and out of the Steam Generators for the Largest Break in the Beaver Valley Unit 1 LBLOCA Break Spectrum Study

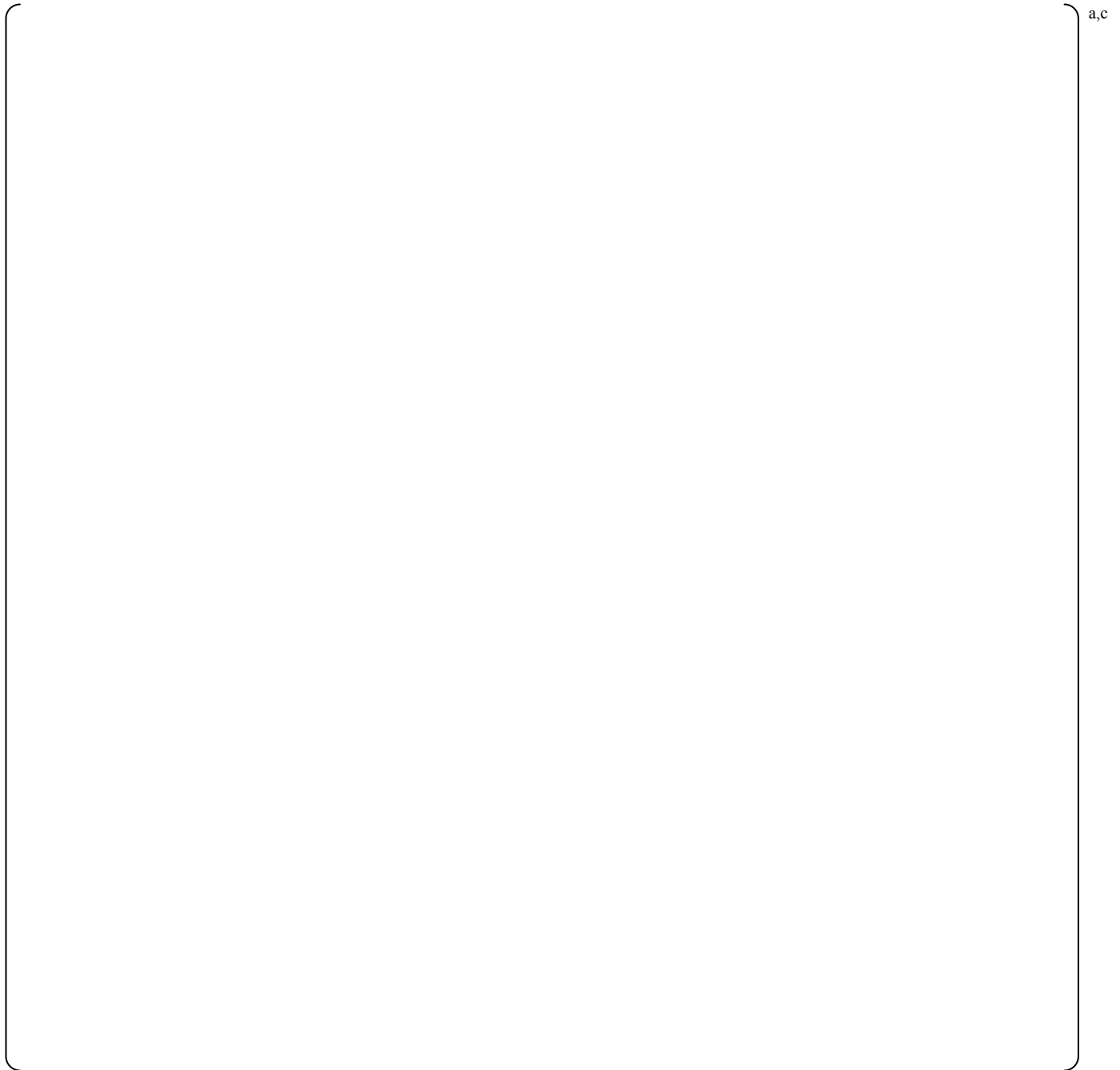


Figure 2-2: Average Post-Blowdown Void Fraction into and out of the Steam Generators for the Smallest Break in the Beaver Valley Unit 1 LBLOCA Break Spectrum Study

3.0 Sensitivity Studies

A sensitivity study on SGTP for SBLOCA was presented in Section 28.2.9 of WCAP-16996-P. It was concluded therein that the [

] ^{a,c}

No LBLOCA sensitivities to SGTP were presented in WCAP-16996-P using WCOBRA/TRAC-TF2; however, there are a number of LBLOCA SGTP sensitivity studies available with WCOBRA/TRAC from the Code Qualification Document (CQD) [2] and Automated Statistical Treatment of Uncertainty Method (ASTRUM) [3] evaluation models. The results from a subset of these studies are presented in Table 3-1; the studies were selected to cover a range of different plant designs (i.e., 2-loop, 3-loop, 4-loop) and a range of different tube plugging levels.

Table 3-1: Steam Generator Tube Plugging Sensitivity Study Results with WCOBRA/TRAC

[

] ^{a,c}

It is observed from Table 3-1 that there is [

] ^{a,c}

The PCT transients associated with these seven LBLOCA SGTP sensitivity studies are presented as Figures 3-1 through 3-7.

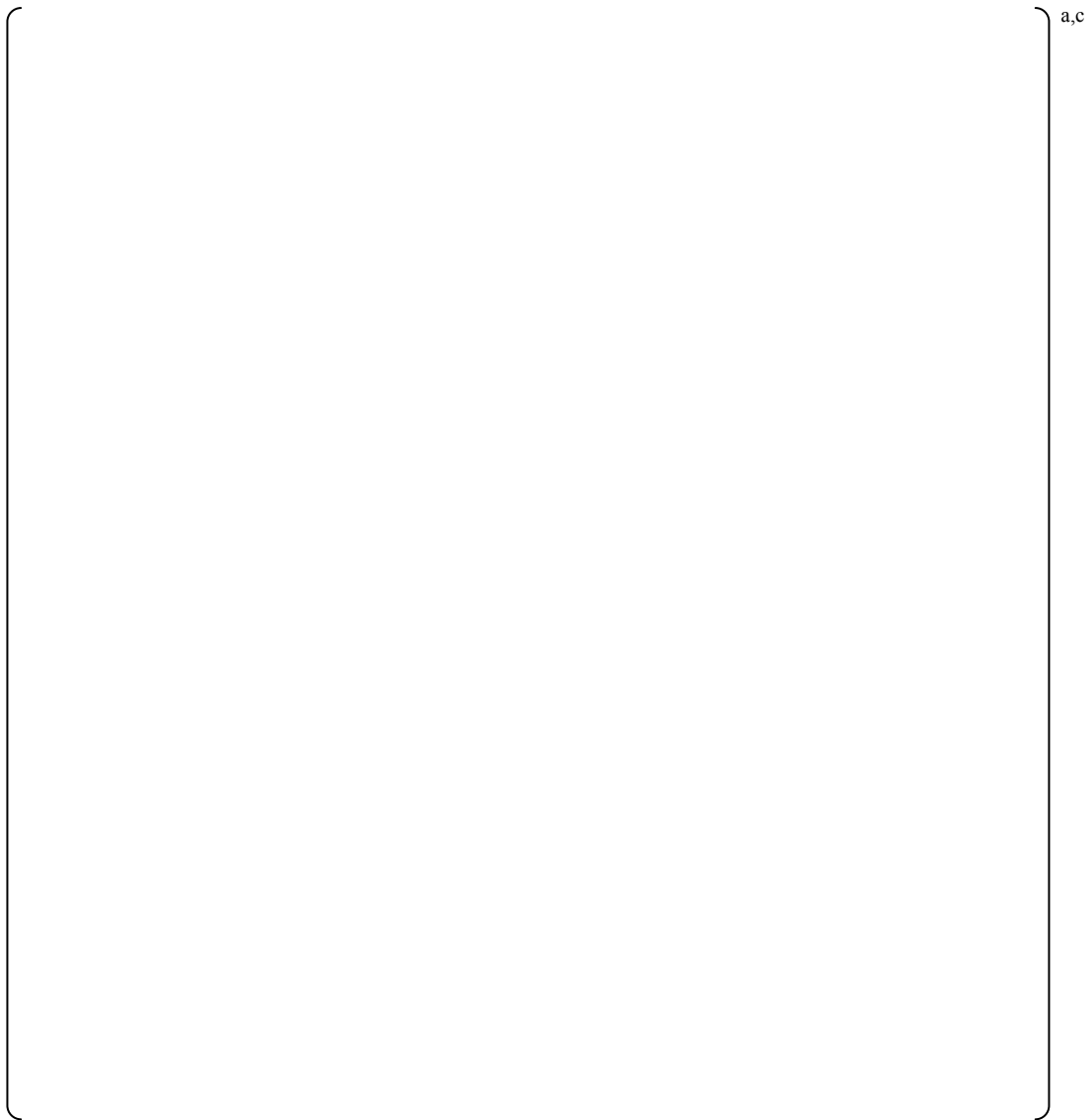


Figure 3-1: Steam Generator Tube Plugging Sensitivity Study for Beaver Valley Unit 1

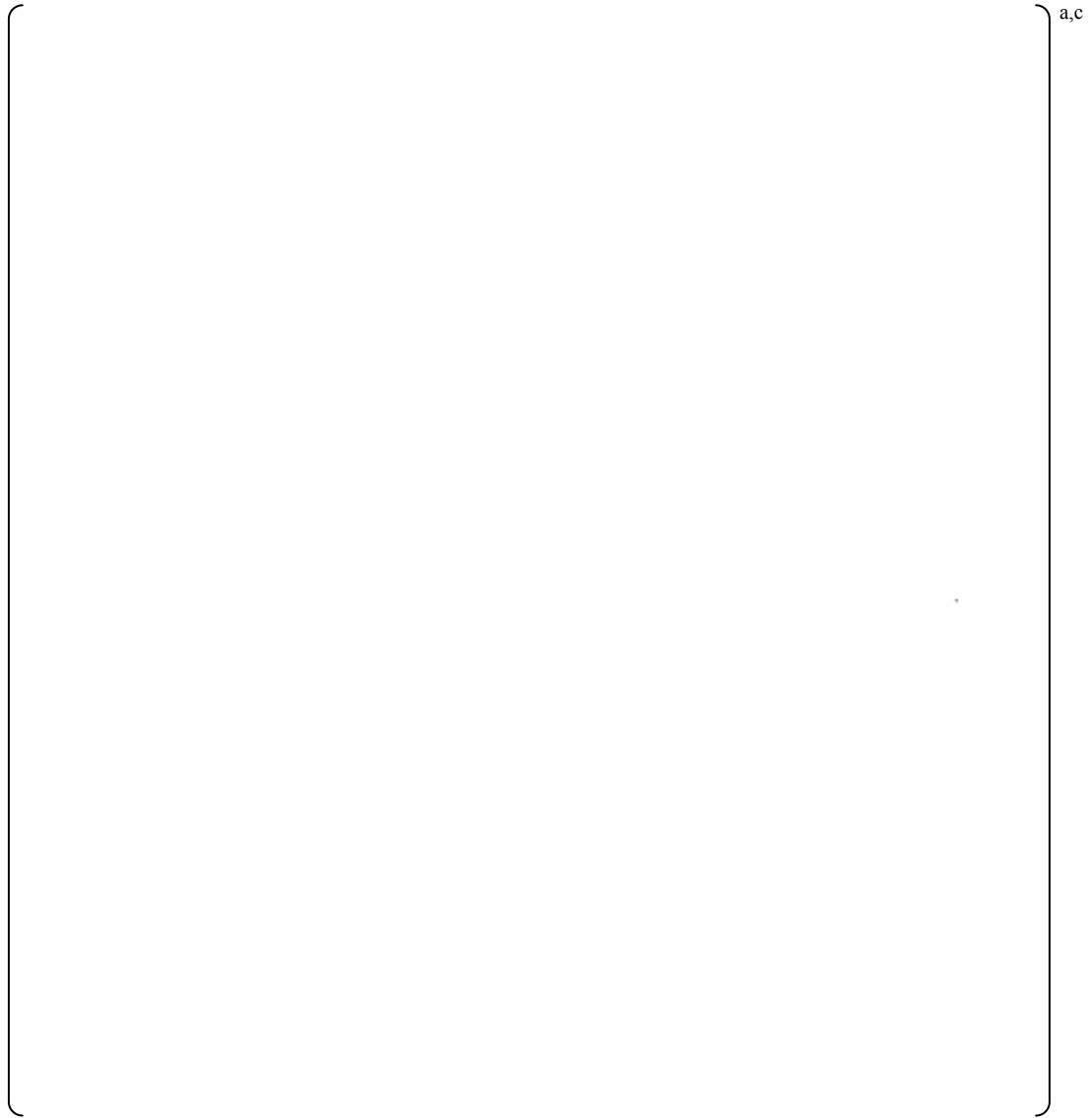


Figure 3-2: Steam Generator Tube Plugging Sensitivity Study for Beaver Valley Unit 2

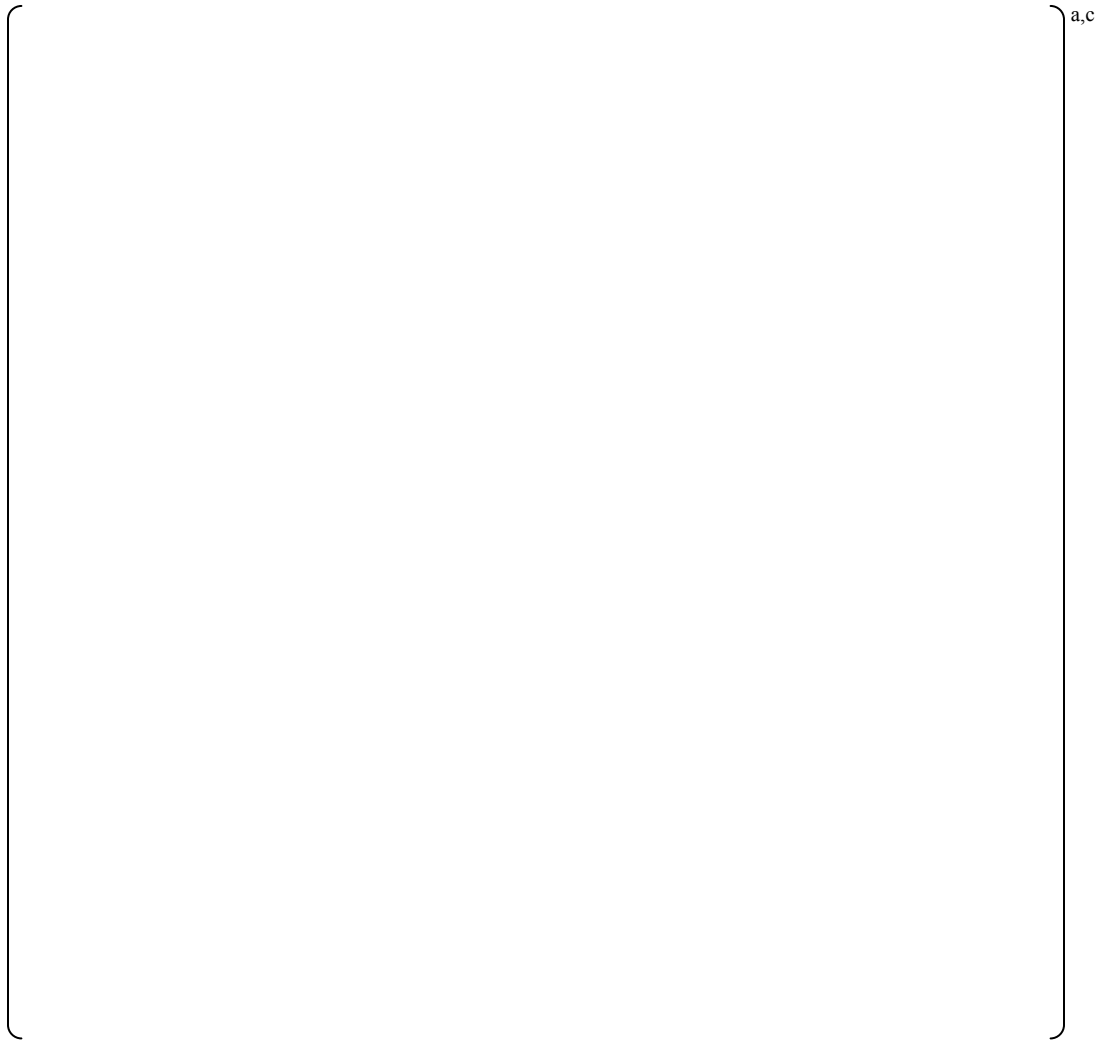


Figure 3-3: Steam Generator Tube Plugging Sensitivity Study for Diablo Canyon Unit 2



Figure 3-4: Steam Generator Tube Plugging Sensitivity Study for Indian Point Unit 3 (Solid line is 10% SGTP, Dashed line is 0% SGTP)



Figure 3-5: Steam Generator Tube Plugging Sensitivity Study for Kewaunee



Figure 3-6: Steam Generator Tube Plugging Sensitivity Study for Seabrook

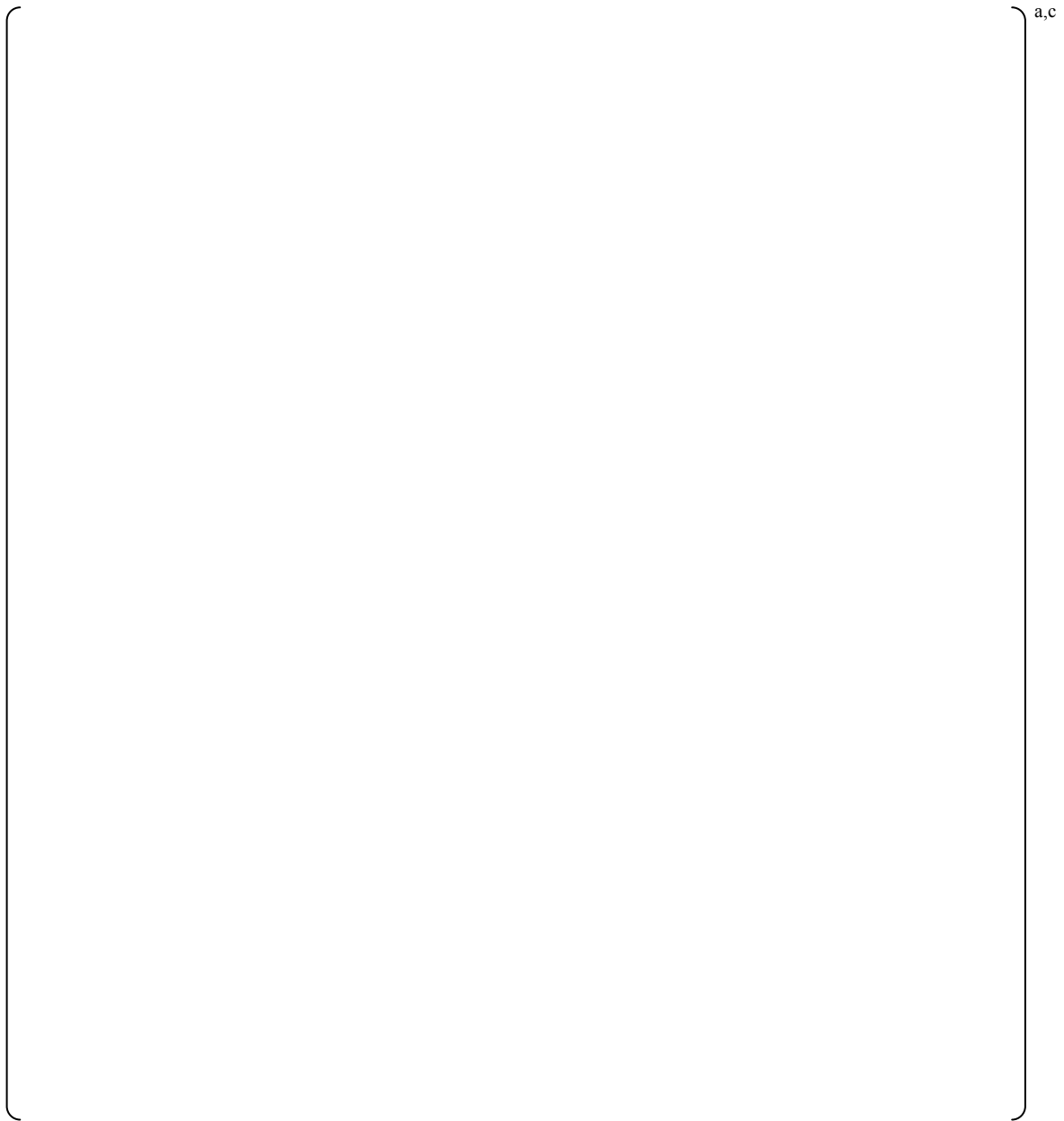


Figure 3-7: Steam Generator Tube Plugging Sensitivity Study for Watts Bar Unit 1

4.0 Summary and Conclusions

It was shown in this RAI response [

] ^{a,c}

5.0 Other Pertinent Information

The steam generator tube plugging level is an input into the FSLOCA EM which is provided by the utility. The utility typically assigns a value that accounts for historical rates of plugging as determined and monitored during outages. For current Westinghouse Best-Estimate EMs, the analyzed plugging level is confirmed every reload to ensure that it remains valid. Any intended changes in the plugging levels beyond the analyzed values are evaluated.

The tube plugging levels provided by the utilities for the FSLOCA scoping studies and demonstration analysis are 22% for Beaver Valley Unit 1 and 10% for V. C. Summer.

6.0 Reference(s)

- 1) WCAP-16996-P, "Realistic LOCA Evaluation Methodology Applied to the Full Spectrum of Break Sizes (FULL SPECTRUM LOCA Methodology)," November 2010.
- 2) WCAP-12945-P-A, Volume 1, Revision 2, Volumes 2 through 5, Revision 1, "Code Qualification Document for Best Estimate LOCA Analysis," March 1998.
- 3) WCAP-16009-P-A, "Realistic Large-Break LOCA Evaluation Methodology Using the Automated Statistical Treatment Of Uncertainty Method (ASTRUM)," January 2005.

RAI Question #138: Safety Injection Pump Flow during Loss-of-Coolant Accidents

WCAP-16996-P/WCAP-16996-NP, Volumes I, II, and III, Revision 0, Section 25, “Plant Sources of Uncertainty,” Subsection 25.3, “Reactor Accident Boundary Conditions,” in summarizing the modeling approach with regard to the SI flow, states that [

]^{a,c} Specifically, it is stated that “safety injection (SI) flow varies depending on the single failure assumed, and on the specific plant pump and injection line configuration. Current methods, which are also used in currently accepted evaluation models, provide conservative estimates of minimum and maximum flow, which take into account several uncertainties.”

Please provide additional information related to the modeling of pumped SI flow in performing LOCA analyses using WCOBRA/TRAC-TF2 as identified below.

- (1) Describe the approach to determine the []^{a,c} that are assumed for LOCA analyses on a plant-specific basis. In particular, please identify and describe these “several uncertainties” that are taken into consideration by the “current methods, which are also used in currently accepted evaluation models” in order to provide conservative estimates as stated in Subsection 25.3, “Reactor Accident Boundary Conditions.” In addition, please explain how the implemented approach accounts for and models the following factors: (a) uncertainties in safety injection pump characteristics, (b) injection line configuration, and (c) flow resistance and pressure drop along the injection lines.
- (2) Please document the parameters identified in Item (1) above and used in the demonstration plant analyses of the FSLOCA™ methodology presented in WCAP-16996-P/WCAP-16996-NP, Volumes I, II, and III, Revision 0, Section 28, “Scoping and Sensitivity Studies,” and in Section 31, “FSLOCA Demonstration Analysis.” State the assumptions and relevant conditions, as implemented in assessing parameters related to the SI pump flow modeling in the performed LOCA analyses. Include graphs of all pump flow characteristics and tables documenting assessments for other relevant parameters, as appropriate.

Response

- (1) The response to RAI #18 provided in LTR-NRC-13-37 [1] on the conservative assumptions / uncertainties the High Head Safety Injection / Charging Pump applies to all the Safety Injection Pumps including the Low Head and Intermediate Head Pumps.

In summary, all Safety Injection (SI) pump performance curves (the High Head Safety Injection / Charging Pump, the low head and the intermediate pump) utilized in the FULL SPECTRUM LOCA (FSLOCA) plant analyses are adjusted to account for uncertainties in measurement of pump developed head and pump flow rate as described in LTR-NRC-13-37.

Additional discussion is provided in this response regarding the assumptions for the injection lines / spilling line configuration and the mini flow (recirculation path around the pump to prevent deadheading) valve treatment.

The assumptions for defining the spilling branch line resistance for the Emergency Core Cooling System (ECCS) LOCA cases are as follows:

- [
-

] ^{a,c}

The high head safety injection pump mini flow path operation during a LOCA varies from plant to plant as follows:

- Automatic isolation signal results in closure of the mini flow path on receiving a safety injection actuation signal ("S" signal), or
- The mini flow paths are locked open to prevent pump deadheading, or
- The system is configured to be automatically open at lower flow rates and closed at high flow rates.

The intermediate head safety injection pump mini flow path is designed to remain open during the RCS injection phase and is automatically closed when switching to the recirculation phase. The residual heat removal (RHR) mini flow valve is automatically controlled by the flow through the RHR pump (i.e., low head pump) and will open on a low RHR pump flow rate and close on a high RHR pump flow rate.

The fluid system hydraulic modeling of the mini flow path being open or closed is based on the individual plant design and is therefore plant-specific. In the safeguards flow cases, the mini flow path is modeled to use the maximum flow orifice tolerance limit plus plant instrument uncertainties in setting the mini flow path resistance in the model. For the minimum ECCS flow cases utilized in the FSLOCA evaluation model, the mini flow path resistance is minimized to maximize the flow through the mini flow path, thereby reducing the RCS injected flows.

(2) The safety injection flows for Beaver Valley Unit 1 are provided by the customer as input into the FSLOCA analysis. The safety injection flows for V. C. Summer are calculated by Westinghouse as input into the FSLOCA analysis. These V. C. Summer safety injection flows are calculated as described in the response to RAI #18 provided in LTR-NRC-13-37 and as described in Part (1) of this response. The V. C. Summer safety injection flows assuming that the spilling line spills to RCS pressure [

] ^{a,c} are provided in Table 138-1. Flows consistent with the spilling line spilling to containment pressure are provided in Table 138-2. As previously discussed, the [

] ^{a,c}

Table 138-1: V. C. Summer Minimum Cold Leg Injection Flows with Spilling to RCS Pressure

a,b,c

Table 138-2: V. C. Summer Minimum Cold Leg Injection Flows with Spilling to Containment Pressure (Assumed to be 0 psig)

a,b,c

Reference(s)

- 1) LTR-NRC-13-37, "Submittal of Westinghouse Responses to 'WCAP-16996-P, 'Realistic LOCA Evaluation Methodology Applied to the Full Spectrum of Break Sizes (FULL SPECTRUM LOCA Methodology)' Request for Additional Information' (Proprietary/Non-Proprietary), Project 700, TAC No. ME5244," June 5, 2013.

RAI Question #139: Asymmetrical Predictions in Modeling of Parallel Flow Configurations

Thermal hydraulic system codes, such as RELAP5, have been found to predict asymmetrical results when modeling parallel flow configurations, usually under low-flow conditions. Recognition of such modeling difficulties is presented by G. W. Johnsen, "RELAP5-3D Development & Application Status," Presentation at the 2002 RELAP5 International User's Seminar, September 4-6, 2001, Park City, Utah. In PWR plant analysis, such flow configurations can be related to parallel flow paths representing the cold legs in the same primary coolant loop of a Combustion Engineering (CE) PWR plant, parallel flow channels representing different azimuthal sections of a reactor vessel downcomer, such representing steam generator secondary side volumes or other regions of the reactor system. A possible solution approach in modeling a simple flow problem between parallel pipes is discussed by D. Lucas, "Recirculating Flow Anomaly Problem Solution Method," Proceedings of 8th International Conference on Nuclear Engineering ICONE8, Paper ID 8479, April 2-6, 2000, Baltimore, Maryland.

Please show that WCOBRA/TRAC-TF2 does not predict anomalous behaviors as described above for other codes when using three- and one-dimensional components. As part of the response, present predictions for an illustrative parallel pipe flow problem as implemented in the RELAP5 dual pipe flow input model presented below.

=Flow Anomaly Test Problem

```
*
*-----
*crdno      problem type    problem option
0000100      new            transnt
*-----
*crdno      input units     output units
0000102      british        british
*-----
*crdno  time 1  time 2
0000105  10.    40.    10000.
*-----
0000110 nitrogen
*-----
*crdno end time  min dt  max dt  control  minor ed  major ed  restart
0000201 5000.  1.0e-6  2.0    3    1    250    500
*****
*****
* minor edit requests
*****
*****
*
*crdno      variable    parameter
*
301 count  0
302 dt      0
303 dternt  0
304 cputime 0
305 errmax  0
306 emass   0
307 tmass   0
310 mflowj 145010000
```

311 mflowj 145020000
 312 mflowj 716000000
 313 mflowj 711000000
 314 mflowj 175010000
 315 mflowj 175020000
 316 tempf 130010000
 317 tempf 160010000
 318 cntrlvar 1
 319 cntrlvar 2
 320 testda 2
 321 testda 3
 322 testda 4
 20800001 testda 2
 20800002 testda 3
 20800003 testda 4

*

* hydrodynamic components

1300000 pmpsuca2 pipe * loop a2 rc pump suction

1300001 1

1300101 4.2761 1

1300301 25.956 1

1300401 0.0 1

1300601 -90. 1

1300701 -25.956 1

1300801 .00030 0. 1

1301001 00 1

1301201 3 2200.0 550.0 0.0 0.0 0.0 1

*

1450000 clbrcha2 branch

1450001 2 0

1450101 10.0 5.4064 0. 0. -90.0 -5.4064 .00015 0.00

1450200 3 2200.0 550.0

1451101 160010000 145000000 4.2761 1.0 1.0 0100

1452101 130010000 145000000 4.2761 1.0 1.0 0100

1451201 0.0 0.0 0.0

1452201 0.0 0.0 0.0

*

1600000 pmpsuca1 pipe

1600001 1

1600101 4.2761 1

1600301 25.956 1

1600401 0.0 1

1600601 -90. 1

1600701 -25.956 1

1600801 .00030 0. 1

1601001 00 1

1601201 3 2200.0 550.0 0.0 0.0 0.0 1

```

*
1750000 clbrchal    branch
1750001 2      0
*1750101 10.0 5.4064    0.  0. -90.0 -5.4064 .00015    0. 00
1750101 10.0 5.4064    0.  0. -90.0 -5.4064 .01000    0. 00
1750200 3 2200.0 550.0
1751101 175010000 1600000000 4.2761 1.0 1.0 0100
1752101 175010000 1300000000 4.2761 1.0 1.0 0100
1751201 0.0 0.0 0.0
1752201 0.0 0.0 0.0
*
*
7100000 lpa1hpit    tmdpv0l
7100101 1.0e6 10.0 0.0 0. -90.0 -10.0 0. 0. 00
7100200 3
7100201 0. 2200.0 90.
*
*
7110000 lpa1hpif    tmdpj0n
7110101 710010000 1750000000 .0246
7110200 1
7110201 0.0 0.0 0.0 0.0
7110202 10.0 96.0 0.0 0.0
*
*
7150000 lpa2hpit    tmdpv0l
7150101 1.0e6 10.0 0.0 0. -90.0 -10.0 0. 0. 00
7150200 3
7150201 0. 2200.0 550.
*
*
7160000 lpa2hpif    snglj0n
7160101 145010000 7150000000 10.0 1.0 1.0 0
7160201 0 0.0 0.0 0.0
*
20500100 dtempf sum 1.0 0.0 1
20500101 0.0 1.0 tempf 160010000 -1.0 tempf 130010000
*
20500200 dtempf sum 1.0 0.0 1
20500201 0.0 1.0 tempf 130010000 -1.0 tempf 160010000
*
. * end of input stream

```

Response:

Six different numerical problems are executed with WCOBRA/TRAC-TF2 to address Request for Additional Information (RAI) 139 on the FULL SPECTRUM™ LOCA (FSLOCA™) evaluation model (EM). First, two 3D (vessel) problems are executed similar to the situation presented in (Lucas, 2000) [1]. Next, two 1D problems are executed with parallel pipes. Finally, an additional 3D and 1D case are executed where the boundary condition flow is ramped down to zero. For all cases zero resistance is used in the hydraulic system.

3D (Vessel) Parallel Channel Low Flow, Zero Resistance Numerical Problems

The noding diagram for the vessel parallel channel problems is presented in Figure 139-1 (dummy 1D components required to execute the code were omitted from the diagram). Four channels were used to model the problem. Vessel Sections 1 and 3, which represent the inlet and outlet of the test section, are both modeled with a single channel. Vessel Section 2, which is in between the inlet and outlet regions, is modeled with two identical channels. No loss coefficients were specified for any of the channels at any elevation.

For the first problem, the boundary conditions were specified as shown in Figure 139-1. A constant flow and enthalpy boundary condition was specified at the bottom of the vessel component, with a mass flow rate of 1 lbm/s and an enthalpy of 500 BTU/lbm. A constant pressure and enthalpy boundary condition was specified at the top of the vessel, with a pressure of 2,000 psia and an enthalpy of 500 BTU/lbm. These boundary conditions cause the flow path to be from the bottom of the vessel to the top of the vessel. For the second problem, the boundary conditions were switched such that the flow was from the top of the vessel to the bottom.

The results for the upward flow case are presented in Figure 139-2. It can be seen that the inlet and outlet flow are both 1 lbm/s, as expected. The flow distributes evenly between the two parallel channels, with half the flow travelling upward through each channel. The results for the downward flow case, presented in Figure 139-3, are similar to the upward flow case. The flow at the inlet and the outlet are 1 lbm/s (negative values indicate flow is downward). The flow distributes evenly between the two parallel channels, with half the flow travelling downward through each channel.

The low flow anomaly presented in (Lucas, 2000) is not observed in either of the 3D vessel low flow, zero resistance numerical problems that were investigated.

1D Parallel Pipe Low Flow, Zero Resistance Numerical Problems

The noding diagram for the vessel parallel channel problems is presented in Figure 139-4. Six different components were used to model the problem. Component 1 is a FILL component, which provides a constant flow and enthalpy condition. The mass flow rate is just less than 1 lbm/s, and the enthalpy is 500 BTU/lbm. Component 2 is a TEE component, which connects the FILL component to two parallel PIPE components. Components 3 and 4 are parallel PIPE components. Component 5 is a TEE component which connects the parallel PIPE components and a BREAK component. Component 6 is a BREAK component which provides a constant pressure condition of 2,000 psia. No loss coefficients or friction entries were specified for any cells of any of the components.

Similar to the 3D numerical problems, for the first 1D problem the components were oriented such that the flow was upward vertically through the components. For the second 1D problem the components were inverted such that the flow was downward vertically through the components.

The results for the 1D components case with upward flow are presented in Figure 139-5. It can be seen that the inlet and outlet flow are both just under 1 lbm/s, as expected. The flow distributes evenly between the two parallel pipe components, with half the flow travelling upward through each pipe. The results for the downward flow case, presented in Figure 139-6, are similar to the upward flow case. The flow at the inlet and the outlet are again just under 1 lbm/s (negative values indicate flow is downward). The flow distributes evenly between the two parallel pipe components, with half the flow travelling downward through each pipe.

No anomalous behavior is observed in either of the 1D component low flow, zero resistance numerical problems that were investigated.

3D and 1D Parallel Channel / Pipe Zero Flow Numerical Problems

Since reasonable results were obtained for the low flow, zero resistance numerical problems, an additional 3D vessel and 1D component case was executed where the boundary condition flow was ramped to zero. For both cases, the boundary condition was held constant for 1,000 seconds, then ramped to zero flow over the next 4,000 seconds, and finally held constant at zero for 5,000 seconds until the end of the problem at 10,000 seconds.

The results for the 3D case are presented in Figure 139-7, and for the 1D case in Figure 139-8. It can be seen for the 3D case, the inlet and outlet flow follow the changes in the boundary conditions, and the flow in the parallel channels follow at half the flow of the boundary conditions. Once the boundary condition flow reaches zero, there is limited, anomalous behavior observed. Rather than the system reaching a state of identically zero flow, there are small flow oscillations observed at the cell faces in the system. However, the nature of the observed instability is different from that presented in the Lucas, 2000 paper.

For the 1D case, the inlet and outlet flow follow the changes in the boundary conditions, and the flow in the parallel pipe components follow at half the flow of the boundary conditions. Once the boundary

condition flow reaches zero, the flow at the cell faces in the system also goes to and remains at zero for the duration of the problem.

Conclusions

The 1D component and 3D vessel low flow numerical problems discussed previously in this response produce the expected solutions and do not exhibit the anomalies observed for similar problems using other thermal-hydraulic codes (e.g. Lucas, 2000). The additional 1D component zero flow numerical problem produces the expected result, as the system settles into a constant state of zero flow. The 3D vessel zero flow numerical problem does exhibit limited numerical noise as it does not settle into a constant state of zero flow. However, this is not a concern for the FSLOCA EM since a sustained zero flow condition will not exist during a LOCA transient. As such, the demonstrated WCOBRA/TRAC-TF2 code performance for these numerical problems is judged to be better than the results presented for other thermal-hydraulic codes, and certainly acceptable relative to the calculation of LOCA transients.

Reference(s)

- 1) Lucas, D. S., "INEEL-Advanced Test Reactor," *Proceedings of ICONE8*, Paper #8479, April 2-6, 2000.

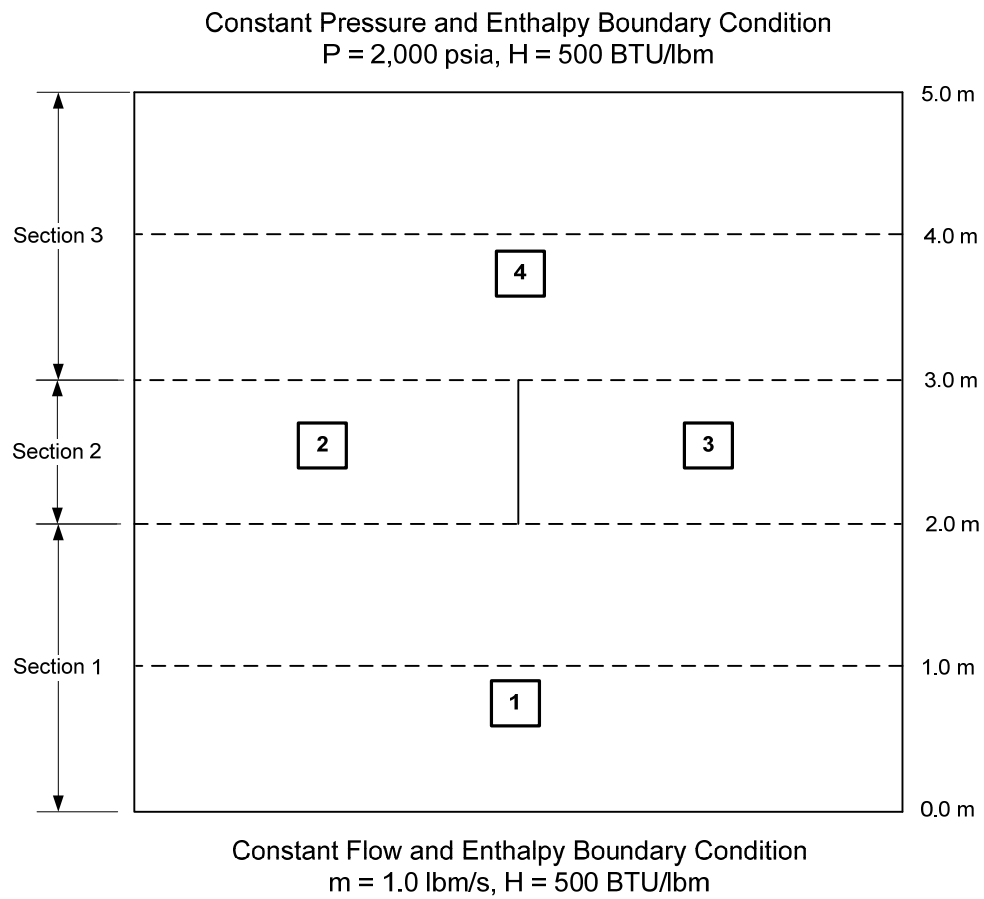
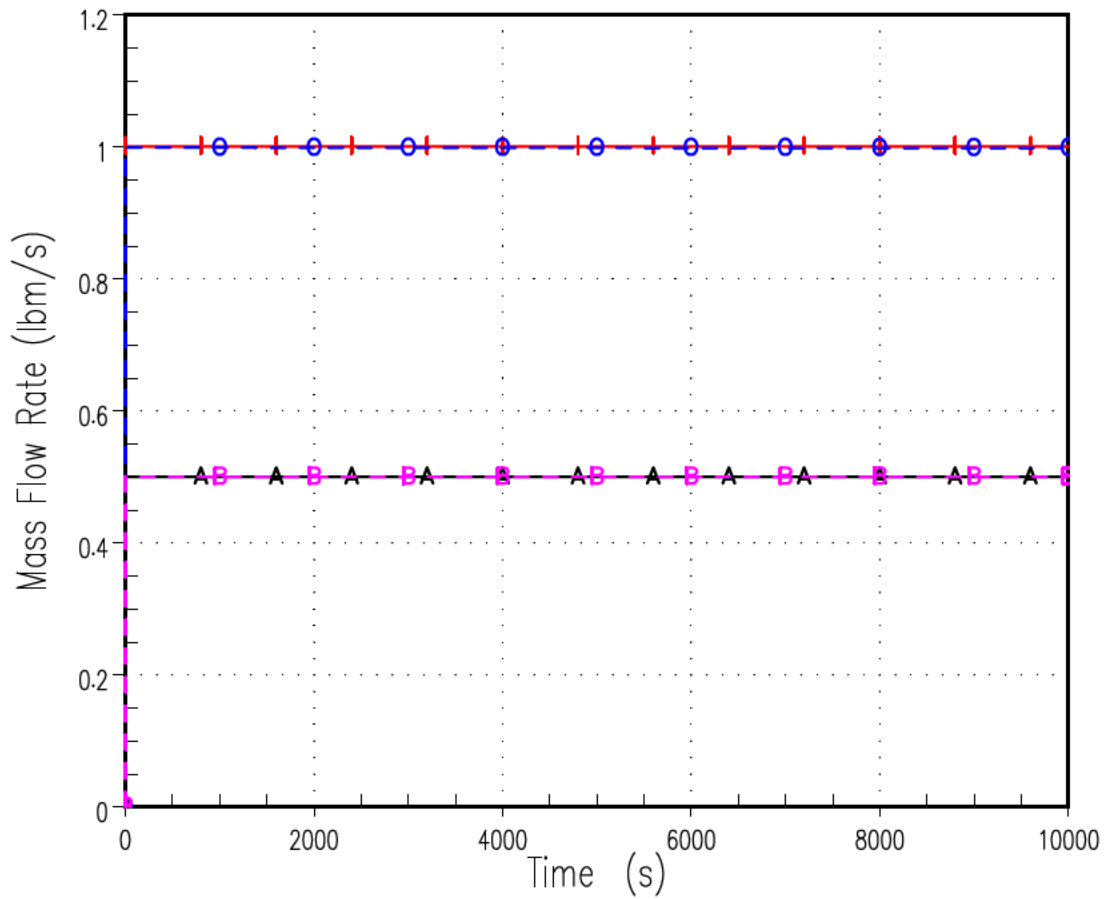


Figure 139-1: Noding Diagram for the 3D (Vessel) Parallel Channel Numerical Problems

3D Parallel Channel Problem – Vertical Upward

1	FLM	1	1	0	Inlet
4	FLM	3	3	0	Outlet
2	FLM	2	2	0	Chnl A
3	FLM	2	2	0	Chnl B

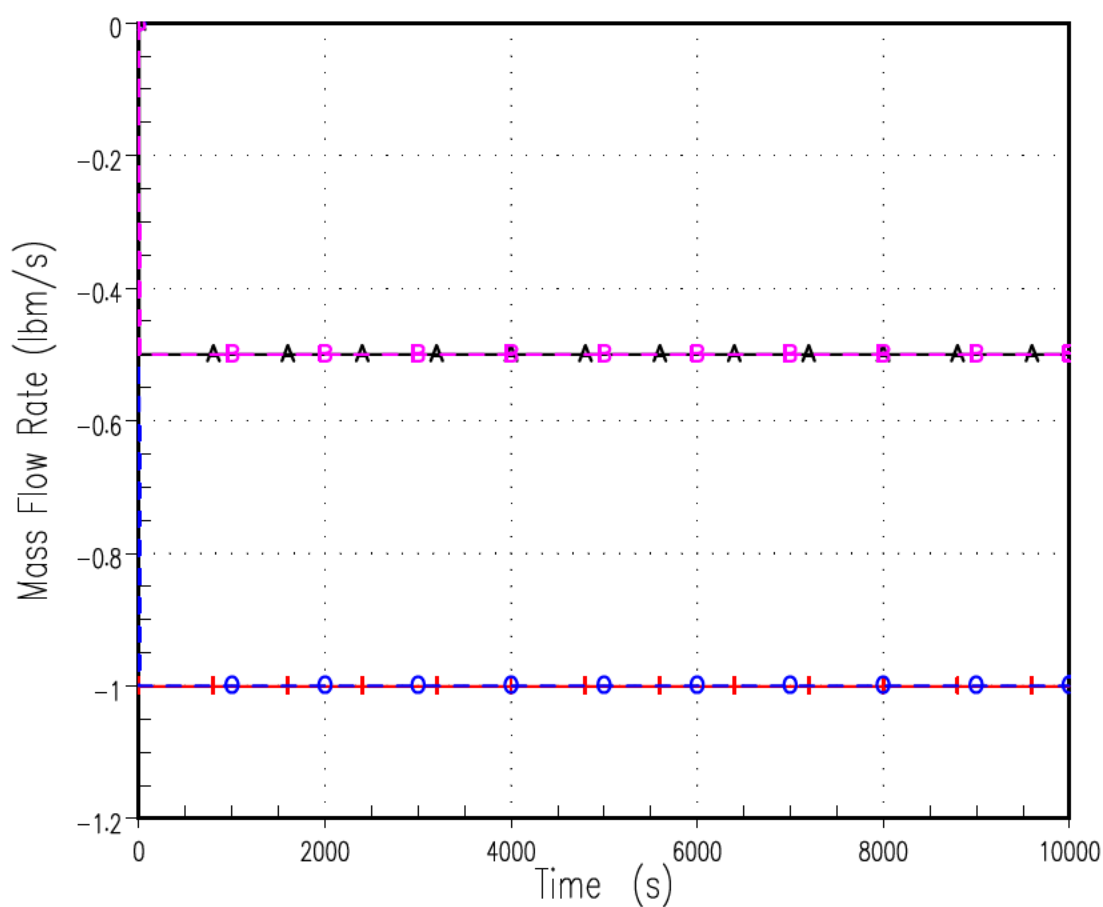


22047988

Figure 139-2: WCOBRA/TRAC-TF2 Results for the 3D Parallel Channel Numerical Problem with Upward Flow through the Vessel Component

3D Parallel Channel Problem – Vertical Downward

—	FLM	4	3	0	Inlet
○	FLM	1	1	0	Outlet
—	FLM	2	2	0	Chnl A
—	FLM	3	2	0	Chnl B



22047988

Figure 139-3: WCOBRA/TRAC-TF2 Results for the 3D Parallel Channel Numerical Problem with Downward Flow through the Vessel Component

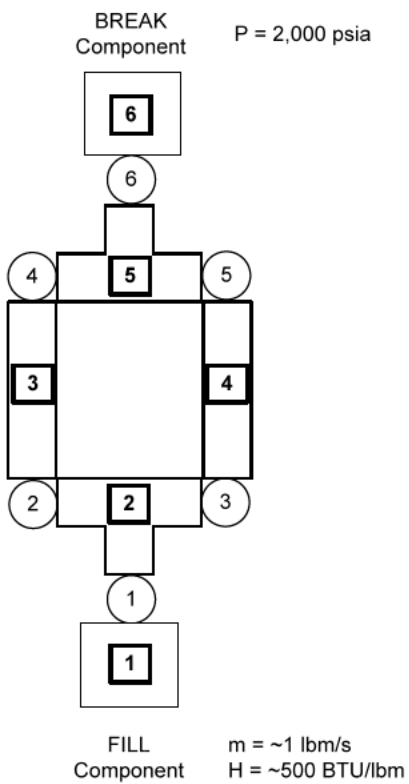
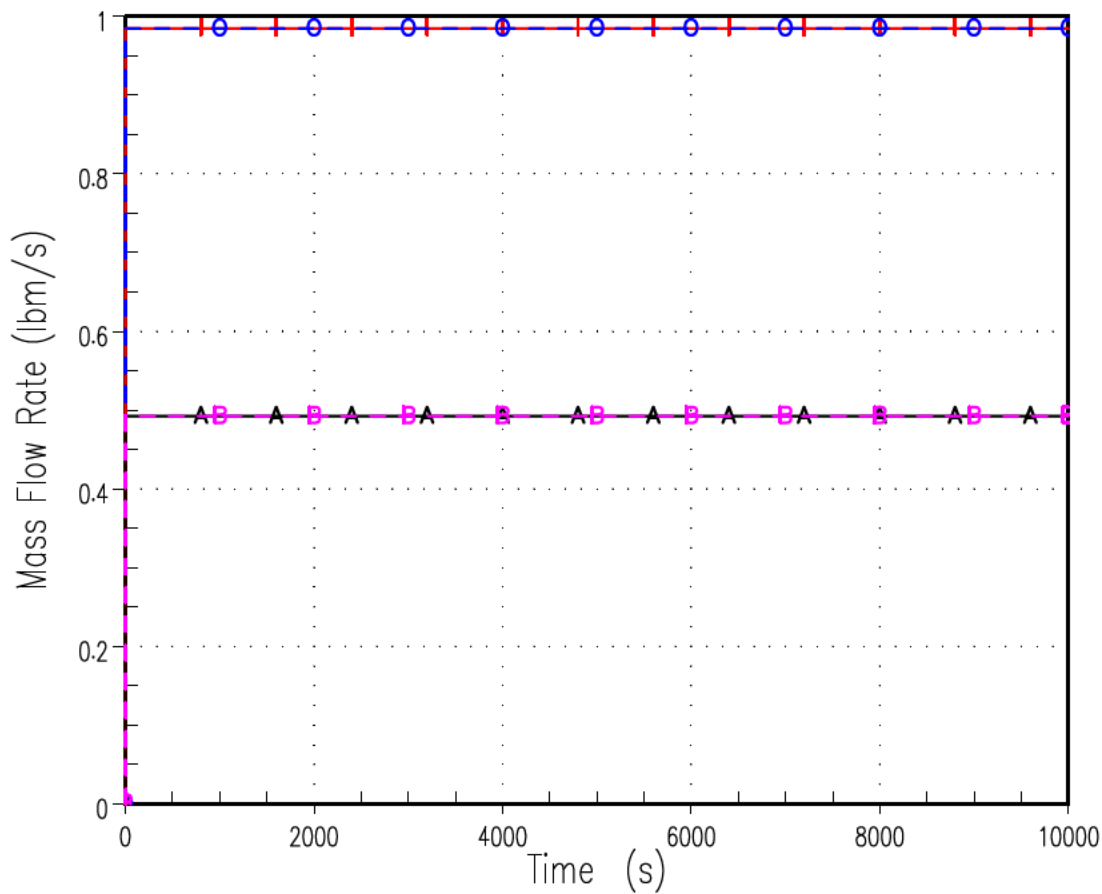


Figure 139-4: Noding Diagram for the 1D Parallel Pipe Numerical Problems

1D Parallel Pipe Problem – Vertical Upward

I	RMVM	2	6	0	Inlet
O	RMVM	5	6	0	Outlet
A	RMVM	3	2	0	Pipe A
B	RMVM	4	2	0	Pipe B

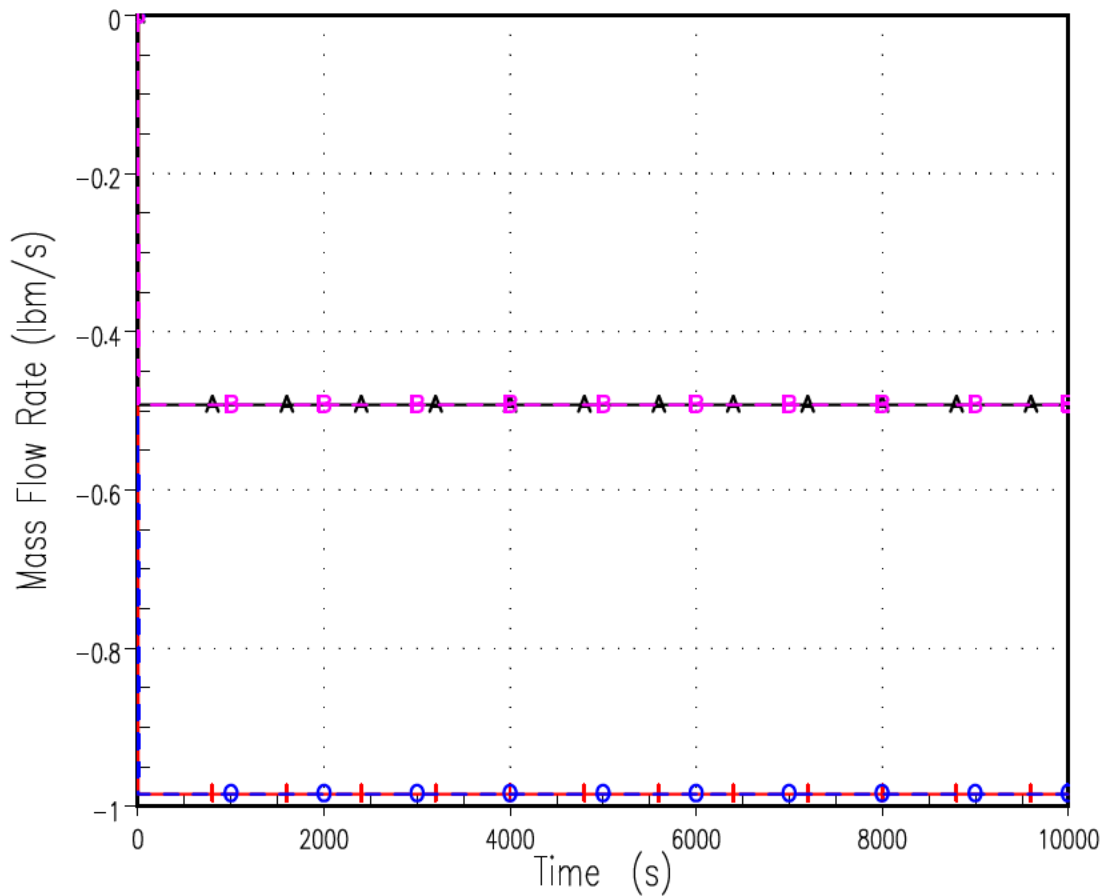


288929177

Figure 139-5: WCOBRA/TRAC-TF2 Results for the 1D Parallel Pipe Numerical Problem with Upward Flow through the 1D Components

1D Parallel Pipe Problem – Vertical Downward

—	RMVM	2	6	0	Inlet
○	RMVM	5	6	0	Outlet
—	RMVM	3	2	0	Pipe A
—	RMVM	4	2	0	Pipe B

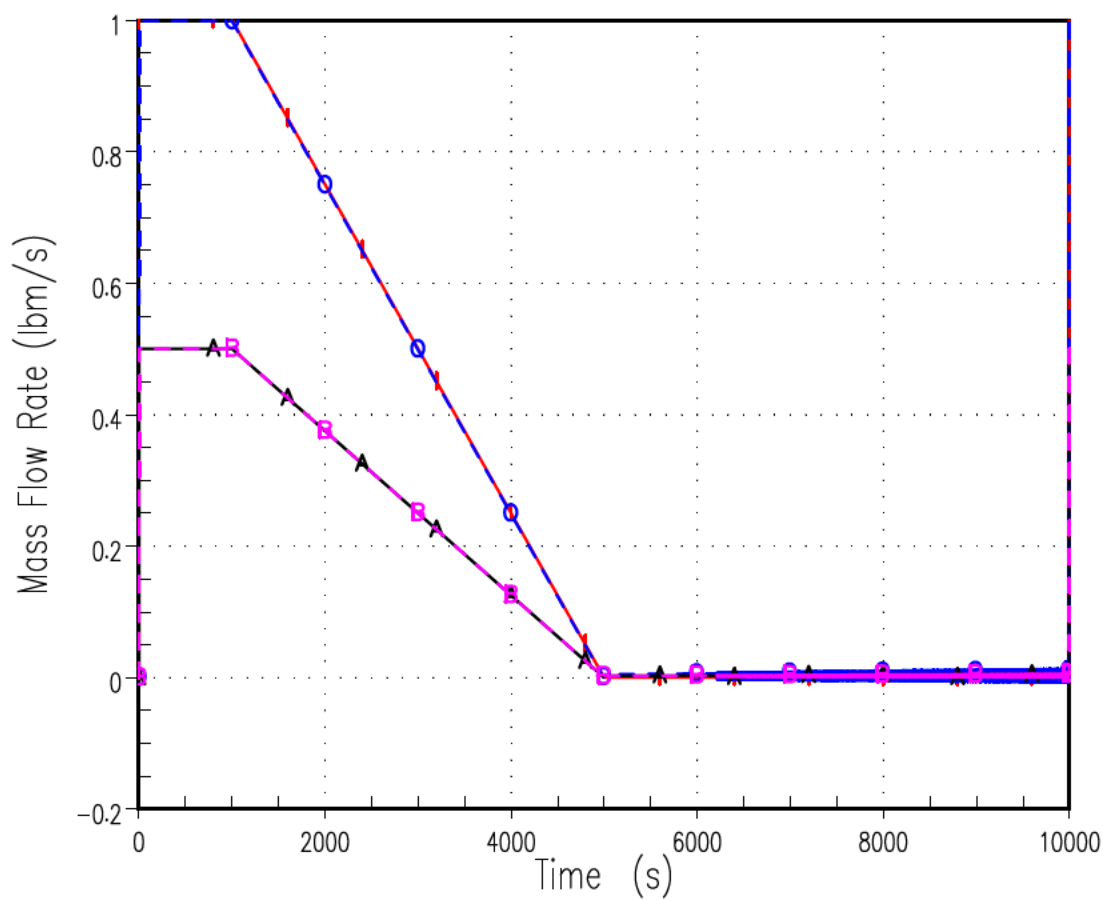


288929177

Figure 139-6: WCOBRA/TRAC-TF2 Results for the 1D Parallel Pipe Numerical Problem with Downward Flow through the 1D Components

3D Parallel Channel Problem – Flow to Zero





—	FLM	1	1	0	Inlet
○	FLM	4	3	0	Outlet
▲	FLM	2	2	0	Chnl A
■	FLM	3	2	0	Chnl B

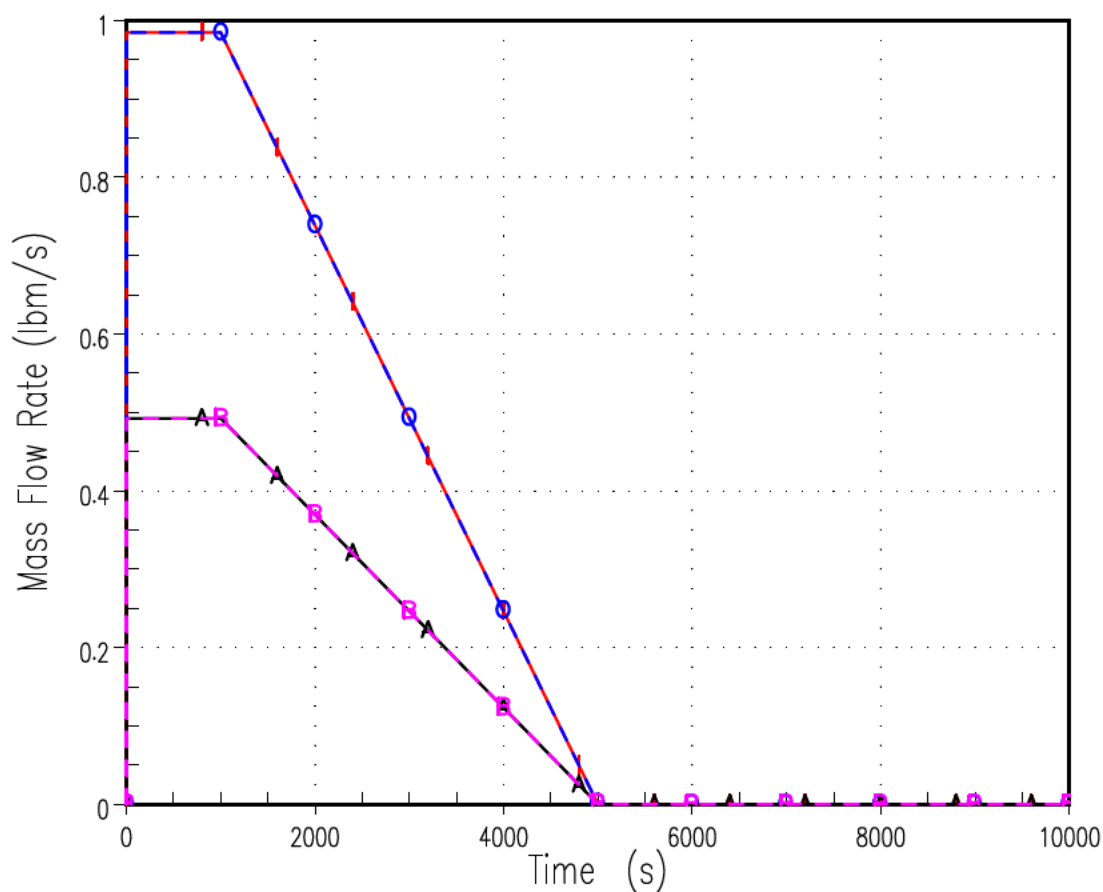


420174754

Figure 139-7: WCOBRA/TRAC-TF2 Results for the 3D Vessel Parallel Channel Numerical Problem with Flow Ramped Down to Zero

1D Parallel Pipe Problem – Flow to Zero

	RMVM	2	6	0	Inlet
	RMVM	5	6	0	Outlet
	RMVM	3	2	0	Pipe A
	RMVM	4	2	0	Pipe B



420174754

Figure 139-8: WCOBRA/TRAC-TF2 Results for the 1D Components Parallel Pipe Numerical Problem with Flow Ramped Down to Zero

B NUCLEAR REGULATORY COMMISSION AUDIT SUMMARIES

This section contains all the summaries of audits which occurred during the licensing of the FSLOCA EM. A list of all the audit summaries and the content discussed in those summaries is contained in Table B1.

Table B1		
Audit Date	Transmittal Document	Subject
July and August 2013	LTR-NRC-13-70	PWR Parametric Studies PWR Steady-State Calibration ROSA SB-CL-02 Transients with Sampling of Uncertainties Updated Region I Break Sampling Impact of YDRAG on FLECHT Crossover Leg Re-plugging Under LBLOCA Conditions Downcomer Steam-Water Interaction for SBLOCA/IBLOCA
February 2014	LTR-NRC-14-55	Interfacial Drag Package Additional IET Validation Methodology Updates for Burnup Method and TCD
May 2014	LTR-NRC-14-29	Semiscale S-07-10D Simulation Loop Seal Clearing Region I Analysis Method PWR Region I Parametric Studies
June 2014	LTR-NRC-14-38	Downcomer Lateral Form Loss Loop-to-Loop Variation Initial Stored Energy
August 2014 (Part 1)	LTR-NRC-14-60	Clarifications Related to RAIs: 23, 36, 37, 36-39, 46, 47, 48, 51, 85, 95, 127, 132, 133, and 134
August 2014 (Part 2)	LTR-NRC-15-6	Clarifications Related to RAIs: 20, 22, 29, 30, 79, 80, 86, 89, 90, 91, 96, 97, 98, 99, 101, 102, 104, 105, 107, 112, 113, 115, and 116
August 2014 (Part 3)	LTR-NRC-15-11	Clarifications Related to RAIs: 26, 51, 52, 53, 54, 55, and 57
June 2015 (Part 1)	LTR-NRC-15-67	Clarifications Related to RAIs: 22, 86, 96, 108, 109, 110, 112, and 122
June 2015 (Part 2)	LTR-NRC-15-70	Clarifications Related to RAIs: 26, 46, 51, 55, 57 ECCS into the Faulted Loop
June 2015 (Part 3)	LTR-NRC-15-85	Clarifications Related to RAI 113 Compilation of Uncertainty Parameter Treatment
September 2015	LTR-NRC-15-82	Offsite Power Availability Method
October 2015	LTR-NRC-15-88	Offsite Power Availability Core-Wide Oxidation Region II Sample Size

**Summary of July 2013 NRC Code Workshop and August 2013 NRC Audit of the FULL
SPECTRUM LOCA (FSLOCA) Evaluation Model (Non-Proprietary)**

October 2013

Westinghouse Electric Company
1000 Westinghouse Drive
Cranberry Township, PA 16066

© 2013 Westinghouse Electric Company LLC
All Rights Reserved

1.0 Introduction

In July 2013, a workshop was held between Westinghouse and the Nuclear Regulatory Commission (NRC) to allow the NRC to specify WCOBRA/TRAC-TF2 cases to be executed as well as to examine the results of existing code cases. In August 2013, the NRC performed an audit of the FULL SPECTRUM™ LOCA (FSLOCA™) evaluation model (EM) submittal.

During the workshop, the NRC reviewed the results of many different level swell calculations. The results from Oak Ridge National Lab (ORNL) level swell and core uncover test simulations were plotted, and additional nodding and timestep studies were executed. These investigations revealed some anomalous behavior at gridded elevations in the G2 level swell test simulations, and also identified an apparent large sensitivity of ORNL Test CC to the []^{a,c}. These items were investigated by Westinghouse and discussed during an NRC audit in August 2013. The NRC also noted the lack of sensitivity for FLECHT SEASET test 31504 to YDRAG, suspicious void fraction dipping in the ORNL simulations, and that the WCOBRA/TRAC-TF2 prediction of the two-phase level for the G2 simulations degraded with additional core nodding. The FLECHT YDRAG sensitivity is discussed later in this summary, and the other two items are still under investigation.

A series of Beaver Valley parametric studies were executed. The results of these studies were presented to the NRC in the August 2013 audit, and additional discussion regarding the studies is included later in this summary.

The NRC discussed concerns with the decay heat sampling, and with the use of the Forslund-Rohsenow model for direct wall-to-droplet heat transfer in the hot wall regime. The decay heat sampling is still under consideration, but Westinghouse has agreed to remove the direct wall-to-droplet heat transfer for the hot wall regime.

The NRC also requested various large runsets with the Beaver Valley Pressurized Water Reactor (PWR) model and the ROSA SB-CL-02 model. The results of these studies were presented to the NRC in the August 2013 audit, and additional discussion regarding these studies is included later in this summary.

Finally, the NRC identified several other considerations which are discussed later in this audit summary.

Additional information to support the licensing of the FSLOCA EM is provided in this attachment. The presentations from the August 2013 NRC audit are included in following attachments.

FULL SPECTRUM™ and FSLOCA™ are trademarks in the United States of Westinghouse Electric Company LLC, its subsidiaries and/or its affiliates. These marks may be used and/or registered in other countries throughout the world. All rights reserved. Unauthorized use is strictly prohibited. Other names may be trademarks of their respective owners.

2.0 Beaver Valley Parametric Studies

A parametric study was executed on run076 from Study C from the response to FSLOCA EM RAIs #9 and #12 (LTR-NRC-13-45 [2-1]).

[

]^{a,c}

Lastly, the complete study is redone with a 25% reduction in safety injection flow. This is performed to study the impact of the parametric study under more severe accident conditions.

2.1 Nominal Safety Injection Cases

[

]^{a,c}

[

]^{a,c}

[

]^{a,c}

2.2 Reduced Safety Injection Cases

[

]^{a,c}

[

]^{a,c}

2.3 Nominal Safety Injection Case with Increase in Decay Heat versus the Reduced Safety Injection Base Case

[

]^{a,c}

2.4 References

- 2-1) LTR-NRC-13-45, "Submittal of Westinghouse Responses to 'WCAP-16996-P, 'Realistic LOCA Evaluation Methodology Applied to the Full Spectrum of Break Sizes (FULL SPECTRUM LOCA Methodology)' Request for Additional Information – RAIs 9 and 12' (Proprietary/Non-Proprietary), Project 700, TAC No. ME5244," June 26, 2013.

a,c

a,c

a,c

a,c

a,c

a,c

a,c

a,c

a,c

a,c

a,c

a,c

a,c

a,c

a,c

a,c

a,c

a,c

a,c

a,c

a,c

a,c

a,c

a,c

a,c

a,c

a,c

a,c

a,c

a,c

a,c

a,c

a,c

a,c

a,c

a,c

a,c

a,c

a,c

a,c

a,c

a,c

a,c

a,c

a,c

a,c

a,c

a,c

a,c

a,c

a,c

a,c

a,c

a,c

a,c

a,c

a,c

a,c

a,c

a,c

a,c

a,c

a,c

a,c

a,c

a,c

a,c

a,c

a,c

a,c

a,c

a,c

a,c

a,c

a,c

a,c

a,c

a,c

a,c

a,c

a,c

a,c

a,c

a,c

a,c

a,c

a,c

a,c

a,c

a,c

a,c

a,c

a,c

a,c

a,c

a,c

a,c

a,c

a,c

a,c

a,c

a,c

a,c

a,c

a,c

a,c

a,c

a,c

a,c

a,c

a,c

a,c

a,c

a,c

a,c

a,c

a,c

a,c

a,c

a,c

a,c

a,c

a,c

a,c

a,c

a,c

a,c

a,c

a,c

a,c

a,c

a,c

a,c

a,c

a,c

a,c

a,c

a,c

a,c

a,c

a,c

a,c

a,c

a,c

a,c

a,c

a,c

a,c

a,c

a,c

a,c

a,c

a,c

a,c

a,c

a,c

a,c

a,c

a,c

a,c

a,c

a,c

a,c

a,c

a,c

a,c

a,c

a,c

a,c

a,c

a,c

a,c

a,c

a,c

a,c

a,c

a,c

a,c

a,c

a,c

a,c

a,c

a,c

a,c

a,c

a,c

a,c

a,c

a,c

a,c

a,c

a,c

a,c

a,c

a,c

a,c

a,c

3.0 Beaver Valley Steady-State Runset

The purpose of the study is to show that there is no large variation in the parameters of interest used for demonstrating a converged steady-state. Section 26.4 of WCAP-16996-P [3-1] discusses the steady-state calculation/calibration process. The distributions of the parameters in Table 26.4-1 of WCAP-16996-P are of interest for this study. The parameters are repeated here in Table 3-1.

[illegible]

In addition, the distributions of the parameters used as part of the automated steady-state process are of interest. These parameters are provided in Table 3-2.

Table 3-2: Parameters Used by Automated Process to Obtain Converged Steady-State		
Parameter		Parameter
[
] ^{a,c}

Lastly, the parameters in Table 3-3 are also of interest, because of their influence on select parameters used to determine if a steady-state has converged.

Table 3-3: Additional Parameters of Interest for Steady-State Convergence		
Parameter		Parameter
[
$\gamma^{a,c}$		

To present the results, data tables and figures are generated. The values for the parameters of interest from the 93 runs were averaged, and the standard deviation was calculated. Table 3-4 includes the values from the nominal case, as well as the values from the 93 runs.

Table 3-5 contains the sampled attribute sets; these are the target values for each of the 93 cases.

Table 3-6 is a summary of the calculated versus target values from the last iteration step output from the automated steady-state process (several parameters in Table 3-1). In addition, the table contains the values for the parameters that are used to obtain the desired steady-state tuned parameters at their target values (parameters in Table 3-2).

Table 3-7 is a listing of the parameters in Table 3-4 at the last time step in each of the 93 steady-state runs.

In addition to extracting the data from the 93 run set, the data was extracted from the Nominal case as well. The data tables (note that there is only one run in these tables) are included as Tables 3-8, 3-9, and 3-10.

[

$\gamma^{a,c}$

[

]^{a,c}

[

]^{a,c}

3.1 References

- 3-1) WCAP-16996-P, Volumes I, II and III, "Realistic LOCA Evaluation Methodology Applied to the Full Spectrum of Break Sizes (FULL SPECTRUM LOCA Methodology)," November 2010.

Table 3-4: List of Values Extracted at the End of the Nominal Case Steady-State Run and the Average of the 93 Cases			
Parameter	Nominal Case Value¹	93 Run Set	
		Average¹	Standard Deviation¹

a,c

Table 3-4: List of Values Extracted at the End of the Nominal Case Steady-State Run and the Average of the 93 Cases

Parameter	Nominal Case Value ¹	93 Run Set	
		Average ¹	Standard Deviation ¹

a,c

¹ Values are presented for loop 1, loop 2 and loop 3 where appropriate.

Table 3-5: Sampled Attribute Sets for the Beaver Valley Steady-State Runset

[

] ^{a,c}

Table 3-5: Sampled Attribute Sets for the Beaver Valley Steady-State Runset

[

] ^{a,c}

Table 3-5: Sampled Attribute Sets for the Beaver Valley Steady-State Runset

[

] ^{a,c}

Table 3-5: Sampled Attribute Sets for the Beaver Valley Steady-State Runset

[

] ^{a,c}

Table 3-5: Sampled Attribute Sets for the Beaver Valley Steady-State Runset

[

] ^{a,c}

Table 3-5: Sampled Attribute Sets for the Beaver Valley Steady-State Runset

[

] ^{a,c}

Table 3-5: Sampled Attribute Sets for the Beaver Valley Steady-State Runset

[

] ^{a,c}

Table 3-5: Sampled Attribute Sets for the Beaver Valley Steady-State Runset

[

] ^{a,c}

Table 3-5: Sampled Attribute Sets for the Beaver Valley Steady-State Runset

[

] ^{a,c}

Table 3-5: Sampled Attribute Sets for the Beaver Valley Steady-State Runset

[

] ^{a,c}

Table 3-5: Sampled Attribute Sets for the Beaver Valley Steady-State Runset

[

] ^{a,c}

Table 3-5: Sampled Attribute Sets for the Beaver Valley Steady-State Runset

[

] ^{a,c}

Table 3-5: Sampled Attribute Sets for the Beaver Valley Steady-State Runset

[

] ^{a,c}

Table 3-5: Sampled Attribute Sets for the Beaver Valley Steady-State Runset

[

] ^{a,c}

Table 3-5: Sampled Attribute Sets for the Beaver Valley Steady-State Runset

[

] ^{a,c}

Table 3-5: Sampled Attribute Sets for the Beaver Valley Steady-State Runset

[

] ^{a,c}

Table 3-6: Calculated and Calibrated Parameter Values for the Beaver Valley Steady-State Runset

[

]^{a,c}

Table 3-6: Calculated and Calibrated Parameter Values for the Beaver Valley Steady-State Runset

[

]^{a,c}

Table 3-6: Calculated and Calibrated Parameter Values for the Beaver Valley Steady-State Runset

[

]^{a,c}

Table 3-6: Calculated and Calibrated Parameter Values for the Beaver Valley Steady-State Runset

[

]^{a,c}

Table 3-6: Calculated and Calibrated Parameter Values for the Beaver Valley Steady-State Runset

[

]^{a,c}

Table 3-6: Calculated and Calibrated Parameter Values for the Beaver Valley Steady-State Runset

[

]^{a,c}

Table 3-6: Calculated and Calibrated Parameter Values for the Beaver Valley Steady-State Runset

[

]^{a,c}

Table 3-6: Calculated and Calibrated Parameter Values for the Beaver Valley Steady-State Runset

[

]^{a,c}

Table 3-6: Calculated and Calibrated Parameter Values for the Beaver Valley Steady-State Runset

[

]^{a,c}

Table 3-6: Calculated and Calibrated Parameter Values for the Beaver Valley Steady-State Runset

[

]^{a,c}

Table 3-6: Calculated and Calibrated Parameter Values for the Beaver Valley Steady-State Runset

[

]^{a,c}

Table 3-6: Calculated and Calibrated Parameter Values for the Beaver Valley Steady-State Runset

[

]^{a,c}

Table 3-6: Calculated and Calibrated Parameter Values for the Beaver Valley Steady-State Runset

[

]^{a,c}

Table 3-6: Calculated and Calibrated Parameter Values for the Beaver Valley Steady-State Runset

[

^{a,c}]

Table 3-6: Calculated and Calibrated Parameter Values for the Beaver Valley Steady-State Runset

[

^{a,c}]

Table 3-6: Calculated and Calibrated Parameter Values for the Beaver Valley Steady-State Runset

[

^{a,c}]

Table 3-6: Calculated and Calibrated Parameter Values for the Beaver Valley Steady-State Runset

[

^{a,c}]

Table 3-6: Calculated and Calibrated Parameter Values for the Beaver Valley Steady-State Runset

[

^{a,c}]

Table 3-6: Calculated and Calibrated Parameter Values for the Beaver Valley Steady-State Runset

[

]^{a,c}

Table 3-7: Table 3-4 Parameters from Last Timestep of Steady-State Calculation for the Beaver Valley Steady-State Runset

[

]^{a,c}

Table 3-7: Table 3-4 Parameters from Last Timestep of Steady-State Calculation for the Beaver Valley Steady-State Runset

[

]^{a,c}

Table 3-7: Table 3-4 Parameters from Last Timestep of Steady-State Calculation for the Beaver Valley Steady-State Runset

[

]^{a,c}

Table 3-7: Table 3-4 Parameters from Last Timestep of Steady-State Calculation for the Beaver Valley Steady-State Runset

[

]^{a,c}

Table 3-7: Table 3-4 Parameters from Last Timestep of Steady-State Calculation for the Beaver Valley Steady-State Runset

[

]^{a,c}

Table 3-7: Table 3-4 Parameters from Last Timestep of Steady-State Calculation for the Beaver Valley Steady-State Runset

[

]^{a,c}

Table 3-7: Table 3-4 Parameters from Last Timestep of Steady-State Calculation for the Beaver Valley Steady-State Runset

[

]^{a,c}

Table 3-7: Table 3-4 Parameters from Last Timestep of Steady-State Calculation for the Beaver Valley Steady-State Runset

[

]^{a,c}

Table 3-7: Table 3-4 Parameters from Last Timestep of Steady-State Calculation for the Beaver Valley Steady-State Runset

[

]^{a,c}

Table 3-7: Table 3-4 Parameters from Last Timestep of Steady-State Calculation for the Beaver Valley Steady-State Runset

[

]^{a,c}

Table 3-7: Table 3-4 Parameters from Last Timestep of Steady-State Calculation for the Beaver Valley Steady-State Runset

[

]^{a,c}

Table 3-7: Table 3-4 Parameters from Last Timestep of Steady-State Calculation for the Beaver Valley Steady-State Runset

[

^{a,c}]

Table 3-7: Table 3-4 Parameters from Last Timestep of Steady-State Calculation for the Beaver Valley Steady-State Runset

[

]^{a,c}

Table 3-7: Table 3-4 Parameters from Last Timestep of Steady-State Calculation for the Beaver Valley Steady-State Runset

[

]^{a,c}

Table 3-7: Table 3-4 Parameters from Last Timestep of Steady-State Calculation for the Beaver Valley Steady-State Runset

[

]^{a,c}

Table 3-7: Table 3-4 Parameters from Last Timestep of Steady-State Calculation for the Beaver Valley Steady-State Runset

[

]^{a,c}

Table 3-7: Table 3-4 Parameters from Last Timestep of Steady-State Calculation for the Beaver Valley Steady-State Runset

[

]^{a,c}

Table 3-7: Table 3-4 Parameters from Last Timestep of Steady-State Calculation for the Beaver Valley Steady-State Runset

[

]^{a,c}

Table 3-7: Table 3-4 Parameters from Last Timestep of Steady-State Calculation for the Beaver Valley Steady-State Runset

[

]^{a,c}

Table 3-7: Table 3-4 Parameters from Last Timestep of Steady-State Calculation for the Beaver Valley Steady-State Runset

[

]^{a,c}

Table 3-7: Table 3-4 Parameters from Last Timestep of Steady-State Calculation for the Beaver Valley Steady-State Runset

[

]^{a,c}

Table 3-7: Table 3-4 Parameters from Last Timestep of Steady-State Calculation for the Beaver Valley Steady-State Runset

[

]^{a,c}

Table 3-7: Table 3-4 Parameters from Last Timestep of Steady-State Calculation for the Beaver Valley Steady-State Runset

[

^{a,c}]

Table 3-7: Table 3-4 Parameters from Last Timestep of Steady-State Calculation for the Beaver Valley Steady-State Runset

[

]^{a,c}

Table 3-7: Table 3-4 Parameters from Last Timestep of Steady-State Calculation for the Beaver Valley Steady-State Runset

[

]^{a,c}

Table 3-7: Table 3-4 Parameters from Last Timestep of Steady-State Calculation for the Beaver Valley Steady-State Runset

[

]^{a,c}

Table 3-7: Table 3-4 Parameters from Last Timestep of Steady-State Calculation for the Beaver Valley Steady-State Runset

[

]^{a,c}

Table 3-7: Table 3-4 Parameters from Last Timestep of Steady-State Calculation for the Beaver Valley Steady-State Runset

[

]^{a,c}

Table 3-7: Table 3-4 Parameters from Last Timestep of Steady-State Calculation for the Beaver Valley Steady-State Runset

[

]^{a,c}

Table 3-7: Table 3-4 Parameters from Last Timestep of Steady-State Calculation for the Beaver Valley Steady-State Runset

[

]^{a,c}

Table 3-7: Table 3-4 Parameters from Last Timestep of Steady-State Calculation for the Beaver Valley Steady-State Runset

[

]^{a,c}

Table 3-8: Attribute Set for the Beaver Valley Steady-State Nominal Case

[

] ^{a,c}

Table 3-9: Calculated and Calibrated Parameter Values for the Beaver Valley Steady-State Nominal Case

[

]^{a,c}

Table 3-10: Table 3-4 Parameters from Last Timestep of Steady-State Calculation for the Beaver Valley Steady-State Nominal Case

[

]^{a,c}



Figure 3-1: Distribution of Hot Leg Temperature (°F)



Figure 3-2: Distribution of Cold Leg Temperature (°F)



Figure 3-3: Distribution of Vessel Average Temperature (°F)



Figure 3-4: Distribution of SG Secondary Side Pressure (psia)

a,c

Figure 3-5: Distribution of Liquid Mass Flowrate in SG Downcomer (lbm/s)

a,c

Figure 3-6: Distribution of Initial Upper Head Enthalpy (BTU/lbm)



Figure 3-7: Distribution of Initial Pressurizer Liquid Volume (ft³)



Figure 3-8: Distribution of Peak Linear Heat Rate (kW/ft)

a,c

Figure 3-9: Distribution of Fuel Rod Gap Thickness (in) for Rod #3

a,c

Figure 3-10: Distribution of Fuel Rod Gap Thickness (in) for Rod #6

a,c

Figure 3-11: Distribution of Fuel Average Temperature at Peak Power Location on Rod #3 (°F)

a,c

Figure 3-12: Distribution of Fuel Average Temperature at Peak Power Location on Rod #6 (°F)

a,c

Figure 3-13: Distribution of Pressurizer Pressure (psia)

a,c

Figure 3-14: Distribution of Core Power (MWt)

4.0 ROSA SB-CL-02 Transient Runset

The FSLOCA uncertainty methodology was applied against Cylindrical Core Test Facility (CCTF) Run 62, which is a prototypical Large Break LOCA (LBLOCA) Integral Effects Test (IET), to demonstrate the code calculations against known, experimental data. It is desirable to do the same for a prototypical Small Break LOCA (SBLOCA) IET. Rig-of-Safety Assessment (ROSA) Large Scale Test Facility (LSTF) test SB-CL-02 was selected since it produces a more significant heatup than many other of the ROSA tests.

Two sets of 311 simulations was executed varying all the experimental uncertainties which could be ranged within a transient runset, as well as all the applicable model uncertainties. These runsets are discussed in Sections 4.1 and 4.2.

4.1 Transient Runset with Full Uncertainty Sampling

[

]^{a,c}

4.2 Transient Runset without Break Discharge Coefficient Sampling

[

]^{a,c}

[

]^{a,c}

[

]^{a,c}

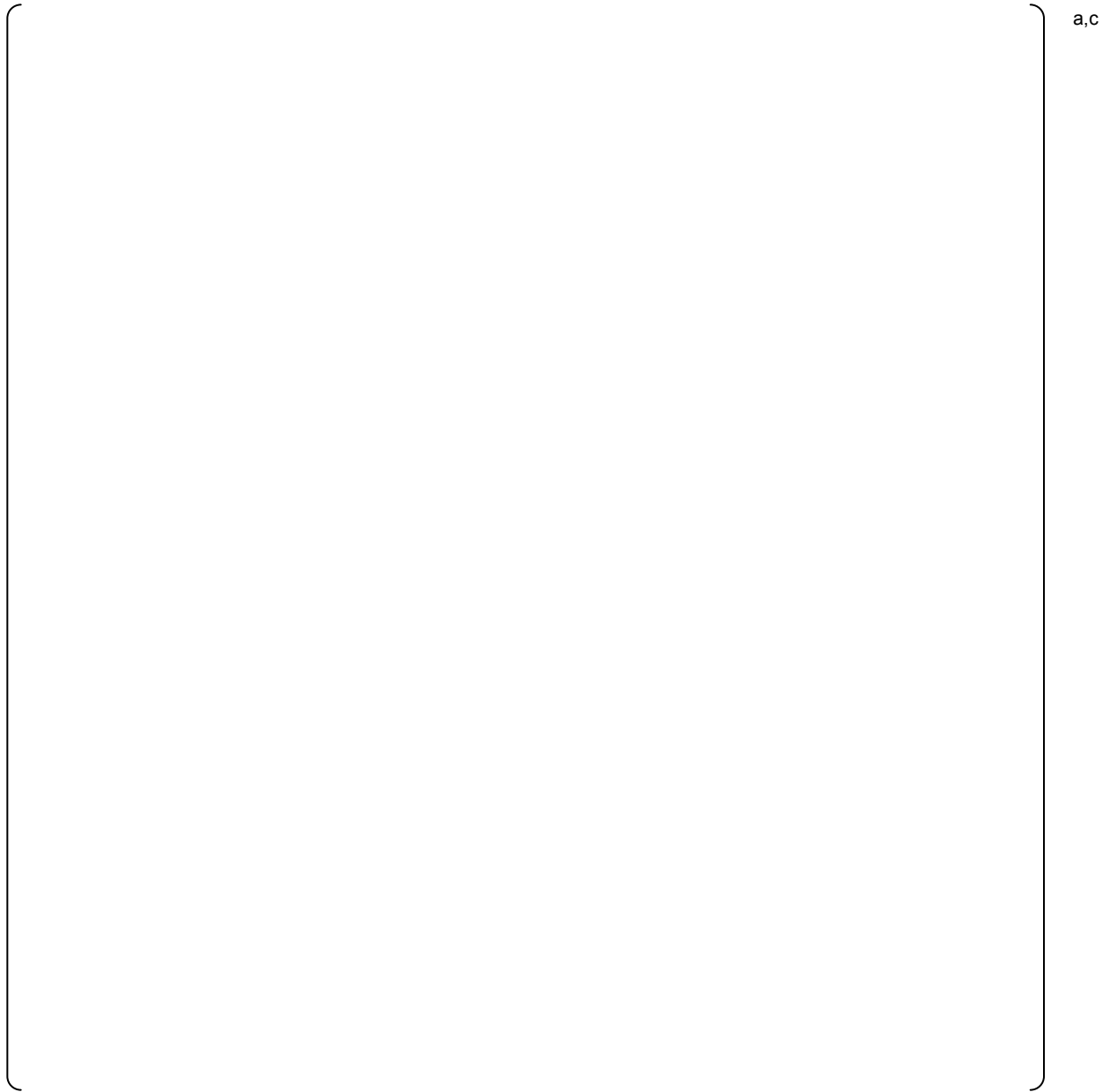


Figure 4-1: Cladding Temperature at the Maximum Measured Cladding Temperature Elevation for the 311 Case ROSA SB-CL-02 Runset

a,c

Figure 4-2: Predicted Minus Measured Cladding Temperature at the Maximum Measured Cladding Temperature Elevation for the 311 Case ROSA SB-CL-02 Runset

[

] ^{a,c}

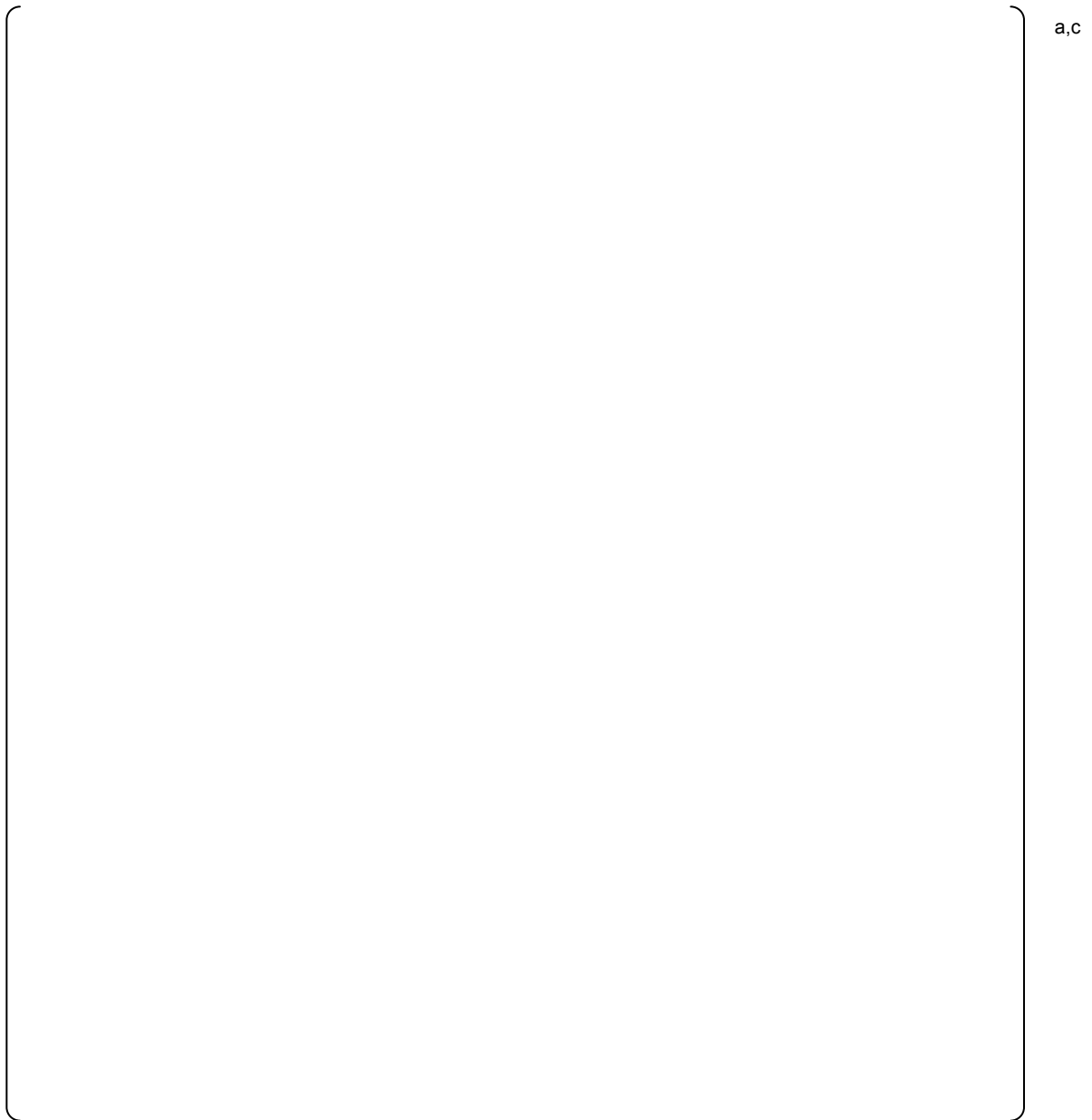


Figure 4-3: Vapor Temperature at the Maximum Measured Cladding Temperature Elevation for the First 100 Cases of the 311 Case ROSA SB-CL-02 Runset

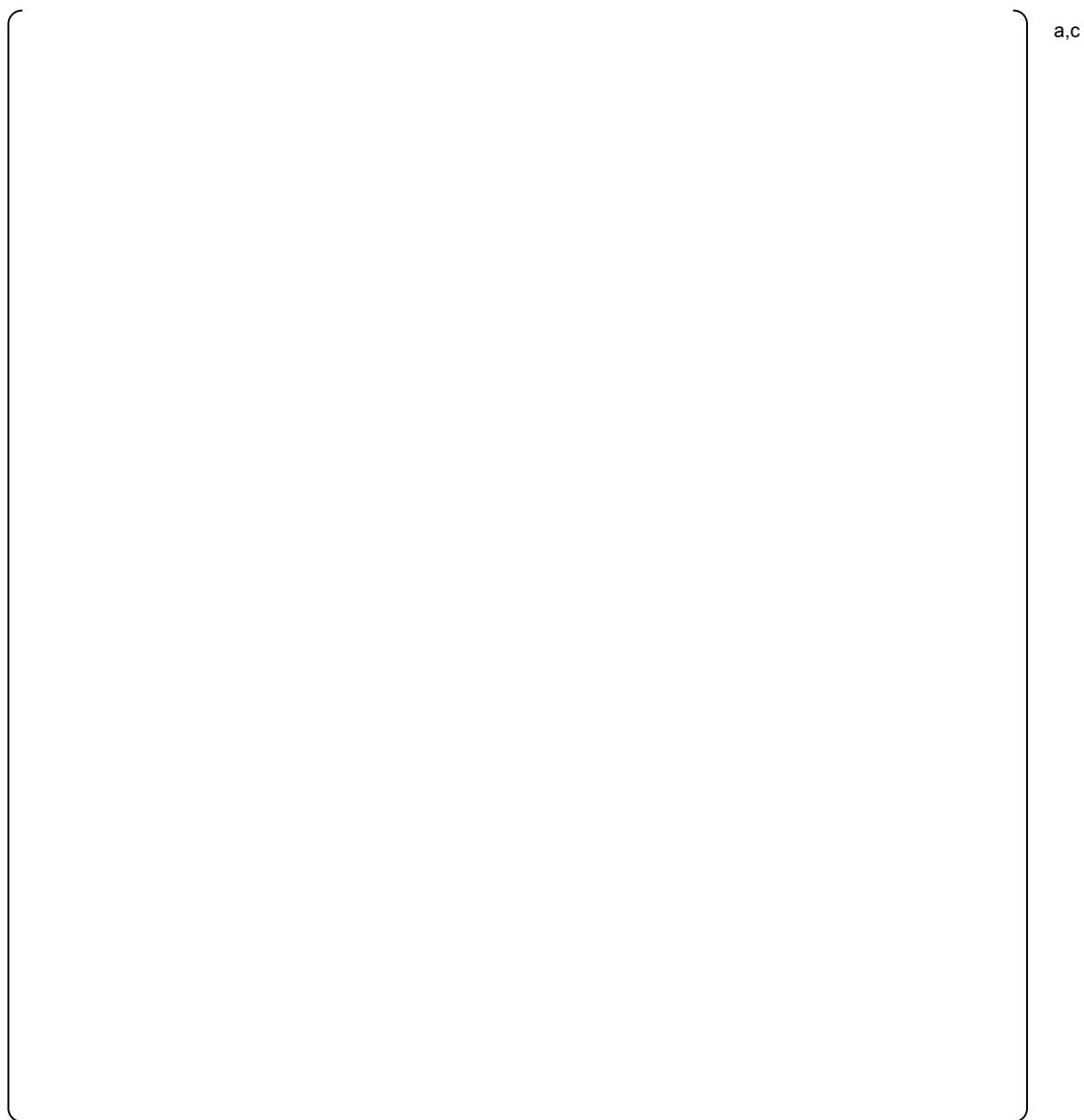


Figure 4-4: Pressurizer Pressure for the First 100 Cases of the 311 Case ROSA SB-CL-02 Runset

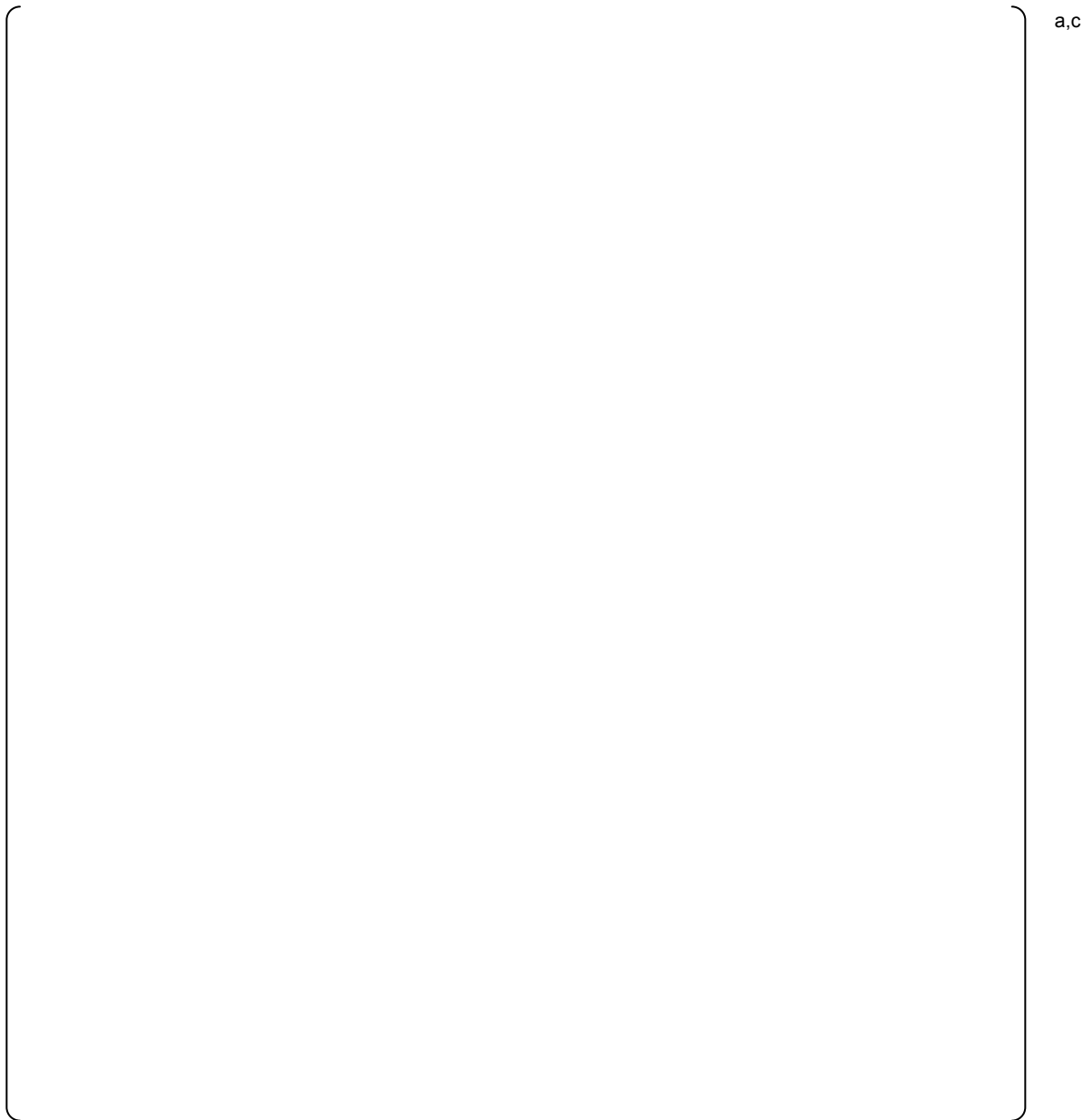


Figure 4-5: Core Differential Pressure for the First 100 Cases of the 311 Case ROSA SB-CL-02 Runset

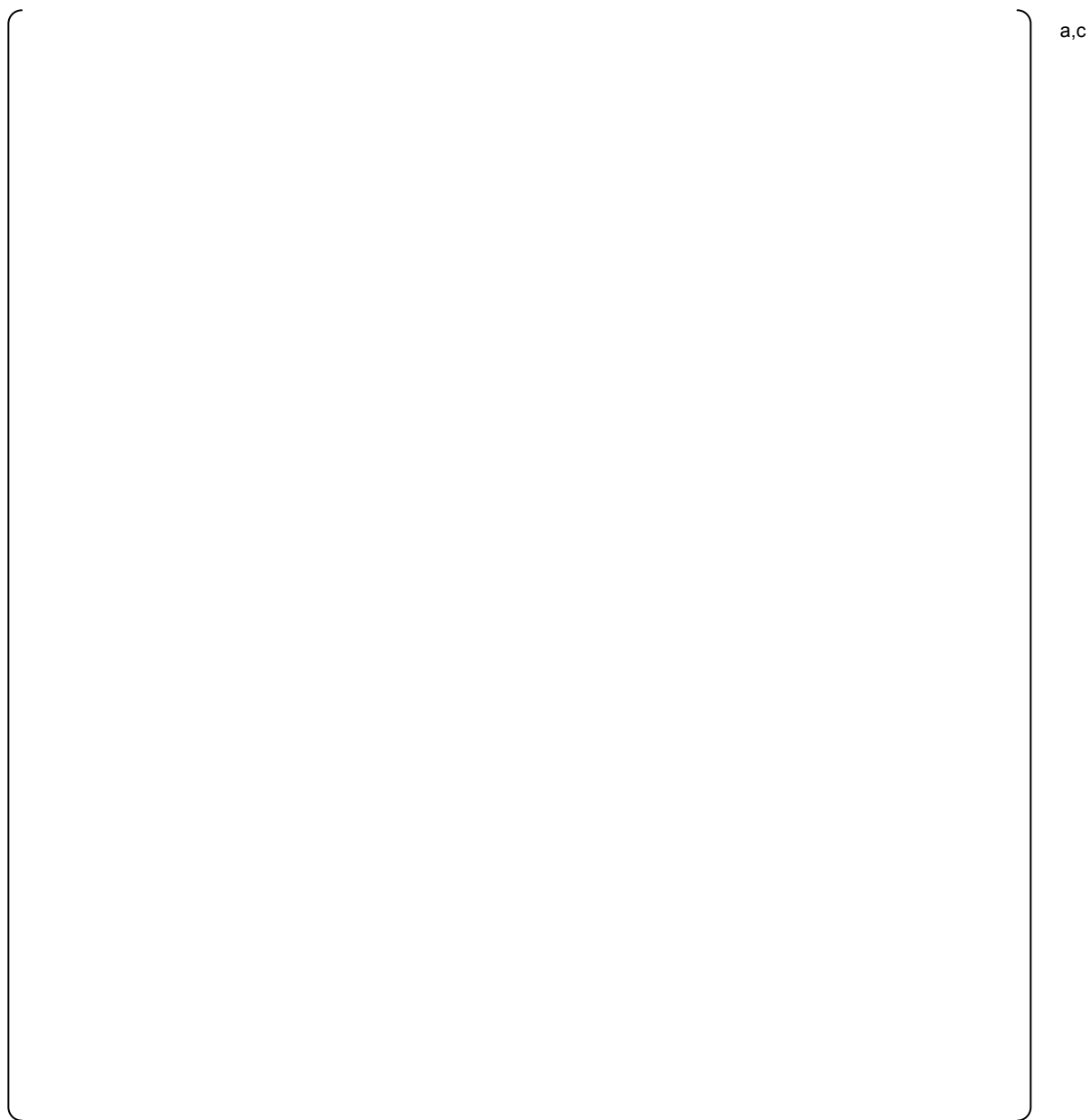


Figure 4-6: Downcomer Differential Pressure for the First 100 Cases of the 311 Case ROSA SB-CL-02 Runset

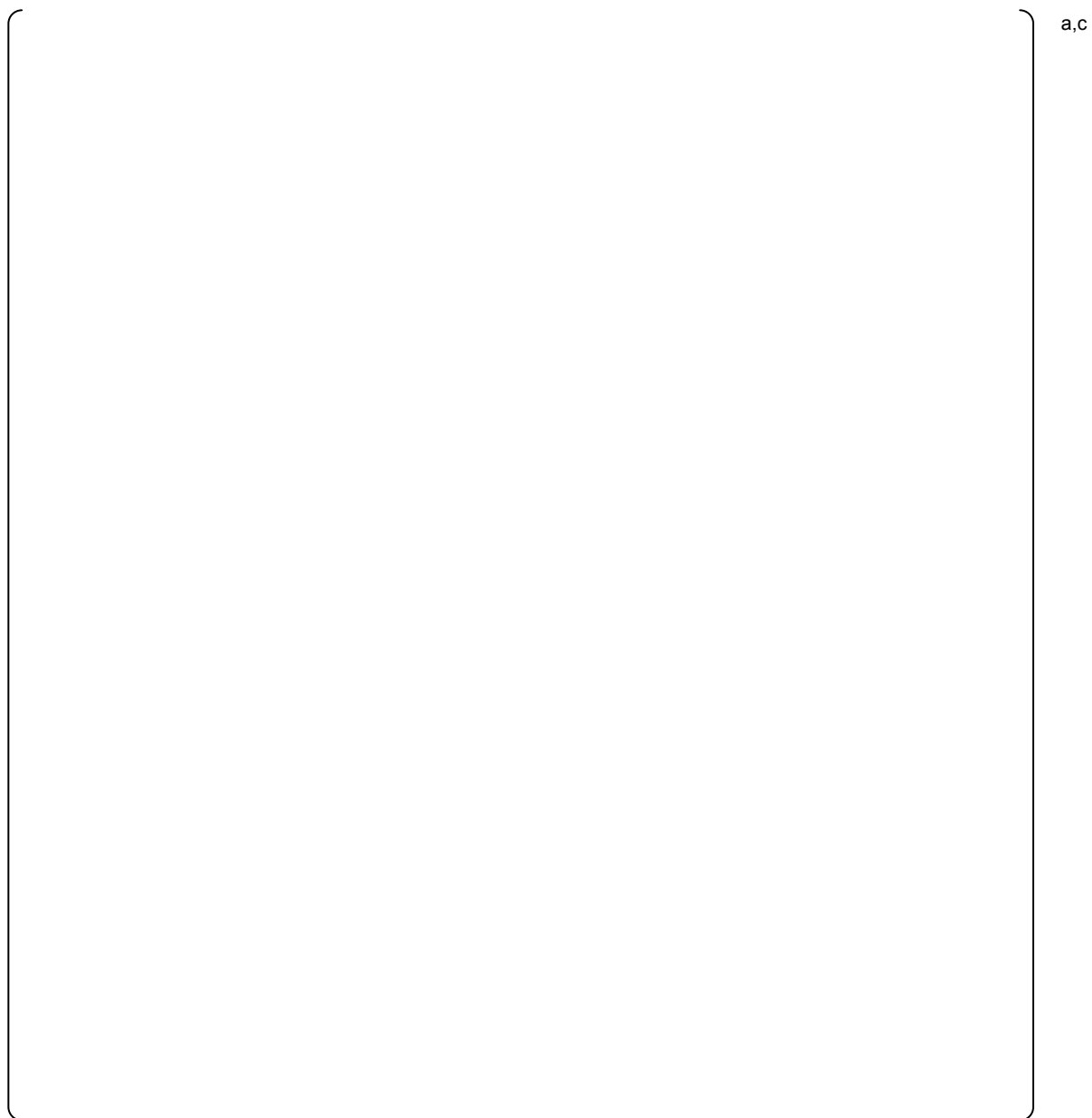


Figure 4-7: Loop Seal A Pump-Side Differential Pressure for the First 100 Cases of the 311 Case ROSA SB-CL-02 Runset

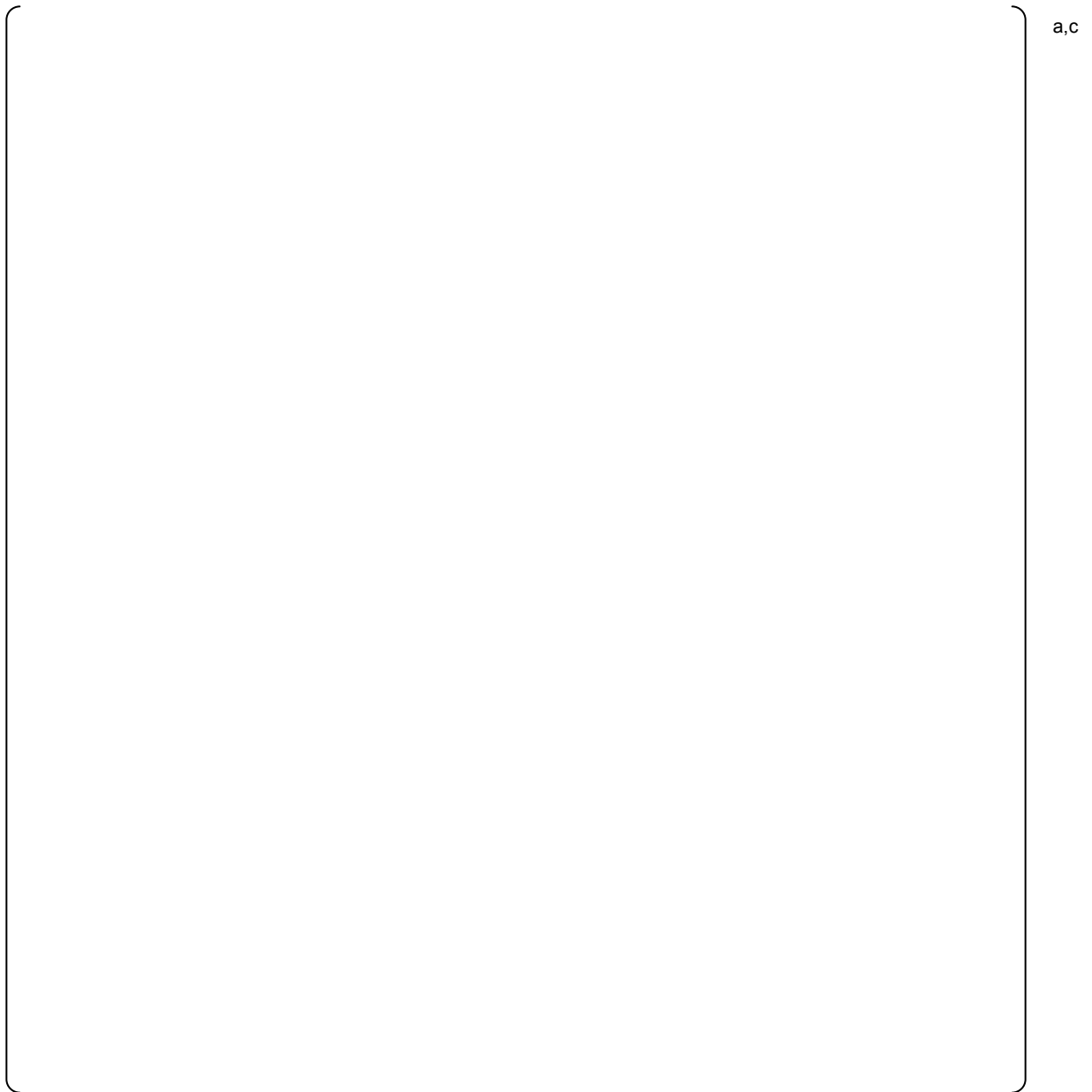


Figure 4-8: Loop Seal B Pump-Side Differential Pressure for the First 100 Cases of the 311 Case ROSA SB-CL-02 Runset



Figure 4-9: Cladding Temperature at the Maximum Measured Cladding Temperature Elevation for the 311 Case ROSA SB-CL-02 Runset without CD Sampling

a,c

Figure 4-10: Predicted Minus Measured Cladding Temperature at the Maximum Measured Cladding Temperature Elevation for the 311 Case ROSA SB-CL-02 Runset without CD Sampling

[

] a,c

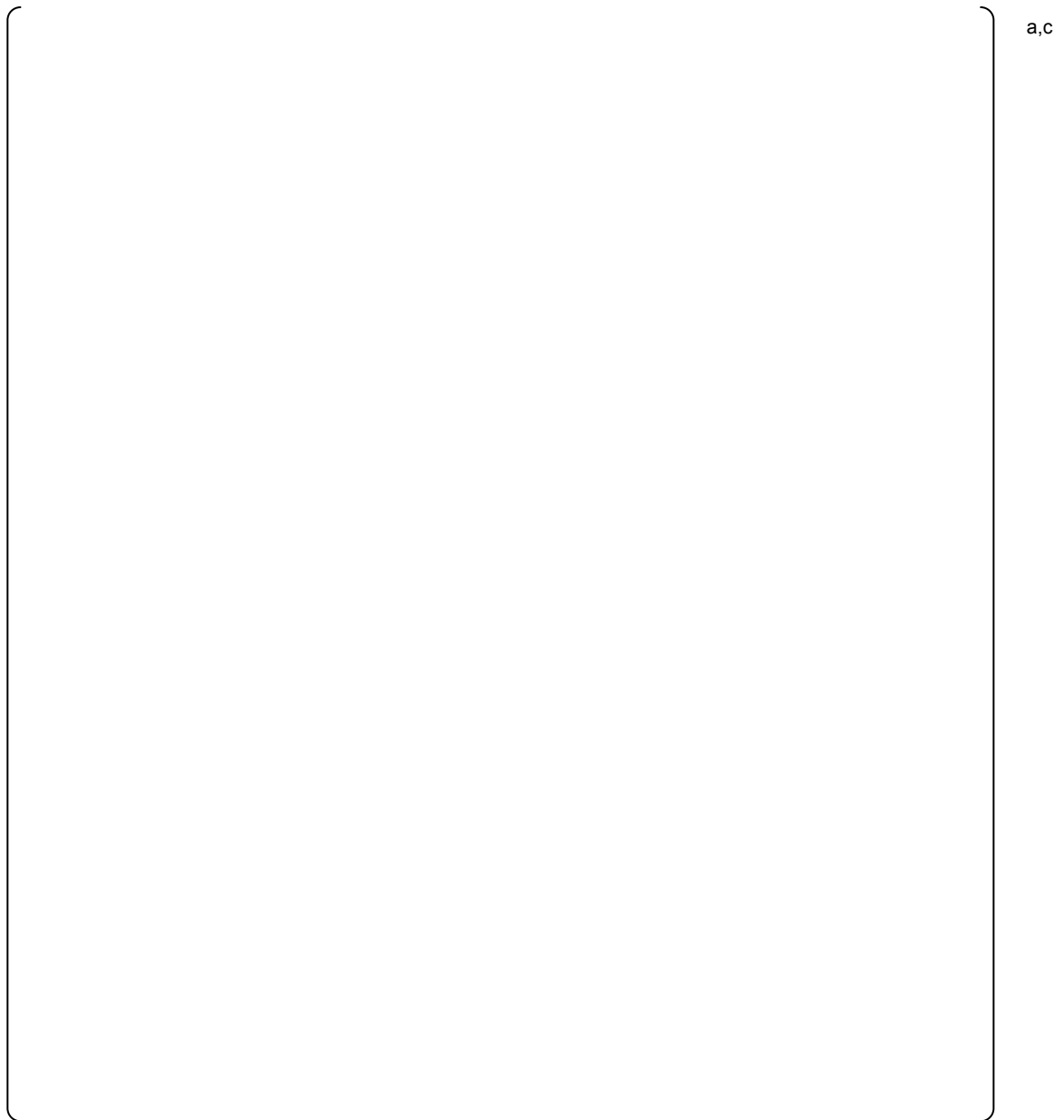


Figure 4-11: Vapor Temperature at the Maximum Measured Cladding Temperature Elevation for the First 100 Cases of the 311 Case ROSA SB-CL-02 Runset without CD Sampling



Figure 4-12: Core Exit Temperatures for the First 100 Cases of the 311 Case ROSA SB-CL-02 Runset without CD Sampling

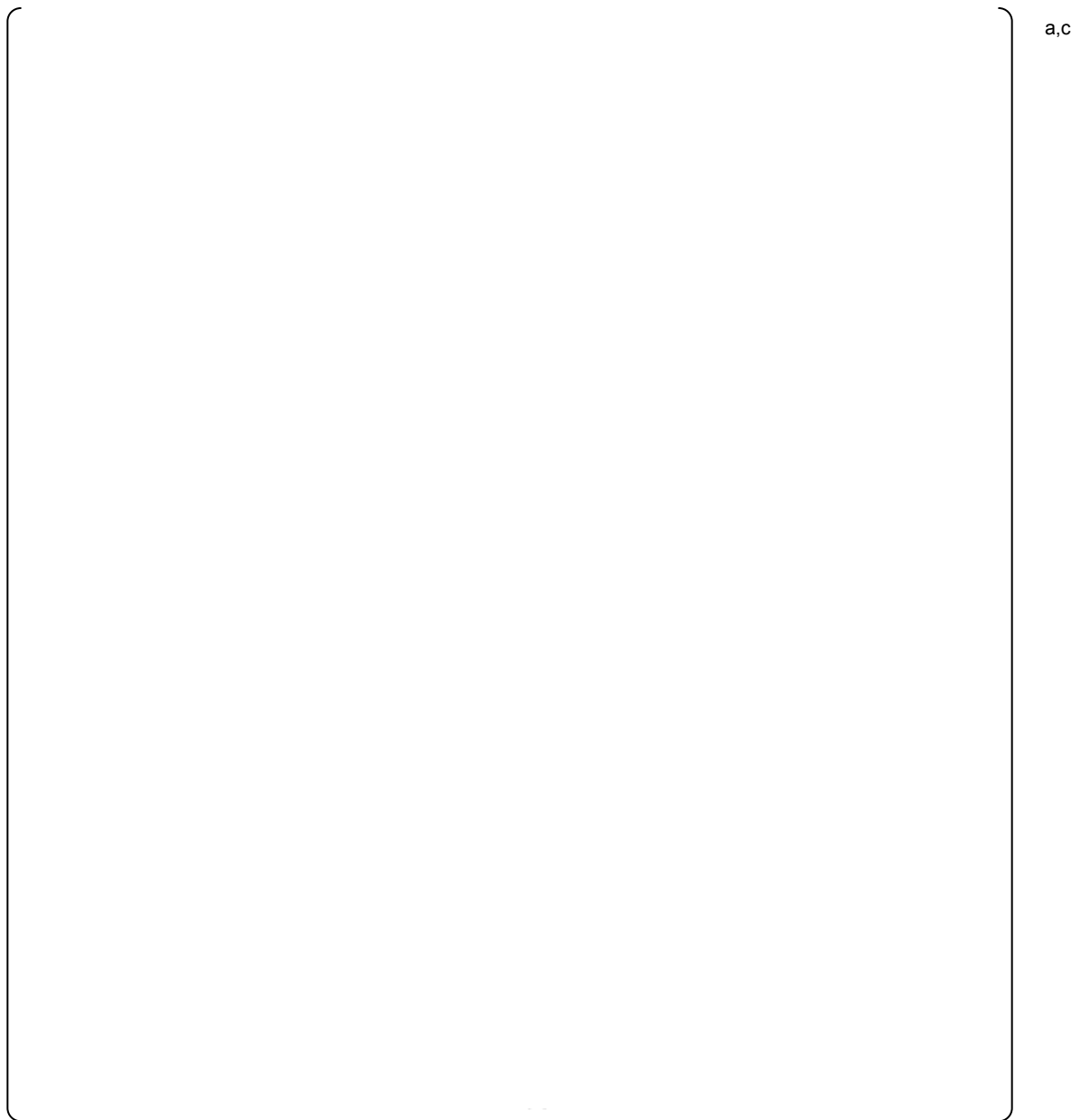


Figure 4-13: Vapor Heat Transfer Coefficient at the Maximum Measured Cladding Temperature Elevation for the First 100 Cases of the 311 Case ROSA SB-CL-02 Runset without CD Sampling

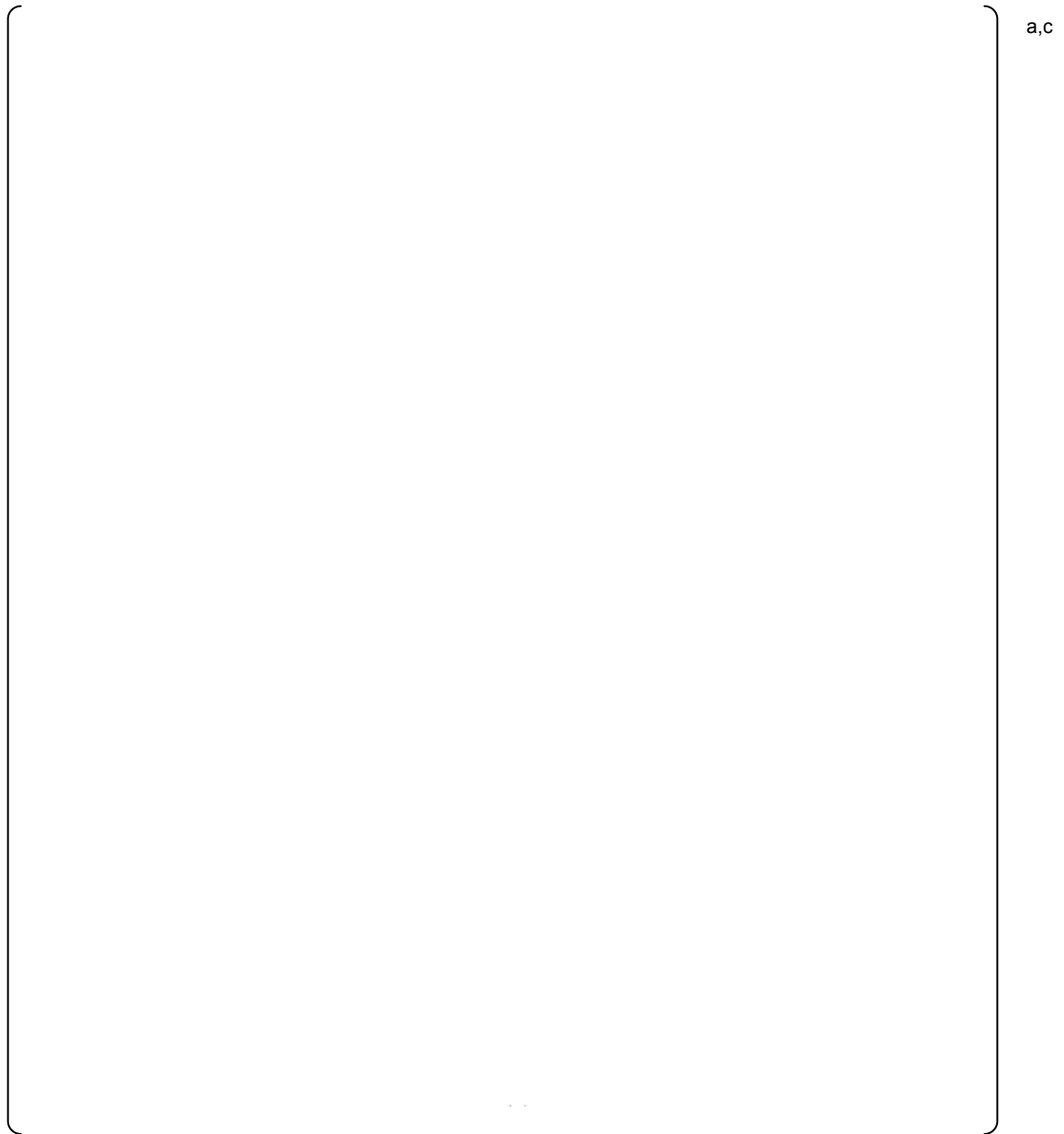


Figure 4-14: Pressurizer Pressure for the First 100 Cases of the 311 Case ROSA SB-CL-02 Runset without CD Sampling

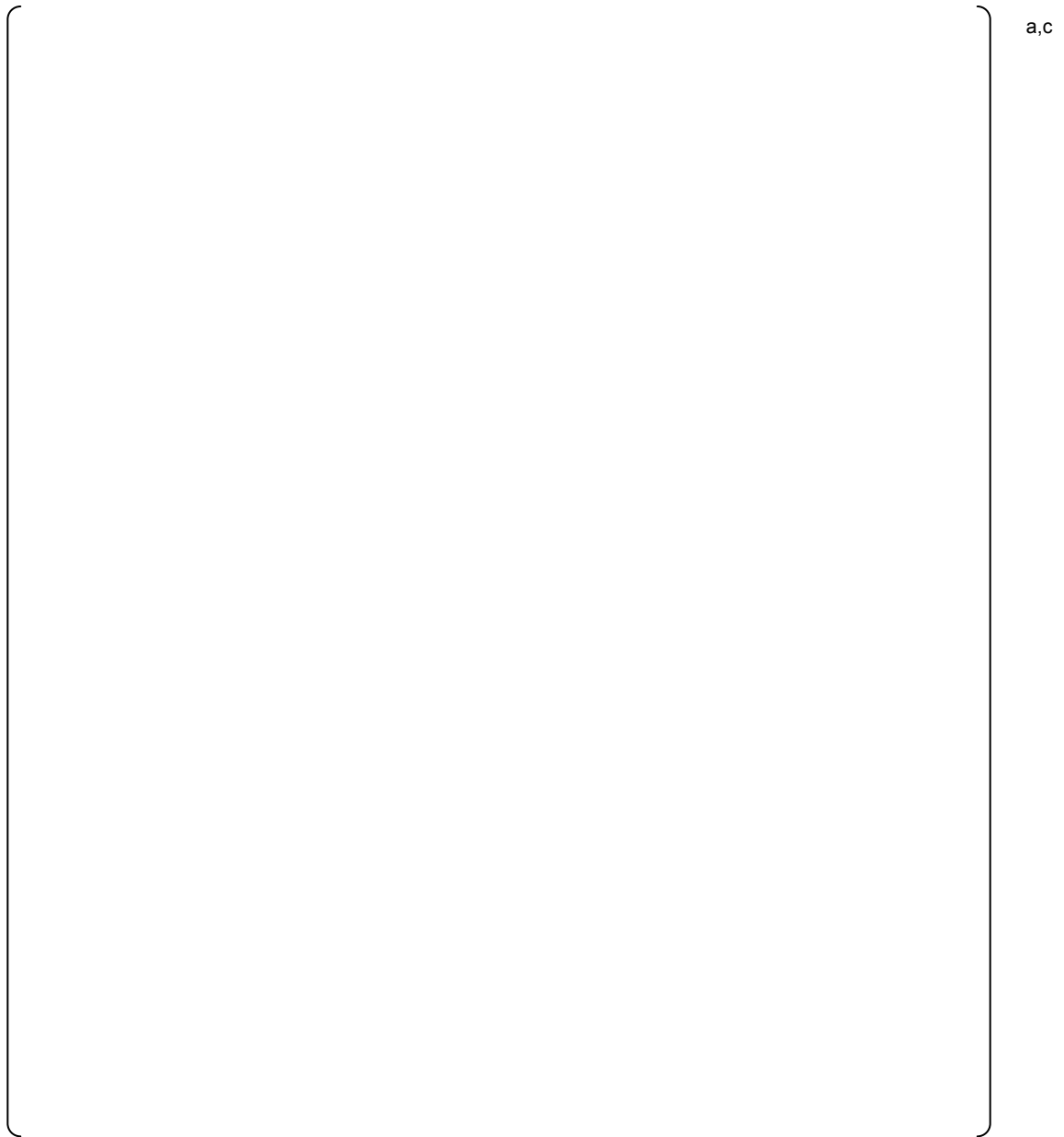


Figure 4-15: Core Differential Pressure for the First 100 Cases of the 311 Case ROSA SB-CL-02 Runset without CD Sampling

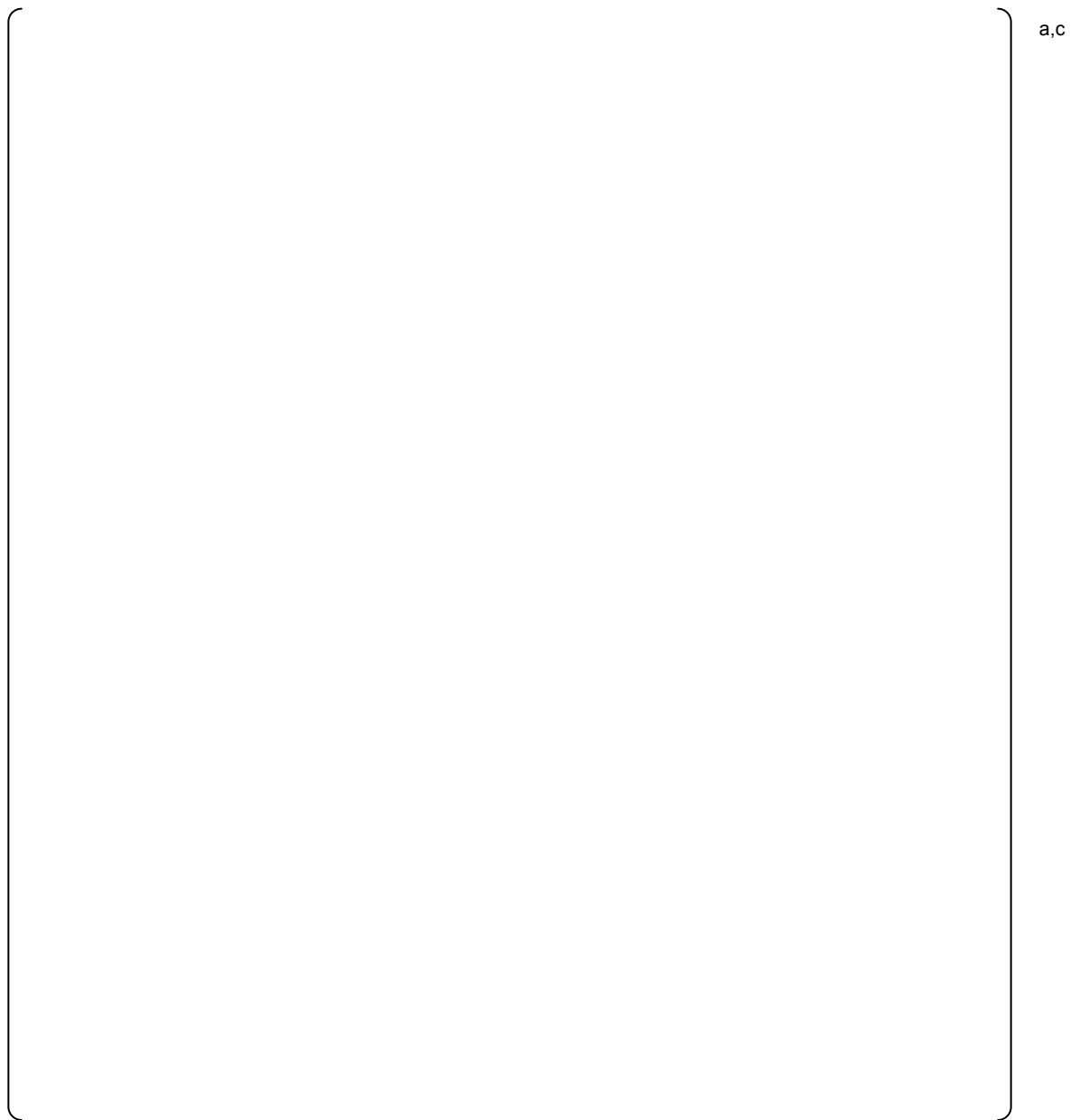


Figure 4-16: Downcomer Differential Pressure for the First 100 Cases of the 311 Case ROSA SB-CL-02 Runset without CD Sampling

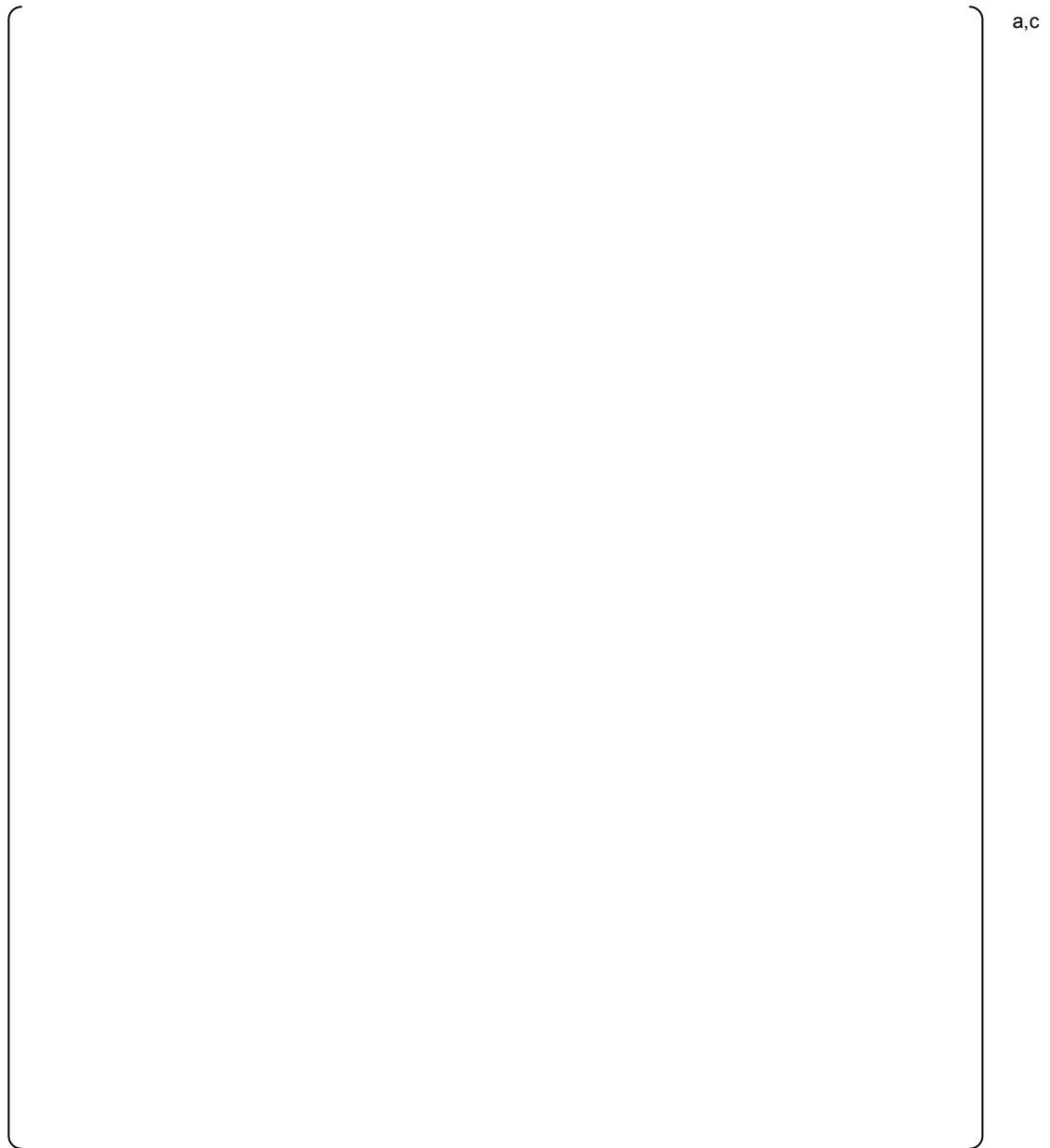


Figure 4-17: Loop Seal A Pump-Side Differential Pressure for the First 100 Cases of the 311 Case ROSA SB-CL-02 Runset without CD Sampling

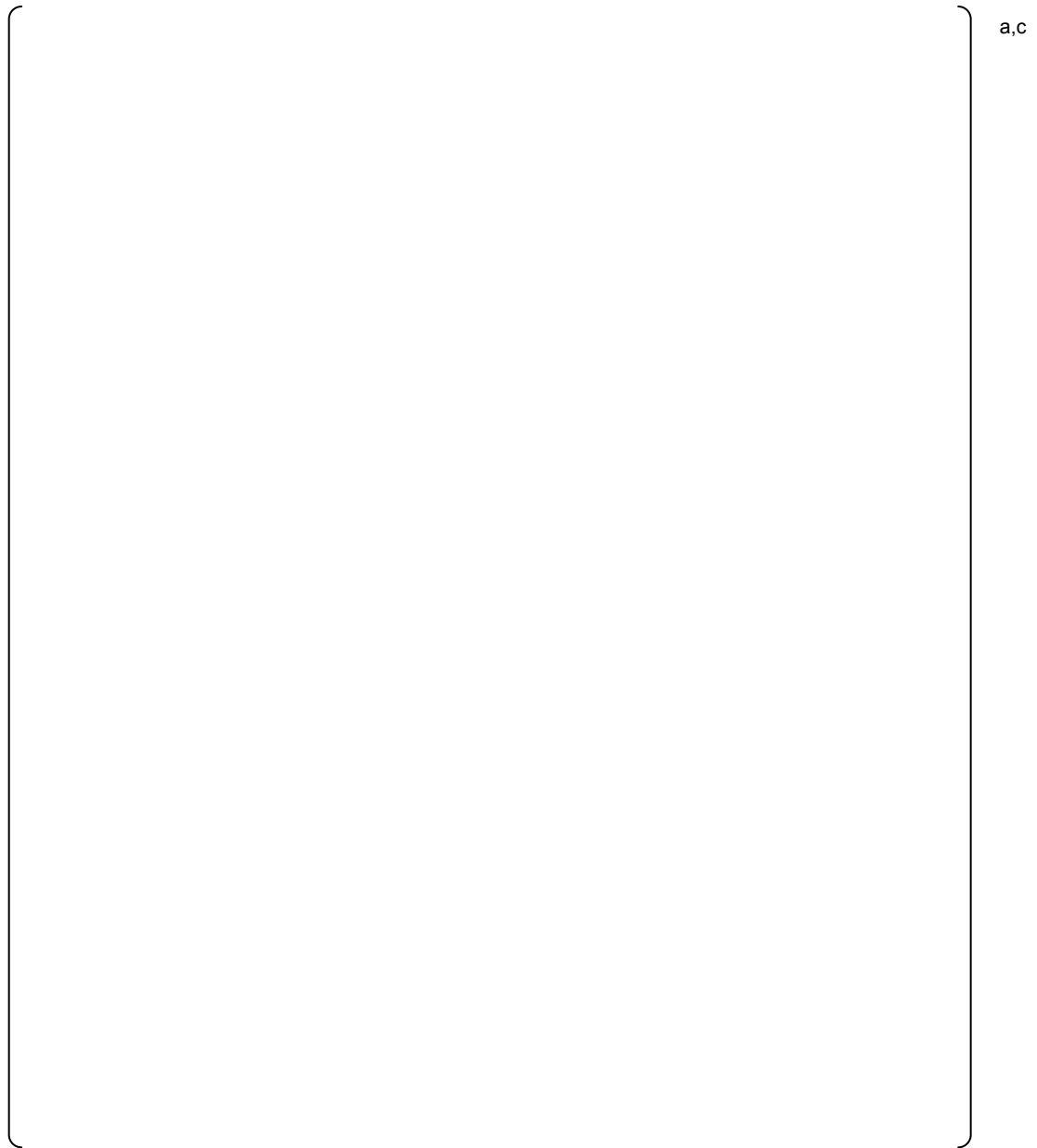


Figure 4-18: Loop Seal B Pump-Side Differential Pressure for the First 100 Cases of the 311 Case ROSA SB-CL-02 Runset without CD Sampling

5.0 Updated Region I Break Sampling Approach

5.1 Background

LTR-NRC-13-45 [5-1] provided the response to RAIs 9 and 12 on the FULL SPECTRUM LOCA methodology topical report [5-2]. During the August 2013 NRC Audit on the FSLOCA methodology, a draft revision to the Region I break area sampling method was presented. The following subsections present the finalized revision to the Region I break area sampling method, which is modified from the approach presented in August 2013.

5.2 Revised Region I Break Area Sampling Method

Section 29.2 of WCAP-16996-P discusses the break area uncertainty treatment for Region I, whereby the break area is sampled []^{a,c} from $A_{I,min}$ to $A_{II,min}$, where $A_{I,min}$ is the smallest break area that the charging pumps can make-up the mass lost out of the break, and $A_{II,min}$ is []^{a,c} As discussed in RAI 9, there exists a small segment (resonance region) between $A_{I,min}$ and $A_{II,min}$ where the core may uncover. The resonance region exists because the transient behavior of a SBLOCA is the result of a race between mass lost out the break and the depressurization of the reactor coolant system (RCS), which results in increased safety injection flow. For the smallest breaks, the mass lost out the break is low, such that the safety injection at the higher pressure (due to the slower depressurization rate) is adequate for keeping the core covered with a two-phase mixture level and mitigating the accident. Likewise, for the larger small breaks, the depressurization rate is fast enough that the increase in safety injection (due to lower pressure) and accumulator actuation are adequate for replenishing the higher mass lost out the break and keeping the core covered with a two-phase mixture level. For the breaks in between (generally 0.0218 ft² (2 inch) to 0.1963 ft² (6 inch)), the depressurization rate is slow enough that the safety injection flow may not be sufficient to keep the core covered with a two-phase mixture level, and core uncover is observed. Since these break areas are most likely to become limiting in Region I, attention should be given to this resonance range within the Region I uncertainty analysis. As such, the Region I break area sampling method, as described in WCAP-16996-P, is revised to []^{a,c}

The revised Region I break area sampling method is divided into two main steps:

[]

[]^{a,c}

The following provides further details for each step.

[]

[]^{a,c}

[

] ^{a,c}

5.3 Example Demonstration of the Revised Region I Break Area Sampling Method

The following provides a sample demonstration of the revised Region I break area sampling method with the Beaver Valley Unit 1 plant model.

[

] ^{a,c}

[

] ^{a,c}**Table 5-2: Results from Step 1 Cases**

a,c



Figure 5-1: Peak Cladding Temperature vs. Effective Break Area for Step 1 Cases

[

] ^{a,c}

a,c

Figure 5-2: Peak Cladding Temperature vs. Effective Break Area for Step 1 and Step 2 Cases

5.4 Conclusions

The revised Region I break area sampling method [

] ^{a,c} In addition, the revised approach adequately captures the large change in PCT with a small change in break area that occurs in the resonance region, and has the ability to demonstrate that the acceptance criteria are met with high probability.

5.5 References

- 5-1) LTR-NRC-13-45, "Submittal of Westinghouse Responses to 'WCAP-16996-P, 'Realistic LOCA Evaluation Methodology Applied to the Full Spectrum of Break Sizes (FULL SPECTRUM LOCA Methodology)' Request for Additional Information – RAIs 9 and 12' (Proprietary/Non-Proprietary), Project 700, TAC No. ME5244," June 26, 2013.
- 5-2) WCAP-16996-P, Volumes I, II and III, "Realistic LOCA Evaluation Methodology Applied to the Full Spectrum of Break Sizes (FULL SPECTRUM LOCA Methodology)," November 2010.
- 5-3) WCAP-12945-P-A, Volume 1, Revision 2, and Volumes 2 through 5, Revision 1, "Code Qualification Document for Best Estimate LOCA Analysis," March 1998.

6.0 Impact of YDRAG on FLECHT SEASET Test 31504

6.1 Background

A question was raised by the NRC Staff during the July 2013 code workshop regarding why the FLECHT-SEASET 31504 case was insensitive to changes in the interfacial drag multiplier (YDRAG). The study's results were examined, and an explanation to the Staff's question is provided below.

6.2 Investigation

Per Section 29.1.5 of WCAP-16996-P [6-1], YDRAG is applied to the []^{a,c}, and is ramped out as the flow transitions to []^{a,c}. As such, YDRAG is not applied when a cell is determined to be in []^{a,c} flow regime.

During reflood (which is at a low system pressure), a cell is determined to be in the hot wall flow regime if any heat transfer node wall temperature in that cell is []^{a,c} above the saturation temperature (Equation 4-1 in WCAP-16996-P). In the FLECHT-SEASET 31504 simulations, the temperature used to determine if a cell is in the hot wall flow regime is []^{a,c} (per Table 14.1-6 of WCAP-16996-P, FLECHT-SEASET 31504 was conducted at a pressure of 40 psia). Since this temperature is lower than the typical quench temperature ([]^{a,c}, Figures 29.1.8-8 to 29.1.8-10 of WCAP-16996-P), a cell is not likely to be in a cold wall flow regime until all the heat transfer nodes in that cell have quenched. This means that the quench front has passed through the cell prior to YDRAG being applied.

This is demonstrated by looking at the void fraction of a cell near the middle of the bundle along with the cladding temperatures near the bottom and top of that cell. Figure 6-1 provides the noding diagram for the FLECHT-SEASET 31504 cases, and Figure 6-2 shows the void fraction for Cell 7 of Channel 2 (inner bundle channel) as well as the cladding temperatures for the heat transfer nodes near the bottom and top of that cell. As seen from the figure, there is []^{a,c}

[]^{a,c}

Figure 24.6.4-7 of WCAP-16996-P compares the void fraction profile of the FLECHT-SEASET 31504 base simulation to test data when the quench front is at 60 inches (5 feet). As seen in Figure 6-2, this also occurs near []^{a,c} in all three YDRAG simulations. A comparison of the void fraction profile at []^{a,c} for the three YDRAG simulations is presented in Figure 6-3, which shows []^{a,c}

[]^{a,c}

Figure 6-4 compares the flow regime through the bundle at []^{a,c}, and shows that []^{a,c}

[]^{a,c}

It is noted that while the void distribution is affected by YDRAG, the [

] ^{a,c} As shown in Figure 6-2, the void fraction in the cell [

] ^{a,c}

Figure 6-5 provides a comparison of the entrained liquid generation rate for cells 6, 7 and 8 of Channel 2. As seen in Figure 6-5, [

] ^{a,c} Based on Figures 6-3 and 6-5, it is concluded that [

] ^{a,c}

6.3 Conclusion

YDRAG is applied to cells which are in [

] ^{a,c}

6.4 References

- 6-1) WCAP-16996-P, Volumes I, II and III, "Realistic LOCA Evaluation Methodology Applied to the Full Spectrum of Break Sizes (FULL SPECTRUM LOCA Methodology)," November 2010.

a,c

Figure 6-1: FLECHT-SEASET 31504 Noding Diagram

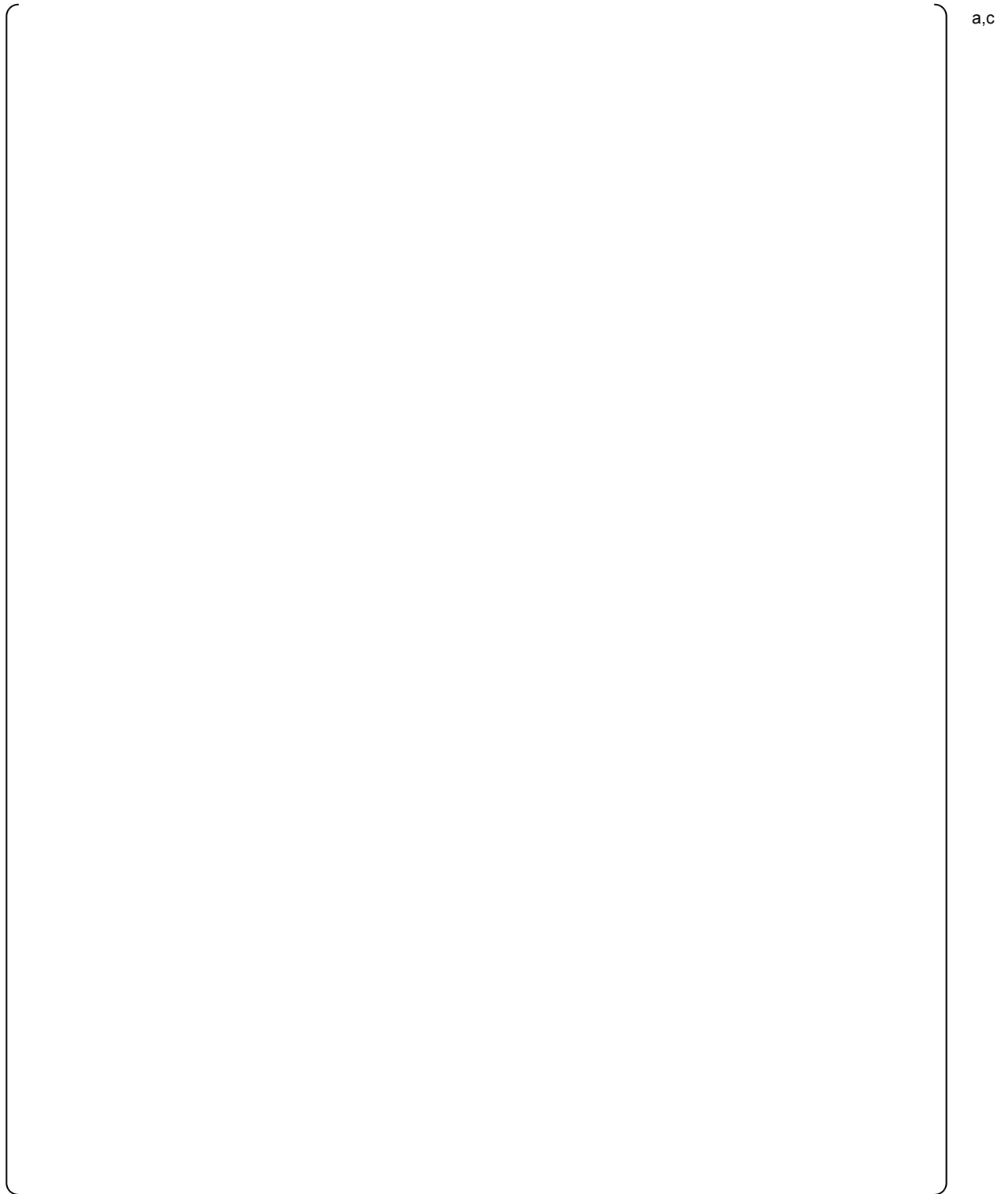


Figure 6-2: Void Fraction and Cladding Temperature for Cell 7 of Channel 2

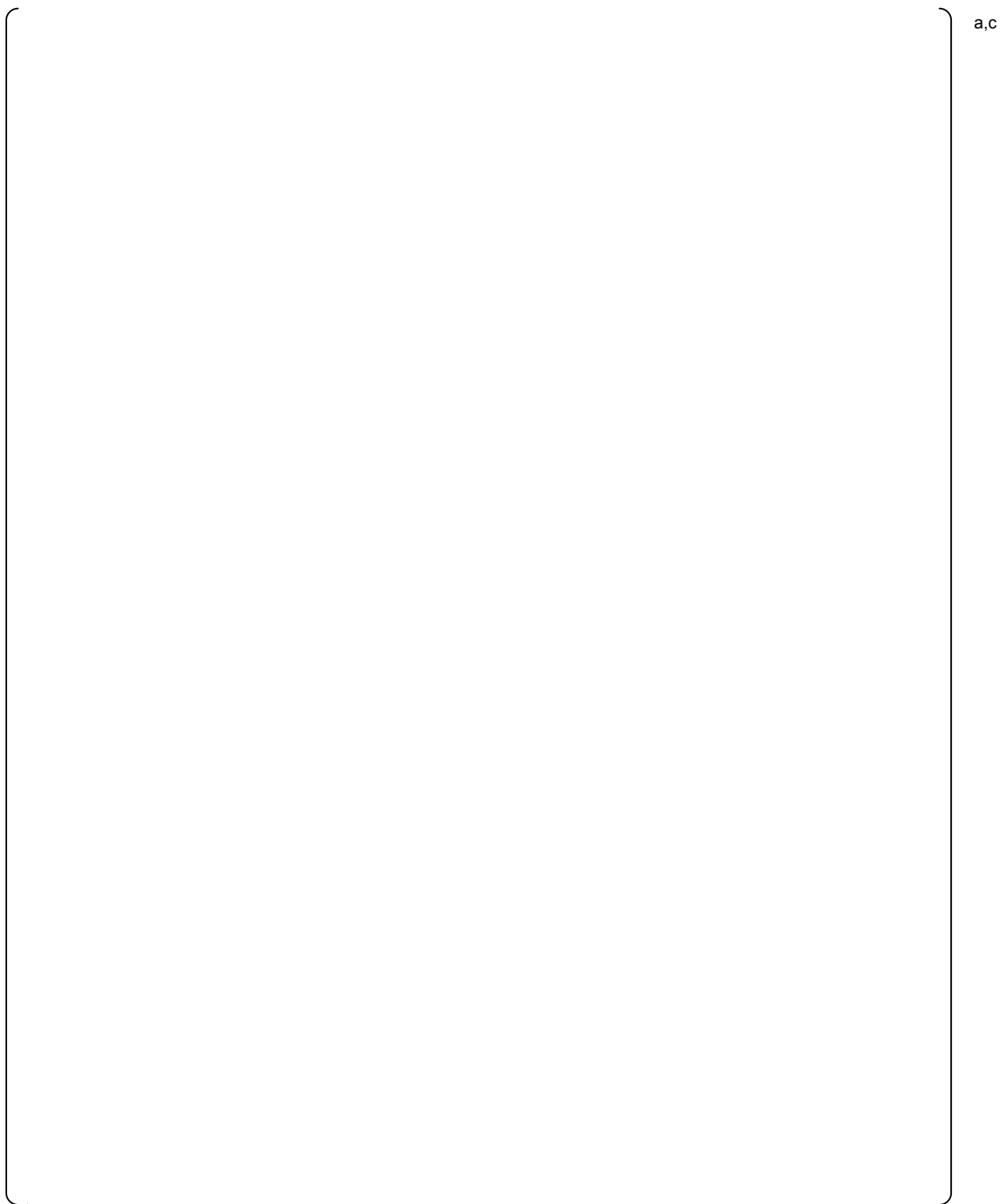


Figure 6-3: Void Fraction Profile for Channel 2 at []^{a,c}

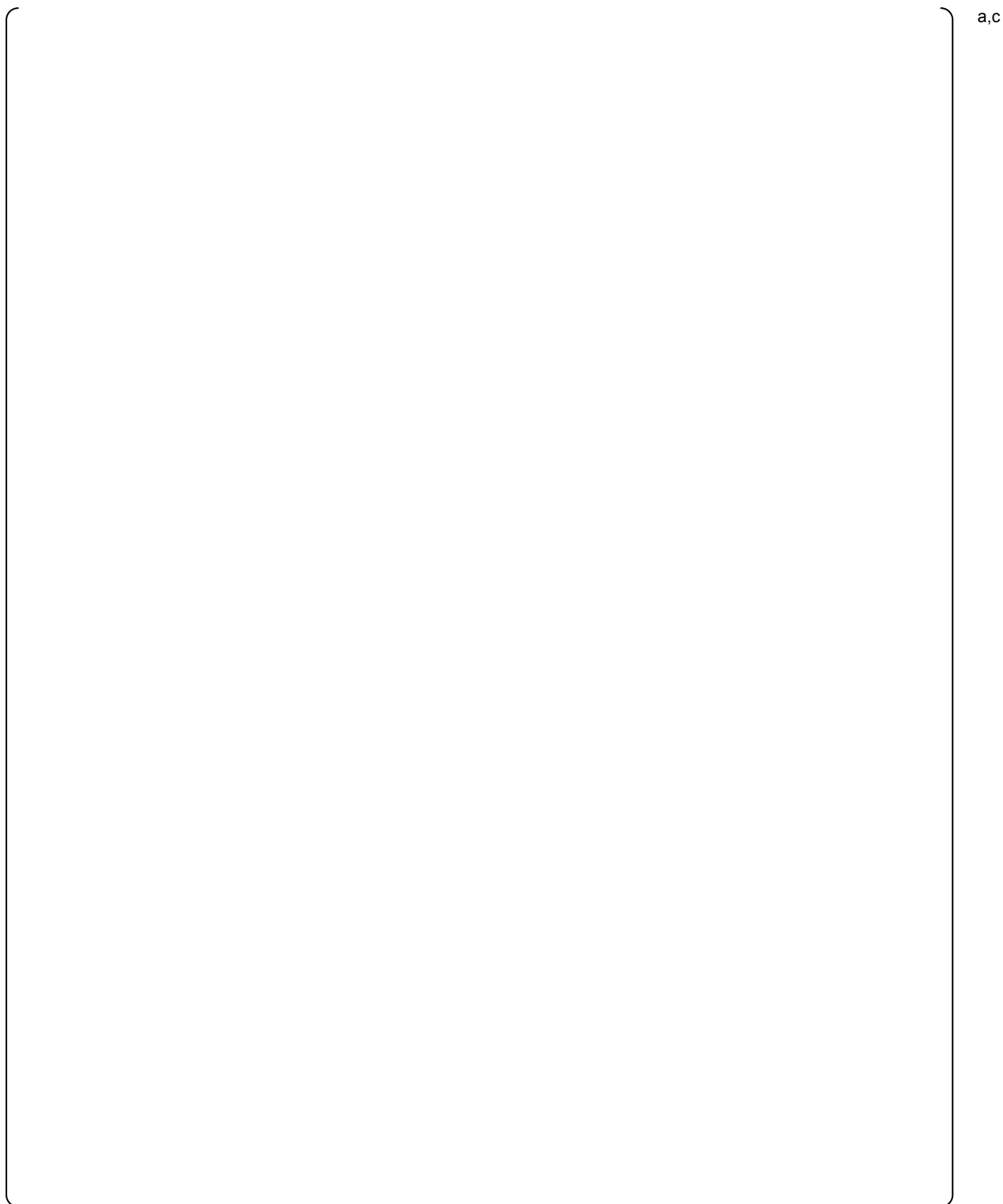


Figure 6-4: Flow Regime Profile for Channel 2 at []^{a,c}

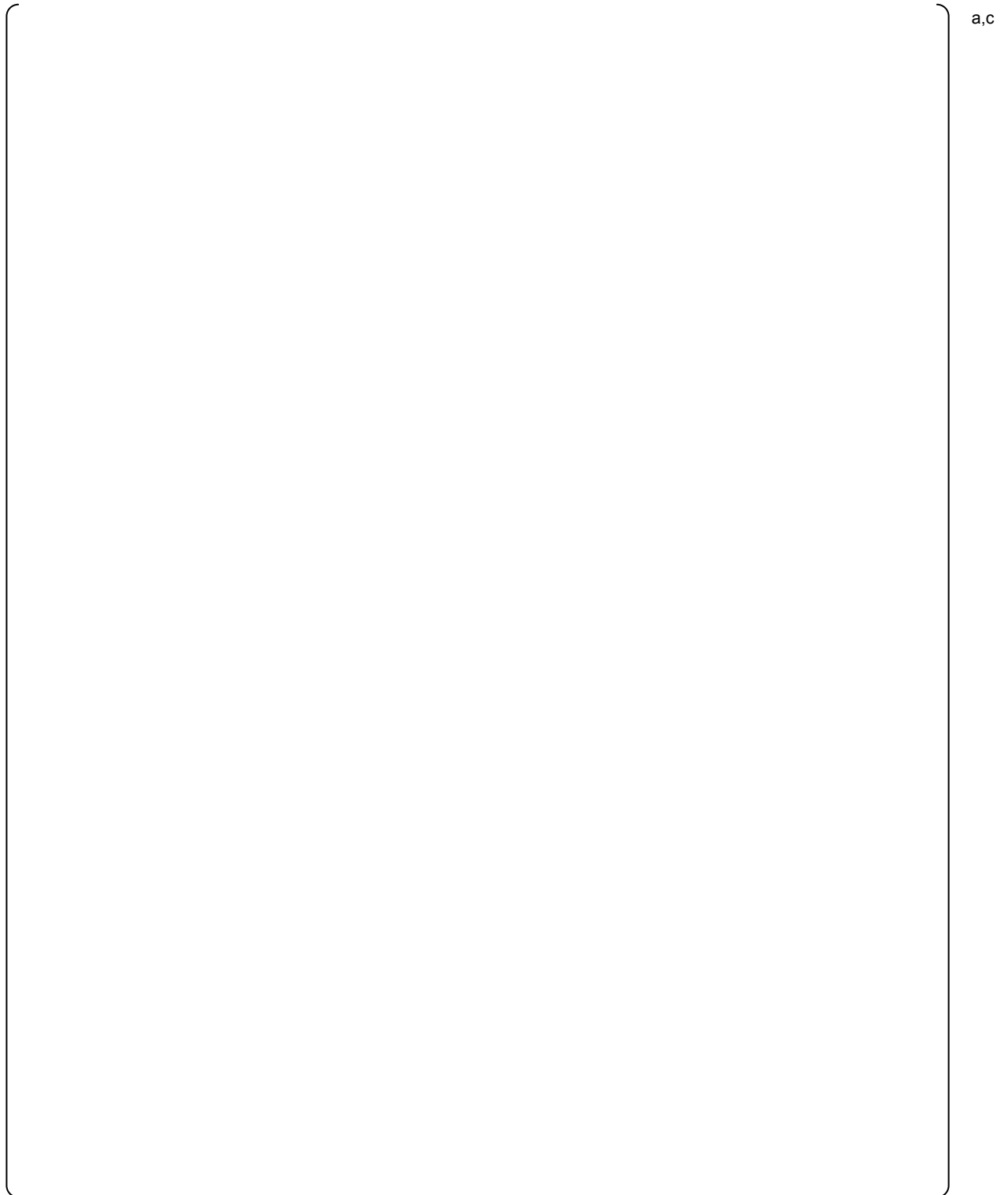


Figure 6-5: Entrained Liquid Generation Rate for Cells 6, 7 and 8 of Channel 2

a,c

Figure 6-6: Total Vessel Mass and PCT

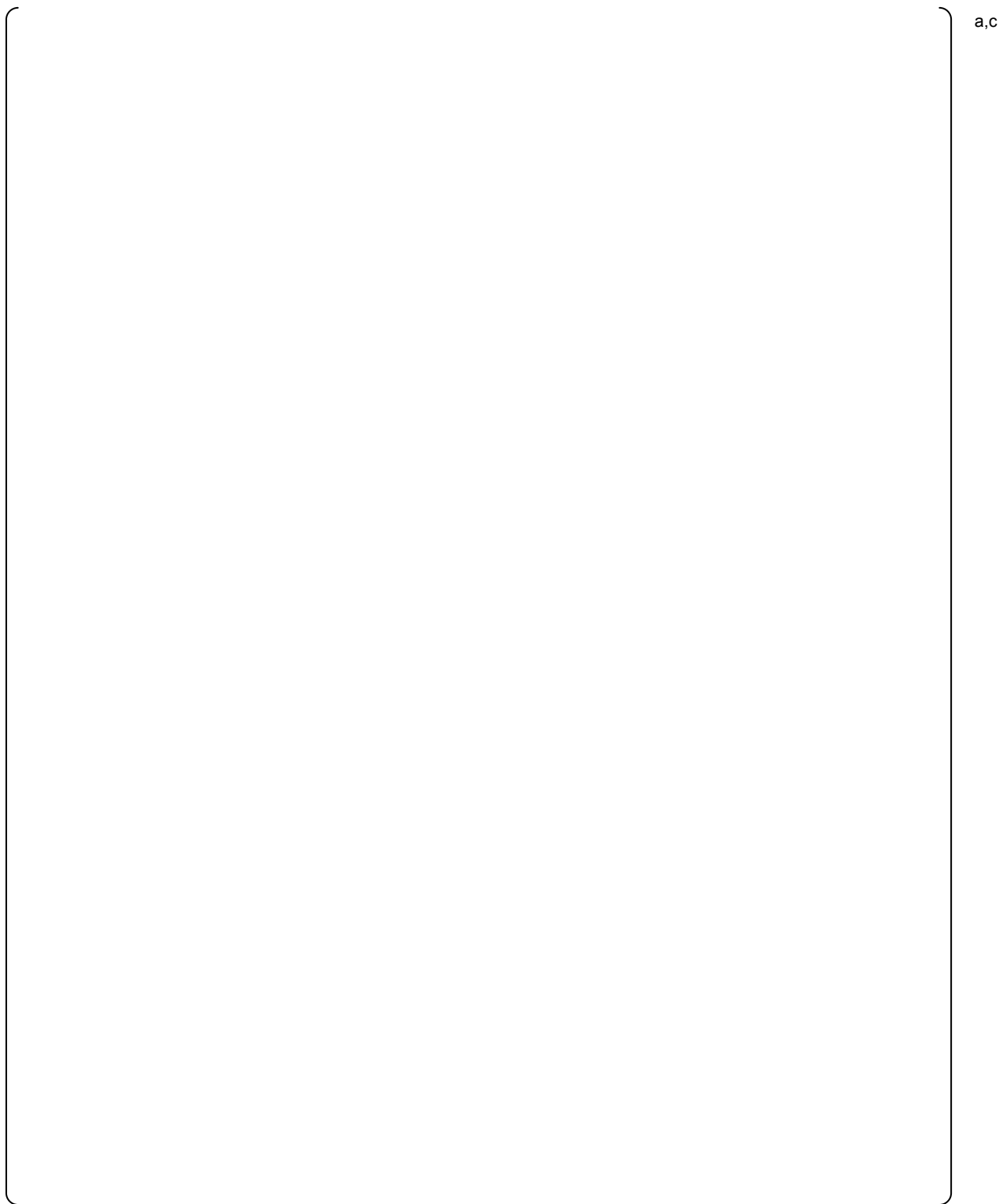


Figure 6-7: Carryover Fraction (Equation 19.5-6 of WCAP-16996-P)

7.0 Crossover Leg Re-Plugging Under LBLOCA Conditions

During the August 2013 NRC audit of the FSLOCA EM, a concern was expressed that the loop seal region could re-plug in the short term under LBLOCA conditions, especially if the break was located at the top of the cold leg piping.

A large split break spectrum was executed for Beaver Valley (presented in Section 27.1.2.1 of WCAP-16996-P [7-1]) with the break oriented at the bottom of the cold leg. This study was then rerun with the break oriented on the top of the pipe.

The resulting split break spectrum studies consider break areas ranging from 1.0 ft² to twice the flow area of the cold leg, with upward and downward oriented breaks. The void fraction at the bottom of the loop seal for all of the base and sensitivity cases was inspected. The figures from the top-oriented break studies with a break area of twice the cold leg area (Figures 7-1 through 7-3) and with a break area of 1.0 ft² (Figures 7-4 through 7-6) are included in this summary.

[

]^{a,c}

7.1 References

- 7-1) WCAP-16996-P, Volumes I, II and III, "Realistic LOCA Evaluation Methodology Applied to the Full Spectrum of Break Sizes (FULL SPECTRUM LOCA Methodology)," November 2010.



Figure 7-1: Void Fraction in the Loop 1 Loop Seal Region for an Upward Oriented Break with a Break Area of Twice the Cold Leg Area



Figure 7-2: Void Fraction in the Loop 2 Loop Seal Region for an Upward Oriented Break with a Break Area of Twice the Cold Leg Area



Figure 7-3: Void Fraction in the Loop 3 Loop Seal Region for an Upward Oriented Break with a Break Area of Twice the Cold Leg Area



Figure 7-4: Void Fraction in the Loop 1 Loop Seal Region for an Upward Oriented Break with a Break Area of 1 Square Foot



Figure 7-5: Void Fraction in the Loop 2 Loop Seal Region for an Upward Oriented Break with a Break Area of 1 Square Foot



Figure 7-6: Void Fraction in the Loop 3 Loop Seal Region for an Upward Oriented Break with a Break Area of 1 Square Foot

8.0 Downcomer Steam-Water Interaction under Intermediate Break LOCA (IBLOCA) and SBLOCA Conditions

The calculation of liquid entrainment and sweepout in the downcomer is important in the simulation of LOCA transients since the downcomer provides the driving head to reflood the core. If the amount of entrainment or liquid sweepout is under-predicted, it could result in increased downcomer inventory, which could lead to an artificially increased liquid level in the core.

Upper Plenum Test Facility (UPTF) Test 25A was designed to study steam-water interaction in the downcomer under LBLOCA reflood conditions. The test was run in four phases, and the test conditions for each phase are presented in Table 19.3-17 of WCAP-16996-P [1]. The test conditions were compared to the conditions for the Beaver Valley Unit 1 SBLOCA and IBLOCA break spectrum cases (Section 27.1.2 of WCAP-16996-P), which covers from 2-inch to 16-inch break diameters. This comparison is presented in Table 8-1.

[

] ^{a,c}

The simulation of UPTF Test 25A with WCOBRA/TRAC-TF2 is discussed in Section 19.3.11 of WCAP-16996-P. [

] ^{a,c}

Some additional information regarding the steam-water interaction in the downcomer under SBLOCA conditions can be extracted from IET facility simulations. For IET facilities, it is recognized that there are a number of phenomena interacting to produce the test data and the simulated result. However, the simulation results can be inspected for indications of an under-prediction of entrainment in the downcomer.

ROSA Test SB-CL-05 is an integral effects test with high head safety injection and a 5% cold leg break. The downcomer differential pressure for the simulation of this experiment is presented as Figure 21.5-15 in WCAP-16996-P. [

] ^{a,c}

ROSA Test SB-CL-14 is an integral effects test without high head safety injection and a 10% cold leg break (no 10% cold leg break test with HHSL was simulated). The downcomer differential pressure cannot be obtained from the available experimental data for this simulation;

however, a comparison of core liquid levels is presented as Figure 21.6-14 in WCAP-16996-P. The concern with excess liquid in the downcomer is that it would provide additional driving head to push liquid into the core. [

] ^{a,c}

8.1 References

- 8-1) WCAP-16996-P, Volumes I, II and III, "Realistic LOCA Evaluation Methodology Applied to the Full Spectrum of Break Sizes (FULL SPECTRUM LOCA Methodology)," November 2010.
- 8-2) Yoon, S. H., et. al., "An Experimental Study of Sweepout and Entrainment in the Advanced Reactor Downcomer," *Proceedings of International Congress on Advanced Nuclear Power Plants (ICAPP)*, Embedded Topical Meeting, June 9-13, 2002.
- 8-3) Yoon, S. H. and Suh, K. Y., "Investigation of Sweepout Mechanism and Critical Void Height in Annular Downcomer," *Journal of Nuclear Science and Technology*, Vol. 40, No. 10, pp. 834-844, October 2003.

Table 8-1: Comparison of Steam Mass Flow Rates, Steam Kinetic Energy, and Kutateladze Numbers between a PWR and UPTF Test 25A

Facility	Intact Loop Steam Flow Rate (lbm/s)	Intact Loop Steam Kinetic Energy (lbm/ft-s ²)	Kutateladze Number (-)	Broken Loop Steam Flow Rate (lbm/s)
[
] ^{a,c}

Presentations from the August NRC Audit

Westinghouse Non-Proprietary Class 3

© 2013 Westinghouse Electric Company LLC. All Rights Reserved.

FULL SPECTRUM LOCA (FSLOCA) Plant Scoping Studies

**Aaron Everhard
Westinghouse Electric Company
August 2013**



Background

- Plant studies were performed to demonstrate code capability
 - List includes studies presented in topical report and response to RAIs

Offsite Power Availability	Break Orientation (SB)
Power Shape	Loop Seal Clearing as function of break size (SB)
Time Step Size	Core Interfacial Drag (YDRAG) (SB)
SG Tube Plugging	Stratification Criterion (HS_SLUG) (SB)
Break Spectrum	Decay Heat (SB)
Accumulator Line Break	Lower SI Flow (SB)
Accumulator Elevation	SG Interfacial Drag (SB)
Break Path Resistance (LB)	Safety Injection Condensation (KCOSI) (SB)
Numerical Perturbations (SB)	SB Limiting Break Size



Studies with V. C. Summer

- []^{a,c} documents the model development

Document	Study Performed
[] ^{a,c}	Break Spectrum (LB, IB, SB)
[] ^{a,c}	Power Shape Offsite Power Availability Time Step Size Accumulator Elevation SG Tube Plugging Break Path Resistance (LB) Lower SI Flow (SB) Break Orientation (SB) Stratification Criterion (HS_SLUG) (SB) Safety Injection Condensation (KCOSI) (SB) Core Interfacial Drag (YDRAG) (SB) Loop Seal Clearing with Break Size (SB) SG Interfacial Drag (SB)
[] ^{a,c}	Demonstration Analysis

Studies with Beaver Valley Unit 1 (1/2)

- []^{a,c} documents the model development

Document	Study Performed
[] ^{a,c}	Break Spectrum (LB, IB, SB)
[] ^{a,c}	Power Shape Offsite Power Availability Time Step Size Accumulator Line Break Break Path Resistance (LB) Break Orientation (SB) Stratification Criterion (SB) Safety Injection Condensation (SB) Core Interfacial Drag (SB) Loop Seal Clearing with Break Size (SB) SG Interfacial Drag (SB)



Studies with Beaver Valley Unit 1 (2/2)

Document	Study Performed
[] ^{a,c}	Numerical Perturbations on stratification criterion and wall drag (SB)
[] ^{a,c}	SB limiting break size
[] ^{a,c}	Parametric study on select parameters (SB) Conservative case (SB)
[] ^{a,c}	Steady-State



Questions



Westinghouse Non-Proprietary Class 3

© 2013 Westinghouse Electric Company LLC. All Rights Reserved.

Full Spectrum LOCA (FSLOCA) Development and Validation of High Importance Phenomena

**Jeffrey Kobelak
Westinghouse Electric Company
August 2013**



Background

- Models were added and/or validation was completed for WCOBRA/TRAC-TF2 to capture several new key phenomena relative to SBLOCA Analysis
 - Mixture Level Swell
 - Loop Seal Clearing
 - Horizontal Stratification
 - Cold Leg Condensation



Mixture Level Swell

- Prediction of two-phase mixture level in the core is significant for the analysis of the SBLOCA transient
- [λ]^{a,c} as described in the response to RAI #17 (LTR-NRC-13-37)
- Code validated against Oak Ridge National Lab (ORNL), G1, G2, Two-Phase Test Facility (TPTF), and Semiscale facilities



Mixture Level Swell

- Facility Models
 - G1 Facility: []^{a,c}
 - G2 Facility: []^{a,c}
 - ORNL Facility: []^{a,c}
 - TPTF Facility: []^{a,c}
- Level Swell Test Simulations and Results
 - All Facilities except Semiscale: []^{a,c}
 - Semiscale SET: []^{a,c}
- Sensitivity Study
 - ORNL/PWR Axial Noding: []^{a,c}
 - ORNL Timestep Size: []^{a,c}



Loop Seal Clearing

- Timing of loop seal clearing, the number of loop seals that clear, and the residual liquid in the loops that clear impact the core uncover progression for a SBLOCA transient
- [
$$]_{a,c}$$
- Code validated against Upper Plenum Test Facility (UPTF) loop seal experiments



Loop Seal Clearing

- []_{a,c}
- Facility Model and Test Simulations
 - UPTF: []_{a,c}



Cold Leg Condensation

- Amount of condensation in the cold leg can influence de-pressurization and core uncover behavior for SBLOCA transients
- Cold leg condensation model added to WCOBRA/TRAC-TF2
- Code validated against COSI and UPTF cold leg condensation experiments
- Details provided in later presentation



Horizontal Stratification

- Model Development
 - Horizontal Stratification Model: []^{a,c}
- Implementation of Model into Code
 - Horizontal Stratification Model: []^{a,c}
- Facility Model and Test Simulations
 - TPTF: []^{a,c}



Conclusions

- Models for High Importance Phenomena have been included in the WCOBRA/TRAC-TF2 code
- Validation of code predictions against experimental data performed for the High Importance Phenomena
 - Confirmed code model performance is acceptable
 - Investigating a few remaining items as part of RAI responses



Questions



Westinghouse Non-Proprietary Class 3

© 2013 Westinghouse Electric Company LLC. All Rights Reserved.

Full Spectrum LOCA (FSLOCA) Modeling Guidance

**Jeffrey Kobelak
Westinghouse Electric Company
August 2013**



Background

- Noding Philosophy
- Model Development
 - Vessel Model
 - Loop Model
 - Containment Model



Noding Philosophy

- [

]a,c

- Overall noding scheme was confirmed to be acceptable and consistent



Production WCOBRA/TRAC Noding

- Evaluation Model Topicals: WCAP-12945-P-A, WCAP-16009-P-A
- Safeguards Engineering Standards

Vessel	Loop
[
]a,c



FSLOCA Noding / Model Development

- During the development of FSLOCA, [
]a,c
- The TF2 User's Manual, [
]a,c was also maintained
- Test Facility and PWR Noding is described in the Evaluation Model Topical: WCAP-16996-P
- []a,c describes the conversion of a production code PWR model to a model for FSLOCA



FSLOCA PWR Models

- Beaver Valley
 - []^{a,c} Production Code Vessel Model
 - []^{a,c} Production Code Loop Model
 - []^{a,c} Model Updates for FSLOCA
- V. C. Summer
 - []^{a,c} Production Code Vessel and Loop Model
 - []^{a,c} Modifications for Upflow Conversion
 - []^{a,c} Model Updates for FSLOCA



Containment Model

- COCO Separate from WCOBRA/TRAC for Production Analyses
 - []^{a,c} COCO_A User's Manual
 - []^{a,c} COCO Input for BASH
 - []^{a,c} Updates to COCO Input for BELOCA
- COCO was incorporated into WCOBRA/TRAC-TF2 for FSLOCA
 - Input Differences Described in the TF2 User's Manual []^{a,c}



Questions



Westinghouse Non-Proprietary Class 3

© 2013 Westinghouse Electric Company LLC. All Rights Reserved.

FULL SPECTRUM LOCA (FSLOCA) Region I Break Sampling

**Aaron Everhard
Westinghouse Electric Company
August 2013**



Outline

- Background
- Previous Region I Break Area Sampling Method
- Revised Region I Break Area Sampling Method



Background (1/2)

- Historically, break size is a legitimate variable during a LOCA event
- Sampling methodology is selected to adequately bound realistic break frequencies
 - A 'realistic' break area sampling would give much more probability weight to smaller break sizes, and this reality is not credited in defining the event



Background (2/2)

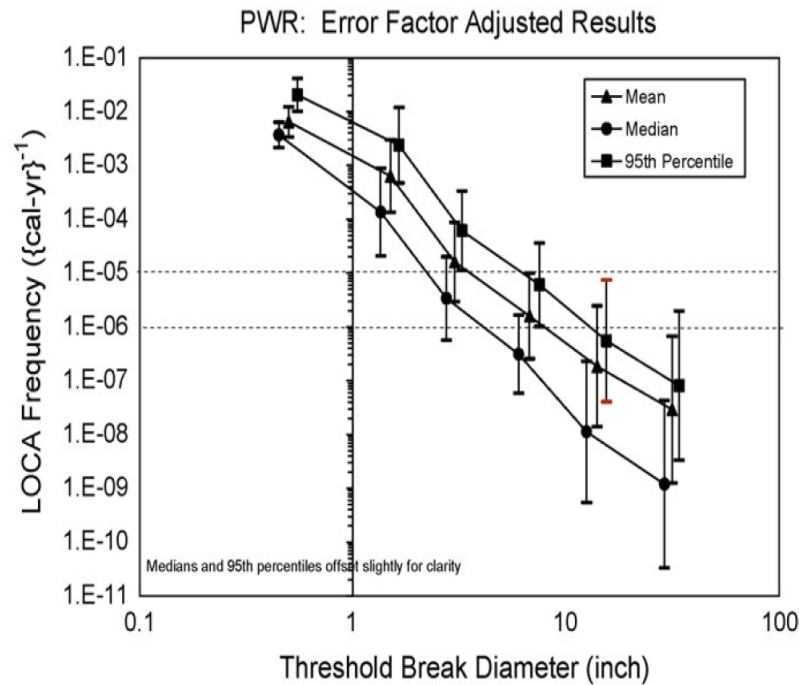
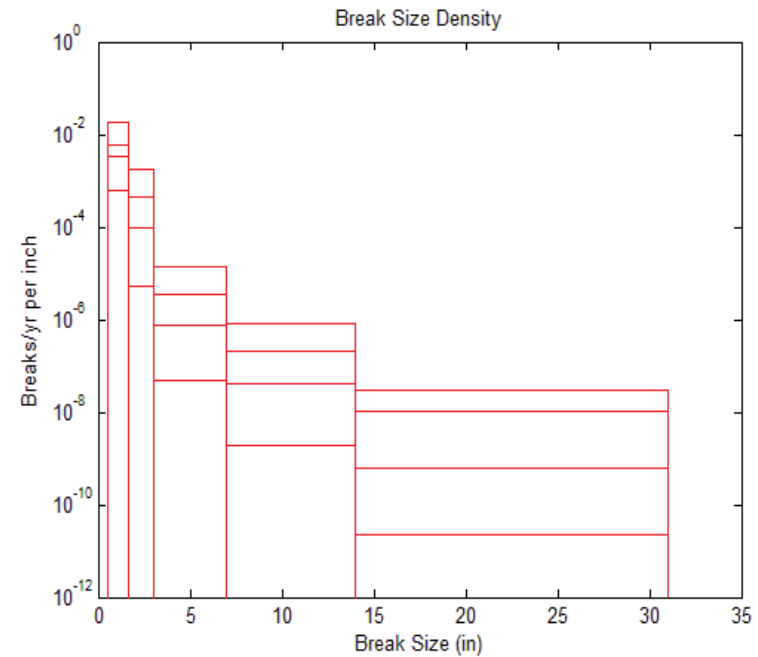


(Figure 7.37 of NUREG-1829 V1)



(from Los Alamos National Lab presentation, May 9, 2012 ACRS transcripts)



Previous Region I Break Area Sampling Method

- Minimum break area defined as the break area where safety injection is adequate to make up loss of mass out the break
 - A_{MIN} , see Section 31.1.1 of WCAP-16996-P for an example
- [

]a,c



Revised Region I Break Area Sampling Method

- [

]a,c



Westinghouse Non-Proprietary Class 3

© 2013 Westinghouse Electric Company LLC. All Rights Reserved.

[



]a,c



Westinghouse Non-Proprietary Class 3

© 2013 Westinghouse Electric Company LLC. All Rights Reserved.

[

]a,c



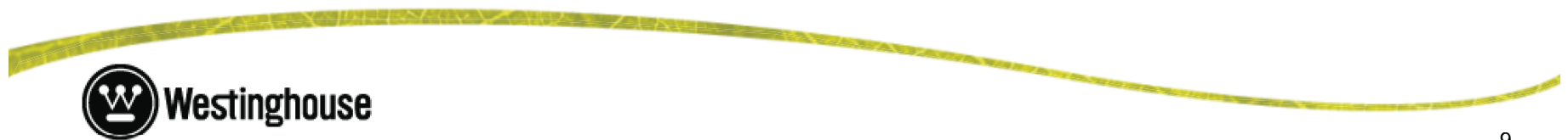
Westinghouse Non-Proprietary Class 3

© 2013 Westinghouse Electric Company LLC. All Rights Reserved.

[



]a,c



Conclusions

- [

]a,c

- Revised method considered adequate for demonstrating that the acceptance criteria are met with a high probability



Questions



Westinghouse Non-Proprietary Class 3

© 2013 Westinghouse Electric Company LLC. All Rights Reserved.

Roadmap of ROSA Large Scale Test Facility Test Simulations for the Westinghouse Full Spectrum LOCA (FSLOCA) Methodology

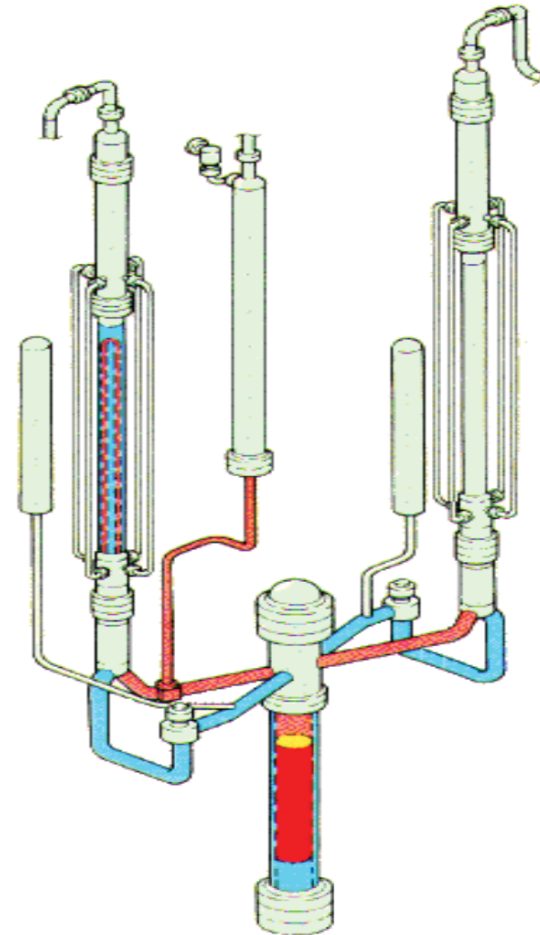
**Nikolay Petkov
Westinghouse Electric Company
August 2013**



JAERI ROSA-IV Large Scale Test Facility

Objectives:

- Conduct large scale integral simulations of PWR SBLOCA and operational transients.
- Provide data to support development and verification of advanced computer codes for PWR accident and transient simulations.
- Investigation of plant recovery methods – operator procedures and equipment to be used on the plant to mitigate SBLOCA transients.



JAERI ROSA-IV Large Scale Test Facility

Design Philosophy:

- Elevations preserved, i.e., one-to-one match to 4-loop Westinghouse PWR.
- Volumes scaled to 1/48 of the PWR volume.
- Flow areas are scaled to 1/48 in the vessel and 1/24 in the steam generators.
- Hot and cold legs scaled to conserve the $L/(D)^{1/2}$ ratio (which is in essence a Froude number) for better manifestation of the flow regime transition in the primary loop.



JAERI ROSA-IV Large Scale Test Facility

Design Philosophy:

- Nominal core power is 10 MW(t) - this is 14% of representative 3423 MW(t) PWR power scaled by a factor of 1/48.
- Core simulator heaters designed to represent 17x17 PWR assembly to preserve the heat transfer characteristics of the core, number of rods scaled to 1/48 of the PWR.
- Pressures (primary and secondary) are similar to PWR.
- Pressure losses designed to match the PWR for the scaled flow rates



JAERI ROSA-IV Large Scale Test Facility

Design Philosophy:

- Each steam generator (SG) has the same height and characteristic elevations as the real PWR steam generator,
- 141 U-tubes with diameter similar to the real SG
- Primary and secondary steam separators,
- SG downcomer is simulated by four pipes, sized to provide a representative downcomer volume and width of the real PWR SG.



ROSA-IV LSTF Model Development and Test Simulations

Topic	Supporting Calcnote
Development of the ROSA-IV LSTF Steady State vessel (3-D) and loop (1-D) model.	[] ^{a,c}
Simulations of the ST-NC-02 natural circulation test	[] ^{a,c}
Various simulations of the 5% cold leg break tests SB-CL-18 and SB-CL-05	[] ^{a,c}
Simulations of ROSA break orientation tests (0.5% and 2.5% breaks)	[] ^{a,c}



Roadmap of Section 21 of the FSLOCA Topical Report WCAP-16996-P

Topical Section	Supporting Calcnote
21.1 - Introduction	N/A
21.2 – Test Facility Description	N/A
21.3 – Description of ROSA Model	[] ^{a,c}
21.4 – Simulation of SB-CL-18	[] ^{a,c}
21.5 – Simulation of SB-CL-05	[] ^{a,c}
21.6 – Simulation of 10% Side Break SB-CL-14	[] ^{a,c}
21.7 – Break Orientation Study	[] ^{a,c}



Roadmap of Section 21 of the FSLOCA Topical Report WCAP-16996-P

Topical Section	Supporting Calcnote
21.8 – Break Spectrum Study	Based on previous sections
21.9 – Simulation of ST-NC-02, 2% Power Natural Circulation Test	[] ^{a,c}
21.10 – CCFL Results and Evaluation	Data extracted from simulations of tests documented in previous sections
21.11 – Bypass Sensitivity Calculations	SB-CL-18 simulations; [] ^{a,c}
21.12 – CD1 Sensitivity	SB-CL-18 simulations; [] ^{a,c}



Roadmap of Section 21 of the FSLOCA Topical Report WCAP-16996-P

Topical Section	Supporting Calcnote
21.13 – CD2 Sensitivity	SB-CL-18 simulations; [] ^{a,c}
21.14 – Broken Loop Pump Resistance	SB-CL-18 simulation; transient in [] ^{a,c}
21.15 – YDRAG Sensitivity	SB-CL-18 simulation; [] ^{a,c}
21.16.1 – HS_SLUG Sensitivity with SB-CL-16	SB-CL-16 simulation; [] ^{a,c}
21.16.2 – HS_SLUG Sensitivity with SB-CL-18	SB-CL-18 simulation; [] ^{a,c}
21.16.3 – HS_SLUG Sensitivity with SB-CL-14	SB-CL-14 simulation; [] ^{a,c}



Roadmap of Section 21 of the FSLOCA Topical Report WCAP-16996-P

Topical Section	Supporting Calcnote
21.17 – KCOSI Sensitivity Calculations	SB-CL-05 simulation; cases from [] ^{a,c}
21.18 – MSSV Setpoint Sensitivity Calculation	Comparison of 0.5% side break SB-CL-15 simulations; Cases from [] ^{a,c}



Questions



Westinghouse Non-Proprietary Class 3

© 2013 Westinghouse Electric Company LLC. All Rights Reserved.

Full Spectrum LOCA (FSLOCA) Overview

**Jeffrey Kobelak
Westinghouse Electric Company
August 2013**



Overview

- Desired Scope of Approval
 - Technical Work for Evaluation Model (EM) Extension
 - Usage Conditions and Limitations
- Westinghouse Status of RAI Responses
- Burnup Methodology



Desired Scope of Approval

a,c



Technical Work Scope for EM Extension

- [

]a,c



Technical Work Scope for EM Extension

- [

]a,c



Applicability Limits

- [

]a,c



Usage Conditions

- [

]a,c



Status of RAI Responses

- Sets 1 Through 4
 - Responses completed and formally transmitted to NRC except RAIs 36-39
 - Ongoing effort to address RAIs 36-39 necessitated changes to the burnup methodology
 - Expect EM updates to be completed along with TR Volume 3 updates by March 2014
 - RAI-45
 - CCTF-62 311-case runset previously transmitted to the NRC (part of LTR-NRC-13-40)
 - Beaver Valley Steady-State cases completed and will be discussed later in audit



Status of RAI Responses

- Set 5 (Primarily Interfacial Drag and Level Swell)
 - Responses completed for RAIs 72 through 74 and 76
 - Developing responses for other Set 5 RAIs
 - Will include pertinent information from the July 2013 code workshop and supplemental investigations
 - RAI-76
 - [

]a,c



Status of RAI Responses

- Set 6
 - Started developing responses to a subset of these RAIs at-risk (ROSA and loop seal clearing)
 - Waiting for formal transmittal of RAI set
- Sets 7 and 8
 - Waiting for formal transmittal of RAI sets
 - Expect subset of RAIs may no longer be relevant based on July and August NRC/Westinghouse discussions
 - E.g. Semiscale-related RAIs 109 to 111



TCD and Burnup Methodology

- Automated Statistical Treatment of Uncertainty Method (ASTRUM) EM modeled the hot rod / hot assembly as fuel in the first cycle of irradiation
- Same modeling approach was used in FSLOCA
 - Approach was developed prior to consideration of fuel pellet TCD
- ASTRUM TCD evaluations and FSLOCA Large Break scoping results indicate that limiting results can occur during first or second cycle of irradiation



TCD and Burnup Methodology

- Methodology updates in-progress to include TCD and revise burnup treatment
 - Use fuel rod performance data which explicitly includes the effect of TCD
 - Analyze fuel in first and second cycle of irradiation
 - [

]a,c

- Neutronics and fuel rod inputs will be updated consistent with the changes to burnup methodology (e.g. peaking factor burndown)
- Limited amount of model improvements
 - e.g. power distribution modeling approach



TCD and Burnup Methodology

- Proactively adding provisions for some burnup-related cladding embrittlement mechanisms in advance of codification
 - Embrittlement mechanisms include
 - Interior cladding oxygen pickup
 - Breakaway oxidation
 - Cladding corrosion
 - Inclusion of these items can only penalize the analysis results, and provide additional assurance that cladding ductility is protected for current 10 CFR 50.46 acceptance criteria



Questions



Westinghouse Non-Proprietary Class 3

© 2013 Westinghouse Electric Company LLC. All Rights Reserved.

Full Spectrum LOCA (FSLOCA) Cold Leg Condensation Model

**Katsuhiro Ohkawa
Westinghouse Electric Company
August 2013**



Background

- Amount of condensation in the cold leg can impact de-pressurization and vessel inventory which would have significant influence on core uncover behavior for SBLOCA transients – TR-Section 2 PIRT
- Models were added in WCT-TF2 to capture condensation enhancement by Safety Injection which was identified as key phenomena relative to SBLOCA Analysis - CNs
- Validation was completed and Uncertainty Range/Distribution was identified - CNs



Cold Leg Condensation

- Cold leg condensation model was developed based on subset of Westinghouse-COSI data and was added to WCOBRA/TRAC-TF2
- Code was validated against
 - COSI data (both Westinghouse and Framatome)
 - ROSA-IV (SET and IET modes)
 - UPTF 8A cold leg condensation experiment
 - UPTF25A cold leg condensation experiment



Cold Leg Condensation Model related Calculation Notes

- Cold Leg Condensation Model Development – [
]a,c
- Implementation of Model into WCOBRA/TRAC-TF2 – [
]a,c
- Facility Test Simulations – [
]a,c
 - Westinghouse Model and COSI (Vertical and Horizontal)
 - Framatome COSI (Co-current and Inverse)
 - JAERI ROSA-IV SB-CL-05 (SET)
 - Development of Uncertainty
- JAERI ROSA-IV SB-CL-05 (IET) – [
]a,c



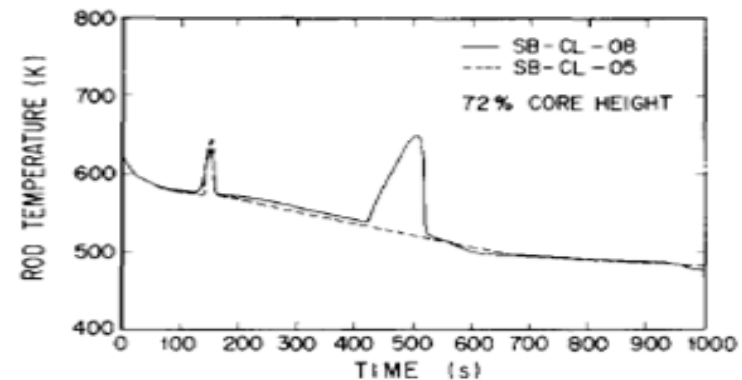
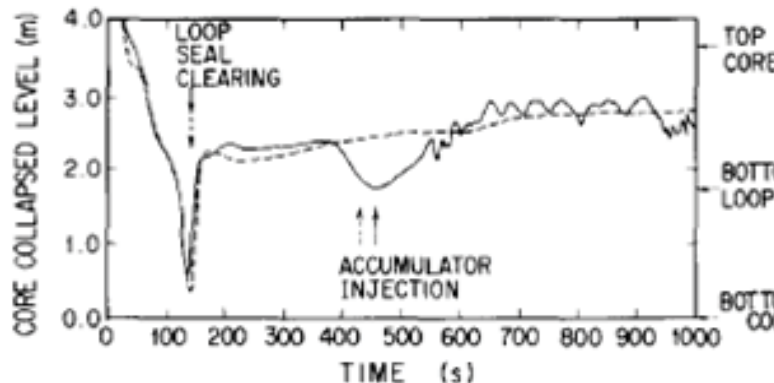
Responses to RAI-30 through 35 and Additional Information

- RAI-30 through 35 addressed additional question of the model applicability for PWR transients: []^{a,c}
- Examination of Scaling of Geometry and other relevant parameters (Dia., Area, Length, Superficial Velocity, Reynolds number of CL and of SI line, Froude number of SI line)
- Moderate Scale Distortion in SI jet Reynolds number – bias accounted for by the KCOSI multiplier
- Scaling analysis + Validation matrix covering wide range of CL diameter, SI flow rate, and SI Reynolds number support scalability to PWR



SI on/off - SB-CL-05 vs. SB-CL-18 in the Topical Report Section 21

- Similar Comparison seen in Tasaka (1988 NED) who compared SB-CL-08 VS. SB-CL-05



- Small impact on the depressurization
- Difference is seen in the coolant inventory in the core



Additional KCOSI Sensitivity Runs

- [

]a,c

a,c



Additional KCOSI Sensitivity Runs

• []^{a,c}

a,c



Additional KCOSI Sensitivity Runs

- [

]a,c

a,c



9

Additional KCOSI Sensitivity Runs

- [

]a,c

a,c



Westinghouse Non-Proprietary Class 3

© 2013 Westinghouse Electric Company LLC. All Rights Reserved.

SI on/off - SB-CL-05 vs. SB-CL-18: Coolant Inventory in Core

a,c



Westinghouse Non-Proprietary Class 3

© 2013 Westinghouse Electric Company LLC. All Rights Reserved.

SI on/off - SB-CL-05 vs. SB-CL-18: Max Cladding Temperature

a,c



Questions



Westinghouse Non-Proprietary Class 3

© 2013 Westinghouse Electric Company LLC. All Rights Reserved.

Issues Discussed in July 2013 NRC Code Workshop

**Jeffrey Kobelak
Aaron Everhard
Westinghouse Electric Company
August 2013**



Overview

- Beaver Valley SS and ROSA Transient Studies
- Anomalous Grid Behavior in G2 Level Swell Test
- []^{a,c}
- Decay Heat Uncertainty Sampling
- Forslund-Rohsenow Model
- Beaver Valley Parametric Study
- Other Issues Still Under Investigation



Beaver Valley and ROSA Studies

- Completed runset of Beaver Valley steady-state cases
 - Results will be presented on Thursday
- Large runset of ROSA transients in-progress



Grid Behavior in G2 Level Swell

- [

]a,c



Grid Behavior in G2 Level Swell



[]^{a,c} Impact on ORNL Test CC

- []

]a,c



[]^{a,c} Impact on ORNL Test CC

a,c



Decay Heat Uncertainty Sampling

- [

]a,c



Decay Heat Uncertainty Sampling

a,c



9

Forslund-Rohsenow Correlation

- Direct contact heat transfer to the entrained field is based on Forslund-Rohsenow
- NRC expressed concern with modeling direct contact heat transfer with droplets
 - Model will be updated to remove the direct heat transfer to droplets
 - Heat transfer multiplier distributions will be revisited



Beaver Valley Study Background

- []^{a,c} presented in February 2013 Meeting
- Performed a parametric study on the following 4 parameters
 - Decay heat increased 20%
 - YDRAG cut in half → []^{a,c}
 - Cold leg condensation at SI location cut in half []^{a,c}
 - Cold leg condensation at SI location turned off []^{a,c}
- Ran an additional case with parameters biased in a conservative direction
- Repeated all 5 cases with the SI reduced by 25%



Main Parameters Varied (1/4)

[
						a,c



Main Parameters Varied (2/4)

[
						a,c



Main Parameters Varied (3/4)

[
						a,c



Main Parameters Varied (4/4)

[
						a,c



Westinghouse Non-Proprietary Class 3

© 2013 Westinghouse Electric Company LLC. All Rights Reserved.

Results – Nominal SI Case

[]^{a,c}

a,c



Westinghouse Non-Proprietary Class 3

© 2013 Westinghouse Electric Company LLC. All Rights Reserved.

Results – Nominal SI Case

[]^{a,c}

a,c



Results – Nominal SI Case

[]a,c

a,c



Results – Nominal SI Case

[]a,c

a,c



Westinghouse Non-Proprietary Class 3

© 2013 Westinghouse Electric Company LLC. All Rights Reserved.

Results – Nominal SI Case

[]a,c

a,c



Results – Nominal SI Case

[]a,c

a,c



21

Westinghouse Non-Proprietary Class 3

© 2013 Westinghouse Electric Company LLC. All Rights Reserved.

Results – Nominal SI Case

[]^{a,c}

a,c



Westinghouse Non-Proprietary Class 3

© 2013 Westinghouse Electric Company LLC. All Rights Reserved.

Results – Nominal SI Case

[]^{a,c}

a,c



Westinghouse Non-Proprietary Class 3

© 2013 Westinghouse Electric Company LLC. All Rights Reserved.

Results – Nominal SI Case

[]a,c

a,c



Westinghouse Non-Proprietary Class 3

© 2013 Westinghouse Electric Company LLC. All Rights Reserved.

[^{a,c} Nominal SI Conservative Case

^{a,c}

25

Westinghouse Non-Proprietary Class 3

© 2013 Westinghouse Electric Company LLC. All Rights Reserved.

[^{a,c} Nominal SI Conservative Case

^{a,c}

Westinghouse Non-Proprietary Class 3

© 2013 Westinghouse Electric Company LLC. All Rights Reserved.

[^{a,c} Nominal SI Conservative Case

^{a,c}

27

Westinghouse Non-Proprietary Class 3

© 2013 Westinghouse Electric Company LLC. All Rights Reserved.

Results – Reduced SI Case

[]^{a,c}

a,c



Results – Reduced SI Case

[]^{a,c}

a,c



Results – Reduced SI Case

[]a,c

a,c



30

Results – Reduced SI Case

[]^{a,c}

a,c



Results – Reduced SI Case

[]^{a,c}

a,c



Results – Reduced SI Case

[a,c]



a,c



33

Westinghouse Non-Proprietary Class 3

© 2013 Westinghouse Electric Company LLC. All Rights Reserved.

Results – Reduced SI Case

[]^{a,c}

a,c



Results – Reduced SI Case

[]^{a,c}

a,c



Results – Reduced SI Case

[]a,c

a,c



36

Westinghouse Non-Proprietary Class 3

© 2013 Westinghouse Electric Company LLC. All Rights Reserved.

[^{a,c} Reduced SI Conservative Case

^{a,c}

Westinghouse Non-Proprietary Class 3

© 2013 Westinghouse Electric Company LLC. All Rights Reserved.

[^{a,c} Reduced SI Conservative Case

^{a,c}

Westinghouse Non-Proprietary Class 3

© 2013 Westinghouse Electric Company LLC. All Rights Reserved.

[^{a,c} Reduced SI Conservative Case

^{a,c}

39

Other Issues

- Several other item identified during July code workshop are being investigated
 - G2 Noding Sensitivity Results
 - Void Fraction Dipping in ORNL Simulations



Questions



Westinghouse Non-Proprietary Class 3

© 2013 Westinghouse Electric Company LLC. All Rights Reserved.

Full Spectrum LOCA (FSLOCA) Uncertainty Contributors and Treatment

**Jeffrey Kobelak
Aaron Everhard
Westinghouse Electric Company
August 2013**



Background (1/2)

- Potential Uncertainty Contributors are generally treated in one of three ways
 - **Nominal without Uncertainty**
 - Parameters which are tightly controlled
 - LOCA transient sensitivity to the parameter is negligible



Background (2/2)

- **Bounded**
 - LOCA transient sensitivity to the parameter is small
 - Effort to develop a detailed uncertainty treatment is judged to exceed the benefit of doing so
 - Intentionally add conservatism to the evaluation model

- **Sampled**
 - Uncertainties are explicitly evaluated
 - Distributions generally either well-characterize the data, or are skewed in a conservative manner



Nominal without Uncertainty

- [

]a,c



Bounded (1/2)

- [

]a,c



Bounded (2/2)

- [

]a,c



Sampled Parameters (1/3)

- Complete list of parameters and ranges provided in response to RAI-45A (from [

]a,c



Sampled Parameters (2/3)

- [

]a,c



Sampled Parameters (3/3)

- [

]a,c



Demonstration of Parameter Ranging

- Large runset with ranging of all applicable uncertainty contributors was previously completed for CCTF Run 62
 - Transmitted to the NRC as part of the Response to RAI-45
- Follow-up demonstration was completed with the Beaver Valley PWR steady-state case



DLW Steady-State Runs – Case Description

- [a,c] documents 93 steady-state runs which randomly sampled all the uncertainty attributes
 - Also includes a case which has the parameters at their nominal/unbiased values

[illegible]

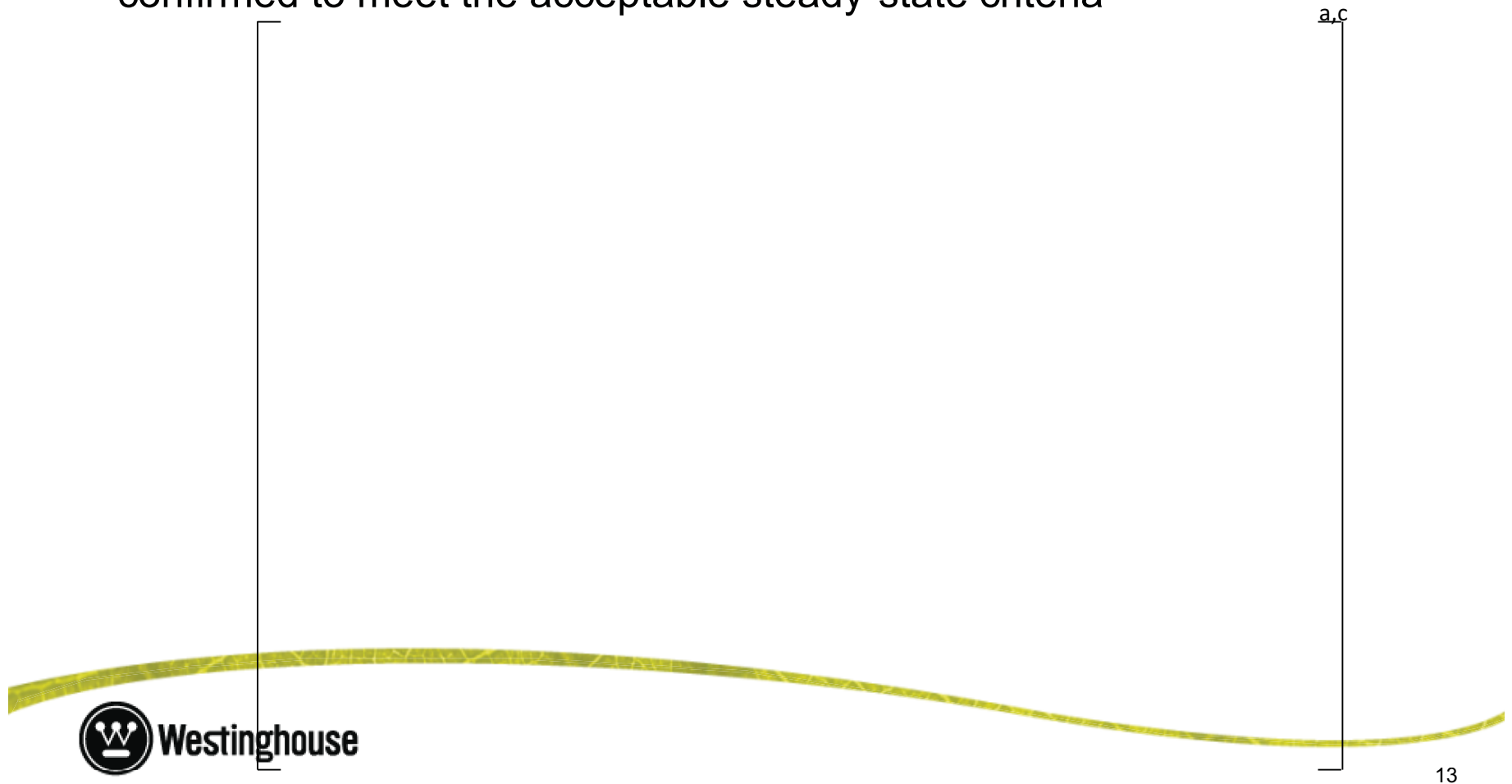
DLW Steady-State Runs – Attributes Sets

- List of Sampled Attribute Sets



DLW Steady-State Runs – SS Convergence

- The parameters defined in Table 26.4-1 of WCAP-16996-P are confirmed to meet the acceptable steady-state criteria



DLW Steady-State Runs – Results (1/7)

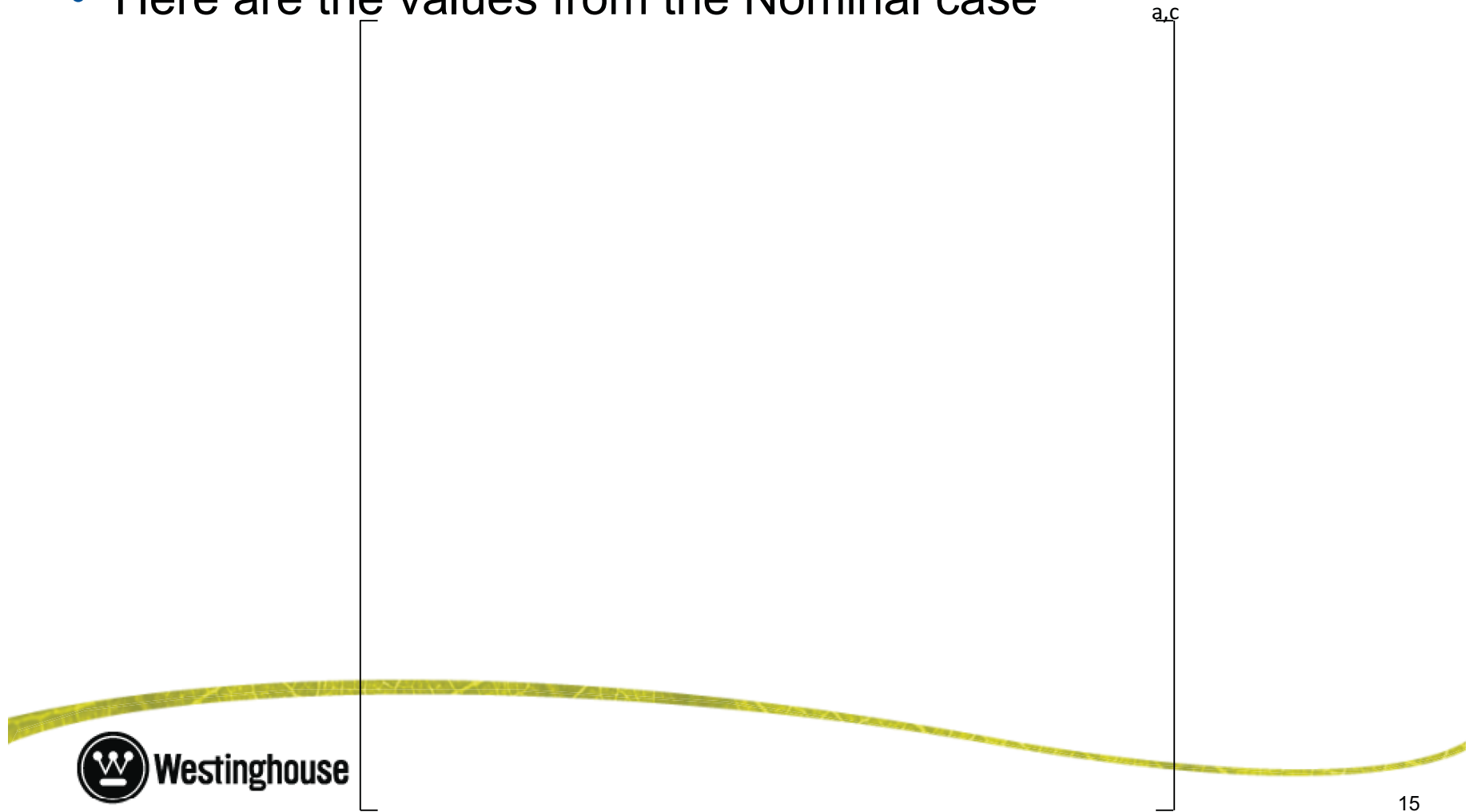
- The following quantities are extracted for each loop from each of the 93 cases, as well as the nominal case.

Hot Leg Temperature (F)	Cold Leg Temperature (F)
Loop Mass Flow Rate (lbm/s)	SG 2 nd Pressure (psia)
SG 2 nd Steam Flow (lbm/s)	SG 2 nd Liquid Flow (lbm/s)
SG Liquid Temperature (F)	Pump Speed (rad/s)
Pump Momentum Source (ft/s ²)	Pump Head (ft)

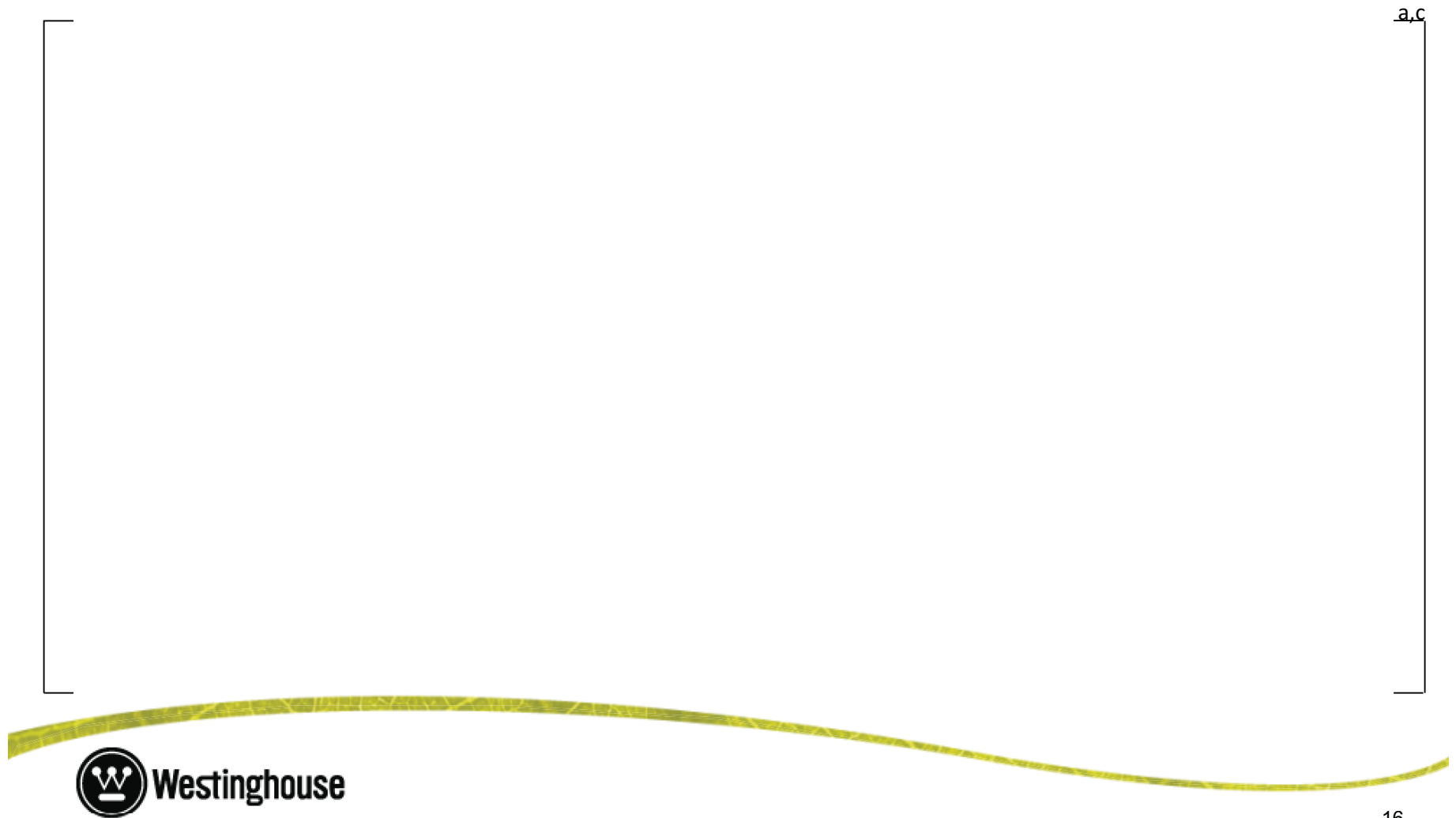


DLW Steady-State Runs – Results (2/7)

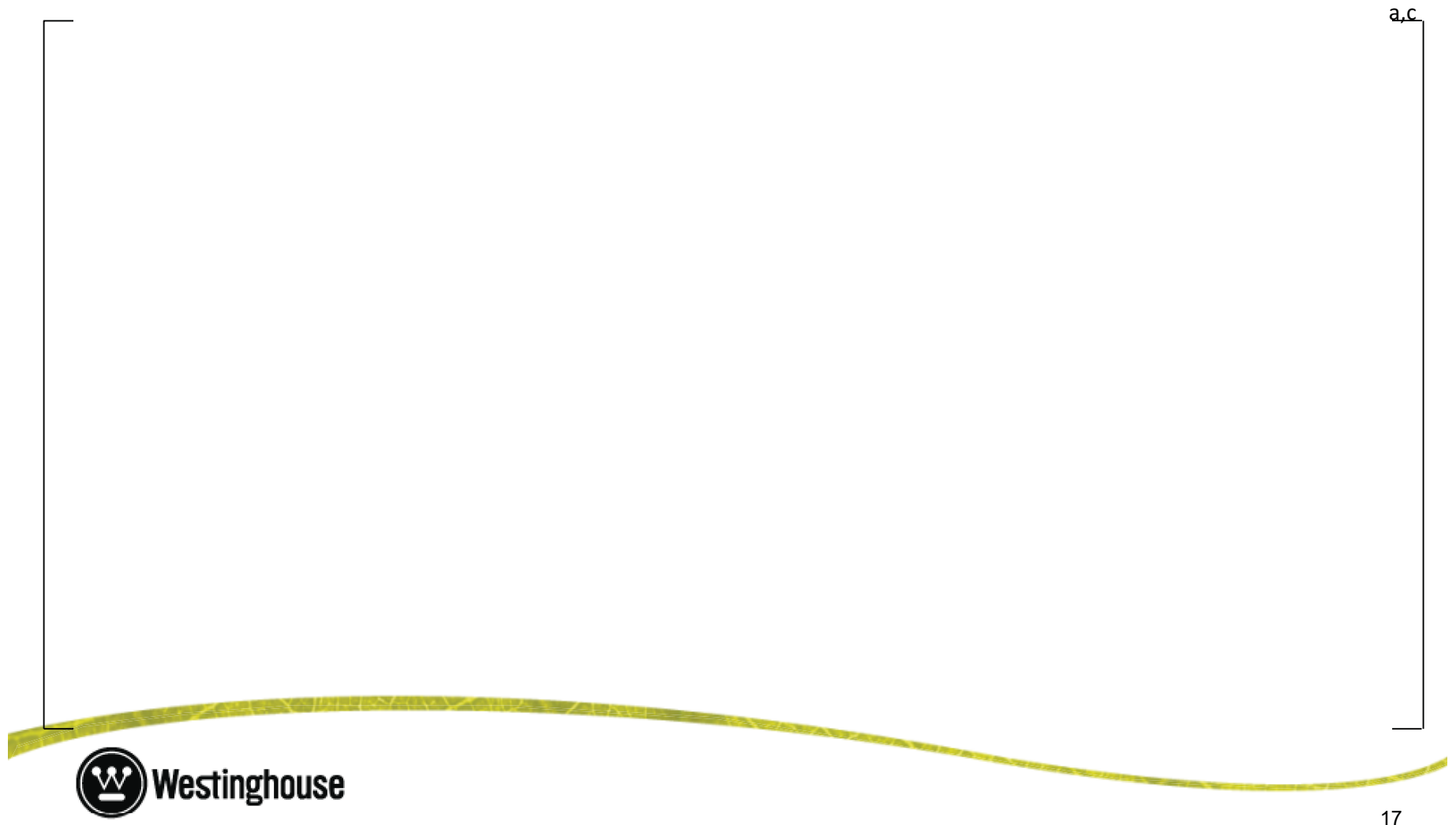
- Here are the values from the Nominal case



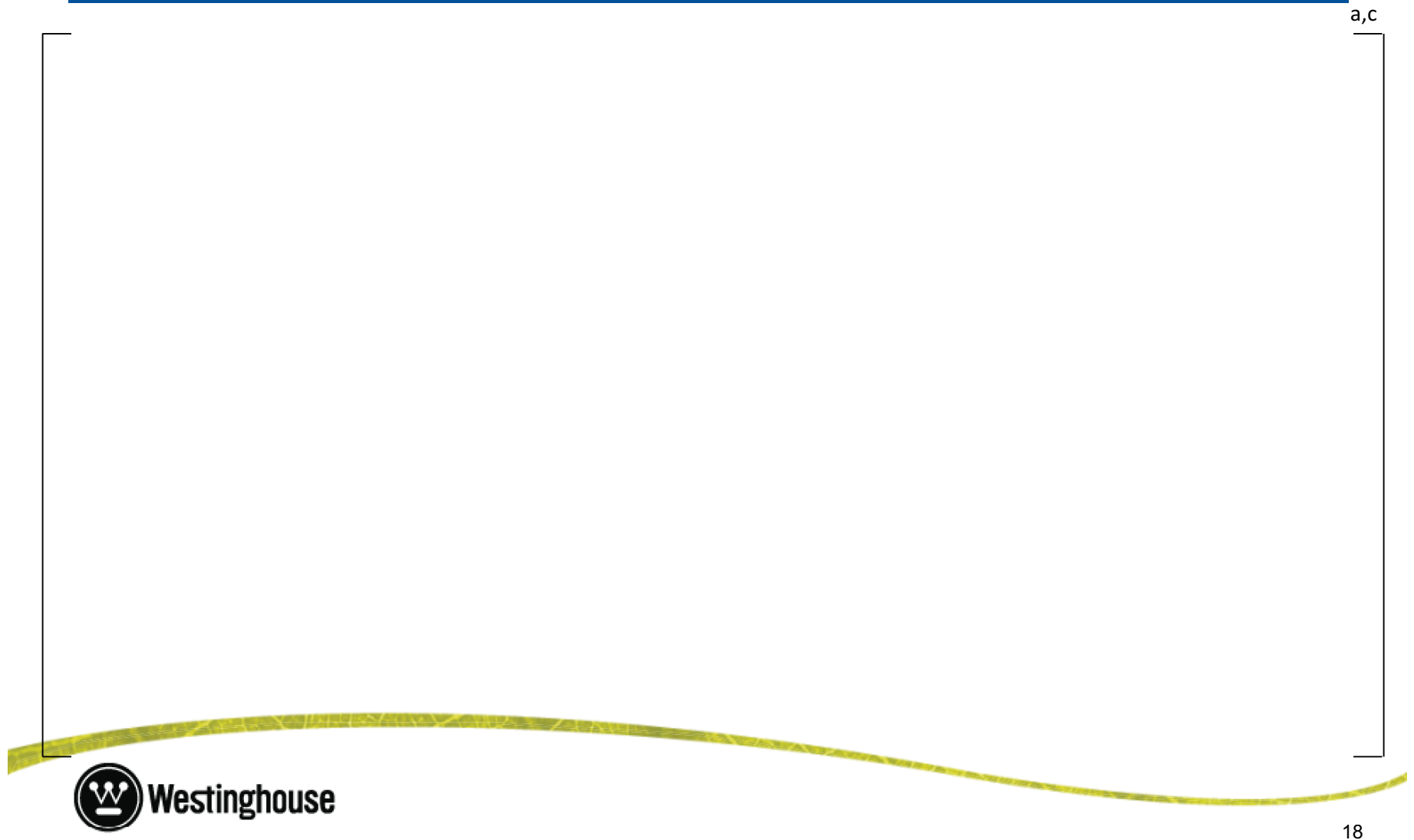
DLW Steady-State Runs – Results (3/7)



DLW Steady-State Runs – Results (4/7)



DLW Steady-State Runs – Results (5/7)

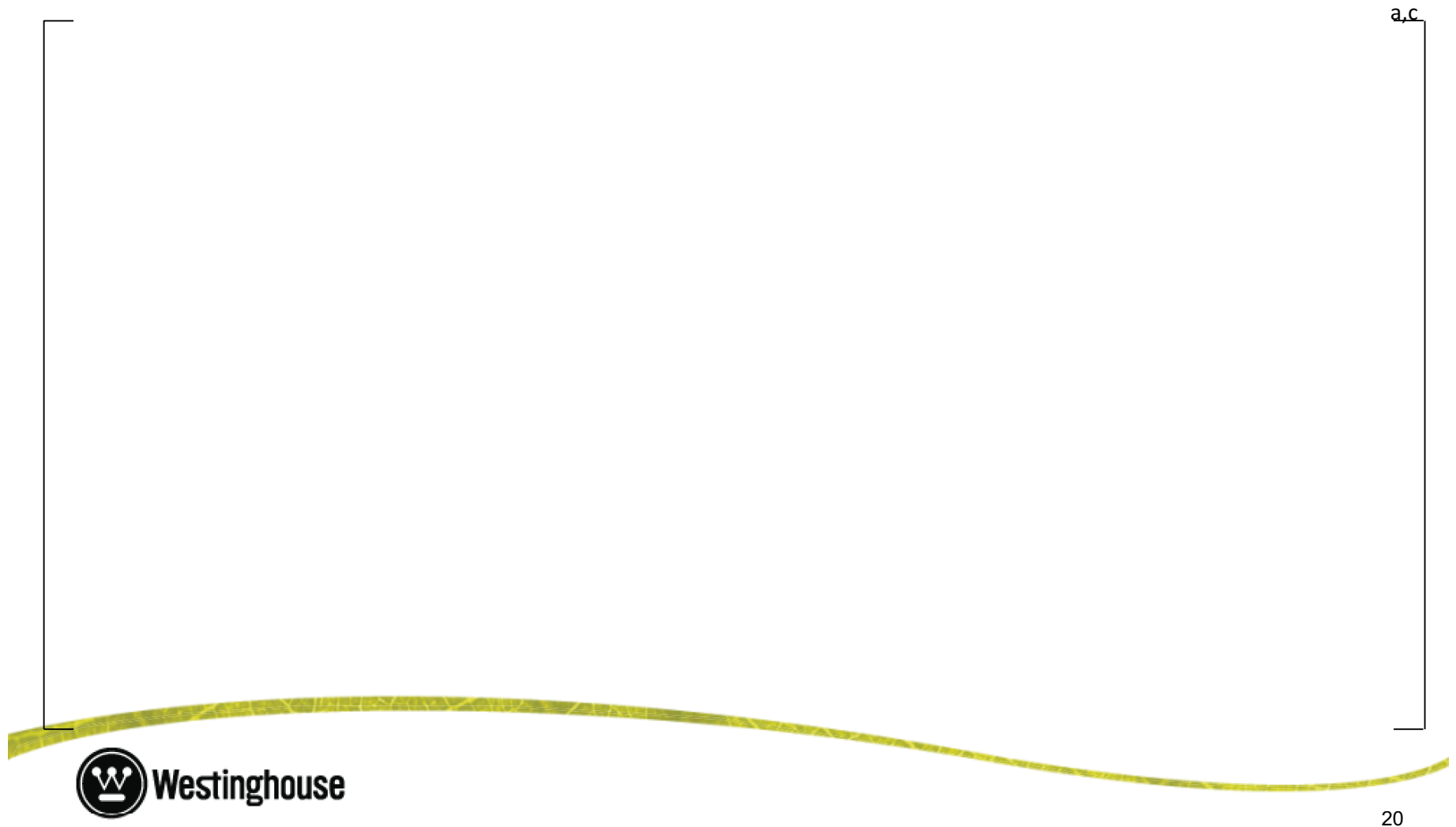


DLW Steady-State Runs – Results (6/7)

a,c



DLW Steady-State Runs – Results (7/7)



DLW Steady-State Runs - Conclusions

- Steady-state criteria met for all 93 cases
- Mean values from the distributions agree very well with the nominal case.
- [

]a,c



Questions



Westinghouse Non-Proprietary Class 3

© 2013 Westinghouse Electric Company LLC. All Rights Reserved.

Full Spectrum LOCA (FSLOCA) CCTF-62 and ROSA SB-CL-02 Runsets

**Jeffrey Kobelak
Westinghouse Electric Company
August 2013**



Overview (1/2)

- Consistency in steady-state (SS) calculation demonstrated with Beaver Valley SS runset
- Code capability for transient calculation demonstrated against IET facilities (data)
 - CCTF Run 62 selected as prototypical LBLOCA test
 - ROSA SB-CL-02 selected as prototypical SBLOCA test



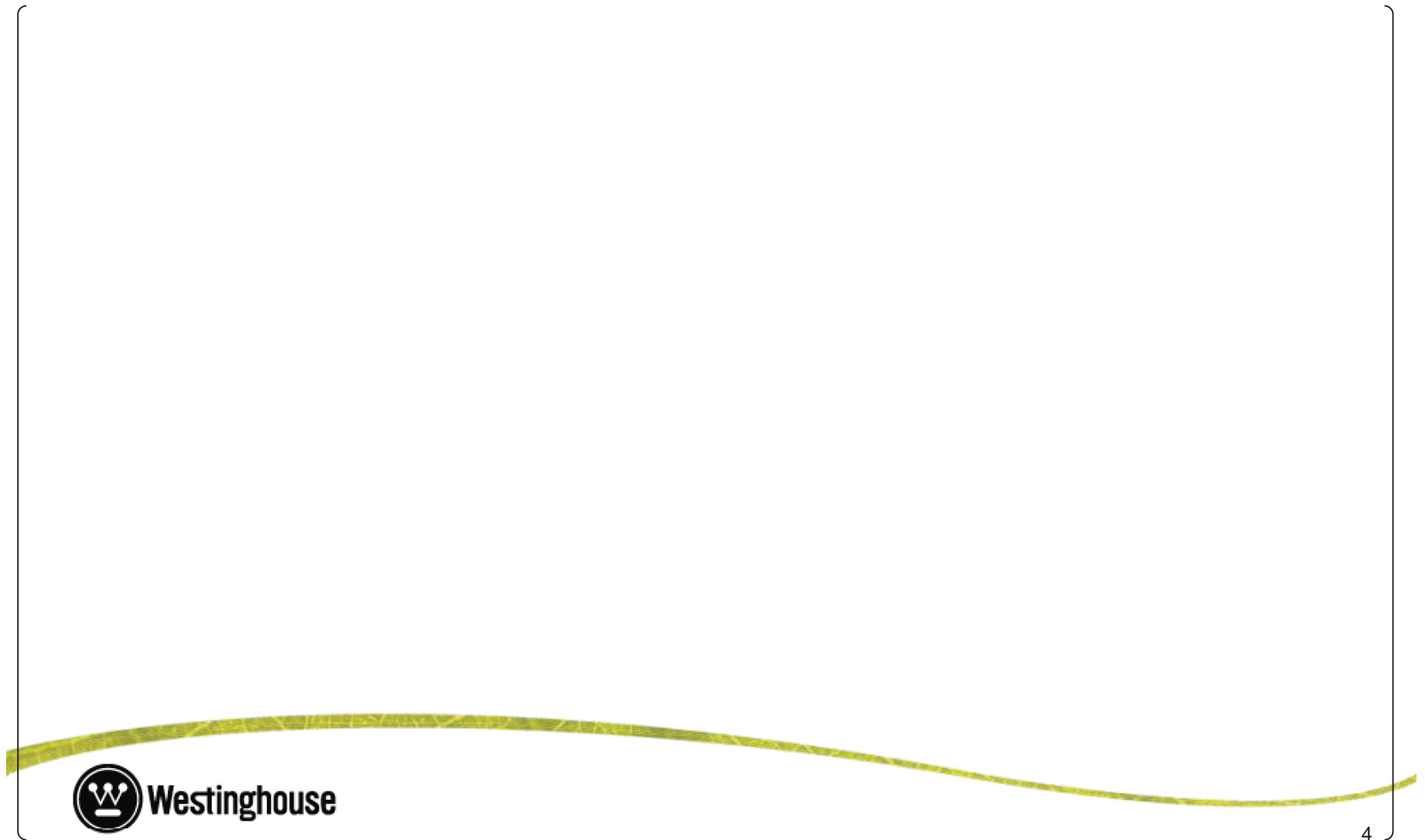
Overview (2/2)

- **CCTF Run 62**
 - Cladding temperature at 6, 8, and 10-ft elevations selected as figures of merit
- **ROSA SB-CL-02**
 - Cladding temperature at PCT elevation selected as figure of merit
 - Plots of other key phenomena presented
- **Both Facilities**
 - Minimum, nominal and maximum code predictions compared against data
 - Distribution for full 311-case runset calculated
 - Histograms show predicted - measured



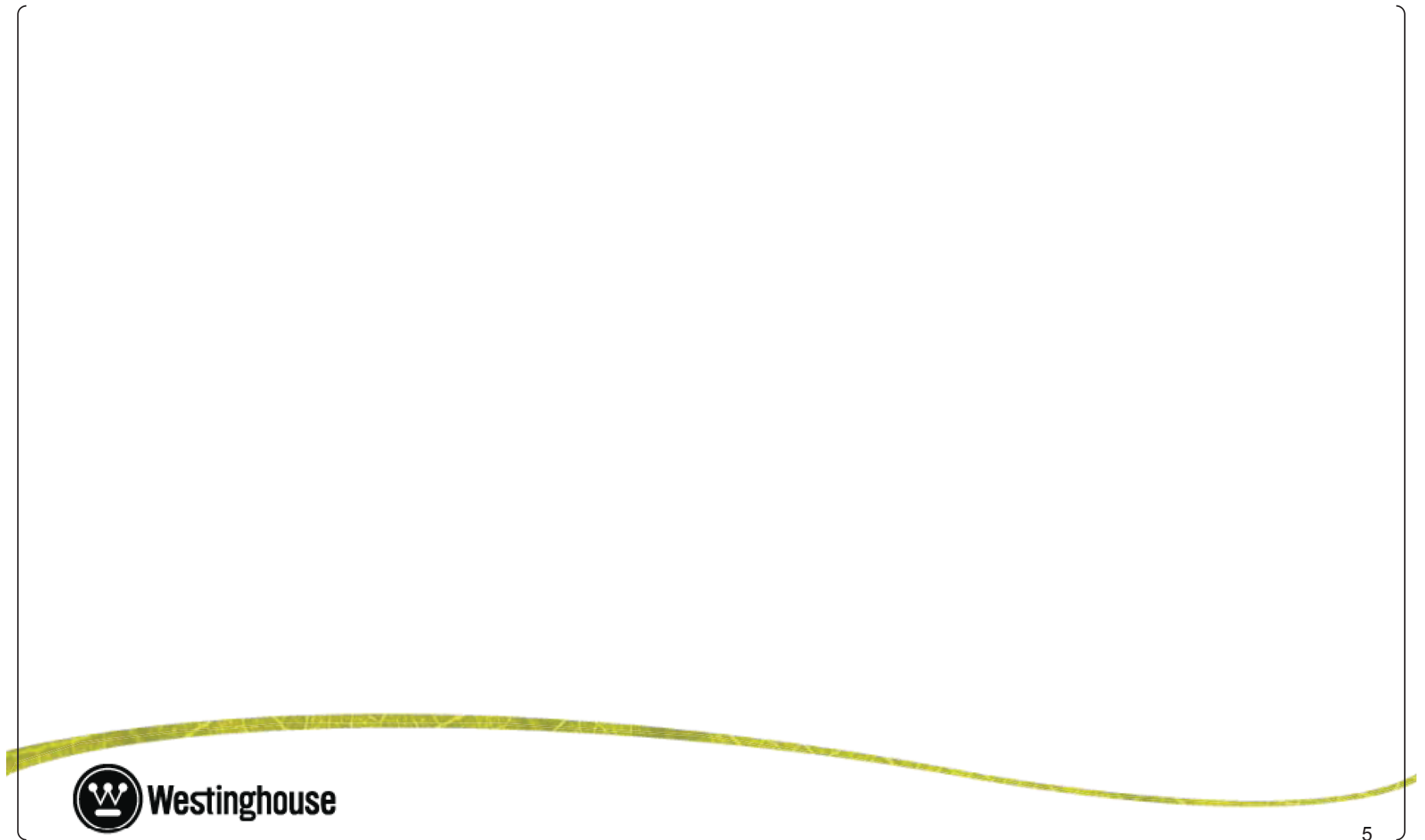
CCTF Run 62 – Tclad at 6 ft

a,c

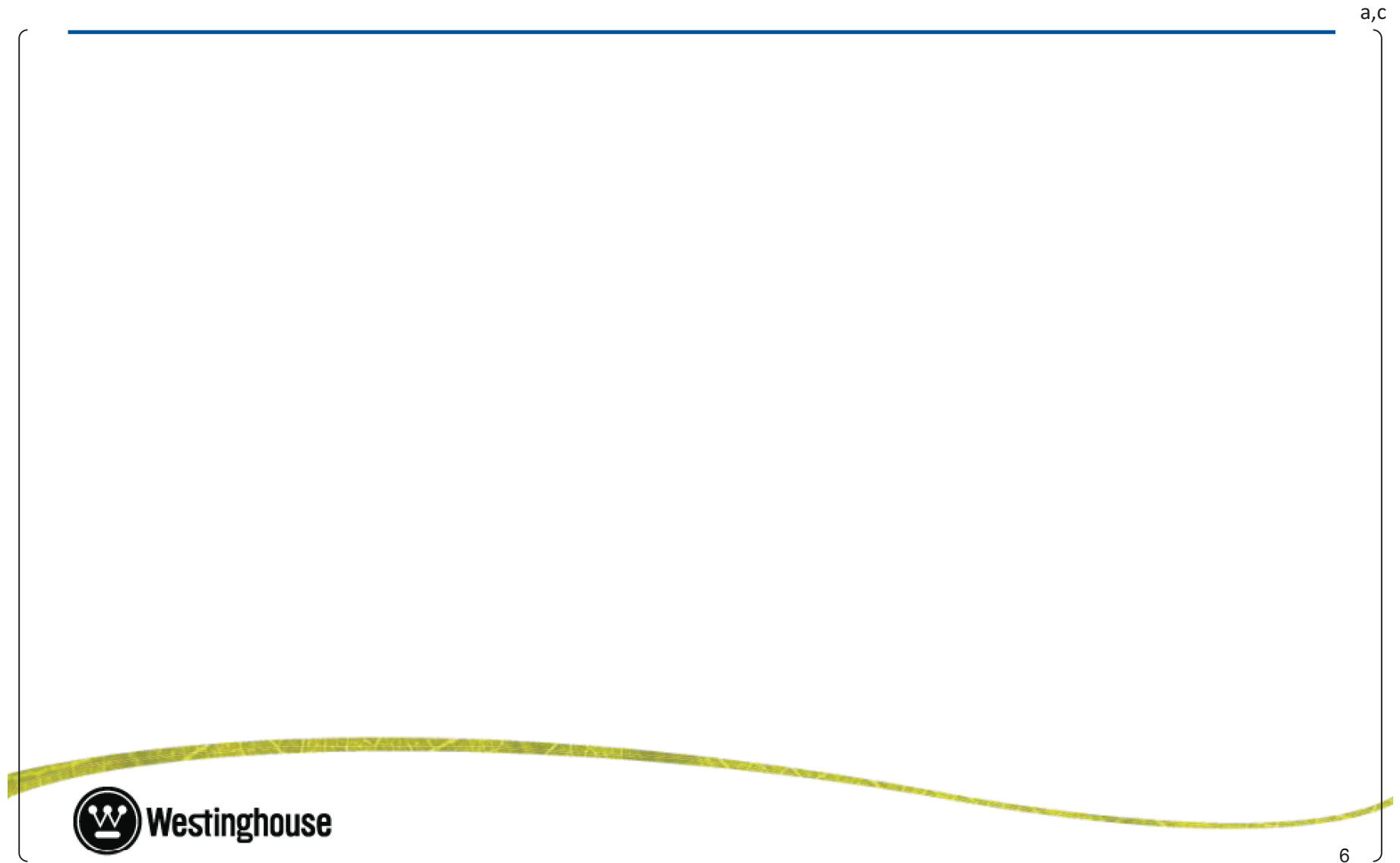


CCTF Run 62 – Tclad at 8 ft

a,c



CCTF Run 62 – Tclad at 10 ft



CCTF Run 62 - Summary

- [

]a,c

Elevation	Number of Cases Over-Predict Maximum Tcld	Number of Cases Under-Predict Maximum Tcld
[
]a,c



ROSA SB-CL-02

- Executed 311 transient runset
- Ranged the following parameters
 - [

]a,c



ROSA SB-CL-02

- Results processed first 100 runs; additional cases not expected to change distribution
- Plots provided for key parameters against data
- [$]^{a,c}$ compared to data for full runset

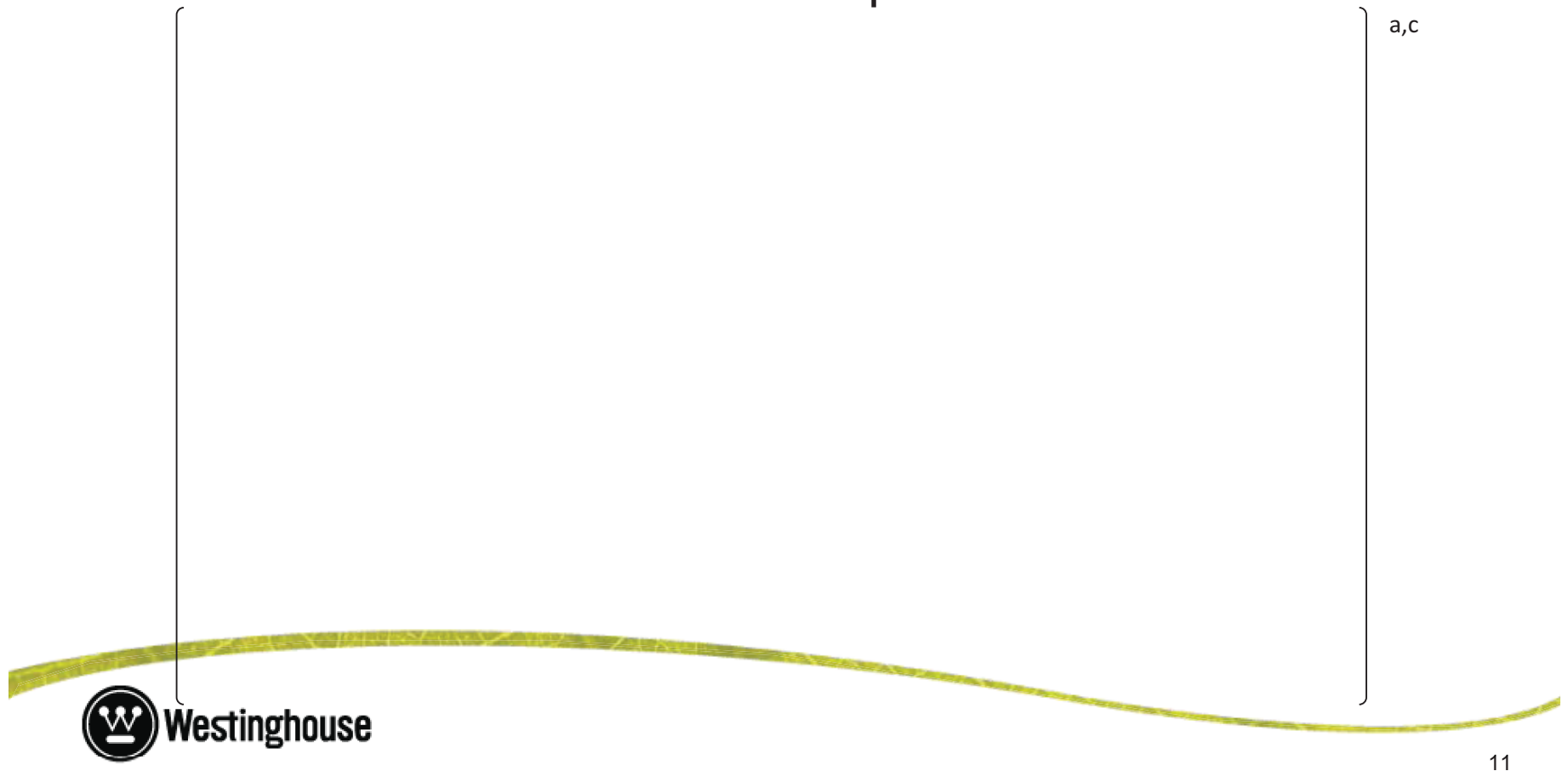


ROSA SB-CL-02



ROSA SB-CL-02 - T_{clad}

- Distribution of predicted cladding temperature at PCT elevation versus data for complete 311 runset



ROSA SB-CL-02 - Observations

- Cladding temperature was [

]a,c



ROSA SB-CL-02



ROSA SB-CL-02 - Tclad

- Distribution of predicted Tclad versus data without CD ranging



ROSA SB-CL-02 - Observations

- [

]a,c



Questions



**Summary of February 2014 NRC Audit of FULL SPECTRUM LOCA (FSLOCA) Evaluation Model
(Non-Proprietary)**

August 2014

Westinghouse Electric Company LLC
1000 Westinghouse Drive
Cranberry Township, PA 16066

©2014 Westinghouse Electric Company LLC
All Rights Reserved

1.0 Summary of Audit

In February 2014, the Nuclear Regulatory Commission (NRC) performed an audit of the FULL SPECTRUM™ LOCA (FSLOCA™) evaluation model (EM) submittal.

During the audit, Westinghouse presented information related to three main topics. One presentation focused on upgrades to the FSLOCA EM to address NRC concerns on the interfacial drag package. Another presentation detailed the plan to include a limited number of Semiscale Integral Effects Test (IET) simulations as part of the code validation package. The final presentation was an overview of the evaluation model changes related to fuel rod models (including thermal conductivity degradation), burnup methodology, and axial power shape generation that resulted from the response to Requests for Additional Information (RAIs) 36 through 39. The first two presentations are included in the audit summary. The last presentation was not included since a more detailed presentation on the same topic was provided in the June 2014 audit and included in LTR-NRC-14-38 [1-1].

1.1 Reference(s)

- 1-1) LTR-NRC-14-38, "Summary of June 2014 NRC Audit of the FULL SPECTRUM LOCA (FSLOCA) Evaluation Model (Proprietary/Non-Proprietary), Project 700, TAC No. ME5244," June 27, 2014.

FULL SPECTRUM and FSLOCA are trademarks of Westinghouse Electric Company LLC, its subsidiaries and/or its affiliates in the United States of America and may be registered in other countries throughout the world. All rights reserved. Unauthorized use is strictly prohibited. Other names may be trademarks of their respective owners.

Presentations from the February 2014 NRC Audit

FULL SPECTRUM and FSLOCA are trademarks of Westinghouse Electric Company LLC, its subsidiaries and/or its affiliates in the United States of America and may be registered in other countries throughout the world. All rights reserved. Unauthorized use is strictly prohibited. Other names may be trademarks of their respective owners.

WCT-TF2 Code Updates for Mixture Level

**Kats Ohkawa
Westinghouse Electric Company
February 2014**

Overview

- July Code Workshop identified Technical Issues - Noding Sensitivity in G2 Boil-off Simulation and Void Fraction Dipping in ORNL Simulation
- Code Updates related to Mixture Level output
- [

]a,c

- Impact on V&V



Mixture Level Code Update

[

]a,c

a,c



Mixture Level Code Update

[

]a,c

a,c



Corrected U_{Γ} for Hot Wall Ramp and application of Hot-Wall Drag

- Response to RAI-67 contains [

]a,c



Liquid Drain Logic

- [

]a,c

a,c



Impact of cumulative updates on V&V

- Examined Subset of V&V cases to evaluate the impact on V&V
 - FLECHT/FLECHT-SEASET
 - ORNL THTF
 - Noding Size Sensitivity
 - G2 Boil-off
 - Noding Size Sensitivity
 - ROSA 2.5% and 5% CL Break Simulations
 - DLW SBLOCA Limiting Cases

Impact of cumulative updates on V&V (cont-1)

FLECHT/FLECHT-SEASET – Slightly higher Peak TCLAD / slightly earlier quench in some transients (1 – Old, 2 – New, Brown - Data)

a,c



Impact of cumulative updates on V&V (cont-2)

ORNL THTF – w/ Correction related to []^{a,c}
Less occurrence of void inversion (**1 – Old**, **2 – New** vs. Data)



Impact of cumulative updates on V&V (cont-3)

ORNL THTF – Noding Size Sensitivity (**1 – 12 in**, **2 – 6 in** vs. Data) →
Detailed noding did not significantly impact the void profile

a,c



Impact of cumulative updates on V&V (cont-4)

G2 Boil-off w/ []_{a,c}

a,c



Impact of cumulative updates on V&V (cont-5)

Noding Size Sensitivity – no significant sensitivity in 3 to 12
inch

a,c



Impact of cumulative updates on V&V (cont-6)

Noding Size Sensitivity improvement relative to Response
to RAI-72 to 74 (LTR-NRC-13-41)

a,c



Impact of cumulative updates on V&V (cont-7)

ROSA 2.5% and 5% CL Break Simulations

a,c



Impact of cumulative updates on V&V (cont-8)

DLW SBLOCA Limiting Case [**a,c**]
(**1 – Old**, **2 – New**)

a,c



Summary Impact of cumulative updates on V&V and Plant Cases

•[

]a,c

- Negligible impact on existing REFLOOD simulations
- Less Void Fraction inversion seen in ORNL THTF
- Consistent heat-up behavior in boil-off
- Negligible node size sensitivity over node sizes used in V&V and plant models

Questions



Overview of Semiscale Plan for Full Spectrum LOCA (FSLOCA)

Jeffrey Kobelak
Westinghouse Electric Company
February 2014

Introduction

- Westinghouse has concluded that the ROSA Large Scale Test Facility (LSTF) was sufficient for SBLOCA Integral Effects Test (IET) facilities
- The staff has stated several concerns with the use of only a single IET facility
- Westinghouse is performing a small subset of SEMISCALE test simulations to confirm code capabilities relative to those concerns

Concerns with use of only ROSA LSTF

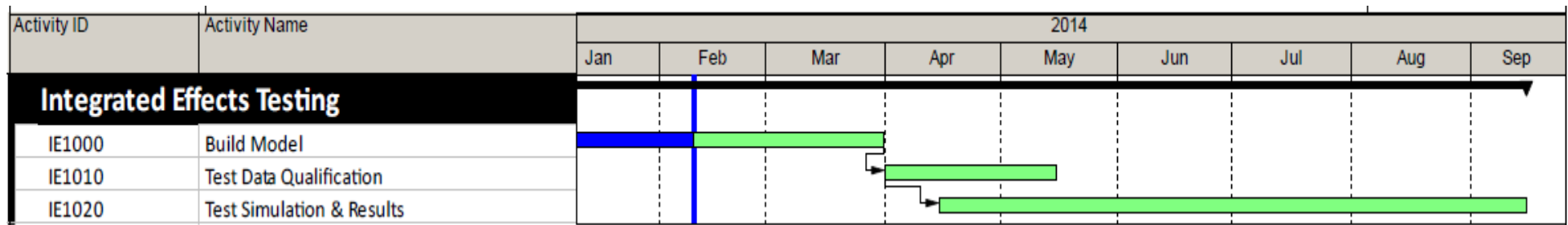
- Only a single scaled SBLOCA IET facility
- No direct bypass sensitivity
- No single test which produced boil-off uncover with high head safety injection
- No cases which produced a deep uncover to exercise the heat transfer package at more severe conditions

SEMISCALE Plan

- Simulate S-LH-1 and S-LH-2 IETs
 - Provide a direct bypass sensitivity
 - Transients experience cladding heatup with safety injection
- Rely on simulation of S-07-10D in SET fashion
 - Simulation as an SET fully exercises the core heat transfer package under more severe conditions
- These SEMISCALE simulations will provide confirmation that WCOBRA/TRAC-TF2 adequately predicts expected behaviors



SEMISCALE Schedule



Questions



**Summary of May 2014 NRC Audit of FULL SPECTRUM LOCA (FSLOCA) Evaluation Model”
(Non-Proprietary)**

June 2014

Westinghouse Electric Company LLC
1000 Westinghouse Drive
Cranberry Township, PA 16066

©2014 Westinghouse Electric Company LLC
All Rights Reserved

1.0 Introduction

In May 2014, the Nuclear Regulatory Commission (NRC) performed an audit of the FULL SPECTRUM™ LOCA (FSLOCA™) evaluation model (EM) submittal.

During the audit, Westinghouse presented information on various topics. The presentations focused on changes to the code and method related to outstanding NRC concerns regarding interfacial drag, cold leg condensation, counter-current flow limitation (CCFL), decay heat, steam cooling, and loop seal clearing; and are included in the following attachments. The code simulations shown in the interfacial drag and CCFL presentations are provided to demonstrate the impact of the updated models described in the associated presentations.

Additional information to support the licensing of the FSLOCA EM is provided in this attachment. Section 2.0 evaluates the Separate Effects Test (SET) simulation of Semiscale test S-07-10D for compensating error. Section 3.0 investigates experimental data and WCOBRA/TRAC-TF2 predictions on loop seal clearing, with a focus on which and how many loops clear. Section 4.0 describes the updated Region I analysis method. Lastly, Section 5.0 provides additional information regarding sensitivity studies for offsite power availability and break orientation.

FULL SPECTRUM™ and FSLOCA™ are trademarks in the United States of Westinghouse Electric Company LLC, its subsidiaries and/or its affiliates. These marks may be used and/or registered in other countries throughout the world. All rights reserved. Unauthorized use is strictly prohibited. Other names may be trademarks of their respective owners.

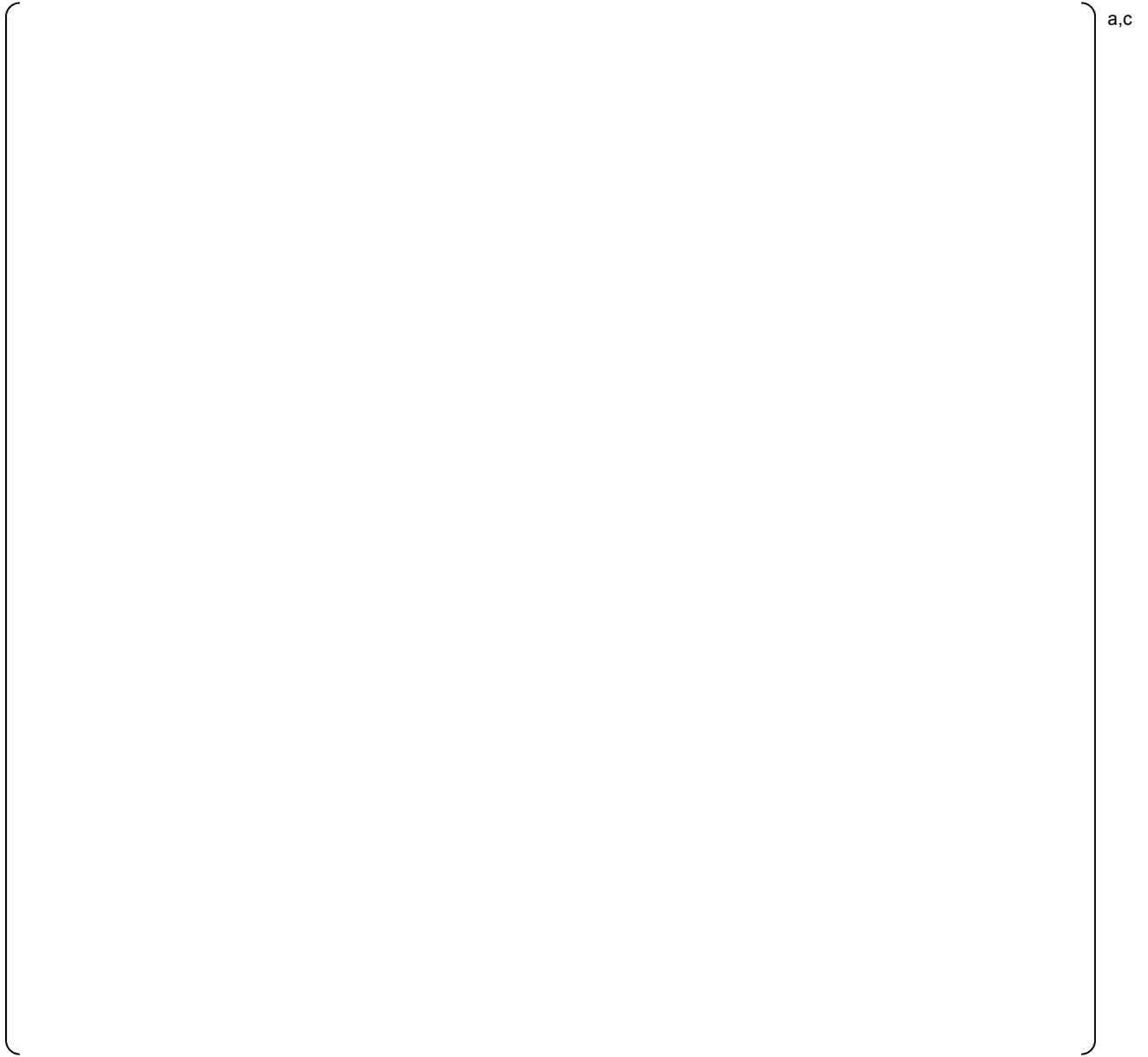
2.0 Semiscale S-07-10D Simulation

The Semiscale S-07-10D experiment was simulated with WCOBRA/TRAC-TF2 in SET mode as presented in Section 23.1.2 of WCAP-16996-P [2-1]. [

]^{a,c}

2.1 References

- 2-1) WCAP-16996-P, "Realistic LOCA Evaluation Methodology Applied to the Full Spectrum of Break Sizes (FULL SPECTRUM LOCA Methodology)," November 2010.
- 2-2) EGG-SEMI-5201, "Analysis of Semiscale MOD-3 Small Break Tests S-07-10 and S-07-10D," July 1980.



a,c

Figure 2-1

3.0 Loop Seal Clearing

3.1 Background / Purpose

Loop seal clearing is an important phenomenon in predicting the plant response to a small break (SB) loss-of-coolant accident (LOCA). Section 3.2 documents a review of available integral effects test data for how many and which loop seals clear for the tests. Section 3.3 documents a review of WCOBRA/TRAC-TF2's capability of predicting how many and which loop seals clear. Section 3.4 documents the revised method for modeling the loop seal region for the Region I uncertainty analysis. Finally, Section 3.5 provides a summary of the conclusions drawn.

3.2 Review of Available Integral Effects Test Data

Several test facilities have executed SBLOCA experiments which have information regarding loop seal clearing behavior. These included ATLAS, BETHSY, ROSA-IV, SEMISCALE and UPTF. Available test reports and published papers were reviewed to obtain information regarding how many loop seals clear and which loop seals clear as a function of break size. This was done in order to support the modeling approach of the loop seal region as part of the FSLOCA methodology, Region I uncertainty analysis.

Table 3-1 provides a summary of the conclusions drawn based on a review of the available information for each facility. As observed in Table 3-1, [

] ^{a,c}

Based on the review of the test facility data, it is expected that the WCOBRA/TRAC-TF2 code should [

] ^{a,c}

3.3 WCOBRA/TRAC-TF2 Trends Based on Sensitivity Studies

To further examine the code behavior regarding loop seal clearing with break size, several sensitivity studies have been performed and previously presented. The studies include:

1. Break spectrum study with [] ^{a,c} (Study B in LTR-NRC-13-45 [3-1])
2. Break spectrum study with [] ^{a,c} (Study C in LTR-NRC-13-45)

3. Parametric studies with []^{a,c} (Section 2.0 of LTR-NRC-13-70 [3-2])

These studies were further reviewed for code behavior regarding the loop seal clearing process, specifically how many and which loop seals are predicted by the code to clear. Two additional studies were also performed (denoted as Study C-1 and Study C-2), whereby Study C of LTR-NRC-13-45 was modified to []

[]^{a,c}

The results from Studies B, C, C-1 and C-2 were segregated into groups of how many and which loop seals were clear at the time of PCT. The results are presented in Figure 3-1, and Figure 3-2 presents the results specifically for Study C-1. (For cases that did not uncover, the PCT was set to 494°F, which is the saturation temperature at the accumulator pressure for these cases.) The following is observed based on Figures 3-1 and 3-2:

[]

[]^{a,c}

Based on the above, []

[]^{a,c}

From the parametric study presented in Section 2.0 of LTR-NRC-13-70, []

[]^{a,c}

3.4 Modeling Approach

Based on the information presented in Sections 3.2 and 3.3, [

] ^{a,c}

3.5 Conclusions

From a review of available integral test facility data, [

] ^{a,c}

Based on sensitivity studies performed with WCOBRA/TRAC-TF2, [

] ^{a,c}

3.6 References

- 3-1) LTR-NRC-13-45, "Submittal of Westinghouse Responses to 'WCAP-16996-P, 'Realistic LOCA Evaluation Methodology Applied to the Full Spectrum of Break Sizes (FULL SPECTRUM LOCA Methodology)' Request for Additional Information – RAIs 9 and 12' (Proprietary/Non-Proprietary), Project 700, TAC No. ME5244," June 26, 2013.
- 3-2) LTR-NRC-13-70, "Summary of July 2013 NRC Code Workshop and August 2013 NRC Audit of the FULL SPECTRUM LOCA (FSLOCA) Evaluation Model (Proprietary/Non-Proprietary)," October 10, 2013.
- 3-3) Kim, Y-S., and Cho, S., "An experimental investigation of loop seal clearings in SBLOCA tests," *Annals of Nuclear Energy*, 2014, Vol. 63, pp. 721-730.
- 3-4) NEA/CSNI/R(R92)20, "ISP-27, OECD/NEA/CSNI International Standard Problem No.27, BETHSY experiment 9.1b, 2" Cold leg break without HPSI and with delayed Ultimate Procedure," R. Deruaz, November 1992.

- 3-5) Asaka, H., et al., "Results of 0.5% Cold-Leg Small-Break LOCA Experiments at ROSA-IV/LSTF: Effect of Break Orientation," *Experimental Thermal and Fluid Science*, 1990, Vol. 3, pp. 588-596.
- 3-6) JAERI-memo 62-399, "ROSA-IV/LSTF 2.5% Cold Leg Break LOCA Experiment, Data Report for Runs SB-CL-01, 02 and 03," Koizumi, Y., et al., November 1987.
- 3-7) JAERI-memo 61-056, "ROSA-IV/LSTF 5% Cold Leg Break LOCA Experiment Data Report, Run SB-CL-05," March 1986.
- 3-8) JAERI-M 89-027, "ROSA-IV/LSTF 5% Cold Leg Break LOCA Experiment, Run SB-CL-18 Data Report," March 1989.
- 3-9) EGG-SEMI-6884, "Quick Look Report for SEMISCALE MOD-2C Experiments S-LH-1 and S-LH-2," May 1985.
- 3-10) NUREG/CR-4945 / EGG-2509, "Summary of the SEMISCALE Program (1965-1986)," G. G. Loomis, July 1987.
- 3-11) NT33/94/011, "Versuch A5, Freiblasen des Pumpenbogens, Einzeleffekt- und Integralversuche," December 1994.

a,c



Figure 3-1: Break Spectrum Studies Segregated Based on the Number and Which Loop Seals Clear



Figure 3-2: Break Spectrum Study C-1 [
]^{a,c}

4.0 Region I Analysis Method

4.1 Background

LTR-NRC-13-45 [4-1] provided the response to RAIs 9 and 12 on the FULL SPECTRUM LOCA methodology topical report [4-2]. During the August 2013 NRC Audit on the FSLOCA methodology, an update to the Region I break area sampling method was proposed as described in Section 5.0 of LTR-NRC-13-70 [4-3]. The following subsections present an updated Region I (SBLOCA) analysis method, including revisions to the break area treatment previously described.

4.2 Revised Region I Analysis Method

As discussed in the response to RAI 9, there exists a small segment (resonance region) of break areas where the core may uncover. The resonance region exists because the transient behavior of a SBLOCA is the result of a race between mass lost out the break and the depressurization of the reactor coolant system (RCS), which results in increased safety injection flow. For the smallest breaks, the mass lost out the break is low, such that the safety injection at the higher pressure (due to the slower depressurization rate) is adequate for keeping the core covered with a two-phase mixture level and mitigating the accident. Likewise, for the larger small breaks, the depressurization rate is fast enough that the increase in safety injection (due to lower pressure) and accumulator actuation are adequate for replenishing the higher mass lost out the break and keeping the core covered with a two-phase mixture level. For the breaks in between about []^{a,c} for Westinghouse 3-loop PWRs, the depressurization rate is slow enough that the safety injection flow may not be sufficient to keep the core covered with a two-phase mixture level, and core uncover is observed. Since these break areas are most likely to become limiting in Region I, attention should be given to this resonance range within the Region I uncertainty analysis. As such, the Region I analysis method is revised to []^{a,c}

The updated Region I analysis method is divided into two main steps:

[]

[]^{a,c}

The following provides further details for each step.

[

] ^{a,c}

Table 4-1: Parameters Biased for Core Uncovery Break Area Study

[
] ^{a,c}

Additionally, the [] ^{a,c} as described in Section 3.4 herein.

A large number of sensitivity studies have indicated that [

] ^{a,c} This is illustrated by Figures 4-1 and 4-2.

The PCT as a function of break diameter from [

$J^{a,c}$

The PCTs versus time for an example break size in the resonance region, and from a larger break diameter are presented in Figure 4-2. [

$J^{a,c}$

[

$J^{a,c}$

[

] ^{a,c}



Figure 4-1: Peak Cladding Temperature vs. Break Diameter



Figure 4-2: Peak Cladding Temperature vs. Time for a Resonance Region Break and a Larger Diameter Break

a,c

Figure 4-3: Overall Peak Cladding Temperature Response Surface

a,c

Figure 4-4: Influence of Mesh Size on the Break Area Scanning

4.3 Example Demonstration of the Revised Region I Analysis Method

The following provides a sample demonstration of the revised Region I analysis method with the Beaver Valley Unit 1 plant model.

[

]^{a,c}

Table 4-2: Limiting Results from the [

]^{a,c}

[

]^{a,c}

[

] ^{a,c}

a,c

**Figure 4-5: Peak Cladding Temperature vs. Decay Heat Uncertainty for Example
Uncertainty Analysis (Step 2 Cases)**

a,c

Figure 4-6: Peak Cladding Temperature vs. High Pressure, Single-Phase Vapor Heat Transfer Multiplier for Example Uncertainty Analysis (Step 2 Cases)

a,c

**Figure 4-7: Peak Cladding Temperature vs. Accumulator Pressure for Example
Uncertainty Analysis (Step 2 Cases)**

a,c

Figure 4-8: Example Uncertainty Analysis Peak Cladding Temperature vs. Number of Cases Executed

4.4 Conclusions

The revised Region I analysis method [

] ^{a,c} In addition, the revised approach adequately captures the large change in PCT with a small change in break area that occurs in the resonance region. The uncertainty analysis then [

] ^{a,c} This approach results in the ability to demonstrate that the acceptance criteria are met with high probability.

4.5 References

- 4-1) LTR-NRC-13-45, "Submittal of Westinghouse Responses to 'WCAP-16996-P, 'Realistic LOCA Evaluation Methodology Applied to the Full Spectrum of Break Sizes (FULL SPECTRUM LOCA Methodology)' Request for Additional Information – RAIs 9 and 12' (Proprietary/Non-Proprietary), Project 700, TAC No. ME5244," June 26, 2013.
- 4-2) WCAP-16996-P, Volumes I, II and III, "Realistic LOCA Evaluation Methodology Applied to the Full Spectrum of Break Sizes (FULL SPECTRUM LOCA Methodology)," November 2010.
- 4-3) LTR-NRC-13-70, "Summary of July 2013 NRC Code Workshop and August 2013 NRC Audit of the FULL SPECTRUM LOCA (FSLOCA) Evaluation Model (Proprietary/Non-Proprietary)," October 10, 2013.

5.0 Supporting Region I Sensitivity Studies

5.1 Offsite Power Availability

A number of Region I offsite power availability sensitivity studies were previously presented. Studies for both V. C. Summer and Beaver Valley Unit 1 were discussed in Sections 28.2.3.1 and 28.2.3.2 of WCAP-16996-P [5-1], respectively. These studies [

Reactor Coolant Pump (RCP) trip time studies were documented as part of the response to various Set 8 RAls. Figure 3.2-33 from LTR-NRC-14-9 [5-2] shows [

A more detailed offsite power availability study was executed, whereby all the Beaver Valley Unit 1 [

5.2 Severed Safety Injection Line

A number of Region I break orientation sensitivity studies were previously presented. Studies for both V. C. Summer and Beaver Valley Unit 1 were discussed in Sections 28.2.7.1 and 28.2.7.2 of WCAP-16996-P, respectively. These studies indicated that [

A more detailed severed SI line study was executed, whereby all the Beaver Valley Unit 1 [

5.3 References

- 5-1) WCAP-16996-P, Volumes I, II and III, "Realistic LOCA Evaluation Methodology Applied to the Full Spectrum of Break Sizes (FULL SPECTRUM LOCA Methodology)," November 2010.
- 5-2) LTR-NRC-14-9, "Submittal of Westinghouse Responses to 'WCAP-16996-P, 'Realistic LOCA Evaluation Methodology Applied to the Full Spectrum of Break Sizes (FULL SPECTRUM LOCA Methodology)' Request for Additional Information – Set 8 RAIs 122-126, 128-131 and 136' (Proprietary/Non-Proprietary), Project 700, TAC No. ME5244," February 12, 2014.

a,c

Figure 5-1: Offsite Power Availability Sensitivity Study with Beaver Valley Unit 1

a,c

Figure 5-2: Severed SI Line Sensitivity Study with Beaver Valley Unit 1

Presentations from the May 2014 NRC Audit

This document is the property of and contains Proprietary Information owned by Westinghouse Electric Company LLC and/or its subcontractors and suppliers. It is transmitted to you in confidence and trust, and you agree to treat this document in strict accordance with the terms and conditions of the agreement under which it was provided to you.

Overview of Westinghouse Approach to Address Remaining NRC Concerns for FULL SPECTRUM LOCA

Jeffrey Kobelak

May 12, 2014



Remaining NRC Concerns

- Decay Heat
- Cold Leg Condensation
- Steam Cooling
- Loop Seal Clearing
- Counter-Current Flow Limitation (CCFL)
- Interfacial Drag

Approach to address each issue is outlined

Decay Heat

- [

]a,c

**Decay Heat issue addressed with
Conservative Bias**

Cold Leg Condensation (1/2)

- Original: Sample KCOSI [a,c]
- Responses to RAIs 30 through 35 addressed model applicability for PWR transients
 - Discussed scaling of geometry and other parameters
 - Concluded scaling analysis and validation matrix support scalability to PWR

Cold Leg Condensation (2/2)

- [

]a,c

- Recognize staff concern with scaling and applicability to PWR

- Proposal: Address with conservative bias

- [

]a,c

**Cold Leg Condensation issue addressed
with Conservative Bias**

Steam Cooling (1/2)

- Staff indicated concern with lack of validation against SBLOCA conditions with deep uncover
- Westinghouse noted S-07-10D simulated in SET fashion
 - Exercised heat transfer package for deep uncover
 - Staff questioned if simulation could be affected by compensating error of mis-predicting high heat transfer with low steam flow

Steam Cooling (2/2)

- Westinghouse confirmed S-07-10D simulation not impacted by compensating error
 - [

]a,c

- S-07-10D simulation in Section 23 of FSLOCA Topical
 - [

]a,c

Current validation matrix adequately covers heat transfer package

Loop Seal Clearing

- Responded to RAIs 83-85, 88-92, 94-95, 113-119
 - Clarify treatment of horizontal stratification
 - Loop seal nodding and modeling is appropriate
- Additional investigation into number of loops / which loops clear
 - Later presentation will provide details
- [

]a,c

**Loop Seal Clearing issue addressed with
Conservative Bias**

CCFL

- Staff indicated concern that CCFL could be violated
- [
-]^{a,c}
- Later presentation will provide details

CCFL enforced in key regions

Interfacial Drag

- Staff indicated concerns
 - Void dipping observed in ORNL simulations
 - Severely oscillatory behavior in GE blowdown simulations
- [
]a,c
 - Issues reconciled
- Proposal: Limited updates to drag package
 - [
]a,c

**Interfacial Drag issue addressed with
code updates and Conservative Bias**

Summary

- **Decay Heat:** Conservative []^{a,c}
- **Cold Leg Condensation:** Conservative []^{a,c}
- **Steam Cooling:** Current approach acceptable
- **Loop Seal Clearing:** Conservative []^{a,c}
- **Counter-Current Flow Limitation (CCFL):** Enforce CCFL in key regions
- **Interfacial Drag:** Mitigated known issues in code and conservative bias

FSLOCA evaluation model has been updated to appropriately address these remaining issues

Questions



This document is the property of and contains Proprietary Information owned by Westinghouse Electric Company LLC and/or its subcontractors and suppliers. It is transmitted to you in confidence and trust, and you agree to treat this document in strict accordance with the terms and conditions of the agreement under which it was provided to you.

Interfacial Drag Modeling

Kats Ohkawa and Jeff Kobelak

May 12, 2014



Overview of Interfacial Drag Model Review, Model Updates and Impact Evaluation

- Review of Identified Issues
 - Excessive oscillation in GE Blowdown
 - Void fraction profile in some cases show exaggerated decrease []^{a,c}
- WCOBRA/TRAC-TF2 Code Model Review and Update
- Simulation Results with Updated Drag Package
 - Separate effects tests
 - Integral effects tests
 - Pressurized water reactor (PWR)

Identified Interfacial Drag Issues Severely Oscillatory Behavior (1/3)

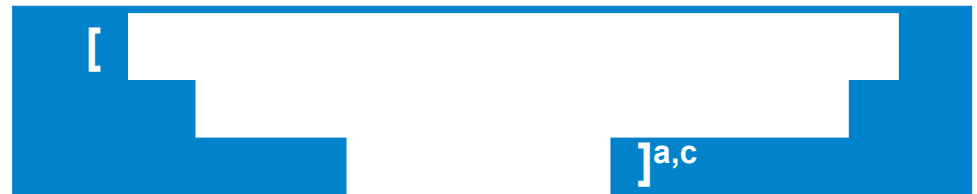
- Severely oscillatory behavior in GE Blowdown simulations

a,c

Identified Interfacial Drag Issues Severely Oscillatory Behavior (2/3)

[

]a,c



Identified Interfacial Drag Issues Severely Oscillatory Behavior (3/3)

[

]a,c

a,c

Identified Interfacial Drag Issues

Void Dipping

Void dipping observed in ORNL simulations

a,c

Impact of []^{a,c} on Void Prediction Profile

[]^{a,c}

(**Red**=orig, **Blue**=removed) in most cases



Review of Interfacial Drag Model: Sensitivity Study with Regime Dependent Multipliers

- Sensitivity study using regime-dependent multipliers with the code version with []^{a,c}
 - Small Bubble Drag (SB)
 - Large Bubble Drag (LB)
 - Film Drag (FD)

Regime Dependent Multiplier Study (1/4)

Small Bubble Regime (LB is set 1.0)

Original code without [

]a,c (Red=1.0, Blue=0.5)

a,c

[

]a,c

Regime Dependent Multiplier Study (2/4)

Large Bubble Regime (SB is set at 0.5)

Original code without [

]a,c (Red=1.0, Blue=0.5)

a,c

[

]a,c

Regime Dependent Multiplier Study (3/4)

Film Drag Regime

[
bound prediction of data

] ^{a,c} provides best-estimate to lower

a,c

Regime Dependent Multiplier Study (4/4)

Summary of Results

Sensitivity study using regime-dependent multipliers with the code version with [

]a,c

Interfacial Drag Model Updates (1/3)

Overview

- [

]a,c

Model updated to eliminate interfacial drag issues

Interfacial Drag Model Updates (2/3)

Model Review and Update

- [

]a,c

a,c

Interfacial Drag Model Updates (3/3)

Implementation of Bestion's Model

- [

]a,c

[

]a,c

Impact of Updated Drag Package

- Impact of the update
 - ORNL
 - G2
 - GE Blowdown
 - ROSA
 - PWR

Impact of Updated Drag Package ORNL Core Uncovery and Level Swell (1/5)

[

]a,c

a,c



Impact of Updated Drag Package

ORNL Core Uncovery and Level Swell (2/5)

a,c

[

]a,c

Impact of Updated Drag Package ORNL Core Uncovery and Level Swell (3/5)

a,c

[

]a,c

Impact of Updated Drag Package ORNL Core Uncovery and Level Swell (4/5)

a,c

[

]a,c

Impact of Updated Drag Package ORNL Core Uncovery and Level Swell (5/5)

[

]a,c

a,c



22

Impact of Updated Drag Package

G2 Boil-Off (1/2)

a,c

Impact of Updated Drag Package

G2 Boil-Off (2/2)

a,c

Noding sensitivity produces
reasonably converged results₂₄

Impact of Updated Drag Package GE Blowdown (1/12)

a,c

Partial mitigation in
2/7 simulations

Impact of Updated Drag Package GE Blowdown (2/12)

a,c

Impact of Updated Drag Package GE Blowdown (3/12)

a,c

Impact of Updated Drag Package GE Blowdown (4/12)

a,c

Impact of Updated Drag Package GE Blowdown (5/12)

a,c

Impact of Updated Drag Package GE Blowdown (6/12)

a,c

Impact of Updated Drag Package GE Blowdown (7/12)

a,c

Full mitigation in
other 5/7 simulations

Impact of Updated Drag Package GE Blowdown (8/12)

a,c

Impact of Updated Drag Package GE Blowdown (9/12)

a,c

Impact of Updated Drag Package GE Blowdown (10/12)

a,c

Impact of Updated Drag Package GE Blowdown (11/12)

a,c

Impact of Updated Drag Package GE Blowdown (12/12)

a,c

Impact of Updated Drag Package ROSA-LSTF (1/2)

a,c

[

]a,c

Impact of Updated Drag Package ROSA-LSTF (2/2)

a,c

Impact of Updated Drag Package Beaver Valley Unit 1 PWR (1/1)

a,c

Summary

- [

]a,c

**FSLOCA evaluation model has been
updated to address interfacial drag
issues**

Reference

- [

]a,c

Questions



This document is the property of and contains Proprietary Information owned by Westinghouse Electric Company LLC and/or its subcontractors and suppliers. It is transmitted to you in confidence and trust, and you agree to treat this document in strict accordance with the terms and conditions of the agreement under which it was provided to you.

Counter-Current Flow Limitation (CCFL)

Jeff Kobelak

May 13, 2014



Overview

- Staff concerned that CCFL was not checked in key areas
 - [
-]^{a,c}
- Westinghouse has taken action to address concern

Approach to address CCFL concern is outlined

CCFL Correlations (1/4)

WCOBRA/TRAC-TF2 Code

- CCFL cards available for application to loop components from TRAC-PF1
- Vessel component modified to accept existing CCFL cards
- Capability to impose CCFL in vessel and loop components

CCFL Correlations (2/4)

[]^{a,c}

- Discussed in Section 21.10.1 of Topical Report

- [

]^{a,c}

CCFL Correlations (3/4)

[]^{a,c}

- Discussed in Section 21.10.2 of Topical Report

- [

]^{a,c}

CCFL Correlations (4/4)

[]^{a,c}

- Discussed in Section 19.4 of Topical Report

- [

]^{a,c}

Code Simulations with CCFL (1/9)

Northwest Lab Perforated Plate

a,c

Code Simulations with CCFL (2/9)

ROSA-LSTF SB-CL-18

a,c

Code Simulations with CCFL (3/9)

ROSA-LSTF SB-CL-18

a,c

Code Simulations with CCFL (4/9)

ROSA-LSTF SB-CL-18

a,c

Code Simulations with CCFL (5/9)

ROSA-LSTF SB-CL-02

a,c

Code Simulations with CCFL (6/9)

ROSA-LSTF SB-CL-02

a,c

Code Simulations with CCFL (7/9)

ROSA-LSTF SB-CL-02

[

] a,c

Code Simulations with CCFL (8/9)

Beaver Valley PWR

a,c

Code Simulations with CCFL (9/9)

Beaver Valley PWR

a,c

Summary

- CCFL enforced in key areas
 - [

]a,c

Concern addressed by enforcing CCFL in key areas

Questions



This document is the property of and contains Proprietary Information owned by Westinghouse Electric Company LLC and/or its subcontractors and suppliers. It is transmitted to you in confidence and trust, and you agree to treat this document in strict accordance with the terms and conditions of the agreement under which it was provided to you.

Discussion Regarding Loop Seal Clearing

Aaron Everhard

May 13, 2014



Outline

- Summary of Code Simulation Results
- Review of Experimental Data
- Comparison of Code Results to Experimental Data
- Conclusions

Code Simulations

- [

]a,c



Sensitivity Study Results

- []^{a,c}

]a,c

[

]a,c

Results with [

]a,c

a,c

[

]a,c

Results from Broken Loop Study

- From parametric studies presented in August 2013



Conclusions from Code Simulations

- [

]a,c

Review of Experimental Data

- Experimental data reviewed for
 - Number of loop seals clear as a function of break size
 - Which loop seals clear (i.e., broken versus intact loop(s))
- Results used to justify acceptability of the []_{a,c}

Review of Experimental Data – Test Facilities

a,c

Review of Experimental Data – Break Size Scaling

a,c

Experimental Loop Seals Clear Results

a,c

Conclusions from Review of Experimental Data

- Transition from one to multiple loop seals clearing occurs between
 - [
 -]
 -]^{a,c}
- In most experiments, the broken loop clears
 - Experimental data does show intact loop can clear

Comparison of Code Results to Experimental Data

a,c

[

]a,c

Conclusions

- [

]a,c

References

- 1) Kim, Y-S., and Cho, S., "An experimental investigation of loop seal clearings in SBLOCA tests," *Annals of Nuclear Energy*, 2014, Vol. 63, pp. 721-730.
- 2) NEA/CSNI/R(R92)20, "ISP-27, OECD/NEA/CSNI International Standard Problem No.27, BETHSY experiment 9.1b, 2" Cold leg break without HPSI and with delayed Ultimate Procedure," R. Deruaz, November 1992.
- 3) Asaka, H., et al., "Results of 0.5% Cold-Leg Small-Break LOCA Experiments at ROSA-IV/LSTF: Effect of Break Orientation," *Experimental Thermal and Fluid Science*, 1990, Vol. 3, pp. 588-596.
- 4) JAERI-memo 62-399, "ROSA-IV/LSTF 2.5% Cold Leg Break LOCA Experiment, Data Report for Runs SB-CL-01, 02 and 03," Koizumi, Y., et al., November 1987.
- 5) JAERI-memo 61-056, "ROSA-IV/LSTF 5% Cold Leg Break LOCA Experiment Data Report, Run SB-CL-05," March 1986.
- 6) JAERI-M 89-027, "ROSA-IV/LSTF 5% Cold Leg Break LOCA Experiment, Run SB-CL-18 Data Report," March 1989.
- 7) EGG-SEMI-6884, "Quick Look Report for SEMISCALE MOD-2C Experiments S-LH-1 and S-LH-2," May 1985.
- 8) NUREG/CR-4945 / EGG-2509, "Summary of the SEMISCALE Program (1965-1986)," G. G. Loomis, July 1987.
- 9) NT33/94/011, "Versuch A5, Freiblasen des Pumpenbogens, Einzeleffekt- und Integralversuche," December 1994.

Questions



BACKUP SLIDES



[

]a,c Results

a,c

[

]a,c

This document is the property of and contains Proprietary Information owned by Westinghouse Electric Company LLC and/or its subcontractors and suppliers. It is transmitted to you in confidence and trust, and you agree to treat this document in strict accordance with the terms and conditions of the agreement under which it was provided to you.

Proposal for FULL SPECTRUM LOCA Analysis Method

Jeffrey Kobelak

May 13, 2014



Overview

- Analysis method for Small Breaks (Region I)
- Staff provided thoughts on possible approach
- Westinghouse's proposal
 - Generally follows outline from staff
 - Differences are explained

Region I Analysis Method

- [

]a,c

- Resolve remaining NRC concerns

Region I []^{a,c} (1/8)

Input Specification

- Parameter Specification
 - [

]^{a,c}

[]^{a,c}

Region I []^{a,c} (2/8) Method

- [

]^{a,c}

- Differences from position paper
 - Additional significant parameters biased
 - Fewer calculations executed for []^{a,c}
 - Resolution shown to be acceptable on later slide
 - Different []^{a,c}

Region I []^{a,c} (3/8)

Influence of Mesh Size

a,c

Region I []^{a,c} (4/8)

Influence of Mesh Size

[

] ^{a,c}

• [

] ^{a,c}

Region I []^{a,c} (5/8) Break Area Range

a,c

Region I []^{a,c} (6/8) Break Area Range

a,c

Region I []^{a,c} (7/8) Break Area Range

- [

]^{a,c}

[]^{a,c}

Region I []^{a,c} (8/8) Summary

- Adequately resolves resonance region
- Scoping studies illustrate no rapid changes in heat-up behavior missed with mesh size
- []^{a,c}



Safety Injection Line Rupture (1/2)

- Executed calculations with SI line rupture
 - [

]a,c



Safety Injection Line Rupture (2/2)

a,c

Offsite Power Availability (1/3)

- [

]a,c

[

]a,c

Offsite Power Availability (2/3)

a,c

Figure 3.2-33: Hot Rod PCT for the Cold Leg Break RCP Trip Time Sensitivity Study

Offsite Power Availability (3/3)

a,c

Uncertainty Analysis (1/4)

- Uncertainty analysis will follow topical report approach with the following changes
 - [

]a,c

- Differences from “position paper”
 - PLHGR would follow RAI 36-39 approach
 - No additional cases (e.g. conservative case)
 - No spreadsheet as part of generic method

Uncertainty Analysis (2/4)

a,c

Uncertainty Analysis (3/4)

a,c

Uncertainty Analysis (4/4)

a,c

Summary

- [

]a,c

- Otherwise analysis would proceed as described in topical report

- [

]a,c

Approach addresses identified NRC concerns

Questions



**Summary of June 2014 NRC Audit of FULL SPECTRUM LOCA (FSLOCA) Evaluation Model”
(Non-Proprietary)**

June 2014

Westinghouse Electric Company LLC
1000 Westinghouse Drive
Cranberry Township, PA 16066

©2014 Westinghouse Electric Company LLC
All Rights Reserved

1.0 Introduction

In June 2014, the Nuclear Regulatory Commission (NRC) performed an audit of the FULL SPECTRUM™ LOCA (FSLOCA™) evaluation model (EM) submittal.

During the audit, Westinghouse presented information related to two main topics. The first presentation focused on an explanation of the evaluation model changes related to fuel rod models (including thermal conductivity degradation), burnup methodology, and axial power shape generation that resulted from the response to Requests for Additional Information (RAIs) 36 through 39 (LTR-NRC-14-17 [1-1]). That presentation is included later in this package.

The second presentation was focused on a limited number of miscellaneous changes to the FSLOCA methodology. Additional information describing the updates to the FSLOCA evaluation model and providing the associated technical basis is included in this attachment. Section 2.0 describes an update to [

] ^{a,c} Section 3.0 describes an update to the accumulator elevation modeling and broken loop sampling.

During the discussion related to the burnup methodology and fuel rod models, more information regarding the initial stored energy was requested. Section 4.0 provides [

] ^{a,c}

1.1 Reference(s)

- 1-1) LTR-NRC-14-17, "Submittal of Westinghouse Responses to 'WCAP-16996-P, 'Realistic LOCA Evaluation Methodology Applied to the Full Spectrum of Break Sizes (FULL SPECTRUM LOCA Methodology)' Request for Additional Information – RAIs 36-39' (Proprietary/Non-Proprietary), Project 700, TAC No. ME5244," March 24, 2014.

ZIRLO is a registered trademark and Optimized ZIRLO, FULL SPECTRUM, and FSLOCA are trademarks of Westinghouse Electric Company LLC, its subsidiaries and/or its affiliates in the United States of America and may be registered in other countries throughout the world. All rights reserved. Unauthorized use is strictly prohibited. Other names may be trademarks of their respective owners.

2.0 Downcomer Lateral Form Loss

The Nuclear Regulatory Commission (NRC) has previously questioned the modeling of lateral losses in the downcomer annulus for best-estimate evaluation models. One example occurred during the licensing of a plant-specific, ASTRUM analysis as described in AEP-NRC-2011-15 [2-1]. Physically, it is expected that the lateral losses could have competing effects on a Large Break LOCA (LBLOCA) transient. An increased loss could promote breakdown of bypass earlier in the transient, but could also serve to reduce mixing in the downcomer later in the transient.

Previously, [

] ^{a,c} As such, the methodology is updated to more appropriately model the azimuthal loss through the downcomer annulus.

[

] ^{a,c}

2.1 Reference(s)

- 2-1) AEP-NRC-2011-15, "Response to Second Request for Additional Information Regarding a License Amendment Request Associated With the Large-Break Loss-Of-Coolant Accident Analysis Methodology (TAC No. ME1017)," February 24, 2011. (ADAMS Accession Number ML110680210)
- 2-2) Idelchik, I. E., 1994, "Handbook of Hydraulic Resistance," 3rd Edition, CRC Press, Inc.

3.0 Modeling of Loop-to-Loop Differences

3.1 Background / Purpose

There are two differences from loop-to-loop that could impact the LOCA analysis for Westinghouse-designed plants. The first is the geometry of the accumulator lines, and the second is the location of the pressurizer. A modeling approach for LBLOCA analysis had been addressed in prior Westinghouse evaluation models.

In the context of the FSLOCA methodology, the loop-to-loop differences must not only be considered for the LBLOCA analysis but also for Small Break LOCA (SBLOCA) analysis. Rather than considering the applicability of the prior LBLOCA modeling approach for SBLOCA, it was proposed that [

] ^{a,c}

However, during the licensing of the FSLOCA evaluation model, it was determined that a [

] ^{a,c} (described in Section 3 of LTR-NRC-14-29 [3-3]). Additionally, a large number of SBLOCA sensitivity study results are available from the licensing of the evaluation model. As such, a [

] ^{a,c} is considered relative to the Region I analysis.

3.2 Prior Region II (LBLOCA) Modeling Approach

3.2.1 Accumulator Line Modeling

The treatment of the accumulator line modeling for the original Westinghouse Code Qualification Document (CQD) Best-Estimate LBLOCA evaluation model is discussed in Section 16-2-4 of WCAP-12945-P-A [3-1]. The following discussion is excerpted from therein:

“Although the accumulators are of the same design for all loops, the lines connecting the accumulator and the cold leg may vary from loop to loop. In the WCOBRA/TRAC PWR plant model, the accumulator and the connecting line in all loops are [

] ^{a,c}

Figure 16-2-7 from WCAP-12945-P-A is included as Figure 3-1 herein. This figure compares the accumulator blowdown behavior [

] ^{a,c}

[

] ^{a,c} was appropriate for LBLOCA analysis. That same modeling approach was maintained for the Automated Statistical Treatment of Uncertainty Method (ASTRUM) LBLOCA evaluation model (WCAP-16009-P-A [3-2]).

3.2.2 Pressurizer Location Modeling

The modeling of the pressurizer location for the Westinghouse ASTRUM Best-Estimate LBLOCA evaluation model is discussed in Section 12-3-1 of WCAP-16009-P-A. The following discussion is excerpted from therein:

“Pressurizer Location: Sensitivity studies have shown that locating the pressurizer [

] ^{a,c}

To summarize, sensitivity studies indicated that the location of the pressurizer relative to the broken loop [

] ^{a,c}

3.3 Consideration of Region I (SBLOCA) Analysis

3.3.1 Accumulator Elevation Modeling

SBLOCA sensitivity studies for the accumulator elevation were included in Section 28.2.5 of the FSLOCA topical report [3-4]. These studies indicate that [

] ^{a,c}

The impact of accumulator elevation on driving head can influence both the initial actuation of the accumulator under SBLOCA transient conditions, as well as the periods of intermittent injection which occur after the initial injection. [

] ^{a,c}

[

] ^{a,c}

[

] ^{a,c}

The Region I analysis method is described in Section 4.0 of LTR-NRC-14-29. [

] ^{a,c}

3.3.2 Pressurizer Location Modeling

A large number of SBLOCA parametric studies were presented and discussed in Section 2 of LTR-NRC-13-70 [3-6]. A number of these studies were performed with the break initiated in all three different loops. The results of the studies show that [

] ^{a,c} This was also noted in the discussion in Section 3 of LTR-NRC-14-29, supported by the results shown on page P-110 therein.

In summary, the Region I (SBLOCA) analysis is [

] ^{a,c}

3.4 Conclusions and FSLOCA Modeling Approach

[

] ^{a,c}

[]^{a,c}

Given these considerations, the FSLOCA evaluation model is updated as follows: [

] ^{a,c}

3.5 Reference(s)

- 3-1) WCAP-12945-P-A, Volume 1, Revision 2, and Volumes 2 through 5, Revision 1, "Code Qualification Document for Best Estimate LOCA Analysis," March 1998.
- 3-2) WCAP-16009-P-A, "Realistic Large-Break LOCA Evaluation Methodology Using the Automated Statistical Treatment Of Uncertainty Method (ASTRUM)," January 2005.
- 3-3) LTR-NRC-14-29, "Summary of May 2014 NRC Audit of the FULL SPECTRUM LOCA (FSLOCA) Evaluation Model (Proprietary/Non-Proprietary), Project 700, TAC No. ME5244," June 5, 2014.
- 3-4) WCAP-16996-P, "Realistic LOCA Evaluation Methodology Applied to the Full Spectrum of Break Sizes (FULL SPECTRUM LOCA Methodology)," November 2010.
- 3-5) LTR-NRC-14-9, "Submittal of Westinghouse Responses to 'WCAP-16996-P, 'Realistic LOCA Evaluation Methodology Applied to the Full Spectrum of Break Sizes (FULL SPECTRUM LOCA Methodology)' Request for Additional Information – Set 8 RAIs 122-126, 128-131 and 136' (Proprietary/Non-Proprietary), Project 700, TAC No. ME5244," February 12, 2014.
- 3-6) LTR-NRC-13-70, "Summary of July 2013 NRC Code Workshop and August 2013 NRC Audit of the FULL SPECTRUM LOCA (FSLOCA) Evaluation Model (Proprietary/Non-Proprietary)," October 10, 2013.



Figure 3-1: Comparison of Detailed Noding with Simplified PWR Noding Prediction of Accumulator Pressure (Figure 16-2-7 from WCAP-12945-P-A)



Figure 3-2: Vessel Fluid Inventory and Integrated Accumulator Injection Flow for the 2.5-inch Hot Leg and Cold Leg Break (Figure 3.2-12 from LTR-NRC-14-9)



Figure 3-3: Hot Rod PCT for the 2.5-inch and 3-inch Hot Leg and Cold Leg Breaks (Figure 3.2-16 from LTR-NRC-14-9)

4.0 Initial Stored Energy

RAI 37 asked for an explanation of the fuel rod initialization, calibration, and the modeling of fuel burnup effects. In the response provided in LTR-NRC-14-17 [4-1], [

] ^{a,c} During the June audit, more information regarding stored energy was requested.

Table 4-1 provides [

] ^{a,c}

Table 4-1: []^{a,c}

[
] ^{a,c}

4.1 Reference(s)

- 4-1) LTR-NRC-14-17, "Submittal of Westinghouse Responses to 'WCAP-16996-P, 'Realistic LOCA Evaluation Methodology Applied to the Full Spectrum of Break Sizes (FULL SPECTRUM LOCA Methodology)' Request for Additional Information – RAIs 36-39' (Proprietary/Non-Proprietary), Project 700, TAC No. ME5244," March 24, 2014.

Presentations from the June 2014 NRC Audit

ZIRLO is a registered trademark and Optimized ZIRLO, FULL SPECTRUM, and FSLOCA are trademarks of Westinghouse Electric Company LLC, its subsidiaries and/or its affiliates in the United States of America and may be registered in other countries throughout the world. All rights reserved. Unauthorized use is strictly prohibited. Other names may be trademarks of their respective owners.

RAI 36-39 Responses and Associated Method Updates

Michael Shockling

Westinghouse Electric Company

June 2014



Overview

- [

]a,c

Objective: Summarize RAI 36-39 Response Package (LTR-NRC-14-17)

[Overview

]a,c

- [

]a,c

[
]a,c

[]^{a,c} Overview

- []

]a,c

[]^{a,c} Overview

- []

]a,c

[

]a,c

[

]a,c

• [

]a,c

[

]a,c

• [

]a,c

[

]a,c

a,c

[

]a,c

Figure RAI37-3 [

]a,c

Figure RAI37-4 [

]a,c

[

]a,c

- [

]a,c

]a,c

- [

]a,c

]a,c

• [

]a,c

]a,c

]a,c

a,c

]a,c

]a,c

]a,c

a,c

]a,c

a,c

]a,c

]a,c

]a,c

• [

]a,c

[

]a,c

]a,c

a,c

]a,c

a,c

]a,c

• [

]a,c

]a,c

]a,c

a,c

[

]a,c

• [

]a,c

[

]a,c

[

]a,c

• [

]a,c

[

]a,c

a,c

[

]a,c

• [

]a,c

[

]a,c

a,c

[

]a,c

• [

]a,c

[

]a,c

]a,c

[

]a,c

a,c

[

]a,c

• [

]a,c

]a,c

]a,c

]a,c

a,c

[
]a,c

• [

]a,c

]a,c

a,c

[

]a,c

• [

]a,c

[

]a,c

[

]a,c

• [

]a,c

]a,c

• [

]a,c

a,c

]a,c

a,c

]a,c

• [

]a,c

a,c

]a,c

]a,c

]a,c

[

]a,c

a,c

[

]a,c

• [

]a,c

[

]a,c

a,c

[

]a,c

a,c

[
]a,c

• [

]a,c

[
]a,c

a,c

Figure 29.4.1-5 [

]a,c

Figure 29.4.1-8 [

]a,c

• [

]a,c

[
]a,c

a,c

Figure 29.4.1-9 Example Bottom Skewed Axial Power Distribution [
]a,c

Figure 29.4.1-10 Example Top Skewed Axial Power Distribution [
]a,c

[

]a,c

• [

]a,c

[

]a,c

• [

]a,c

Questions / Backup



Fuel Rod Behavior vs Burnup

a,c

Allowable Transient Oxidation

a,c

[

]a,c

a,c

Figure RAI37-6

[

]a,c

**Summary of August 2014 NRC Audit Part 1 of FULL SPECTRUM LOCA (FSLOCA) Evaluation Model”
(Non-Proprietary)**

September 2014

Westinghouse Electric Company LLC
1000 Westinghouse Drive
Cranberry Township, PA 16066

©2014 Westinghouse Electric Company LLC
All Rights Reserved

August 2014 FULL SPECTRUM LOCA Audit Summary – Part 1

Introduction

The review of the FULL SPECTRUM™ LOCA (FSLOCA™) evaluation model has spanned a four year period. During that time, there were a series of interactions with the Nuclear Regulatory Commission (NRC) that included draft Requests for Additional Information (RAIs), formal RAIs, periodic meetings and audits.

During the recent August 2014 audit, a plan to close all of the open items related to the RAI responses was established. The plan is to provide additional information to the NRC in a two part audit summary. Part one of the audit summary, provided herein, transmits the additional information that was requested for a subset of the open items. The remaining information will be transmitted in the part two audit summary.

Considerable effort is required to prepare the audit summaries. This requires a diversion of resources resulting in an impact to the current schedule for updating the topical report. Westinghouse is re-evaluating the schedule to determine a revised delivery date of the updated volumes.

RAI-23

It is clarified that the maximum assembly []^{a,c}
and the maximum peak rod []^{a,c}

RAI-36

[]^{a,c}

FULL SPECTRUM and FSLOCA are trademarks of Westinghouse Electric Company LLC, its subsidiaries and/or its affiliates in the United States of America and may be registered in other countries throughout the world. All rights reserved. Unauthorized use is strictly prohibited. Other names may be trademarks of their respective owners.

[

]^{a,c}

Rod stored energy was shown to be []^{a,c} in Section 4.0 of LTR-NRC-14-38 [3].

RAI-37

Regarding the conformance of the results shown in Figures RAI37-1 through 37-4 of LTR-NRC-14-17 with the proposed []^{a,c} please see the discussion on page P-16 of LTR-NRC-14-17. Specifically, see the passage: [

]^{a,c}

It is clarified that “Average temperatures” for WCOBRA/TRAC-TF2 and PAD5 are volume-averaged quantities. The rod stored energy was shown to be []^{a,c} in Section 4.0 of LTR-NRC-14-38.

The fuel thermal conductivity and gap conductance models in WCOBRA/TRAC-TF2 are [

]^{a,c}

RAIs 36 through 39 – Gap Conductance

During the audit, the NRC requested additional information related to the fuel rod initialization process discussed in the response to RAIs 36 and 37, originally provided in LTR-NRC-14-17. [

]^{a,c}

RAIs 36 through 39 – Processing of Axial Power Distributions

[

]^{a,c}

[

]^{a,c}

[

]^{a,c}

[

] ^{a,c}

Conclusions

[

] ^{a,c}

RAI-46**Code Version and Input**

The version of COCO that is coupled to WCOBRA/TRAC-TF2 is COCO_A Version 1.4. COCO_A Version 1.4 was released in September 2001. As such, COCO_A Version 1.4 has been used for all Automated Statistical Treatment of Uncertainty Method (ASTRUM) analyses (WCAP-16009-P-A [6]) that included a re-calculation of the containment back-pressure for dry containment designs.

A list of updates for coupling COCO_A Version 1.4 to WCOBRA/TRAC-TF2 and references to the theoretical bases are given in the response to Question 1 of RAI 46 (see LTR-NRC-13-73 [7]). They are summarized as follows:

- WCAP-8327-P [8]: This document contains a description of the models in COCO.
- WCAP-8471-P-A [9]: This document contains NRC approval of COCO for use with the 1974 Appendix K Evaluation Model (EM).
- WCAP-8339 [10]: Appendix A of this document contains guidance for application of COCO. Much of this guidance still applies, but an updated list of inputs and assumptions is given in the response to Question 4 of RAI 46 (see LTR-NRC-13-73).
- WCAP-9220-P-A, Revision 1 [11]: This document contains a discussion of the modeling of paint in COCO.
- WCAP-10266-P-A, Revision 2 [12]: This document contains NRC approval of COCO for use with the BASH Appendix K EM.

The most complete user's manual is that for containment integrity analyses, which explains all inputs. For Large Break LOCA (LBLOCA) analyses to confirm emergency core cooling system (ECCS) performance, some generic inputs and additional user guidance are given in guidance documents.

Standalone Version Comparison to Coupled Version

A Double-Ended Guillotine (DEG) break case and a split break case were performed to compare the results of a standalone COCO run with those of a coupled COCO run. In each of these test cases, a case is first run with the coupled COCO model. Then, the mass and energy releases (M&Es) from the reactor coolant system (RCS) for that run are used as input for a standalone COCO_A Version 1.4 run. The pressure comparisons for the test cases are included in Figures 19 and 20. These figures show that [

] ^{a,c}

Containment Leakage

[

] ^{a,c}

[

] ^{a,c}**Non-Condensable Gas Treatment**

[

] ^{a,c}**Paint/Coating Qualification**

A proposed methodology for Generic Safety Issue 191 (GSI-191) analysis was created by industry representatives in NEI-04-07 [13]. From Section 3.4.3.3.4 of Volume I of NEI-04-07, all indeterminate and design basis accident (DBA)-unqualified and unacceptable coatings are considered to fail. In NEI-04-07, the definitions of DBA-qualified/acceptable, DBA-unqualified/unacceptable, and indeterminate coatings are taken from ASTM D5144-00; however, this document has been superseded, and the most appropriate document is Regulatory Guide 1.54, Revision 2 [14]. In addition to the DBA-unqualified/unacceptable and indeterminate coatings, any DBA-qualified/acceptable coatings within the Zone of Influence (ZOI) of the break are considered to fail.

ZOIs were proposed in NEI-04-07, but the issue was finally resolved in Reference [15], in which the NRC allows a ZOI with a radius of 4 times the pipe diameter for epoxy coatings, and a ZOI with a radius of 10 times the pipe diameter for un-topcoated inorganic zinc coatings.

In order to conform to the standards for GSI-191, unqualified or indeterminate coatings throughout containment and qualified coatings within the ZOI will not be credited in FSLOCA analyses. Although the DBA-qualification testing makes use of a containment pressure/temperature transient that is at significantly higher temperature and pressure than is expected for a LBLOCA ECCS performance analysis (see ANSI N101.2-1972 [16] for an example of DBA-qualification testing), data is not readily available to justify use of unqualified coatings. As such, no attempt will be made to credit these coatings, which is conservative.

Typographical Error

In the response to Question 2 in LTR-NRC-13-73, the statement in modelling assumption c) should be changed to: "...only multilayered flat walls are considered and heat transfer is neglected in any direction **except** perpendicular to the wall surface."

Heat Sink Noding

Each layer of a heat sink requires inputs for the number of nodes in the layer, the thickness of the layer, the thermal conductivity of the layer, the volumetric heat capacity of the layer, and the heat transfer coefficient/emissivity with the next layer. Based on this, a layer can simply be considered a section with user-supplied thickness and number of nodes which is used to model a change in heat transfer characteristics, whereas a node is simply a subdivision of a layer to perform the heat transfer calculations across the walls.

[]^{a,c}

Interior Walls

[]^{a,c}

Initial Containment Temperature

For the FSLOCA methodology, a plant-specific initial containment temperature value will be determined based on customer input, and the assumption of []^{a,c} for initial containment temperature will not be used.

Generic End of Blowdown Time and Energy Released

The directions of conservatism for the []^{a,c} are explained in the response to Question 5 in LTR-NRC-13-73. However, the magnitudes of the values are considered below. A representative set of plants was used to determine the bounding nature of these values by checking the plant-specific COCO values that are currently used for several analyses.

- []

] ^{a,c}

Based on these investigations, the []

] ^{a,c}

Tagami Equation Exponential Decay

The Tagami correlation is based on the work done in (Tagami, 1966) [17]. The heat transfer coefficient is given by (units are BTU/hr-ft²-°F):

$$h_s = h_{stag} + (h_{max} - h_{stag})e^{-0.05(t-t_p)}, t > t_p$$

Where:

$$h_{stag} = 2 + 50x, x = \text{steam to air weight ratio in containment}$$

Based on review of (Tagami, 1966), it is apparent that this correlation is based on Section 4 of (Tagami, 1966). The h_{stag} correlation is from a linear curve fit to the data in Figure 4.3. For the remainder of the heat transfer coefficient equation, Figures 4.6 and 4.7 are used. Using the heat transfer coefficient equation above, a curve was created for all the points after blowdown in Figure 4.6. In addition, a curve was created with the same equation with []^{a,c} (this is the method currently used for FSLOCA analyses). In both of these equations, a constant h_{stag} set to the end of transient value was used in order to simplify the calculations.

These curves are both presented in Figure 21, along with the data from (Tagami, 1966). Based on Figure 21, []

] ^{a,c}

Emissivity of Exterior Containment Walls

The basis for the []^{a,c} emissivity is explained in the response to Question 4 in LTR-NRC-13-73. A sensitivity study is shown herein that justifies the use of the []

] ^{a,c}

RAI-47

It is clarified that the input flag []^{a,c} within the FSLOCA evaluation model.

[]

] ^{a,c}

RAI-48

The steam generator nodding was primarily derived from the simulation of the Rig-of-Safety Assessment (ROSA) Large Scale Test Facility (LSTF) natural circulation tests. The original steam generator nodding utilized a []

] ^{a,c} Various nodding sensitivity studies were executed to examine the impact on the simulation results, including the loop circulation flows and liquid holdup in the uphill side of the generator at different fluid inventories.

The nodding sensitivity studies included the addition of a []

] ^{a,c}

[

]^{a,c}

It is clarified that the statement that the single-pipe steam generator model produces conservative results is based on the liquid holdup behavior in the steam generator. It was shown that the single-pipe model tends to retain excess liquid in the uphill side of the steam generator tubes relative to the measured data, which results in increased pressure drop through the steam generator and hangs up the primary side pressure under SBLOCA conditions.

RAI-51

The data from (Lee and Ryley, 1968) [19] are presented against the code predictions in Figure 23. It can be seen that the code [

]^{a,c} The (Yuen and Chen, 1978) [20] data are presented against the code predictions in Figure 24, which indicates that [

]^{a,c}

RAI-85

It is clarified that the meaning of [

]^{a,c} Since the interfacial drag decreases significantly with flow stratification, the lack of stratification ensures that the interfacial drag will remain higher, which is more likely to result in limiting the liquid downflow against the forward vapor flow. It is also noted that the methodology was updated to []^{a,c} as described in the presentation attached to LTR-NRC-14-29, and discussed more in the following paragraph.

[

]^{a,c}

[

]^{a,c}

RAI-95

After the FSLOCA evaluation model is approved, a working level procedure will be written for analysts that details the implementation of the approved method for production. This is the same approach that was employed for prior, approved best-estimate evaluation models such as ASTRUM (WCAP-16009-P-A) and Code Qualification Document (CQD) (WCAP-12945-P-A [23]).

RAI-127

It is clarified that for Region I (small breaks), the [

]^{a,c}

RAI-132

It is clarified that the pressure drop from the steam generator secondary side to the Main Steam Safety Valves (MSSVs) will be [^{a,c}

RAI-133

[

]^{a,c}

The steam generator secondary-side conditions control the vessel average temperature. Since the plants control to a target vessel average temperature, the reduction in the heat transfer coefficient on the outside of the tubes impacts the steam generator secondary-side conditions (pressure, temperature) in order to maintain the desired vessel average temperature. Hand

calculations were performed that indicate [

] ^{a,c} This behavior is consistent with that expected for plant operation when fouling accrues on the secondary side.

It is clarified that Figure 133-3 in the response to RAI 133 in LTR-NRC-14-4 [24] shows the steam generator secondary-side pressure. From Table 132-1 in the response to RAI 132 in LTR-NRC-14-4, the setpoint pressure is [

] ^{a,c}

RAI-134

The plant-specific steam generator tube plugging (SGTP) level to be analyzed is provided as input to the FSLOCA analysis as described in Section 5.0 of LTR-NRC-14-4.

The impact of the SGTP level on the PCT during the blowdown phase of a LBLOCA was discussed in Section 2.1 of LTR-NRC-14-4. To summarize, it was stated that the [

] ^{a,c}

References

- 1) NUREG/CR-6534, Volume 4, "FRAPCON-3 Updates, Including Mixed-Oxide Fuel Properties," May 2005.
- 2) LTR-NRC-14-17, "Submittal of Westinghouse Responses to 'WCAP-16996-P, 'Realistic LOCA Evaluation Methodology Applied to the Full Spectrum of Break Sizes (FULL SPECTRUM LOCA Methodology)' Request for Additional Information – RAIs 36-39' (Proprietary/Non-Proprietary), Project 700, TAC No. ME5244," March 24, 2014.
- 3) LTR-NRC-14-38, "Summary of June 2014 NRC Audit of the FULL SPECTRUM LOCA (FSLOCA) Evaluation Model (Proprietary/Non-Proprietary), Project 700, TAC No. ME5244," June 27, 2014.
- 4) WCAP-8385 (P), "Power Distribution Control and Load Following Procedures," 1974.
- 5) LTR-NRC-14-29, "Summary of May 2014 NRC Audit of the FULL SPECTRUM LOCA (FSLOCA) Evaluation Model (Proprietary/Non-Proprietary), Project 700, TAC No. ME5244," June 5, 2014.
- 6) WCAP-16009-P-A, "Realistic Large-Break LOCA Evaluation Methodology Using the Automated Statistical Treatment Of Uncertainty Method (ASTRUM)," January 2005.
- 7) LTR-NRC-13-73, "Submittal of Westinghouse Responses to 'WCAP-16996-P, 'Realistic LOCA Evaluation Methodology Applied to the Full Spectrum of Break Sizes (FULL SPECTRUM LOCA Methodology)' Request for Additional Information – RAIs 46-58, 75, and 77' (Proprietary/Non-Proprietary), Project 700, TAC No. ME5244," October 2013.
- 8) WCAP-8327-P, "Containment Pressure Analysis Code (COCO)," July 1974
- 9) WCAP-8471-P-A, "The Westinghouse ECCS Evaluation Model: Supplementary Information," April 1975.
- 10) WCAP-8339, "Westinghouse Emergency Core Cooling System Evaluation Model – Summary," June 1974.
- 11) WCAP-9220-P-A, Revision 1, "Westinghouse ECCS Evaluation Model 1981 Version," February 1982.
- 12) WCAP-10266-P-A, Revision 2, "The 1981 Version of the Westinghouse ECCS Evaluation Model Using the BASH Code," March 1987.
- 13) NEI-04-07, "Pressurized Water Reactor Sump Performance Evaluation Methodology," December 2004. (ADAMS Accession Numbers ML050550138 for Volume I, ML050550156 for Volume II)

- 14) Regulatory Guide 1.54, Revision 2, "Service Level I, II, and III Protective Coatings Applied to Nuclear Power Plants," October 2010.
- 15) NRC Letter, "Revised Guidance Regarding Coatings Zone of Influence for Review of Final Licensee Responses to Generic Letter 2004-02, 'Potential Impact of Debris Blockage on Emergency Recirculation During Design Basis Accidents at Pressurized-Water Reactors,'" April 2010. (ADAMS Accession Number ML100960495)
- 16) ANSI N101.2-1972, "Protective Coatings (Paints) for Light Water Nuclear Reactor Containment Facilities," May 1972.
- 17) Tagami, Takashi, "Interim Report on Safety Assessments and Facilities Establishment Project in Japan for Period Ending June, 1965 (No. 1)," February 28, 1966.
- 18) WCAP-16996-P, "Realistic LOCA Evaluation Methodology Applied to the Full Spectrum of Break Sizes (FULL SPECTRUM LOCA Methodology)," November 2010.
- 19) Lee, Kwan and Ryley, D. J., "The Evaporation of Water Droplets in Superheated Steam," *Journal of Heat Transfer*, Vol. 90, pp. 445-451, 1968.
- 20) Yuen, M. C. and Chen, L. W., "Heat-Transfer Measurements of Evaporating Liquid Droplets," *Int. J. Heat Mass Transfer*, Volume 21, pp. 537-542, 1978.
- 21) Glaeser, H. and Karwat, H., "The contribution of UPTF experiments to resolve some scale-up uncertainties in countercurrent two phase flow," *Nuclear Engineering and Design*, 145, pp. 63 - 84, 1993.
- 22) Mayinger, F., et al., "Two-phase flow phenomena in full-scale reactor geometry," *Nuclear Engineering and Design*, 145, pp. 47 - 61, 1993.
- 23) WCAP-12945-P-A, "Code Qualification Document for Best Estimate LOCA Analysis," March 1998.
- 24) LTR-NRC-14-4, "Submittal of Westinghouse Responses to 'WCAP-16996-P, 'Realistic LOCA Evaluation Methodology Applied to the Full Spectrum of Break Sizes (FULL SPECTRUM LOCA Methodology)' Request for Additional Information – Set 8 RAIs 127, 132-135 and 137-139' (Proprietary/Non-Proprietary), Project 700, TAC No. ME5244," January 30, 2014.

Table 1: Average Blowdown PCT as a Function of the Steam Generator Tube Plugging

	a,c
--	-----

a,c

Figure 1: [

]^{a,c}

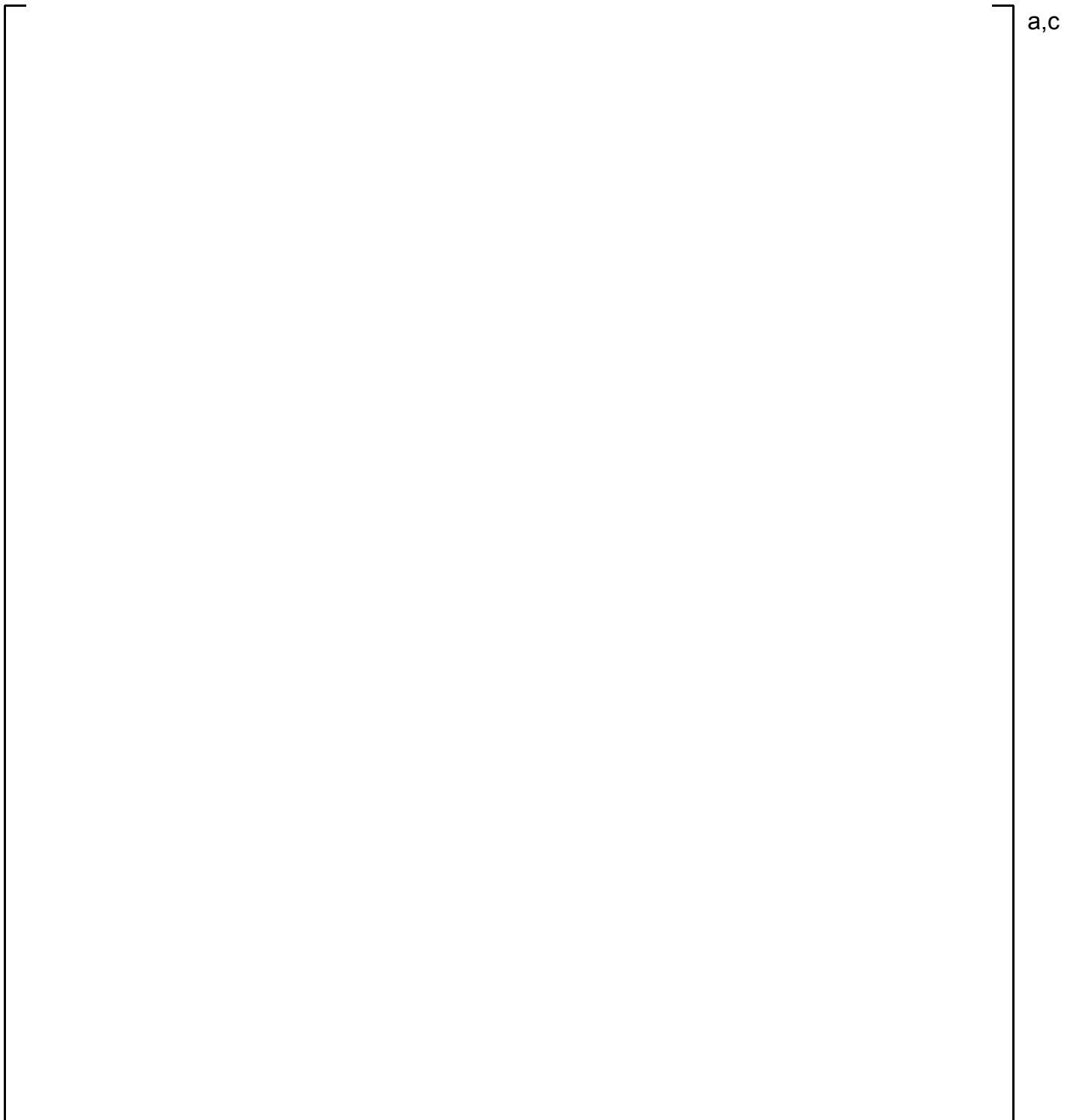


Figure 2: [

]^{a,c}

a,c

Figure 3: [

]^{a,c}

a,c

Figure 4: [

]^{a,c}

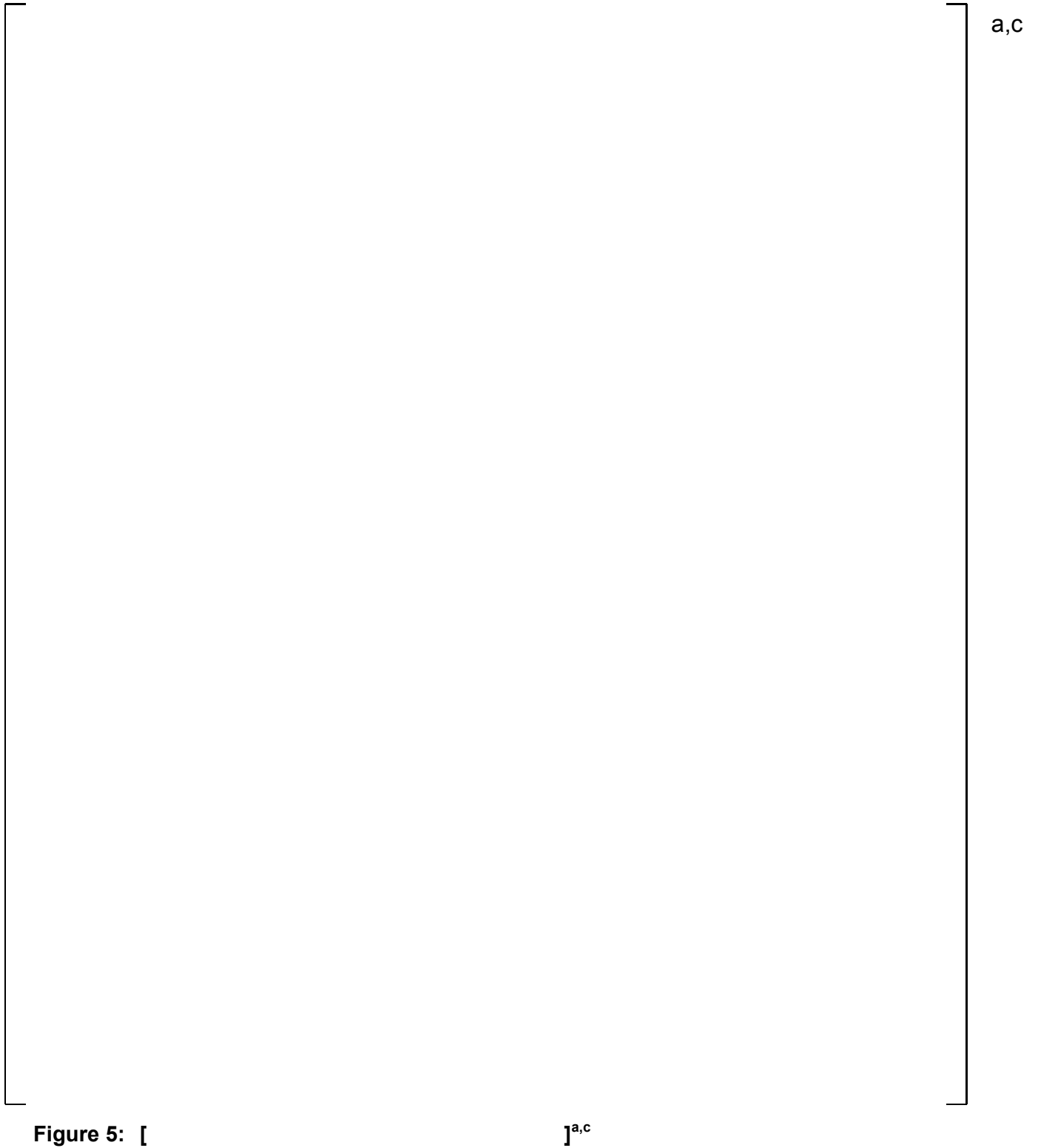


Figure 5: [

]^{a,c}

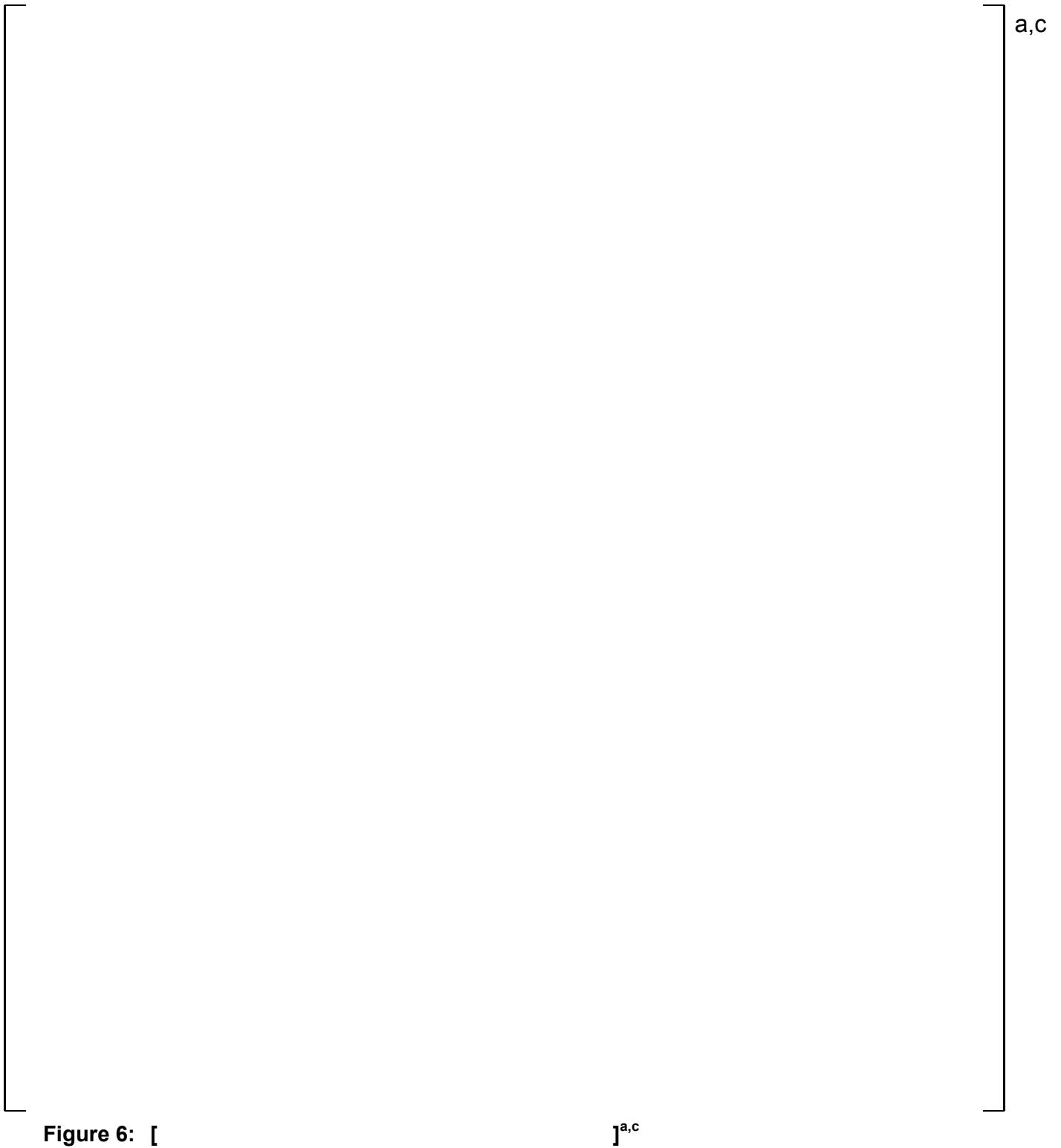


Figure 6: [

a,c

Figure 7: [

]^{a,c}

a,c

Figure 8: [

]^{a,c}

a,c

Figure 9: [

]^{a,c}

a,c

Figure 10: [

]^{a,c}

a,c

Figure 11: [

]^{a,c}

a,c

Figure 12: [

]^{a,c}

a,c

Figure 13:

]^{a,c}

a,c

Figure 14: [

]^{a,c}



Figure 15: []^{a,c}

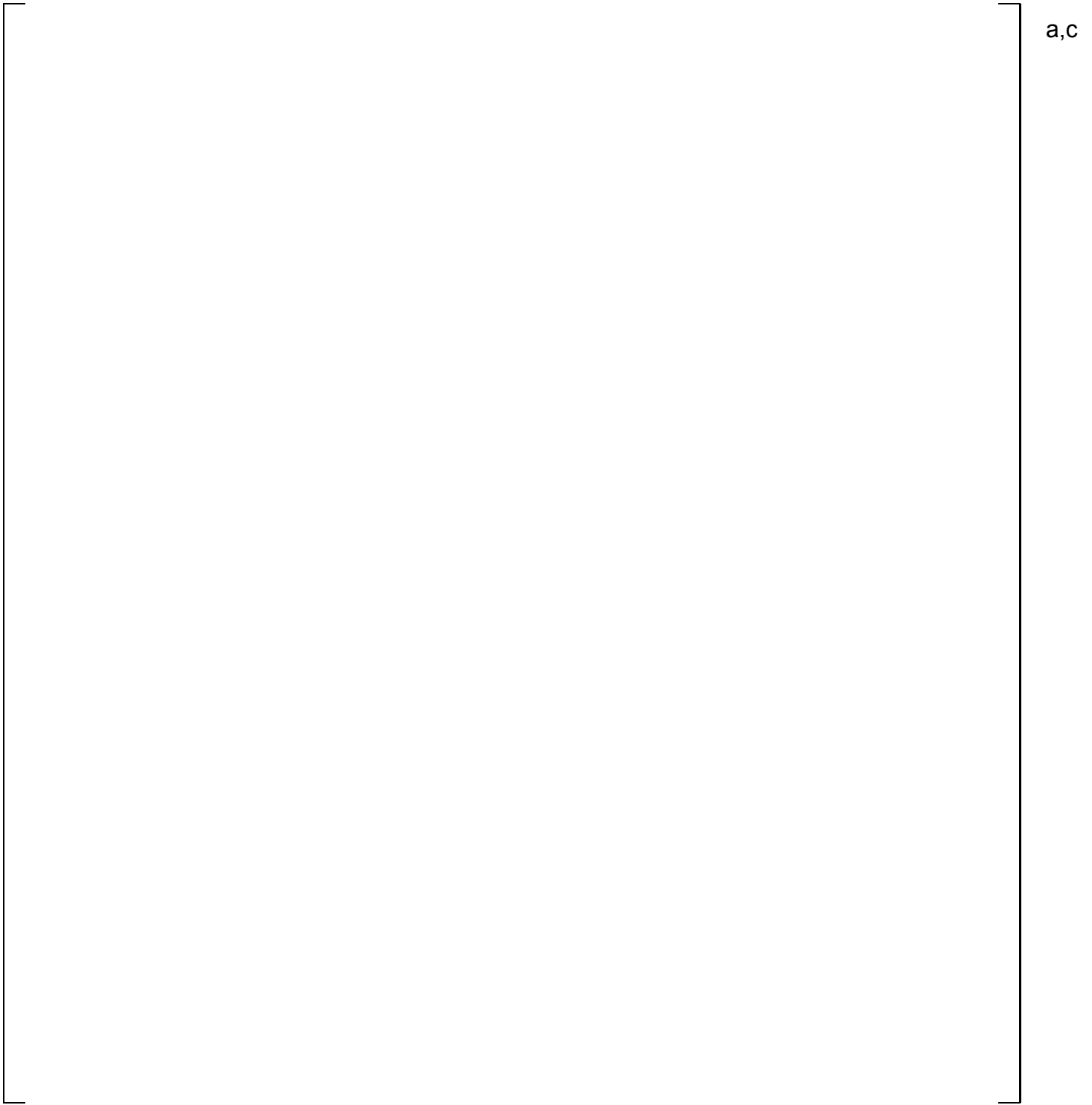


Figure 16: []^{a,c}

a,c

Figure 17: [

]^{a,c}

a,c

Figure 18: [

]^{a,c}

a,c

Figure 19: Double-Ended Guillotine Break Containment Pressure Comparison between Calculations with COCO Integrated into WCOBRA/TRAC-TF2 and Calculations with COCO_A Version 1.4

a,c

Figure 20: Split Break Containment Pressure Comparison between Calculations with COCO Integrated into WCOBRA/TRAC-TF2 and Calculations with COCO_A Version 1.4

a,c

Figure 21: Tagami Data and Calculated Heat Transfer Coefficients

a,c

Figure 22: Emissivity Sensitivity Study Results

a,c

Figure 23: Comparison of WCOBRA/TRAC-TF2 DFFB Interfacial Heat Transfer to the Data from Lee and Ryley, 1968

a,c

Figure 24: Comparison of WCOBRA/TRAC-TF2 DFFB Interfacial Heat Transfer to the Data from Yuen and Chen, 1978

a,c

Figure 25: Cumulative Distribution Function of the Region II Blowdown PCT Results for Different Steam Generator Tube Plugging Levels

**Summary of August 2014 NRC Audit Part 2 of FULL SPECTRUM LOCA (FSLOCA) Evaluation Model”
(Non-Proprietary)**

January 2015

Westinghouse Electric Company LLC
1000 Westinghouse Drive
Cranberry Township, PA 16066

©2015 Westinghouse Electric Company LLC
All Rights Reserved

August 2014 FULL SPECTRUM LOCA Audit Summary – Part 2

Introduction

During the August 2014 audit of the FULL SPECTRUM™ LOCA (FSLOCA™) evaluation model (EM), a plan to close all of the open items related to the Request for Additional Information (RAI) responses was established. The plan was to provide additional information to the Nuclear Regulatory Commission (NRC) via an audit summary. Part one of the audit summary, previously transmitted in LTR-NRC-14-60 [1], contained the additional information that was requested for a subset of the open items. The majority of the remaining information is transmitted in the part two audit summary herein. A few remaining items will be transmitted later in a part three audit summary.

RAI-20, 22

The responses to RAIs 20 through 29 were sent to the NRC in LTR-NRC-13-33 [2]. In the response to RAI 22, Figures RAI-22-1 through RAI-22-3 show a comparison between the WCOBRA/TRAC-TF2 uncertainty prediction and the ANSI 1979 decay heat standard ANSI/ANS-5.1-1979 [3]. In response, the NRC questioned decay heat uncertainty prediction during the first second after the break, since there is no data given in ANSI/ANS-5.1-1979. The approach to examine this question is to first examine the data and determine a conservative approximation of the uncertainty for the first second. After this approximation, WCOBRA/TRAC-TF2 runs will be used to assess the impact of the increased decay heat.

In order to produce extrapolations of the decay heat uncertainty data, the data for the first 10 seconds after shutdown from ANSI/ANS-5.1-1979 was plotted for each isotope. For U235, the largest change over time is present in the first 2 points; thus, a [

] ^{a,c} for conservatism. The result is shown in Figure 20-1.

For Pu239, the largest change over time is also present in [

] ^{a,c} for conservatism. The result is shown in

Figure 20-2. For U238, the curve [

] ^{a,c} The result is shown in Figure 20-3. Based on visual inspection of Figures 20-1 through 20-3, the extrapolations are all reasonable, but conservative.

The equations given in Figures 20-1 through 20-3 are integrated over 0 to 1 seconds and divided by the interval (1 second) to obtain the average power increase for 2σ uncertainty over

FULL SPECTRUM and FSLOCA are trademarks of Westinghouse Electric Company LLC, its subsidiaries and/or its affiliates in the United States of America and may be registered in other countries throughout the world. All rights reserved. Unauthorized use is strictly prohibited. Other names may be trademarks of their respective owners.

the first second for each isotope. The results are [

]^{a,c} It is noted that U238 has a small fission fraction throughout the life of the fuel, and a vast majority of the total decay heat is provided by U235 or Pu239, depending on burnup (the higher the burnup, the larger the Pu239 contribution; see Figures 9-1 to 9-3 of WCAP-16996-P [4]). As such, although U238 has the highest uncertainty, it has little impact on the overall decay heat.

A sensitivity study is performed using an input deck for an early reflood limited case. For this study, 2 cases are needed:

- A new baseline case, which turns off the LUCIFER reactor kinetics calculations and instead uses a manually-input power versus time curve.
- A case with the decay heat contribution to the total power increased by []^{a,c} for the first second. This percentage is chosen because it bounds the calculations above with ample conservatism.

[

]^{a,c}

RAI-29

It is clarified that the decay heat uncertainty is sampled only from the positive side of a normal distribution from 0 to 2σ for the Region II analysis. This is same approach as used for the Region I analysis per Section 4.2 of LTR-NRC-14-29 [5].

RAI-30

Development of the cold leg condensation model in WCOBRA/TRAC-TF2 is based on experimental observation and measurement of the Condensation on Safety Injection (COSI) tests that when cold safety injection (SI) water is injected into the cold leg with stratified flow, a majority of the condensation occurs in the mixing zone in the vicinity of the SI injection due to the turbulence by the SI jet as it impinges on the stratified liquid layer in the cold leg agitating the bulk liquid. Equation 6-227 from WCAP-16996-P is based on the primary contribution from the mixing zone and other factors are only secondary effects. The validation cases that cover a wide range of geometry scale and pressure support scalability of the developed cold leg condensation model.

[

]^{a,c}

RAI-79

[

] ^{a,c}**RAI-80**

It is clarified that the Japanese Atomic Energy Research Institute (JAERI) test reports referenced in the RAI response are those cited in Table 21.1-1 of WCAP-16996-P.

RAI-86

It is clarified that the inclination angle of a cell face refers to the angle of the cell face relative to horizontal. For example, a cell face which was horizontal would have an inclination angle of 0°, whereas a cell face that was vertical would have an inclination angle of 90°.

Guidance on the specification of STRTX/STRTX1/STRTX2 will be included in the document described under the supplemental information for RAI-95 provided in LTR-NRC-14-60.

RAI-89

Additional figures are provided herein that show the calculation results of the loop seal (LS) nodding sensitivity study performed in response to RAI-89, transmitted in LTR-NRC-14-19 [10].

The figures compare key loop seal clearance parameters calculated for the LS noding sensitivity against the base case.

[

] ^{a,c}

RAI-90

The effect of the HS_SLUG parameter on the Upper Plenum Test Facility (UPTF) loop seal Separate Effects Test (SET) simulation results is shown in Figures 29.1.11-1 and 29.1.11-2 of WCAP-16996-P. These results are discussed further in the clarifications provided for RAI-113 herein. The effect of the HS_SLUG parameter on select Rig-of-Safety Assessment (ROSA) Large Scale Test Facility (LSTF) simulations was investigated with sensitivity studies presented in Section 21.16 of WCAP-16996-P.

RAI-91

It is clarified that there is no significance in the differing angles at the middle of the loop seal bend for the UPTF SET, the ROSA Integral Effects Test (IET), and the PWR models. For all these facilities, the modeling approach [

] ^{a,c}

[

] ^{a,c}

General Bypass Flow Discussion

[

] ^{a,c}

[

]^{a,c}

[

] ^{a,c}**RAI-96**

The spray nozzle bypass quantity is defined as the percentage of the total flow from all the reactor coolant system (RCS) loops that passes through the spray nozzles.

Ranges in the spray nozzle bypass capacities for a constant flow area and loss coefficient are caused by differences in the vessel and fuel design. The flow passing through the spray nozzles is a balance between the resistance through the upper head into the upper plenum, and the resistance through the downcomer, lower head/plenum, and core into the upper plenum. As such, any differences in resistance in the later path will impact the flow percentage in the former.

[

] ^{a,c}

The impact of different power levels on the bypass capacity within the maximum expected core power uncertainty (+/- 2%) is negligible.

RAI-97

The 10% tolerance allows for calibration within the stated uncertainty.

RAI-98

[

] ^{a,c}

[

]^{a,c}

RAI-99

A table of the spray nozzle reference areas and loss coefficients based on design data for forward flow is presented in Table 99-1. Additionally, the [

]^{a,c}

RAI-101

[

]^{a,c}

[

] ^{a,c}

RAI-102

The Semiscale test S-LH-1 and S-LH-2 simulations were transmitted to the NRC in LTR-NRC-14-70.

RAI-104

It is clarified that the FE010-HLA and FE150-HLB measurements, discussed on page P-31 of LTR-NRC-14-21, record the measured flows in the hot leg-to-downcomer (HL-to-DC) leakage lines installed at the ROSA-IV LSTF.

The total HL-to-DC leakage of 0.124 kg/sec, reported on page P-31 of LTR-NRC-14-21, is based on the steady-state leakage flows as recorded by the FE010-HLA and FE150-HLB, which are part of the SB-CL-18 electronic data set in the possession of Westinghouse.

RAI-105

See the ROSA bypass discussion in the "General Bypass Flow Discussion," and the supplemental information provided for the response to RAI-101.

RAI-107

The effect of flow reversal on the hot leg nozzle gap bypass capacity under SBLOCA conditions has not been quantified. The updated approach described in the “General Bypass Flow Discussion” accounts for the reverse flow through the spray nozzles. [

] ^{a,c}

A better quality rendition of Figure 107-2 has been included herein.

RAI-112

The steam generator (SG) model used in the PWR examples in the FSLOCA Topical Report is based on a combination of PIPE, TEE, and HTSTR components. A single PIPE component is used to model the entire primary side U-tube bundle. The primary-to-secondary heat transfer is modeled by using a HTSTR component that connects the primary side PIPE and the secondary side, which is modeled by a TEE component. This steam generator model has been validated against test data from the ROSA-IV LSTF as shown in Section 21 of the Topical Report. In the original response to RAI 112 (LTR-NRC-14-12), two sensitivity studies have been performed to assess the impact of different steam generator nodalization to the PWR SBLOCA transient. The first sensitivity study is to refine the noding in the steam generator tubes, and the second one utilizes three parallel PIPE components instead of one PIPE to model the steam generator tubes.

The PWR SBLOCA case used in the sensitivity studies in the original response to RAI 112 was taken from the SBLOCA parametric study to support the NRC audit on FSLOCA (LTR-NRC-13-70 [17]). The postulated split break occurs in the cold leg of loop 1 with the break size of [

] ^{a,c}. To comply with the proposed loop seal model for the region I analysis (LTR-NRC-14-29), [

] ^{a,c}

Reviewing the base case for the sensitivity study in the original RAI 112 response in LTR-NRC-14-12 indicates that [

] ^{a,c}

The figures in the original RAI 112 response have been updated and presented in this document. In addition, the collapsed liquid levels in the loop seal uphill and downhill sides are plotted instead of void fraction. The collapsed liquid level is measured from the bottom of the loop seal. The flow rates (liquid and gas) through each loop seal and SG primary PIPE components are plotted as well.

The first sensitivity study is to refine the noding in the steam generator tubes, and the second one utilizes three parallel PIPE components instead of one PIPE to model the steam generator tubes. The figures will replace the corresponding figure in the original RAI 112 response with additional figures for liquid and vapor flow rates.

Sensitivity Study 1: Double the Nodes in the Steam Generator Tubes

In the first sensitivity study, the node size of the vertical tubes (both uphill and downhill) is reduced to a half of the original node size in the base case as shown in Figure 112-1.

The results of this sensitivity study are presented in Figures 112-2 through 112-29. Figures 112-2, 112-3 and 112-4 show the average void fraction at the uphill side of U-tubes in the respective steam generator 1, steam generator 2, and steam generator 3. The SG noding difference only creates [

J^{a,c}

[

] ^{a,c}**Sensitivity Study 2: Three Parallel Pipes Modeling the Steam Generator Tubes**

In this nodding sensitivity study, the U-tube PIPE component is replaced by three parallel PIPE components. The three parallel Pipes are merged to the steam generator inlet and outlet plenums similar to the physical layout of the steam generator as shown in Figure 112-30.

[

] ^{a,c}

The results of this sensitivity study are presented in Figures 112-31 through 112-58. Similar to the first sensitivity study, average void fraction is used to demonstrate the water distribution in the steam generators and the collapsed liquid level of the loop seals is shown. Figures 112-31, 112-32 and 112-33 show the average void fraction at the uphill side of U-tubes in the respective steam generator 1, steam generator 2, and steam generator 3. [

] ^{a,c}

[

]^{a,c}

Conclusions

The sensitivity studies on the steam generator nodalization indicate that in general the SBLOCA transient is not sensitive to the noding changes studied herein. [

]^{a,c}

RAI-113

During a recent NRC Audit on the FSLOCA methodology, the NRC requested clarification regarding the impact of [^{a,c} the residual liquid in the UPTF SETs.

While the request for additional information is directed at the residual liquid predictions, the response here considers the two most significant impacts of loop seal clearing, namely:

1. Residual liquid – an indicator of how much liquid is expelled out the loop seal region which may end up in the vessel
2. Pressure drop – the resistance for venting vapor generated in the core

The results presented in Figure 113-1 through 113-4 in LTR-NRC-14-19 are from cases that [

] ^{a,c}

As described in the response to RAI 114 of LTR-NRC-14-19, [

] ^{a,c}

[

]^{a,c}

RAI-115

It is clarified that []^{a,c} was used in the base case calculations presented in the response to RAI 115 in LTR-NRC-14-19.

RAI-116

The NRC requested that the plots from one or two cases presented in the response to RAI 116 in LTR-NRC-14-19 be re-submitted one-per-page to increase the readability of the figures.

Plots from the 3-bar / $Jg^* = 0.076$ and case 15-bar / $Jg^* = 0.178$ were selected which illustrate the transient behavior described in the RAI response. The figures are provided as Figures 116-1 through 116-7, Figures 116-47 and 116-48, Figures 116-29 through 116-35, and Figures 116-55 and 116-56. The cell / cell face noding is detailed in Figure 116-0.

References

- 1) LTR-NRC-14-60, "Summary of August 2014 NRC Audit Part 1 of the FULL SPECTRUM LOCA (FSLOCA) Evaluation Model (Proprietary/Non-Proprietary), Project 700, TAC No. ME5244," September 17, 2014.
- 2) LTR-NRC-13-33, "Submittal of Westinghouse Responses to 'WCAP-16996-P, 'Realistic LOCA Evaluation Methodology Applied to the Full Spectrum of Break Sizes (FULL SPECTRUM LOCA Methodology)' Request for Additional Information – Second Set' (Proprietary/Non-Proprietary), Project 700, TAC No. ME5244," May 31, 2013.
- 3) ANSI/ANS-5.1-1979, "Decay Heat Power in Light Water Reactors," American Nuclear Society, August 29, 1979.
- 4) WCAP-16996-P, "Realistic LOCA Evaluation Methodology Applied to the Full Spectrum of Break Sizes (FULL SPECTRUM LOCA Methodology)," November 2010.
- 5) LTR-NRC-14-29, "Summary of May 2014 NRC Audit of the FULL SPECTRUM LOCA (FSLOCA) Evaluation Model (Proprietary/Non-Proprietary), Project 700, TAC No. ME5244," June 5, 2014.
- 6) Bestion D., and Gros d'Aillon, L., "Condensation tests analysis and correlation for the CATHARE code," *Proceeding of 4th International Topical Meeting on Nuclear Reactor Thermal-Hydraulics*, Karlsruhe, Germany, 1989.
- 7) Janicot, A., and Bestion, D., "Condensation Modeling for ECC injection," *Nuclear Engineering and Design*, Vol. 145, pp. 37-45, 1993.
- 8) LTR-NRC-14-12, "Submittal of Westinghouse Responses to 'WCAP-16996-P, 'Realistic LOCA Evaluation Methodology Applied to the Full Spectrum of Break Sizes (FULL SPECTRUM LOCA Methodology)' Requests for Additional Information – RAIs 77 - 82, 86 - 87, 93 and 112,' (Proprietary/Non-Proprietary)," March 12, 2014.
- 9) [] a,c
- 10) LTR-NRC-14-19, "Submittal of Westinghouse Responses to 'WCAP-16996-P, 'Realistic LOCA Evaluation Methodology Applied to the Full Spectrum of Break Sizes (FULL SPECTRUM LOCA Methodology)' Request for Additional Information – RAIs 83-85, 88-

92, 94-95 and 113-119' (Proprietary/Non-Proprietary), Project 700, TAC No. ME5244," April 2, 2014.

- 11) LTR-NRC-14-70, "Submittal of Westinghouse Responses to 'WCAP-16996-P, 'Realistic LOCA Evaluation Methodology Applied to the Full Spectrum of Break Sizes (FULL SPECTRUM LOCA Methodology)' Request for Additional Information – RAIs 109-111' (Proprietary/Non-Proprietary), Project 700, TAC No. ME5244," October 31, 2014.
- 12) LTR-NRC-14-21, "Submittal of Westinghouse Responses to 'WCAP-16996-P, 'Realistic LOCA Evaluation Methodology Applied to the Full Spectrum of Break Sizes (FULL SPECTRUM LOCA Methodology)' Request for Additional Information – RAIs 96-105 and 107' (Proprietary/Non-Proprietary), Project 700, TAC No. ME5244," April 4, 2014.
- 13) Tasaka, K., et al., 1988, "The Results of 5% Small Break LOCA Tests and Natural Recirculation Tests at the ROSA-IV LSTF," *Nuclear Engineering and Design*, Vol.108, 1988, pp 37-44.
- 14) JAERI-M 89-220, "Data Report for ROSA-IV LSTF 5% Cold Leg Break LOCA Experiment Run SB-CL-08," January 1990.
- 15) [] ^{a,c}
- 16) JAERI-M 89-113, "Supplemental Description of ROSA-IV/LSTF with No. 1 Simulated Fuel-Rod Assembly," September 1989.
- 17) LTR-NRC-13-70, "Summary of July 2013 NRC Code Workshop and August 2013 NRC Audit of the FULL SPECTRUM LOCA (FSLOCA) Evaluation Model (Proprietary/Non-Proprietary)," October 10, 2013.
- 18) LTR-NRC-13-73, "Submittal of Westinghouse Responses to 'WCAP-16996-P, 'Realistic LOCA Evaluation Methodology Applied to the Full Spectrum of Break Sizes (FULL SPECTRUM LOCA Methodology)' Requests for Additional Information – RAIs 46 - 58, 75 and 77,' (Proprietary)," October 28, 2013.

Table 99-1: Spray Nozzle Area and Loss Coefficients

[]

a,c

a,c

Figure 20-1: Extrapolation of Decay Heat Uncertainty Data for U235



Figure 20-2: Extrapolation of Decay Heat Uncertainty Data for Pu239



Figure 20-3: Extrapolation of Decay Heat Uncertainty Data for U238

a,c

Figure 20-4: Core Power Comparison

a,c

Figure 20-5: PCT Comparison

a,c

Figure 20-6: Blowdown PCT Comparison

a,c

Figure 20-7: Reflood PCT Comparison

a,c

Figure 89-1 Cross-Over Leg Differential Pressures

a,c

Figure 89-3 Rod 1 Peak Cladding Temperatures



Figure 89-4 Core Differential Pressures and Rod 1 Peak Cladding Temperatures

a,c

Figure GBFD-1: Loop Seal Clearance in the Intact Cross-Over Leg for Bypass Sensitivity

a,c

Figure GBFD-2: Loop Seal Clearance in the Broken Cross-Over Leg for Bypass Sensitivity

a,c

Figure GBFD-3: SB-CL-05 Core Differential Pressures for Bypass Sensitivity

a,c

Figure GBFD-4: Semiscale Vessel (Core) Differential Pressures



a,c

**Figure GBFD-5: Hot Rod Peak Cladding Temperature for the Beaver Valley Unit 1
2.5-inch Break Bypass Sensitivity Study**



a,c

**Figure GBFD-6: Hot Rod Peak Cladding Temperature for the Beaver Valley Unit 1
2.4-inch Break Bypass Sensitivity Study**



a,c

Figure GBFD-7: Hot Rod Peak Cladding Temperature for the V. C. Summer 2.5-inch Break Bypass Sensitivity Study

a,c

Figure GBFD-8: Hot Rod Peak Cladding Temperature for the V. C. Summer 2.4-inch Break Bypass Sensitivity Study

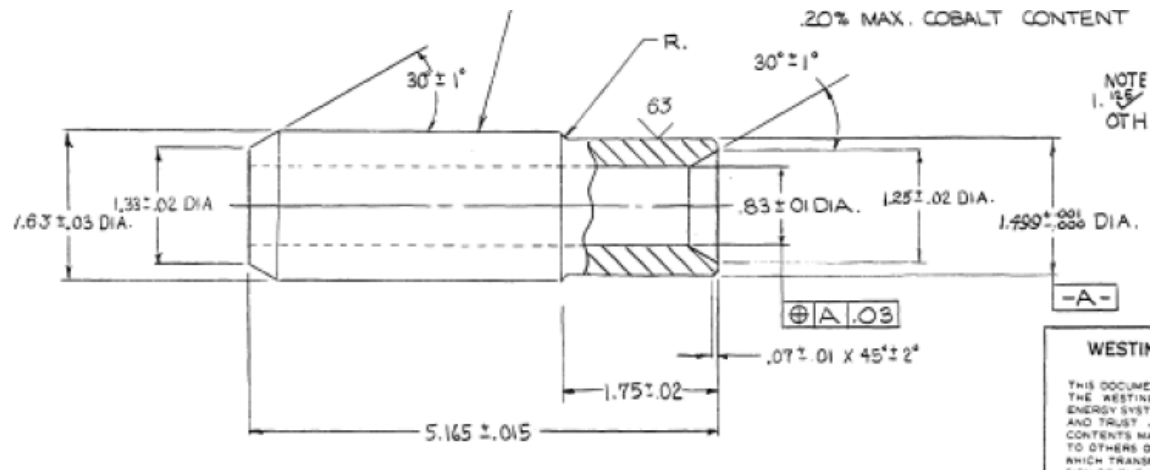


Figure 107-2: Typical Nozzle Design



a,c

Figure 112-1. Comparison of SG nodalization in the base case (left) and the revised one with doubled SG tube nodes (right). (Sensitivity Study 1)



a,c

Figure 112-2. Comparison of SG 1 U-tube uphill average void fraction. (Sensitivity Study 1)

a,c

Figure 112-3. Comparison of SG 2 U-tube uphill average void fraction. (Sensitivity Study 1)



a,c

Figure 112-4. Comparison of SG 3 U-tube uphill average void fraction. (Sensitivity Study 1)



a,c

**Figure 112-5. Comparison of SG 1 U-tube downhill average void fraction.
(Sensitivity Study 1)**

**a,c**

**Figure 112-6. Comparison of SG 2 U-tube downhill average void fraction.
(Sensitivity Study 1)**

**a,c**

**Figure 112-7. Comparison of SG 3 U-tube downhill average void fraction.
(Sensitivity Study 1)**

**a,c**

**Figure 112-8. Comparison of loop seal 1 downhill collapsed liquid level.
(Sensitivity Study 1)**

**a,c**

**Figure 112-9. Comparison of loop seal 2 downhill collapsed liquid level.
(Sensitivity Study 1)**



a,c

**Figure 112-10. Comparison of loop seal 3 downhill collapsed liquid level.
(Sensitivity Study 1)**

**a,c**

Figure 112-11. Comparison of loop seal 1 uphill collapsed liquid level. (Sensitivity Study 1)

**a,c**

Figure 112-12. Comparison of loop seal 2 uphill collapsed liquid level. (Sensitivity Study 1)

**a,c**

Figure 112-13. Comparison of loop seal 3 uphill collapsed liquid level. (Sensitivity Study 1)



a,c

Figure 112-14. Liquid flow rate to steam generator 1. (Sensitivity Study 1)



a,c

Figure 112-15. Vapor flow rate to steam generator 1. (Sensitivity Study 1)



a,c

Figure 112-16. Liquid flow rate to steam generator 2. (Sensitivity Study 1)

**a,c**

Figure 112-17. Vapor flow rate to steam generator 2. (Sensitivity Study 1)



a,c

Figure 112-18. Liquid flow rate to steam generator 3. (Sensitivity Study 1)



a,c

Figure 112-19. Vapor flow rate to steam generator 3. (Sensitivity Study 1)

**a,c**

Figure 112-20. Liquid flow rate to loop seal 1. (Sensitivity Study 1)

**a,c**

Figure 112-21. Vapor flow rate to loop seal 1. (Sensitivity Study 1)

**a,c**

Figure 112-22. Liquid flow rate to loop seal 2. (Sensitivity Study 1)

**a,c**

Figure 112-23. Vapor flow rate to loop seal 2. (Sensitivity Study 1)

**a,c**

Figure 112-24. Liquid flow rate to loop seal 3. (Sensitivity Study 1)



a,c

Figure 112-25. Vapor flow rate to loop seal 3. (Sensitivity Study 1)

a,c

Figure 112-26. Comparison of core collapsed liquid level. (Sensitivity Study 1)

**a,c**

Figure 112-27. Comparison of core void fraction. (Sensitivity Study 1)

**a,c**

Figure 112-28. Comparison of downcomer collapsed liquid level. (Sensitivity Study 1)



a,c

Figure 112-29. Comparison of PCT. (Sensitivity Study 1)

**a,c**

Figure 112-30. Comparison of SG nodalization in the base case (left) and the revised one with three steam generator tube components (right). (Sensitivity Study 2)



a,c

**Figure 112-31. Comparison of SG 1 U-tube uphill average void fraction.
(Sensitivity Study 2)**



a,c

**Figure 112-32. Comparison of SG 2 U-tube uphill average void fraction.
(Sensitivity Study 2)**

a,c

**Figure 112-33. Comparison of SG 3 U-tube uphill average void fraction.
(Sensitivity Study 2)**



a,c

**Figure 112-34. Comparison of SG 1 U-tube downhill average void fraction.
(Sensitivity Study 2)**



a,c

**Figure 112-35. Comparison of SG 2 U-tube downhill average void fraction.
(Sensitivity Study 2)**

**a,c**

**Figure 112-36. Comparison of SG 3 U-tube downhill average void fraction.
(Sensitivity Study 2)**



a,c

**Figure 112-37. Comparison of loop seal 1 downhill collapsed liquid level.
(Sensitivity Study 2)**

**a,c**

**Figure 112-38. Comparison of loop seal 2 downhill collapsed liquid level.
(Sensitivity Study 2)**

a,c

**Figure 112-39. Comparison of loop seal 3 downhill collapsed liquid level.
(Sensitivity Study 2)**

**a,c**

Figure 112-40. Comparison of loop seal 1 uphill collapsed liquid level. (Sensitivity Study 2)



a,c

Figure 112-41. Comparison of loop seal 2 uphill collapsed liquid level. (Sensitivity Study 2)



a,c

Figure 112-42. Comparison of loop seal 3 uphill collapsed liquid level. (Sensitivity Study 2)



a,c

Figure 112-43. Liquid flow rate to steam generator 1. (Sensitivity Study 2)



a,c

Figure 112-44. Vapor flow rate to steam generator 1. (Sensitivity Study 2)



a,c

Figure 112-45. Liquid flow rate to steam generator 2. (Sensitivity Study 2)



a,c

Figure 112-46. Vapor flow rate to steam generator 2. (Sensitivity Study 2)

**a,c**

Figure 112-47. Liquid flow rate to steam generator 3. (Sensitivity Study 2)



a,c

Figure 112-48. Vapor flow rate to steam generator 3. (Sensitivity Study 2)

**a,c**

Figure 112-49. Liquid flow rate to loop seal 1. (Sensitivity Study 2)

**a,c**

Figure 112-50. Vapor flow rate to loop seal 1. (Sensitivity Study 2)



a,c

Figure 112-51. Liquid flow rate to loop seal 2. (Sensitivity Study 2)



a,c

Figure 112-52. Vapor flow rate to loop seal 2. (Sensitivity Study 2)

**a,c**

Figure 112-53. Liquid flow rate to loop seal 3. (Sensitivity Study 2)



a,c

Figure 112-54. Vapor flow rate to loop seal 3. (Sensitivity Study 2)



a,c

Figure 112-55. Comparison of core collapsed liquid level. (Sensitivity Study 2)



a,c

Figure 112-56. Comparison of core void fraction. (Sensitivity Study 2)



a,c

Figure 112-57. Comparison of downcomer collapsed liquid level. (Sensitivity Study 2)



a,c

Figure 112-58. Comparison of PCT. (Sensitivity Study 2)



Figure 116-0.a: Momentum Cell Noding Diagram for WCOBRA/TRAC-TF2 Input for UPTF Loop Seal Test Simulations

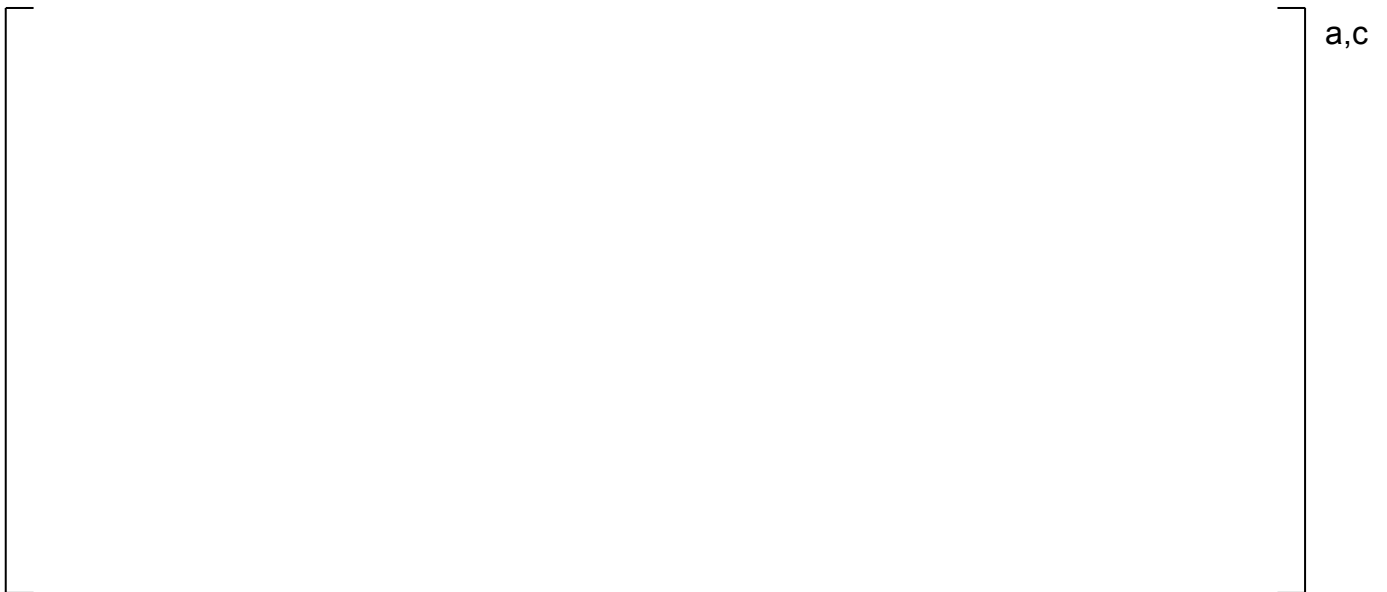


Figure 116-0.b: Continuity Cell Noding Diagram for WCOBRA/TRAC-TF2 Input for UPTF Loop Seal Test Simulations

a,c

Figure 116-1.a: 3-bar, $Jg^*=0.076$ – Mass Flow Rate

a,c

Figure 116-1.b: 3-bar, $J_{g^*}=0.076$ – Mass Flow Rate

a,c

Figure 116-1.c: 3-bar, $J_g^*=0.076$ – Mass Flow Rate

a,c

Figure 116-2: 3-bar, $J_g^*=0.076$ – Total System Mass

a,c

Figure 116-3.a: 3-bar, $J_g^*=0.076$ – Void Fraction

a,c

Figure 116-3.b: 3-bar, $Jg^*=0.076$ – Void Fraction

a,c

Figure 116-3.c: 3-bar, $Jg^*=0.076$ – Void Fraction

a,c

Figure 116-3.d: 3-bar, $J_g^*=0.076$ – Void Fraction

a,c

Figure 116-3.e: 3-bar, $Jg^*=0.076$ – Void Fraction

a,c

Figure 116-4.a: 3-bar, $Jg^*=0.076$ – Phasic Velocity

a,c

Figure 116-4.b: 3-bar, $J_g^*=0.076$ – Phasic Velocity

a,c

Figure 116-4.c: 3-bar, $Jg^*=0.076$ – Phasic Velocity

a,c

Figure 116-4.d: 3-bar, $J_g^*=0.076$ – Phasic Velocity

a,c

Figure 116-4.e: 3-bar, $Jg^*=0.076$ – Phasic Velocity

a,c

Figure 116-5.a: 3-bar, $Jg^*=0.076$ – Liquid Entrainment Fraction

a,c

Figure 116-5.b: 3-bar, $Jg^*=0.076$ – Liquid Entrainment Fraction

a,c

Figure 116-5.c: 3-bar, $Jg^*=0.076$ – Liquid Entrainment Fraction

a,c

Figure 116-6.a: 3-bar, $Jg^*=0.076$ – Flow Regime

a,c

Figure 116-6.b: 3-bar, $Jg^*=0.076$ – Flow Regime



a,c

Figure 116-6.c: 3-bar, $Jg^*=0.076$ – Flow Regime

a,c

Figure 116-6.d: 3-bar, $J_g^*=0.076$ – Flow Regime

a,c

Figure 116-7.a: 3-bar, $Jg^*=0.076$ – Interfacial Friction Force

a,c

Figure 116-7.b: 3-bar, $J_g^*=0.076$ – Interfacial Friction Force

a,c

Figure 116-7.c: 3-bar, $Jg^*=0.076$ – Interfacial Friction Force

a,c

Figure 116-7.d: 3-bar, $J_g^*=0.076$ – Interfacial Friction Force

a,c

Figure 116-47.a: 3-bar, $Jg^*=0.076$ – Horizontal Stratification and Wavy Dispersed Criteria

a,c

Figure 116-47.b: 3-bar, $Jg^*=0.076$ – Horizontal Stratification and Wavy Dispersed Criteria

a,c

Figure 116-47.c: 3-bar, $Jg^*=0.076$ – Horizontal Stratification and Wavy Dispersed Criteria

a,c

Figure 116-48.a: 3-bar, $Jg^*=0.076$ – Kutateladze Number

a,c

Figure 116-48.b: 3-bar, $Jg^*=0.076$ – Kutateladze Number

a,c

Figure 116-48.c: 3-bar, $Jg^*=0.076$ – Kutateladze Number

a,c

Figure 116-29.a: 15-bar, $J_g^*=0.178$ – Mass Flow Rate

a,c

Figure 116-29.b: 15-bar, $J_g^*=0.178$ – Mass Flow Rate

a,c

Figure 116-29.c: 15-bar, $J_g^*=0.178$ – Mass Flow Rate

a,c

Figure 116-30: 15-bar, $Jg^*=0.178$ – Total System Mass

a,c

Figure 116-31.a: 15-bar, $Jg^*=0.178$ – Void Fraction

a,c

Figure 116-31.b: 15-bar, $Jg^*=0.178$ – Void Fraction

a,c

Figure 116-31.c: 15-bar, $Jg^*=0.178$ – Void Fraction

a,c

Figure 116-31.d: 15-bar, $J_g^*=0.178$ – Void Fraction

a,c

Figure 116-31.e: 15-bar, $Jg^*=0.178$ – Void Fraction

a,c

Figure 116-32.a: 15-bar, $Jg^*=0.178$ – Phasic Velocity

a,c

Figure 116-32.b: 15-bar, $Jg^*=0.178$ – Phasic Velocity

a,c

Figure 116-32.c: 15-bar, $Jg^*=0.178$ – Phasic Velocity

a,c

Figure 116-32.d: 15-bar, $Jg^*=0.178$ – Phasic Velocity

a,c

Figure 116-32.e: 15-bar, $Jg^*=0.178$ – Phasic Velocity

a,c

Figure 116-33.a: 15-bar, $Jg^*=0.178$ – Liquid Entrainment Fraction

a,c

Figure 116-33.b: 15-bar, $Jg^*=0.178$ – Liquid Entrainment Fraction

a,c

Figure 116-33.c: 15-bar, $J_{g^*}=0.178$ – Liquid Entrainment Fraction

a,c

Figure 116-34.a: 15-bar, $Jg^*=0.178$ – Flow Regime

a,c

Figure 116-34.b: 15-bar, $Jg^*=0.178$ – Flow Regime

a,c

Figure 116-34.c: 15-bar, $Jg^*=0.178$ – Flow Regime

a,c

Figure 116-34.d: 15-bar, $Jg^*=0.178$ – Flow Regime

a,c

Figure 116-35.a: 15-bar, $J_g^*=0.178$ – Interfacial Friction Force

a,c

Figure 116-35.b: 15-bar, $J_g^*=0.178$ – Interfacial Friction Force

a,c

Figure 116-35.c: 15-bar, $J_g^*=0.178$ – Interfacial Friction Force

a,c

Figure 116-35.d: 15-bar, $J_g^*=0.178$ – Interfacial Friction Force

a,c

Figure 116-55.a: 15-bar, $Jg^*=0.178$ – Horizontal Stratification and Wavy Dispersed Criteria

a,c

Figure 116-55.b: 15-bar, $J_g^*=0.178$ – Horizontal Stratification and Wavy Dispersed Criteria

a,c

Figure 116-55.c: 15-bar, $J_g^*=0.178$ – Horizontal Stratification and Wavy Dispersed Criteria

a,c

Figure 116-56.a: 15-bar, $Jg^*=0.178$ – Kutateladze Number

a,c

Figure 116-56.b: 15-bar, $Jg^*=0.178$ – Kutateladze Number

a,c

Figure 116-56.c: 15-bar, $Jg^*=0.178$ – Kutateladze Number

**Summary of August 2014 NRC Audit Part 3 of FULL SPECTRUM LOCA (FSLOCA) Evaluation Model
(Non-Proprietary)**

February 2015

Westinghouse Electric Company LLC
1000 Westinghouse Drive
Cranberry Township, PA 16066

©2015 Westinghouse Electric Company LLC
All Rights Reserved

August 2014 FULL SPECTRUM LOCA Audit Summary – Part 3

Introduction

During the August 2014 audit of the FULL SPECTRUM™ LOCA (FSLOCA™) evaluation model (EM), a plan to close all of the open items related to the Request for Additional Information (RAI) responses was established. The plan was to provide additional information to the Nuclear Regulatory Commission (NRC) via an audit summary. Parts one and two of the audit summary, previously transmitted in LTR-NRC-14-60 [1] and LTR-NRC-15-6 [2], contained the additional information that was requested for a majority of the open items. The remaining information is transmitted in the part three audit summary herein.

RAI-26

Request for Additional Information

“Per RAI response, [

]^{a,c}

Revised Response to RAI 26

In order to demonstrate that [

]^{a,c} it is necessary to quantify the relative contributions from fission products, ²³⁹U and ²³⁹Np actinides, and from the other excluded actinides, in both a time dependent and equilibrium manner. [

]^{a,c}

Tables RAI-26-1 through RAI-26-12 provide comparison results from a selection of limiting power increase transient case scenarios. The results shown in Tables RAI-26-1 through RAI-26-12 demonstrate that [

]^{a,c} The time scale of interest in a LOCA PCT analysis is less than 10,000 seconds. The data shown in Tables RAI-26-1 through RAI-26-12 also confirms that [

]^{a,c}

FULL SPECTRUM and FSLOCA are trademarks of Westinghouse Electric Company LLC, its subsidiaries and/or its affiliates in the United States of America and may be registered in other countries throughout the world. All rights reserved. Unauthorized use is strictly prohibited. Other names may be trademarks of their respective owners.

[]^{a,c} In the earliest part of the transient, when the decay heat power level is highest, [

] ^{a,c}

The methods used to obtain the data shown in Tables RAI-26-1 through RAI-26-12 are described below.

A study was performed using shapes from the Beaver Valley Unit 1 power shape library with peak power density. For each cycle burnup included in the power shape library, the most limiting daily load follow power transients were identified, based on which transients generated the peak local power density. The peak local power history as a function of time was obtained for the load follow maneuver associated with the limiting shape. Figure RAI-26-1 shows an example for one of the limiting case power histories that was studied. [

] ^{a,c}

For the decay heat contribution from actinides other than ²³⁹U and ²³⁹Np, the data shown on Figure 9-33 of WCAP-16996 provides example decay heat power data as a function of enrichment and burnup, due to the other actinides excluded from the decay heat model. [

] ^{a,c}

[

^{a,c} The actual data points and the bounding line are shown in Figure RAI-26-2.

To quantify the behavior of the ²³⁹U and ²³⁹Np decay heat [^{a,c} it is necessary to solve the differential equations (9-12) and (9-13) given in Section 9.4 of WCAP-16996-P Revision 0. These equations are repeated below as equations (1) and (2):

$$\frac{dP_u}{dt} = \bar{R}\alpha_u[v\Sigma_F n(t)] - \lambda_u P_u(t) \quad (1)$$

$$\frac{dP_n}{dt} = \frac{\lambda_u P_u(t)\alpha_n}{\alpha_u} - \lambda_n P_n(t) \quad (2)$$

where:

$v\Sigma_F n(t)$ = time-dependent fission rate (proportional to power density),

λ_u = ²³⁹U decay constant = 4.91E-4 sec⁻¹,

λ_n = ²³⁹Np decay constant = 3.41E-6 sec⁻¹,

$\bar{R}(\text{BU}, \epsilon)$ = ²³⁸U capture-to-fission ratio, function of initial enrichment ϵ , and burnup (BU),

$P_u(t)$ = time dependent decay power due to ²³⁹U decay,

q_u = energy release per ²³⁹U decay = 0.474 MeV,

$P_n(t)$ = time dependent decay power due to ²³⁹Np decay,

q_n = energy release per ²³⁹Np decay = 0.419 MeV,

$\alpha_u = q_u \lambda_u$ decay power yield per capture (MeV/sec/capture) for ²³⁹U, and

$\alpha_n = q_n \lambda_n$ decay power yield per capture (MeV/sec/capture) for ²³⁹Np.

[

^{a,c}^{a,c}

(3)

(4)

Equations (1) and (2) can be readily solved if one assumes a constant fission rate over a short time step Δt . If we specify the constant fission rate as Q, the solutions for the time dependent decay powers over the time step are given by the following expressions:

$$\left[\begin{array}{c} \text{a,c} \\ \text{a,c} \\ \text{a,c} \end{array} \right] \quad (5)$$

As a demonstration of the time dependent behavior of ^{239}U and ^{239}Np actinide decay heat, the above equations were solved for a hypothetical step change in power density from a relative power density of 1.0 to 1.4, i.e., Q in the above expression increases instantaneously from a steady state value of 1.0 to 1.4 at time 0 and then remains at this value. (This is analogous to the local $F_Q \cdot \text{Power}$ value increasing, e.g., from a steady state value of 1.8 to 2.52 since $2.52/1.8 = 1.4$). Figure RAI-26-3 shows the resulting time dependent decay heat values for ^{239}U and ^{239}Np and for the sum of both. [

^{a,c} This figure assumes an \bar{R} value (^{238}U capture/fission ratio) of 0.6, corresponding to low burnup, high enrichment fuel. Calculations have confirmed that using different values for \bar{R} is not important to the relative difference between [

$\mathbf{J}^{a,c}$

The above step change is not a realistic case since such a large increase in local power density above the natural steady-state value cannot be maintained for such an extended period, i.e., days. It is however useful to demonstrate the lag in the time dependent actinide decay heat associated with a simple power change.

The solution for []^{a,c} fission product decay power in Tables RAI-26-1 through RAI-26-12 was obtained by solving the ANSI/ANS 5.1-1979 exponential equation, using the methods described in Section 9.2 of WCAP-16996. The capture correction term (G(T)) was also included per the requirements of ANSI/ANS 5.1-1979, as described in

Section 9.9.3 of WCAP-16996. [

]^{a,c}

In every case demonstrated below in Tables RAI-26-1 through RAI-26-12, [

]^{a,c} This conclusion holds out to at least 10,000 seconds after shutdown. The time scale of interest in a LOCA PCT analysis is less than 10,000 seconds. In addition, it can be observed from the results in Tables RAI-26-1 through RAI-26-12 that [

]^{a,c}

It is therefore concluded based on this study that [

]^{a,c} provides sufficient conservatism to assure that the actual decay heat power will be bounded in the LOCA analysis.

Table RAI-26-1
Decay Heat After Shutdown for 5% Enriched Fuel at 10 GWD/MTU
10% Power Increase 24-Hours Prior to Shutdown

a,c

Table RAI-26-2
Decay Heat After Shutdown for 5% Enriched Fuel at 10 GWD/MTU
20% Power Increase 24-Hours Prior to Shutdown

a,c

Table RAI-26-3
Decay Heat After Shutdown for 5% Enriched Fuel at 10 GWD/MTU
40% Power Increase 24-Hours Prior to Shutdown

a,c

Table RAI-26-4
Decay Heat After Shutdown for 5% Enriched Fuel at 10 GWD/MTU
60% Power Increase 24-Hours Prior to Shutdown

a,c

Table RAI-26-5
Decay Heat After Shutdown for 5% Enriched Fuel at 30 GWD/MTU
10% Power Increase 24-Hours Prior to Shutdown

a,c

Table RAI-26-6
Decay Heat After Shutdown for 5% Enriched Fuel at 30 GWD/MTU
20% Power Increase 24-Hours Prior to Shutdown

a,c

Table RAI-26-7
Decay Heat After Shutdown for 5% Enriched Fuel at 30 GWD/MTU
40% Power Increase 24-Hours Prior to Shutdown

a,c

Table RAI-26-8
Decay Heat After Shutdown for 5% Enriched Fuel at 30 GWD/MTU
60% Power Increase 24-Hours Prior to Shutdown

a,c

Table RAI-26-9
Decay Heat After Shutdown for 5% Enriched Fuel at 60 GWD/MTU
10% Power Increase 24-Hours Prior to Shutdown

a,c

Table RAI-26-10
Decay Heat After Shutdown for 5% Enriched Fuel at 60 GWD/MTU
20% Power Increase 24-Hours Prior to Shutdown

a,c

Table RAI-26-11
Decay Heat After Shutdown for 5% Enriched Fuel at 60 GWD/MTU
40% Power Increase 24-Hours Prior to Shutdown

a,c

Table RAI-26-12
Decay Heat After Shutdown for 5% Enriched Fuel at 60 GWD/MTU
60% Power Increase 24-Hours Prior to Shutdown

a,c

Figure RAI-26-1 Example of a Typical Limiting $Q(t)$ Profile used for Study of Transient Decay Heat

a,c

Note: Q is the relative local power density or fission rate where a Q of 1 corresponds to operating at the nominal rated thermal power or local fission rate.

Figure RAI-26-2 Bounding Decay Heat Power from Actinides Other than ^{239}U and ^{239}Np

a,c

Figure RAI-26-3 Relative Decay Heat for ^{239}U and ^{239}Np for a Step Change in Relative Power Density from 1.0 to 1.4

a,c

Note: Equilibrium values are for a Q of 1.4

Figure RAI-26-4 Relative Decay Heat for Fission Products for a Step Change in Relative Power Density from 1.0 to 1.4

a,c

Note: Equilibrium values are for a Q of 1.4

RAIs-51, 52, 53, 54, 55, and 57**Background**

In the August 2014 audit on the FSLOCA EM, the NRC requested additional information regarding the responses to RAIs on the interfacial heat transfer models in WCOBRA/TRAC-TF2. The additional information which was requested is summarized as follows:

RAI 51

Discuss the statement [

]^{a,c}

RAI 52

Discuss the statement [

]^{a,c}

RAI 53

(1) Discuss the statement [

]^{a,c}

(2) Discuss the statement [

]^{a,c}

RAI 54

(1) Explain if Equations (6-26) and (6-49) describe the same heat transfer process (superheated vapor to liquid droplets) and clarify its treatment in specific flow regimes [

]^{a,c}

(2) Discuss the statement [

]^{a,c}

(3) Discuss the statement [

]^{a,c}

RAI 55

(1) Explain the basis for []^{a,c}.

(2) Explain why [

]^{a,c} (see Figures 15.9.2-22 and 15.9.2-23).

(3) All predicted results []^{a,c} of the droplet diameter data points in Figure 15.9.2-35. Explain why this is acceptable.

RAI 57

Discuss the following statements:

Table 57-1 (SPL): [

]^{a,c}

Table 57-2 (SUBC/NUCB): [

]^{a,c}

Table 57-3 (CHF): Refers to Section 15.3, which concludes: [

]^{a,c}

Table 57-4 (TRAN): [

]^{a,c}

Table 57-5 (IAFB/IADF): [

]^{a,c}

Table 57-6 (DFFB): [

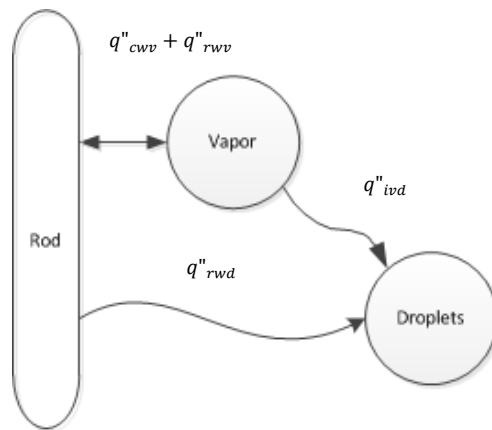
]^{a,c}

Clarification for Responses to RAIs 51, 52, 53(1) and 54(2)

The discussion that follows addresses the requested clarifications related to [

]^{a,c}

Reflood heat transfer is a complicated network between the rods and the vapor and liquid phases. Above the quench front where the flow is in dispersed flow film boiling (DFFB), the overall heat transfer is a function of heat transfer between the rods and the vapor (convection (cwv) and radiation (rwv)), the rods and the liquid (radiation to droplets (rwd)) and between the vapor and the droplets (interfacial heat transfer (ivd)). This is pictorially shown in Figure 1. In DFFB, the droplet temperature will be lower than the vapor and wall temperatures. As such, the heat is transferred from the wall or vapor to the droplet and is shown with a one-way arrow in Figure 1. Since the vapor temperature near the top of the core may exceed the wall temperature due to low rod power and high vapor superheating, the heat transfer between the wall and the vapor is represented by a two-way arrow in Figure 1.



$$q'' = q''_{cwv} + q''_{rwv} + q''_{rwd} + q''_{ivd}$$

cwv – convection between wall and vapor

rwv – radiation between wall and vapor

rwd – radiation between wall and droplet

ivd – interfacial heat transfer between vapor and droplet

Figure 1: Cartoon of the Reflood Heat Transfer Network

The assessment of reflood heat transfer includes the impacts of interfacial heat transfer by virtue of [

]^{a,c}

[

] ^{a,c}

[

] ^{a,c}

a,c

Figure 2a: FLECHT 31805 Measured (red solid lines) vs. Predicted (blue dashed lines), Heat Transfer Coefficient Comparison at 6ft

a,c

Figure 2b: FLECHT 31805 Measured (red solid lines) vs. Predicted (blue dashed lines), Heat Flux Comparison at 6ft

[

]^{a,c}



Figure 3a: Demonstration of Heat Transfer Coefficient Determination for FLECHT 31504 Data



Figure 3b: Demonstration of Heat Transfer Coefficient Determination for FLECHT 31504 Code Simulations



Figure 3c: Code Predicted Heat Transfer Regimes during Evaluation Period for FLECHT 31504



Figure 3d: Code Predicted Void Fraction and Heat Transfer Regimes during Evaluation Period for FLECHT 31504

[

]^{a,c}

a,c

Figure 4: Measured vs. Predicted Peak Cladding Temperature

a,c

Figure 5: Measured vs. Predicted Turnaround Time

a,c

Figure 6: Measured vs. Predicted Time Above 1600°F

Clarification for Response to RAI 53(2)

Figures 29.1.8-8 through 29.1.8-10 of WCAP-16996-P provide a comparison of predicted versus measured quench temperatures for the FLECHT experiments (SEASET, low flooding rate, Skewed) simulated in Section 15.6 of WCAP-16996-P. The data values are the individual thermocouples located within the inner channel modeled by WCOBRA/TRAC-TF2. As can be seen from the figures, WCOBRA/TRAC-TF2 tends to [

] ^{a,c}

Clarification for Response to RAI 54(1)

Yes, the two equations describe the general heat transfer process of superheated vapor to liquid droplets. However, the flow regimes for which these two equations are applied are different. Equation (6-26) of WCAP-16996-P is applied to the Churn-Turbulent regime, which is a Normal Wall regime (i.e., wall is wet with a superheated vapor core region), in which the wall temperature is less than [^{a,c} Equation (6-49) of WCAP-16996-P is applied to the Inverted Annular regime if the liquid is sub-cooled and to the

Inverted Slug regime if the liquid is saturated or superheat and is applied to the dispersed droplet flow regime. All three of these flow regimes are Hot Wall flow regimes (i.e., wall is dry), in which the wall temperature is at least []^{a,c}

Clarification for Response to RAI 54(3)

The statement given is a concluding statement in the response to RAI 54 to the arguments used to justify the use of the Lee and Ryley (1968) [6] correlation for the description of heat transfer mechanism in the case of []

[]^{a,c} As stated in the RAI 54 response [5], []

[]^{a,c}

Clarification for Response to RAI 55

The creation of Figure 15.9.2-22, 15.9.2-23 and 15.9.2-35 was reviewed, and it was concluded that []

[]^{a,c}

[

] ^{a,c}] ^{a,c}

Figure 7: FLECHT 31701 Droplet Velocity vs. Droplet Diameter – 3ft



Figure 8: FLECHT 31701 Droplet Velocity vs. Droplet Diameter – 9ft



Figure 9: FLECHT 31805 Droplet Velocity vs. Droplet Diameter – 6ft



Figure 10: FLECHT 31504 Droplet Velocity vs. Droplet Diameter – 6ft

Clarification for Response to RAI 57

The statements made in Table 57-1 and Table 57-2 reflect the statements made in Section 2.3.2.2 of WCAP-16996-P (under Heat Transfer to a Covered Core) which provide the rationale for the low ranking of these heat transfer regimes. And as described in Section 2.3 of WCAP-16696-P, for a low ranking, [

]^{a,c}

[

] ^{a,c}] ^{a,c}

Figure 11: FLECHT 31504, Cladding Temperature at 6 ft



Figure 12: FLECHT 31504, Cladding Temperature at 10 ft



Figure 13: FLECHT 31805, Cladding Temperature at 6 ft

a,c

Figure 14: FLECHT 31805, Cladding Temperature at 10 ft

a,c

Figure 15: ORNL i, Void Fraction Profile



Figure 16: ORNL j, Void Fraction Profile

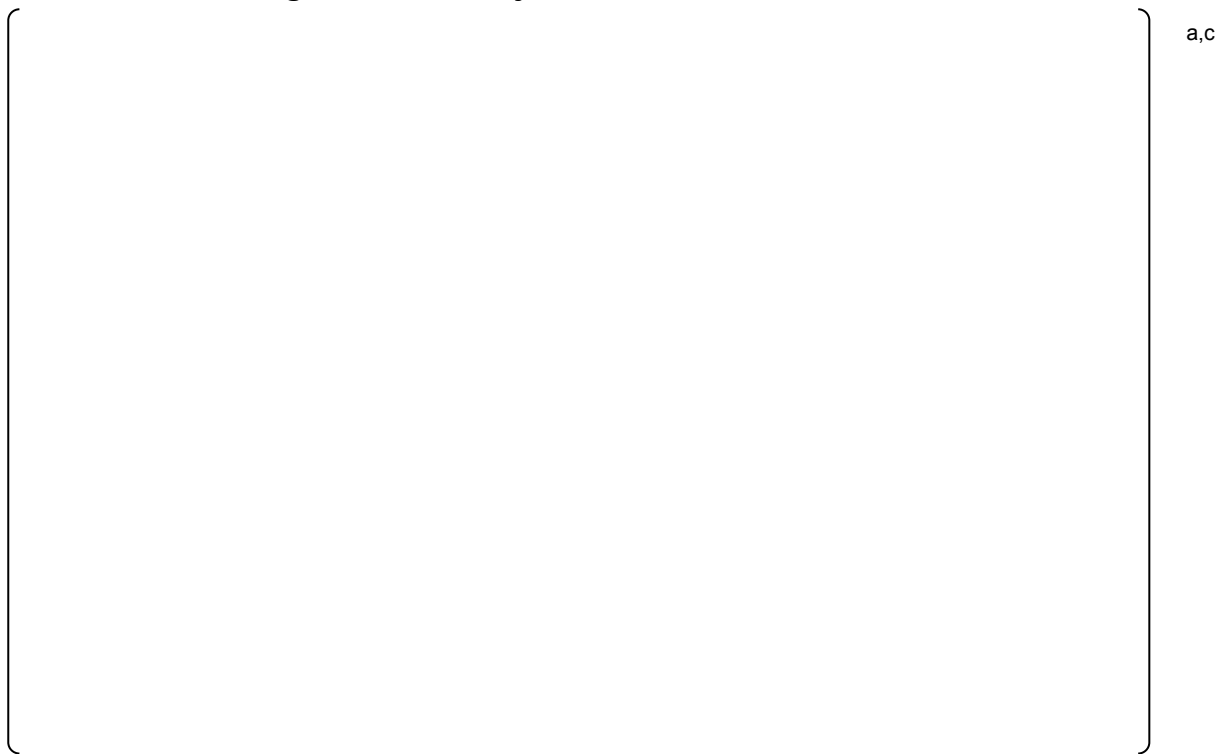


Figure 17: ORNL k, Void Fraction Profile

References

- 1) LTR-NRC-14-60, "Summary of August 2014 NRC Audit Part 1 of the FULL SPECTRUM LOCA (FSLOCA) Evaluation Model (Proprietary/Non-Proprietary), Project 700, TAC No. ME5244," September 17, 2014.
- 2) LTR-NRC-15-6, "Summary of August 2014 NRC Audit Part 2 of the FULL SPECTRUM LOCA (FSLOCA) Evaluation Model (Proprietary/Non-Proprietary), Project 700, TAC No. ME5244," January 30, 2015.
- 3) WCAP-12945-P-A, Revision 2 (Volume 1), and Revision 1 (Volumes 2 through 5), "Code Qualification Document for Best Estimate LOCA Analysis," March 1998.
- 4) WCAP-16996-P, "Realistic LOCA Evaluation Methodology Applied to the Full Spectrum of Break Sizes (FULL SPECTRUM LOCA Methodology)," November 2010.
- 5) LTR-NRC-13-73, "Submittal of Westinghouse Responses to 'WCAP-16996-P, 'Realistic LOCA Evaluation Methodology Applied to the Full Spectrum of Break Sizes (FULL SPECTRUM LOCA Methodology)' Request for Additional Information – RAIs 46 – 58, 75 and 77' (Proprietary/Non-Proprietary), Project 700, TAC No. ME5244," October 28, 2013.
- 6) Lee, K., and Ryley, D. J., "The Evaporation of Water Droplets in Superheated Steam," *Trans A.S.M.E. J Heat Transfer*, Vol. 90, 1968, pp. 445-451.

**Summary of June 2015 NRC Audit Part 1 of FULL SPECTRUM LOCA (FSLOCA) Evaluation Model
(Non-Proprietary)**

July 2015

Westinghouse Electric Company LLC
1000 Westinghouse Drive
Cranberry Township, PA 16066

©2015 Westinghouse Electric Company LLC
All Rights Reserved

Clarifications from June 2015 FULL SPECTRUM LOCA Discussion – Part 1

Summaries of the requested clarifications from each Request for Additional Information (RAI) are first presented in italics, followed by the clarification itself.

RAI-22

The response to RAI-21 reported three WCOBRA/TRAC-TF2 code errors related to decay heat uncertainty. Were the errors corrected to perform the provided additional information? Please append Figures 20-4 (core power), 20-6 (blowdown PCT) and 20-7 (reflood PCT) to show the results calculated with the corrected nominal decay heat model in WCOBRA/ TRAC-TF2 (the nominal-case results should be easily obtainable).

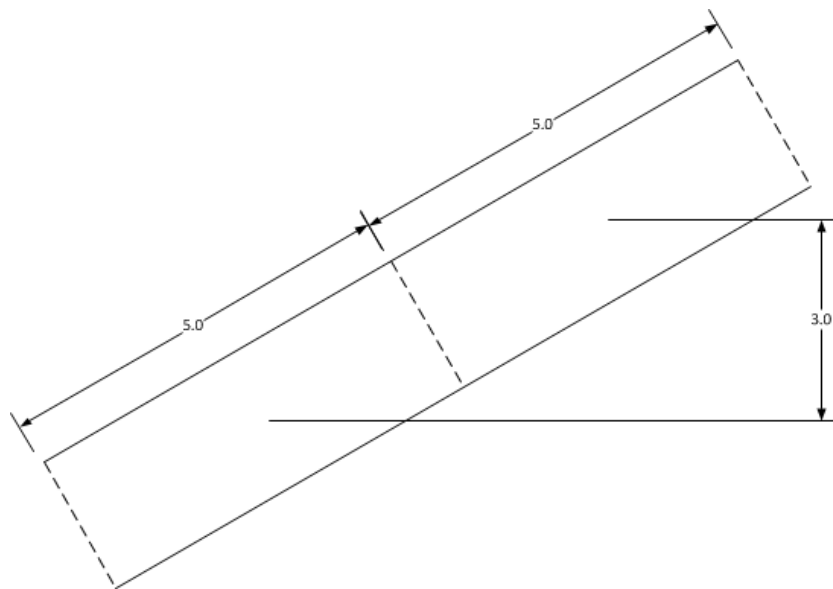
It is clarified that the errors identified in the response to Request for Additional Information (RAI)-21 were all corrected prior to providing the additional information for RAI-22.

As discussed in the June 8, 2015 meeting, a direct comparison cannot be provided with the full use of the decay heat package in WCOBRA/TRAC-TF2. The manually input power-versus-time curve was used so that the desired power change could be exactly controlled. The execution of the LUCIFER package includes other models (e.g. gamma redistribution) that would result in a different power than was input.

RAI-86

The provided definition for “a cell face inclination angle” is unclear. In 1D formalization of a cell to represent a section of the fluid conduit, the cell is defined by its fluid volume, length, and the flow areas of both cell faces that communicate with adjacent volumes. In the force balance for momentum conservation, additional input is needed to determine the acting gravitational force component (usually provided in terms of an angle relative to a chosen orientation). The mathematical expressions that define “a cell face inclination angle” in terms of input quantities for 1D description of fluid conduit represented by a number of interconnected cells can clarify this quantity.

The input which determines the elevation change, from which the inclination angle is defined, is referred to as GRAV. GRAV is input for each cell face, and is defined as the ratio of the elevation difference to the flow length between the centers of two cells. Take the following illustration for example:



There are two cells both of length 5.0, and the elevation difference between the two cell centers is 3.0. The GRAV input for the cell face between these two cells is then:

$$\text{GRAV} = \frac{3.0}{0.5(5.0 + 5.0)} = 0.6$$

The inclination angle of the cell face is then defined as:

$$\text{Inclination Angle} = \sin^{-1}(\text{GRAV}) = \sin^{-1}(0.6) = \sim 37^\circ$$

Physically, this inclination angle is the orientation of the cell face relative to a horizontal line.

RAI-96

Given a functional relationship between the pressure drop, flow rate, and hydraulic resistance across a flow path, it remains unclear how 15% uncertainty in the hydraulic resistance of the bypass path and a 15% uncertainty on the pressure drop across it result in 10% uncertainty for the bypass capacity (defined as a flow rate). Clarify the derivation of the uncertainty for the bypass capacity given the uncertainties for the contributing parameters.

It is noted that given the updated modeling approach for the bypass described in the “General Bypass Flow Discussion” section of LTR-NRC-15-6 [1] (i.e., the maximum of the estimated forward and reverse loss through the spray nozzles is modeled, and the hot leg nozzle gap flow path is not modeled), the significance of the uncertainty is greatly diminished. However, for completeness, the derivation is as follows.

$$\Delta P = K \frac{\rho V^2}{2}$$

Rearranging yields:

$$V = \sqrt{\frac{2\Delta P}{\rho K}}$$

Where: ΔP = pressure drop

K = hydraulic resistance

ρ = density

V = velocity

$$\dot{m} = \rho VA$$

Substituting for velocity:

$$\dot{m} = \rho A \sqrt{\frac{2\Delta P}{\rho K}} = \sqrt{\frac{2\Delta P \rho A^2}{K}}$$

Where: \dot{m} = mass flow rate

A = flow area

Per Chapter 8 of Green and Bourne (1972) [2], a first-order Taylor series expansion may be used to approximately express the mass flow rate as a function of the variates for small deltas as follows:

$$\partial \dot{m} \approx \frac{\partial \dot{m}}{\partial K}(\partial K) + \frac{\partial \dot{m}}{\partial \Delta P}(\partial \Delta P) + \frac{\partial \dot{m}}{\partial A}(\partial A) + \frac{\partial \dot{m}}{\partial \rho}(\partial \rho)$$

The flow area is known with negligible uncertainty therefore:

$$\frac{\partial \dot{m}}{\partial A}(\partial A) \rightarrow 0$$

The density is specified for each case so there is no associated uncertainty:

$$\frac{\partial \dot{m}}{\partial \rho}(\partial \rho) \rightarrow 0$$

Since the uncertainty is expressed as a fraction of a given value, the remaining terms are all divided by the mass flow rate to obtain the uncertainty as a fraction of the mass flow rate:

$$\frac{\partial \dot{m}}{\dot{m}} \approx \frac{1}{\dot{m}} \frac{\partial \dot{m}}{\partial K}(\partial K) + \frac{1}{\dot{m}} \frac{\partial \dot{m}}{\partial \Delta P}(\partial \Delta P)$$

Solve for the terms:

$$\frac{1}{\dot{m}} \frac{\partial \dot{m}}{\partial K} = -\frac{1}{2} \frac{(2\Delta P \rho A^2)^{0.5} K^{-1.5}}{(2\Delta P \rho A^2)^{0.5} K^{-0.5}} = -\frac{1}{2K}$$

$$\frac{1}{\dot{m}} \frac{\partial \dot{m}}{\partial \Delta P} = \frac{1}{2} \frac{(2\rho A^2)^{0.5} (\Delta P K)^{-0.5}}{(2\Delta P \rho A^2)^{0.5} K^{-0.5}} = \frac{1}{2\Delta P}$$

Substitute back into the equation:

$$\frac{\partial \dot{m}}{\dot{m}} \approx -\frac{1}{2K}(\partial K) + \frac{1}{2\Delta P}(\partial \Delta P)$$

Assuming that all the variables are independent, and the uncertainties are normally distributed, the square root of the sum of the squares can be used:

$$\left(\frac{\partial \dot{m}}{\dot{m}}\right)^2 \leq \frac{1}{4} \left(\frac{\partial K^2}{K^2} + \frac{\partial \Delta P^2}{\Delta P^2} \right)$$

$$\frac{\partial \dot{m}}{\dot{m}} \leq \frac{1}{2} \sqrt{\left(\frac{\partial K}{K}\right)^2 + \left(\frac{\partial \Delta P}{\Delta P}\right)^2}$$

Substitute uncertainties:

$$\frac{\partial \dot{m}}{\dot{m}} \leq \frac{1}{2} \sqrt{(0.15)^2 + (0.15)^2} = \frac{1}{2} \sqrt{2(0.15)^2} = 0.106$$

This yields approximately a 10% uncertainty on flow rate.

RAI-108

The description of the CCFL models that will be applied at the three critical locations (hot leg elbow, SG tubes, upper core plate) needs to be provided.

The assessment of the final WCOBRA/TRAC-TF2 version with the new CCFL modeling features implemented needs to be presented. This information is necessary to demonstrate the applicability of the three implemented models.

To demonstrate proper implementation of the hot leg CCFL model in WCOBRA/TRAC-TF2, the RAI asked for a specific assessment study using data from a very simple test setup with well-defined boundary conditions (Costigan's experiment). Given the pedigree of the newly implemented CCFL model and if opted so by Westinghouse, an assessment for the 2D/3D UPTF Hot Leg SB LOCA Test No. 11 would be acceptable for the Staff in lieu of the Costigan's experiment assessment.

To resolve questions related to: a) effects of hot leg nodalization, and b) sensitivities to the HS_SLUG parameter ranging, the assessment discussed above can be easily used to provide the relevant sensitivity results needed to resolve these questions.

The countercurrent flow limitation (CCFL) models applied at all three locations are described in revision 1 of the topical report. A summary for each is provided below: [

]^{a,c}

As discussed in the June 8, 2015 meeting, plots of the flooding curves versus code predictions for the reference pressurized water reactor (PWR) will be provided in revision 1 of the topical report in lieu of additional experimental simulations. These plots will provide assurance that the code is properly enforcing the CCFL in key areas.

RAI-109 and RAI-110

The NRC Staff needs to understand the causes for the predicted negative flow in the intact hot leg between 100 s and 200 s of the transient as seen in Figure 3.2.1-5 in the RAI response.

The NRC Staff needs to understand the causes for the predicted negative flow in the intact hot leg between 100 s and 250 s of the transient as and evident from Figure 3.2.2-5 in the RAI response. The test data show significant positive hot leg flow during this period.

As shown in Figures 3.2.1-5 and 3.2.2-5 of LTR-NRC-14-70 [7], the predicted volumetric flow (FLOW) is calculated as

$$\text{FLOW} = \frac{\text{Mass Flowrate}}{\text{Mixture Density}} = \frac{\rho_v \cdot \alpha_v \cdot V_v \cdot F_A + \rho_l \cdot (1 - \alpha_v) \cdot V_l \cdot F_A}{\rho_m} = V_m \cdot F_A = \frac{\rho_v}{\rho_m} \cdot \alpha_v \cdot V_v \cdot F_A + \frac{\rho_l}{\rho_m} \cdot (1 - \alpha_v) \cdot V_l \cdot F_A$$

In the above equation, ρ is density (kg/m³), V is velocity (m/sec), F_A is flow area (m²) and α is void fraction. The subscripts v , l and m denote vapor phase, liquid phase, and mixture, respectively.

Note that the volumetric flow as defined by the above equation is a weighted mean mixture volumetric flow rate. The total volumetric flow determined as the sum of the predicted phasic volumetric flow is more appropriate for the comparison. Therefore, Figures 3.2.1-5b, 3.2.2-5b, 3.2.1-6b and 3.2.2-6b from LTR-NRC-14-70 are re-plotted using VFLOW defined as the sum of the vapor (FLOW_VAP) and liquid (FLOW_LIQ) volumetric flows, as,

$$\text{VFLOW} = \text{FLOW_VAP} + \text{FLOW_LIQ} = \alpha_v \cdot V_v \cdot F_A + (1 - \alpha_v) \cdot V_l \cdot F_A$$

In the above calculation, the determining of the void fraction α is determined for each phase depending on the direction of the respective velocity.

The next two sets of figures (109-1,2,3 and 110-1,2,3) show calculated (vapor, liquid and mixture) velocities and void fractions in the intact loop hot legs, as well as the updated intact and broken loop hot leg (HL) volumetric flows for S-LH-1 and S-LH-2, respectively.

As seen in Figures 109-1 and 110-1, showing the calculated velocities and void fractions in the broken loop HL, [

]^{a,c}

RAI-112

The response did not clarify if the three-PIPE component model of the U-tube bundle accounted for gravitational effects due to elevation differences between the arc regions of the inner, middle, and outer PIPE components.

The three-PIPE model of the steam generator U-tubes, used for the PWR sensitivity study for RAI-112 used [

]^{a,c}

It was not explained how angle change in the arc regions was accounted for in the adopted nodding schemes for both SG U-tube bundle models.

The primary impact of the angle change in the arc region for the different length pipes is the elevation difference, [

]^{a,c}

Which analyses were considered by Westinghouse in concluding that [

]^{a,c} How can it be shown that WCOBRA/TRAC-TF2 assessment of Semiscale Tests S-LH-1 and S-LH-2 supports this statement and the implemented SG modeling approach (single-PIPE component model of the SG U-tube bundle)? Which WCOBRA/TRAC-TF2 assessments of ROSA LSTF tests support this statement and the implemented SG modeling approach [

]^{a,c}

The simulation results of the Rig-of-Safety Assessment IV (ROSA-IV) and Semiscale integral effects test (IET) facilities were considered in concluding that WCOBRA/TRAC-TF2 tends to predict [

]^{a,c} hold-

up is demonstrated by the code predictions for the SB-CL-18 test simulations, Figures 21.4-7 and 21.4-8 in Section 21.4.3 of WCAP-16996-P, Revision 1 [8], the SB-CL-05 test simulations, Figures 21.5-8(a) and 21.5-9(a) in Section 21.5.2 of WCAP-16996-P, Revision 1, and the SB-CL-14 simulations, Figures 21.6-9 and 21.6-10 in Section 21.6.2 of WCAP-16996-P, Revision 1. []^{a,c} was predicted in the Semiscale test simulations as well, Figures 3.2.1-3(a) and 3.2.1-4(a) of LTR-NRC-14-70 for the S-LH-1 simulation, and Figures 3.2.2-3(a) and 3.2.2-4(a) of LTR-NRC-14-70, for the S-LH-2 simulation.

In both the ROSA-IV (WCAP-16996-P, Revision 1) and the Semiscale simulations (LTR-NRC-14-70), the primary side of the U-tube bundle in each steam generator was modeled using a []^{a,c}

RAI-122

Confirm the LOOP logic for RCP trip that is implemented in WCOBRA/TRAC-TF2 and explain the reason for changing it from the one in the approved ASTRUM EM. What technical basis demonstrates that timing variability in an operator action to manually trip the RCPs following applicable procedures will not infringe upon the validity of the obtained FSLOCA™ results for any given plant (these results will represent the licensing basis)? This item needs to be addressed for both LOCA Region I, where the realistic FSLOCA EM and WCOBRA/TRAC-TF2 will be applied for first time, and Region II where the proposed modeling approach differs drastically from the approved ASTRUM EM.

Region I: A significant amount of information regarding the treatment of offsite power availability and reactor coolant pump (RCP) trip for Region I was previously provided in the FSLOCA topical report, the RAI responses transmitted in LTR-NRC-14-9 [9], and Section 5.1 of LTR-NRC-14-29 [10]. A concise explanation of the resultant modeling approach for Region I is provided, with the technical basis supported by the referenced documents.

[

] ^{a,c}

FULL SPECTRUM and FSLOCA are trademarks of Westinghouse Electric Company LLC, its subsidiaries and/or its affiliates in the United States of America and may be registered in other countries throughout the world. All rights reserved. Unauthorized use is strictly prohibited. Other names may be trademarks of their respective owners.

Region II: The operation of the RCPs relative to the power availability assumption for the FSLOCA evaluation model is as follows. [

] ^{a,c}

References

- 1) LTR-NRC-15-6, "Summary of August 2014 NRC Audit Part 2 of the FULL SPECTRUM LOCA (FSLOCA) Evaluation Model (Proprietary/Non-Proprietary), Project 700, TAC No. ME5244," January 30, 2015.
- 2) Green, A. E. and Bourne, A. J., 1972, Reliability Technology, John Wiley and Sons.
- 3) LTR-NRC-14-33, "Submittal of Westinghouse Responses to 'WCAP-16996-P, 'Realistic LOCA Evaluation Methodology Applied to the Full Spectrum of Break Sizes (FULL SPECTRUM LOCA Methodology)' Request for Additional Information – RAIs 108, 120 and 121' (Proprietary/Non-Proprietary), Project 700, TAC No. ME5244," June 13, 2014.
- 4) LTR-NRC-14-60, "Summary of August 2014 NRC Audit Part 1 of the FULL SPECTRUM LOCA (FSLOCA) Evaluation Model (Proprietary/Non-Proprietary), Project 700, TAC No. ME5244," September 17, 2014.
- 5) Vallée, C., et al., 2012, "Counter-current flow limitation in a model of the hot leg of a PWR-Comparison between air/water and steam/water experiments," *Nuclear Engineering and Design* 245, pp. 113-124.
- 6) Kukita, Y., et al., 1991, "Summary of ROSA-IV LSTF First-phase Test Program - Integral Simulation of PWR Small-break LOCAs and Transients," *Nuclear Engineering and Design*, 131, pp. 101-111.
- 7) LTR-NRC-14-70, "Submittal of Westinghouse Responses to 'WCAP-16996-P, 'Realistic LOCA Evaluation Methodology Applied to the Full Spectrum of Break Sizes (FULL SPECTRUM LOCA Methodology)' Request for Additional Information – RAIs 109-111' (Proprietary/Non-Proprietary), Project 700, TAC No. ME5244," October 31, 2014.
- 8) WCAP-16996-P, Volume II, Revision 1, "Realistic LOCA Evaluation Methodology Applied to the Full Spectrum of Break Sizes (FULL SPECTRUM LOCA Methodology)," June 2015.
- 9) LTR-NRC-14-9, "Submittal of Westinghouse Responses to 'WCAP-16996-P, 'Realistic LOCA Evaluation Methodology Applied to the Full Spectrum of Break Sizes (FULL SPECTRUM LOCA Methodology)' Request for Additional Information – Set 8 RAIs 122-126, 128-131 and 136' (Proprietary/Non-Proprietary), Project 700, TAC No. ME5244," February 12, 2014.
- 10) LTR-NRC-14-29, "Summary of May 2014 NRC Audit of the FULL SPECTRUM LOCA (FSLOCA) Evaluation Model (Proprietary/Non-Proprietary), Project 700, TAC No. ME5244," June 5, 2014.
- 11) WCAP-16009-P-A, "Realistic Large-Break LOCA Evaluation Methodology Using the Automated Statistical Treatment Of Uncertainty Method (ASTRUM)," January 2005.

Figure 108-1: Comparison of UPTF Test 11 and TOPFLOW Hot Leg Flooding Results (Figure 12b from Vallée et al., 2012)



Figure 109-1: Calculated Intact Hot Leg Fluid Velocities and Void Fractions for S-LH-1

Figure 109-2: Intact Loop Hot Leg Volumetric Flows for S-LH-1 (Updated Figure 3.2.1-5b of LTR-NRC-14-70)



Figure 109-3: Broken Loop Hot Leg Volumetric Flows for S-LH-1 (Updated Figure 3.2.1-6b of LTR-NRC-14-70)



Figure 110-1: Calculated Intact Hot Leg Fluid Velocities and Void Fractions for S-LH-2

Figure 110-2: Intact Loop Hot Leg Volumetric Flows for S-LH-2 (Updated Figure 3.2.2-5b of LTR-NRC-14-70)



Figure 110-3: Broken Loop Hot Leg Volumetric Flows for S-LH-2 (Updated Figure 3.2.2-6b of LTR-NRC-14-70)



Figure 112-1: U-tube Bend Noding for the Three-PIPE Steam Generator Model

**Summary of June 2015 NRC Audit Part 2 of FULL SPECTRUM LOCA (FSLOCA) Evaluation Model
(Non-Proprietary)**

September 2015

Westinghouse Electric Company LLC
1000 Westinghouse Drive
Cranberry Township, PA 16066

©2015 Westinghouse Electric Company LLC
All Rights Reserved

Clarifications from June 2015 FULL SPECTRUM LOCA Discussion – Part 2

Section 1: Introduction

Section 2 of this letter contains a subset of the clarifications requested by the Nuclear Regulatory Commission (NRC) staff relative to specific Requests for Additional Information (RAIs) on the FULL SPECTRUM™ LOCA (FSLOCA™) evaluation model. Summaries of the requested clarifications from each RAI are first presented in italics, followed by the clarification itself. Section 3 of this letter contains additional discussion regarding the emergency core cooling system (ECCS) injection into the faulted loop. Section 4 of this letter contains a list of cited references.

Section 2: RAI Clarifications

RAI-26

Figure RAI-26-1 from LTR-NRC-15-11 [1] shows three cycles for a [

]^{a,c}

Figure RAI-26-1 from LTR-NRC-15-11 shows how the local power varies in a single 3D core location that reaches the highest power during a load follow transient (i.e., the “hot spot” core location). In this example, the hot spot core location is located at approximately the 3-ft core elevation. The local power in this 3D core location thus follows both the core average power level and the axial power shape. When the axial power shape becomes more bottom skewed, the local power in the hot spot location increases. When the axial power shape changes to a more top skewed shape, the local power in the hot spot location decreases.

At approximately hour 58 in the transient simulation shown in Figure RAI-26-1, a control rod insertion occurred, because the predicted Axial Flux Difference (AFD) reached the positive side of the technical specification allowed AFD limit. In accordance with the Constant Axial Offset Control (CAOC) operating strategy being simulated in this particular case, the control rods were inserted to restore the AFD to the target value. Since the axial power distribution was pushed more toward the bottom of the core as a result of this control rod motion, this increased the local power in the hot spot core location, starting at approximately hour 58, before the core average power was increased. The reason that a similar trend did not occur in the first and second day

FULL SPECTRUM and FSLOCA are trademarks of Westinghouse Electric Company LLC, its subsidiaries and/or its affiliates in the United States of America and may be registered in other countries throughout the world. All rights reserved. Unauthorized use is strictly prohibited. Other names may be trademarks of their respective owners.

of the load follow simulation was that the AFD in these cases did not quite reach the positive side of the AFD band before the core power was increased.

The data shown in Figure RAI-26-1 has been confirmed accurate.

Why (does) the third cycle in Figure RAI-26-1 of LTR-NRC-15-11 produce a hot spot power shape much different from the one predicted for the first two cycles?

Again, this is due to control rod motions that occurred to control the AFD in accordance with the CAOC operating strategy being simulated in this particular case. In the first two days of the load follow cycle, at approximately hours 18 and 43, the AFD reached the negative side of the technical specification allowed AFD limit. In accordance with the CAOC operating strategy being simulated in this particular case, the control rods were withdrawn to restore AFD to the target value appropriate for that power level. Since the axial power distribution was skewed more toward the top of the core as a result of this control rod motion, this decreased the local power in the hot spot core location at the 3-ft elevation at approximately hours 18 and 43. After the third day of load follow, the AFD did not quite reach the negative side of the technical specification allowed AFD limit before the xenon transient reversed the trend in AFD. As a result, a similar rod motion did not occur after the third day of operation.

Figures RAI-26-3 and RAI-26-4 of LTR-NRC-15-11 plot relative decay heat results for ^{239}U and ^{239}Np and for fission products for a step change in relative power density (Q) from 1.0 to 1.4 for low-burnup high-enriched fuel. These figures do not agree with any of the data in Tables RAI-26-1 through RAI-26-12 of LTR-NRC-15-11. Clarify how the plotted results correspond to the data in Tables RAI-26-1 through RAI-26-12 of LTR-NRC-15-11.

Figures RAI-26-3 and RAI-26-4 of LTR-NRC-15-11 show how the dominant actinide and fission product components of decay heat change after a step power change of 40% followed by continued operation after the power change. The purpose of these figures was to illustrate the time dependence of the effects, in order to demonstrate how long it takes for the individual components of decay heat to approach equilibrium values, following a step change in power.

As noted in the text describing Figure RAI-26-3 of LTR-NRC-15-11, the data was generated assuming a specific \bar{R} value (^{238}U capture-to-fission ratio). However, investigation revealed that this \bar{R} value was actually []^{a,c} as originally described. Therefore, the value of \bar{R} used in the initial presentation of Figure RAI-26-3 in LTR-NRC-15-11 did not match any of the data listed in Tables RAI-26-1 through RAI-26-12 of LTR-NRC-15-11. However, as noted in the RAI-26 text, it has been confirmed that different values of \bar{R} will scale both the equilibrium and transient actinide decay heat terms by the same relative amounts. Thus the re-regeneration of the data plotted in Figure RAI-26-3 with an \bar{R} value that matches one of the data tables still shows the same relative time dependence. As an example of this, the data in Figure RAI-26-3 of LTR-NRC-15-11 was regenerated using the same value of \bar{R} that was used to generate the

actinide data in Table RAI-26-7 of LTR-NRC-15-11 [

]^{a,c} The revised data using [

]^{a,c} consistent with Table RAI-26-7 of LTR-NRC-15-11, is shown in Figure RAI-26-3a herein. This confirms that the plotted actinide data shows the same relative time dependence shown in the original version of Figure RAI-26-3 in LTR-NRC-15-11, but the data can now be matched up with the actinide results shown in Table RAI-26-7 of LTR-NRC-15-11 for time zero after shutdown ($t=0$). Specifically, in Figure RAI-26-3a, the equilibrium ^{239}U and ^{239}Np and the equilibrium Sum of $^{239}\text{U} + ^{239}\text{Np}$ match exactly the $t=0$ data in Table RAI-26-7 of LTR-NRC-15-11 for the equilibrium initial condition assumption. The transient data at 24 hours after the step power change also matches the transient data shown in Table RAI-26-7 of LTR-NRC-15-11 for time zero after shutdown. Since Figure RAI-26-3a does not plot the time dependence after shutdown, none of the other data from Table RAI-26-7 of LTR-NRC-15-11 (i.e., with $t>0$) is applicable in this comparison.

The data provided in the original version of Figure RAI-26-4 of LTR-NRC-15-11 was generated for []^{a,c} and can therefore be compared to the fission product decay heat data in Table RAI-26-7 of LTR-NRC-15-11 at time zero after shutdown.

The change made to Figure RAI-26-3a herein puts this figure on a directly comparable basis with both the data in Table RAI-26-7 of LTR-NRC-15-11 and Figure RAI-26-4 of LTR-NRC-15-11. However, the original points made with respect to the relative time dependent variation of the dominant actinides in Figure RAI-26-3 are still valid.

*Figure RAI-26-1 of LTR-NRC-15-11 shows a Q value of 2.4 at the F_Q limit. In explaining the step increase in Q used in Figures RAI-26-3 and RAI-26-4, a " F_Q *Power value" of 2.52 was used (see page P-5). How do these values interrelate and does their choice have any impact on the generality of the conclusions supported by the results in the response?*

The value of $F_Q = 2.4$ is shown in Figure RAI-26-1 because this is the F_Q limit associated with the specific plant for which the transient was run. The example discussed on page 5 of the response of F_Q increasing 40% from 1.8 to 2.52 was just an example of what a 40% power increase might correlate to in F_Q space. There is no intended inter-relationship. A 40% power step increase results in the same relative time dependence of the fission product and actinide decay heat terms, regardless of whether the 40 % increase is from 1.0 to 1.4, 1.71 to 2.40, or 1.80 to 2.52. This has no impact on the conclusions made in the response.

RAI-46

The assumption of modeling the containment atmosphere in COCO as []^{a,c} is not found in the final response for RAI-46 provided by Westinghouse in LTR-NRC-13-73 [2]. Considering this new information, it is found necessary to clarify the following items that are relevant to this assumption.

1) *The impact on containment pressurization by modeling the containment [*
]^{a,c}

2) *Relevance to modeling of steam condensation on liquid droplets, films and pool surfaces inside containment.*

3) *Relevance to the effect of the initial containment humidity on containment pressure.*

4) *Relevance to the applicability of COCO validation results.*

[

]^{a,c}

[

] ^{a,c}

It is therefore concluded that the existing COCO validation remains valid.

RAI-51

What is the basis for using only thermocouples [
] ^{a,c} for a facility?

[

] ^{a,c}

[

] ^{a,c}

[

] ^{a,c}

RAI-55

Explain why Figure 10 in LTR-NRC-15-11 shows [

]^{a,c} What is the time interval for the shown code results and how was it determined? Identify WCAP-9699 on page P-36 in the response and WCAP-9891 in Figure 10 and in Figure 24.6.4-8.

Several code changes have occurred which may have influenced the transient behavior. For example, [

^{a,c} WCAP-9699 [5] cited on page P-36 of LTR-NRC-15-11 refers to the data report for the FLECHT 31504 experimental results, while WCAP-9891 [6] cited in Figure 10 of LTR-NRC-15-11 and in Figure 24.6.4-8 of Revision 0 to Volume II of WCAP-16996-P refers to the evaluation and analysis report where the data droplet vs. velocity values were obtained.

Clarify the statement: "in the case of the FLECHT 31805 results, there are [

^{a,c}

The statement regarding [

^{a,c}

RAI-57

A PCT impact of [
is this impact negligible?

^{a,c} *Why*

[

] ^{a,c}

A [*why is this impact negligible?*

] ^{a,c} *What causes the void drop and*

For the ORNL case shown in Figure 15 of LTR-NRC-15-11, [

] ^{a,c}

The response did not discuss the impact on the thermal energy stored initially in the core at steady-state (prior to LOCA).

Section 4.0 of LTR-NRC-14-38 [10] provided a clarification regarding the response to RAI 37 related to stored energy. As stated in Section 4.0 of LTR-NRC-14-38, [

] ^{a,c}

Section 3: ECCS into Faulted Loop

Since the FSLOCA EM evolved during the licensing process, Westinghouse took the initiative to revalidate a number of prior conclusions to ensure they remained intact. It was previously stated that [

] ^{a,c}

Section 4: References

- 1) LTR-NRC-15-11, "Summary of August 2014 NRC Audit Part 3 of the FULL SPECTRUM LOCA (FSLOCA) Evaluation Model (Proprietary/Non-Proprietary), Project 700, TAC NO. ME5244," February 24, 2015.
- 2) LTR-NRC-13-73, "Submittal of Westinghouse Responses to 'WCAP-16996-P, 'Realistic LOCA Evaluation Methodology Applied to the Full Spectrum of Break Sizes (FULL SPECTRUM LOCA Methodology)' Request for Additional Information – RAIs 46 – 58, 75

and 77' (Proprietary/Non-Proprietary), Project 700, TAC No. ME5244," October 28, 2013.

- 3) WCAP-8327-P, "Containment Pressure Analysis Code (COCO)," July 1974.
- 4) WCAP-16996-P, Volume II, Revision 1, "Realistic LOCA Evaluation Methodology Applied to the Full Spectrum of Break Sizes (FULL SPECTRUM LOCA Methodology), Volume II, WCOBRA/TRAC-TF2 Assessment", June 2015.
- 5) NUREG/CR-1532, WCAP-9699, "PWR FLECHT SEASET Unblocked Bundle, Forced and Gravity Reflood Task Data Report," June 1980.
- 6) NUREG/CR-2256, WCAP-9891, "PWR FLECHT SEASET Unblocked Bundle, Forced and Gravity Reflood Task Data Evaluation and Analysis Report," November 1981.
- 7) WCAP-16996-P, Volume II, Revision 0, "Realistic LOCA Evaluation Methodology Applied to the Full Spectrum of Break Sizes (FULL SPECTRUM LOCA Methodology), Volume II, WCOBRA/TRAC-TF2 Assessment", November 2010.
- 8) WCAP-16996-P, Volume I, Revision 1, "Realistic LOCA Evaluation Methodology Applied to the Full Spectrum of Break Sizes (FULL SPECTRUM LOCA Methodology), Volume I, WCOBRA/TRAC-TF2 Models and Correlations", April 2015.
- 9) Chen, J. C., 1963, "Correlation for Boiling Heat Transfer to Saturated Fluids in Convective Flow," ASME 63-HT-34.
- 10) LTR-NRC-14-38, "Summary of June 2014 NRC Audit of the FULL SPECTRUM LOCA (FSLOCA) Evaluation Model (Proprietary/Non-Proprietary), Project 700, TAC No. ME5244," June 27, 2014.

a,c

**Figure RAI-26-3a: Relative Decay Heat for ^{239}U and ^{239}Np for a Step Change in
Relative Power Density from 1.0 to 1.4**

**5% Enriched Fuel at 30 GWD/MTU
(Compare to Table RAI-26-7 of LTR-NRC-15-11, t=0 Data)**

a,c



Figure 46-1: Containment Pressure Response Comparison between Modeling Air (Red Line) and Modeling Nitrogen (Blue Line)



Figure 51-1: Predicted vs. Measured Time Cladding Temperature is Greater than 1,600°F

a,c

Figure 51-2: Updated Predicted vs. Measured Time Cladding Temperature is Greater than 1,600°F

a,c

Figure 57-1: FLECHT 31805 Vapor Temperature at 10ft

a,c

Figure 57-2: FLECHT 31805 Entrained Liquid Fraction at 10ft

a,c



Figure 57-3: FLECHT 31805 Entrainment Generation at Quench Front

a,c



Figure 57-4: FLECHT 31805 Vapor Generation at Quench Front



Figure 57-5: FLECHT 31805 Liquid Temperature at and Below Quench Front



Figure 57-6: ORNL I Liquid Temperature in Cells 2 and 3 of Channel 2 vs. Saturation Temperature



Figure 57-7: ORNL I Heat Transfer Mode for Representative Nodes in Cells 2 and 3 of Channel 2



Figure 57-8: ORNL I Vapor Generation in Cells 2 and 3 of Channel 2



Figure 57-9: ORNL I Liquid and Saturation Temperature in Cell 4 of Channel 2



Figure 57-10: ORNL I Vapor Generation in Cell 4 of Channel 2



Figure S3-1: Time-at-Temperature for Region I 2.5-inch Break LOCA Transients with and without ECC into the Faulted Loop

a,c

Figure S3-2: Time-at-Temperature for Region I 2.5-inch Break LOCA Transients with and without ECC into the Faulted Loop; Transient Time Shifted such that the Boiloff Uncovery Starts at the Same Time for Both Transients

**Summary of June 2015 NRC Audit Part 3 of FULL SPECTRUM LOCA (FSLOCA) Evaluation Model
(Non-Proprietary)**

October 2015

Westinghouse Electric Company LLC
1000 Westinghouse Drive
Cranberry Township, PA 16066

©2015 Westinghouse Electric Company LLC
All Rights Reserved

RAI-113 Clarification

As discussed in Section 4.0 of LTR-NRC-14-29 [1], []^{a,c} The assessments which support the use of []^{a,c} are the Upper Plenum Test Facility (UPTF) loop seal separate effects test (SET) and pressurized water reactor (PWR) studies. Figure 29.1.11-1 of Revision 1 of the topical report [2] shows that the []

PWR sensitivity studies varying HS_SLUG were presented in Section 28.2.12 of Revision 1 of the topical report, for both Beaver Valley Unit 1 and V. C. Summer. []^{a,c}

[]^{a,c}

FULL SPECTRUM and FSLOCA are trademarks of Westinghouse Electric Company LLC, its subsidiaries and/or its affiliates in the United States of America and may be registered throughout the world. All rights reserved. Unauthorized use is strictly prohibited. Other names may be trademarks of their respective owners.

Description:

There are two tables created in this letter. The first table provides a comprehensive description of the code input multipliers/parameters/flags in the WCOBRA/TRAC-TF2 code and relevant uncertainty elements in the FSLOCATM EM. The table integrates Tables 50-1, 50-2, and 50-3 in response to Request for Additional Information (RAI) 50[1], Table I in the response to RAI 77[1], information in the response to RAI 86[2], and Table 87-1 from the response to RAI 87[2]. The table is sorted alphabetically to better retrieve the information.

The second table summarizes the parameters treated as bounded in the FSLOCA EM, which are from Table 2 in the response to RAI 77[1].

Some correction and updates are added to the tables.

List of Acronyms

CDF	cumulative distribution function
DEG	double ended guillotine
ECCS	emergency core cooling system
HFP	hot full power
LOCA	loss of coolant accident
LOOP	loss of offsite power
MTC	moderator temperature coefficient
OPA	offsite power availability
PWR	pressurized water reactor
RCS	reactor coolant system
SGTP	steam generator tube plugging
SI	safety injection
UPI	upper plenum injection
<u>W</u> CT-TF2	<u>W</u> COBRA/TRAC-TF2

References:

1. LTR-NRC-13-73, Submittal of Westinghouse Response to “WCAP-16996-P, ‘Realistic LOCA Evaluation Methodology Applied to the Full Spectrum of Break Sizes (FULL SPECTRUM LOCA Methodology)’ Request for Additional Information - RAIs 46 – 58, 75 and 77” (Proprietary/Non-Proprietary), Project 700, TAC No. ME5244, October 2013.
2. LTR-NRC-14-12, Submittal of Westinghouse Response to “WCAP-16996-P, ‘Realistic LOCA Evaluation Methodology Applied to the Full Spectrum of Break Sizes (FULL SPECTRUM LOCA Methodology)’ Request for Additional Information - RAIs 77-82, 86-87, 93 and 112” (Proprietary/Non-Proprietary), Project 700, TAC No. ME5244, March 2014.

Table I Combined Table for Multipliers/Parameters/Flags Relevant to FSLOCA EM

a,c

a,c



a,c

a,c

[

]

a,c

Table II Parameters Treated as Bounded in FSLOCA EM**a,c**

a,c

a,c

a,c

**Summary of September 2015 NRC Audit of FULL SPECTRUM LOCA (FSLOCA) Evaluation Model
(Non-Proprietary)**

September 2015

Westinghouse Electric Company LLC
1000 Westinghouse Drive
Cranberry Township, PA 16066

©2015 Westinghouse Electric Company LLC
All Rights Reserved

Clarifications from September 14, 2015 Meeting on FULL SPECTRUM LOCA EM: Offsite Power Availability

1: Introduction

This letter serves to document and provide further clarification on the information provided by Westinghouse during a September 14, 2015 meeting with the Nuclear Regulatory Commission (NRC) staff relative to the treatment of offsite power availability in Region II (large break) analyses in the FULL SPECTRUM™ LOCA (FSLOCA™) evaluation model (EM).

The following request for clarification on the response to request for additional information (RAI) 136 [1] was provided to Westinghouse [

J^{a,c}

FULL SPECTRUM and FSLOCA are trademarks of Westinghouse Electric Company LLC, its subsidiaries and/or its affiliates in the United States of America and may be registered in other countries throughout the world. All rights reserved. Unauthorized use is strictly prohibited. Other names may be trademarks of their respective owners.

[

] ^{a,c} are described in Section

2. Section 2.1 considers [

] ^{a,c}

Throughout the response, references are made to figures and information provided in the slide package discussed in the September 14, 2015 meeting, which are provided in Attachment P2.

2: [

]^{a,c}

[

] ^{a,c}

2.1 [

] ^{a,c}

3: References

1. LTR-NRC-14-9, "Submittal of Westinghouse Responses to 'WCAP-16996-P, 'Realistic LOCA Evaluation Methodology Applied to the Full Spectrum of Break Sizes (FULL SPECTRUM LOCA Methodology)' Request for Additional Information – Set 8 RAIs 122-126, 128-131 and 136' (Proprietary/Non-Proprietary), Project 700, TAC No. ME5244," February 12, 2014.
2. Wilks, S. S., 1941, "Determination of Sample Sizes for Setting Tolerance Limits," The Annals of Mathematical Statistics, Vol. 12, pp.91-96.

Offsite Power Availability: FULL SPECTRUM™ LOCA (FSLOCA™) []]a,c

September 14, 2015
Michael A. Shockling

FULL SPECTRUM and FSLOCA are trademarks of Westinghouse Electric Company LLC, its affiliates and/or subsidiaries in the United States of America and may be registered in other countries throughout the world. All rights reserved. Unauthorized use is strictly prohibited. Other names may be trademarks of their respective owners.



NRC Request for Clarification on Offsite Power Treatment

[

]a,c



Refresher: FSLOCA EM Analysis Method

a,c



]a,c

a,c



Outline

[

]a,c



[[REDACTED]] a,c

a,c



[[REDACTED]] a,c

[REDACTED]

]a,c

a,c



[REDACTED]a,c

[

]a,c

[

]a,c



]a,c

a,c



[

]a,c

[

]a,c

a,c



[

]a,c

]a,c

a,c

[

[

]a,c

]a,c



[
]a,c

a,c

]a,c

]a,c



]a,c

Conclusions

[

]a,c

Questions?



[REDACTED]

]a,c

a,c

[REDACTED]

[REDACTED]

]a,c



**Summary of October 2015 NRC Audit of FULL SPECTRUM LOCA (FSLOCA) Evaluation Model
(Non-Proprietary)**

October 2015

Westinghouse Electric Company LLC
1000 Westinghouse Drive
Cranberry Township, PA 16066

©2015 Westinghouse Electric Company LLC
All Rights Reserved

Attachment 1

Clarifications from October 7, 2015 Meeting on FULL SPECTRUM LOCA EM: []^{a,c}

1: Introduction

This letter serves to document and provide further clarification on the information provided by Westinghouse during a October 7, 2015 meeting with the Nuclear Regulatory Commission (NRC) staff relative to the []

[]^{a,c}

Item (1) above is []^{a,c} and is addressed in Section 2 of this document and in Section 2.1 in [1]. Item (3) above is []^{a,c} and is addressed in Section 3 of this document. Item (2) is []^{a,c} and is addressed in Section 4 of this document.

Throughout the response, references are made to figures and information provided in the slide package discussed in the October 7, 2015 meeting, which is provided in Attachment 2.

[]

[]^{a,c}

FULL SPECTRUM and FSLOCA are trademarks of Westinghouse Electric Company LLC, its subsidiaries and/or its affiliates in the United States of America and may be registered in other countries throughout the world. All rights reserved. Unauthorized use is strictly prohibited. Other names may be trademarks of their respective owners.

Updated topical sections to address the resolution of these issues are provided in Attachment 3 and Attachment 4, with changes identified relative to Revision 1 of the topical report.

2: Offsite Power Availability

[

]^{a,c}

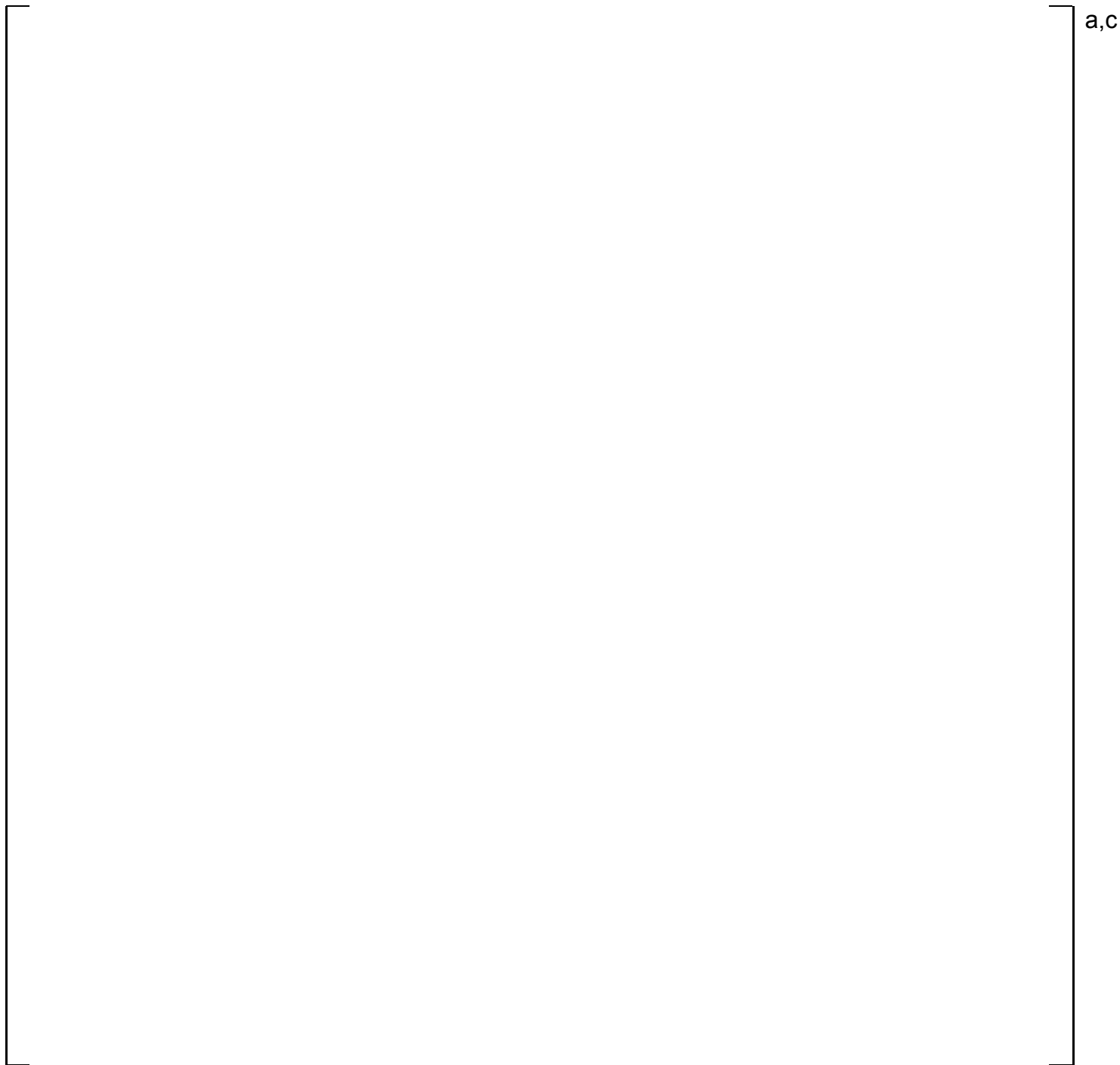


Figure 1: [

]^{a,c}

a,c

Figure 2: [

]^{a,c}

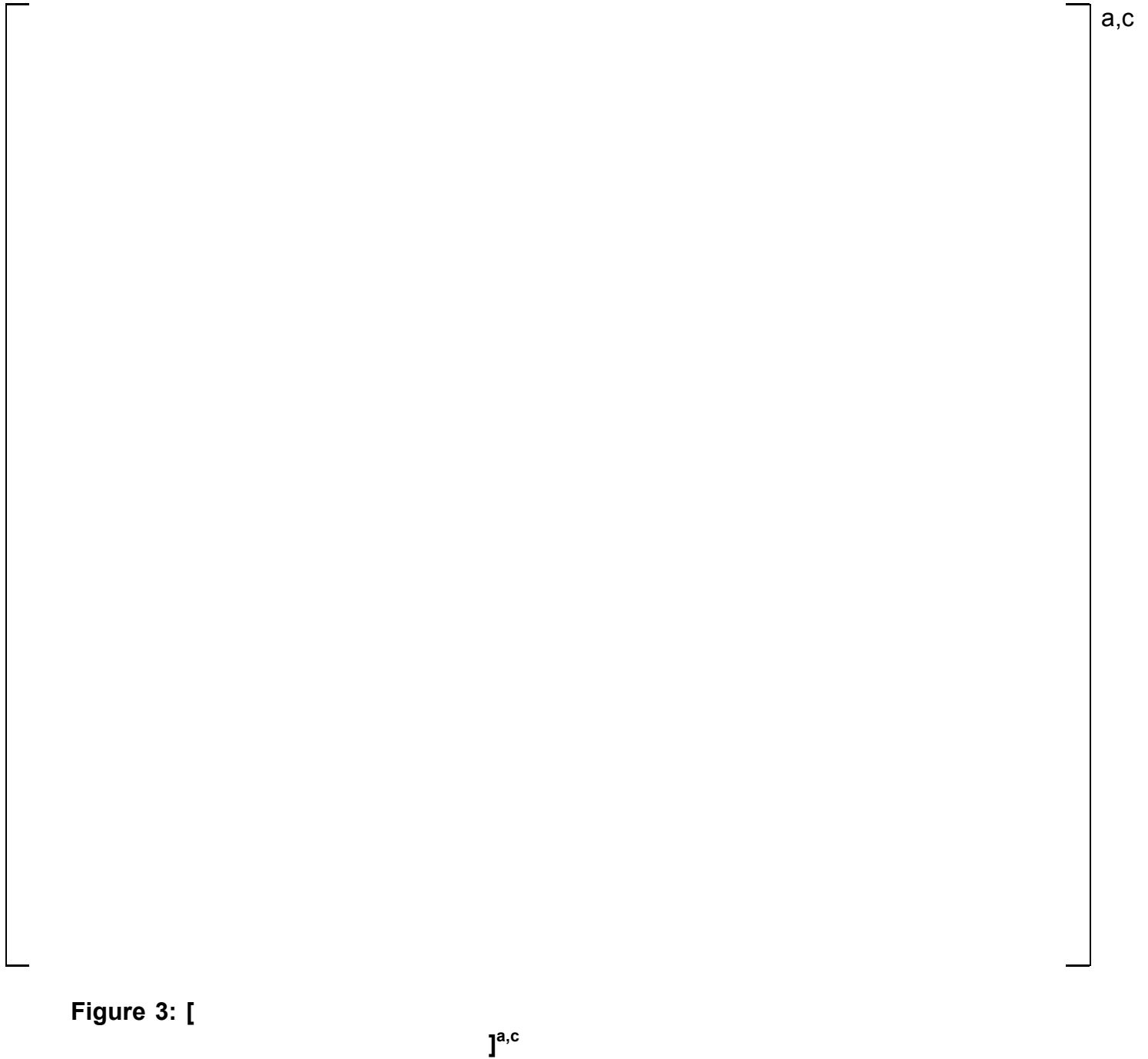


Figure 3: [

3: [

] ^{a,c}

[

] ^{a,c} in Attachment 3 and Attachment 4 of this document, respectively.

4: [] ^{a,c}

[

] ^{a,c}

[

] ^{a,c}

5: Conclusions

First, the FSLOCA EM [

]^{a,c}

The main changes to Revision 1 of the topical report [6] necessary [

]^{a,c} are identified in Attachment 3 and Attachment 4 of this document.

6: References

1. LTR-NRC-15-82, "Summary of September 2015 NRC Audit of the FULL SPECTRUM LOCA (FSLOCA) Evaluation Model (Proprietary/Non-Proprietary)," September 28, 2015.
2. WCAP-16009-P-A, "Realistic Large-Break LOCA Evaluation Methodology Using the Automated Statistical Treatment Of Uncertainty Method (ASTRUM)," January 2005.
3. WCAP-16996-P, Revision 0, "Realistic LOCA Evaluation Methodology Applied to the Full Spectrum of Break Sizes (FULL SPECTRUM LOCA Methodology)," November 2010.
4. Wilks, S. S., "Determination of Sample Sizes for Setting Tolerance Limits," *The Annals of Mathematical Statistics*, Vol. 12, pp. 91-96, 1941.
5. NEA/CSNI/R(2011)4, "BEMUSE Phase VI Report, Status Report on the area, classification of the methods, conclusions and recommendations," 2011.
6. WCAP-16996-P, Volume III, Revision 1, "Realistic LOCA Evaluation Methodology Applied to the Full Spectrum of Break Sizes (FULL SPECTRUM LOCA Methodology) – Volume III: FULL SPECTRUM LOCA Uncertainty Methodology and Demonstration Plant Analysis," October 2015.

Attachment 2

*©2015 Westinghouse Electric Company LLC
All Rights Reserved*



[[REDACTED]]a,c

FULL SPECTRUM™ LOCA (FSLOCA™) Analyses

October 7, 2015

Michael A. Shockling

FULL SPECTRUM and FSLOCA are trademarks of Westinghouse Electric Company LLC, its affiliates and/or subsidiaries in the United States of America and may be registered in other countries throughout the world. All rights reserved. Unauthorized use is strictly prohibited. Other names may be trademarks of their respective owners.



Outline

- [

]a,c



[

]a,c

• [

]a,c



[

]a,c

a,c

[

]a,c

[

]a,c



[

]a,c

- Background
- []a,c
- FSLOCA EM Illustration
- Conclusions



]a,c

• [

]a,c



[

]a,c

• [

]a,c



[

]a,c

]a,c



[

]a,c

[

]a,c

a,c



[

]a,c

a,c



11



[

]a,c

• [

]a,c



[

]a,c

a,c



[

]a,c

[

]a,c

a,c



[

]a,c

[

]a,c

• [

]a,c



LOCA Analysis: The FSLOCA EM Approach

a,c



FSLOCA EM Illustration: Beaver Valley Unit 1 WCOBRA/TRAC-TF2 Runs

a,c



FSLOCA EM Illustration: Beaver Valley Unit 1 WCOBRA/TRAC-TF2 Runs

a,c



18

FSLOCA EM Illustration: Beaver Valley Unit 1: [

]a,c

a,c

]a,c



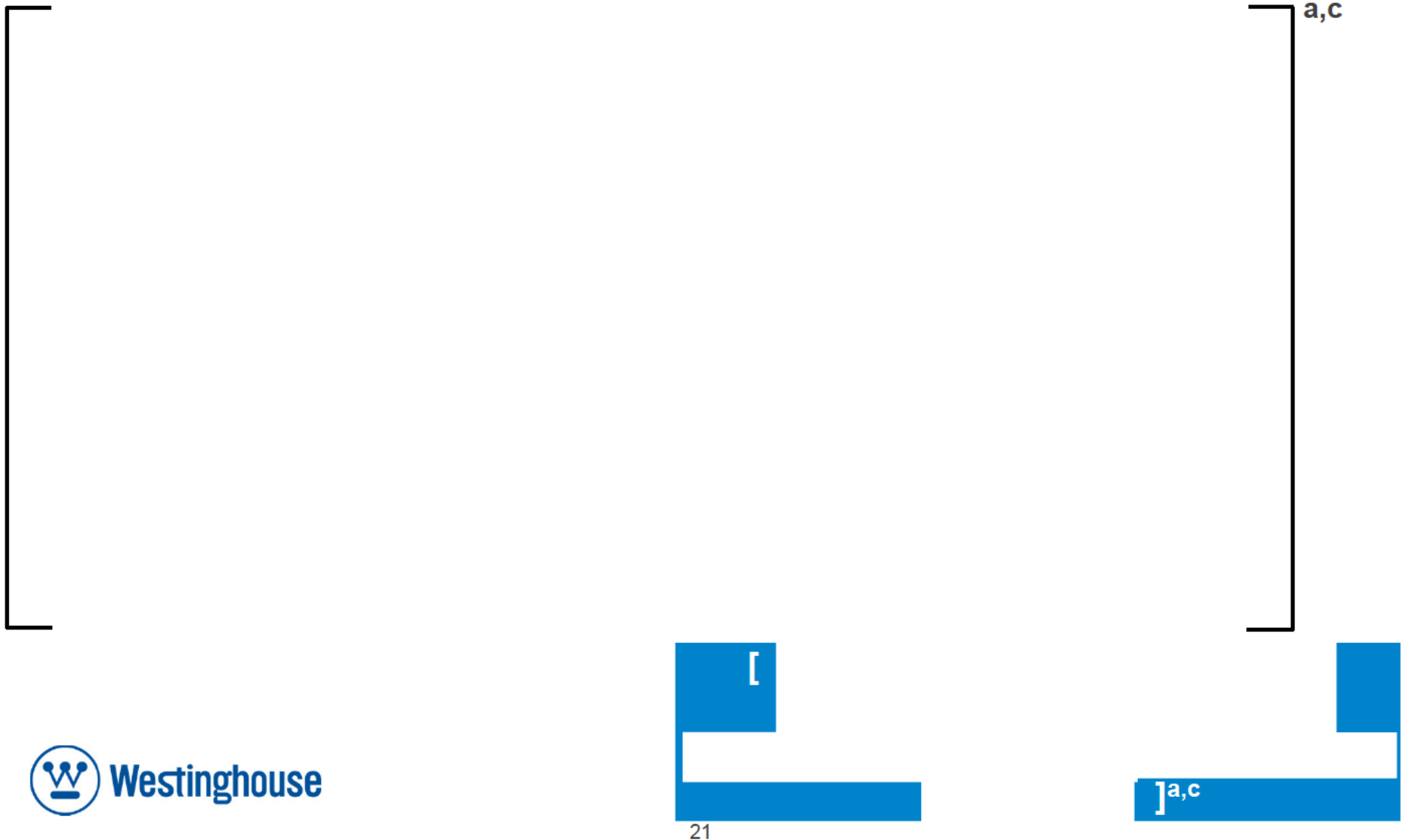
FSLOCA EM Illustration

- [

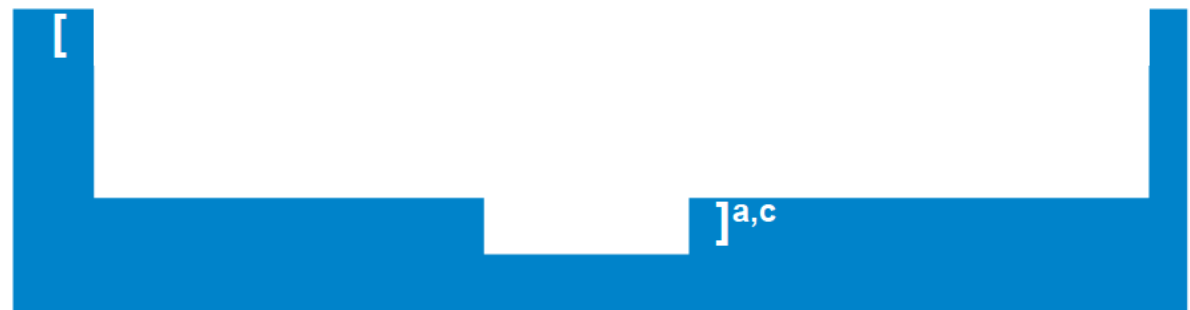
]a,c



FSLOCA EM Illustration



FSLOCA EM Illustration



[

]a,c

a,c



[[REDACTED]]^{a,c}

Conclusions & “Lessons Learned”

[[REDACTED]]^{a,c}

[[REDACTED]]^{a,c}



Conclusions

- [

]a,c



Attachment 3

Updates to Section 30 of WCAP-16996-NP, Revision 1

©2015 Westinghouse Electric Company LLC
All Rights Reserved

30 TECHNICAL BASIS OF STATISTICAL PROCEDURES APPLIED IN FULL SPECTRUM LOCA UNCERTAINTY METHODOLOGY

30.1 STATISTICAL METHODOLOGY ROADMAP

A realistic (best-estimate) safety analysis asks for the assessment of uncertainties associated with physical models, data uncertainties, and plant initial and boundary condition variability. The current safety regulations of the United States Nuclear Regulatory Commission (US NRC) are stipulated in the Code of Federal Regulations (CFR) 10 CFR Part 50, Section 50.46. Based on the 10 CFR 50.46 rule, an emergency core cooling system (ECCS) design is required to satisfy prescriptive criteria. The regulation identifies the following five criteria:

1. Peak cladding temperature (PCT) shall be less than 2200°F
2. Maximum local oxidation (MLO) shall be less than 17%
3. Core-wide oxidation (CWO) shall be less than 1% (to limit the maximum amount of hydrogen generated)
4. The core shall maintain a coolable geometry
5. Long term cooling shall be demonstrated

NRC Information Notice 98-29 (Roe, 1998) provides further clarification that the 10 CFR 50.46(b)(2) MLO criterion “includes both pre-accident oxidation and oxidation occurring during a LOCA.” In the FULL SPECTRUM LOCA (FSLOCA) uncertainty methodology, therefore, ‘MLO’ results are the sum of the two.

Code Scaling, Applicability, and Uncertainty (CSAU) Element 3, the sensitivity and uncertainty analysis element, aims to provide a simple Best-Estimate Plus Uncertainty (BEPU) statement (Boyack et al., 1989) that satisfies the first three criteria above. To accomplish this objective, the effects of the important uncertainty contributors are determined. The uncertainty statement is based on the combined effect of the contributors.

The objective of a Loss-of-Coolant Accident (LOCA) analysis is to directly address criteria (b)(1), (b)(2) and (b)(3) of 10 CFR 50.46; the determination of peak cladding temperature, maximum local oxidation, and core-wide oxidation. [

|]^{a,c} Criterion (b)(4) (coolable geometry) is satisfied by meeting the first three criteria, and accounting for grid deformation if calculated to occur in the in-board assemblies. Typically the last criterion (long-term cooling) is satisfied outside the LOCA analysis.

Regarding the treatment of uncertainties within the CSAU framework, the most straightforward approach is to combine the uncertainties with a direct Monte Carlo simulation. The procedure is designed to first generate a sample of the predicted short term LOCA population (which for the FSLOCA evaluation model is designed to be more severe than the expected LOCA response). Then non-parametric statistical inference procedures are applied to develop probabilistic statements based on the predicted LOCA population, which are in turn used to show a high probability of compliance with the 10 CFR 50.46 criteria.

The code (WCOBRA/TRAC-TF2) is the ‘black-box’ which receives as input a set of random values, one for each uncertainty parameter, and outputs the three values that characterize a specific LOCA scenario (PCT, MLO and CWO). [

]^{a,c}

Several cases (scenarios) are executed until the sample size is large enough to represent the population and provide the estimates of the key parameters of interest. The issue is how results are interpreted to demonstrate compliance with the 10 CFR 50.46 requirements.

10 CFR 50.46 states that “[...] *uncertainty must be accounted for, so that, when the calculated ECCS cooling performance is compared to the criteria set forth in paragraph (b) of this section, there is a high level of probability that the criteria would not be exceeded.*” Paragraph (b) of 10 CFR 50.46 contains the list of the acceptance criteria. 10 CFR 50.46 does not explicitly specify how this probability should be evaluated or what its value should be.

Additional clarification as to the US NRC expectations on the acceptable implementation of the “high probability” requirement is provided in Section 4 of Regulatory Guide 1.157 (Best-Estimate Calculations of Emergency Core Cooling System Performance) that states: “*a 95% probability is considered acceptable to the NRC staff [...].*” Further, Regulatory Guide 1.157 introduced the concept of confidence level as a possible refinement to the uncertainty treatment, but did not expand further on this concept.

As statistical methods are implemented to perform LOCA safety analyses, a statistical statement which estimates or bounds the 95th quantile of the population with a 95% confidence level has been suggested by the NRC as acceptable to demonstrate the required “high probability.” In the previous approved Automated Statistical Treatment of Uncertainty Method (ASTRUM, Nissley et al., 2005), the 95th quantile of the joint-distribution of PCT, MLO and CWO is bounded with at least 95% confidence level. The Safety Evaluation Report (SER) of the Westinghouse Best-Estimate Large Break LOCA methodology (ASTRUM) states the following: “*the staff determined that a 95th percentile probability level based on best approximations of the constituent parameter distributions and the statistical approach used in the methodology is appropriately high for this application.*”

Consistent with the previously approved methodology, the 95/95 criterion is also considered for the FSLOCA methodology. [

] ^{a,c}

One key difference between the previous Large Break LOCA methodology (ASTRUM, Nissley et.al, 2005) and the FSLOCA EM is that the FSLOCA methodology extends the break area spectrum considered in the analysis to cover the full range from what is historically defined as Small Breaks (SB) to Large Breaks (LB) including break sizes typically not analyzed and classified as Intermediate Breaks (IB). As discussed in Section 29.2, a simple extension of the ASTRUM approach to smaller break sizes was considered not appropriate because SBLOCA would not be properly considered in the sample by simply extending a uniform probability distribution of the split break sizes in the SB region. A more balanced approach has been developed and was discussed in Section 29.2.

[

|

|

|

] ^{a,c}

[

]^{a,c}

30.2 STATISTICAL SAMPLING APPROACH (MONTE CARLO)

The run matrix is generated by using random numbers. The random numbers are obtained using a generator from Press et al. (1992). This particular generator has a period of approximately 2.3×10^{18} , that is, the series of numbers generated would not be repeated before 2.3×10^{18} random numbers are used. For all practical purposes, this number is quite large and period exhaustion is considered impossible.

In addition, according to Press et al. (1992), the output from this random number generator has passed standard statistical tests intended to detect lack of randomness (especially certain subtle serial correlations).

The random number generator returns a value, RND, between 0 and 1. To alter the range to [a,b] instead, a linear mapping is applied.:

$$\text{VALUE} = a + (b-a) \cdot \text{RND}$$

The generation of normal (Gaussian) random variables is done by first generating RND and then using a rejection method that is efficient for distributions that have symmetric unimodal probability density functions (PDFs).

The random number generator depends on an initial seed to select the starting point in a random sequence. Having such algorithms allows for repeatability of results without compromising randomness. In the analysis, the initial seed is obtained randomly from the configuration control system. This system assigns a random identifier to each run, so that they can be uniquely identified. If the run matrix needs to be repeated or extended, repeatability is ensured by using the same seed.

30.3 NON-PARAMETRIC ORDER-STATISTICS TOLERANCE LIMITS FORMULATION

The consideration of nonparametric tolerance limits was originally presented by Wilks (Wilks, 1941). Wilks showed that for continuous populations, the distribution of $P(i,j)$, the proportion of the population between the i -th and j -th order statistics, is independent of the population sampled.

The assumption of continuity is a rather mild one. In the present context, it means that the probability of getting two runs with precisely the same [result](#) is zero. Formally, we require that the cumulative distribution function (CDF) of the outcomes be continuous; the PDF, which is the derivative of the CDF, need not be continuous for the relevant results to hold.

Derivation of non-parametric tolerance limits is presented next. This derivation is based on the non-parametric multivariate tolerance limits formulation first proved by Wald (1943) and more recently adapted by Guba-Makai (Guba, et al., 2003) to the problem of making safety inferences based on the output of models of complex systems. The derivation provided here of the non-parametric tolerance limits follows the formulation by Guba-Makai.

For the sake of simplicity the case with a single output variable y with a probability density function $g(y)$ is considered first. Assume that nothing is known about the probability density function $g(y)$ except that it is continuous. If N runs are carried out with random input(s), then a sample $\{y_1, y_2, \dots, y_N\}$ of the random output y will be obtained.

Two functions $L = L(y_1, y_2, \dots, y_N)$ and $U = U(y_1, y_2, \dots, y_N)$ called tolerance limits can be defined such that:

$$P\left(\int_L^U g(y)dy > \gamma\right) = \beta \quad (30-1)$$

where β represents the probability that a fraction γ of the random output variable y population falls within the tolerance limits U and L .

Now arrange the values y_1, y_2, \dots, y_N in increasing order (the probability of equal values of y occurring is neglected since $g(y)$ has been assumed to be a continuous function), and denote by y_k the k^{th} of these ordered value.

Thus, in particular:

$$y(1) = \min_{1 \leq k \leq N} y_k \quad \text{and} \quad y(N) = \max_{1 \leq k \leq N} y_k \quad (30-2)$$

and let by definition $y(0) = -\infty$ and $y(N+1) = +\infty$.

In this case, for some positive $\gamma < 1$ and $\beta < 1$, it can be demonstrated that there can be constructed two functions $L = L(y_1, y_2, \dots, y_N)$ and $U = U(y_1, y_2, \dots, y_N)$, such that the probability β that

$$\int_L^U g(y) dy > \gamma \quad (30-3)$$

can be determined, as demonstrated in Guba, et al. (2003), as:

$$\beta = 1 - I(\gamma, s - r, N - s + r + 1) = \sum_{j=0}^{s-r-1} \binom{N}{j} \gamma^j (1 - \gamma)^{N-j} \quad (30-4)$$

where,

$$I(\gamma, j, k) = \int_0^\gamma \frac{u^{j-1} (1-u)^{k-1}}{B(j, k)} du \quad (30-5)$$

$$B(j, k) = \frac{(j-1)!(k-1)!}{(j+k-2)!} \quad (30-6)$$

$$0 \leq r < s \leq N, \text{ and } L = y(r), U = y(s)$$

Equation 30-4 can be used to provide an answer to the question “for a given $L = y(r)$ and $U = y(s)$, what is the sampling size N of the output variable y that has to be collected so that there is a probability β that a fraction γ of the random output variable y population falls within the specified tolerance limits U and L ?” It can be observed that Equation 30-4 does not depend on the probability density function $g(y)$ or the number of input variables in the process.

In the particular case that the tolerance limits are selected such that $r = 1$ and $s = N$ (i.e., the maximum and minimum value of the samples $y(k)$ of the output variable y are used to define L and U), the two-sided tolerance level can be obtained as¹:

$$\beta = 1 - \gamma^N - N(1 - \gamma)\gamma^{N-1} \quad (30-7)$$

If interest is limited only to the upper tolerance limit ($r = 0$ and $s = N$),

$$\beta = 1 - \gamma^N \quad (30-8)$$

1. Note that Guba, et al. (2003) Equation 18 contains a typographical error in the definition of β for the two-sided case that is corrected in Equation 30-7.

Guba, et al. (2003) also provides an extension of the single output variable formulation for the case of multiple variables. For this case, some additional definitions are required. Consider an output comprised of p variables, y_1, y_2, \dots, y_p . Let $g(y_1, \dots, y_p)$ be the joint distribution of the output variables and let \underline{Y} be defined as:

$$\underline{Y} = \begin{pmatrix} y_{11} & y_{12} & \dots & y_{1N} \\ y_{21} & y_{22} & \dots & y_{2N} \\ \dots & \dots & \dots & \dots \\ y_{p1} & y_{p2} & \dots & y_{pN} \end{pmatrix} \quad (30-9)$$

Analogous to the single output case, the problem of setting tolerance limits for y_1, \dots, y_p can be formulated as follows: for some given positive values $\gamma < 1$ and $\beta < 1$, there can be constructed two random functions $L_j = L_j(y_1, y_2, \dots, y_N)$ and $U_j = U_j(y_1, y_2, \dots, y_N)$, such that there is a probability β that:

$$\int_{L_1}^{U_1} \dots \int_{L_p}^{U_p} g(y_1, \dots, y_p) dy_1 \dots dy_p > \gamma \quad (30-10)$$

If $g(y_1, \dots, y_p)$ is continuous, it can be assumed that no two elements in \underline{Y} are equal. The sequence of rows in \underline{Y} is arbitrary, reflecting the fact that we number the output variables arbitrarily. Let us consider the first row of the sample matrix and arrange its elements in order of increasing magnitude $y_1(1), y_1(2), \dots, y_1(N)$. Select now between these $y_1(r_1)$ as L_1 and $y_1(s_1) > y_1(r_1)$ as U_1 . Let $i_1, i_2, \dots, i_{s_1-r_1-1}$ stand for the original columns of the elements $y_1(r_1 + 1), y_1(r_1 + 2), \dots, y_1(s_1 - 1)$. Next, the N observed values of the output variable y_2 are considered, and the part $y_{2,i_1}, y_{2,i_2}, \dots, y_{2,i_{s_1-r_1-1}}$ of its elements are arranged in increasing order to obtain $y_2(1), y_2(2), \dots, y_2(s_1 - r_1 - 1)$. Select now between these $y_2(r_2)$ as L_2 and $y_2(s_2) > y_2(r_2)$ as U_2 , where evidently $r_2 \geq r_1$ and $s_2 \leq s_1 - r_1 - 1$. If this process is applied to the end of the sample matrix, a p -dimensional space will be defined:

$$V_p = \{[L_1, U_1] * [L_2, U_2] * \dots * [L_p, U_p]\} \quad (30-11)$$

where,

$$\begin{aligned} L_j &= y_j(r_j) \\ U_j &= y_j(s_j) \end{aligned}$$

$$\begin{aligned} r_j &\geq r_{j-1} \geq \dots \geq r_1, & \text{for } j = 2, \dots, p \\ r_j &< s_j \leq s_{j-1} - r_{j-1} - 1, & \text{for } j = 2, \dots, p \end{aligned}$$

As demonstrated by Guba, et al. (2003), in the case of $p \geq 2$ dependent output variables with continuous joint distribution function $g(y_1, \dots, y_p)$ it is then possible to construct p -pairs of random intervals $[L_i, U_i]$, $i = 1, \dots, p$ such that the probability of the inequality:

$$\int_{L_1}^{U_1} \dots \int_{L_p}^{U_p} g(y_1, \dots, y_p) dy_1 \dots dy_p > \gamma \quad (30-12)$$

is free of $g(y_1, \dots, y_p)$ and is given by

$$P \left(\int_{L_1}^{U_1} \dots \int_{L_p}^{U_p} g(y_1, \dots, y_p) dy_1 \dots dy_p > \gamma \right) = 1 - I(\gamma, s_p - r_p, N - s_p + r_p + 1) \quad (30-13)$$

As demonstrated in Guba, et al. (2003), where $I(\dots, \dots, \dots)$ is the incomplete beta function ratio defined in Equation 30-5 and

$$s_p \leq s_{p-1} - r_{p-1} - 1 \leq s_1 - \sum_{j=1}^{p-1} (r_j + 1) \quad (30-14)$$

$$r_p \geq r_{p-1} \geq r_1 \quad (30-15)$$

In several practical applications, $r_1 = r_2 = \dots = r_p = 1$, and $s_p = N - 2(p - 1)$, and the probability β from Equation 30-13 can be expressed as:

$$\beta = 1 - I(\gamma, N - 2p + 1, 2p) = \sum_{j=0}^{N-2p} \binom{N}{j} \gamma^j (1 - \gamma)^{N-j} \quad (30-16)$$

And for a one sided confidence level ($r_1 = r_2 = \dots = r_p = 0$) and $s_p = N - p + 1$, then²:

$$\beta = 1 - I(\gamma, N - p + 1, p) = \sum_{j=0}^{N-p} \binom{N}{j} \gamma^j (1 - \gamma)^{N-j} \quad (30-17)$$

2. Note that Guba, et al. (2003) Equation 25 contains a typographical error in the definition of β for the single-sided case that is corrected in Equation 30-17.

[

 $]^{a,c}$

$$\left[\begin{array}{c} \text{ } \end{array} \right]^{a,c} \quad (30-18)$$

where,

$$\left[\begin{array}{c} \text{ } \end{array} \right]^{a,c} \quad (30-19)$$

which can be expanded as follows:

$$\left[\begin{array}{c} \text{ } \end{array} \right]^{a,c} \quad (30-20)$$

Equation 30-18 can be expressed as follows:

$$\left[\begin{array}{c} \text{ } \end{array} \right]^{a,c} \quad (30-21)$$

[

 $]^{a,c}$

However, there are important disadvantages of the distribution-free upper confidence bounds. First, the extreme order statistics generally tend to have high variance, so different sets of computer runs can give

very high upper confidence bounds. The variance of the estimator can be reduced by extending the sample size. The effect of the sample size on the variance of the estimator is discussed next.

30.3.1 Tolerance Intervals and Sample Size

The approach discussed in Section 30.3 is the so-called '*tolerance interval method*.' The procedure is used to determine an upper bound estimate of a given quantile of the population, say the 95th quantile Q_{95} . The k-th estimator/rank (Table 30-1) bounds the proportion $\gamma = 95\%$ of the population for the considered output variables []^{a,c} with at least $\beta = 95\%$ confidence.

Call this estimate $Q_{95/95}$. The procedure is known to be conservative (bounding) and the risk of excessively overestimating the fraction of the population of interest is very high, especially if the estimator is based on the extreme case, rank $k=1$.

[

] ^{a,c}

30.4 [

] ^{a,c}

[

] ^{a,c}

[

] ^{a,c}

30.5 OVERVIEW OF FULL SPECTRUM LOCA STATISTICAL PROCEDURE

Sections 30.3 and 30.4 provided the theoretical basis for the various statistical procedures needed to:

1. Generate a representative sample of the LOCA scenarios population;
2. Analyze the results and infer figures of merit that can satisfy compliance with the 10 CFR 50.46 design criteria.

[

] ^{a,c}

[

|

|

|

|

] ^{a,c}

30.6 CONCLUSIONS ON COMPLIANCE WITH 10 CFR 50.46 ACCEPTANCE CRITERIA

The previous sections described the statistical theory used to determine the number of cases required to assure that there is a high probability that the first two acceptance criteria are met, consistent with the 10 CFR 50.46 requirements and Regulatory Guide 1.157 guidance. Further insights on the full compliance with the 10 CFR 50.46 criteria are described below.

30.6.1 []^{a,c}

[

] ^{a,c}

30.6.2 []^{a,c}

[

] ^{a,c}

[

] ^{a,c}

[

] ^{a,c}

30.7 REFERENCES

1. Boyack, B., et al., 1989, "Quantifying Reactor Safety Margins," NUREG/CR-5249.
2. [Glaeser, H., et al., 2011, "BEMUSE Phase VI Report, Status report on the area, classification of the methods, conclusions and recommendations," NEA/CSNI/R\(2011\)4.](#)
3. Guba, A., et al., 2003, "Statistical Aspects of Best Estimate Method-I," *Reliability Engineering and System Safety*, 80, pp. 217-232.
4. Nissley, M.E., et al., 2005, "Realistic Large Break LOCA Evaluation Methodology Using Automated Statistical Treatment of Uncertainty Method (ASTRUM)," WCAP-16009-P-A, Revision 0, and WCAP-16009-P-NP-A, Revision 0 (Non-Proprietary).
5. Press, W. H., et al., 1992, Numerical Recipes in FORTRAN: The Art of Scientific Computing, 2nd Edition, Cambridge University Press, Chapter 7.
6. Roe, J., 1998, "NRC Information Notice 98-29: Predicted Increase in Fuel Rod Cladding Oxidation."
7. Wald, A., 1943, "An Extension of Wilks' Method for Setting Tolerance Limits," *The Annals of Mathematical Statistics*, Vol. 14, pp. 45-55.
8. Wilks, S. S., 1941, "Determination of Sample Sizes for Setting Tolerance Limits," *The Annals of Mathematical Statistics*, Vol. 12, pp. 91-96.

[illegible]

a,c

Table 30-3 Generic Rod Power Census Used for Core-Wide Oxidation Assessment

a,c

Attachment 4

Updates to Section 31 of WCAP-16996-NP, Revision 1

©2015 Westinghouse Electric Company LLC
All Rights Reserved

31 FULL SPECTRUM LOCA DEMONSTRATION ANALYSIS

The nuclear power plant selected for the demonstration analysis of the FULL SPECTRUM LOCA (FSLOCA) methodology is Beaver Valley Unit 1 (DLW), a three-loop Westinghouse pressurized water reactor.

The development of the plant input model and input parameters were documented in Section 26. In Section 27, this plant model was exercised in the representative loss-of-coolant accident (LOCA) scenarios covering the full spectrum of break sizes to demonstrate that the dominant phenomena identified in the phenomena identification and ranking table (PIRT) (Section 2) were properly captured.

To perform a realistic (best-estimate) safety analysis for an emergency core coolant system (ECCS), the associated uncertainties in the physical models, experimental data and plant initial and boundary conditions needed to first be identified and assessed as outlined in Section 29. With regard to the treatment of the identified uncertainties, Section 30 introduces the approach to combine the identified uncertainties along with the technical basis for doing so.

In this section, the demonstration plant model is exercised using the WCOBRA/TRAC-TF2 code to demonstrate the FSLOCA analysis methodology.

31.1 DEVELOPMENT OF INITIAL MATRIX

As discussed in Section 30, a Monte Carlo simulation is to be carried out to combine the uncertainties and generate a representative sample of LOCA scenarios. The uncertainty attributes sampled include plant initial and boundary conditions and global and local model uncertainty variables (Section 29), and the plant response to a LOCA scenario is computed with the WCOBRA/TRAC-TF2 computer code.

[

|

J^{a,c}

Among all the uncertainty attributes, [

] ^{a,c}.

31.1.1 Break Area Ranges

The break size is [

] ^{a,c}

31.1.2 Plant Operating Range

In Section 29, the uncertainty contributors or parameters that are explicitly considered in the FSLOCA evaluation model (EM) are listed in Tables 29-1 through 29-5. As discussed there, the uncertainty contributors are grouped as:

1. [^{a,c}, break type (DEG vs. Split), Split break area (Table 29-1)
2. Thermal-hydraulic (T/H) global models (Table 29-2)
3. Local models for the Dummy Rod (Tables 29-3a and 29-3b)
4. Power related uncertainty parameters (Table 29-4)
5. Initial and boundary conditions (Table 29-5)

Table 31.1-1 summarizes the plant operating range over which the uncertainty evaluation is to be performed for the demonstration plant.

[

] ^{a,c}

[

] ^{a,c}**Table 31.1-1 Nominal and Uncertainty Range of Plant Specific Uncertainty Contributors**

] ^{a,c}

Table 31.1-2a []^{a,c}

a,c

Table 31.1-2b []^{a,c}

a,c

Table 31.1-2c []^{a,c}

a,c

Table 31.1-3 [] ^{a,c}		

a,c

a,c

Figure 31.1-1 Description of Break Area Regions

31.2 ANALYSIS EXECUTION

Section 30.5 outlines the statistical procedures used to:

1. Generate a representative sample of the LOCA population;
2. Analyze the results and infer figures of merit that address compliance with the Code of Federal Regulation (CFR) 10 CFR 50.46 design criteria.

The purpose of this section is to describe the generation of the LOCA database. The statistical analysis of the results and reporting relative to 10 CFR 50.46 acceptance criteria will be discussed in Section 31.5.

[

30.5.

] ^{a,c} discussed in Section

31.2.1 [

] ^{a,c}

[

] ^{a,c}

[illegible]

a,c

Figure 31.2-1 [] ^{a,c}

a,c

Figure 31.2-2 [

] a,c

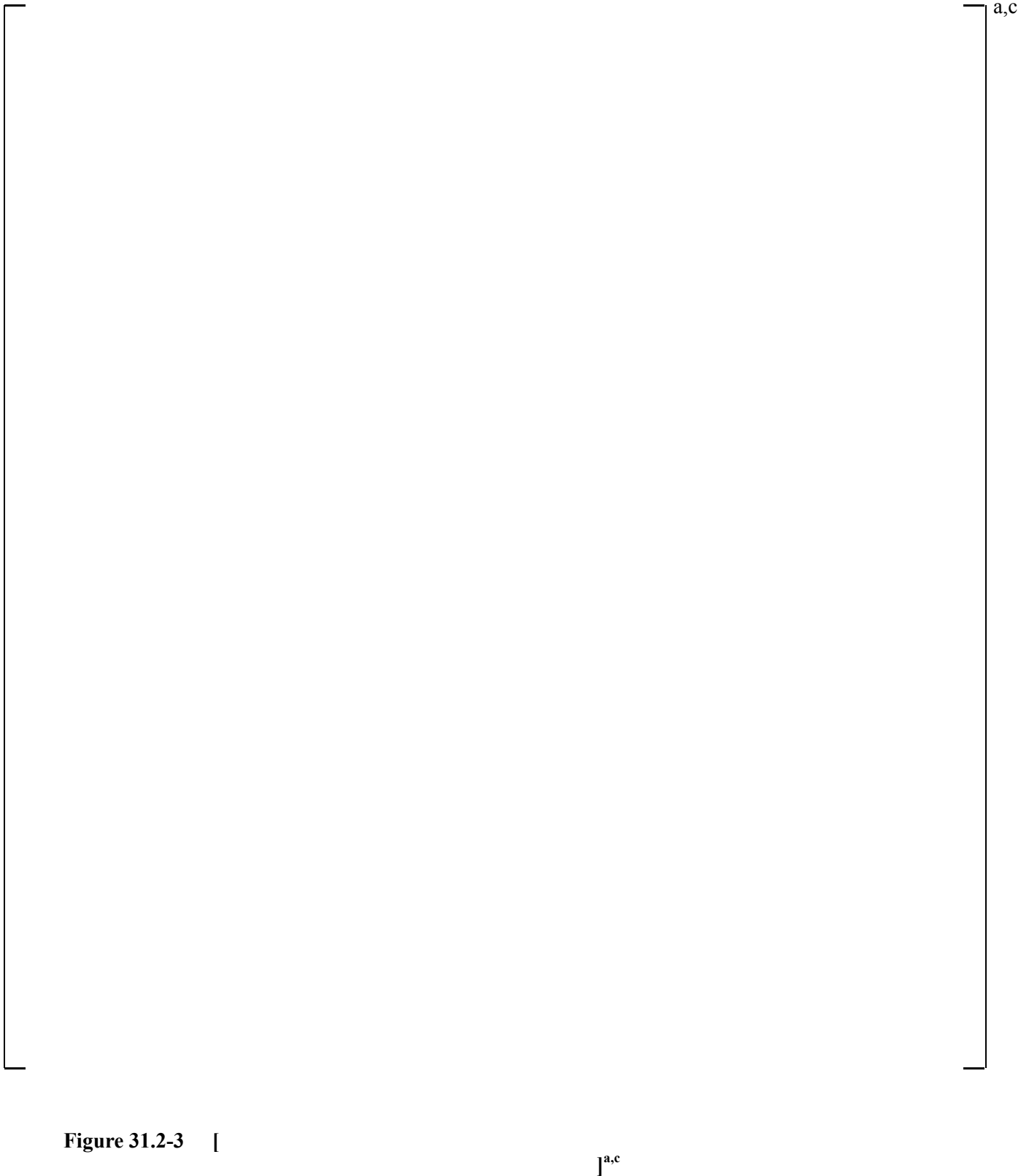


Figure 31.2-3 [

] ^{a,c}

a,c

Figure 31.2-4 [

] a,c

31.2.2 [

] ^{a,c}

[

] ^{a,c}

Table 31.2-2a [] ^{a,c}	

a,c

Table 31.2-2b [] ^{a,c}	

a,c

31.2.3 Conclusion

The analysis shows that [

] ^{a,c} Details of the results are provided in Section 31.3.

| [

] ^{a,c} Details of the results are provided in
Section 31.4.

31.3 ANALYSIS OF RESULTS [] ^{a,c}

| [

|

|

] ^{a,c}

| The predicted PCTs for [] ^{a,c} are provided in Figure 31.3-1 as a function of
[] ^{a,c}

[

] ^{a,c}

(31-1)

The [

] ^{a,c} Tables 31.3-1a and 31.3-1b provide the uncertainty attributes and
the results for the [] ^{a,c}

Figure 31.3-3 shows the PCT sensitivity to [

] ^{a,c}

[illegible]

[illegible][illegible]

a,c

Figure 31.3-1 [

] a,c

a,c

Figure 31.3-2 [

] a,c

a,c

Figure 31.3-3 [

] a,c

a,c

Figure 31.3-4 [**]**^{a,c}

a,c

Figure 31.3-5 [] ^{a,c}

a,c

Figure 31.3-6 [**]**^{a,c}

a,c

Figure 31.3-7 [**]**^{a,c}

a,c

Figure 31.3-8 [**]**^{a,c}

a,c

Figure 31.3-9 [**]**^{a,c}

a,c

Figure 31.3-10 [] ^{a,c}

a,c

Figure 31.3-11 [

] a,c

a,c

Figure 31.3-12 [

] a,c

a,c

Figure 31.3-13 [**]**^{a,c}

a,c

Figure 31.3-14 [**]**^{a,c}

a,c

Figure 31.3-15 [**]**^{a,c}

a,c

Figure 31.3-16 [**]**^{a,c}

a,c

Figure 31.3-17 [

] a,c

a,c

Figure 31.3-18 [**]**^{a,c}

a,c

Figure 31.3-19 [**]**^{a,c}

a,c

Figure 31.3-20 [**] a,c**

a,c

Figure 31.3-21 [

] a,c

a,c

Figure 31.3-22 [**]**^{a,c}

31.4 ANALYSIS OF RESULTS []^{a,c}

[

|

] ^{a,c}

Table 31.4-1a provides the uncertainty attributes for the 10 most limiting []^{a,c} while Table 31.4-1b shows the PCT and MLO results. Figure 31.4-1 shows the influence of the effective break area [] as

[

] ^{a,c} In the case of a DEG break,

] ^{a,c} Figure 31.4-4 shows the influence of [

] ^{a,c}

[]^{a,c} Appreciable transient oxidation is expected to occur only above approximately []

[]^{a,c}

Figure 31.4-8 shows the peak cladding temperatures []

[]^{a,c} Each case indicates rod quench has occurred by []^{a,c}
A comparison of the []^{a,c} and the nominal DEG reference transient from Section 27.2.1 is provided in Figure 31.4-9, where the peak cladding temperature for the hot rod is shown []

[]^{a,c}

Section 30.3.1 discusses the concept of tolerance intervals and sample size in the context of order statistics, while Section 30.5 describes []

[]^{a,c} Figure 31.4-11 shows the upper bound predictor of the 95th quantile PCT with 95% confidence (95/95) []

[]^{a,c}

Table 31.4-1a Uncertainty Attributes [

$$J^{a,c}$$
[illegible]

a,c

Table 31.4-1a Uncertainty Attributes [**] ^{a,c} (cont.)**

a,c

Table 31.4-1b Results [**] ^{a,c}**

a,c

a,c

Figure 31.4-1 [**]**^{a,c}

a,c

Figure 31.4-2 [**]**^{a,c}

a,c

Figure 31.4-3 [**]**^{a,c}

a,c

Figure 31.4-4 [

] a,c

a,c

Figure 31.4-5 [

] a,c

a,c

Figure 31.4-6 [

] a,c

a,c

Figure 31.4-7 [] ^{a,c}

a,c

Figure 31.4-8 [

] a,c

a,c

| **Figure 31.4-9** |] ^{a,c}

a,c

Figure 31.4-10 [

] a,c

a,c

Figure 31.4-11 [

] a,c

31.5 SUMMARY REPORT AND COMPLIANCE WITH 10 CFR 50.46 CRITERIA

The objective of the LOCA safety analysis is to provide upper bound values of PCT, MLO and core-wide oxidation (CWO) that can be directly compared against (b)(1), (b)(2) and (b)(3) of the 10 CFR 50.46 acceptance criteria. It is written that the “[...] uncertainty must be accounted for, so that, when the calculated ECCS cooling performance is compared to the criteria set forth in paragraph (b) of this section, there is a high level of probability that the criteria would not be exceeded.”

The method chosen to accomplish such objectives was discussed in Section 30.6. [

] ^{a,c}

As discussed in Section 30.6.2, [

] ^{a,c}

Table 31.5-1 [^{a,c}			

] ^{a,c}

C MISCELLANEOUS LICENSING DOCUMENTS

This section contains all the other, miscellaneous licensing documents associated with the FSLOCA EM. A summary of all the miscellaneous licensing documents associated with the FSLOCA EM is contained in Table C1.

Note that the proprietary markings on the draft SER, transmitted as part of LTR-NRC-16-14 and LTR-NRC-16-58, are not included in this document.

Table C1	
Transmittal Document	Subject
LTR-NRC-15-91	Compilation of Changes During the Licensing of the FSLOCA EM
LTR-NRC-15-96	Initial Discussion on Draft Limitations and Conditions
LTR-NRC-15-102, Revision 2	Additional Discussion on Draft Limitations and Conditions Supplemental Information on the FSLOCA EM
LTR-NRC-16-14	Comments on Draft SER
LTR-NRC-16-58	Comments on Draft of Final SER

**Compilation of Changes During the Licensing of the FULL SPECTRUM LOCA (FSLOCA) Methodology
(Non-Proprietary)**

October 2015

Westinghouse Electric Company LLC
1000 Westinghouse Drive
Cranberry Township, PA 16066

©2015 Westinghouse Electric Company LLC
All Rights Reserved

Updates to Obsolete Information in the RAI Responses and Audit Summaries
Resulting from Changes During the Licensing of the FULL SPECTRUM LOCA
Methodology

Information contained in the request for additional information (RAI) responses and audit summaries which has become obsolete during the licensing of the FULL SPECTRUM™ LOCA (FSLOCA™) evaluation model (EM) is identified in this letter, along with references to where the updated information is presented (generally either a later audit summary and/or in the updated Topical Report). The term updated Topical Report used throughout this letter refers to WCAP-16996-P, Revision 1¹. It should be noted that this letter does not cover all instances where supplemental information was provided, but it is intended to cover all instances of obsolete information.

A number of the original RAI responses and/or audit summaries reference specific equation numbers. Those equation numbers refer to revision 0 of the Topical Report (unless otherwise noted). In this letter, equation numbers refer to Revision 1 of the Topical Report as noted in the text. There are numerous sensitivity studies that were executed during the licensing of the FSLOCA EM with code versions prior to obtaining the frozen code version. The exact numerical results from these studies would be expected to change with the frozen code version, but the conclusions drawn from studies are expected to remain valid unless otherwise discussed herein.

Response to RAI Question #3 (LTR-NRC-13-37 [1])

It is clarified that the discussion in Section 2-2-5 Hot Leg relative to counter-current flow limitation (CCFL) is intended to state that the [

] ^{a,c} Supporting discussion was included in the response to RAI-108 in LTR-NRC-14-33 [2].

Also, the phenomena identification and ranking table (PIRT) was updated since this RAI response was developed. The final PIRT is presented as Table 2-1 in the updated Topical Report.

Response to RAI Question #4 (LTR-NRC-13-37)

The general discussion in this RAI response relative to the heat transfer multiplier development based on the heat transfer regime rather than the LOCA transient period remains valid. However, the details of the heat transfer multiplier development and application were updated as described in the supplemental information provided for RAIs-51, 52, 53, 54, 55, and 57 in LTR-NRC-15-11 [3], and in Section 29.4.3 of the updated Topical Report.

¹ The updated Topical Report refers to WCAP-16996-P, Revision 1, with the expectation that the references will be identical to those in the approved version of the Topical Report.

FULL SPECTRUM and FSLOCA are trademarks of Westinghouse Electric Company LLC, its affiliates and/or its subsidiaries in the United States of America and may be used and/or registered in other countries throughout the world. All rights reserved. Unauthorized use is strictly prohibited. Other names may be trademarks of their respective owners.

Response to RAI Question #6 (LTR-NRC-13-37)

It is stated in the response that offsite power availability is [

] ^{a,c}

Response to RAI Question #8 (LTR-NRC-13-37)

It is stated in the response to RAI-8 that [

] ^{a,c} However, during the licensing process, the sampling range for several Region I uncertainty parameters was updated. The modified sampling ranges (or fixed values) are described in Section 4.0 of LTR-NRC-14-29 [4].

It is also stated in the response that the intent of the two regions is to develop probabilistic statements with respect to peak cladding temperature and maximum local oxidation for the possible break sizes within each region of the spectrum. Per LTR-NRC-15-88 [5], a [

] ^{a,c}

Response to RAI Question #9 (LTR-NRC-13-45 [7])

It is stated in the response to RAI-9 that the [

] ^{a,c} A modified Region I analysis approach was first described in Section 5.0 of LTR-NRC-13-70, but later revised in Section 4.0 of LTR-NRC-14-29 and Section 29.2 of the updated Topical Report.

Response to RAI Question #10 (LTR-NRC-13-37)

It is stated in the response to RAI-10 that for offsite power available (OPA), an upper bound operator action time to trip the reactor coolant pumps (RCPs) of [] ^{a,c} from the time of reactor trip is assumed. The time assumed for operator action to trip the RCPs with offsite power available was modified as described in LTR-NRC-14-9 [8]. To summarize, the [] ^{a,c}

[]^{a,c}
The use of the generic versus a plant-specific time was clarified in LTR-NRC-15-67 [9].

It is also stated in the response to RAI-10 that [

] ^{a,c}

Response to RAI Question #11 (LTR-NRC-13-37)

It is stated in the response to RAI-11 that the FSLOCA approach adopted is to not restrict loop seal clearing to a single loop. However, as discussed in LTR-NRC-14-29 and Section 29.1.11 of the updated Topical Report, the FSLOCA methodology was updated such that [

] ^{a,c}

Response to RAI Question #13 (LTR-NRC-13-37)

It is stated in the response to RAI-13 that decay powers less than 1.0 can be sampled if the sampling is consistent with the uncertainty distribution. While that statement technically remains correct, it is noted that the decay heat uncertainty range for both Region I and Region II []^{a,c} as reflected in Index 7 of Table I of LTR-NRC-15-85 [11] and Table 29-4 in the updated Topical Report.

Response to RAI Question #14 (LTR-NRC-13-37)

As discussed in Section 3 of LTR-NRC-15-88, the []^{a,c}
discussed in the response to RAI-14).

Response to RAI Question #17 (LTR-NRC-13-37)

It is stated in the response to RAI-17 that []^{a,c} as discussed in the presentation attached

to LTR-NRC-14-55 [12]. The WCOBRA/TRAC-TF2 determination of the mixture level is discussed in Sections 5.14 and 13.3 of the updated Topical Report.

It is also stated in the response to RAI-17 that WCOBRA/TRAC-TF2 is [

] ^{a,c}

That statement was accurate relative to the level swell separate effects test simulations presented in WCAP-16996-P, Revision 0 [13]. However, elements of the interfacial drag package were updated during the licensing process. The updated drag package [

] ^{a,c}

Finally, it is stated several places in the response to RAI-17 that the transition to single-phase vapor occurs at [^{a,c} The transition was modified to occur at [^{a,c} as shown in the presentation attached to LTR-NRC-14-55, and discussed in Section 7.2.8 of the updated Topical Report.

Response to RAI Question #18 (LTR-NRC-13-37)

It is stated in the RAI-18 response that the [

] ^{a,c} would be assumed.

Response to RAI Question #19 (LTR-NRC-13-37)

The process to generate power distributions described in Section 2 of the response to RAI-19, and several statements regarding the power shape generation in Sections 3 and 4 of the response are obsolete due to changes during the licensing process. The approach used to generate the power distributions in the FULL SPECTRUM LOCA methodology is described in Section 4 of the introduction to the responses to RAIs 36 through 39 transmitted in LTR-NRC-14-17 [14]. Additional details are available in the response to RAI-38, and Sections 25.2.1 and 29.4.1 of the updated Topical Report.

Response to RAI Question #26 (LTR-NRC-13-33 [15])

A revised response to RAI-26 (Actinides Decay Heat Power) was provided in LTR-NRC-15-11, and further clarifications were provided in Section 2 of LTR-NRC-15-70 [16].

Response to RAI Question #33 (LTR-NRC-13-31 [17])

It is stated in the response to RAI-33 that KCOSI is []^{a,c}. KCOSI was subsequently updated per LTR-NRC-14-29 to be []^{a,c} per Section 29.1.6 of the updated Topical Report.

Response to RAI Question #40 (LTR-NRC-13-32 [18])

The response to RAI 40 states:

The FSLOCA EM may need to be updated to reflect the changes of the fuel performance code, as well as the 10 CFR 50.46 rule change. The rod burnup sampling method is expected to be revised based on PAD 5.0, however, the compliance to the burnup limitation will be strictly maintained.

The changes to the FSLOCA EM to account for PAD5, including changes to the rod burnup sampling method, are discussed in the responses to RAIs 36 through 39 transmitted in LTR-NRC-14-17 (as well as in Section 29.4 of the updated Topical Report).

Response to RAI Question #41 (LTR-NRC-13-32)

It is clarified that the []^{a,c} this is discussed in Section 8.6 of the updated Topical Report. Also, it is noted that select fuel rod deformation and rupture models were updated as part of the response to RAIs 36 through 39 as described in LTR-NRC-14-17 and Section 29.4.2 of the updated Topical Report.

Response to RAI Question #42 (LTR-NRC-13-32)

It is stated in the response to RAI-42 that the initial calibration of the fuel average temperature and rod internal pressure are against the PAD 4.0 or FATES3B fuel performance codes; however, per LTR-NRC-14-17, the FSLOCA EM will use the PAD5 fuel performance code.

Response to RAI Question #43 (LTR-NRC-13-32)

The response to RAI-43 discusses []

[]^{a,c} The differences between the HOTSPOT models and WCOBRA/TRAC-TF2 models are specifically called out in the RAI response. However, there were some additional changes to the cladding deformation and

rupture models and associated uncertainties implemented as discussed in the responses to RAIs 36 through 39 transmitted in LTR-NRC-14-17, and Section 29.4.2 of the updated Topical Report.

Response to RAI Question #44 (LTR-NRC-13-32)

The impact of fuel pellet thermal conductivity degradation was address via the responses to RAIs 36 through 39 transmitted in LTR-NRC-14-17, and Section 11.4.1 of the updated Topical Report.

Response to RAI Question #45 (LTR-NRC-13-40 [20])

In the response to RAI 45, an uncertainty analysis was performed for the Cylindrical Core Test Facility (CCTF) Run 62 integral effects test (IET) simulation. The uncertainties considered via sampling were the following:

[

] ^{a,c}

Since that response, the treatment for several of the uncertainty parameters was updated. The updates are expected to change the exact numerical results from the CCTF Run 62 simulations, but are not expected to impact the conclusions drawn from the simulations.

Response to RAI Question #46 (LTR-NRC-13-73 [21])

In the response to Question 2, Part c of RAI-46, an incorrect modeling assumption is stated. The correct statement is: "...only multilayered flat walls are considered and heat transfer is neglected in any direction **except** perpendicular to the wall surface" as clarified in LTR-NRC-14-60 [22].

In response to Question 4 of RAI-46, it is stated under "Initial Conditions" that the initial containment air temperature for LOCA evaluations is typically set to [] ^{a,c} for dry-atmospheric containments.

However, this position was updated in LTR-NRC-14-60 where it is stated that the FSLOCA methodology will use a plant-specific initial containment temperature based on customer input.

In the response to Part b of Question 1 of RAI-46, the following potentially confusing statement was identified:

At the end of each WC/T-TF2 time-step, the following boundary conditions are provided to COCO: [

]^{a,c} In addition, COCO provides the following boundary conditions back to WC/T-TF2 for its next time step: [

]^{a,c}

The following revised statement is provided in LTR-NRC-14-60:

At the end of each WCOBRA/TRAC-TF2 time-step, the following boundary conditions are provided to COCO: [

]^{a,c} In addition, COCO provides the following boundary conditions back to WCOBRA/TRAC-TF2 for its next time step: [

]^{a,c}

Additionally, throughout the response, the use of [^{a,c} could be better described as the [^{a,c}

Finally, the demonstration analysis in the updated Topical Report used a blowdown energy release consistent with the evaluation model position as described in the response to Question 5.

Response to RAI Question #47 (LTR-NRC-13-73)

The discussion under item 8 (TEE component), sub-items d and f is not entirely correct. New IENTRN = 2, 3, and 4 options were added to the code. [

^{a,c}

Response to RAI Question #50 (LTR-NRC-13-73)

Updated tables which contain the treatment for all the potential uncertainty contributors, input flags, etc. were documented in LTR-NRC-15-85. The tables from LTR-NRC-15-85 supersede the tables transmitted in the response to RAI-50.

Response to RAI Question #52 (LTR-NRC-13-73)

The pressure delimiter between the []^{a,c} as discussed in Section 29.4.3 of the updated Topical Report.

Response to RAI Question #58 (LTR-NRC-13-73)

In the response to RAI-58, sensitivity studies were run with Rig-of-Safety Assessment (ROSA) Test SB-CL-02 and the Beaver Valley Unit 1 pressurized water reactor (PWR) to illustrate the impact of T_{CHF} value used for selection of the flow regime under Small Break LOCA (SBLOCA) conditions. The conclusions drawn from those sensitivity studies are not expected to change as a result of code or method changes made after the sensitivity study was executed. As such, the existing study remains valid.

Responses to RAIs #59 through # 71 (LTR-NRC-13-75 [23])Section 2 of LTR-NRC-13-75

Core nodding and timestep sensitivity studies with the Oak Ridge National Laboratory (ORNL) core uncovering and level swell tests, along with core nodding sensitivity studies for the Beaver Valley Unit 1 PWR were presented in Section 2 of LTR-NRC-13-75. There were updates made to the interfacial drag package after these studies were executed, but they were not expected to impact the conclusions from these studies.

To confirm that the conclusions from the studies remain valid, a subset of the ORNL timestep studies was rerun with the frozen WCOBRA/TRAC-TF2 code. The results are presented as Figures 1 and 2. It can be seen that the code calculations are []^{a,c}

G2 boiloff simulations were also executed with the majority of the interfacial drag package updates; the simulations were run with bundle node sizes of 12-inches, 6-inches, and 3-inches. The results were previously presented in LTR-NRC-14-55, and have been included as Figure 3 herein. It can be seen that the []^{a,c}

Section 3 of LTR-NRC-13-75

The 'hot wall ramp' is described in Section 3 of LTR-NRC-13-75. The final 'hot wall ramp' implemented into the frozen code is described in Section 5.4 of the updated Topical Report. The conclusions drawn from the ORNL and PWR sensitivity studies regarding the hot wall ramp are judged to remain applicable given the model discussed in the updated Topical Report.

A subset of the hot wall ramp study was repeated with the updated interfacial drag package. The study was presented in LTR-NRC-14-29, and the results support the conclusion of LTR-NRC-13-75.

Response to RAI Question #63 (LTR-NRC-13-75)

The information contained in Table 1 of the RAI response is updated as shown in the following Table 1, which is consistent with the updates to the small bubble regime drag in the core region and the annular film drag.

Table 1: WCOBRA/TRAC-TF2 Approach to Interfacial Drag for Vessel Component "Cold Wall" Two-Phase Flow Regimes

Flow Regime	Void Fraction α (%)	Major Constitutive Correlations	Note (Equation #s from updated Topical Report)
Small Bubble ¹ (non-rod bundle)	$0 < \alpha \leq 20$	$C_{Db} = (24/Re_b)(1+0.1Re_b^{0.75})$ $C_{Db} = (2/9)^{1/2} N_\mu Re'_b (1-\alpha_v)^2$ $C_{Db} = (8/3) (1-\alpha_v)^2$	Equation (5-50) Equation (5-53) Equation (5-57)
Small-to-Large Bubble	$20 < \alpha \leq 50$	$C'_{Db} = C_{Db} (1-\alpha_v)^2$ $C_{Db} = (24/Re_b)(1+0.1Re_b^{0.75}) = 0.45 (1-\alpha_v)^2$ Interpolation between small bubble drag and large bubble drag at local void fraction, using the interpolation factor defined as $F_{SB} = \alpha_{SB} (1-\alpha_v) / [(1-\alpha_{SB}) \alpha_v]$, where $\alpha_{SB} = [\quad]^{a,c}$	Equation (5-75) Equations (5-50) and 5-58) Equation (5-80)
Churn-Turbulent	$50 < \alpha \leq \alpha_{crit}$	Interpolation between small-to-large bubble drag (at local void fraction) and film/drop interfacial drag (at α_{crit}), using the factor defined as $F_{CT} = (\alpha_v - \alpha_{LB}) / (\alpha_{crit} - \alpha_{LB})$, where $\alpha_{LB} = [\quad]^{a,c}$	Equation (5-82) Equation (5-83)
Film/Drop	$\alpha_{crit} < \alpha \leq 100$	$f_{i,w} = 0.005[1+75(1-\alpha_v)]$	Equation (5-96)

¹For rod bundle geometry, the interfacial drag is calculated based on Bestion's drift velocity as described in Section 5.4.1.2 of the updated Topical Report.

Response to RAI Question #65 (LTR-NRC-13-75)

The correction to Equation 5-103 identified in Part 3 of the RAI response was unintentionally omitted in the updated Topical Report (Equation 5-107). It was also noted that the same typographical correction should be included in Equation 5-67c of the updated Topical Report. These corrections are included in Attachment 2 of this letter.

Response to RAI #66 (LTR-NRC-13-75)

The interfacial drag package was updated during the licensing process, and is described in Section 5.4 of the updated Topical Report. It is clarified here that [

]^{a,c} as described in

Section 5.6.2 of the updated Topical Report.

Response to RAI Question #67 (LTR-NRC-13-75)

The 'hot wall ramp' is discussed in the response to RAI 67. The description of the final 'hot wall ramp' implemented into the frozen code is contained in Section 5.4 of the updated Topical Report.

Response to RAI Question #68 (LTR-NRC-13-75)

Equations 5-67 through 5-69 in Section 5.4.1 of the updated Topical Report describe the hot wall ramp. The justification and supporting demonstration comparisons contained in the original response to RAI-68 remain valid. LTR-NRC-14-55 contains a subset of hot wall sensitivity runs with the updated interfacial drag package which supports the conclusion.

The error identified in Part 1 of the response to RAI-68 was corrected in the updated Topical Report. The original response to Parts 2 and 3 remains applicable with the updated interfacial drag package, except that []^{a,c} as described in LTR-NRC-14-29 and the
updated Topical Report, and $K_{iX,v_{iSB}}$ is defined by Bestion for the rod bundle geometry.

Response to RAI Question #69 (LTR-NRC-13-75)

It is clarified that this RAI response is applicable for non-rod bundle geometry.

Updated plots were provided as Figures 5-3a and 5-3b in the updated Topical Report. Updated tables are presented as Tables 2 and 3 herein.

a,c

a,c

Response to RAI Questions #70 and #71 (LTR-NRC-13-75)

It is stated in the response to RAIs 70 and 71 that []^{a,c} is used in the core region. It was then later determined that []^{a,c} (interfacial drag presentation from the May 2014 NRC audit included in LTR-NRC-14-29). Later, the interfacial drag package was updated as part of the licensing process, with the changes described in Section 5 of the updated Topical Report. Based on these updates, a []^{a,c} as discussed in Section 29.1.5 of the updated Topical Report. Figures 13.4.2-4 through 13.4.2-15 in the updated Topical Report show the sensitivity of the ORNL simulations to different []^{a,c} values.

Response to RAI Questions #72, #73 and #74 (LTR-NRC-13-41 [24])

A discussion of the possibility of regime-dependent interfacial drag multipliers is provided in Section 3.0 of LTR-NRC-13-41. After the RAI response was written, regime-dependent multipliers were developed as discussed in the presentation attached to LTR-NRC-14-29. []^{a,c}

The use of []^{a,c} is noted in several places within the RAI response. The []^{a,c} as discussed in Section 29.1.5 of the updated Topical Report.

The specific YDRAG ranges discussed in this response are obsolete; the final uncertainty treatment is to use []^{a,c} as discussed in Section 29.1.5 of the updated Topical Report.

It was also implied in Section 3.3 of the response that the transition to single-phase vapor occurs at []^{a,c}. The transition was modified to occur at []^{a,c} as shown in the presentation attached to LTR-NRC-14-55, and discussed in Section 7.2.8 of the updated Topical Report.

The sensitivity of the G2 boil-off calculations to the fluid cell mesh was evaluated with the updated drag package as previously discussed herein; the results are shown in Figure 3. It was concluded that the simulations were stable relative to the core node size.

The ROSA ST-NC-01 and ST-NC-06E SET simulations were also rerun with the frozen code.

The void fraction profiles for ST-NC-01 and ST-NC-06E with nominal YDRAG are shown in Figures 4 and 5, respectively. The void fraction profiles for the simulation of both ST-NC-01 and ST-NC-06E are reasonably predicted. The predicted void fractions lower in the bundle are []^{a,c}

[]^{a,c}

YDRAG sensitivity studies were conducted for both ST-NC-01 and ST-NC-06E, and the results are presented in Figures 6 and 7, respectively. It can be seen that (except at the top of the bundle where all cases are comparable) reducing YDRAG tends to [

] ^{a,c}

Response to RAI Question #75 (LTR-NRC-13-73)

The updated minimum YDRAG value is [

] ^{a,c} the YDRAG sensitivity study range will exceed the minimum value in order to illustrate a more significant change in the interfacial drag.

Response to RAI Question #76 (LTR-NRC-13-41)

Relative to Part 3 of the response, it is noted that the Semiscale S-LH-1 and S-LH-2 tests were simulated as described in the response to RAIs 109 through 111 in LTR-NRC-14-70 [25].

Response to RAI Question #77 (LTR-NRC-13-73)

Updated tables which contain the treatment for all the potential uncertainty contributors, input flags, etc. were documented in LTR-NRC-15-85. The tables from LTR-NRC-15-85 supersede the tables transmitted in the response to RAI-77.

Response to RAI Question #80 (LTR-NRC-14-12 [26])

The response to RAI-80 references Japanese Atomic Energy Research Institute (JAERI) test reports. LTR-NRC-15-6 [27] confirms that these JAERI reports are those cited in Table 21.1-1 of WCAP-16996-P, Revision 0. The updated Topical Report Table 21.1-1 contains the same information, but is more readable.

Response to RAI Question #83 (LTR-NRC-14-19 [28])

The response to Part 7 of RAI-83 notes that the [

] ^{a,c} The FSLOCA methodology was updated (as discussed in LTR-NRC-14-29, the response to RAI-108 in LTR-NRC-14-33, the clarification related to the RAI-85 response in LTR-NRC-14-60, the clarification related to the RAI-108 response in LTR-NRC-15-67, and the updated Topical Report) to [^{a,c}

Response to RAI Question #85 (LTR-NRC-14-19)

The response to RAI-85 provides information on the interfacial drag assumed with the stratified flow model and how the actual modeled flow piping inclination is accounted for. The FSLOCA methodology was updated (as discussed in LTR-NRC-14-29, the response to RAI-108 in LTR-NRC-14-33, the clarification related to the RAI-85 response in LTR-NRC-14-60, the clarification related to the RAI-108 response in LTR-NRC-15-67, and the updated Topical Report) to [^{a,c}

Response to RAI Question #91 (LTR-NRC-14-19)

It is clarified that the statement regarding [

] ^{a,c} discussed in Section 3.4 of LTR-NRC-14-29 and Section 29.1.11 of the updated Topical Report.

Response to RAI Questions #96 through #99 and #107 (LTR-NRC-14-21 [29])

The response to RAIs 96 through 99 and 107 describes the upper head spray nozzle bypass modeling. A change in the bypass loss coefficient modeling, relative to the information provided in LTR-NRC-14-21, is described under the “General Bypass Flow Discussion” in LTR-NRC-15-6.

Response to RAI Questions #106 (N/A)

It is noted that there were two RAIs numbered 77, and there is no RAI number 106.

Response to RAI Questions #109 and #110 (LTR-NRC-14-70)

The base Semiscale S-LH-1 and S-LH-2 simulations were rerun with the frozen code. The results are presented in Figures 3.2.1-1 through 3.2.1-13 for S-LH-1, Figures 3.2.2-1 through 3.2.2-13 for S-LH-2, and Figures 3.2.3-1 through 3.2.3-13 for the comparison of S-LH-1 and S-LH-2 (figure numbers were retained from original RAI response). It can be seen that the simulations results are similar to the prior simulations in LTR-NRC-14-70, and all the conclusions drawn from LTR-NRC-14-70 remain valid.

Response to RAI Question #111 (LTR-NRC-14-70)

The results of the base Semiscale simulations as discussed previously for RAIs 109 and 110 were similar to the prior results, and all the prior conclusions remain valid. Likewise, it is expected that the steam generator sensitivity studies would produce similar results. As such, the prior results are judged to remain valid and all the sensitivity studies are not rerun.

Response to RAI Question #112 (LTR-NRC-14-12)

The response to RAI-112 provides information on the sensitivity of WCOBRA/TRAC-TF2 SBLOCA predictions to steam generator nodalization. This sensitivity study was re-executed with [

] ^{a,c} An updated response to RAI-112, including replacement figures, are presented in LTR-NRC-15-6. The results of the updated sensitivity study show [

] ^{a,c}

Response to RAI Question #115 (LTR-NRC-14-19)

It is clarified in LTR-NRC-15-6 that the base case calculations presented in the RAI-115 response model the default value of STFRU.

Response to RAI Question #116 (LTR-NRC-14-19)

During the licensing process, the NRC requested that plots from one or two of cases presented in the response to RAI-116 be re-submitted one-per-page to increase the readability of the figures. These revised figures are presented in LTR-NRC-15-6.

Response to RAI Questions #122 through 126, 128, 129, and 136 (LTR-NRC-14-9)

The use of the generic versus a plant-specific RCP trip time, and the treatment of the offsite power availability for SBLOCA were clarified in LTR-NRC-15-67.

[]^{a,c} as described in LTR-NRC-15-67.

The offsite power configuration for the []^{a,c} using the approach described in LTR-NRC-15-82 and Section 30.4 of the updated Topical Report.

Response to RAI Question #127 (LTR-NRC-14-4 [30])

The response to RAI-127 provides a summary of the single failure assumptions in the loss-of-coolant accident analyses. It is stated in LTR-NRC-14-4 that for Region I (small breaks), []^{a,c} LTR-NRC-14-60 clarifies that the Region I (small breaks) []

[]^{a,c}

July and August 2013 Audit Summary (LTR-NRC-13-70)

The []^{a,c} The updated modeling approach for defining []^{a,c} is described under the “General Bypass Flow Discussion” in LTR-NRC-15-6.

An uncertainty analysis was performed for the ROSA SB-CL-02 IET simulation in Section 4 of the audit summary. The uncertainties considered via sampling were the following:

[]

[]^{a,c}

Since that response, the treatment for several of the uncertainty parameters was updated. The updates are expected to change the exact numerical results from the ROSA SB-CL-02 simulations, but are not expected to impact the conclusions drawn from the simulations.

The modified Region I analysis approach described in Section 5.0 was later revised in Section 4.0 of LTR-NRC-14-29.

February 2014 Audit Summary (LTR-NRC-14-55)

Relative to the third bullet of the attached presentation on page 5, the [

] ^{a,c}

August 2014 Audit Summary Part 3 (LTR-NRC-15-11)

Figure 6 in LTR-NRC-15-11 was updated as Figure 51-1 in LTR-NRC-15-70.

The pressure delimiter between the [

] ^{a,c} as discussed in

Section 29.4.3 of the updated Topical Report.

June 2015 Audit Summary Part 1 (LTR-NRC-15-67)

The plots of the flooding curves versus code predictions for the reference PWR which were committed to be provided to the staff in the clarification of RAI-108 were provided in Section 31.3 of the updated Topical Report.

Impact on Topical Report

During the development of the roadmap letter, a few errata were discovered in Revision 1 of the Topical Report. Additionally, there were a few other miscellaneous updates required to reflect the changes for the core-wide oxidation treatment previously described in LTR-NRC-15-88. Attachment 2 contains the Topical Report updates to correct the errata and reflect the updated core-wide oxidation treatment (except for Sections 30 and 31 which were transmitted in LTR-NRC-15-88). All of the updates from LTR-NRC-15-88 and herein will be reflected in the approved version of the Topical Report.

References

1. LTR-NRC-13-37, "Submittal of Westinghouse Responses to 'WCAP-16996-P, 'Realistic LOCA Evaluation Methodology Applied to the Full Spectrum of Break Sizes (FULL SPECTRUM LOCA Methodology)' Request for Additional Information' (Proprietary/Non-Proprietary), Project 700, TAC No. ME5244," June 5, 2013.
2. LTR-NRC-14-33, "Submittal of Westinghouse Responses to 'WCAP-16996-P, 'Realistic LOCA Evaluation Methodology Applied to the Full Spectrum of Break Sizes (FULL SPECTRUM LOCA Methodology)' Request for Additional Information – RAIs 108, 120 and 121' (Proprietary/Non-Proprietary), Project 700, TAC No. ME5244," June 13, 2014.
3. LTR-NRC-15-11, "Summary of August 2014 NRC Audit Part 3 of the FULL SPECTRUM LOCA (FSLOCA) Evaluation Model (Proprietary/Non-Proprietary), Project 700, TAC NO. ME5244," February 24, 2015.
4. LTR-NRC-14-29, "Summary of May 2014 NRC Audit of the FULL SPECTRUM LOCA (FSLOCA) Evaluation Model (Proprietary/Non-Proprietary), Project 700, TAC No. ME5244," June 5, 2014.
5. LTR-NRC-15-88, "Summary of October 2015 NRC Audit of the FULL SPECTRUM LOCA (FSLOCA) Evaluation Model (Proprietary/Non-Proprietary)," October 12, 2015.
6. LTR-NRC-13-70, "Summary of July 2013 NRC Code Workshop and August 2013 NRC Audit of the FULL SPECTRUM LOCA (FSLOCA) Evaluation Model (Proprietary/Non-Proprietary)," October 10, 2013.
7. LTR-NRC-13-45, "Submittal of Westinghouse Responses to 'WCAP-16996-P, 'Realistic LOCA Evaluation Methodology Applied to the Full Spectrum of Break Sizes (FULL SPECTRUM LOCA Methodology)' Request for Additional Information - RAIs 9 and 12' (Proprietary/Non-Proprietary), Project 700, TAC No. ME5244," June 26, 2013.
8. LTR-NRC-14-9, "Submittal of Westinghouse Responses to 'WCAP-16996-P, 'Realistic LOCA Evaluation Methodology Applied to the Full Spectrum of Break Sizes (FULL SPECTRUM LOCA Methodology)' Request for Additional Information – Set 8 RAIs 122-126, 128-131 and 136' (Proprietary/Non-Proprietary), Project 700, TAC No. ME5244," February 12, 2014.
9. LTR-NRC-15-67, "Summary of June 2015 NRC Audit Part 1 of the FULL SPECTRUM LOCA (FSLOCA) Evaluation Model (Proprietary/Non-Proprietary)," July 24, 2015.
10. LTR-NRC-15-82, "Summary of September 2015 NRC Audit of the FULL SPECTRUM LOCA (FSLOCA) Evaluation Model (Proprietary/Non-Proprietary)," September 28, 2015.
11. LTR-NRC-15-85, "Summary of June 2015 NRC Audit Part 3 of the FULL SPECTRUM LOCA (FSLOCA) Evaluation Model (Proprietary/Non-Proprietary)," October 1, 2015.
12. LTR-NRC-14-55, "Summary of February 2014 NRC Audit of the FULL SPECTRUM LOCA (FSLOCA) Evaluation Model (Proprietary/Non-Proprietary), Project 700, TAC No. ME5244," August 21, 2014.
13. WCAP-16996-P, Revision 0, "Realistic LOCA Evaluation Methodology Applied to the Full Spectrum of Break Sizes (FULL SPECTRUM LOCA Methodology)," November 2010.

14. LTR-NRC-14-17, "Submittal of Westinghouse Responses to 'WCAP-16996-P, 'Realistic LOCA Evaluation Methodology Applied to the Full Spectrum of Break Sizes (FULL SPECTRUM LOCA Methodology)' Request for Additional Information – RAIs 36-39' (Proprietary/Non-Proprietary), Project 700, TAC No. ME5244," March 24, 2014.
15. LTR-NRC-13-33, "Submittal of Westinghouse Responses to 'WCAP-16996-P, 'Realistic LOCA Evaluation Methodology Applied to the Full Spectrum of Break Sizes (FULL SPECTRUM LOCA Methodology)' Request for Additional Information – Second Set' (Proprietary/Non-Proprietary), Project 700, TAC No. ME5244," May 31, 2013.
16. LTR-NRC-15-70, "Summary of June 2015 NRC Audit Part 2 of the FULL SPECTRUM LOCA (FSLOCA) Evaluation Model (Proprietary/Non-Proprietary)," September 16, 2015
17. LTR-NRC-13-31, "Submittal of Westinghouse Responses to 'WCAP-16996-P, 'Realistic LOCA Evaluation Methodology Applied to the Full Spectrum of Break Sizes (FULL SPECTRUM LOCA Methodology)' Request for Additional Information – Third Set' (Proprietary/Non-Proprietary), Project 700, TAC No. ME5244," May 30, 2013.
18. LTR-NRC-13-32, "Submittal of Westinghouse Responses to 'WCAP-16996-P, 'Realistic LOCA Evaluation Methodology Applied to the Full Spectrum of Break Sizes (FULL SPECTRUM LOCA Methodology)' Request for Additional Information - Fourth Set' (Proprietary/Non-Proprietary), Project 700, TAC No. ME5244," May 30, 2013.
19. WCAP-16009-P-A, "Realistic Large-Break LOCA Evaluation Methodology Using the Automated Statistical Treatment Of Uncertainty Method (ASTRUM)," January 2005.
20. LTR-NRC-13-40, "Submittal of Westinghouse Responses to 'WCAP-16996-P, 'Realistic LOCA Evaluation Methodology Applied to the Full Spectrum of Break Sizes (FULL SPECTRUM LOCA Methodology)' Request for Additional Information' (Proprietary/Non-Proprietary), Project 700, TAC No. ME5244," June 13, 2013.
21. LTR-NRC-13-73, "Submittal of Westinghouse Responses to 'WCAP-16996-P, 'Realistic LOCA Evaluation Methodology Applied to the Full Spectrum of Break Sizes (FULL SPECTRUM LOCA Methodology)' Request for Additional Information - RAIs 46 – 58, 75 and 77' (Proprietary/Non-Proprietary), Project 700, TAC No. ME5244," October 28, 2013.
22. LTR-NRC-14-60, "Summary of August 2014 NRC Audit Part 1 of the FULL SPECTRUM LOCA (FSLOCA) Evaluation Model" (Proprietary/Non-Proprietary), Project 700, TAC No. ME5244," September 17, 2014.
23. LTR-NRC-13-75, "Submittal of Westinghouse Responses to 'WCAP-16996-P, 'Realistic LOCA Evaluation Methodology Applied to the Full Spectrum of Break Sizes (FULL SPECTRUM LOCA Methodology)' Request for Additional Information – RAIs 59 – 71' (Proprietary/Non-Proprietary), Project 700, TAC No. ME5244," November 7, 2013.
24. LTR-NRC-13-41, "Submittal of Westinghouse Responses to 'WCAP-16996-P, 'Realistic LOCA Evaluation Methodology Applied to the Full Spectrum of Break Sizes (FULL SPECTRUM LOCA Methodology)' Request for Additional Information - RAIs 72, 73, 74 and 76' (Proprietary/Non-Proprietary), Project 700, TAC No. ME5244," June 21, 2013.
25. LTR-NRC-14-70, "Submittal of Westinghouse Responses to 'WCAP-16996-P, 'Realistic LOCA Evaluation Methodology Applied to the Full Spectrum of Break Sizes (FULL SPECTRUM

- LOCA Methodology)’ Request for Additional Information - RAIs 109-111’ (Proprietary/Non-Proprietary), Project 700, TAC No. ME5244,” October 31, 2014.
26. LTR-NRC-14-12, “Submittal of Westinghouse Responses to ‘WCAP-16996-P, ‘Realistic LOCA Evaluation Methodology Applied to the Full Spectrum of Break Sizes (FULL SPECTRUM LOCA Methodology)’ Request for Additional Information - RAIs 77-82, 86-87, 93 and 112’ (Proprietary/Non-Proprietary), Project 700, TAC No. ME5244,” March 12, 2014.
 27. LTR-NRC-15-6, “Summary of August 2014 NRC Audit Part 2 of the FULL SPECTRUM LOCA (FSLOCA) Evaluation Model (Proprietary/Non-Proprietary), Project 700, TAC NO. ME5244,” January 30, 2015.
 28. LTR-NRC-14-19, “Submittal of Westinghouse Responses to ‘WCAP-16996-P, ‘Realistic LOCA Evaluation Methodology Applied to the Full Spectrum of Break Sizes (FULL SPECTRUM LOCA Methodology)’ Request for Additional Information – RAIs 83-85, 88-92, 94-95 and 113-119’ (Proprietary/Non-Proprietary), Project 700, TAC No. ME5244,” April 2, 2014.
 29. LTR-NRC-14-21, “Submittal of Westinghouse Responses to ‘WCAP-16996-P, ‘Realistic LOCA Evaluation Methodology Applied to the Full Spectrum of Break Sizes (FULL SPECTRUM LOCA Methodology)’ Request for Additional Information – RAIs 96-105 and 107’ (Proprietary/Non-Proprietary) Project 700, TAC No. ME5244,” April 4, 2014.
 30. LTR-NRC-14-4, “Submittal of Westinghouse Responses to ‘WCAP-16996-P, ‘Realistic LOCA Evaluation Methodology Applied to the Full Spectrum of Break Sizes (FULL SPECTRUM LOCA Methodology)’ Request for Additional Information – Set 8 RAIs 127, 132-135 and 137-139’ (Proprietary/Non-Proprietary), Project 700, TAC No. ME5244,” January 30, 2014.

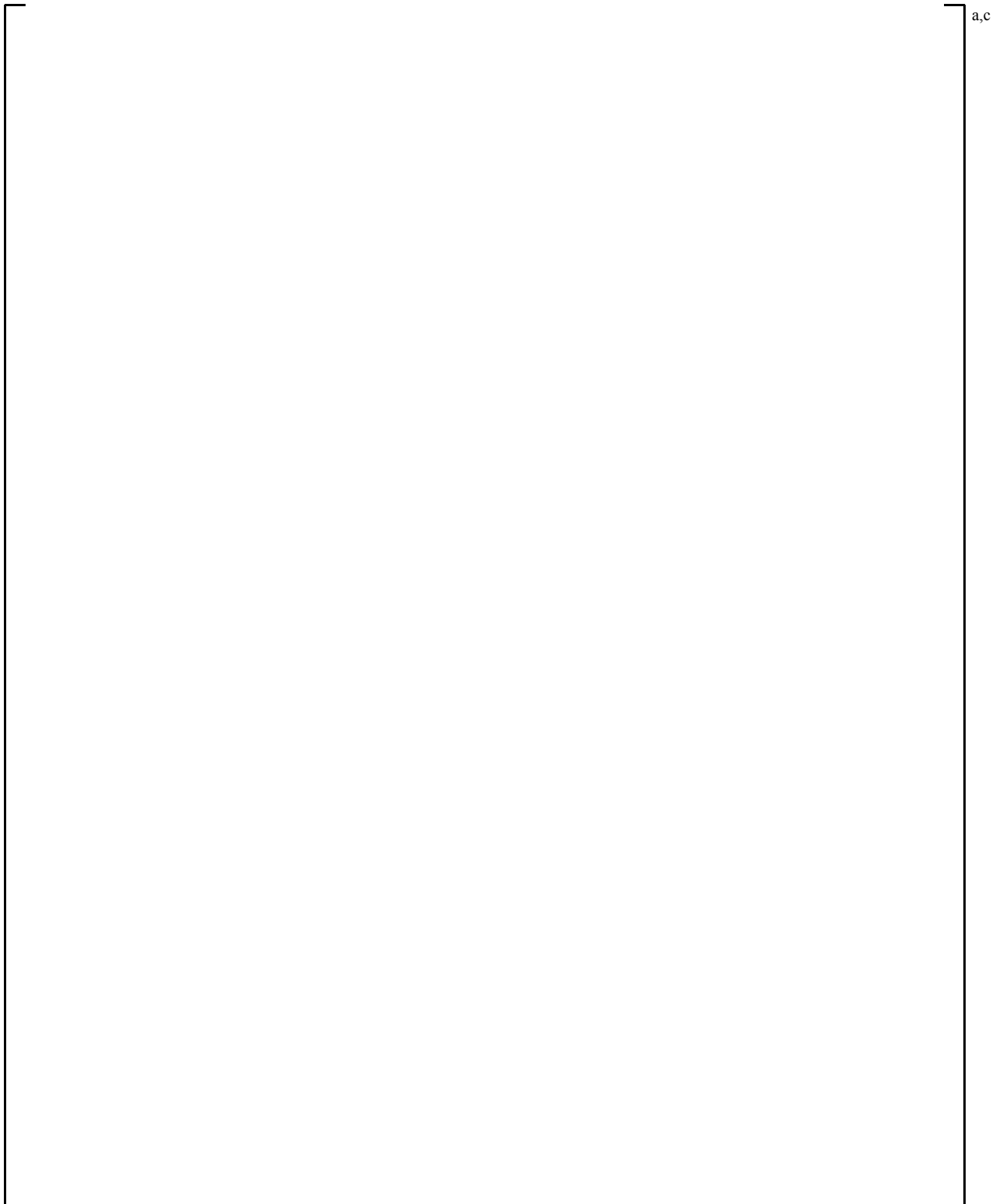


Figure 1: Comparison of Predicted and Measured Void Profiles for Timestep Study, ORNL – THTF Test 3.09.10I (Solid, red line = 5ms max timestep; Dashed, green line = 0.5ms max timestep)

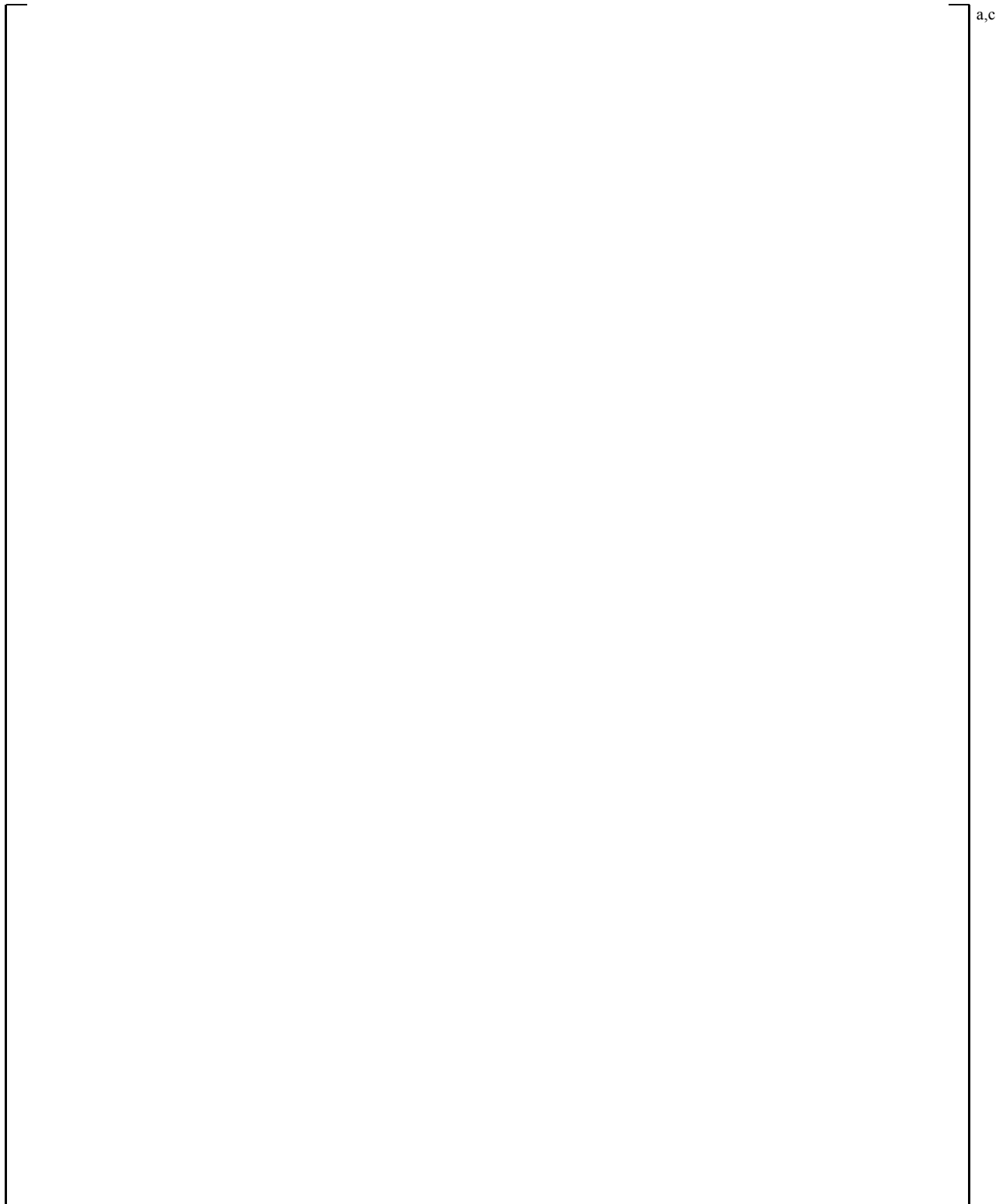


Figure 2: Comparison of Predicted and Measured Void Profiles for Timestep Study, ORNL – THTF Test 3.09.10CC (Solid, red line = 5ms max timestep; Dashed, green line = 0.5ms max timestep)

a,c

Figure 3: Predicted versus Measured Level Swell for G2 Boiloff Noding Sensitivity Studies



Figure 4: Void Fraction Profile Comparison for Nominal ROSA ST-NC-01 Simulation



Figure 5: Void Fraction Profile Comparison for Nominal ROSA ST-NC-06E Simulation



Figure 6: Void Fraction Profile Comparison for the ROSA ST-NC-01 YDRAG Study



Figure 7: Void Fraction Profile Comparison for the ROSA ST-NC-06E YDRAG Study

a,c

Figure 3.2.1-1 Pressurizer and Steam Generator Secondary Side Pressures

a,c

Figure 3.2.1-2 Break Flows

a,c

Figure 3.2.1-3 Intact Loop Steam Generator U-tube Differential Pressures

a,c

Figure 3.2.1-4 Broken Loop Steam Generator U-tube Differential Pressures

a,c

Figure 3.2.1-5 Intact Loop Hot Leg Draining

a,c

Figure 3.2.1-6 Broken Loop Hot Leg Draining

a,c

Figure 3.2.1-7 Cross-over Leg Differential Pressures



Figure 3.2.1-8 Downcomer Differential Pressures



Figure 3.2.1-9 Inner Vessel (Core) Differential Pressures

Figure 3.2.1-10 Upper Head Differential Pressures

a,c

Figure 3.2.1-11 Core Mixture Level Comparison

a,c

Figure 3.2.1-12 Calculated Rod 1 Heatup (located under guide tube) vs. Test Data

a,c

Figure 3.2.1-13 Calculated Rod 2 Heatup (located under open hole) vs. Test Data

a,c

Figure 3.2.2-1 Pressurizer and Steam Generator Secondary Side Pressures

a,c

Figure 3.2.2-2 Break Flows

a,c

Figure 3.2.2-3 Intact Loop Steam Generator U-tube Differential Pressures

a,c

Figure 3.2.2-4 Broken Loop Steam Generator U-tube Differential Pressures

a,c

Figure 3.2.2-5 Intact Loop Hot Leg Draining

a,c

Figure 3.2.2-6 Broken Loop Hot Leg Draining

a,c

Figure 3.2.2-7 Cross-over Leg Differential Pressures

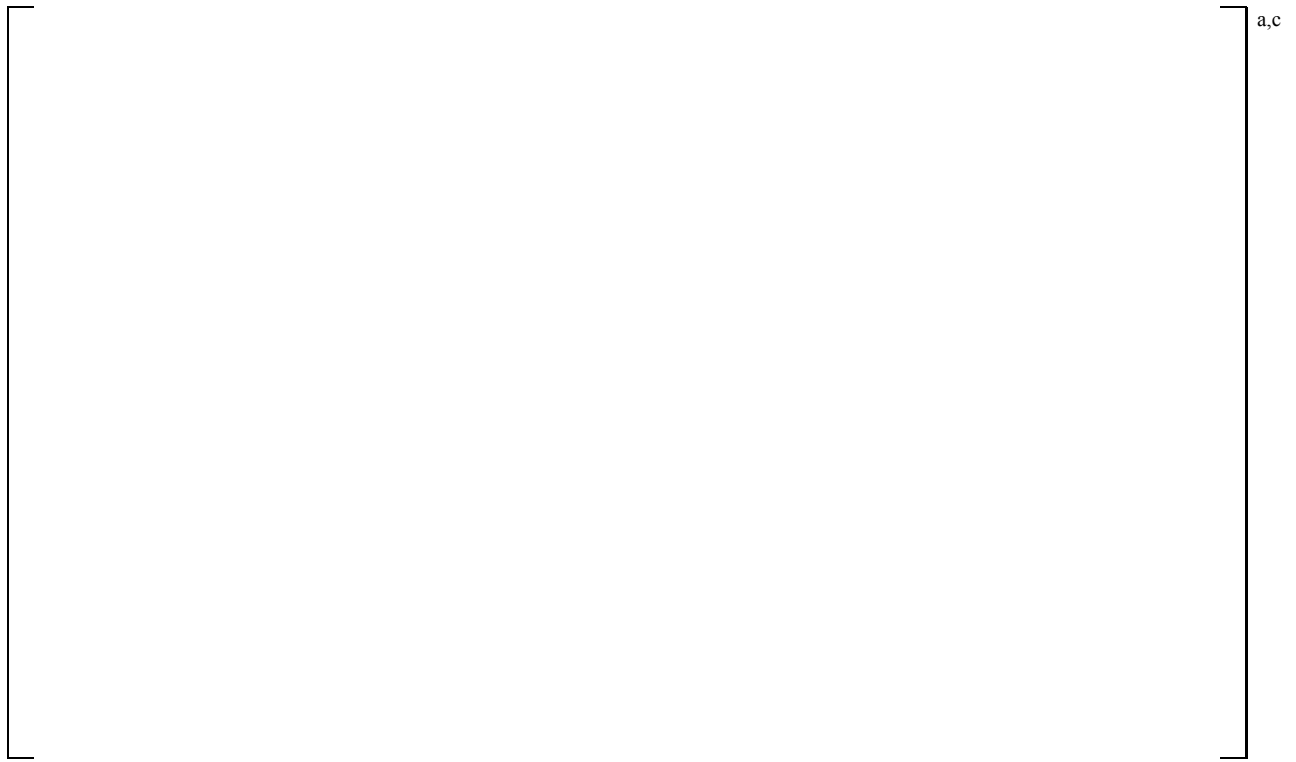


Figure 3.2.2-8 Downcomer Differential Pressures

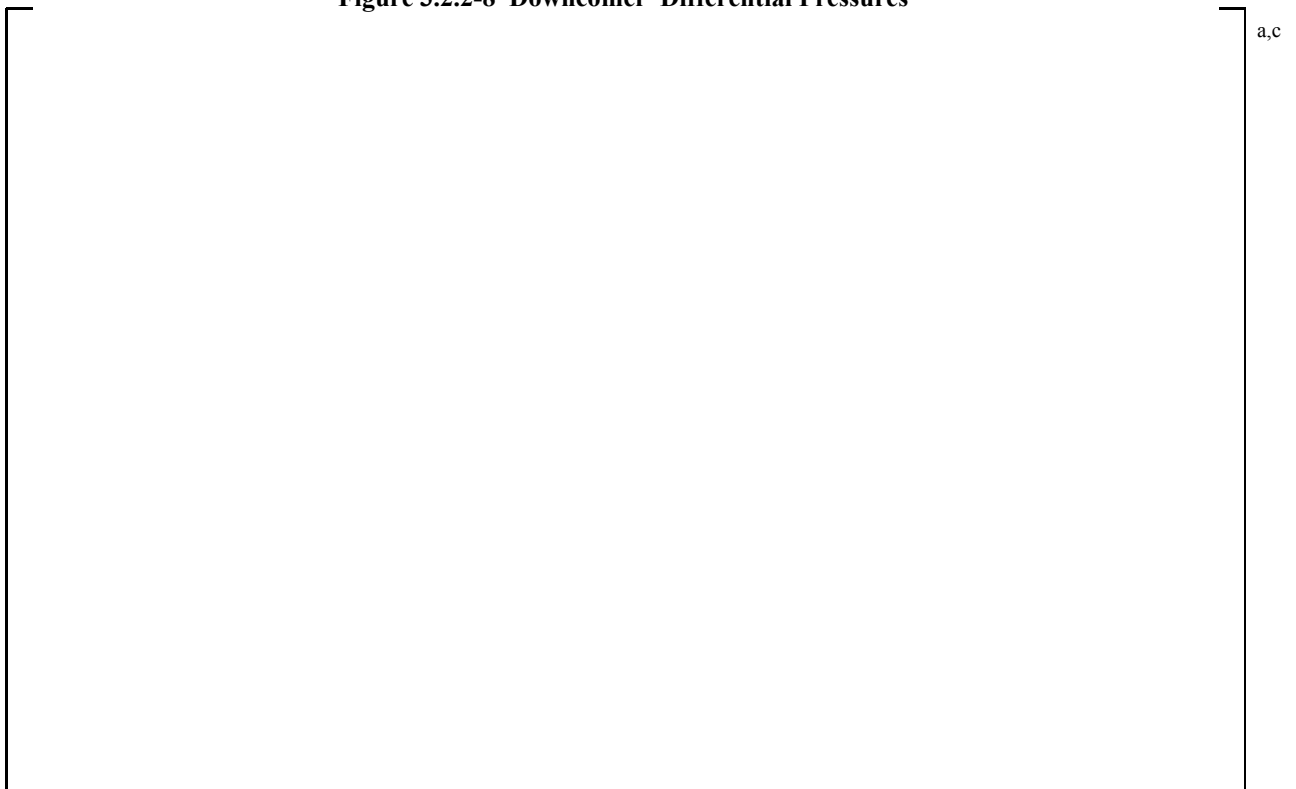


Figure 3.2.2-9 Vessel (Core) Differential Pressures



Figure 3.2.2-10 Upper Head Differential Pressure

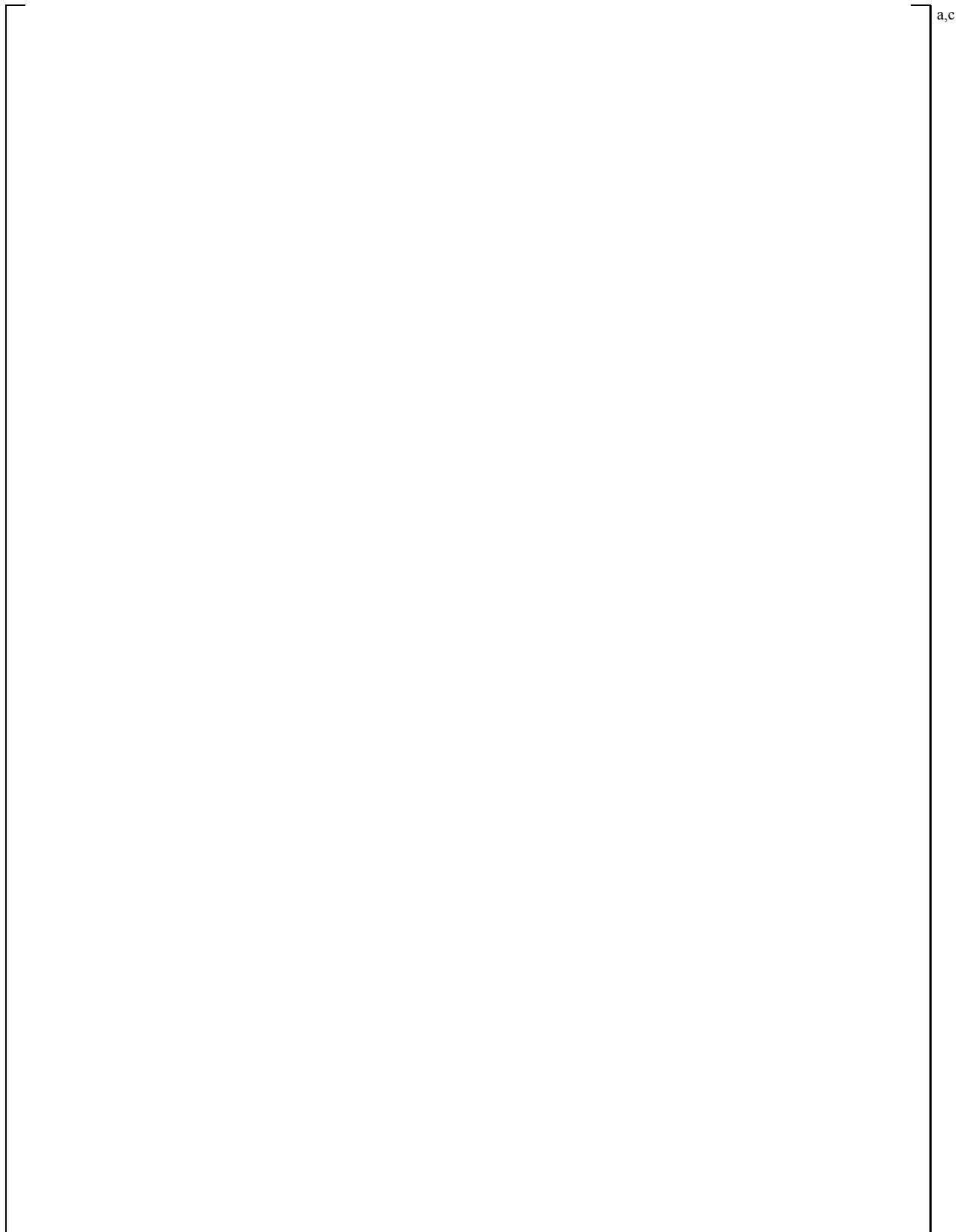


Figure 3.2.2-11 Core Mixture Level Comparison

a,c

Figure 3.2.2-12 Calculated Rod 1 Heatup (located under guide tube) vs. Test Data

a,c

Figure 3.2.2-13 Calculated Rod 2 Heatup (located under open hole) vs. Test Data

a,c

Figure 3.2.3-1 Break Flows

a,c

Figure 3.2.3-2 Integrated Break Flows

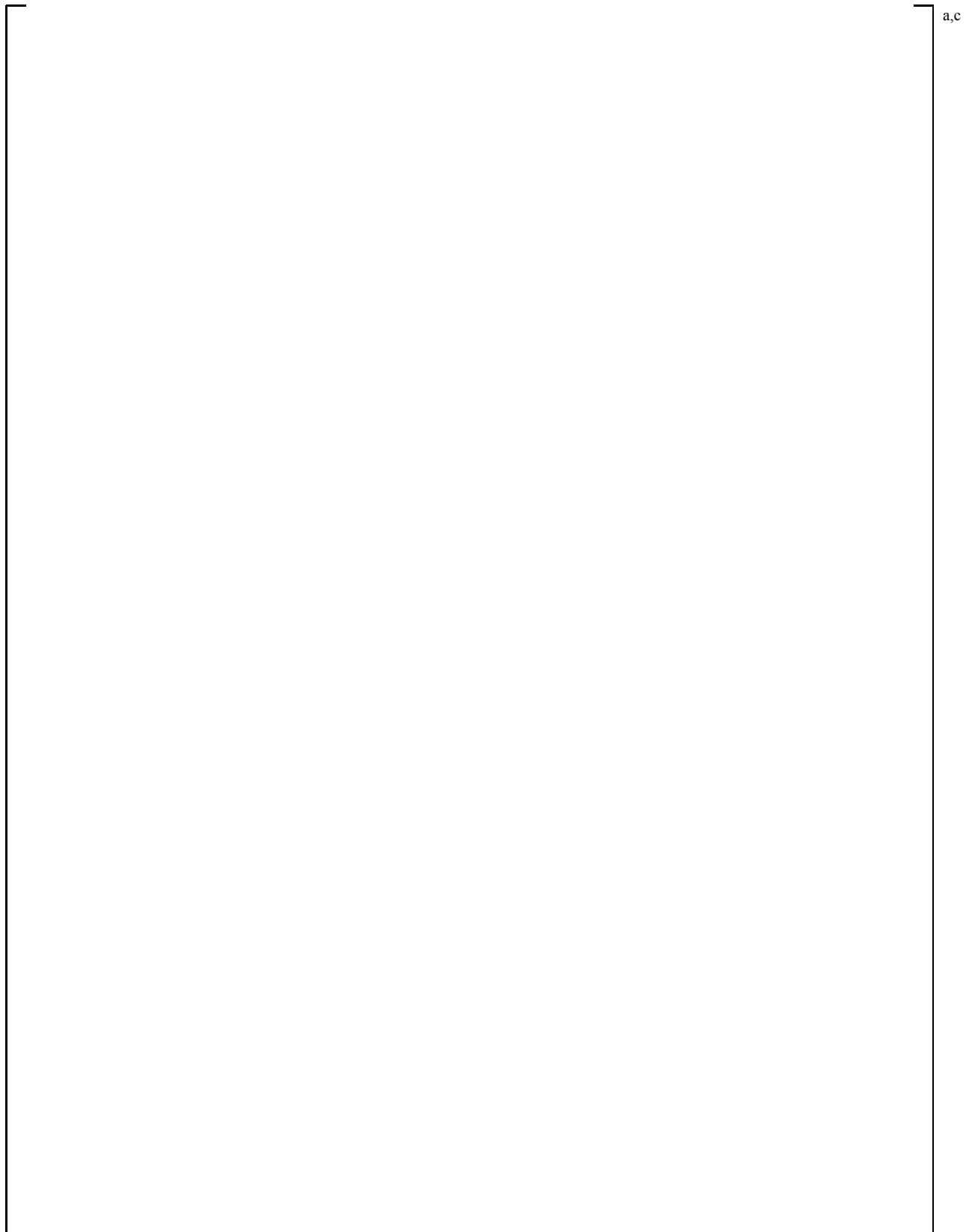


Figure 3.2.3-3 Upper Head Differential Pressures

a,c

Figure 3.2.3-4 Downcomer Differential Pressures

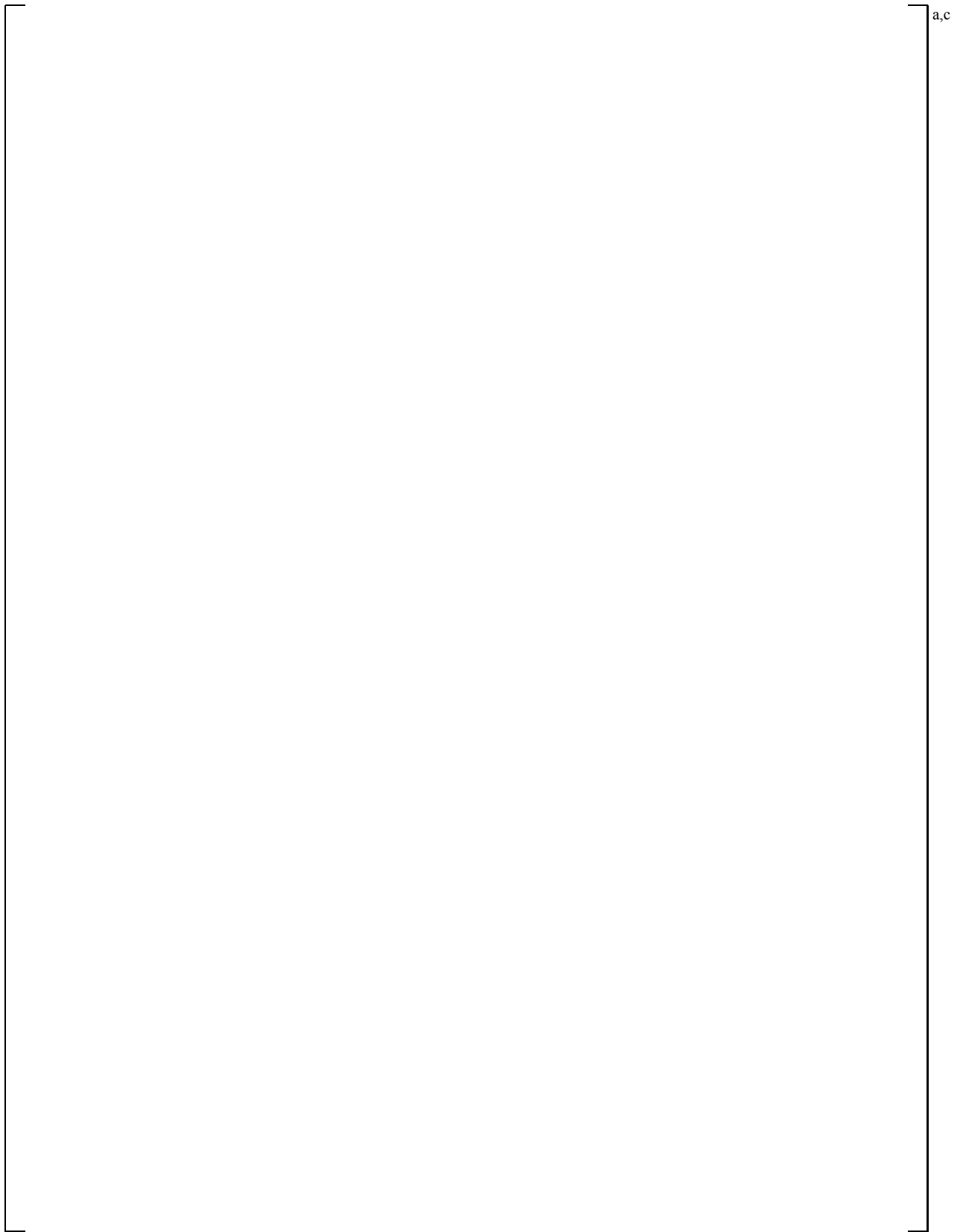


Figure 3.2.3-5 Inner Vessel (Core) Differential Pressures

a,c

Figure 3.2.3-6 Rod Cladding Temperatures at 207 cm Elevation

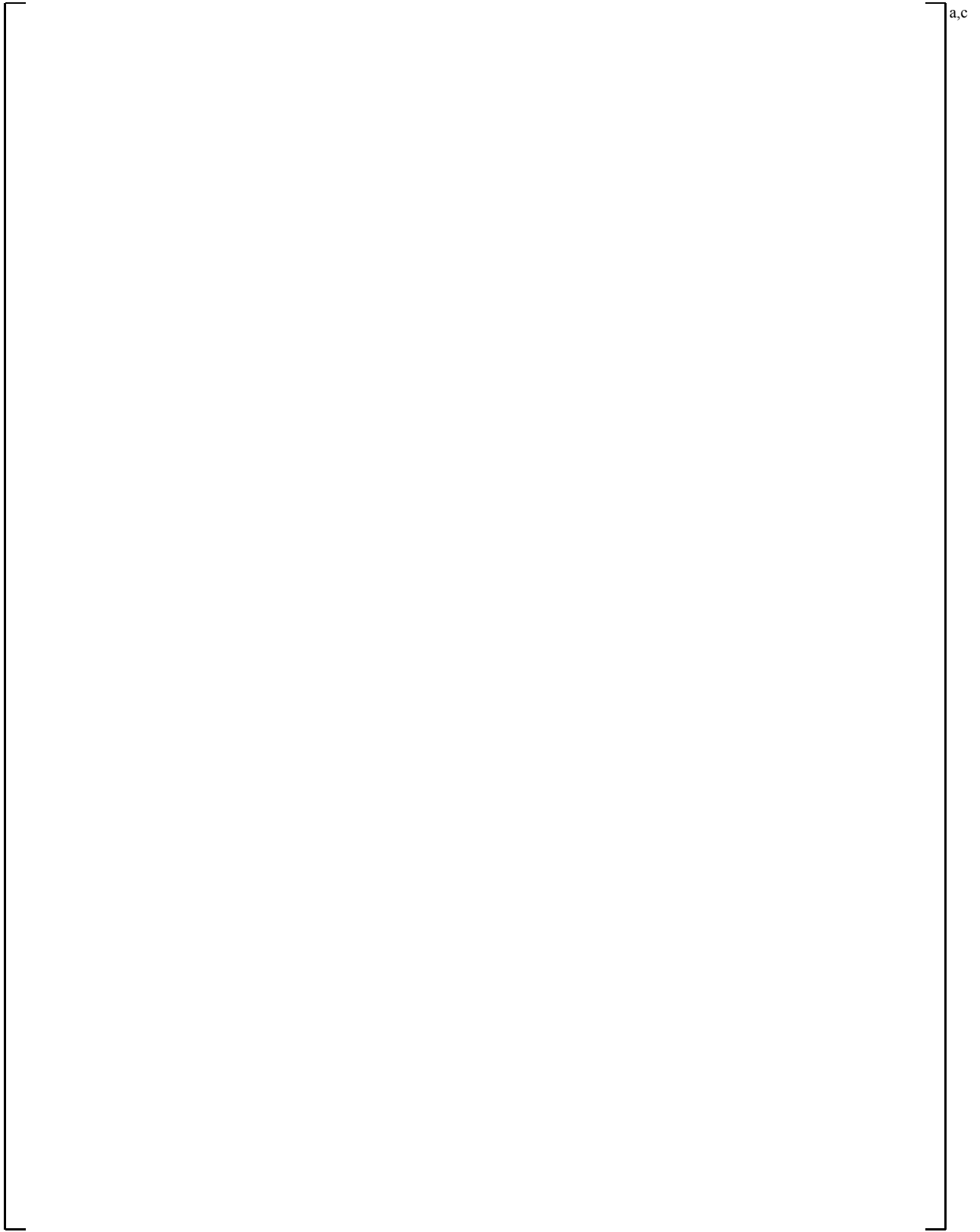


Figure 3.2.3-7 Core Mixture Levels

a,c

Figure 3.2.3-8 Intact Loop SG U-tube Uphill Differential Pressures

a,c

Figure 3.2.3-9 Intact Loop SG U-tube Downhill Differential Pressures

a,c

Figure 3.2.3-10 Broken Loop SG U-tube Uphill Differential Pressures

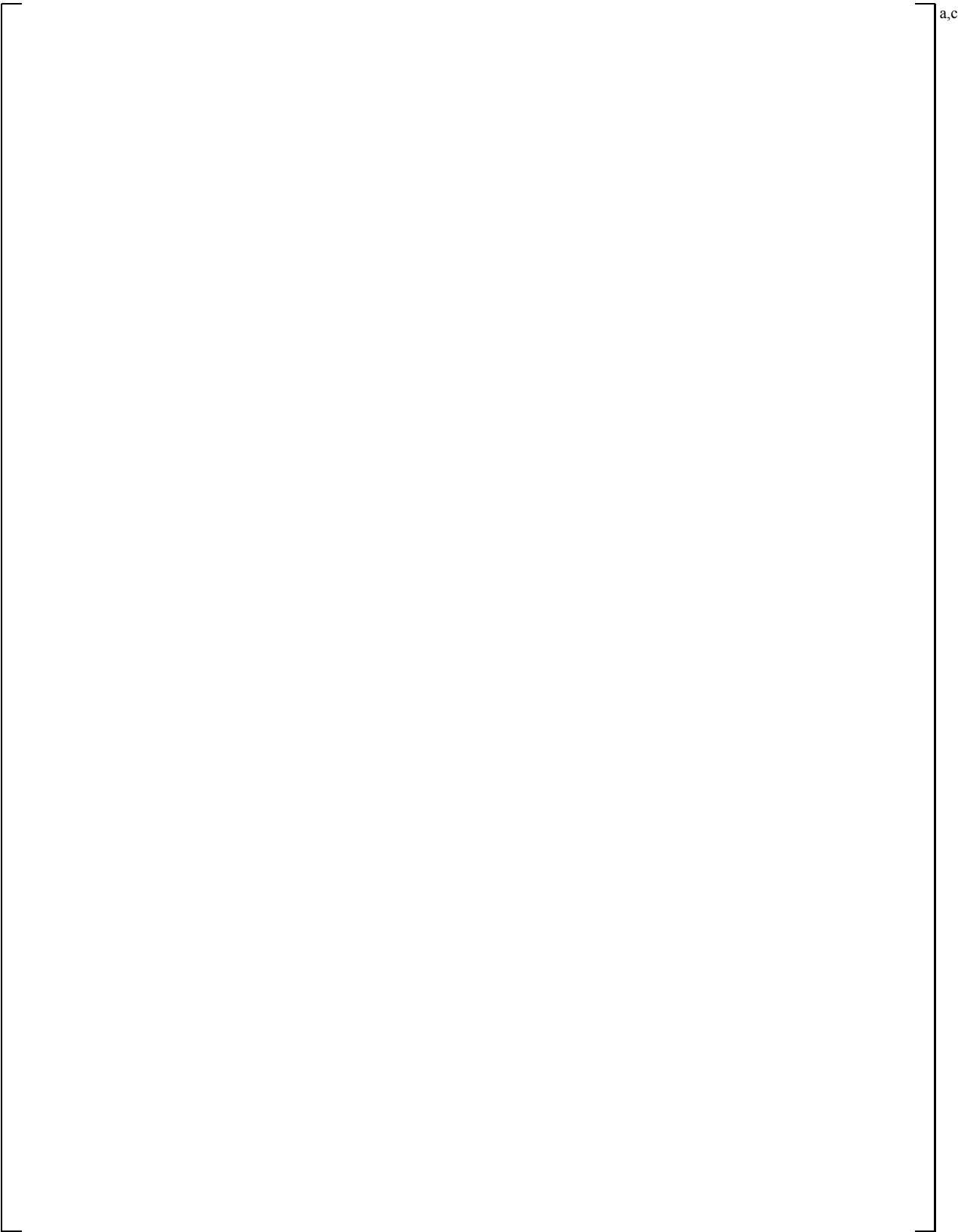


Figure 3.2.3-11 Broken Loop SG U-tube Downhill Differential Pressures

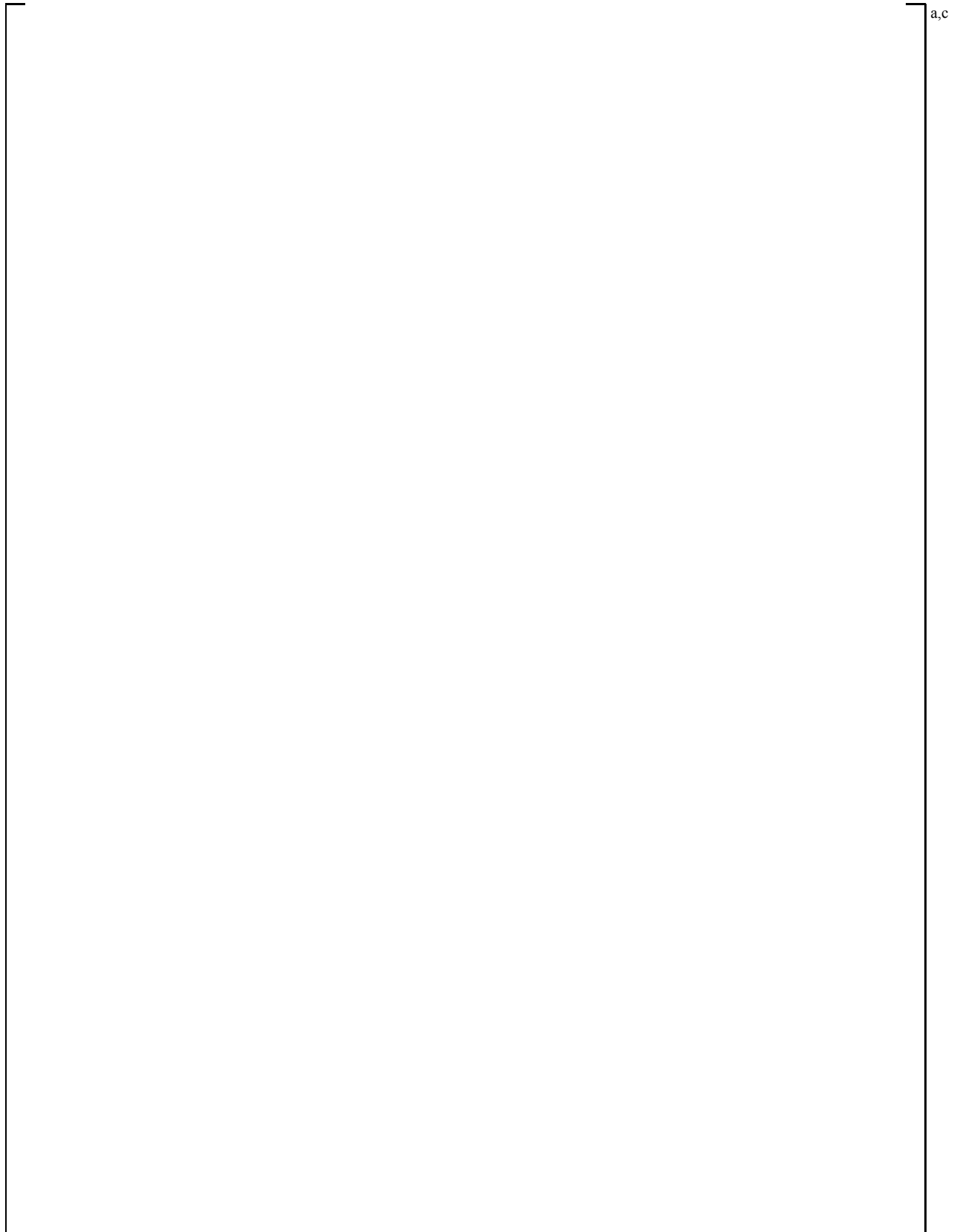


Figure 3.2.3-12 Intact Loop Cross-over Leg Differential Pressures

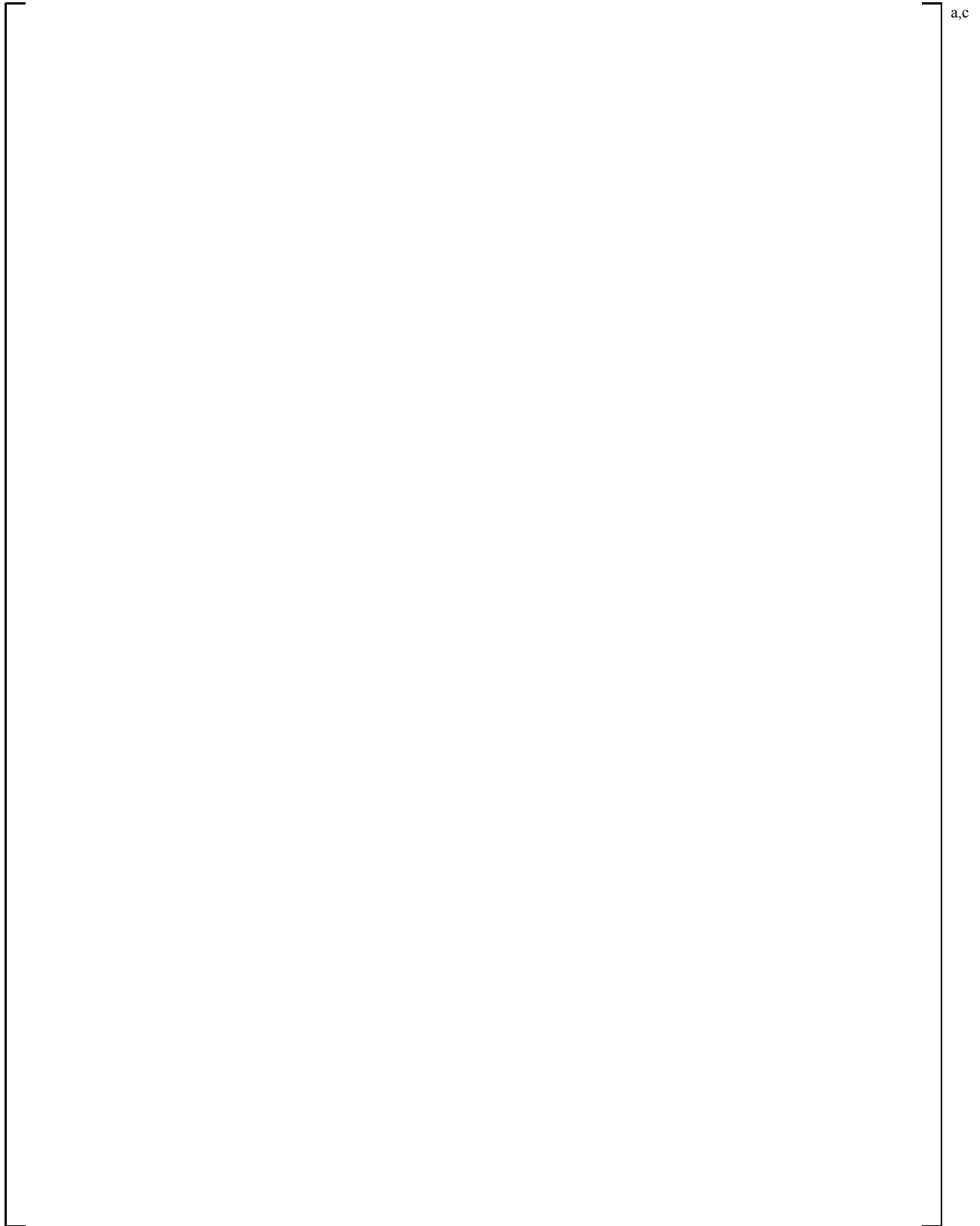


Figure 3.2.3-13 Broken Loop Cross-over Leg Differential Pressures

Updated Topical Report Pages

TABLE OF CONTENTS

LIST OF TABLES	ix
----------------------	----

LIST OF FIGURES	xii
-----------------------	-----

EXECUTIVE SUMMARY	xxii
-------------------------	------

VOLUME I

1	ROADMAP OF FULL SPECTRUM LOCA (FSLOCA) METHODOLOGY	1-1
1.1	BACKGROUND	1-1
1.2	MAPPING OF FSLOCA EM DEVELOPMENT TO REGULATORY GUIDANCE, REGULATORY GUIDE 1.203 (EMDAP)	1-2
1.2.1	EMDAP Element 1 (Step 1): Analysis Purpose, Transient Class and Power Plant Class	1-4
1.2.2	EMDAP Element 1 (Step 2): Specification of Figures of Merit	1-5
1.2.3	EMDAP Element 1 (Steps 3 and 4): Phenomena Identification and Ranking Table	1-5
1.2.4	EMDAP Element 2 (Step 5): Specify Objectives for Assessment Base	1-5
1.2.5	EMDAP Element 2 (Steps 6, 7 and 8): Definition of the Assessment Base and Applicability	1-5
1.2.6	EMDAP Element 2 (Step 9): Determine Experimental Uncertainties as Appropriate	1-6
1.2.7	EMDAP Element 3 (Steps 10, 11 and 12): Develop Evaluation Model	1-6
1.2.8	EMDAP Element 4 (Steps 13, 14 and 15): Bottom-Up Evaluation of Models	1-7
1.2.9	EMDAP Element 4 (Steps 16, 17, 18 and 19): Top-Down Evaluation of Models	1-7
1.2.10	EMDAP Element 4 (Step 20): Determine Evaluation Model Biases and Uncertainties	1-8
1.3	ORGANIZATION OF THE REPORT	1-9
1.4	REFERENCES	1-12
2	EVALUATION MODEL FUNCTIONAL REQUIREMENTS	2-1
2.1	INTRODUCTION	2-1
2.2	FIGURES OF MERIT (EMDAP STEP 2)	2-1
2.3	PHENOMENA IDENTIFICATION AND RANKING TABLE (EMDAP STEPS 3 AND 4)	2-1
2.3.1	LOCA Scenario Specification	2-2
2.3.2	Identification of System, Components, Processes and Ranking	2-7
2.3.3	PIRT: Summary and Conclusions	2-42

If $\left[\begin{array}{c} \alpha_v \\ \alpha_\ell \end{array} \right]^{a,c}$, an inverted pool is assumed and the void fractions used to determine the flow regime and interfacial terms in cell (i, j) are:

$$\left[\begin{array}{c} \alpha_v \\ \alpha_\ell \end{array} \right]^{a,c} \quad (4-9)$$

$$\left[\begin{array}{c} \alpha_v \\ \alpha_\ell \end{array} \right]^{a,c} \quad (4-10)$$

and

$$\left[\begin{array}{c} \alpha_v \\ \alpha_\ell \end{array} \right]^{a,c} \quad (4-11)$$

When a large void gradient between two cells is not present, the void fractions at the momentum cell center are assumed to be $\left[\begin{array}{c} \alpha_v \\ \alpha_\ell \end{array} \right]^{a,c}$. That is:

$$\left[\begin{array}{c} \alpha_v \\ \alpha_\ell \end{array} \right]^{a,c} \quad (4-12)$$

$$\left[\begin{array}{c} \alpha_v \\ \alpha_\ell \end{array} \right]^{a,c} \quad (4-13)$$

and

$$\left[\begin{array}{c} \alpha_v \\ \alpha_\ell \end{array} \right]^{a,c} \quad (4-14)$$

After these volume fractions (α_v , α_ℓ , α_e) are determined, the flow regime and interfacial terms are calculated. The following sections describe the flow regimes and the determination of interfacial area for each regime. The subsections for each normal wall flow regime follow in order of increasing void fraction. First the small bubble regime is described, followed by the small-to-large bubble regime, the churn-turbulent regime, and then the film/drop regime.

The flow regime is indicated by the code for each computational node following the numbering scheme shown in Table 4.2-1:

Table 4.2-1 Summary of Flow Regime Number in Vessel Components	
Flow Regime Indicator and Number	Flow Regime
ISIJ = 1:	Small Bubble
ISIJ = 2:	Large Bubble
ISIJ = 5:	Film/Drop
ISIJ = 6:	Hot Wall
ISIJ = 11:	Top Deluge

4.4.5 Horizontal Stratified Flow

Model Basis

At low liquid and vapor velocities, the individual phases may separate and form a relatively smooth interface. The schematic plot of horizontal stratified flow is shown in Figure 4-9. Due to the effect of gravity, the two-phase flow is separated with the heavier liquid phase at the bottom and the lighter gas phase at the top. A flat horizontal liquid-gas interface separates the two phases. One characteristic of the horizontal stratified flow is that the interfacial area between two phases is minimal compared with other flow regimes, such as bubbly-slug, annular-mist, etc. A low interfacial area consistent with stratified flow allows for increased gas venting capability during a small break LOCA scenario. However, the structure of horizontal stratified flow is unstable if the relative velocity between the two phases is large. According to the Kelvin-Helmholtz stability theory, a large relative velocity causes the interface to become unstable and interfacial waves to grow. The growing interfacial waves eventually destroy the stratified flow structure.

The transition criterion from horizontal stratification to other regimes is based on a modified version of the Kelvin-Helmholtz theory and is discussed in the following. The theory presented is supported by theoretical studies and experiments (Taitel and Dukler, 1976; Anoda et al., 1989; Crowley et al., 1992; Barnea and Taitel, 1994). The criterion is based on dimensionless parameters and is shown to have a relatively minor dependence on the pipe diameter, system pressure, and fluid properties, as well as the fluid superficial velocities.

It is recognized that the transition criterion developed here is based on a steady state condition which lacks proper treatment relative to transient behavior such as an explicit relaxation model to account for settling of the separation process and changing of the interface level. Taitel et al. (1978) discussed a delay in transition to non-stratified flow due to gravity wave propagation when the level changes due to a liquid flow increase. They also demonstrated that the delay characteristics are different when the separated liquid flow is subcritical or supercritical. Transition from the non-stratified flow pattern to the stratified flow pattern also shows a delay, since it takes place when the two phases are completely separated. The settling of the separation process takes time, since the turbulence in liquid flow interferes with the merging and rising of the bubbles. These phenomena are not explicitly modeled in the transition model, although the transition criterion based on the local variables partially captures the transition process from the stratified flow to non-stratified flow. It is noted that the highly transient behavior, which likely happens in loop seal clearance, was simulated reasonably well for Integral Effects Tests, such as the Rig-of-Safety Assessment (ROSA) 0.5% break, 2.5% break, 5% break, and 10% break. Details are given in Section 21.

Transition Criteria

Taitel and Dukler (1976) represents the first complete semi-theoretical horizontal flow regime transition theory. In the original Taitel-Dukler work, boundaries of smooth stratified, wavy stratified, intermittent, annular, and dispersed bubbles regimes are derived assuming steady state flows.

The Taitel-Dukler stratification transition criterion was developed using Kelvin-Helmholtz stability theory. The Kelvin-Helmholtz theory provides a stability criterion for waves of infinitesimal amplitude

formed on a flat surface of liquid flow between horizontal parallel plates. Considering a round pipe geometry and pipe inclination angle, Taitel and Dukler gave a semi-empirical neutral stability condition for horizontal stratified flow.

$$u_g = \left(1 - \frac{h_l}{D}\right) \sqrt{\frac{(\rho_l - \rho_g)g \cos \beta A_g}{\rho_g S_i}} \quad (4-106)$$

where h_l is the depth of the liquid layer, D is the pipe diameter, ρ_l and ρ_g are the respective liquid phase density and gas phase density, g is the gravitational constant, A_g and A_l are the areas of the pipe occupied by the respective gas phase and liquid phase, S_i is the interfacial length in the cross section of pipe (Figure 4-9), and β is the pipe inclination angle.

If the gas phase velocity is higher than the critical gas velocity given in Equation 4-103, the stratified flow is no longer stable and the transition happens. The critical gas velocity is determined by the pipe diameter, the void fraction, the pipe inclination angle, and fluid densities. However, Taitel-Dukler assumed liquid phase velocity is much smaller than the gas phase velocity in their criterion, which is only reasonable for low mass flux flow.

Asaka et al. (1991) analyzed Two-Phase Test Facility (TPTF) experiments using the TRAC-PF1/MOD1 code to assess the adequacy of the Taitel-Dukler flow regime transition criterion and code's interfacial drag models. The code predicted slug or transitional flow regime for tests conducted for relatively high flow rates, whereas the experimental flow regime was stratified flow. This resulted in a large over-prediction of the interfacial drag for these tests. As a result, Asaka suggested the use of a modified version of the Taitel-Dukler model to better describe the flow regime transition (Anoda et al., 1989). The difference between Equation 4-107 and Equation 4-106 is the gas phase velocity u_g is replaced by relative velocity $|u_g - u_l|$.

$$\Delta u_c = |u_g - u_l| = \left(1 - \frac{h_l}{D}\right) \sqrt{\frac{(\rho_l - \rho_g)g \cos \beta A_g}{\rho_g S_i}} \quad (4-107)$$

Beside TRAC-PF1/MOD1, the modified Taitel-Dukler (1976) criterion for the transition and its variations were also implemented in other LOCA safety evaluation codes. A similar approach was also implemented in the RELAP5/MOD3 code (INEL, 1995). The model included in CATHARE was described by Bestion (1990). A review of these models was presented in the paper by Yudov (2002) which in particular described how the horizontal stratified flow regime is formulated in the KORSAR code.

Asaka's (1991) approach, with the sound physical base of the modified Taitel-Dukler criterion, has been considered for the 1D module of WCOBRA/TRAC-TF2. There are other more sophisticated transition criteria (Barnea and Taitel, 1994; Crowley, et al., 1992) that consider viscous effects of the Kelvin-Helmholtz stability analysis. The viscous transition models improve accuracy of the transition criteria by incorporating the viscous Kelvin-Helmholtz instability into the two-fluid model. However, the implementation of the viscous transition model into a computer code is cumbersome. The original inviscid Taitel-Dukler (1976) criterion is suggested over the viscous transition model for

WCOBRA/TRAC-TF2. However, the predictions from the viscous transition model are utilized to calibrate the transition model developed here.

The modified Taitel-Dukler transition criterion can be presented in dimensionless form. A modified Wallis number j_{gl}^* is defined using the liquid velocity, the vapor velocity, the void fraction, the pipe diameter, gravitational constant, and fluid densities.

$$j_{gl}^* = \frac{|u_g - u_l| \alpha}{\sqrt{\frac{\rho_l - \rho_g}{\rho_g} D g}} \quad (4-108)$$

Therefore, Equation 4-107 is regrouped as:

$$j_{gl,c}^*(\alpha) = \left(1 - \frac{h_l}{D}\right) \sqrt{\frac{\alpha^3 \pi D \cos \beta}{4 S_i}} \quad (4-109)$$

Here $\cos \beta$ is the effect of pipe inclination angle on the transition criterion. In the WCOBRA/TRAC-TF2 regime map, horizontal flow is only allowed when the pipe inclination angle is less than $[\quad]^{a,c}$. Since $[\quad]^{a,c}$ the value can be approximated as 1.0 for simplicity, and $\cos \beta$ is removed from the stratification transition criterion. This simplification will slightly stabilize the stratified flow in an inclined pipe flow. The new transition criterion is given by:

$$j_{gl,c}^*(\alpha) = \left(1 - \frac{h_l}{D}\right) \sqrt{\frac{\alpha^3 \pi D}{4 S_i}} \quad (4-110)$$

In Equation 4-110, j_{gl}^* is only a function of void fraction for a round pipe since h_l/D and S_i/D are both functions of void fraction. Trends with pressure and hydraulic diameter are shown in Figure 4-10 and Figure 4-11. Figure 4-12 shows the modified Taitel-Dukler transition line in the $j_{gl}^* - \alpha$ plot together with various transition boundary data. The data points in Figure 4-12, and also used in Figure 4-13, Figure 4-14, and Figure 4-17, include the stratified flow to slug flow transition boundary observed in the TPTF tests (Nakamura et al., 1995), the transition boundaries from the offtake experiments of Moon (Moon and No, 2003), and from Smoglie, which data points were presented by Moon and No (2003), gas-liquid experimental data from Crowley et al. (1992). The data sources for Figure 4-13 are summarized in Table 4.4.5-1. The data considered include pressures from 0.1 MPa to 7.3 MPa as well as pipe diameter up to 0.295 m.

The transition boundary data of Crowley et al (1992) were given in the format of gas superficial velocity and liquid superficial velocity. The superficial velocities are transformed to the modified Wallis number by assuming the equilibrium state void fraction.

[

] ^{a,c}

] ^{a,c}
--	------------------

(4-118)

[

|

] ^{a,c}

[

] ^{a,c}**Conclusions**

A hybrid transition model [

model was developed assuming a cylindrical pipe. The uncertainty of these models is accounted for in the overall WCOBRA/TRAC-TF2 code bias and uncertainty discussed in Section 29.

Table 4.4.5-1 [^{a,c}				

] ^{a,c}**4.4.6 Wavy-Dispersed Flow****Model Basis**

A wavy-dispersed flow regime is a particular horizontal stratified flow characterized by a significant amount of liquid entrained in a vapor core (pictorial representation below). This flow was observed in high pressure (3~12 MPa) steam/water experiments using the TPTF facility (Nakamura, 1995). It was observed that when pressure is above 8.6 MPa, the slug flow regime could not be established and was completely replaced by the wavy-dispersed flow instead. The occurrence of wavy-dispersed flow instead of slug flow potentially has a significant influence on the coolant distribution during a small break LOCA.

Conclusions

The model for the wavy-dispersed regime is verified through its use in the 1D components of the ROSA and LOFT integral effects tests, as documented in Volume 2. The uncertainty in modeling this regime is accounted for in the overall WCOBRA/TRAC-TF2 code bias and uncertainty.

4.5 REFERENCES

1. Anoda, Y., Kukita, Y., Nakamura, H. and Tasaka, K., 1989, "Flow Regime Transition in High-Pressure Large-Diameter Horizontal Two-Phase Flow," *Proceeding of 26th ASME/AICHE/ANS National Heat Transfer Conference*, Philadelphia, pp 61-68.
2. Asaka, H., Kukita, Y., Anoda, Y., Nakamura, H. and Tasaka, K., 1991, "Improvement of TRAC-PF1 Interfacial Drag Model for Analysis of High-Pressure Horizontally-Stratified Two-Phase Flow," *Journal of Nuclear Science and Technology*, Vol. 28, No. 1, pp. 33-44.
3. Bajorek, S. M., et al., 1998, "Code Qualification Document for Best Estimate LOCA Analysis," WCAP-12945-P-A, Volume 1, Revision 2, and Volumes 2 through 5, Revision 1, and WCAP-14747 (Non-Proprietary).
4. Barnea, D. and Taitel, Y., 1994, "Interfacial and Structural Stability of Separated Flow," *Int. J. Multiphase Flow*, Vol. 20, Suppl., pp. 387-414.
5. Bestion, D., 1990, "The physical closure laws in the CATHARE code," *Nuclear Engineering and Design*, Vol. 124, pp. 229-245.
6. Choe, W. G., Weinberg, L. and Weisman, J., 1976, "Observation and Correlation of Flow Pattern Transitions in Horizontal, Cocurrent Gas-Liquid Flow," *Two-Phase Transport and Reactor Safety*, Veziroglu, T. N. and Kakac, S., editors, Vol. IV, pp. 1357-1393.
7. Chow, S. K., et al., 1989, "Assessment of Scaling Uncertainties for PWR Plant Large-Break LOCA Analysis," EPRI NP-6602.
8. Crowley, C. J., Wallis, G. B. and Barry, J. J., 1992, "Validation of a One-Dimensional Wave Model for the Stratified-to-Slug Flow Regime Transition, with Consequences for Wave Growth and Slug Frequency," *Int. J. Multiphase Flow*, Vol. 18, No. 2, pp. 249-271.
9. DeJarlais, G., 1983, "An Experimental Study of Inverted Annular Flow Hydrodynamics Utilizing an Adiabatic Simulation," ANL-83-44, NUREG/CR-3339.
10. Dukler, A. E., 1977, "Two Phase Interactions in Countercurrent Flow Studies of the Flooding Mechanism," NUREG-0214.
11. Griffith, P. and Snyder, G. A., 1964, "The Bubbly-Slug Transition in a High Velocity Two Phase Flow," MIT Report 5003-29 (TID-20947).

a,c

Figure 4-12 [] ^{a,c}

a,c

Figure 4-13 [] ^{a,c}

a,c

Figure 4-14 The Hybrid Horizontal Stratification Criterion

a,c

Figure 4-17 Horizontal Stratified Flow Regime Transition and Relevant Data

[

 $]^{a,c}$

Next, the bubble drag coefficient is calculated, using Equations 5-50, 5-53, 5-57, and 5-58. [

 $]^{a,c}$

The interfacial drag between the continuous liquid and the vapor in the small bubble regime is calculated as:

$$\left[\right]^{a,c} \quad (5-67a)$$

where the interfacial area $A_{i,SB}$ is given in Equation 4-17. If there is significant vapor generation at the wall, the interfacial drag is ramped between the small bubble value calculated from Equation 5-67a and the inverted slug value as:

$$\left[\right]^{a,c} \quad (5-67b)$$

The hot wall drag coefficient, $K_{iX,v\ell,HW}$ is calculated similar to Equation 5-109 as:

$$K_{iX,v\ell,HW} = \text{maximum} \begin{cases} K_{iX,v\ell,IVS} \text{ as defined by Equation 5-107} \\ 0.125 \rho_v A_{i,IVS} \end{cases} \quad (5-67c)$$

The value of F'_T is given as:

$$\left[\right]^{a,c} \quad (5-68a)$$

Where,

$$\left[\right]^{a,c} \quad (5-68b)$$

[

 $\alpha_v^{a,c}$

For stable films, the annular flow interfacial correlation developed by Wallis (1969) is used:

$$f_{i,W} = 0.005 [1 + 75 (1 - \alpha_v)] \quad (5-96)$$

[

 $\alpha_v^{a,c}$

As discussed in Section 4, the transition to churn-turbulent (large bubble) regime begins at a void fraction of $\alpha_v^{a,c}$ percent and continues until a stable film is achieved. The void fraction at which a stable liquid film will exist depends on the flow channel size and the vapor velocity. The critical void fraction is determined from a force balance between the disruptive force of the pressure gradient over the crest of waves on the film and the restraining force of surface tension. The resulting expression for the critical vapor fraction is:

$$\left[\frac{1}{\alpha_v^{a,c}} \right] \quad (5-97)$$

The critical void fraction is limited to a minimum value of $\alpha_v^{a,c}$, the value below which waves can be expected to bridge across the flow channel and cause a transition to churn-turbulent flow.

The interfacial drag logic for the lateral flow is simplified relative to the vertical flow since the film flow between the gaps is assumed to be stable and the Wallis interfacial friction factor given in Equation 5-96 is used. [

 $\alpha_v^{a,c}$

Model as Coded

[

$\alpha_v^{a,c}$ The interfacial drag is calculated as,

$$\left[\frac{2}{\pi} \frac{A_{i, \text{film}}}{D} \right]^{a,c} \quad (5-98)$$

where the interfacial area $A_{i, \text{film}}$ is given by Equation 4-51.

For lateral flow through the gaps, the interfacial friction factor is calculated using:

$$\left[\frac{2}{\pi} \frac{A_{i, \text{film}}}{D} \right]^{a,c} \quad (5-99)$$

where the factor of 2 in Equation 5-89 has been taken into account, and giving a lateral drag coefficient of:

$$\left[\frac{2}{\pi} \frac{A_{i, \text{film}}}{D} \right]^{a,c} \quad (5-100)$$

Scaling Considerations

The Wallis friction factor for film, Equation 5-96 has been examined for horizontal and vertical flow from pipe sizes ranging from 1-inch to 3-inch diameter as shown in Figure 5-4. The Hanstock and Hanratty film friction model has also been compared to vertical film flow data on diameter of 0.503 inches to 2.5 inches over a range of different fluid velocities and pressures. The comparison of their correlation to data is shown in Figure 5-5. This comparison shows that the correlation provides a good fit to the data over a range of scales.

Conclusions

The film wall drag models have been compared for both horizontal and vertical flows over a range of geometries and hydraulic diameters. WCOBRA/TRAC-TF2 has been used with these models to calculate the two-phase pressure drops in an annular film flow regime.

5.4.5 Inverted Annular Flow Regime

Model Basis

An inverted annular flow regime is assumed if the continuous liquid phase is subcooled and the surrounding surface is hot and dry. This regime consists of a liquid core surrounded by a vapor film.

For inverted annular flow, the interfacial friction factor is []^{a,c}:

$$\left[\frac{2}{\pi} \frac{A_{i, \text{film}}}{D} \right]^{a,c} \quad (5-101)$$

no scaling effects. The experimental conditions were varied over wide ranges to ensure that the PWR plant conditions were covered.

Conclusions

The inverted annular interfacial drag model used in WCOBRA/TRAC-TF2 is derived from the annular film flow model used for high void fraction wetted wall flows. The inverted annular interfacial drag model is assessed with full-scale prototypical rod bundle experiments for different rod arrays.

5.4.6 Inverted Liquid Slug Regime

Model Basis

As the liquid flow in the inverted annular flow regime is heated by wall heat transfer, the liquid core is accelerated by the increased vapor content of the flow. When the liquid reaches the saturation temperature, it no longer can condense the vapor and the liquid begins breaking into ligaments or chunks into a dispersed droplet flow as it progresses up along the heated channel. The interfacial friction is calculated assuming an unstable liquid film surface exists on the large liquid ligaments or drops as:

$$\left[\right]^{a,c} \quad (5-106)$$

This equation is $\left[\right]^{a,c}$ times the Wallis (1969) equation for stable liquid films discussed earlier, given as Equation 5-96.

The interfacial area is calculated assuming that the liquid slugs are spherical, and have a diameter $\left[\right]^{a,c}$ of the channel diameter, as described in Section 4.3.3.

Model as Coded

The axial flow interfacial drag coefficient is calculated as:

$$K_{iX,v\ell,IVS} = f_{i,IVS} \frac{\rho_v |U_{v\ell}|}{2} A_{i,IVS} / \Delta X \quad (5-107)$$

where the friction factor is calculated from Equation 5-106 and the interfacial area $A_{i,IVS}$ for the liquid slug regime is from Equation 4-60 as:

$$A_{i,IVS} = \frac{8.04\alpha_\ell}{D_h} A_X \Delta X \approx \frac{8\alpha_\ell}{D_h} A_X \Delta X \quad (5-108)$$

where α_ℓ is the minimum of the liquid void fraction in the mesh cell $\alpha_\ell(i,j)$ and the average liquid void is given by Equation 4-13.

This is further modified by:

a,c

Figure 7.2-3 Heat Transfer Regime Map for Vessel Component

14.2.3.5 G-2 Reflood Experiments

The low pressure, forced reflood tests performed at the Westinghouse G-2 test facility were simulated using the WCOBRA/TRAC-TF2 computer code. Comparisons of the WCOBRA/TRAC-TF2 results to the reflood test data can be used to help assess the capability of WCOBRA/TRAC-TF2 to accurately predict rod bundle reflood heat transfer behavior including spacer grid effects on dispersed flow film boiling heat transfer. [

] ^b

14.2.3.5.1 Facility Description

The facility is the same as that described in Section 14.2.2.3.

14.2.3.5.2 Test Procedure

[

|

] ^b

Table 14.2.3.5-1 G-2 Reflood Tests and Conditions

b

18.2.2 PWS 2.3 Loop Seal Tests

Scaled U-tube experiments designed to examine the hydraulic behavior of a U-tube under conditions similar to those encountered during a small break LOCA were performed as part of the ECTHOR (an acronym from French “Ecoulements dans des Tuyauteries Horizontales en Eau-Air” which stands for Air-Water Flow in Horizontal Pipes) Program (Boileau and Bourteele, 1985). The vapor flow required to clear the U-tube was a specific focus of the tests.

18.2.2.1 Test Facility Description

The tests were run in a plexiglass facility with air and water at atmospheric pressure. The facility, illustrated schematically in Figure 18.2.2-1, consists of a blower, a run of horizontal piping from the blower, a U-tube, and a catch tank.

The pipe diameter chosen for the facility was $[]^{a,c}$. This corresponds to approximately $[]^{a,c}$ scale compared with a pressurized water reactor (PWR), which has a pipe diameter of 2.58 feet. The air and water flow rates were scaled so that approximate similitude was maintained for the Froude number, shown to define the flow regime transition from stratified to intermittent and annular flow by (Taitel and Dukler, 1976). Figure 18.2.2-2 shows the predicted flow regime transition using the Taitel and Dukler flow regime map for atmospheric pressure, $[]^{a,c}$ scale, compared with the transition for steam at 1000 psia, full-scale geometry. This figure indicates that the transition from stratified to annular flow occurs at a higher vapor flux in the air-water tests. While better similitude could have been obtained with a smaller pipe, the chosen diameter also assures that the vertical pipes of the U-tube are sufficiently large so that any countercurrent flow limits (CCFL) that occur will not be affected by the pipe diameter. According to (Richter, 1981), the critical vapor flux for CCFL in pipes larger than approximately 2 inches in diameter depends only on pressure, not on pipe diameter.

Pressure drop across the U-tube was measured. In the horizontal and in the downstream vertical sections, several independent measurements of void fraction were made using pressure drops, optical probes, and gamma densitometers.

18.2.2.2 Test Procedures

Several test series were performed, as described below:

- Limit Line Tests

These tests were designed to obtain the liquid level in the horizontal portion of the U-tube, which produces significant liquid entrainment for a given air flow rate. This is equivalent in some ways to the CCFL limit and is termed the U-tube limit line. The tests were performed as follows:

[

$]^{a,c}$

Figure 21.6-9 Comparison of Steam Generator A U-tube Inlet-to-top Differential Pressures

a,c

Figure 21.18-2 Calculated Break Flows

data. [

] ^{a,c}

The assessment of the thermal-hydraulic models in WCOBRA/TRAC-TF2 used a large number of test comparisons to ensure that estimates of the model uncertainties were well-founded, and included potential scaling effects. Models were grouped in some cases as a package when it was considered more meaningful to validate a specific model package against experiments. For example, the WCOBRA/TRAC-TF2 simulations of the FLECHT reflooding experiments in Sections 14 and 15 were used to validate many aspects of the heat transfer package, including specific heat transfer correlations, the prediction of the minimum film boiling temperature, the entrainment model, the heat flux split between evaporation and superheating, and calculated dispersed droplet flow behavior (drop sizes and velocities). The FLECHT and FLECHT-SEASET tests have sufficient independent sources of data that can be used to validate the computer code such that one is confident that the correct answer is being calculated for the correct reasons. A compensating error analysis is also provided in Section 24.

The plant conditions uncertainty contributors calculations account for the different possible operating conditions and accident initial conditions that the plant could experience. The plant specific sources of uncertainty are discussed in Section 25. Similar to the code model uncertainty contributors, some are explicitly ranged in the uncertainty methodology, others are bounded to ease the analysis when it is not practical or desirable to treat these conditions in a statistical fashion.

10 CFR 50.46 states that “[...] *uncertainty must be accounted for, so that, when the calculated ECCS cooling performance is compared to the criteria set forth in paragraph (b) of this section, there is a high level of probability that the criteria would not be exceeded.*” 10 CFR 50.46 does not explicitly specify how this probability should be evaluated or what its value should be. However, additional clarification as to the US NRC expectations on the acceptable implementation of the “high probability” requirement is provided in Regulatory Position 4.1 that states: “*a 95% probability is considered acceptable by the NRC staff [...]*”. Further, Regulatory Guide 1.157 introduced the concept of confidence level as a possible refinement to the uncertainty treatment, but did not expand further on this concept.

As statistical methods are implemented to perform LOCA safety analyses, a statistical statement which estimates or bounds the 95th quantile of the population with a 95% confidence level has been suggested by the NRC as acceptable to demonstrate the required “high probability.” In the previous approved methodology (ASTRUM, Nissley et al., 2005) the 95th quantile of the joint-distribution of PCT, MLO and core-wide oxidation (CWO) is bounded with at least 95% confidence level. [

] ^{a,c}



Fuel Behavior

Uncertainties in the lead fuel rod initial conditions and its behavior during the LOCA transient are explicitly accounted for. These uncertainties include hot rod peaking, initial fuel temperature, cladding burst temperature, burst strain, fuel density after burst due to relocation, and metal-water reaction rates. The treatment of fuel behavior in the Westinghouse methodology is considered to be more complete than that used in the CSAU methodology, in that [

] ^{a,c}

Other Variables

Uncertainties in decay heat and break flowrate are included in the overall uncertainty assessment. The metal-water reaction rate uncertainty is also considered as one of the fuel rod uncertainty parameters, as noted in the Regulatory Position 4.3.2 Compliance Discussion.

Statistical Treatment of Overall Computational Uncertainty

The overall calculational uncertainty statement is determined using a non-parametric statistical method. Uncertainties in [

|

|

] ^{a,c}

The FULL SPECTRUM LOCA methodology used by Westinghouse addresses the PCT, maximum cladding oxidation, maximum hydrogen generation, and coolable geometry criteria defined in 10 CFR 50.46(b)(1) through (b)(4). [

] ^{a,c} Coolable geometry is demonstrated by ensuring that the [] ^{a,c} criteria are satisfied, including any effects of combined LOCA and Safe-Shutdown Earthquake (SSE) loads on core geometry.

The Westinghouse methodology used to satisfy the long-term cooling criterion defined in 10 CFR 50.46(b)(5) is unaffected by the use of best-estimate techniques for the short-term transient calculation.

32.4 METHODOLOGY LIMITATIONS

The maximum assembly [

] ^{a,c}

The FULL SPECTRUM LOCA evaluation model cannot be applied for transient times longer than 10,000 seconds following shutdown unless the decay heat model is shown to be acceptable for the analyzed core conditions.

32.5 REFERENCES

1. Bajorek, S. M., et al., 1998, "Code Qualification Document for Best Estimate LOCA Analysis," WCAP-12945-P-A, Appendix C (Proprietary).
2. Nissley, M. E., et al., 2005, "Realistic Large Break LOCA Evaluation Methodology Using Automated Statistical Treatment of Uncertainty Method (ASTRUM)," WCAP-16009-P-A, Revision 0, and WCAP-16009-NP-A, Revision 0 (Non-Proprietary).
3. Roe, J., 1998, "NRC Information Notice 98-29: Predicted Increase in Fuel Rod Cladding Oxidation."
4. USNRC, 1989, "Best-Estimate Calculations of Emergency Core Cooling System Performance," Regulatory Guide 1.157.
5. USNRC, 2005, "Transient and Accident Analysis Methods," Regulatory Guide 1.203.

**Summary of November 2015, December 2015 and January 2016 Discussions of Draft Limitations and Conditions and Supplemental Information for the FULL SPECTRUM LOCA (FSLOCA) Evaluation Model
(Non-Proprietary)**

January 2016

Westinghouse Electric Company LLC
1000 Westinghouse Drive
Cranberry Township, PA 16066

©2016 Westinghouse Electric Company LLC
All Rights Reserved

Summary of November 2015, December 2015, and January 2016 Discussions on Draft Limitations and Conditions and Supplemental Information for the FULL SPECTRUM LOCA (FSLOCA) Evaluation Model

In order to provide context for the discussion in this letter, the draft limitations and conditions proposed by the Nuclear Regulatory Commission (NRC) for the FULL SPECTRUM™ LOCA (FSLOCA™) evaluation model (EM) as discussed in the November 2015 meeting are included here in italics.

Draft Item #1

The FSLOCA EM applicability for performing PWR LOCA analyses is defined in terms of applicable accident transient phases so that the FSLOCA EM cannot be applied for analyzing the long-term core cooling phase of LOCA transients for the purpose of demonstrating compliance with the long-term core cooling requirement set forth in 10 CFR 50.46(b)(5). This limitation specifically addresses the condition that the FSLOCA EM does [

] ^{a,c}

Draft Item #2

The FSLOCA EM applicability for performing PWR LOCA analyses is defined in terms of applicable types of PWR plants so that the EM can be applied for LOCA analyses of Westinghouse designed three-loop and four-loop PWR plants only.

Draft Item #3

The coupled WCOBRA/TRAC-TF2 and COCO codes will be applied to calculate the containment backpressure in PWR LOCA analyses for Region II so that a conservatively low, although not explicitly bounded, containment pressure will be predicted and used. For this purpose, the input to the COCO model and its prediction results will be based on appropriate plant-specific containment design parameters and initial conditions and will simulate accordingly engineered safety features and installed systems capable of affecting the containment pressure including their actuation, performance, and associated processes. The following specific limitations will apply for Region II analyses using the FSLOCA EM: [

] ^{a,c} (2) an acceptable plant-specific

FULL SPECTRUM and FSLOCA are trademarks of Westinghouse Electric Company LLC, its subsidiaries and/or its affiliates in the United States of America and may be registered in other countries throughout the world. All rights reserved. Unauthorized use is strictly prohibited. Other names may be trademarks of their respective owners.

initial containment temperature will be determined based on input from the utility for the purpose of modeling the containment pressure response with COCO; (3) unqualified or indeterminate coatings throughout containment and qualified coatings within the break jet zone-of-influence will not be credited for the purpose of modeling the containment pressure response using COCO consistent with the bounding treatment of this parameter (conservatively low containment pressure).

Draft Item #4

[

]^{a,c}

Draft Item #5

The maximum assembly average burnup will be limited to []^{a,c} and the maximum peak rod length-average burnup will be limited to []^{a,c} within the FSLOCA EM.

Draft Item #6

In the FSLOCA EM applications for PWR LOCA analyses, an NRC approved version of the PAD 5.0 code will be used as a fuel performance code interfaced with WCOBRA/TRAC-TF2.

Draft Item #7

[

] ^{a,c}

Draft Item #8

[

] ^{a,c}

Draft Item #9

[

] ^{a,c}

[

] ^{a,c}

Draft Item #10

[

] ^{a,c}

Draft Item #11

[

] ^{a,c}

Draft Item #12

[

] ^{a,c}Draft Item #13

[

] ^{a,c}Draft Item #14

Use of the Cathcart-Pawel correlation for oxidation will require the maximum local oxidation limit to be set at 13%.

Westinghouse had no comments regarding draft items 1, 2, 4, 5, 7, 8, 12, and 13. Discussion of draft items 3, 6, 9, 10, 11, and 14 follows.

Draft Limitation and Condition #3

The discussion in the November 2015 meeting was focused on the following aspect of the draft limitation and condition:

[

]^{a,c}

In the meeting, Westinghouse agreed to provide supporting information regarding the removal of this aspect of the draft limitation and condition. That information is provided as follows.

LOTIC2 Code Version

When the Automated Statistical Treatment of Uncertainty Method (ASTRUM) EM [1] was approved, the LOTIC2 code version was 5.0. Due to maintenance of the code, there were two versions (6.0 and 7.0) that were released subsequent to the approval of the ASTRUM EM. The changes that were implemented in Versions 6.0 and 7.0 were reported to the NRC in LTR-NRC-12-37 [2] (LOTIC2 Error Corrections) and LTR-NRC-13-16 [3] (General Code Maintenance), and were estimated to have a negligible impact on peak cladding temperature (PCT) calculations.

The D. C. Cook Unit 2 ASTRUM analysis (transmitted to the NRC in AEP-NRC-2009-23 [4]) utilized LOTIC2 Version 5.0. The LOTIC2 calculation with Version 5.0 (shown on page 26 of Enclosure 2 to AEP-NRC-2009-23) was repeated with Version 7.0, with no changes to the input. The result is presented in Figure 3-1; it can be seen that the [

]^{a,c}

Method to Determine Containment Pressure

For analyses with the ASTRUM EM, there was a step to perform a confirmatory study prior to executing the uncertainty analysis. The transient that resulted in the limiting configuration from the confirmatory study was referred to as the reference transient. The [

]^{a,c} For the D. C. Cook Unit 2 ASTRUM analysis, the WCOBRA/TRAC reference transient input containment pressure and the associated LOTIC2-calculated containment pressure are shown in the figure on page 26 of Enclosure 2 to AEP-NRC-2009-23.

A flow map of the method to calculate the containment pressure for ice condenser containment designs is presented as Figure 3-2. The same method is used for ice condenser containment

designs within the FULL SPECTRUM methodology. Since there is no confirmatory study or “reference transient” in the FSLOCA methodology, a representative transient is used as a surrogate for the ASTRUM reference transient, with key parameters set to minimize the mass and energy releases (hence the containment pressure). For example, the representative transient is based on a low vessel average temperature (less fluid energy) and a maximum steam generator tube plugging (less reactor coolant system (RCS) primary side fluid volume).

Review of Changes in COCO Modeling Assumptions Relative to LOTIC2

During the licensing of the FULL SPECTRUM LOCA EM, there was a Request for Additional Information (RAI) 46 regarding COCO, and several later clarifications regarding the RAI response that were transmitted to the NRC staff. As discussed in the RAI response and subsequent clarifications, a number of changes to the COCO code and modeling assumptions were made either due to the coupling with WCOBRA/TRAC-TF2 or as a result of the licensing process. These changes were reviewed to identify any differences relative to LOTIC2, which are discussed in the following paragraphs.

LTR-NRC-13-73 [5]: Several updates were made to the standalone COCO code in order to couple it with WCOBRA/TRAC-TF2 as described in the letter. The LOTIC2 code is not coupled with WCOBRA/TRAC-TF2 in any way; as such, no such changes were made to the standalone LOTIC2 code.

LTR-NRC-13-73: Generic values were determined for the *end-of-blowdown time* and *integral of break energy released to containment during blowdown* COCO inputs as described in the letter. No such values need be determined by the user for LOTIC2 because the blowdown calculation is different (refer to Sections 2 and 4.1 of the approved LOTIC2 topical report WCAP-8354-P-A, Supplement 1 [6]) and there are no corresponding inputs in LOTIC2.

LTR-NRC-13-73: Consistent with the prior approved best-estimate EMs, [

]^{a,c}

LTR-NRC-14-60: The modeling of paint on containment structures and the initial containment temperature for LOTIC2 will follow the same approach described in LTR-NRC-14-60 for COCO.

LTR-NRC-14-60: The generic end-of-blowdown time and integral of break energy released to containment during blowdown are not applicable to LOTIC2 as discussed under LTR-NRC-13-73.

LTR-NRC-15-70 [8]: The [

]^{a,c}

Example Ice Condenser Containment Pressure Calculation

The LOTIC2 code has no direct interface with the thermal-hydraulic code. The mass and energy releases from the thermal-hydraulic code (WCOBRA/TRAC for the ASTRUM EM or WCOBRA/TRAC-TF2 for the FSLOCA EM) are extracted by the analyst and then entered via tables into the LOTIC2 code. It was previously shown that the current version of LOTIC2 produces the [

] ^{a,c}

As previously mentioned, the D. C. Cook Unit 2 WCOBRA/TRAC reference transient input containment pressure and the associated LOTIC2-calculated containment pressure are shown in the figure on page 26 of Enclosure 2 to AEP-NRC-2009-23 for the ASTRUM analysis. This figure has been included herein as Figure 3-3.

The process previously outlined was used to determine an appropriate containment pressure boundary condition for WCOBRA/TRAC-TF2 within the FSLOCA EM. A WCOBRA/TRAC-TF2 transient with conditions as similar to the ASTRUM reference transient as reasonably achievable was used (recognizing that there will be some differences in the mass and energy releases from the ASTRUM case). A comparison of the assumed WCOBRA/TRAC-TF2 containment pressure boundary condition versus the LOTIC2-calculated containment pressure is given in Figure 3-4. It can be seen that [

] ^{a,c}

Additional Information from January 2016 Discussion

1) Initial Containment Pressure: The initial containment pressure for the results presented in Figure 3-4 was set to [] ^{a,c} psia simply for consistency with the initial pressure analyzed in the ASTRUM analysis (presented in Figure 3-3). However, for analyses with the FSLOCA EM, the containment pressure will be initialized as described in Appendix A, Section A.1, Item I.A. of WCAP-8339 [21] (discussion is applicable for both COCO and LOTIC2 as identified at the beginning of the appendix). Specifically, the [

] ^{a,c}

2) Increase in Calculated Containment Pressure During Transient: It was observed that the LOTIC2-calculated containment pressure presented in Figure 3-4 based on WCOBRA/TRAC-TF2 (for the FSLOCA methodology) increases from about 40 to 80 seconds. This increase is primarily due to the injection of the accumulators. The accumulator injection is capable of pushing liquid into the bottom of the core, which then contacts the hot fuel rods and generates steam. This steam causes a re-pressurization in the reactor coolant system and results in additional mass and energy release into containment. Additionally, and perhaps even more

important, is that once the accumulators empty, the non-condensable cover gas enters into containment.

A sensitivity case was executed with LOTIC2 where the only difference from the result presented in Figure 3-4 was to not model the injection of the accumulator cover gas into containment (the mass and energy releases were not modified, as it is not easy to separate the contribution from the accumulators). The resulting LOTIC2-calculated containment pressures from the base case and the sensitivity study are compared in Figure 3-5. It can be seen that the LOTIC2-calculated containment pressure for the sensitivity study without the accumulator cover gas modeled does not show the same pressure increase that was observed in the base case, which supports the assertion that the increase in the calculated containment pressure is the result of accumulator injection.

3) Convergence of Results: There was a question during the discussion as to whether convergence has been obtained between the WCOBRA/TRAC-TF2 and LOTIC2 codes. It was pointed out that the [

] ^{a,c}

Draft Limitation and Condition #6

In the November 2015 meeting it was discussed that there is an expectation that fuel performance codes would be updated over time to account for new data and potentially new phenomena that were not previously recognized. This draft limitation and condition (as currently written) would restrict the FULL SPECTRUM LOCA evaluation model to an NRC-approved version of the PAD5 code. The concern with the limitation is that it would not allow for the use of newer versions of the PAD fuel performance code which may be reviewed and approved by the NRC.

In the November 2015 meeting, the NRC took an action to modify the restriction in recognition that fuel performance codes will be updated over time. The updated language would allow the use of newer PAD versions which are reviewed and approved by the NRC.

In revising the draft limitation and condition, it is requested that implementation of the draft limitation and condition be considered from the perspective that review of plant-specific LOCA submittals as well as methodology topical reports can both span several years. As such, the limitation and condition should accommodate plant-specific analysis submittals which use a prior approved version of the PAD fuel performance code, should a newer PAD version be approved during the review of the plant analysis submittal.

Draft Limitation and Condition #9

In the November 2015 meeting, Westinghouse discussed that this draft limitation and condition should be removed based on supplemental information which would be provided to the NRC, and similarities of the effect of the parameters studied across various plant classes. The NRC noted that certain plant classes have unique features and questioned whether the information based on a Westinghouse-designed 3-loop pressurized water reactor (PWR) may be different for other plant classes. Upon further consideration, Westinghouse agrees that the draft limitation with respect to the model uncertainty contributors is appropriate for plant classes other than Westinghouse-designed 3-loop PWRs. As such, Westinghouse does not request the removal of this draft limitation and condition. Rather, Westinghouse proposes several modifications to the draft language [

J^{a,c}

[

] ^{a,c}

Break Area Sampling, Background

In order to provide context around the sensitivity studies that were executed regarding the break size sampling, some background is first provided regarding the break sampling approach within the FSLOCA EM.

[

] ^{a,c}

[

] ^{a,c}

¹ The effect of sampling the break discharge coefficients was assessed because they directly influence the sampled break area, resulting in what is generally referred to as the “effective break area”. The impact of sampling these uncertainties is described in 29.1.1 of WCAP-16996-P, Revision 1.

[

] ^{a,c}**Break Area Sampling, Sensitivity Studies**

Given that background, additional break area sampling sensitivity studies were executed based on the Region I demonstration analysis in WCAP-16996-P, Revision 1 [12] (the same studies which were previously discussed in the context of the [

] ^{a,c}

[

] ^{a,c}

The peak cladding temperature from the limiting transient for each sensitivity study with biased uncertainty parameters is shown in Figure 9-4, with the time scale shifted such that boiloff uncover starts at the same time for all 4 transients. It can be seen that the [

] ^{a,c}

Less Prescriptive Means to Demonstrate Uncertainty Parameter Sensitivities

The current language in the draft limitation and condition is very prescriptive. It would preclude the use of parametric sensitivity studies, or other means of being able to assess the sensitivity of the uncertainty contributors individually. As such, it is requested that the language be written in a manner that is less prescriptive for how to demonstrate the desired sensitivities.

Conclusion

[

] ^{a,c}

The topical report will be updated prior to issuing the approved version to reflect this change.

Draft Limitation and Condition #10

The discussion in the November 2015 meeting focused on three different aspects of the draft limitation and condition.

- 1) First, it was discussed that this limitation and condition should not apply to Westinghouse-designed 3-loop plants since it was already demonstrated as part of the methodology licensing. Additional information is also provided herein relative to the three-loop Westinghouse designed plant.

[

] ^{a,c}

3) Third, Westinghouse requested [

]^{a,c}

Draft Limitation and Condition #11

The following was proposed after the November 2015 discussion with the NRC.

The FSLOCA EM uncertainty methodology is described in Section 30 of the topical report (WCAP-16996-P, Revision 1). Following the submittal of Revision 1 of the topical report, and in part stemming from an October 7, 2015 meeting between Westinghouse and the NRC, adjustments to the uncertainty methodology were made to [

] ^{a,c} The summary of the meeting and these updates were provided in LTR-NRC-15-88 [13].

In general, the FSLOCA EM uncertainty methodology relies on non-parametric order statistics, [

] ^{a,c} The population of calculated results arises from the geometric model of the PWR being analyzed, the predictive tool (WCOBRA/TRAC-TF2), and the various uncertainty contributors and their associated distributions. Uncertainty contributors include the postulated accident scenario and boundary conditions, plant initial conditions, and code or model uncertainties.

Because it is impractical to fully resolve the population of predicted results, manageable sample sizes are used to make a bounding estimate of the 95th quantile. Assuring that this bounding estimate of the 95th quantile for each of the outcomes meets its acceptance criterion, and since the population of predictions known to be conservative relative to experimental benchmarks, "high probability" is assured that the acceptance criteria would be met in the event of an accident.

A consequence of making only a bounding prediction is that a confidence level must be specified. In the FSLOCA EM, consistent with prior licensed EMs, a 95% confidence level is used; in each analysis, it is assured with 95% confidence that the bounding prediction succeeds and bounds the true 95th quantile of the population of predicted results. The bounding predictor is referred to as the 95/95 predictor.

[

] ^{a,c}

- [

] ^{a,c}

[

] ^{a,c}

The topical report will be also be updated prior to issuing the approved version to reflect this change.

In the January 2016 phone call, the NRC asked for a concise explanation of how Westinghouse would comply with this draft limitation and condition.

[

] ^{a,c}

[

] ^{a,c}

- [

] ^{a,c}

[

]^{a,c}

[

]^{a,c}

- [

] ^{a,c}

Draft Limitation and Condition #14

In the November 2015 discussion, the NRC staff indicated that this limitation stemmed from the use of the Baker-Just correlation to convert the time-at-temperature into equivalent cladding reacted for the data which resulted in the current 10 CFR 50.46 oxidation criterion of 17%. The discussion in RIL 0202 [14] indicated that the use of Cathcart-Pawel considering the same data would result in a limit of approximately 13%. Westinghouse did not agree that this limitation and condition was appropriate for the FULL SPECTRUM LOCA evaluation model, and provided several supporting reasons in the November 2015 discussion. The NRC staff requested that Westinghouse provide those reasons for consideration, which is done in the following paragraphs.

- 1) At beginning-of-life (BOL), NRC-sponsored research indicates that cladding ductility is maintained beyond 17% Cathcart-Pawel (CP) equivalent cladding reacted (ECR). The NRC has sponsored post-quench ductility (PQD) testing at Argonne National Laboratory (ANL) in support of the 10 CFR 50.46c rulemaking. A summary of the results from this testing is presented on page 40775 of the Federal Register [15]. It can be seen that at BOL, cladding ductility is maintained for data points up to roughly 20% CP-ECR. A ductile-to-brittle CP-ECR level was presented in Figure 2 of the update to RIL 0801 [16], which shows a transition of just over 18% at BOL. Finally, an acceptable analytical limit for CP-ECR presented in Figure 2 of a draft of RG 1.224 [17] is 18% CP-ECR at BOL.
- 2) After beginning-of-life, the upper bound, steady-state corrosion accounted for in the FSLOCA EM is transparent to the correlation used to translate the LOCA transient time-at-temperature to an ECR. Prior Westinghouse best-estimate LOCA EMs only accounted for the LOCA transient oxidation when comparing against the 17% acceptance criterion. However, for the FSLOCA EM, the sum of the LOCA transient oxidation and the upper bound steady-state corrosion is compared against the current 10 CFR 50.46 acceptance criterion of 17% consistent with the recommendation in IN 98-29 [18]. The contribution of the steady-state corrosion, which []^{a,c} (e.g. Figure 31.4-6 of WCAP-16996-P, Revision 1), is transparent to the selection of the correlation used to convert the transient time-at-temperature to an ECR. The comparison of the total oxidation to anything other than a 17% acceptance criterion is inconsistent with the guidance in IN 98-29 regarding the treatment of the pre-existing corrosion.
- 3) The current regulation (10 CFR 50.46) does not require the use of Baker-Just for best-estimate EMs, and regulatory guidance indicates the use of Cathcart-Pawel for best-estimate EMs is acceptable. A review of the 10 CFR 50.46 regulation indicates that the use of Baker-Just is required for Appendix K EMs. However, there is no stated requirement to use the Baker-Just correlation for best-estimate EMs in the regulation. A review of associated Regulatory Guide (RG) 1.157 indicates that the use of Cathcart-Pawel is acceptable under certain conditions. As such, the regulatory guidance associated with LOCA analysis supports the use of the Cathcart-Pawel correlation.

- 4) The NRC has previously found acceptable and approved best-estimate LOCA EMs which use correlations such as Cathcart Pawel (or other correlations besides Baker Just) to convert the transient time-at-temperature into an ECR and then compare against a 17% oxidation criterion.
- 5) The 17% versus 13% is based on LOCA transient oxidation at 2,200°F. The use of 13% as mentioned in RIL 0202 versus the 17% acceptance criterion is believed to be specific to the conversion of LOCA transient time-at-temperature to ECR based on oxidation at 2,200°F. A comparison of the Baker-Just weight gain normalized to Cathcart-Pawel is presented in Figure 2 of an Argonne National Laboratory report from June 2002 [19]. At 2,200°F, the ratio of Baker-Just to Cathcart-Pawel weight gain is about 1.3 to 1 (17% / 1.3 = ~13%). As the oxidation temperature decreases from 2,200°F the two correlations begin to converge (i.e., the difference becomes smaller). The [

J^{a,c}

Proposed Updates to Select Limitations and Conditions

This section contains the proposed updates to the draft limitations and conditions based on the previous discussion in this letter. Additions are shown in **blue, bolded text** and removals are shown in **red text** with strikeouts.

Draft Item #3

[

]^{a,c}

Draft Item #6

NRC action

Draft Item #9

[

]^{a,c}

[

]^{a,c}

Draft Item #10

[

]^{a,c}

Draft Item #11

Propose replacement of draft limitation and condition with the following

[

]^{a,c}

Draft Item #14

Propose replacement of draft limitation and condition with the following, which has the same intent as the NRC-proposed wording but more detail for completeness:

[

] ^{a,c}

References

- 1) WCAP-16009-P-A, "Realistic Large-Break LOCA Evaluation Methodology Using the Automated Statistical Treatment Of Uncertainty Method (ASTRUM)," January 2005.
- 2) LTR-NRC-12-37, "10 CFR 50.46 Annual Notification and Reporting for 2011," July 9, 2012.
- 3) LTR-NRC-13-16, "10 CFR 50.46 Annual Notification and Reporting for 2012," April 1, 2013.
- 4) AEP-NRC-2009-23, "License Amendment Request Regarding Large Break Loss-of-Coolant Accident Analysis Methodology," March 19, 2009 (ADAMs accession # ML090930453).
- 5) LTR-NRC-13-73, "Submittal of Westinghouse Responses to 'WCAP-16996-P, 'Realistic LOCA Evaluation Methodology Applied to the Full Spectrum of Break Sizes (FULL SPECTRUM LOCA Methodology)' Request for Additional Information - RAIs 46 – 58, 75 and 77' (Proprietary/Non-Proprietary), Project 700, TAC No. ME5244," October 28, 2013.
- 6) WCAP-8354-P-A, Supplement 1, "Long Term Ice Condenser Containment Code – LOTIC Code," April 1976.
- 7) LTR-NRC-14-60, "Summary of August 2014 NRC Audit Part 1 of the FULL SPECTRUM LOCA (FSLOCA) Evaluation Model" (Proprietary/Non-Proprietary), Project 700, TAC No. ME5244," September 17, 2014.
- 8) LTR-NRC-15-70, "Summary of June 2015 NRC Audit Part 2 of the FULL SPECTRUM LOCA (FSLOCA) Evaluation Model (Proprietary/Non-Proprietary)," September 16, 2015.
- 9) LTR-NRC-13-70, "Summary of July 2013 NRC Code Workshop and August 2013 NRC Audit of the FULL SPECTRUM LOCA (FSLOCA) Evaluation Model (Proprietary/Non-Proprietary)," October 10, 2013.
- 10) WCAP-16996-P, Revision 0, "Realistic LOCA Evaluation Methodology Applied to the Full Spectrum of Break Sizes (FULL SPECTRUM LOCA Methodology)," November 2010.
- 11) LTR-NRC-14-29, "Summary of May 2014 NRC Audit of the FULL SPECTRUM LOCA (FSLOCA) Evaluation Model (Proprietary/Non-Proprietary), Project 700, TAC No. ME5244," June 5, 2014.
- 12) WCAP-16996-P, Revision 1, "Realistic LOCA Evaluation Methodology Applied to the Full Spectrum of Break Sizes (FULL SPECTRUM LOCA Methodology)," 2015.
- 13) LTR-NRC-15-88, "Summary of October 2015 NRC Audit of the FULL SPECTRUM LOCA (FSLOCA) Evaluation Model (Proprietary/Non-Proprietary)," October 12, 2015.
- 14) Research Information Letter 0202, "Revision of 10 CFR 50.46 and Appendix K," June 20, 2002.

- 15) Federal Register, Volume 74, Number 155, "Proposed Rules: Performance-Based Emergency Core Cooling System Acceptance Criteria," August 13, 2009.
- 16) Letter from B. W. Sheron to E. J. Leeds and M. R. Johnson, "Update to Research Information on Cladding Embrittlement Criteria in 10 CFR 50.46," December 29, 2011(ADAMS accession ML113050484).
- 17) RG 1.224 (Preliminary Draft), "Establishing Analytical Limits for Zirconium-Alloy Cladding Material," 2015 (ADAMS accession ML15281A192).
- 18) Information Notice 98-29, "Predicted Increase in Fuel Rod Cladding Oxidation," August 3, 1998.
- 19) Letter from M. C. Billone to H. H. Scott, "Steam Oxidation Kinetics of Zirconium Alloys," June 2002 (ADAMS accession ML021680052).
- 20) NUREG-1475, Revision 1, "Applying Statistics," March 2011.
- 21) WCAP-8339, "Westinghouse Emergency Core Cooling System Evaluation Model – Summary," June 1974.
- 22) WCAP-12610-P-A & CENPD-404-P-A, Addendum 2-A, "Westinghouse Clad Corrosion Model for ZIRLO and *Optimized ZIRLO*," October 2013.
- 23) LTR-NRC-15-82, "Summary of September 2015 NRC Audit of the FULL SPECTRUM LOCA (FSLOCA) Evaluation Model (Proprietary/Non-Proprietary)," September 28, 2015.
- 24) LTR-NRC-13-40, "Submittal of Westinghouse Responses to 'WCAP-16996-P, 'Realistic LOCA Evaluation Methodology Applied to the Full Spectrum of Break Sizes (FULL SPECTRUM LOCA Methodology)' Request for Additional Information' (Proprietary/Non-Proprietary), Project 700, TAC No. ME5244," June 13, 2013.

Figure 3-1: Comparison of Containment Pressure from LOTIC2 Version 5.0 and 7.0 with Identical Inputs



Figure 3-2: Process for Calculating Containment Pressure for Ice Condenser Containment

a,c

Figure 3-3: Figure 17 from AEP-NRC-2009-23, D. C. Cook Unit 2 ASTRUM Analysis Containment Pressure Comparison

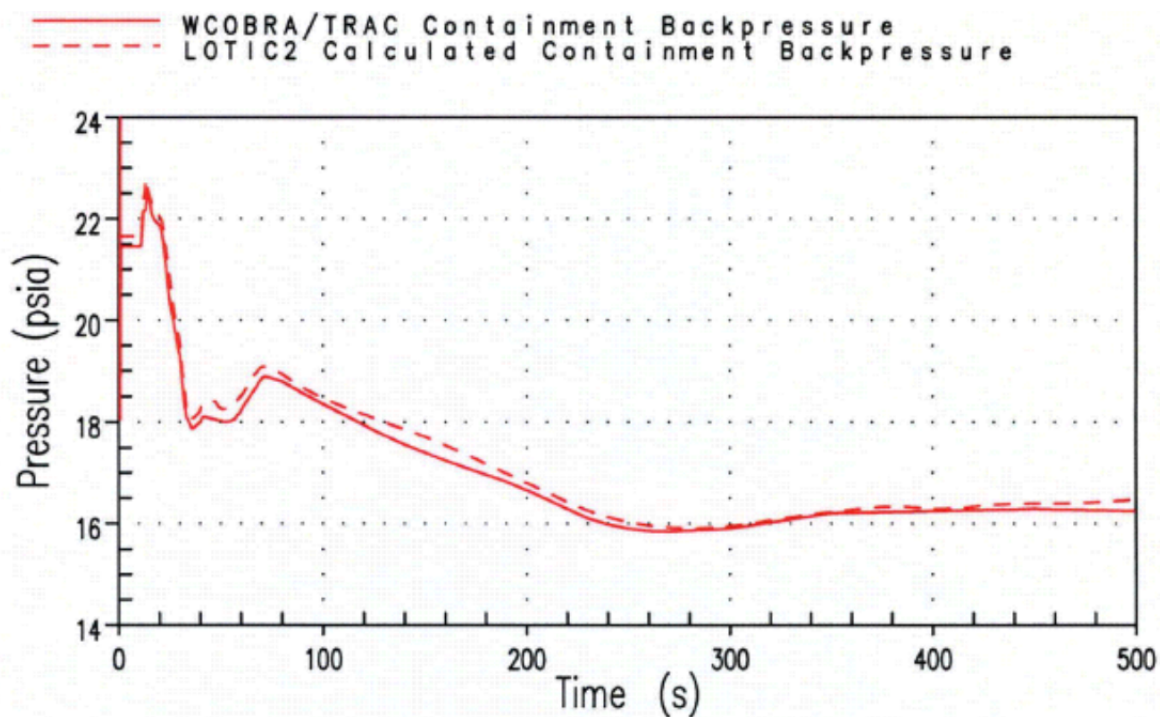


Figure 3-4: D. C. Cook Unit 2 Containment Pressure Comparison with Mass and Energy Releases from WCOBRA/TRAC-TF2

a,c

Figure 3-5: Comparison of LOTIC2-Calculated Containment Pressure with and without Accumulator Cover Gas Modeled

a,c

a,c

Figure 3-7: Comparison of WCOBRA/TRAC-TF2 Containment Pressure Boundary Condition and LOTIC2-Calculated Containment Pressure for All Three Iterations

a,c

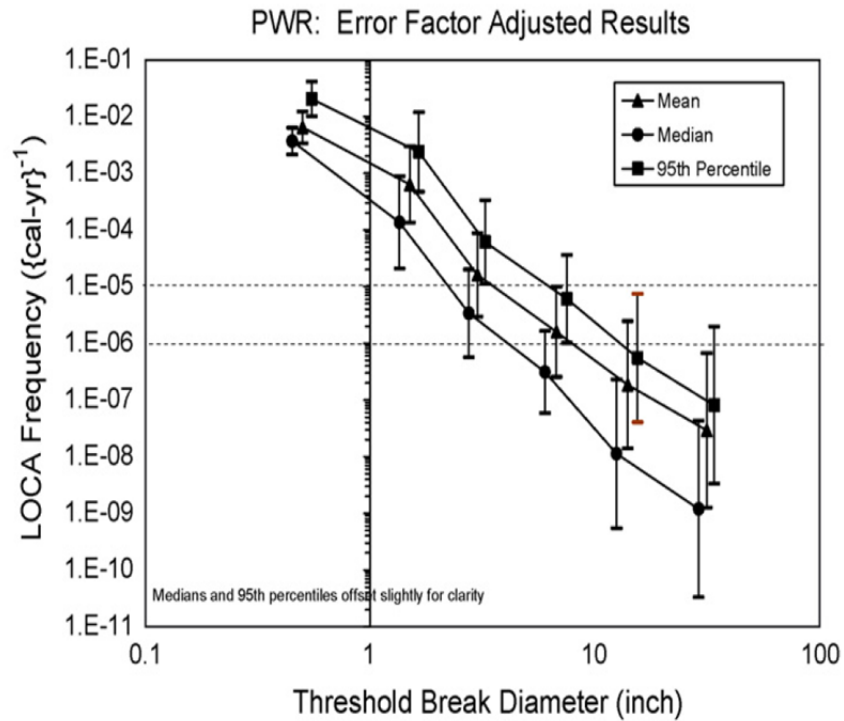
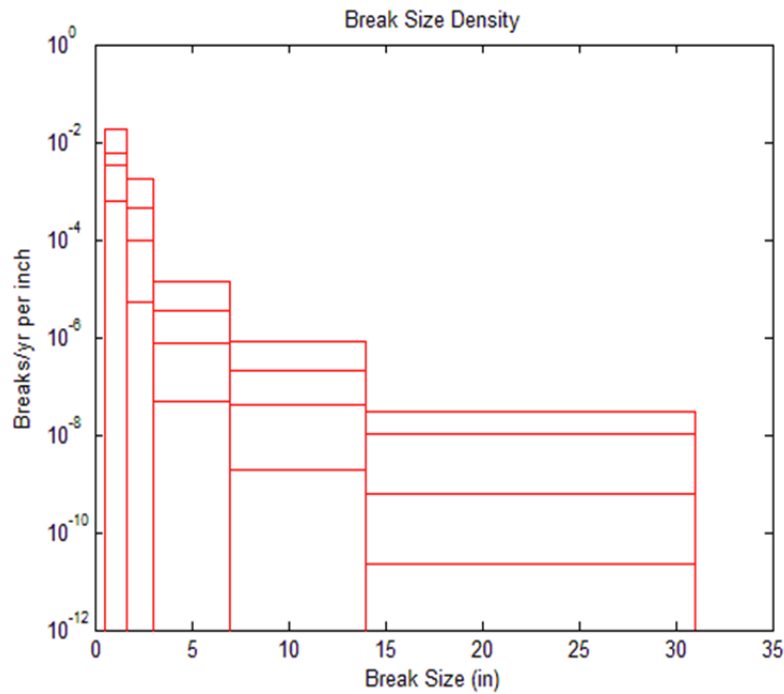
Figure 9-1: Figure 7.37 of NUREG-1829 V1**Figure 9-2: From Los Alamos National Lab presentation, May 9, 2012 ACRS transcripts**

Figure 9-3A: Analysis Peak Cladding Temperature for Region I Studies with Different Break Area Sampling Ranges Compared to the Region I Break Spectrum Study

a,c

Figure 9-3B: Average Transient Peak Cladding Temperature for Region I Studies with Different Break Area Sampling Ranges

a,c

Figure 9-4: Peak Cladding Temperature for the Limiting Transient from Each Break Area Sampling Sensitivity Study with [

]^{a,c}

^{a,c}

Figure 10-1: Peak Cladding Temperature vs. Break Diameter
(Figure 4-1 from LTR-NRC-14-29)



Figure 10-2: Peak Cladding Temperature vs. Time for a Resonance Region Break and a Larger Diameter Break (Figure 4-2 from LTR-NRC-14-29)



Figure 10-3: Peak Cladding Temperature vs. Effective Break Diameter from Demonstration Analysis



Figure 10-4: Peak Cladding Temperature vs. Time for the Limiting Region I Break, Several Smaller Region II Breaks, and the Limiting Region II Large Break

a,c

Figure 11-1: Illustration of Perceived Concern

Figure 11-2: Result Not Demonstrating Compliance

a,c

Figure 11-3: Result Demonstrating Compliance

a,c

Figure 11-4 – Predicted [

]^{a,c}

^{a,c}

Proprietary Markings and Comments on the Draft Safety Evaluation for WCAP-16996-P/WCAP-16996-NP, Volumes I, II and III, Revision 1, 'Realistic LOCA Evaluation Methodology Applied to the Full Spectrum of Break Sizes (FULL SPECTRUM LOCA Methodology) (Non-Proprietary)

April 2016

Westinghouse Electric Company LLC
1000 Westinghouse Drive
Cranberry Township, PA 16066

©2016 Westinghouse Electric Company LLC
All Rights Reserved

1.0 Editorial Comments

Page	Line	Comment
i,ii,iii	-	Page numbers in table of contents are incorrect
2	22	of → Of (the 'O' is capitalized in the ASTRUM TR title)
3	8	<u>W</u> COBR/TRAC → <u>W</u> COBRA/TRAC (missing an 'A')
6	20	regulations → regulation
7	31-34	Font and character spacing looks different than rest of document
8	10	50 50.46 → 50.46
10	2	...describes uncertainty determination <u>and</u> provides...
10	16	2003 → 2007
11	7	June → March (date on approved version of CQD TR is March 1998)
11	15	bellow → below
12	4-5	and in <u>a subset of</u> the currently approved
18	2	Summary for item 10: suite → suit
20	2	SBLOCA (ROSA) → SBLOCA (ROSA, LOFT)
22	36	August 13-15 → August 12-15
22	40	of the of the → of the (remove duplicate instance)
24	14	RAI No. 45 was issued to Westinghouse as part of NRC RAI Set No. 4 as opposed to being issued individually
25	3	NRC RAI Set No. 4 included RAIs No. 36 through No. 45 (as opposed to only No. 44)
27	16	Some listed RAIs are double-counted; for example, current list includes 58-71, 63, 65-77. Westinghouse calculates the total number of RAIs as 69 with the double counting removed.
28	6	There is an excess space in LTR-NRC-14-55 between 'NRC-' and '14' in the second column of the tables
30	3	There is an excess space in LTR-NRC-14-55 between 'NRC-' and '14' in the second column of the tables
31	4	There is a space missing between 'Revision' and '1' in the last row, fourth column of the table
37	9	The LOFT facility was also initially selected for SBLOCA (in addition to the ROSA facility).
37	41	Full Spectrum → FULL SPECTRUM
38	33	24 → 23 (Revision 0 of the TR had erroneously numbered the table items which was corrected in Revision 1, but the total number was 23 in both revisions)
40	25	"justified on <u>a</u> case by case basis..." <u>a</u> was added in Rev.1
41	42	WCAP-16996-P\WCAP-16996-NP → WCAP-16996-P\WCAP-16996-NP
42	46	Table A-I → Table A-1
42	47	Tables I-I → Tables 1-1 and A-I → A-1
43	14	"... phase <u>of</u> a LBLOCA ..."

Page	Line	Comment
43	44,46	SETs and IETs → SET and IET facilities
43	49	raw → row
44	2	The ASTRUM EM TR is WCAP-16009-P-A
45	7	COBRA/TRAC-TF2 → <u>W</u> COBRA/TRAC-TF2
45	30	LTR-NRC-14-17 → LTR-NRC-14-70
47	11	CQD methodology → and CQD methodologies
48	5	ASTRUM CQD EM → ASTRUM and CQD EMs
48	28	“... well compared <u>to</u> test data ...”
48	36	1,000 → 1,000 psia
49	8	that that → that (remove duplicate instance)
49	31	Referenced ‘Section 4.2.2.4 in this SE’ does not exist
49	44	ASTRUM-FS → the FSLOCA™ EM
49	44	ASTRUM CQD EM → ASTRUM and CQD EMs
51	2	... necessary for understanding the basis... (remove first ‘the’)
51	50	“50.46 and Appendix K” → “50.46 Appendix K”
52	4	liming → limiting
53	33	one facility, ROSA-IV → two facilities, ROSA-IV and LOFT
53	35	eight → ten (9 ROSA-IV and 1 LOFT = 10)
53	36	900°F → 940K (1,232°F)
54	4	No attached figures (as referenced in text) were found
55	42	ASTRUM CQD EM → ASTRUM EM
56	15	LTR-NRC-15-50 → LTR-NRC-15-70
56	27	ASTRUM CQD EM → ASTRUM EM
56	28,29	LOTIC → LOTIC2
57	6	ASTRUM CQD EM → ASTRUM EM
58	17	Open Times → Open Items
58	22	Open them → Open Items
60	33	expensive → extensive
62	16	<u>W</u> COBR/TRAC-TF2 → <u>W</u> COBRA/TRAC-TF2 (missing an ‘A’)
62	17	it → its
62	23	4.2.1 → 4.3
62	40	SEMCA-2005-323 → SEMCA-2005-313
62	49	temperate → temperature
63	41	assigned a power → assigned power (remove ‘a’)
63	42	represent → represented
64	37	24.4.1-1 → 29.4.1-1
65	18	though → through
65	45	supresses → suppress
65	49	June 3-4, 2014 → August 6-8, 2014
66	1	May 12-13, → May 12-13, 2014,
66	10	update <u>to</u> employ

Page	Line	Comment
66	27	Remove the word “parameter”
66	39	RIAs → RAIs
68	33	Center “Small Bubble” in first cell of second row of table 15
69	7	“The selected tests cover a ...”
69	9	TNTF → THTF
71	35	horizontal SI injection → with a 45° injection angle
71	39	[(UPTF)] → (UPTF)
71	42	Westinghouse Vertical COSI Test Facility → High-Pressure Cold Leg Condensation Test Facilities
71	43	cm → m (first column, third row of table)
72	-	cm → m (first column, first row of table on this page)
73	31	Delete “COSI”
75	12-13	“... to the latter criterion with the gas phase velocity being replaced by the relative velocity at lower void fractions.” → “... to the latter criterion at lower void fractions with the gas phase velocity being replaced by the relative velocity.”
75	33	0.7 m → 0.295 m (this correction was shown on page P-80 of LTR-NRC-15-91)
77	2	FSLOCA ^{TR} → FSLOCA TM
77	5	Unit 1that → Unit 1that
77	33	transitioning to stratified → transitioning from stratified
78	12	Sections 28.2.12 29.1.7 → Sections 28.2.12 and 29.1.7
80	30	RAI Nos. 98, 90, and 91 → RAI Nos. 89, 90, and 91
80	35	RAI Nos. 88 through 91 → RAI Nos. 88 through 92
82	5	WCOBR/TRAC → WCOBRA/TRAC (missing an ‘A’)
82	40	pp.1773-1997July, 1997 → pp. 1753-1793, May 1997
85	19	request → requested
85	22	LTR-NRC-13-33 → LTR-NRC-13-73
87	10	EM ASTRUM → ASTRUM EM
87	25	uncover → uncover
87	38	upper limiting break size → upper limit of break sizes
87	45	Region II → Region I
87	46	Region I → Region II
87	51	for the for the → for the (remove duplicate instance)
88	4	“... 2.1 percent of CL area for 3-loop plants.”
88	39	other that a DEG → other than a DEG
90	32	reflected → reflecting
90	38	Delete “were”
91	17	NRC-LTR-13-37 → LTR-NRC-13-37
91	39	analyses → calculations
91	47	(KCOSI), → (KCOSI,
91	48	(HS_SLUG), → (HS_SLUG,

Page	Line	Comment
91	49	(SPV1 and SPV2), → (SPV1 and SPV2,
91	50	(PACC), → (PACC,
92	42	“The NRC staff finds the proposed...”
93	24	the sample size → the minimum sample size
94	12	reelects → reflects
94	49	in a in a → in a (remove duplicate instance)
96	40	NRC-LTR-15-82 → LTR-NRC-15-82
98	17	Delete “in the table”
98	39	settled in → settled on
100	-	tract → track (in draft L&C number 1)
101	-	<u>W</u> COBR/TRAC-TF2 → <u>W</u> COBRA/TRAC-TF2 (missing an ‘A’)
105	5	cold leg side injection → cold leg injection
105	7	is → are
106	-	Several WEC TR review documents cited on pages 26-31 (Tables 8-13) in the draft safety evaluation are missing from the reference list.
107	1-5	LTR-NRC-13-42 was not referenced in the draft safety evaluation, but is included in the reference list.
108	4-7	This document was not referenced in the draft safety evaluation, but is included in the reference list.
108	-	WCAP-10079-P-A / WCAP-10080-A and WCAP-14449-P-A, Revision 1 should be added to the list of WEC Technical Documents section since they are cited in the draft safety evaluation (e.g. in Tables 2 and 3).
108	-	RIL 02-02 and NUREG-1230 should be added to the list of U.S. NRC Technical Documents since they are cited in the SE.

The 'W' in WCOBRA/TRAC and WCOBRA/TRAC-TF2 should be underlined in all instances. Noted places missing the underline are:

PiiL38	P2L23	P2L25	P3L8	P18L2 (x2)
P33L40	P33L44	P34L8	P34L12	P34L13
P36L24	P38L25	P39L51	P41L24	P45L5
P53L31	P53L42	P53L47	P54L6	P56L37
P59L42	P62L12	P62L16	P62L18	P70L38
P75L7	P78L45	P80L22	P80L39	P80L48
P81L30	P81L35 (x2)	P81L48	P82L5	P82L7
P82L11	P82L29	P101 (x2)	P103	

PAD5 should be referred to as such in all instances, rather than PAD 5.0. Noted places include:

P61L39	P61L40	P61L45	P61L49	P62L2 (x2)
P62L9	P101 (x2)			

At least the first instance of the AP1000 plant should be referred to as the AP1000[®] plant, since it is a registered trademark of Westinghouse Electric Company. Noted instances of the AP1000 plant include:

P3L17 (x2) P12L2 (4th row, 7th column)

At least the first instance of ZIRLO cladding should be referred to as ZIRLO[®] cladding, since it is a registered trademark of Westinghouse Electric Company. In several places ZIRLO cladding is cited as a trademark as opposed to a registered trademark. Noted instances of ZIRLO cladding include:

P5L23	P62L51	P63L3	P63L7	P63L28
-------	--------	-------	-------	--------

Optimized ZIRLO[™] cladding was correctly marked throughout the entire document.

The audit which occurred in August 2014 is in some places cited as 'August 6-7, 2014,' and in other places as 'August 7-8, 2014.' According to Westinghouse records the audit occurred from August 6-8, 2014. The cited dates should be consistent throughout the document. Noted instances of the cited dates include:

P22L37	P22L40	P28L6 (x4)	P29L3 (x2)	P30L3 (x2)
P56L5	P57L39	P58L1	P60L27	P61L10
P67L7	P67L8	P73L14	P77L12	P77L17
P79L48	P80L29	P85L25		

2.0 Factual Comments

Page	Line	Comment
2	25	Suggest replacing “extends the applicability of the <u>W</u> COBRA/TRAC code” to “replaced the 1D portion of the code, and extends the applicability of the resulting WCOBRA/TRAC-TF2 code”
3	2	The following large break EMs are missing from Table 1: 1981 EM (Appendix K EM) WCAP-10266-P-A, Revision 2 with BASH code CQD (BE EM) WCAP-12945-P-A, <u>W</u> COBRA/TRAC MOD7A Rev.1
3 12 13 18	2 2 2 2	The frozen code associated with the FULL SPECTRUM LOCA evaluation model is <u>W</u> COBRA/TRAC-TF2 Version 1.3 as identified on page 2-52 of WCAP-16996-P, Volume I, Revision 1. <u>W</u> COBRA/TRAC-TF2 Version 1.1 was the as-submitted version.
24	10,12	There are references to Appendices A and B which do not appear to be included in the draft safety evaluation.
47	11	‘and removing’ → ‘in lieu of using’; the TRAC vessel component technically still exists in the code, but it is not used as part of the FSLOCA EM.
56	28-30	Westinghouse did not couple the LOTIC2 code with <u>W</u> COBRA/TRAC-TF2, but has included LOTIC2 within the FSLOCA EM, utilized in a similar manner as the ASTRUM EM.
65	20,22	“TS” should be removed before each instance of FQ owing to the fact that the [] ^{a,c}
67	31-32	“In addressing RAI Nos. 72 through 72, nodding sensitivity results for ORNL THTF and G2 tests.” The cited RAI numbers appear to be incorrect, and the sentence does not appear to be complete. It is believed that the sentence was intended to read as: In addressing RAIs Nos. 59 through 71, nodding sensitivity results for ORNL THTF and G2 tests were presented.
67	45-47	The 3 changes cited on lines 43 through 50 were all implemented into the code at the time of the cited audit. However, after that audit, it was discovered that only the first and third changes were required to remedy the unwanted behavior in the level swell predictions. As such, the second change was removed from the code downstream of the audit. Revision 1 of the topical report was updated to reflect the first and third changes (including model descriptions, validation, plant application, etc.), but the second change was absent from the updates.
82	19	The [] ^{a,c}

Page	Line	Comment
87 91 92 92	24-26 31-35 13-17 33-35	The cited pages and lines in the draft SER indicate that the [] ^{a,c} (refer to page P-17 of LTR-NRC-15-102, Revision 2.) As such, the discussion on the cited pages and lines should be updated to reflect the finalized approach.
89	1-5	The discussion leading to limitation and condition #10 should reflect the 1 ft ² limitation for the lower end of the Region II break area sampling (which is consistent with the approved ASTRUM EM).
97	14 to 47	Westinghouse understands that the NRC staff found the proposed approach for Region II offsite power availability to be unacceptable; however, the proposed approach is mischaracterized on the cited page and lines in several regards. Given that the proposed approach is superseded in its entirety by limitation and condition 15, Westinghouse suggests removing the cited text from the draft SER to eliminate the mischaracterizations.
100	5-6	“Table 22 also includes references to sections of this SE where the individual limitations and conditions were introduced.” No evidence of these references was found in Table 22.

The text for a number of the draft limitations and conditions (1, 2, 3, 6, 8, 10, 11, 15) in the body of the draft SER was inconsistent with Table 22. Suggest updating the text of the draft limitations and conditions in the body of the SER to exactly match that in Table 22.

3.0 Clarifications

Page	Line	Clarification
3	35	It is clarified that the 2-loop UPI and CE extension of the FSLOCA EM may be pursued with an addendum or on a plant-specific basis. As such, “in a future revision” would be better characterized as “in the future.”
6	37	“This is based on the Baker-Just equation” is taken to mean for use in converting the time-at-temperature to ECR.
38	37-39	In Table 32-1 of Revision 0 of the topical report, all 23 phenomena groups were assigned reasonable agreement. However, in Revision 1 of the topical report, 21 of the 23 phenomena groups were assigned reasonable agreement while the other two phenomena groups (Items 1 and 4) were assigned excellent agreement. Item No. 14 is “Spilling Flow Treatment (Pumped SI)” and Item No. 23 is “Containment Pressure” in Revision 1 of the topical report.
51	16	The passage from pg. 51, line 16 to pg. 55, line 15 is incorporated from the “white paper” without adjustment for context. The passage is written as though the issues have not been addressed, although the issues have been addressed and the analysis methodology has been updated. The text which is extracted from the “white paper” should be delineated from the surrounding text, and it should be acknowledged that the final methodology, which was updated to address the cited issues, is not entirely consistent with the discussion extracted from the “white paper.”
63	34	It is clarified that the design limit is intended to be the plant-specific design limit, which is confirmed on a reload basis.
65	22 - 28	It is clarified that the [
68	14-30	It is clarified that the [] ^{a,c} multipliers are applied only to the core region.

Page	Line	Clarification
92	47	It is stated that certain controlling parameters were [<p style="text-align: right;">] ^{a,c} which better characterizes the rationale and is consistent with language elsewhere in the draft SER (e.g. for the decay heat treatment characterization on line 4 of page 93).</p>
94	21	It is clarified that the quote “if the calculated [<p style="text-align: right;">] ^{a,c}</p>
95 96	25 5	The two paragraphs beginning on these lines should be placed before the Limitation No. 11 to be clear on the progression of the methodology licensing leading to Limitation No. 11.
101	-	Based on a phone call with the NRC staff, it was clarified that “maximize the initial fuel stored energy and gap pin pressure” refers to the nominal values, and the uncertainty treatment would proceed as described in revision 1 of the topical report.
105	3-5	The cited statement could be interpreted to mean that the ASTRUM EM has only been applied to Westinghouse 3-loop and 4-loop PWR designs. However, the ASTRUM EM has been successfully utilized for 2-loop PWRs equipped with upper plenum injection, advanced plant designs such as the AP1000 [®] plant, and was approved for CE-designed plants.
105	26	The intent of the following text is not clear: “prior to generic application and prior to any specific plant licensing application...” Changes to the FSLOCA EM may be justified for application either on a generic or a plant-specific basis. In either case, “the process and all of its elements, including a description of its intended use and justification,” would be submitted for review and approval.

AP1000 is a registered trademark of Westinghouse Electric Company LLC, its subsidiaries and/or its affiliates in the United States of America and may be registered in other countries throughout the world. All rights reserved. Unauthorized use is strictly prohibited. Other names may be trademarks of their respective owners.

Proprietary Markings and Comments on the Draft of the Final Safety Evaluation for WCAP-16996-P/WCAP-16996-NP, Volumes I, II and III, Revision 1, 'Realistic LOCA Evaluation Methodology Applied to the Full Spectrum of Break Sizes (FULL SPECTRUM LOCA Methodology) (Non-Proprietary)

August 2016

Westinghouse Electric Company LLC
1000 Westinghouse Drive
Cranberry Township, PA 16066

©2016 Westinghouse Electric Company LLC
All Rights Reserved

Westinghouse reviewed the draft of the final SER for proprietary information, and found several instances where information is considered proprietary but is not marked as such. This information has been identified in the attachment to this letter using track changes.

During Westinghouse review of the draft of the final SER for proprietary information, several inconsistencies within the SER were discovered. These inconsistencies are as follows (along with associated SER page numbers):

Incorrect document references: WCAP-16996-P, Revision 2 (page 56) and LTR-NRC-15-201, Revision 2 (page 91). Westinghouse requests that the document references be updated to WCAP-16996-P, Revision 1, and LTR-NRC-15-102, Revision 2, respectively.

Limitations and conditions (L&Cs) in the body of the SER are inconsistent with Table 22: L&C #1 (page 41), L&C #2 (page 41), L&C #6 (page 65), L&C #8 (page 82), L&C #10 (page 93), L&C #11 (pages 98-99), and L&C #15 (page 101). Westinghouse requests that the discussion of the limitations and conditions in the body of the SER be updated for consistency with Table 22.

Inconsistent description of the treatment of break size in Region I: Various passages still state or imply that the [

] ^{a,c} (as is correctly explained in L&C #8). Such statements are made on pages 91, 95, 96 (several places), and as part of L&C #7 (pages 75 and 106).

Lack of clarity regarding excerpt from 'white paper': An excerpt from a 'white paper' (ADAMS Accession No. ML15343A002) was included in the SER, starting on page 51 and ending on page 56. While the final methodology [

] ^{a,c}

FULL SPECTRUM and FSLOCA are trademarks of Westinghouse Electric Company LLC, its affiliates and/or its subsidiaries in the United States of America and may be registered in other countries throughout the world. All rights reserved. Unauthorized use is strictly prohibited. Other names may be trademarks of their respective owners.